Biocatalytic P450 Oxidative Phenolic Coupling Reactions for Biaryl-bond Formation

by

Jessica A. Yazarians

A dissertation submitted in partial fulfillment
of the requirements for the degree of
Doctor of Philosophy
(Chemistry)
in the University of Michigan
2022

Doctoral Committee:

Professor Alison R. H. Narayan, Chair
Professor Robert Kennedy
Professor Roland Kersten
Professor Melanie S. Sandford

Jessica A. Yazarians

jyazaria@umich.edu

ORCID iD: 0000-0001-8129-8483

To my life partner and husband, Colton. Thank you for being the One.

To my father Emanoel, my mother Audrey and mother-in-law Kay, I miss you and may you both rest in peace. Thank you for thinking I'm smart while "college" has reminded me how much I have to learn.

To my dear friends and family who have loved and supported me unconditionally through this. Thank you for the beers, the cheers, and the tears.

Acknowledgements

They say never forget where you came from. While I think this statement is meant to instill humility and help us honor our roots, it also can be an imposition to remember to stay in your lane or make it difficult to see yourself in a new role in life. I've experienced both sides of that statement, as I have felt humbled by my tenure in grad school and grounded by my life's experiences and exceptionally grateful for the people that have shaped me along the way. I've also at times been afraid of moving forward and found it difficult to see myself as a scientist and take on that new identity. This work would not have been possible without my history and journey, or the love and support of my friends, family, and mentors. I have grown and learned so much because of this shared experience, and I am endlessly grateful for it. As I reflect on this accomplishment, I am truly astonished I made it this far. If you told me 10 years ago if I would be getting a PhD, I'm not sure I could have envisioned it. Not because I was incapable, but because I didn't know the path forward, or how to start climbing the mountain that was getting an education and realizing my life's dream of becoming a scientist. The first person I must thank for helping me close that gap and climb is Dr. Gregory Boyce, my undergraduate advisor at FGCU. Dr. Boyce saw potential in me and gave me the research opportunities and mentorship that I know got me to the next step. He truly helped open the possibility of grad school for me, and I wouldn't have had the courage to go for it without that guidance.

Secondly, I must thank my advisor, Professor Alison Narayan, for recruiting me, and giving me the freedom to let curiosity be the guide and to allow it to lead my research with all the "I wonder what if's…" Thank you for believing in me, for encouraging me and caring. Thank you for being open minded and allowing our group's values to evolve and grow, and for letting me be a part of that process. Thank you for holding space for me, and for others. I know it has not been easy, but it has been worth it, and I am so grateful that you continued to support and believe in me.

I also must thank my co-workers, past and present! #NarayanLabTries! I've been lucky to build some of the best friendships of my life in this lab, and I value the opportunity to get to know you all. Specifically, I want to thank Dr. Meagan Hinze, who taught me so much about science, from how to perfectly pack a column to sharing all your little chemistry tricks with openness and glee, and selflessly helping those around you. I will cherish our friendship, and the early 2000s playlists I'm sure no one else liked but us!

Shout out to the first classes of Naraynlab who were a part of what I fondly call the formative years, we are nearly all Doctors now! As I remember the first few years as a small group together, it was an unparalleled experience getting to live, laugh, and learn together. Thank you to all the scientists I have learned with and learned from while in this lab – all our postdocs and lab managers, and all the friendly neighbors in the LSI in the Mapp, Wang, and Sherman Labs.

I especially want to thank the P450 team: Meagan, April, Suman, Lara, and Lauren. I am so proud of the work we did together on a difficult but ultimately rewarding project. We did it! Thank you to Dr. Wendy Feng for teaching me so much about LC-MS, I could not have done my research without you and the instruments! I grew to love LC-MS, and you made a huge impact on the way I used the instruments –I will always filter my solvents and samples! Lastly, I want to thank Professor Melanie Sanford for your wisdom and support, and my entire committee for your suggestions and guidance throughout my career at Michigan.

The last thing I want to share here is one of the fondest memories of my mom. When I was beginning elementary school, I remember hating to read. My mom took me to the library, and she let me take out anything, any book I wanted. I started by reading about Nature – I had an obsession with birds, dinosaurs, black holes, weird animals and who knows what else. She encouraged me to learn to read by learning about the things I was interested in, giving me the freedom to develop the deep thirst for knowledge and exploration I have been fortunate to have throughout my life. These early experiences hooked me on science, starting this lifelong passion, which I am now able to finally pursue as my life's work. Thank you, mom, pop, and grandpa George, for encouraging curiosity and creativity from the start and ensuring those things were a part of my childhood. I am me because of you, and because of those trips to the library.

Table of Contents

List of Tables

List of Figures

List of Abbreviations

LC	liquid chromatography
ToF	time of flight
MS	mass spectrometry
HRMS	High-resolution mass spectrometry
EIC	extracted ion chromatogram
UPLC	ultra-performance liquid chromatography
DAD	diode array detector
AU	absorbance unit
NMR	nuclear magnetic resonance
TLC	thin layer chromatography
R_f	retention factors
THF	tetrahydrofuran
DMF	dimethyl formamide
DCM	dichloromethane
HFIP	hexafluoroisopropanol
NBS	*N*-bromosuccinimide
NIS	*N*-iodosuccinimide
HCL	hydrochloric acid
NHC	N-heterocyclic carbene
PCET	proton coupled electron transfer
µM	micromolar
mM	millimolar
mL	milliliter
µL	microliter
L	liter
Å	angstrom

xg	g force
OD	optical density
BMM	minimal media
LB	Luria broth
H^-	histidine dropout media
E. coli	*Escherichia coli*
S. cerevisiae	*Saccharomyces cerevisiae*
P. pastoris	*Pichia pastoris*
FI	fold improvement

Abstract

Atropisomers, derived from the Greek word "*atropos,*" meaning "without turn", are chiral molecules that possess a bond that is sterically hindered, impeding free rotation around that bond. This structural feature impacts the three-dimensional shape of atropisomers, which can influence the physical and biological properties of the compounds that contain this form of stereoisomerism. Atropisomers are structurally diverse, found in natural products, drugs, materials, and privileged scaffolds in asymmetric catalysis. The selective formation of chiral biaryl bonds in the form of sterically hindered atropisomers persists as an open challenge in modern synthesis. Synthetic strategies to forge hindered biaryl bonds often require either prefunctionalization at the desired site of bond formation, or the direct transformation of two C–H bonds into a C–C bond through oxidative coupling. However, control over the chemoselectivity, site-selectivity and atroposelectivity in direct oxidative coupling reactions remains challenging. Nature employs site- and stereoselective oxidative coupling in the synthesis of atropoisomeric natural products with enzymes such as cytochromes P450 (P450s) implicated in the intermolecular dimerization reactions of phenols.[1] Despite the growing number of enzymes capable of catalyzing oxidative coupling reactions site- and stereoselectively, most are not studied beyond their native reactivity, with few examples of enzymatic cross-coupling reactions reported.

The catalyst-controlled site-selectivity displayed by the P450 enzymes KtnC and DesC in the oxidative dimerization of coumarins provided inspiration for developing an enzymatic platform for oxidative phenolic coupling reactions.[2] We hypothesized that this class of enzymes could be developed into tunable biocatalysts for intermolecular fragment coupling, with the potential to overcome the limitations inherent to established synthetic methods for the direct oxidative coupling of phenolic compounds. Furthermore, applying P450s in biocatalysis for atroposelective cross-coupling reactions has the potential to compliment current methods but remains underexplored.

In Chapter 2, a biocatalytic platform for oxidative phenolic coupling catalyzed by the fungal P450s KtnC and DesC is disclosed. The engineering and heterologous expression of the genes encoding P450s in *Saccharomyces cerevisiae* and *Pichia pastoris* are described. Analytical methods for reaction profiling by liquid chromatography mass spectrometry were developed allowing for rapid method optimization. In chapter 3, the substrate scope of KtnC was further explored. The ability to catalyze atroposelective oxidative dimerization and cross-coupling reactions on a panel of coumarin substrates is demonstrated, with wild-type KtnC displaying promiscuity with non-native coumarins and phenolic substrates.

In Chapter 4, a directed evolution strategy was developed to engineer P450 variants with improved activity and selectivity, overcoming the challenges accessing cross-coupled coumarin products bearing the 6,6'-connectivity. Enzyme libraries were generated through semi-rational mutagenesis,[3] wherein beneficial mutations were identified through site-scanning saturation mutagenesis of active site residues.[4] Over two rounds of evolution, the chemoselectivity and site-selectivity of the KtnC-mediated reaction were enhanced in comparison to wild-type. A variant possessing two substitutions, P333G and L422V, provided a 3-fold increase in the percent yield of the desired product. This biocatalytic method for constructing sterically hindered biaryl bonds provides an engineerable platform for assembling molecules with catalyst-controlled reactivity and selectivity.

1. Huttel, W.; Muller, M., *Nat. Prod. Rep.* **2021**, 38, 1408-1408.
2. Mazzaferro, L. S.; Huttel, W.; Fries, A.; Muller, M., *J. Am. Chem. Soc.* **2015**, 137, 12289-12295.
3. Lutz, S., *Curr. Opin. Biotech.* **2010**, 21, 734-743.
4. Chen, M. M. Y.; Snow, C. D.; Vizcarra, C. L.; Mayo, S. L.; Arnold, F. H., *Protein Eng. Des. Sel.* **2012**, 25, 171-178.

Chapter 1: Biocatalytic Oxidative Cross-coupling of Coumarins and Phenols

1.1 Summary

The selective formation of chiral biaryl bonds in the form of sterically hindered atropisomers persists as an open challenge in modern synthesis. Atropisomers are represented by structurally diverse natural products, are found in drugs and materials, and are privileged scaffolds in asymmetric catalysis. The most commonly employed strategies to forge sterically hindered biaryl bonds require prefunctionalization at the site of bond formation or directly transform two C–H bonds into a C–C bond through oxidative coupling. Prefunctionalization strategies employing transition metal cross-coupling reactions dictate the site-selectivity by preinstallation of functional groups at the desired site of bond formation, at the expense of additional synthetic steps, the need for protecting group manipulations, and require screening to identify suitable conditions for each new pair of arenes coming together. Direct oxidative coupling of phenols allows for the coupling of two fragments without preinstalled functional groups, however, control over the chemoselectivity, site-selectivity, and atroposelectivity in reactions involving sterically hindered systems remains challenging. Examples of direct oxidative coupling in Nature in the synthesis of atropoisomeric natural products provide inspiration for leveraging the site- and stereoselectivity of enzymes such as cytochrome P450s and multicopper oxidases, including laccases and peroxidases. Cytochrome P450 enzymes are implicated in the selective intermolecular dimerization reactions of phenols in the biosynthesis of atropisomeric natural products, but few examples of cross-coupling reactions have been reported. Despite the numerous examples of enzymes capable of catalyzing oxidative coupling reactions site- and stereoselectively, many have not been studied beyond their native reactivity. Applying P450s in biocatalysis for atroposelective cross-coupling reactions has the potential to compliment current synthetic methods but has been underexplored.

1.2: Introduction

Axially chiral atropisomers are an important class of molecules possessing an axis of chirality around a sterically hindered biaryl bond.[1-2] This barrier to free rotation gives molecules a three-dimensional architecture that imparts the biological activity of natural products[3-4] and stereo-induction in asymmetric catalysis.[5-7] With a propensity to racemize in a temperature dependent manner, a compound is defined as an atropisomer if at a specified temperature it possesses a half-life of 1000 seconds or more.[8] For tetra-*ortho*-substituted biaryl compounds, the molecules are often configurationally stable and exist as two distinct, observable, and isolable isomers. Racemization can occur thermally, through photoinduction, and chemically, especially under acidic or basic conditions[8-9]. LaPlante and coworkers assigned three categories to compounds defined by the energetic barrier and rotational half-life of molecules to assess if atropisomers were possible and described the time-scale for interconversion, developing a computational model using quantum mechanical calculations to predict the rotational barrier and rate of racemization (Figure 1.1).[10] This method was developed as a tool to identify atropisomers in the drug discovery pipeline, relating the energy barrier and the rate of interconversion between isomers. Class I compounds freely rotate around a biaryl bond, with a barrier of rotation up to 20 kcal/mol, and experience fast axial rotation rates of seconds or less and are not classified as atropisomers. Class II compounds, with barriers of rotation between 20 and 30 kcal/mol and rotation half-life of minutes to hours, have the potential to form atropisomers, but with lower energy barriers and fast rates of interconversion, these compounds are prone to racemization. Class III compounds possess rotational energy barriers above 30 kcal/mol with rotational half-lives on the order of months to years and are considerably more stable.

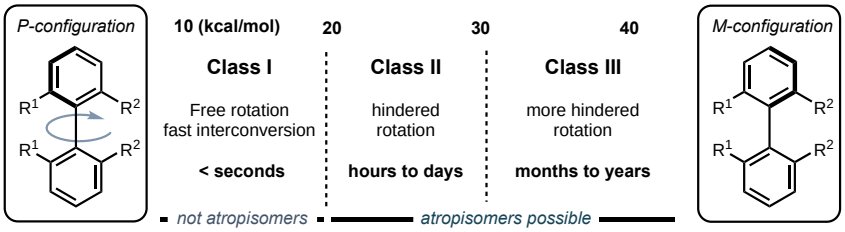

Figure 1.1: Rotational barrier in axially chiral compounds.
Class I-III describes the energetic barrier for the interconversion of atropisomers (kcal/mol) and the time scale for the half-life of torsional rotation.

Biaryl scaffolds are ubiquitous in drugs and diversely represented in the core structures of natural products (Figure 1.2A). [11-13] With a combination of traditional stereogenic centers and a biaryl bond which creates an atropomeric axis of chirality, the antibiotic vancomycin, **1**, possesses a three-dimensional structure that selectivity interacts with a biological target to convey its potent antibiotic activity.[8, 14-15] Ancistrocladine, **2**, also contains stereogenic and atropoisomeric centers, and is representative of a large class of isoquinoline alkaloids isolated[16] from tropical vining liana from the *Ancistrocladus* genus displaying promising antiplasmodic and anti-HIV activity.[4, 17-18] The pharmacological differences between enantiomers of drugs[19] have been well documented, including for atropisomers, suggesting the importance for considering atropisomerism in drug development and design.[3, 20-21] For example, greater activity has been attributed to (*M*)-gossypol[22] (a more potent Bcl-2 inhibitor with undesirable side-effects compared to *P*-gossypol), telenzepine[23] (an antimuscarinic, FDA approved drug with a 500-fold increased activity in the (+)-isomer), and cholchicine[24] (an antimicrotubule agent with greater activity exhibited by the *M*-isomers of cholchicinoid atropisomers[25]).[3, 20, 26]

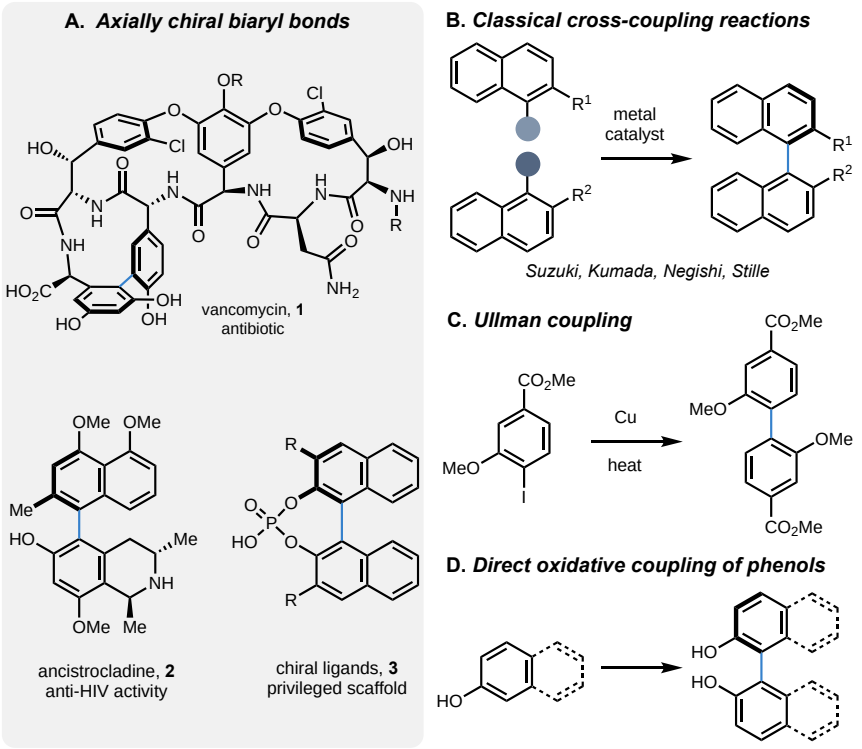

Figure 1.2: A. Axially chiral biaryl bonds in natural products and ligands. B-D. Chemical methods for biaryl bond formation.

Beyond natural products, drugs, and materials,[27-28] the C_2-symmetric substituted 2,2'-binaphthalenes are a privileged ligand scaffold for asymmetric metal catalysis and organocatalysis.[11] BINOL-type scaffolds comprise a large class of chiral ligands

employed for a wide range of transformations, with installation of different groups at the C3, C4, and C7-positions to modify their steric and electronic properites.[6, 29] Appending larger groups with extended π-systems, or with more electron-rich or electron-withdrawing properties allow for tunable stereoelectronic properties that can be tailored to the desired reactivity and starting materials in a transformation, regulating the stereochemical outcome.[5] For example, chiral phosphoric acids, such as **3** (Figure 1.2A), are employed as organocatalysts in a growing number of reactions, from reductive aminations,[30] Friedel-Crafts alkylations,[31] and hetero-Diels-Alder reactions.[32]

Forging hindered biaryl bonds chemo-, site- and atroposelectively remains an outstanding challenge in modern synthesis.[8, 15, 33-35] Numerous methods have been developed including cross-coupling reactions that join two pre-functionalized aryl fragments with transition metal catalysts[7, 36-37] (Figure 1.2B), reductive coupling of aryl halides through the Ullman reaction (Figure 1.2C),[38-40] and the direct oxidative coupling of phenols (Figure 1.2D).[41-42] Of the methods reported for atroposelective biaryl bond formation, many are categorized into one of two strategies: (1) reaction which require prefunctionalization or (2) direct oxidative coupling reactions, each with unique advantages and constraints.

1.3 Prefunctionalization Strategies

Prefunctionalization strategies are documented and include transition metal catalyzed reactions such as the Kumada,[43-44] Negishi,[45-48] Stille,[49] and Suzuki-Miyaura[37, 50-51] cross-coupling reactions (Figure 1.2B-D).[21, 36, 45, 52-54] These reactions share the advantage of preprogrammed site-selectivity, forging the desired biaryl bond between fragments at the site of preinstalled functional groups, and can achieve enantioselectivity with chiral ligands or auxiliaries. Synthesis of prefunctionalized coupling partners adds additional steps in a synthetic campaign, particularly redox and protecting group manipulations. In some cases, installation of a functional handle at the desired site of bond formation is not achievable, limiting access to the desired connectivity in the final product.[55] Additionally, reactions are limited by functional group tolerance, especially when utilizing organomagnesium and organozinc species, while each reaction class

requires screening to identify suitable conditions for each new pair of coupling partners.[56-62]

General reactivity in the formation of hindered biaryl bonds suffers with the addition of substituents *ortho* to the site of bond formation, with tetra-*ortho*-substituted motifs the most challenging to access. [13, 60, 63] Of these classes of reactions, palladium catalyzed Suzuki-Miyaura cross-couplings are the most utilized due to tolerance of a wider range of functional groups, milder reaction conditions, and stable starting materials such as aryl halides, triflates, and boronic acids derivatives.[50, 64] Identification of cross-coupling conditions that allow the synthesis of sterically hindered biaryl bonds are reported but are few in comparison to more general Suzuki cross-coupling reactions that are less sterically demanding.[37, 62, 65-67] The first example of an asymmetric tetra-*ortho*-substituted Suzuki cross-coupling by Cammidge in 2000 (Figure 1.3A) leveraged a mono-phosphine ferrocene ligand to achieve modest yield and ee's, however, this required extended reaction times (6 days), and substantial competing deborylation was observed.[68] To reduce this undesirable side reaction, two equivalents of the boronic ester, anhydrous conditions with careful drying of all reagents, and the use of an aryl iodide electrophile were required for catalysis. Buchwald developed biaryl phosphine ligands in 2002 bearing a bulky phenanthrene group on the southern ring and bicyclohexyl

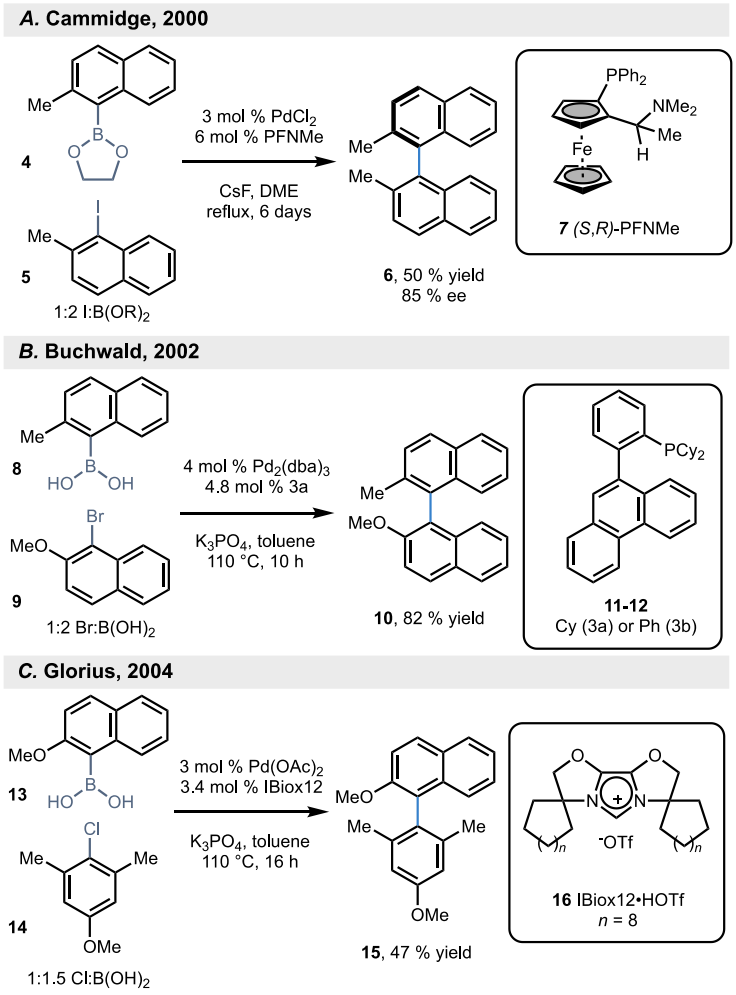

Figure 1.3: Tetra-*ortho*-substituted Suzuki cross-coupling reactions.

substituted phosphine **11** on the northern ring, reporting 16 examples of tetra-*ortho*-substituted products with moderate to excellent yields (Figure 1.3B).[67] The negative effects of traces of water in the reactions leading to debromination rather than deborylation are documented in these studies. Glorius and coworkers developed a class of *N*-heterocyclic carbene (NHC) ligands with a rigid tricyclic bioxazoline core, appended with flexible cycloalkyl rings that could be tuned to improve reactivity.[69] Ligand IBiox12 (**16**) with dodecyl-cycloalkyl substituents enabled sterically demanding cross-couplings, with several examples reported with hindered aryl chlorides and boronic acids (Figure 1.3C).

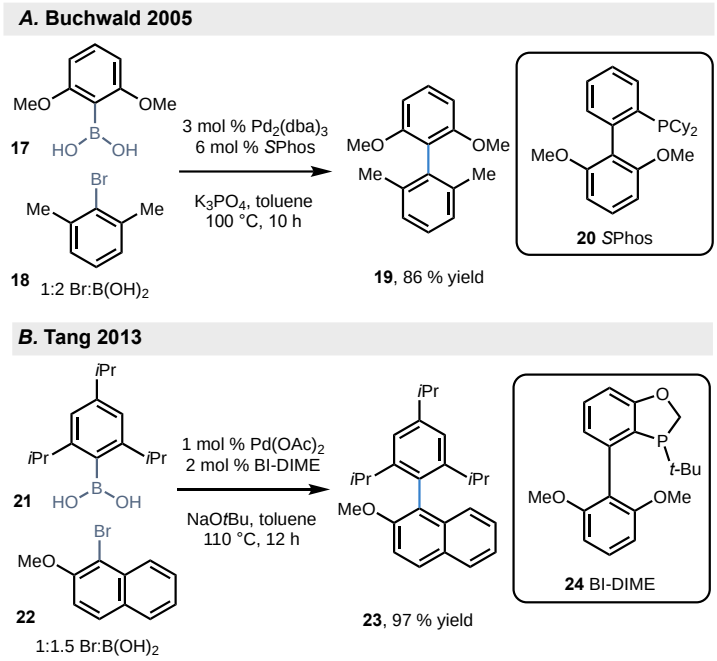

Figure 1.4: Improved ligands for tetra-*ortho*-substituted Suzuki cross-coupling reactions.

In 2005, a bicyclohexyl phosphine ligand *S*Phos (**20**) was reported by Buchwald and coworkers that enabled reactions to proceed at lower temperatures with aryl chlorides and a greater range of functional groups for tri-substituted couplings, while remaining effective for tetra-*ortho*-couplings (Figure 1.4A).[64] With similarities to the structural motif of electron-rich biaryl *S*Phos, Tang developed a new class of biaryl monophosphorous BI-DIME ligands with an oxaphosphole moiety that provided greater rigidity of the top biaryl ring preventing rotation of the phosphonyl group (**24**, Figure 1.4B).[65, 70] This feature locks the palladium-BI-DIME complex into one confirmation, compared to *S*Phos that can freely rotate around the unhindered biaryl bond and adopt multiple conformations. It has been postulated that steric constraints provide a rigid ligand backbone which leads to greater activity by stabilizing the reactive $L_1Pd(0)$ after dissociation of one ligand and subsequent oxidative addition in the catalytic cycle in both phosphine and NHC ligands, supported by experimental evidence based on X-ray crystallography and computational studies of the Pd complexes.[71-73] The BI-DIME catalyst was effective in sterically

demanding Suzuki cross-couplings, with over 20 examples of tetra-*ortho*-substituted products reported.[65]

Although progress has been made in achieving general reactivity in forming sterically hindered tetra-*ortho*-substituted biaryl bonds through Suzuki cross-coupling, most examples do not report catalyst controlled atroposelectivity. Cammidge observed changes in the enantioselectivity based on the boronic ester used, postulating that the enantio-determining step was transmetalation.[58, 68, 74] Other examples for controlling atroposelectivity required proximal coordinating groups on the aryl halide (Tang, 2012)[75] and linking an imidazoindole phosphine ligand to a PEG polymer (Ouzomi, 2009).[76] More recently in a collaborative effort between the Kozlowski and Garg groups, progress towards asymmetric Suzuki and Negishi cross-coupling reactions with *P*-chiral dihydro-benzooxaphosphole (BOP) ligands were disclosed (**30** and **36**, Figure 1.5).[45] Supported by computational studies of the mechanism of both reactions, the enantiodetermining step was reductive elimination for the Negishi reactions, with transmetalation and reductive elimination accounting for the greatest contribution to stereoselectivity in Suzuki reactions, although they note all steps of the Suzuki catalytic cycle playing a role in enantioselectivity.

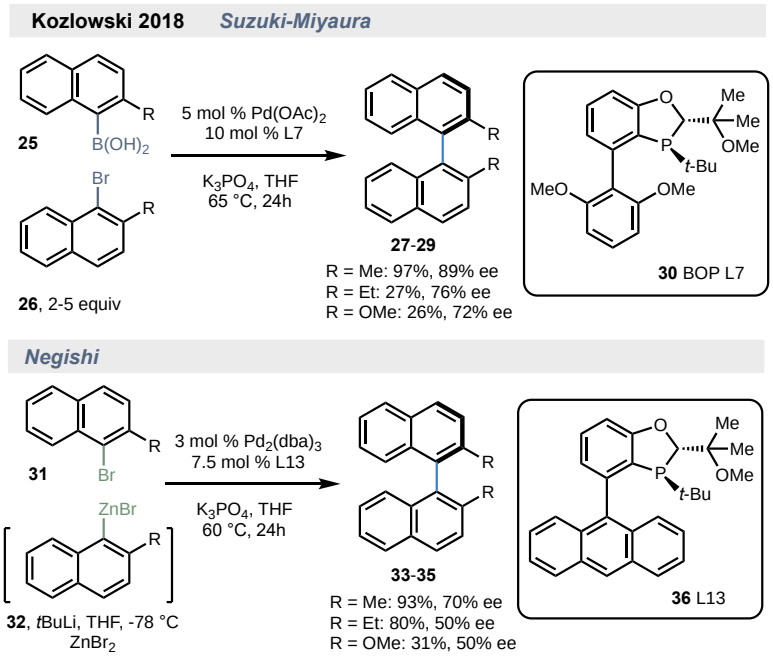

Figure 1.5: Improved ligands for tetra-*ortho*-substituted Suzuki cross-coupling reactions.

Despite these advances, to date, no general conditions or catalysts have been discovered that have wide generality for different substrates in sterically demanding cross-couplings, making it difficult to rely on convergent strategies for selective synthesis of atropisomers through classical cross-coupling reactions. Minor changes that alter the stereoelectronic properties of substituents on either aryl coupling partner can reduce or

eliminate reactivity and erode enantioselectivity (Figure 1.5), percent yield and percent ee shown for different R groups, necessitating screening for new conditions with each unique pair.[45] A general lack of chemical diversity and complexity is also apparent, with few examples of heterocycles or densely functionalized aromatic rings populating substrate scopes. However, from methods developed over the last 20 years, some trends for successful tetra-*ortho*-cross-couplings have emerged (Figure 1.6A). The exclusion of water has been shown to prevent undesired proto-deborylation of the boronic acid and the proto-dehalogenation of aryl halides. Addition of excess boronic acid species, with a preference for boronic acids over esters, is often required to mitigate these undesired side reactions, with two to five equivalents typically added.[45, 58, 67, 71] Electron-poor boronic acids undergo more facile transmetalation and can improve the reaction.[73] Optimization of the base has largely been empirically derived, but K_3PO_4 stands out as the base of choice in many examples of sterically hindered cross-couplings.[71] Solvents such as toluene, xylenes, and THF are common, with higher temperature and longer reactions times typical. The palladium(II) source and ratio of palladium to ligand can be crucial, with evidence that dissociation of one ligand and stabilization of the mono-ligand $L_1Pd(0)$ species for oxidative addition are critical for successful catalysis.[71-72] Features of ligands that improve yield and enantioselectivity have advanced through empirical evidence, X-ray crystallography, and computational studies, providing insight into catalytic intermediates to inform the design of new ligands that are increasingly effective at this difficult transformation (Figure 1.6B).[71-72, 77-78]

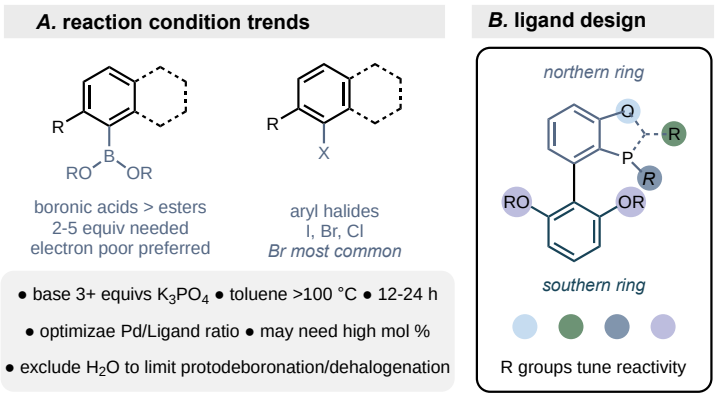

Figure 1.6: Reaction condition trends and ligand design.

1.4 Direct oxidative coupling of phenols

Oxidative coupling provides an attractive strategy for convergent fragment coupling through the net transformation of two C–H bonds into a C–C bond through the favorable one-electron oxidation of phenols.[79] Additional synthetic steps to install functional groups at the desired site of bond formation is unnecessary, and phenols are coupled directly without protecting groups.[55, 80] However, these advantages come at the expense of the yield and selectivity, which is dictated by the intrinsic steric and electronic properties of each substrate, thereby limiting the versatility of this transformation.[55, 81-83] Numerous metal catalyst and metal-free oxidants have been reported for the dimerization and cross-coupling of phenolic substrates; however, the application of these methods is commonly restricted to electron-rich phenols or those bearing only mildly electron-withdrawing groups such as halides (Figure 1.7A).[81-98] Reports featuring V,[92, 99-101] Cr,[82, 102] and Co[103] catalysts are disclosed in the literature, with copper[33, 96, 104-108] and iron[109-116] catalysts representing the majority of methods for this chemistry. Metal-free conditions explored by Kita and coworkers employ hypervalent iodide reagents such as PIDA and PIFA for oxidative coupling, mainly in dimerization reactions.[117-118] Electrochemical

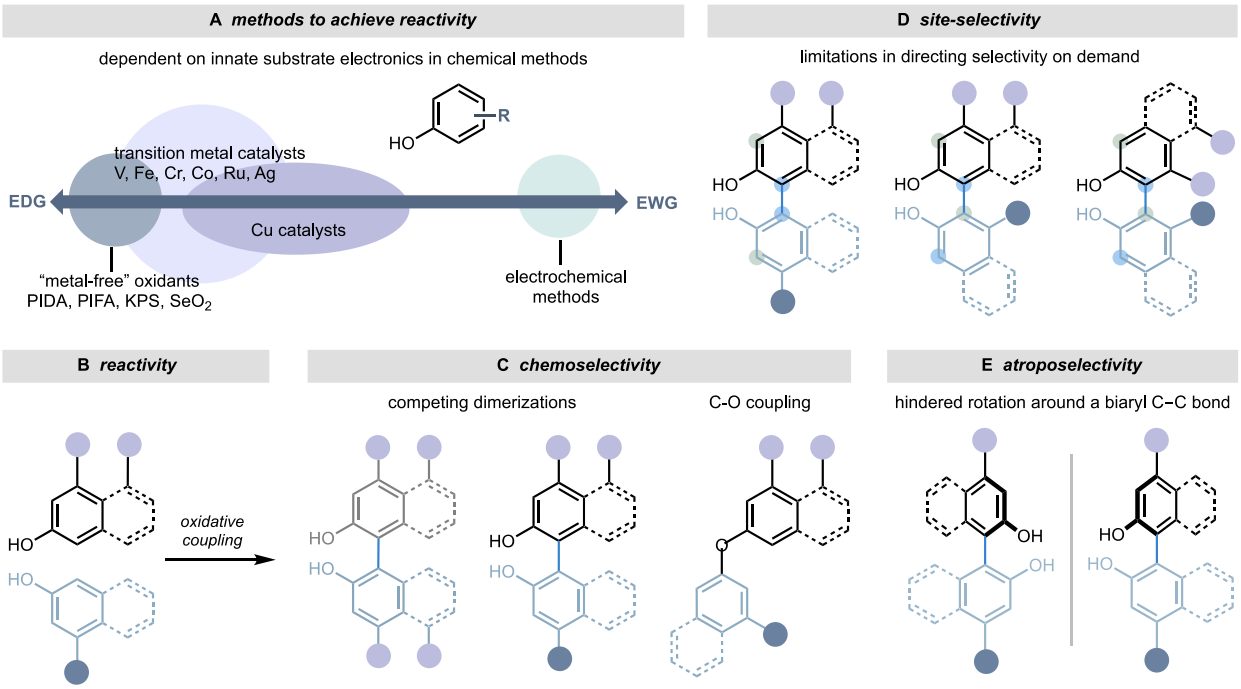

Figure 1.7: Control over selectivity in oxidative coupling of phenols.

methods have been developed for the dimerization of phenols with electron-withdrawing groups such as nitrenes, oximes, and sulfones, with limited scope for cross-coupling phenols to naphthalene.[88, 119] When general reactivity can be achieved, controlling the selectivity of the oxidative coupling reaction presents several additional layers of difficulty with the need to exert control over chemo-, site-, and atroposelectivity to form sterically hindered biaryl bonds (Figure 1.7B-E). Through the phenoxyl radical intermediate formed from one-electron oxidation, controlling chemoselectivity to favor dimerization, cross-coupling, or C-O coupling is challenging and often is not under catalyst control (Figure 1.7C). If more than one site for bond formation is available, the electronic properties of substituents dictate the site-selectivity, favoring carbon atoms with an accumulation of spin density *ortho* or *para* to the phenol, with *meta* positions typically inaccessible (Figure 1.7D).[41, 120] This electronic bias can be advantageous if only one site is activated for bond formation, resulting in excellent site-selectivity. However, if there are multiple electronically ambiguous reactive sites, isomeric products can form in an unselective manner. Site-selectivity can also be influenced by reaction conditions, with solvents such as hexafluoroisopropanol (HFIP) capable of changing selectivity by altering the mechanism.[115]

Lastly, controlling enantioselectivity in sterically hindered systems (Figure 1.7E) is similarly difficult in comparison to prefunctionalization strategies. Methods can be atroposelective if chiral ligands are employed; however, achieving high enantioselectivities across a broad range of substrates remains elusive.[8] Copper oxidants with chiral amines as ligands were developed to afford dimers of 2-naphthol with high yields and atroposelectivity.[104, 108] An alternative approach utilizes chiral auxiliaries, especially chiral ethers, as intramolecular tethers followed by auxiliary cleavage after biaryl-bond formation.[121] Enantioenrichment can also be achieved through dynamic kinetic resolution, with a notable example using $CuCl_2$ and amphetamine to achieve enantiopure material.[106]

Whereas reports of dimerization of phenols outnumber oxidative cross-coupling reactions, early examples of selective oxidative cross-coupling reactions were reported by Smrčina with the synthesis of C_1-symmetric ligand NOBIN and other unsymmetrical binaphthalenes (Figure 1.8A).[122] Kozlowski used computer modeling to predict new

ligands for asymmetric coupling reactions and developed a catalytic system with a 1,5-diaza-*cis*-decalin copper complex for asymmetric dimerization of C3 substituted 2-naphthols.[123-125] Smrčina and coworkers later hypothesized that cross-coupling of phenols would proceed preferentially with a sufficient difference in oxidation potential between two phenols ($\Delta E_p \geq 0.25$ V), proposing the coupling partner with lower oxidation potential (more negative) is oxidized first, then captures the less oxidizable partner (higher oxidation potential) to form the cross-coupled product.[120, 122, 126] When the oxidation potentials of the two phenols are similar, the reactions are not chemoselective and result in mixtures of dimers and cross-coupled products. Over two decades later, site- and chemoselective oxidative coupling methods are still being developed and utilized in synthesis, with Porco's creative approach using blocking groups in the late-stage oxidative dimerization with VOF_3 as a key step in the total synthesis of gonytolide A (**42**, Figure 1.8B).[127] The Kozlowski group has made major contributions developing new catalysts over this time for oxidative coupling reactions, particularly chiral copper, vanadium, and chromium catalysts for asymmetric dimerizations.[33, 82, 124, 128] A 2014 study of 36 metal-Salen/an complexes uncovered optimized conditions for oxidative cross-coupling and discussed the origin of site-selectivity in *ortho-ortho*, *ortho-para*, and *para-para* coupling reactions of phenols.[102] A chromium-Salen catalyst with cyclohexyl

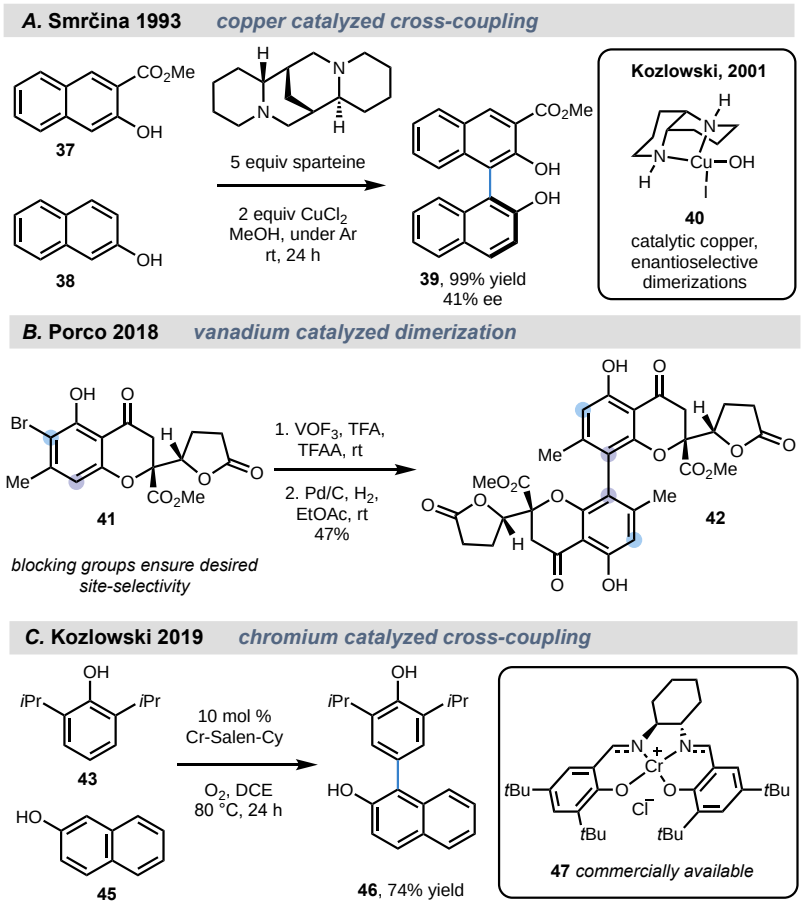

Figure 1.8: Metal catalyzed oxidative coupling reactions.

diamine backbone (**47**) emerged as the most general and useful catalyst and was the subject of additional studies that expanded the substrate scope of oxidative cross-coupling reactions (Figure 1.8C). A 2019 investigation disclosed over 20 examples of oxidative cross-coupling with moderate to excellent yields.[82] However, there was limited chemical diversity (primarily *ortho*-substituted phenols bearing one hydroxyl group with 2-naphthol derivatives). A follow up paper in 2020 included aminonaphthalenes and anilines as coupling partners to phenols and naphthols, enhanced by changing the solvent from DCE to HFIP with *t*BuOOH as the terminal oxidant.[97] Across more than 40 cross-coupled products reported, only three examples were tetra-*ortho*-substituted and none of the methods were enantioselective, highlighting the continued need for atroposelective oxidative cross-coupling reactions.

1.5 Iron-catalyzed direct oxidative coupling of phenols

The Pappo group has focused on investigating oxidative phenolic dimerization and cross-coupling reactions, making considerable progress in understanding the mechanisms of different iron catalysts and exploring the basis of control over chemo and site-selectivity in cross-coupling reactions (Figure 1.8). Building on the work of Smrčina[120] and Katsuki[109, 129] to understand the chemoselectivity of cross-coupling of phenols, in 2015, Pappo and coworkers developed a predictive model based on mechanistic studies, experimentally measured oxidation potential (E_{ox}), and the computationally calculated nucleophilicity (N) of different phenols (Figure 1.9A, top panel).[114] Grouped into two categories, Group A possessed lower oxidation potentials and were selectively oxidized by the iron catalyst, while group B were more nucleophilic, attacking phenoxyl radical electrophiles. Using this model, they predicted that cross-coupling would be preferred if two conditions were met, $E_{ox}A < E_{ox}B$ and NB > NA. In cases where the oxidation potential or nucleophilicity created a mismatch between phenols, the chemoselectivity of the reaction was diminished. Based on detailed kinetic studies, they proposed two potential mechanisms to explain the chemoselectivity observed in this reaction and others: 1) a radical-radical mechanism via radical recombination of two *para*-phenoxyl radicals, which results in homocoupling of the group A phenol in a *para-para* site-selective manner, or 2)

a radical-anion mechanism characterized by reversible chelation of A and B to the iron center through formation of one phenoxyl radical, and addition to the coupling partner A or B. Through this mode, homocoupling or cross-coupling can occur, favoring cross-coupling by pairing two “matched” phenols from A and B groups, while less chemoselectivity occurs when the phenols are not complimentary.

In efforts to develop an enantioselective method (Figure 1.9A, lower panel), the cross-coupling of substituted 2-naphthol and phenol substrates was investigated in 2016 with a chiral iron-phosphoric acid complex.[113] Although this method was successful in cross-coupling C_1-symmetric BINOL type products with some variation, the yields were low, hovering around 50%, with ee’s ranging from to 62% to 92%. This catalyst system was proposed to proceed through a radical-anion mechanism, and while atroposelective,

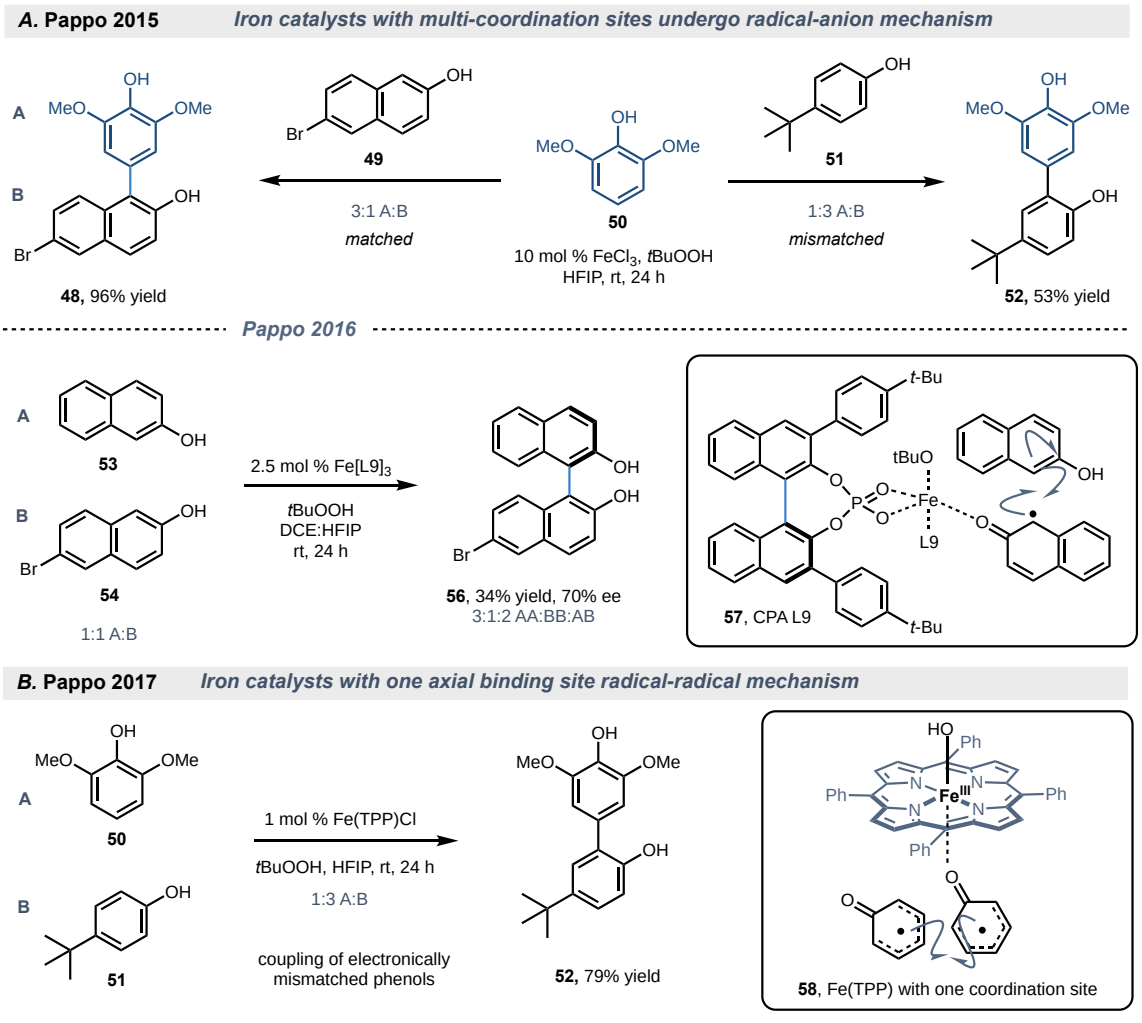

Figure 1.9: Selectivity in iron catalyzed oxidative cross-coupling reactions of phenols.

the reaction was not chemoselective, resulting in mixtures of dimers in addition to the cross-coupled products. Interestingly, racemization of the BINOL type biaryl products was observed with catalytic amounts of both iron(III) and coper(II) salts, proposed to occur through a reversible process due to binding of the product to two open coordination sites at the metal, with single electron transfer forming a binaphthyl radical that undergoes racemization.

To develop a reaction that did not require electronically complimentary phenols to achieve an efficient cross-coupling reaction, biomimetic iron-porphyrin complexes were investigated (Figure 1.9B).[112] Previous kinetic studies indicated that the number of coordination sites open for phenol binding influenced the mechanism, for example, with $FeCl_3$, both phenols are coordinated to iron and can proceed through an intramolecular radical-anion mechanism. Stoichiometry studies with iron and phosphate ligands to optimize **57** provided evidence that the active catalytic species was a biphosphate, potentially leaving two open *cis*-coordination sites, however, this was not definitively verified. In contrast, porphyrin-iron complexes allow only one axial coordination site, potentially impacting the operative mechanism. NMR, EPR, and competitive binding studies of the porphyrin-metal complex suggested electron transfer between a ligated phenol (B) and the iron complex, similar to the electron “push” mediated by axial ligands in heme-containing enzymes. This promoted the oxidation and liberation of phenol (A), followed by diradical combination of A and B. With this unique mechanism, two electronically and/or nucleophilic mismatched phenols were cross-coupled in higher yield **52**, 79%, (Figure 1.9B) compared to chiral iron-phosphate catalyst **52**, 53%, (Figure 1.9A).

Comprehensive studies using kinetic data, computational modeling, and NMR/EPR to investigate the mechanistic basis of reaction selectivity in different redox active iron complexes has built a framework to predict reactivity in oxidative phenolic coupling reactions.[110] Despite these advances in gaining catalyst control, considerable hurdles remain in expanding the scope to include more diverse phenols and reliably synthesize a specific product isomer.[8, 15, 83, 93, 127, 130] If the intrinsic steric and electronic properties of the reacting phenols, together with the operative mechanism in the coupling reaction preclude access to certain product isomers, synthesis of unfavored products remains an unsolved problem.

1.6 Enzymatic oxidative phenolic coupling reactions

Nature has evolved catalysts for oxidative dimerization of phenolic compounds to generate biaryl natural products with control over site- and atroposelectivity.[4, 131] Examples of natural products containing biaryl phenolic bonds are plentiful, such as melanin,[132] flavonoids,[133] and coumarin dimers.[134-138] A growing number of these catalysts have been identified in the biosynthetic pathways of biaryl natural products,[135, 139-151] including laccases,[151-152] peroxidases,[153] multicopper oxidases (MCOs),[154] and cytochrome P450 monooxygenases (P450s)[155-157] from bacteria, fungi, and plants. Although laccases have been employed in biocatalysis, these enzymes have only been shown to exert control over the selectivity of the C–C bond-forming event following the initial oxidation in a limited number of examples,[151, 158] and more commonly afford complex product mixtures.[152, 159] In contrast, P450s associated with secondary metabolite biosynthesis often exhibit excellent control over the site- and atroposelectivity in oxidative coupling reactions.[160] Intramolecular biaryl bond forming reactions have been studied in greater depth, though intermolecular reactions have the potential to be more impactful in the application of biocatalysis and synthesis. Like chemical methods for direct oxidative coupling, these enzymes are hypothesized to similarly proceed through hydrogen atom

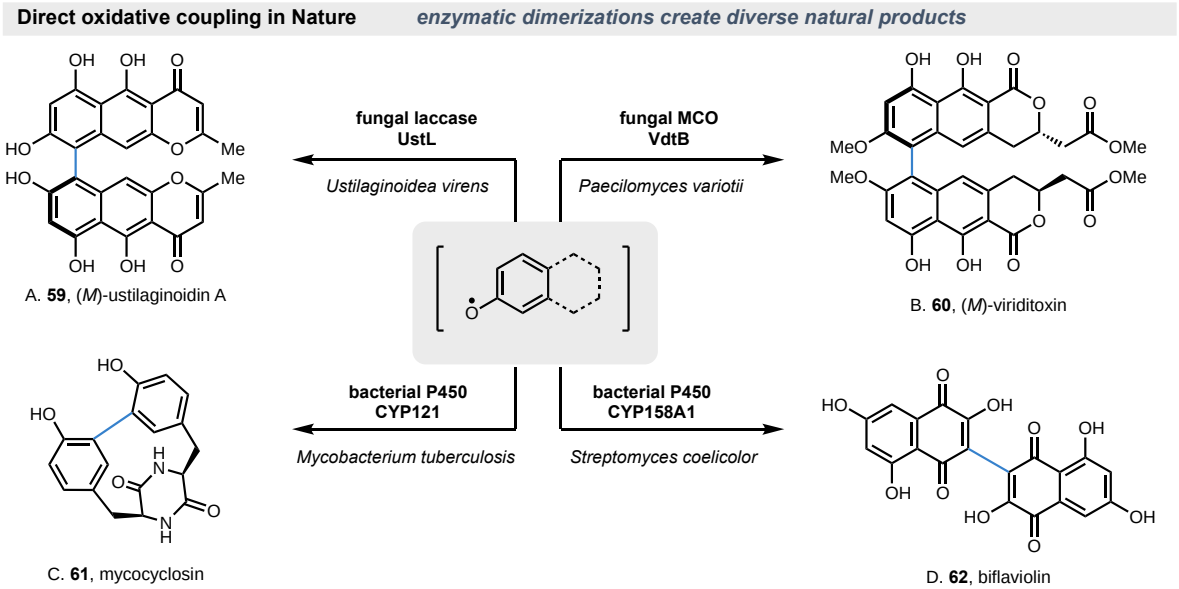

Figure 1.10: Enzymatic oxidative dimerizations of phenols.

abstraction and generation of a phenoxyl radical species in both intra- and intermolecular processes (Figure 1.10).[131, 151, 154, 161-162] To date, most reports for enzymatic oxidative phenolic coupling consist of either intramolecular coupling, or dimerization reactions with few examples of enzymatic phenolic cross-coupling described.[163]

In a rare example of the selective oxidative phenolic coupling catalyzed by a laccase, Müller and coworkers described the oxidative dimerization of γ-naphthopyrones to the natural product (*M*)-ustilaginoidin A (**59**, Figure 1.10A).[151] Laccases, copper-containing enzymes adept at generating phenoxyl radicals through a one-electron oxidation, typically act as an oxidant without control over the site- or stereoselectivity of the reaction. Through characterizing the biosynthetic pathway using cell lysate of the heterologous host *Aspergillus niger* expressing UstL, dimeric product **59** was observed as the major product in a site- and atroposelective reaction, selectivity which is usually attributed to the presence of noncatalytic dirigent proteins.[164] Chooi and coworkers reported the activity of a multicopper oxidase enzyme, VdtB, and a dirigent protein, VdtD, that imparts site- and atroposelectivity in the dimerization of naphthopyrones in the biosynthesis of (*M*)-viriditoxin (**60**, Figure 1.10B).[150] The MCO is implicated in the oxidation, while VdtD, a unique example of a fungal dirigent protein, controls the selectivity in the C–C bond forming event.

In contrast, cytochromes P450 can exhibit more control over the selectivity in oxidative dimerization reactions, without the need for dirigent proteins. Numerous examples of P450 catalyzed intramolecular oxidative phenolic coupling reactions have been reported, such as the C–C *ortho-para* coupling in (*R*)-reticuline in the endogenous mammalian biosynthesis of morphine by human P450 2D6 reported by Grobe,[165] and the P450 salutaridine synthase in morphine biosynthesis in the opium poppy *Papaver somniferum*.[166-167] The intramolecular *ortho-ortho* C–C phenolic coupling in the biosynthesis of cyclic natural product mycocyclosin (**61**) was reported to be catalyzed by the P450 CYP121, an enzyme essential for viability of the producing organism *Mycobacterium tuberculosis* (Figure 1.10C).[168]

Of the enzymes known to catalyze intermolecular oxidative phenolic coupling reactions, the bacterial P450 enzymes CYP158A1 & 2 that are responsible for the dimerization of flaviolin have been the most comprehensively studied from a structural

basis (**62**, Figure 1.10D).[146, 162] High resolution X-ray diffraction of single crystals containing flaviolin substrate bound in the active site of CYP158A2 show two molecules of flaviolin co-localized and stacked together, as well as the location of hydrogen bond networks between amino acid residues and water molecules in the active site.[169] The hydrogen bond networks position the substrates in the active site, forming a polar environment for catalysis at the heme cofactor. Whereas no definitive evidence for a specific mechanism is presented, both a diradical recombination and cationic mechanism have been proposed.[170-171]

Since the co-crystallization of flaviolin and CYP158A2 in the early 2000's, no detailed spectroscopic or kinetic studies of oxidative phenolic coupling P450 enzymes have been disclosed, thus mechanistic insight is lacking. In addition, isolation and purification of fungal P450 enzymes, which are often membrane bound and rely on electron transport from an external reductase partner, is expressly difficult, limiting the ability to conduct *in vitro* experiments.[156] Despite these limitations, two main mechanistic proposals are most commonly invoked: 1) a diradical recombination mechanism 2) a radical-addition mechanism (Figure 1.11). Both mechanisms begin with hydrogen-atom abstraction by the iron(IV)oxo species oxidant, which is formed by substrate binding,

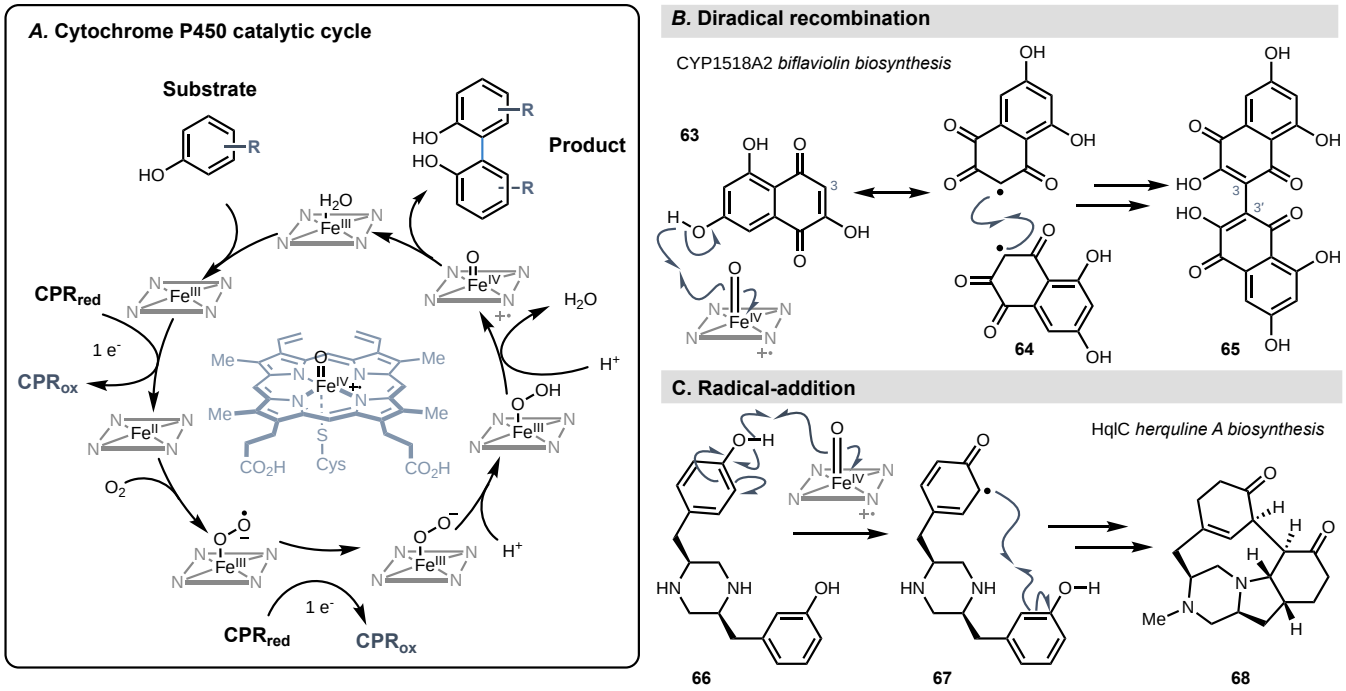

Figure 1.11: Cytochrome P450 catalytic cycle and proposed mechanisms.

delivery of one electron from a cytochrome P450 reductase (CPR) to the iron center, binding of O_2, a second electron transfer from the CPR, and finally protonation and cleavage of ferric hydroperoxide to the active catalytic species (Figure 1.11A).[172] In the diradical mechanistic proposal, hypothesized in the biosynthesis of biflaviolin and other dimeric natural products, two hydrogen-abstraction occur within the enzyme active site and C–C bond formation occurs with a radical-radical recombination. Alternatively, in a radical-addition mechanism, only one radical is formed within the enzyme active site, and C–C bond formation occurs with the radical attacking a closed-shell, neutral or ionic species.

In the absence of structural information, computational studies have expanded to fill the gap in mechanistic understanding of P450 mediated oxidative coupling reactions. In 2016, the Houk and Tang groups disclosed studies utilizing DFT and relative Gibbs free energy calculations of intermediates and products proposed in the biosynthesis of several phenolic biaryl natural products, the spirocyclic antifungal griseofulvin[173-175] and cyclic piperazine alkaloid herquline A.[161, 176] Coupled with experimental data, plausible mechanisms were proposed in two studies which provide computational evidence for a radical-addition mechanism for the intramolecular P450 catalyzed oxidative phenolic biaryl couplings of griseofulvin and herquline A. Both P450s, GsfF in the formation of a spirocyclic C–O bond, and HqlC in the formation of a C–C bond between the tyrosine sidechain of a diketopiperazine of herquline A are proposed to proceed through a radical-addition mechanism, with one phenoxyl radical generated through H-atom abstraction, followed by radical addition to a neutral phenolic partner. This mechanism is in contrast to the computational studies that support the diradical mechanism in the intramolecular C–C coupling in the biosynthesis of the related compound mycocyclosin. Through high resolution X-ray diffraction of the co-crystallized P450 enzyme with its diketopiperazine substrate[168] and QM/MM modeling,[177] a mechanistic proposal for oxidative coupling was proposed as an initial hydrogen-atom abstraction, proton-coupled electron transfer (PCET), a second hydrogen atom abstraction, and diradical recombination. Finally, a radical-radical mechanism is proposed in the biosynthesis of communesin by P450 CnsC for the cross-coupling of non-equivalent indoles through two N-H atom abstractions and formation of a radical and combination to form a quaternary C–C bond.[178]

Promisingly, P450s that mediate intermolecular oxidative dimerization chemistry have recently been identified but have not been investigated as biocatalysts capable of chemistry beyond their native reactivity.[135, 139-148] Among the P450s previously characterized to perform oxidative dimerization reactions in the biosynthesis of biaryl natural products, we were initially drawn to a small cluster of *Aspergillus* P450s, KtnC and DesC, that each imparts a unique site-selectivity in the oxidative dimerization of coumarin **69**, as demonstrated by Müller and coworkers.[135] This catalyst-controlled site-selectivity provided a tantalizing starting point for developing an enzymatic platform for oxidative coupling reactions. We hypothesized that this class of enzymes could be developed into tunable biocatalysts for convergent, intermolecular fragment coupling, providing a paradigm for oxidative cross-coupling reactions with catalyst-controlled selectivity. Developing a biocatalytic oxidative cross-coupling reaction would have the potential to overcome the limitations inherent to established methods for direct oxidative coupling of phenols.

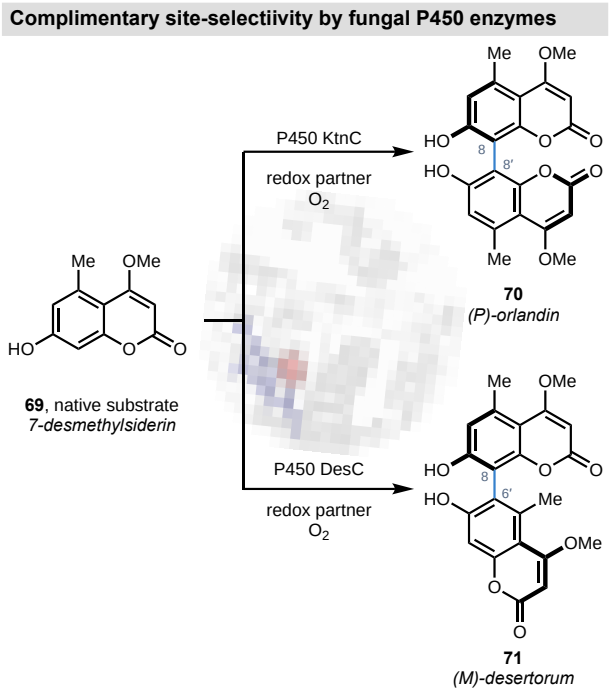

Figure 1.12: Catalyst controlled site- and atroposelectivity by fungal P450s KtnC and DesC.

1.7 Conclusions

Biaryl bonds with hindered rotation are abundant in natural products, drugs, materials, and ligands. Their three-dimensional structure impacts the function of this diverse group, but in medicinal chemistry, atroposelectivity is often overlooked as a source of stereoisomerism.[8, 10, 26] Atroposelective biaryl bond formation remains a challenging transformation in modern chemistry.[179] Although numerous methods have been developed, each has limitations that impede their reliable incorporation into synthetic routes and into target compounds. The most widely utilized routes, transition

metal catalyzes cross-coupling reactions, excel in building biaryl C–C bonds that are less sterically demanding, with methods for cross-coupling arenes with mono, di, and tri-*ortho*-substituents disclosed.[71-72] Tetra-*ortho*-substitution patterns are considerably more challenging and can be difficult to identify suitable conditions for coupling a specific pair of molecules and are typically not general.[45, 73]

In contrast, direct oxidative coupling of phenols provides a more direct route to the formation of sterically hindered biaryl bonds but is overrepresented with examples of dimerizations while cross-coupling reactions are more challenging.[41] Direct oxidative coupling can be achieved with a wide range of transition metal catalyst and metal free oxidants and offers an attractive alternative without the need for additional synthetic steps to install functional handles at the site of bond formation or protecting group manipulations but are impeded by the need to control multiple layers of selectivity. To be effective, control over the chemoselectivity (homocoupling *vs.* cross-coupling, and C–C *vs.* C–O or C–N coupling), site-selectivity (in the formation of one desired product isomer), and atroposelectivity of the reactions must be achieved for formation of the desired biaryl bond on demand. This requirement for different forms of selectivity, which is dictated by innate stereoelectronic properties of the starting materials in small molecule catalyzed cross-coupling reactions, has limited the use of direct oxidative coupling in the formation of sterically hindered and electronically unfavorable combinations.[86, 110, 120] However, Nature has developed numerous enzymes capable of selective direct oxidative coupling reactions, controlling the chemo, site- and atroposelectivity through binding of the substrates within an enzyme active site, or in the case of some laccases, with dirigent proteins.[180] Although examples of oxidative coupling enzymes have been identified and characterized, these enzymes are rarely investigated beyond their native reactivity for synthesis of compounds outside the biosynthetic pathway of the host organism. The investigation and development of oxidative coupling biocatalysts for non-native dimerization reactions and cross-coupling of phenols remains an underexplored and underutilized tool in synthesis.[156]

1.8 References

1. Chavan, R. R.; Hosamani, K. M., Microwave-assisted synthesis, computational studies and antibacterial/ anti-inflammatory activities of compounds based on coumarin-pyrazole hybrid. *R Soc Open Sci* **2018,** *5* (5), 172435.

2. Christie, G. H.; Kenner, J., The molecular configurations of polynuclear aromatic compounds. Part I. The resolution of gamma-6 : 6'-dinitro- and 4 : 6 : 4': 6'-tetranitro-diphenic acids into optically active components. *J Chem Soc* **1922,** *121*, 614-620.

3. Zask, A.; Murphy, J.; Ellestad, G. A., Biological Stereoselectivity of Atropisomeric Natural Products and Drugs. *Chirality* **2013,** *25* (5), 265-274.

4. Bringmann, G.; Günther, C.; Ochse, M.; Schupp, O.; Tasler, S., Biaryls in nature: A multi-facetted class of stereochemically, biosynthetically, and pharmacologically intriguing secondary metabolites. In *Progress in the Chemistry of Organic Natural Products*, Bringmann, G.; Günther, C.; Ochse, M.; Schupp, O.; Tasler, S.; Herz, W.; Falk, H.; Kirby, G. W.; Moore, R. E., Eds. Springer Vienna: Vienna, 2001; pp 1-249.

5. Terada, M., Chiral Phosphoric Acids as Versatile Catalysts for Enantioselective Carbon-Carbon Bond Forming Reactions. *B Chem Soc Jpn* **2010,** *83* (2), 101-119.

6. Chen, Y.; Yekta, S.; Yudin, A. K., Modified BINOL ligands in asymmetric catalysis. *Chem. Rev.* **2003,** *103* (8), 3155-3211.

7. Cherney, A. H.; Kadunce, N. T.; Reisman, S. E., Enantioselective and Enantiospecific Transition-Metal-Catalyzed Cross-Coupling Reactions of Organometallic Reagents To Construct C-C Bonds. *Chem Rev* **2015,** *115* (17), 9587-652.

8. Bringmann, G.; Mortimer, A. J. P.; Keller, P. A.; Gresser, M. J.; Garner, J.; Breuning, M., Atroposelective synthesis of axially chiral biaryl compounds. *Angew. Chem.-Int. Edit.* **2005,** *44* (34), 5384-5427.

9. Kyba, E. P.; Gokel, G. W.; Dejong, F.; Koga, K.; Sousa, L. R.; Siegel, M. G.; Kaplan, L.; Sogah, G. D. Y.; Cram, D. J., Host-Guest Complexation .7. Binaphthyl Structural Unit in Host Compounds. *J. Org. Chem.* **1977,** *42* (26), 4173-4184.

10. LaPlante, S. R.; Edwards, P. J.; Fader, L. D.; Jakalian, A.; Hucke, O., Revealing Atropisomer Axial Chirality in Drug Discovery. *Chemmedchem* **2011,** *6* (3), 505-513.

11. Yoon, T. P.; Jacobsen, E. N., Privileged chiral catalysts. *Science* **2003,** *299* (5613), 1691-1693.

12. Yet, L., Biaryls. In *Privileged Structures in Drug Discovery*, First ed.; John Wiley & Sons, Inc.: Hoboken, NJ, 2018; pp 83-154.

13. Brown, D. G.; Boström, J., Analysis of past and present synthetic methodologies on medicinal chemistry: where have all the new reactions gone? *J. Med. Chem.* **2016,** *59* (10), 4443-4458.

14. Williams, D. H.; Bardsley, B., The vancomycin group of antibiotics and the fight against resistant bacteria. *Angew. Chem.-Int. Edit.* **1999,** *38* (9), 1173-1193.

15. Bringmann, G.; Gulder, T.; Gulder, T. A.; Breuning, M., Atroposelective total synthesis of axially chiral biaryl natural products. *Chem Rev* **2011,** *111* (2), 563-639.

16. Govindachari, T. R.; Parthasarathy, P. C., Ancistrocladine, a New Type of Isoquinoline Alkaloid from Ancistrocladus-Heyneanus. *Tetrahedron* **1971,** *27* (5), 1013-+.

17. Bringmann, G.; Jansen, J. R.; Rink, H. P., Acetogenic Isoquinoline Alkaloids .11. Regioselective and Atropoisomeric-Selective Aryl Coupling to Give Naphthyl Isoquinoline Alkaloids - the 1st Total Synthesis of (-)-Ancistrocladine. *Angew. Chem.-Int. Edit. Engl.* **1986,** *25* (10), 913-915.

18. Bringmann, G.; Irmer, A.; Feineis, D.; Gulder, T. A. M.; Fiedler, H.-P., Convergence in the biosynthesis of acetogenic natural products from plants, fungi, and bacteria. *Phytochemistry* **2009,** *70* (15-16), 1776-1786.

19. Eichelbaum, M. G., Annette S., Stereochemical aspects of drug action and disposition. *Advances in Drug Research* **1996,** *28*, 1-64.

20. Toenjes, S. T.; Gustafson, J. L., Atropisomerism in medicinal chemistry: challenges and opportunities. *Future Med Chem* **2018,** *10* (4), 409-422.

21. Boström, J.; Brown, D. G.; Young, R. J.; Keserü, G. M., Expanding the medicinal chemistry synthetic toolbox. *Nat. Rev. Drug Discov.* **2018,** *17* (10), 709-727.

22. Qiu, J. P.; Levin, L. R.; Buck, J.; Reidenberg, M. M., Different pathways of cell killing by gossypol enantiomers. *Exp Biol Med* **2002,** *227* (6), 398-401.

23. Eveleigh, P.; Hulme, E. C.; Schudt, C.; Birdsall, N. J. M., The Existence of Stable Enantiomers of Telenzepine and Their Stereoselective Interaction with Muscarinic Receptor Subtypes. *Mol Pharmacol* **1989,** *35* (4), 477-483.

24. Pietra, F., Why colchicine does not show mutarotation. With M05-2X density functional in the realm of tricky natural products. *Journal of Physical Organic Chemistry* **2007,** *20* (12), 1102-1107.

25. Berg, U.; Deinum, J.; Lincoln, P.; Kvassman, J., Stereochemistry of Colchicinoids - Enantiomeric Stability and Binding to Tubulin of Desacetamidocolchicine and Desacetamidoisocolchicine. *Bioorg Chem* **1991,** *19* (1), 53-65.

26. Clayden, J.; Moran, W. J.; Edwards, P. J.; LaPlante, S. R., The Challenge of Atropisomerism in Drug Discovery. *Angew. Chem.-Int. Edit.* **2009,** *48* (35), 6398-6401.

27. Abourahma, H.; Bodwell, G. J.; Lu, J. J.; Moulton, B.; Pottie, I. R.; Walsh, R. B.; Zaworotko, M. J., Coordination polymers from calixarene-like [Cu-2(dicarboxylate)(2)](4) building blocks: Structural diversity via atropisomerism. *Cryst Growth Des* **2003,** *3* (4), 513-519.

28. Rizzo, S.; Arnaboldi, S.; Mihali, V.; Cirilli, R.; Forni, A.; Gennaro, A.; Isse, A. A.; Pierini, M.; Mussini, P. R.; Sannicolo, F., "Inherently Chiral" Ionic-Liquid Media: Effective Chiral Electroanalysis on Achiral Electrodes. *Angew. Chem.-Int. Edit.* **2017,** *56* (8), 2079-2082.

29. Brunel, J. M., BINOL: A versatile chiral reagent. *Chem. Rev.* **2005,** *105* (3), 857-897.

30. Storer, R. I.; Carrera, D. E.; Ni, Y.; MacMillan, D. W. C., Enantioselective organocatalytic reductive amination. *J. Am. Chem. Soc.* **2006,** *128* (1), 84-86.

31. Itoh, J.; Fuchibe, K.; Akiyama, T., Chiral phosphoric acid catalyzed enantioselective Friedel-Crafts alkylation of indoles with nitroalkenes: Cooperative effect of 3 angstrom molecular sieves. *Angew. Chem.-Int. Edit.* **2008,** *47* (21), 4016-4018.

32. Liu, H.; Cun, L. F.; Mi, A. Q.; Jiang, Y. Z.; Gong, L. Z., Enantioselective direct aza hetero-Diels-Alder reaction catalyzed by chiral Bronsted acids. *Org. Lett.* **2006,** *8* (26), 6023-6026.

33. Kozlowski, M. C.; Morgan, B. J.; Linton, E. C., Total synthesis of chiral biaryl natural products by asymmetric biaryl coupling. *Chem. Soc. Rev.* **2009,** *38* (11), 3193-3207.

34. Ashenhurst, J. A., Intermolecular oxidative cross-coupling of arenes. *Chem. Soc. Rev.* **2010,** *39* (2), 540-548.

35. Wencel-Delord, J.; Panossian, A.; Leroux, F. R.; Colobert, F., Recent advances and new concepts for the synthesis of axially stereoenriched biaryls. *Chem. Soc. Rev.* **2015,** *44* (11), 3418-3430.

36. Yin; Liebscher, J., Carbon−carbon coupling reactions catalyzed by heterogeneous palladium catalysts. *Chem. Rev.* **2007,** *107* (1), 133-173.

37. Zhang, D.; Wang, Q. R., Palladium catalyzed asymmetric Suzuki-Miyaura coupling reactions to axially chiral biaryl compounds: Chiral ligands and recent advances. *Coordination Chemistry Reviews* **2015,** *286*, 1-16.

38. Mondal, S., Recent advancement of Ullmann-type coupling reactions in the formation of C–C bond. *ChemTexts* **2016,** *2* (4).

39. Sambiagio, C.; Marsden, S. P.; Blacker, A. J.; McGowan, P. C., Copper catalysed Ullmann type chemistry: from mechanistic aspects to modern development. *Chem. Soc. Rev.* **2014,** *43* (10), 3525-3550.

40. Fanta, P. E., THE ULLMANN SYNTHESIS OF BIARYLS. *Chem. Rev.* **1946,** *38* (1), 139-196.

41. Kozlowski, M. C., Oxidative Coupling in Complexity Building Transforms. *Accounts Chem. Res.* **2017,** *50* (3), 638-643.

42. Grzybowski, M.; Sadowski, B.; Butenschon, H.; Gryko, D. T., Synthetic Applications of Oxidative Aromatic Coupling-From Biphenols to Nanographenes. *Angew Chem Int Ed Engl* **2020,** *59* (8), 2998-3027.

43. Organ, M. G.; Abdel-Hadi, M.; Avola, S.; Hadei, N.; Nasielski, J.; O'Brien, C. J.; Valente, C., Biaryls made easy: PEPPSI and the Kumada-Tamao-Corriu reaction. *Chem-Eur J* **2007,** *13* (1), 150-157.

44. Martin, R.; Buchwald, S. L., Pd-catalyzed Kumada-Corriu cross-coupling reactions at low temperatures allow the use of Knochel-type Grignard reagents. *J. Am. Chem. Soc.* **2007,** *129* (13), 3844-+.

45. Patel, N. D.; Sieber, J. D.; Tcyrulnikov, S.; Simmons, B. J.; Rivalti, D.; Duvvuri, K.; Zhang, Y.; Gao, D. A.; Fandrick, K. R.; Haddad, N.; Lao, K. S.; Mangunuru, H. P. R.; Biswas, S.; Qu, B.; Grinberg, N.; Pennino, S.; Lee, H.; Song, J. J.; Gupton, B. F.; Garg, N. K.; Kozlowski, M. C.; Senanayake, C. H., Computationally Assisted Mechanistic Investigation and Development of Pd-Catalyzed Asymmetric Suzuki-Miyaura and Negishi Cross-Coupling Reactions for Tetra-ortho-Substituted Biaryl Synthesis. *ACS Catal* **2018,** *8* (11), 10190-10209.

46. Genov, M.; Fuentes, B.; Espinet, P.; Pelaz, B., Asymmetric Negishi reaction for sterically hindered couplings: synthesis of chiral binaphthalenes. *Tetrahedron-Asymmetry* **2006,** *17* (18), 2593-2595.

47. Milne, J. E.; Buchwald, S. L., An extremely active catalyst for the Negishi cross-coupling reaction. *J. Am. Chem. Soc.* **2004,** *126* (40), 13028-13032.

48. Dai, C. Y.; Fu, G. C., The first general method for palladium-catalyzed Negishi cross-coupling of aryl and vinyl chlorides: Use of commercially available Pd(P(t-BU)(3))(2) as a catalyst. *J. Am. Chem. Soc.* **2001,** *123* (12), 2719-2724.

49. Saa, J. M.; Martorell, G., Palladium-Catalyzed Cross-Coupling Synthesis of Hindered Biaryls and Terphenyls - Cocatalysis by Copper(I) Salts. *J. Org. Chem.* **1993,** *58* (7), 1963-1966.

50. Han, F. S., Transition-metal-catalyzed Suzuki-Miyaura cross-coupling reactions: a remarkable advance from palladium to nickel catalysts. *Chem. Soc. Rev.* **2013,** *42* (12), 5270-5298.

51. Kotha, S.; Lahiri, K.; Kashinath, D., Recent applications of the Suzuki-Miyaura cross-coupling reaction in organic synthesis. *Tetrahedron* **2002,** *58* (48), 9633-9695.

52. Roughley, S. D.; Jordan, A. M., The medicinal chemist's toolbox: an analysis of reactions used in the pursuit of drug candidates. *J. Med. Chem.* **2011,** *54* (10), 3451-3479.

53. Fu, G. C., The development of versatile methods for palladium-catalyzed coupling reactions of aryl electrophiles through the use of P(t-Bu)3 and PCy3 as ligands. *Acc Chem Res* **2008,** *41* (11), 1555-64.

54. Stanforth, S. P., Catalytic cross-coupling reactions in biaryl synthesis. *Tetrahedron* **1998,** *54* (3-4), 263-303.

55. Kozlowski, M. C., Oxidative coupling in complexity building transforms. *Acc. Chem. Res.* **2017,** *50* (3), 638-643.

56. Patel, N. D.; Sieber, J. D.; Tcyrulnikov, S.; Simmons, B. J.; Rivalti, D.; Duvvuri, K.; Zhang, Y.; Gao, D. A.; Fandrick, K. R.; Haddad, N.; Lao, K. S.; Mangunuru, H. P. R.; Biswas, S.; Qu, B.; Grinberg, N.; Pennino, S.; Lee, H.; Song, J. J.; Gupton, B. F.; Garg, N. K.; Kozlowski, M. C.; Senanayake, C. H., Computationally assisted mechanistic investigation and development of Pd-catalyzed asymmetric Suzuki–Miyaura and Negishi cross-coupling reactions for tetra-*ortho*-substituted biaryl synthesis. *ACS Catal.* **2018,** *8* (11), 10190-10209.

57. Yin, J.; Rainka, M. P.; Zhang, X.-X.; Buchwald, S. L., A highly active Suzuki catalyst for the synthesis of sterically hindered biaryls: novel ligand coordination. *J. Am. Chem. Soc.* **2002,** *124* (7), 1162-1163.

58. Cammidge, A. N.; Crépy, K. V. L., Synthesis of chiral binaphthalenes using the asymmetric Suzuki reaction. *Tetrahedron* **2004,** *60* (20), 4377-4386.

59. Organ, M. G.; Çalimsiz, S.; Sayah, M.; Hoi, K. H.; Lough, A. J., Pd-PEPPSI-IPent: an active, sterically demanding cross-coupling catalyst and its application in the synthesis of tetra-*ortho*-substituted biaryls. *Angew. Chem. Int. Ed.* **2009,** *48* (13), 2383-2387.

60. Valente, C.; Çalimsiz, S.; Hoi, K. H.; Mallik, D.; Sayah, M.; Organ, M. G., The development of bulky palladium NHC complexes for the most-challenging cross-coupling reactions. *Angew. Chem. Int. Ed.* **2012,** *51* (14), 3314-3332.

61. Wu, L.; Drinkel, E.; Gaggia, F.; Capolicchio, S.; Linden, A.; Falivene, L.; Cavallo, L.; Dorta, R., Room-temperature synthesis of tetra-*ortho*-substituted biaryls by NHC-catalyzed Suzuki–Miyaura couplings. *Chem. Eur. J.* **2011,** *17* (46), 12886-12890.

62. Ackermann, L.; Potukuchi, H. K.; Althammer, A.; Born, R.; Mayer, P., Tetra-*ortho*-substituted biaryls through palladium-catalyzed Suzuki−Miyaura couplings with a diaminochlorophosphine ligand. *Org. Lett.* **2010,** *12* (5), 1004-1007.

63. Brown, D. G.; Gagnon, M. M.; Boström, J., Understanding our love affair with *p*-chlorophenyl: present day implications from historical biases of reagent selection. *J. Med. Chem.* **2015,** *58* (5), 2390-2405.

64. Barder, T. E.; Walker, S. D.; Martinelli, J. R.; Buchwald, S. L., Catalysts for Suzuki−Miyaura Coupling Processes: Scope and Studies of the Effect of Ligand Structure. *J. Am. Chem. Soc.* **2005,** *127* (13), 4685-4696.

65. Zhao, Q.; Li, C.; Senanayake, C. H.; Tang, W., An efficient method for sterically demanding Suzuki-Miyaura coupling reactions. *Chemistry* **2013,** *19* (7), 2261-5.

66. Wu, L.; Drinkel, E.; Gaggia, F.; Capolicchio, S.; Linden, A.; Falivene, L.; Cavallo, L.; Dorta, R., Room-temperature synthesis of tetra-ortho-substituted biaryls by NHC-catalyzed Suzuki-Miyaura couplings. *Chemistry* **2011,** *17* (46), 12886-90.

67. Yin, J.; Rainka, M. P.; Zhang, X. X.; Buchwald, S. L., A highly active Suzuki catalyst for the synthesis of sterically hindered biaryls: novel ligand coordination. *J Am Chem Soc* **2002,** *124* (7), 1162-3.

68. Cammidge, A. N.; Crépy, K. V. L., The first asymmetric Suzuki cross-coupling reaction. *Chemical Communications* **2000,** (18), 1723-1724.

69. Altenhoff, G.; Goddard, R.; Lehmann, C. W.; Glorius, F., Sterically demanding, bioxazoline-derived N-heterocyclic carbene ligands with restricted flexibility for catalysis. *J Am Chem Soc* **2004,** *126* (46), 15195-201.

70. Tang, W.; Capacci, A. G.; Wei, X.; Li, W.; White, A.; Patel, N. D.; Savoie, J.; Gao, J. J.; Rodriguez, S.; Qu, B.; Haddad, N.; Lu, B. Z.; Krishnamurthy, D.; Yee, N. K.; Senanayake, C. H., A general and special catalyst for Suzuki-Miyaura coupling processes. *Angew Chem Int Ed Engl* **2010,** *49* (34), 5879-83.

71. Martin, R.; Buchwald, S. L., Palladium-catalyzed Suzuki-Miyaura cross-coupling reactions employing dialkylbiaryl phosphine ligands. *Acc Chem Res* **2008,** *41* (11), 1461-73.

72. Barder, T. E.; Biscoe, M. R.; Buchwald, S. L., Structural Insights into Active Catalyst Structures and Oxidative Addition to (Biaryl)phosphine−Palladium Complexes via Density Functional Theory and Experimental Studies. *Organometallics* **2007,** *26* (9), 2183-2192.

73. Wurtz, S.; Glorius, F., Surveying Sterically Demanding N-Heterocyclic Carbene Ligands with Restricted Flexibility for Palladium-catalyzed Cross-Coupling Reactions. *Accounts Chem. Res.* **2008,** *41* (11), 1523-1533.

74. Cammidge, A. N.; Crepy, K. V., Application of the Suzuki reaction as the key step in the synthesis of a novel atropisomeric biphenyl derivative for use as a liquid crystal dopant. *J Org Chem* **2003,** *68* (17), 6832-5.

75. Tang, W. J.; Patel, N. D.; Xu, G. Q.; Xu, X. B.; Savoie, J.; Ma, S. L.; Hao, M. H.; Keshipeddy, S.; Capacci, A. G.; Wei, X. D.; Zhang, Y. D.; Gao, J. J.; Li, W. J.; Rodriguez, S.; Lu, B. Z.; Yee, N. K.; Senanayake, C. H., Efficient Chiral Monophosphorus Ligands for Asymmetric Suzuki-Miyaura Coupling Reactions. *Org. Lett.* **2012,** *14* (9), 2258-2261.

76. Uozumi, Y.; Matsuura, Y.; Arakawa, T.; Yamada, Y. M. A., Asymmetric Suzuki-Miyaura Coupling in Water with a Chiral Palladium Catalyst Supported on an Amphiphilic Resin. *Angew. Chem.-Int. Edit.* **2009,** *48* (15), 2708-2710.

77. Lundgren, R. J.; Stradiotto, M., Addressing Challenges in Palladium-Catalyzed Cross-Coupling Reactions Through Ligand Design. *Chem-Eur J* **2012,** *18* (32), 9758-9769.

78. Yang, H.; Tang, W., Efficient Enantioselective Syntheses of Chiral Natural Products Facilitated by Ligand Design. *Chem Rec* **2020,** *20* (1), 23-40.

79. Yang, Y. D.; Lan, J. B.; You, J. S., Oxidative C-H/C-H Coupling Reactions between Two (Hetero)arenes. *Chem. Rev.* **2017,** *117* (13), 8787-8863.

80. Grzybowski, M.; Sadowski, B.; Butenschön, H.; Gryko, D. T., Synthetic applications of oxidative aromatic coupling—from biphenols to nanographenes. *Angew. Chem. Int. Ed.* **2020,** *59* (8), 2998-3027.

81. Lee, Y. E.; Cao, T.; Torruellas, C.; Kozlowski, M. C., Selective oxidative homo- and cross-coupling of phenols with aerobic catalysts. *J. Am. Chem. Soc.* **2014,** *136* (19), 6782-6785.

82. Nieves-Quinones, Y.; Paniak, T. J.; Lee, Y. E.; Kim, S. M.; Tcyrulnikov, S.; Kozlowski, M. C., Chromium-Salen Catalyzed Cross-Coupling of Phenols: Mechanism and Origin of the Selectivity. *J Am Chem Soc* **2019,** *141* (25), 10016-10032.

83. Shalit, H.; Dyadyuk, A.; Pappo, D., Selective oxidative phenol coupling by iron catalysis. *J. Org. Chem.* **2019,** *84* (4), 1677-1686.

84. Scott, A. I., Oxidative coupling of phenolic compounds. *Q. Rev. Chem. Soc.* **1965,** *19* (1), 1-35.

85. McDonald, P. D.; Hamilton, G. A., CHAPTER II - Mechanisms of phenolic oxidative coupling reactions. In *Organic Chemistry*, Trahanovsky, W. S., Ed. Elsevier: 1973; Vol. 5, pp 97-134.

86. Libman, A.; Shalit, H.; Vainer, Y.; Narute, S.; Kozuch, S.; Pappo, D., Synthetic and predictive approach to unsymmetrical biphenols by iron-catalyzed chelated radical–anion oxidative coupling. *J. Am. Chem. Soc.* **2015,** *137* (35), 11453-11460.

87. Shalit, H.; Libman, A.; Pappo, D., *meso*-Tetraphenylporphyrin iron chloride catalyzed selective oxidative cross-coupling of phenols. *J. Am. Chem. Soc.* **2017,** *139* (38), 13404-13413.

88. Wiebe, A.; Riehl, B.; Lips, S.; Franke, R.; Waldvogel, S. R., Unexpected high robustness of electrochemical cross-coupling for a broad range of current density. *Sci. Adv.* **2017,** *3* (10), eaao3920.

89. Kang, H.; Herling, M. R.; Niederer, K. A.; Lee, Y. E.; Vasu Govardhana Reddy, P.; Dey, S.; Allen, S. E.; Sung, P.; Hewitt, K.; Torruellas, C.; Kim, G. J.; Kozlowski, M. C., Enantioselective vanadium-catalyzed oxidative coupling: development and mechanistic insights. *J. Org. Chem.* **2018,** *83* (23), 14362-14384.

90. Yu, Q.; Fu, Y.; Huang, J.; Qin, J.; Zuo, H.; Wu, Y.; Zhong, F., Enantioselective oxidative phenol-indole [3 + 2] coupling enabled by biomimetic Mn(III)/Brønsted acid relay catalysis. *ACS Catal.* **2019,** *9* (8), 7285-7291.

91. Reiss, H.; Shalit, H.; Vershinin, V.; More, N. Y.; Forckosh, H.; Pappo, D., Cobalt(II)[salen]-catalyzed selective aerobic oxidative cross-coupling between electron-rich phenols and 2-naphthols. *J. Org. Chem.* **2019,** *84* (12), 7950-7960.

92. Sako, M.; Aoki, T.; Zumbrägel, N.; Schober, L.; Gröger, H.; Takizawa, S.; Sasai, H., Chiral dinuclear vanadium complex-mediated oxidative coupling of resorcinols. *J. Org. Chem.* **2019,** *84* (3), 1580-1587.

93. Tian, J.-M.; Wang, A.-F.; Yang, J.-S.; Zhao, X.-J.; Tu, Y.-Q.; Zhang, S.-Y.; Chen, Z.-M., Copper-complex-catalyzed asymmetric aerobic oxidative cross-coupling of 2-naphthols: enantioselective synthesis of 3,3′-substituted C1-symmetric BINOLs. *Angew. Chem. Int. Ed.* **2019,** *58* (32), 11023-11027.

94. Xu, W.; Huang, Z.; Ji, X.; Lumb, J.-P., Catalytic aerobic cross-dehydrogenative coupling of phenols and catechols. *ACS Catal.* **2019,** *9* (5), 3800-3810.

95. Hayashi, H.; Ueno, T.; Kim, C.; Uchida, T., Ruthenium-catalyzed cross-selective asymmetric oxidative coupling of arenols. *Org. Lett.* **2020,** *22* (4), 1469-1474.

96. Neuhaus, W. C.; Kozlowski, M. C., Total synthesis of pyrolaside B: phenol trimerization through sequenced oxidative C−C and C−O coupling. *Angew. Chem. Int. Ed.* **2020,** *59* (20), 7842-7847.

97. Paniak, T. J.; Kozlowski, M. C., Aerobic Catalyzed Oxidative Cross-Coupling of N,N-Disubstituted Anilines and Aminonaphthalenes with Phenols and Naphthols. *Org Lett* **2020,** *22* (5), 1765-1770.

98. Röckl, J. L.; Schollmeyer, D.; Franke, R.; Waldvogel, S. R., Dehydrogenative anodic C−C coupling of phenols bearing electron-withdrawing groups. *Angew. Chem. Int. Ed.* **2020,** *59* (1), 315-319.

99. Kang, H.; Herling, M. R.; Niederer, K. A.; Lee, Y. E.; Vasu Govardhana Reddy, P.; Dey, S.; Allen, S. E.; Sung, P.; Hewitt, K.; Torruellas, C.; Kim, G. J.; Kozlowski, M. C., Enantioselective Vanadium-Catalyzed Oxidative Coupling: Development and Mechanistic Insights. *J Org Chem* **2018,** *83* (23), 14362-14384.

100. Guo, Q. X.; Wu, Z. J.; Luo, Z. B.; Liu, Q. Z.; Ye, J. L.; Luo, S. W.; Cun, L. F.; Gong, L. Z., Highly enantioselective oxidative couplings of 2-naphthols catalyzed by chiral bimetallic oxovanadium complexes with either oxygen or air as oxidant. *J. Am. Chem. Soc.* **2007,** *129* (45), 13927-13938.

101. Hirao, T., Vanadium in modern organic synthesis. *Chem. Rev.* **1997,** *97* (8), 2707-2724.

102. Lee, Y. E.; Cao, T.; Torruellas, C.; Kozlowski, M. C., Selective Oxidative Homo- and Cross-Coupling of Phenols with Aerobic Catalysts. *J. Am. Chem. Soc.* **2014,** *136* (19), 6782-6785.

103. Reiss, H.; Shalit, H.; Vershinin, V.; More, N. Y.; Forckosh, H.; Pappo, D., Cobalt(II)[salen]-Catalyzed Selective Aerobic Oxidative Cross-Coupling between Electron-Rich Phenols and 2-Naphthols. *J Org Chem* **2019,** *84* (12), 7950-7960.

104. Tian, J. M.; Wang, A. F.; Yang, J. S.; Zhao, X. J.; Tu, Y. Q.; Zhang, S. Y.; Chen, Z. M., Copper-Complex-Catalyzed Asymmetric Aerobic Oxidative Cross-Coupling of 2-Naphthols: Enantioselective Synthesis of 3,3'-Substituted C1 -Symmetric BINOLs. *Angew Chem Int Ed Engl* **2019,** *58* (32), 11023-11027.

105. Allen, S. E.; Walvoord, R. R.; Padilla-Salinas, R.; Kozlowski, M. C., Aerobic Copper-Catalyzed Organic Reactions. *Chem. Rev.* **2013,** *113* (8), 6234-6458.

106. Brussee, J.; Groenendijk, J. L. G.; Tekoppele, J. M.; Jansen, A. C. A., ON THE MECHANISM OF THE FORMATION OF "S(-)-(1,1'-BINAPHTHALENE)-2,2'-DIOL VIA COPPER(II)AMINE COMPLEXES. *Tetrahedron* **1985,** *41* (16), 3313-3319.

107. Noji, M.; Nakajima, M.; Koga, K., A New Catalytic-System for Aerobic Oxidative Coupling of 2-Naphthol Derivatives by the Use of Cucl-Amine Complex - a Practical Synthesis of Binaphthol Derivatives. *Tetrahedron Letters* **1994,** *35* (43), 7983-7984.

108. Smrcina, M.; Polakova, J.; Vyskocil, S.; Kocovsky, P., Synthesis of enantiomerically pure binaphthyl derivatives. Mechanism of the enantioselective, oxidative coupling of naphthols and designing a catalytic cycle. *The Journal of Organic Chemistry* **2002,** *58* (17), 4534-4538.

109. Egami, H.; Katsuki, T., Iron-Catalyzed Asymmetric Aerobic Oxidation: Oxidative Coupling of 2-Naphthols. *J. Am. Chem. Soc.* **2009,** *131* (17), 6082-+.

110. Shalit, H.; Dyadyuk, A.; Pappo, D., Selective Oxidative Phenol Coupling by Iron Catalysis. *J Org Chem* **2019,** *84* (4), 1677-1686.

111. Brutting, C.; Fritsche, R. F.; Kutz, S. K.; Borger, C.; Schmidt, A. W.; Kataeva, O.; Knolker, H. J., Synthesis of 1,1'- and 2,2'-Bicarbazole Alkaloids by Iron(III)-Catalyzed Oxidative Coupling of 2- and 1-Hydroxycarbazoles. *Chemistry* **2018,** *24* (2), 458-470.

112. Shalit, H.; Libman, A.; Pappo, D., meso-Tetraphenylporphyrin Iron Chloride Catalyzed Selective Oxidative Cross-Coupling of Phenols. *J. Am. Chem. Soc.* **2017,** *139* (38), 13404-13413.

113. Narute, S.; Parnes, R.; Toste, F. D.; Pappo, D., Enantioselective Oxidative Homocoupling and Cross-Coupling of 2-Naphthols Catalyzed by Chiral Iron Phosphate Complexes. *J Am Chem Soc* **2016,** *138* (50), 16553-16560.

114. Libman, A.; Shalit, H.; Vainer, Y.; Narute, S.; Kozuch, S.; Pappo, D., Synthetic and Predictive Approach to Unsymmetrical Biphenols by Iron-Catalyzed Chelated Radical-Anion Oxidative Coupling. *J. Am. Chem. Soc.* **2015,** *137* (35), 11453-11460.

115. Gaster, E.; Vainer, Y.; Regev, A.; Narute, S.; Sudheendran, K.; Werbeloff, A.; Shalit, H.; Pappo, D., Significant Enhancement in the Efficiency and Selectivity of Iron-Catalyzed Oxidative Cross-Coupling of Phenols by Fluoroalcohols. *Angew. Chem.-Int. Edit.* **2015,** *54* (14), 4198-4202.

116. Huang, Z. L.; Jin, L. Q.; Feng, Y.; Peng, P.; Yi, H.; Lei, A. W., Iron-Catalyzed Oxidative Radical Cross-Coupling/Cyclization between Phenols and Olefins. *Angew. Chem.-Int. Edit.* **2013,** *52* (28), 7151-7155.

117. Morimoto, K.; Sakamoto, K.; Ohshika, T.; Dohi, T.; Kita, Y., Organo-Iodine(III)-Catalyzed Oxidative Phenol-Arene and Phenol-Phenol Cross-Coupling Reaction. *Angew Chem Int Ed Engl* **2016,** *55* (11), 3652-6.

118. Morimoto, K.; Sakamoto, K.; Ohnishi, Y.; Miyamoto, T.; Ito, M.; Dohi, T.; Kita, Y., Metal-free oxidative para cross-coupling of phenols. *Chemistry* **2013,** *19* (27), 8726-31.

119. Rockl, J. L.; Schollmeyer, D.; Franke, R.; Waldvogel, S. R., Dehydrogenative Anodic C-C Coupling of Phenols Bearing Electron-Withdrawing Groups. *Angew Chem Int Ed Engl* **2020,** *59* (1), 315-319.

120. Kocovsky, P.; Vyskocil, S.; Smrcina, M., Non-symmetrically substituted 1,1'-binaphthyls in enantioselective catalysis. *Chem Rev* **2003,** *103* (8), 3213-46.

121. Lipshutz, B. H.; Kayser, F.; Liu, Z. P., ASYMMETRIC-SYNTHESIS OF BIARYLS BY INTRAMOLECULAR OXIDATIVE COUPLINGS OF CYANOCUPRATE INTERMEDIATES. *Angew. Chem.-Int. Edit. Engl.* **1994,** *33* (18), 1842-1844.

122. Smrcina, M.; Polakova, J.; Vyskocil, S.; Kocovsky, P., Synthesis of Enantiomerically Pure Binaphthyl Derivatives - Mechanism of the Enantioselective, Oxidative Coupling of Naphthols and Designing a Catalytic Cycle. *J. Org. Chem.* **1993,** *58* (17), 4534-4538.

123. Hewgley, J. B.; Li, X. L.; Kozlowski, M. C., Mechanistic study of enantioselective oxidative biaryl coupling by the 1,5-diaza-cis-decalin/cui/O-2 catalyst system. *Abstr Pap Am Chem S* **2004,** *228*, U883-U883.

124. Kozlowski, M. C.; Li, X. L.; Carroll, P. J.; Xu, Z. R., Copper(II) complexes of novel 1,5-diaza-cis-decalin diamine ligands: An investigation of structure and reactivity. *Organometallics* **2002,** *21* (21), 4513-4522.

125. Kozlowski, M. C.; Hewgley, J. B.; Mulrooney, C. M.; Li, X. L., Synthesis of chiral 3,3 '-binol derivatives using a 1,5-diaza-cis-decalin copper catalyst: Examination of scope and mechanism. *Abstr Pap Am Chem S* **2002,** *224*, U178-U178.

126. Smrcina, M.; Vyskocil, S.; Maca, B.; Polasek, M.; Claxton, T. A.; Abbott, A. P.; Kocovsky, P., Selective Cross-Coupling of 2-Naphthol and 2-Naphthylamine Derivatives - a Facile Synthesis of 2,2',3-Trisubstituted and 2,2',3,3'-Tetrasubstituted 1,1'-Binaphthyls. *J. Org. Chem.* **1994,** *59* (8), 2156-2163.

127. Wu, X.; Iwata, T.; Scharf, A.; Qin, T.; Reichl, K. D.; Porco, J. A., Asymmetric synthesis of gonytolide A: strategic use of an aryl halide blocking group for oxidative coupling. *J. Am. Chem. Soc.* **2018,** *140* (18), 5969-5975.

128. Neuhaus, W. C.; Jemison, A. L.; Kozlowski, M. C., Vanadium-Catalyzed Selective Oxidative Homocoupling of Alkenyl Phenols to Synthesize Lignan Analogs. *ACS Catal* **2019,** *9* (12), 11067-11073.

129. Egami, H.; Matsumoto, K.; Oguma, T.; Kunisu, T.; Katsuki, T., Enantioenriched Synthesis of C-1-Symmetric BINOLs: Iron-Catalyzed Cross-Coupling of 2-Naphthols and Some Mechanistic Insight. *J. Am. Chem. Soc.* **2010,** *132* (39), 13633-13635.

130. Nieves-Quinones, Y.; Paniak, T. J.; Lee, Y. E.; Kim, S. M.; Tcyrulnikov, S.; Kozlowski, M. C., Chromium-salen catalyzed cross-coupling of phenols: mechanism and origin of the selectivity. *J. Am. Chem. Soc.* **2019,** *141* (25), 10016-10032.

131. Aldemir, H.; Richarz, R.; Gulder, T. A., The biocatalytic repertoire of natural biaryl formation. *Angew. Chem. Int. Ed.* **2014,** *53* (32), 8286-8293.

132. Funa, N.; Funabashi, M.; Ohnishi, Y.; Horinouchi, S., Biosynthesis of hexahydroxyperylenequinone melanin via oxidative aryl coupling by cytochrome P-450 in Streptomyces griseus. *J Bacteriol* **2005,** *187* (23), 8149-55.

133. Zhao, B.; Bellamine, A.; Lei, L.; Waterman, M. R., The role of Ile87 of CYP158A2 in oxidative coupling reaction. *Arch Biochem Biophys* **2012,** *518* (2), 127-32.

134. Hugentobler, K. G.; Muller, M., Towards semisynthetic natural compounds with a biaryl axis: Oxidative phenol coupling in Aspergillus niger. *Bioorg Med Chem* **2018,** *26* (7), 1374-1377.

135. Mazzaferro, L. S.; Huttel, W.; Fries, A.; Muller, M., Cytochrome P450-Catalyzed Regio- and Stereoselective Phenol Coupling of Fungal Natural Products. *J. Am. Chem. Soc.* **2015,** *137* (38), 12289-12295.

136. Huttel, W.; Muller, M., Regio- and stereoselective intermolecular oxidative phenol coupling in kotanin biosynthesis by Aspergillus niger. *ChemBioChem* **2007,** *8* (5), 521-9.

137. Nozawa, K.; Nakajima, S.; Kawai, K.; Udagawa, S.; Miyaji, M., Bicoumarins from Ascostromata of Petromyces-Alliaceus. *Phytochemistry* **1994,** *35* (4), 1049-1051.

138. Laakso, J. A.; Narske, E. D.; Gloer, J. B.; Wicklow, D. T.; Dowd, P. F., Isokotanins Ac - New Bicoumarins from the Sclerotia of Aspergillus-Alliaceus. *J. Nat. Prod.* **1994,** *57* (1), 128-133.

139. Gil Girol, C.; Fisch, K. M.; Heinekamp, T.; Günther, S.; Hüttel, W.; Piel, J.; Brakhage, A. A.; Müller, M., Regio-and stereoselective oxidative phenol coupling in Aspergillus niger. *Angew. Chem. Int. Ed.* **2012,** *51*, 9788-9791.

140. Präg, A.; Grüning, B. A.; Häckh, M.; Lüdeke, S.; Wilde, M.; Luzhetskyy, A.; Richter, M.; Luzhetska, M.; Günther, S.; Müller, M., Regio- and stereoselective intermolecular oxidative phenol coupling in *Streptomyces*. *J. Am. Chem. Soc.* **2014,** *136* (17), 6195-6198.

141. Thiele, W.; Froede, R.; Steglich, W.; Müller, M., Enzymatic formation of rufoschweinitzin, a binaphthalene from the basidiomycete *Cortinarius rufoolivaceus*. *ChemBioChem* **2020,** *21* (10), 1423-1427.

142. Obermaier, S.; Muller, M., Biaryl-forming enzymes from *Aspergilli* exhibit substrate-dependent stereoselectivity. *Biochemistry* **2019,** *58* (22), 2589-2593.

143. Griffiths, S.; Mesarich, C. H.; Saccomanno, B.; Vaisberg, A.; De Wit, P. J. G. M.; Cox, R.; Collemare, J., Elucidation of cladofulvin biosynthesis reveals a cytochrome P450 monooxygenase required for anthraquinone dimerization. *Proc. Natl. Acad. Sci.* **2016,** *113* (25), 6851.

144. Matsuda, Y.; Gotfredsen, C. H.; Larsen, T. O., Genetic characterization of neosartorin biosynthesis provides insight into heterodimeric natural product generation. *Org. Lett.* **2018,** *20* (22), 7197-7200.

145. Funa, N.; Funabashi, M.; Ohnishi, Y.; Horinouchi, S., Biosynthesis of hexahydroxyperylenequinone melanin via oxidative aryl coupling by cytochrome P-450 in Streptomyces griseus. *J. Bacteriol.* **2005,** *187* (23), 8149-8155.

146. Zhao, B.; Lamb, D. C.; Lei, L.; Kelly, S. L.; Yuan, H.; Hachey, D. L.; Waterman, M. R., Different binding modes of two flaviolin substrate molecules in cytochrome P450 158A1 (CYP158A1) compared to CYP158A2. *Biochemistry* **2007,** *46* (30), 8725-8733.

147. Zhao, B.; Guengerich, F. P.; Bellamine, A.; Lamb, D. C.; Izumikawa, M.; Lei, L.; Podust, L. M.; Sundaramoorthy, M.; Kalaitzis, J. A.; Reddy, L. M.; Kelly, S. L.; Moore, B. S.; Stec, D.; Voehler, M.; Falck, J. R.; Shimada, T.; Waterman, M. R., Binding of two flaviolin substrate

molecules, oxidative coupling, and crystal structure of Streptomyces coelicolor A3(2) cytochrome P450 158A2. *J. Biol. Chem.* **2005,** *280* (12), 11599-11607.

148. Lim, Y.-R.; Han, S.; Kim, J.-H.; Park, H.-G.; Lee, G.-Y.; Le, T.-K.; Yun, C.-H.; Kim, D., Characterization of a biflaviolin synthase CYP158A3 from *Streptomyces avermitilis* and its role in the biosynthesis of secondary metabolites. *Biomol. Ther.* **2017,** *25* (2), 171-176.

149. Effenberger, I.; Zhang, B.; Li, L.; Wang, Q.; Liu, Y.; Klaiber, I.; Pfannstiel, J.; Wang, Q.; Schaller, A., Dirigent proteins from cotton (*Gossypium* sp.) for the atropselective synthesis of gossypol. *Angew. Chem. Int. Ed.* **2015,** *54* (49), 14660-14663.

150. Hu, J.; Li, H.; Chooi, Y.-H., Fungal dirigent protein controls the stereoselectivity of multicopper oxidase-catalyzed phenol coupling in viriditoxin ciosynthesis. *J. Am. Chem. Soc.* **2019,** *141* (20), 8068-8072.

151. Obermaier, S.; Thiele, W.; Fürtges, L.; Müller, M., Enantioselective phenol coupling by laccases in the biosynthesis of fungal dimeric naphthopyrones. *Angew. Chem. Int. Ed.* **2019,** *58* (27), 9125-9128.

152. Engelmann, C.; Illner, S.; Kragl, U., Laccase initiated C–C couplings: Various techniques for reaction monitoring. *Process Biochem.* **2015,** *50* (10), 1591-1599.

153. Hu, X. J.; Wang, X. B.; Kong, L. Y., alpha-Glucosidase inhibitors via green pathway: biotransformation for bicoumarins catalyzed by Momordica charantia peroxidase. *J Agric Food Chem* **2013,** *61* (7), 1501-8.

154. Hu, J.; Li, H.; Chooi, Y. H., Fungal Dirigent Protein Controls the Stereoselectivity of Multicopper Oxidase-Catalyzed Phenol Coupling in Viriditoxin Biosynthesis. *J Am Chem Soc* **2019,** *141* (20), 8068-8072.

155. Zhang, X.; Guo, J.; Cheng, F.; Li, S., Cytochrome P450 enzymes in fungal natural product biosynthesis. *Nat Prod Rep* **2021,** *38* (6), 1072-1099.

156. Huttel, W.; Muller, M., Regio- and stereoselective intermolecular phenol coupling enzymes in secondary metabolite biosynthesis. *Natural Product Reports* **2021,** *38* (5), 1011-1043.

157. Podust, L. M.; Sherman, D. H., Diversity of P450 enzymes in the biosynthesis of natural products. *Natural Product Reports* **2012,** *29* (10), 1251-1266.

158. Sagui, F.; Chirivì, C.; Fontana, G.; Nicotra, S.; Passarella, D.; Riva, S.; Danieli, B., Laccase-catalyzed coupling of catharanthine and vindoline: an efficient approach to the bisindole alkaloid anhydrovinblastine. *Tetrahedron* **2009,** *65* (1), 312-317.

159. Ciecholewski, S.; Hammer, E.; Manda, K.; Bose, G.; Nguyen, V.; Langer, P.; Schauer, F., Laccase-catalyzed carbon-carbon bond formation: oxidative dimerization of salicylic esters by air in aqueous solution. *Tetrahedron* **2005,** *61*, 4615-4619.

160. Zhang, X.; Guo, J.; Cheng, F.; Li, S., Cytochrome P450 enzymes in fungal natural product biosynthesis. *Nat. Prod. Rep.* **2021,** *38* (6), 1072-1099.

161. Yu, X.; Liu, F.; Zou, Y.; Tang, M. C.; Hang, L.; Houk, K. N.; Tang, Y., Biosynthesis of Strained Piperazine Alkaloids: Uncovering the Concise Pathway of Herquline A. *J. Am. Chem. Soc.* **2016,** *138* (41), 13529-13532.

162. Zhao, B.; Guengerich, F. P.; Bellamine, A.; Lamb, D. C.; Izumikawa, M.; Lei, L.; Podust, L. M.; Sundaramoorthy, M.; Kalaitzis, J. A.; Reddy, L. M.; Kelly, S. L.; Moore, B. S.; Stec, D.; Voehler, M.; Falck, J. R.; Shimada, T.; Waterman, M. R., Binding of two flaviolin substrate molecules, oxidative coupling, and crystal structure of Streptomyces coelicolor A3(2) cytochrome P450 158A2. *Journal of Biological Chemistry* **2005,** *280* (12), 11599-11607.

163. Matsuda, Y.; Gotfredsen, C. H.; Larsen, T. O., Genetic Characterization of Neosartorin Biosynthesis Provides Insight into Heterodimeric Natural Product Generation. *Org Lett* **2018,** *20* (22), 7197-7200.

164. Davin, L. B.; Wang, H. B.; Crowell, A. L.; Bedgar, D. L.; Martin, D. M.; Sarkanen, S.; Lewis, N. G., Stereoselective bimolecular phenoxy radical coupling by an auxiliary (dirigent) protein without an active center. *Science* **1997,** *275* (5298), 362-366.

165. Grobe, N.; Zhang, B.; Fisinger, U.; Kutchan, T. M.; Zenk, M. H.; Guengerich, F. P., Mammalian cytochrome P450 enzymes catalyze the phenol-coupling step in endogenous morphine biosynthesis. *J Biol Chem* **2009,** *284* (36), 24425-31.

166. Li, Y.; Li, S.; Thodey, K.; Trenchard, I.; Cravens, A.; Smolke, C. D., Complete biosynthesis of noscapine and halogenated alkaloids in yeast. *Proceedings of the National Academy of Sciences of the United States of America* **2018,** *115* (17), E3922-E3931.

167. Gesell, A.; Rolf, M.; Ziegler, J.; Chavez, M. L. D.; Huang, F. C.; Kutchan, T. M., CYP719B1 Is Salutaridine Synthase, the C-C Phenol-coupling Enzyme of Morphine Biosynthesis in Opium Poppy. *Journal of Biological Chemistry* **2009,** *284* (36), 24432-24442.

168. Belin, P.; Le Du, M. H.; Fielding, A.; Lequin, O.; Jacquet, M.; Charbonnier, J. B.; Lecoq, A.; Thai, R.; Courcon, M.; Masson, C.; Dugave, C.; Genet, R.; Pernodet, J. L.; Gondry, M., Identification and structural basis of the reaction catalyzed by CYP121, an essential cytochrome P450 in Mycobacterium tuberculosis. *Proceedings of the National Academy of Sciences of the United States of America* **2009,** *106* (18), 7426-7431.

169. Zhao, B.; Guengerich, F. P.; Voehler, M.; Waterman, M. R., Role of active site water molecules and substrate hydroxyl groups in oxygen activation by cytochrome P450 158A2 - A new mechanism of proton transfer. *Journal of Biological Chemistry* **2005,** *280* (51), 42188-42197.

170. Stadler, R.; Zenk, M. H., The Purification and Characterization of a Unique Cytochrome-P-450 Enzyme from Berberis-Stolonifera Plant-Cell Cultures. *Journal of Biological Chemistry* **1993,** *268* (2), 823-831.

171. Guengerich, F. P., Common and uncommon cytochrome P450 reactions related to metabolism and chemical toxicity. *Chem Res Toxicol* **2001,** *14* (6), 611-650.

172. Guengerich, F. P., Mechanisms of Cytochrome P450-Catalyzed Oxidations. *ACS Catal.* **2018,** *8* (12), 10964-10976.

173. Grandner, J. M.; Cacho, R. A.; Tang, Y.; Houk, K. N., Mechanism of the P450-Catalyzed Oxidative Cyclization in the Biosynthesis of Griseofulvin. *ACS Catal.* **2016,** *6* (7), 4506-4511.

174. Petersen, A. B.; Ronnest, M. H.; Larsen, T. O.; Clausen, M. H., The Chemistry of Griseofulvin. *Chem. Rev.* **2014,** *114* (24), 12088-12107.

175. Cacho, R. A.; Chooi, Y. H.; Zhou, H.; Tang, Y., Complexity Generation in Fungal Polyketide Biosynthesis: A Spirocycle-Forming P450 in the Concise Pathway to the Antifungal Drug Griseofulvin. *Acs Chem Biol* **2013,** *8* (10), 2322-2330.

176. Omura, S.; Hirano, A.; Iwai, Y.; Masuma, R., Herquline, a New Alkaloid Produced by Penicillium-Herquei Fermentation, Isolation and Properties. *J Antibiot* **1979,** *32* (8), 786-790.

177. Dumas, V. G.; Defelipe, L. A.; Petruk, A. A.; Turjanski, A. G.; Marti, M. A., QM/MM study of the C-C coupling reaction mechanism of CYP121, an essential Cytochrome p450 of Mycobacterium tuberculosis. *Proteins* **2014,** *82* (6), 1004-1021.

178. Lin, H. C.; McMahon, T. C.; Patel, A.; Corsello, M.; Simon, A.; Xu, W.; Zhao, M. X.; Houk, K. N.; Garg, N. K.; Tang, Y., P450-Mediated Coupling of Indole Fragments To Forge Communesin and Unnatural Isomers. *J. Am. Chem. Soc.* **2016,** *138* (12), 4002-4005.

179. Bringmann, G.; Gulder, T.; Gulder, T. A. M.; Breuning, M., Atroposelective total synthesis of axially chiral biaryl natural products. *Chem. Rev.* **2011,** *111* (2), 563-639.

180. Huttel, W.; Muller, M., Regio- and stereoselective intermolecular phenol coupling enzymes in secondary metabolite biosynthesis (vol 38, pg 1011, 2021). *Natural Product Reports* **2021,** *38* (7), 1408-1408.

Chapter 2: Developing a Biocatalytic Platform for KtnC and DesC Catalyzed Selective Oxidative Phenolic Coupling Reactions

2.1 Summary

Direct oxidative coupling provides an attractive strategy for the assembly of biaryl cores through the net transformation of two C–H bonds into a C–C, C–N, or C–O bond, rapidly building molecular complexity.[1-2] This approach confers advantages such as greater efficiency in synthesis, but at the expense of the transformation's selectivity which is often dictated by the steric and electronic properties of the coupling fragments.[3-5] Nature has evolved enzymes for the oxidative coupling of phenolic compounds to generate structurally diverse biaryl natural products such as melanin and flavonoids,[6-7] and forge key bonds in the biosynthesis of the drugs morphine and vancomycin.[8-10] Whereas a growing number of enzymes, especially laccases and cytochromes P450, have been identified in the biosynthetic pathways of biaryl natural products, many remain uncharacterized and assigned only putative function.[11-12] The catalyst-controlled site-selectivity displayed by the P450 enzymes KtnC and DesC in the oxidative dimerization of coumarins provided inspiration for developing an enzymatic platform for oxidative phenolic coupling reactions.[13] We hypothesized that this class of enzymes could be developed into tunable biocatalysts for intermolecular fragment coupling, with the potential to overcome the limitations inherent to established synthetic methods for the direct oxidative coupling of phenolic compounds.[11, 14]

Here, we disclose a biocatalytic platform for oxidative phenolic coupling catalyzed by the fungal cytochromes P450 KtnC and DesC. The engineering and heterologous expression of the genes encoding fungal P450s *Saccharomyces cerevisiae* and *Pichia pastoris* are described, and we demonstrate the ability to catalyze atroposelective oxidative dimerization and cross-coupling reactions on a panel of coumarin substrates.

2.2 Introduction

Among the P450s characterized to perform oxidative dimerization reactions in the biosynthesis of biaryl natural products, we were initially drawn to a small cluster of *Aspergillus* P450 enzymes, KtnC and DesC, that each imparts a unique site- and atroposelectivity in the oxidative dimerization of coumarin **1**, as demonstrated by Müller and coworkers in 2015 (Figure 2.1A).[13, 15-18] Bicoumarin natural products joined by a biaryl bond with different connectivities have been isolated from multiple species of *Aspergilli* fungi, representing diversity formed through the phenolic oxidative coupling of monomeric coumarins.[17-22] While the natural products of phenolic biaryl coupling enzymes have been known to science for decades, researchers weilding the tools of modern genomics have only in the last 10 years been capable of identifying the enzymes responsible for this transformation.[12, 23-25] For example, the two P450 enzymes BicC and AfvE have been identified in the biosynthetic pathways of *A. alliaceus* and *A. flavus*, respectively, and are speculated to be responsible for the phenolic coupling step in the biosynthesis of biaryl

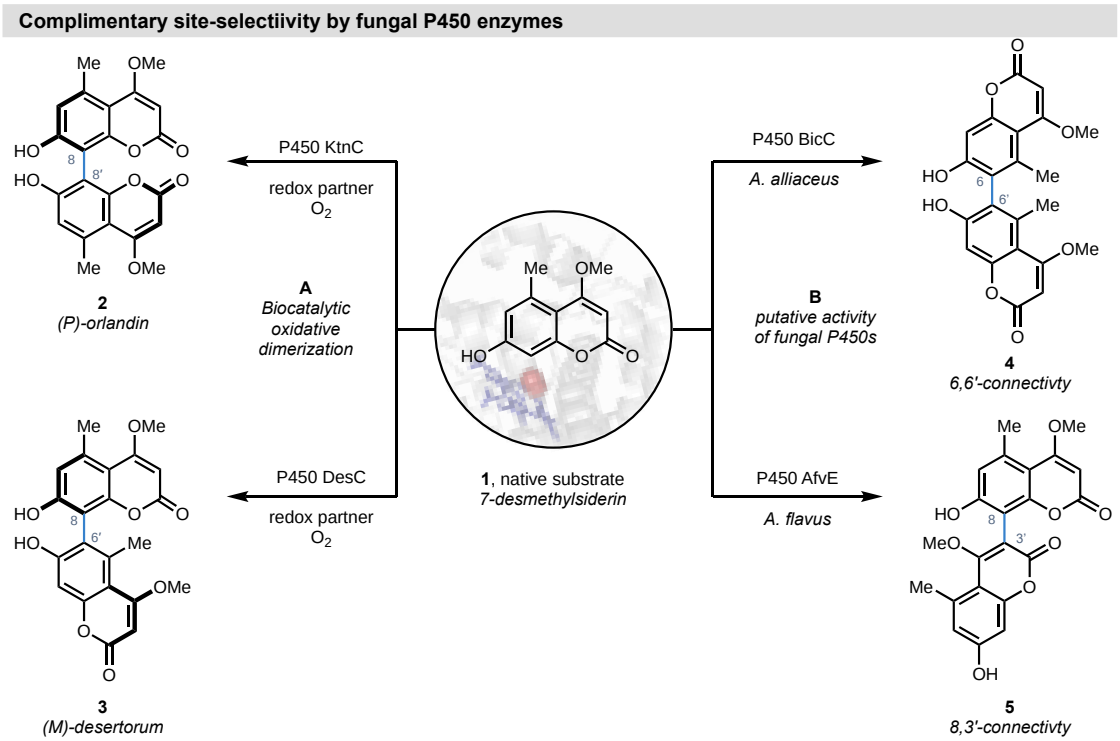

Figure 2.1: Complimentary site-selectivity of fungal P450s.
A. KtnC and DesC catalyze the oxidative dimerization of coumarin **1** with complimentary catalyst-controlled site-selectivity. B. Putative activity of fungal P450s identified in biosynthetic gene clusters of bicoumarin producing *Aspergilli.*

natural products **3** and **4**, but have not been unequivecally verified to catalyze this reaction (Figure 2.1B).[13-19]

Intermolecular biaryl coupling of phenols by enzymes is hypothesized to occur through one of two mechanisms (Figure 2.2).[10, 24, 26-34] Both proposals proceed through an initial hydrogen atom abstraction on the phenolic hydroxyl group by **6** within the enzyme active site to form a phenoxy radical, represented by the delocalized resonance contributors **7**-**10**. (Figure 2.2A). The more commonly invoked mechanistic proposal (Figure 2.2B), diradical recombination, presumes the formation of two radicals within the enzyme active site through a second hydrogen-atom abstraction event on the colocalized

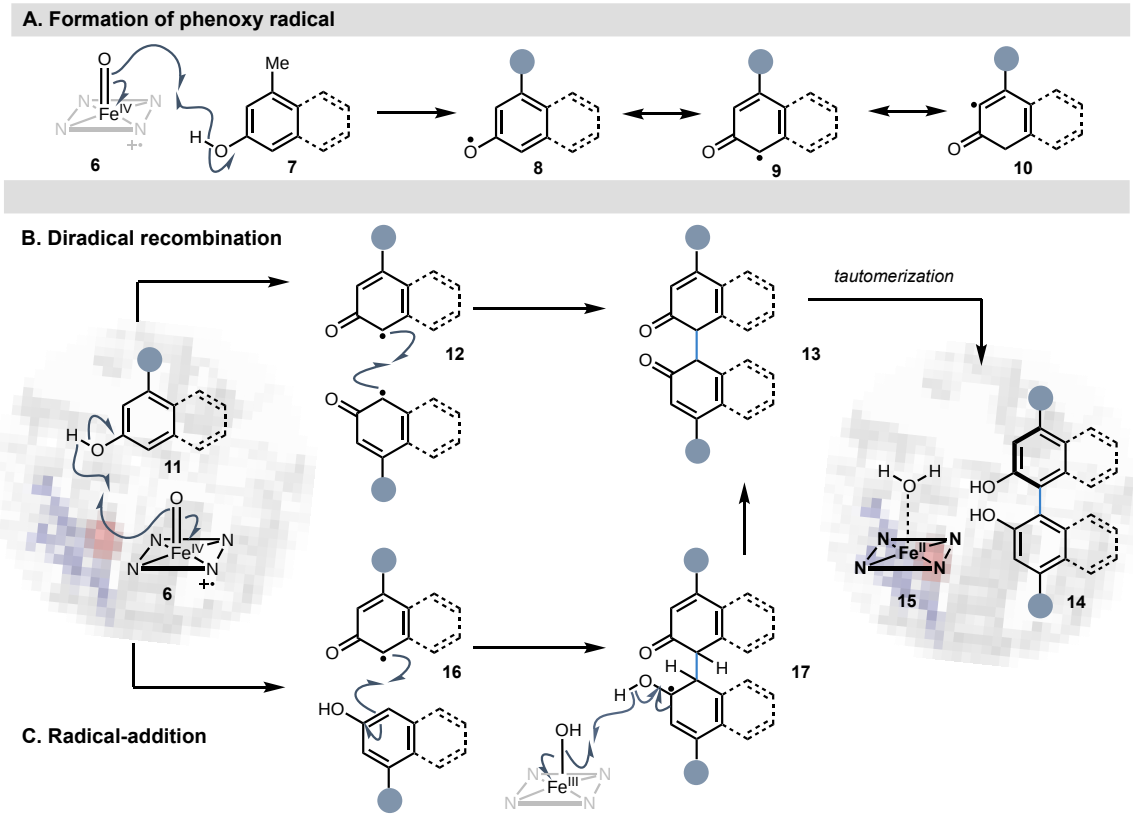

Figure 2.2: Proposed mechanism in KtnC catalyzed oxidative dimerizations.
A. Hydrogen atom abstraction and radical delocalization. B. Di-radical mechanism: formation of two radicals colocalized within the enzyme active site, followed by radical recombination. C. Radical–addition mechanism: formation of one radical and addition to a neutral coupling partner.

phenolic substrate (**12**), followed by C–C bond formation to **13,** and tautomerization to yield the biaryl product **14**.[27] The second mechanistic proposal (Figure 2.2C), radical–addition, is envisioned to proceed by addition of a neutral, nucleophilic phenol (**16**) to the phenoxyl radical to form the C–C bond (**17**), then a second hydrogen atom abstraction to form intermediate **13**, and re-aromatization to product **14**. These two enzymatic

mechanistic proposals share similarities with iron catalysts for the direct oxidative coupling of phenols proposed by the Pappo group and others.[4, 35-38] For example, a diradical mechanism was proposed for the reactions with single coordinate, biomimetic iron-porphyrin catalyst, Fe(TPP)Cl, and a radical–anion addition mechanism was proposed for iron catalysts bearing multiple coordination sites, such as $FeCl_3$ and a chiral iron-phosphoric acid catalyst. In these reactions, the chemo- and site-selectivity of the reactions were controlled by the mechanism and the steric and electronic attributes of the phenols, and selectivity was challenging to achieve.[4, 35] However, the origin of selectivity in P450 catalyzed oxidative coupling reactions is understood to be governed by substrate positioning within the enzyme active site rather than the intrinsic stereoelectronic properties of the substrates.[27, 32]

Of the P450 enzymes known to carry out oxidative dimerization reactions, to our knowledge, none have been developed into biocatalysts for chemistry beyond their native reactions, although the first step towards this goal was accomplished by Hugentobler and Müller in 2018.[14, 24] *Aspergillus niger* was engineered to synthesize **3** by deletion of the gene encoding KtnC and the insertion of the gene encoding DesC to switch the biosynthesis from bicoumarin **2** naturally produced by *A. niger* to **3**, the bicoumarin formed by the fungi *Emericella desertorum*.[14] The heterologous expression of the gene encoding DesC in *A. niger* was verified by LC-MS analysis of the fungal cultures and isolation of **3**, however the yields from the reactions were not disclosed and the platform was not developed further. Although KtnC and DesC exhibit exquisite site- and atroposelectivity for their native substrate **1**, the promiscuity of these enzymes towards non-native coumarins and phenolic compounds was unknown. Our initial studies sought to establish the general reactivity, selectivity, and substrate scope of the oxidative coupling reactions catalyzed by wild-type KtnC and DesC. To accomplish this goal of building a P450 catalyzed oxidative phenolic coupling platform, we aspired to develop and optimize three areas (1) heterologous expression of KtnC and DesC in yeast amenable to analytical and preparative scale reactions, (2) protocols for whole cell biocatalytic reactions, and (3) methods for the reliable analysis and quantification of analytical scale biotransformations. Once established, these methods would allow us to gain insight into and potentially expand the chemistry of P450s KtnC and DesC.

2.3 Whole cell biocatalysis

One reason for the lack of detailed structural and mechanistic studies of P450 enzymes that catalyze oxidative coupling reactions relates to the logistical problems encountered purifying and characterizing the enzymes through traditional techniques employed by chemical biologists.[24, 39] In particular, fungal P450s are often membrane bound which can complicate the isolation and purification of a desired protein, and furthermore, the expressed protein may not be soluble or active.[40-41] The factors that compound the isolation of fungal P450 enzymes for structural and mechanistic characterization can also impact their use as biocatalysts *in vitro*.[42-43] Alternatively, whole cell platforms for the heterologous expression of fungal P450 enzymes in yeast allow the study of enzyme reactivity without the need for purification and isolation of the biocatalysts.[44-45]

Advantages of heterologous expression of fungal P450s in yeast has been extensively documented with different strains employed for this purpose, especially *S. cerevisiae* and *P. pastoris*.[46-48] Several of the benefits of heterologous expression in yeast are the presence of endogenous cytochrome P450 reductases (CPRs) absent in bacterial hosts such as *E. coli*.[49] These coupling partners deliver the electrons necessary for catalytic activity, and can be co-expressed with the enzyme of interest.[42, 47, 50-51] Simple protocols that utilize fermentation an aerobic processes have been extensively developed and described, and both yeast species hold GRAS status (generally regarded as safe) making them ideal heterologous expression hosts.[50, 52] For example, in the first iterations of our biocatalytic platform, biotransformations in yeast were performed according to a standard procedure (Figure 2.3) starting with the inoculation and growth of a culture with the engineered strain, then induction of protein expression by the change of the carbon source accomplished by harvesting the cells and resuspending in the induction media.. Once protein expression was induced, our workflow included the addition of substrates to the cultures, incubation of the biotransformations, and reaction analysis and quantification. This procedure was adapted from standard protocols for the heterologous expression of enzymes in yeast and was further refined as the biocatalytic method evolved.[42, 46-47, 50-51, 53]

Initially, *S. cerevisiae* was engineered as the heterologous host expressing the genes encoding KtnC and DesC employed for biocatalytic reactions, however, we encountered several limitations with this platform. Biotransformations in *S. cerevisiae* displayed an intolerance for high substrate concentrations indicated by a drop in product formation in reactions with substrate concentrations increasing up 0.5 mM (see Supplemental Figure S2.8B), thus, the general protocol was not amenable to preparative-scale reactions and initially imposed limitations in exploring the selectivity of the enzymes. Additionally, low levels of protein expression after induction were observed, with the protein undetectable by Western blot, (Lara Zetzsche, Supplemental Figure S2.8A). However, the expression of the biocatalysts was verified by the formation of natural products **2** and **3** in biotransformations with coumarin **1**. Nevertheless, reactions in *S. cerevisiae* allowed for the investigation of the reactivity of KtnC and DesC with analysis carried out on analytical scale by LC-MS. Attempts to optimize the whole-cell biotransformations in *S. cerevisiae* revealed some minor improvements when increasing the cell density at the time of induction of protein expression (Figure 2.4). Typical

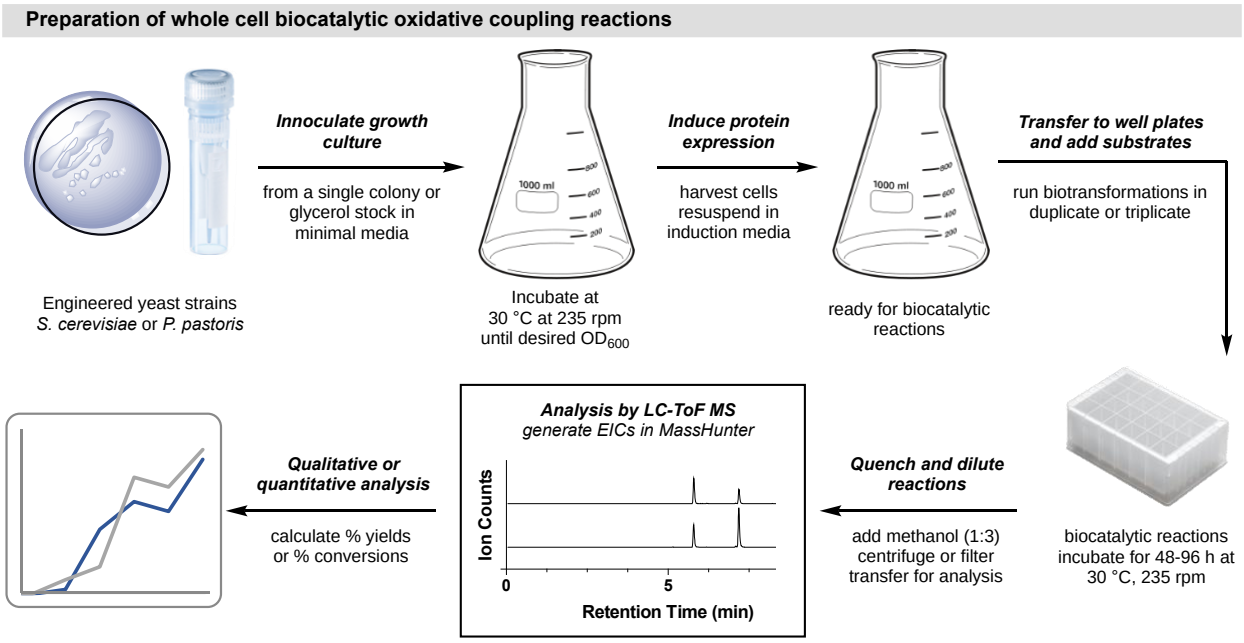

Figure 2.3: General method for heterologous expression in yeast for biocatalytic reactions.
The standard protocols for the functional expression of genes encoding P450 enzymes KtnC and DesC are illustrated. This workflow was applied to biotransformations of *S. cerevisiae* (SC) and *P. pastoris* (PP) expression systems. Minimal media used: H- (SC) and BMM (PP), with recipes in experimental section 2.14. Analytical scale reactions were quenched and diluted with methanol (1:3) then analyzed by LC-MS. Detailed experimental protocols are in experimental section 2.15.

expression protocols favor induction in the log phase of growth, usually between an optical density (OD_{600}) of 0.3 and 0.8 measured spectrophotometrically at 600 nm.[47, 50, 54] However, we observed favorable relative percent yields when growth cultures were allowed to reach an OD_{600} 3-6. For example, dimerization reactions with KtnC were carried out with minimal media cultures containing 4% glucose grown to low and high cell densities and the relative percent yields of coumarin dimers were compared. To induce protein expression, the cells were harvested after reaching the desired OD_{600} by centrifugation and resuspended in a minimal media containing 6% galactose.[54-55] Protocol 2 (high cell density) was found to provide equal or better relative percent conversions of coumarin dimers **1** and **21**-**24**, however, lower cell density was preferred for coumarin **22**. Given that growing cultures to higher cell densities allowed for greater flexibility in preparing the biotransformations and was not usually deleterious to the reaction, attaining higher cell densities was adopted for the general biotransformation protocol in *P. pastoris*.

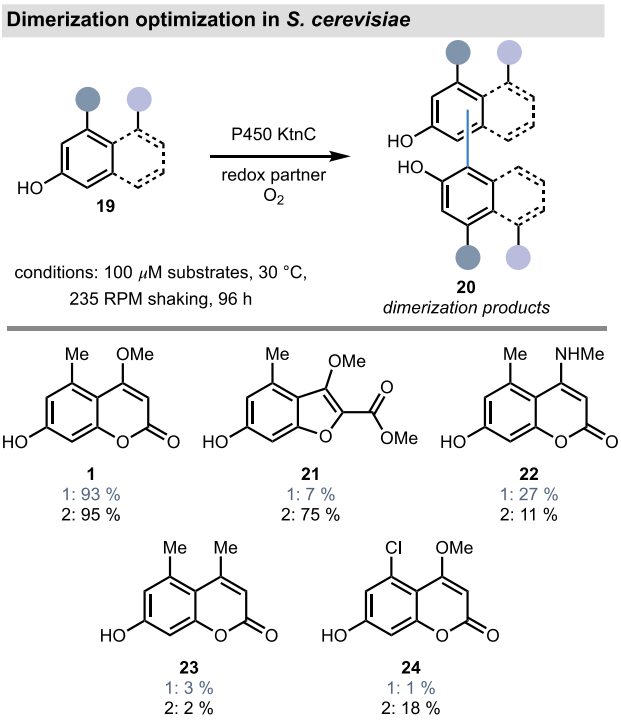

Figure 2.4: KtnC dimerization in *S. cerevisiae*. Comparison of relative percent yield between the general protocol (1) induction at low OD and protocol (2) high OD.

Additional attempts to enhance protein expression in *S. cerevisiae* were not impactful and added unnecessary steps to the procedure. For example, because protein induction occurs by a metabolic shift from *S. cerevisiae* utilizing glucose to galactose for metabolism, we attempted to eliminate residual glucose that could inhibit protein expression. This process, also known as a diauxic shift,[46] happens naturally in yeast when the primary carbon source is exhausted: growth slows, and metabolism switches to the available carbon source such as ethanol or an alternative sugar. With this rationale, several induction procedures were tested by Lara Zetsche to eliminate residual glucose

(Figure 2.5A). The first implemented a washing step by resuspending harvested yeast cells in 6% galactose media, then harvesting, decanting, and resuspending again in fresh galactose media two to three times. Next, incubation with media containing an alternative semi-fermentable sugar, raffinose, was probed, in which the growth media was resuspended in media containing 2% raffinose,[54] allowed to incubate until reaching the desired OD_{600}, then the cells were harvested and resuspended in 6% galactose media for the biotransformations. Biotransformations were then performed for the KtnC and DesC catalyzed dimerization of coumarin **1** (0.1mM, 30 C, 235 rpm, 96 h), and the relative percent yield to dimer **2** was calculated over the course of 96 h and plotted. Both methods provided relatively high percent relative yields of 90 and 73% for KtnC and 51 and 47% for DesC after 96 h incubation. To qualitatively analyze protein expression under different induction protocols, Western blot experiments were conducted (Figure 2.5B). KtnC, with a molecular weight of 60 kD, was not observed, suggesting the induction protocols did not enhance protein expression. These addition steps were ultimately not adopted, offering no benefit to the conversion to desired products or protein expression, while adding complexity to the biotransformation protocol.

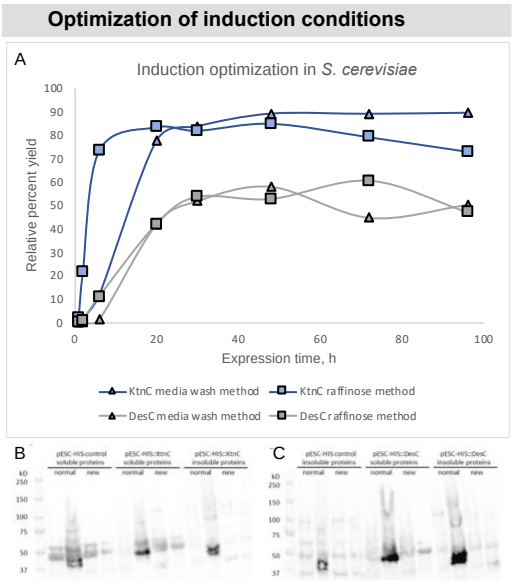

Figure 2.5: KtnC optimization in *S. cerevisiae*. *Data by Lara Zetzsche*. A. Comparison of two induction protocols for KtnC and DesC biotransformations. B-C. Western blots of KtnC and DesC under two induction protocols. Bands should appear at approximately 60 kD.

With limited success in improving product conversion in *S. cerevisiae*, an alternative expression system was desired. We hypothesized that the low levels of protein expression observed in *S. cerevisiae* could be improved by heterologous expression in *P. pastoris*.[49, 51-53] In addition to higher protein expression in *P. pastoris*, other advantages include the yeast's almost entirely aerobic respiration, allowing cultures to reach extremely high cell densities up to 150 g of cells per liter of culture.[51-52] Originally sold as a protein-rich supplement for livestock in the 80's by Phillips Petroleum Company and later developed into a platform for heterologous yeast expression by the Salk Institute, *P.*

pastoris was licensed to Invitrogen as a protein expression system.[56] *P. pastoris* possess promoters that allow for the inducible expression of heterologous proteins by the addition of methanol. The oxidation of methanol to formaldehyde, which is ultimately used as a carbon source, is encoded by two alcohol oxidase genes, AOX1 and AOX2.[49, 53] Of several promoters used for gene expression, alcohol oxidase AOX1 has greater promoter strength in most applications and can achieve concentrations of heterologously expressed protein up to 20 g/L of culture in industrial applications.[51, 53, 57] Alternatively, constitutive promoters such as the glyceraldehyde-3-phosphate dehydrogenase (P_{GAP}) promoter allow for the continuous expression of proteins on carbon sources such as glucose and glycerol without the need for the addition of methanol to induce protein expression, and can achieve comparable levels of protein expression with glucose as the carbon source.[58-59]

A whole cell expression system for KtnC in *P. pastoris* was developed to take advantage of the higher titers achievable compared to *S. cerevisiae.* We hypothesized this would enhance the synthetic utility of KtnC catalyzed oxidative coupling reactions. Two commercially available strains, KM71[60] (His^+Mut^S phenotype) and GS115[53, 61] (His^+Mut^+), were engineered by Lara Zetzsche to express KtnC (see experimental procedures, section 2.14).[49, 62] Both strains were evaluated for their activity in whole cell biotransformations by calculating the relative percent yields of the reactions at time points over 48 h (Figure 2.6A-B). KM71 and GS115 cultures were grown to cell densities of 3-6 OD_{600}. The cultures were then diluted to a final OD_{600} of approximately 1.0 with induction media containing 0.5% methanol. The

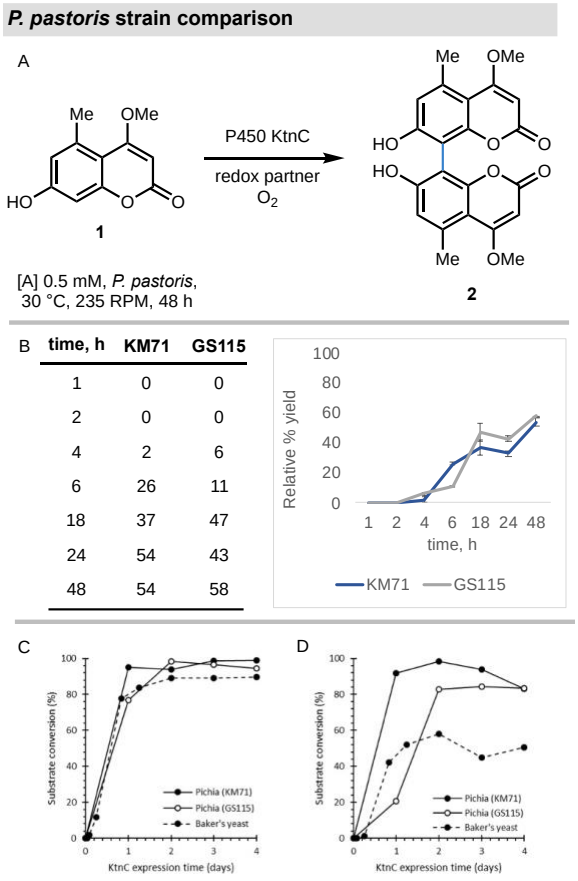

Figure 2.6: P450 catalyzed dimerization in yeast strains KM71, GS115, and *S. cerevisiae*.
A-B. Biotransformations were carried out in culture tubes with 0.5 mM **1**, 30 °C, 235 rpm. The reactions were monitored over 48 h for formation of **2**. C-D. Data by Lara Zetzsche: Biotransformations with three engineered yeast strains containing 0.1 mM **1** were monitored over 4 days and compared.

coumarin substrate **1** was added to the expression cultures (0.5 mM) and incubated at 30 °C for 48 h in culture tubes. The reactions were quenched by the addition of methanol, filtered, then analyzed by LC-MS. There was little difference observed between the relative percent yields of the two strains for biocatalyst KtnC. In 48 h, both whole cell biotransformations reached nearly the same relative percent yield of dimer **2**, 54% for KM71 and 58% for GS115 (Figure 2.6B). Comparing the three different yeast strains in biotransformations carried out at 0.1 mM **1** over 4 days (Figure 2.6C-D), biocatalyst KtnC produced excellent relative percent yields in all three strains, reaching above 80% within 48 h, results consistent with our observations of percent conversion of KtnC-catalyzed dimerizations of **1** in *S. cerevisiae.* Due to the high conversion of this native reaction in all three strains, potential differences in reactivity between strains was not apparent. In DesC, however, which typically achieves lower yields compared to KtnC, the differences in activity between *P. pastoris* strains KM71 and DS115 and *S. cerevisiae* was more obvious (panel D). In *S. cerevisiae*, DesC a maximum yield of approximately 50%, while the reaction climbed to 80% with *P. pastoris*.

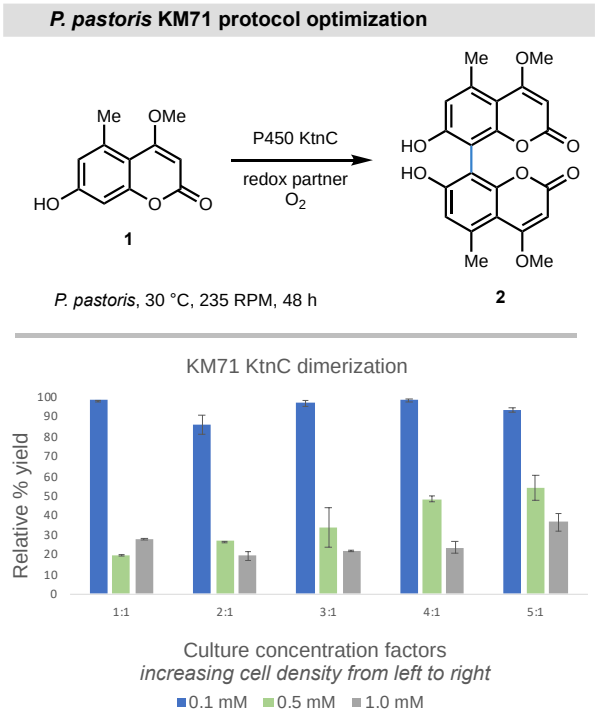

Figure 2.7: KtnC dimerization in KM71.
Comparison of relative percent yield with different cell densities and substrate concentrations.

Optimization of the induction procedure for KtnC catalyzed dimerization reactions in whole cell KM71 biotransformations was investigated next. Unlike *S. cerevisiae*, *P. pastoris* can achieve high cell densities, and we anticipated that this would result in an increase in the biocatalyst, thus enhancing product yields. To test this hypothesis, different cell densities of KM71 were prepared and monitored for the formation of coumarin dimer **2**. Following the general procedure, growth cultures of KM71 were harvested and resuspended to the desired cell densities. Biotransformation cultures were prepared by concentrating a specified

volume of the growth cultures and then resuspending the cell pellets in different volumes of induction media to achieve concentrations from 1:1 to 5:1 (Figure 2.7). For example, the cells from 50 mL of the growth culture were harvested and resuspended in 10 mL of the induction media, concentrating the cell mass by a factor of 5:1. Additionally, the concentration of the coumarin substrate **1** was increased from the concentrations of 0.1 mM, 0.5 mM, up to 1.0 mM to observe the change in relative percent yield with increasing substrate concentration at each cell density. After addition of coumarin **1**, the reactions were incubated for 48 h, quenched with methanol (1:3 dilution), and then analyzed by LC-MS to calculate the relative percent yields of **2**. Little difference in relative percent yield was observed at low concentrations (0.1 mM, blue bars) across the different culture preparations, with all the media preparations achieving high relative percent yields above 80% to nearly quantitative as anticipated. Increasing the substrate concentration typically leads to a decrease in percent yield in all the expression systems tested, however, increasing cell densities had a positive effect on relative percent yield (bars in green, 0.5 mM, and grey, 1.0 mM). Specifically, increasing substrate concentration to 0.5 mM from 0.1 mM caused a drop from 95% to 20% conversion in the 1:1 preparation, however, percent yield more than doubled to 54% in the 5:1 preparation. The same trend was observed in the highest substrate concentration (grey bars), and although the increase in cell density from 1:1 to 5:1 was beneficial, this reaction maxed out at a relative yield of 36% as the boost from higher cell density did not overcome the suppression of reactivity from high substrate concentrations.

2.4 P450 catalyzed oxidative dimerizations of coumarins

With the successful engineering and optimization of the biocatalytic P450 platform, we sought to investigate the scope of the oxidative dimerization reactions catalyzed by KtnC and DesC. To benchmark the native dimerization reaction of coumarin **1** by KtnC and DesC, we compared the P450-catalyzed oxidative phenolic coupling to established methods employing small molecule oxidants (Figure 2.8).[63-66] Coumarin **1** was subjected to conditions known to instigate oxidative coupling reactions with phenols, and extensive screening of conditions was completed by Dr. Meagan Hinze (see Supplemental Figure

S2.2, entries 1-5 for experimental details), only two chemical conditions were identified for the dimerization of electron-deficient coumarin **1** (entries 5 and 6). Specifically, in reaction entries 1-3 with oxidants $Pb(OAc)_4$,[23, 67] Phenyliodine bis(trifluoroacetate) (PIFA),[68-69] and vanadium(V)oxychloride ($VOCl_3$)[70] all failed to produce the expected products. Next, vanadium(V)oxyfluoride (VOF_3) was screened (entries 4-5).[66, 71] In a blend of trifluoroacetic acid (TFA) and dichloromethane (DCM) cooled to 0 °C with 2.0 equiv VOF_3 (entry 5) afforded a mixture of isomeric products composed of the 8,8'-dimer (**2**, 18%), the 8,6'-dimer (**3**, 13%), and the 6,6'-dimer (**4,** 1%). Finally, stoichiometric copper coordinated to tetramethylethylenediamine in hexafluoroisopropanol (HFIP, entry 6) provided solely the 8,8'-dimer (**2**) in a 13% yield.[72] These results illustrate the electronically biased selectivity of reactions mediated with small molecule oxidants of substrates such as electron-poor coumarin **1**. In contrast, P450s KtnC and DesC outperformed small molecule oxidants, resulting in the selective, catalyst-controlled oxidative coupling of **1**. Complete characterization of the atroposelectivity of **2** and **3** demonstrated that KtnC afforded the 8,8'-dimer **2** exclusively in 95% yield and >99:1 er (Figure 2.9A), and DesC biotransformations delivered a complementary product, 8,6'-dimer **3**, in 35% yield and 93:7 er.

Direct oxidative coupling strategies

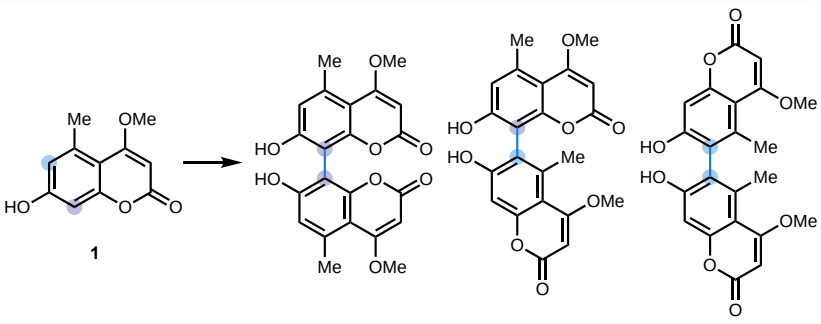

Entry	Conditions	8,8'	8,6'	6,6'
1	$Pb(OAc)_4$ (0.55 equiv), BF_3OEt_2, MeCN, rt	–	–	–
2	PIFA (1.1 equiv), BF_3OEt_2, DCM, 0 °C	–	–	–
3	$VOCl_3$ (2.0 equiv), TFA, DCM, 0 °C	–	–	–
4	VOF_3 (2.2 equiv), TFA, TFAA, 0 °C	–	–	–
5	VOF_3 (2.0 equiv), TFA, DCM, 0 °C to rt, 14 h	18%	13%	<1%
6	Cu(OH)Cl TMEDA (1.0 equiv), HFIP, air, rt, 24 h	13%	–	–
7	P450 KtnC, O_2, BMM, 235 rpm, 30 °C, 48 h	95%	0%	0%
8	P450 DesC, O_2, BMM, 235 rpm, 30 °C, 48 h	<1%	35%	0%

Figure 2.8: Methods for oxidative dimerizations.
Entries 1-6: Small molecule oxidants investigated for the direct oxidative dimerization of coumarin **1**. Entries 7-8: KtnC and DesC catalyze chemically challenging oxidative dimerization reactions with complimentary catalyst-controlled site selectivity. Reaction conditions: *P. pastoris* cells expressing KtnC or DesC in BMM minimal media containing 500 µM coumarin **1** at 30 °C, 235 RPM for 48 h; reported as percent yields. See section 2.14, Figure S2.2 for experimental details.

Next, a panel of non-native 7-hydroxycoumarins were synthesized to probe the substrate scopes of KtnC and DesC. Both enzymes showed promiscuity towards coumarins with different substitution patterns (Figure 2.9). Biotransformations were performed on analytical scale, quenched with methanol (1:3) then analyzed by LC-MS. Although the biocatalysts showed exquisite site- and atroposelectivity towards their native substrate (Figure 2.9A), with non-native coumarins, multiple product peaks were

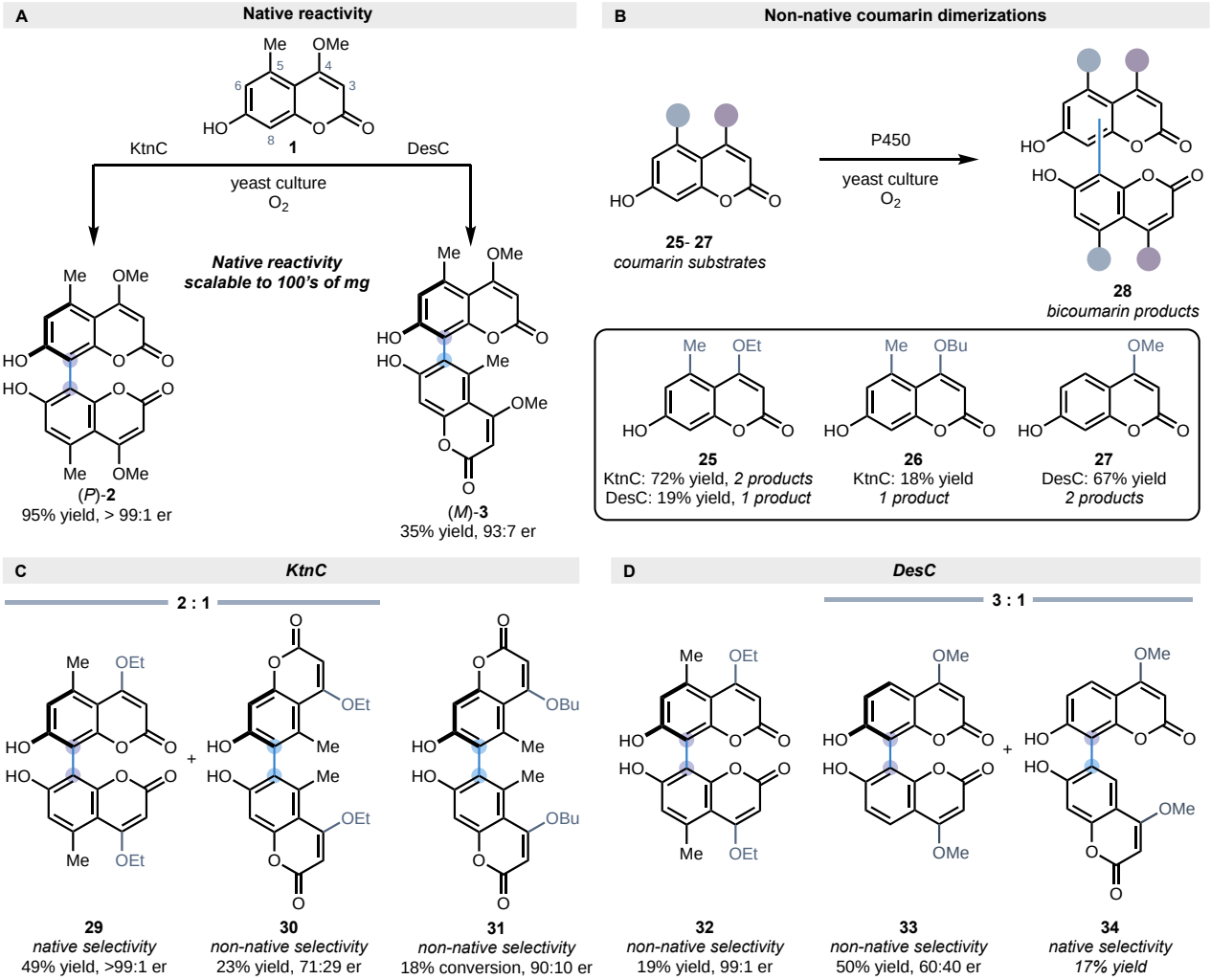

Figure 2.9: Selectivity of dimerization reactions.
Reaction conditions: *P. pastoris* cells expressing KtnC or DesC in BMM minimal media containing 500 µM coumarin **1**, **25**-**27** at 30 °C, 235 RPM for 48 h; reported as percent yields measured by product standard curves in LC-MS. *Relative percent yield.

observed in the extracted ion chromatograms of some of the biotransformations (Figure 2.9B-D). For example, the dimerization reaction of **25** formed two product peaks with KtnC, and **27** formed two products with DesC (Figure 2.9B). To determine the product distribution, site- and enantioselectivity of non-native coumarin dimers produced by KtnC

and DesC, the biotransformations were conducted on preparative-scale (100 of mgs) for product isolation and characterization (see section 2.15 for experimental details for preparative scale reactions carried out by Dr. Meagan Hinze). In reactions with KtnC, the 8,8'-isomer could be obtained exclusively, except in the case of substrates possessing increased steric bulk at the C4 position. For example, increasing steric bulk induced a shift from the selective formation of the 8,8'-isomer (**2**) with coumarin **1** in the native reaction, to mixtures of 8,8'-isomer **29** and 6,6-isomer **30** in the dimerization of C4-ethyl ester **25**. Interestingly, the enantioselectivity for the 8,8'-isomer remained high with a 99:1 er, however an erosion of enantioselectivity was observed with the “non-natural” 6,6'-isomer (71:29 er) **30**. Increasing the steric bulk further to a butyl ester **26**, a complete switch in site-selectivity to the 6,6'-isomer **31** was observed, and while the yield dropped to 18%, the enantioselectivity remained high at 90:10 er. This unexpected substrate-controlled site-selectivity observed in reactions catalyzed by KtnC provided access to 6,6'-isomers, which remains elusive by direct chemical oxidative coupling methods. The potential to switch the site-selectivity by increasing the steric bulk of the C4-ester in KtnC catalyzed dimerization reactions provided an advantage over small molecule oxidants for the synthesis of coumarin dimers bearing the 6,6'-connectivity.

Reactions mediated by DesC also displayed selectivity trends according to the change in functional group at the C4 and C5-substituent. A site-selectivity switch from the native 8,6'-isomer **3** to the 8,8'-isomer **32** as the sole product with increasing steric bulk at C4 ester of coumarin **25** was observed. Removal of the methyl group at C5, coumarin **27**, resulted in a mixture of 8,8' and 8,6'-isomers in 2:1 ratio. While the non-native coupling to the 8,8'-configuration of dimer **32** was highly enantioselective with 99:1 er, the loss of the C5 methyl group of **27**, resulted in dimer **33** in a 50% yield and 60:40 er, suggesting that the coumarin substituents could play a role in substrate binding within the active site, potentially influencing the site- and enantioselectivity of the reaction.

With promising results achieved in demonstrating the promiscuity of KtnC and DesC in the oxidative dimerization of coumarins, we sought to expand this chemistry beyond coumarins. Nearly all non-coumarin phenolic substrates such as 2-naphthols, quinolines, and simple phenols with a single aromatic ring tested in the dimerization reaction were unsuccessful, highlighting a potential limitation of the scope of the wild-type

enzymes. However, we identified one example of a non-coumarin dimerization in the reaction of benzofuran **21** (Figure 2.10) which possesses similar structural features to the native substrate. We observed the formation of two different product peaks by LC-MS in both DesC and KtnC that shared the same retention times and noticed a switch in the major product peaks. This suggested complimentary site-selectivity in the dimerization reaction, however, efforts to scale up and isolate the products for characterization were unsuccessful. For example, in preparative scale reactions following the standard conditions developed for coumarin dimerization biotransformations, product formation corresponding to dimeric products represented by **35** were observed, however the conversion was low with the formation of two products in a ratio of approximately 3:1 (8% and 3% relative yield, two product peaks). The reaction culture was extracted with ethyl acetate and concentrated, however, by LC-MS, much of the product remained in the pelleted cells after extraction, and the concentrated organic extracts did not show the formation of product by ^{1}H NMR. Additional attempts provided similar results. Efforts to synthesize the dimeric product standards by Dr. Meagan Hinze were not fruitful due to a lack of stability of the vinylogous methyl ester, a feature of the dimeric products that may also have contributed to the difficulty in product isolation from biotransformation cultures.

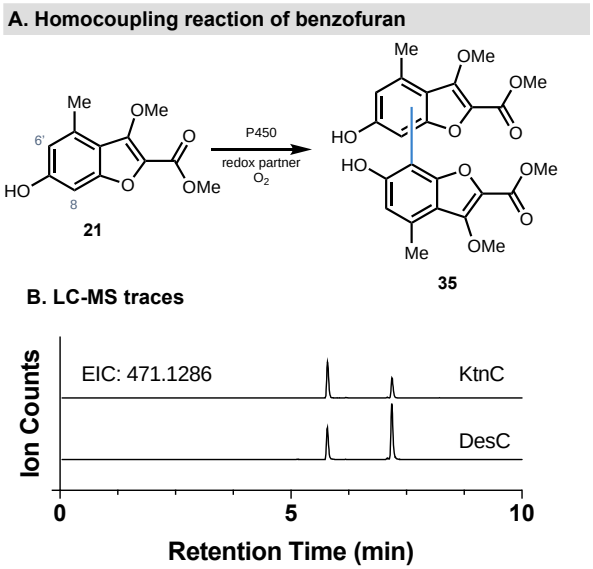

Figure 2.10: Benzofuran dimerization reactivity. Reaction conditions: *P. pastoris* cells expressing KtnC or DesC in BMM minimal media containing 100 µM benzofuran **21** at 30 °C, 235 RPM for 48 h.

2.5 P450 KtnC catalyzed oxidative cross-coupling of phenols

Focusing on the biocatalyst KtnC, which exhibited higher percent yields in most dimerization reactions compared to DesC while still maintaining excellent enantioselectivity with non-native substrates, we sought to investigate the potential for

KtnC to carry out oxidative chemistry beyond the native dimerization reaction. From exploration of the substrate scope of KtnC catalyzed dimerization reactions, we observed that non-native coumarins could be efficiently converted to dimeric products. We speculated that cross-coupling reactions might be possible by the initial hydrogen atom abstraction of one unit of coumarin **1**, and the colocalization of a different phenolic coupling partner within the enzyme active site through a radical–addition mechanism (Figure 2.11A). To test this hypothesis, a proof-of-principle cross-coupling experiment was completed in which the (**1**) and a phenolic substrate that does not dimerize, 2-naphthol (**39**), were combined with KtnC under the standard dimerization conditions (Figure 2.11B). Unsurprisingly, the major product at >95% relative yield was the coumarin dimer **2.** However, the cross-coupled coumarin-naphthol products were detected by LC-MS as minor products in a 3% total relative yield (**40**). This early result demonstrated that KtnC could mediate a cross-coupling reaction to produce unsymmetrical biaryl products in addition to symmetrical dimers, albeit in low amounts. To further investigate the potential for KtnC to function as a biocatalyst capable of cross coupling a wider range of phenols, we sought to optimize the KtnC reaction in the *P. pastoris* platform.

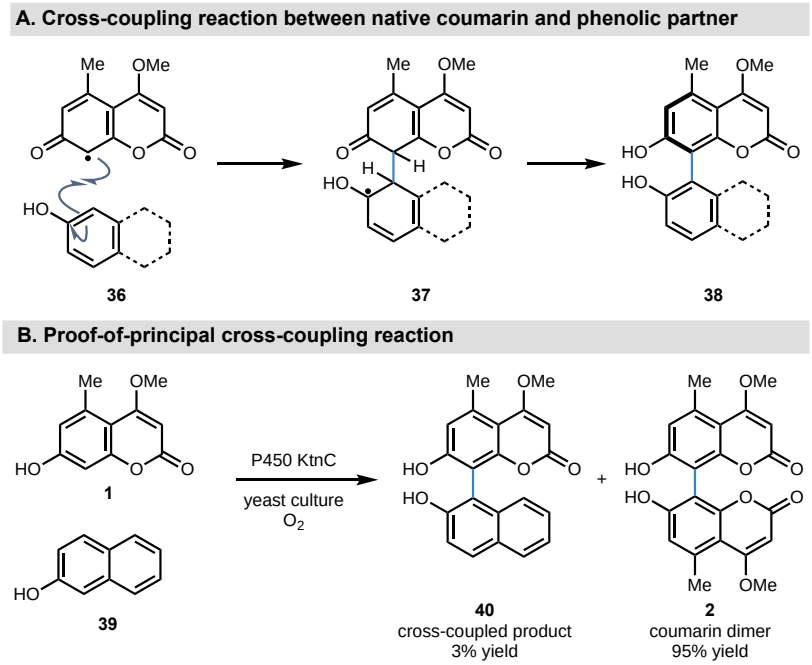

Figure 2.11: KtnC catalyzed oxidative cross-coupling.
A. Radical–addition proposed for the cross-coupling reaction. B. Preliminary evidence for KtnC cross-coupling. Reaction conditions: *P. pastoris*, BMM, 100 µM coumarin **1**, 1000 µM **39** at 30 °C, 235 RPM for 48 h.

2.6 Whole cell cross-coupling biotransformation optimization

As dimerization of the native substrate **1** was favored, we hypothesized that the product distribution could be biased toward cross-coupled product by increasing the concentration of the coupling partner relative to the native substrate. This strategy is employed in the direct oxidative cross-coupling of phenols mediated by small molecule oxidants to overcome the electronic bias leading to preferential dimerization of phenols with higher oxidation potentials.[4, 37, 73-75] We considered that rather than overcoming an electronic bias in chemoselectivity, we could suppress dimerization by out-competing the binding of two units of the native substrate within the active site by increasing the relative concentration of the coupling partner to favor cross-coupling. To test this hypothesis, analytical scale biotransformations with increasing concentrations from 0.1 mM to 1.0 mM of the coupling partner were carried out (Figure 2.12), changing the coumarin substrate ratio from 1:1 up to a 1:10 relative to coumarin **1**. We observed this trend as an increase in the relative percent yield of the cross-coupled product as the concentration of the non-native aminocoumarin **22** was increased. At concentrations above 0.4 mM of **22** (entry 3), formation of cross-coupled product was favored, reaching up to 70% relative yield of the cross-coupled product (entries 5 and 6). Encouraged by this result, cross-coupling reactions were carried out in a 1:10 ratio of **1**:**22** coupling partners as standard conditions to compare reactivity across a wide range of cross-coupling reactions.

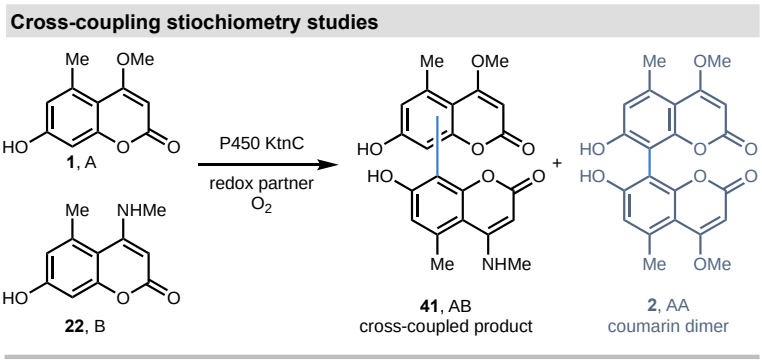

entry	[A]	[B]	% AA	% AB	AA:AB
1	0.1	0.1	68	24	3:1
2	0.1	0.2	59	30	2:1
3	0.1	0.4	49	38	1:1
4	0.1	0.6	14	67	1:5
5	**0.1**	**0.8**	**10**	**70**	**1:7**
6	**0.1**	**1.0**	**9**	**70**	**1:7**

[A] & [B] in mM, *P. pastoris*, 30 °C, 235 RPM, 48 h

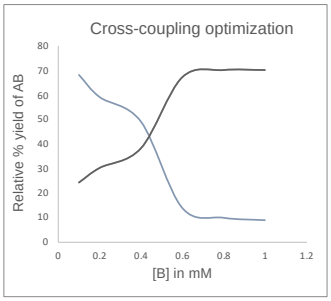

Figure 2.12: KtnC oxidative cross-coupling optimization.
Increasing the concentration of the coupling partner, **22** (B), relative to the concentration of **1** (A) resulted in more cross-coupled product, **41** (AB).

2.7 Quantification strategies for analytical scale reactions

With the ability to run reactions in a high throughput or semi-high throughput format (in 96 or 24 well plates), a method for rapid analysis was desired. Reactions conducted on analytical scale were monitored by LC-MS. Whole cell biotransformations were quenched by the addition of methanol or acetonitrile suitable for HPLC, typically in a 1:3 dilution (reaction:organic solvent), or to a final substrate concentration between 10 and

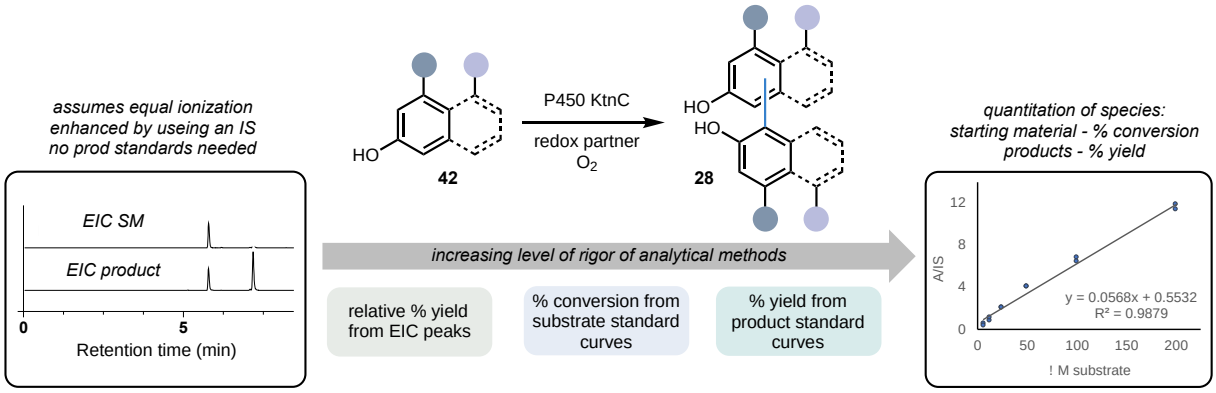

Figure 2.13: KtnC dimerization in KM71.
Comparison of relative percent yield with different cell densities and substrate concentrations.

50 µM. The addition of organic solvent crashed out biomolecules and salts from the whole cell biotransformation media, and the cells and debris were then pelleted by centrifugation. The supernatant was then analyzed directly or could be further diluted and filtered if desired. With analysis of the biotransformations by LC-MS, data was generated quickly and provided insight into the general reactivity of the biotransformations, which allowed for rapid method development and protocol optimization. Several strategies were developed for reaction analysis and quantification by LC-MS, with varying degrees of rigor. The advantages and limitations are discussed here in order from the least to most rigorous.

2.8 Relative percent yields

Relative percent yields were calculated by extracting the exact masses of the starting materials and products in Agilent's MassHunter software. The extracted ion

chromatograms (EICs) were integrated, and the peak areas for the relevant species were compared directly or normalized with an internal standard. This method was most useful when all species, starting materials and potential products, ionized similarly, and assumed negligible degradation or off-target reactivity of the different species compared. Positive and negative controls were built into the experiment, and all biotransformations were run either in duplicate or triplicate. The desired product peak areas were compared to all the species present, including remaining starting materials and additional products formed (equations 1-4, Figure 2.14). Using relative percent yields, the general reactivity of dimerization and cross-coupling reactions was characterized in initial screens to investigate the substrate scope of KtnC. This level of analysis gave a rough estimate of the relative amount of the products formed in comparison to starting materials remaining. These screens allowed the comparison of reactions across different sets of conditions and could be reliably used for coumarin dimerization and coumarin-coumarin cross-coupling reactions. We found this analysis especially useful when initially characterizing substrate scope for oxidative coupling reactions, when authentic product standards were not accessible synthetically, or when reactivity was low, and products could not be isolated.

Relative percent yields calculated by the following equations:

Dimerization biotransformations:

$$Eq.1 \quad [A]_{start} = [A]_{remaining} + 2 \times [AA]_{formed}$$

$$Eq.2 \quad [AA]_{total} = \frac{(\sum [AA]_{formed})}{(\sum [AA]_{formed} + 0.5 \times [A]_{remaining})} \times 100\%$$

Cross-coupling biotransformations:

$$Eq.3 \quad [A]_{start} = [A]_{remaining} + 2 \times [AA]_{formed} + [AB]_{formed}$$

$$Eq.4 \quad [AB]_{total} = \frac{(\sum [AB]_{formed})}{(\sum [AB]_{formed} + (2 \times \sum [AA]_{formed}) + [A]_{remaining})} \times 100\%$$

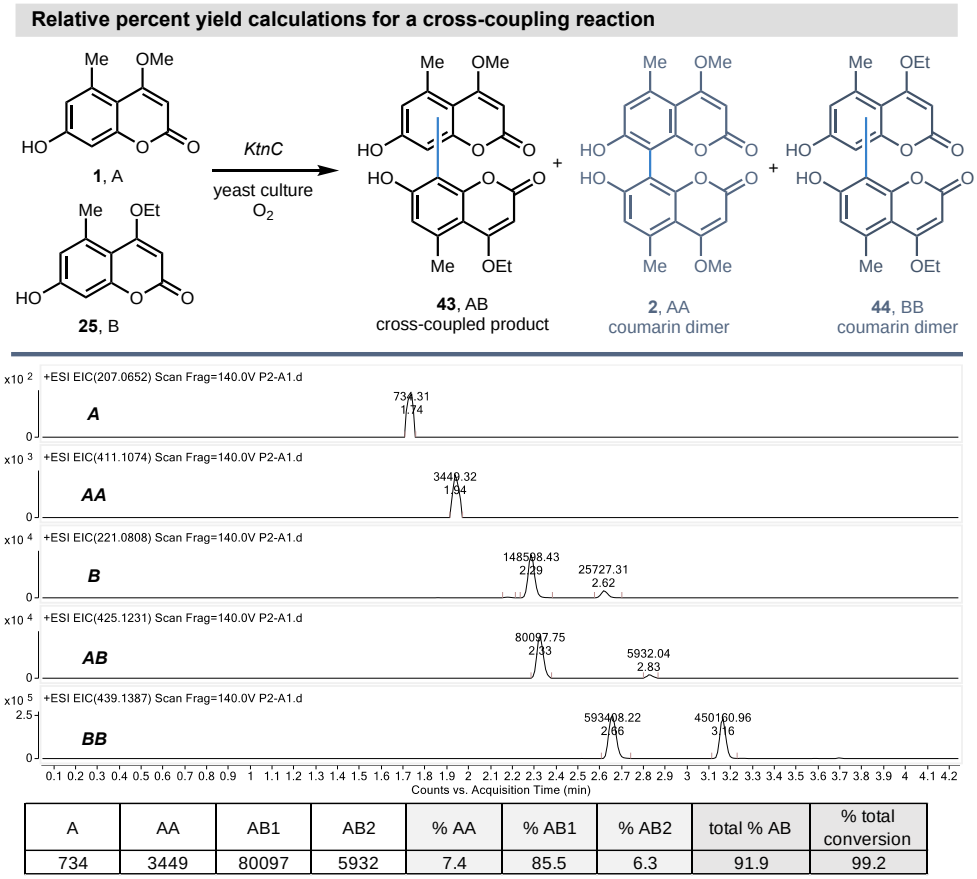

A	AA	AB1	AB2	% AA	% AB1	% AB2	total % AB	% total conversion
734	3449	80097	5932	7.4	85.5	6.3	91.9	99.2

Figure 2.14: KtnC oxidative coupling reactions.
Notation shows A and B starting materials, AA, AB, and BB products, with A as the limiting reagent. Biotransformation in *P. pastoris*, 25 µM **1**, 250 µM **25**, 30 C, 48 h. Relative percent yield calculated for each species from the EIC peak areas by Eq. 1-4. Positive mode, phase A = deionized water with 2 mM ammonium formate, pH = 3.5 and phase B = 95:5 acetonitrile: deionized water, v/v with 2 mM ammonium formate, pH = 3.5; method = 80% A held for 0.5min, to 45% A over 2.75 min, 10% A 100% A for 1.0 min, 254, 275, and 308 nm UV detection and 0.7 mL/min flow rate. Each injection was followed by equilibration at 80% A for 1 min.

If more than one product peak was present, each individual peak was assessed relative to the other species in the same manner, for example, AB_{total} would be replaced by AB_1.

Generally, similar relative percent yields were calculated for repeated biotransformations with the same reaction conditions and substrates that ionize similarly (Figure 2.15). This analysis was less reliable for reactions with non-coumarin phenolic substrates for example, with naphthols and nitrogen heterocycles, as either a reduction or enhancement in ionization would give reduced or increased relative percent yields, respectively. In figure 2.15, reactions 1-3 were run with identical conditions, and included cross-coupling of both coumarins **25** and **26** to **1**. Although variation was observed, the trends in reactivity remained the same. In the cross-coupling reaction of **1** and **25**,

reactions 1 and 2, were nearly identical with high relative yield of the cross-coupled products. Reaction 3 had lower relative percent yield, however the ratio of cross-coupled products to dimers was nearly the same as reactions 1 and 2. With this level of analysis, we obtained an understanding of the general trends in reactivity and product distribution and could identify reactions to further investigate and characterize by more rigorous analytical methods.

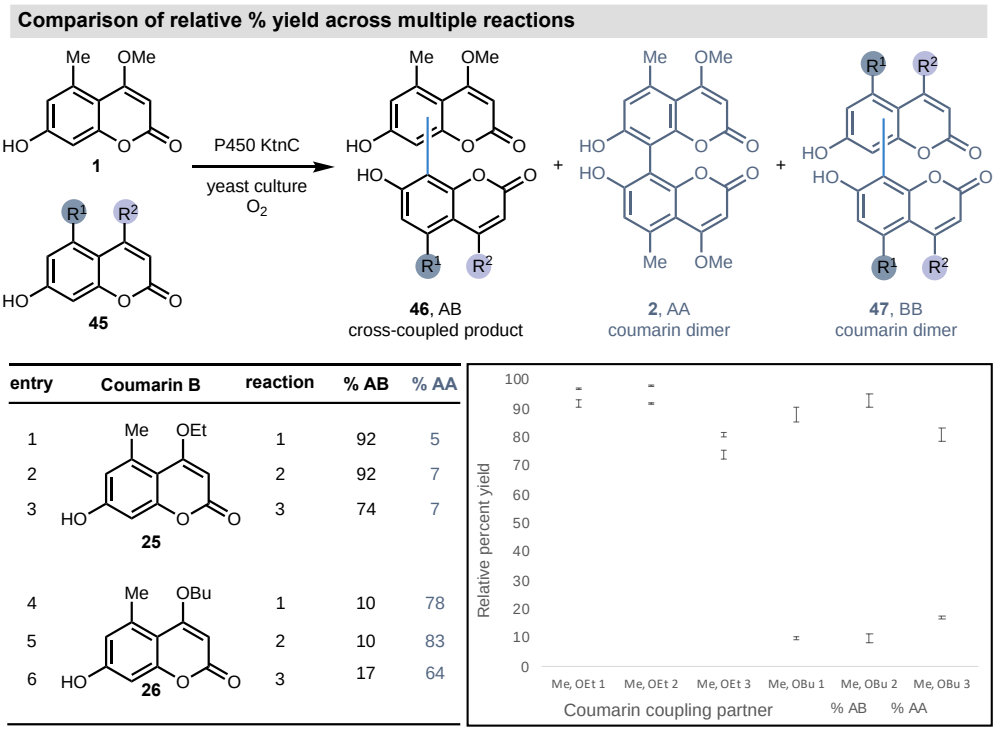

entry	Coumarin B	reaction	% AB	% AA
1	25	1	92	5
2		2	92	7
3		3	74	7
4	26	1	10	78
5		2	10	83
6		3	17	64

Figure 2.15: Relative percent yield comparisons.
Three sets of biotransformation in *P. pastoris*, 25 µM A, 250 µM B, 30 C, 48 h, 1 mL reactions in 24 well plates. Relative percent yield calculated for each species from the EIC peak areas by Eq. 4. Means of total AB and AA products calculated for reactions carried out in triplicates and compared (entries 1-6).

2.9 Percent conversions by standard curves of known species

Due to the limitations in analysis by relative percent yield, we sought to develop a more robust method for quantification of KtnC catalyzed oxidative coupling reactions on analytical scale. Methods were developed for both dimerization and cross-coupling reactions based on standard curves of known species in the biotransformations. For dimerization reactions, calculating percent conversions was relatively straightforward (Figure 2.16). A standard curve of the starting material was generated by serial dilutions

of the substrate in triplicate, normalized with an internal standard, and all reactions were quenched and analyzed in one experiment. The standard curve was used to calculate the remaining, unreacted substrate concentration with the assumption that all the coumarin substrate consumed formed dimerized products. This method could by applied using integrated EIC peak areas of the substrates and internal standard, or the same analysis by peak integration in UV chromatograms.

Percent conversion by standard curve

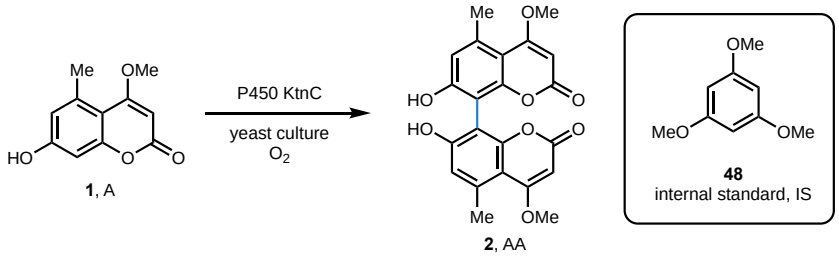

#	[A]	A	IS	A/IS
B1	0.2	1662320	861764	1.93
B2	0.2	1555453	884233	1.76
B3	0.2	1691602	756771	2.24
B4	0.1	628487	881675	0.71
B5	0.1	802130	790968	1.01
B6	0.1	752907	843104	0.89
C1	0.05	375601	825737	0.45
C2	0.05	467831	796224	0.59
C3	0.05	464115	770056	0.60
C4	0.025	195623	823456	0.24
C5	0.025	194230	841404	0.23
C6	0.025	220411	833843	0.26
D1	0.0125	98131	840734	0.12
D2	0.0125	89505	947025	0.09
D3	0.0125	88353	947101	0.09
D4	0.00625	37500	920660	0.04
D5	0.00625	47887	955365	0.05
D6	0.00625	51194	915688	0.06

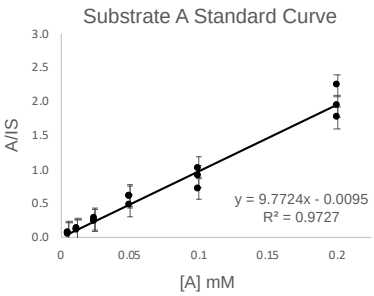

Reaction		LC-MS EIC Peak Area		Calculations				
well #	[A] mM	A	IS	A/IS	$A_{remaining}$	AA_{formed}	% AA	average
A1	0.1	105689	808593	0.131	0.0144	0.0428	85.6	87.1
A2	0.1	75791	746980	0.101	0.0114	0.0443	88.6	

Figure 2.16: Relative percent conversion by standard curve.
Biotransformations were carried out in duplicate in cultures of *P. pastoris* with 0.1 mM **1** in 24 well plates. The standard curve was prepared in triplicates by serial dilution of coumarin **1** in DMSO**,** then addition to KM71 no-enzyme control cultures in 24 well plates and incubated at 30 C, 235 rpm, 48 h. All yeast cultures were prepared with 0.3 mM as the internal standard **48,** then transferred in 1 mL aliquots into 24 well plates containing the substrates. The plates were incubated at 30 °C, 235 rpm, for 48 h. All reactions and standard curve were quenched with methanol (1:3) and analyzed by LC-MS. Calculations made with EIC peak areas.

When the native substrate **1** (A) was used as the limiting reagent in a cross-coupling reaction, we observed the formation of the native dimer **2** (AA) and cross-coupled products, resulting in mixtures of starting materials, dimers, and cross-coupled products. An analytical method was developed to quantify the formation of cross-coupled products indirectly through quantification of the known species formed in the reactions, A and AA. The percent conversion to the cross-coupled AB products was calculated by determining the concentration of the remaining native coumarin **1** by standard curve of A, and the amount of coumarin dimer **2** formed by standard curve of AA. The concentration of the desired

cross-coupled AB products was assumed to be comprised of the remaining coumarin species according to the formulas:

$$Eq.5 \quad [A]_{start} = [A]_{remaining} + 2 \times [AA]_{formed} + [AB]_{formed}$$

$$Eq.6 \quad [AB]_{formed} = [A]_{remaining} + 2 \times [AA]_{formed} - [A]_{start}$$

$$Eq.7 \quad \%\ conversion\ to\ AB = \frac{[AB]_{formed}}{[A]_{start}} \times 100\%$$

Calculating percent conversion by standard curve

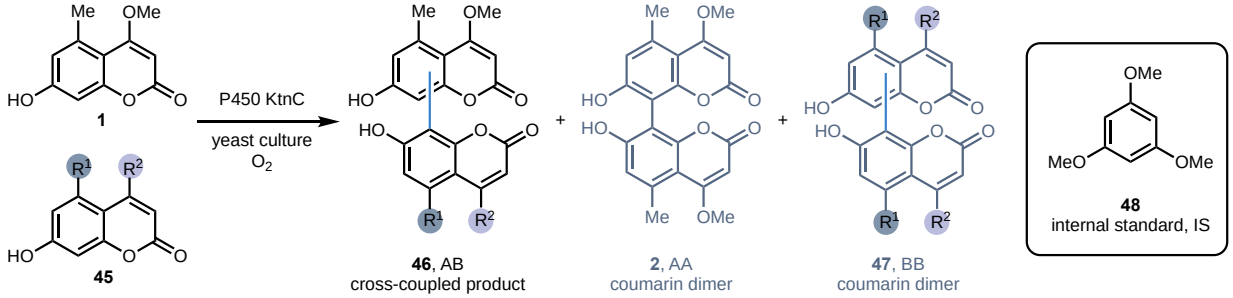

well	[A]	[AA]	A	IS	A/IS	AA	IS	A/IS
A1	100	0	197152	78144	2.52	0	78144	0.00
A2	100	0	197152	78144	2.52	0	78144	0.00
A3	100	0	183612	76419	2.40	0	76419	0.00
A4	50	0.78125	99189	77906	1.27	2828	77906	0.04
A5	50	0.78125	90774	77346	1.17	3699	77346	0.05
A6	50	0.78125	87508	81024	1.08	4253	81024	0.05
B1	25	1.5625	35762	74128	0.48	7400	74128	0.10
B2	25	1.5625	43885	74288	0.59	6914	74288	0.09
B3	25	1.5625	37380	84870	0.44	7155	84870	0.08
B4	12.5	3.125	17397	78475	0.22	17719	78475	0.23
B5	12.5	3.125	17961	75909	0.24	17816	75909	0.23
B6	12.5	3.125	33610	75079	0.45	16247	75079	0.22
C1	6.25	6.25	8190	76368	0.11	34776	76368	0.46
C2	6.25	6.25	9323	73484	0.13	36209	73484	0.49
C3	6.25	6.25	14727	74461	0.20	36094	74461	0.48
C4	3.125	12.5	3920	77423	0.05	79390	77423	1.03
C5	3.125	12.5	5210	75879	0.07	104678	75879	1.38
C6	3.125	12.5	10954	74988	0.15	90314	74988	1.20
D1	1.5625	25	2052	74676	0.027	172734	74676	2.31
D2	1.5625	25	3900	74915	0.052	163183	74915	2.18
D3	1.5625	25	2344	75820	0.031	164248	75820	2.17

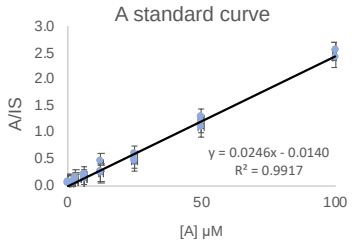

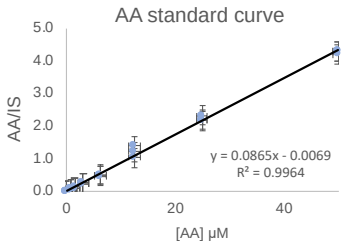

Substrate	LC-MS EIC Peak Area						calculations						
R1, R2	A	IS	A/IS	AA	IS	AA/IS	$[A]_{remaining}$	$[AA]_{present}$	$[AB]_{formed}$	% conv AB	average	% AA	average
Me, OEt	734	71880	0.010	3449	71880	0.048	0.98	0.63	22.75	91.0	90.1	5.1	4.6
	1933	74378	0.026	2862	74378	0.038	1.63	0.52	22.33	89.3		4.2	
Me, OPr	17816	74738	0.238	15449	74738	0.207	10.26	2.47	9.80	39.2	40.7	19.8	17.9
	18069	74479	0.243	12424	74479	0.167	10.43	2.01	10.55	42.2		16.1	
Me, OBu	4980	75922	0.066	25476	75922	0.336	3.24	3.96	13.85	55.4	52.5	31.7	34.5
	5029	75559	0.067	29934	75559	0.396	3.27	4.66	12.41	49.6		37.3	

Figure 2.17: Relative percent conversion by standard curve.
Biotransformations were carried out in duplicates in cultures of *P. pastoris* with 25 µM and 250 µM B in 24 well plates. The standard curve was prepared in triplicates by serial dilution of coumarin **1** in DMSO**,** then addition to KM71 no-enzyme control cultures then incubated at 30 C, 235 rpm, 48 h. All yeast cultures were prepared with 0.3 mM **48** as the internal standard, then transferred in 1 mL aliquots into 24 well plates containing the substrates. The plates were incubated at 30 °C, 235 rpm, for 48 h. All reactions were quenched with methanol (1:3) and analyzed by LC-MS. Calculations made with EIC peak areas. The percent conversion was calculated according to Eq. 5-8.

$$Eq.8 \quad \%\, yield\ to\ AA\ = \frac{[AA]_{formed}}{[AA]_{theoretical\ max}} \times 100\%$$

Initial attempts at generating the standard curves of both coumarin monomer **1** (A) and dimer **2** (AA) species were unsuccessful, with the calculated concentrations of **1** well above the actual starting concertation added to the biotransformations. The standard curve for AA also overestimated the concentration of the dimer **2**. Several problems were uncovered and resulted in refinement of standard curve generation and development of best practices that were useful for other analytical quantitation methods by LC-MS in the project. The need for matching the whole cell biotransformation matrix in the standard curve samples was crucial, which required the standard curves to be run in whole cell yeast cultures in either *S. cerevisiae* or *P. pastoris* no enzyme control under the standard reaction conditions. Initially, biotransformations were carried out with substrate concentrations of 0.1 mM **1** and 1.0 mM coupling partner B or 25 µM **1**and 250 µM B, and standard curves were generated with a concentration range from zero up to double the maximum starting concentration of **1**.

In reactions containing the internal standard 4,4'-dihydroxybenzophenone, a gradual increase of the peak area was observed, with a difference of up to 400% from the initial samples injected to the end of the sequence, on average 50 injections or more. This was attributed to carry-over from previous injections and was improved by both reducing the concentration of the internal standard and modifying the LC-MS method to increase the length of the post-run to 1 minute from 0.25 minutes and increasing the needle washing to 10 seconds from 4 seconds. Alternatively, different internal standards such as 1,3,5-trimethoxybenzene could be used successfully and were less prone to carry-over, however this internal standard could only be used in positive ion mode while 4,4'-dihydroxybenzophenone ionized well in both positive and negative modes. The last factors that were crucial in obtaining standard curve data were (1) modifying the method to separate the **1** and **2** so there was no overlap in the peak retention times and (2) purifying the native substrate **1** by prep HPLC to remove an impurity that co-eluted with the dimeric product **2** (see experimental section 2.14). Once all these requirements were implemented, the quantitation of both A and AA species was more consistent across experiments and provided reliable quantitation (Figure 2.17).

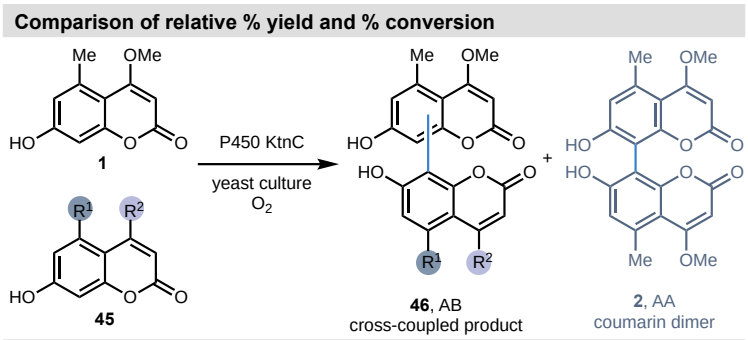

			Relative % yield				% conversion			
entry	Coumarin B	equiv B	% AB		% AA		% AB		% AA	
1	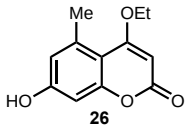	1.0	35	±4	60	±2	12	±4	75	±2
2		2.5	47	<1	44	±1	53	±2	32	<1
3		5.0	75	±2	15	±2	61	±1	19	±1
4	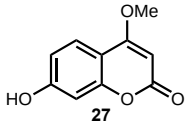	1.0	12	±1	77	±1	1	±2	76	±1
5		2.5	17	<1	55	±1	13	±5	45	±1
6		5.0	16	<1	27	<1	18	±2	20	<1
7	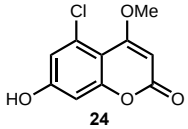	1.0	5	±1	51	±2	8	±2	37	±3
8		2.5	6	<1	30	±2	8	<1	22	±2
9		5.0	5	±1	16	±5	9	±3	12	±3

Figure 2.18: Comparison of analysis methods.
Conditions: Biotransformations in 24 well plates well plates, *P. pastoris*, BMM, 100 µM **1**. Coupling partner B added in 1.0, 2.5, or 5.0 equiv (100, 250, or 500 µM), 30 °C, 235 RPM, 48 h.

Generating this data set allowed for the comparison of the relative percent yield analysis to a more rigorous quantification by standard curve. Comparing the quantification methods, there was fair agreement between the methods although variation between percent conversion and yield was greater when competing dimerization was higher, notably in entries 1 and 4 (Figure 18). Some of this variation could be rationalized as random, however, error in the quantification of coumarin dimer **2** by standard curve could also account for the differences; in this example, the R^2 values of the standard curves for **1** and **2** were 0.9697 and 0.9550 respectively. However, the general trends are apparent in both quantification approaches, for example, as the equivalents of B are increased from 1 to 5, the increasing formation of cross-coupled product is observed in both quantification methods, and similar conclusions about the reactivity of each set of the reactions and conditions could be drawn.

2.10 Percent yield by product standard curves

When products could be directly isolated from yeast biotransformations or synthesized, the preferred method of analysis on analytical scale was quantitation by product standard curves. This method was the most rigorous for analytical quantitation.

We were able to quantify multiple product species formed in dimerization reactions catalyzed by both KtnC and DesC (see Figure 2.2). Gratifyingly, we found good agreement between all three methods for quantitation of coumarin dimers (Figure 19), suggesting that all methods were reliable for qualitative analysis of the biotransformations, and quantification by standard curve was attainable by two different approaches.

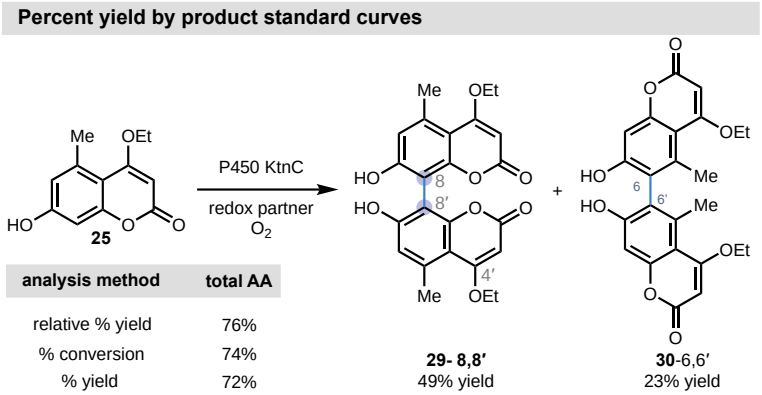

Figure 2.19: Comparison of analysis methods.
Conditions: 1 mL reactions in 24 well plates, *P. pastoris,* BMM, 250 µM **25**, 30 °C, 235 RPM, 48 h. The percent yields were calculated by standard curves of **25** or **29** and **30**. The percent conversion was calculated from the standard curve of **25**. Relative percent yields were calculated from the EIC peak areas.

2.11 Summary of analytical scale quantification methods by LC-MS

Three different methods for analytical scale quantification of biocatalytic oxidative coupling reactions by LC-MS were developed. All methods had different advantages and applications, with some assumptions and limitations noted. In the first two methods presented, relative percent yield and percent conversion, both assume that the formation of dimers and/or cross-coupled products proceed cleanly with negligible degradation of the starting materials or the products. We assume no undesired side reactions occur, such as the formation of trimers or hydroxylated products. The masses for these potential off-target compounds were not observed by LC-MS, however, while this does not exclude the existence of undesirable reactivity, it does suggest that this is not a major pathway. When products are not isolable or cannot be synthesized, the first two approaches provide useful methods for assessing reactivity in biocatalytic reactions resulting in complex mixtures and help identify reactions of potential interest for further investigation.

Analysis of biotransformations by relative percent yield was the fastest way to get a sense of the general reactivity of biotransformations studied involving the reactions of KtnC and DesC. By extracting exact masses of the starting materials and products, we

could immediately compare the peak areas to assess the ratio of products to one another, and to roughly estimate the percent yield. This analysis was applied to screening conditions for reaction optimization and induction protocols and allowed for the rapid development of the scope of reactivity of KtnC and DesC in dimerization and cross-coupling reactions, quickly revealing if product was forming and the relative amount. This method served as an excellent comparative tool to get a sense for how different substrates compared across the panel of compounds tested, and analysis could be completed with or without the addition of an internal standard. In this context, relative percent yield analysis was a reliable tool to study the general reactivity of the biocatalysts and especially useful for exploratory campaigns of new enzymes.

The main limitation of analysis by relative percent yield was the observation that differences in ionization between compounds, and enhancement or suppression of ionization due to matrix effects could artificially inflate or reduce the relative percent yields. This effect was notable in non-coumarin aromatic compounds, especially naphthols and nitrogen containing molecules. In these cases, relative percent yields could still be useful when comparing different protocols for the same reactions, but the results should be verified with other methods.

For more rigorous quantification, percent conversions based on standard curves were used to estimate the conversion from starting material to products. This strategy could be applied to both dimerization and cross-coupling reactions, however, quantification of more than one species was difficult and increased the amount of error in the calculations. This could be particularly problematic in reactions with low conversion, typically under 10%, but results were improved by increasing the number of replicants in a reaction and running biotransformations at lower concentrations. One advantage of analysis by percent conversions for cross-coupling reactions was the well characterized behavior of the native substrate **1** and dimer **2**, for which standard curves were built. However, this method could not be extended to reactions with different limiting reagents beyond the native substrate, unless no dimerization was observed.

Finally, the most rigorous analysis was by quantification of percent yield of products by product standard curves. Unlike the first two methods, without authentic standards, the selectivity of oxidative coupling reactions remains unknown which is

challenging if multiple products are formed. Comparison to authentic standards provides detailed information on the site-selectivity of products formed in a new reaction but is only feasible if standards are accessible. Comparison of each analysis method across the same reactions revealed that all could be reliable and provide good estimations of reactivity when applied in the right context.

2.12 Conclusions

Extensive optimization studies in *S. cerevisiae* and *P. pastoris* developed a new platform for oxidative coupling by heterologously expressed fungal P450 enzymes KtnC and DesC. Initial exploration of the substrate scopes of KtnC and DesC revealed the enzymes were promiscuous and could be employed for oxidative dimerizations of coumarins, in some cases with good site- and enantioselectivity. Site-selectivity trends were observed in the dimerization of coumarins with increasing steric bulk of vinylogous ester functional groups, leading to the discovery of novel selectivity in wild-type KtnC in the formation of 6,6'-isomers in non-natural substrates bearing large groups at the C4 position. New reactivity was discovered in wild-type KtnC for the oxidative cross-coupling of coumarins, a promising proof-of-concept outside the native functionality of the enzymes. Refinement of three analysis methods for analytical scale reactions provided tools to quantify and compare product formation in dimerization and cross-coupling reactions.

2.13. Experimental

Chemical synthesis

All reagents were used as received unless otherwise noted. Reactions were carried out under a nitrogen atmosphere using standard Schlenck techniques unless otherwise noted. Solvents were degassed and dried over aluminum columns on an MBraun solvent system (Innovative Technology, Inc., Model PS-00-3). Reactions were monitored by thin layer chromatography using Machery-Nagel 60 F_{254} precoated silica TLC plates (0.25 mm) or Merck Silica Gel 60 F_{254} precoated silica TLC plates (0.25 mm) which were visualized using UV, *p*-anisaldehyde, CAM, DNP, or bromocresol green stain. Flash column chromatography was performed using Machery-Nagel 60 μm (230-400 mesh) silica gel. All compounds purified by column chromatography were sufficiently pure for use in further experiments unless otherwise indicated. ^{1}H and ^{13}C NMR spectra were obtained in $CDCl_3$ at rt (25 ˚C), unless otherwise noted, on Varian 400 MHz or Varian 600 MHz spectrometers. Chemical shifts of ^{1}H NMR spectra were recorded in parts per million (ppm) on the δ scale. High resolution electrospray mass spectra were obtained on an Agilent UPLC-QTOF at the University of Michigan Life Sciences Institute or Agilent UPLC-TOF at the University of Michigan Life Sciences Institute. IR spectra were recorded on a Perkin-Elmer Spectrum BX FT-IR spectrometer. SFC spectra were obtained on a Waters SCF Investigator SFC system. Circular dichroism spectra were obtained on a JASCO J-1500 CD Spectrometer.

Synthesis of substrates

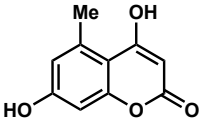

4,7-dihydroxy-5-methyl-*2H*-chromen-2-one (50):

To a mixture of 5-methylresorcinol (3.000 g, 24.16 mmol, 1.0 equiv), malonic acid (2.514 g, 24.16 mmol, 1.0 equiv) and $ZnCl_2$ flame-dried under vacuum (10.21 g, 74.91 mmol, 3.1 equiv) was added $POCl_3$ (60.0 mL). The reaction was heated at 60 °C and stirred for 14.5 h. The reaction was quenched by pouring into ice water and induced the precipitation of

a solid, which was isolated by vacuum filtration. The crude solid was purified by flash column chromatography (5:6:1 toluene/EtOAc/formic acid v/v) to afford a 3.38 g of the title compound (73% yield) as a yellow solid with minor impurities. R_f = 0.37 (8:3:1 toluene/EtOAc/formic acid v/v); **^{1}H NMR** (400 MHz, $(CD_3)_2SO$) δ 12.06 (s, 1H), 10.39 (s, 1H), 6.54 (s,1H), 6.50 (s, 1H), 5.33 (s, 1H), 2.57 (s, 3H);**^{13}C NMR** (150 MHz, $(CD_3)_2SO$) δ 169.1, 161.9, 160.4, 157.0, 138.7, 115.6, 106.4, 100.4, 88.0, 22.8; **HRMS** (ESI) *m/z* calculated for $C_{10}H_9O_4^+$ $[M+H]^+$ 193.0495, found 193.0505. All spectra obtained were constant with literature values.[76]

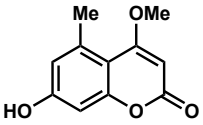

7-hydroxy-4-methoxy-5-methyl-*2H*-chromen-2-one (1):

To a solution of 4,7-dihydroxy-5-methyl-*2H*-chromen-2-one (**50**, 1.450 g, 7.546 mmol, 1.0 equiv) in MeOH (84.0 mL) was added H_2SO_4 (8.4 mL). The reaction was heated at 75 °C for 6.2 h. Incubation at 0 °C induced the precipitation of a white solid which was isolated by vacuum filtration to afford 1.070 g of the title compound (69% yield). R_f = 0.43 (8:3:1 toluene/EtOAc/formic acid v/v); **^{1}H NMR** (400 MHz, $(CD_3)_2SO$) δ 10.46 (s, 1H), 6.57 (d, *J* = 2.4, 1H), 6.54 (d, *J* = 2.4, 1H), 5.59 (s, 1H), 3.92 (s, 3H), 2.53 (s, 3H); **HRMS** (ESI) *m/z* calculated for $C_{11}H_{11}O_4^+$ $[M+H]^+$ 207.0652, found 207.0657. All spectra obtained were constant with literature values.[77]

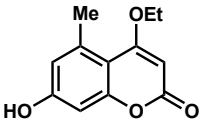

4-ethoxy-7-hydroxy-5-methyl-*2H*-chromen-2-one (25):

To a solution of 4,7-dihydroxy-5-methyl-*2H*-chromen-2-one (**50**, 510.0 mg, 2.650 mmol, 1.0 equiv) in EtOH (29.6 mL) was added H_2SO_4 (2.9 mL). The reaction was heated at 75 °C for 9.5 h. Incubation at 0 °C induced the precipitation of a pale yellow solid which was isolated by vacuum filtration to afford 237.6 mg of the title compound (41% yield). MP 276.5-278.2 °C; R_f = 0.58 (8:3:1 toluene/EtOAc/formic acid v/v); **^{1}H NMR** (600 MHz, $(CD_3)_2SO$) δ 10.40 (br s, 1H), 6.54 (d, *J* = 2.4, 1H), 6.51 (d, *J* = 2.4, 1H), 5.50 (s, 1H),

4.12 (q, *J* = 7.0, 2H), 2.51 (s, 3H), 1.40 (t, *J* = 7.0, 3H); **^{13}C NMR** (150 MHz, $(CD_3)_2SO$) δ 168.3, 161.8, 160.2, 156.1, 138.2, 116.0, 106.0, 100.5, 86.8, 65.2, 23.1, 13.9; **IR** (thin film, cm^{-1}) 3189, 1697, 1612, 1558, 1459, 1403; **HRMS** (ESI) *m/z* calculated for $C_{12}H_{13}O_4^+$ $[M+H]^+$ 221.0808, found 221.0813.

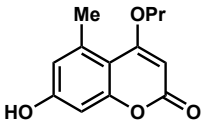

7-hydroxy-5-methyl-4-propoxy-*2H*-chromen-2-one (34):

To a solution of 4,7-dihydroxy-5-methyl-*2H*-chromen-2-one (**50**, 500.0 mg, 2.602 mmol, 1.0 equiv) in PrOH (29.0 mL) was added H_2SO_4 (2.9 mL). The reaction was heated at 75 °C for 8.6 h. The solution was partially concentrated under reduced pressure, diluted with H_2O, and extracted with EtOAc (3x). The organic layers were combined, washed with brine, dried over Na_2SO_4, filtered, and evaporated under reduced pressure to afford a solid. The crude solid was purified by flash column chromatography (8:3:1 toluene/EtOAc/formic acid v/v) and subjected to trituration (3x, 8:3:1 toluene/EtoAc/formic acid v/v) to afford 167.1 mg of the title compound (27% yield) as a tan solid. MP 198.2-199.5 °C; R_f = 0.50 (8:3:1 toluene/EtOAc/formic acid v/v); **^{1}H NMR** (600 MHz, $(CD_3)_2CO$) δ 9.26 (s, 1H), 6.63 (dd, *J* = 2.6, 1.0, 1H), 6.57 (d, *J* = 2.5, 1H), 5.48 (s, 1H), 4.14 (t, *J* = 6.3, 2H), 2.63 (s, 3H), 1.98-1.87 (m, 2H), 1.10 (t, *J* = 7.4, 3H); **^{13}C NMR** (150 MHz, $(CD_3)_2CO$) δ 169.7, 162.6, 161.1, 157.8, 139.7, 116.8, 108.0, 101.7, 88.2, 72.1, 23.9, 22.8, 11.1; **IR** (thin film, cm^{-1}) 3148, 3090, 2974, 2935, 1709, 1697, 1689, 1625, 1451; **HRMS** (ESI) *m/z* calculated for $C_{13}H_{15}O_4^+$ $[M+H]^+$ 235.0965, found 235.0960.

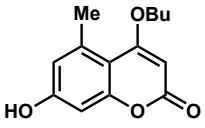

4-butoxy-7-hydroxy-5-methyl-*2H*-chromen-2-one (26):

To a solution of 4,7-dihydroxy-5-methyl-*2H*-chromen-2-one (**50**, 400.0 mg, 2.081 mmol, 1.0 equiv) in BuOH (23.3 mL) was added H_2SO_4 (2.3 mL). The reaction was heated at 75 °C for 5.1 h. The solution was partially concentrated under reduced pressure, diluted with H_2O, and extracted with EtOAc (3x). The organic layers were combined, washed with

brine, dried over Na_2SO_4, filtered, and evaporated under reduced pressure to afford a solid. The crude solid was purified by flash column chromatography (9:2:1 to 8:3:1 toluene/EtOAc/formic acid v/v) and subjected to trituration (3x, 8:3:1 toluene/EtOAc/formic acid v/v) to afford 105.2 mg of the title compound (21% yield) as a white solid. MP 196.7-197.8 °C; R_f = 0.54 (8:3:1 toluene/EtOAc/formic acid v/v); **^{1}H NMR** (600 MHz, CD_3OD) δ 6.58 (d, *J* = 2.2, 1H), 6.54 (d, *J* = 2.2, 1H), 5.55 (s, 1H), 4.15 (t, *J* = 6.3, 2H), 2.61 (s, 3H), 1.92-1.84 (m, 2H), 1.57 (q, *J* = 7.5, 2H), 1.02 (t, *J* = 7.4); **^{13}C NMR** (150 MHz, CD_3OD) δ 171.5, 166.1, 162.2, 158.0. 140.2, 117.5, 108.0, 101.7, 87.5, 70.9, 31.8, 23.9, 20.5, 14.1; **IR** (thin film, cm^{-1}) 3279, 3122, 2957, 2872, 1675, 1610, 1555, 1448, 1409; **HRMS** (ESI) *m/z* calculated for $C_{14}H_{17}O_4^+$ $[M+H]^+$ 249.1121, found 249.1124.

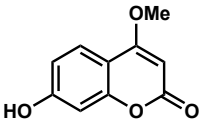

7-hydroxy-4-methoxy-*2H*-chromen-2-one (27):

To a solution of 4,7-dihydroxycoumarin (250.0 mg, 1.403 mmol, 1.0 equiv) in MeOH (15.6 mL) was added H_2SO_4 (1.6 mL). The reaction was heated at 75 °C for 2.8 h. Incubation at 0 °C induced the precipitation of a white solid which was isolated by vacuum filtration to afford 226.2 mg of the title compound (84% yield). **^{1}H NMR** (600 MHz, $(CD_3)_2SO$) δ 7.61 (d, *J* =8.7, 1H), 6.78 (dd, *J* = 8.7, 2.3, 1H), 6.69 (d, *J* = 2.3, 1H), 5.67 (s, 1H), 3.96 (s, 3H); **HRMS** (ESI) *m/z* calculated for $C_{10}H_9O_4^+$ $[M+H]^+$ 193.0495, found 193.0503. All spectra obtained were constant with literature values.[78]

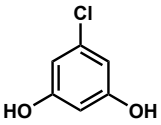

5-chlororesorcinol (51):

To a solution of 1-chloro-3,5-dimethoxybenzene (1.00 g, 5.79 mmol, 1 equiv) dissolved in DCM (6.0 mL) was added a 1M solution of BBr_3 in DCM (12.2 mL, 12.1 mmol, 2.1 equiv) at -78 °C. The reaction was allowed to warm to rt and stirred for 14 h. The reaction was quenched with the addition of water (4.0 mL). The aqueous phase was extracted with EtOAc (3x). The organic layers were combined, washed with brine, dried over Na_2SO_4,

filtered, and evaporated under reduced pressure to afford an oil. The crude residue was purified by flash column chromatography (4:1 hexanes/EtOAc v/v) to afford 661 mg of the title compound (79% yield) as a pink solid. **^{1}H NMR** (400 MHz, $(CD_3)_2CO$) δ 8.63 (s, 2H), 6.37 (d, *J* = 2.1, 2H), 6.30 (t, *J* = 2.1, 1H). All spectra obtained were constant with literature values.[79]

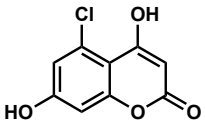

5-chloro-4,7-dihydroxy-*2H*-chromen-2-one (52)

To a mixture of 5-chlororesorcinol (**S4**, 300.0 mg, 2.075 mmol, 1equiv), malonic acid (215.9 mg, 2.075 mmol, 1 equiv) and $ZnCl_2$ flame-dried under vacuum (876.7 mg, 6.432 mmol, 3.1 equiv) was added $POCl_3$ (5.2 mL). The reaction was heated at 60 °C and stirred for 14.5 h. The reaction was quenched by pouring into ice water and induced the precipitation of a solid, which was isolated by vacuum filtration. The crude solid was purified by flash column chromatography (8:3:1 toluene/EtOAc/formic acid v/v) to afford a 108.3 mg of the title compound (24% yield) as a tan solid with minor impurities. MP 250.1-252.9 °C; R_f = 0.45 (8:3:1 toluene/EtOAc/formic acid v/v); **^{1}H NMR** (600 MHz, $(CD_3)_2CO$) δ 6.88 (d, *J* = 2.4, 1H), 6.70 (d, *J* = 2.4, 1H), 5.51 (s, 1H);**^{13}C NMR** (150 MHz, $(CD_3)_2CO$) δ 166.9, 161.6, 161.2, 158.5, 132.8, 116.5, 107.0, 103.2, 91.0; **IR** (thin film, cm^{-1}) 3254, 3080, 2940, 1617, 1547, 1436; **HRMS** (ESI) *m/z* calculated for $C_9H_6ClO_4^+$ $[M+H]^+$ 212.9949, found 212.9953.

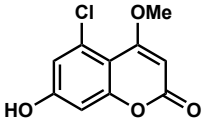

5-chloro-7-hydroxy-4-methoxy-*2H*-chromen-2-one (24):

To a solution of 5-chloro-4,7-dihydroxy-*2H*-chromen-2-one (**52**, 88.0 mg, 0.414 mmol, 1.0 equiv) in MeOH (4.6 mL) was added H_2SO_4 (0.46 mL). The reaction was heated at 75 °C for 3.7 h. Incubation at 0 °C induced the precipitation of a white solid which was isolated by vacuum filtration to afford 56.9 mg of the title compound (61% yield). MP >310 °C; R_f = 0.49 (8:3:1 toluene/EtOAc/formic acid v/v); **^{1}H NMR** (600 MHz, $(CD_3)_2SO$) δ 10.98 (br

s, 1H), 6.82 (d, *J* = 2.3, 1H), 6.68 (d, *J* = 2.3, 1H), 5.71 (s, 1H), 3.93 (s, 3H); **^{13}C NMR** (150 MHz, $(CD_3)_2SO$) δ 166.8, 160.9, 160.5, 156.2, 130.6, 115.9, 105.1, 102.2, 88.0, 56.8; **IR** (thin film, cm^{-1}) 3139, 2728, 2161, 2033, 1698, 1613, 1593,1522, 1449, 1433; **HRMS** (ESI) *m/z* calculated for $C_{10}H_8ClO_4^+$ $[M+H]^+$ 227.0106, found 227.0112.

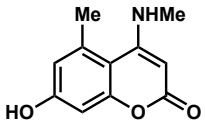

7-hydroxy-5-methyl-4-(methylamino)-*2H*-chromen-2-one (22):

To a solution of 4,7-dihydroxy-5-methyl-*2H*-chromen-2-one (**50)**, 423.0 mg, 2.213 mmol, 1.0 equiv) in MeCN (8.8 mL) was added benzyltriethylammonium chloride (2.010 g, 8.854 mmol, 4.0 equiv). The solution was heated at 40 °C for 10 min then $POCl_3$ (910.0 µL, 9.739 mmol, 4.4 equiv) was added. The reaction was heated at 90 °C for 1.0 h. The reaction was quenched by pouring into ice water and extracted with EtOAc (3x). The organic layers were combined, washed with brine, dried over Na_2SO_4, filtered, and evaporated under reduced pressure to afford an oil, which was carried forward without further purification and dissolved in EtOH (12.7 mL) in a pressure vessel. To the crude solution was added TEA (4.2 mL) and methylamine hydrochloride (1.490 g, 22.13 mmol, 10 equiv). The reaction was heated at 80 °C for 14.5 h. The reaction was quenched by pouring into 1M HCl and extracted with EtOAc (3x). The organic layers were combined, washed with brine, dried over Na_2SO_4, filtered, and evaporated under reduced pressure to afford 88.7 mg of the title compound (20% yield) as an orange solid. MP 279.3-283.6 °C; R_f = 0.17 (8:3:1 toluene/EtOAc/formic acid v/v); **^{1}H NMR** (600 MHz, (CD_3OD) δ 8.46 (s, 1H), 6.59 (d, *J* = 2.5, 1H), 6.54 (d, *J* = 2.6, 1H), 5.08 (s, 1H), 2.95 (s, 3H), 2.71 (s, 3H); **^{13}C NMR** (150 MHz, CD_3OD) δ 166.6, 161.5, 160.2, 157.9, 137.9, 117.8, 107.5, 102.5, 80.5, 30.5, 23.4; **HRMS** (ESI) *m/z* calculated for $C_{11}H_{12}NO_3^+$ $[M+H]^+$ 206.0812, found 206.0820.

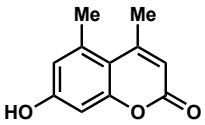

7-hydroxy-4,5-dimethyl-*2H*-chromen-2-one (23):

7-hydroxy-4,5-dimethyl-*2H*-chromen-2-one (**23**) was prepared from 5-methylbenzene-1,3-diol according to the procedure described by Zav'yalov et al.[80] **^{1}H NMR** (600 MHz, $(CD_3)_2SO$) δ 10.53 (s, 1H), 6.62 (s, 1H), 6.57 (s, 1H), 6.05 (s, 1H), 2.54 (s, 3H), 2.27 (s, 3H); **HRMS** (ESI) *m/z* calculated for $C_{11}H_{11}O_3^+$ $[M+H]^+$ 191.0703, found 191.0707. All spectra obtained were constant with literature values.[81]

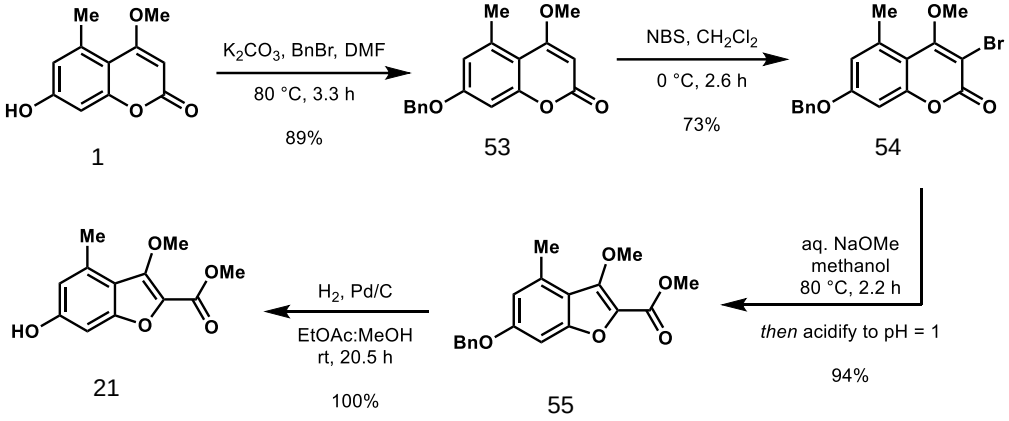

Figure S2.1. Synthesis of benzofuran **21**.

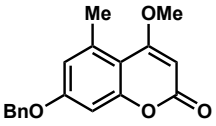

7-(benzyloxy)-4-methoxy-5-methyl-*2H*-chromen-2-one (53)

To a solution of 7-hydroxy-4-methoxy-5-methyl-*2H*-chromen-2-one (**1**, 1.07 g, 5.19 mmol, 1.00 equiv) in DMF (52.0 mL) was added K_2CO_3 (1.07 g, 7.78 mmol, 1.50 equiv) and BnBr (740 µL, 6.23 mmol, 1.20 equiv). The reaction was heated at 80 °C and stirred for 3.3 h. The reaction was quenched with MeOH (1 mL). Water was added and the aqueous phase was extracted with EtOAc (3 x). The organic layers were combined, washed with brine, dried over Na_2SO_4, filtered, and evaporated under reduced pressure afford 1.37 g of the title compound (89% yield) as a white solid. **MP** 137.5-138.7 °C; **R_f** = 0.17 (2:1 hexanes/EtOAc v/v); **^{1}H NMR** (600 MHz, $CDCl_3$) δ 7.41-7.34 (m, 4H), 7.33-7.29 (m, 1H), 6.65 (d, *J* = 2.6, 1H), 6.63 (d, *J* = 2.5, 1H), 5.47 (s, 1H), 5.03 (s, 2H), 3.86 (s, 3H), 2.55 (s, 3H); **^{13}C NMR** (150 MHz, $CDCl_3$) δ 169.6, 163.0, 160.9, 156.5, 138.5, 135.9, 128.7, 128.2, 127.5, 116.1, 108.0, 99.6, 87.5, 70.1, 55.9, 23.4; **IR** (thin film, cm^{-1}) 3089, 3063, 3032, 2975, 2935, 1711, 1601, 1555, 1497, 1455, 1423; **HRMS** (ESI) *m/z* calculated for $C_{18}H_{17}O_4^+$ $[M+H]^+$ 297.1121, found 297.1122.

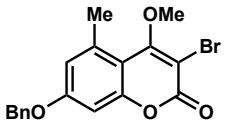

7-(benzyloxy)-3-bromo-4-methoxy-5-methyl-*2H*-chromen-2-one (54)

To a solution of 7-(benzyloxy)-4-methoxy-5-methyl-*2H*-chromen-2-one (**53**, 600 mg, 2.02 mmol, 1.00 equiv) in DCM (25.0 mL) was added recrystallized N-bromosuccinimide (378.0, 2.126 mmol, 1.05 equiv) at 0 °C. The reaction was stirred for 2.6 h. The reaction was quenched with saturated $Na_2S_2O_3$ (5 mL). The aqueous phase was extracted with DCM (3 x). The organic layers were combined, washed with brine, dried over Na_2SO_4, filtered, and evaporated under reduced pressure afford 555 mg of the title compound (73% yield) as a white solid. **MP** 118.3-121.5 °C; **R_f** = 0.53 (2:1 hexanes/EtOAc v/v); **^{1}H NMR** (600 MHz, $CDCl_3$) δ 7.42-7.33 (m, 5H), 6.76 (d, 2H), 5.11 (s, 2H), 4.09 (s, 3H), 2.65 (s, 3H); **^{13}C NMR** (150 MHz, $CDCl_3$) δ 168.5, 161.4, 159.6, 155.4, 137.9, 135.7, 128.9, 128.5, 127.6, 117.2, 110.2, 99.9, 97.4, 70.5, 61.0, 22.6; ; **IR** (thin film, cm^{-1}) 3089, 3063, 3032, 2972, 2939, 1715, 1612, 1588, 1538, 1497, 1453; **HRMS** (ESI) *m/z* calculated for $C_{18}H_{16}BrO_4^+$ $[M+H]^+$ 375.0226, found 375.0218.

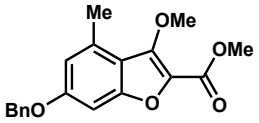

Methyl 6-(benzyloxy)-3-methoxy-4-methylbenzofuran-2-carboxylate (55):

To a suspension of 7-(benzyloxy)-3-bromo-4-methoxy-5-methyl-*2H*-chromen-2-one (**54**, 418 mg, 1.11 mmol, 1.00 equiv) in MeOH (44.6 mL) was added freshly prepared 1M solution of NaOMe in MeOH (11.1 mL, 11.1 mmol, 10.0 equiv). The reaction was heated at 80 °C and stirred for 2.2 h. The reaction was poured into 122 mL of 0.1 M HCl. The acidifed aqueous phase was extracted with EtOAc (3 x). The organic layers were combined, washed with brine, dried over Na_2SO_4, filtered, and evaporated under reduced pressure to afford 342 mg of the title compound (94% yield) as an off-white solid. **MP** 57.9-58.8 °C; **R_f** = 0.62 (2:1 hexanes/EtOAc v/v); **^{1}H NMR** (400 MHz, $CDCl_3$) δ 7.45-7.30 (m, 5H), 6.81 (d, *J* = 2.1, 1H), 6.74 (d, *J* = 2.1, 1H), 5.08 (s, 2H), 4.12 (s, 3H), 3.96 (s, 3H), 2.59 (s, 3H); **^{13}C NMR** (100 MHz, $CDCl_3$) δ 160.3, 159.6, 154.8, 152.4, 136.5, 134.5,

131.2, 128.8, 128.2, 127.5, 115.3, 94.4, 70.4, 63.1, 52.0, 18.2; **IR** (thin film, cm^{-1}) 3033, 2950, 2851, 1708, 1621, 1598, 1573, 1498, 1446; **HRMS** (ESI) *m/z* calculated for $C_{19}H_9O_5^+$ $[M+H]^+$ 327.1227, found 327.1231.

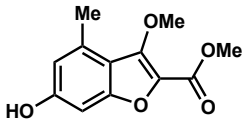

Methyl 6-hydroxy-3-methoxy-4-methylbenzofuran-2-carboxylate (21):

A solution of methyl 6-(benzyloxy)-3-methoxy-4-methylbenzofuran-2-carboxylate (**55**, 502 mg, 0.923 mmol, 1.00 equiv) in MeOH (30.0 mL) was sparged with N_2 for 15 min then 10% Pd/C (30 mg, 10% w/w) as a slurry in EtOAc (1.0 mL). The reaction was sparged with N_2 for 10 min then sparged with H_2 for 10 min and stirred for 20.5 h under H_2 balloon atmosphere. The reaction was filtered through a plug of celite, rinsed with EtOAc, and the organic solution evaporated under reduced pressure. The crude solid was purified through a silica plug with flash chromatography (EtOAc) to afford 220 mg of the title compound (quantitative yield) as a light pink solid. **MP** 137.6-140.2 °C; $\mathbf{R_f}$ = 0.45 (2:1 hexanes/EtOAc v/v); **^{1}H NMR** (600 MHz, CD_3OD) δ 6.58 (d, *J* = 1.0, 1H), 6.54 (d, *J* = 1.0, 1H), 4.04 (s, 3H), 3.89 (s, 3H), 2.51 (s, 3H); **^{13}C NMR** (150 MHz, CD_3OD) δ 161.2, 160.6, 156.5, 153.6, 135.4, 131.8, 115.7, 115.1, 96.0, 63.5, 52.1, 18.1; **IR** (thin film, cm^{-1}) 3365, 2952, 2852, 1682, 1619, 1600, 1575, 1448; **HRMS** (ESI) *m/z* calculated for $C_{12}H_{13}O_5^+$ $[M+H]^+$ 237.0757, found 237.0762.

Figure S2.2. Condition screen for oxidative dimerization (Figure 2.8).

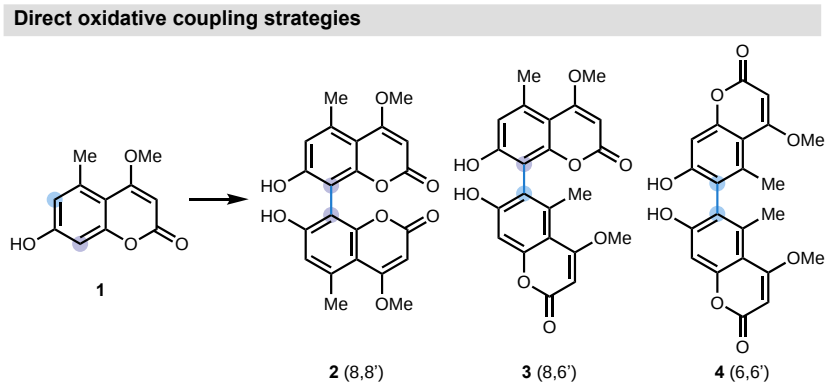

Entry	Conditions	8,8'	8,6'	6,6'
1	$Pb(OAc)_4$ (0.55 equiv), BF_3OEt_2, MeCN, rt	–	–	–
2	PIFA (1.1 equiv), BF_3OEt_2, DCM, 0 °C	–	–	–
3	$VOCl_3$ (2.0 equiv), TFA, DCM, 0 °C	–	–	–
4	VOF_3 (2.2 equiv), TFA, TFAA, 0 °C	–	–	–
5	VOF_3 (2.0 equiv), TFA, DCM, 0 °C to rt, 14 h	18%	13%	<1%
6	Cu(OH)Cl TMEDA (1.0 equiv), HFIP, air, rt, 24 h	13%	–	–
7	P450 KtnC, O_2, BMM, 235 rpm, 30 °C, 48 h	95%	0%	0%
8	P450 DesC, O_2, BMM, 235 rpm, 30 °C, 48 h	<1%	35%	0%

VOF_3 general procedure (entries 3–5): To a solution of 7-hydroxy-4methoxy-5-methyl-*2H*-chromen-2-one (**1**, 10.3 mg, 0.050 mmol, 1.0 equiv) in DCM (0.4 mL) and TFA (0.1 mL) was added VOF_3 (equivalents specified in entries 12–17) at 0 °C. The reaction was stirred for the specified duration of time. The reaction was quenched with H_2O (2 mL). The aqueous phase was extracted with EtOAc (3x). The organic layers were combined, washed with brine, dried over Na_2SO_4, filtered, and evaporated under reduced pressure. Yields were determined using 1,3,5-trimethoxybenzene as an internal standard in $(CD_3)SO$.

Entry 5: The reaction was performed using 2.0 equiv of VOF_3 (12.4 mg, 0.100 mmol) and stirred for 14 h. Based on 0.0107 mmol IS, the reaction afforded 18% **3** (0.00449 mmol), 13% **3** (0.00321 mmol), and 1% **4** (0.00032 mmol) with 14% of starting material **1** recovered (0.00706 mmol), as shown in S2.67.

Entry 6: To a solution of 7-hydroxy-4-methoxy-5-methyl-*2H*-chromen-2-one (**1**, 100 mg, 0.4831 mmol, 1.0 equiv) in HFIP (4.8 mL, 0.1 M) was added Cu(OH)Cl*TMEDA (116 mg, 0.4831 mmol, 1.0 equiv) at room temperature and stirred for 24. Upon addition of copper

complex, reaction mixture turned a deep navy blue. The reaction was quenched with 1M HCl, changing in color from navy to green to light yellow. The reaction was diluted with deionized H_2O (10 mL), extracted with EtOAc (15 mL x 3) and 70% *i*PrOH was added to aid in separating emulsion (2 mL x 2). Combined organic extracts were washed with brine, dried over Na_2SO_4, then concentrated to a pale yellow solid, 121 mg of crude material. Yield was calculated using 20 mg of crude reaction mixture in 1 mL of D_6-DMSO as 13% (0.0317 mmol) by ^1H NMR using 0.0200 mmol 1,2,3,5-tetramethoxybenzene as an internal standard, see S2.68. (400 MHz, $(CD_3)_2SO$) δ 10.37 (s, 2H), 6.79 (s, 2H), 5.55 (s, 2H), 3.92 (s, 6H), 2.57 (s, 6H); **HRMS** (ESI) *m/z* calculated for $C_{22}H_{19}O_8^+$ $[M+H]^+$ 411.1074, found 411.1082.

Determination of site-selectivity on analytical scale: The sample of crude reaction mixture (**entry 5**) was prepared by diluting 50 µL of the reaction mixture with 1.0 mL of methanol. The reaction was compared to authentic standards. The samples were subjected to liquid chromatography PDA spectrometry (UPLC) analysis performed on an Agilent 6230 time of flight mass spectrometer with a Dual AJS ESI source and an Agilent 1290 Infinity Series II diode array detector, autosampler, and binary pump, using a Waters Acquity UPLC HSS T3 1.8 µm C18, 2.1x50 mm column under the following conditions: Positive mode, phase A = 95:5 deionized water:acetonitrile with 0.1% formic acid, B = 95:5 acetonitrile:deionized water with 0.1% formic acid; method = 80% A held for 0.5min, to 45% A over 2.75 min, 10% A 100% A for 1.0 min, 254, 275, and 308 nm UV detection and 0.7 mL/min flow rate. Each injection was followed by equilibration at 80% A for 1 min.

Figure S2.3. Chemical dimerization site-selectivity assignment

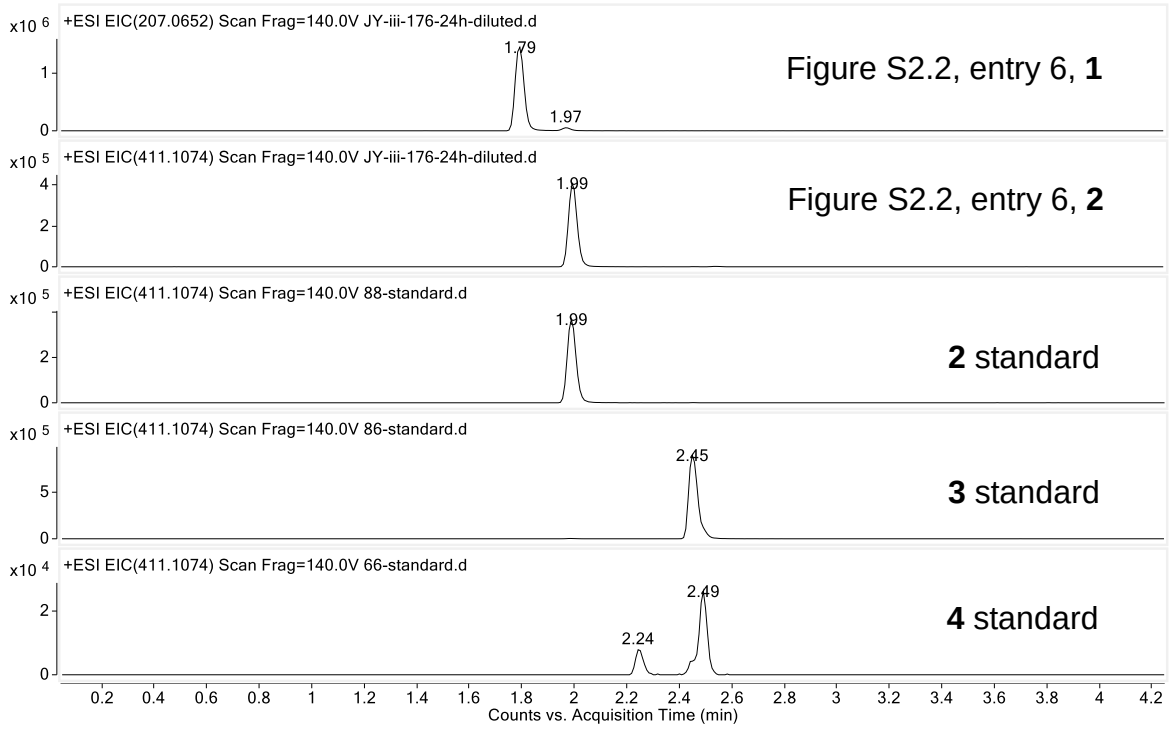

Synthesis of racemic dimer product standards

Note: Some scaffolds could be accessed in greater amounts via the biotransformations, and the full characterization can be found in that section.

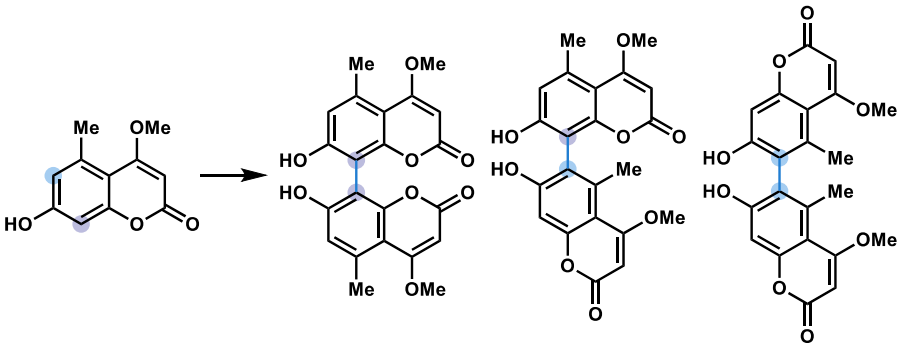

Figure S2.4.

Racemic chemical dimerization of 7-hydroxy-4-methoxy-5-methyl-*2H*-chromen-2-one (1): To a solution of 7-hydroxy-5-methyl-4-propoxy-*2H*-chromen-2-one (**1**, 51.5 mg, 0.250 mmol, 1.0 equiv) in DCM (1.0 mL) and TFA (0.25 mL) was added VOF_3 (123.95 mg, 0.375 mmol, 1.5 equiv) at 0 °C. The reaction was stirred for 4.0 h. The reaction was quenched with H_2O (2 mL). The aqueous phase was extracted with EtOAc (3x). The organic layers were combined, washed with brine, dried over Na_2SO_4, filtered, and evaporated under reduced pressure. The crude solid was purified by flash column chromatography (8:3:1 toluene/EtOAc/formic acid v/v) then reversed-phase HPLC (Phenomenex Kinetex 5 µm C18, 150 x 21.2 mm column) under the following conditions: mobile phase A = deionized water + 0.1% formic acid and B = acetonitrile + 0.1% formic acid; method = 75% A for 5.0 min, 75% A to 70% A over 2.0 min, 70% A for 7.0 min, 70% A to 65% A over 2.0 min, 65% A for 5.0 min, 65% A to 50% A over 3.0 min, 50% A for 1.0 min, 254 and 308 nm UV detection and 14 mL/min flow rate. A retention time of 12.65-14.77 min afforded 7.0 mg of 8,8' product **2** (14% yield), and a retention time of 18.44-20.07 min afforded 6.6 mg of 6,8' product **3** (13% yield).

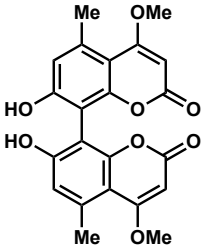

7,7'-dihydroxy-4,4'-dimethoxy-5,5'dimethyl-*2H*,*2H'*-[8,8'-bichromene]-2,2'-dione (2): **^{1}H NMR** (400 MHz, $(CD_3)_2SO$) δ 6.69 (s, 2H), 5.55 (s, 2H), 3.94 (s, 6H), 2.59 (s, 6H); **HRMS** (ESI) *m/z* calculated for $C_{22}H_{19}O_8^+$ $[M+H]^+$ 411.1074, found 411.1070. All spectra obtained were agreement with literature values.[82]

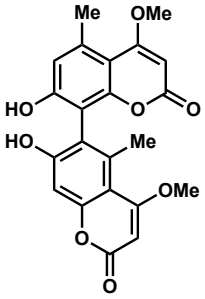

7,7'-dihydroxy-4,4'-dimethoxy-5,5'dimethyl-*2H*,*2H'*-[6,8'-bichromene]-2,2'-dione (3): **^{1}H NMR** (400 MHz, $(CD_3)_2SO$) δ 6.70 (s, 1H), 6.68 (s, 1H), 5.63 (s, 1H), 5.57 (s, 1H), 3.93 (s, 6H), 2.58 (s, 3H), 2.23 (s, 3H); **HRMS** (ESI) *m/z* calculated for $C_{22}H_{19}O_8^+$ $[M+H]^+$ 411.1074, found 411.1088. All spectra obtained were in agreement with literature values.[83-84]

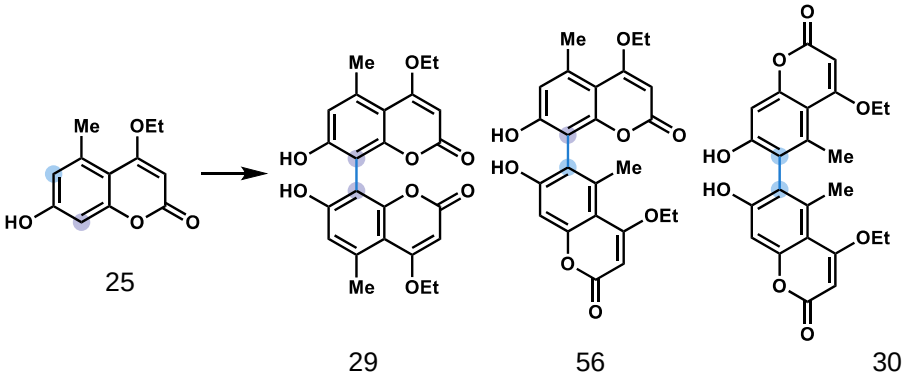

Figure S2.5.

Racemic chemical dimerization of 4-ethoxy-7-hydroxy-5-methyl-*2H*-chromen-2-one (25): To a solution of 4-ethoxy-7-hydroxy-5-methyl-*2H*-chromen-2-one (**17**, 85.1 mg,

0.3864 mmol, 1.0 equiv) in DCM (1.5 mL) and TFA (0.4 mL) was added VOF_3 (95.8 mg, 0.7728 mmol, 2.0 equiv) at 0 °C. The reaction was stirred for 3.2 h. The reaction was quenched with H_2O (2 mL). The aqueous phase was extracted with EtOAc (3x). The organic layers were combined, washed with brine, dried over Na_2SO_4, filtered, and evaporated under reduced pressure. The crude solid was purified by flash column chromatography (8:3:1 toluene/EtOAc/formic acid v/v) then reversed-phase HPLC (Phenomenex Kinetex 5 µm C18, 150 x 21.2 mm column) under the following conditions: mobile phase A = deionized water + 0.1% formic acid and B = acetonitrile + 0.1% formic acid; method = 67.5% A for 45 min, 254 and 308 nm UV detection and 14 mL/min flow rate. A retention time of 17.50-21.42 min afforded 2.1 mg of 8,8' product **29** (2% yield), and a retention time of 33.31-40.72 min afforded 4.2 mg of 6,8' product **56** (5% yield).

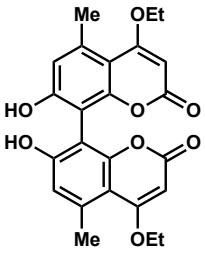

4,4'-diethoxy-7,7'-dihydroxy-5,5'dimethyl-*2H*,*2H'*-[8,8'-bichromene]-2,2'-dione (29): **^{1}H NMR** (400 MHz, $(CD_3)_2CO$) δ 6.76 (s, 2H), 5.44 (s, 2H), 4.25 (q, *J* = 7.0, 4H), 2.67 (s, 6H), 1.54 (t, *J* = 7.0, 6H); **HRMS** (ESI) *m/z* calculated for $C_{24}H_{23}O_8^+$ $[M+H]^+$ 439.1387, found 439.1394.

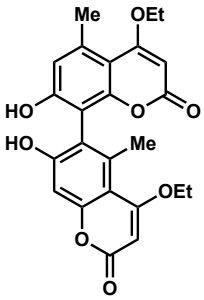

4,4'-diethoxy-7,7'-dihydroxy-5,5'dimethyl-*2H*,*2H'*-[6,8'-bichromene]-2,2'-dione (56): MP >310 °C; (8:3:1 toluene/EtOAc/formic acid v/v); **^{1}H NMR** (600 MHz, $(CD_3)_2CO$) δ 6.75 (s, 1H), 6.72 (s, 1H), 5.52 (s, 1H), 5.41 (s, 1H), 4.25 (dq, *J* = 14.1, 7.0, 4H), 2.66 (s, 3H), 2.36 (s, 3H), 1.53 (t, *J* = 6.8, 3H), 1.50 (t, *J*= 7.0, 3H); **^{13}C NMR** (150 MHz, $(CD_3)_2SO$) δ

168.9, 162.0, 162.0, 155.5, 153.9, 137.3, 136.4, 120.0, 116.5, 110.0, 105.4, 105.2, 100.7, 86.6, 86.1, 65.3, 65.2, 23.4, 19.4, 14.0, 14.0; **IR** (thin film, cm^{-1}) 3204, 2925, 1686, 1591, 1448; **HRMS** (ESI) *m/z* calculated for $C_{24}H_{23}O_8^+$ $[M+H]^+$ 439.1387, found 439.1391.

Racemic chemical dimerization of 4-ethoxy-7-hydroxy-5-methyl-*2H*-chromen-2-one (25): To a solution of 4-ethoxy-7-hydroxy-5-methyl-2H-chromen-2-one (**17**, 55 mg, 0.25 mmol, 1.0 equiv) in DCM (1.0 mL) and TFA (250 µL) was added VOF_3 (31 mg, 0.25 mmol, 1.0 equiv) at 0 °C. The reaction was stirred for 2.5 h. The reaction was quenched with H_2O (2 mL). The aqueous phase was extracted with EtOAc (3x). The organic layers were combined, washed with brine, dried over Na2SO4, filtered, and evaporated under reduced pressure. The crude solid was purified by flash column chromatography (8:3:1 toluene/EtOAc/formic acid v/v) then reversed-phase HPLC (Phenomenex Kinetex 5 µm C18, 150 x 10.0 mm column) under the following conditions: mobile phase A = deionized water + 0.1% formic acid and B = acetonitrile + 0.1% formic acid; method = 95% A for 5 min, 95% A to 70% A over 6 min, 70% A to 40% A over 12 min, 40% A to 5% A over 5 min, 5% A for 3 min, 5% A to 95% A over 5 min, 95% A over 2 min, 254 and 214 nm UV detection and 5 mL/min flow rate. The 6,8'-product **56** and 6,6'-product **30** co-eluted (1:1 ratio, 1H NMR) from 15.8-16.5 min to provide 1.2 mg (2% yield).

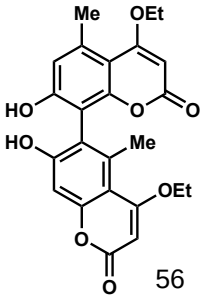

56

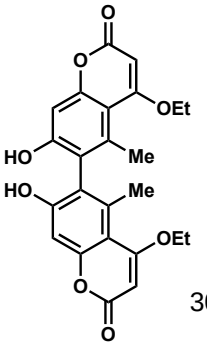

30

4,4'-diethoxy-7,7'-dihydroxy-5,5'dimethyl-*2H*,*2H'*-[6,8'-bichromene]-2,2'-dione (56) and 4,4'-diethoxy-7,7'-dihydroxy-5,5'dimethyl-*2H*,*2H'*-[6,6'-bichromene]-2,2'-dione (30) 1:1 mixture: **^{1}H NMR** (600 MHz, $(CD_3)_2CO$) δ 6.81 (s, 1H), 6.76 (s, 2H), 6.73 (s, 1H), 5.52 (s, 2H), 5.51 (s, 1H), 5.46 (s, 1H), 4.28-4.23 (m, 8H), 2.69 (s, 3H), 2.40 (s, 3H), 2.36 (s, 6H), 1.54 (t, *J* = 6.9, 3H), 1.50 (t, *J* = 6.9, 6H), 1.50 (t, *J* = 6.9, 3H). **HRMS** (ESI) *m/z* calculated for $C_{24}H_{23}O_8^+$ $[M+H]^+$ 439.1387, (6,6' product) found 439.1390.

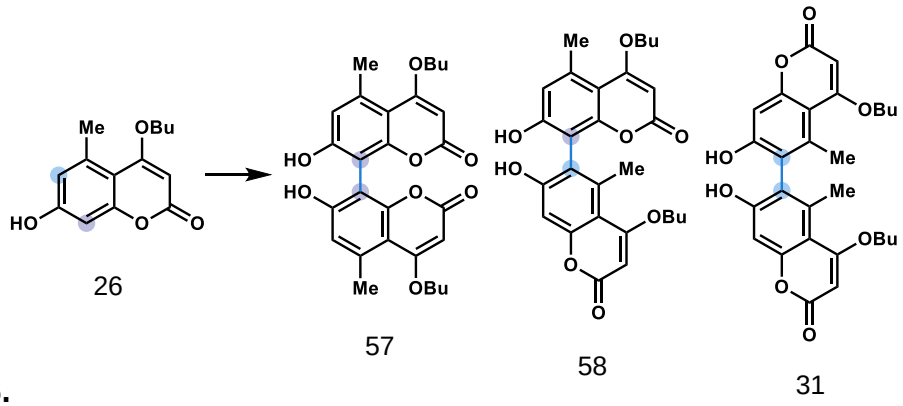

Figure S2.6.

Racemic chemical dimerization of 4-butoxy-7-hydroxy-5-methyl-*2H*-chromen-2-one (26): To a solution of 4-butoxy-7-hydroxy-5-methyl-*2H*-chromen-2-one (**26**, 117.3 mg, 0.470 mmol, 1.0 equiv) in DCM (2.0 mL) and TFA (0.5 mL) was added VOF_3 (92.9 mg, 0.750 mmol, 1.5 equiv) at 0 °C. The reaction was stirred for 3.0 h. The reaction was quenched with H_2O (2 mL). The aqueous phase was extracted with EtOAc (3x). The organic layers were combined, washed with brine, dried over Na_2SO_4, filtered, and evaporated under reduced pressure. The crude solid was purified by flash column chromatography (8:3:1 toluene/EtOAc/formic acid v/v) then reversed-phase HPLC (Phenomenex Kinetex 5 µm C18, 150 x 21.2 mm column) under the following conditions: mobile phase A = deionized water + 0.1% formic acid and B = acetonitrile + 0.1% formic acid; method = 55% A for 5 min, 55% A to 50% A over 1.5 min, 50% A for 5 min, 50% A to 45% A over 1.5 min, 45% A for 5 min, 45% A to 40% A over 1.5 min, 40% A for 3.5 min, 40% A to 30% A over 3 min, 30% A for 4 min, 254 and 308 nm UV detection and 14 mL/min flow rate. A retention time of 14.32-16.66 min afforded 4.7 mg of 8,8' product **57** (4% yield). A mixture of 6,8' product **58** and 6,6' product **31** co-eluted (in approximately a 3:1 ratio, ^{1}H NMR) with a retention time of 20.24-23.18 min to afford 10.4 mg as an off-white solid. This mixture was rinsed with MeOH (3x) to afford 6.8 mg of 6,8' product **58** (6% yield) as an off-white solid.

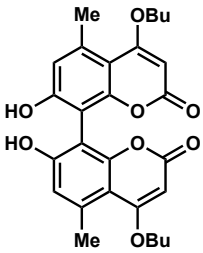

4,4'-dibutoxy-7,7'-dihydroxy-5,5'dimethyl-*2H*,*2H'*-[8,8'-bichromene]-2,2'-dione (57): MP decomposition at 302.6 °C; R_f = 0.43 (8:3:1 toluene/EtOAc/formic acid v/v); **^{1}H NMR** (600 MHz, $(CD_3)_2CO$) δ 6.77 (s, 2H), 5.47 (s, 2H), 4.20 (t, *J* = 6.3, 4H), 2.68 (s, 6H), 1.96-1.87 (m, 4H), 1.59 (h, *J* = 7.5, 4H), 1.02 (t, *J* = 7.4, 6H); **^{1}H NMR** (600 MHz, $(CD_3)_2SO$) δ 10.35 (s, 2H), 6.70 (s, 2H), 5.55 (s, 2H), 4.14 (t, *J* = 6.3, 4H), 2.61 (s, 6H), 1.81 (p, *J* = 6.7, 4H), 1.49 (h, *J* = 7.4, 4H), 0.96 (t, *J* = 7.4, 6H); **^{13}C NMR** (150 MHz, $(CD_3)_2SO$) δ 168.9, 161.8, 158.8, 154.0, 136.9, 115.8, 106.1, 105.9, 86.7, 69.3, 30.1, 23.4, 18.9, 13.6; **IR** (thin film, cm^{-1}) 3177, 2728, 2161, 2012, 1675, 1559, **HRMS** (ESI) *m/z* calculated for $C_{28}H_{31}O_8^+$ $[M+H]^+$ 495.2013, found 495.2020.

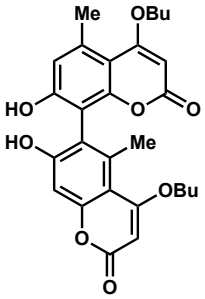

4,4'-dibutoxy-7,7'-dihydroxy-5,5'dimethyl-*2H*,*2H'*-[6,8'-bichromene]-2,2'-dione (58): MP 293.2-294.6 °C; R_f = 0.34 (8:3:1 toluene/EtOAc/formic acid v/v); **^{1}H NMR** (400 MHz, $(CD_3)_2CO$) δ 6.80 (s, 1H), 6.72 (s, 1H), 5.54 (s, 1H), 5.49 (s, 1H), 4.21 (t, *J* = 6.4, 4H), 2.69 (s, 3H), 2.40 (s, 3H), 1.97-1.83 (m, 4H), 1.6-1.47 (m, 4H), 1.02 (t, *J* = 7.4, 3H), 0.97 (t, *J* = 7.4, 3H); **^{1}H NMR** (600 MHz, $(CD_3)_2SO$) δ 10.24 (s, 2H), 6.71 (s, 1H), 6.70 (s, 1H), 5.62 (s, 1H), 5.56 (s, 1H), 4.13 (t, *J* = 6.3, 4H), 2.60 (s, 3H), 2.26 (s, 3H), 1.81 (q, *J* = 7.1, 2H), 1.75 (q, *J* = 7.1, 2H), 1.49 (p, *J* = 7.7, 2H), 1.43 (p, *J* = 7.8, 2H), 0.96 (t, *J* = 7.4, 3H), 0.91 (t, *J* = 7.5, 3H); **^{13}C NMR** (150 MHz, $(CD_3)_2SO$) δ 168.8, 168.8, 161.8, 161.8, 158.9, 158.1, 155.4, 153.8, 137.3, 136.8, 119.0, 115.6, 109.4, 106.3, 106.2, 100.3, 87.2, 86.8, 69.3, 69.3, 30.2, 30.1, 23.4, 19.1, 18.9, 18.9, 13.6, 13.6; **IR** (thin film, cm^{-1}) 3263, 3165, 2961, 2936, 2875, 1680, 1590, 1551, 1453, 1438; **HRMS** (ESI) *m/z* calculated for $C_{28}H_{31}O_8^+$ $[M+H]^+$ 495.2013, found 495.2027.

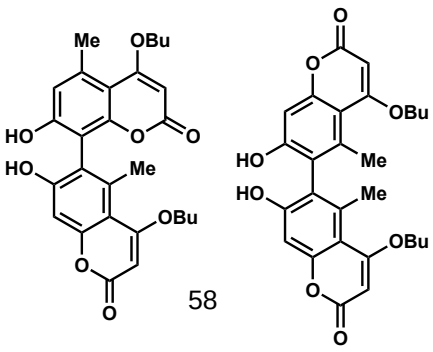

4,4'-dibutoxy-7,7'-dihydroxy-5,5'dimethyl-*2H*,*2H'*-[6,8'-bichromene]-2,2'-dione (58) and 4,4'-dibutoxy-7,7'-dihydroxy-5,5'dimethyl-*2H*,*2H'*-[6,6'-bichromene]-2,2'-dione (31) 1:0.3 mixture: ^{1}**H NMR** (600 MHz, $(CD_3)_2CO$) δ 6.81 (s, 1H), 6.75 (s, 0.6 H), 6.72 (s, 1H), 5.55 (s, 0.6 H), 5.53 (s, 1H), 5.49 (s, 1H), 4.20 (q, *J* = 6.1, 5.4H), 2.69 (s, 3H), 2.40 (s, 3H), 2.36 (s, 1.8H), 1.95-1.84 (m, 5.8H), 1.64-1.48 (m, 5.8H), 1.02 (t, *J* = 7.4), 0.97 (td, *J* = 7.4, 1.9, 4.8H). **HRMS** (ESI) *m/z* calculated for $C_{28}H_{31}O_8^+$ $[M+H]^+$ 495.2013, found (6,8' product) 495.2020 and found (6,6' product) 495.2022.

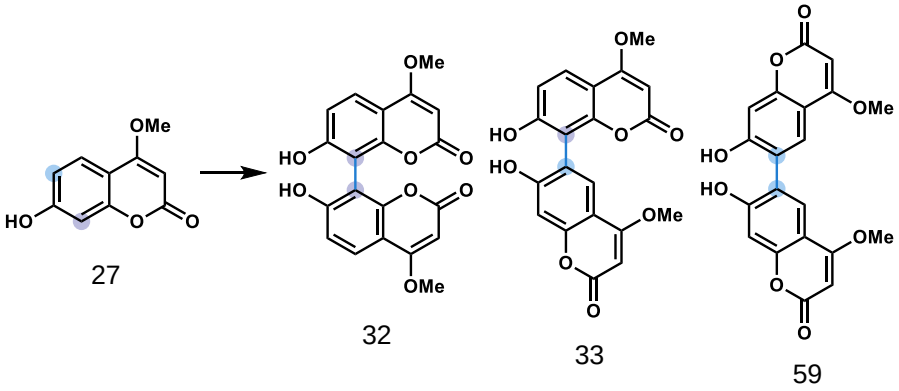

Figure S2.7

Racemic chemical dimerization of 7-hydroxy-4-methoxy-*2H*-chromen-2-one (21):

To a solution of 7-hydroxy-4-methoxy-*2H*-chromen-2-one (**21**, 48.1 mg, 0.250 mmol, 1.0 equiv) in DCM (1.0 mL) and TFA (0.25 mL) was added VOF_3 (46.5 mg, 0.375 mmol, 1.5 equiv) at 0 °C. The reaction was stirred for 5.0 h. The reaction was quenched with H_2O (2 mL). The aqueous phase was extracted with EtOAc (3x). The organic layers were combined, washed with brine, dried over Na_2SO_4, filtered, and evaporated under reduced pressure. The crude solid was purified by flash column chromatography (8:3:1 toluene/EtOAc/formic acid v/v) then reversed-phase HPLC (Phenomenex Kinetex 5 µm C18, 150 x 21.2 mm column) under the following conditions: mobile phase A = deionized

water + 0.1% formic acid and B = acetonitrile + 0.1% formic acid; method = 80% A for 5 min, 80% A to 75% A over 2.5 min, 75% A for 5 min, 75% A to 70% A over 2.5 min, 70% A for 5 min, 70% A to 50% A over 5 min, 254 and 308 nm UV detection and 14 mL/min flow rate. A retention time of 13.08-14.92 min afforded 2.4 mg of 8,8' product **32** (5% yield), and a retention time of 18.92-20.87 afforded 2.9 mg of 6,8' product **33** (6% yield).

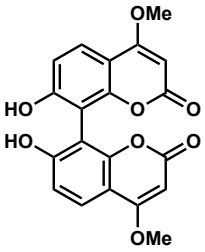

7,7'-dihydroxy-4,4'-dimethoxy-*2H*,*2H'*-[8,8'-bichromene]-2,2'-dione (32): MP >310 °C; R_f = 0.15 (8:3:1 toluene/EtoAc/formic acid v/v); **^{1}H NMR** (600 MHz, (CD_3OD) δ 7.80 (d, *J* = 8.8, 2H), 6.95 (d, *J* = 8.8, 2H), 5.65 (s, 2H), 4.04 (s, 6H); **^{13}C NMR** (150 MHz, CD_3OD) δ 169.7, 166.3, 161.5, 154.4, 125.0, 113.8, 109.3, 108.6, 87.3, 57.3; **IR** (thin film, cm^{-1}) 3411, 3187, 1681, 1604, 1572, 1506, 1442; **HRMS** (ESI) *m/z* calculated for $C_{20}H_{15}O_8^+$ $[M+H]^+$ 383.0761, found 383.0773.

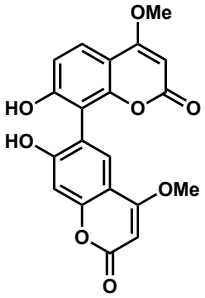

7,7'-dihydroxy-4,4'-dimethoxy-*2H*,*2H'*-[6,8'-bichromene]-2,2'-dione (33): MP >310 °C; R_f = 0.14 (8:3:1 toluene/EtoAc/formic acid v/v); **^{1}H NMR** (400 MHz, $(CD_3)_2CO$) δ 7.73 (d, *J* = 8.7, 1H), 7.63 (s, 1H), 7.03 (d, *J* = 8.8, 1H), 6.89 (s, 1H), 5.61 (s, 1H), 5.58 (s, 1H), 4.06 (s, 3H), 4.03 (s, 3H); **^{1}H NMR** (600 MHz, $(CD_3)_2SO$) δ 10.73 (br s, 2H), 7.64 (d, *J* = 8.4, 1H), 7.48 (s, 1H), 6.92 (br s, 1H), 6.83 (s, 1H), 5.70 (s, 1H), 5.66 (s, 1H), 3.98 (s, 3H), 3.95 (s, 3H); **^{13}C NMR** (150 MHz, $(CD_3)_2SO$) δ 166.7, 166.4, 162.3, 162.2, 160.4, 159.9, 154.0, 152.4, 126.1, 122.9, 117.4, 112.6, 111.9, 106.9, 106.6, 102.2, 86.9, 86.6, 56.8,

56.8; **IR** (thin film, cm^{-1}) 3412, 3186, 2730, 1688, 1602, 1443; **HRMS** (ESI) *m/z* calculated for $C_{20}H_{15}O_8^+$ $[M+H]^+$ 383.0761, found 383.0778.

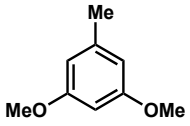

1,3-dimethoxy-5-methylbenzene (60): 1,3-dimethoxy-5-methylbenzene (**60**) was prepared from 5-methylbenzene-1,3-diol according to the procedure described by Trost et al.[85] The crude oil was purified by flash column chromatography (19:1 hexanes/EtOAc v/v) to afford a 6.24 g of the title compound (85% yield) as a colorless liquid. **^{1}H NMR** (600 MHz, $CDCl_3$) δ 6.34 (d, *J* = 2.1, 2H), 6.29 (t, *J* = 2.3, 1H), 3.78 (s, 6H), 2.31 (s, 3H); **HRMS** (ESI) *m/z* calculated for $C_9H_{13}O_2^+$ $[M+H]^+$ 153.0910, found 153.0898. All spectra obtained were constant with literature values.

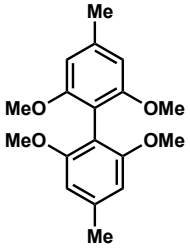

2,2',6,6'-tetramethoxy-4,4'-dimethyl-1,1'-biphenyl (61): 2,2',6,6'-tetramethoxy-4,4'-dimethyl-1,1'-biphenyl (**61**) was prepared from 1,3-dimethoxy-5-methylbenzene (**60**) according to the procedure described by Li et al.[86] **^{1}H NMR** (400 MHz, $CDCl_3$) δ 6.47 (s, 4H), 3.71 (s, 12H), 2.39 (s,6H); **HRMS** (ESI) *m/z* calculated for $C_{18}H_{23}O_4^+$ $[M+H]^+$ 303.1591, found 303.1595. All spectra obtained were constant with literature values.

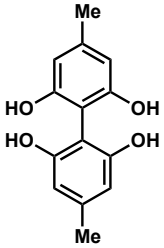

4,4'-dimethyl-[1,1'-biphenyl]-2,2',6,6'tetraol (62): To a solution of 2,2',6,6'-tetramethoxy-4,4'-dimethyl-1,1'-biphenyl (**61**, 973.1 mg, 3.218 mmol, 1 equiv) dissolved

in DCM (3.2 mL) was added a 1M solution of BBr_3 in DCM (13.20 mL, 13.19 mmol, 4.1 equiv) at -78 °C. The reaction was allowed to warm to rt and stirred for 17.4 h. The reaction was quenched with the addition of water (5.0 mL). The aqueous phase was extracted with EtOAc (3x). The organic layers were combined, washed with brine, dried over Na_2SO_4, filtered, and evaporated under reduced pressure to afford 736.1 mg of the title compound (91%) as a yellow solid. MP 75.7-77.1 °C; R_f = 0.45 (1:1 hexanes/EtOAc v/v); **^{1}H NMR** (600 MHz, (CD_3OD) δ 6.31 (s, 4H), 2.24 (s, 6H); **^{13}C NMR** (150 MHz, (CD_3OD) δ 157.1, 140.2, 109.2, 106.6, 21.5; **IR** (thin film, cm^{-1}) 3331, 2921, 1623, 1573, 1503, 1450, 1417; **HRMS** (ESI) *m/z* calculated for $C_{14}H_{15}O_4^+$ $[M+H]^+$ 247.0965, found 247.0963.

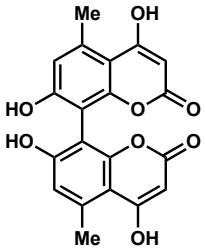

4,4',7,7'-tetrahydroxy-5,5'-dimethyl-*2H,2H'*-[8,8'-bichromene]-2,2'-dione (63): To a mixture of 4,4'-dimethyl-[1,1'-biphenyl]-2,2',6,6'tetraol (**62**), 658.8 mg, 2.632 mmol, 1equiv), malonic acid (547.8 mg, 5.264 mmol, 2 equiv) and $ZnCl_2$ flame-dried under vacuum (2.224 g, 16.32 mmol, 6.2 equiv) was added $POCl_3$ (13.2 mL). The reaction was heated at 60 °C and stirred for 13.3 h. The reaction was quenched by pouring into ice water and induced the precipitation of a solid. The precipitate was isolated by vacuum filtration to afford 820.7 mg of the title compound (82% yield) as a yellow solid. MP 287.9-290.7 °C; R_f = 0.05 (8:3:1 toluene/EtOAc/formic acid v/v); **^{1}H NMR** (600 MHz, $(CD_3)_2SO$) δ 6.70 (s, 2H), 5.34 (s, 2H), 2.64 (s, 6H);**^{13}C NMR** (150 MHz, $(CD_3)_2SO$) δ 169.5, 162.0, 158.0, 154.9, 137.5, 115.2, 106.5, 105.9, 87.9, 23.1; **IR** (thin film, cm^{-1}) 3194, 2976, 2935, 1725, 1660, 1609, 1578, 1492, 1450; **HRMS** (ESI) *m/z* calculated for $C_{20}H_{15}O_8^+$ $[M+H]^+$ 383.0761, found 383.0757.

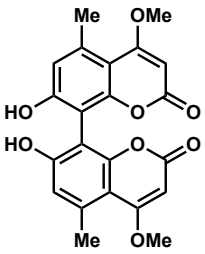

7,7'-dihydroxy-4,4'-dimethoxy-5,5'dimethyl-*2H*,*2H'*-[8,8'-bichromene]-2,2'-dione (2): To a suspension of 4,4',7,7'-tetrahydroxy-5,5'-dimethyl-*2H,2H'*-[8,8'-bichromene]-2,2'-dione (**S20**, 1.116 g, 2.919 mmol, 1 equiv) in MeOH (32.0 mL) was added H_2SO_4 (3.2 mL). The reaction was heated at 75 °C and stirred for 5.7 h. The reaction was cooled, and water added to induce the precipitation of a solid. The precipitate was isolated by vacuum filtration to afford 707.3 mg of the title compound (59% yield) as a tan solid. **^{1}H NMR** (600 MHz, $(CD_3)_2SO$) δ 10.20 (s, 2H), 6.72 (s, 2H), 5.57 (s, 2H), 3.94 (s, 6H), 2.60 (s, 6H); **HRMS** (ESI) *m/z* calculated for $C_{22}H_{19}O_8^+$ $[M+H]^+$ 411.1074, found 411.1076. All spectra were consistent with literature values.[83]

Plasmids and sequences

The genes encoding *ktnC* (A2QK67.1) and *desC* (A0A0N9HKQ7.1) in a pJET1.2 cloning plasmid and a pESC-HIS expression plasmid were generous gifts from Professor Michael Müller's lab at the Albert-Ludwigs-Universität Freiburg. The genes for *ktnC and desC* were amplified and cloned into a pPIC3.5 plasmid (Invitrogen) for functional expression in *P. pastoris*.

***ktnC* sequence:**

ATGGCAGTTCATGTACCATTCAGCATCCACCACGTCGTGGATATCGGCATTTCCAC
CGGCCCGGTAGTCATTGTCCTCGTTCTCCTATTCGGGTTGGCTGTCGTGGGATCC
GACAGCCTTGATGGATGGTGGCAGAAAAGAGCCTTGAGAGGCATTCCGATTGTAG
ACGAGGGTAGCTACATGCGGCCAAAGCTACGATGGAAGCGCTTCGATGCGGAGA
AAGAGTATGCGAGAGCATATCAGCAGTACACAAAAGCAGGGAAACCTTATGCGAT
CCGGATGCAGAATGATAATTATGGCATTGTGCTTCCCTTAAACTCAGCAAAGGAAT
GGAGGTCTCTACCACACGACCAGCTGAGCTTTCTTCAAGCCTTGGCAGAGTTTGC
GGATATGAACATGTACTGCGACGTCACGGACAGGACACCCATTGAAGCTGTTCATA
GTTGCAACAACGCTGAATCATTAAACATCCTCAATAAGCTTCTCGCCCGGGAAACC
GATACAGCCTTATCTCAGATTTTCGAGCAGCCTACAGGAAAAGACTGGAAGGAATT
GAACACACTGCAGACAATCCTCTCCTTATGCTCAACGGTTACTATGGCCTTGCTCC
TCGGACCAGATACAGCCCCTGACCCGGTGCTCCACCACCATTCGACGTCTTTTGG
CGAAGCAATTATGAGCAGTTGTTATCGACGAACGGGATATCCGCGCATCCTGCGG
CCATTCGTGTGGCGCTTTTCGTCCGAATGCCGAAATCTGAGGAAACACTTATCTCT
CGTGAGAGAGAGACTTGTTCCTGAGGTTGCGCGCCGTGTCGCAGCTGCACGAGC
GGCGGATAAAACCAAGGACGTACGCCCATCTTCATTGTTGGACGCACTGATCGCG
GCGGCCTTCGACAACGGCAGCTTAAGCCCAGATGACCAAGGCAGAAATGATGCAG
CACAGGTACAGTTGCTGGCAGATGATCTCATTTTCTACCATTTCGAACTCTGTAAAC
CGACCGCATTCAACATCATCTTCCAGCTGTATGCCATCATGGACCACCCAGAGTAC
AAGGCTCCTCTCCGAGAGGAGGCACTCCAAGCCTTGAAGCTCACCAATGGTGACT
GGACCGTTGAAACTCTGAAGCACGCTCCCAAGTTAGAAAGCTTTACAAAGGAGAC
CTTTCGACTGTACGATATCTCCGGTTTTGTCAGCTTTCGCCGTGTCATGAAACCTCT

TACTCTAAACTCCATCGGCCTGTCTCTTCGTCCCGGTACAATCTTATTGTCTCCATG
TCGGAATGTCCATTTGGATCCCGAGATCTATGAAGACCCGACAACTTTCAATGGCT
ACCGCTTCTACGACTCCAGCCGCGAGGTCTGCTCTCCACGCGTGGCAACCACCTC
GCTCACGTTCTTGACATTTTCTCATGGAGCGGGCAGCTGTCCCGCGCGGGTTCTC
GCTACTCAAATTTGTCGGACGATCTTCATCAAGTTCCTGTTGCAGTACGACGTAGA
ACCTGTGCAGAAGGAGATACTACCCTATGGATTCACCAGTGGTCCGGTCTATATGC
CTAATCCATCAGTGATGATGAGAATCCGGCCAAGAAGTGACGGGAAG

KtnC protein sequence:

MAVHVPFSIHHVVDIGISTGPVVIVLVLLFGLAVVGSDSLDGWWQKRALRGIPIVDEGSY
MRPKLRWKRFDAEKEYARAYQQYTKAGKPYAIRMQNDNYGIVLPLNSAKEWRSLPHD
QLSFLQALAEFADMNMYCDVTDRTPIEAVHSCNNAESLNILNKLLARETDTALSQIFEQ
PTGKDWKELNTLQTILSLCSTVTMALLLGPDTAPDPVLHHHSTSFGEAIMSSCYRRTGY
PRILRPFVWRFSSECRNLRKHLSLVRERLVPEVARRVAAARAADKTKDVRPSSLLDALI
AAAFDNGSLSPDDQGRNDAAQVQLLADDLIFYHFELCKPTAFNIIFQLYAIMDHPEYKA
PLREEALQALKLTNGDWTVETLKHAPKLESFTKETFRLYDISGFVSFRRVMKPLTLNSI
GLSLRPGTILLSPCRNVHLDPEIYEDPTTFNGYRFYDSSREVCSPRVATTSLTFLTFSH
GAGSCPARVLATQICRTIFIKFLLQYDVEPVQKEILPYGFTSGPVYMPNPSVMMRIRPR
SDGK

***desC* sequence:**

ATGGGCGCTCTATCAGAGATATTCACGGCGGGCTATGTCGCCCTCGCAGGGATCA
CTGGGTTCTTCCTCGTCTTCCTCGGTTTTCTCGTGGTCATCTCCGACTACATTGAC
GGATGGCGTAGCAGAAGGGCATTGGGAGATATCCCCATCGTGGATGAGGGAAGC
AATCTGAGTCCCATACTACGATGGAACTCCCAACCATATGACGCCGAGGCAGAGTT
CACCAGGGCCTATTACAAGTATAGCAAGAACGGGAAGCCCTTTGCTGCCCGGATC
CAGCACGGCGGCTATGCCATTGTCCTCCCGCCGAGCGCTTGCAGAAAAGTCCGTT
CAATCGGCCATGAGCAGTTGAGCTTCTTGGATGCTCTGGCGGAGTTTGCGGATCT
TTCCCTACACATGGACGTGACCAGCCGGAGAGTCATTGAAGCGACCCACGCGTGC
AACAACGAGACCACGATAAAGAATTTCCAGGAACGGCTTGCCCTCGAGTGCGGAA
AACACTTGGCCCCCGTCTTCGACCCCCCACAAGAACAGGAGTCAACCGAGCTCAA

AACCTTGAAATCGGTCTTTGCTGCGATCTCAGCGGTGGCCACGGCCCTGATTCTTG
GGCCTGACTGCCCGGAGGCCCTGGTATCCGAGGTCACGGCCGGGGCCACCGCAT
ACAACGAGGTCATGATACAGTGCCGCATTCTGCGTGCGCAGTATCCCAAGATTCT
GAAGCCACTTGTCTGGCGGTTCTCCCGCACCGCTCGTGAGCTGAGGGCCATTCTC
TCGCGTCTCAAAGCGCGGCTGGTCCCTGAGATTAAGCGGCGGATTGCCTACCTCG
AGGCCCACTCTACGAGCGAGAATCAAGCAGAATCCGCCGGCTCATTCTCGCTACT
CGACATCCTCATCCAGACCAGCTTCAAGAACAGGCACCTGCCCAGCACACCCGTA
GAGAACGACAAATGGGCTGATCTCCTCTGCCAACAGGCCCTCCTGTATCACTTCAA
ACTCAGCAGGGCTCCAGGAACCAGCGTTACCTTTATGCTCTACAGAGTCATGAACC
ACCCAGAGTACGCCACAATGCTCCGCGACGAAATGATAGCAGCTCTAAAGCCGTC
GGGTGGTAATTGGACGGCTGATATCCTGCAGCGCGCGCCCAAGCTGGAGAGTTTC
AATAAAGAGACCTTTCGCATGCATGATATCTCGAATTTCGTCGGCCTCCGCGTCGC
CATGCGCCCGGTCGATCTCAGATCCGTCTCGCCTCCCCTGCATCTCAAGCCAGGA
ACAATGATCATGACCCCCTCCCGAACAGTCCATTACGACGCGGAGCACTACGTTG
ACCCGCTGACCTTCAACGGGTTGCGCTTCTACGACGCCACCAGCAACACCTGCAC
TCCCCGCGTGTTCACCACCTCGCCAACCTACCTGCCCTTCAGCCACGGGACGGGC
TCGTGCCCCGCACGCAACTTCGCGACGCAGATTGCGCGCATGCTGTTTATCCGAC
TGCTGATGGGGTATGAGTTTGAGCTGGCCAATGAGGAAATGCCGGCTTATGGGCT
GATGGATGGGACGGCGTATTTTCCGAATCCGGAGGTTAGGATGAGAGTCAGGGTG
AGGGGGAAG

DesC protein sequence:

MGALSEIFTAGYVALAGITGFFLVFLGFLVVISDYIDGWRSRRALGDIPIVDEGSNLSPIL
RWNSQPYDAEAEFTRAYYKYSKNGKPFAARIQHGGYAIVLPPSACRKVRSIGHEQLSF
LDALAEFADLSLHMDVTSRRVIEATHACNNETTIKNFQERLALECGKHLAPVFDPPQEQ
ESTELKTLKSVFAAISAVATALILGPDCPEALVSEVTAGATAYNEVMIQCRILRAQYPKIL
KPLVWRFSRTARELRAILSRLKARLVPEIKRRIAYLEAHSTSENQAESAGSFSLLDILIQT
SFKNRHLPSTPVENDKWADLLCQQALLYHFKLSRAPGTSVTFMLYRVMNHPEYATML
RDEMIAALKPSGGNWTADILQRAPKLESFNKETFRMHDISNFVGLRVAMRPVDLRSVS
PPLHLKPGTMIMTPSRTVHYDAEHYVDPLTFNGLRFYDATSNTCTPRVFTTSPTYLPFS
HGTGSCPARNFATQIARMLFIRLLMGYEFELANEEMPAYGLMDGTAYFPNPEVRMRV

RVRGK

Functional expression in yeast

Functional expression of P450s in *S. cerevisiae*: *S. cerevisiae* strain BY4742 cells were prepared for transformation with pESC-HIS expression plasmids harboring *ktnC* and *desC* through a standard protocol for lithium acetate transformations.[87] Transformed cells were plated on histidine dropout plates containing 2% glucose. After 2-3 d of growth at 30 °C, colonies were inoculated in histidine dropout minimal medium containing 2% glucose and grown overnight at 30 °C with shaking at 235 rpm. Cultures were induced for expression by resuspension (1:1) in histidine dropout minimal media containing 6% galactose. Expression cultures were grown at 30 °C with shaking at 235 rpm for 2-5 days. For biotransformations, substrate was spiked into the expression culture at the point of induction.

Cloning and functional expression of P450s in *P. pastoris*: The open reading frames for *ktnC* and *desC* were amplified from a pJET1.2 cloning plasmid with primers that incorporated a 5' EcoRI restriction site, Kozak sequence, and FLAG tag, and a 3' AvrII restriction site. PCRs were performed with NEB reagents in 50 µL reaction volumes containing 1X HF Phusion buffer, 0.2 mM dNTPs, 0.5 µM of each of the primers, 20 units of Phusion DNA polymerase, and 5 µL template plasmid DNA. The reaction conditions were programmed as follows: 95 °C denaturation for 2 min; 30 cycles of 95 °C for 30 sec, 61 °C for 1 min, 72 °C for 3 min; and a final 72 °C extension for 5 min. PCR products were extracted from a 0.8% agarose gel.

Supplemental Table S2.1. Primers used in amplification of the genes for KtnC and DesC.

	Forward primer (5'-3')	Reverse primer (5'-3')
ktnC	CATGATGAATTCAATAATGTCTGACTACAAAGACGAT GACGACAAGATTGATCCCTTCACCATGGCAGTTCAT GTACCATTC	CATGTACCTAGGCTTCCCGTCA CTTCTTGG

desC	CATGATGAATTCAATAATGTCTGACTACAAAGACGATG ACGACAAGATTGATCCCTTCACCATGGGCGCTCTATC AGAG	CATGTACCTAGGCTTCCCCCT CACCCTG

The amplified genes were cloned into a pPIC3.5 plasmid (Invitrogen) for expression in the *P. pastoris*. Digestion reactions contained 3 µg of DNA in 1X Cutsmart buffer and 2 µL each of EcoRI and AvrII restriction enzymes (NEB) in a 50 µL reaction volume. Reactions were incubated at 37 °C for 2.5 h before quenching and purification of the DNA with a PCR clean-up. Ligation reactions contained 100 ng of plasmid DNA and 100 ng of insert were incubated with 1X T4 DNA ligase buffer and 1 unit of T4 DNA ligase enzyme (NEB) in 10 µL reaction volumes for 1 h at room temperature, followed by a 65 °C heat inactivation for 10 min. Ligations were transformed in DH5α *E. coli* cells and transformants were confirmed for gene integration by Sanger sequencing. The expression plasmids harboring *ktnC* and *desC* were linearized with SalI-HF restriction enzyme (NEB) using the same digestion procedures as previously described. *P. pastoris* strain KM71 electrocompetent cells were prepared as described by Madden et al.[88] and transformed with 0.1-2 µg of linearized DNA by electroporation. Electroporated cells were immediately recovered in PERS (1 M sorbitol and YPD, 1:1 v/v) and incubated for 1-4 h at 30 °C with shaking at 100 rpm before plating cells on MD plates (1.34% YNB, 4 x 10^{-5} % biotin, 2% dextrose, 1.5% agar). After 2 d of growth at 30 °C, colonies were inoculated in BMG medium (100 mM potassium phosphate pH 6.0, 1.34% YNB, 4 x 10^{-5} % biotin, 1% glycerol) and grown overnight at 30 °C with shaking at 235 rpm. Cultures were induced for expression by resuspension (5:1) in BMM medium (100 mM potassium phosphate pH 6.0, 1.34% YNB, 4 x 10^{-5} % biotin, 0.5% methanol). Expression cultures were grown at 30 °C with shaking at 235 rpm for 2-5 days and supplemented daily with methanol to maintain 0.5% methanol in the cultures. For biotransformations, substrate was spiked into the expression culture at the point of induction.

Comparison of yeast systems for whole-cell biocatalysis: To compare *S. cerevisiae* and *P.* pastoris as hosts for whole-cell biocatalysis of heterologous P450s, the heterologous expression levels of the P450s was assessed by Western blot

(Supplemental Figure S2.8A) and the relative conversions achievable by biotransformations was assessed by mass spectrometry (Supplemental Figure S2.8B).

Supplemental Figure S2.8A. Relative heterologous expression levels of KtnC and DesC (60-kDa membrane-bound P450s) in *S. cerevisiae* (**a**) and *P. pastoris* (**b**). Proteins were expressed for three days at 30 °C. Insoluble proteins from approximately 9 x 10^7 cells were resolved by SDS-PAGE and detected through anti-FLAG-HRP Western blots.

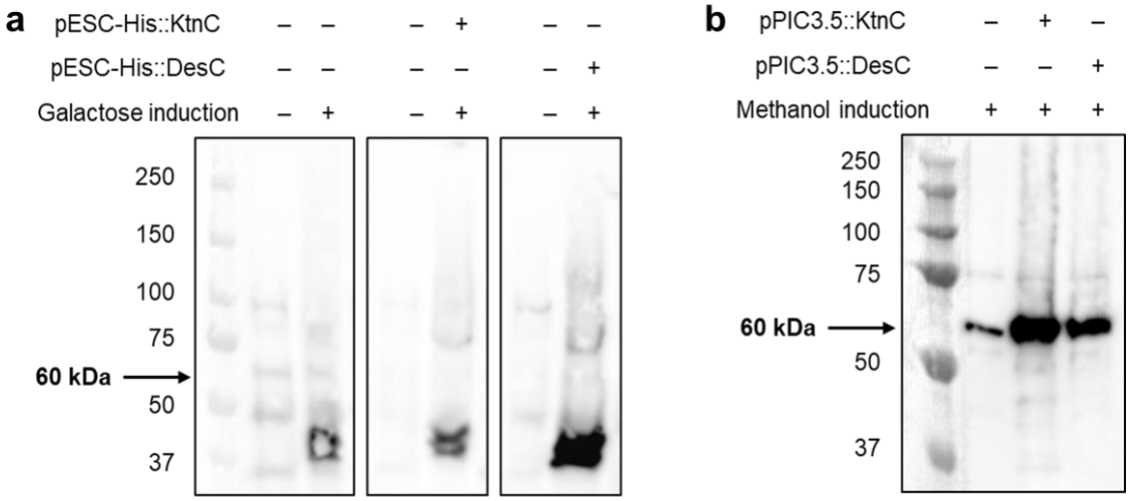

Supplemental Figure S2.8B. Substrate concentration screen. Relative conversions in whole-cell biotransformations in *S. cerevisiae* and *P. pastoris* when increased substrate is added at the point of induction. For each timepoint, an aliquot of the biotransformation was quenched with excess methanol and analyzed by TOF-LC/MS for relative conversion of coumarin **1** to the major dimer (**14** for KtnC and **15** for DesC).

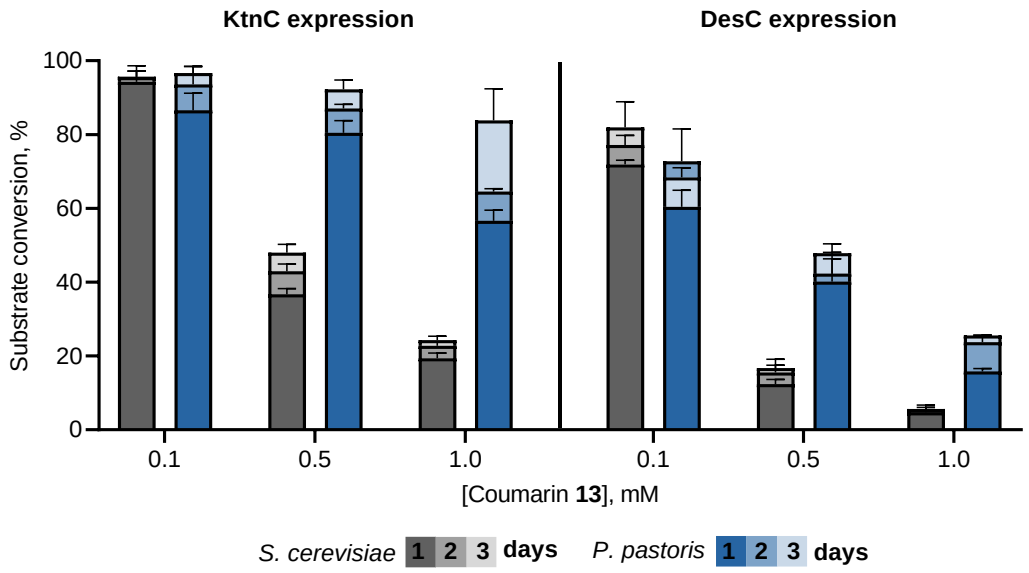

Biotransformations

Stock solutions: Stock solutions of each substrate (50 mM) were prepared by dissolving in DMSO. UPLC solvents were prepared from a stock (1.26 g ammonium formate, 500 µL formic acid, 100 mL deionized water).

Analytical-scale whole-cell biotransformations for dimerization

General protocol: A colony of *S. cerevisiae* strain BY4742 containing KtnC or Desc was inoculated in 5 mL histidine dropout minimal medium containing 4% glucose and grown overnight at 30 °C with shaking at 235 rpm to OD_{600} of 3-6. Cultures were induced for expression by resuspension (1:1) in histidine dropout minimal media containing 6% galactose. Expression cultures were grown at 30 °C with shaking at 235 rpm for 2-4 days. For biotransformations, substrate was spiked into the expression culture at the point of induction.

General protocol: A colony of *P. pastoris* KM71 containing KtnC or Desc was inoculated in 5 mL BMG medium and grown overnight at 30 °C with shaking at 235 rpm. The culture was added to BMG medium (50 mL) and grown at 30 °C with shaking at 235 rpm until the optical density at 600 nm was in the range of 10-16. Cultures were induced for expression by resuspension in BMM medium (20 mL). Expression cultures were portioned in 1 mL aliquots, and substrate was added from a 50 mM stock in DMSO. Cultures were grown at 30 °C with shaking at 235 rpm for 48-60 h and supplemented with 100 µL of 10X methanol (5% MeOH, 95% water) after 24 h.

Determination of percent conversion for dimerization (Figure 2.16): Percent conversion was determined based on consumption of starting material compared to a calibration curve. To generate the calibration curve, a colony of *P. pastoris* KM71 was inoculated in 5 mL BMG medium and grown overnight at 30 °C with shaking at 235 rpm. The culture was added to BMG medium (100 mL) and grown at 30 °C with shaking at 235 rpm until the optical density at 600 nm was in the range of 9-14. Cultures were induced

for expression by resuspension in BMM medium (40 mL). Expression cultures were portioned in 1 mL aliquots, and substrate was added from a 50 mM stock in DMSO. Cultures were grown at 30 °C with shaking at 235 rpm for 48-60 h and supplemented with 100 µL of 10X methanol (5% MeOH, 95% water) after 24 h. For analysis, the cultures were subjected to chemical lysis by the addition of 200 µL CelLytic Y Cell Lysis Reagent (Sigma) and 24 µL of 500 mM DTT then incubated at 30 °C with shaking at 235 rpm for 30 min. The samples underwent vortexing then 28 µL was removed and diluted with a solution (1:1, MeOH: 2 mM ammonium formate, pH=3.5) containing either 1,3,5-trimethoxybenzene or 1,2,3,5-tetramethoxybenzene for a final concentration of 300 µM in internal standard. Precipitated yeast cells were pelleted by centrifugation (17,000 x *g*, 10 min). The supernatant was transferred and liquid chromatography PDA spectrometry (UPLC) analysis was performed on an Agilent 6230 time of flight mass spectrometer with a Dual AJS ESI source and an Agilent 1290 Infinity Series II diode array detector, autosampler, and binary pump using a Waters Acquity UPLC HSS T3 1.8 µm C18, 2.1x50 mm column under the following conditions:

Using a Waters Acquity UPLC HSS T3 1.8 µm C18, 2.1x50 mm column under the following conditions:

Method A: phase A = deionized water with 2 mM ammonium formate pH = 3.5 (10 mL stock, 990 mL deionized water) and phase B = 9:1 acetonitrile: deionized water, v/v with 2 mM ammonium formate pH = 3.5 (10 mL stock, 90 mL deionized water, 900 mL acetonitrile); method = 80% A for 0.5 min, 80% A to 30% A over 1.8 min, 30% A for 0.2 min, 275 and 308 nm UV detection and 0.7 mL/min flow rate. Each injection was followed by equilibration at 80% A for 1 min.

Method B: phase A = deionized water with 2 mM ammonium formate, pH = 3.5 and phase B = 95:5 acetonitrile: deionized water, v/v with 2 mM ammonium formate, pH = 3.5; method = 80% A to 20% A over 2.3 min, 20% A for 0.2 min, 275 and 308 nm UV detection and 0.7 mL/min flow rate. Each injection was followed by equilibration at 80% A for 1 min.

Using a Waters XBridge 3.5 µm C18, 2.1x150 mm column under the following conditions:

Method C: phase A = deionized water with 0.1% formic acid and phase B = acetonitrile with 0.1% formic acid; method = 55% A for 5 min, 55% A to 5% A over 2 min, 5% A for 0.5 min, 5% A to 55% A over 1 min, 55% A for 1.5 min and 0.4 mL/min flow rate.

The percent conversion of the substrate to oxidative dimer product was calculated with $AUC_{substrate}/AUC_{internal\ standard}$ at 275 nm for both substrate and internal standard or 308 nm for the substrate and 275 nm for the internal standard. All biotransformations were performed in triplicate, and each KtnC and DesC reaction sampled and analyzed in duplicate.

Determination of percent yield for dimerization (Figure 2.9): Percent yield was determined by comparison to a calibration curve of authentic standards of the dimerization products. To generate the calibration curve, a colony of either *P. pastoris* KM71, KtnC, or DesC was inoculated in 6 mL BMG medium and grown overnight at 30 °C with shaking at 235 rpm. The culture was added to BMG medium (75-250 mL) and grown at 30 °C with shaking at 235 rpm until the optical density at 600 nm was in the range of 5-16. Cultures were induced for expression by resuspension in BMM medium to a final optical density of 30. Solutions of products were prepared in DMSO by serial dilution of 25 mM stock solutions in DMSO prepared in triplicate. The stock solutions of authentic standards were added to 24 well plates, followed with 1 mL aliquots of expression cultures with final concentrations of analyte from 0 to 250 µM. Dimerization reactions were run in triplicate alongside calibration curve and were prepared with identical expression cultures of either KtnC or DesC in 24-well plates with coumarin substrate concentrations from 200 to 500 µM. The 24 well plates were sealed with an adhesive cover and grown at 30 °C with shaking at 235 rpm for 48 h and supplemented with 100 µL of 10X methanol (5% MeOH, 95% water) after 24 h.

For analysis, the cultures were subjected to chemical lysis by the addition of 200 µL CelLytic Y Cell Lysis Reagent (Sigma) then incubated at 30 °C with shaking at 235 rpm

for 30 min. 50 µL of the samples were removed and diluted with 150 µL methanol containing an internal standard, either 1,3,5-trimethoxybenzene for a final concentration of 300 µM, or 4,4-dihydroxybenzophenone for a final concentration of 40 µM. Precipitated yeast cells were pelleted by centrifugation (17,000 x *g*, 10 min) in 1.5 mL Eppendorf tubes, or filtered through Pall AcroPrep Advance 350 µL 0.2 um GHP Short Tip Natural PP 96-well filter plates by centrifugation (2000 rpm, 3 minutes). The samples were subjected to liquid chromatography PDA spectrometry (UPLC) analysis performed on an Agilent 6230 time of flight mass spectrometer with a Dual AJS ESI source and an Agilent 1290 Infinity Series II diode array detector, autosampler, and binary pump using a Waters Acquity UPLC HSS T3 1.8 µm C18, 2.1x50 mm column under the following conditions:

Method A: Positive mode, phase A = deionized water with 2 mM ammonium formate, pH = 3.5 and phase B = 95:5 acetonitrile: deionized water, v/v with 2 mM ammonium formate, pH = 3.5; method = 80% A held for 0.5min, to 45% A over 2.75 min, 10% A 100% A for 1.0 min, 254, 275, and 308 nm UV detection and 0.7 mL/min flow rate. Each injection was followed by equilibration at 80% A for 1 min.

Method B: Negative mode, phase A = 95:5 deionized water:acetonitrile B = 95:5 acetonitrile:deionized water; method = 80% A held for 0.5min, to 45% A over 2.75 min, 10% A 100% A for 1.0 min, 254, 275, and 308 nm UV detection and 0.7 mL/min flow rate. Each injection was followed by equilibration at 80% A for 1 min.

Protocol used in site-selectivity analysis of benzofuran (21) dimerization (Fig 2.10): 12 mL 10% glucose H- media was prepared fresh by combining 9.6 mL H- media, 1.2 mL 20% glucose, 1.2 mL sterile water and sterile filtering by syringe. 6 mL media was transferred to culture tubes was inoculated with a single colony of *S. cerevisiae* (BY4742) cells harboring the plasmids for KtnC or DesC and incubated overnight, to an optical density at 600 nm between 5 and 8. The cells were harvested by centrifugation (3000 RPM) and resuspended in **1** mL 4% galactose media, freshly prepared by combining 24 mL H- media, 6 mL sterile water, and 1.8 g galactose, then sterile filtered. Substrates were added to sterile culture tubes as 50 mM stock solutions in DMSO (2 µL, final

concentration of 0.1 mM), then 1 mL aliquots of DesC or KtnC were added. Reactions were incubated for 2-4 days at 30 ˚C, 235 RPM. Reactions were quenched with methanol in a 1:3 dilution and filtered or pelleted 10,000 x *g* for 10 minutes. The supernatant was removed and liquid chromatography PDA spectrometry (UPLC) analysis was performed on an Agilent 6230 time of flight mass spectrometer with a Dual AJS ESI source and an Agilent 1290 Infinity Series II diode array detector, autosampler, and binary pump using under the following conditions:

Using a Waters XBridge 3.5 µm C18, 2.1x150 mm column under the following conditions:

Method D: Positive mode, phase A = deionized water with 2 mM ammonium formate pH = 3.5 (10 mL stock, 990 mL deionized water) and phase B = 9:1 acetonitrile: deionized water, v/v with 2 mM ammonium formate pH = 3.5 (10 mL stock, 90 mL deionized water, 900 mL acetonitrile); method = 85% A held for 1 min, 85% A to 20% A over 7 min, 20% A held for 1.5 min, and 0.4 mL/min flow rate, with either no UV detection or 254, 275, and 308 nm UV detection.

Analytical-scale whole-cell biotransformations for cross-coupling

General protocol: A colony of *P. pastoris* KM71 containing KtnC was inoculated in 6 mL BMG medium and grown overnight at 30 °C with shaking at 235 rpm. The culture was added to BMG medium (125 mL) and grown at 30 °C with shaking at 235 rpm until the optical density at 600 nm was in the range of 10-16. Cultures were induced for expression by resuspension in BMM medium to a final optical density of 30. Substrates were added to 24 well plates from a 50 mM stock in DMSO, followed by 1 mL aliquots of expression cultures. The 24 well plates were sealed with an adhesive cover and grown at 30 °C with shaking at 235 rpm for 48h and supplemented with 100 µL of 10X methanol (5% MeOH, 95% water) after 24 h. Reactions were carried out with final substrate concentrations of 25 µM coumarin **1**, and 250 µM coupling partner or 100 µM **1** and 1000 µM coupling partner.

Determination of percent conversion by calibration curve and relative percent conversions for oxidative cross-coupling biotransformations (Figures 2.17): Percent conversion was determined based on consumption of coumarin starting material **1** and formation of coumarin dimer **2** compared to a calibration curve with an internal standard. To generate the calibration curves, a colony of *P. pastoris* KM71 was inoculated in 6 mL BMG medium and grown overnight at 30 °C with shaking at 235 rpm. The culture was added to BMG medium (125 to 200 mL) and grown at 30 °C with shaking at 235 rpm until the optical density at 600 nm was in the range of 9-14. Cultures were induced for expression by resuspension in BMM medium to a final optical density of 30. Solutions of starting material coumarin **1** and dimer product **2** were prepared in triplicate by serial dilution with DMSO. The stock solutions of standards were added to 24 well plates, followed by 1 mL aliquots of expression cultures with final concentrations from 0 up to 100 µM coumarin **1** and 0 to 50 µM dimer **2**. The 24 well plates were sealed with an adhesive cover and grown at 30 °C with shaking at 235 rpm for 48 h and supplemented with 100 µL of 10X methanol (5% MeOH, 95% water) after 24 h.

For analysis, the cultures were subjected to chemical lysis by the addition of 200 µL CelLytic Y Cell Lysis Reagent (Sigma) then incubated at 30 °C with shaking at 235 rpm for 30 min. 50 µL of the samples were removed and diluted with 150 µL methanol containing an internal standard, either 1,3,5-trimethoxybenzene for a final concentration of 300 µM, or 4,4-dihydroxybenzophenone for a final concentration of 40 µM. Precipitated yeast cells were pelleted by centrifugation (17,000 x *g*, 10 min), or filtered through Pall AcroPrep Advance 350 µL 0.2 um GHP Short Tip Natural PP 96-well filter plates by centrifugation (2000 rpm, 3 minutes). The samples were subjected to liquid chromatography PDA spectrometry (UPLC) analysis performed on an Agilent 6230 time of flight mass spectrometer with a Dual AJS ESI source and an Agilent 1290 Infinity Series II diode array detector, autosampler, and binary pump, using the specified columns under the following conditions:

<u>Using a Waters Acquity UPLC HSS T3 1.8 µm C18, 2.1x50 mm column under the following conditions:</u>

Method A: Positive mode, phase A = deionized water with 2 mM ammonium formate, pH = 3.5 and phase B = 95:5 acetonitrile: deionized water, v/v with 2 mM ammonium formate, pH = 3.5; method = 80% A held for 0.5min, to 45% A over 2.75 min, 10% A 100% A for 1.0 min, 254, 275, and 308 nm UV detection and 0.7 mL/min flow rate. Each injection was followed by equilibration at 80% A for 1 min.

Method B: Negative mode, phase A = 95:5 deionized water:acetonitrile B = 95:5 acetonitrile:deionized water; method = 80% A held for 0.5min, to 45% A over 2.75 min, 10% A 100% A for 1.0 min, 254, 275, and 308 nm UV detection and 0.7 mL/min flow rate. Each injection was followed by equilibration at 80% A for 1 min.

Method C: Negative mode, phase A = 100% deionized water with 0.1% formic acid: B = 95:5 acetonitrile:deionized water with 0.1% formic acid; method = 80% A held for 0.5min, to 45% A over 2.75 min, 10% A 100% A for 1.0 min, 254, 275, and 308 nm UV detection and 0.7 mL/min flow rate. Each injection was followed by equilibration at 80% A for 1 min.

Using a Waters XBridge 3.5 µm C18, 2.1x150 mm column under the following conditions:

Method D: Positive mode, phase A = deionized water with 0.1% formic acid and phase B = 95:5 acetonitrile:deionized water with 0.1% formic acid; method = 85% A held for 1 min, 85% A to 20% A over 7 min, 20% A held for 1.5 min, and 0.4 mL/min flow rate, with either no UV detection or 254, 275, and 308 nm UV detection.

The percent conversion of the cross-coupled AB products was calculated with respect to the native coumarin **1** coupling partner by quantifying the concentration of remaining starting material A (native coumarin **1**) by calibration curve, and the amount of coumarin dimer AA (dimer **14**) formed by calibration curve. The concentration of the desired cross-coupled AB products was assumed to be comprised of the remaining. A species according to the formula:

1. $[A]_{start} = [A]_{remaining} + 2 \times [AA]_{formed} + [AB]_{formed}$

2. where $[AB]_{formed} = [A]_{start} - [A]_{remaining} - 2 \times [AA]_{formed}$

3. $\%\ AB = [AB]_{formed} / [A]_{start} * 100\%$

4. $\%\ AA = [AA]_{formed} / [AA]_{max} * 100\%$ where $[AA]_{max}$ is the theoretical maximum concentration possible.

Calibration curves for $[A]_{remaining}$ and $[AA]_{formed}$ were generated by using MassHunter software to process the raw data files. Extracted Ion Chromatograms to find peak integration of each species A, AA, and the internal standard (IS) with the peak integrations normalized by the internal standard:

A/IS and AA/IS

Determination of relative percent conversion for cross-coupling (Figure 4):
Using the general procedure for analytical oxidative cross-coupling in *P. pastoris*, peaks for each species A, AA, and AB, were integrated from the EICs of each species in MassHunter software. The peak areas were used to calculate the relative percent conversion by the formula:

$\%\ \text{conversion to AA} = (2*AA_{area})/(A_{area}+(2*AA_{area})+AB_{area})*100\%$

$\%\ \text{conversion to AB} = (AB_{area})/(A_{area}+(2*AA_{area})+AB_{area})*100\%$

Determination of oxidative cross-coupling site-selectivity (Figure 2.17):
A colony of *P. pastoris* KM71 was inoculated in 6 mL BMG medium and grown overnight at 30 °C with shaking at 235 rpm. The culture was added to BMG medium (100 or 200 mL) and grown at 30 °C with shaking at 235 rpm until the optical density at 600 nm was in the range of 9-11. Cultures were induced for expression by resuspension in BMM

medium to a final optical density of 30. Substrates were added to 24 well plates from 50 mM stock in DMSO, followed by 1 mL aliquots of expression cultures. The 24 well plates were sealed with an adhesive cover and grown at 30 °C with shaking at 235 rpm for 48h and supplemented with 100 µL of 10X methanol (5% MeOH, 95% water) after 24 h. Reactions were carried out with final substrate concentrations of 100 µM of coumarin **1** and 1000 µM coupling partner.

For analysis, the cultures were subjected to chemical lysis by the addition of 200 µL CelLytic Y Cell Lysis Reagent (Sigma) then incubated at 30 °C with shaking at 235 rpm for 30 min. 100 µL of the samples were removed and diluted with 300 µL methanol containing 4,4-dihydroxybenzophenone for a final concentration of 40 µM as internal standard. Precipitated yeast cells were pelleted by centrifugation (17,000 x *g*, 10 min). The samples were subjected to liquid chromatography PDA spectrometry (UPLC) analysis performed on an Agilent 6230 time of flight mass spectrometer with a Dual AJS ESI source and an Agilent 1290 Infinity Series II diode array detector, autosampler, and binary pump, using the specified columns under the following conditions:

Using a Waters Acquity UPLC HSS T3 1.8 µm C18, 2.1x50 mm column under the following conditions:

Method B: Negative mode, phase A = 95:5 deionized water:acetonitrile B = 95:5 acetonitrile:deionized water; method = 80% A held for 0.5min, to 45% A over 2.75 min, 10% A 100% A for 1.0 min, 254, 275, and 308 nm UV detection and 0.7 mL/min flow rate. Each injection was followed by equilibration at 80% A for 1 min.

Using a Waters XBridge 3.5 µm C18, 2.1x150 mm column under the following conditions:

Method D: Positive mode, phase A = deionized water with 0.1% formic acid and phase B = 95:5 acetonitrile:deionized water with 0.1% formic acid; method = 85% A held for 1 min, 85% A to 20% A over 7 min, 20% A held for 1.5 min, and 0.4 mL/min flow rate, with either no UV detection or 254, 275, and 308 nm UV detection.

Preparative-scale whole-cell biotransformations for dimerization

General protocol: Preparative-scale biotransformations were conducted on 0.1 or 0.2 mmol substrate under the following conditions: A colony of *P. pastoris* KM71 containing KtnC or DesC was inoculated in 5 or 10 mL BMG medium and grown overnight at 30 °C with shaking at 235 rpm. The culture was added to BMG medium (500 or 1000 mL) and grown at 30 °C with shaking at 235 rpm until an acceptable optical density at 600 nm was obtained. Cultures were induced for expression by resuspension in BMM medium (200 or 400 mL), and 2.0 or 4.0 mL substrate was added from a 50 mM stock in DMSO. Cultures were grown at 30 °C with shaking at 235 rpm for 2-3 d and supplemented with 20 or 40 mL or of 10X methanol (5% MeOH, 95% water) after each 24 h period.

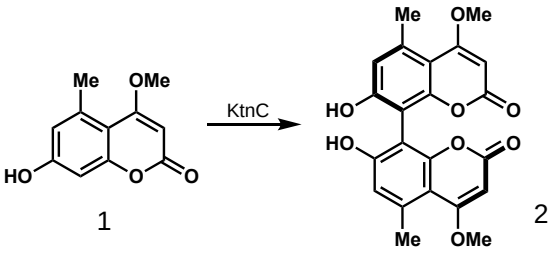

1 2

Supplemental Figure S2.9.

7,7'-dihydroxy-4,4'-dimethoxy-5,5'dimethyl-*2H*,*2H'*-[8,8'-bichromene]-2,2'-dione (2): Cultures containing KtnC were grown to an optical density at 600 nm of 11. The biotransformation on 0.1 mmol substrate was halted after 44 h. The cell pellet was separated from the supernatant and frozen with liquid nitrogen. The aqueous supernatant was partially concentrated under reduced pressure, acidified with 1 M HCl (5 mL), and extracted with EtOAc (3x). The organic layers were combined, washed with brine, dried over Na_2SO_4, filtered, and evaporated under reduced pressure. The pellet was ground with a cold mortar and pestle (chilled at –78 °C) and extracted with EtOAc by stirring for 2 h. The organic layer was decanted, washed with brine, dried over Na_2SO_4, filtered, and evaporated under reduced pressure. The crude solids were purified by flash column chromatography (8:3:1 toluene/EtOAc/formic acid v/v) then reversed-phase HPLC (Phenomenex Kinetex 5 µm C18, 150 x 21.2 mm column) under the following conditions: mobile phase A = deionized water + 0.1% formic acid and B = acetonitrile + 0.1% formic

acid; method = 70% A for 5 min, 70% A to 65% A over 2.0 min, 65% A for 5 min, 65% A to 60% A over 2.0 min, 60% A for 5 min, 60% A to 40% A over 5 min, 40% A for 5 min, 254 and 308 nm UV detection and 12 mL/min flow rate. A retention time of 6.98-14.37 min afforded 3.7 mg of the title compound **2** (18% yield). **^{1}H NMR** (400 MHz, $(CD_3)_2SO$) δ 6.71 (s, 2H), 5.57 (s, 2H), 4.94 (s, 6H), 2.59 (s, 6H); **^{1}H NMR** (400 MHz, CD_3OD) δ 6.75 (s, 2H), 5.59 (s, 2H), 4.00 (s, 6H), 2.67 (s, 6H); **HRMS** (ESI) *m/z* calculated for $C_{22}H_{19}O_8^+$ $[M+H]^+$ 411.1074, found 411.1077. All spectra obtained were in agreement with literature values.

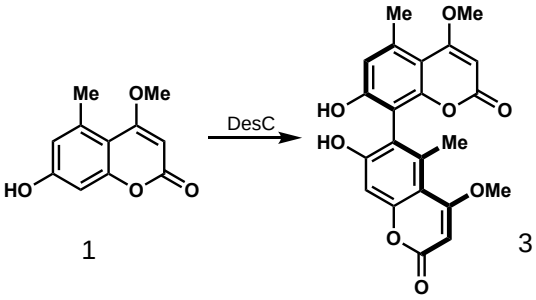

Supplemental Figure S2.10.

7,7'-dihydroxy-4,4'-dimethoxy-5,5'dimethyl-*2H*,*2H'*-[6,8'-bichromene]-2,2'-dione (3): Cultures containing DesC were grown to an optical density at 600 nm of 11.4. The biotransformation on 0.1 mmol substrate was halted after 68.5 h. The cell pellet was separated from the supernatant and frozen with liquid nitrogen. The aqueous supernatant was partially concentrated under reduced pressure, acidified with 1 M HCl (5 mL), and extracted with EtOAc (3x). The organic layers were combined, washed with brine, dried over Na_2SO_4, filtered, and evaporated under reduced pressure. The pellet was ground with a cold mortar and pestle (chilled at –78 °C) and extracted with EtOAc by stirring for 2 h. The organic layer was decanted, washed with brine, dried over Na_2SO_4, filtered, and evaporated under reduced pressure. The crude solids were purified by reversed-phase HPLC (Phenomenex Kinetex 5 µm C18, 150 x 21.2 mm column) under the following conditions: mobile phase A = deionized water + 0.1% formic acid and B = acetonitrile + 0.1% formic acid; method = 70% A for 5 min, 70% A to 65% A over 2.0 min, 65% A for 5 min, 65% A to 60% A over 2.0 min, 60% A for 5 min, 60% A to 40% A over 5 min, 40% A for 5 min, 254 and 308 nm UV detection and 12 mL/min flow rate. A retention time of 10.85-14.31 min afforded 4.4 mg of the title compound **3** (21% yield). **^{1}H NMR** (400 MHz,

$(CD_3)_2SO$) δ 6.71 (s, 1H), 6.69 (s, 1H), 5.63 (s, 1H), 5.57 (s, 1H), 3.94 (s, 3H), 3.93 (s, 3H), 2.58 (s, 3H), 2.23 (s, 3H); **^{1}H NMR** (600 MHz, (CD_3OD) δ 6.74 (s, 1H), 6.71 (s, 1H), 5.63 (s, 1H), 5.60 (s, 1H), 4.00 (s, 3H), 3.98 (s, 3H), 2.68 (s, 3H), 2.35 (s, 3H); **HRMS** (ESI) *m/z* calculated for $C_{22}H_{19}O_8^+$ $[M+H]^+$ 411.1074, found 411.1083. All spectra obtained were in agreement with literature values.

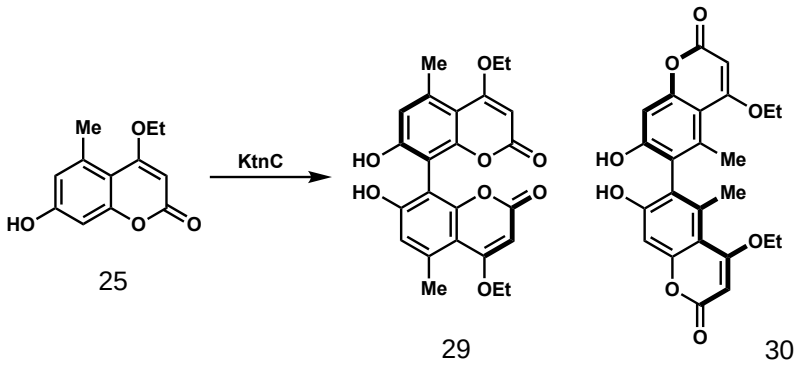

25 29 30

Supplemental Figure S2.11.

KtnC dimerization of 4-ethoxy-7-hydroxy-5-methyl-*2H*-chromen-2-one (25): Cultures were grown to an optical density at 600 nm of 1. The biotransformation on 0.2 mmol substrate was halted after 72 h. The cell pellet was separated from the supernatant and frozen with liquid nitrogen. The aqueous supernatant was partially concentrated under reduced pressure, acidified with 1 M HCl (5 mL), and extracted with EtOAc (3x). The organic layers were combined, washed with brine, dried over Na_2SO_4, filtered, and evaporated under reduced pressure. The pellet was ground with a cold mortar and pestle (chilled at –78 °C) and extracted with EtOAc by stirring for 2 h. The organic layer was decanted, washed with brine, dried over Na_2SO_4, filtered, and evaporated under reduced pressure. The crude solids were purified reversed-phase HPLC (Phenomenex Kinetex 5 µm C18, 150 x 21.2 mm column) under the following conditions: mobile phase A = deionized water + 0.1% formic acid and B = acetonitrile + 0.1% formic acid; method = 70% A for 5 min, 70% A to 65% A over 2.0 min, 65% A for 5 min, 65% A to 60% A over 2.0 min, 60% A for 5 min, 60% A to 40% A over 5 min, 40% A for 5 min, 254 and 308 nm UV detection and 12 mL/min flow rate. The 8,8'-product **31** eluted from 15.4-17.5 min to provide 4.4 mg (10% yield), and the 6,6'-product **32** eluted from 20.2-23.1 min to provide 10.5 mg (24% yield).

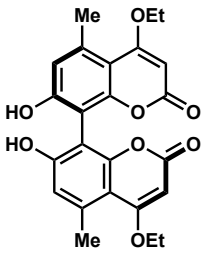

4,4'-diethoxy-7,7'-dihydroxy-5,5'dimethyl-*2H*,*2H'*-[8,8'-bichromene]-2,2'-dione (29): MP >310 °C; **^{1}H NMR** (600 MHz, CD_3OD) δ 6.75 (s, 2H), 5.55 (s, 2H), 4.24 (q, *J* = 7.1, 4H), 2.71 (s, 6H), 1.55 (t, *J* = 7.2, 6H); **^{1}H NMR** (600 MHz, $(CD_3)_2CO$) δ 6.75 (s, 2H), 5.43 (s, 2H), 4.24 (q, *J* = 6.9, 4H), 2.67 (s, 6H), 1.54 (t, *J* = 7.0, 6H); **^{13}C NMR (**150 MHz, $(CD_3)_2CO$) δ 169.7, 162.5, 159.9, 155.8, 138.8, 116.9, 107.9, 106.8, 87.7, 66.1, 23.9, 14.5; **IR** (thin film, cm^{-1}) 3114, 2980, 2933, 1673, 1609, 1554, 1470, 1452**; HRMS** (ESI) *m/z* calculated for $C_{24}H_{23}O_8^+$ $[M+H]^+$ 439.1387, found 439.1398

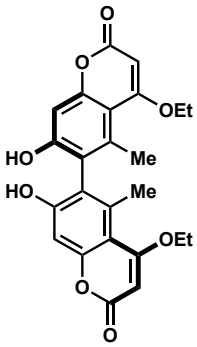

4,4'-diethoxy-7,7'-dihydroxy-5,5'dimethyl-*2H*,*2H'*-[6,6'-bichromene]-2,2'-dione (30): Decomposition 276.4-277.5 °C; R_f = 0.24 (8:3:1 toluene/EtOAc/formic acid v/v); **^{1}H NMR** (600 MHz, CD_3OD) δ 6.71 (s, 2H), 5.61 (s, 2H), 4.23 (q, *J* = 7.0, 4H), 2.33 (s, 6H), 1.50 (t, *J* = 7.9, 6H); **^{13}C NMR** (150 MHz, CD_3OD) δ 171.7, 166.0, 160.3, 157.3, 139.4, 124.4, 108.3, 101.5, 87.8, 67.0, 19.5, 14.5; **IR** (thin film, cm^{-1}) 3229, 2985, 2941, 1690, 1591, 1558, 1450; **HRMS** (ESI) *m/z* calculated for $C_{24}H_{23}O_8^+$ $[M+H]^+$ 439.1387, found 439.1392.

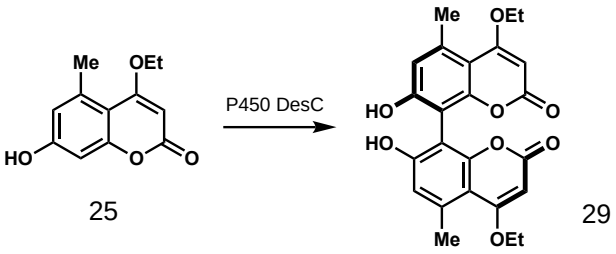

25 29

Supplemental Figure S2.12.

4,4'-diethoxy-7,7'-dihydroxy-5,5'dimethyl-*2H*,*2H'*-[8,8'-bichromene]-2,2'-dione (29): Cultures containing DesC were grown to an optical density at 600 nm of 15. The biotransformation on 0.1 mmol substrate was halted after 63 h. The cell pellet was separated from the supernatant and frozen with liquid nitrogen. The aqueous supernatant was partially concentrated under reduced pressure, acidified with 1 M HCl (5 mL), and extracted with EtOAc (3x). The organic layers were combined, washed with brine, dried over Na_2SO_4, filtered, and evaporated under reduced pressure. The pellet was ground with a cold mortar and pestle (chilled at –78 °C) and extracted with EtOAc by stirring for 2 h. The organic layer was decanted, washed with brine, dried over Na_2SO_4, filtered, and evaporated under reduced pressure. The crude solids were purified by reversed-phase HPLC (Phenomenex Kinetex 5 µm C18, 150 x 21.2 mm column) under the following conditions: mobile phase A = deionized water + 0.1% formic acid and B = acetonitrile + 0.1% formic acid; method = 70% A for 5 min, 70% A to 65% A over 2.0 min, 65% A for 5 min, 65% A to 60% A over 2.0 min, 60% A for 5 min, 60% A to 40% A over 5 min, 40% A for 5 min, 254 and 308 nm UV detection and 12 mL/min flow rate. A retention time of 15.14-17.70 min afforded 1.1 mg of the title compound **31** (5% yield). **^{1}H NMR** (600 MHz, CD_3OD) δ 6.75 (s, 2H), 5.56 (s, 2H), 4.24 (q, *J* = 7.2, 4H), 2.71 (s, 6H), 1.55 (t, *J* = 7.2, 6H); **HRMS** (ESI) *m/z* calculated for $C_{24}H_{23}O_8^+$ $[M+H]^+$ 439.1387, found 439.1394.

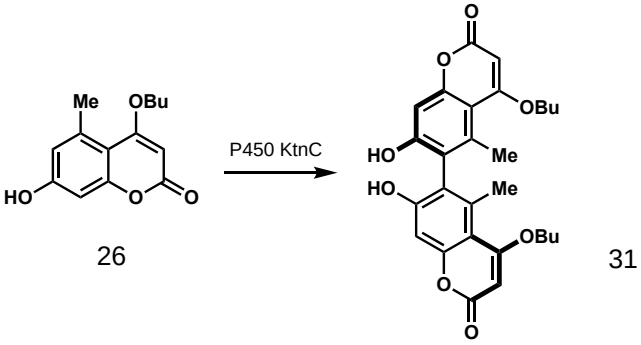

26 31

Supplemental Figure S2.13.

4,4'-butoxy-7,7'-dihydroxy-5,5'dimethyl-*2H*,*2H'*-[6,6'-bichromene]-2,2'-dione (31):

Cultures containing KtnC were grown to an optical density at 600 nm of 9. The biotransformation on 0.2 mmol substrate was halted after 55.8 h. The cell pellet was separated from the supernatant and frozen with liquid nitrogen. The aqueous supernatant was partially concentrated under reduced pressure, acidified with 1 M HCl (5 mL), and extracted with EtOAc (3x). The organic layers were combined, washed with brine, dried over Na_2SO_4, filtered, and evaporated under reduced pressure. The pellet was ground with a cold mortar and pestle (chilled at –78 °C) and extracted with EtOAc by stirring for 2 h. The organic layer was decanted, washed with brine, dried over Na_2SO_4, filtered, and evaporated under reduced pressure. The crude solids were purified by reversed-phase HPLC (Phenomenex Kinetex 5 µm C18, 150 x 21.2 mm column) under the following conditions: mobile phase A = deionized water + 0.1% formic acid and B = acetonitrile + 0.1% formic acid; method = 55% A for 5 min, 55% A to 50% A over 1.5 min, 50% A for 5 min, 50% A to 45% A over 1.5 min, 45% A for 5 min, 45% A to 40% A over 1.5 min, 40% A for 3.5 min, 40% A to 30% A over 3 min, 30% A for 4 min, 254 and 308 nm UV detection and 14 mL/min flow rate. A retention time of 20.42-21.15 min afforded 1.1 mg of the title compound **33** (2% yield) with minor impurities. R_f = 0.34 (8:3:1 toluene/EtOAc/formic acid v/v); **^{1}H NMR** (600 MHz, CD_3OD) δ 6.72 (s, 2H), 5.63 (s, 2H), 4.19 (t, *J* = 6.3, 4H), 2.33 (s, 6H), 1.87 (q, *J* = 7.0, 6.5, 4H, 1.54 (q, *J* =7.7, 4H), 1.00 (t, *J* = 7.4, 6H); **^{1}H NMR** (700 MHz, $(CD_3)CO$) δ 6.75 (s, 2H), 5.54 (s, 2H), 4.21 (t, *J* = 6.4, 4H), 2.36 (s, 6H), 1.88 (p, *J* = 6.6, 4H), 1.60-1.51 (m, 4H), 0.98 (t, *J* = 7.4, 6H); **^{13}C NMR** (175 MHz, $(CD_3)CO$) δ 169.9, 162.4, 159.5, 157.1, 138.8, 122.9, 108.3, 101.7, 88.4, 70.3, 31.4, 20.1, 19.5, 14.0; **IR** (thin film, cm^{-1}) 3401, 2957, 2930, 1587, 1451; **HRMS** (ESI) *m/z* calculated for $C_{28}H_{31}O_8^+$ $[M+H]^+$ 495.2013, found 495.2024.

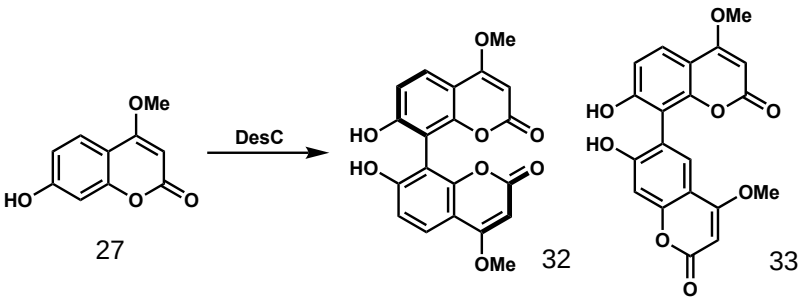

27 32 33

Supplemental Figure S2.14.

DesC dimerization of 7-hydroxy-4-methoxy-*2H*-chromen-2-one (27):

Cultures were grown to an optical density at 600 nm of 13.2. The biotransformation on 0.2 mmol substrate was halted after 95 h. The cell pellet was separated from the supernatant and frozen with liquid nitrogen. The aqueous supernatant was partially concentrated under reduced pressure, acidified with 1 M HCl (5 mL), and extracted with IPA and EtOAc (3x). The organic layers were combined, washed with brine, dried over Na_2SO_4, filtered, and evaporated under reduced pressure. The pellet was ground with a cold mortar and pestle (chilled at –78 °C) and extracted with IPA and EtOAc by stirring for 2 h. The organic layer was decanted, washed with brine, dried over Na_2SO_4, filtered, and evaporated under reduced pressure. The crude solids were purified by flash column chromatography (8:3:1 toluene/EtOAc/formic acid v/v) then reversed-phase (Phenomenex Kinetex 5 µm C18, 150 x 21.2 mm column) under the following conditions: mobile phase A = deionized water + 0.1% formic acid and B = acetonitrile + 0.1% formic acid; method = 80% A for 5 min, 80% A to 75% A over 2.5 min, 75% A for 5 min, 75% A to 70% A over 2.5 min, 70% A for 5 min, 70% A to 50% A over 5 min, 254 and 308 nm UV detection and **2** mL/min flow rate. A retention time of 13.41-15.06 min afforded 1.1 mg of the 8,8’ product **32** (3% yield), and a retention time of 19.28-20.27 afforded 0.3 mg of 6,8’ product **33** (1% yield).

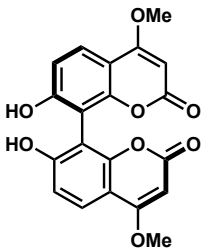

7,7'-dihydroxy-4,4'-dimethoxy-*2H*,*2H'*-[8,8'-bichromene]-2,2'-dione (32):

^{1}H NMR (400 MHz, CD_3OD) δ 7.80 (d, *J* = 8.8, 2H), 6.95 (d, *J* = 8.8, 2H), 5.64 (s, 2H), 4.05 (s, 6H); **HRMS** (ESI) *m/z* calculated for $C_{20}H_{15}O_8^+$ $[M+H]^+$ 383.0761, found 383.0765.

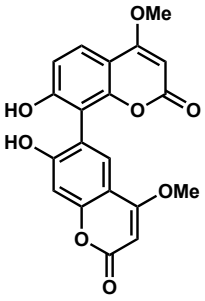

7,7'-dihydroxy-4,4'-dimethoxy-*2H*,*2H'*-[6,8'-bichromene]-2,2'-dione (33):

^{1}H NMR (400 MHz, $(CD_3)_2CO$) δ 7.70 (d, *J* = 8.8, 1H), 7.66 (s, 1H), 6.97 (d, *J* = 8.8, 1H), 6.84 (s, 1H), 5.59 (s, 1H), 5.56 (s, 1H), 4.05 (s, 3H), 4.02 (s, 3H); **HRMS** (ESI) *m/z* calculated for $C_{20}H_{15}O_8^+$ $[M+H]^+$ 383.0761, found 383.0768.

Synthetic modifications after biotransformation to access product standards

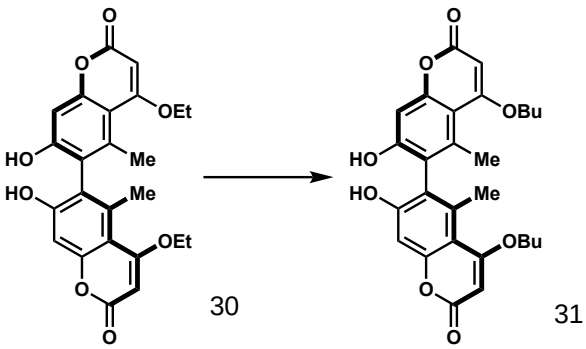

Supplemental Figure S2.15.

4,4'-butoxy-7,7'-dihydroxy-5,5'dimethyl-*2H*,*2H'*-[6,6'-bichromene]-2,2'-dione (31):

To a suspension of 4,4'-diethoxy-7,7'-dihydroxy-5,5'-dimethyl-*2H, 2H'*-[6,6'-bichromene]-2,2'-dione (**30**, 1.0 mg, 0.002 mmol, 1.0 equiv) in *n*BuOH (400 µL) was added ground 3 Å molecular sieves and H_2SO_4 (10 µL). The reaction was heated at 75 °C for 12.2 h. The reaction was quenched by diluting with EtOAc and pouring into water. The aqueous layer was extracted with EtOAc (3 x), washed with brine, dried over Na_2SO_4, filtered, and evaporated under reduced pressure. The crude solids were purified by reversed-phase HPLC (Phenomenex Kinetex 5 µm C18, 150 x 21.2 mm column) under the following conditions: mobile phase A = deionized water + 0.1% formic acid and B = acetonitrile + 0.1% formic acid; method = 55% A for 5 min, 55% A to 50% A over 1.5 min, 50% A for 5 min, 50% A to 45% A over 1.5 min, 45% A for 5 min, 45% A to 40% A over 1.5 min, 40% A for 3.5 min, 40% A to 30% A over 3 min, 30% A for 4 min, 254 and 308 nm UV detection and 14 mL/min flow rate. The 6,6'-product **31** eluted from 19.1-22.9 min to provide 0.1 mg (10% yield) with minor impurities. **^{1}H NMR** (600 MHz, $(CD_3)CO$) δ 6.74 (s, 2H), 5.55 (s, 2H), 4.21 (t, *J* = 6.3, 4H), 2.36 (s, 6H), 1.92-1.85 (m, 4H), 1.60-1.50 (m, 4H), 0.98 (t, *J* = 7.4, 6H); **HRMS** (ESI) *m/z* calculated for $C_{28}H_{31}O_8^+$ $[M+H]^+$ 495.2013, found 495.2023. Full characterization of 6,6'-product **33** can be found on page S248.

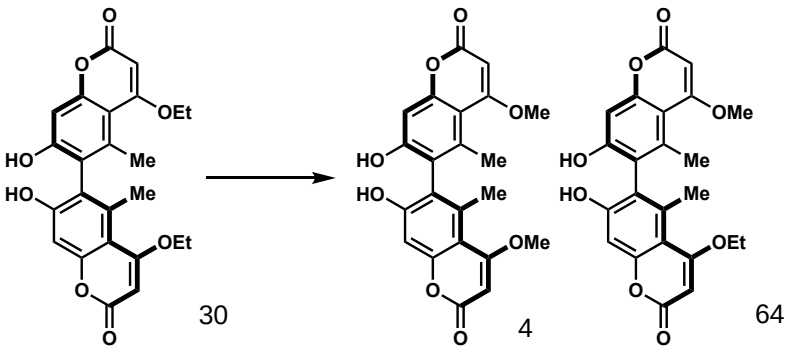

Supplemental Figure S2.16.

Transesterification with 4,4'-diethoxy-7,7'-dihydroxy-5,5'dimethyl-*2H*,*2H'*-[6,6'-bichromene]-2,2'-dione (31): To a suspension of 4,4'-diethoxy-7,7'-dihydroxy-5,5'-dimethyl-*2H, 2H'*-[6,6'-bichromene]-2,2'-dione (**31**, 10.0 mg, 0.023 mmol, 1.0 equiv) in MeOH (2.5 mL) and EtOH (2.5 mL) was added ground 3 Å molecular sieves (40.0 mg) and H_2SO_4 (250 µL). The reaction was heated at 75 °C for 10.6 h. The reaction was quenched by diluting with EtOAc and pouring into water. The aqueous layer was extracted with EtOAc (3x), washed with brine, dried over Na_2SO_4, filtered, and evaporated under reduced pressure. The crude solids were purified by reversed-phase (Phenomenex Kinetex 5 µm C18, 150 x 21.2 mm column) under the following conditions: mobile phase A = deionized water + 0.1% formic acid and B = acetonitrile + 0.1% formic acid; method = 70% A for 5 min, 70% A to 65% A over 2.0 min, 65% A for 5.0 min, 65% A to 60% A over 2.0 min, 60% A for 5.0 min, 60% A to 40% A over 5.0 min, 40% A for 2.0 min, 40% A to 10% A over 4.0 min, 10% A for 1.0 min, 254 and 308 nm UV detection and 12 mL/min flow rate. A retention time of 12.05-14.55 min afforded 1.5 mg of 6,6' product **4** (16% yield), and a retention time of 16.57-19.55 afforded 2.0 mg of 6,6' cross-product **64** (20% yield).

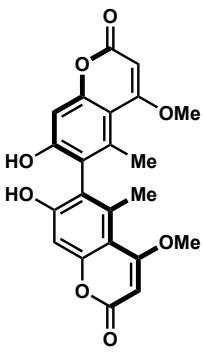

7,7’-dihydroxy-4,4’-dimethoxy-5,5’-dimethyl-*2H*,*2H’*-[6,6’-bichromene]-2,2’-dione (4): ^{1}H NMR (400 MHz, CD_3OD) δ 6.71 (s, 2H), 5.65 (s, 2H), 3.99 (s, 6H), 2.30 (s, 6H); **HRMS** (ESI) *m/z* calculated for $C_{22}H_{19}O_8^+$ $[M+H]^+$ 411.1074, found 411.0990. All spectra obtained were in agreement with literature values.[89]

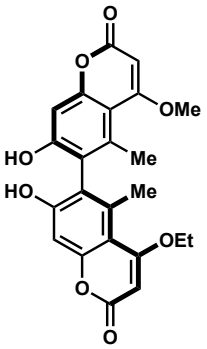

4-ethoxy-7,7'-dihydroxy-4'methoxy-5,5'-dimethyl-*2H,2H*'-[6,6'-bichromene]2,2'-dione (64). ^{1}H NMR (600 MHz, CD_3OD) δ 6.71 (s, 2H), 5.65 (s, 1H), 5.61 (s, 1H), 4.24 (q, *J* = 7.0, 2H), 3.99 (s, 3H), 2.33 (s, 3H), 2.30 (s, 3H), 1.51 (t, *J* = 7.0, 3H); **^{13}C NMR** (200 MHz, CD_3OD) δ 172.6 171.7, 166.1, 165.9, 160.4, 160.4, 157.4, 157.3, 139.4, 139.3, 124.4, 108.4, 101.6, 101.5, 87.8, 87.5, 66.9, 56.9, 40.4, 19.4, 19.3, 14.5. **HRMS** (ESI) *m/z* calculated for $C_{23}H_{21}O_8^+$ $[M+H]^+$ 425.1231, found 425.1255.

Calibration curves

Supplemental Figure S2.17 Oxidative dimerization of **1** by KtnC and DesC (**Figure 2.9**).

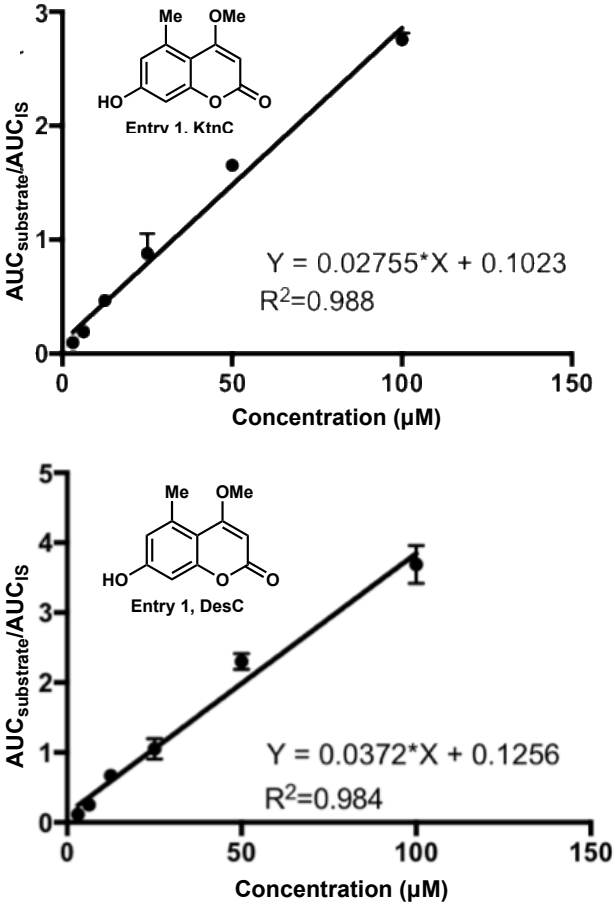

Supplemental Figure S2.18. Oxidative dimerization of **1 by** KtnC (**Figure 2.9**).

Supplemental Figure S2.19. Oxidative dimerization of **1** by DesC (**Figure 2.9**).

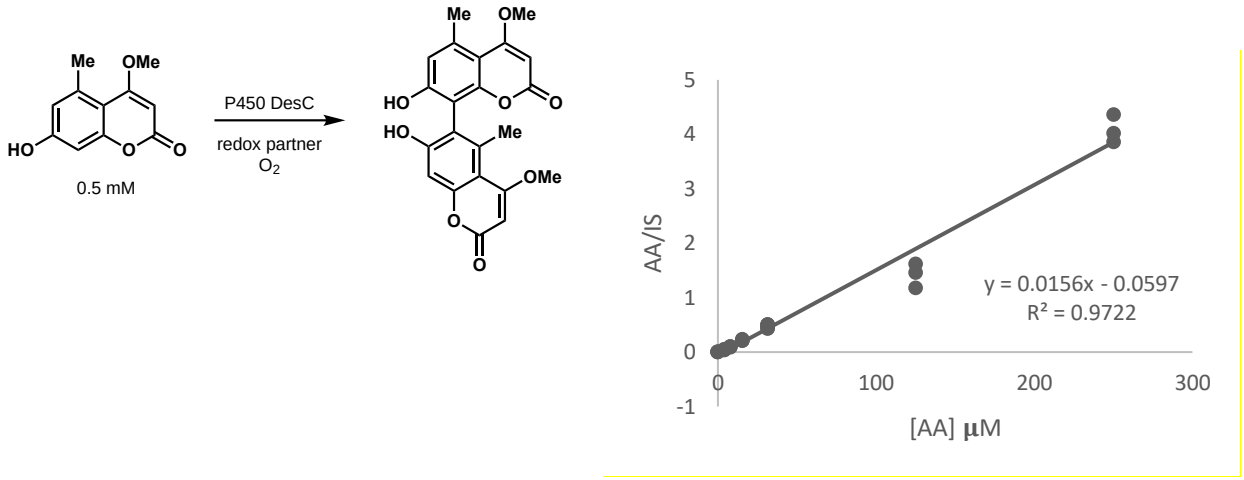

Supplemental Figure S2.20. Oxidative dimerization of **25** by KtnC (**Figure 2.9**).

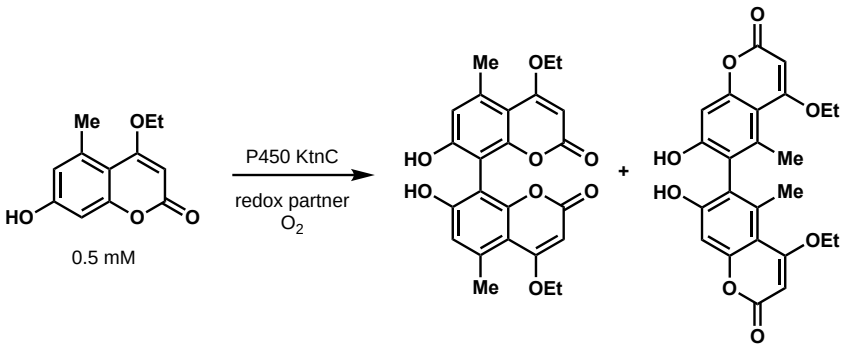

8,8 6,6

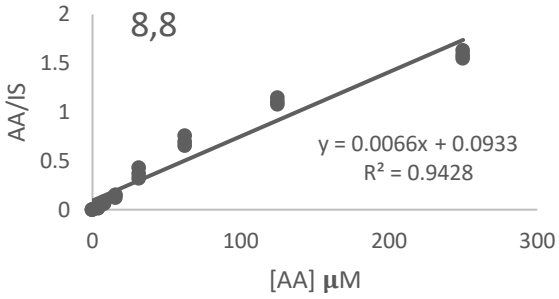

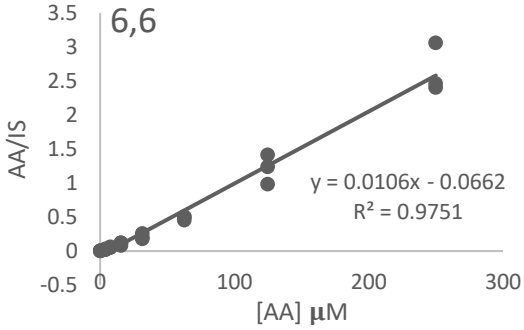

Supplemental Figure S2.21. Oxidative dimerization of **25** by DesC (**Figure 2.9**).

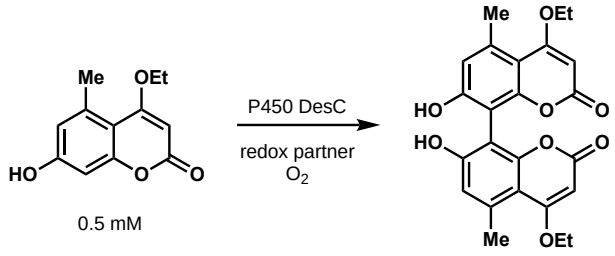

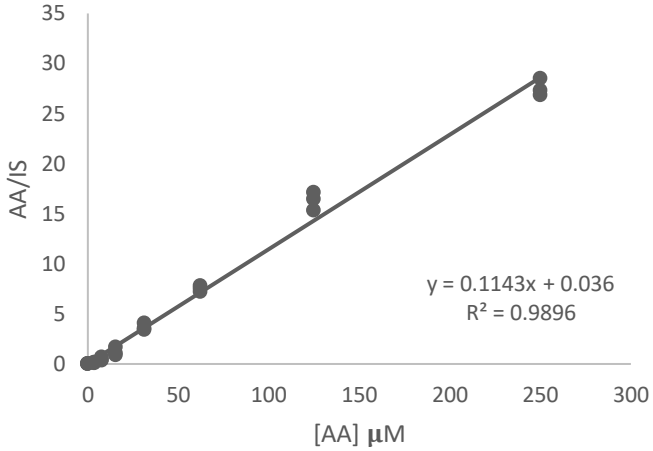

Supplemental Figure S2.22. Oxidative dimerization of **27** by DesC (**Figure 2.9**).

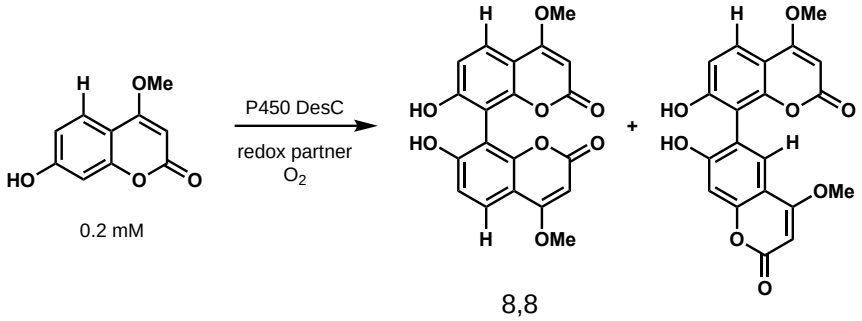

8,8

8,6

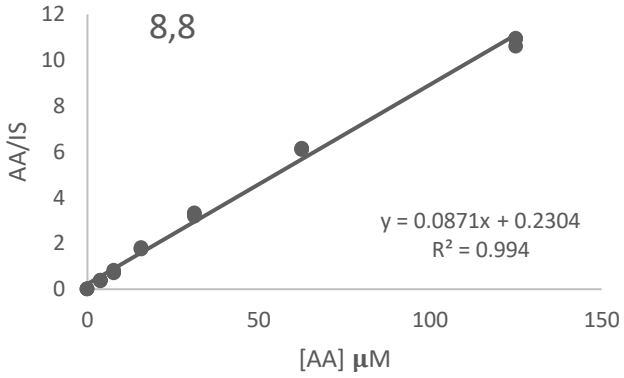

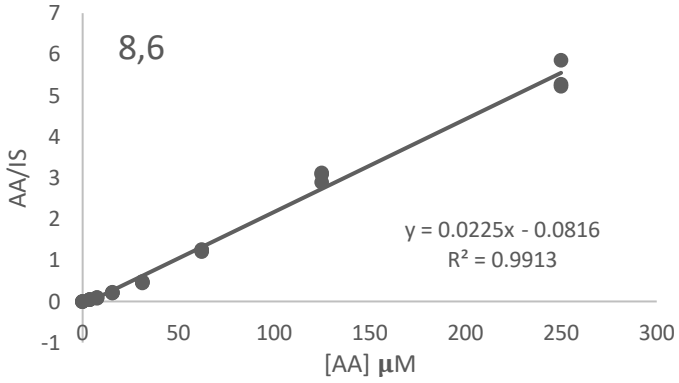

Standard curves for oxidative cross-coupling reactions

Supplemental Figure S2.23. Oxidative cross-coupling of **1** (A) with non-native partner (B) catalyzed by KtnC (Figure 2.17 and 2.18).

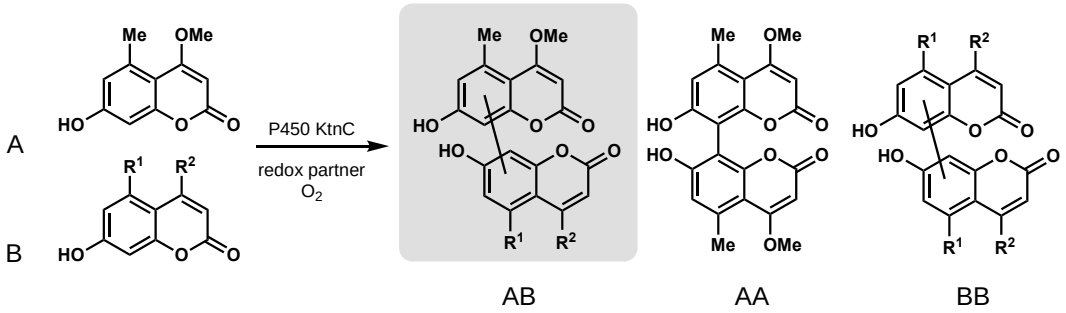

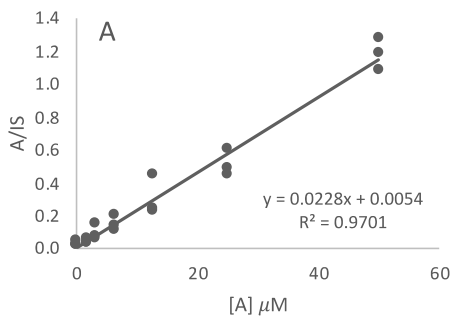

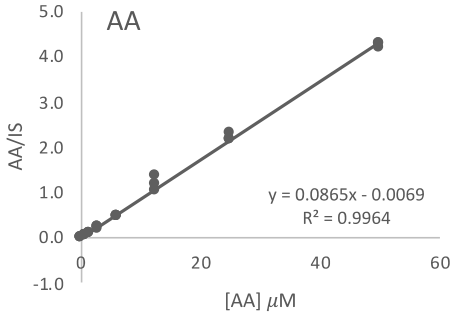

R1	R2	entry #	A/IS	AA/IS	$[A]_{remaining}$	$[AA]_{present}$	AB	% conv AB	average	% conv AA	average
Me	OEt	A1	0.01	0.05	1.67	0.64	22.05	88.19	87.3	5.12	4.7
		A2	0.03	0.04	2.32	0.53	21.62	86.49		4.24	
Me	OPr	A3	0.24	0.21	11.00	2.47	9.06	36.22	37.7	19.79	17.9
		A4	0.24	0.17	11.17	2.01	9.80	39.22		16.10	
Me	OBu	B1	0.07	0.34	3.94	3.96	13.14	52.56	49.7	31.70	34.5
		B2	0.07	0.40	3.97	4.66	11.70	46.80		37.30	

Supplemental Figure S2.24. Oxidative cross-coupling of **1** (A) with non-native partner (B) catalyzed by KtnC (**2.18**).

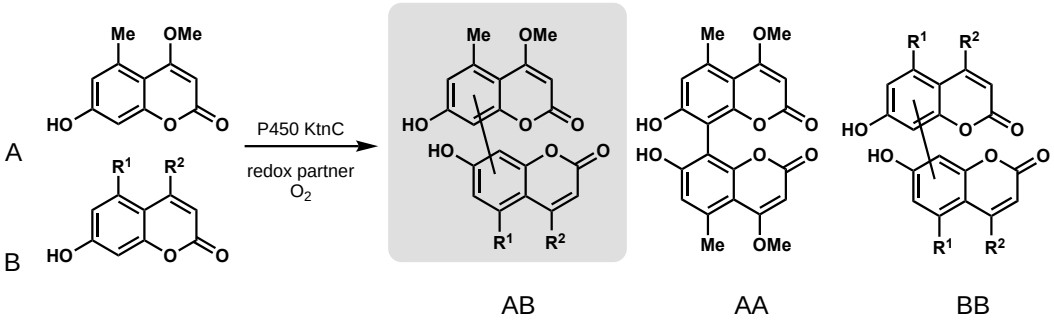

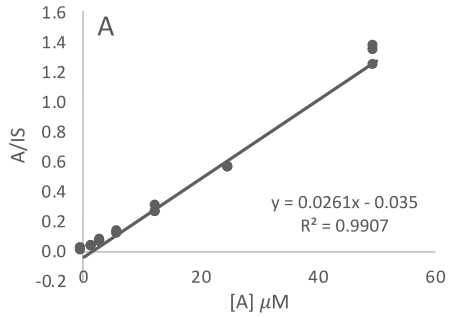

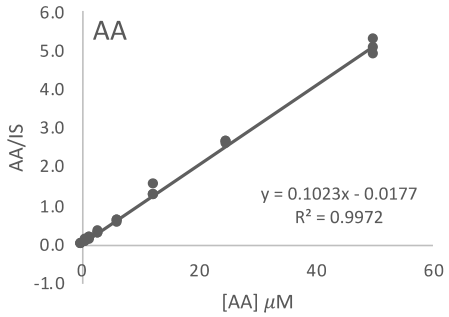

R1	R2	entry #	A/IS	AA/IS	$[A]_{remaining}$	$[AA]_{present}$	AB	% conv AB	average	% conv AA	average
H	OMe	A5	0.156	0.141	7.31570	1.54898	14.586	58.3	67.3	12.4	14.1
		A6	0.016	0.185	1.97117	1.98662	19.056	76.2		15.9	
Cl	OMe	C5	0.515	0.027	21.08830	0.43675	3.038	12.2	21.2	3.5	4.0
		C6	0.391	0.041	16.31739	0.57053	7.542	30.2		4.6	

Supplemental Figure S2.25. Oxidative cross-coupling of **1** (A) with non-native partner (B) catalyzed by KtnC (**Figure 2.11**).

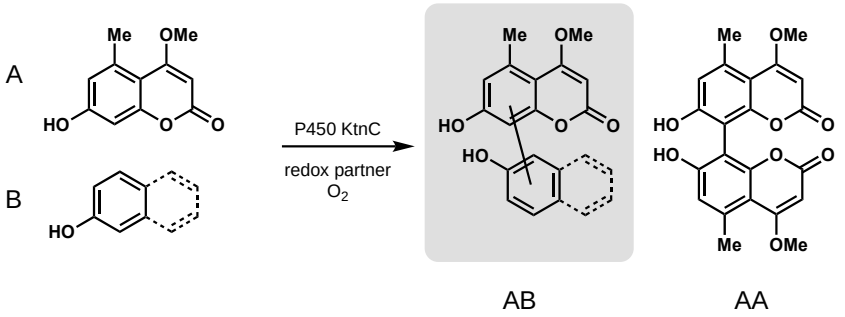

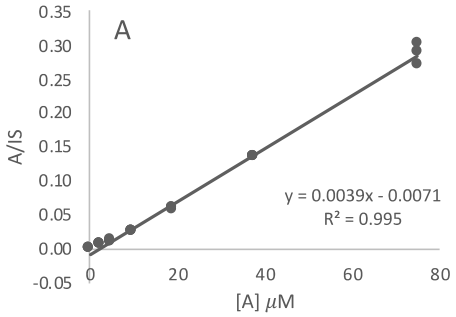

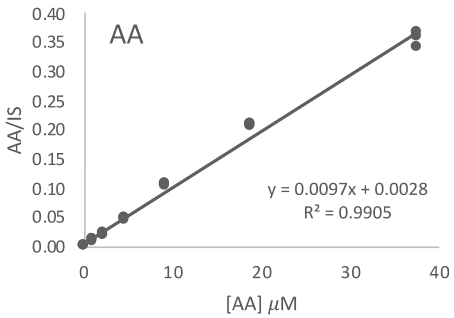

Phenol	entry #	A/IS	AA/IS	$[A]_{remaining}$	$[AA]_{present}$	AB	% conv AB	average	% conv AA	average
quinoline	C3	0.051	0.340	15.02189	34.84561	15.287	15.3	14.2	69.7	72.1
	C4	0.041	0.363	12.31828	37.27717	13.127	13.1		74.6	
2-naphthol	D1	0.121	0.322	33.02458	33.02720	0.921	0.9	2.0	66.1	65.1
	D2	0.119	0.314	32.72324	32.12063	3.035	3.0		64.2	

TOF traces of dimerization biotransformations

Note: Traces are scaled to highest peak in each line.

Data acquired by Dr. Meagan Hinze

Supplemental Figure S2.26. Oxidative dimerization of **1** to **2** by KtnC (**Figure 2.9**). EIC trace of biotransformation and control using separation method A. DAD trace (275 nm) of biotransformation using 1,3,5-trimethoxybenzene as the IS.

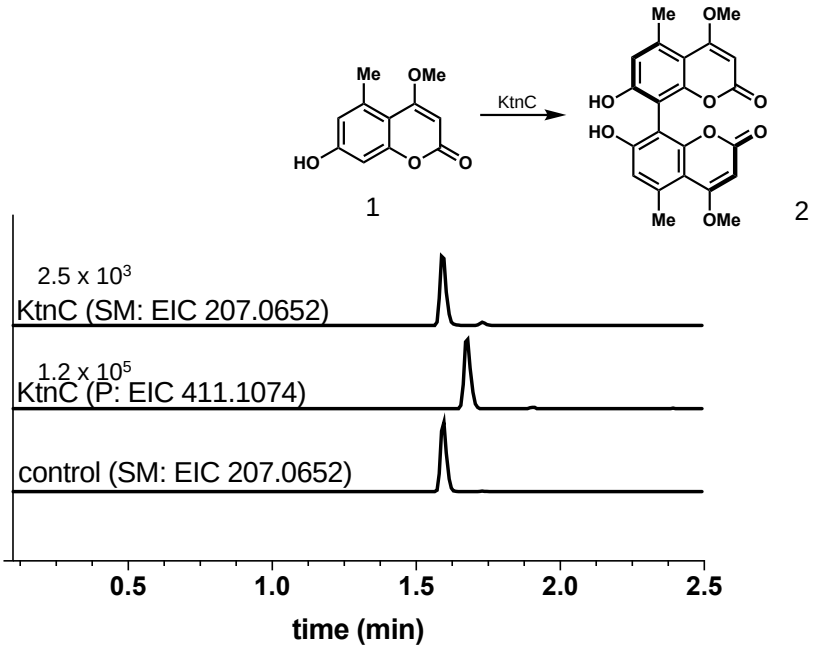

Peak	Ret. Time	Area
1	1.540	0.22
2	1.627	7.95
3	2.100	6.34

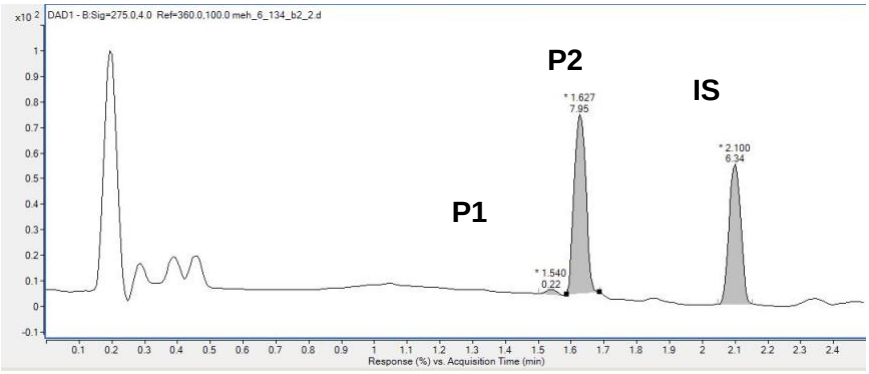

Supplemental Figure S2.27. Oxidative dimerization of **1** to **3** by DesC (**Figure 2.9**). EIC trace of biotransformation and control using separation method A. DAD trace (275 nm) of biotransformation using 1,3,5-trimethoxybenzene as the IS.

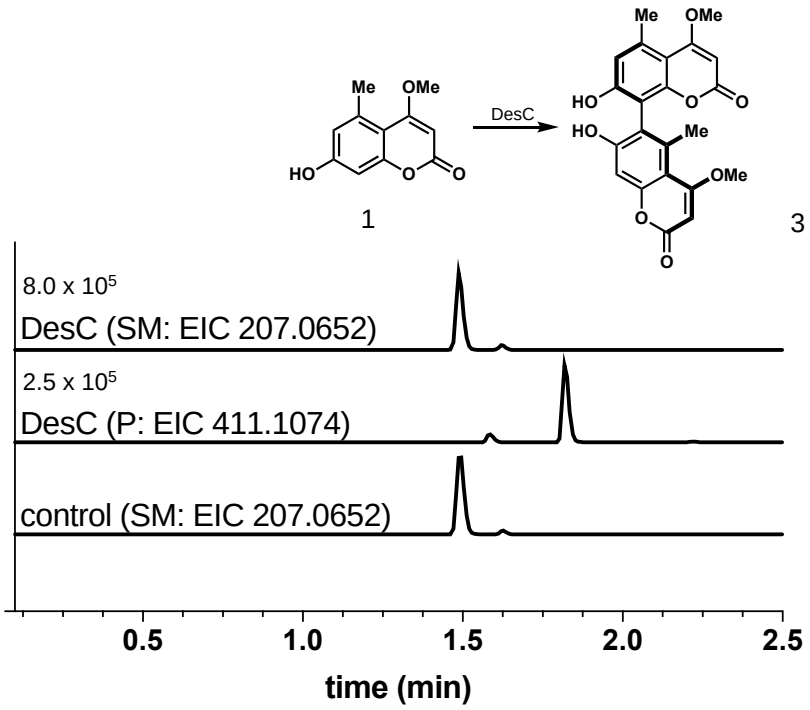

Peak	Ret. Time	Area
1	1.447	7.01
2	1.780	3.42
3	2.000	6.60

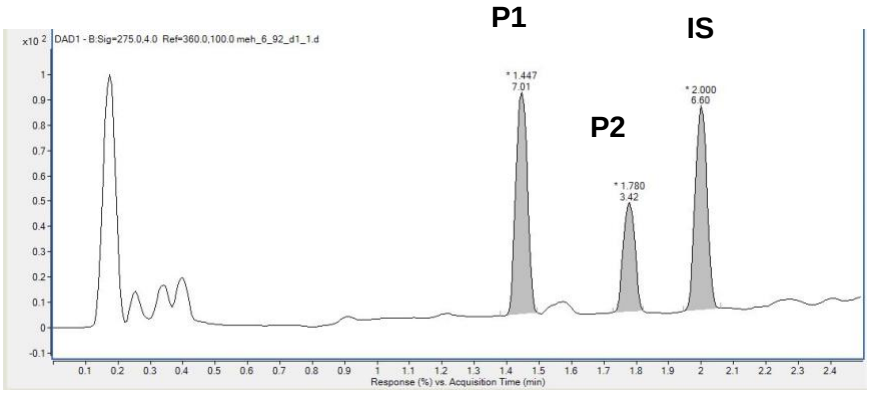

Supplemental Figure S2.28. Oxidative dimerization of **25** to **29** and **30** by KtnC (**Figure 2.9**). EIC trace of biotransformation and control using separation method A. DAD trace (275 nm) of biotransformation using 1,3,5-trimethoxybenzene as the IS.

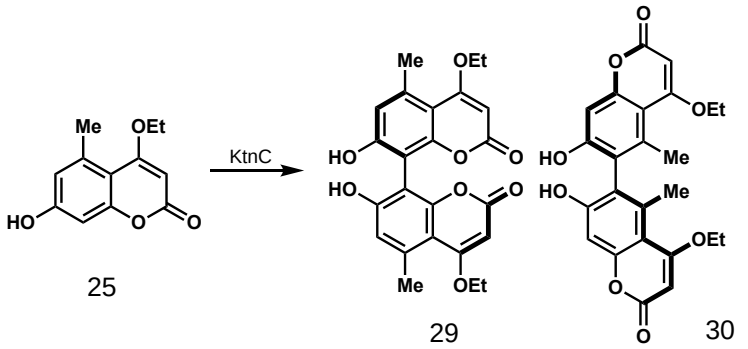

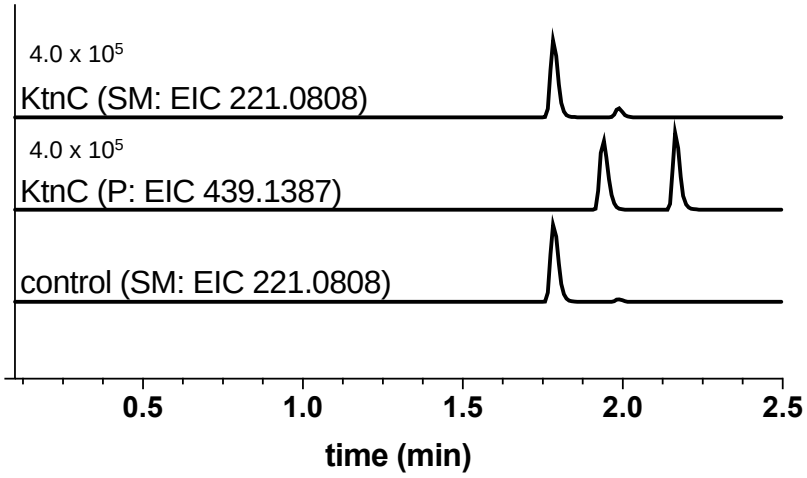

Peak	Ret. Time	Area
1	1.747	2.80
2	1.900	2.52
3	2.007	5.87
4	2.127	1.98

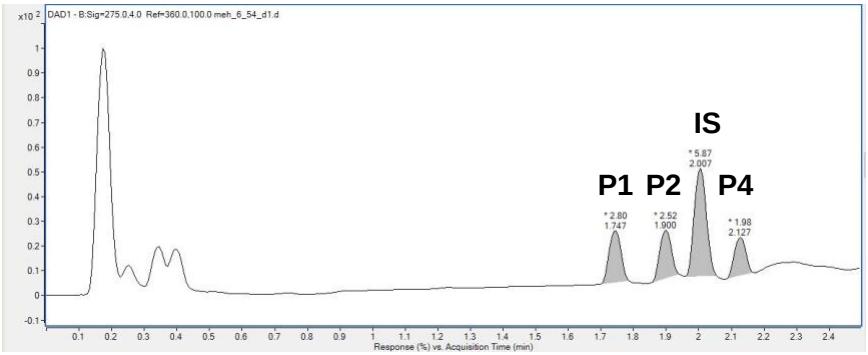

Supplemental Figure S2.29. Oxidative dimerization of **25** to **29** by DesC (**Figure 2.9**). EIC trace of biotransformation and control using separation method A. DAD trace (275 nm) of biotransformation using 1,3,5-trimethoxybenzene as the IS.

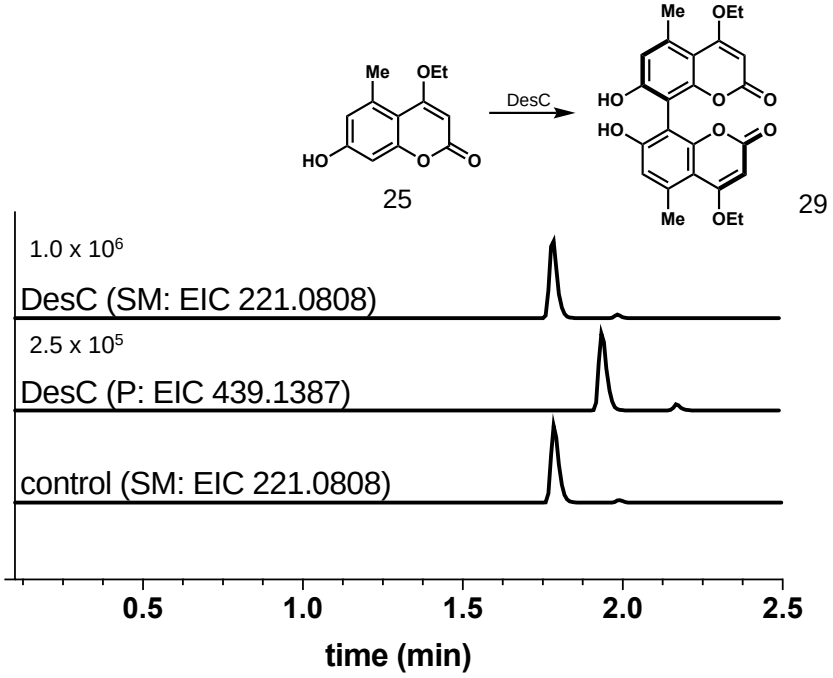

Peak	Ret. Time	Area
1	1.747	8.41
2	1.900	1.27
3	2.007	6.09

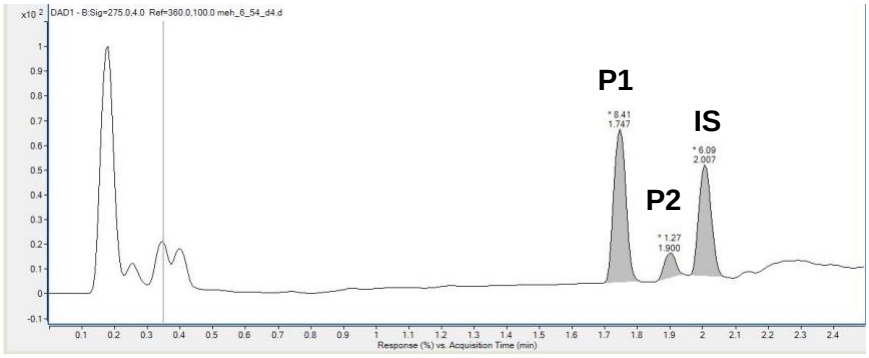

Supplemental Figure S2.30. Oxidative dimerization of **26** to **31** by KtnC (**Figure 2.9**). EIC trace of biotransformation and control using separation method B. DAD trace (275 nm) of biotransformation using 1,3,4,5-tetramethoxybenzene as the IS.

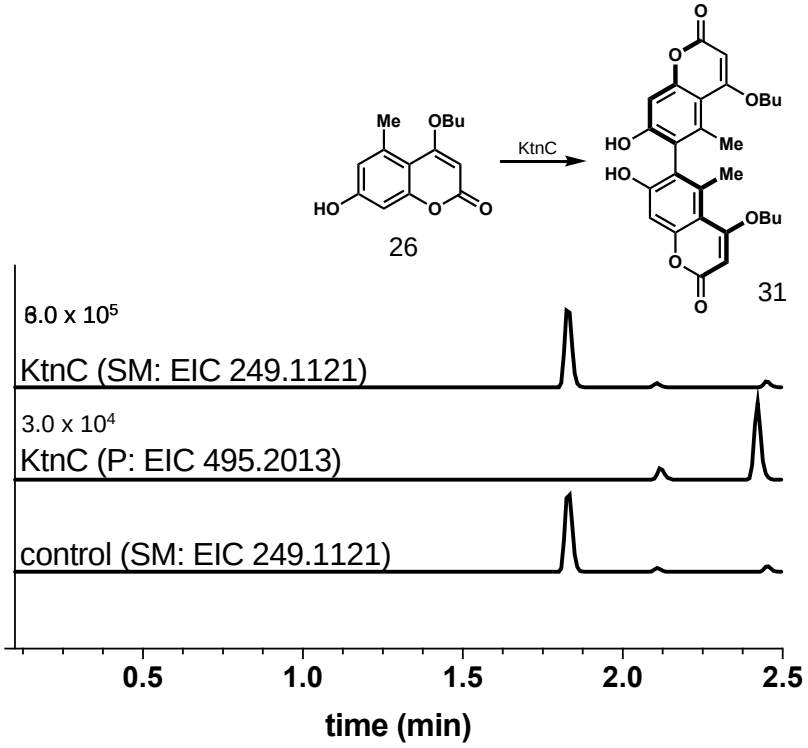

Peak	Ret. Time	Area
1	1.280	31.29
2	1.793	3.95

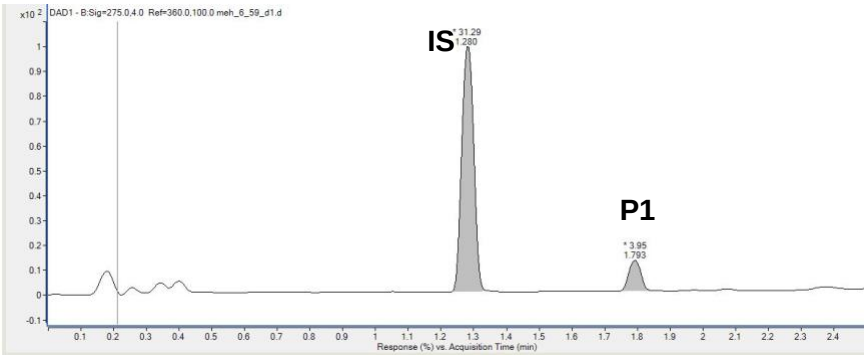

Supplemental Figure S2.31. Oxidative dimerization of **26** to **57** by DesC (**Figure 2.9)**. EIC trace of biotransformation and control using separation method B. DAD trace (275 nm) of biotransformation using 1,3,4,5-tetramethoxybenzene as the IS.

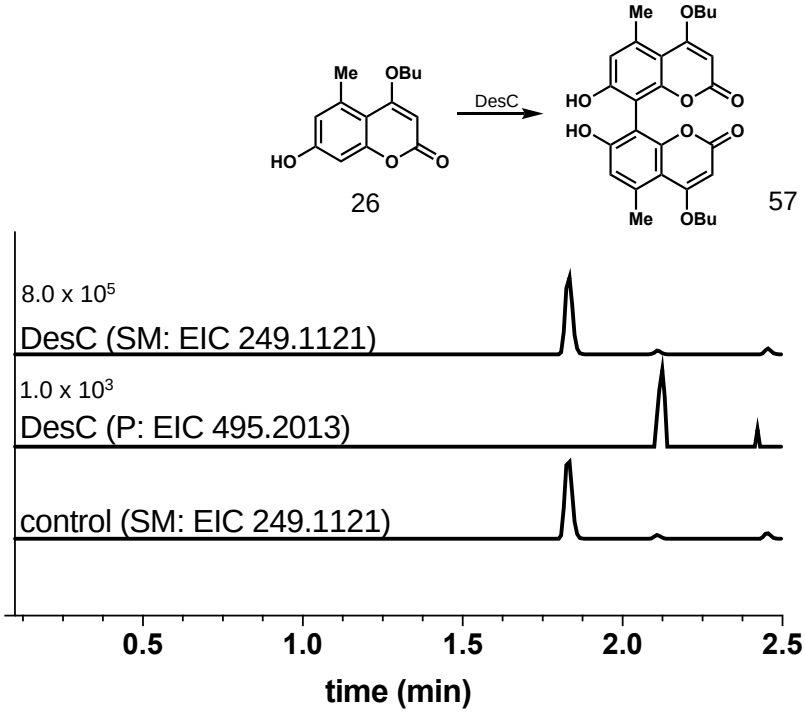

Peak	Ret. Time	Area
1	1.280	30.01
2	1.793	5.15

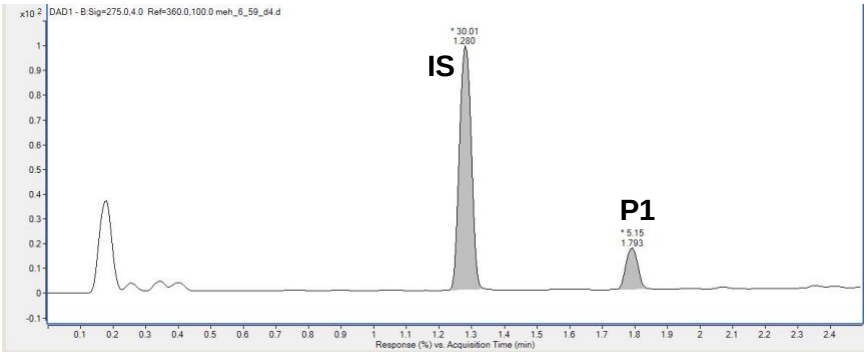

Supplemental Figure S2.32. Oxidative dimerization of **27** to **32** by KtnC (**Figure 2.9**). EIC trace of biotransformation and control using separation method A. DAD trace (275 nm) of biotransformation using 1,3,5-trimethoxybenzene as the IS.

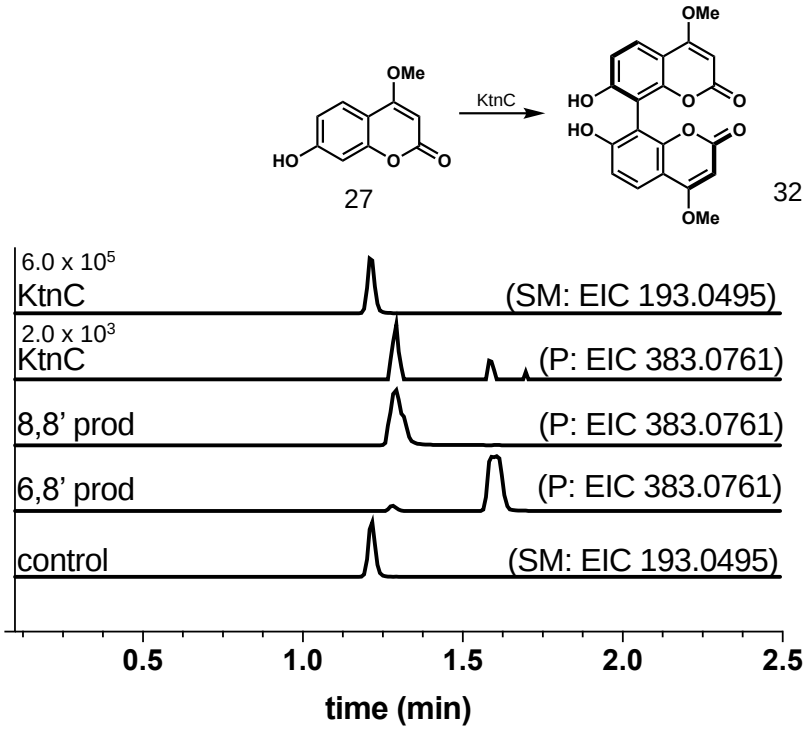

Peak	Ret. Time	Area
1	1.173	7.88
2	2.007	6.53

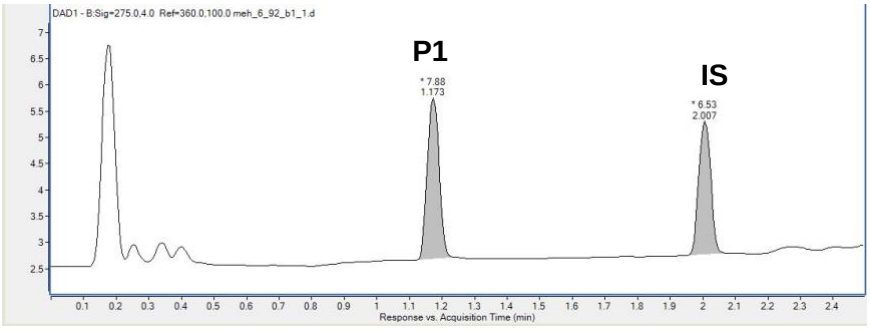

Supplemental Figure S2.33. Oxidative dimerization of **27** to **32** and **33** by DesC (**Figure 2.9**). EIC trace of biotransformation and control using separation method A. DAD trace (275 nm) of biotransformation using 1,3,5-trimethoxybenzene as the IS.

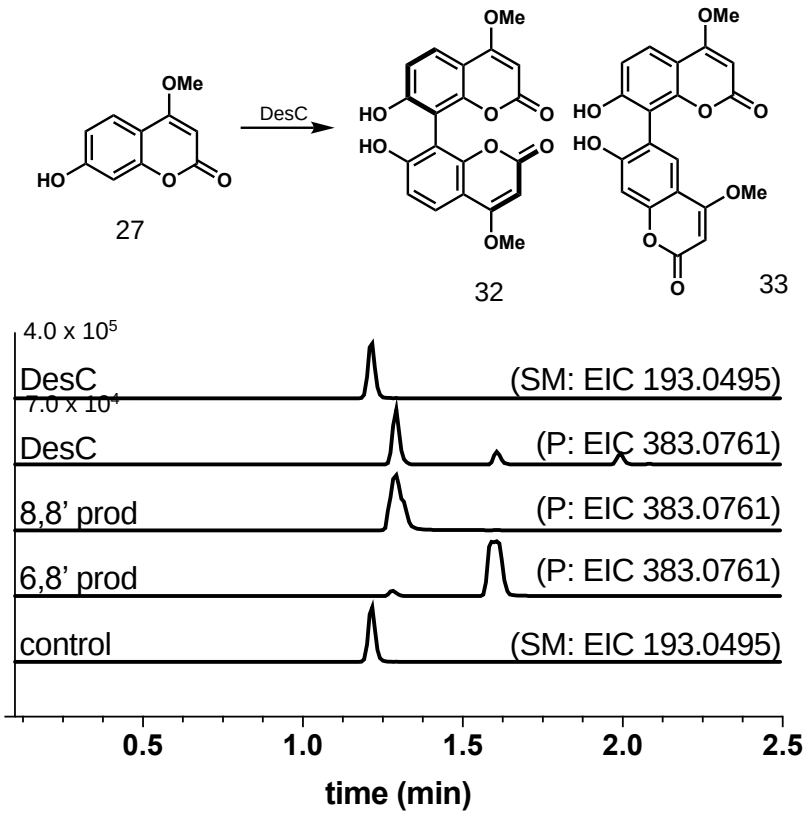

Peak	Ret. Time	Area
1	1.167	3.90
2	1.247	1.32
3	2.007	6.33

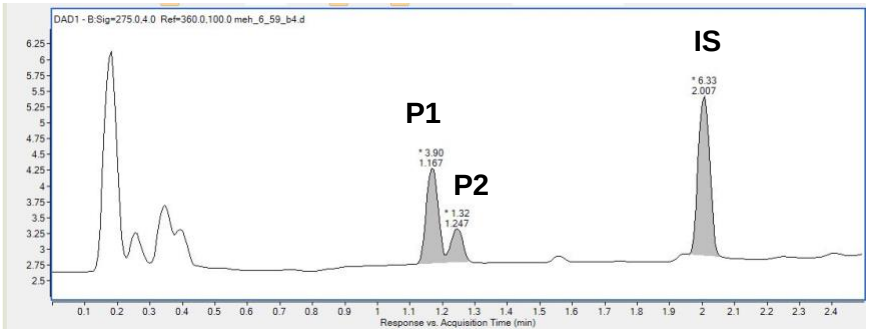

Supplemental Figure S2.34. Oxidative dimerization of **22** by KtnC (**Figure 2.4**). EIC trace of biotransformation and control using separation method A. DAD trace (275 nm) of biotransformation using 1,3,5-trimethoxybenzene as the IS.

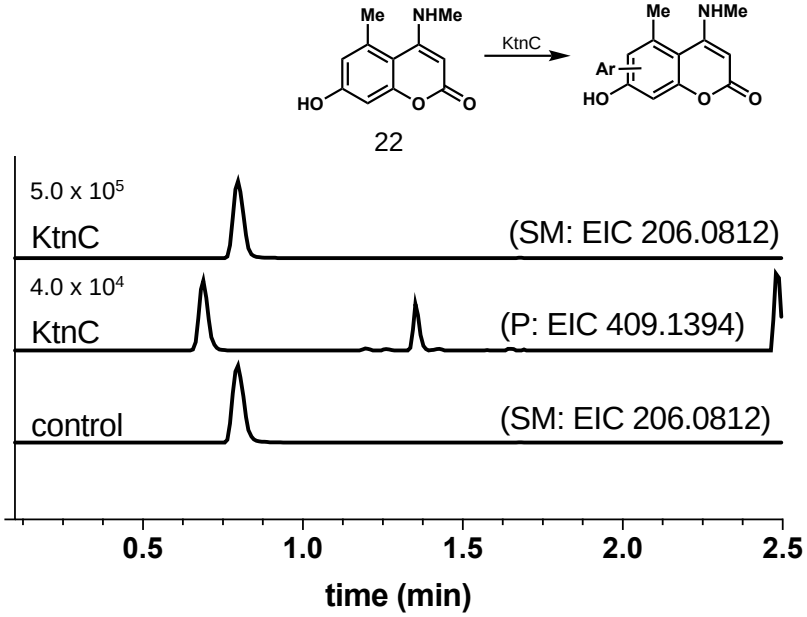

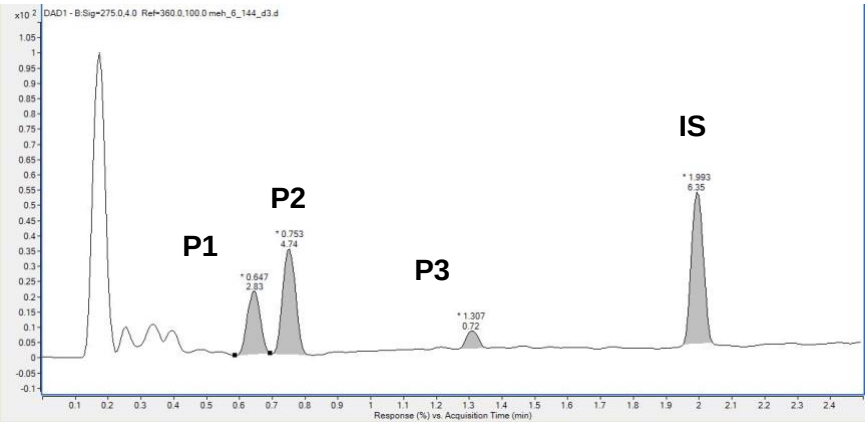

Peak	Ret. Time	Area
1	0.647	2.83
2	0.753	4.74
3	1.307	0.72
4	1.993	6.35

Supplemental Figure S2.35. Oxidative dimerization of **23** by KtnC (**Figure 2.4**). EIC trace of biotransformation and control using separation method A. DAD trace (308 nm and 275 nm) of biotransformation using 1,3,4,5-tetramethoxybenzne as the IS.

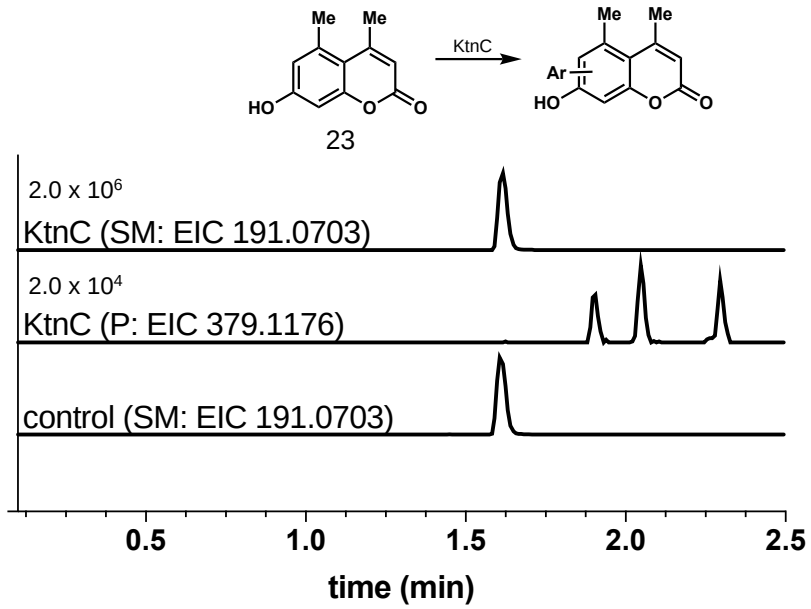

Peak	Ret. Time	Area
1	1.567	28.14
2	1.693	29.96

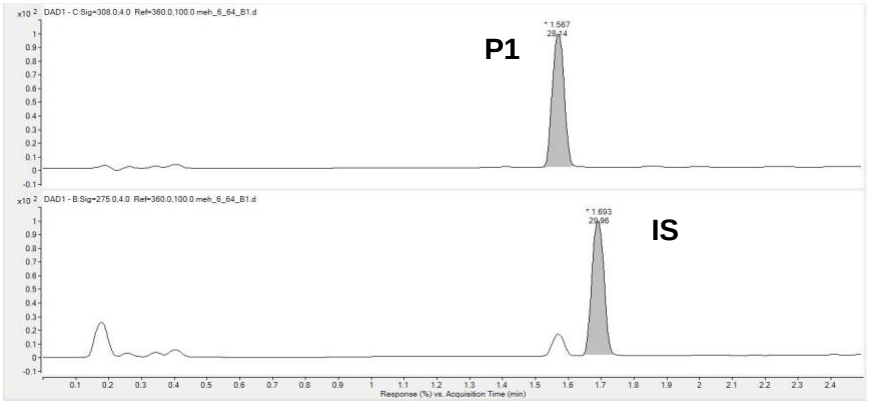

Supplemental Figure S2.36. Oxidative dimerization of **21** by KtnC (**Figure 2.4**). EIC trace of biotransformation and control using separation method A. DAD trace (275 nm and 308 nm) of biotransformation using 1,3,5-trimethoxybenzene as the IS.

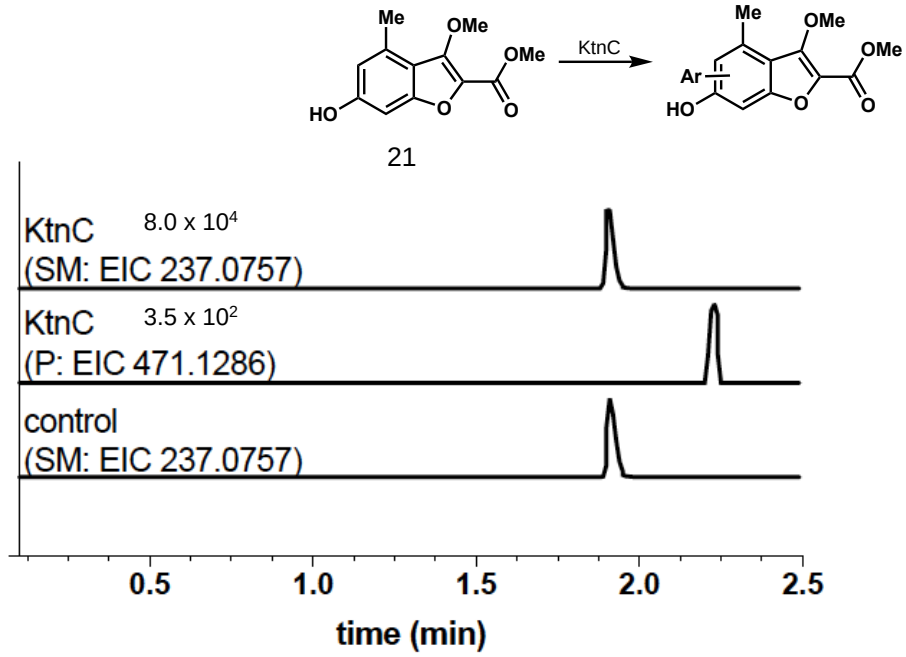

Peak	Ret. Time	Area
1	1.87	39.41
2	1.99	6.49

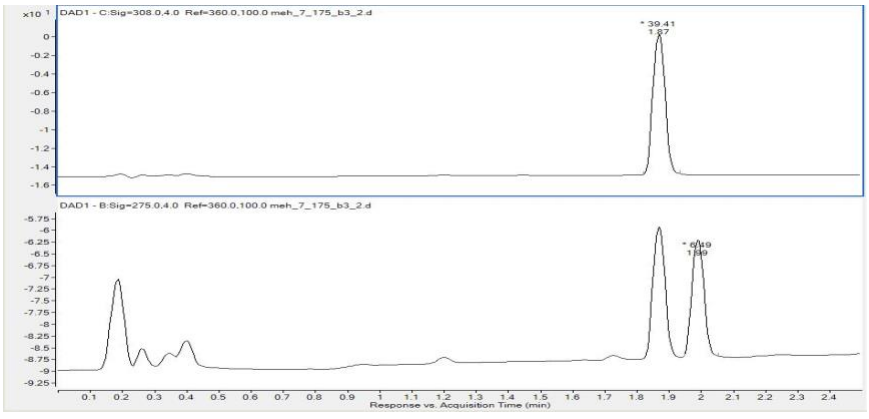

Supplemental Figure S2.37. Oxidative dimerization of **21** by DesC (**Figure 2.4**). EIC trace of biotransformation and control using separation method A. DAD trace (275 nm and 308 nm) of biotransformation using 1,3,5-trimethoxybenzene as the IS.

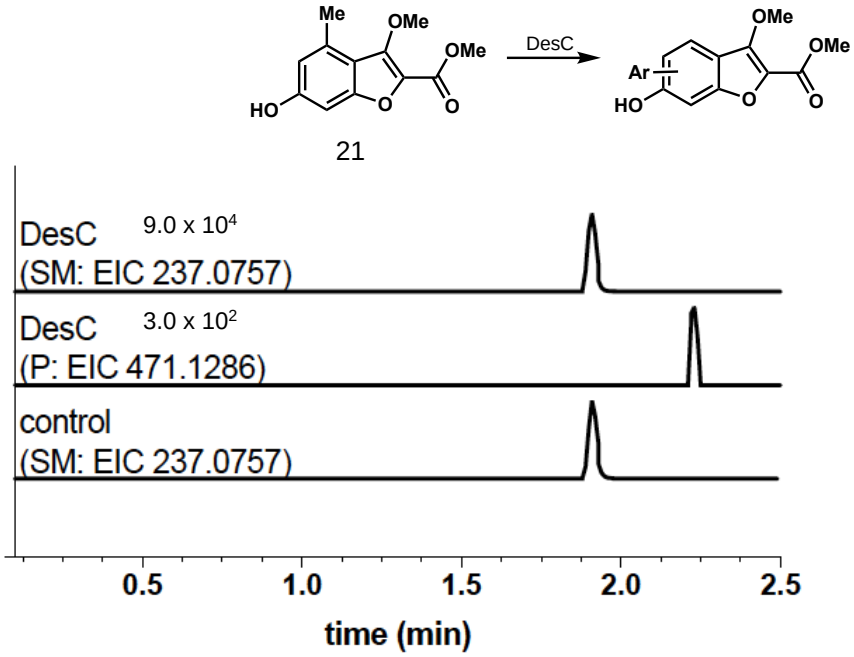

Peak	Ret. Time	Area
1	1.87	33.77
2	1.99	6.73

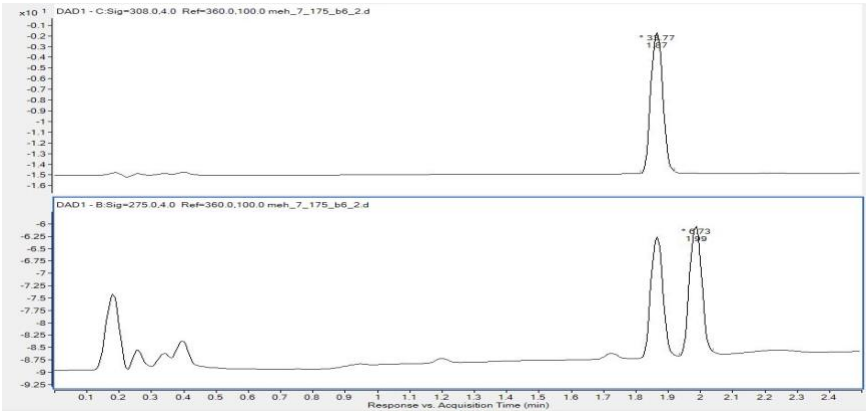

Supplemental Figure S2.38. Complementary site-selectivity of KtnC and DesC in the oxidative dimerization of **21**.

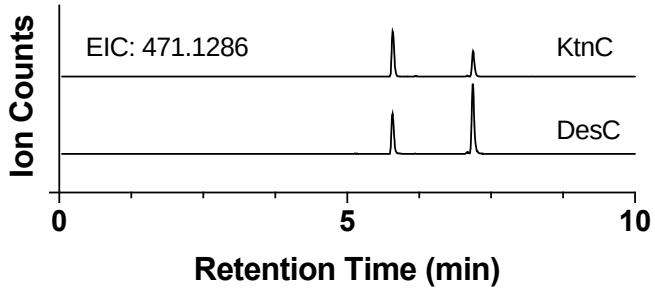

TOF traces for oxidative cross-coupling biotransformations

EIC's shown for starting materials and products.

Supplemental Figure S2.39. Oxidative cross-coupling of **1** and **25** by KtnC. (**Figure 2.17**).

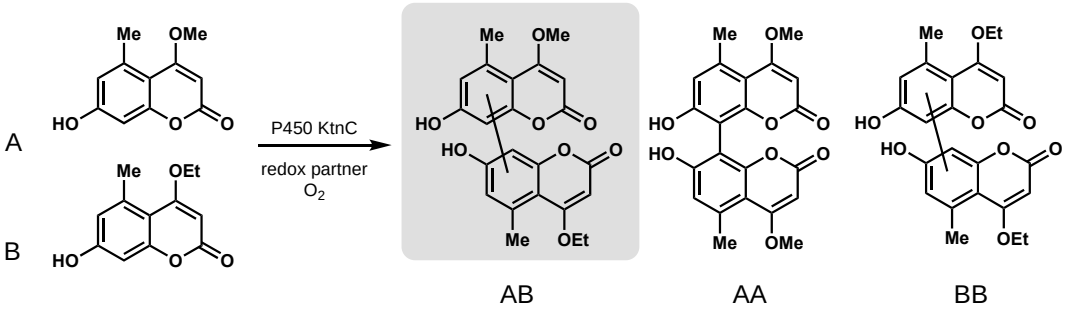

KtnC

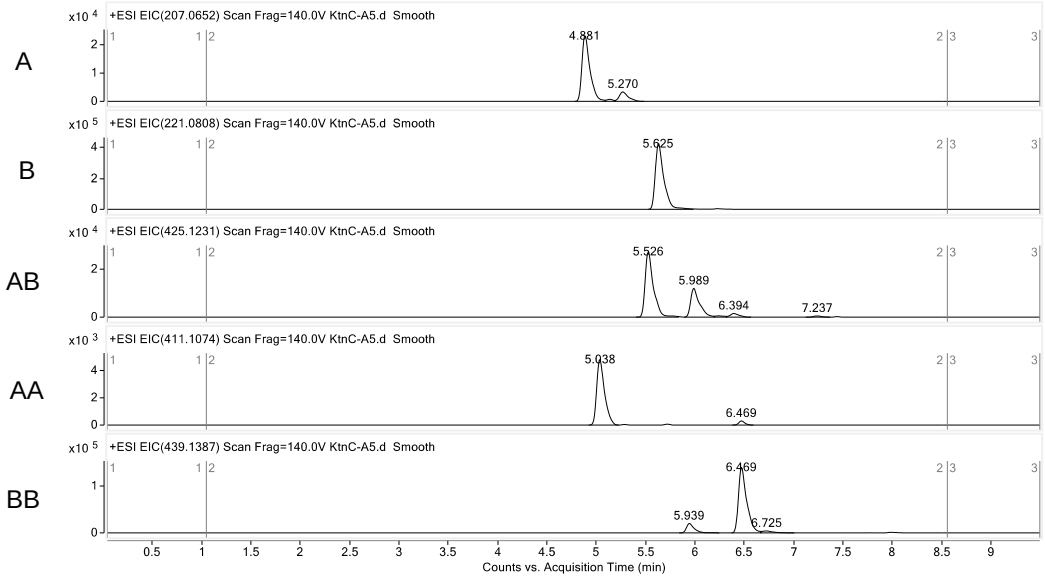

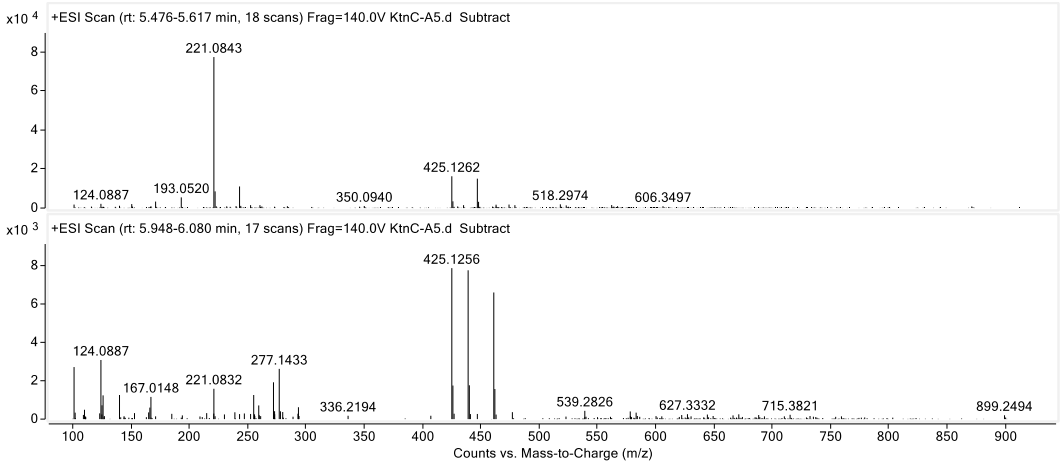

No Enzyme control

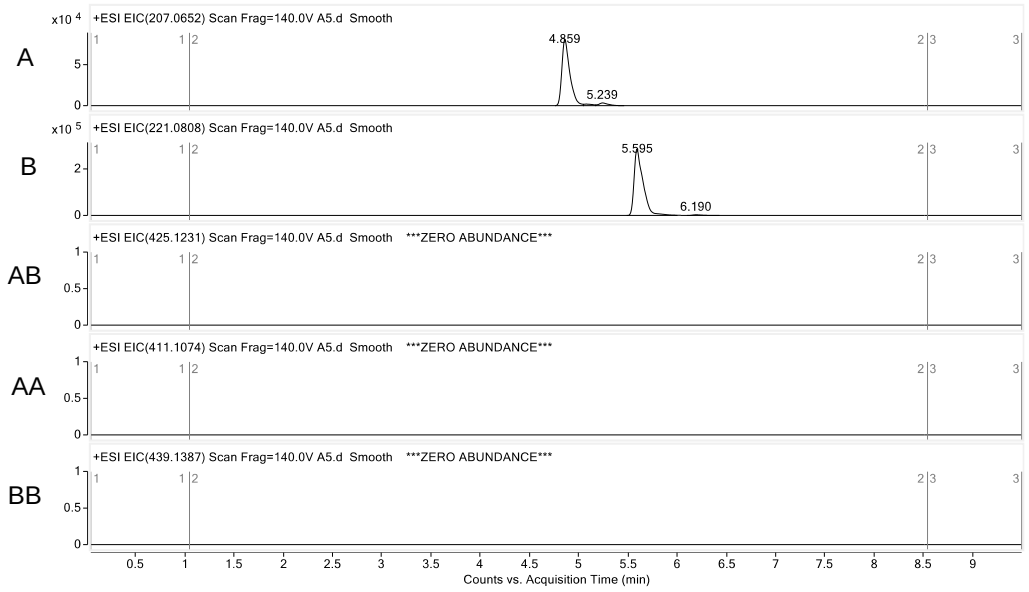

Supplemental Figure S2.40. Oxidative cross-coupling of **1** and **18** by KtnC. (**Figure 2.17**).

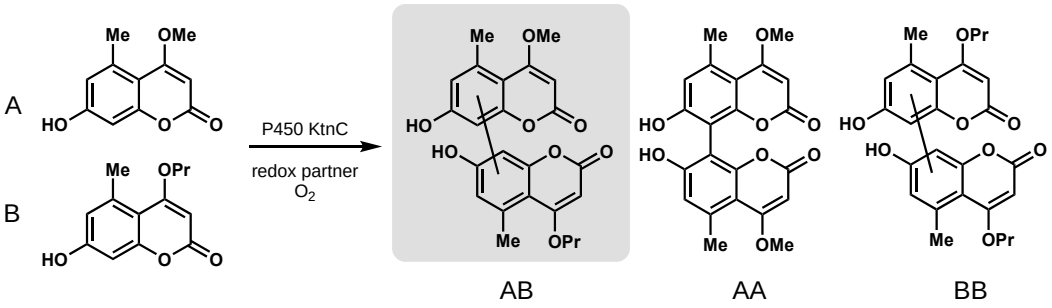

KtnC

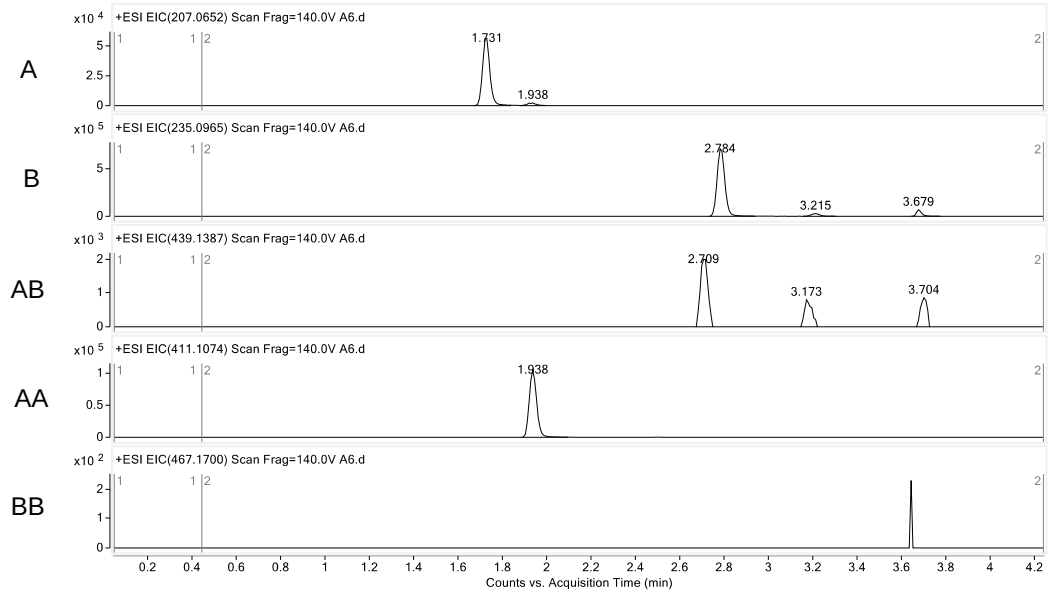

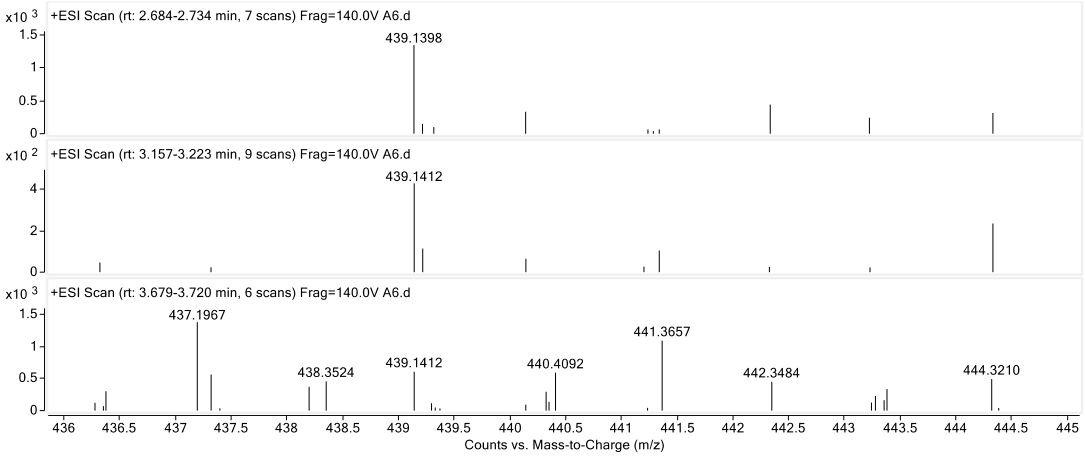

No Enzyme control

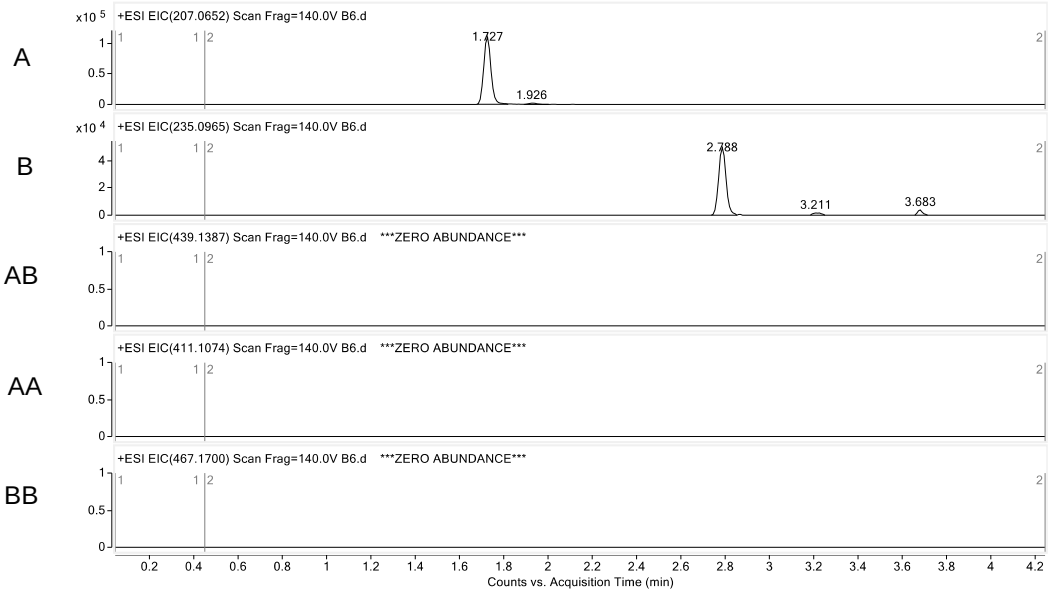

Supplemental Figure S2.41. Oxidative cross-coupling of **1** and **20** by KtnC (**Figure 2.17**).

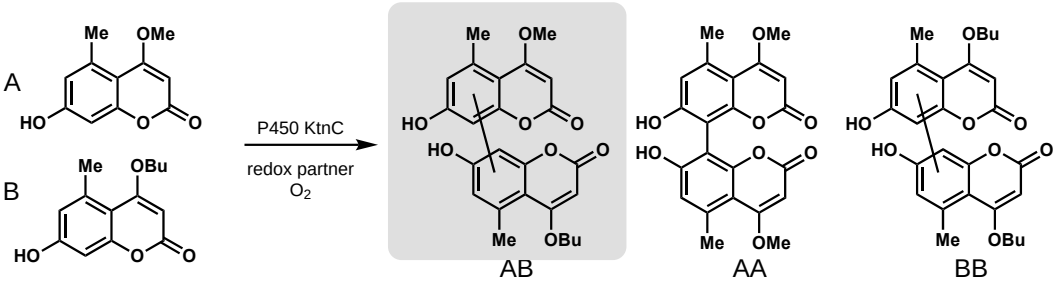

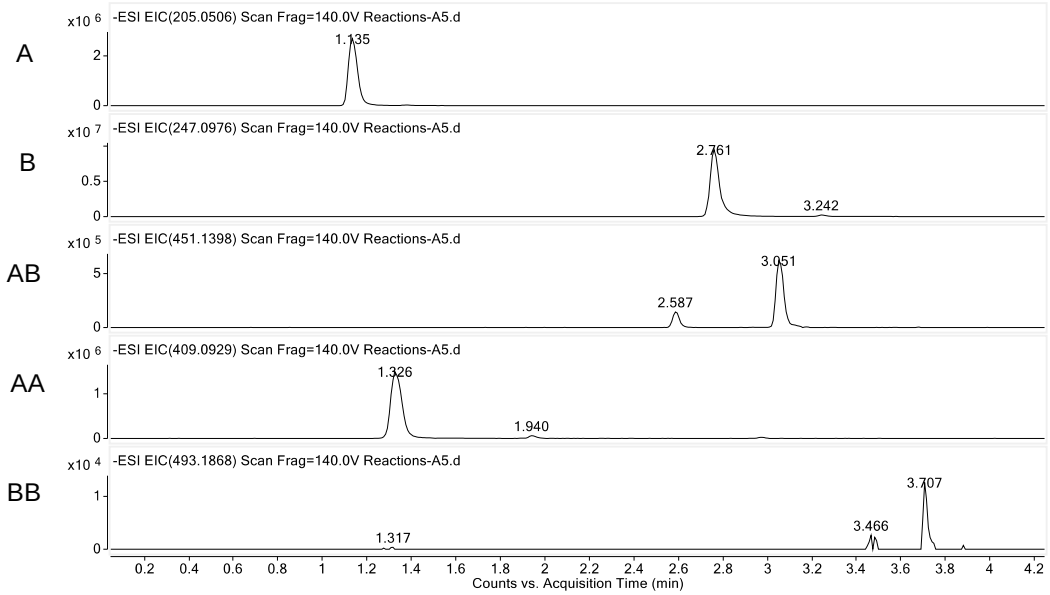

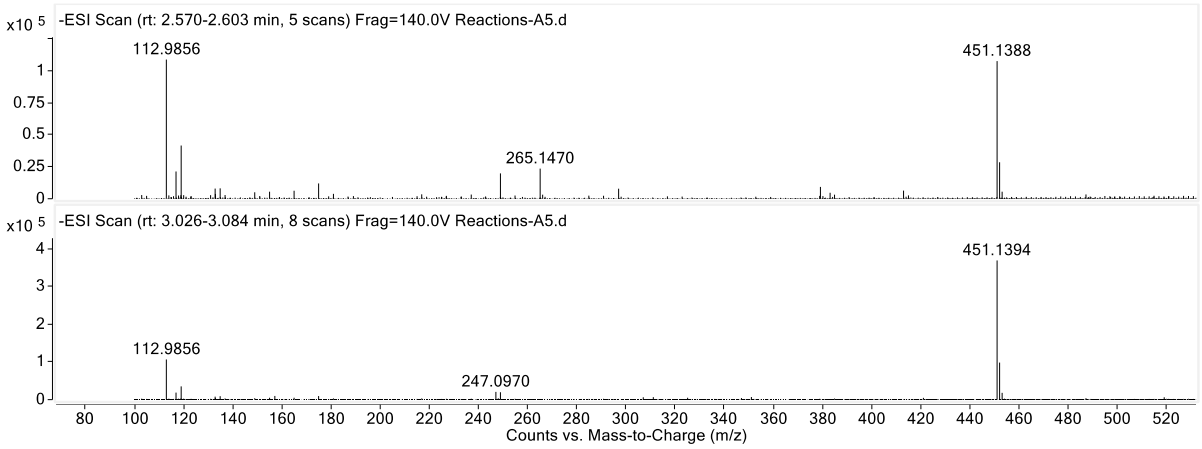

No Enzyme control

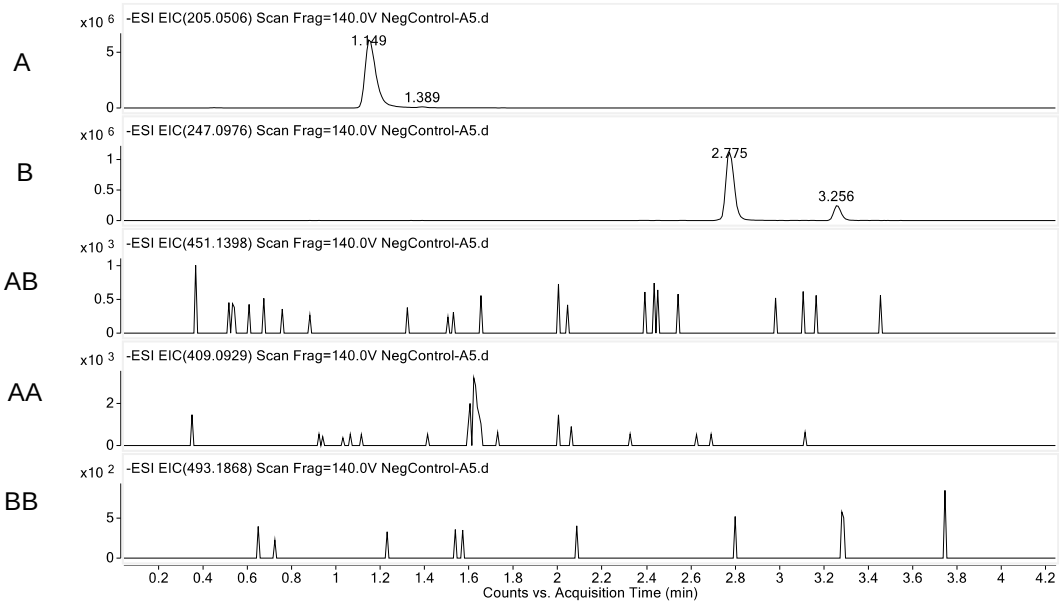

Supplemental Figure S2.42. Oxidative cross-coupling of **1** and **21** by KtnC (**Figure 2.18**).

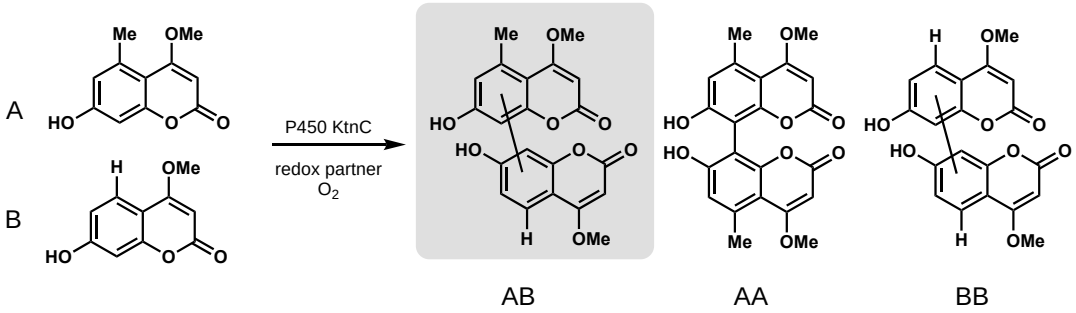

KtnC

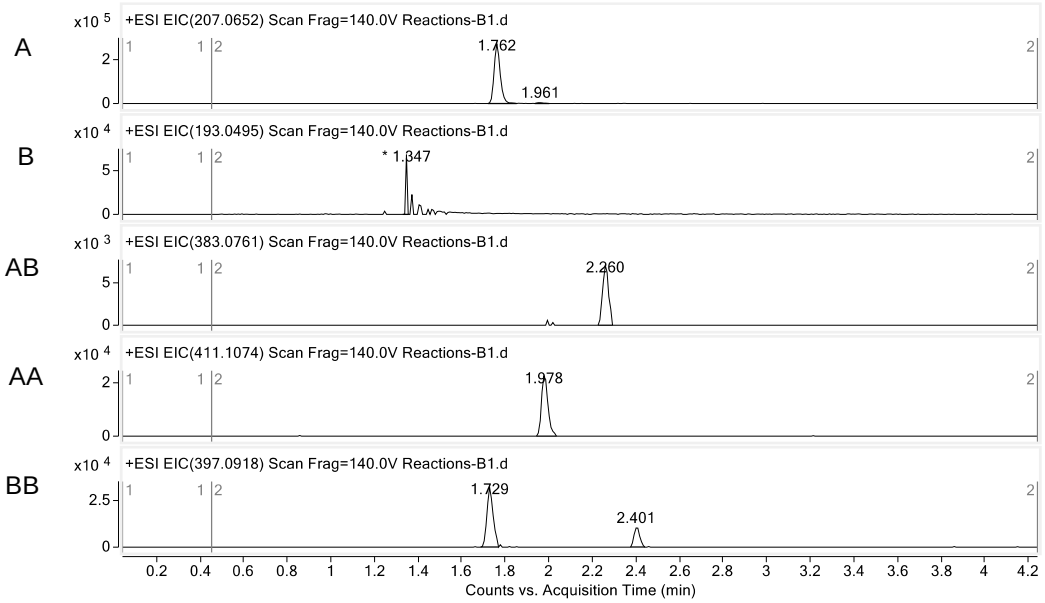

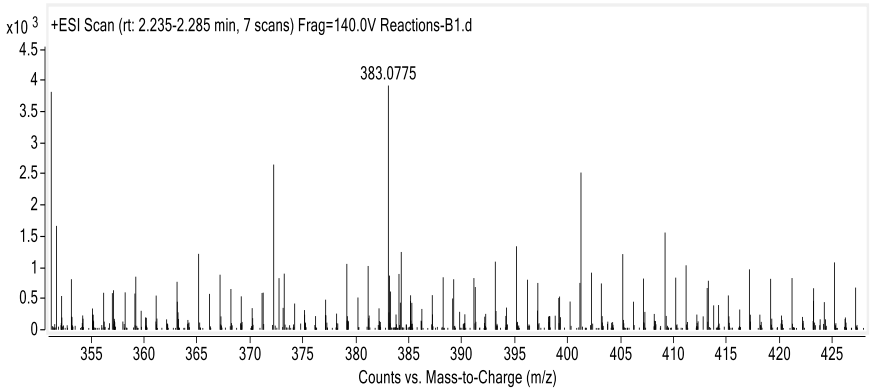

No Enzyme control

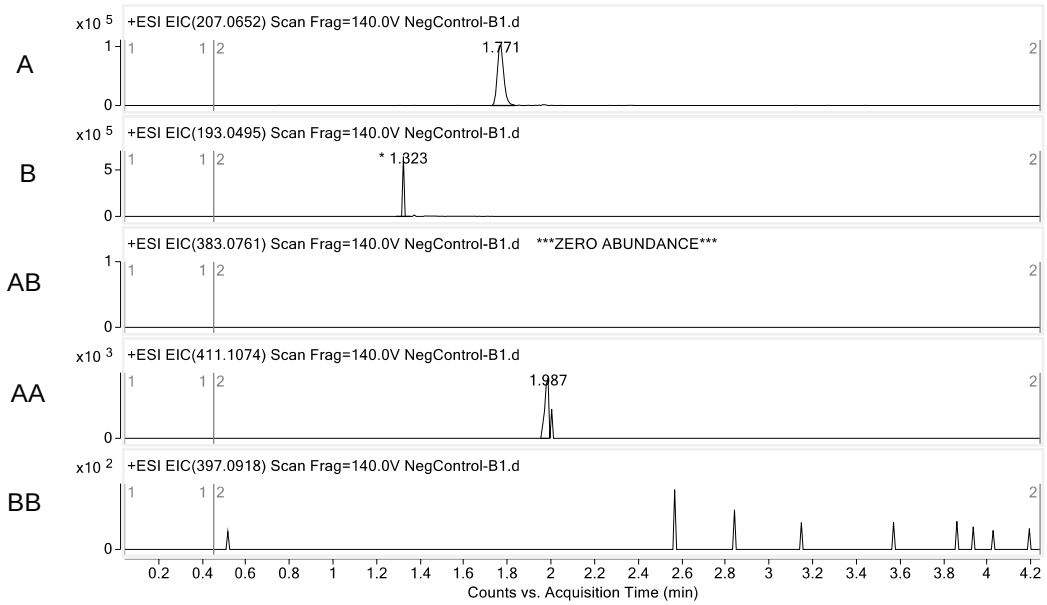

Supplemental Figure S2.43. Oxidative cross-coupling of **1** and **24** by KtnC (**Figure 2.18**).

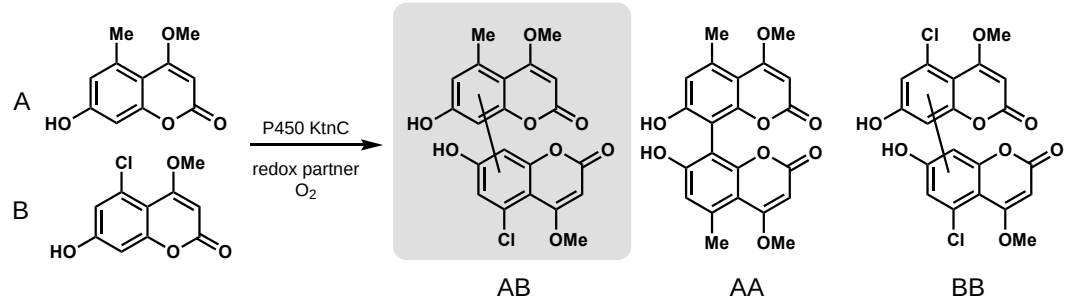

KtnC

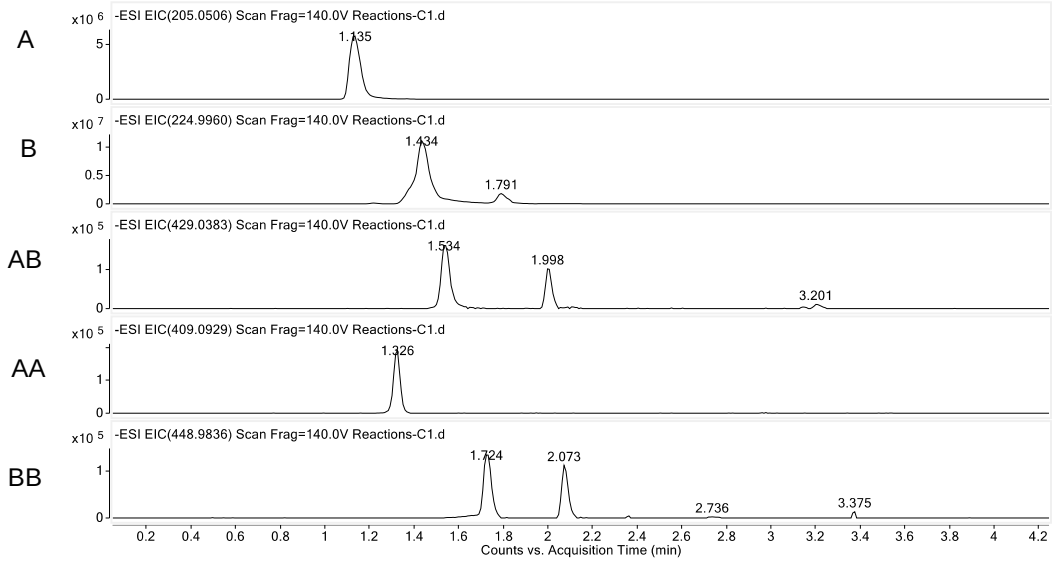

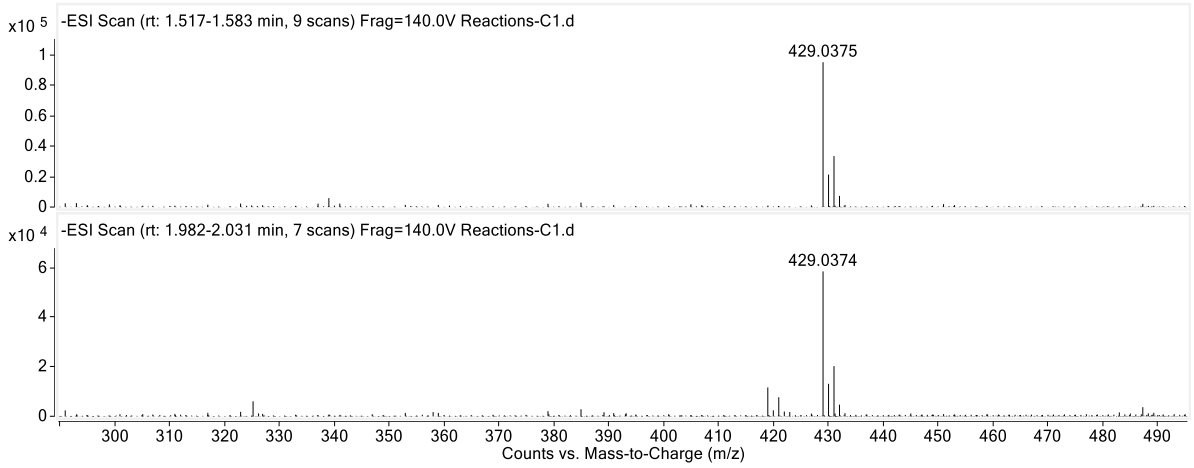

No Enzyme control

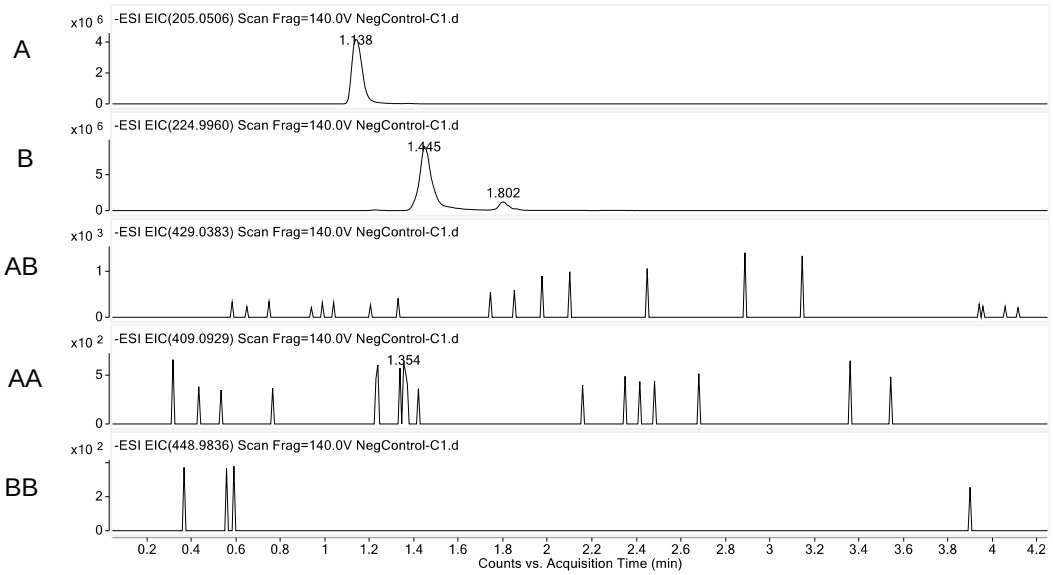

Supplemental Figure S2.44. Oxidative cross-coupling of **1** and **22** by KtnC (**Figure 2.12**).

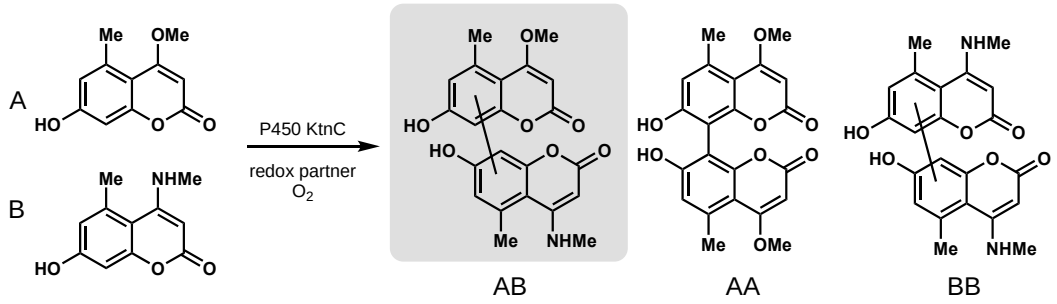

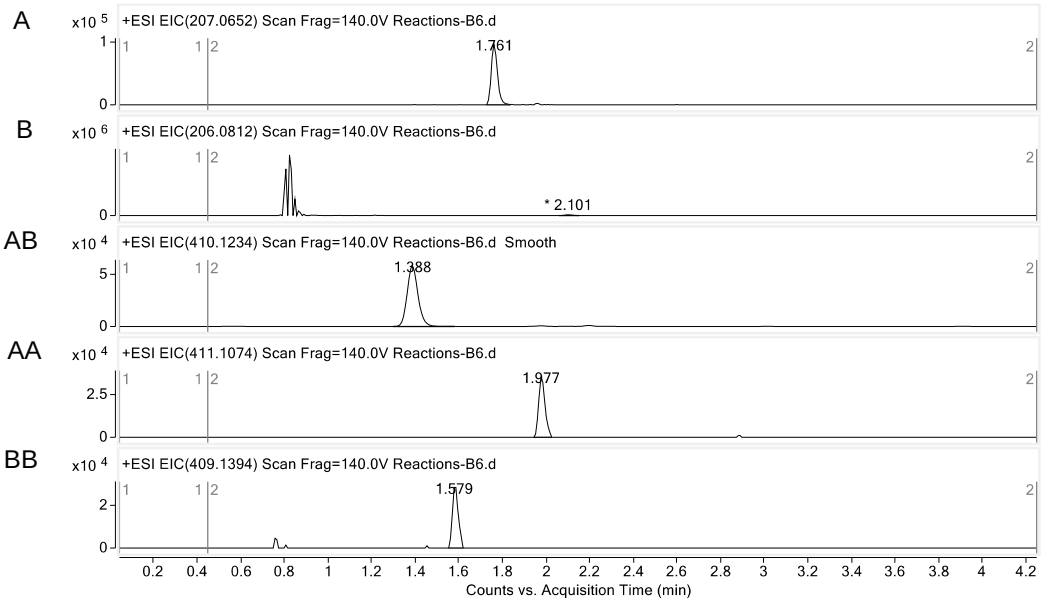

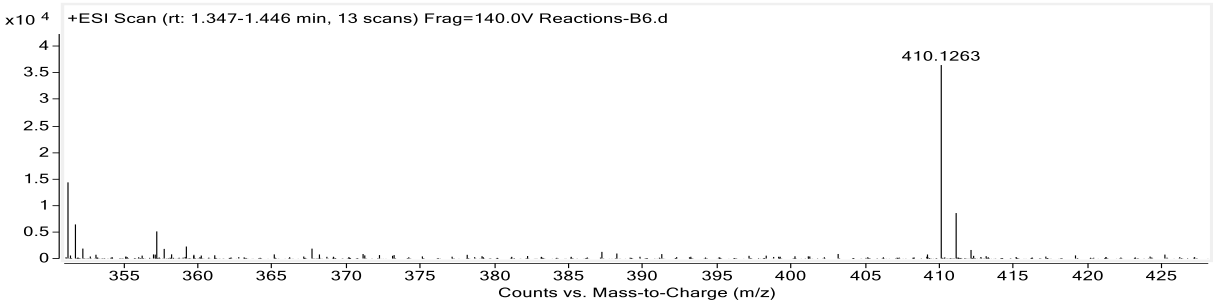

No Enzyme control

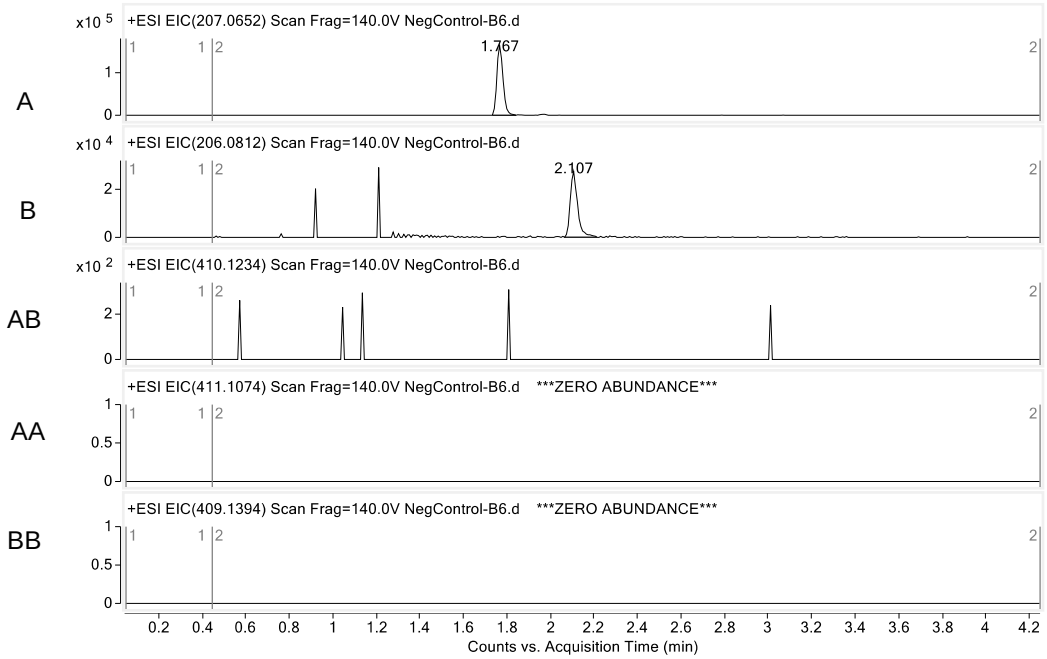

Supplemental Figure S2.45. Oxidative cross-coupling of **1** and **39** by KtnC (**Figure 2.11**).

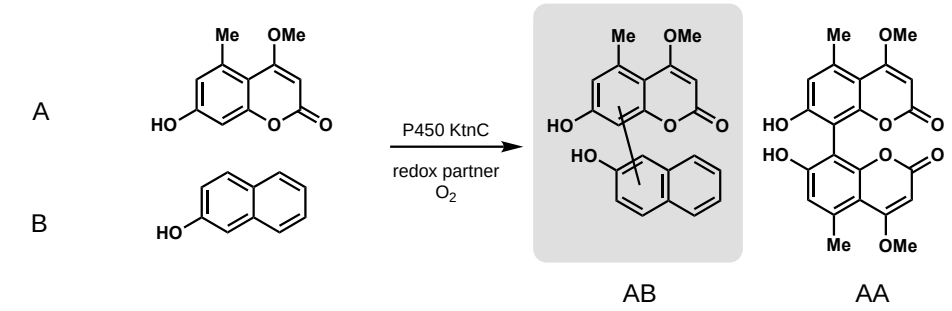

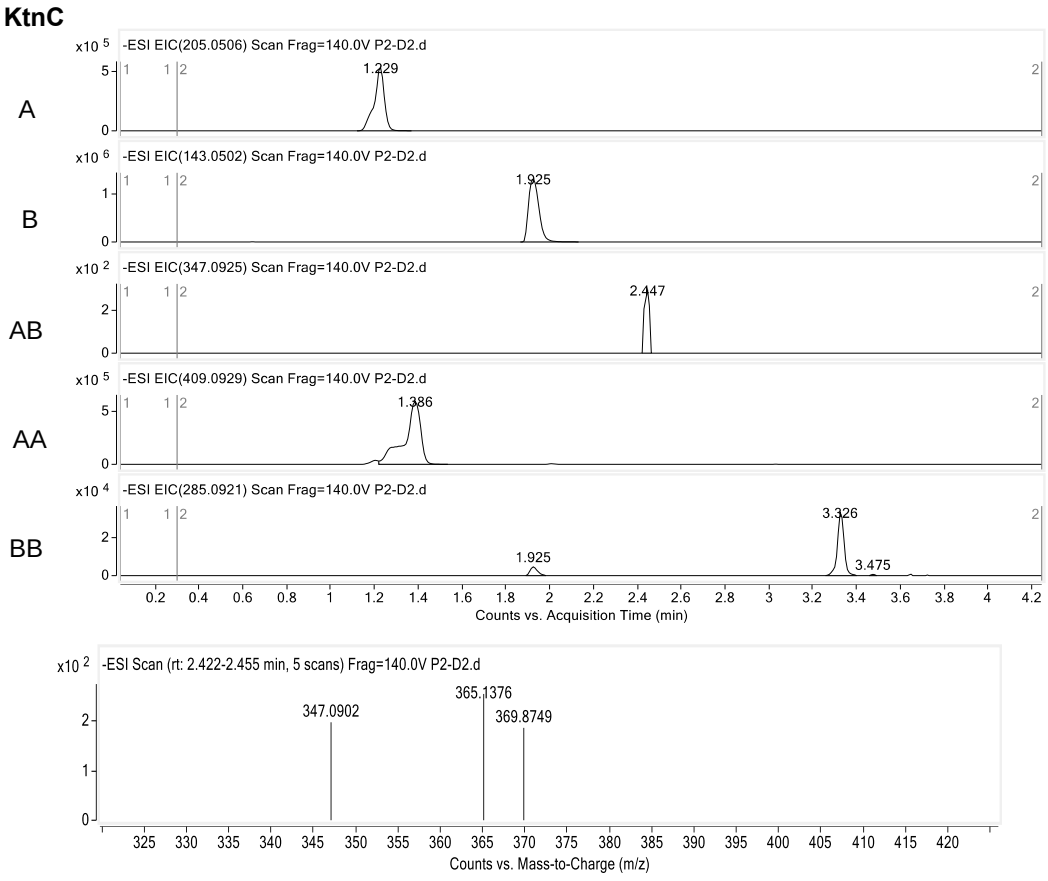

No Enzyme control

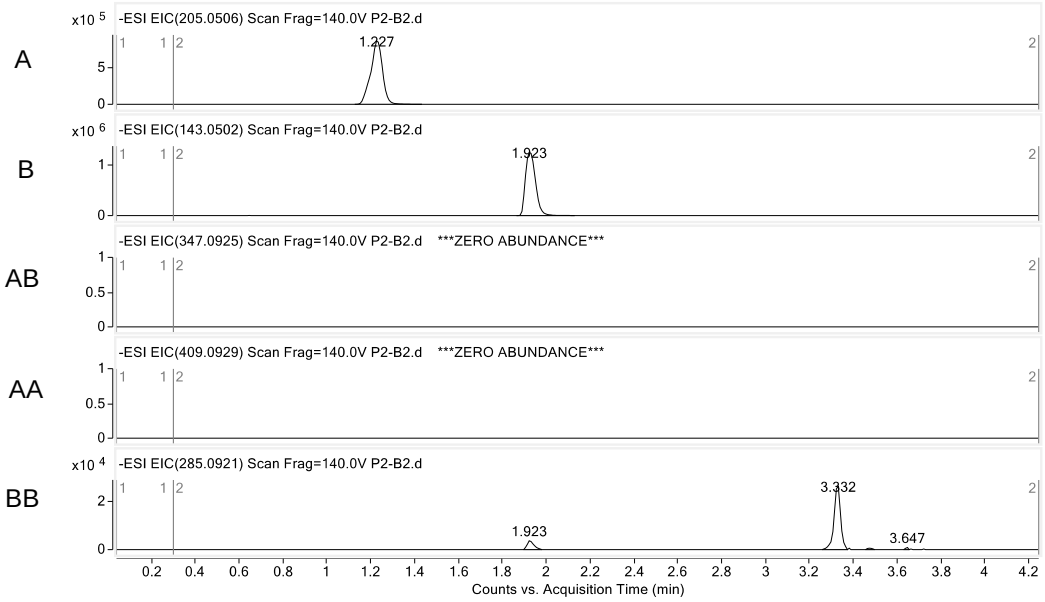

Site-selectivity of oxidative cross-coupling biotransformations

Supplemental Figure S2.46. Site-selectivity of oxidative cross-coupling of **1** and **25** by KtnC (**Figure 2.17**).

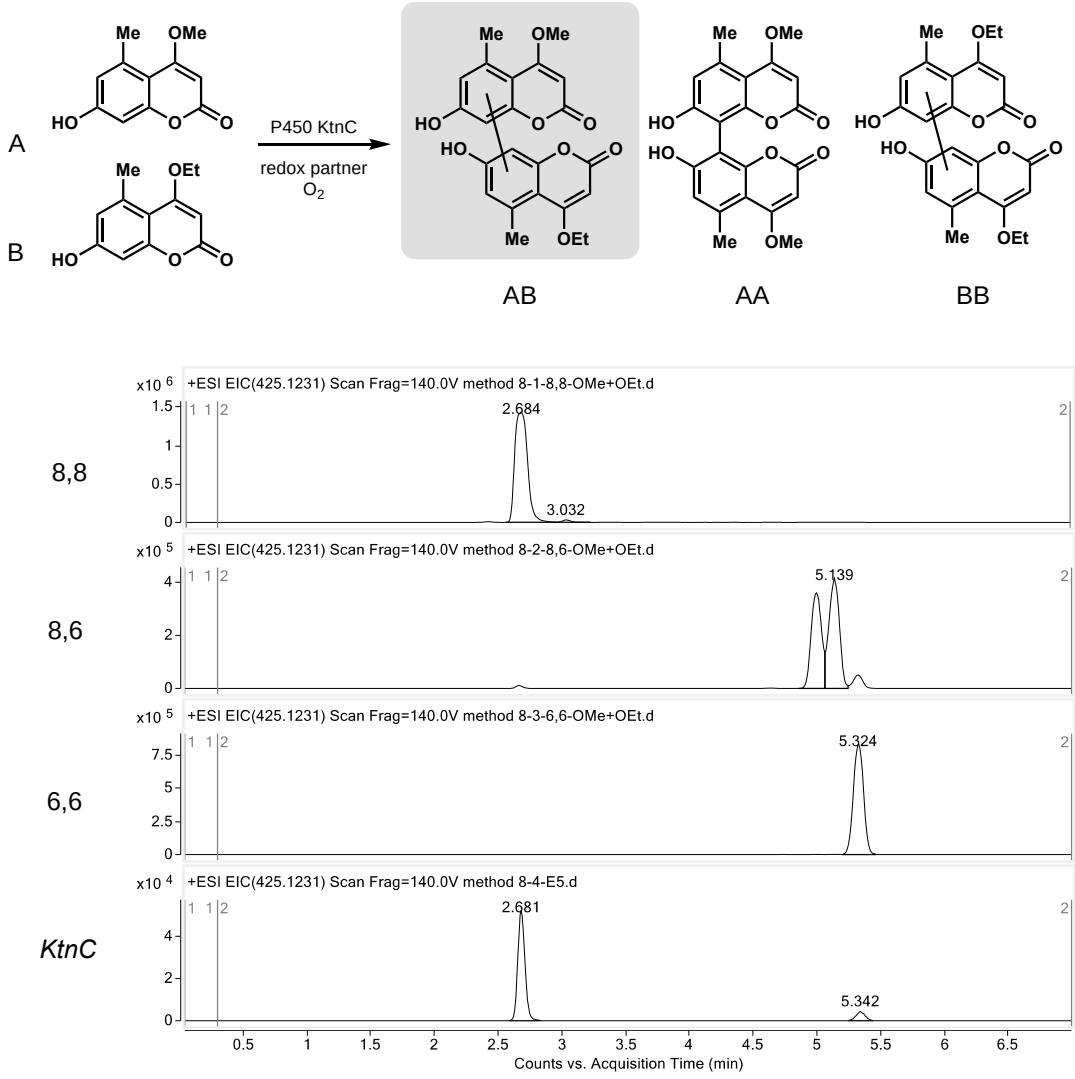

Supplemental Figure S2.47. Site-selectivity of oxidative cross-coupling of **1** and **26** by KtnC (**Figure 2.17**).

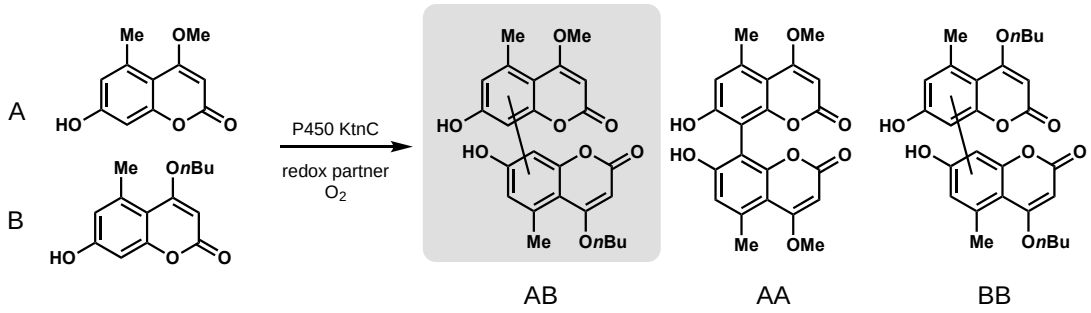

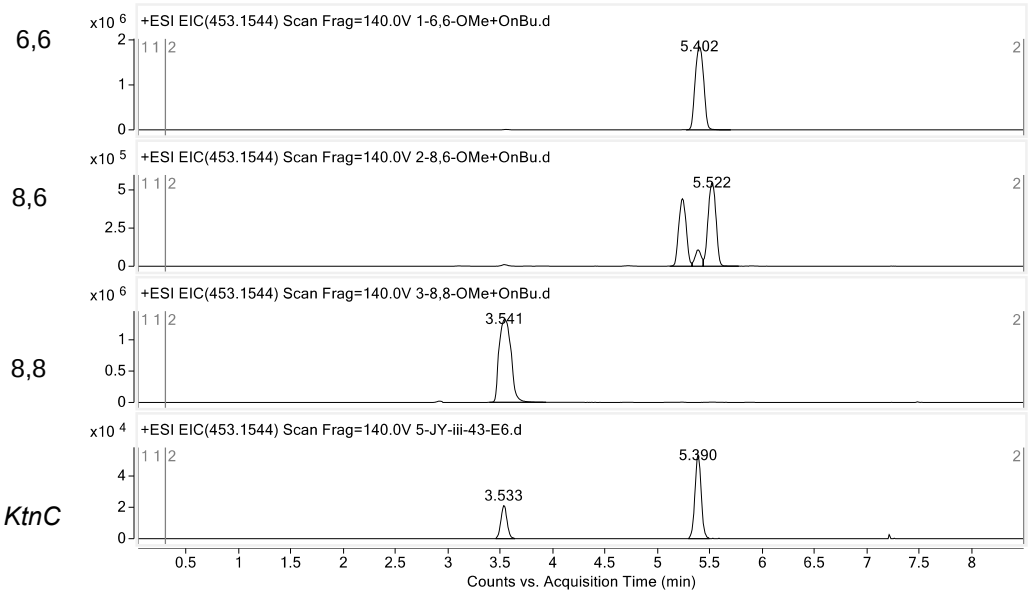

SFC traces of isolated products

Data acquired by Dr. Meagan Hinze

Supplemental Figure S2.48. PDA traces of racemic **2** obtained from VOF_3 oxidative dimerization and KtnC-mediated oxidative dimerization (CHIRALPAK OJ-H, 20% MeOH, CO_2, 3.5 mL/min).

Racemic standard

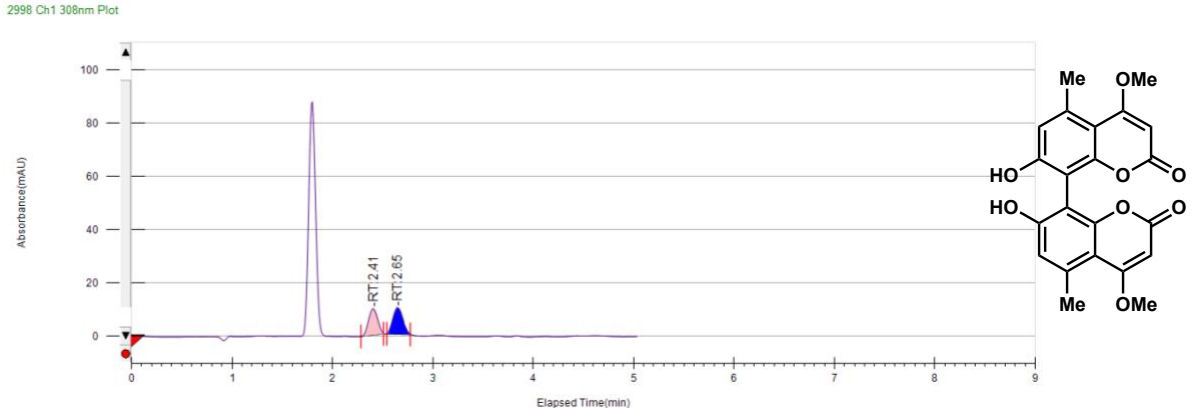

Run Information

Instrument Method	Inj. Vol.	Solvent	Column	Sample	Temp.	Flow	% Modifier	Pressure
OJ-H-MeOH20%	10	MeOH	OJ-H Chiral Analytical	meh-3-10588	40	3.5	20	120

Peak Information

Peak No.	% Area	Area	Ret. Time	Height
1	47.7285	59.8685	2.41 min	9.8095
2	52.2715	65.5671	2.65 min	9.907

14 from KtnC reaction

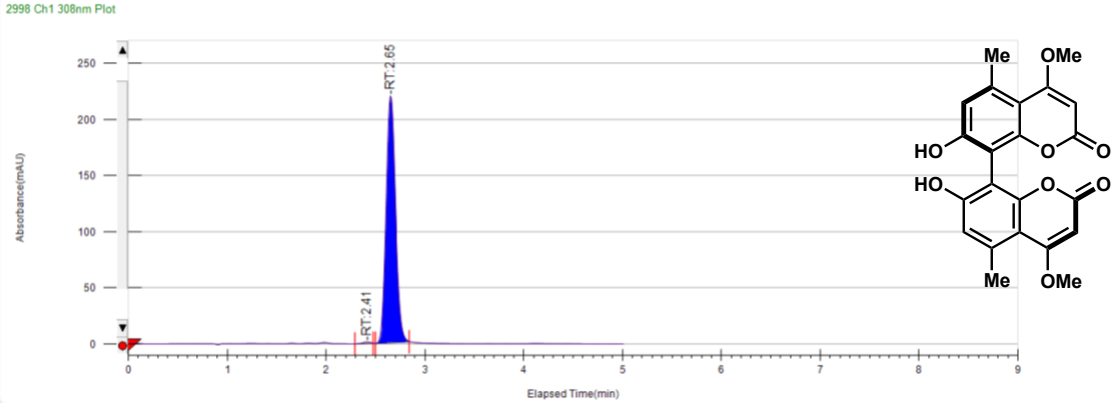

Run Information

Instrument Method	Inj. Vol.	Solvent	Column	Sample	Temp.	Flow	% Modifier	Pressure
OJ-H-MeOH20%	2	MeOH	OJ-H Chiral Analytical	meh-6_100	40	3.5	20	120

Peak Information

Peak No.	% Area	Area	Ret. Time	Height
1	0.4241	5.9559	2.41 min	1.2717
2	99.5759	1398.4688	2.65 min	219.9764

Supplemental Figure S2.49. PDA traces of racemic **31** obtained from VOF_3 oxidative dimerization and KtnC-mediated oxidative dimerization (CHIRALPAK OD-H, 30% MeOH, CO_2, 3.5 mL/min).

Racemic Standard

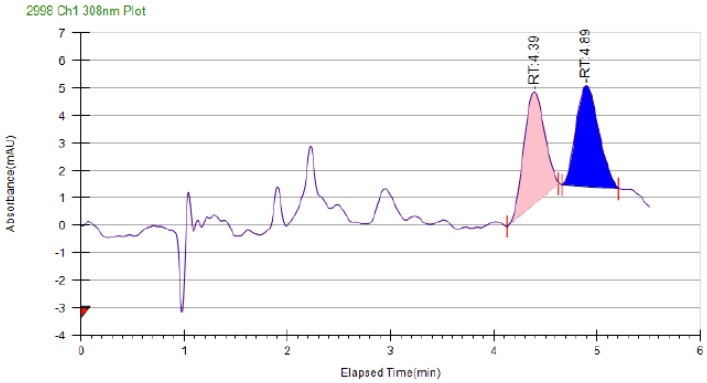

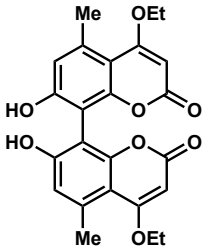

Run Information

Instrument Method	Inj. Vol.	Solvent	Column	Sample	Temp.	Flow	% Modifier	Pressure
OD-H_MeOH30%	10	MeOH	OD-H Chiral Analytical	meh-6_88rac	40	3.5	30	120

Peak Information

Peak No.	% Area	Area	Ret. Time	Height
1	50.1356	56.0581	4.39 min	4.0889
2	49.8644	55.7548	4.89 min	3.6728

31 from KtnC reaction

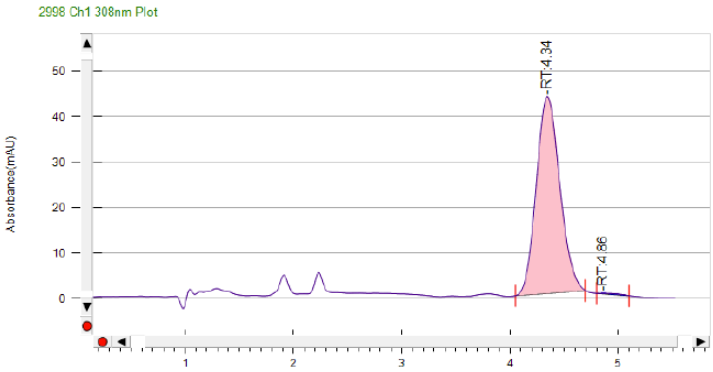

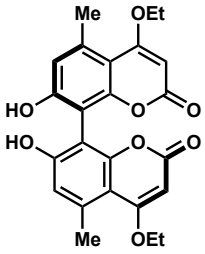

Run Information

Instrument Method	Inj. Vol.	Solvent	Column	Sample	Temp.	Flow	% Modifier	Pressure
OD-H_MeOH30%	10	MeOH	OD-H Chiral Analytical	meh-6-66-88	40	3.5	30	120

Peak Information

Peak No.	% Area	Area	Ret. Time	Height
1	99.5926	648.7717	4.34 min	43.3822
2	0.4074	2.6537	4.86	0.123

Supplemental Figure S2.50. PDA traces of racemic **31** obtained from VOF_3 oxidative dimerization and KtnC-mediated oxidative dimerization (CHIRALPAK OD-H, 40% MeOH, CO_2, 3.5 mL/min).

Racemic Standard

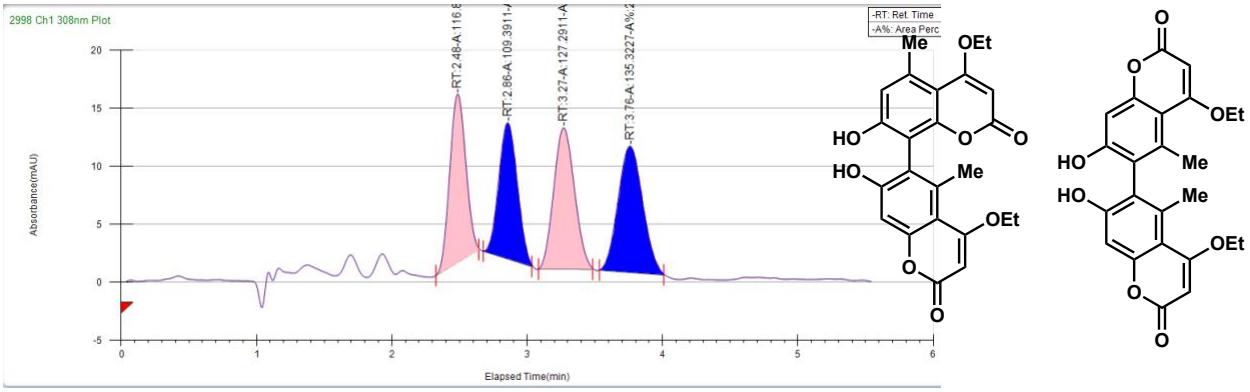

Run Information

Instrument Method	Inj. Vol.	Solvent	Column	Sample	Temp.	Flow	% Modifier	Pressure
OD-H_MeOH40%	10	MeOH	OD-H Chiral Analytical	meh-5-18-6866rac	40	3.5	40	120

Peak Information

Peak No.	% Area	Area	Ret. Time	Height
1	23.9105	116.8993	2.48 min	14.5448
2	22.3748	109.3911	2.86 min	11.7207
3	26.036	127.2911	3.27 min	12.19
4	27.6788	135.3227	3.76 min	10.8893

32 from KtnC reaction

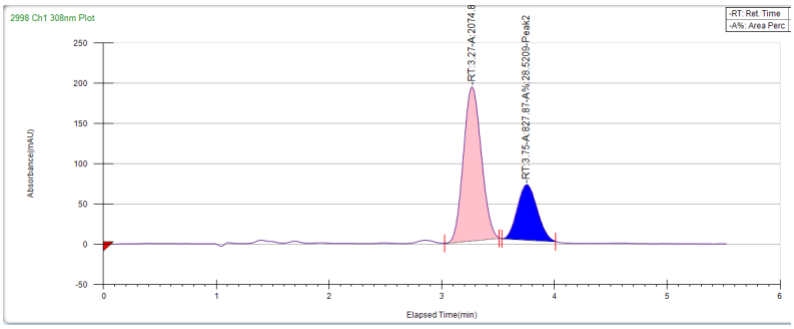

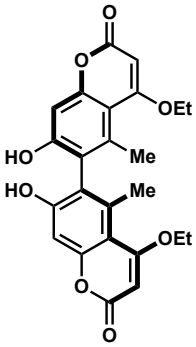

Run Information

Instrument Method	Inj. Vol.	Solvent	Column	Sample	Temp.	Flow	% Modifier	Pressure
OD-H_MeOH40%	10	MeOH	OD-H Chiral Analytical	meh-6-66-66prod	40	3.5	40	120

Peak Information

Peak No.	% Area	Area	Ret. Time	Height
1	71.4791	2074.8101	3.27 min	191.2852
2	28.5209	827.87	3.75 min	68.6818

Supplemental Figure S2.51. PDA traces of racemic **31** obtained from VOF_3 oxidative dimerization and KtnC-mediated oxidative dimerization (CHIRALPAK OD-H, 40% MeOH, CO_2, 3.5 mL/min).

Racemic Standard

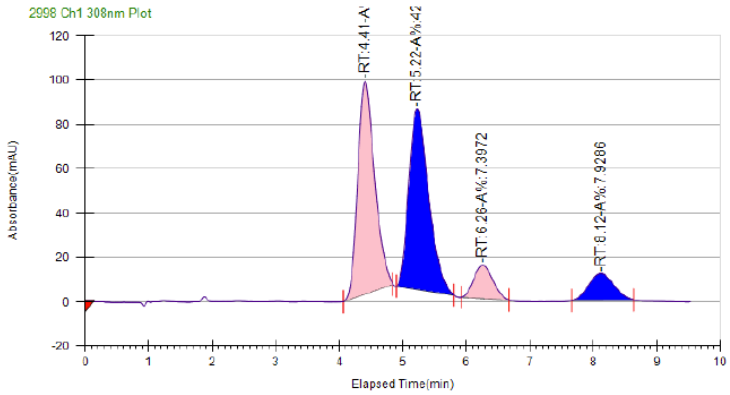

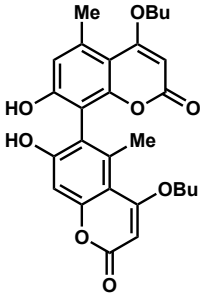

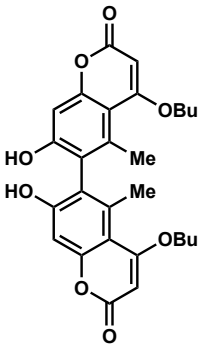

Run Information

Instrument Method	Inj. Vol.	Solvent	Column	Sample	Temp.	Flow	% Modifier	Pressure
OD-H_ MeOH30%	7	MeOH	OD-H Chiral Analytical	meh-6-113 _6866mixed_30 %	40	3.5	30	120

Peak Information

Peak No.	% Area	Area	Ret. Time	Height
1	42.5238	1767.0118	4.41	96.1671
2	42.1503	1751.4913	5.22	81.601
3	7.3972	307.381	6.26	14.9744
4	7.9286	329.4627	8.12	11.9942

31 from KtnC reaction

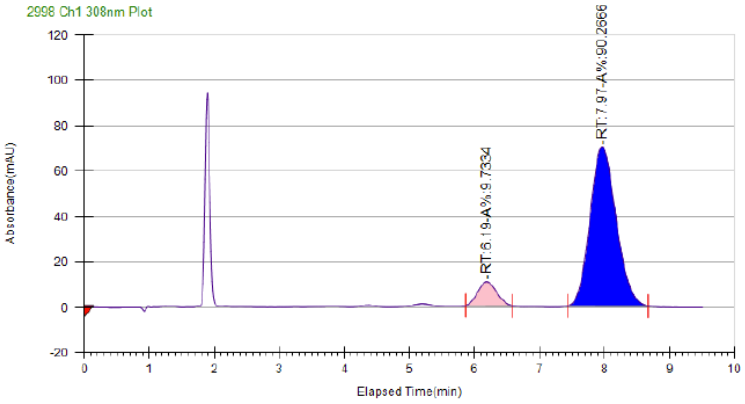

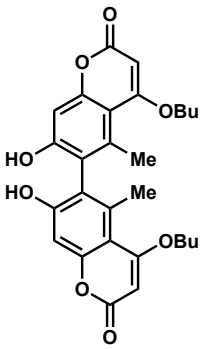

Run Information

Instrument Method	Inj. Vol.	Solvent	Column	Sample	Temp.	Flow	% Modifier	Pressure
OD-H_ MeOH30%	7	MeOH	OD-H Chiral Analytical	meh_6_142_ 66prod_30%	40	3.5	30	120

Peak Information

Peak No.	% Area	Area	Ret. Time	Height
1	9.7334	208.8304	6.19	10.4784
2	90.2666	1936.6834	7.97	70.2415

Supplemental Figure S2.52. PDA traces of racemic **3** obtained from VOF_3 oxidative dimerization and DesC-mediated oxidative dimerization (CHIRALPAK OD-H, 40% MeOH, CO_2, 3.5 mL/min).

Racemic Standard

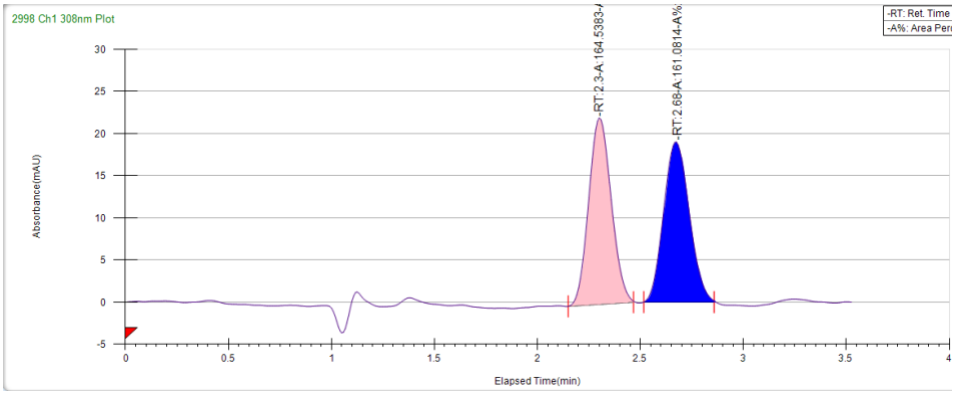

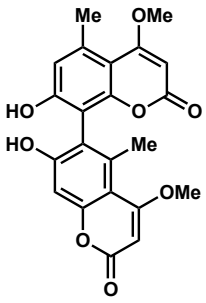

Run Information

Instrument Method	Inj. Vol.	Solvent	Column	Sample	Temp.	Flow	% Modifier	Pressure
OD-H_MeOH40%	10	MeOH	OD-H Chiral Analytical	native-68-rac	40	3.5	40	120

Peak Information

Peak No.	% Area	Area	Ret. Time	Height
1	50.5308	164.5383	2.3 min	22.1636
2	49.4692	161.0814	2.68 min	19.0192

15 from DesC reaction

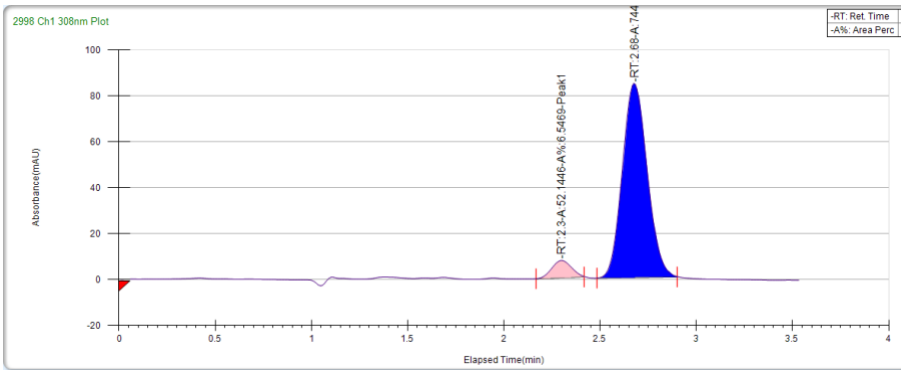

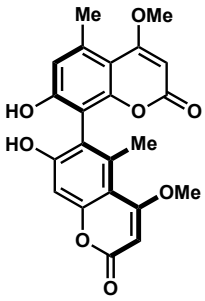

Run Information

Instrument Method	Inj. Vol.	Solvent	Column	Sample	Temp.	Flow	% Modifier	Pressure
OD-H_MeOH40%	4	MeOH	OD-H Chiral Analytical	Meh-6-58-68prod	40	3.5	40	120

Peak Information

Peak No.	% Area	Area	Ret. Time	Height
1	6.5469	52.1446	2.3 min	7.5636
2	93.4531	744.3314	2.68 min	84.6462

Supplemental Figure S2.53. PDA traces of racemic **29** obtained from VOF_3 oxidative dimerization and DesC-mediated oxidative dimerization (CHIRALPAK OD-H, 30% MeOH, CO_2, 3.5 mL/min).

Racemic Standard

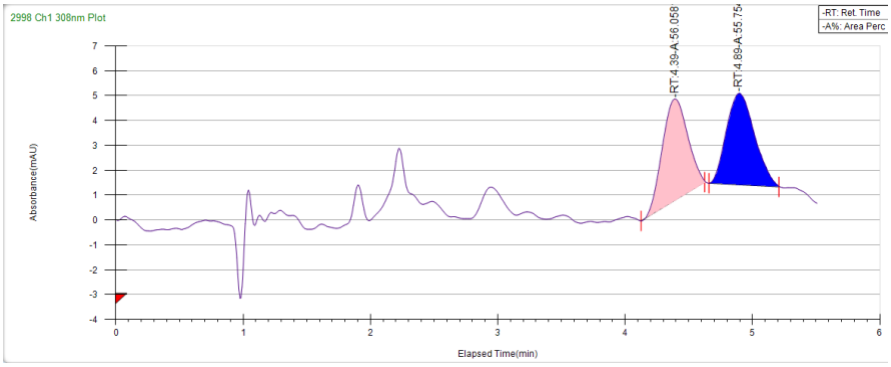

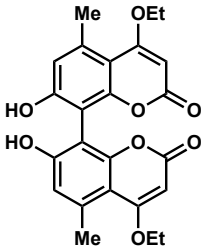

Run Information

Instrument Method	Inj. Vol.	Solvent	Column	Sample	Temp.	Flow	% Modifier	Pressure
OD-H_MeOH30%	10	MeOH	OD-H Chiral Analytical	meh-6-88rac	40	3.5	30	120

Peak Information

Peak No.	% Area	Area	Ret. Time	Height
1	50.1356	56.0581	4.39	4.0889
2	49.8644	55.7548	4.89	3.6728

29 from DesC reaction

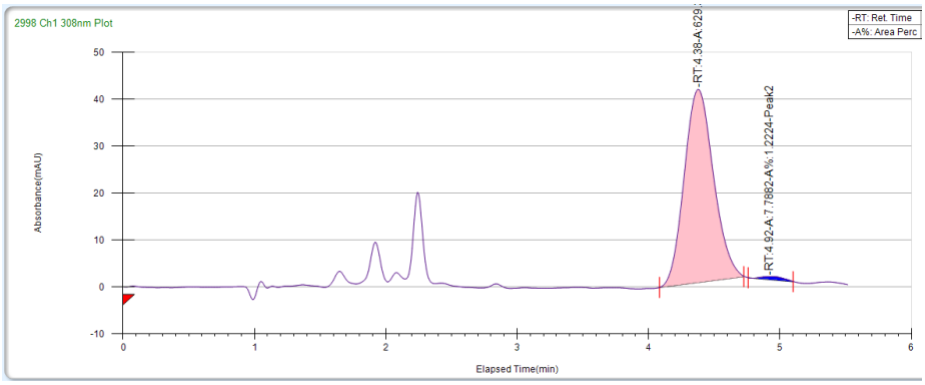

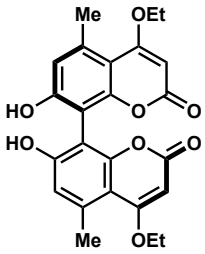

Run Information

Instrument Method	Inj. Vol.	Solvent	Column	Sample	Temp.	Flow	% Modifier	Pressure
OD-H_MeOH30%	10	MeOH	OD-H Chiral Analytical	meh-6-56-88prod	40	3.5	30	120

Peak Information

Peak No.	% Area	Area	Ret. Time	Height
1	98.7776	629.3395	4.38	41.1804
2	1.2224	7.7882	4.92	0.637

Supplemental Figure S2.54. PDA traces of racemic **32** obtained from VOF_3 oxidative dimerization and DesC-mediated oxidative dimerization (CHIRALPAK OD-H, 20% MeOH, CO_2, 3.5 mL/min).

Racemic Standard

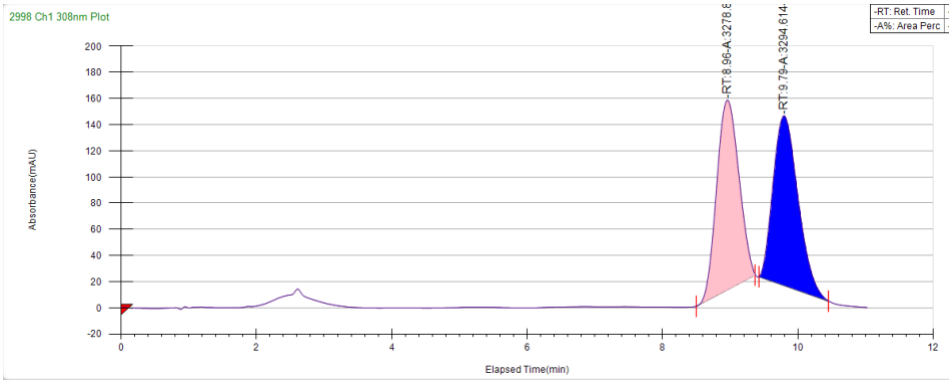

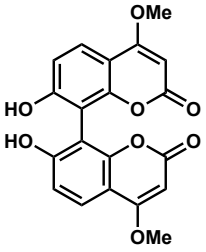

Run Information

Instrument Method	Inj. Vol.	Solvent	Column	Sample	Temp.	Flow	% Modifier	Pressure
OD-H_MeOH20%	10	MeOH	OD-H Chiral Analytical	meh-6	40	3.5	20	120

Peak Information

Peak No.	% Area	Area	Ret. Time	Height
1	49.8799	3278.8189	8.96 min	145.1216
2	50.1201	3294.614	9.79 min	129.7135

32 from DesC reaction

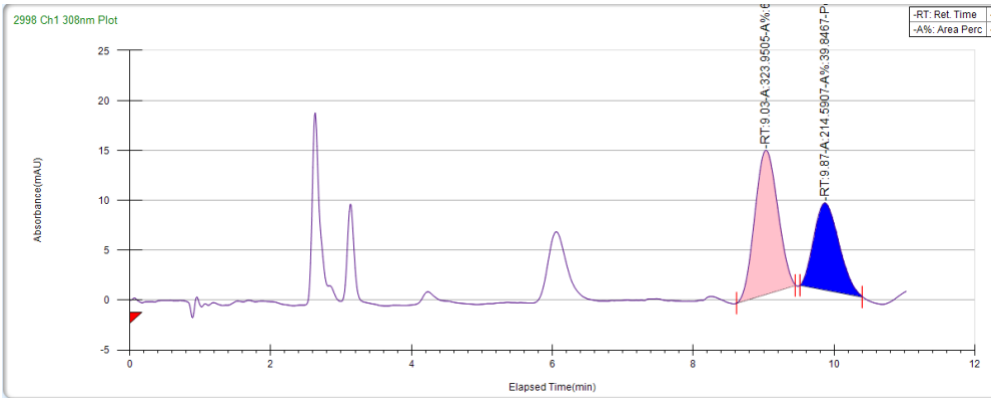

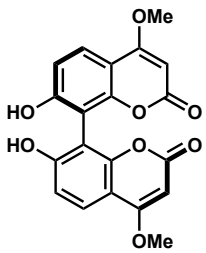

Run Information

Instrument Method	Inj. Vol.	Solvent	Column	Sample	Temp.	Flow	% Modifier	Pressure
OD-H_MeOH20%	10	MeOH	OD-H Chiral Analytical	meh-6-86-peak2	40	3.5	20	120

Peak Information

Peak No.	% Area	Area	Ret. Time	Height
1	60.1533	323.9505	9.03 min	14.4411
2	39.8467	214.5907	9.87 min	8.7105

Assignment of absolute configuration of enzymatic products

ECD Methodology

The general approach for absolute configuration assignment using ECD, including the detailed computational workflow, has been published elsewhere.[90-92] A subset of the details of the computational methodology is provided here. Conformers of each test structure were geometry optimized at the B3LYP/6-31G** level and stationary points were confirmed by performing frequency calculations.[93-101] All calculations were performed using Gaussian 09. Output conformers were ranked according to DFT energy and a clustering was performed in order to remove duplicates. Initial duplicate identification was performed solely on an electronic energy basis where two compounds were considered identical if the difference in Hartrees was less than 0.01. Rounding the differences led to inconsistencies in identification of duplicates. It became better to cluster the DFT minima by energy and then re-cluster each energy bucket by structure using an all atom RMS of 0.6 Å. This process removed just identical compounds. Two Boltzmann distributions were calculated based on the free energy (G) and the electronic energy (E).

To calculate UV and ECD spectra, B3LYP geometries were used as input. The spectra were then calculated using either the B3LYP or CAM-B3LYP[102] functionals, along with the 6-31++G** basis set in vacuo.[103] Only conformers which contributed more than 5.0% to the total in vacuo conformer distribution were selected for UV and ECD calculation. Time-dependent Density Functional Theory (TDDFT)[104] methodology was employed using the following keywords: TD=full,singlet, Nstates=100, and integral=ultrafinegrid. Spectral display, Boltzmann weighting, and curve fitting were carried out using SpecDis,[105] and were displayed with a wavelength shift and band broadening sigma values in order to best match the calculated and experimental UV spectra. This shift and band broadening were then applied to the ECD spectra, and the area under the curve fit was determined by SpecDis. Conformers were visualized using CYLview Version 1.0.

Compound 2

Calculations of the ECD and UV spectra (CAM-B3LYP/6-31++G**) involved modeling the (*P*)- enantiomer of the compound. Hence, the (*P*)-enantiomer had a positive dihedral angle about the atropisomeric bond. Since the atropisomeric bond represents the only stereochemical element in the molecule, the (*M*)-enantiomer is assumed to have a spectrum that will be equal and opposite at all wavelengths.

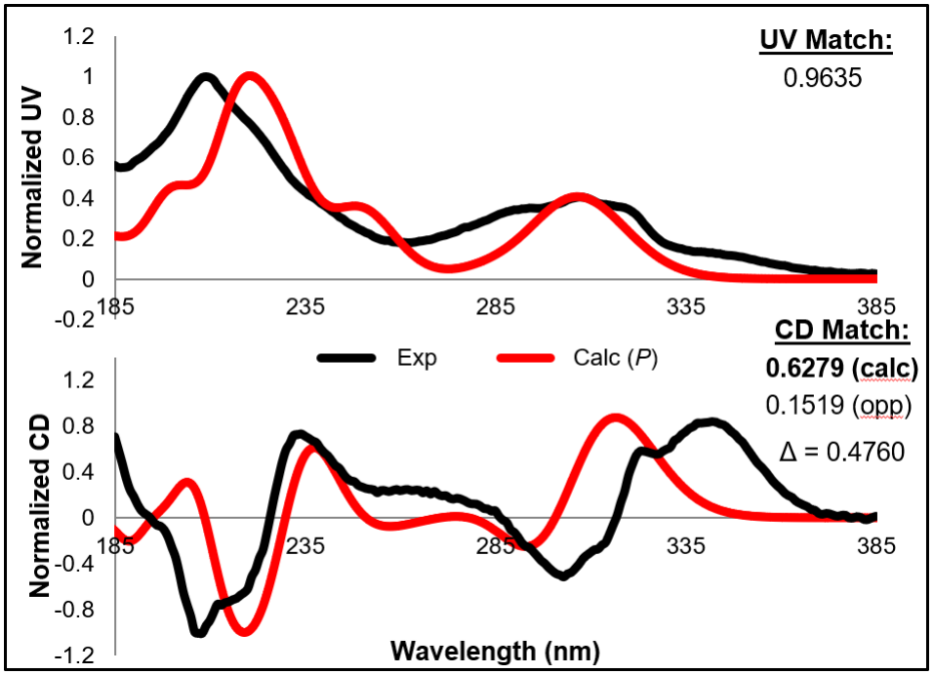

Supplemental Figure S2.55. Comparison between compound **2** experimental (black) and calculated (red) UV (top) and ECD (bottom) spectra. The calculated (*P*)-enantiomer is the better match to the experimental spectrum, with a large difference in fits (Δ=0.4760) suggesting a confident assignment. The calculated spectrum has been shifted 25 nm, and a band broadening of 0.25 eV has been applied.

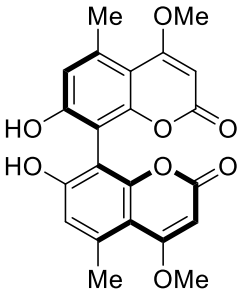

Supplemental Figure S2.56. Assigned absolute configuration of compound **2** based on ECD analysis. One conformer of the (*P*)-enantiomer of compound **2** that contributes >2% to the Boltzmann distribution. Note the percentage shown above based is on *in vacuo* electronic energies.

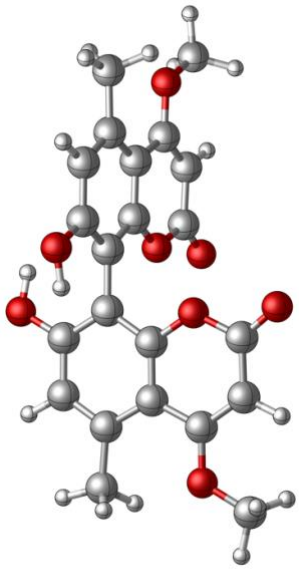

Conformer 1 : 98.4%

Supplemental Table S2.2. Coordinates and electronic energies for B3LYP/6-31G** conformational minima contributing >2% to the *in vacuo* Boltzmann distribution.

Conformer 1: -1451.009545 hartrees

6	-2.441	1.9261	-1.7144
6	-1.1174	1.9309	-1.2545
6	-0.7066	1.0582	-0.2383
6	-1.6647	0.1655	0.2749
6	-3.0021	0.1348	-0.1802
6	-3.3889	1.0482	-1.2065
6	0.7066	1.0582	0.2383
6	1.1174	1.9309	1.2545
6	2.441	1.9261	1.7144
6	3.3888	1.0482	1.2065
6	3.0021	0.1348	0.1802
6	1.6647	0.1655	-0.2749
8	-1.2069	-0.6596	1.2512
6	-2.0119	-1.6193	1.8856
6	-3.3776	-1.6815	1.4338
6	-3.8582	-0.8569	0.4571
6	3.8582	-0.8569	-0.4571
6	3.3776	-1.6815	-1.4338
6	2.012	-1.6193	-1.8856
8	1.2069	-0.6596	-1.2512
8	-1.4944	-2.2943	2.7443
8	1.4944	-2.2943	-2.7442
8	-0.2634	2.8131	-1.8249
8	0.2634	2.8131	1.8249
6	-4.784	1.1202	-1.7855

6	4.784	1.1202	1.7855
8	-5.1331	-0.8942	0.017
6	-6.0279	-1.8499	0.5841
8	5.1331	-0.8942	-0.017
6	6.0279	-1.8499	-0.5841
1	-5.5301	1.343	-1.0187
1	-4.8272	1.9006	-2.5487
1	-5.0786	0.1723	-2.2427
1	5.0786	0.1723	2.2427
1	5.5301	1.3431	1.0187
1	4.8272	1.9006	2.5487
1	-6.9802	-1.699	0.0758
1	-6.1531	-1.6836	1.6595
1	-5.6744	-2.8718	0.4104
1	6.9802	-1.699	-0.0758
1	6.1531	-1.6836	-1.6595
1	5.6744	-2.8718	-0.4104
1	-2.7069	2.624	-2.5006
1	2.7069	2.624	2.5006
1	-3.9885	-2.4258	1.9228
1	3.9885	-2.4257	-1.9228
1	0.622	2.6629	-1.4553
1	-0.622	2.6629	1.4553

Compound 3

Calculations of the ECD and UV spectra (CAM-B3LYP/6-31++G**) involved modeling the (*M*)-enantiomer of the compound. Hence, the (*M*)-enantiomer had a negative dihedral angle about the atropisomeric bond. Since the atropisomeric bond represents the only stereochemical element present in this compound, the (*P*)-enantiomer is assumed to have a spectrum that will be equal and opposite at all wavelengths.

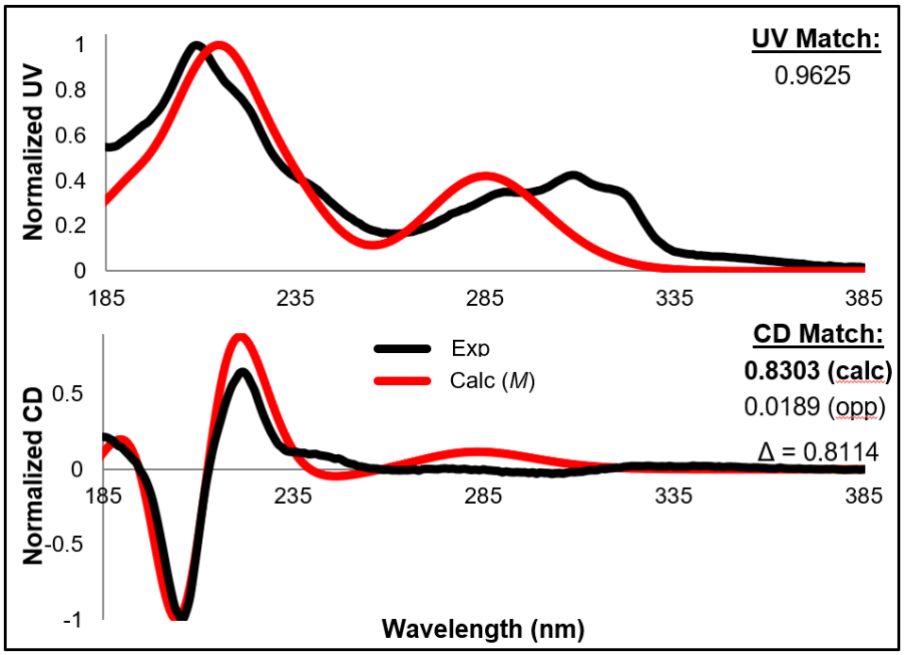

Supplemental Figure S2.57. Comparison between compound **3** experimental (black) and calculated (red) UV (top) and ECD (bottom) spectra. The calculated (*M*)-enantiomer is the better match to the experimental spectrum, with a large difference in fits (Δ=0.4760) suggesting a confident assignment. The calculated spectrum has been shifted 15 nm, and a band broadening of 0.34 eV has been applied.

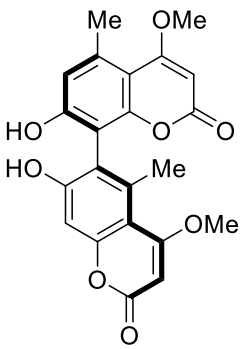

Supplemental Figure S2.58. Assigned absolute configuration of compound **3** based on ECD analysis. Two conformers of the (*M*)-enantiomer of compound **3** that contribute >2% to the Boltzmann distribution. Note the percentage shown above based is on *in vacuo* electronic energies.

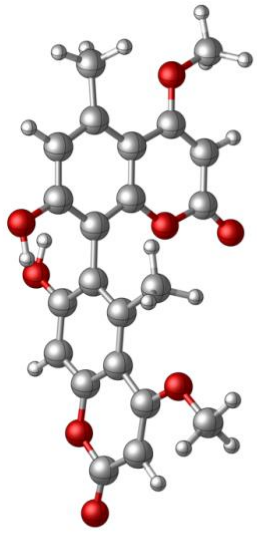

Conformer 1 : 93.5%

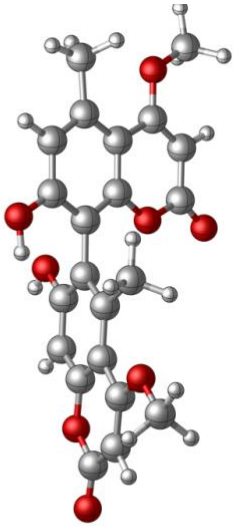

Conformer 2 : 6.2%

Supplemental Table S2.3. Coordinates and electronic energies for B3LYP/6-31G** conformational minima contributing >2% to the *in vacuo* Boltzmann distribution.

Conformer 1: -1451.006913 hartrees

6	-2.26397	1.32304	-1.81171	6	1.89957	-0.00671	-0.13883
6	-0.94194	1.40207	-1.40244	6	4.13733	-0.94655	-0.23642
6	-0.51667	0.803317	-0.1881	6	3.63053	-2.05329	-0.85512
6	-1.43248	0.089407	0.606382	6	2.2263	-2.19746	-1.13973
6	-2.78992	-0.01152	0.185085	8	1.41535	-1.11616	-0.75497
6	-3.16918	0.623084	-1.02306	8	1.68024	-3.13699	-1.66731
6	0.92831	0.963257	0.172799	8	0.509039	3.10264	1.19058
6	1.36838	2.12099	0.831744	8	-0.08255	2.08132	-2.19966
6	2.72231	2.30306	1.14517	6	-3.86125	-0.72515	0.873751
6	3.68147	1.35025	0.828533	6	-5.131	-0.73911	0.371865
6	3.27079	0.153653	0.167648	6	-5.48696	-0.0641	-0.85061

8	-4.44076	0.598618	-1.50328
8	-6.58176	-0.01496	-1.36104
6	5.11289	1.6505	1.2138
6	-0.93451	-0.55208	1.88334
8	-3.51417	-1.35843	2.01348
6	-4.50992	-2.09661	2.72001
8	5.44741	-0.7875	0.041619
6	6.35989	-1.81985	-0.33203
1	5.51737	0.891309	1.88758
1	5.76975	1.67535	0.340709
1	5.16491	2.62049	1.71351
1	-1.51744	-0.22936	2.74809
1	-1.02375	-1.64013	1.83297
1	0.111851	-0.30215	2.05639
6	-2.08204	-1.37141	-1.69424
6	-0.80206	-0.85393	-1.58108
6	-0.50308	0.156212	-0.63216
6	-1.51543	0.6375	0.217837
6	-2.84503	0.128989	0.091087
6	-3.08799	-0.87996	-0.86648
6	0.903446	0.659505	-0.57677
6	1.23962	1.91072	-1.10343
6	2.56161	2.37466	-1.07679
6	3.59413	1.61345	-0.54672
6	3.29074	0.325388	-0.01372
6	1.9474	-0.11452	-0.047
6	4.24198	-0.60854	0.571563
6	3.839	-1.82526	1.04385
6	2.46306	-2.24681	0.995087
8	1.56574	-1.32422	0.44404
8	2.00929	-3.30028	1.38027
8	0.306184	2.73015	-1.65009
8	0.215688	-1.27591	-2.37242
1	-4.00079	-2.52451	3.5836
1	-4.92016	-2.89887	2.0976
1	-5.32172	-1.44267	3.05655
1	7.3432	-1.47095	-0.017
1	6.35326	-1.97758	-1.41577
1	6.12116	-2.76006	0.176462
1	-2.59074	1.78324	-2.73548
1	3.00649	3.21757	1.65375
1	4.24779	-2.88378	-1.1639
1	-5.94329	-1.25832	0.858345
1	-0.38982	2.8265	0.94486
1	0.809834	2.00439	-1.82601

Conformer 2: -1451.004345 hartrees

6	-4.0131	0.541878	0.863114
6	-5.23232	-0.03915	0.657269
6	-5.44143	-1.07298	-0.32354
8	-4.30856	-1.44279	-1.0623
8	-6.47846	-1.64044	-0.57583
6	4.98438	2.20887	-0.57312
6	-1.15221	1.66532	1.26942
8	-3.81035	1.52319	1.76591
6	-4.91173	1.97125	2.55493
8	5.52455	-0.18831	0.608922
6	6.51322	-1.05145	1.16724
1	5.40473	2.30152	0.431462
1	5.67904	1.58966	-1.14636
1	4.9515	3.20207	-1.02723
1	-1.65851	2.61887	1.09741
1	-1.45545	1.32647	2.26153
1	-0.07729	1.83931	1.27803
1	-4.51027	2.74932	3.2041
1	-5.3183	1.15606	3.16285
1	-5.70424	2.38852	1.92445

1	7.45494	-0.50745	1.09325
1	6.58318	-1.9883	0.603937
1	6.29627	-1.27278	2.21788
1	-2.33017	-2.14656	-2.41199
1	2.76328	3.35495	-1.49452
1	4.52254	-2.53952	1.47836
1	-6.11338	0.246638	1.2123
1	-0.54428	2.26234	-1.64973
1	-0.08929	-2.01065	-2.92182

Compound 29

Calculations of the ECD and UV spectra (CAM-B3LYP/6-31++G**) involved modeling the (*P*) -enantiomer of the compound. Hence, the (*P*)-enantiomer had a negative dihedral angle about the atropisomeric bond. Since the atropisomeric bond represents the only stereochemical element present in this compound, the (*M*)-enantiomer is assumed to have a spectrum that will be equal and opposite at all wavelengths.

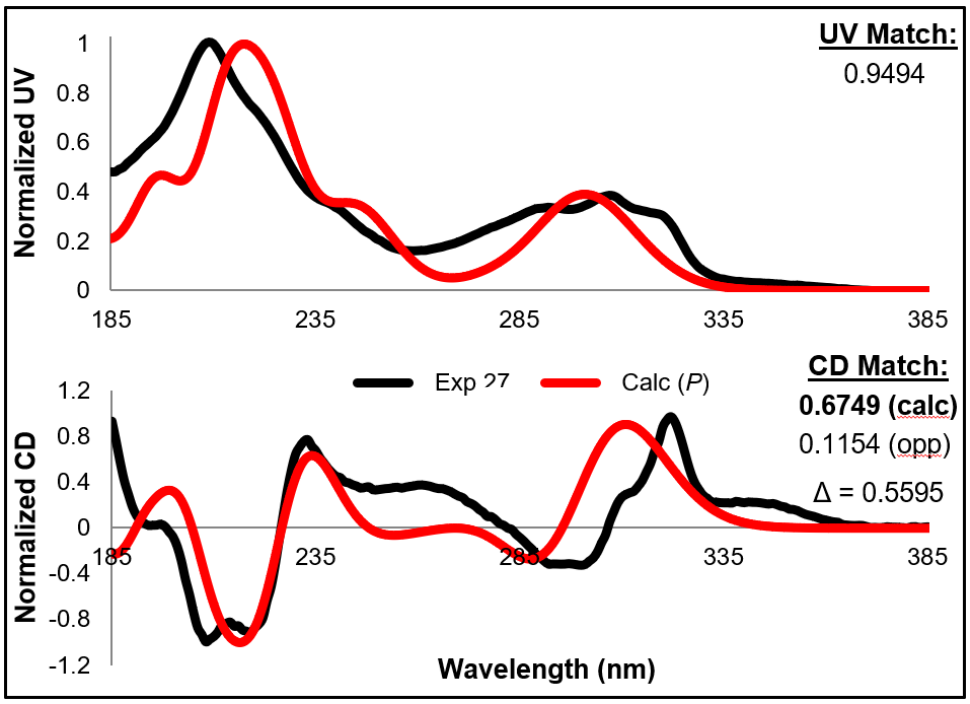

Supplemental Figure S2.59. Comparison between compound **29** experimental (black) and calculated (red) UV (top) and ECD (bottom) spectra. The calculated (*P*)-enantiomer is the better match to the experimental spectrum, with a large difference in fits (Δ=0.5595)

suggesting a confident assignment. The calculated spectrum has been shifted 23 nm, and a band broadening of 0.25 eV has been applied.

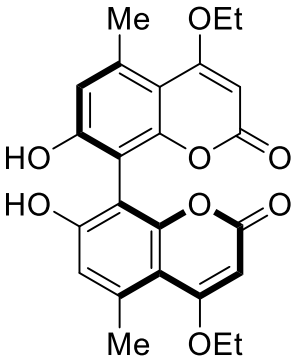

Supplemental Figure S2.60. Assigned absolute configuration of compound **31** based on ECD analysis. Three conformers of the (*P*)-enantiomer of *c*ompound **31** that contributes >2% to the Boltzmann distribution. Note the percentage shown above based is on *in vacuo* electronic energies.

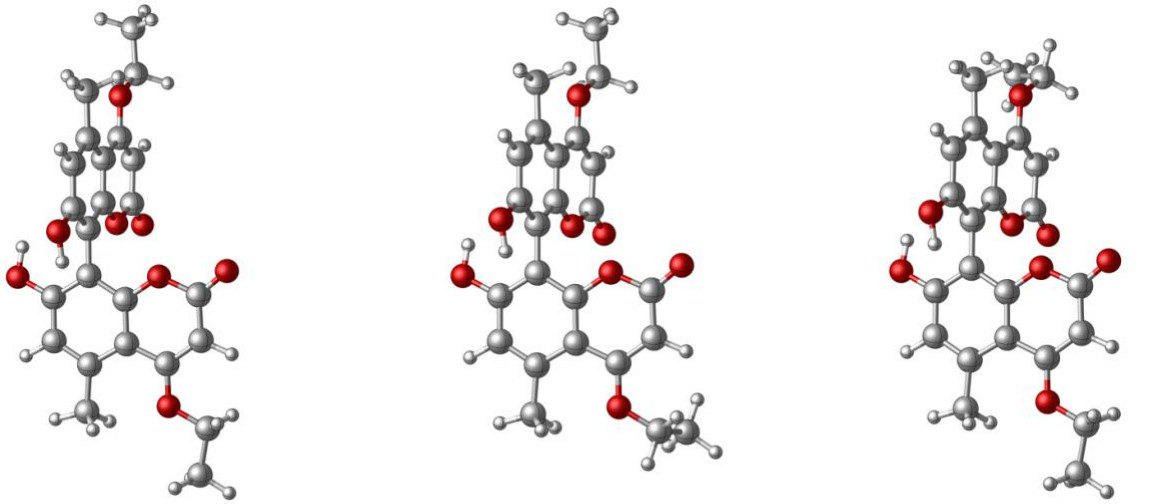

Conformer 1 : 81.4% **Conformer 2** : 8.8% **Conformer 3** : 8.4%

Supplemental Table S2.4. Coordinates and electronic energies for B3LYP/6-31G** conformational minima contributing >2% to the *in vacuo* Boltzmann distribution.

Conformer 1: -1529.653712 hartrees 6 2.4461 2.0336 1.7069

6	1.1207	2.038	1.2527
6	0.7076	1.1678	0.2357
6	1.6651	0.2786	-0.2848
6	3.005	0.2485	0.1635
6	3.3934	1.1592	1.1917
8	1.2032	-0.5432	-1.2619
6	2.0069	-1.4986	-1.904
6	3.3747	-1.5602	-1.46
6	3.8615	-0.739	-0.4823
8	0.2675	2.9172	1.8292
6	-0.7076	1.1678	-0.2356
6	-1.1208	2.0382	-1.2524
6	-2.4462	2.0338	-1.7067
6	-3.3934	1.1592	-1.1916
6	-3.005	0.2483	-0.1636
6	-1.6651	0.2784	0.2848
6	-3.8614	-0.7392	0.4822
6	-3.3745	-1.5606	1.4596
6	-2.0066	-1.4995	1.9031
8	-1.2031	-0.5436	1.2616
8	-0.2676	2.9176	-1.8287
8	1.4857	-2.1719	-2.7621
8	-1.4857	-2.1721	2.762
8	5.1387	-0.7768	-0.0517
8	-5.1388	-0.7768	0.0517
6	6.0446	-1.7307	-0.6302
6	7.3925	-1.5503	0.0419
6	-6.0447	-1.7308	0.6302
6	-7.3927	-1.55	-0.0417
6	4.7899	1.2328	1.7669
6	-4.79	1.233	-1.7667
1	8.1106	-2.2623	-0.3754
1	7.7765	-0.5393	-0.1193
1	7.3181	-1.727	1.1183
1	-8.1108	-2.2621	0.3756
1	-7.7765	-0.539	0.1198
1	-7.3184	-1.7264	-1.1181
1	5.5332	1.4598	0.9989
1	4.833	2.0108	2.5326
1	5.088	0.2843	2.2199
1	-5.0881	0.2845	-2.22
1	-5.5333	1.4597	-0.9986
1	-4.8332	2.0112	-2.5321
1	5.6524	-2.7426	-0.4715
1	6.112	-1.5553	-1.7111
1	-5.6525	-2.7427	0.4711
1	-6.1118	-1.5556	1.7111
1	2.7142	2.729	2.4945
1	3.9828	-2.3016	-1.9561
1	-2.7143	2.7294	-2.494
1	-3.9827	-2.302	1.9558
1	-0.6188	2.7669	1.4618
1	0.6187	2.7672	-1.4614

Conformer 2: -1529.651618 hartrees

6	2.5292	2.194	1.5112
6	1.1854	2.219	1.1147
6	0.6912	1.287	0.193
6	1.5862	0.3118	-0.2843
6	2.9408	0.2561	0.1132
6	3.4144	1.2351	1.0378
8	1.0476	-0.567	-1.1668
6	1.7781	-1.614	-1.7499
6	3.158	-1.7066	-1.351
6	3.7225	-0.8277	-0.4702
8	0.3964	3.1806	1.6526
6	-0.7403	1.3134	-0.2217
6	-1.1907	2.2341	-1.1766

6	-2.5345	2.2585	-1.5732
6	-3.4637	1.3599	-1.0669
6	-3.0357	0.3922	-0.1083
6	-1.6801	0.3995	0.2894
6	-3.8687	-0.6329	0.5103
6	-3.3437	-1.5047	1.4223
6	-1.9635	-1.4572	1.8261
8	-1.1833	-0.4692	1.2055
8	-0.3576	3.1377	-1.7475
8	1.1919	-2.3309	-2.527
8	-1.4133	-2.1689	2.634
8	5.0122	-0.8939	-0.082
8	-5.1598	-0.6354	0.1212
6	5.8443	-1.9463	-0.5967
6	7.2244	-1.7789	0.0104
6	-6.0802	-1.6154	0.6378
6	-5.9785	-2.9459	-0.0953
6	4.8375	1.2943	1.5456
6	-4.8832	1.4716	-1.5773
1	7.8877	-2.5664	-0.3594
1	7.6546	-0.8109	-0.2603
1	7.1815	-1.8484	1.1006
1	-6.7392	-3.6345	0.2865
1	-6.15	-2.8046	-1.1659
1	-4.9989	-3.4107	0.0376
1	5.5546	1.409	0.7291
1	4.9508	2.1393	2.2287
1	5.1126	0.3802	2.0772
1	-5.205	0.554	-2.0758
1	-5.5922	1.6515	-0.7655
1	-4.9547	2.2963	-2.2902
1	5.4057	-2.9154	-0.3294
1	5.8797	-1.8767	-1.691
1	-5.9359	-1.7256	1.7178
1	-7.0613	-1.1615	0.4778
1	2.8613	2.9416	2.2231
1	3.7093	-2.52	-1.7983
1	-2.8314	2.9957	-2.3108
1	-3.9275	-2.2816	1.8929
1	-0.5161	3.0287	1.3573
1	0.5465	2.9547	-1.4439

Conformer 3: -1529.651567 hartrees

6	-2.3755	1.9137	-1.8918
6	-1.0598	1.9624	-1.4122
6	-0.6651	1.182	-0.3178
6	-1.6304	0.3329	0.2536
6	-2.9592	0.2561	-0.2207
6	-3.3296	1.0778	-1.3276
8	-1.1869	-0.4007	1.3058
6	-1.9998	-1.3051	2.0072
6	-3.3558	-1.4158	1.5373
6	-3.824	-0.6832	0.4833
8	-0.1976	2.7945	-2.0442
6	0.7395	1.2262	0.1804
6	1.1567	2.2387	1.0539
6	2.4733	2.2769	1.5322
6	3.4062	1.3088	1.1862
6	3.0126	0.2531	0.309
6	1.6827	0.2424	-0.1684
6	3.8561	-0.8446	-0.1502
6	3.3645	-1.7968	-0.9982
6	2.0061	-1.7788	-1.4718
8	1.216	-0.7153	-1.009
8	0.3164	3.2186	1.4647
8	-1.4958	-1.8981	2.9323
8	1.4834	-2.5695	-2.2225
8	-5.0895	-0.77	0.0255

8	5.1173	-0.8392	0.327
6	-5.9998	-1.6869	0.6546
6	-7.3294	-1.5829	-0.068
6	6.0446	-1.8784	-0.0398
6	6.701	-1.6172	-1.3888
6	-4.7135	1.0944	-1.9365
6	4.793	1.4427	1.775
1	-8.0503	-2.2689	0.3865
1	-7.731	-0.5681	-0.0024
1	-7.2211	-1.8469	-1.1235
1	7.4448	-2.3943	-1.5919
1	5.9731	-1.6201	-2.2035
1	7.2093	-0.649	-1.3838
1	-5.4752	1.3741	-1.2047
1	-4.7454	1.8097	-2.7616
1	-4.9948	0.1107	-2.3199
1	5.056	0.5743	2.3839
1	5.5574	1.5225	0.9982
1	4.842	2.3346	2.4039
1	-5.5899	-2.7023	0.591
1	-6.101	-1.4246	1.7151
1	6.789	-1.8587	0.7599
1	5.5424	-2.8508	-0.0048
1	-2.6293	2.5402	-2.7396
1	-3.9706	-2.1191	2.0785
1	2.7454	3.0831	2.2041
1	3.9618	-2.6171	-1.3668
1	0.6844	2.6719	-1.6567
1	-0.5696	3.0264	1.1168

Compound 30

Calculations of the ECD and UV spectra (CAM-B3LYP/6-31++G**) involved modeling the (*P*)-enantiomer of the compound. Hence, the (*P*)-enantiomer had a negative dihedral angle about the atropisomeric bond. Since the atropisomeric bond represents the only stereochemical element present in this compound, the (*M*)-enantiomer is assumed to

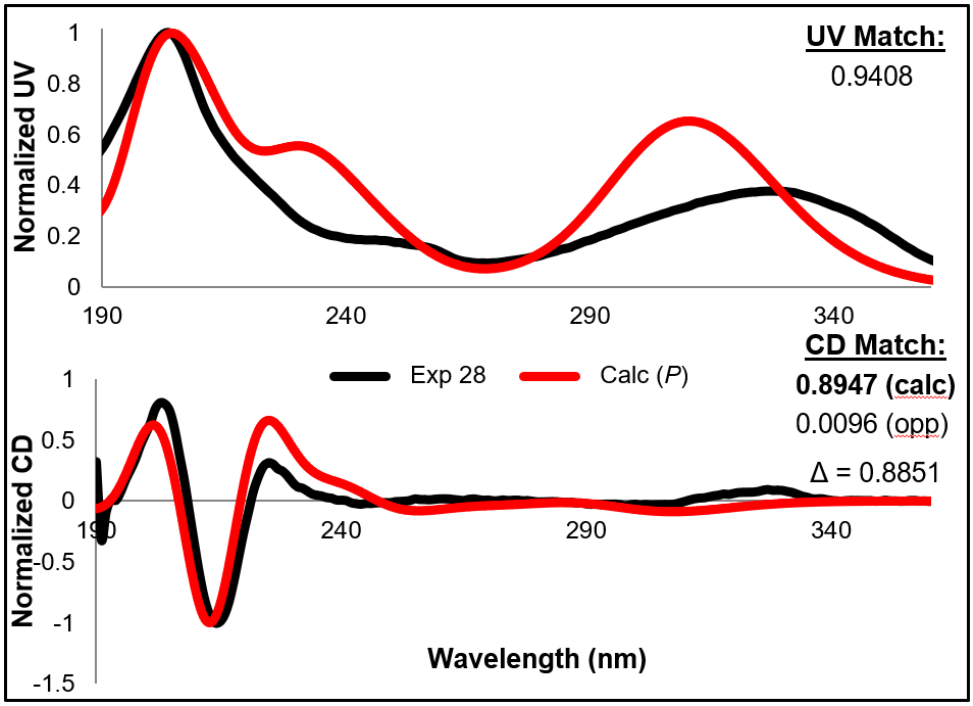

have a spectrum that will be equal and opposite at all wavelengths.

Supplemental Figure S2.61. Comparison between compound **30** experimental (black) and calculated (red) UV (top) and ECD (bottom) spectra. The calculated (*P*)-enantiomer is the better match to the experimental spectrum, with a large difference in fits (Δ=0.8851) suggesting a confident assignment. The calculated spectrum has been shifted 26 nm, and a band broadening of 0.27 eV has been applied.

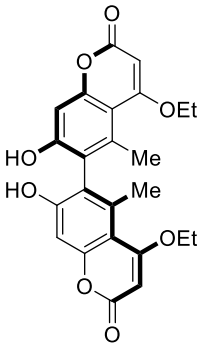

Supplemental Figure S2.62. Assigned absolute configuration of compound **32** based on ECD analysis. One conformer of the (*P*)-enantiomer of compound **30** that contributes >2% to the Boltzmann distribution. Note the percentage shown above based is on *in vacuo* electronic energies.

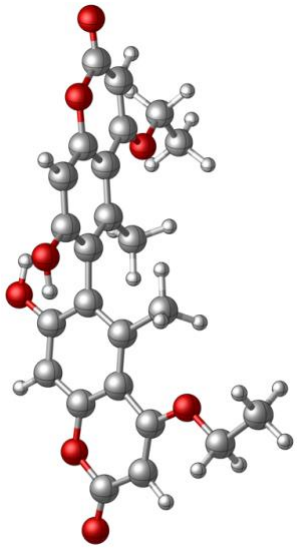

Conformer 1 : 98.6%

Supplemental Table S2.5. Coordinates and electronic energies for B3LYP/6-31G** conformational minima contributing >2% to the *in vacuo* Boltzmann distribution.

Conformer 1: -1529.649257 hartrees

6	0.993835	-1.36762	1.58732
6	2.27617	-1.88631	1.67206
6	3.29272	-1.28967	0.934152
6	3.06548	-0.16998	0.097387
6	1.73861	0.345697	0.003389
6	0.708267	-0.25201	0.755957
6	-0.70827	0.252022	0.755954
6	-1.73862	-0.34569	0.00339
6	-3.06548	0.169983	0.097381
6	-3.29273	1.28968	0.934138
6	-2.27617	1.88633	1.67205
6	-0.99384	1.36764	1.5873
6	-4.2485	-0.34451	-0.58928
6	-5.46615	0.252746	-0.42561
6	-5.65864	1.40231	0.421597
8	-4.51421	1.86567	1.08361
8	4.51421	-1.86565	1.08364
6	5.65864	-1.40229	0.421629
6	5.46615	-0.25275	-0.4256
6	4.2485	0.344502	-0.58928
6	1.38819	1.51207	-0.89724
6	-1.3882	-1.51207	-0.89723
8	0.026	-1.96831	2.31866

8	-0.02601	1.96833	2.31865
8	-6.69337	1.99488	0.618899
8	-4.05868	-1.42719	-1.36976
6	-5.18126	-1.99717	-2.06479
6	-4.67607	-3.19131	-2.85185
8	6.69336	-1.99489	0.618902
8	4.05869	1.42718	-1.36978
6	5.18127	1.99715	-2.0648
6	4.67611	3.19129	-2.85187
1	1.6966	1.31773	-1.92614
1	0.314337	1.6956	-0.88677
1	1.90001	2.42719	-0.58903
1	-1.90002	-2.42719	-0.58901
1	-1.69661	-1.31774	-1.92613
1	-0.31435	-1.69561	-0.88675
1	-5.50678	-3.65248	-3.39403
1	-3.91746	-2.88772	-3.57828
1	-4.24055	-3.94167	-2.18658
1	5.50682	3.65245	-3.39405
1	3.91749	2.88769	-3.5783
1	4.24058	3.94166	-2.18661
1	-5.94351	-2.29435	-1.33418
1	-5.61833	-1.23939	-2.72658
1	5.94353	2.29432	-1.33418
1	5.61834	1.23936	-2.72657
1	2.49284	-2.73967	2.30216
1	-2.49285	2.73969	2.30214
1	-6.35891	-0.10275	-0.91771
1	6.35891	0.102734	-0.91772
1	-0.80855	-1.49468	2.16741
1	0.808541	1.4947	2.1674

Compound 31

Calculations of the ECD and UV spectra (CAM-B3LYP/6-31++G**) involved modeling the (*P*) -enantiomer of the compound. Hence, the (*P*)-enantiomer had a negative dihedral angle about the atropisomeric bond. Since the atropisomeric bond represents the only stereochemical element present in this compound, the (*M*)-enantiomer is assumed to have a spectrum that will be equal and opposite at all wavelengths.

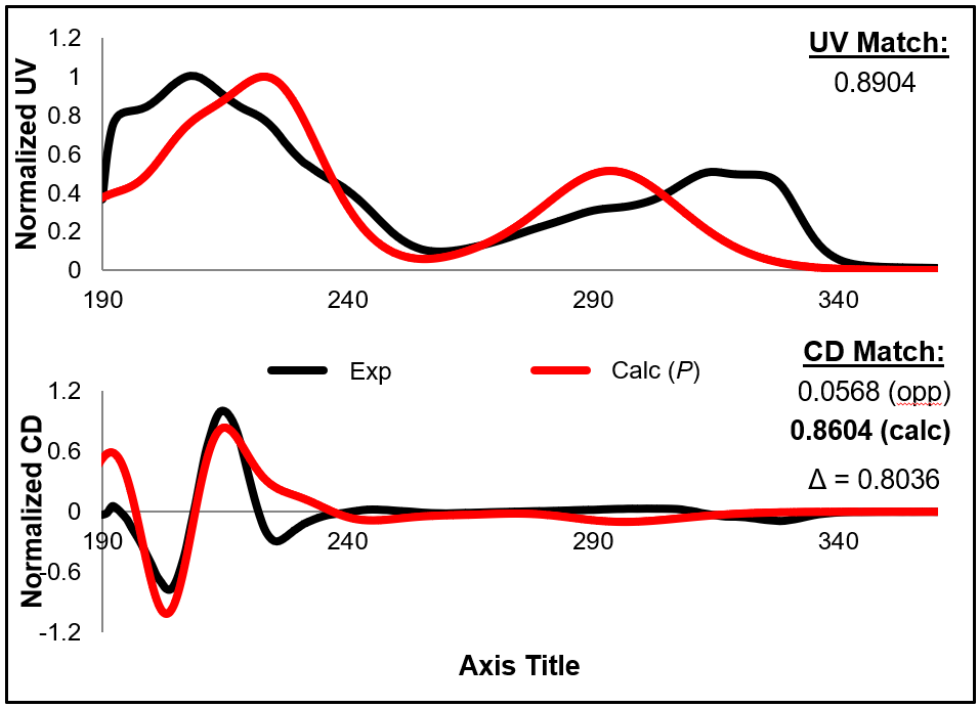

Supplemental Figure S2.63. Comparison between compound **31** experimental (black) and calculated (red) UV (top) and ECD (bottom) spectra. The calculated (*P*)-enantiomer is the better match to the experimental spectrum, with a large difference in fits (Δ=0.8036) suggesting a confident assignment. The calculated spectrum has been shifted 15 nm, and a band broadening of 0.27 eV has been applied.

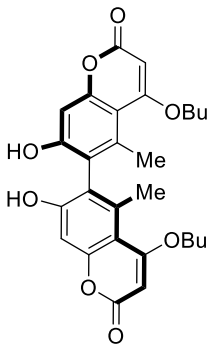

Supplemental Figure S2.64. Assigned absolute configuration of compound **31** based on ECD analysis. Four conformers of the (*P*)-enantiomer of compound **31** that contribute >2% to the Boltzmann distribution. Note the percentage shown above based is on *in vacuo* electronic energies.

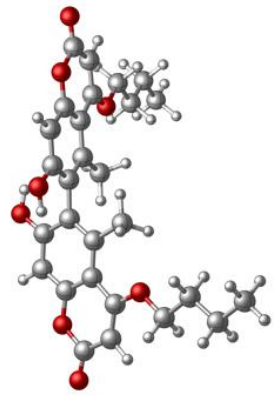

Conformer 1 : 41.7%

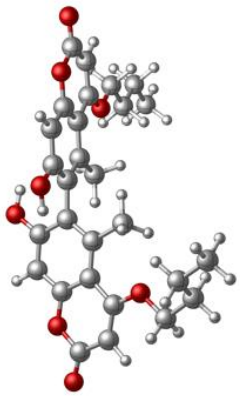

Conformer 2 : 32.0%

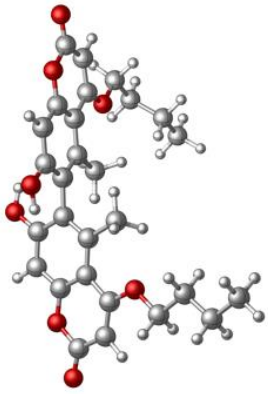

Conformer 3 : 14.5%

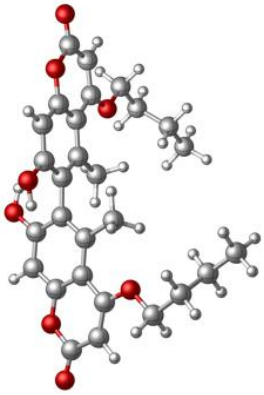

Conformer 4 : 10.8%

Supplemental Table S2.6. Coordinates and electronic energies for B3LYP/6-31G** conformational minima contributing >2% to the *in vacuo* Boltzmann distribution.

Conformer 1: -1686.915126 hartrees			
6	0.628404	0.412323	-1.25861
6	0.63998	1.57158	-2.07905
6	1.75947	2.38532	-2.15067
6	2.8877	2.04367	-1.41268
6	2.93581	0.890784	-0.59173
6	1.77171	0.07055	-0.50917
8	-0.44186	1.92929	-2.81013
8	3.93339	2.9009	-1.54636
6	5.15158	2.7227	-0.87756
6	5.24171	1.54736	-0.04922
6	4.20672	0.667349	0.094586

8	6.01029	3.55446	-1.05577
8	4.28542	-0.444	0.85314
6	-0.62851	-0.41281	-1.2585
6	-0.64038	-1.57194	-2.07912
6	-1.75989	-2.38567	-2.15048
6	-2.88792	-2.04405	-1.41218
6	-2.93578	-0.89123	-0.59112
6	-1.77159	-0.07111	-0.5087
8	0.441242	-1.92957	-2.81058
8	-3.93366	-2.90125	-1.54564
6	-5.15174	-2.72297	-0.87664
6	-5.24164	-1.54763	-0.04828
6	-4.2066	-0.66765	0.095322
8	-6.01052	-3.55467	-1.05473
8	-4.28515	0.443799	0.853749
6	-5.51156	0.737943	1.54369
6	-5.32424	2.04625	2.2962
6	-6.58355	2.45165	3.07368
6	-6.41179	3.77138	3.83137
6	5.51177	-0.73762	1.54341
6	5.3245	-2.0455	2.29668
6	6.58368	-2.45009	3.0748
6	6.41224	-3.76967	3.8328
6	1.71098	-1.15469	0.379231
6	-1.71049	1.15391	0.37999
1	-7.32328	4.03679	4.37532
1	-5.59576	3.70724	4.55947
1	-6.18077	4.59429	3.14619
1	7.32363	-4.03447	4.37723
1	5.59587	-3.70573	4.56054
1	6.18193	-4.59289	3.14777
1	1.96213	-0.9019	1.41108
1	0.713021	-1.59108	0.363496
1	2.42865	-1.91633	0.064509
1	-1.9619	0.900991	1.41174
1	-0.71235	1.58989	0.364465
1	-2.42778	1.91594	0.065332
1	-5.74635	-0.08445	2.23174
1	-6.32732	0.81517	0.813446
1	-5.05691	2.83291	1.5801
1	-4.47654	1.94316	2.9847
1	-6.84775	1.65501	3.78175
1	-7.43004	2.53632	2.37933
1	5.7464	0.085203	2.23099
1	6.32762	-0.81521	0.813303
1	5.05757	-2.83268	1.58101
1	4.47658	-1.94215	2.98486
1	6.8472	-1.65311	3.78275
1	7.43051	-2.53455	2.38083
1	1.76569	3.2732	-2.77023
1	6.19165	1.41251	0.445762
1	-1.76629	-3.27349	-2.77014
1	-6.19152	-1.41268	0.446793
1	-1.13707	1.26531	-2.67073
1	1.1365	-1.2656	-2.6713

Conformer 2: -1686.914872 hartrees

6	-0.47596	-0.51215	-1.12047
6	-0.43572	-1.77156	-1.77574
6	-1.55084	-2.59346	-1.81392
6	-2.72462	-2.16306	-1.20481
6	-2.82263	-0.91327	-0.5459
6	-1.66497	-0.08091	-0.49914
8	0.691454	-2.21745	-2.37878
8	-3.76293	-3.03476	-1.29593
6	-5.02373	-2.77464	-0.74302
6	-5.16239	-1.50444	-0.07745
6	-4.13399	-0.61099	0.024323

8	-5.87387	-3.62376	-0.87396
8	-4.25514	0.58368	0.636345
6	0.779238	0.314532	-1.15676
6	0.845646	1.3437	-2.13309
6	1.97041	2.14439	-2.25119
6	3.0506	1.91631	-1.40537
6	3.04561	0.891577	-0.42753
6	1.8728	0.090094	-0.297
8	-0.18764	1.58697	-2.97321
8	4.10412	2.75282	-1.59601
6	5.27702	2.68134	-0.83376
6	5.31518	1.63368	0.154556
6	4.27465	0.771112	0.355389
8	6.14562	3.48716	-1.07283
8	4.31217	-0.22732	1.26054
6	5.488	-0.38784	2.07604
6	5.28536	-1.59337	2.98132
6	5.23173	-2.93743	2.2443
6	5.04867	-4.12557	3.19263
6	-5.52066	0.955121	1.20828
6	-5.3666	2.33551	1.82773
6	-6.67172	2.8361	2.46046
6	-6.52788	4.22409	3.09145
6	-1.66077	1.25515	0.214365
6	1.74827	-0.99159	0.755536
1	5.01875	-5.07107	2.64269
1	5.86949	-4.18719	3.91602
1	4.1145	-4.04115	3.759
1	-7.47098	4.55667	3.5354
1	-5.76918	4.22319	3.88169
1	-6.22909	4.96909	2.34593
1	-1.96721	1.1434	1.25621
1	-0.6661	1.69889	0.192561
1	-2.36441	1.95649	-0.24067
1	1.97815	-0.60107	1.74806
1	0.738147	-1.39964	0.768328
1	2.44849	-1.81124	0.573944
1	5.63945	0.526338	2.66298
1	6.36082	-0.52814	1.42539
1	4.37075	-1.44578	3.56931
1	6.1166	-1.60105	3.69877
1	6.15697	-3.06626	1.66659
1	4.41493	-2.9191	1.51397
1	-5.80927	0.212377	1.96312
1	-6.28588	0.956961	0.421397
1	-5.03285	3.03712	1.05344
1	-4.57371	2.29917	2.58484
1	-7.00629	2.12038	3.22318
1	-7.46136	2.86084	1.69785
1	-1.51903	-3.5552	-2.31017
1	-6.14233	-1.31111	0.332391
1	2.01786	2.93543	-2.9889
1	6.2341	1.57695	0.718157
1	1.37705	-1.53554	-2.28586
1	-0.89298	0.946879	-2.78234

Conformer 3: -1686.914784 hartrees

6	-0.477	0.9263	1.0324
6	-0.5378	2.3129	1.3335
6	-1.7017	3.0378	1.1322
6	-2.8247	2.3831	0.6379
6	-2.8231	0.9999	0.3339
6	-1.6152	0.2664	0.5278
8	0.5379	2.9779	1.8167
8	-3.9163	3.1753	0.4743
6	-5.1383	2.6932	-0.013
6	-5.1771	1.2849	-0.3145
6	-4.0941	0.4679	-0.1537

8	-6.0416	3.4875	-0.1315
8	-4.123	-0.8532	-0.4189
6	0.8249	0.2247	1.3043
6	0.9284	-0.4902	2.527
6	2.0984	-1.147	2.8736
6	3.1826	-1.0944	2.0043
6	3.1351	-0.3949	0.7735
6	1.9237	0.272	0.4234
8	-0.1095	-0.561	3.3933
8	4.2843	-1.7633	2.4342
6	5.4746	-1.8169	1.6978
6	5.4629	-1.1112	0.4419
6	4.3664	-0.4354	-0.0145
8	6.3946	-2.4407	2.1725
8	4.3489	0.2277	-1.1884
6	5.5449	0.258	-1.9896
6	5.2635	1.0647	-3.248
6	4.2626	0.4131	-4.2103
6	4.029	1.2457	-5.4738
6	-5.3471	-1.4513	-0.8779
6	-5.0957	-2.9383	-1.0745
6	-6.3519	-3.6817	-1.5469
6	-6.1124	-5.1813	-1.7446
6	-1.5027	-1.2063	0.1916
6	1.7666	1.0238	-0.8815
1	3.3133	0.7587	-6.1433
1	4.9604	1.3916	-6.0325
1	3.6326	2.237	-5.2278
1	-7.0232	-5.6863	-2.0802
1	-5.7916	-5.6575	-0.8117
1	-5.3347	-5.3635	-2.4944
1	-2.1707	-1.8123	0.8086
1	-0.4816	-1.5559	0.34
1	-1.786	-1.3941	-0.8458
1	2.4905	1.8371	-0.968
1	0.7634	1.4394	-0.968
1	1.9393	0.3627	-1.7336
1	6.3528	0.7124	-1.4034
1	5.8365	-0.7704	-2.2394
1	4.9159	2.0643	-2.9584
1	6.2244	1.2079	-3.76
1	4.6293	-0.5844	-4.488
1	3.3102	0.256	-3.6915
1	-6.1349	-1.2783	-0.1334
1	-5.6544	-0.9733	-1.817
1	-4.2864	-3.0699	-1.8032
1	-4.742	-3.3658	-0.1282
1	-7.1594	-3.5336	-0.8177
1	-6.706	-3.2406	-2.4883
1	-1.7459	4.0962	1.3557
1	-6.1288	0.924	-0.6743
1	2.1775	-1.6924	3.8055
1	6.3881	-1.1594	-0.112
1	1.2693	2.346	1.9137
1	-0.8496	-0.0508	3.0252

Conformer 4: -1686.914499 hartrees

6	-0.6753	1.3538	-0.3304
6	-0.8376	2.1979	-1.461
6	-2.0545	2.285	-2.1181
6	-3.1266	1.5321	-1.6515
6	-3.0209	0.6755	-0.5283
6	-1.7622	0.589	0.1375
8	0.1873	2.9413	-1.9398
8	-4.2767	1.6895	-2.3575
6	-5.4638	1.0211	-2.0325
6	-5.3931	0.1444	-0.8915
6	-4.2471	-0.0361	-0.1695

8	-6.4301	1.2343	-2.7266
8	-4.1739	-0.856	0.8984
6	0.6756	1.3538	0.3304
6	0.838	2.1979	1.4609
6	2.0548	2.2849	2.1181
6	3.1269	1.5319	1.6515
6	3.0211	0.6753	0.5283
6	1.7624	0.5889	-0.1374
8	-0.1869	2.9413	1.9398
8	4.277	1.6893	2.3575
6	5.4641	1.0208	2.0324
6	5.3933	0.144	0.8915
6	4.2472	-0.0363	0.1696
8	6.4304	1.2339	2.7265
8	4.1739	-0.8563	-0.8984
6	5.3603	-1.5504	-1.3273
6	5.0094	-2.404	-2.5363
6	4.0582	-3.5691	-2.2365
6	3.7493	-4.4142	-3.4755
6	-5.3606	-1.5499	1.3272
6	-5.01	-2.4036	2.5363
6	-4.059	-3.5689	2.2365
6	-3.7506	-4.4141	3.4756
6	-1.5432	-0.3151	1.3322
6	1.5435	-0.3152	-1.3321
1	3.0721	-5.2393	-3.2347
1	4.6624	-4.8467	-3.8997
1	3.2744	-3.8121	-4.2581
1	-3.0735	-5.2394	3.2348
1	-4.6638	-4.8463	3.8997
1	-3.2755	-3.8121	4.2582
1	-2.2103	-0.0598	2.1584
1	-0.5135	-0.2483	1.6817
1	-1.752	-1.3559	1.0752
1	2.2106	-0.0601	-2.1583
1	0.5139	-0.2485	-1.6817
1	1.7522	-1.3561	-1.075
1	6.1318	-0.8117	-1.5767
1	5.7322	-2.1715	-0.5022
1	4.5851	-1.7579	-3.315
1	5.953	-2.7952	-2.9394
1	4.5031	-4.2043	-1.4586
1	3.1252	-3.1773	-1.8158
1	-6.1319	-0.8111	1.5765
1	-5.7325	-2.1709	0.502
1	-4.5855	-1.7575	3.315
1	-5.9537	-2.7945	2.9393
1	-4.5041	-4.204	1.4586
1	-3.1259	-3.1775	1.8159
1	-2.1789	2.9279	-2.9803
1	-6.3164	-0.361	-0.6523
1	2.1793	2.9279	2.9803
1	6.3165	-0.3614	0.6523
1	0.9656	2.785	-1.3799
1	-0.9652	2.7851	1.3799

Compound 32

Calculations of the ECD and UV spectra (CAM-B3LYP/6-31++G**) involved modeling the (*P*)- enantiomer of the compound. Hence, the (*P*)-enantiomer had a negative dihedral angle about the atropisomeric bond. Since the atropisomeric bond represents the only stereochemical element present in this compound, the (*M*)-enantiomer is assumed to have a spectrum that will be equal and opposite at all wavelengths.

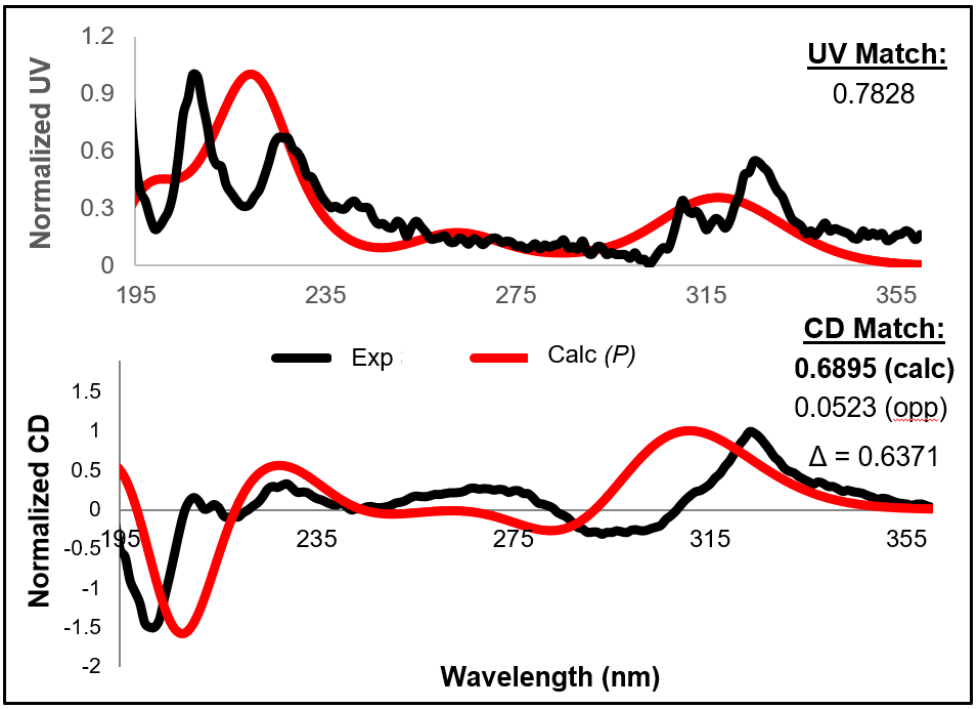

Supplemental Figure S2.65. Comparison between compound **32** experimental (black) and calculated (red) UV (top) and ECD (bottom) spectra. The calculated (*P*)-enantiomer is the better match to the experimental spectrum, with a large difference in fits (Δ=0.6371) suggesting a confident assignment. The calculated spectrum has been shifted 23 nm, and a band broadening of 0.27 eV has been applied.

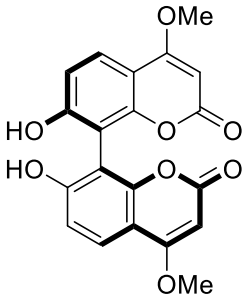

Supplemental Figure S2.66. Assigned absolute configuration of compound **32** based on ECD analysis. One conformer of the (*P*)-enantiomer of compound **32** that contributes >2% to the Boltzmann distribution. Note the percentage shown above based is on *in vacuo* electronic energies.

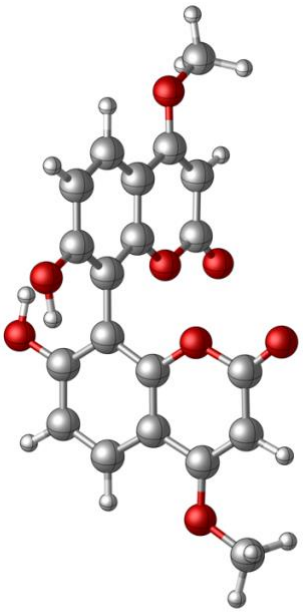

Conformer 1 : 97.4%

Supplemental Table S2.7. Coordinates and electronic energies for B3LYP/6-31G** conformational minima contributing >2% to the *in vacuo* Boltzmann distribution.

Conformer 1: -1372.377848 hartrees

6	2.31394	2.02338	1.89126	6	1.67274	0.229013	-0.15375
6	1.02614	2.01804	1.32742	6	2.96203	0.216559	0.406028
6	0.688352	1.13213	0.287947	6	3.26247	1.12913	1.4338

8	1.31721	-0.61885	-1.15131
6	2.20633	-1.57434	-1.68586
6	3.53343	-1.60616	-1.11385
6	3.90356	-0.75375	-0.11538
8	0.128796	2.90377	1.82103
6	-0.68836	1.13213	-0.28794
6	-1.02615	2.01806	-1.3274
6	-2.31395	2.0234	-1.89123
6	-3.26248	1.12914	-1.43378
6	-2.96202	0.216545	-0.40604
6	-1.67274	0.228997	0.153743
6	-3.90355	-0.75377	0.115366
6	-3.53342	-1.60621	1.11381
6	-2.2063	-1.57443	1.68577
8	-1.3172	-0.61889	1.15128
8	-0.12881	2.9038	-1.82098
8	1.78499	-2.27601	-2.57392
8	-1.78499	-2.27603	2.5739
8	5.11786	-0.71581	0.466646
6	6.10971	-1.6432	0.026224
8	-5.11787	-0.71581	-0.46664
6	-6.10972	-1.64317	-0.02618
1	6.99507	-1.43832	0.627694
1	6.34095	-1.49606	-1.03433
1	5.78198	-2.6753	0.190171
1	-6.99512	-1.43823	-0.62759
1	-6.34089	-1.49606	1.03439
1	-5.78204	-2.67528	-0.19018
1	2.53014	2.72423	2.68914
1	4.25637	1.11657	1.86547
1	4.19646	-2.34756	-1.53589
1	-2.53016	2.72426	-2.68909
1	-4.25638	1.11658	-1.86545
1	-4.19645	-2.3476	1.53585
1	-0.72741	2.74724	1.39056
1	0.727394	2.74726	-1.39053

[1]H NMR and [13]C NMR spectra of compounds

Supplemental Figure S2.67. Crude ^{1}H NMR (600 MHz, $(CD_3)_2SO$, 1.5-4.5 ppm) from oxidative dimerization of **1** (**Figure 2.8, Entry 5**).

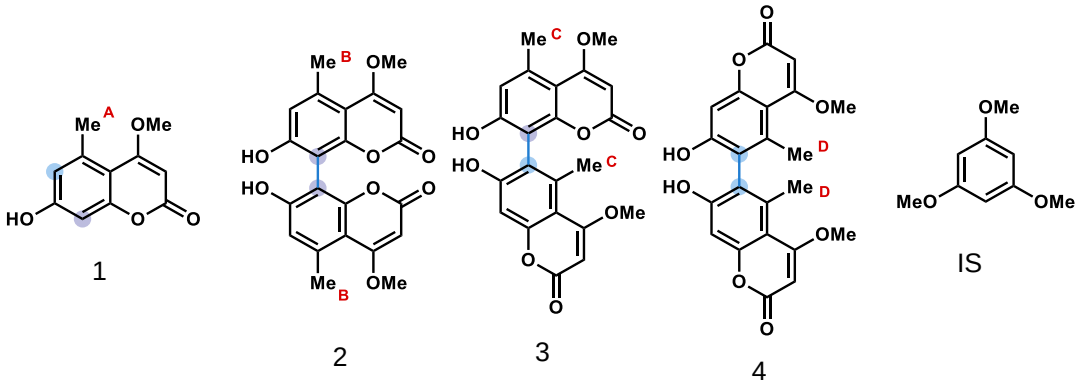

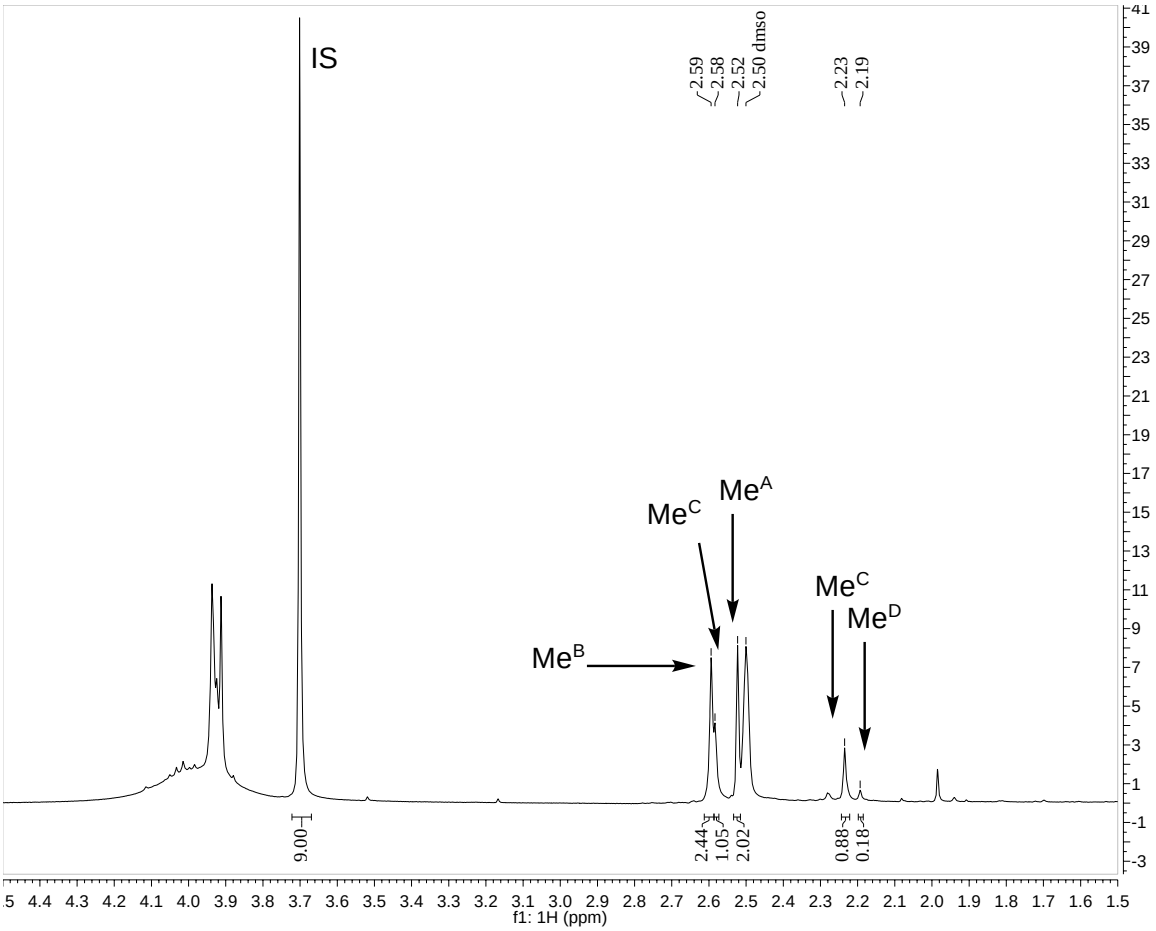

Supplemental Figure S2.68. Crude 1H NMR (600 MHz, (CD3)2SO, 1.5-4.5 ppm) from oxidative dimerization of **1** (**Figure 2.8, Entry 6**).

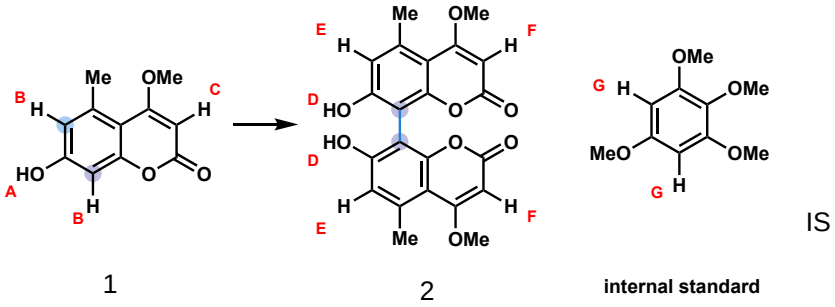

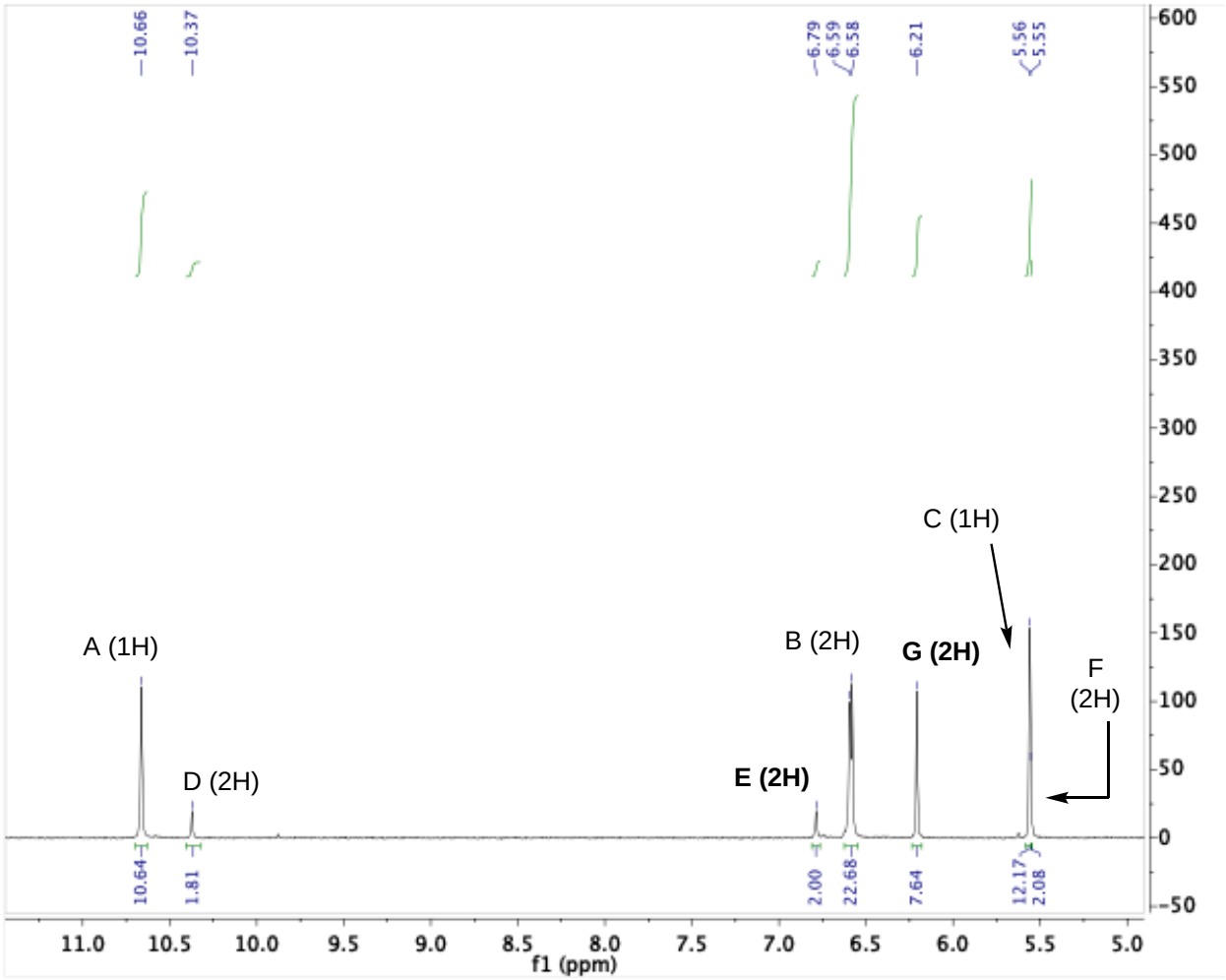

Peaks E and G used for calculating % yield.

Supplemental Figure S2.69. (**50**) ^{1}H NMR (400 MHz, $(CD_3)_2SO$)

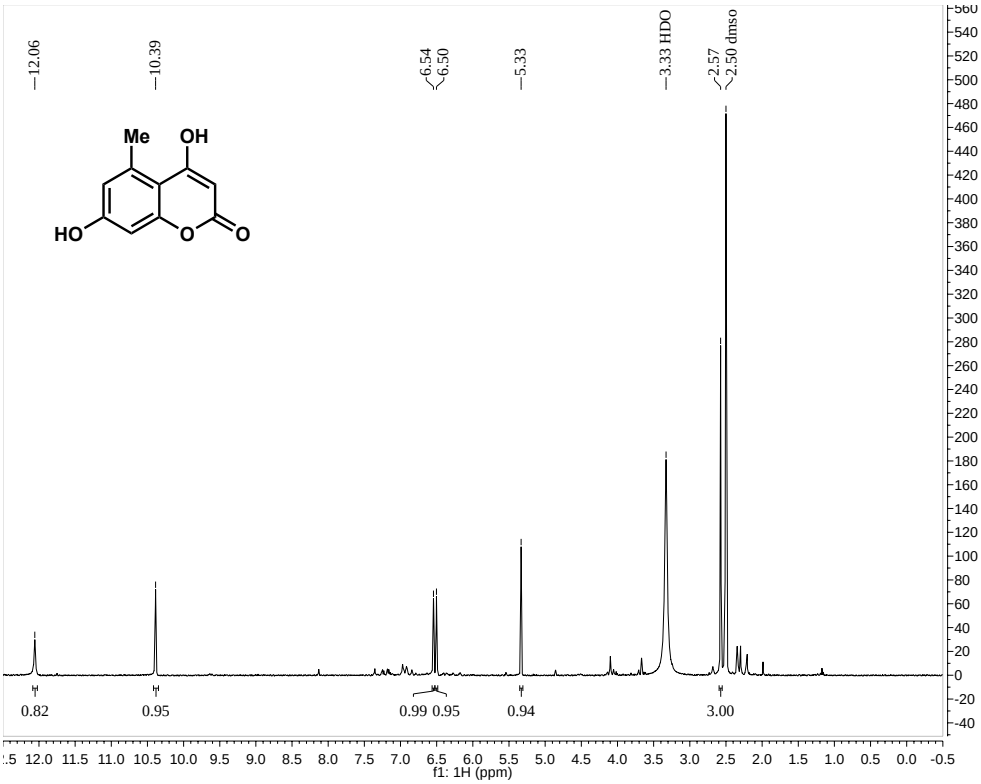

^{13}C NMR (150 MHz, $(CD_3)_2SO$)

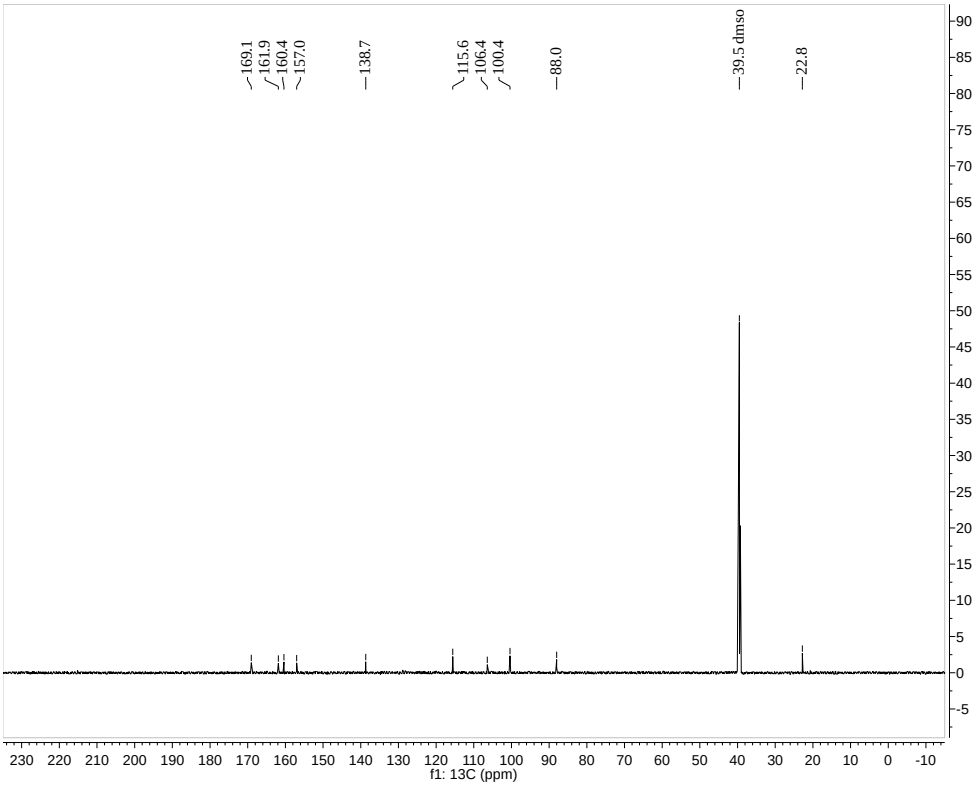

Supplemental Figure S2.70. (**1**) ^{1}H NMR (400 MHz, $(CD_3)_2SO$)

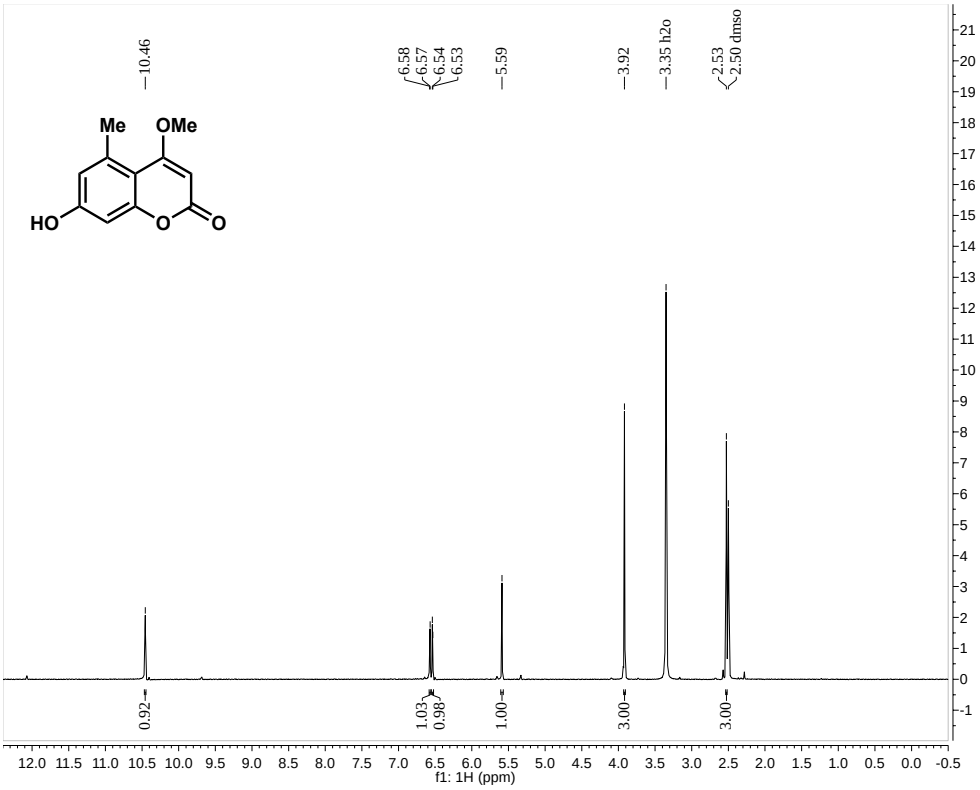

Supplemental Figure S2.71. (**25**) ^{1}H NMR (600 MHz, $(CD_3)_2SO$)

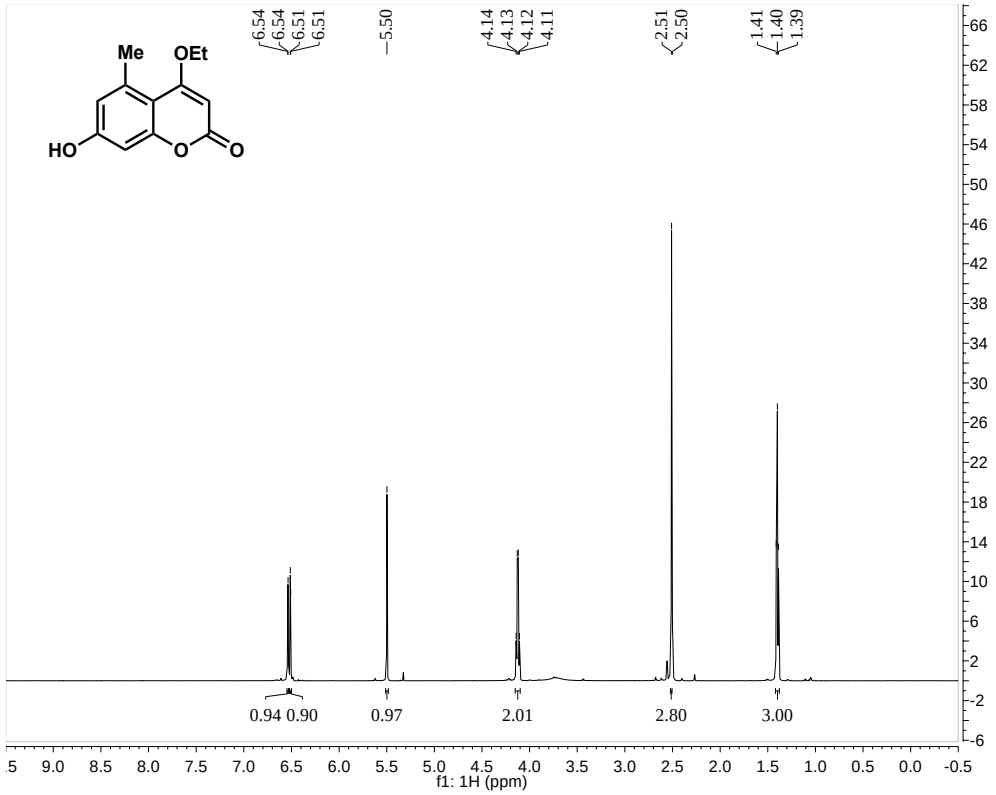

^{13}C NMR (150 MHz, $(CD_3)_2SO$)

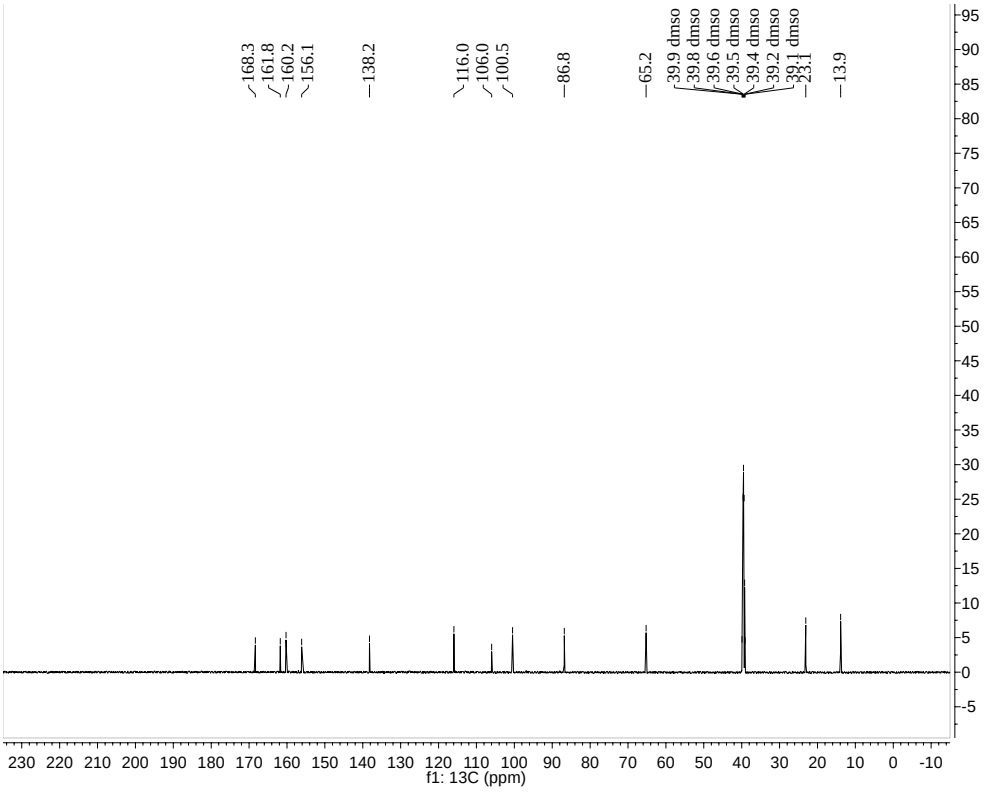

Supplemental Figure S2.72. (**34**) ^{1}H NMR (600 MHz, $(CD_3)_2CO$)

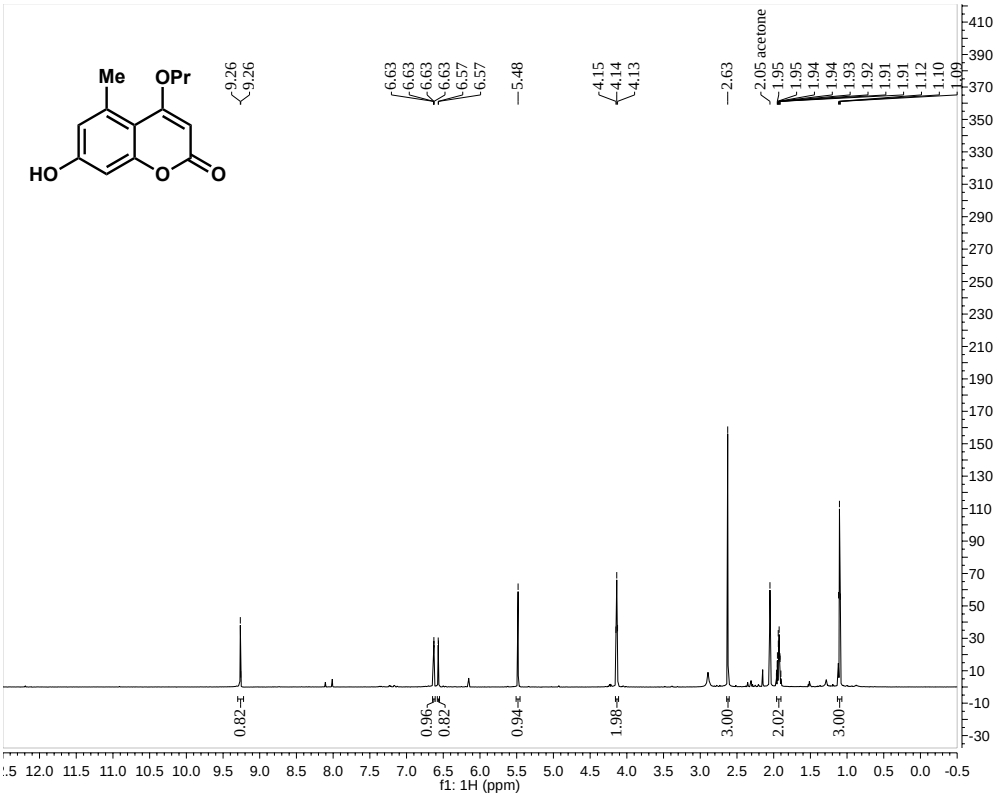

^{13}C NMR (150 MHz, $(CD_3)_2CO$)

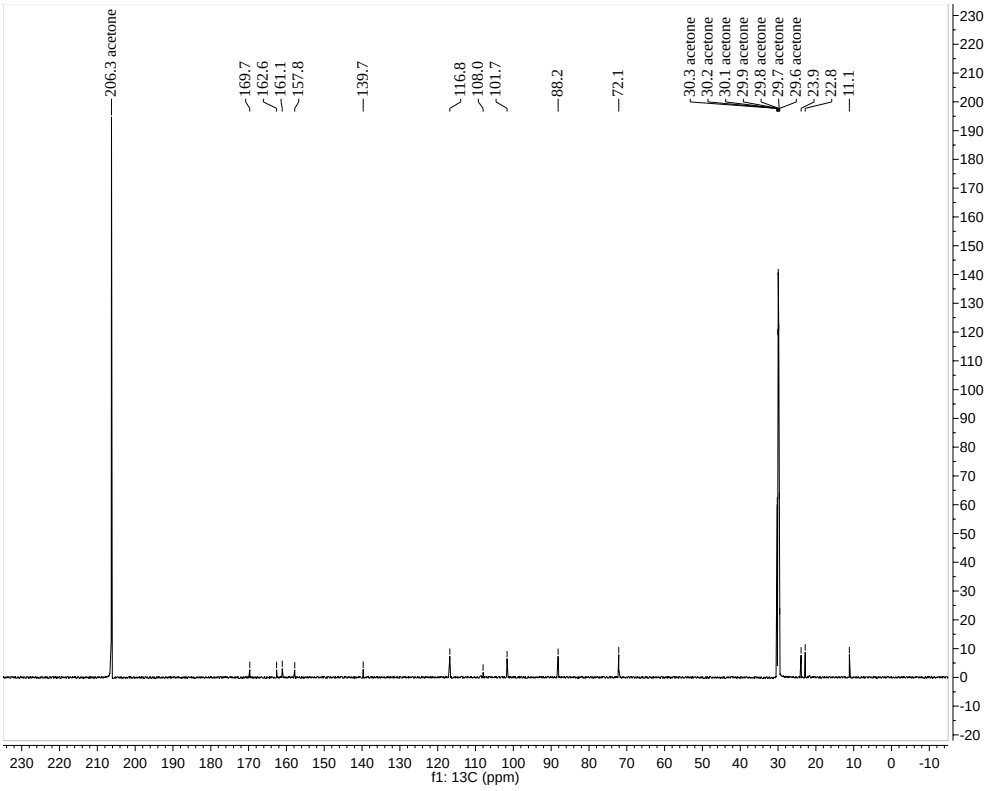

Supplemental Figure S2.73. (**26**)^{1}H NMR (600 MHz, CD_3OD)

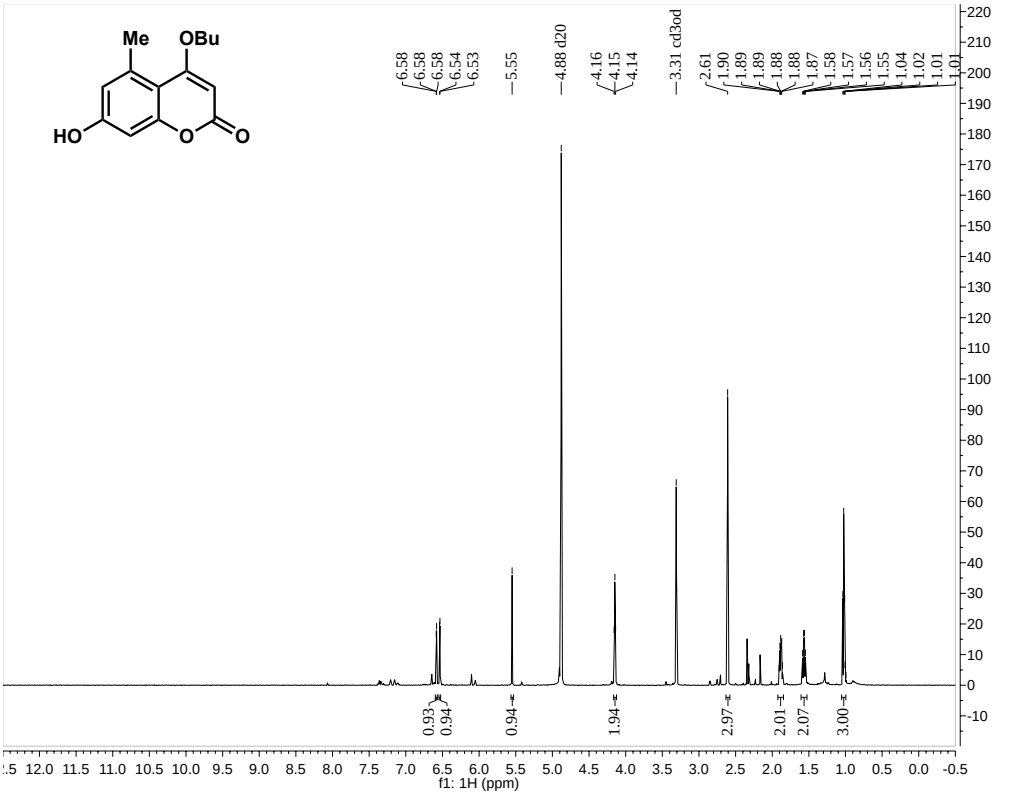

^{13}C NMR (150 MHz, CD_3OD)

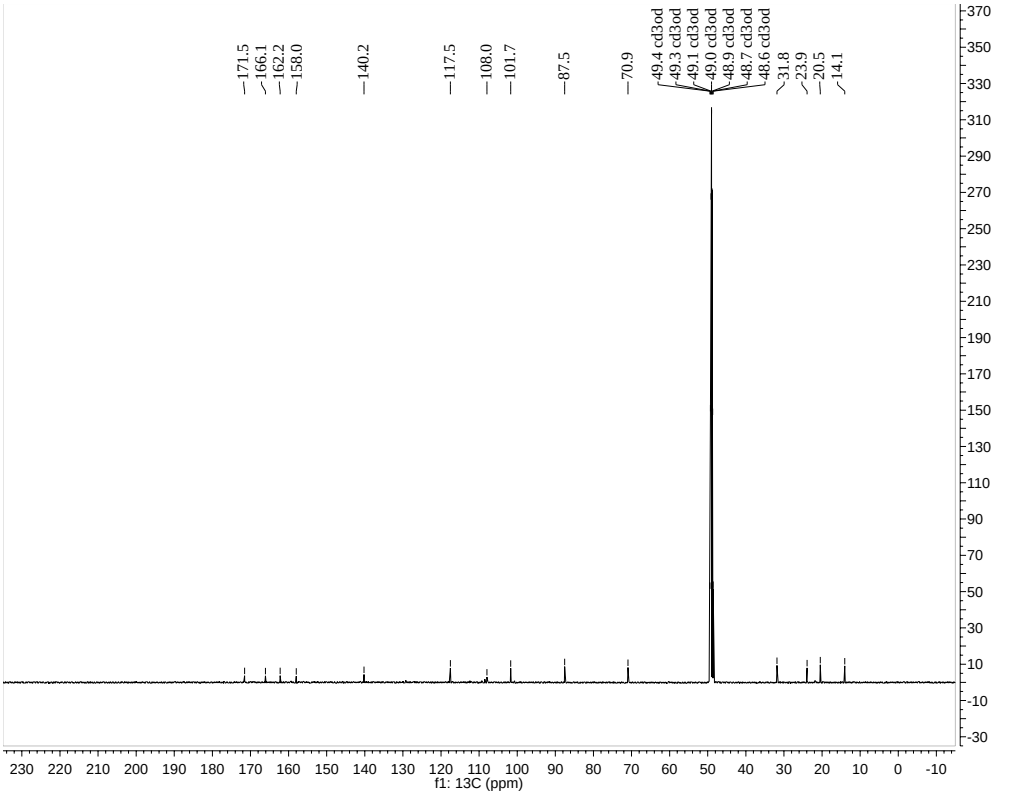

Supplemental Figure S2.74. (**27**) ^{1}H NMR (600 MHz, $(CD_3)_2SO$)

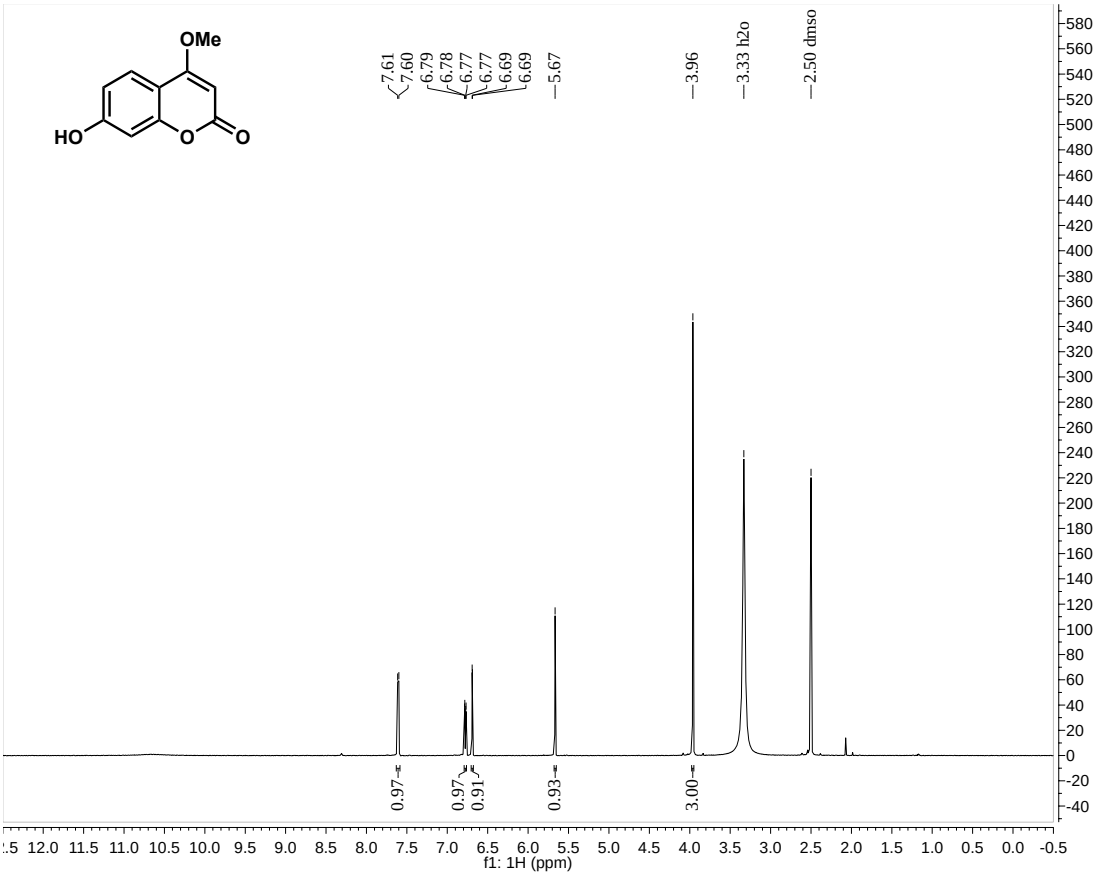

Supplemental Figure S2.75. (**51**) ^{1}H NMR (400 MHz, $(CD_3)_2CO$)

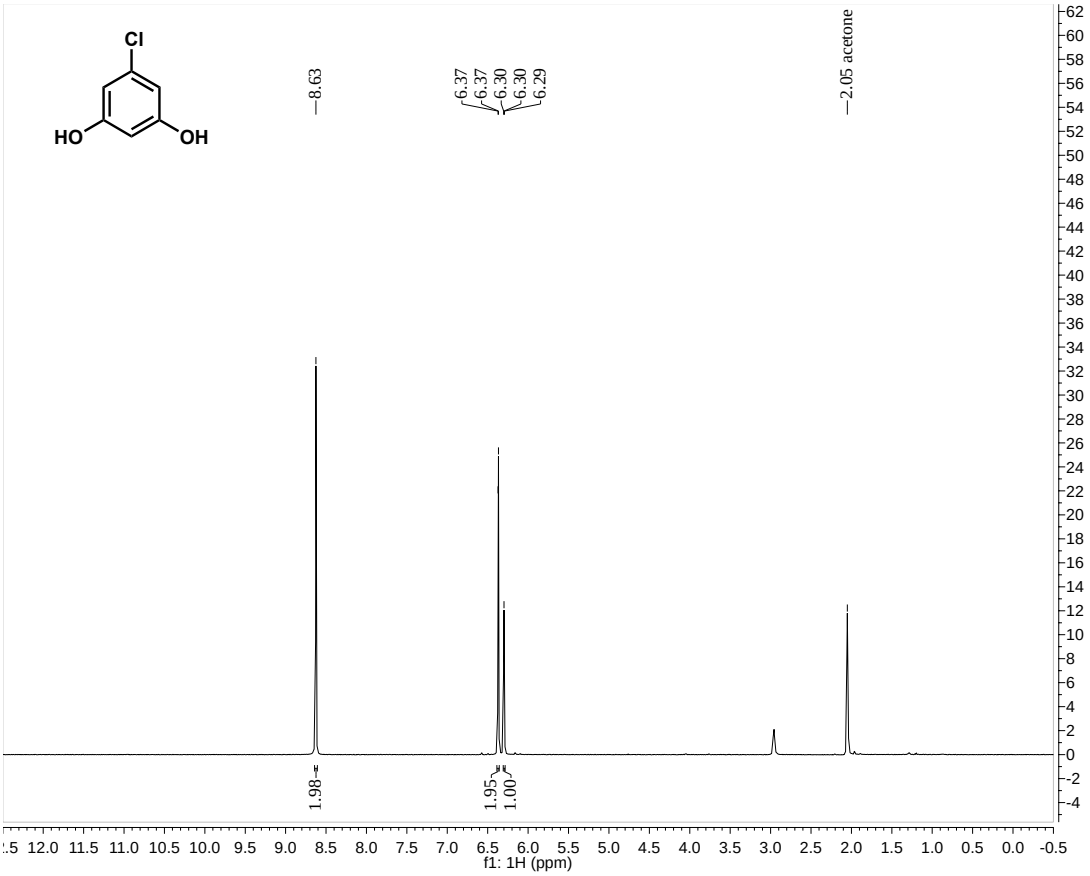

Supplemental Figure S2.76. (**52**) ^{1}H NMR (600 MHz, $(CD_3)_2CO$)

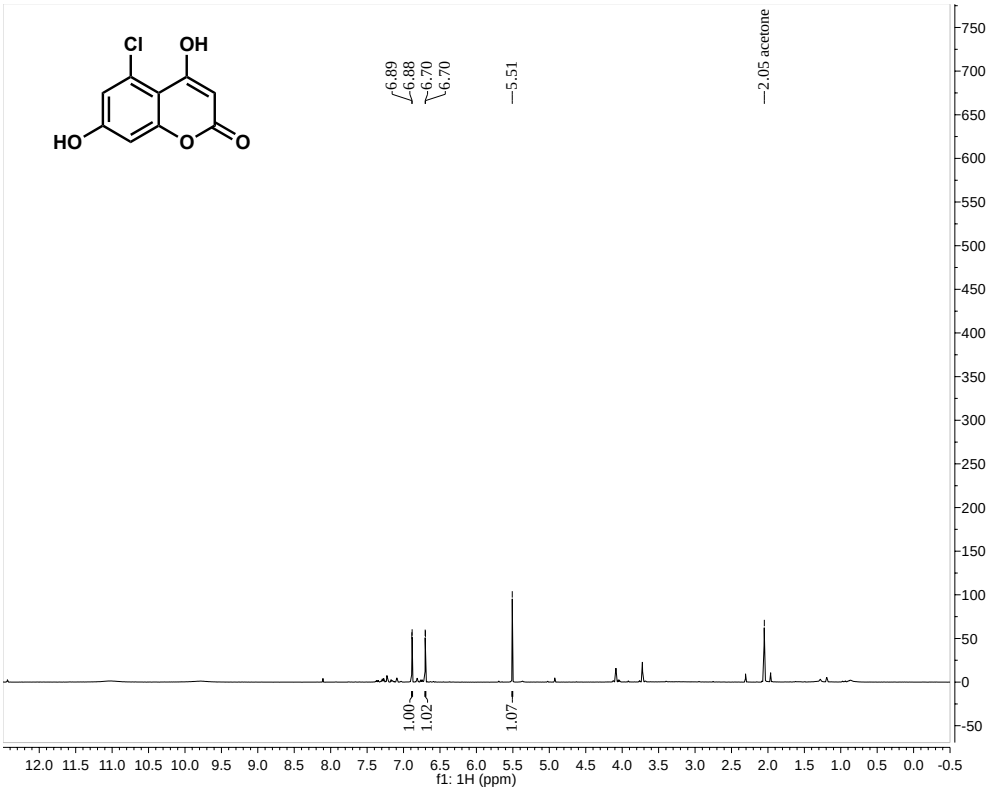

^{13}C NMR (150 MHz, $(CD_3)_2CO$)

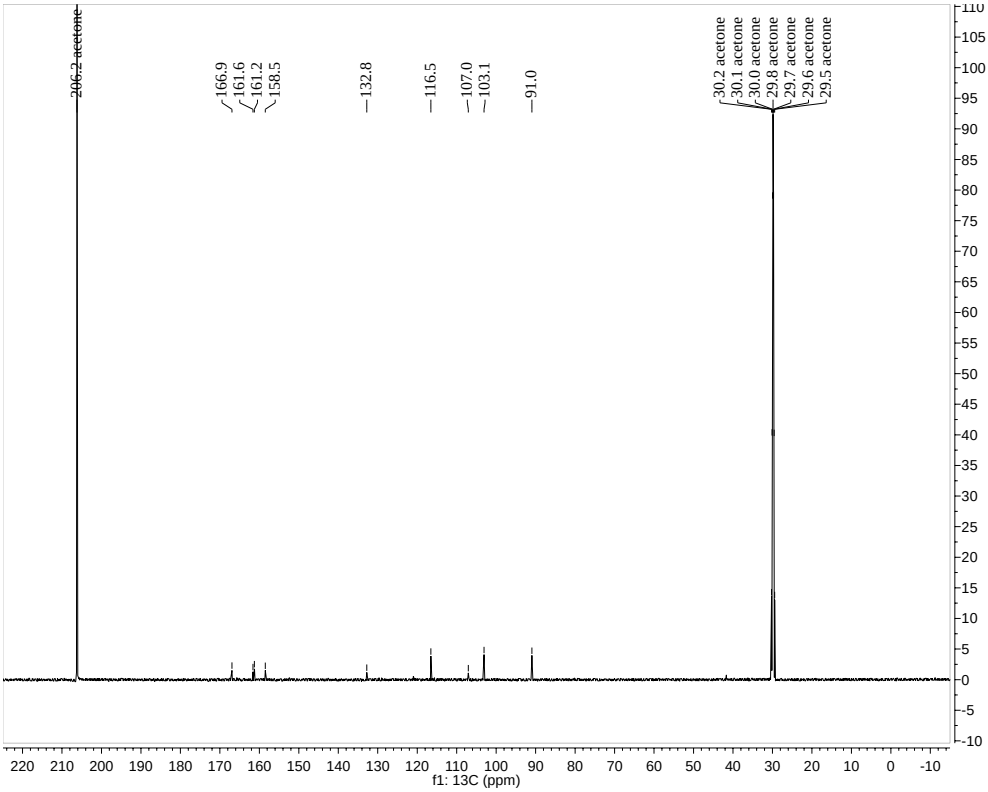

Supplemental Figure S2.77. (**24**) ^{1}H NMR (600 MHz, $(CD_3)_2SO$)

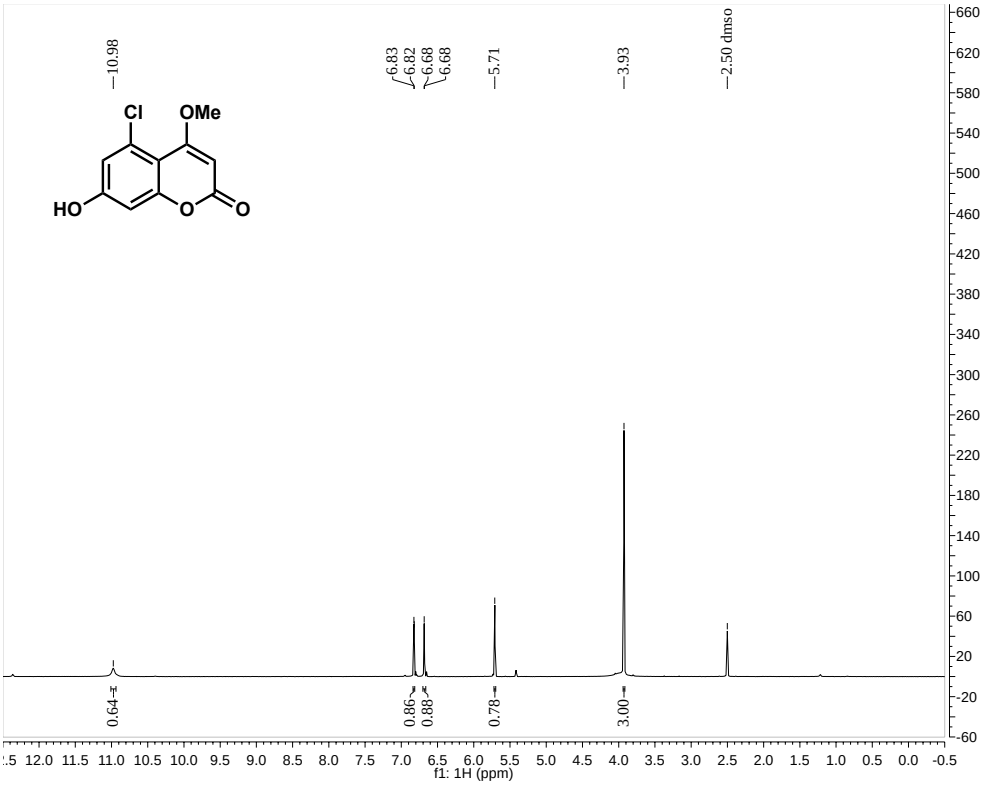

^{13}C NMR (150 MHz, $(CD_3)_2SO$)

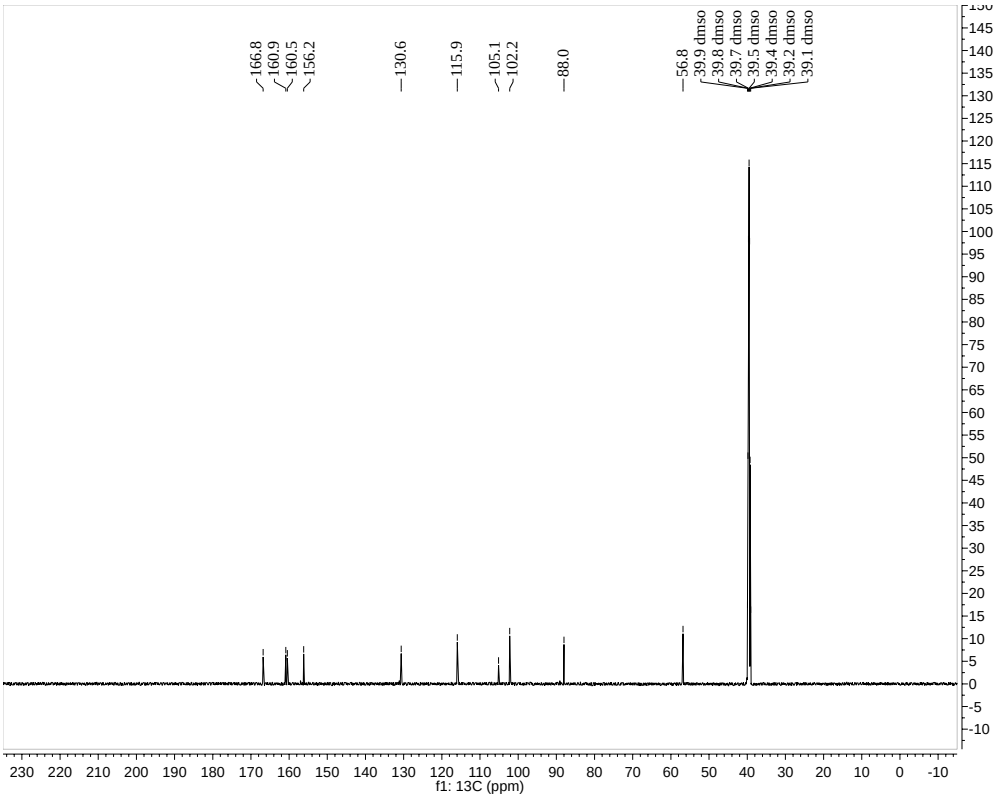

Supplemental Figure S2.78. (**23**) ^{1}H NMR (600 MHz, $(CD_3)_2SO$)

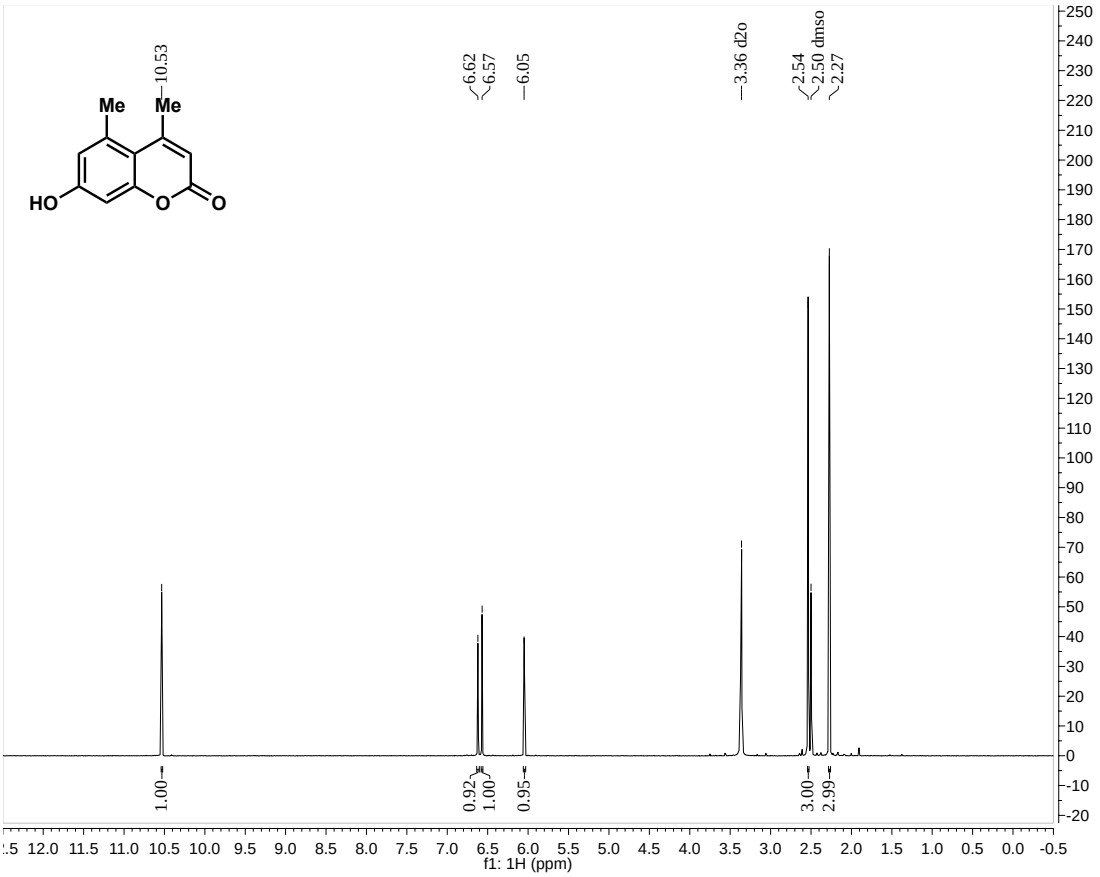

Supplemental Figure S2.79. (**22**) ^{1}H NMR (600 MHz, CD_3OD)

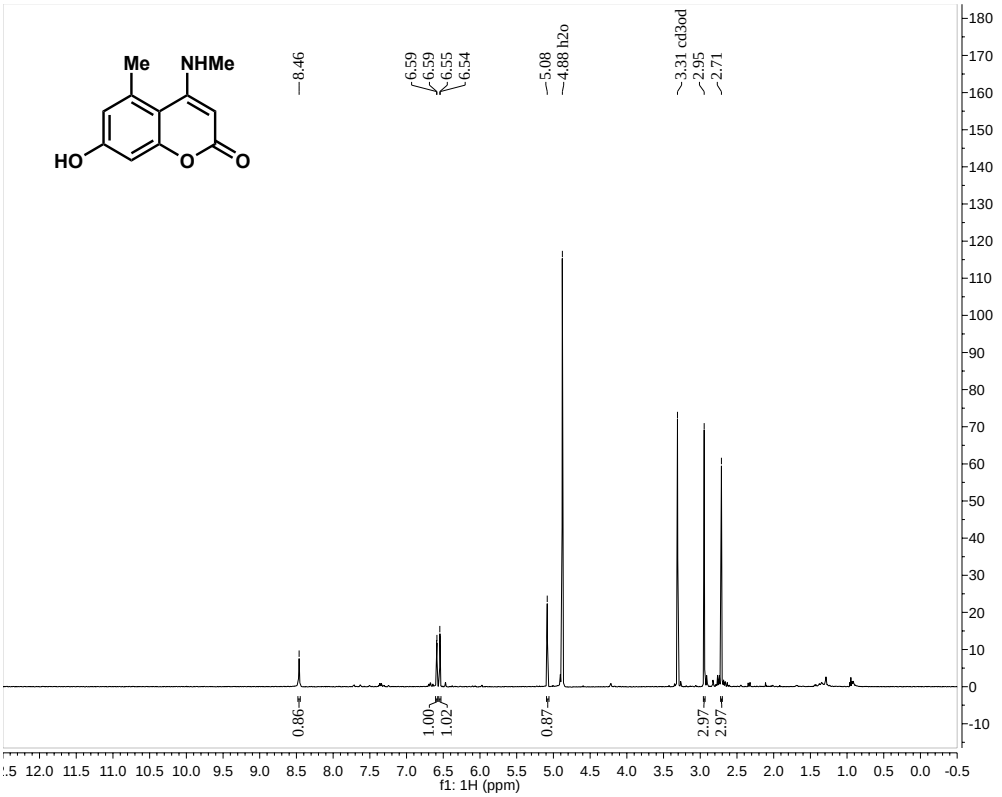

^{13}C NMR (150 MHz, CD_3OD)

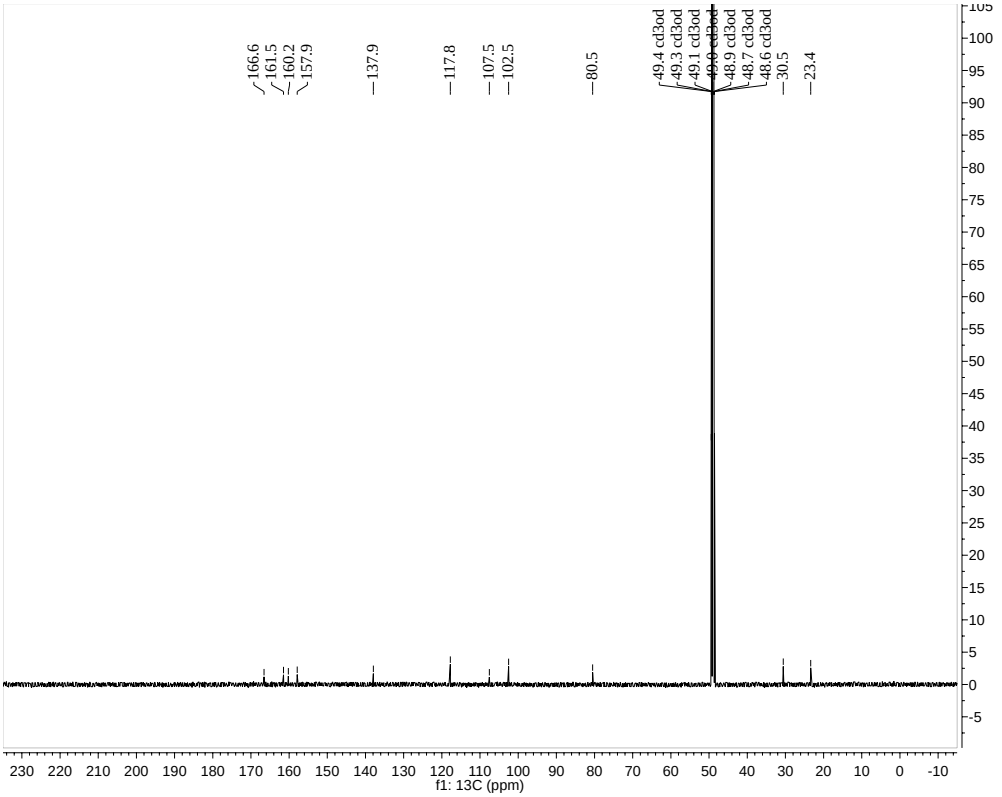

Supplemental Figure S2.80. (**53**) ^{1}H NMR (600 MHz, $CDCl_3$)

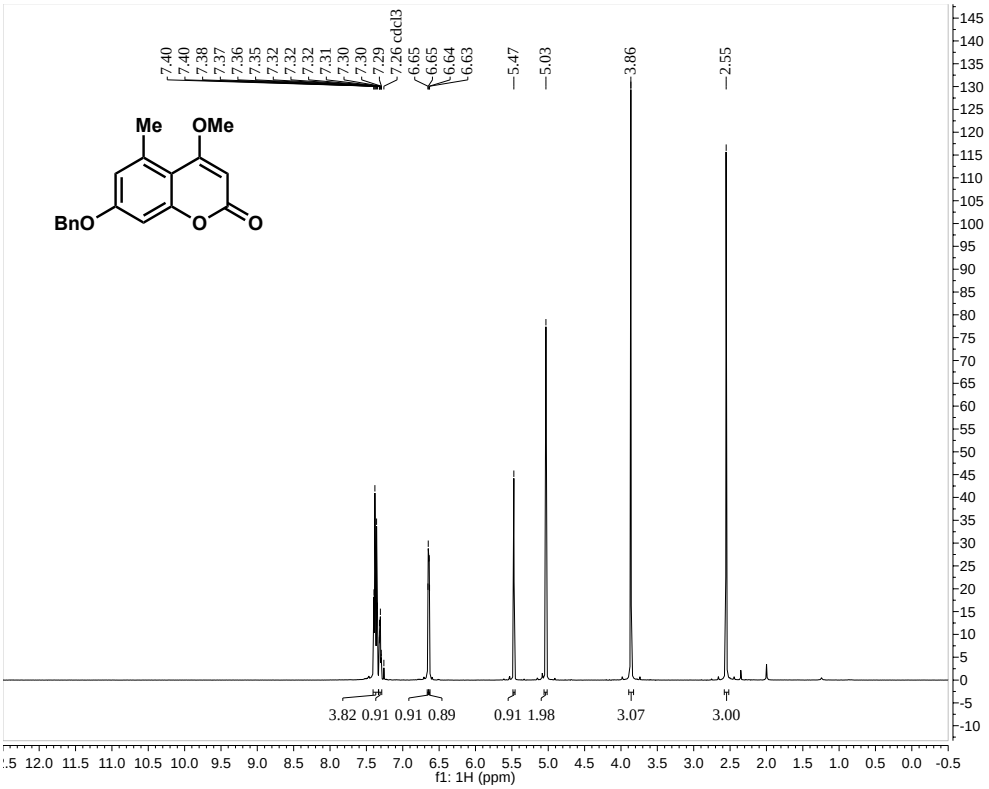

^{13}C NMR (150 MHz, $CDCl_3$)

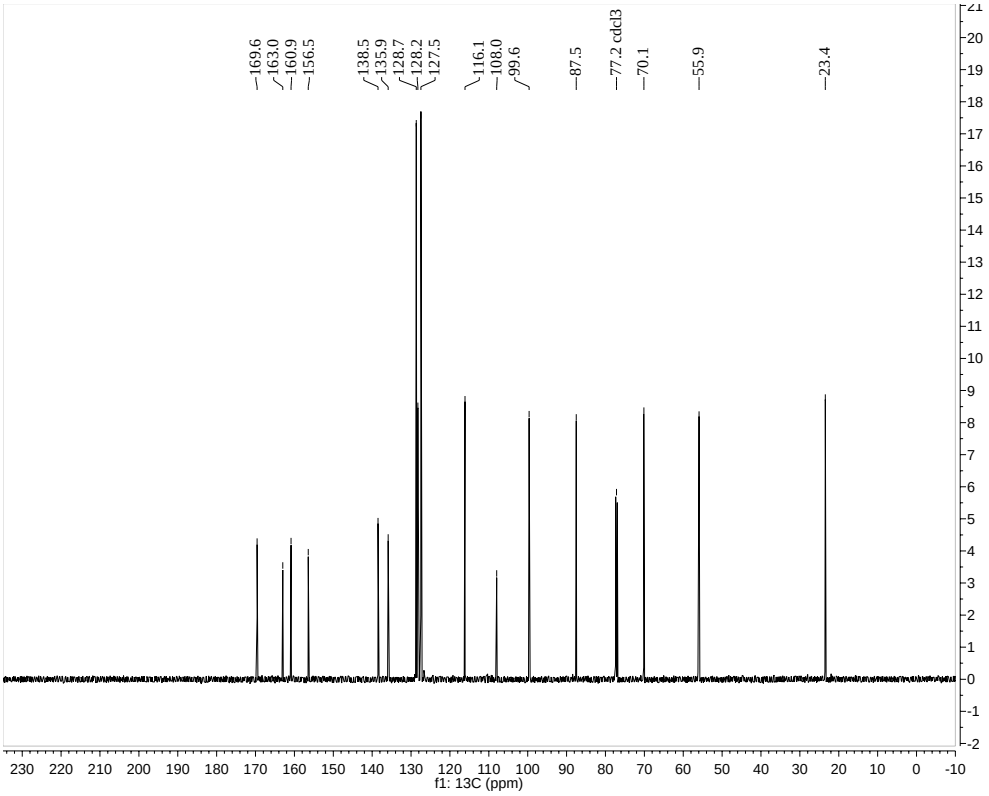

Supplemental Figure S2.81. (**54**) ^{1}H NMR (600 MHz, $CDCl_3$)

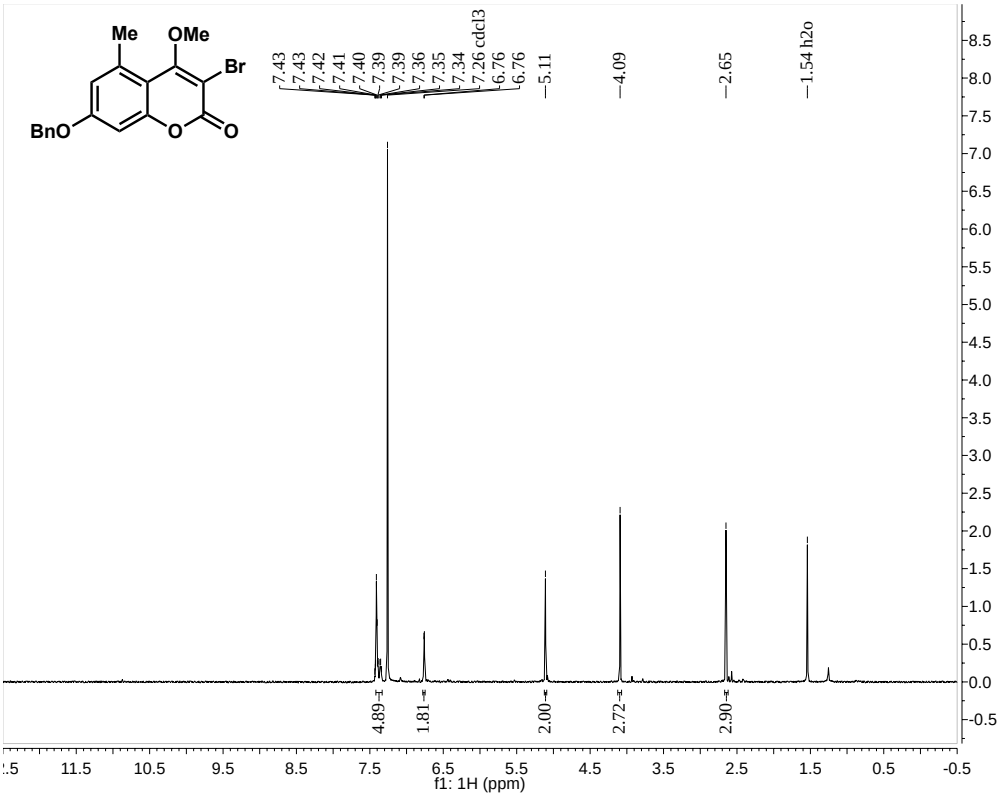

^{13}C NMR (150 MHz, $CDCl_3$)

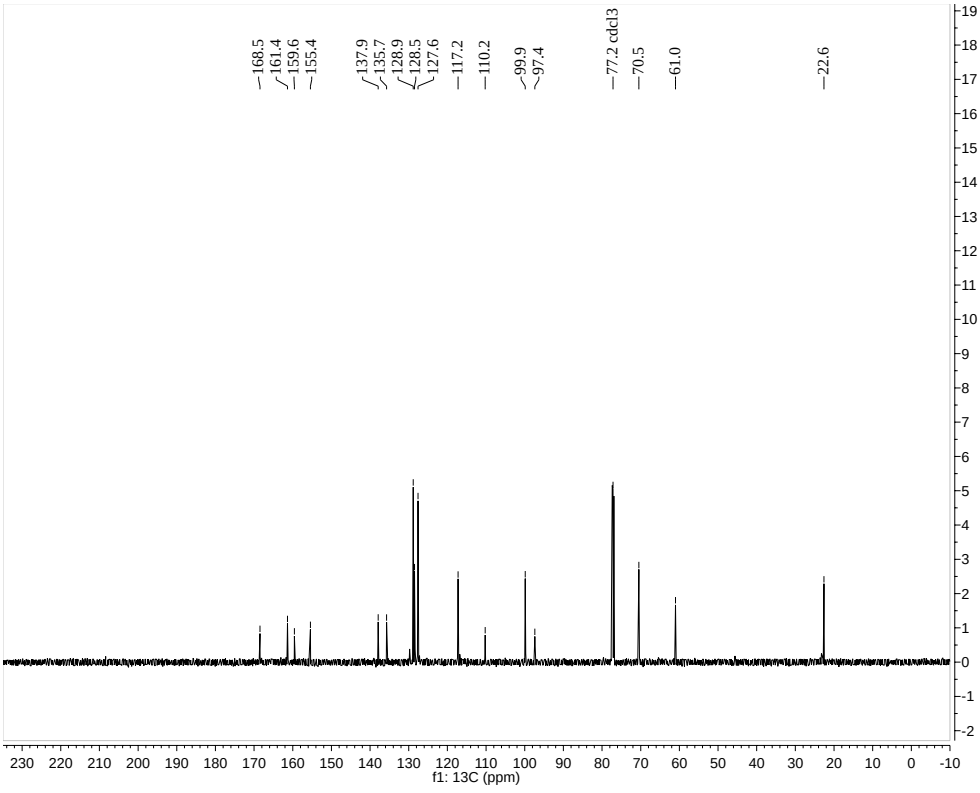

Supplemental Figure S2.82. (**55**) ^{1}H NMR (400 MHz, $CDCl_3$)

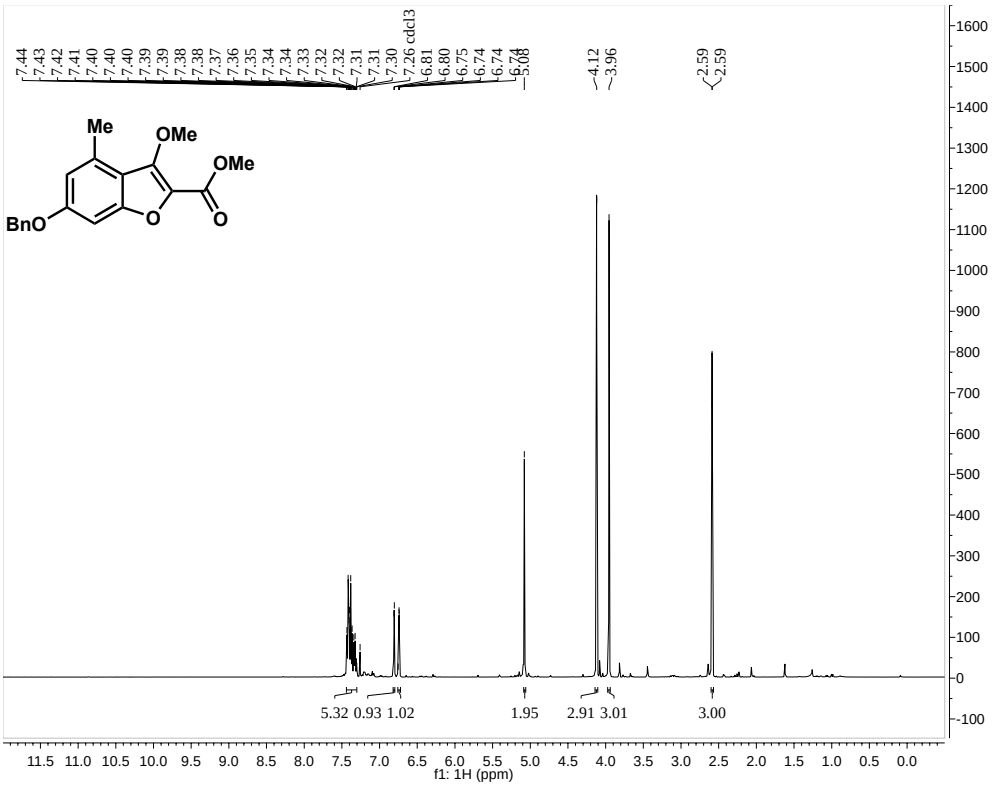

^{13}C NMR (100 MHz, $CDCl_3$)

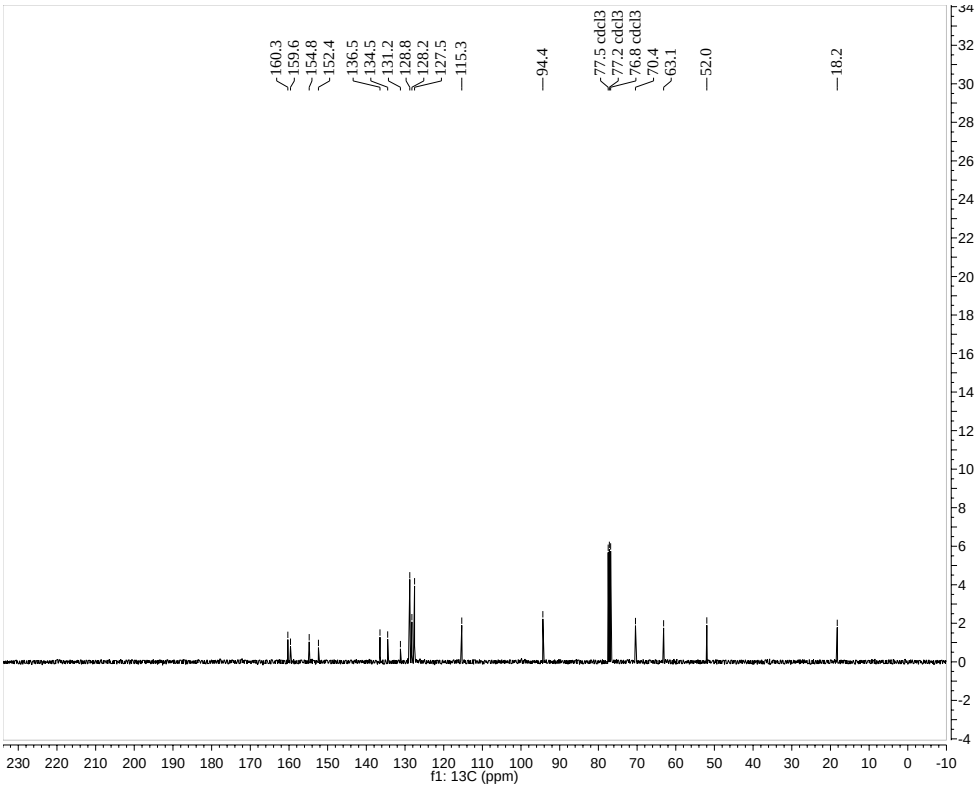

Supplemental Figure S2.83. (**21**) ^{1}H NMR (600 MHz, CD_3OD)

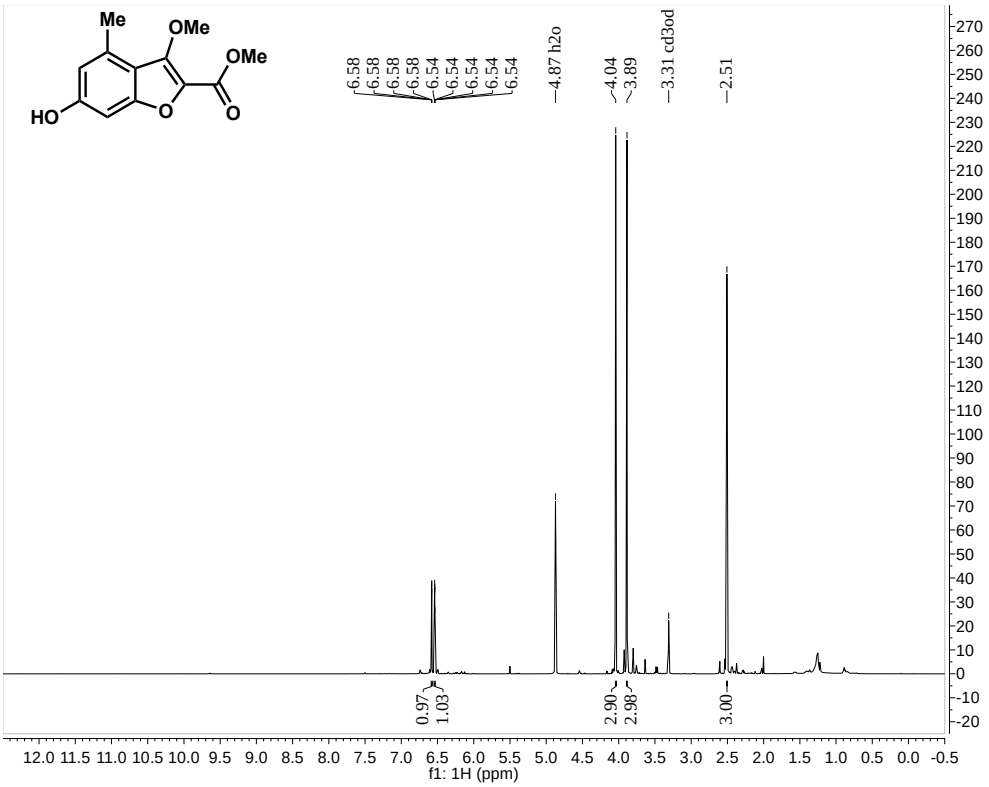

^{13}C NMR (150 MHz, CD_3OD)

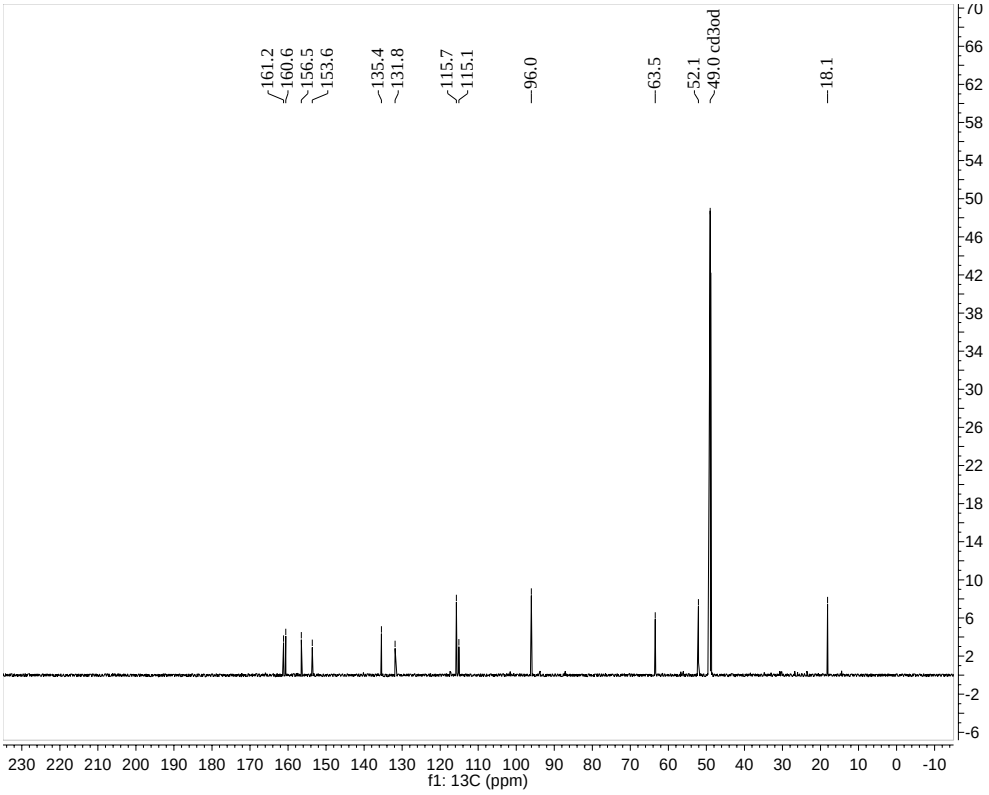

Supplemental Figure S2.84. (**2**) ^{1}H NMR (400 MHz, $(CD_3)_2SO$)

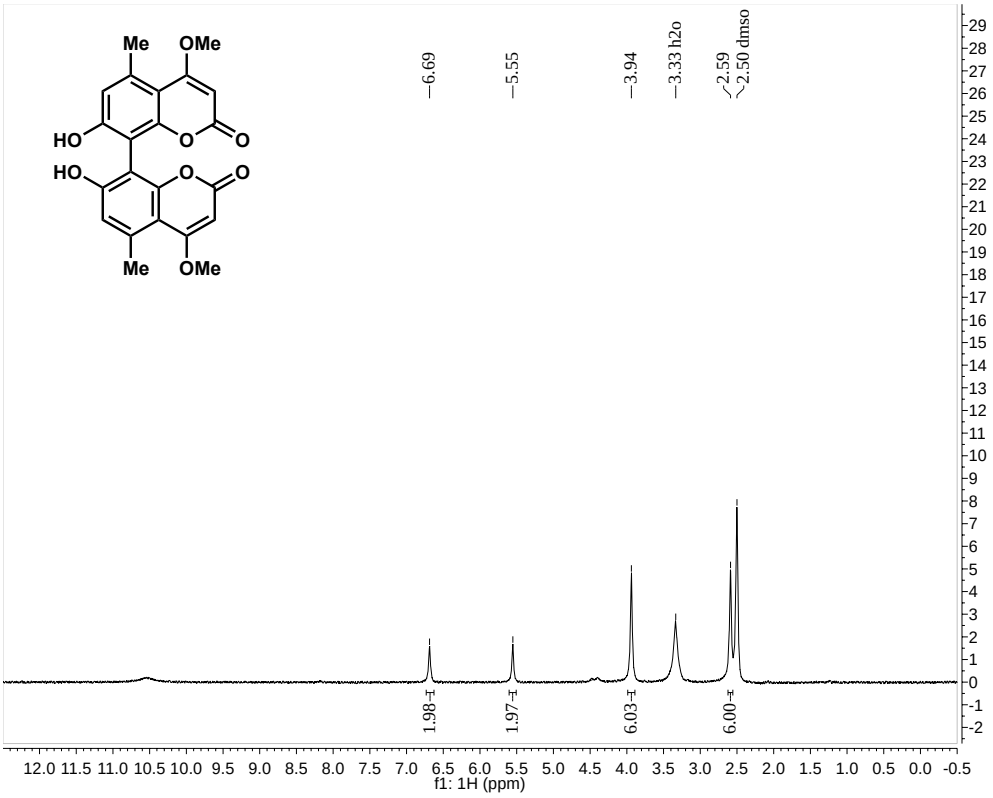

Supplemental Figure S2.85. (**3**) ^{1}H NMR (400 MHz, $(CD_3)_2SO$)

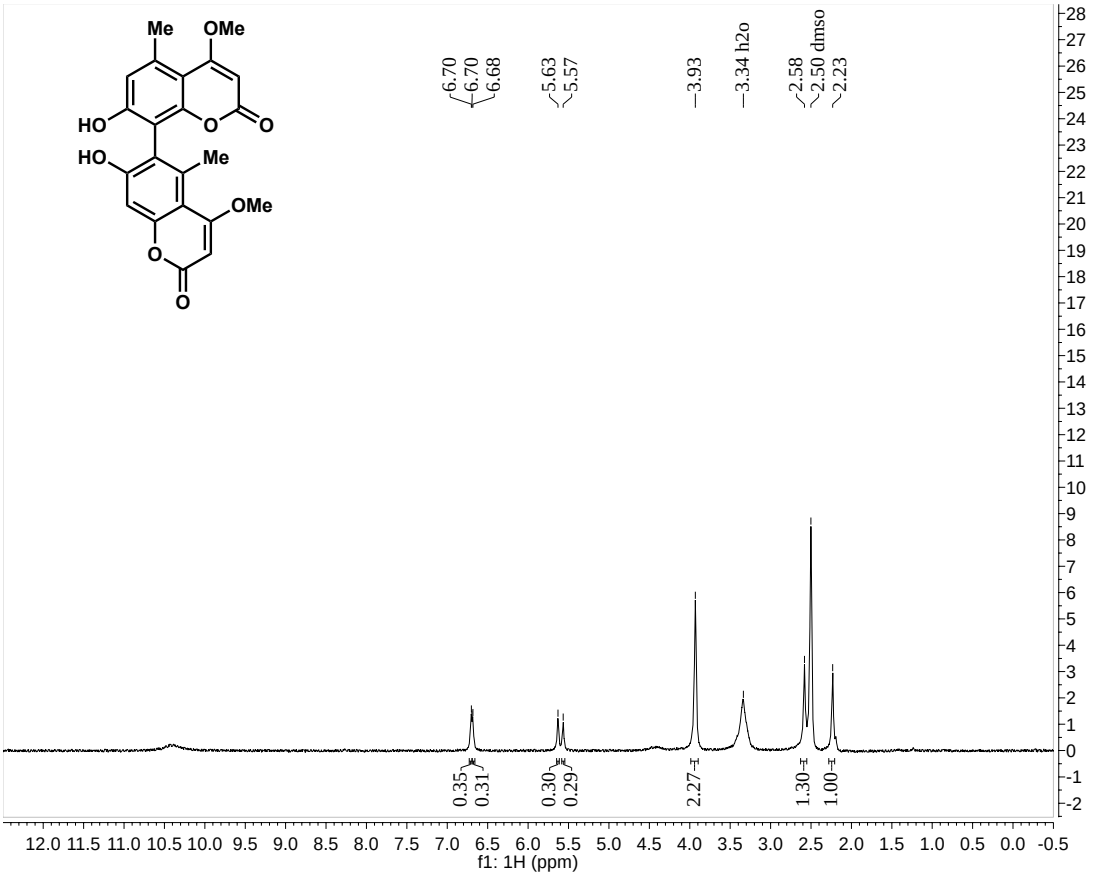

Supplemental Figure S2.86. (**29**) ^{1}H NMR (400 MHz, $(CD_3)_2CO$)

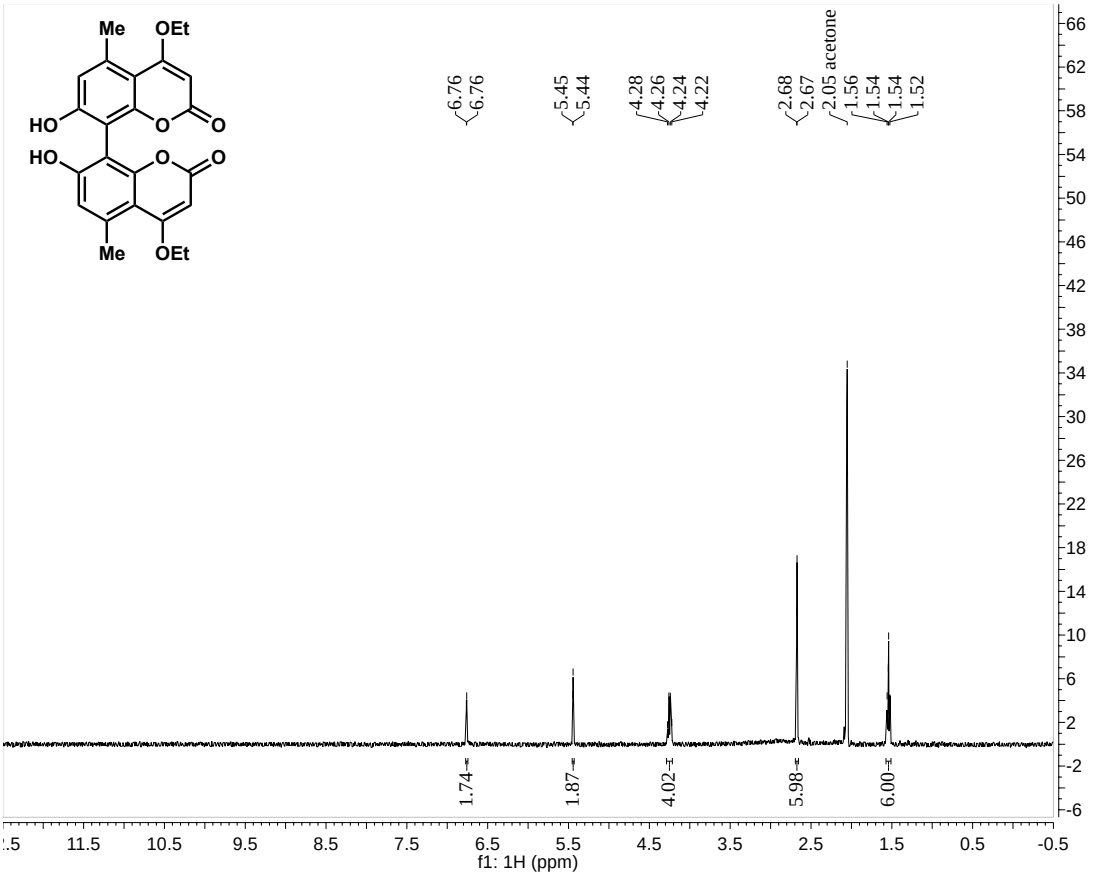

Supplemental Figure S2.87. (**56**) ^{1}H NMR (600 MHz, $(CD_3)_2CO$)

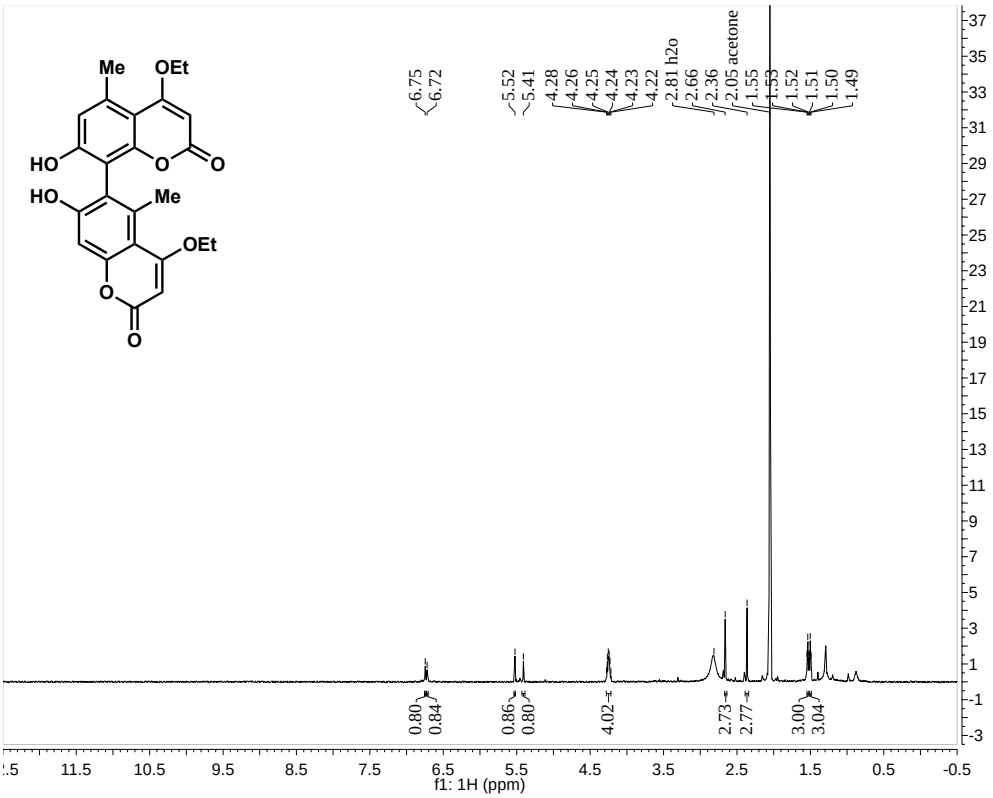

^{13}C NMR (150 MHz, $(CD_3)_2SO$)

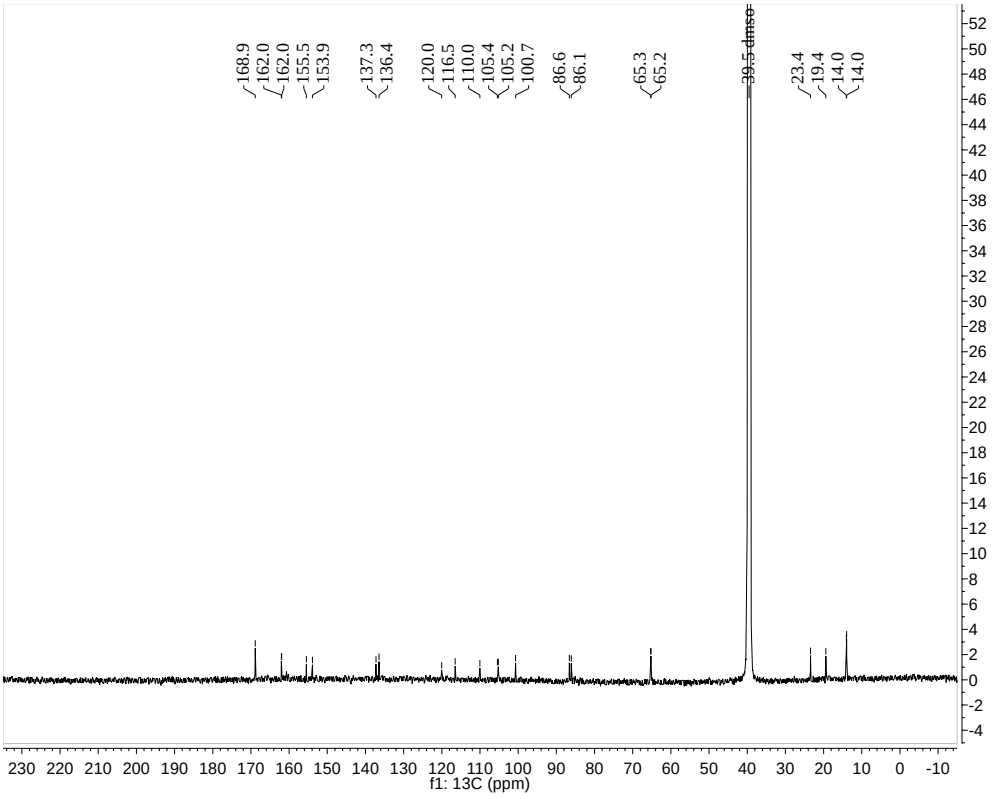

Supplemental Figure S2.88. (**56** and **30**) ^{1}H NMR (150 MHz, CD_3OD)

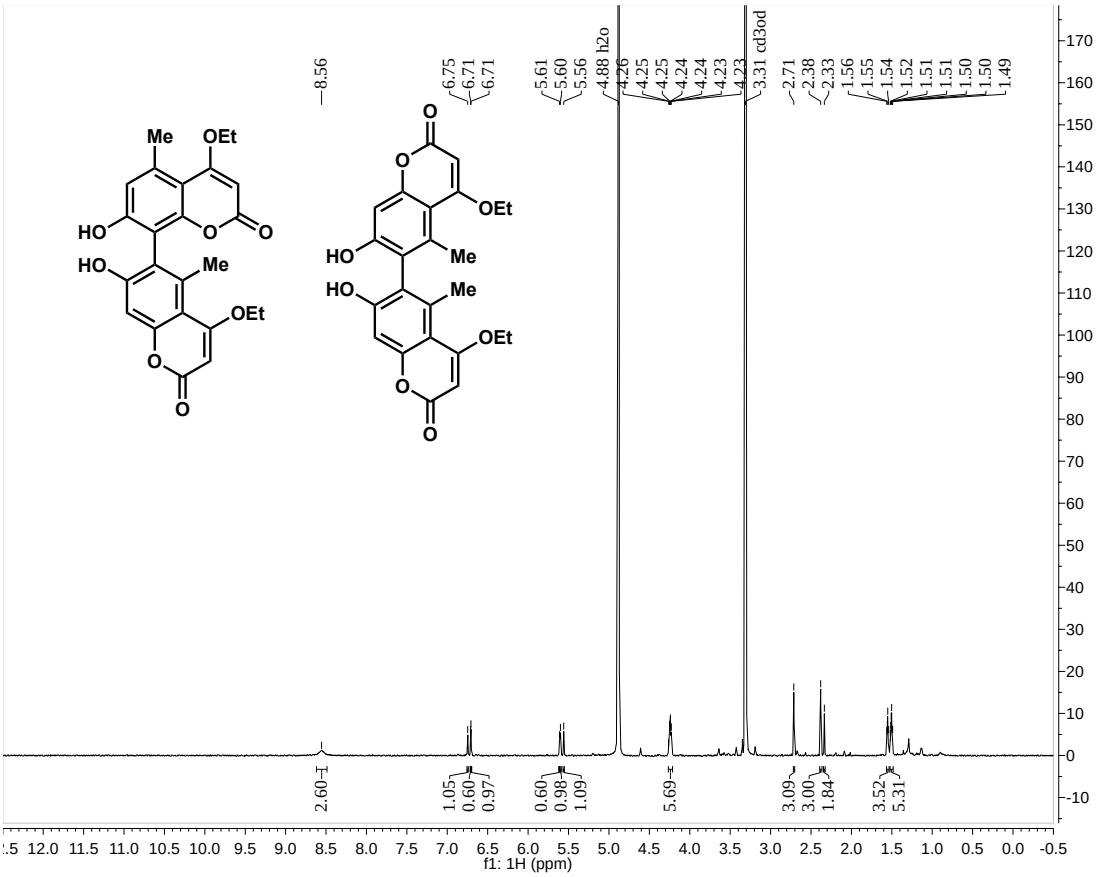

Supplemental Figure S2.89. (**57**) ^{1}H NMR (600 MHz, $(CD_3)_2CO$)

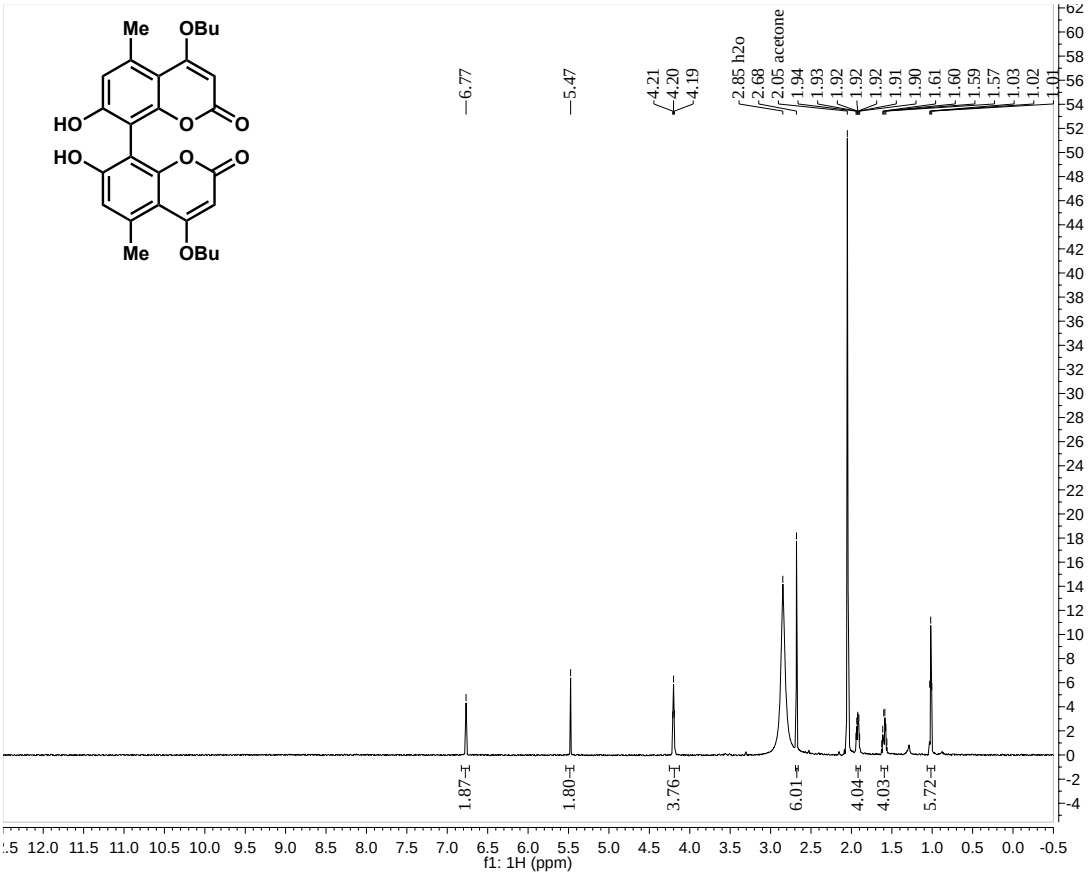

Supplemental Figure S2.90. (**57**) ^{1}H NMR (600 MHz, $(CD_3)_2SO$)

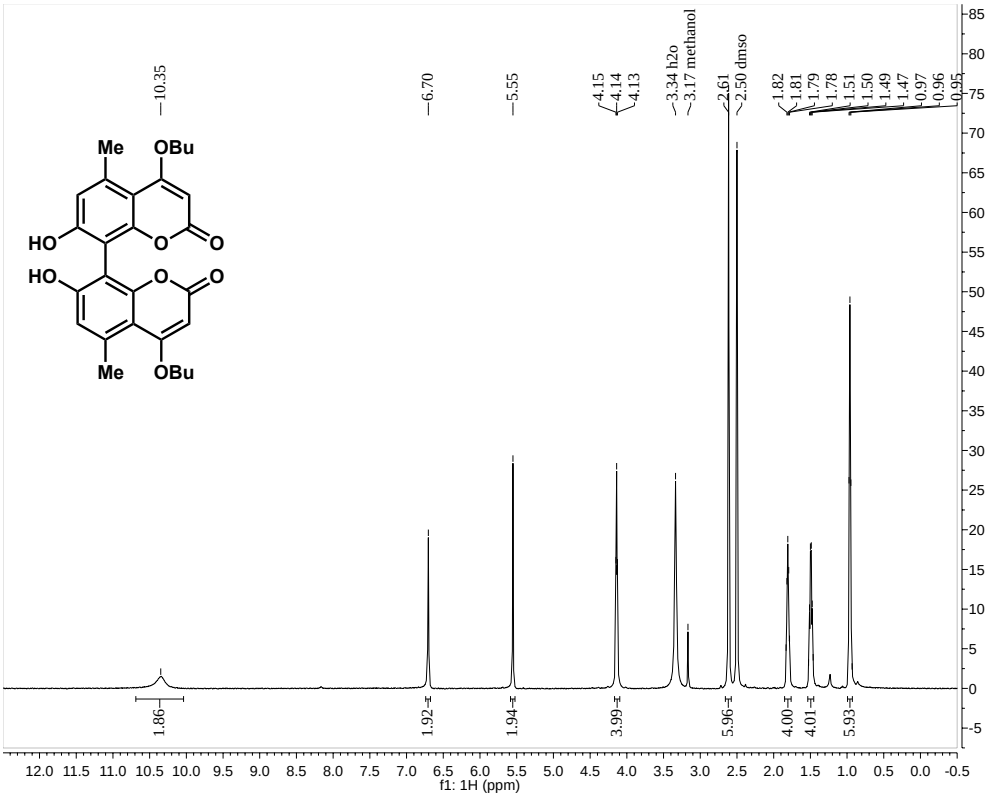

^{13}C NMR (150 MHz, $(CD_3)_2SO$)

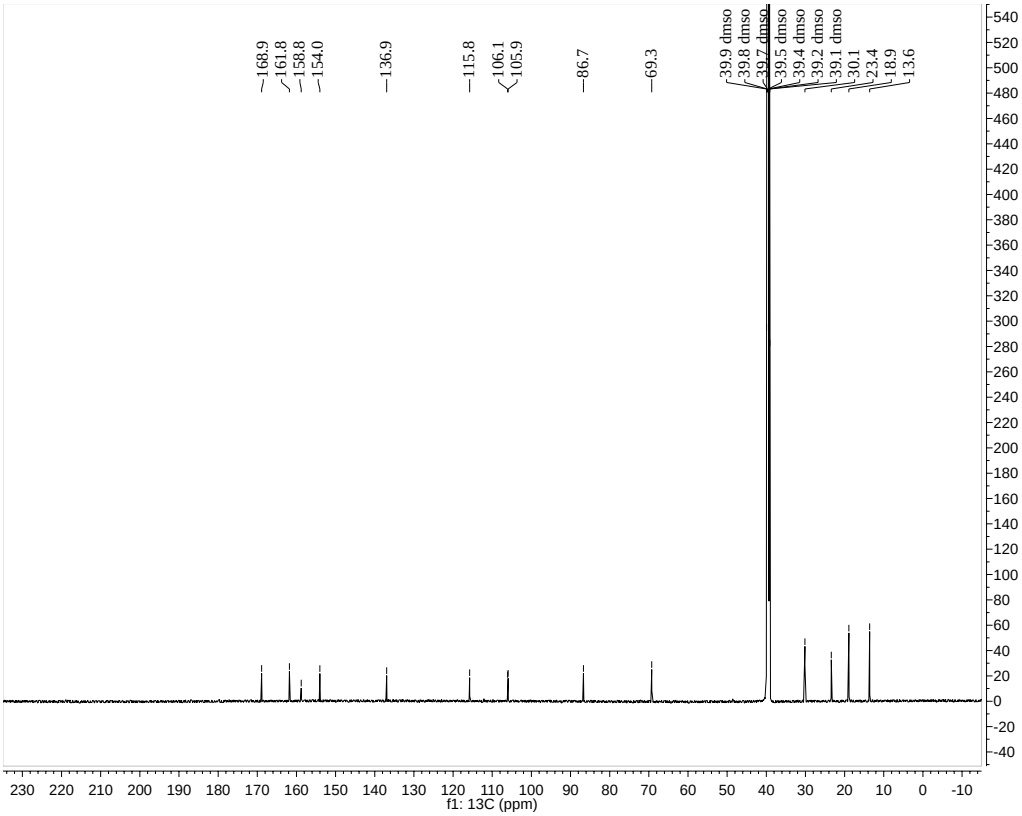

Supplemental Figure S2.91. (**58**) ^{1}H NMR (400 MHz, $(CD_3)_2CO$)

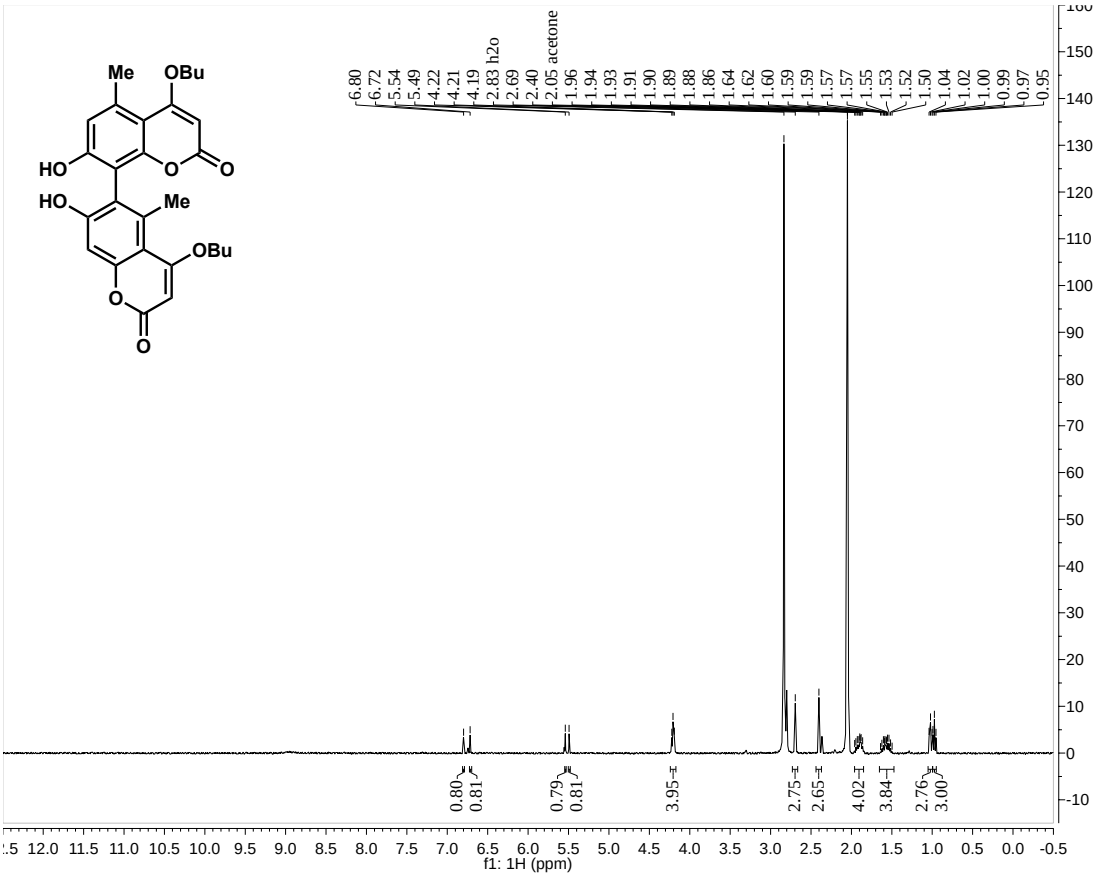

Supplemental Figure S2.92. (**58**) ^{1}H NMR (600 MHz, $(CD_3)_2SO$)

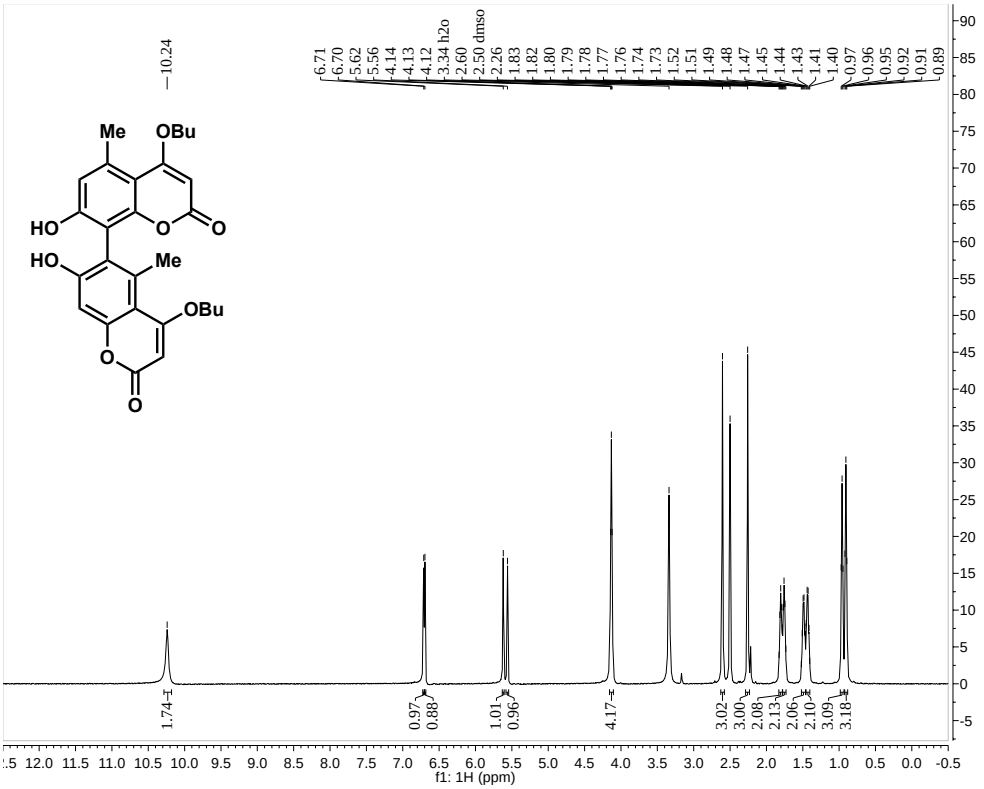

^{13}C NMR (150 MHz, $(CD_3)_2SO$)

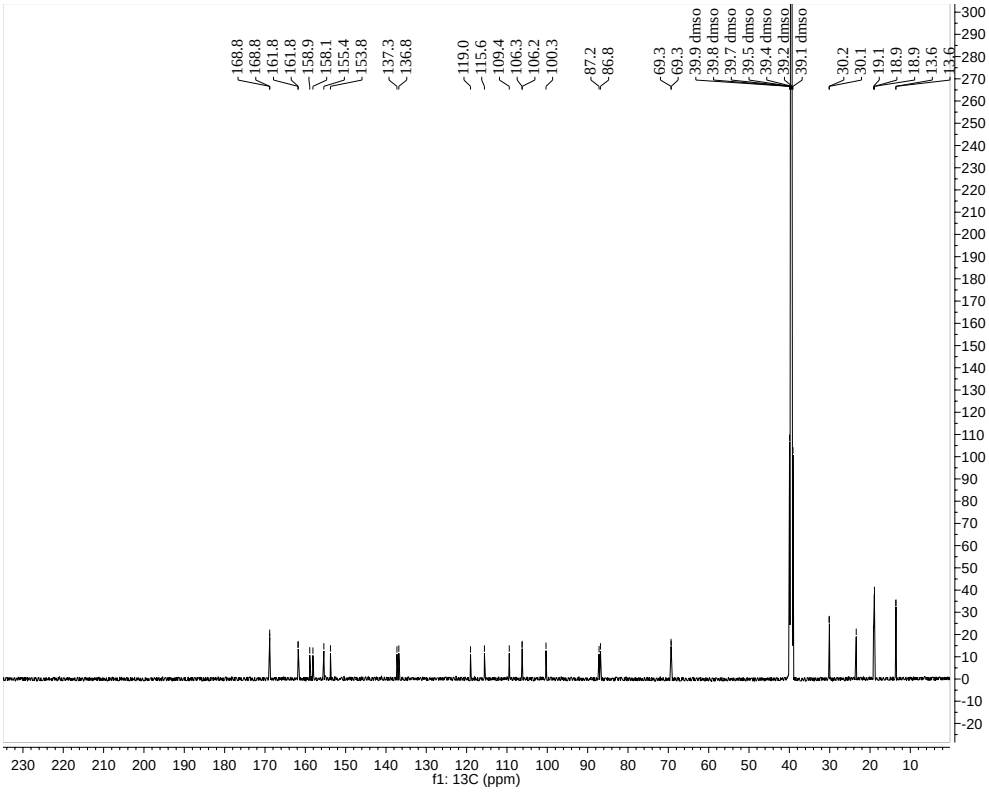

Supplemental Figure S2.93. (**58** and **31**) ^{1}H NMR (600 MHz, $(CD_3)_2CO$)

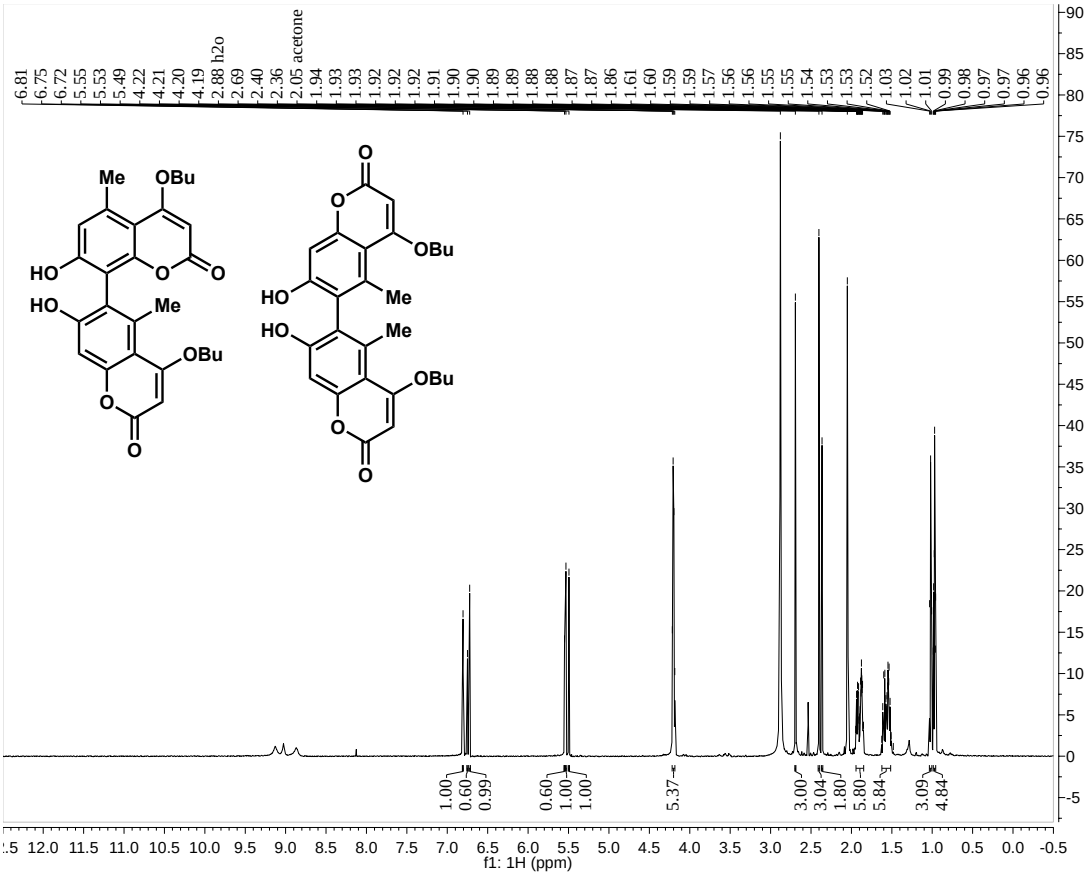

Supplemental Figure S2.94. (**32**) ^{1}H NMR (600 MHz, CD_3OD)

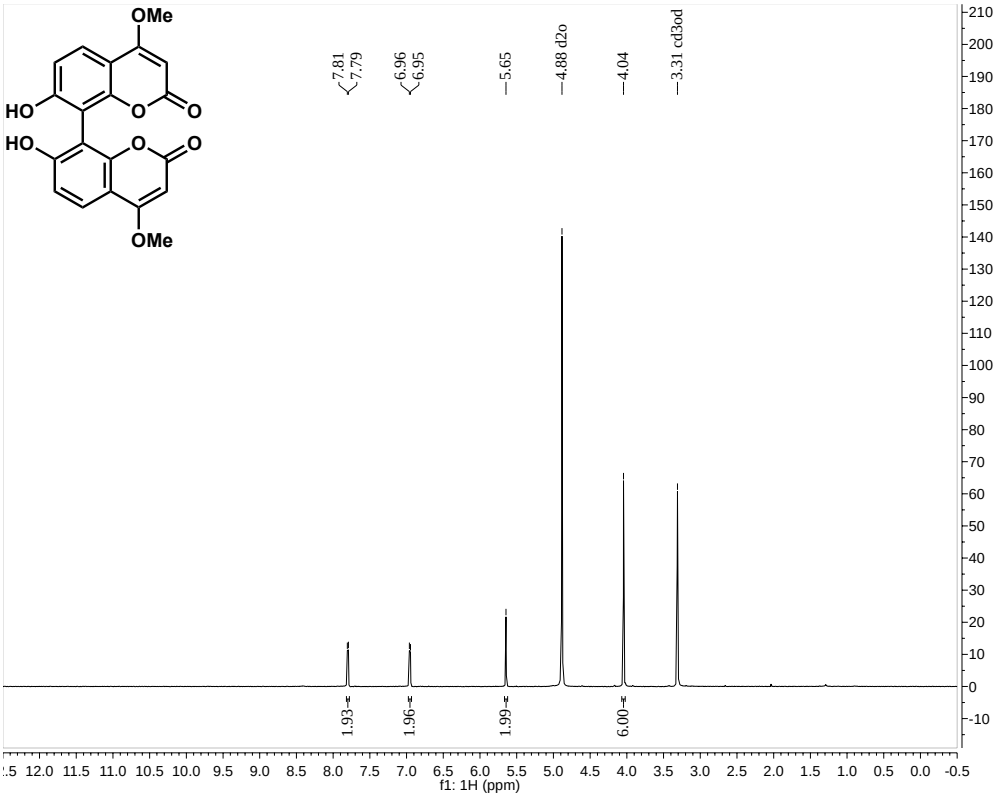

^{13}C NMR (150 MHz, CD_3OD)

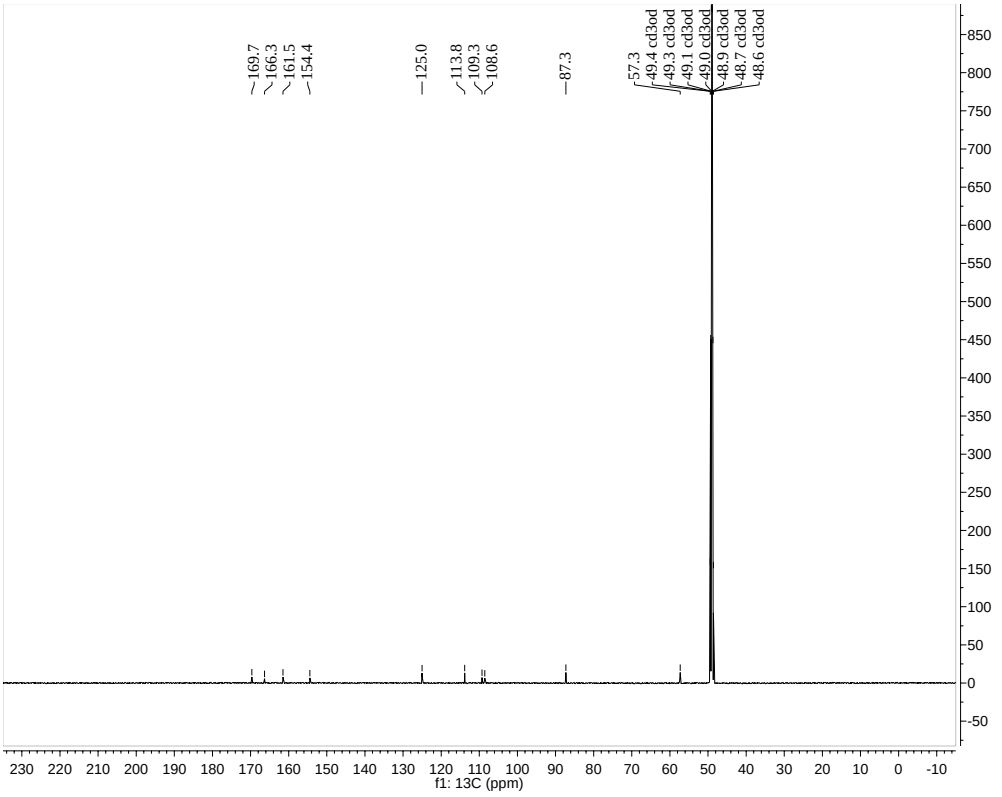

Supplemental Figure S2.95. (**33**) ^{1}H NMR (400 MHz, $(CD_3)_2CO$)

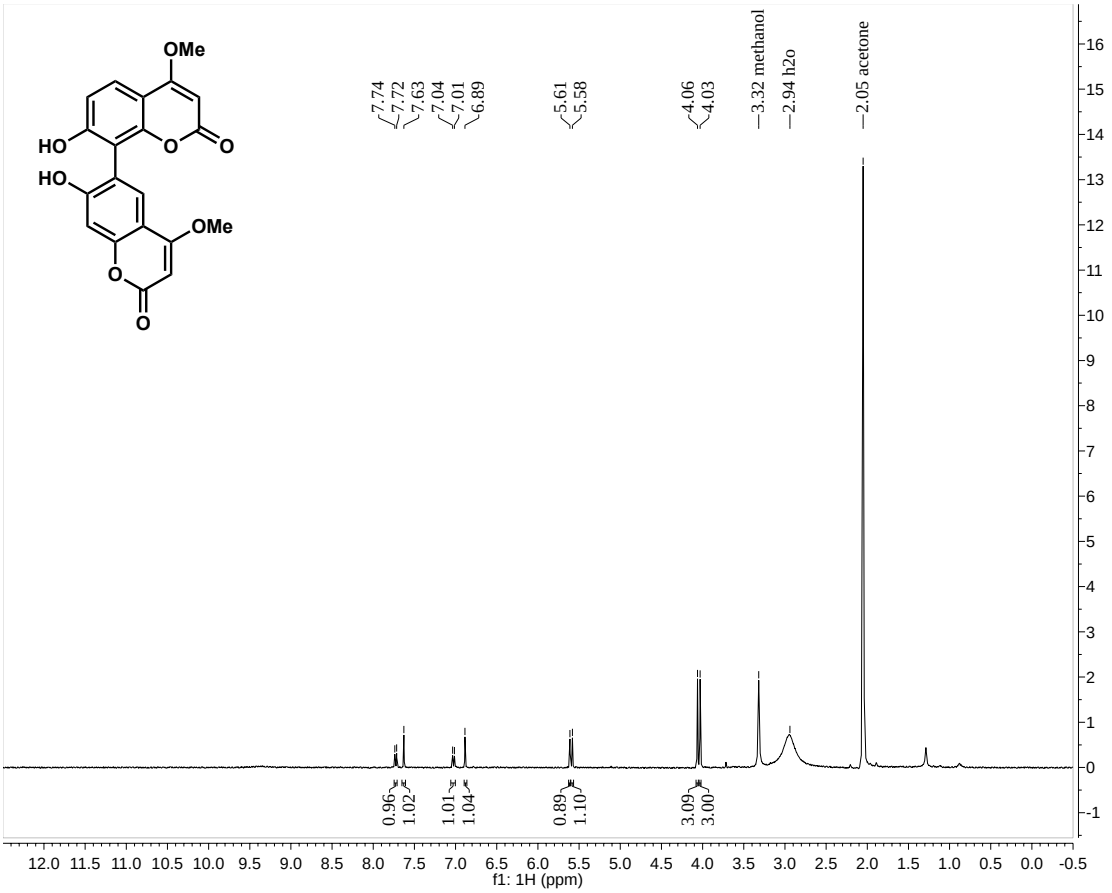

Supplemental Figure S2.96. (**33**) ^{1}H NMR (600 MHz, $(CD_3)_2SO$)

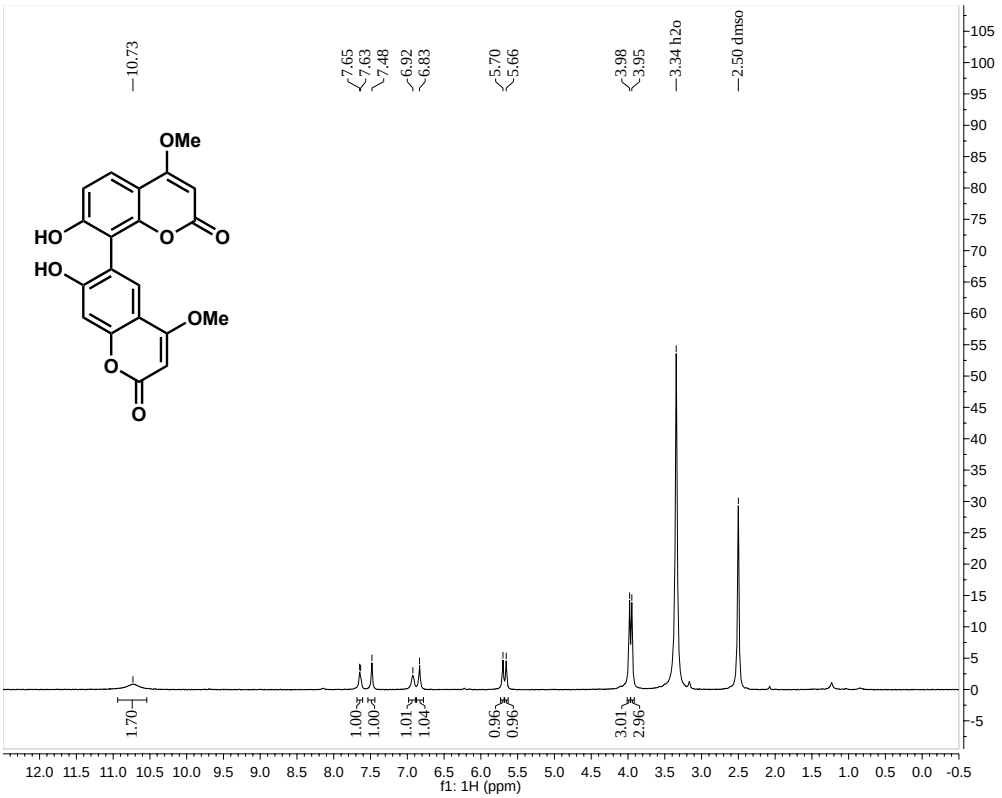

^{13}C NMR (150 MHz, $(CD_3)_2SO$)

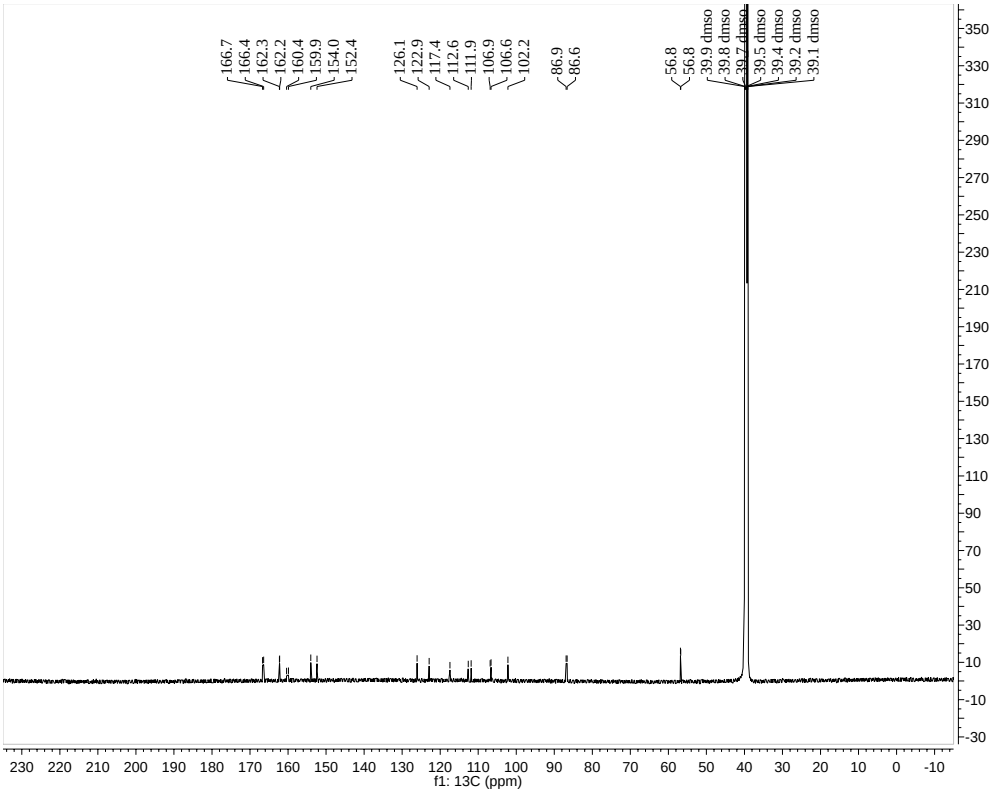

Supplemental Figure S2.97. (**60**) ^{1}H NMR (600 MHz, $CDCl_3$)

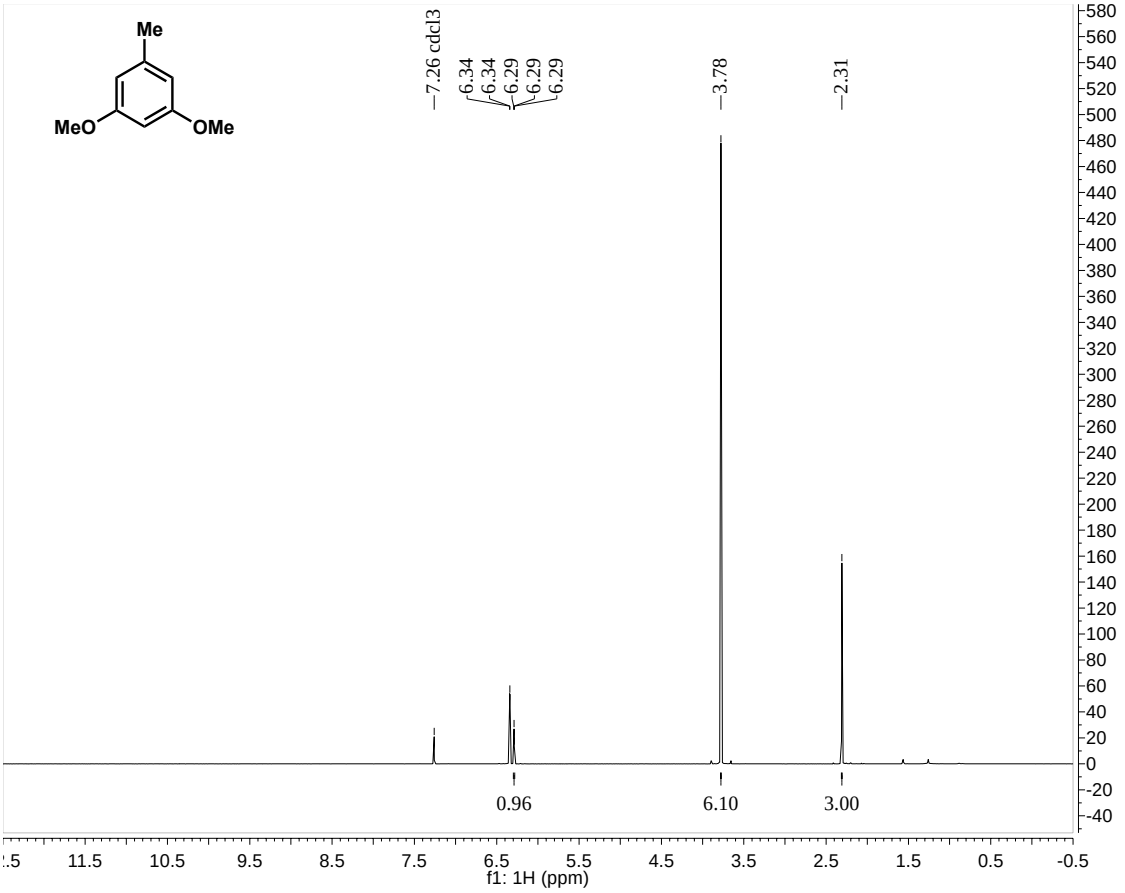

Supplemental Figure S2.98. (**61**) ^{1}H NMR (400 MHz, $CDCl_3$)

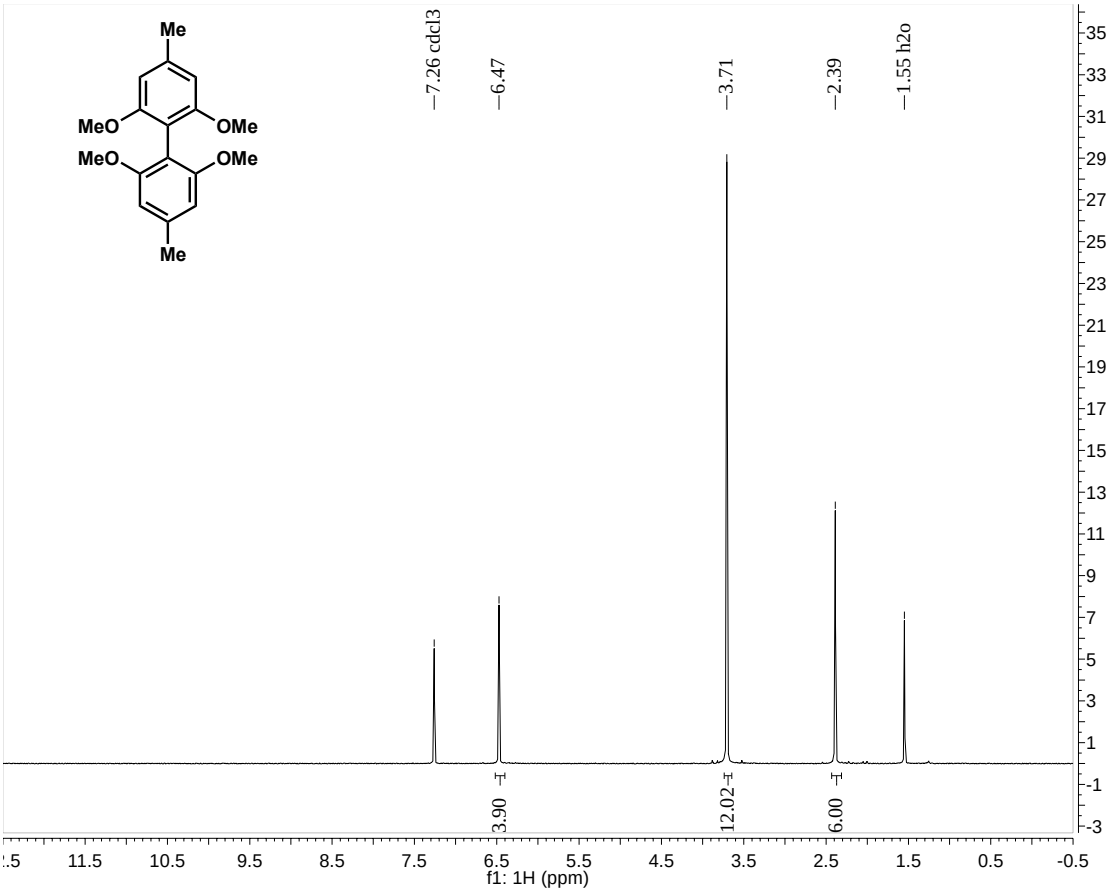

Supplemental Figure S2.99. (**62**) ^{1}H NMR (600 MHz, CD_3OD)

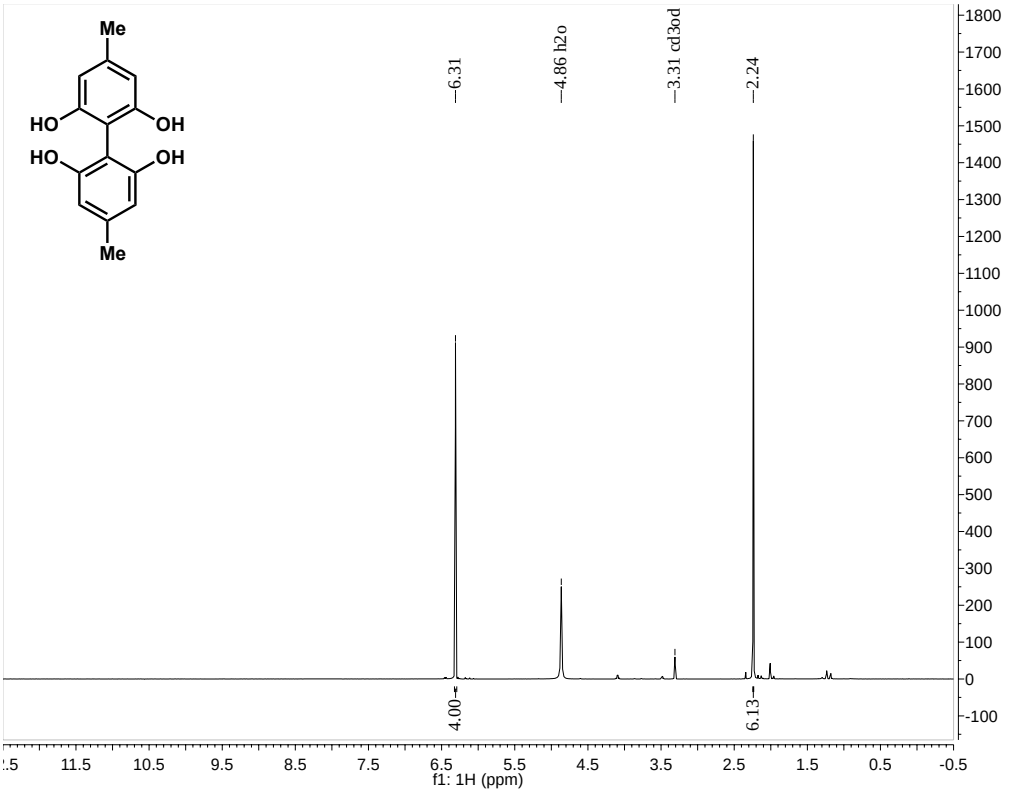

^{13}C NMR (150 MHz, CD_3OD)

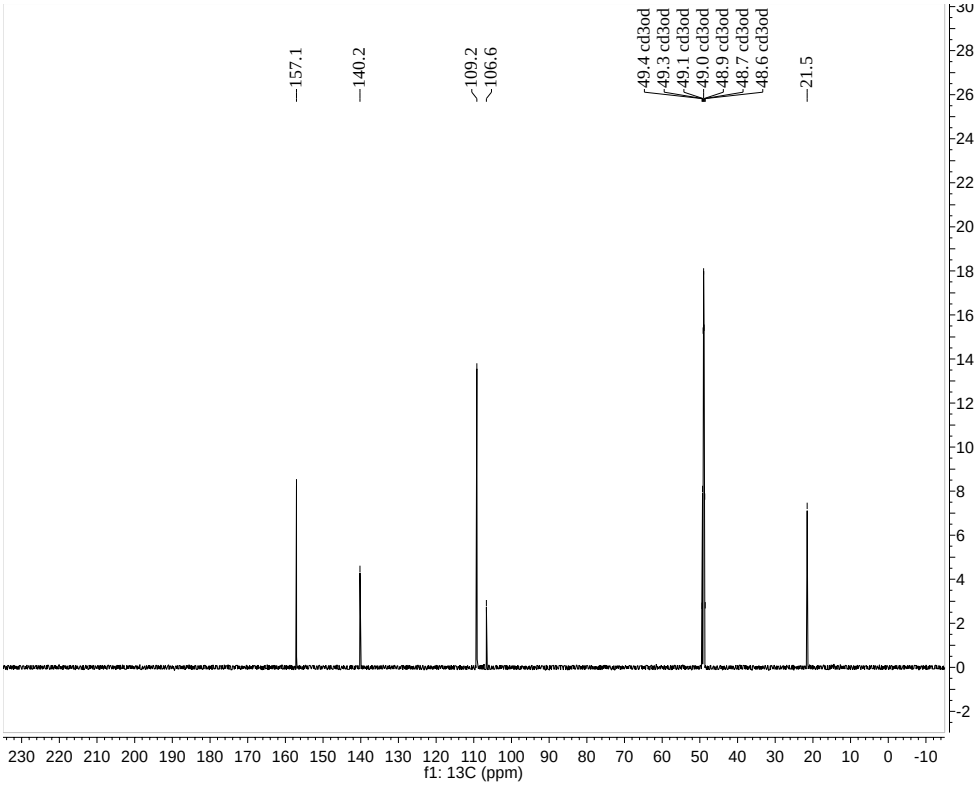

Supplemental Figure S2.100. (**63**) ^{1}H NMR (600 MHz, $(CD_3)_2SO$)

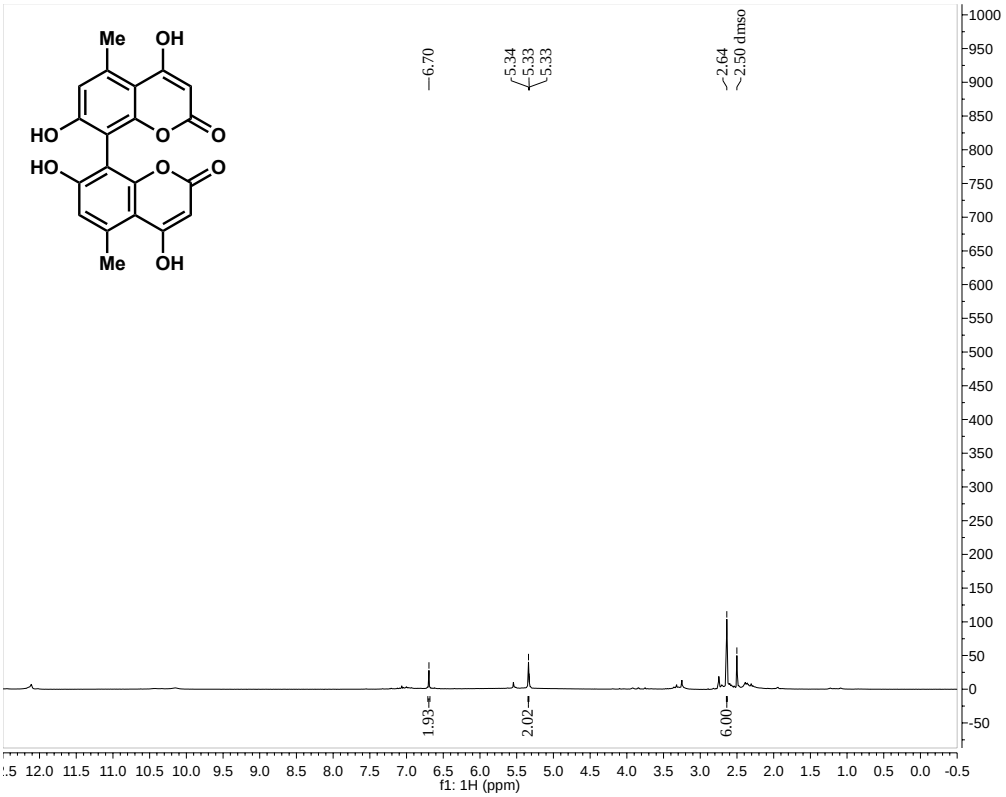

^{13}C NMR (150 MHz, $(CD_3)_2SO$)

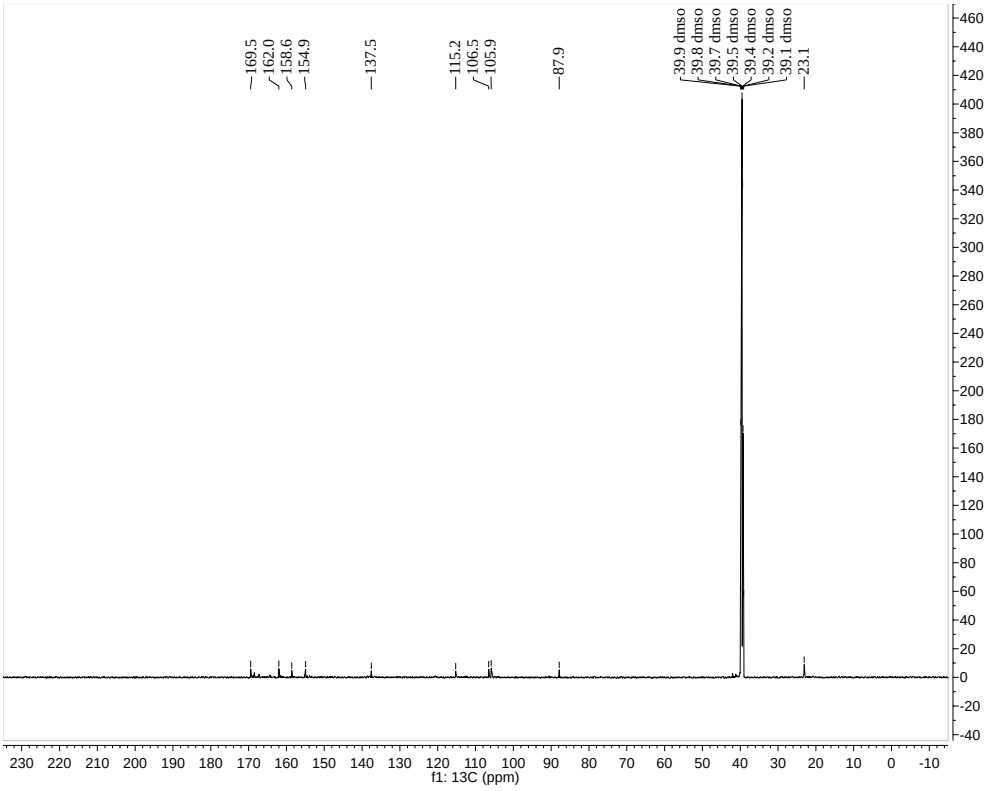

Supplemental Figure S2.101. (**2**) ^{1}H NMR (600 MHz, $(CD_3)_2SO$)

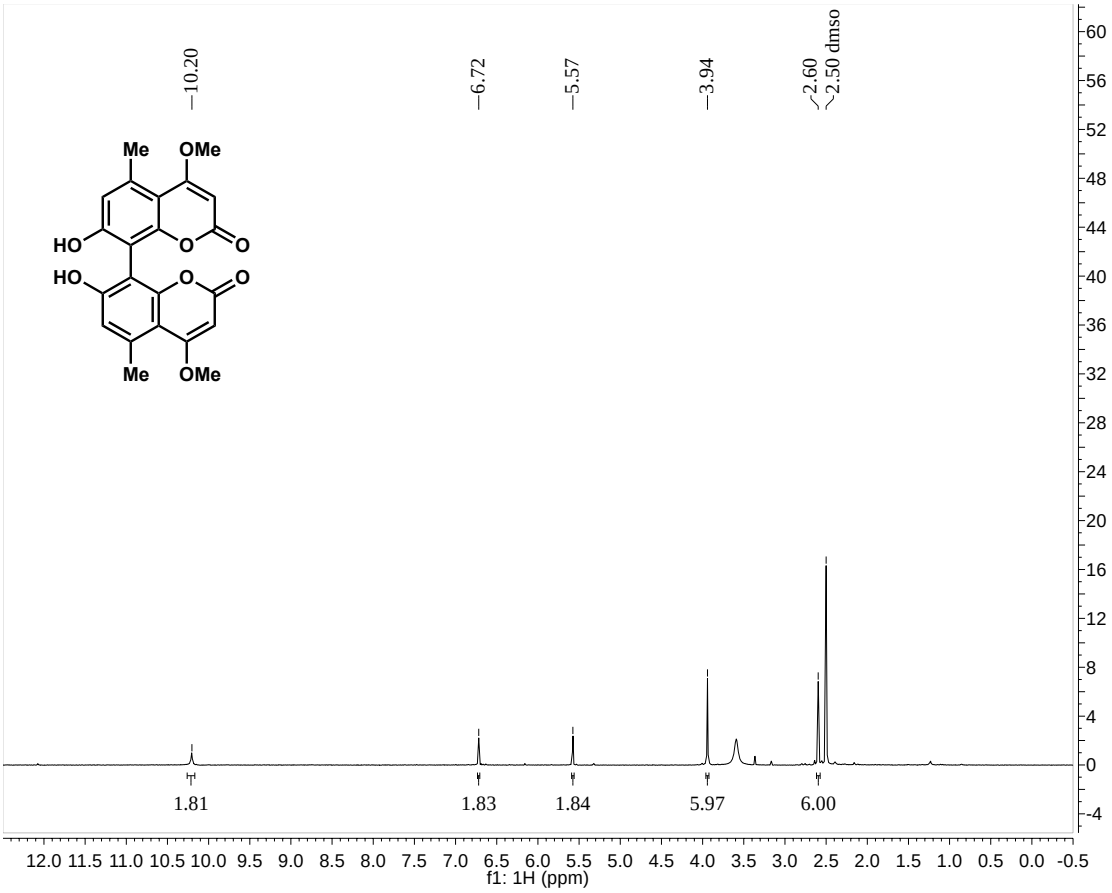

[1]H NMR and [13]C NMR spectra from biotransformation isolations

Supplemental Figure S2.102. (**2**) ^{1}H NMR (400 MHz, $(CD_3)_2SO$)

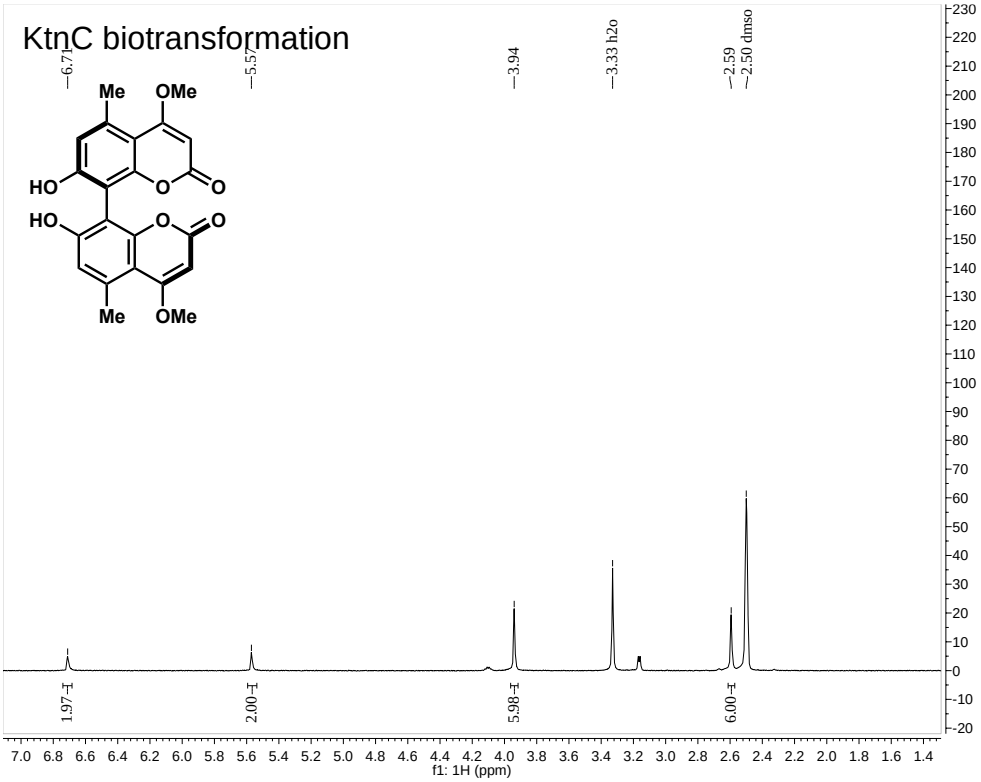

^{1}H NMR (400 MHz, CD_3OD)

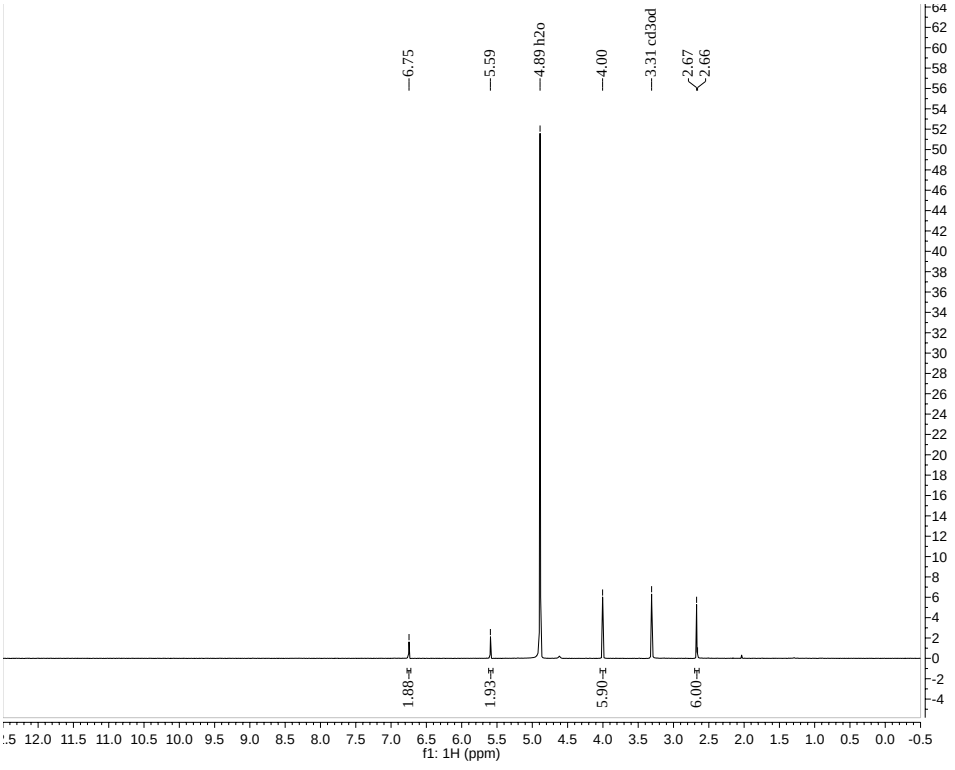

Supplemental Figure S2.103. (**3**) ^{1}H NMR (400 MHz, $(CD_3)_2SO$)

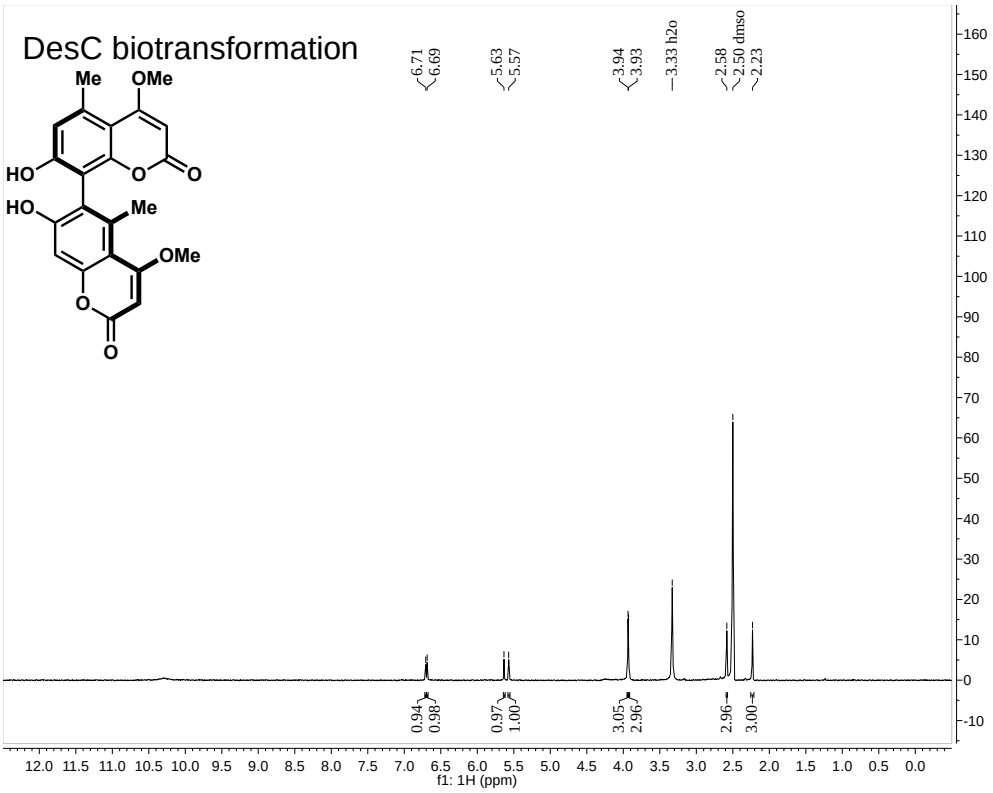

^{1}H NMR (600 MHz, CD_3OD)

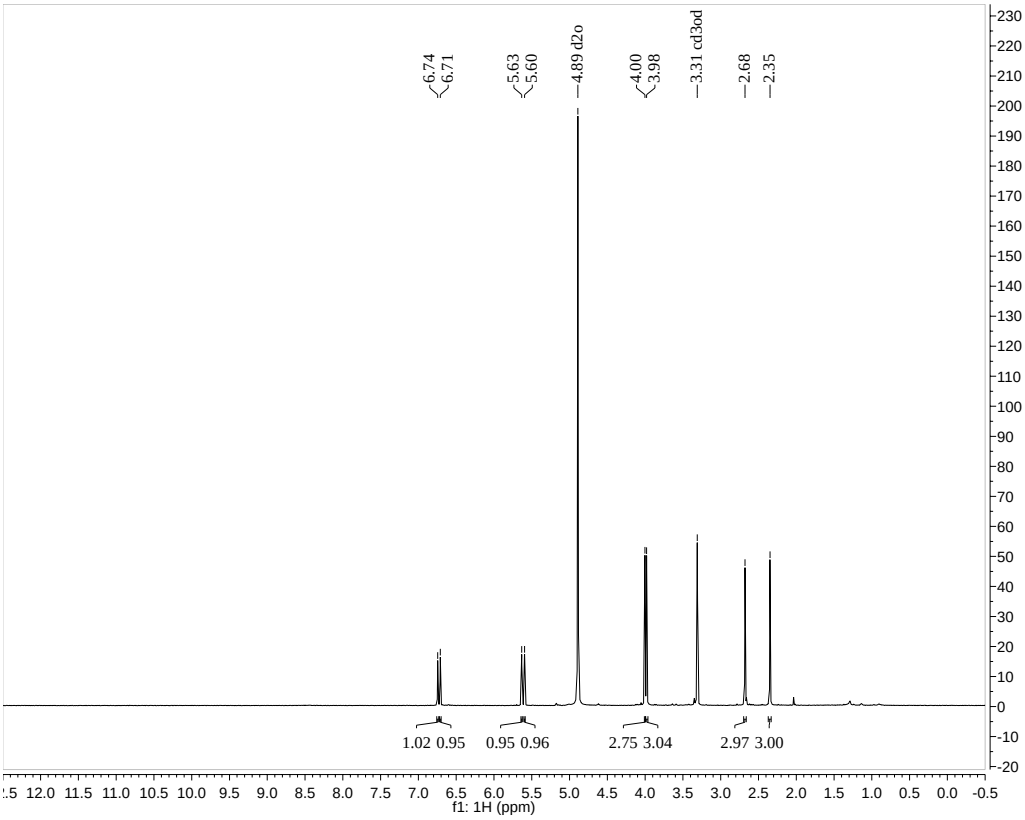

Supplemental Figure S2.104. (**29**) ^{1}H NMR (600 MHz, CD_3OD)

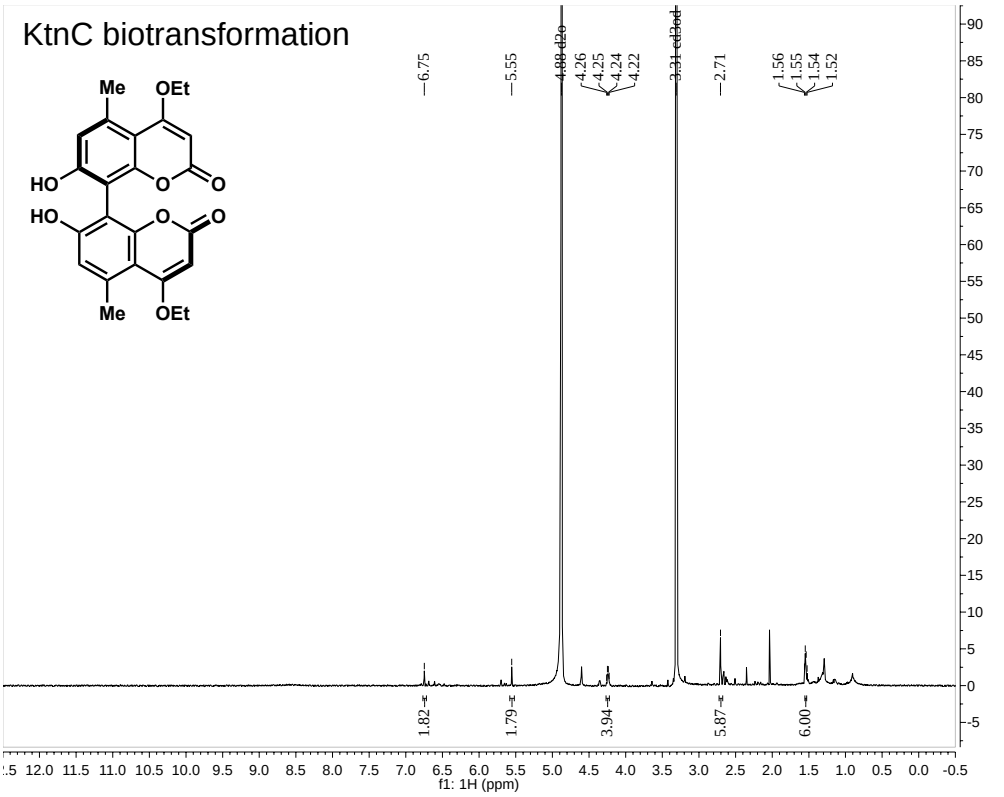

^{1}H NMR (600 MHz, $(CD_3)_2CO$)

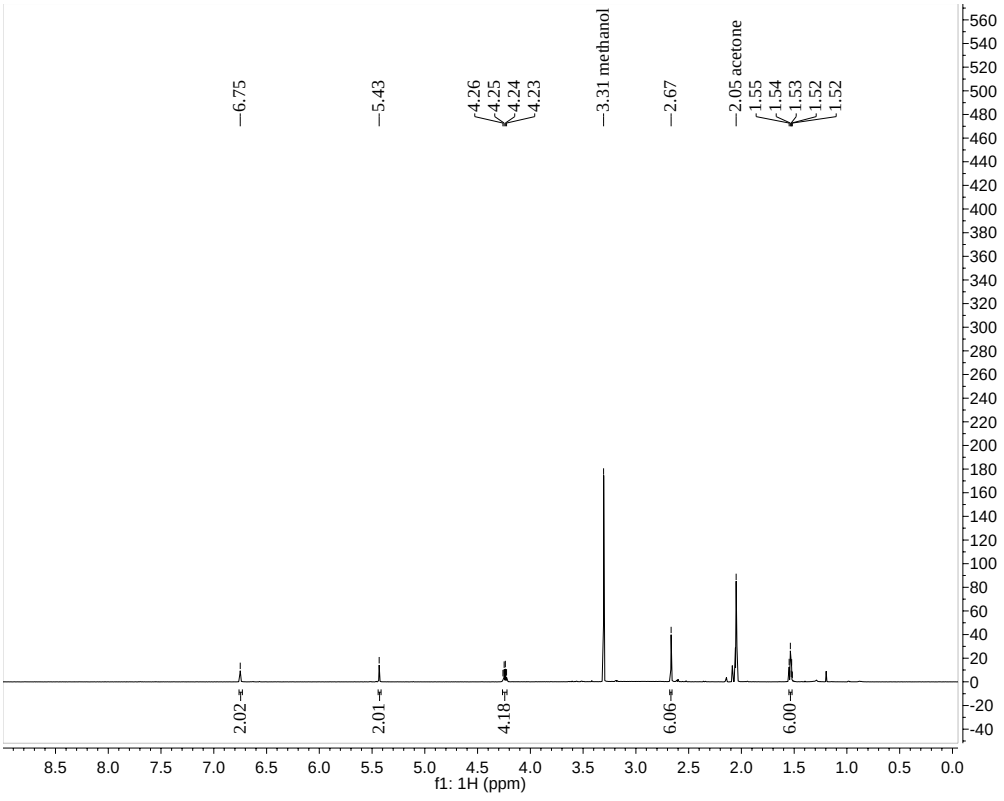

^{13}C NMR (150 MHz, $(CD_3)_2CO$)

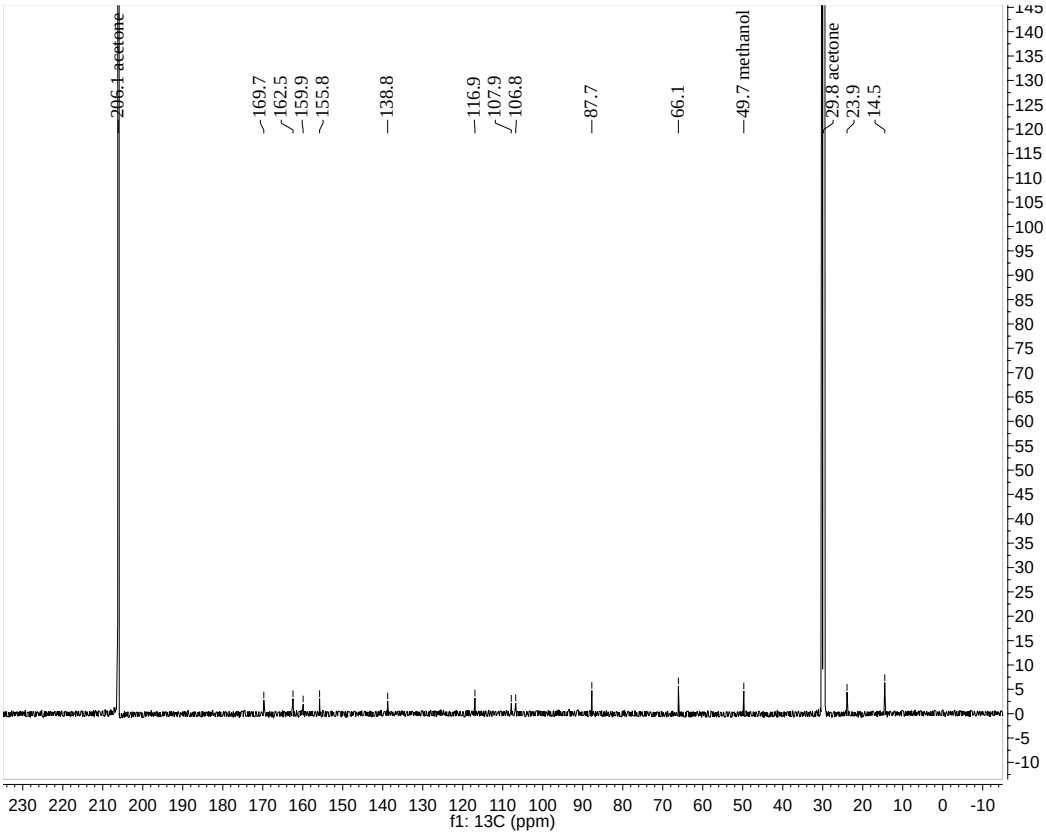

Supplemental Figure S2.105. (**30**) ^{1}H NMR (600 MHz, CD_3OD)

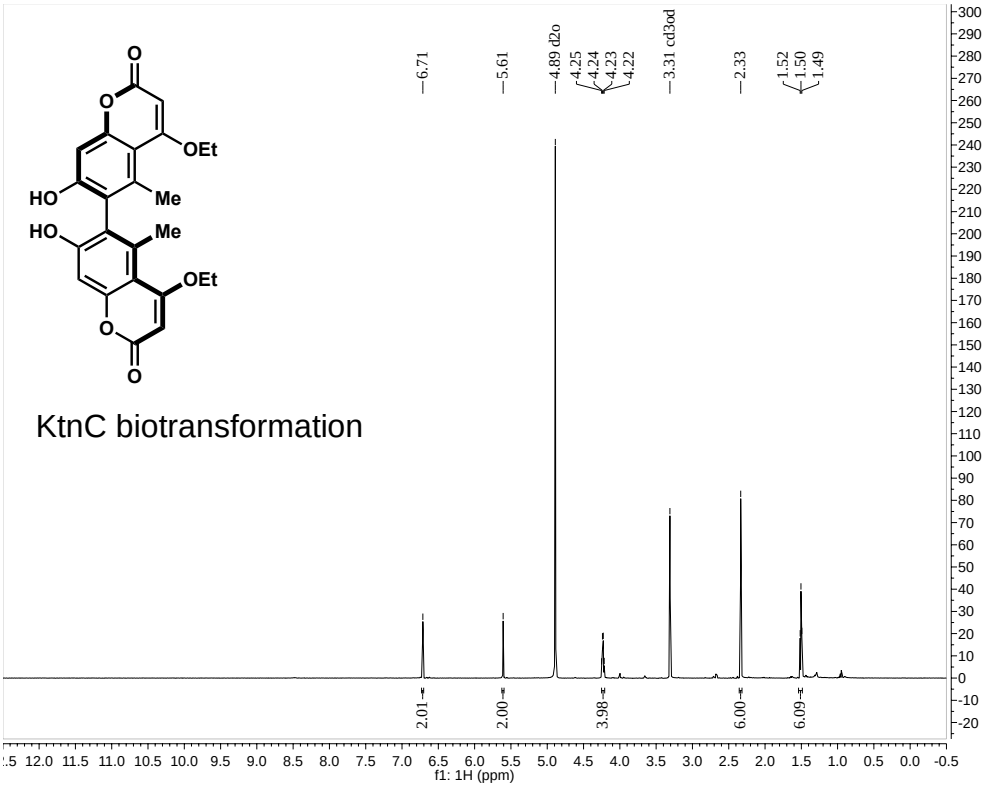

^{13}C NMR (150 MHz, CD_3OD)

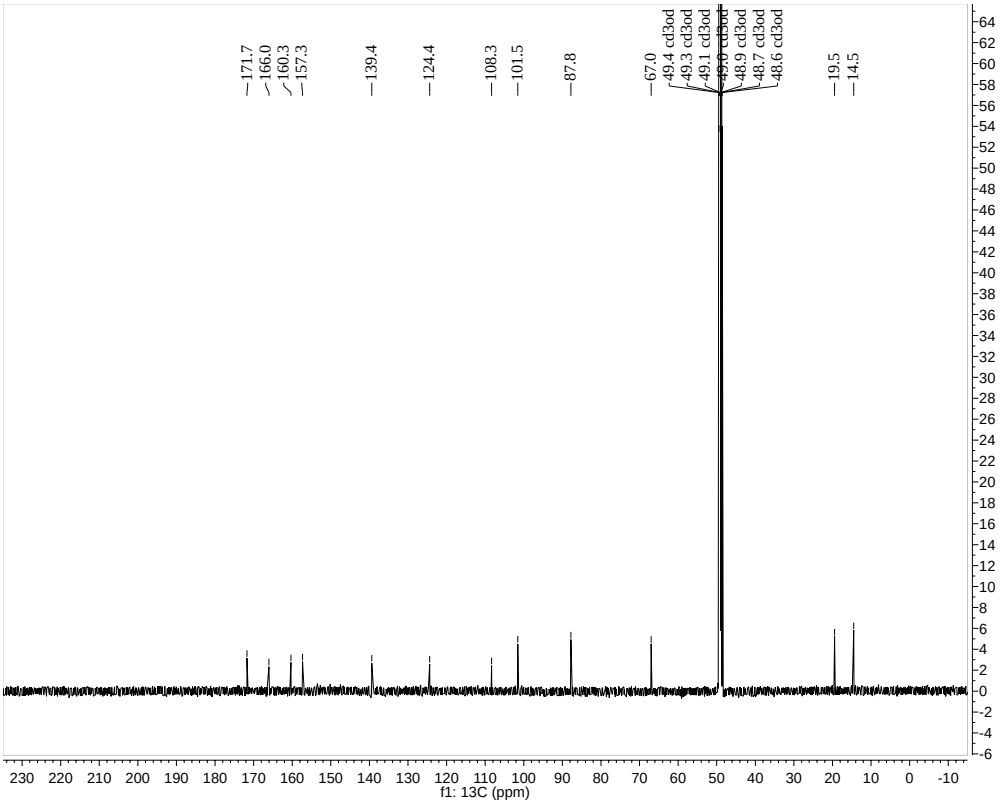

Supplemental Figure S2.106. (**29**) ^{1}H NMR (600 MHz, CD_3OD)

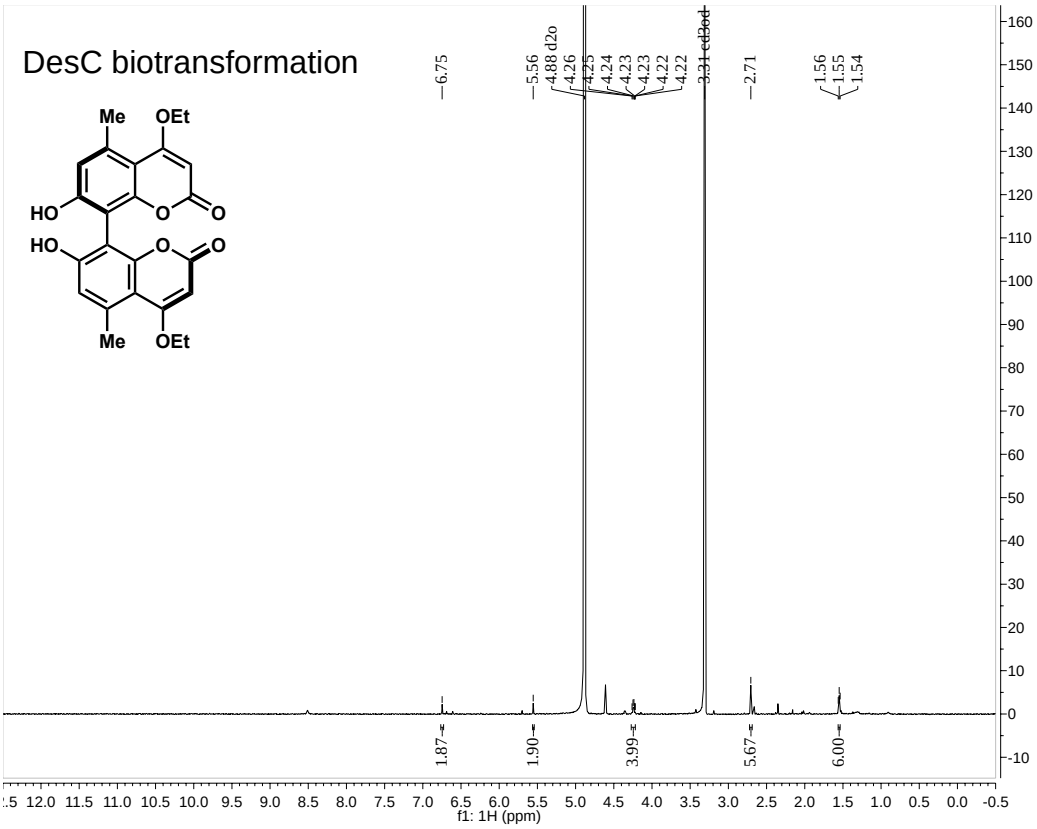

Supplemental Figure S2.107. (**31**) ^{1}H NMR (600 MHz, CD_3OD)

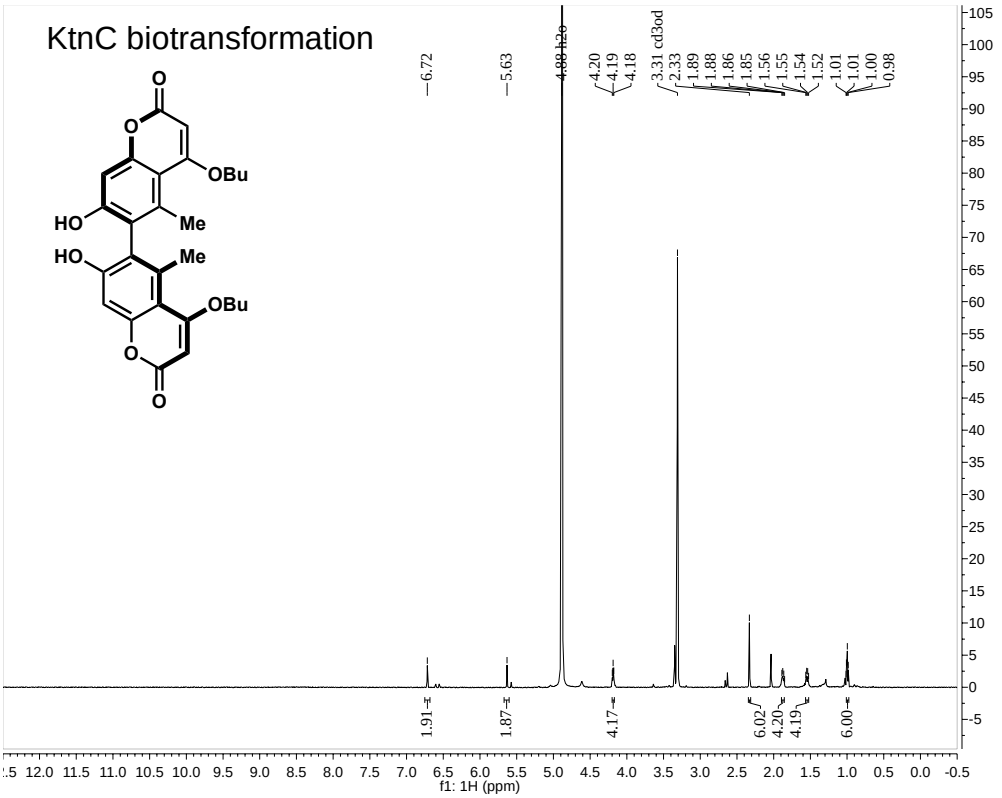

^{1}H NMR (700 MHz, $(CD_3)_2CO$)

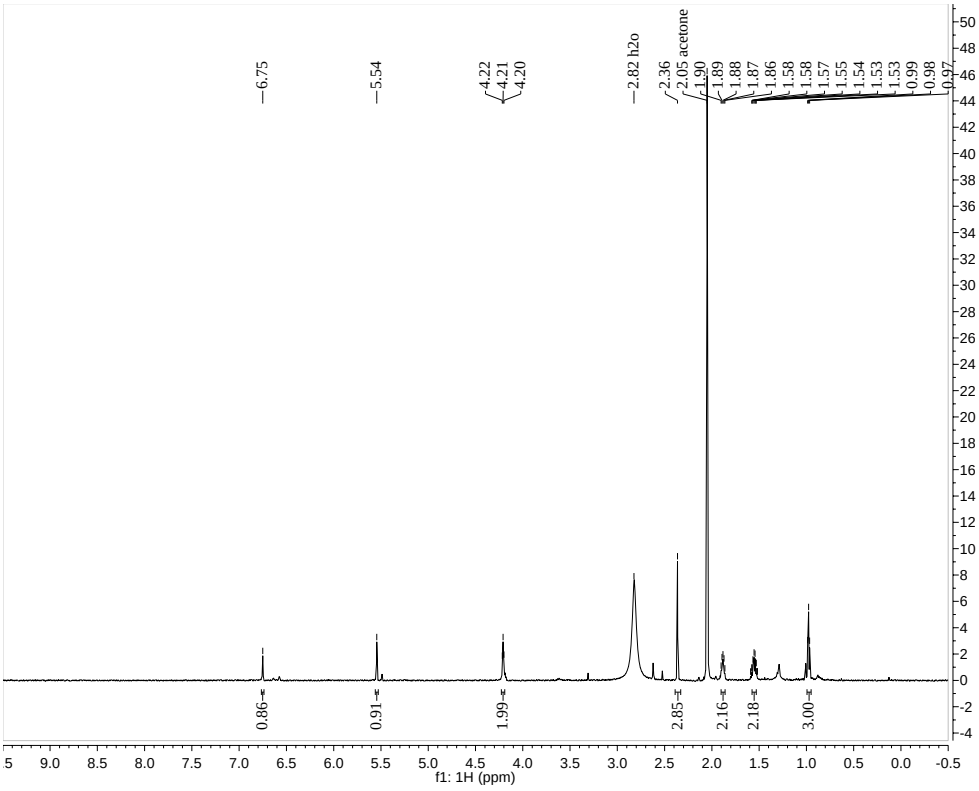

^{13}C NMR (175 MHz, $(CD_3)_2CO$)

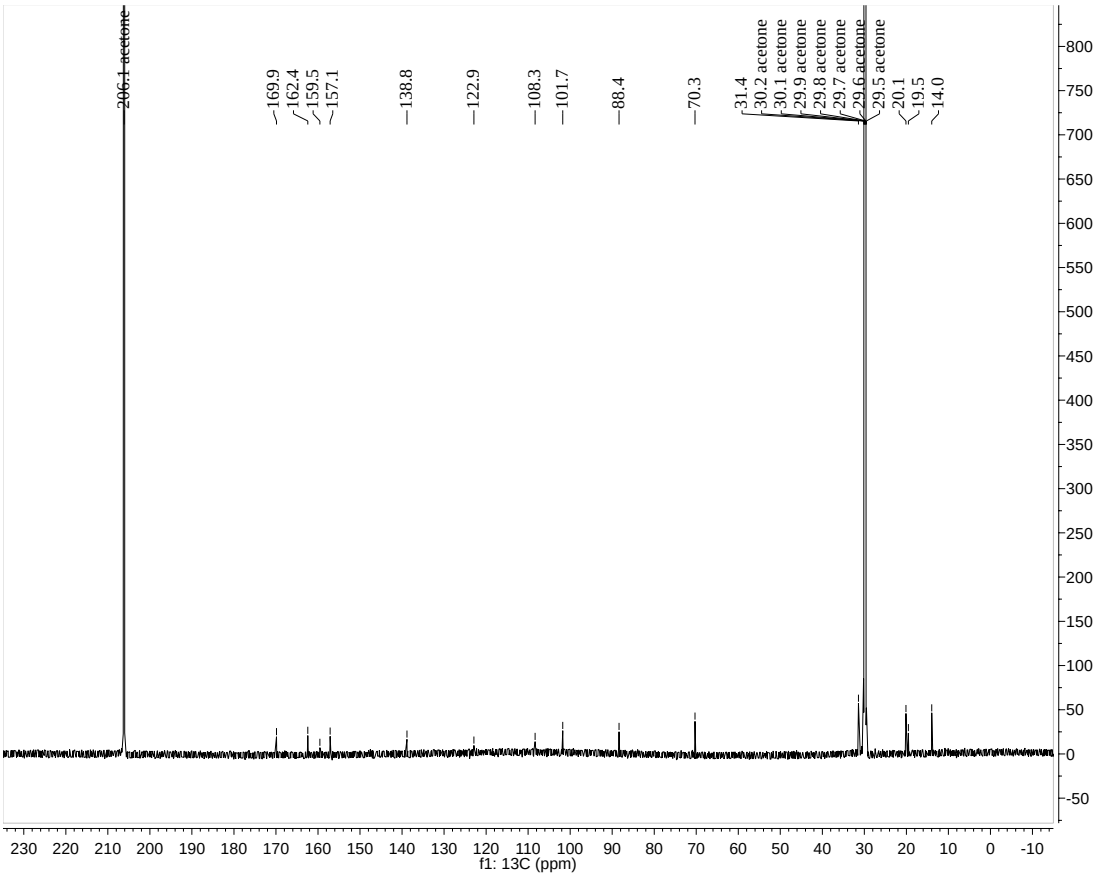

Supplemental Figure S2.108. (**32**) ^{1}H NMR (600 MHz, $(CD_3)_2CO$)

DesC biotransformation

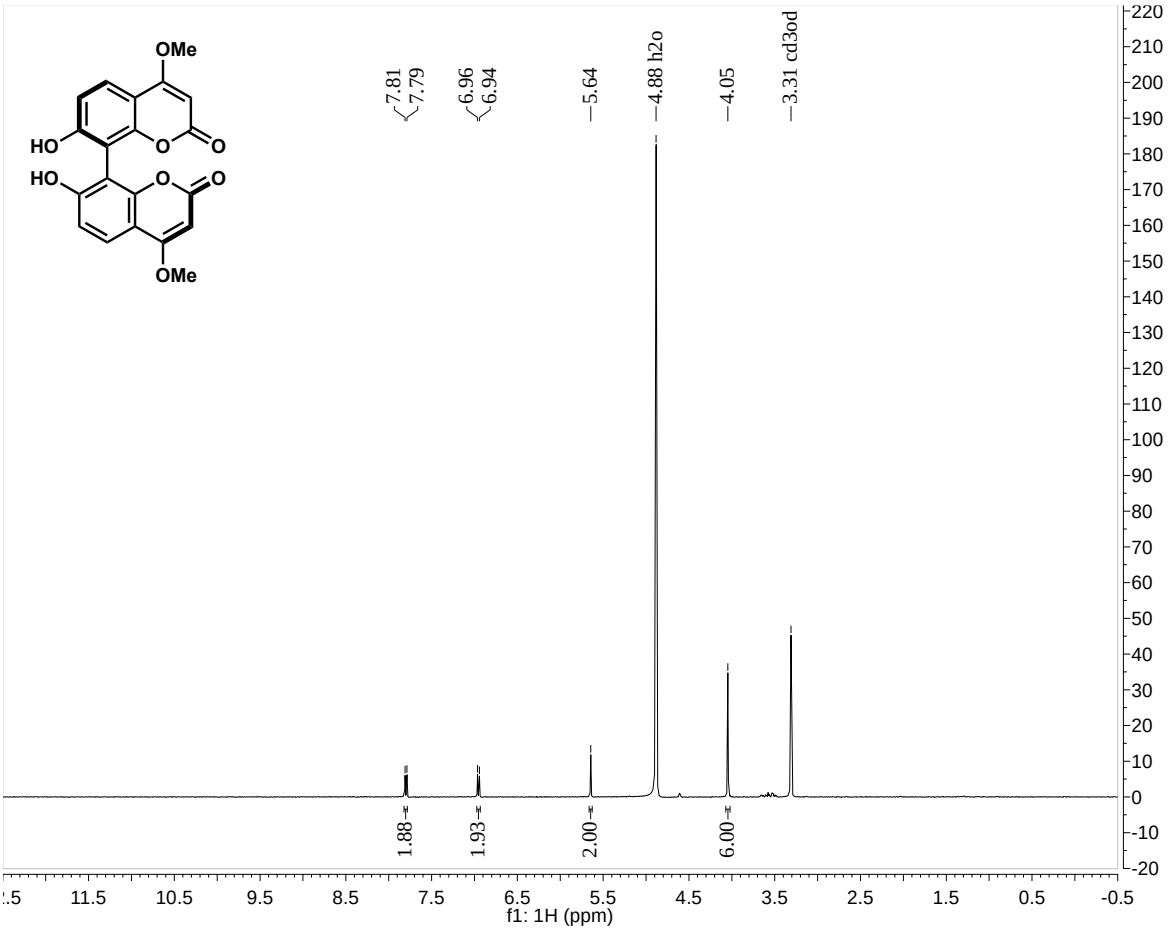

Supplemental Figure S2.109. (**33**) ^{1}H NMR (400 MHz, $(CD_3)_2CO$)

DesC biotransformation

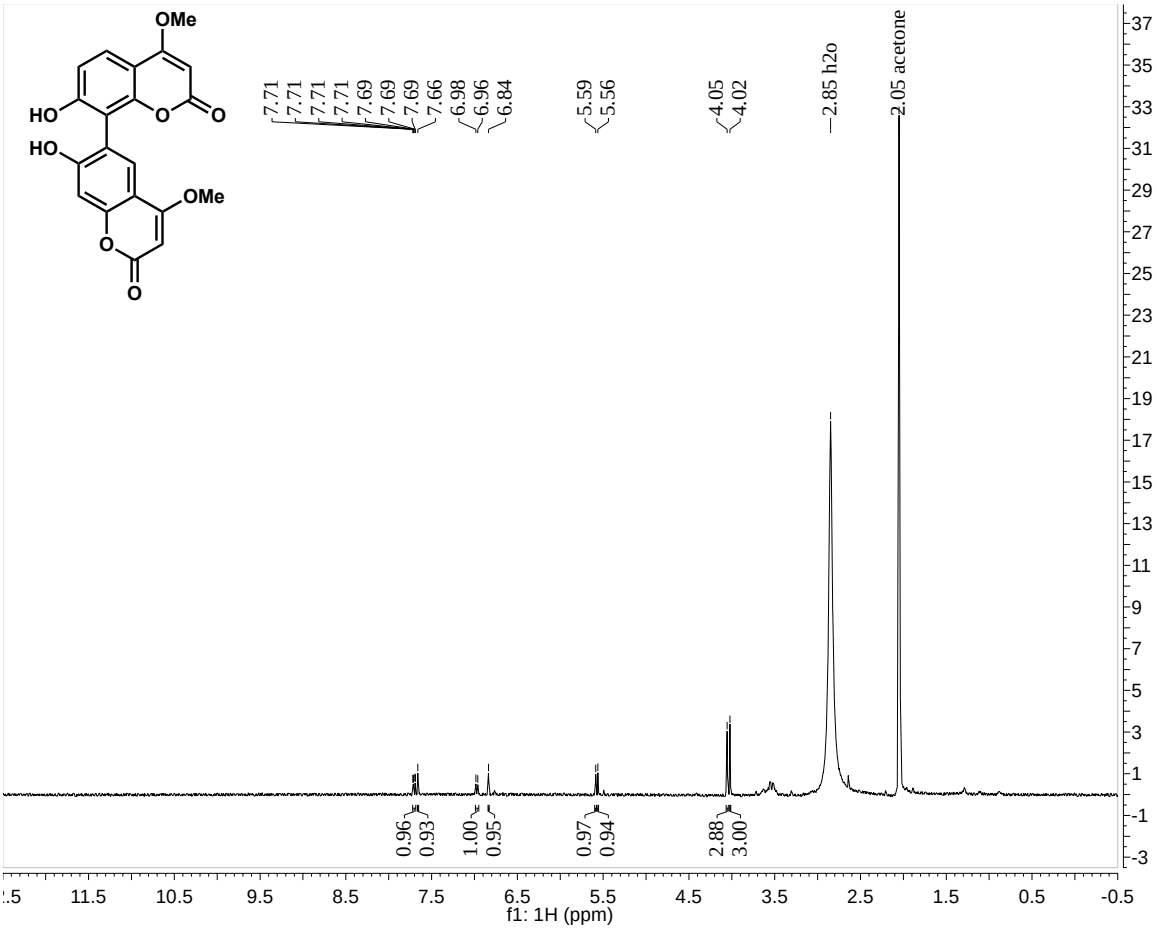

Supplemental Figure S2.110. (**31**) ^{1}H NMR (600 MHz, $(CD_3)_2CO$)

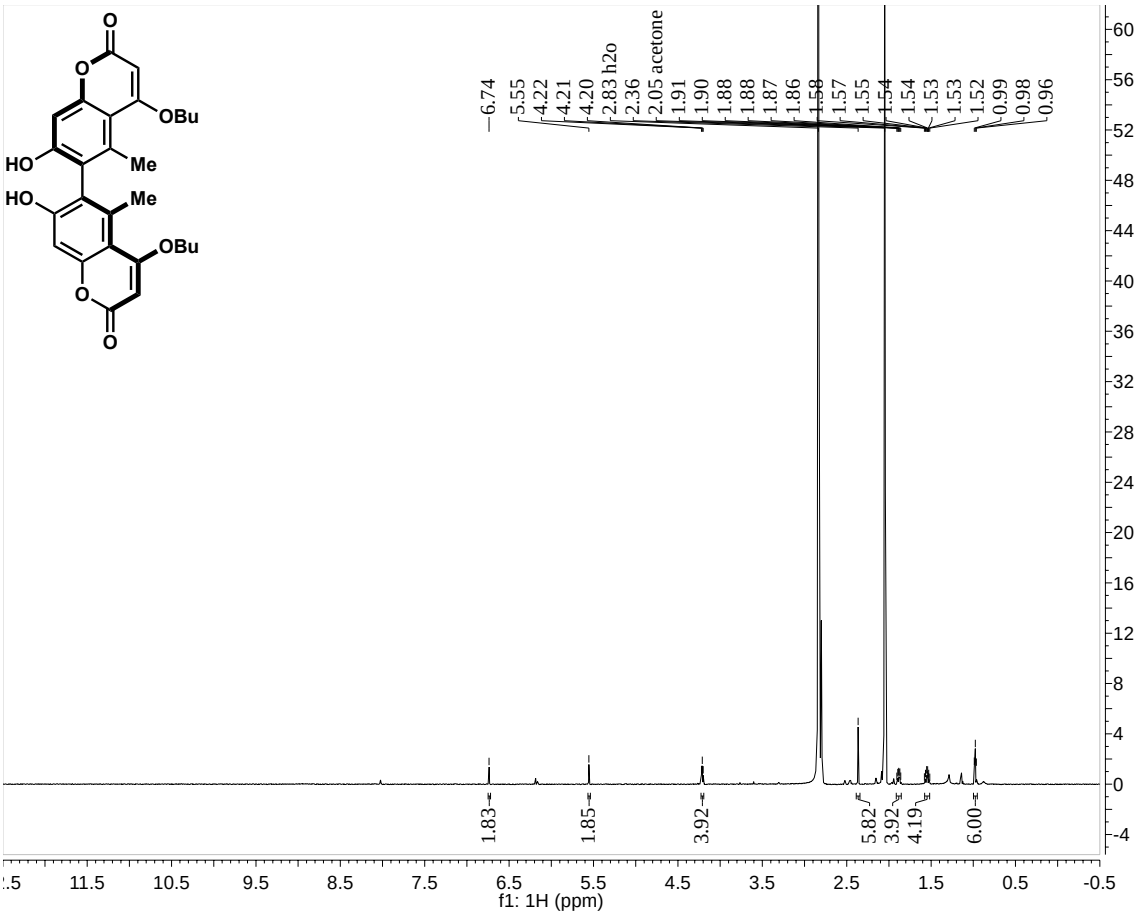

Supplemental Figure S2.111. Transesterification product (**4**) ^{1}H NMR (400 MHz, CD_3OD)

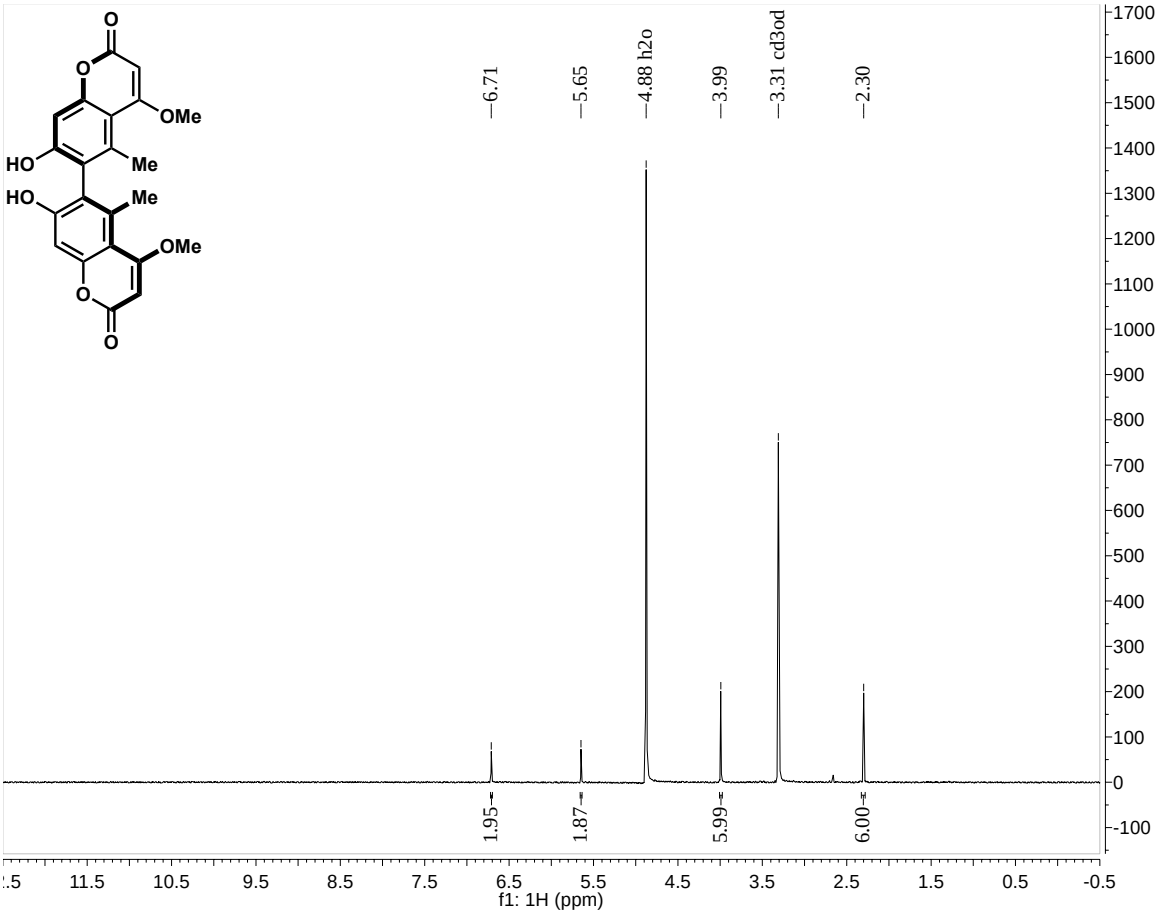

Supplemental Figure S2.112. (**64**) ^{1}H NMR (400 MHz, CD_3OD)

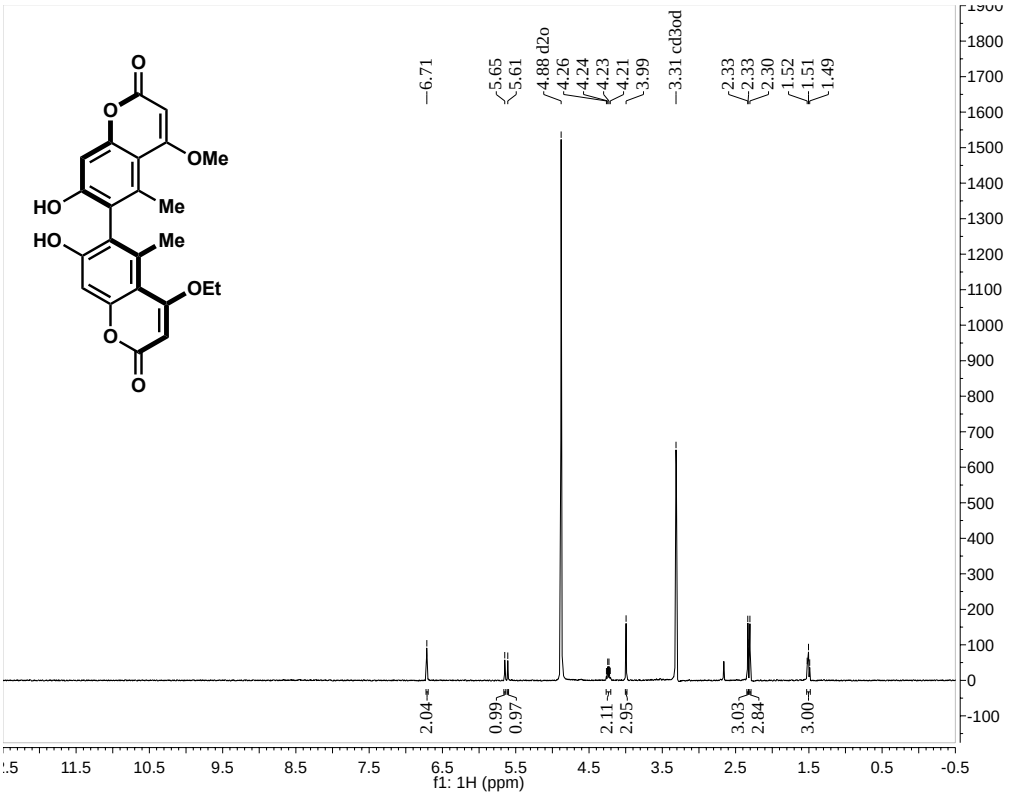

^{13}C NMR (150 MHz, CD_3OD)

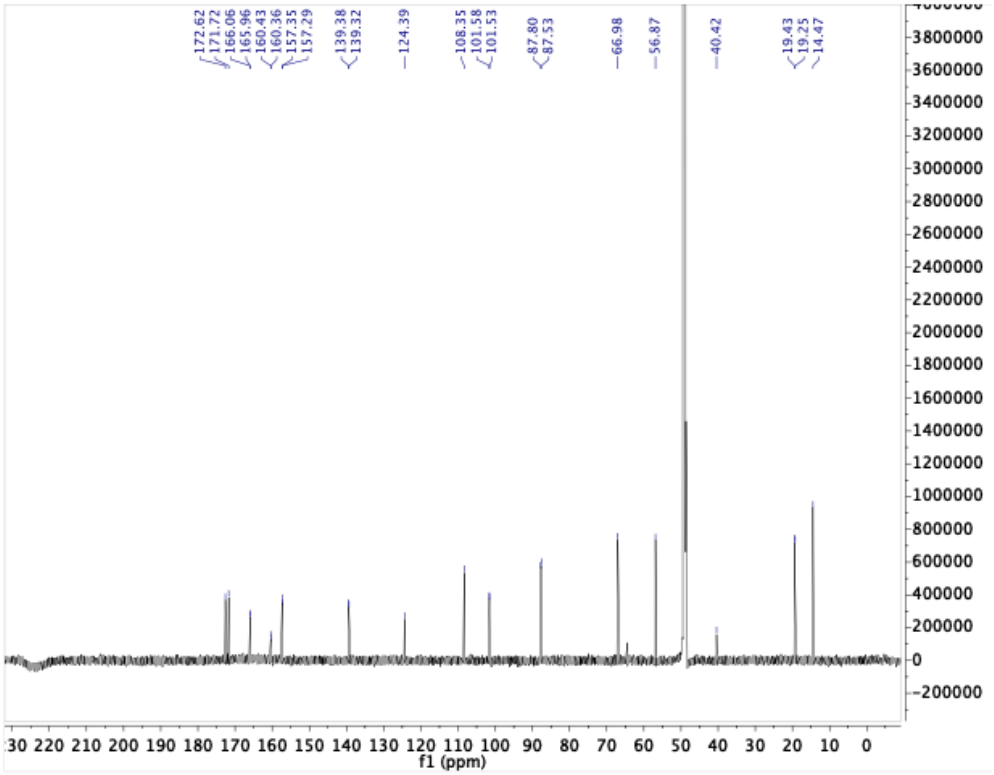

2.14 References

1. Kozlowski, M. C., Oxidative Coupling in Complexity Building Transforms. *Accounts Chem. Res.* **2017,** *50* (3), 638-643.

2. Yang, Y. D.; Lan, J. B.; You, J. S., Oxidative C-H/C-H Coupling Reactions between Two (Hetero)arenes. *Chem. Rev.* **2017,** *117* (13), 8787-8863.

3. Grzybowski, M.; Sadowski, B.; Butenschon, H.; Gryko, D. T., Synthetic Applications of Oxidative Aromatic Coupling-From Biphenols to Nanographenes. *Angew Chem Int Ed Engl* **2020,** *59* (8), 2998-3027.

4. Shalit, H.; Dyadyuk, A.; Pappo, D., Selective Oxidative Phenol Coupling by Iron Catalysis. *J Org Chem* **2019,** *84* (4), 1677-1686.

5. More, N. Y.; Jeganmohan, M., Oxidative Cross-Coupling of Two Different Phenols: An Efficient Route to Unsymmetrical Biphenols. *Org Lett* **2015,** *17* (12), 3042-5.

6. Carletti, G.; Nervo, G.; Cattivelli, L., Flavonoids and Melanins: A Common Strategy across Two Kingdoms. *Int J Biol Sci* **2014,** *10* (10), 1159-1170.

7. Wheeler, M. H.; Stipanovic, R. D., Melanin Biosynthesis and the Metabolism of Flaviolin and 2-Hydroxyjuglone in Wangiella-Dermatitidis. *Arch Microbiol* **1985,** *142* (3), 234-241.

8. Forneris, C. C.; Seyedsayamdost, M. R., In Vitro Reconstitution of OxyC Activity Enables Total Chemoenzymatic Syntheses of Vancomycin Aglycone Variants. *Angew Chem Int Ed Engl* **2018,** *57* (27), 8048-8052.

9. Grobe, N.; Zhang, B.; Fisinger, U.; Kutchan, T. M.; Zenk, M. H.; Guengerich, F. P., Mammalian cytochrome P450 enzymes catalyze the phenol-coupling step in endogenous morphine biosynthesis. *J Biol Chem* **2009,** *284* (36), 24425-31.

10. Gesell, A.; Rolf, M.; Ziegler, J.; Chavez, M. L. D.; Huang, F. C.; Kutchan, T. M., CYP719B1 Is Salutaridine Synthase, the C-C Phenol-coupling Enzyme of Morphine Biosynthesis in Opium Poppy. *Journal of Biological Chemistry* **2009,** *284* (36), 24432-24442.

11. Huttel, W.; Muller, M., Regio- and stereoselective intermolecular phenol coupling enzymes in secondary metabolite biosynthesis (vol 38, pg 1011, 2021). *Natural Product Reports* **2021,** *38* (7), 1408-1408.

12. Aldemir, H.; Richarz, R.; Gulder, T. A., The biocatalytic repertoire of natural biaryl formation. *Angew. Chem. Int. Ed.* **2014,** *53* (32), 8286-8293.

13. Mazzaferro, L. S.; Huttel, W.; Fries, A.; Muller, M., Cytochrome P450-Catalyzed Regio- and Stereoselective Phenol Coupling of Fungal Natural Products. *J. Am. Chem. Soc.* **2015,** *137* (38), 12289-12295.

14. Hugentobler, K. G.; Muller, M., Towards semisynthetic natural compounds with a biaryl axis: Oxidative phenol coupling in Aspergillus niger. *Bioorg Med Chem* **2018,** *26* (7), 1374-1377.

15. Kjaerbolling, I.; Vesth, T.; Frisvad, J. C.; Nybo, J. L.; Theobald, S.; Kildgaard, S.; Petersen, T. I.; Kuo, A.; Sato, A.; Lyhne, E. K.; Kogle, M. E.; Wiebenga, A.; Kun, R. S.; Lubbers, R. J. M.; Makela, M. R.; Barry, K.; Chovatia, M.; Clum, A.; Daum, C.; Haridas, S.; He, G. F.; LaButti, K.; Lipzen, A.; Mondo, S.; Pangilinan, J.; Riley, R.; Salamov, A.; Simmons, B. A.; Magnuson, J. K.; Henrissat, B.; Mortensen, U. H.; Larsen, T. O.; de Vries, R. P.; Grigoriev, I. V.; Machida, M.; Baker,

S. E.; Andersen, M. R., A comparative genomics study of 23 Aspergillus species from section Flavi. *Nature Communications* **2020,** *11* (1).

16. Cary, J. W.; Han, Z.; Yin, Y.; Lohmar, J. M.; Shantappa, S.; Harris-Coward, P. Y.; Mack, B.; Ehrlich, K. C.; Wei, Q.; Arroyo-Manzanares, N.; Uka, V.; Vanhaecke, L.; Bhatnagar, D.; Yu, J.; Nierman, W. C.; Johns, M. A.; Sorensen, D.; Shen, H.; De Saeger, S.; Di Mavungu, J. D.; Calvo, A. M., Transcriptome Analysis of Aspergillus flavus Reveals veA-Dependent Regulation of Secondary Metabolite Gene Clusters, Including the Novel Aflavarin Cluster. *Eukaryot. Cell* **2015,** *14* (10), 983-997.

17. Gil Girol, C.; Fisch, K. M.; Heinekamp, T.; Günther, S.; Hüttel, W.; Piel, J.; Brakhage, A. A.; Müller, M., Regio-and stereoselective oxidative phenol coupling in Aspergillus niger. *Angew. Chem. Int. Ed.* **2012,** *51*, 9788-9791.

18. Huttel, W.; Muller, M., Regio- and stereoselective intermolecular oxidative phenol coupling in kotanin biosynthesis by Aspergillus niger. *ChemBioChem* **2007,** *8* (5), 521-9.

19. Obermaier, S.; Muller, M., Biaryl-forming enzymes from *Aspergilli* exhibit substrate-dependent stereoselectivity. *Biochemistry* **2019,** *58* (22), 2589-2593.

20. Laakso, J. A.; Narske, E. D.; Gloer, J. B.; Wicklow, D. T.; Dowd, P. F., Isokotanins Ac - New Bicoumarins from the Sclerotia of Aspergillus-Alliaceus. *J. Nat. Prod.* **1994,** *57* (1), 128-133.

21. Huttel, W.; Nieger, M.; Muller, M., A short and efficient total synthesis of the naturally occurring coumarins siderin, kotanin, isokotanin A and desertorin C. *Synthesis-Stuttgart* **2003,** (12), 1803-1808.

22. Nozawa, K.; Nakajima, S.; Kawai, K.; Udagawa, S.; Miyaji, M., Bicoumarins from Ascostromata of Petromyces-Alliaceus. *Phytochemistry* **1994,** *35* (4), 1049-1051.

23. Scott, A. I., Oxidative coupling of phenolic compounds. *Q. Rev. Chem. Soc.* **1965,** *19* (1), 1-35.

24. Huttel, W.; Muller, M., Regio- and stereoselective intermolecular phenol coupling enzymes in secondary metabolite biosynthesis. *Natural Product Reports* **2021,** *38* (5), 1011-1043.

25. Davin, L. B.; Wang, H. B.; Crowell, A. L.; Bedgar, D. L.; Martin, D. M.; Sarkanen, S.; Lewis, N. G., Stereoselective bimolecular phenoxy radical coupling by an auxiliary (dirigent) protein without an active center. *Science* **1997,** *275* (5298), 362-366.

26. Zhang, X.; Guo, J.; Cheng, F.; Li, S., Cytochrome P450 enzymes in fungal natural product biosynthesis. *Nat Prod Rep* **2021,** *38* (6), 1072-1099.

27. Guengerich, F. P., Mechanisms of Cytochrome P450-Catalyzed Oxidations. *ACS Catal.* **2018,** *8* (12), 10964-10976.

28. Grandner, J. M.; Cacho, R. A.; Tang, Y.; Houk, K. N., Mechanism of the P450-Catalyzed Oxidative Cyclization in the Biosynthesis of Griseofulvin. *ACS Catal.* **2016,** *6* (7), 4506-4511.

29. Dumas, V. G.; Defelipe, L. A.; Petruk, A. A.; Turjanski, A. G.; Marti, M. A., QM/MM study of the C-C coupling reaction mechanism of CYP121, an essential Cytochrome p450 of Mycobacterium tuberculosis. *Proteins* **2014,** *82* (6), 1004-1021.

30. Zhao, B.; Bellamine, A.; Lei, L.; Waterman, M. R., The role of Ile87 of CYP158A2 in oxidative coupling reaction. *Arch Biochem Biophys* **2012,** *518* (2), 127-32.

31. Zhao, B.; Lamb, D. C.; Lei, L.; Kelly, S. L.; Yuan, H.; Hachey, D. L.; Waterman, M. R., Different binding modes of two flaviolin substrate molecules in cytochrome P450 158A1 (CYP158A1) compared to CYP158A2. *Biochemistry* **2007,** *46* (30), 8725-8733.

32. Zhao, B.; Guengerich, F. P.; Bellamine, A.; Lamb, D. C.; Izumikawa, M.; Lei, L.; Podust, L. M.; Sundaramoorthy, M.; Kalaitzis, J. A.; Reddy, L. M.; Kelly, S. L.; Moore, B. S.; Stec, D.; Voehler, M.; Falck, J. R.; Shimada, T.; Waterman, M. R., Binding of two flaviolin substrate molecules, oxidative coupling, and crystal structure of Streptomyces coelicolor A3(2) cytochrome P450 158A2. *Journal of Biological Chemistry* **2005,** *280* (12), 11599-11607.

33. Zhao, B.; Guengerich, F. P.; Voehler, M.; Waterman, M. R., Role of active site water molecules and substrate hydroxyl groups in oxygen activation by cytochrome P450 158A2 - A new mechanism of proton transfer. *Journal of Biological Chemistry* **2005,** *280* (51), 42188-42197.

34. Guengerich, F. P., Common and uncommon cytochrome P450 reactions related to metabolism and chemical toxicity. *Chem Res Toxicol* **2001,** *14* (6), 611-650.

35. Shalit, H.; Libman, A.; Pappo, D., meso-Tetraphenylporphyrin Iron Chloride Catalyzed Selective Oxidative Cross-Coupling of Phenols. *J. Am. Chem. Soc.* **2017,** *139* (38), 13404-13413.

36. Narute, S.; Parnes, R.; Toste, F. D.; Pappo, D., Enantioselective Oxidative Homocoupling and Cross-Coupling of 2-Naphthols Catalyzed by Chiral Iron Phosphate Complexes. *J Am Chem Soc* **2016,** *138* (50), 16553-16560.

37. Libman, A.; Shalit, H.; Vainer, Y.; Narute, S.; Kozuch, S.; Pappo, D., Synthetic and Predictive Approach to Unsymmetrical Biphenols by Iron-Catalyzed Chelated Radical-Anion Oxidative Coupling. *J. Am. Chem. Soc.* **2015,** *137* (35), 11453-11460.

38. Egami, H.; Matsumoto, K.; Oguma, T.; Kunisu, T.; Katsuki, T., Enantioenriched Synthesis of C-1-Symmetric BINOLs: Iron-Catalyzed Cross-Coupling of 2-Naphthols and Some Mechanistic Insight. *J. Am. Chem. Soc.* **2010,** *132* (39), 13633-13635.

39. Guengerich, F. P.; Waterman, M. R.; Egli, M., Recent Structural Insights into Cytochrome P450 Function. *Trends Pharmacol Sci* **2016,** *37* (8), 625-640.

40. Bernhardt, R.; Urlacher, V. B., Cytochromes P450 as promising catalysts for biotechnological application: chances and limitations. *Applied Microbiology and Biotechnology* **2014,** *98* (14), 6185-6203.

41. Byme, B., Pichia pastoris as an expression host for membrane protein structural biology. *Current Opinion in Structural Biology* **2015,** *32*, 9-17.

42. Jiang, L. H.; Huang, L.; Cai, J.; Xu, Z. N.; Lian, J. Z., Functional expression of eukaryotic cytochrome P450s in yeast. *Biotechnol Bioeng* **2021,** *118* (3), 1050-1065.

43. O'Reilly, E.; Kohler, V.; Flitsch, S. L.; Turner, N. J., Cytochromes P450 as useful biocatalysts: addressing the limitations. *Chemical Communications* **2011,** *47* (9), 2490-2501.

44. Garzon-Posse, F.; Becerra-Figueroa, L.; Hernandez-Arias, J.; Gamba-Sanchez, D., Whole Cells as Biocatalysts in Organic Transformations. *Molecules* **2018,** *23* (6).

45. Lin, B. X.; Tao, Y., Whole-cell biocatalysts by design. *Microbial Cell Factories* **2017,** *16*.

46. Peng, B. Y.; Williams, T. C.; Henry, M.; Nielsen, L. K.; Vickers, C. E., Controlling heterologous gene expression in yeast cell factories on different carbon substrates and across the diauxic shift: a comparison of yeast promoter activities. *Microbial Cell Factories* **2015,** *14*.

47. Liu, Z. H.; Tyo, K. E. J.; Martinez, J. L.; Petranovic, D.; Nielsen, J., Different expression systems for production of recombinant proteins in Saccharomyces cerevisiae. *Biotechnol Bioeng* **2012,** *109* (5), 1259-1268.

48. Muller, S.; Sandal, T.; Kamp-Hansen, P.; Dalboge, H., Comparison of expression systems in the yeasts Saccharomyces cerevisiae, Hansenula polymorpha, Klyveromyces lactis, Schizosaccharomyces pombe and Yarrowia lipolytica. Cloning of two novel promoters from Yarrowia lipolytica. *Yeast* **1998,** *14* (14), 1267-1283.

49. Cereghino, J. L.; Cregg, J. M., Heterologous protein expression in the methylotrophic yeast Pichia pastoris. *Fems Microbiol Rev* **2000,** *24* (1), 45-66.

50. Byrne, L. J.; O'Callaghan, K. J.; Tuite, M. F., Heterologous gene expression in yeast. *Methods Mol Biol* **2005,** *308*, 51-64.

51. Ahmad, M.; Hirz, M.; Pichler, H.; Schwab, H., Protein expression in Pichia pastoris: recent achievements and perspectives for heterologous protein production. *Applied Microbiology and Biotechnology* **2014,** *98* (12), 5301-5317.

52. Juturu, V.; Wu, J. C., Heterologous Protein Expression in Pichia pastoris: Latest Research Progress and Applications. *ChemBioChem* **2018,** *19* (1), 7-21.

53. Looser, V.; Bruhlmann, B.; Bumbak, F.; Stenger, C.; Costa, M.; Camattari, A.; Fotiadis, D.; Kovar, K., Cultivation strategies to enhance productivity of Pichia pastoris: A review. *Biotechnology Advances* **2015,** *33* (6), 1177-1193.

54. Bergman, L. W., Growth and maintenance of yeast. *Methods Mol Biol* **2001,** *177*, 9-14.

55. Searle, B. A.; Kirsop, B. H., Sugar Utilization by a Brewing Yeast in Relation to the Growth and Maintenance Phases of Metabolism. *J I Brewing* **1979,** *85* (6), 342-345.

56. www.pichia.com.

57. Hasslacher, M.; Schall, M.; Hayn, M.; Bona, R.; Rumbold, K.; Luckl, J.; Griengl, H.; Kohlwein, S. D.; Schwab, H., High-level intracellular expression of hydroxynitrile lyase from the tropical rubber tree Hevea brasiliensis in microbial hosts. *Protein Expres Purif* **1997,** *11* (1), 61-71.

58. Heyland, J.; Fu, J. A.; Blank, L. M.; Schmid, A., Quantitative Physiology of Pichia pastoris During Glucose-Limited High-Cell Density Fed-Batch Cultivation for Recombinant Protein Production. *Biotechnol Bioeng* **2010,** *107* (2), 357-368.

59. Zhang, A. L.; Luo, J. X.; Zhang, T. Y.; Pan, Y. W.; Tan, Y. H.; Fu, C. Y.; Tu, F. Z., Recent advances on the GAP promoter derived expression system of Pichia pastoris. *Mol Biol Rep* **2009,** *36* (6), 1611-1619.

60. Cregg, J. M.; Cregg, J. M., *Pichia protocols*. 2nd ed.; Humana Press: Totowa, N.J., 2007; p xi, 268 p.

61. De Schutter, K.; Lin, Y. C.; Tiels, P.; Van Hecke, A.; Glinka, S.; Weber-Lehmann, J.; Rouze, P.; Van de Peer, Y.; Callewaert, N., Genome sequence of the recombinant protein production host Pichia pastoris. *Nature Biotechnology* **2009,** *27* (6), 561-+.

62. Madden, K.; Tolstorukov, I.; Cregg, J., Electroporation of Pichia pastoris. In *Genetic Transformation Systems in Fungi, Volume 1*, Springer: 2015; pp 87-91.

63. Grzybowski, M.; Sadowski, B.; Butenschön, H.; Gryko, D. T., Synthetic applications of oxidative aromatic coupling—from biphenols to nanographenes. *Angew. Chem. Int. Ed.* **2020,** *59* (8), 2998-3027.

64. Lee, Y. E.; Cao, T.; Torruellas, C.; Kozlowski, M. C., Selective Oxidative Homo- and Cross-Coupling of Phenols with Aerobic Catalysts. *J. Am. Chem. Soc.* **2014,** *136* (19), 6782-6785.

65. Ashenhurst, J. A., Intermolecular oxidative cross-coupling of arenes. *Chem. Soc. Rev.* **2010,** *39* (2), 540-548.

66. Kozlowski, M. C.; Morgan, B. J.; Linton, E. C., Total synthesis of chiral biaryl natural products by asymmetric biaryl coupling. *Chem. Soc. Rev.* **2009,** *38* (11), 3193-3207.

67. Boyd, E. M.; Sperry, J., Biomimetic Synthesis of Dendridine A. *Org. Lett.* **2015,** *17* (5), 1344-1346.

68. Morimoto, K.; Sakamoto, K.; Ohshika, T.; Dohi, T.; Kita, Y., Organo-Iodine(III)-Catalyzed Oxidative Phenol-Arene and Phenol-Phenol Cross-Coupling Reaction. *Angew Chem Int Ed Engl* **2016,** *55* (11), 3652-6.

69. Morimoto, K.; Sakamoto, K.; Ohnishi, Y.; Miyamoto, T.; Ito, M.; Dohi, T.; Kita, Y., Metal-free oxidative para cross-coupling of phenols. *Chemistry* **2013,** *19* (27), 8726-31.

70. Hirao, T., Vanadium in modern organic synthesis. *Chem. Rev.* **1997,** *97* (8), 2707-2724.

71. Wu, X.; Iwata, T.; Scharf, A.; Qin, T.; Reichl, K. D.; Porco, J. A., Asymmetric synthesis of gonytolide A: strategic use of an aryl halide blocking group for oxidative coupling. *J. Am. Chem. Soc.* **2018,** *140* (18), 5969-5975.

72. Noji, M.; Nakajima, M.; Koga, K., A New Catalytic-System for Aerobic Oxidative Coupling of 2-Naphthol Derivatives by the Use of Cucl-Amine Complex - a Practical Synthesis of Binaphthol Derivatives. *Tetrahedron Letters* **1994,** *35* (43), 7983-7984.

73. Kocovsky, P.; Vyskocil, S.; Smrcina, M., Non-symmetrically substituted 1,1'-binaphthyls in enantioselective catalysis. *Chem Rev* **2003,** *103* (8), 3213-46.

74. Smrcina, M.; Vyskocil, S.; Maca, B.; Polasek, M.; Claxton, T. A.; Abbott, A. P.; Kocovsky, P., Selective Cross-Coupling of 2-Naphthol and 2-Naphthylamine Derivatives - a Facile Synthesis of 2,2',3-Trisubstituted and 2,2',3,3'-Tetrasubstituted 1,1'-Binaphthyls. *J. Org. Chem.* **1994,** *59* (8), 2156-2163.

75. Smrcina, M.; Polakova, J.; Vyskocil, S.; Kocovsky, P., Synthesis of Enantiomerically Pure Binaphthyl Derivatives - Mechanism of the Enantioselective, Oxidative Coupling of Naphthols and Designing a Catalytic Cycle. *J. Org. Chem.* **1993,** *58* (17), 4534-4538.

76. Hubbard, J. S.; Harris, T. M., Condensations at the 6-Position of the Methyl-Ester and Dimethylamide of 3,5-Dioxohexanoic Acid Via 2,4,6-Trianions. *J. Org. Chem.* **1981,** *46* (12), 2566-2570.

77. Gil Girol, C.; Fisch, K. M.; Heinekamp, T.; Günther, S.; Hüttel, W.; Piel, J.; Brakhage, A. A.; Müller, M., Regio‐ and stereoselective oxidative phenol coupling in Aspergillus niger. *Angew. Chem. Int. Ed.* **2012,** *51*, 9788-9791.

78. Xie, S. S.; Wang, X. B.; Jiang, N.; Yu, W. Y.; Wang, K. D. G.; Lan, J. S.; Li, Z. R.; Kong, L. Y., Multi-target tacrine-coumarin hybrids: Cholinesterase and monoamine oxidase B inhibition properties against Alzheimer's disease. *Eur J Med Chem* **2015,** *95*, 153-165.

79. Conradt, D.; Schatzle, M. A.; Haas, J.; Townsend, C. A.; Muller, M., New Insights into the Conversion of Versicolorin A in the Biosynthesis of Aflatoxin B-1. *J. Am. Chem. Soc.* **2015,** *137* (34), 10867-10869.

80. Zav'yalov, S. I.; Dorofeeva, O. V.; Rumyantseva, E. E.; Zavozin, A. G., Synthesis of hydroxyderivatives of 4-methylcoumarin. *Pharmaceutical Chemistry Journal* **1996,** *30* (3), 204-205.

81. Karimi, B.; Zareyee, D., Design of a highly efficient and water-tolerant sulfonic acid nanoreactor based on tunable ordered porous silica for the von Pechmann reaction. *Org. Lett.* **2008,** *10* (18), 3989-3992.

82. Cutler, H. G.; Crumley, F. G.; Cox, R. H.; Hernandez, O.; Cole, R. J.; Dorner, J. W., Orlandin - Nontoxic Fungal Metabolite with Plant-Growth Inhibiting Properties. *J Agr Food Chem* **1979,** *27* (3), 592-595.

83. Mazzaferro, L. S.; Huttel, W.; Fries, A.; Muller, M., Cytochrome P450-Catalyzed Regio- and Stereoselective Phenol Coupling of Fungal Natural Products. *J. Am. Chem. Soc.* **2015,** *137* (38), 12289-12295.

84. Nozawa, K.; Seyea, H.; Nakajima, S.; Udagawa, S.; Kawai, K., Studies on Fungal Products .10. Isolation and Structures of Novel Bicoumarins, Desertorin-a, Desertorin-B, and Desertorin-C, from Emericella-Desertorum. *J Chem Soc Perk T 1* **1987,** (8), 1735-1738.

85. Trost, B. M.; Pissot-Soldermann, C.; Chen, I., A short and concise asymmetric synthesis of hamigeran B. *Chem-Eur J* **2005,** *11* (3), 951-959.

86. Li, J. W.; Ren, Y. W.; Qi, C. R.; Jiang, H. F., Fully meta-Substituted 4,4 '-Biphenyldicarboxylate-Based Metal-Organic Frameworks: Synthesis, Structures, and Catalytic Activities. *Eur J Inorg Chem* **2017,** (11), 1478-1487.

87. Gietz, R. D.; Woods, R. A., Transformation of yeast by lithium acetate/single-stranded carrier DNA/polyethylene glycol method. *Method Enzymol* **2002,** *350*, 87-96.

88. Cregg, J. M.; Cregg, J. M., *Pichia protocols*. 2nd ed.; Humana Press: Totowa, N.J., 2007; p xi, 268 p.

89. Laakso, J. A.; Narske, E. D.; Gloer, J. B.; Wicklow, D. T.; Dowd, P. F., Isokotanins Ac - New Bicoumarins from the Sclerotia of Aspergillus-Alliaceus. *J. Nat. Prod.* **1994,** *57* (1), 128-133.

90. Sherer, E. C.; Lee, C. H.; Shpungin, J.; Cuff, J. F.; Da, C. X.; Ball, R.; Bach, R.; Crespo, A.; Gong, X. Y.; Welch, C. J., Systematic Approach to Conformational Sampling for Assigning Absolute Configuration Using Vibrational Circular Dichroism. *J Med Chem* **2014,** *57* (2), 477-494.

91. Joyce, L. A.; Nawrat, C. C.; Sherer, E. C.; Biba, M.; Brunskill, A.; Martin, G. E.; Cohen, R. D.; Davies, I. W., Beyond optical rotation: what's left is not always right in total synthesis. *Chemical Science* **2018,** *9* (2), 415-424.

92. Liu, Z. Q.; Shultz, C. S.; Sherwood, C. A.; Krska, S.; Dormer, P. G.; Desmond, R.; Lee, C.; Sherer, E. C.; Shpungin, J.; Cuff, J.; Xu, F., Highly enantioselective synthesis of anti aryl beta-hydroxy alpha-amino esters via DKR transfer hydrogenation. *Tetrahedron Letters* **2011,** *52* (14), 1685-1688.

93. Petersson, G. A.; Allaham, M. A., A Complete Basis Set Model Chemistry .2. Open-Shell Systems and the Total Energies of the 1st-Row Atoms. *J Chem Phys* **1991,** *94* (9), 6081-6090.

94. Petersson, G. A.; Bennett, A.; Tensfeldt, T. G.; Allaham, M. A.; Shirley, W. A.; Mantzaris, J., A Complete Basis Set Model Chemistry .1. The Total Energies of Closed-Shell Atoms and Hydrides of the 1st-Row Elements. *J Chem Phys* **1988,** *89* (4), 2193-2218.

95. Rassolov, V. A.; Ratner, M. A.; Pople, J. A.; Redfern, P. C.; Curtiss, L. A., 6-31G*basis set for third-row atoms. *J Comput Chem* **2001,** *22* (9), 976-984.

96. Rassolov, V. A.; Pople, J. A.; Ratner, M. A.; Windus, T. L., 6-31G* basis set for atoms K through Zn. *J Chem Phys* **1998,** *109* (4), 1223-1229.

97. Francl, M. M.; Pietro, W. J.; Hehre, W. J.; Binkley, J. S.; Gordon, M. S.; Defrees, D. J.; Pople, J. A., Self-Consistent Molecular-Orbital Methods .23. A Polarization-Type Basis Set for 2nd-Row Elements. *J Chem Phys* **1982,** *77* (7), 3654-3665.

98. Hehre, W. J.; Ditchfield, R.; Pople, J. A., Self-Consistent Molecular-Orbital Methods .12. Further Extensions of Gaussian-Type Basis Sets for Use in Molecular-Orbital Studies of Organic-Molecules. *J Chem Phys* **1972,** *56* (5), 2257-+.

99. Becke, A. D., Density-Functional Thermochemistry .3. The Role of Exact Exchange. *J Chem Phys* **1993,** *98* (7), 5648-5652.

100. Lee, C. T.; Yang, W. T.; Parr, R. G., Development of the Colle-Salvetti Correlation-Energy Formula into a Functional of the Electron-Density. *Phys Rev B* **1988,** *37* (2), 785-789.

101. Miehlich, B.; Savin, A.; Stoll, H.; Preuss, H., Results Obtained with the Correlation-Energy Density Functionals of Becke and Lee, Yang and Parr. *Chem Phys Lett* **1989,** *157* (3), 200-206.

102. Marenich, A. V.; Cramer, C. J.; Truhlar, D. G., Universal Solvation Model Based on Solute Electron Density and on a Continuum Model of the Solvent Defined by the Bulk Dielectric Constant and Atomic Surface Tensions. *J Phys Chem B* **2009,** *113* (18), 6378-6396.

103. Yanai, T.; Tew, D. P.; Handy, N. C., A new hybrid exchange-correlation functional using the Coulomb-attenuating method (CAM-B3LYP). *Chem Phys Lett* **2004,** *393* (1-3), 51-57.

104. Bauernschmitt, R.; Ahlrichs, R., Treatment of electronic excitations within the adiabatic approximation of time dependent density functional theory. *Chem Phys Lett* **1996,** *256* (4-5), 454-464.

105. Bruhn, T.; Schaumloffel, A.; Hemberger, Y.; Bringmann, G., SpecDis: Quantifying the Comparison of Calculated and Experimental Electronic Circular Dichroism Spectra. *Chirality* **2013,** *25* (4), 243-249.

Chapter 3: Biocatalytic Oxidative Cross-coupling of Coumarins and Phenols

Reprinted (adapted) from Zetzsche, L. E.; Yazarians, J. A.; Chakrabarty, S.; Hinze, M. E.; Murray, L. A. M.; Lukowski, A. L.; Joyce, L. A., Narayan, A. R. H. Biocatalytic oxidative cross-coupling reactions for biaryl bond formation. *ChemRxiv*. **2021**; DOI:10.33774/chemrxiv-2021-v0bv6-v2. Accepted to *Nature*, December 14, 2021.

3.1 Summary

Despite their varied applications, many indispensable molecules in medicine, materials, and asymmetric catalysis share a biaryl core.[1-2] The necessity of joining arene building blocks to access these compounds has inspired multiple approaches for biaryl bond formation and has challenged chemists to develop increasingly concise and robust methods for this task.[3] Oxidative coupling of two C–H bonds offers an efficient strategy for the formation of a biaryl C–C bond, however, fundamental challenges remain in controlling the reactivity and selectivity for uniting a given pair of substrates.[4-5] Biocatalysis offers compelling advantages in synthesis, often becoming the method of choice for the enhanced sustainability, safety, and selectivity profiles.[6-7] Biocatalytic oxidative cross-coupling reactions have the potential to overcome limitations inherent to small molecule-mediated methods by providing a complementary, engineerable approach for catalyst-controlled selectivity.[8] Here, a strategy for biocatalytic cross-coupling of coumarins and phenolic compounds through oxidative C–C bond formation using cytochrome P450 enzyme KtnC is disclosed. Analytical methods for reaction profiling by LC-Tof MS were developed for screening of biocatalytic reactions, allowing for rapid method optimization and investigation of the substrate scope of KtnC. The reactivity, site-, and atroposelectivity of selected cross-coupling reactions were investigated by the comparison of enzymatic reactions to synthetic product standards on

analytical scale, and by the isolation and characterization of biocatalytic products on preparative scale.

The ability to catalyze cross-coupling reactions on a panel of substrates using P450 catalysts was demonstrated, with wild-type KtnC displaying promiscuity with non-native coumarins and phenolic substrates. Notably, KtnC provided access to the 6,6'-connectivity by cross-coupling the native substrate **6** to coumarins bearing greater steric bulk at the C4 position, products otherwise difficult to obtain through traditional synthetic methods. The promiscuity observed in the oxidative cross-coupling of coumarins and phenolic substrates by KtnC provides a foundation for further enhancement of selectivity and yields through protein engineering. This biocatalytic method for constructing sterically hindered biaryl bonds offers an engineerable platform for assembling molecules with catalyst-controlled reactivity and selectivity.

3.2: Introduction

Biaryl bonds are ubiquitous in drugs, materials, and ligands for asymmetric catalysis (Figure 3.1A).[1-2] The most commonly employed strategy to construct these molecules relies on metal-catalyzed cross-coupling of prefunctionalized aryl fragments, thereby offering preprogrammed site-selectivity, albeit at the expense of adding extra steps in a synthetic campaign (Figure 3.1B).[9-10] These reactions can require extensive screening to identify suitable conditions for each new pair of coupling partners and are

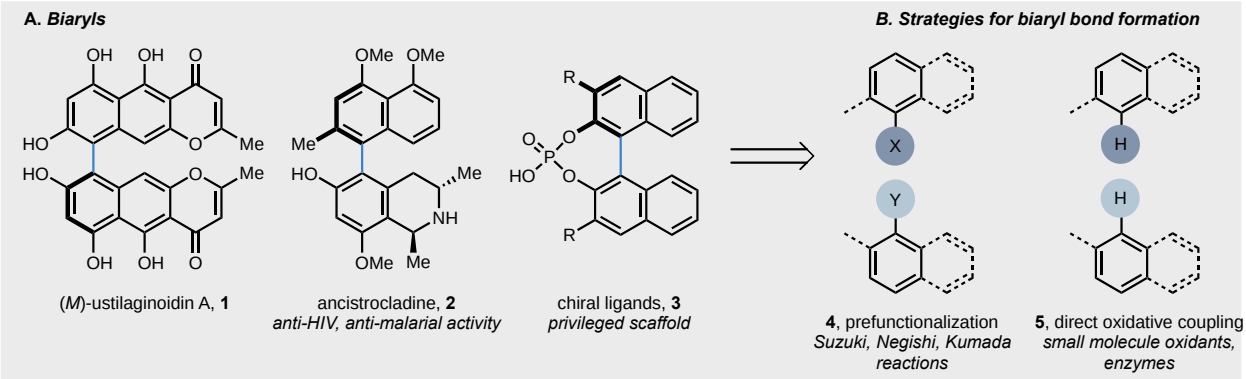

Figure 3.1: Biaryl natural products and biaryl synthetic strategies.
A. Biaryl natural products and privileged scaffolds in asymmetric catalysis. B. Different approaches to building sterically-hindered biaryl bonds, Prefunctionalization or direct oxidative coupling.

still restricted in the connectivities which are readily accessible,[11-15] with the formation of

tetra-*ortho*-substituted biaryl bonds remaining an outstanding challenge.[16-17] Oxidative coupling provides an alternative strategy for biaryl bond formation through the net transformation of two C–H bonds into a C–C bond (Figure 3.1B).[4-5] However, these advantages come at the expense of the efficiency and selectivity of this transformation, which is typically dictated by the intrinsic steric and electronic properties of each substrate, thereby limiting the versatility of this transformation (Chapter 1, Figure 1.7A-E).[4, 18-20] Numerous metal catalysts and metal-free oxidants have been reported for the dimerization and cross-coupling of phenolic substrates; however, the application of these methods is commonly restricted to electron-rich phenols while oxidative coupling with electron deficient phenols remains more broadly challenging.[18-29] When general reactivity can be achieved, controlling the chemo-, site-, and atroposelectivity of the oxidative coupling presents a considerable hurdle, particularly in cases where the intrinsic steric and electronic properties of the reacting phenols prohibit access to the desired product isomer.[19-20, 30-34]

Biocatalytic oxidative cross-coupling reactions have the potential to overcome the limitations inherent to small molecule-mediated methods for direct oxidative coupling by providing catalyst-controlled selectivity. Nature has evolved oxidative enzymes, including laccases and cytochromes P450 (P450s), that mediate the dimerization of phenolic compounds in the biosynthesis of biaryl natural products.[35] The application of laccases in selective catalysis has been limited by the scarcity of examples in which these enzymes exert control over the selectivity of the bond formation following the initial oxidation, such as in the biosynthesis of the natural product (*M*)-ustilaginoidin, **1**, (Figure 3.1A).[36-38] In contrast, an ever-expanding repertoire of P450s mediate highly selective oxidation reactions,[39] among which exist a small subset of enzymes that catalyze site- and atroposelective dimerizations.[8] This subset of wild-type P450s that perform oxidative coupling chemistry are yet to be explored as biocatalysts for unnatural cross-coupling reactions. We hypothesized that this class of enzymes could be developed into biocatalysts for convergent oxidative cross-coupling reactions with catalyst-controlled reactivity, site-selectivity, and atroposelectivity.

3.3 KtnC catalyzed cross-coupling substrate scope

The site- and enantioselectivity documented in the KtnC catalyzed oxidative dimerization reactions provided a tantalizing starting point for developing an enzymatic platform for oxidative cross-coupling reactions. We envisioned developing a biocatalytic method for the site- and atroposelective oxidative cross-coupling of coumarins and phenols. To further investigate the potential for KtnC to function as a biocatalyst for cross-coupling a range of phenolic substrates, we sought to explore the scope of the cross-coupling reaction with a panel of coumarins and other phenolic compounds.

Using optimized conditions for KtnC-catalyzed cross-couplings (see Chapter 2, section 2.3-2.9) native coumarin **6** was paired with a range of phenolic substrates to form cross-coupled products (Figure 3.2). Substrate promiscuity in KtnC-catalyzed cross-coupling reactions was observed with a panel of coumarin substrates (Figure 3.2A) in modest to excellent percent conversions. Initial cross-coupling reactions between **6** and coumarins **11**–**16** demonstrated that maintaining similar substitution patterns to **6** at the C4 and C5 positions of the coumarin was beneficial but not required for activity. Additionally, KtnC tolerated a range of electron-rich and electron-deficient substituents (**17**–**21**), diverging from the electronic restrictions often hindering small molecule-catalyzed oxidative cross-couplings.[19-20] Added steric bulk at the C4 and C5 positions of coumarins **22**–**26** was readily accepted, as observed in dimerization reactions. In contrast to the high levels of reactivity achieved in coumarin cross-couplings with KtnC, modest to no cross-coupling reactivity was observed when coumarins were subjected to established methods for the oxidative coupling of phenolic substrates (see section 3.8 and experimental Figure 3.S1).[5, 24, 40-45] In a model cross-coupling reaction between coumarins **6** and **22**, the most productive chemical cross-coupling gave a 23% conversion with vanadium oxyfluoride compared to an 87% conversion with KtnC.[46] Moreover, the vanadium-catalyzed reaction resulted in an inseparable mixture of isomeric coumarin–coumarin cross-coupled products and dimers (experimental Figure S14).

In addition to forming a range of unsymmetrical bicoumarin products, a panel of more diverse phenolic substrates were cross-coupled to coumarin **6** (Figure 3.2B). In general, superior reactivity was observed with phenolic substrates that more closely

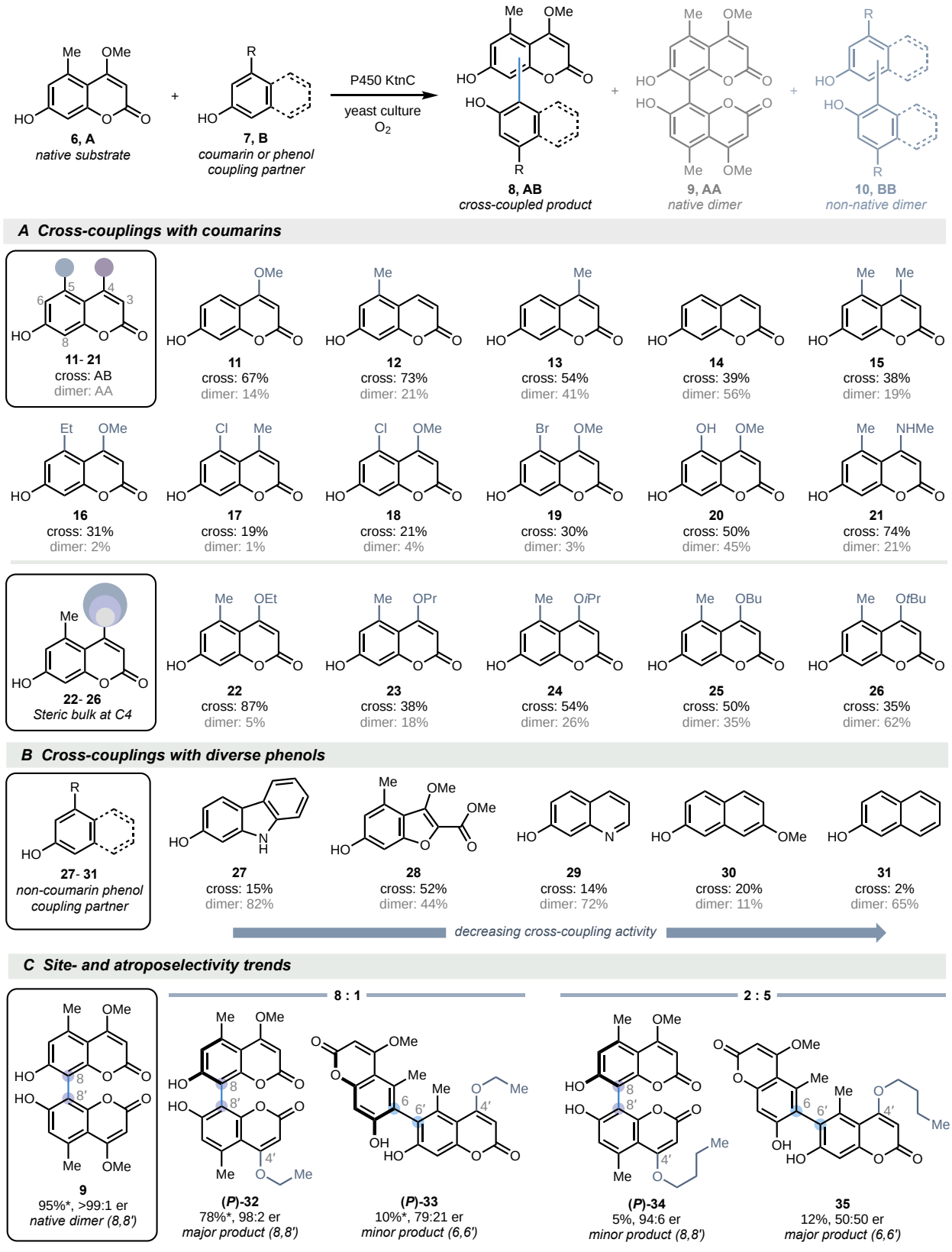

Figure 3.2: KtnC catalyzed oxidative cross-coupling of coumarins and phenols.
Reactivity expressed as percent conversions of total percent AB and AA products calculated by standard curves of A and AA. Reaction conditions: *P. pastoris*, BMM, at 30 °C, 235 RPM for 48 h. **a** Coumarin–coumarin coupling, 25 µM coumarin **6**, 250 µM; b: Coumarin–phenol coupling, 100 µM coumarin **6**, 1000 µM. **c** Site- and atroposelectivity of selected reactions. [a] relative percent yield, 200 µM A and B.

resembled the native substrate (**6**), such as benzofuran **28** which afforded a 52% conversion to cross-coupled product. Additionally, naphthol **30** which possesses similar stereoelectronic properties to coumarin **6** was substantially more reactive than 2-naphthol (**31**), with conversions of 20% and 2% to cross-coupled products, respectively. Although the undesirable formation of the native substrate dimer (AA) and dimers of the coupling partners (BB) were observed, it was notable that the cross-coupled products were often favored over dimers of the limiting substrate coumarin **6**.

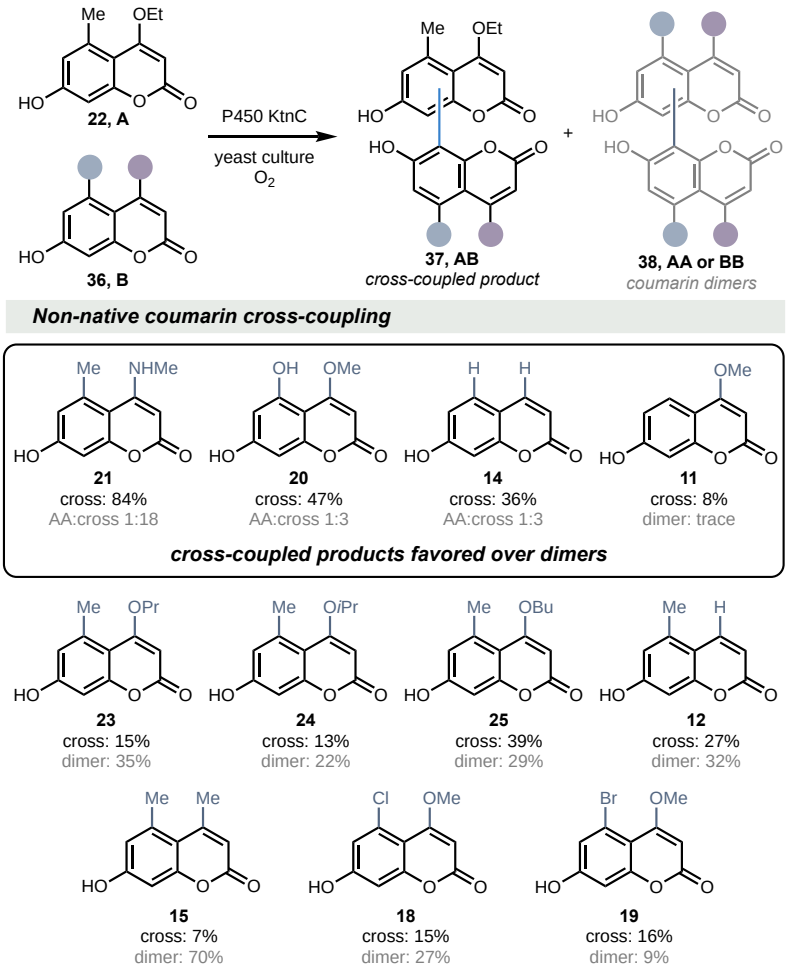

Figure 3.3: KtnC cross-coupling of non-native coumarins. Reactivity expressed as relative percent yields, total percent AB and AA products. Reaction conditions: *P. pastoris*, BMM, 100 µM **22**, 1000 µM B at 30 °C, 235 RPM for 48 h.

To investigate the selectivity of KtnC mediated cross-coupling, we fully characterized both the site- and atroposelectivity for selected coumarin pairs. In reactions with coumarins harboring increased steric bulk at the C4 vinylogous ester (see **32**–**35**), the formation of a second cross-coupled product in addition to the expected 8,8'-product (Figure 3.2C) was observed. For example, in the reaction between **6** and ethyl ester-bearing **22**, two products were formed in an 8:1 ratio, with the major product harboring the 8,8'-connectivity (**32**) and the minor product possessing the 6,6'-connectivity (**33**). In a similar trend observed in dimerization reactions, as the steric bulk of the coumarin coupling partner was further increased to a butyl ester (see **25**), the site-selectivity of the reaction was altered, giving a 2:5 ratio of the 8,8'-product (**34**) to the 6,6'-

product (**35**). The atroposelectivity in the formation of the 8,8'-products was excellent (see **9**, **32**, and **34**), whereas the formation of the 6,6'-products with increased steric bulk showed erosion of atroposelectivity (see **33** and **35**). Notably, both prefunctionalization and direct oxidative coupling synthetic strategies were unsuccessful in generating the 6,6'-isomer in these coumarin–coumarin cross-coupling reactions, highlighting the steric and electronic biases that impede access to a specific connectivity using small molecule-based strategies (Supplemental Figures S3.21-22 and S3.24-25).[19-20]

Seeking to move beyond reactions requiring the native substrate as a coupling partner, and previously demonstrating promiscuity in the dimerization reactions with KtnC and DesC, we tested combinations of non-native coumarins and phenolic substrates to find new reactivity with KtnC (Figures 3.4-6). The screening of reactions was approached by categorizing the substrates that would be the limiting reagent, partner A, and which would be provided in excess as coupling partner, B. Two classes of coumarins were chosen to be screened against the panel of substrates: (1) a coumarin that dimerized readily ("native substrate like") and (2) a coumarin that is not dimerized by KtnC. The limiting reagent A was also varied in two experiments with non-coumarin phenols as the coupling partner B. We anticipated identifying substrate combinations that would instigate greater chemoselectivity in favor of cross-coupling over the formation of dimers. Substrate combinations were screened in 24-well plate format and analyzed by LC-MS, which allowed for rapid generation of data on the general reactivity of the reactions.

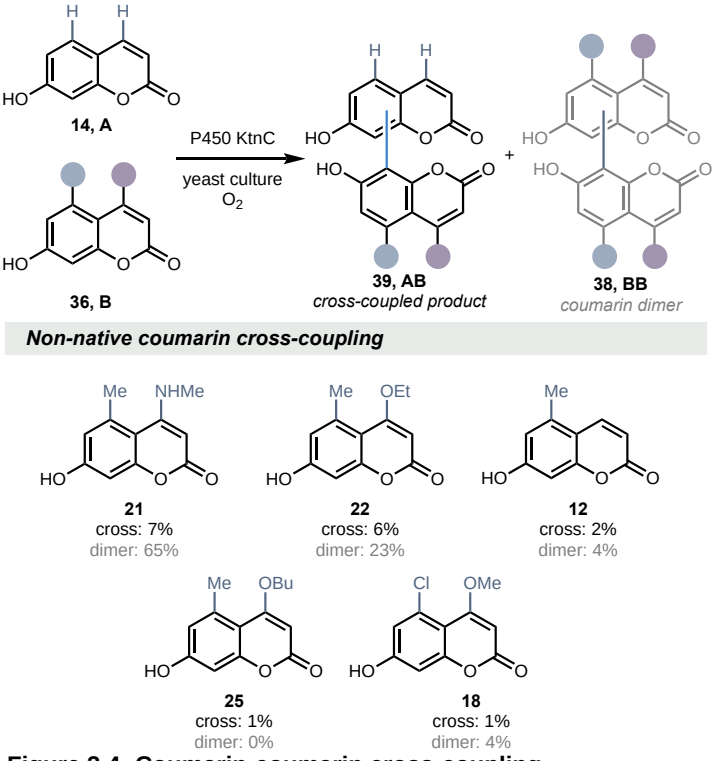

Figure 3.4: Coumarin-coumarin cross-coupling. Reactivity expressed as relative percent yields, total percent AB and AA products. Reaction conditions: *P. pastoris*, BMM, 100 µM A, 1000 µM B at 30 °C, 235 RPM for 48 h.

A panel of coumarin-coumarin cross coupling reactions were examined with C4-ethyl ester coumarin **22** (dimerizes, see Chapter 2, Figure 2.9) as the limiting reagent A (Figure 3.3) and a panel with 7-hydroxycoumarin **14** (does not dimerize, see experimental Figures S3.55, S3.75, and S3.84-90) as the A partner (Figure 3.4) to satisfy the two categories of coumarins. Different A coupling partners were screened against 7-hydroxyquinoline **29** (Figure 3.5) and 2-naphthol (Figure 3.6). New combinations that formed cross-coupled products beyond the native substrate were identified, adding to the diversity of KtnC cross-coupled non-native coumarins and phenolic substrates. Unsurprisingly, less promiscuity was observed with non-native substrates compared to combinations with coumarin **6** (reactions detailed in Figure 3.2), and in general the most reactivity was observed with coumarin-coumarin combinations. However, notable examples were identified where cross-coupled products were the major products in the reactions in at least a 1:3 ratio of AA:AB products (Figure 3.3). Specifically, in reactions pairing coumarin **22,** which dimerizes almost as efficiently as the native substrate, and coumarins **14**, **20**, and **21**, greater chemoselectivity was observed for cross-coupling in comparison to the analogous reactions with the native substrate (Figure 3.2A). Similar relative percent yield was obtained in the reactions of **22** and **20**–**21** compared to the same reaction combinations with the native substrate. Investigating

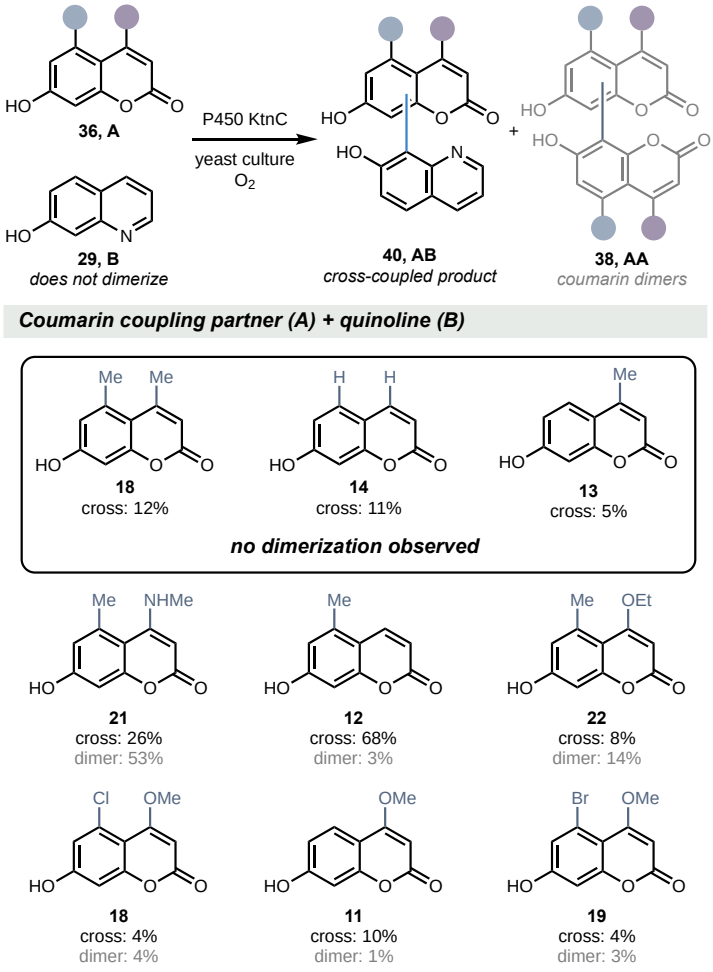

Figure 3.5: Coumarin and quinoline cross-coupling. Reactivity expressed as relative percent yields, total percent AB and AA products. Reaction conditions: *P. pastoris*, BMM, 100 µM A, 1000 µM B at 30 °C, 235 RPM for 48 h.

7-hydroxycoumarin **14** (a substrate that does not dimerize, Figure 3.4), a sharp reduction in general reactivity was observed, with relative yields reaching nor more than 7%. A reduction in the dimerization of coumarins that typically dimerize well, for example, **14** with **22**, was also observed in this series of reactions.

The most intriguing cases found were between phenolic substrate combinations that achieve complete chemoselectivity for cross-coupling with no dimerization products detected. Pairing different coumarins and an excess of 7-hydroxyquinoline **29**, several examples were identified where the cross-coupled products were formed without dimerization of the coumarin substrate A or B (Figure 3.5, **13**–**14**, **18**). The relative percent yields were low but are promising examples of non-native chemoselective cross-coupling. Of particular interest is the cross-coupling observed between two substrates that do not dimerize individually, 7-hydroxycoumarin and 7-hydroxyquinoline (Figure 3.5, **14**). This example suggested that H-atom abstraction was occurring at one of the coupling partners, and the assumption that abstraction occurred preferentially on substrates that were capable of dimerizing initially guided our thinking about reactivity, however, in this example, it was not clear which substrate, or if both, undergo H-atom abstraction to form the cross-coupled product. Of the reaction combinations explored in Figure 3.5, coupling between coumarin **12** and 7-hydroxyquinoline **29** was especially intriguing. In this example, a combined 68% relative yield (as the sum of four cross-coupled product peaks, consisting of two major and two minor product peaks, see traces in Supplemental Figure S3.93) was observed. Finally, coupling reactions with different coumarins (A) to 2-naphthol (B) was explored (Figure 3.6), and similar low relative percent yield in comparison to the analogous reaction with the native substrate was observed, with few reactions forming cross-coupled products. Low dimerization was concurrent with low cross-coupling, except in the case of coumarin **21** bearing an amine at the C4 position with 38% dimer AA and 5% cross-coupled AB product.

While some trends in the reactivity of the KtnC catalyzed cross-coupling reactions were identified (selectivity trends with increased steric demand at the C4 position, Figure 3.2C), generally, we could not predict which substrate combinations would result in favorable cross-coupling reactions. Examples in all reaction combination types with a preference for cross-coupled products over dimers were identified, and in some cases

with relatively high yields. From these reactions, several were chosen to investigate further as targets for full characterization.

Reactions detailed in Figures 3.1–3.5 showed the range of the general reactivity in the KtnC catalyzed cross-coupling reaction, with some examples achieving chemoselectivity for cross-coupling. However, most of the reactions were not selective, and multiple cross-coupled and dimerized products were observed across the substrate scope, determined by the number of product peaks observed by LC-MS. Understanding the additional layers of selectivity within these reactions required characterizing the site- and enantioselectivity of the products. Two strategies for product characterization were developed and applied to reactions in which we sought to further understand selectivity (1) the synthesis of authentic standards for the determination of selectivity on analytical scale biotransformations and (2) isolation of products from preparative scale reactions. Preparative scale reactions provided sufficient material for characterization in cross-coupling reactions that were approximately 40% yield or higher, but the protocols were not generally applicable to substrate combinations when reactivity was low or with the formation of inseparable mixtures of products. In these cases, we relied on the synthesis of product standards and comparison of the standards to enzymatic reactions by LC-MS. Product standards were prepared by palladium catalyzed Suzuki-Miyaura cross-coupling reactions or the transesterification of coumarin dimers.

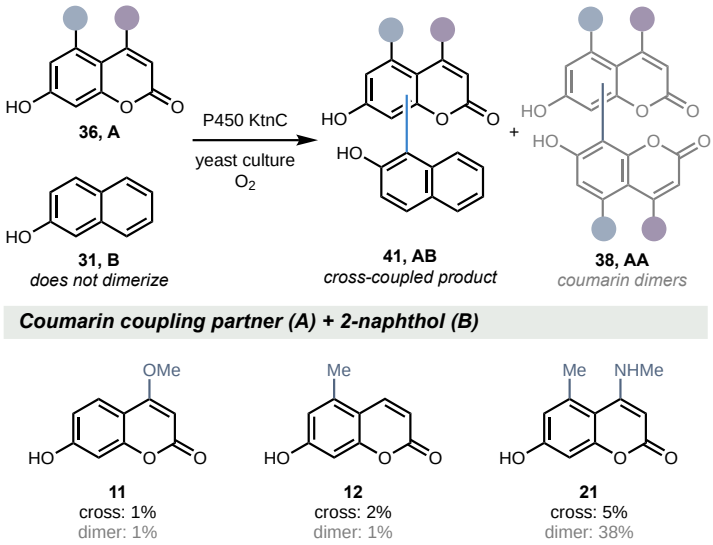

Figure 3.6: Coumarin and 2-naphthol cross-coupling. Reactivity expressed as relative percent yields, total percent AB and AA products. Reaction conditions: *S. cerevisiae*, 50 µM A, 500 µM B at 30 °C, 235 RPM for 48 h.

3.4 Synthesis of authentic standards by Suzuki-Miyaura cross-coupling

One strategy employed for the synthesis of authentic standards was the development of Suzuki-Miyaura cross-coupling reactions for coumarin-naphthol cross-coupling reactions. The first synthetic targets were the isomeric products of the cross-coupling between coumarin **12** and 2-naphthol, a reaction selected for a protein engineering campaign carried out by Lara Zetzsche (Figure 3.7). In the wild-type KtnC catalyzed cross-coupling, this reaction was low yielding (2.7% conversion) and unselective, producing up to four isomeric products indicated by LC-MS in addition to 1.7% conversion to multiple coumarin dimers. To identify the reaction products, and to aid in the protein engineering goal of enhancing the selectivity of wild-type KtnC, authentic standards were required.

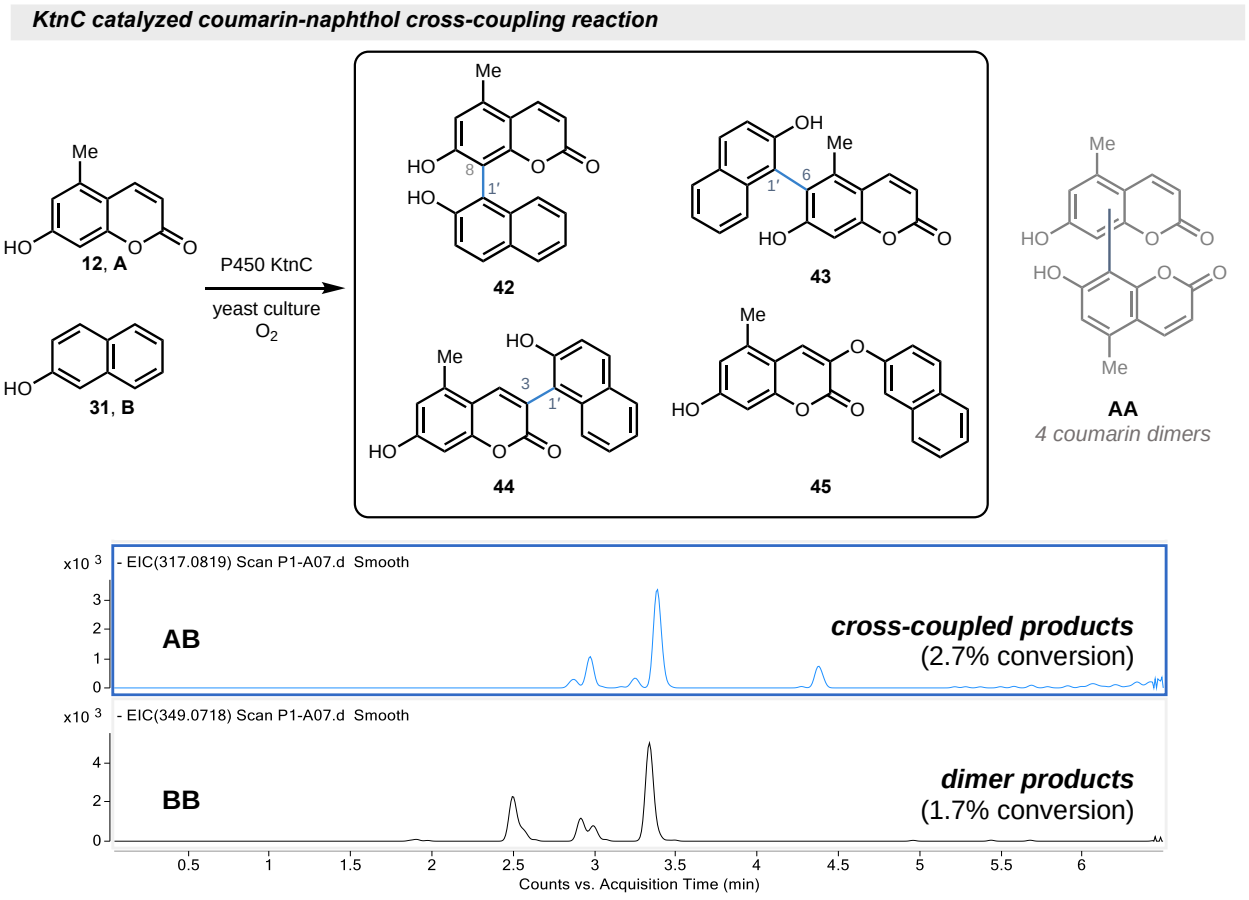

Figure 3.7: KtnC catalyzed coumarin and 2-naphthol cross-coupling.
Reactivity expressed as relative percent yields, total percent AB and AA products. Reaction conditions: *P. pastoris*, BMM, 100 µM A, 300 µM B at 30 °C, 235 RPM for 48 h. Traces are EICs in negative mode.

The first target selected was the 8,1'-isomer **42**, possessing a BINOL type architecture analogous to the 8,8'-connectivity of the native dimerization product, which we hypothesized would be the major product in the KtnC catalyzed cross-coupling reaction. We envisioned forging the tetra-*ortho*-substituted C–C bond joining prefunctionalized coumarin and naphthol fragments through a palladium catalyzed Suzuki-Miyaura cross-coupling reaction (Figure 3.8).[12, 47] The coumarin aryl-iodide **46** was prepared through regioselective iodination of **12** followed by methyl protection (see Supplemental Figure S3.4) and screened palladium catalyzed Suzuki-Miyaura cross-coupling conditions with a commercially available boronic acid **47**.

I anticipated screening to identify productive reaction conditions for **46** and **47**, as sterically demanding Suzuki cross-coupling remains challenging and lacks generality.[48] Reaction conditions were guided by examples of hindered Suzuki cross-couplings disclosed over the last two decades.[12, 47, 49-53] (see Chapter 1 for a discussion on ligand trends). Summarizing the commonly employed reaction conditions and trends represented in the literature, the most commonly implemented conditions utilize $Pd(OAc)_2$ or $Pd_2(dba)_3$ as the palladium sources. Ligand choice spans different classes, with dialkyl biaryl monophosphines[47, 49-51] and the BiDIMES[54-56] showing better reactivity profiles in more recent examples. Boronic acids derivatives were compared by Cammidge and Kozlowski, with boronic acid and esters productively coupled with an excess of 1.5-5.0 equivalents, while triflouroborate salts were reported as unreactive.[12, 48, 53] The most common bases employed were potassium phosphate, sodium carbonate and cesium fluoride, in excess of 2.0-5.0 equiv, with dry toluene or THF as the solvents of choice. Longer reaction times and elevated temperatures were often necessary, with seminal examples by Cammidge and coworkers employing reactions times of up to 6 days, although more commonly 18-24 h reaction times are reported in the literature.[53]

Considering there were few examples of sterically-hindered cross-coupling reactions with coumarins, I conducted initial screening based on some of the trends detailed above. I chose to start with $Pd(OAc)_2$ and $Pd_2(dba)_3$ in toluene with 4 Å mol sieves (Figure 3.8), monophosphine ligand *S*Phos (entries **1**-**2**), and bidentate diphosphine ligands DPEPhos (entries **3**-**6**) and XantPhos (entries **7**-**10**).[47, 50, 57-58] Success with *S*Phos was anticipated, and was demonstrated as one of the most general

Suzuki-Miyaura cross-coupling screen

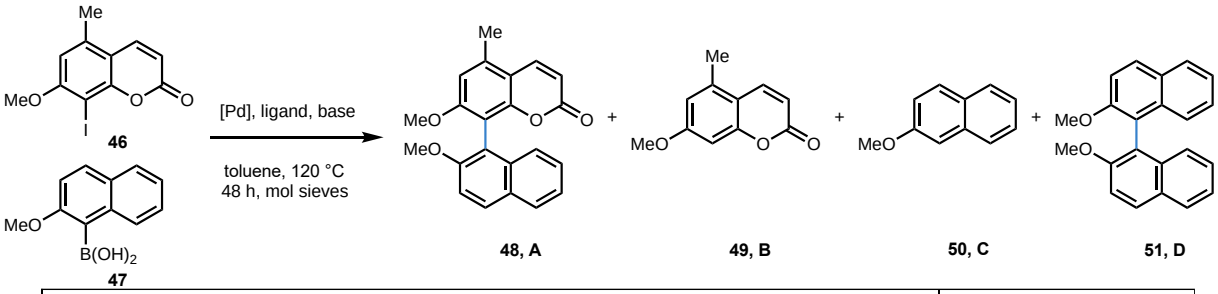

Conditions							Products	
entry	**Pd**	**mol %**	**ligand**	**mol %**	**base**	**equiv**	**A**	**Major species**
1	*$Pd(OAc)_2$*	*5*	*SPhos*	*10*	*K_3PO_4*	*3*	*yes*	*A*
2	$Pd(OAc)_2$	5	*SPhos*	10	Na_2CO_3	3	no	Ar-I
3	$Pd_2(dba)_3$	10	DPEPhos	12	K_3PO_4	3	trace	1:1 B:Ar-I
4	$Pd_2(dba)_3$	10	DPEPhos	12	K_2CO_3	3	no	C
5	$Pd_2(dba)_3$	10	DPEPhos	12	Na_2CO_3	3	no	C
6	$Pd_2(dba)_3$	10	DPEPhos	12	CsF	5	trace	B
7	$Pd_2(dba)_3$	10	XantPhos	12	K_3PO_4	3	minor	D
8	$Pd_2(dba)_3$	10	XantPhos	12	K_2CO_3	3	trace	Ar-I
9	$Pd_2(dba)_3$	10	XantPhos	12	Na_2CO_3	3	trace	Ar-I
10	$Pd_2(dba)_3$	10	XantPhos	12	CsF	5	yes	D

Figure 3.8: Tetra-*ortho*-substituted Suzuki cross-coupling reaction screen.
5.0 mg scale Ar-I **46**, 3.0 equiv boronic acid **47**, 4 Å mol sieves, dry toluene, 110 °C, 48 h. Stock solutions of Pd source and ligands in toluene were added to vials containing **46**, **47**, and base and capped with PTFE screw caps. Monitored by TLC and compared to standards of byproducts B, C, and D. Reactions were quenched with an aqueous workup and extracted with ethyl acetate. Crude reaction mixtures were analyzed by ^{1}H NMR to determine the major species.

ligands for tetra- and tri-*ortho*-substituted Suzuki cross-coupling reactions of aryl fragments with the greatest variety in function groups and electronics. In addition to several catalysts, five bases, K_3PO_4, K_2CO_3, Na_2CO_2, and CsF were chosen for initial screening, and reactions were carried out with boronic acid 3.0 equiv **47** in toluene at 120 °C. Reactions were carried out on 5.0 mg scale, and care was taken to exclude water known to hinder sterically demanding cross-coupling reactions.[53, 59-60] The reactions were monitored by TLC and analyzed by ^{1}H NMR for the formation of the desired product over 48 h (Figure 3.7). As discussed by Cammidge,[12] Buchwald,[51] and Kozlowski,[48] byproducts were observed resulting from both proto-dehalogenation (**49**) and deboronation (**50**), as well as a dimeric product of the boronic acid (**51**).[61] All the reactions contained remaining unreacted **46** after 48 h. The consumption of the boronic acid which was added in excess in a 3:1 ratio with the aryl iodide to form either deboronated **50** or dimeric product **51** predominated (entries 4, 5, 7, and 10). The condition found to be the

most promising was the addition of 5 mol % $Pd(OAc)_2$, 10 mol % *S*Phos, and 3.0 equiv K_3PO_4, to a solution of toluene containing **46** and **47**, stirred at 120 °C for 48 h (entry 1), forming the cross-coupled product as the major product, although the formation of dimer **51** and unreacted aryl iodide remaining was observed. This reaction was ultimately performed on 66.9 mg to afford the target product in 30% yield.

With this successful result, we sought to access additional targets, both the 6,1'-isomer **43** (Figure 3.-3.11) and 3,1'-isomer **44** (Figure 3.12). In the next campaign to

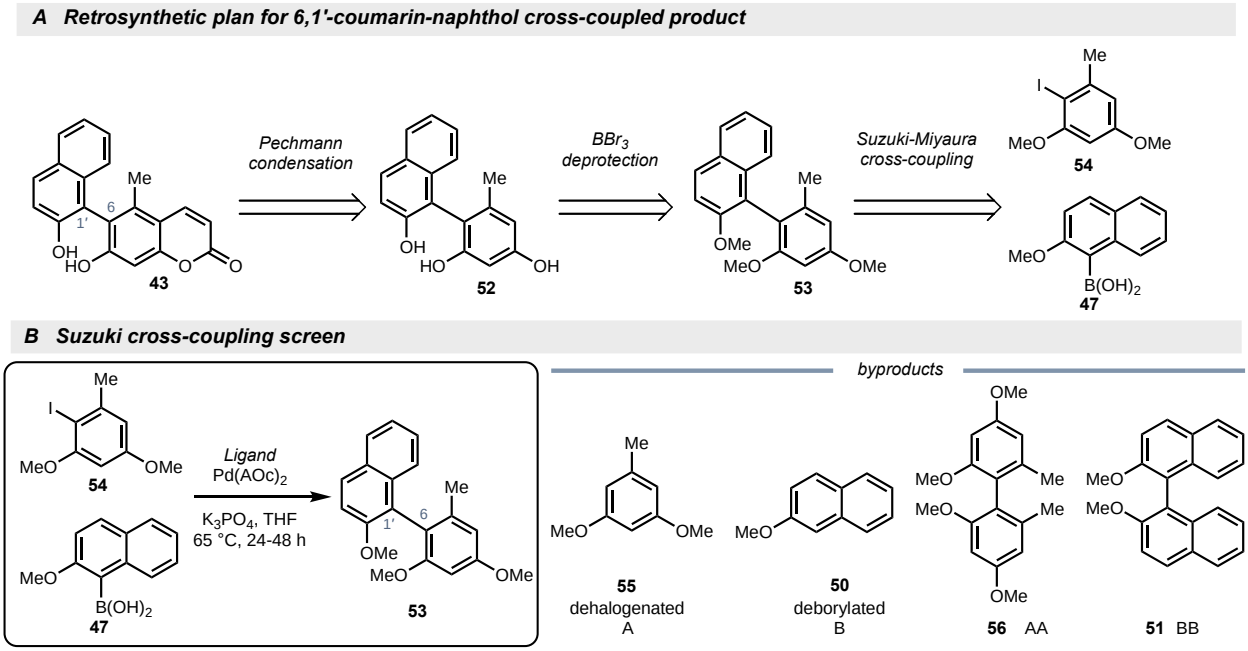

Peak areas from exact mass EICs $[M+H]^+$								
starting materials				**product**	**byproducts**			
entry	ligand	Ar-I	$B(OH)_2$	AB	A	B	AA	BB
1	**XantPhos**	**1841**	**3047**	**121753**	**0**	**3389**	**3189**	**6134**
2	XPhos	498	0	388	0	726	6349	0
3	DavePhos	1480	750	9738	0	884	497	1105
4	DPEPhos	4005	0	1735	0	1493	0	822
5	*R*-BINOL	1873	0	34566	0	651	971	7826
6	***i*Pr-BiDIME**	**890**	**495**	**464114**	**0**	**665**	**1714**	**17633**
7	*S*Phos	2627	0	60904	0	268	0	9471

Figure 3.9: Suzuki cross-coupling reaction screen towards the synthesis of 6,1'-standard 43.
A. Retrosynthetic plan to access the 6,1'-isomer **43** through Suzuki coupling and Pechmann condensation. **B**. Reactions carried out on 2.0 mg scale of Ar-I **54**, 3.0 equiv boronic acid **47**, 5 equiv K_3PO_4, 4 Å mol sieves, 300 µL dry THF, 65 °C, 48 h. Stock solutions of $Pd(OAc)_2$ (20 mol percent) and ligands (40 mol percent) in THF were added to vials containing **54**, **47**, and base, then capped with PTFE caps and heated. **C**. Reactions were monitored by LC-MS, EIC peak areas of possible byproducts recorded and relative percent yields were calculated.

synthesize the 6,1'-isomer **43**, we envisioned a retrosynthetic plan with a Pechmann condensation reaction[62-63] to build the coumarin ring and a tetra-*ortho*-substituted cross-

coupling reaction as the key disconnections (Figure 3.9A). Methods for installing a functional handle at the 6-position of coumarin **12** were not trivial, and although we identified methods to selectively halogenate at the 8 and 3-positions to synthesize prefunctionalized coumarin building blocks, identifying a method to install a functional handle at the 6-position of **12** was initially challenging. In contrast, we could easily access aryl iodide **54** which would position the halide at the desired site of C–C bond formation for a Suzuki cross-coupling prior to ring closing of the coumarin hemisphere of the molecule.

In the synthesis of the 8,1'-isomer **48**, screening reaction conditions on 5.0 to 10.0 mg scale and analysis by ^{1}H NMR after an aqueous workup provided information on the major species present in the crude reaction mixtures. In cross-coupling reactions with aryl fragments (and the resultant byproducts) that possessed similar R_f's and structure, TLC and ^{1}H NMR were not the best methods for reaction monitoring due to unresolved TLC spots and NMR peaks. Instead, I found monitoring reactions by LC-MS (Figure 3.9B) provided a solution and allowed us to search for possible byproducts by mass. Identifying more favorable reaction conditions across a screen by comparing peak areas of the same species simplified the identification of promising conditions but could not be used as a method for quantification. Subsequently, Suzuki cross-coupling condition screening was carried out in this fashion going forward.

Conditions for a tetra-*ortho*-substituted cross-coupling reaction were screened with the aryl halide fragment **54** and boronic acid **47** (Figure 3.9B-C) using a panel of phosphine ligands, *R*-BINOL, and *P*-chiral oxaphosphole ligand *i*Pr-BIDIME with $Pd(OAc)_2$ and K_3PO_4 in dry THF.[64] Several promising reaction conditions were identified screening by LC-MS, entries 1 (XantPhos) and 6 (*i*Pr-BIDIME) which showed higher amounts of cross-coupled product compared across the set of reactions. These two reactions appeared to have similar reaction profiles, however, entry **6** had the largest absolute peak area for the desired cross-coupled product and these conditions were used in subsequent reactions for this transformation. Upon scaling the reaction up (Figure 3.10), the cross-coupling reaction resulted in a mixture of products, an outcome which was indicated by observing byproducts by LC-MS on analytical scale, however, the major byproduct **51** was isolated along with the desired cross-coupled product **53** as an

inseparable mixture. I anticipated that the products of a BBr_3 deprotection would be separable and was delighted to recover 3.5 mg of **52** in a 12% yield across two steps. Biaryl **52** was then subjected to the same Pechmann condensation conditions employed to build the coumarin monomer **12** but disappointingly, the formation of two product isomers were observed by LC-MS in a 1:1 ratio. I reasoned that the two products were different regioisomers that have previously been observed in the synthesis of the coumarin monomer **12** resulting from ring closing at the two different positions on the orcinol ring. Although this exploratory route was successful in forming the desired cross-coupled product in modest amounts, the formation of inseparable byproducts and the lack of selectivity in the last step was undesirable, and this route was ultimately abandoned.

Dr. Suman Chakrabarty developed a second route (Figure 3.11) to access **43** by a similar strategy through an initial Suzuki cross-coupling reaction, followed by the construction of the coumarin ring after C–C bond formation. Due to the lack of selectivity in the first route, building the coumarin ring was accomplished over two steps by a Vilsmeier–Haack formylation and Wittig olefination, followed by a BBr_3 deprotection and

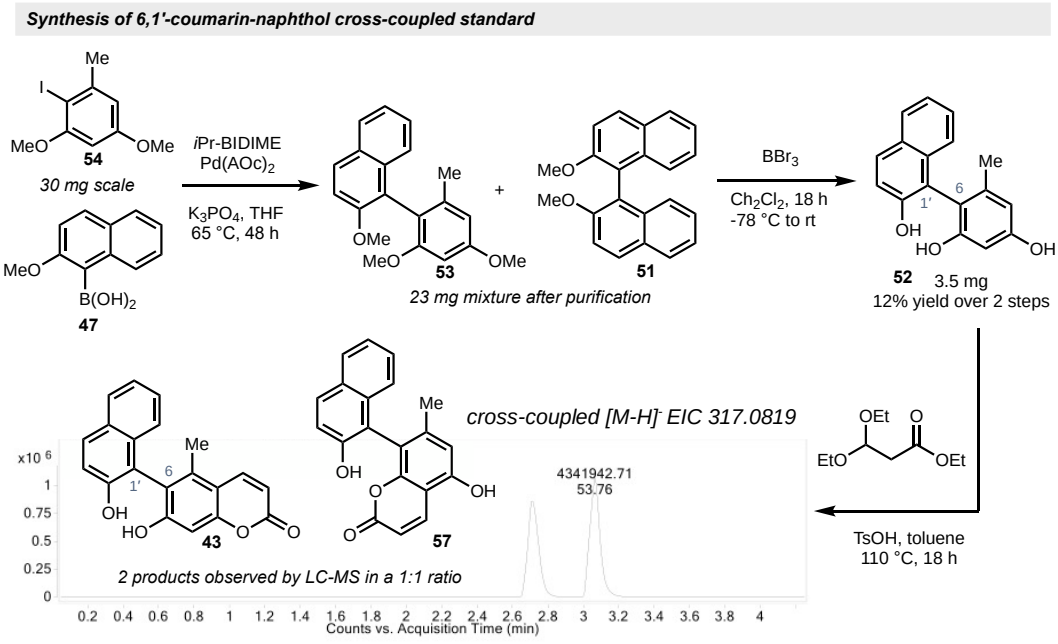

Figure 3.10: Efforts towards the synthesis of 6,1'-standard 43.
A. Palladium catalyzed Suzuki cross-coupling resulted in a mixture of products. B. BBr_3 deprotection allowed the separation of the product mixture. C. Pechmann condensation resulted in a mixture of product isomers.

cyclization to afford the desired product. Notably, the Suzuki cross-coupling proceeded in a 70% yield with aldehyde **58** using *S*Phos as a ligand and 1.5 equiv of the boronic acid.

From developing two synthetic routes for tetra-*ortho*-substituted Suzuki cross-coupling reactions to join coumarin and naphthol fragments, we found that *S*Phos was the ligand of choice for synthesis of both the 8,1'- and 6,1'-isomer standards, providing the best yields of the ligands that were screened. Determining conditions for the tri-*ortho*-substituted 3,1'-isomer **44** was less challenging due to the less sterically demanding biaryl bond formed by Suzuki cross-coupling and cross-coupling conditions were quickly identified that provided good yields (Figure 3.12). Synthesis of the prefunctionalized coumarin halide **61** was straightforward, [65-66] proceeding through a regioselective electrophilic bromination of the C3 position with *N*-bromosuccinimide on the methyl protected coumarin **49**, followed by Suzuki cross-coupling with the XantPhos ligand and $Pd(OAc)_2$ to afford the target biaryl product in 77% yield under the standard conditions developed for the synthesis of authentic standard isomers. The presence of the deboronated and 2,2-bismethoxy-binaphthalene byproducts were confirmed by ^1H NMR of the purified fractions, as well as traces of the dehalogenated coumarin, with complete consumption of the coumarin halide observed. Due to the presence of unreacted boronic acid and boronic acid byproducts, purification was difficult and isolating the desired compound required multiple purifications by column chromatography, suggesting it would be

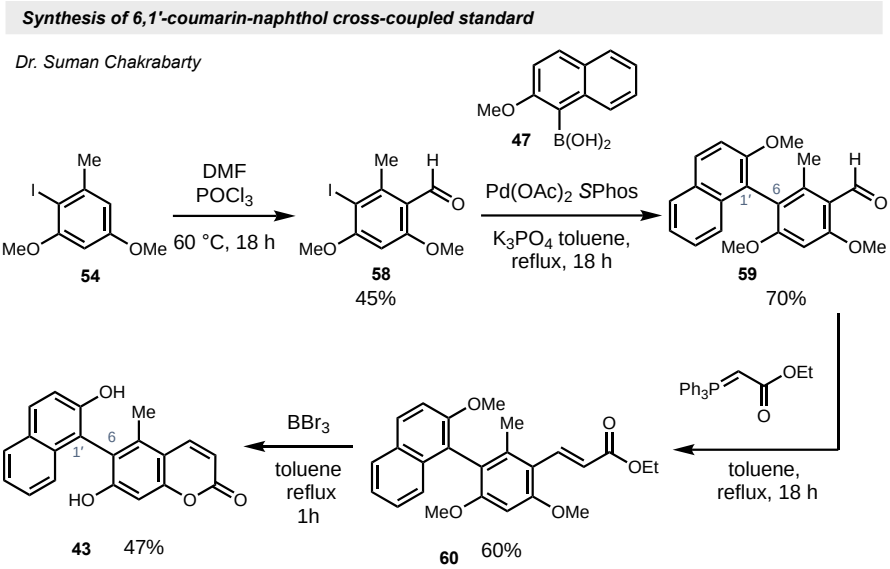

Figure 3.11: Synthesis of 6,1'-standard 43.
Installation of the aldehyde by Vilsmeier-Haack formylation, tetra-*ortho*-substituted Suzuki cross-coupling: 20 mol % $Pd(OAc)_2$, 40 mol % *S*Phos,1.5 equiv boronic acid, 6 equiv K_3PO_4, toluene, 18 h. Wittig olefination, BBr_3 deprotection and cyclization.

advantageous to reduce the equivalents of the boronic acid, however further optimization was not attempted given the initial success in synthesis of the desired 3,1-isomer **44**.

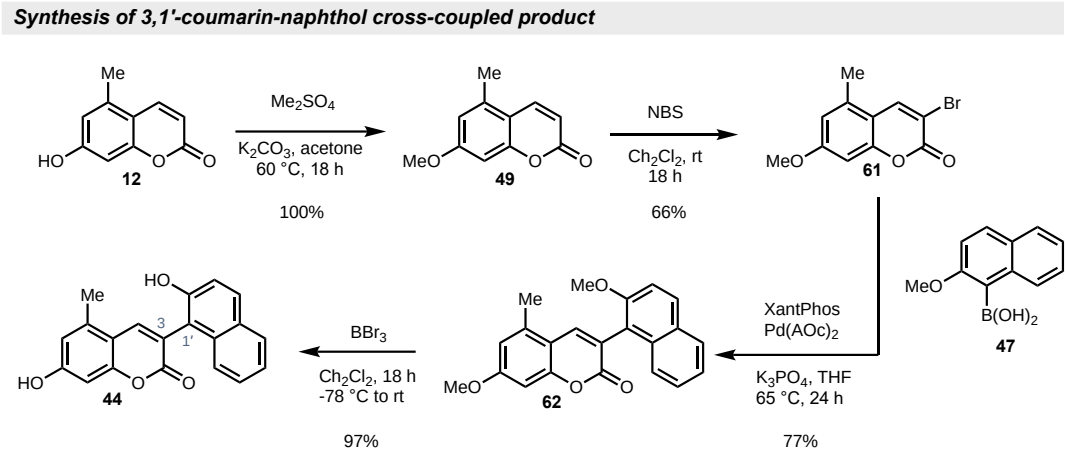

Figure 3.12: Synthesis of 3,1'-standard 44.
Methyl protecting the coumarin phenol followed by electrophilic bromination with NBS for the regioselective bromination at the C3 position. Suzuki cross-coupling: 20 mol % $Pd(OAc)_2$, 40 mol % XantPhos, 3.0 equiv boronic acid, 5 equiv K_3PO_4, 65 °C in dry THF for 24 h. BBr_3 deprotection affords 3,1'-isomer **44** in a 49% yield over 4 steps from coumarin **12**.

3.5 Site-selectivity of KtnC catalyzed cross-coupling of coumarin 12 and 2-naphthol

With the all three isomers 42-44 in hand, the KtnC catalyzed oxidative cross-coupling of coumarin **12** and 2-naphthol were compared by LC-MS (Figure 3.13). Initial attempts to identify the major species by comparison to the product standards were misleading due to changes in the retention times of the products between the whole cell enzymatic reaction and the standards initially prepared in methanol. A spiking experiment with the KtnC reaction and the standards solved this problem, with the peaks of the standards matching the retention times of enzymatic products (traces, Figure 3.13). The samples were prepared by diluting the biocatalytic reactions 1:3 with methanol containing 15 µM internal standard with a final volume of 400 µL. Solutions of 25 µM of the authentic standards in methanol were prepared, and 2 µL of the standard solutions were added to the 100 µL of the diluted KtnC reactions and analyzed by LC-MS.

The two major products were identified as the 3,1'-**42** and 8,1'-**44**, with one of two minor products identified as the 6,1'-isomer **43**. These results were surprising, as the major product was anticipated to retain the 8,1'-connectivity of the native reaction of wild type KtnC, and bond formation at the C3 carbon in any previously characterized oxidative

coupling products from KtnC biotransformations had not been observed. Later, a C–O coupled product was synthesized by Suman Chakrabarty and identified the remaining minor product as the C-O cross-coupled product.

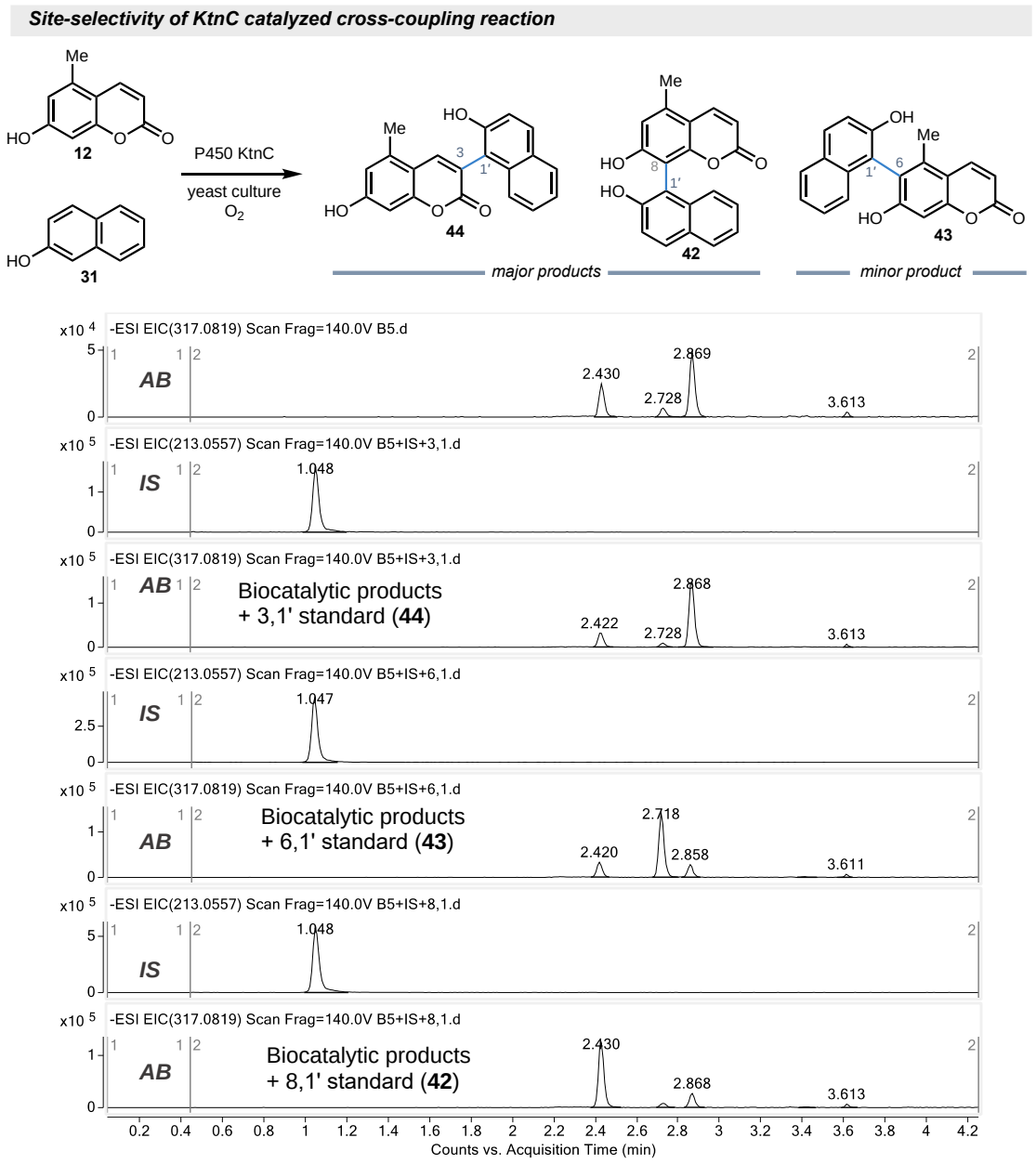

Figure 3.13: Spiking experiment determining major product in KtnC catalyzed cross-coupling reaction. Spiking of authentic standards into KtnC biotransformation to determine site-selectivity.

3.6 Transesterification of dimers

In coumarin dimerization reactions that included the native substrate or a related species with a vinylogous ester at the C4 position, such as **6** and **22**, only the 8,8' and 8,6'-isomers were readily synthesized.[67] Access to the 6,6'-isomer was best achieved by the preparative scale re actions leveraging the selectivity switch observed in the dimerization of C4-ethyoxy coumarin **22** by KtnC, where the 6,6'-isomer was formed in addition to the 8,8'-isomer, and all species were separable (See Chapter 2, Figure 2.9). Given the difficulty in synthesizing the 6,6'-isomer through traditional synthetic methods,

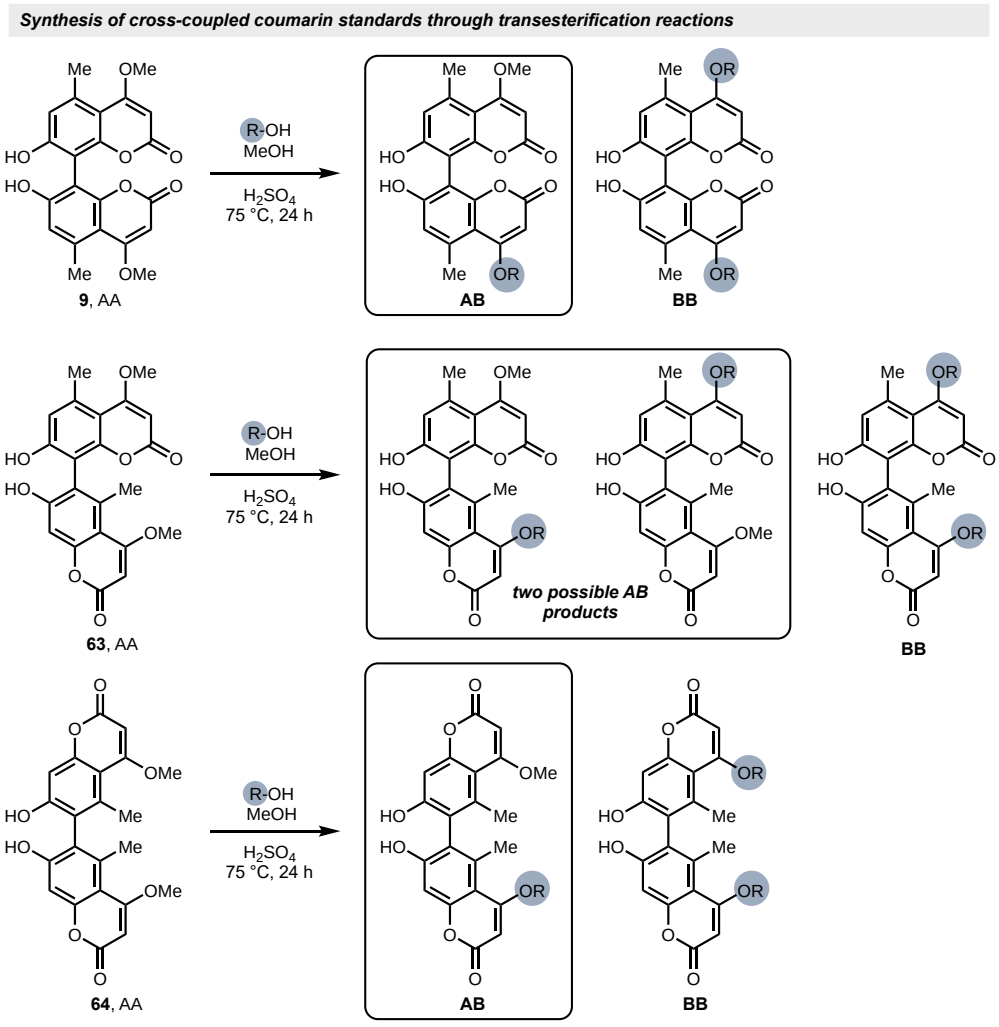

Figure 3.14: Transesterification of coumarin dimers to access cross-coupled products.
Conditions: coumarin dimers were dissolved in a blend of ROH:MeOH (1:1 ratio, 0.09 M), 0.9 M or catalytic H_2SO_4, heated, and monitored by LC-MS. See Supplementary Figures S3.9-20.

we were inspired to use the KtnC dimerized product as a starting point for the synthesis of cross-coupled coumarin products through a transesterification reaction. Subjecting dimers containing a labile vinylogous methyl ester to a given alcohol in the presence of acid and heat created mixtures of dimers and cross-coupled coumarin compounds that were used as analytical standards for analysis by LC-MS without the need for isolation of

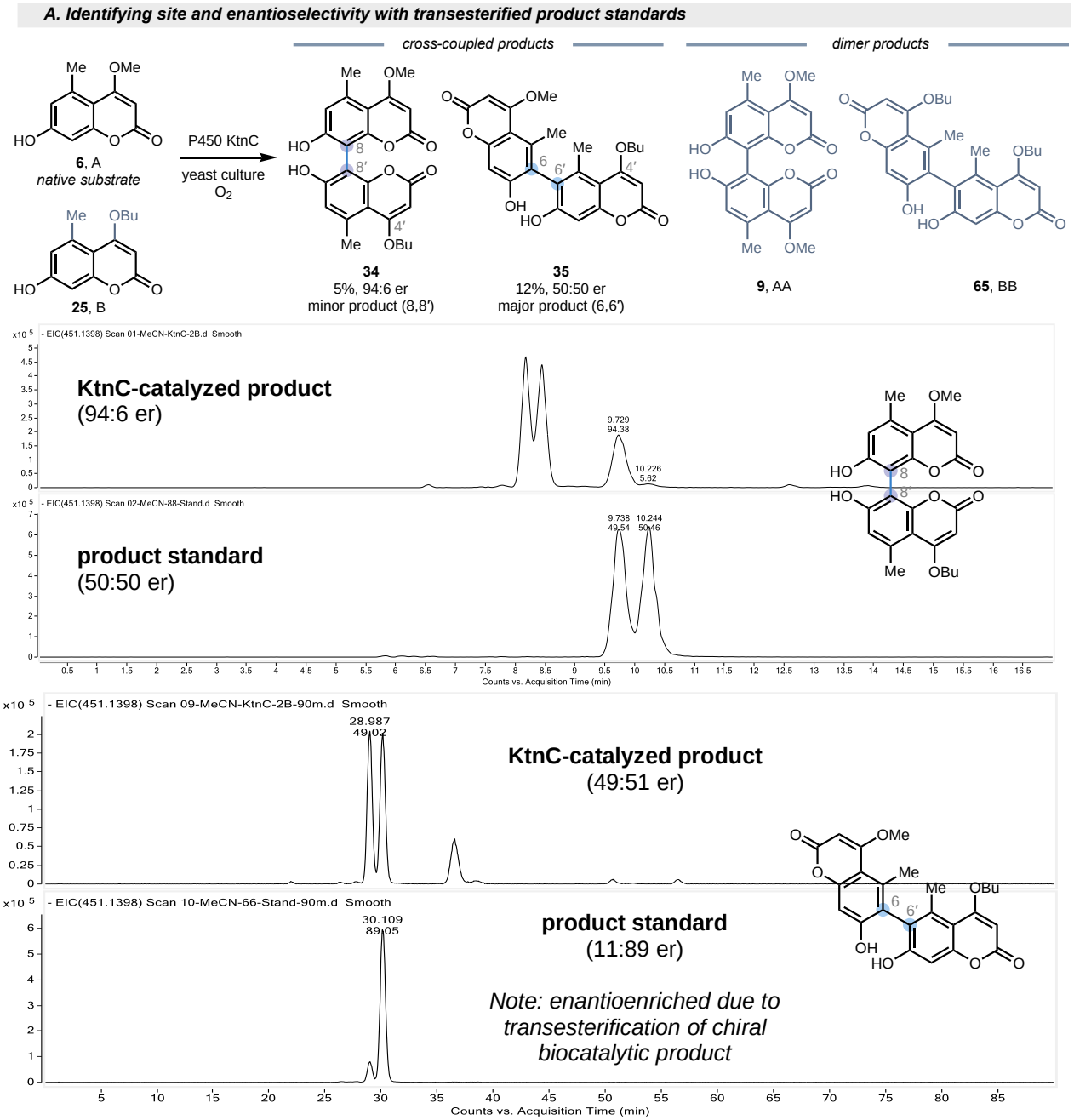

Figure 3.15: Determining site and enantioselectivity by LC-MS.
A. KtnC biotransformation: analytical scale, *P. pastoris*, 100 uM A and 100 uM B, BMM media, 30 °C, 48 h.
B. Chiral separation by LC-MS and EIC traces of crude enzymatic reaction compared to cross-coupled standards

individual species (Figure 3.14). This strategy allowed for the rapid access to standards with known connectivity for comparison to KtnC catalyzed cross-coupled biotransformations and was used to identify the site-selectivity of cross-coupled products **32**-**35** (see Figure 3.2C).

Using coumarin dimers of known connectivity, we subjected the 8,8', 8,6', and 6,6' dimers **9**, **63**-**64** to heat, acid, and blends of alcohols to obtain a statistical mixture of the starting material AA, the cross-coupled product AB, and the dimer BB (Figure 3.14). This strategy was successful with as little as nanograms of the starting materials and generated cross-coupled standards for assignment of the site-selectivity of KtnC biotransformations on an analytical scale. The 8,8'-native dimer **9** was readily accessed through several synthetic approaches developed within our group. The 8,6'-dimer **63** was also accessible through synthesis. The 6,6'-dimer **64** was best obtained through the isolation from KtnC preparative-scale dimerization reactions carried out by Dr. Meagan Hinze. The dimers isolated from biotransformations were enantioenriched, thus cross-coupled standards prepared from biocatalytic dimerization products were not racemic, retaining enantiomeric ratios under the transesterification reaction conditions (see the bottom trace of 3.15B). This approach was utilized to determine the site-selectivity and enantioselectivity of the two products formed in the cross-coupling reaction between native coumarin **6** and the C4-butyl ester **22**, which formed two cross-coupled products. In this reaction, the major product was determined to be the 6,6'-cross-coupled isomer, and with a chiral column (Diacel, Chiralpak IC-3, 4.6 x 150 mm, 3 μm), the enantiomeric ratio of both the 8,8' and 6,6'-isomeric products formed in the KtnC biotransformation were determined by LC-MS (Figure 3.15B). Whereas the minor 8,8'-product isomer was formed in a 94:6 er, the major 6,6'-isomer was racemic (49:51 er), a trend observed in the erosion of enantioselectivity in the dimerization reactions of coumarins harboring bulky C4 groups.

Using a chiral column with mass spectrometry conferred a major advantage in determining the selectivity of the coumarin cross-coupling reactions, which could result in mixtures of products that were not isolable and otherwise difficult to characterize. Analysis on analytical-scale became the method of choice in determining the site- and enantioselectivity of reactions that resulted in complex mixtures.

3.7 Preparative-scale cross-coupling biotransformations

Initially, developing a biocatalytic method for the oxidative cross-coupling of phenols motivated us to not only understand the substrate scope of KtnC cross-coupling reactions, but also to create a synthetically useful platform to compliment current chemical methods of a transformation that still poses significant challenges in controlling selectivity. To reach this goal, preparative scale reactions allowing the direct access of new atropisomers was imperative. Additionally, as we sought to understand the selectivity of the biocatalytic reactions by characterizing products, the difficulty encountered in synthesizing product standards further highlighted the need for this chemistry. Given our desire to demonstrate the scalability of the platform and characterize new enzymatic products, we initially began scaling up selected reactions that performed well on analytical scale. Our initial trials efforts scaling up the biotransformations did not immediately solve this problem, as we were constrained by several limitations of the expression system in *S. cerevisiae.* As discussed in Chapter 2, biocatalytic reactions with KtnC were constrained by low substrate concentrations, which hindered exploring preparative-scale reactions in this format. Although *P. pastoris* did provide an improvement in substrate concentration tolerance, both expression systems were challenging for isolating products from whole cell biotransformations.

The main obstacles encountered in whole cell biotransformations in *S. cerevisiae* followed from the constraint on substrate concentration, leading to a large volume of media required to carry out the reactions. For example, the maximum volume practical for manual liquid-liquid extraction in a separatory funnel was up to 1 L of the biotransformation cultures. Thus, the concentration of total coumarins added could not be increased without a substantial loss of reactivity, resulting in a steady decline in product formation from 0.25 mM to 0.5 mM coumarin substrate (approximately 50 to 100 mg per liter of culture, see discussion on biotransformation optimization in Chapter 2). Early attempts in the native dimerization preparative scale reactions showed that while the complete consumption of the starting material coumarin **6** was observed, extracting the product gave low isolated yields (see experimental details in Chapter 2) and similar problems with cross-coupling reactions on preparatory scale were encountered.

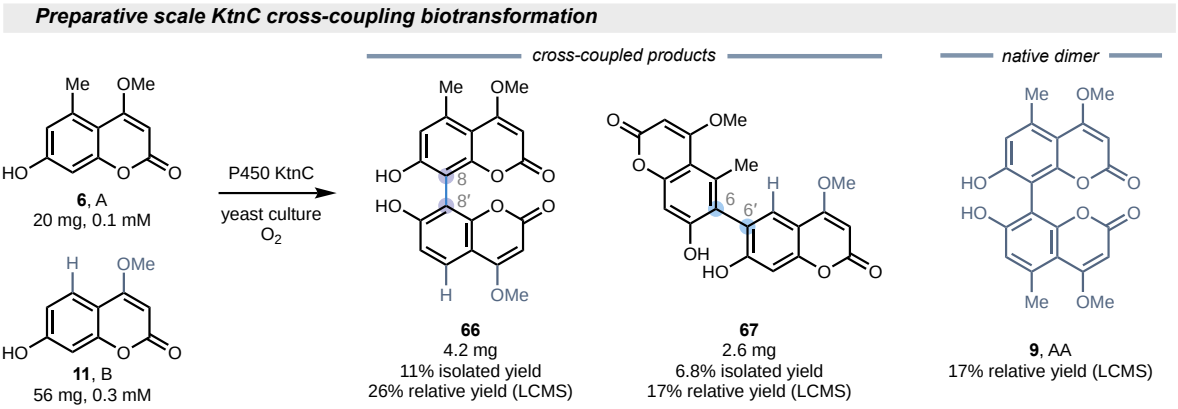

	Relative % yield calculations			
Whole cell extraction components	% AA	% 8,8′-AB	% 6,6′-AB	total % AB
Combined organic extracts	16.9	25.9	16.6	42.6
Aqueous supernatant	31.9	31.9	9.9	41.8
Pelleted cell debris	21.1	10.5	9.4	19.9

Figure 3.16: Preparative scale reactions in *S. cerevisiae.*
A. Conditions: *S. cerevisiae* in H^- minimal media, 6% galactose, 20 mgs A, 0.1 mM, 56 mg B, 0.3 mM, 30 °C, 96 h, 235 RPM shaking. Reaction monitored by LC-MS, no additional product formation after 72 h.
B. Analysis of product distribution in different components of the whole cell biotransformation after extraction with ethyl acetate. The combined organic extracts were purified by column chromatography over silica gel and reverse phase prep-HPLC to afford the 8,8' and 6,6'-product isomers.

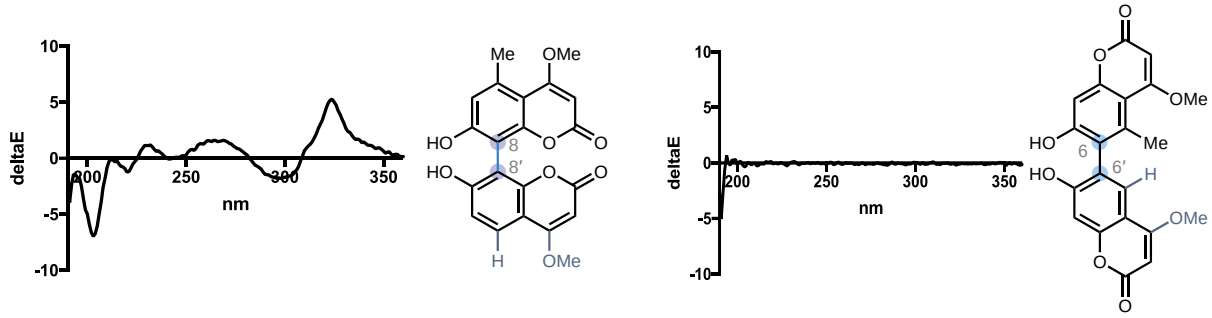

Figure 3.17: CD spectra of 8,8' and 6,6'-isomers.

The formation of two cross-coupled products were observed in the KtnC catalyzed biotransformation with native coumarin **6** and **11** (Figure 3.16) and the reaction was scaled up to 20 mg of the limiting reagent, which was dissolved in 1 L of yeast culture. The biotransformation was monitored by LC-MS over 4 days, and no additional product formation was observed after 72 h. The crude whole cell reaction was separated into supernatant and pellet fractions by centrifugation, then the aqueous supernatant was extracted with ethyl acetate exhaustively (10 x 200 mL ethyl acetate, then washes with brine) and concentrated to an off-white solid with an uncanny yeast aroma.

The combined organic layers were analyzed by LC-MS to ensure the presence of

cross-coupled products in the residue, then purified in a two-step process. The first purification was accomplished through column chromatography over silica gel and served to separate the unreacted starting materials and most of the coumarin dimer from the desired cross-coupled products. The second purification step was accomplished by reverse phase preparatory-HPLC (prep-HPLC), which separated the isomeric cross-coupled products and removed most of the minor contaminating impurities. However, it is notable that the coumarin compounds are not soluble in most organic solvents, with the exception of DMSO. Unless sufficiently diluted with water and methanol, heated, and filtered, the compounds would crash out upon loading the crude reaction solution onto the prep-HPLC, posing a logistical challenge by limiting the amount of material that could be loaded for each separation to approximately 10 mg. Successive prep-HPLC runs, followed by a tier-two screen of fractions by LC-Tof MS, then pooling of fractions that contained the desired products was accomplished over two runs. Analysis by ^{1}H NMR identified the first peak as the 8,8'-isomer **66** (4.2 mg, 10.9% isolated yield), and the second peak as the 6,6'-isomer (2.6 mg, 6.8% isolated yield). Analysis of the atroposelectivity of the two product isomers by circular dichroism (CD) spectroscopy revealed that the 8,8'-isomer **66** was enantioenriched, although measuring the er of this product was achieved due to difficulty in synthesizing the racemic authentic standard (Figure 3.16). The 6,6'-isomer **67** was not enantioenriched due to the free rotation around the unhindered biaryl bond in this molecule.

With the low recovery of the desired products in comparison to the relative percent yields that were calculated by LC-Tof MS, we sought understand the difference in mass balance and to improve the recovery of the products from preparatory scale biotransformations. We suspected one confounding problem was from attempting to recover small amounts (10’s of mgs) of products from large volumes of media. In the reaction detailed in Figure 3.15, a 100% yield would produce 38 mg of the cross-coupled products. We observed a 43% conversion to two cross-coupled products, posing a substantial challenge in isolating less than 20 mg of products from a total volume of 1 L of media also containing yeast, sugars, and biomolecules.

Upon analysis of the different reaction components by LC-Tof MS, we observed the product mass in all portions of the reaction components (organic extracts, aqueous

layer, and cell pellet). Although it was difficult to quantify the exact amounts of products in each partition, there were differences in the distribution of products, for example, in the combined organic extracts (which were subsequently purified), the native dimer **9** and both cross-coupled products in roughly a 2:1 ratio of AB:AA were found. In the remaining aqueous layer, this ratio was 1.3:1, and 1:1 in the pelleted cell debris. This data suggested different product species had different propensity to stay within the media, pellet, or be successfully extracted into the organic layer. Furthermore, we reasoned that the poor mass balance and recovery of products could be explained by the dimer and cross-coupling products remaining in the aqueous layer and in the pelleted yeast cells. Additionally, material loss from dilution and filtering to load samples for prep-HPLC was an ongoing problem that could not be ruled out as impacting recovery.

Next, scaling up and isolating products was attempted in the *P. pastoris* expression system, which posed several advantages, most importantly, the ability to run reactions at higher substrate concentrations and to use higher cell densities for the reactions. Efforts to improve the recovery of products over the *S. cerevisiae* preparative-scale biotransformations included collecting the cells by centrifugation and separating the solids from the supernatant, treating each reaction component separately and then combining crude extracts for purification. The supernatant was reduced in volume to roughly 300 mL by rotary evaporation to concentrate products and then extract with ethyl acetate and isopropanol as described. The pelleted cells were frozen in liquid nitrogen and physically lysed by grinding in a mortar and pestle. This crude cell lysate, containing the desired products, was then extracted by first dissolving in ethyl acetate, then stirred vigorously for several hours at room temperature before filtering and washing with water and brine. The organic extracts from both the aqueous supernatant and the pellet were then combined and purified. Additionally, the protocol for extracting the supernatant with ethyl acetate was improved by the addition of approximately 10% of the extraction volume of 70% isopropanol, which served to tame emulsions that made extraction laborious.

Even with these improvements, significant challenges remained in scaling up and isolating products directly from biotransformations carried out in yeast. Whereas the efforts to improve recovery detailed above did help improve the isolated yields of whole cell yeast biotransformations (see a comparison of the unoptimized dimerization

biotransformation preparative scale protocol in *S. cerevisiae* compared to optimized in *P. pastoris*), when reactions were unselective, forming multiple products with similar R_f's and retention times, separating the compounds was not always possible. Mixtures of products were often recovered after rounds of prep-HPLC, and isolated yields remained low in these reactions (Figure 3.17).

For example, in the reaction of coumarins **6** and **22** on an analytical-scale, up to 87% total cross-coupled products was observed, with the 8,8'-**32** and 6,6'-**33** products forming in a ratio of 8:1 at concentrations of 0.1 and 1.0 mM A and B (see figure 3.2C).

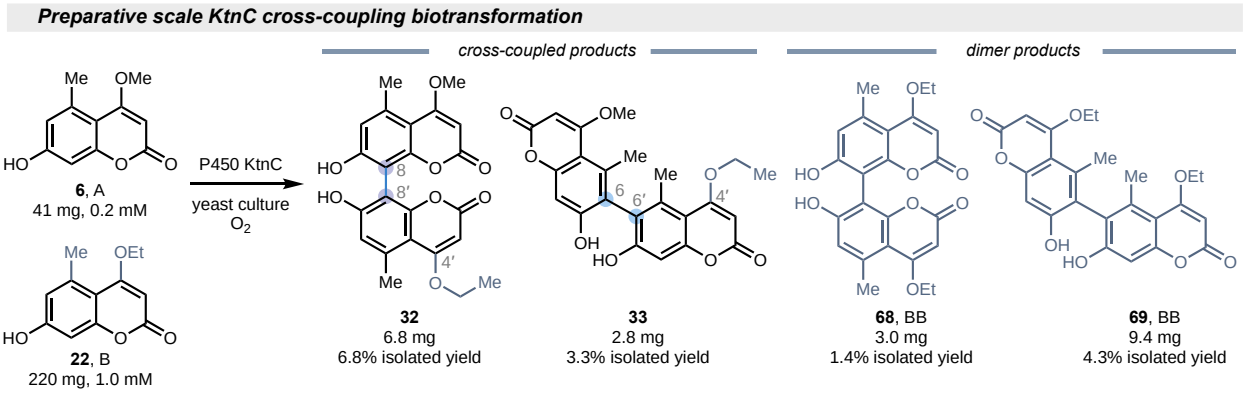

Figure 3.18: Preparative scale biocatalytic oxidative cross-coupling reaction.
Conditions: *P. pastoris*, BMM media, 0.2 mM A, 1.0 mM B, 30 °C, 48 h.

On preparative-scale, the reaction was carried out with 0.2 mM A and 5 equiv of B (1.0 mM). The reaction was not selective, with formation of the coumarin dimer from the coupling partner **22** used in excess. The retention times are similar for the 8,8'-cross-coupled product **32** and the non-native coumarin **22** starting material, as well as the 8,8'-coumarin dimer **9** and cross-coupled product 6,6'-cross coupled product **33**, which were isolated as mixtures after purification by prep-HPLC. This reaction highlights the difficulty in isolating compounds from mixtures, especially with coumarin-coumarin cross-coupling reactions where the starting materials and the isomeric products can have similar retention times.

3.8 Direct oxidative coupling

After investigating the substrate scope of KtnC and the selectivity of several biocatalytic cross-coupling reactions in further detail, we sought to compare the enzymatic

cross-coupling reaction to commonly employed small molecule transition metal catalysts (Figure 3.18).[5, 24, 40-45] Three categories of representative examples of coumarin–coumarin (entries 1A-1E), coumarin–naphthol (entries 2A-2E), and naphthol–naphthol cross-coupling (entries 3A-3E) reactions were chosen. Reactions that were either previously explored by synthesizing standards for comparison to KtnC (entries 1A-1E and 2A-2E), or, in the case of naphthol-naphthol cross-coupling, a combination that had been characterized and reported,[68-69] such that accessing at least one of the isomeric products would be achievable, were selected. The small molecule catalysts and reagents were chosen from frequently cited examples of oxidative dimerization and cross-coupling reactions. Specifically, the copper catalyst reported by Nakajima and coworkers,[41, 70] vanadium oxyfluoride utilized by the Porco group in an elegant synthesis of gonytolide B,[42] iron catalysts detailed mechanistically by the Pappo[71-73] and Katsuki[74-75] groups, and a chromium-Salen-complex reported by the Kozlowski[76-77] group with wide substrate scope were chosen. All the metal catalysts were commercially available and purchased from TCI America or Strem Chemicals. For all the reactions, the substrates were

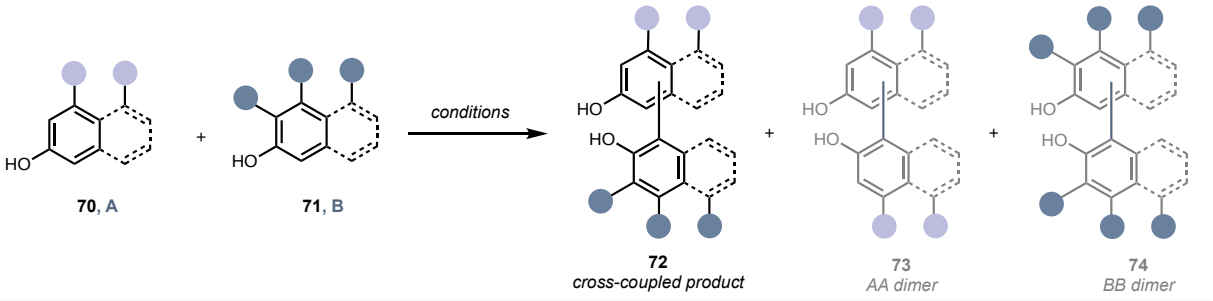

Entry	Phenols	(A) Cu(OH)Cl•TMEDA	(B) VOF_3	(C) $FeCl_3$	(D) Fe(TPP)Cl	(E) Cr-Salen-Cy
1	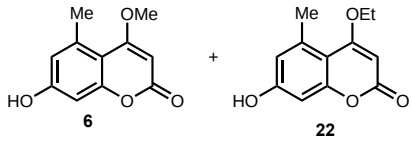	5% [a]	23% [a]	trace	trace	0%
2	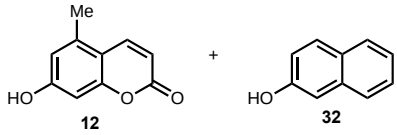	19% [b]	trace	0%	decomposition	trace
3	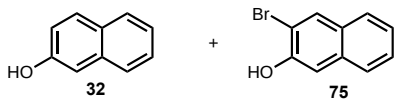	23%	5% [b]	6% [b]	decomposition	5%

Figure 3.19: Direct oxidative coupling with small molecule transition metal catalysts.
Percent yields for isolated cross-coupled products are reported unless noted otherwise.
[a]Relative percent conversion calculated by LC-MS. [b]Percent yield calculated by NMR.

combined in a 1:1 molar ratio and set up under air. All reactions were first screened on an analytical scale (5 mg) and monitored by LC- MS over 48 h to determine the general reactivity profile of the starting material combinations. Reactions that showed relative percent yields of >5% to cross-coupled products were selected for further investigation by scaling up, and again monitored by LC-MS over 48 h. Reactions that formed products were then quenched, extracted, and concentrated. The crude material was either purified by flash chromatography over silica gel, taken up into a solution of $CDCl_3$ to calculate percent yield by 1H NMR with an internal standard of 1,3,5-trimethoxybenzene, or compared to product standards by LC-MS to determine relative percent yield and site-selectivity. LC-Tof MS traces (Supplemental Figures S8-S25) detail the extracted ion chromatograms of the remaining starting materials, dimerized, and cross-coupled products formed in the reactions.

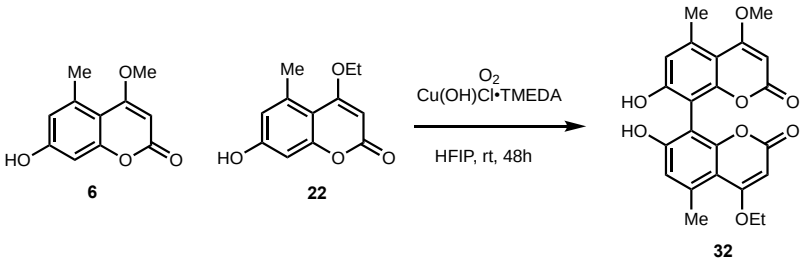

Entry 1A: The coumarin substrates **6** and **22** were added to a solution of Cu(OH)Cl•TMEDA (1 equiv) suspended in HFIP (0.1 M) at room temperature. The reaction was monitored over the course of 48 h, then quenched with dilute HCL and extracted with ethyl acetate. The crude material was first analyzed by LC-MS to calculate a relative percent yield, then further comparison to product standards to determine site-selectivity. The reaction formed a mixture of and cross-coupled product, each mass with only one peak indicating the reaction was site-selective but not chemoselective. The relative percent yield was calculated from LC-MS traces as 5% of product **32** with 8,8'-connectivity, identified by comparison to product standards.

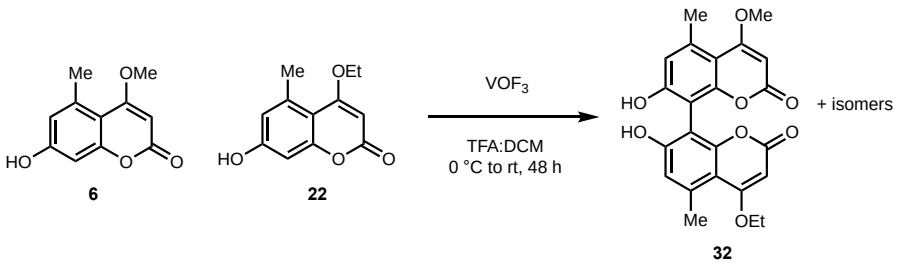

Entry 1B: The coumarin substrates **6** and **22** were dissolved in a blend of dry CH_2CH_2 (0.125 M) and trifluoroacetic acid (0.5 M), and cooled to 0 °C, then VO_3 (2.0 equiv) was added under air. The reaction was monitored over the course of 48 h, then quenched with dilute HCL and extracted with ethyl acetate. The reaction formed multiple products as a mixture of dimers and cross-coupled products, with a total of 23% relative percent yield for the cross-coupled products. The distribution of products followed the same trend observed in dimerization reactions under these conditions, with 8,8'-**32**, 8,6'-AB-isomer, and 6,6'-**33** isomers formed, with **32** formed as the major product and the minor product was 6,6'-isomer **33**.

Entries 1C-E: No or only trace product formed.

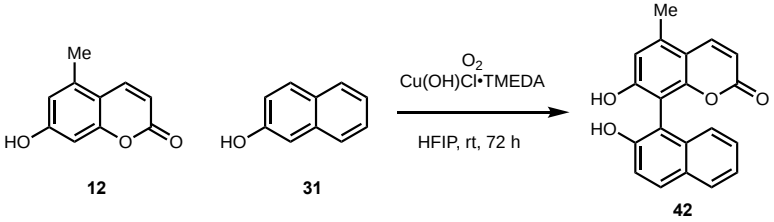

Entry 2A: Coumarin **12** and 2-naphthol **31** were added to a solution of Cu(OH)Cl•TMEDA (1 equiv) suspended in HFIP (0.1 M) at room temperature under air. The reaction was monitored over the course of 48 h, then quenched with dilute HCL and extracted with ethyl acetate. The crude material was dissolved in $CDCl_3$, with product **42** obtained as a 19% yield calculated by ^1H NMR. The crude material was compared by LC-MS to a product standard of **42,** with matching retention times observed (see Figure S3.23). The reaction was not chemoselective, forming multiple dimeric products of coumarin **12** and one dimer of 2-naphthol. For this substrate combination, this was the only conditions that produced cross-coupled product.

Entries 2B-E: Only trace product formation or decomposition observed.

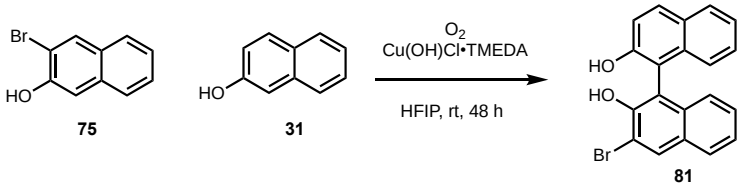

Entry 3A: Naphthols **75** and **31** were added to a solution of Cu(OH)Cl•TMEDA (1 equiv) suspended in HFIP (0.1 M) at room temperature under air. The reaction was monitored over the course of 48 h, then quenched with dilute HCL and extracted with ethyl acetate. The crude material was purified over silica gel with a gradient of 5% to 30% ethyl acetate in hexanes afforded **81** in a 23% yield. All spectra obtained was consistent for product **81**. This reaction was not chemoselective, forming one dimeric species of each coupling partner.

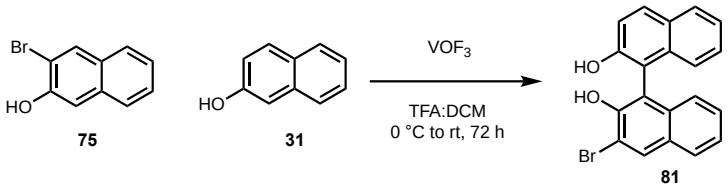

Entry 3B: Naphthols **75** and **31** were dissolved in a blend of dry CH_2CH_2 (0.125 M) and trifluoroacetic acid (0.5 M), and cooled to 0 °C, then VO_3 (2.0 equiv) was added under air. The reaction was monitored over the course of 48 h, then quenched with dilute HCL and extracted with ethyl acetate. The crude material was dissolved in $CDCL_3$, with product **81** obtained as a 6% yield calculated by ^{1}H NMR. All spectra obtained was consistent for product **81**. This reaction was not chemoselective, forming one dimeric species of each coupling partner.

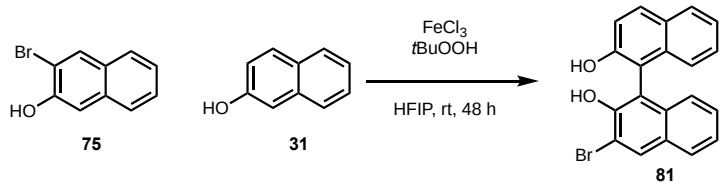

Entry 3C: Naphthols **75** and **31** were dissolved in HFIP (0.1 M). Anhydrous $FeCl_3$ (0.2 equiv) was added under inert atmosphere, followed by *t*-BuOOH added as 70% solution (1.1 equiv) and stirred at rt. The reaction was monitored over the course of 48 h, then quenched with dilute HCL and extracted with ethyl acetate. The crude material was purified over silica gel with a gradient of 5% to 30% ethyl acetate in hexanes, resulting in mixed fractions of related biaryl compounds. The fractions containing the cross-coupled product mass were combined and dissolved in $CDCL_3$, with product **81** obtained as a 6% yield calculated by ^{1}H NMR. This reaction was not chemoselective, forming one dimeric species of each coupling partner. By LC-MS, the cross-coupled product peak appeared to have a shoulder, suggesting the formation of an additional cross-coupled product.

Entry 3D: Decomposition observed.

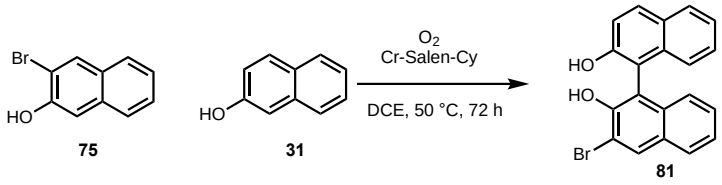

Entry 3E: Naphthols **75** and **31** were dissolved in 1,2-dichloroethane (0.1 M), and the Cr-Salen-Cy (0.1 equiv) catalyst was added under air, then the reaction was heated to 60 °C. The reaction was monitored over the course of 72 h, then quenched with dilute HCL and extracted with ethyl acetate. The crude material was purified over silica gel with a gradient of 0% to 20% ethyl acetate in hexanes, with product **81** obtained in a 5% yield. All spectra obtained was consistent for product **81**. This reaction was not chemoselective, forming one dimeric species of each coupling partner. By LC-MS, the cross-coupled product peak appeared to have a shoulder, suggesting the formation of an additional cross-coupled product.

General discussion: Achieving reactivity, chemoselectivity and site-selectivity were challenging across the scope of representative reactions studied in Figure 3.18. Generally, we observed low overall reactivity, with isolated yields of cross-coupled products from 5% (Entry 3E) to 23% in the best scenario (Entry 3A). In all cases, the reactions resulted in mixtures of multiple species including unreacted starting materials, dimers, and cross-coupled products, and in some cases, multiple regioisomers of each species (1B). Analysis of these complex mixtures has been an ongoing challenge; however, we have found success using LC-MS as a screening tool to quickly identify reactions that show desirable chemoselectivity and determine the site-selectivity when authentic standards are accessible. Using relative percent conversions was useful in providing an estimate of the reactivity observed for a given set of substrates under established conditions and serve as an indication for the reactions that should be scaled up for further analysis. Verification of the formation of meaningful amounts of cross-coupled products was attained by either purification and isolation of products, or by ^{1}H NMR analysis of mixtures and comparison to internal standards. When these two options were not feasible due to low yields of the desired cross-coupled products or the formation

of inseparable mixtures of products, percent conversion to cross-coupled products calculated by LC-MS remained the best indication of reactivity.

Of the phenolic substrates selected for direct oxidative coupling, coumarin–coumarin cross-coupling reactions (Entries 1A-1E) were the most challenging to achieve with the panel of metal catalysts, whereas naphthol–naphthol cross-coupling reactions (3A-3E) were more broadly accessible with the oxidants investigated. When reactivity was achieved, the formation of multiple products rendered isolation a challenge, with several rounds of purification required to isolate characterizable products. The most versatile catalyst for cross-coupling was Cu(OH)Cl•TMEDA (column A), which formed cross-coupled products with each substrate pair with low to moderate reactivity. Whereas this copper-mediated method generally led to the formation of only one major cross-coupled product, the reactions suffered from competing dimerization and overall low yields. In general, iron and chromium catalysts resulted in mixtures of products, with no reactivity in coumarin–coumarin and coumarin–naphthol coupling reactions. In reactions with Fe(TPP)Cl (column C), decomposition of starting materials in each case was observed. For coumarin–coumarin coupling, VOF_3 (Entry 1B) achieved modest conversions to cross-coupled products and was the only oxidant capable of forming 8,6'-isomers and trace amounts of 6,6'-isomers. However, individual isomers were not isolable from the complex reaction mixtures as isomers were inseparable.

3.9 Comparison of KtnC, DesC, and copper cross-coupling reactions

With a greater understanding of the reactivity for oxidative cross-coupling of coumarins and phenols with small molecule catalysts, we sought to make a more accurate comparison to enzymatic methods and the most versatile metal catalyst uncovered in screening, Cu(OH)Cl•TMEDA. In the KtnC catalyzed cross-coupling reaction, Fig 3.1, the combinations of substrates were carried out in a molar ratio of 1:10 (A:B), which favored the cross-coupling products. Though using an excess of the less oxidizable coupling partner is routinely encountered in direct oxidative coupling reactions (see Chapter 1 for a discussion on chemically catalyzed oxidative coupling of phenolic substrates), the reactions were evaluated with substrates coupled in a 1:1 ratio to make

a direct comparison across the enzymatic and chemical methods. Additionally, we included DesC, which had not been extensively investigated for oxidative cross-coupling reactions (Figure 3.20).

In coumarin-coumarin combinations, the copper catalyst was found to be inefficient for cross-coupling, with moderate reactivity of up to a relative percent yield of 19% observed (entry 2, Me, OPr). The major products in most of the reactions were the native coumarin dimer **9**, with the exception of entries 5 and 10). In entry 5, the major product was the dimer of coupling partner B, which is more electron rich in comparison to the native substrate **6**, however, it was not clear why coumarin **12** in entry 10 was preferentially dimerized over the native substrate.

Surprisingly, in a 1:1 ratio of substrates, DesC consistently outperformed KtnC in the relative percent yield of cross-coupled products, while also forming less dimeric product of both coumarins. In the native dimerization reaction, lower percent conversion

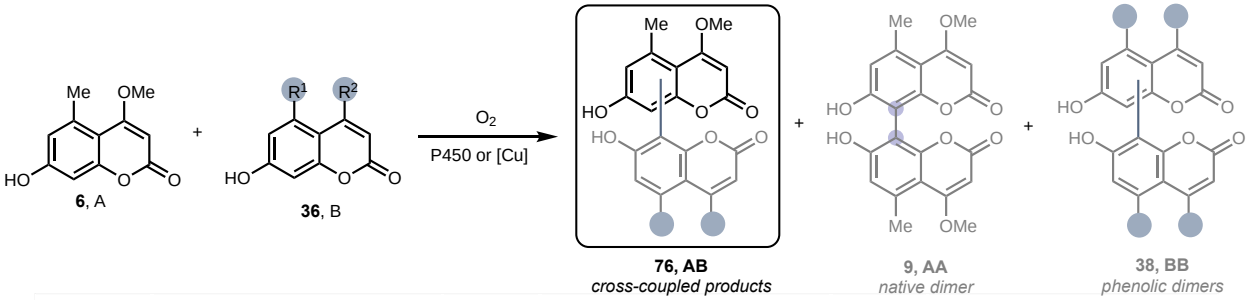

B substrate		KtnC			DesC			Cu(OH)Cl•TMEDA		
R1, R2	**% AB**	**% AA**	**%BB**	**% AB**	**% AA**	**%BB**	**% AB**	**% AA**	**%BB**
Me, OEt	28	68	63	32	15	30	4	3	4
Me, OPr	2	96	2	20	59	1	19	11	20
Me, OBu	2	98	0	2	75	0	10	20	24
Me, NHMe	11	83	50	3	61	0	5	8	6
OH, OMe	5	83	trace	9	63	trace	1	trace	34
H, OMe	19	71	22	28	37	36	5	26	4
Et, OMe	9	82	46	19	44	37	14	11	12
Cl, OMe	2	76	0	20	30	0	1	31	3
Br, OMe	4	62	0	8	20	0	1	32	0
Me, H	11	76	20	21	50	14	5	8	16
H, Me	8	92	2	16	56	4	4	25	1
H, H	1	99	trace	2	74	trace	4	24	4

Figure 3.20: Comparison of direct oxidative coupling methods – coumarin-coumarin couplings.
Conditions: KtnC and DesC: *P. pastoris*, analytical scale, BMM media, 0.1 mM substrate concentrations (A and B), 30 °C, 48 h. Chemical reactions: 5 mg scale, 1 equiv [Cu], 0.1 M HFIP, rt, 48 h. Relative analyzed by LC-MS, relative percent yields calculated by EIC peak areas. Green highlights highest total relative percent AB conversion

to the dimeric products has been regularly observed with DesC with more starting material left unconsumed, where in comparison, the KtnC dimerization reaction of the native substrate is fast and goes to full conversion and is also more robust with dimerization of non-native coumarins. This data suggests that DesC may be an efficient catalyst for oxidative cross-coupling reactions, but the selectivity of DesC is limited to a few examples in the dimerization reaction (Chapter 2). Looking at the distribution of the cross-coupled products by LC-MS, DesC and KtnC reaction traces possessed similar product peaks, but with different major products, while the copper catalyst forms one product peak (Figure 3.20).

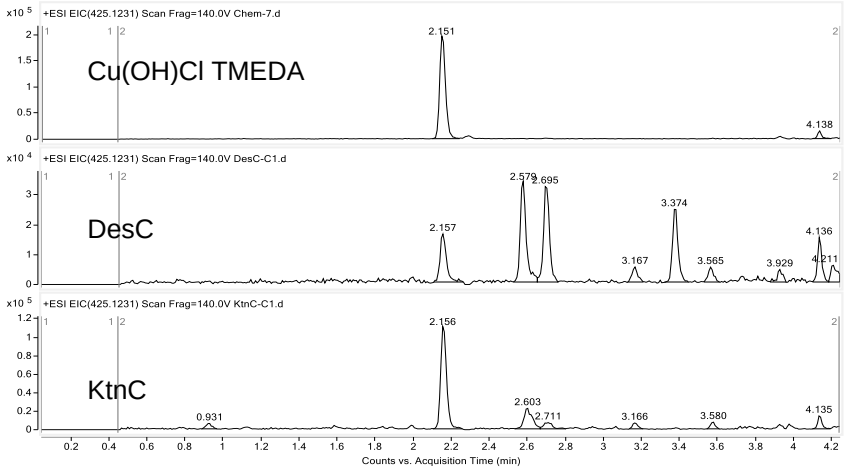

Figure 3.21: Cross-coupled product peaks oxidative coupling reactions. Comparison of LC-MS EIC traces of the exact AB mass.
[Cu] reactions are selective for one isomer. KtnC and DesC form multiple products, with different distribution of major products.

Next, we tested the same catalysts with coumarin-phenol cross-coupling reactions under the same reaction conditions (Figure 3.21). Here, the copper catalyst provided the most product, but was also capable of dimerizing both A and B (entries 4-8), which KtnC and DesC cannot do with the exception of benzofuran **28** (entries 5 and 6). This trend was anticipated as KtnC and DesC poorly couple non-coumarin phenolic substrates, while the copper catalyst oxidized these compounds more readily. With a substrate ratio of 1:1, the enzymatic reactions with non-coumarin phenolic substrates formed 10% or less cross-coupled products. These reactions could be improved upon with protein engineering and could offer a reasonable starting point for enhancing a desired reaction. With DesC unexpectedly outperforming KtnC in substrate ratios of 1:1, future exploration of the DesC cross-coupled substrate scope is warranted, and based on this preliminary data, optimization of substrate concentrations may reveal promising leads.

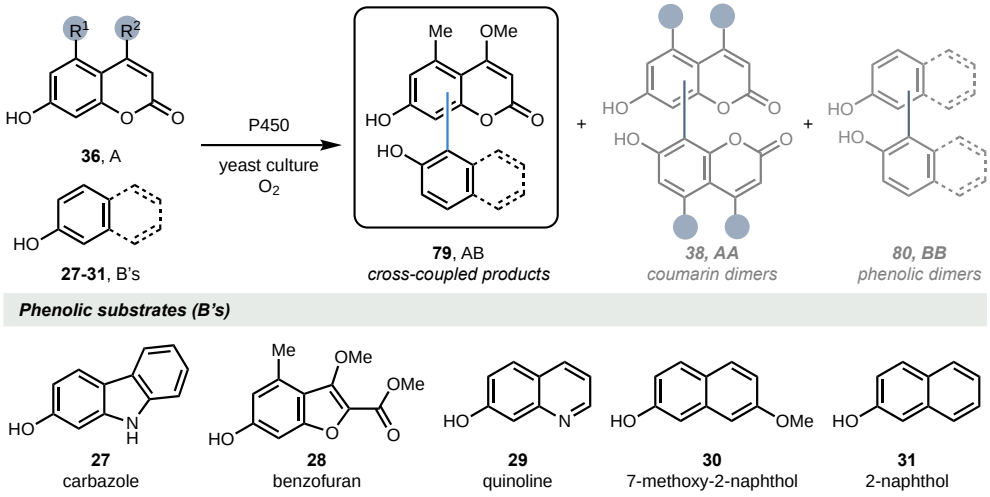

A substrate	B substrate	KtnC			DesC			Cu(OH)Cl•TMEDA		
R1, R2	**name**	**% AB**	**% AA**	**BB?**	**% AB**	**% AA**	**BB?**	**% AB**	**% AA**	**BB?**
Me, OMe	2-naphthol	trace	99	no	0	78	no	12	2	no
Me, OMe	7-Methoxy-2-naphthol	0	99	no	0	77	no	17	9	no
Me, OMe	quinoline	1	98	no	1	77	no	37	22	no
Me, OMe	carbazole	trace	99	no	trace	79	no	trace	18	yes
Me, OMe	benzofuran	5	86	yes	10	56	yes	7	40	yes
OH, Ome	benzofuran	trace	32	yes	0	34	yes	trace	22	yes
Me, H	7-Methoxy-2-naphthol	2	36	no	trace	32	no	14	3	yes
Me, H	quinoline	3	48	no	0	40	no	76	4	yes
H, Ome	quinoline	3	25	no	trace	64	no	31	1	yes
Me, NHMe	quinoline	9	57	no	trace	76	no	24	2	yes
H, H	quinoline	trace	trace	no	0	trace	no	35	3	yes

Figure 3.22: Comparison of direct oxidative coupling methods – coumarin-phenol couplings.
Conditions: KtnC and DesC: *P. pastoris*, analytical scale, BMM media, 0.1 mM substrate concentrations (A and B), 30 °C, 48 h. Chemical reactions: 5 mg scale, 1 equiv [Cu], 0.1 M HFIP, rt, 48 h. Relative analyzed by LC-MS, relative percent yields calculated by EIC peak areas. Green highlights highest total relative percent AB conversion.

3.10 Conclusions

The substrate scope of KtnC was investigated and found to be surprisingly promiscuous, with numerous examples of cross-coupling between coumarins and phenolic compounds (Figures 3.2-3.6). By developing methods for reaction analysis, including analytical and preparative scale reaction strategies, we have successfully profiled the reactivity of wild-type KtnC, and created a toolbox to apply to additional P450 enzymes (Figures 3.20-22). Specifically, strategies to determine site and

enantioselectivity on analytical scale reactions enables the rapid profiling of P450 enzymes heterologously expressed in *P. pastoris*, circumventing limitations in the scalability of the reaction observed with wild-type KtnC. We identified conditions for challenging, sterically demanding Suzuki-cross coupling reactions on unique coumarin scaffolds, allowing the synthesis of product standards to aid in the characterization of biocatalytic products.

We uncovered evidence that the biocatalytic method exerts control over the chemo, site-selectivity and atroposelectivity in some cases. For example, we observed excellent enantioselectivity in the cross-coupling of coumarins **6** and **22** to form (*P*)-**32** in a 78% conversion and 98:2 er and (*P*)-**33** in a 10% conversion and 79:21 er. This result suggests that the enzyme exerts control in the coupling reaction step, whereas the analogous reaction with oxidant VOF_3 provides a racemic distribution of products that differs from the major isomers observed in the biocatalytic reaction (see Figure 3.19 and experimental traces). While not perfect, this example highlights that there is catalyst-control in this biocatalytic reaction and suggests the possibility for improvement through engineering campaigns, a result demonstrated by Lara Zetzsche in the development of KtnC variants with enhanced yield and site selectivity, and the ability to change the atroposelectivity with iterative rounds of evolution. (see Figure 3.7).

3.11 Experimental

Chemical synthesis

General considerations. All reagents were used as received unless otherwise noted. Reactions were carried out under a nitrogen atmosphere using standard Schlenck techniques unless otherwise noted. Solvents were degassed and dried over aluminum columns on an MBraun solvent system (Innovative Technology, Inc., Model PS-00-3). Reactions were monitored by thin layer chromatography using Machery-Nagel 60 F_{254} precoated silica TLC plates (0.25 mm) or Merck Silica Gel 60 F_{254} precoated silica TLC plates (0.25 mm) which were visualized using UV, *p*-anisaldehyde, CAM, DNP, or bromocresol green stain. Flash column chromatography was performed using Machery-Nagel 60 μm (230-400 mesh) silica gel. All compounds purified by column chromatography were sufficiently pure for use in further experiments unless otherwise indicated. ^{1}H and ^{13}C NMR spectra were obtained in $CDCl_3$ at rt (25 °C), unless otherwise noted, on Varian 400 MHz or Varian 600 MHz spectrometers. Chemical shifts of ^{1}H NMR spectra were recorded in parts per million (ppm) on the δ scale. High resolution electrospray mass spectra were obtained on an Agilent UPLC-QTOF at the University of Michigan Life Sciences Institute or Agilent UPLC-TOF at the University of Michigan Life Sciences Institute. IR spectra were recorded on a Perkin-Elmer Spectrum BX FT-IR spectrometer. SFC spectra were obtained on a Waters SCF Investigator SFC system. Circular dichroism spectra were obtained on a JASCO J-1500 CD Spectrometer. Compounds **13**, **14**, **27,** and **29**-**31** were commercially available and purchased from TCI chemicals or Sigma Aldrich. Synthesis of substrates **6**, **11**, **15**, **18**, **21**-**23**, and **25** were reported in Chapter 2 experimental sections 2.13 (experimental details).

Synthesis of substrates

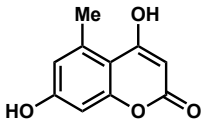

4,7-dihydroxy-5-methyl-*2H*-chromen-2-one (82). To a mixture of 5-methylresorcinol (3.000 g, 24.16 mmol, 1.000 equiv), malonic acid (2.514 g, 24.16 mmol, 1.000 equiv) and

$ZnCl_2$ flame-dried under vacuum (10.21 g, 74.91 mmol, 3.100 equiv) was added $POCl_3$ (60.0 mL). The reaction was heated at 60 °C and stirred for 14.5 h. The reaction was quenched by pouring into ice water and induced the precipitation of a solid, which was isolated by vacuum filtration. The crude solid was purified by flash column chromatography (5:6:1 toluene/ethyl acetate/formic acid v/v) to afford 3.38 g of the title compound (73% yield) as a yellow solid with minor impurities. $\mathbf{R_f}$ = 0.37 (8:3:1 toluene/ethyl acetate/formic acid v/v); **^{1}H NMR** (400 MHz, DMSO-*d*$_6$) δ 12.06 (s, 1H), 10.39 (s, 1H), 6.54 (s,1H), 6.50 (s, 1H), 5.33 (s, 1H), 2.57 (s, 3H); **^{13}C NMR** (150 MHz, DMSO-*d*$_6$) δ 169.1, 161.9, 160.4, 157.0, 138.7, 115.6, 106.4, 100.4, 88.0, 22.8; **HRMS** (ESI) *m/z* calculated for $C_{10}H_9O_4^+$ $[M+H]^+$ 193.0495, found 193.0505. All spectra obtained were constant with literature values.[78]

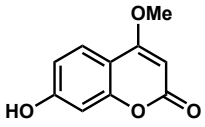

7-hydroxy-4-methoxy-*2H*-chromen-2-one (11). To a solution of 4,7-dihydroxycoumarin (250.0 mg, 1.403 mmol, 1.000 equiv) in MeOH (15.6 mL) was added H_2SO_4 (1.6 mL). The reaction was heated at 75 °C for 2.8 h. Incubation at 0 °C induced the precipitation of a white solid which was isolated by vacuum filtration to afford 226.2 mg of the title compound (84% yield). **^{1}H NMR** (600 MHz, DMSO-*d*$_6$) δ 7.61 (d, *J* =8.7, 1H), 6.78 (dd, *J* = 8.7, 2.3, 1H), 6.69 (d, *J* = 2.3, 1H), 5.67 (s, 1H), 3.96 (s, 3H); **HRMS** (ESI) *m/z* calculated for $C_{10}H_9O_4^+$ $[M+H]^+$ 193.0495, found 193.0503. All spectra obtained were constant with literature values.[79]

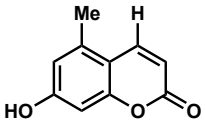

7-hydroxy-5-methyl-*2H*-chromen-2-one (12). Ethyl(3,3)-diethoxypropanoate (0.36 mL, 1.8 mmol, 1.0 equiv) was added neat to 5-methylresorcinol (250 mg, 2.0 mmol, 1.1 equiv). The reaction was heated at 120 °C and stirred until dissolved for 1 h. Toluene (5.0 mL) and toluene sulfonic acid monohydrate (77 mg, 0.40 mmol, 0.200 equiv) were added to the solution. The reaction was heated at 110 °C and stirred for 16 h. The reaction was quenched by pouring into ice water and further induced the precipitation of a solid, which

was isolated by vacuum filtration to afford 320.0 mg of the title compound (99% yield).**^{1}H NMR** (400 MHz, DMSO-*d_6*) δ 10.45 (s, 1H), 8.05 (d, *J* = 9.7, 1H0, 6.64 (d, *J* = 2.0, 1H), 6.55 (d, *J* = 2.0, 1H), 6.19 (d, *J* = 9.7, 1H), 2.42 (s, 3H); **HRMS** (ESI) *m/z* calculated for $C_{10}H_9O_3^+$ $[M+H]^+$ 177.0546, found 177.0556. All spectra obtained were constant with literature values.[80]

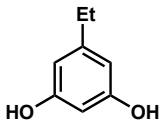

5-ethylbenzene-1,3-diol (83). The title compound was prepared from 1-(3,5-dihydroxyphenyl)ethan-1-one according to the procedure described by Linusson et al.[81] **^{1}H NMR** (400 MHz, acetone-*d_6*) δ 8.01 (s, 2H), 6.19 (d, *J* = 1.9, 2H), 6.17 (d, *J* = 2.1, 1H), 2.46 (q, *J* = 7.6, 2H), 1.14 (t, *J* = 7.6, 3H). All spectra obtained were consistent with literature values.[81]

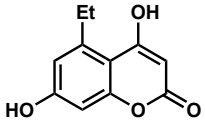

5-ethyl-4,7-dihydroxy-*2H*-chromen-2-one (84). To a mixture of 5-ethylbenzene-1,3-diol (**83**, 800.2 mg, 5.791 mmol, 1.000 equiv), malonic acid (602.6 mg, 5.791 mmol, 1.000 equiv) and $ZnCl_2$ flame-dried under vacuum (2.446 g, 17.95 mmol, 3.100 equiv) was added $POCl_3$ (14.5 mL). The reaction was heated at 60 °C and stirred for 14.5 h. The reaction was quenched by pouring into ice water and induced the precipitation of a solid, which was isolated by vacuum filtration. The crude solid was purified by flash column chromatography (8:3:1 to 6:5:1 toluene/ethyl acetate/formic acid v/v) to afford a 183.5 mg of the title compound (15% yield) as a tan solid with minor impurities. **MP** = 234.1-236.8 °C; **R_f** = 0.43 (8:3:1 toluene/ethyl acetate/formic acid v/v); **^{1}H NMR** (600 MHz, DMSO-*d_6*) δ 12.11 (s, 1H), 10.41 (s, 1H), 6.57 (d, *J* = 2.4, 1H), 6.51 (d, *J* = 2.4, 1H), 5.36 (s, 1H), 2.99 (q, *J* = 7.4, 2H), 1.15 (t, *J* = 7.4, 3H); **^{13}C NMR** (150 MHz, DMSO-*d_6*) δ 168.7, 161.8, 160.6, 157.2, 145.2, 114.4, 105.7, 100.6, 88.3, 28.2, 16.5; **IR** (thin film, cm^{-1}) 3086, 2971, 2599, 1646, 1598, 1555, 1510, 1437; **HRMS** (ESI) *m/z* calculated for $C_{11}H_{11}O_4^+$ $[M+H]^+$ 207.0652, found 207.0651.

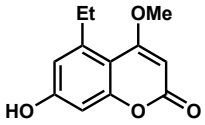

5-ethyl-7-hydroxy-4-methoxy-*2H*-chromen-2-one (16). To a solution of 5-ethyl-4,7-dihydroxy-*2H*-chromen-2-one (**84**, 141.7 mg, 0.691 mmol, 1.000 equiv) in MeOH (7.7 mL) was added H_2SO_4 (0.77 mL). The reaction was heated at 75 °C for 4.4 h. Incubation at 0 °C induced the precipitation of an orange solid which was isolated by vacuum filtration to afford 78.8 mg of the title compound (52% yield) as a tan solid with minor impurities. **MP** = 267.4-269.5 °C; **R_f** = 0.48 (8:3:1 toluene/ethyl acetate/formic acid v/v); **^{1}H NMR** (600 MHz, DMSO-d_6) δ 10.45 (br s, 1H), 6.58 (d, *J* = 2.3, 1H), 6.54 (d, *J* = 2.3, 1H), 5.60 (s, 1H), 3.93 (s, 3H), 2.91 (q, *J* = 7.3, 2H), 1.12 (t, *J* = 7.4, 3H); **^{13}C NMR** (150 MHz, DMSO-d_6) δ 169.0, 161.7, 160.5, 156.2, 144.5, 114.7, 105.3, 100.6, 86.9, 56.5, 28.6, 16.1; **IR** (thin film, cm^{-1}) 3286, 1689, 1621, 1606, 1560, 1421; **HRMS** (ESI) *m/z* calculated for $C_{12}H_{13}O_4^+$ $[M+H]^+$ 221.0808, found 221.0818.

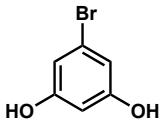

5-bromoresorcinol (85). To a solution of 1-bromo-3,5-dimethoxybenzene (2.00 g, 8.33 mmol, 1.00 equiv) in CH_2Cl_2 (8.3 mL) was added 1 M BBr_3 solution in CH_2Cl_2 (25.0 mL, 25.0 mmol, 3.00 equiv) at –78 °C. The reaction was warmed to rt and stirred for 16 h. The reaction was quenched by slow addition of water (10 mL) at 0 °C and extracted with ethyl acetate (3x). The organic layers were combined, washed with brine, dried over Na_2SO_4, filtered, and evaporated under reduced pressure to afford an oil. The crude product was purified by flash column chromatography (9:1 to 7:3 hexanes/ethyl acetate v/v) to afford 1.846 g of the title compound (85% yield) as an off-white solid. **^{1}H NMR** (400 MHz, CD_3OD) δ 6.42 (d, *J* = 2.1, 2H), 6.19 (t, *J* = 2.1, 1H). All spectra obtained were constant with literature values.[82]

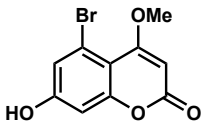

5-bromo-7-hydroxy-4-methoxy-*2H*-chromen-2-one (19). To a mixture of 5-bromoresorcinol (**85**, 422.0 mg, 2.232 mmol, 1.000 equiv), malonic acid (232.3 mg, 2.232 mmol, 1.000 equiv) and $ZnCl_2$ flame-dried under vacuum (943.0 g, 6.919 mmol, 3.100

equiv) was added $POCl_3$ (5.6 mL). The reaction was heated at 60 °C and stirred for 15.1 h. The reaction was quenched by pouring into ice water and induced the precipitation of a solid, which was isolated by vacuum filtration. The crude material was used without further purification due to decomposition under flash column chromatography conditions. To a solution of crude 5-bromo-4,7-dihydroxy-*2H*-chromen-2-one (459.0 mg, 1.785 mmol, 1.000 equiv) in MeOH (20.0 mL) was added H_2SO_4 (2.0 mL). The reaction was heated at 75 °C for 7.1 h. Partial concentration of the solution and incubation at 0 °C induced the precipitation of a white solid which was isolated by vacuum filtration to afford 34.3 mg of the title compound (13% yield). **MP** = 207.4-212.0 °C; **R_f** = 0.41 (8:3:1 toluene/ethyl acetate/formic acid v/v); **^{1}H NMR** (600 MHz, DMSO-*d_6*) δ 7.04 (d, *J* = 2.4, 1H), 6.71 (d, *J* = 2.4, 1H), 5.71 (s, 1H), 3.92 (s, 3H); **^{13}C NMR** (150 MHz, DMSO-*d_6*) δ 166.4, 160.9, 160.7, 156.2, 119.7, 117.6, 106.2, 102.7, 87.9, 56.6; **IR** (thin film, cm^{-1}) 3406, 3147, 1694, 1611, 1589, 1550, 1433; **HRMS** (ESI) *m/z* calculated for $C_{10}H_8BrO_4^+$ $[M+H]^+$ 270.9600, found 270.9607.

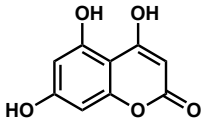

4,5,7-trihydroxy-*2H*-chromen-2-one (86). 86 was prepared from phloroglucinol and cyanoacetic acid according to the procedure described by Pandey et al.[83] **MP** = >310 °C; **R_f** = 0.38 (8:3:1 toluene/ethyl acetate/formic acid v/v); **^{1}H NMR** (600 MHz, DMSO-*d_6*) δ 10.40 (s, 1H), 6.17 (s, 2H), 5.19 (s, 1H); **^{13}C NMR** (150 MHz, DMSO-*d_6*) δ 168.3, 162.2, 161.9, 156.9, 156.3, 98.6, 96.6, 94.7, 86.6; **IR** (thin film, cm^{-1}) 3097, 2707, 2600, 1634, 1569, 1471, 1415; **HRMS** (ESI) *m/z* calculated for $C_9H_7O_5^+$ $[M+H]^+$ 195.0288, found 195.0295.

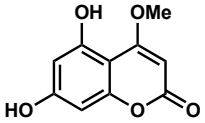

5,7-dihydroxy-4-methoxy-*2H*-chromen-2-one (20). To a solution of 4,5,7-trihydroxy-*2H*-chromen-2-one (**86**, 67.6 mg, 0.35 mmol, 1.00 equiv) in MeOH (3.0 mL) was added H_2SO_4 (0.35 mL). The reaction was heated at 80 °C for 1.5 h. Incubation at 0 °C induced

the precipitation of a tan solid which was isolated by vacuum filtration to afford 19.0 mg of the title compound (26% yield). **MP** = 224.2-226.5 °C; **R_f** = 0.42 (8:3:1 toluene/ethyl acetate/formic acid v/v); **^{1}H NMR** (600 MHz, DMSO-*d_6*) δ 6.20 (d, *J* = 2.1, 1H), 6.17 (d, *J* = 2.5, 1H), 5.49 (s, 1H), 3.90 (s, 3H); **^{13}C NMR** (150 MHz, DMSO-*d_6*) δ 168.8, 161.8, 161.6, 156.7, 156.0, 99.5, 96.5, 94.6, 85.2, 56.7; **IR** (thin film, cm^{-1}) 3402, 3234, 3089, 1700, 1642, 1609, 1579, 1521, 1464, 1443, 1405; **HRMS** (ESI) *m/z* calculated for $C_{10}H_9O_5^+$ $[M+H]^+$ 209.0444, found 209.0452.

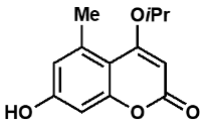

7-hydroxy-4-isopropoxy-5-methyl-*2H*-chromen-2-one (24). To a solution of 4,7-dihydroxy-5-methyl-*2H*-chromen-2-one (**82**, 550.0 mg, 2.862 mmol, 1.000 equiv) in *i*-PrOH (32.0 mL) was added H_2SO_4 (3.2 mL). The reaction was heated at 75 °C for 4.7 h. The solution was partially concentrated under reduced pressure, diluted with H_2O and extracted with ethyl acetate (3x). The organic layers were combined, washed with brine, dried over Na_2SO_4, filtered, and evaporated under reduced pressure to afford a solid. The crude solid was purified by flash column chromatography (9:2:1 to 8:3:1 toluene/ethyl acetate/formic acid v/v) to afford 51.8 mg of the title compound (8% yield) as a tan solid. **MP** = 215.1-217.1 °C; **R_f** = 0.51 (8:3:1 toluene/ethyl acetate/formic acid v/v); **^{1}H NMR** (600 MHz, acetone-*d_6*) δ 6.61 (d, *J* = 2.2, 1H), 6.56 (d, *J* = 2.5, 1H), 5.48 (s, 3H), 4.84 (heptd, *J* = 6.0, 2.7, 1H), 2.61 (s, 3H), 1.46 (d, *J* = 6.0, 6H); **^{13}C NMR** (150 MHz, acetone-*d_6*) δ 168.2, 162.7, 160.9, 157.8, 139.8, 116.7, 108.2, 101.5, 88.2, 73.0, 24.0, 21.8; **IR** (thin film, cm^{-1}) 3207, 2980, 2933, 1683, 1599, 1556, 1452; **HRMS** (ESI) *m/z* calculated for $C_{13}H_{15}O_4^+$ $[M+H]^+$ 235.0965, found 235.0973.

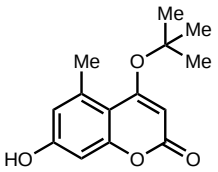

26

4-(*tert*-butoxy)-7-hydroxy-5-methyl-2*H*-chromen-2-one (26). To a solution of 4,7-dihydroxy-5-methyl-*2H*-chromen- 2-one (**82**, 25.0 mg, 0.121 mmol) in *t*-butanol (1.20 mL,

0.10 M) was added H_2SO_4 (0.120 mL, 1.0 M) in a 10 mL cuvette. The reaction was heated at 120 °C for 1 hr in a microwave reactor, rapidly forming a biphasic mixture. The reaction was quenched by the addition of water and extracted with ethyl acetate (3x). The organic layers were combined, washed with brine, dried over Na_2SO_4, and evaporated under reduced pressure to afford a yellow solid. The crude solid was purified over silica gel by flash chromatography (2% to 20% ethyl acetate in dichloromethane), to afford 8.9 mg (28% yield) of coumarin **21** as a glassy yellow film. **^{1}H NMR** (600 MHz, Acetone-d_6) δ 6.60 (d, J = 2.5 Hz, 1H), 6.48 (d, J = 2.4 Hz, 1H), 6.16 (s, 1H), 2.53 (s, 3H), 1.01 (s, 9H). **^{13}C NMR** (150 MHz, Acetone-d_6) δ 191.5, 167.4, 159.6, 159.3, 143.8, 116.1, 108.3, 102.0, 100.6, 67.0, 28.7, 21.9. **HRMS** (ESI) *m/z* calculated for $C_{14}H_{17}O_4^+$ $[M+H]^+$ 249.1121, found 249.1123.

Synthesis of authentic product standards

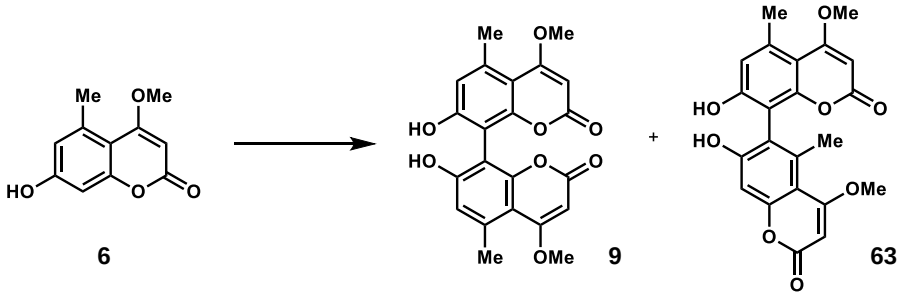

Supplemental Figure S3.1. Chemical dimerization of 7-hydroxy-4-methoxy-5-methyl-*2H*-chromen-2-one (6) to produce racemic product mixtures (9 and 63). To a solution of 7-hydroxy-5-methyl-4-propoxy-*2H*-chromen-2-one (**6**; 51.5 mg, 0.250 mmol, 1.00 equiv) in CH_2Cl_2 (1.0 mL) and trifluoroacetic acid (0.25 mL) was added VOF_3 (124 mg, 0.375 mmol, 1.50 equiv) at 0 °C. The reaction was stirred for 4.0 h. The reaction was quenched with H_2O (2 mL). The aqueous phase was extracted with ethyl acetate (3x). The organic layers were combined, washed with brine, dried over Na_2SO_4, filtered, and evaporated under reduced pressure. The crude solid was purified by flash column chromatography (8:3:1 toluene/ethyl acetate/formic acid v/v) then reverse-phase HPLC (Phenomenex Kinetex 5 µm C18, 150 x 21.2 mm column) under the following conditions: mobile phase A = deionized water + 0.1% formic acid and B = acetonitrile + 0.1% formic acid; method = 75% A for 5.0 min, 75% A to 70% A over 2.0 min, 70% A for 7.0 min, 70%

A to 65% A over 2.0 min, 65% A for 5.0 min, 65% A to 50% A over 3.0 min, 50% A for 1.0 min, 254 and 308 nm UV detection and 14 mL/min flow rate. A retention time of 12.65-14.77 min afforded 7.0 mg of 8,8'-product **9** (14% yield), and a retention time of 18.44-20.07 min afforded 6.6 mg of 6,8'-product **63** (13% yield).

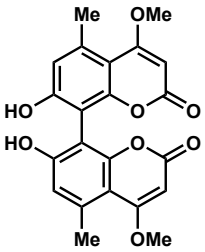

7,7'-dihydroxy-4,4'-dimethoxy-5,5'dimethyl-*2H*,*2H*'-[8,8'-bichromene]-2,2'-dione (9). **^{1}H NMR** (400 MHz, DMSO-d_6) δ 6.69 (s, 2H), 5.55 (s, 2H), 3.94 (s, 6H), 2.59 (s, 6H); **HRMS** (ESI) *m/z* calculated for $C_{22}H_{19}O_8^+$ $[M+H]^+$ 411.1074, found 411.1070. All spectra obtained were agreement with literature values.[84]

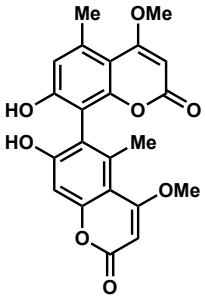

7,7'-dihydroxy-4,4'-dimethoxy-5,5'dimethyl-*2H*,*2H*'-[6,8'-bichromene]-2,2'-dione (63). **^{1}H NMR** (400 MHz, DMSO-d_6) δ 6.70 (s, 1H), 6.68 (s, 1H), 5.63 (s, 1H), 5.57 (s, 1H), 3.93 (s, 6H), 2.58 (s, 3H), 2.23 (s, 3H); **HRMS** (ESI) *m/z* calculated for $C_{22}H_{19}O_8^+$ $[M+H]^+$ 411.1074, found 411.1088. All spectra obtained were in agreement with literature values.[85]

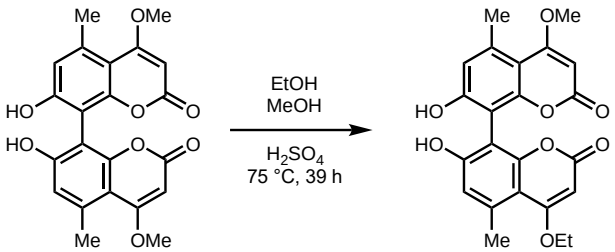

9, AA **32**

Supplemental Figure S3.2. 4-ethoxy-7,7'-dihydroxy-4'methoxy-5,5'-dimethyl-*2H,2H*'-[8,8'-bichromene]-2,2'-dione (32). To a suspension of 7,7'-dihydroxy-4,4'-dimethoxy-5,5'dimethyl-*2H*,*2H*'-[8,8'-bichromene]-2,2'-dione (**9**, 25 mg, 0.061 mmol, 1.000 equiv) in MeOH (5.0 mL) and EtOH (5.0 mL) was added ground 3 Å molecular sieves (100 mg) and H_2SO_4 (500 µL). The reaction was heated at 75 °C and stirred for 38.7 h. The reaction was cooled, diluted with ethyl acetate, and poured into water. The aqueous phase was extracted with ethyl acetate (3x). The organic layers were combined, washed with brine, dried over Na_2SO_4, filtered, and evaporated under reduced pressure. The crude solid was purified by reverse-phase HPLC (Phenomenex Kinetex 5 µm C18, 150 x 21.2 mm column) under the following conditions: mobile phase A = deionized water + 0.1% formic acid and B = acetonitrile + 0.1% formic acid; method = 70% A for 5 min, 70% A to 65% A over 2.0 min, 65% A for 5 min, 65% A to 60% A over 2.0 min, 60% A for 5 min, 60% A to 40% A over 5 min, 40% A for 2 min, 40% A to 10% A over9min, 10% A for 1 min, 254 and 308 nm UV detection and 12 mL/min flow rate. The 8,8'-product, **32**, eluted from 9.8-12.0 min to provide 7 mg of material (27% yield) with minor impurities. **^{1}H NMR** (400 MHz, acetone-d_6) δ 6.77 (s, 2H), 5.50 (s, 1H), 5.45 (s, 1H), 4.25 (q, *J* = 7.0, 2H), 4.02 (s, 3H), 2.68 (s, 3H), 2.64 (s, 3H), 1.54 (t, *J* = 7.0, 3H); **HRMS** (ESI) *m/z* calculated for $C_{23}H_{21}O_8^+$ $[M+H]^+$ 425.1231, 425.1235; **^{13}C NMR** (150 MHz, DMSO-d_6) δ 169.7, 168.7, 161.8, 161.7, 158.7, 158.7, 154.0, 154.0, 137.1, 137.0, 115.7, 115.7, 106.0, 106.0, 105.8, 105.8, 86.6, 86.4, 65.3, 56.5, 23.4, 23.2, 14.0.

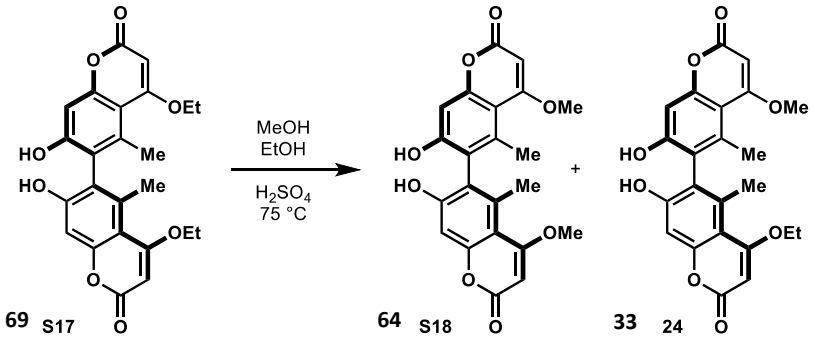

Supplemental Figure S3.3. 4-ethoxy-7,7'-dihydroxy-4'methoxy-5,5'-dimethyl-*2H,2H*'-[8,8'-bichromene]-2,2'-dione (32).7,7'-dihydroxy-4,4'-dimethoxy-5,5'-dimethyl-*2H*,*2H*'-[6,6'-bichromene]-2,2'-dione (64) and 4-ethoxy-7,7'-dihydroxy-4'methoxy-5,5'-dimethyl-*2H,2H*'-[6,6'-bichromene] -2,2'-dione (33). To a suspension of 4,4'-diethoxy-7,7'-dihydroxy-5,5'-dimethyl-*2H, 2H*'-[6,6'-bichromene]-2,2'-dione (**69**, 10 mg, 0.023 mmol, 1.0 equiv) in MeOH (2.5 mL) and EtOH (2.5 mL) was added ground 3 Å molecular sieves (40.0 mg) and H_2SO_4 (250 µL). The reaction was heated at 75 °C for 10.6 h. The reaction was quenched by diluting with ethyl acetate and pouring into water. The aqueous layer was extracted with ethyl acetate (3x), washed with brine, dried over Na_2SO_4, filtered, and evaporated under reduced pressure. The crude solids were purified by reverse-phase (Phenomenex Kinetex 5 µm C18, 150 x 21.2 mm column) under the following conditions: mobile phase A = deionized water + 0.1% formic acid and B = acetonitrile + 0.1% formic acid; method = 70% A for 5 min, 70% A to 65% A over 2.0 min, 65% A for 5.0 min, 65% A to 60% A over 2.0 min, 60% A for 5.0 min, 60% A to 40% A over 5.0 min, 40% A for 2.0 min, 40% A to 10% A over 4.0 min, 10% A for 1.0 min, 254 and 308 nm UV detection and 12 mL/min flow rate. A retention time of 12.05-14.55 min afforded 1.5 mg of 6,6' product **64** (16% yield), and a retention time of 16.57-19.55 afforded 2.0 mg of 6,6' cross-coupled product **33** (20% yield).

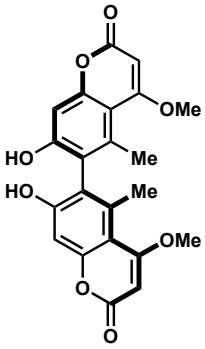

7,7'-dihydroxy-4,4'-dimethoxy-5,5'-dimethyl-*2H*,*2H*'-[6,6'-bichromene]-2,2'-dione (64). **^{1}H NMR** (400 MHz, CD_3OD) δ 6.71 (s, 2H), 5.65 (s, 2H), 3.99 (s, 6H), 2.30 (s, 6H); **HRMS** (ESI) *m/z* calculated for $C_{22}H_{19}O_8^+$ $[M+H]^+$ 411.1074, found 411.0990. All spectra obtained were in agreement with literature values.[86]

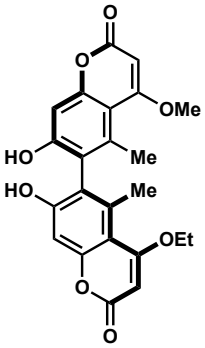

4-ethoxy-7,7'-dihydroxy-4'methoxy-5,5'-dimethyl-*2H,2H*'-[6,6'-bichromene]2,2'-dione (33). **^{1}H NMR** (600 MHz, CD_3OD) δ 6.71 (s, 2H), 5.65 (s, 1H), 5.61 (s, 1H), 4.24 (q, *J* = 7.0, 2H), 3.99 (s, 3H), 2.33 (s, 3H), 2.30 (s, 3H), 1.51 (t, *J* = 7.0, 3H); **^{13}C NMR** (200 MHz, CD_3OD) δ 172.6 171.7, 166.1, 165.9, 160.4, 160.4, 157.4, 157.3, 139.4, 139.3, 124.4, 108.4, 101.6, 101.5, 87.8, 87.5, 66.9, 56.9, 40.4, 19.4, 19.3, 14.5. **HRMS** (ESI) *m/z* calculated for $C_{23}H_{21}O_8^+$ $[M+H]^+$ 425.1231, found 425.1255.

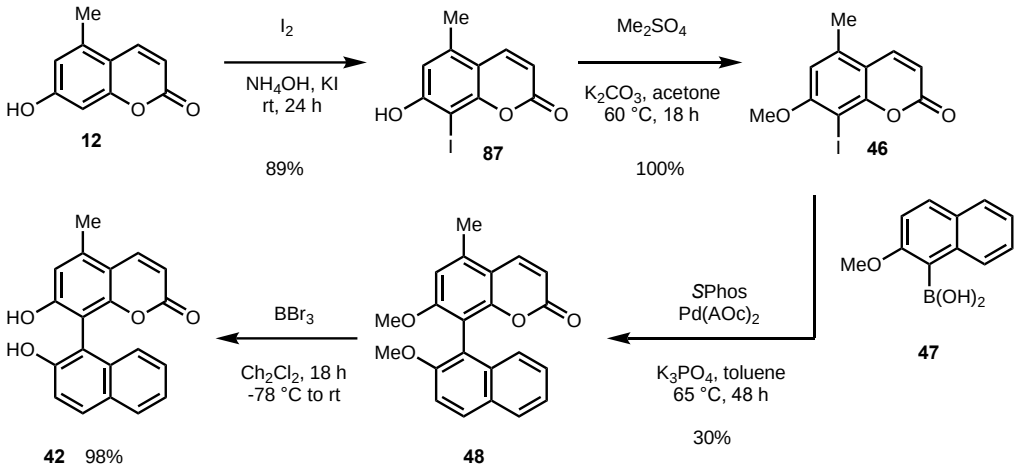

Supplemental Figure S3.4. Synthesis of 8,1'-cross-coupled product **42**.

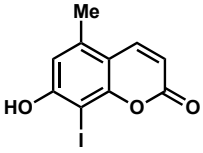

7-hydroxy-8-iodo-5-methyl-2*H*-chromen-2-one (87). Coumarin (**12**; 750 mg, 4.26 mmol, 1.00 equiv) was dissolved in 20% aqueous solution of NH_4OH (17.0 mL, 0.250 M) at room temperature in a round bottom flask open to air. I_2 (1.08 g, 4.26 mmol, 1.000 equiv) was dissolved in an 5.0% KI solution (8.50 mL, 0.125 M), and added dropwise to the reaction flask. The reaction was stirred at rt for 48 h, until complete by TLC. The reaction was acidified to a pH of approximately 2.0 with 6M H_2SO_4, where the product precipitated as an off-white solid. The solid was collected by vacuum filtration and dried under vacuum and carried forward without further purification, 1.15 g, 89% yield. **^{1}H NMR** (600 MHz, DMSO-d_6) δ 11.29 (s, 1H), 8.02 (d, J = 9.7 Hz, 1H), 6.75 (s, 1H), 6.23 (d, J = 9.6 Hz, 1H), 2.41 (s, 3H); **^{13}C NMR** (151 MHz, DMSO-d_6) δ 160.6, 160.2, 155.4, 141.8, 137.9, 113.2, 111.2, 111.1, 71.3, 18.0; **HRMS** (ESI) *m/z* calculated for $C_{10}H_8IO_3^+$ $[M+H]^+$ 302.9513, found 302.9513.[87]

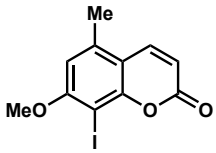

8-iodo-7-methoxy-5-methyl-2*H*-chromen-2-one (46). Iodocoumarin (**87**; 100 mg, 0.33 mmol, 1.0 equiv) and K_2CO_3 (183 mg, 1.32 mmol, 4.00 equiv) were added to a dry 1 dram vial. Dry acetone (0.7 mL, 0.5 M) was added at rt followed by Me_2SO_4 (79 µL, 0.83 mmol,

2.5 equiv). The reaction was heated to reflux and allowed to stir overnight 16 h. The reaction was cooled to rt, and quenched by stirring with dilute HCl (1 mL) for 10 min at rt. The reaction was then extracted with ethyl acetate (20 mL x 3), the extracts were combined, washed with brine, dried over Na_2SO_4, and concentrated to an off-white solid, (104 mg, quantitative yield). The product was carried forward to the next step without further purification. **^{1}H NMR** (600 MHz, $CDCl_3$) δ 7.76 (d, J = 9.7 Hz, 1H), 6.65 (s, 1H), 6.24 (d, J = 9.7 Hz, 1H), 3.97 (s, 3H), 2.51 (s, 3H); **^{13}C NMR** (150 MHz, $CDCl_3$) δ 161.2, 160.7, 155.4, 140.3, 137.9, 113.3, 112.8, 109.3, 73.0, 57.0, 19.0; **HRMS** (ESI) *m/z* calculated for $C_{11}H_{10}IO_3^+$ $[M+H]^+$ 316.9669, found 316.9671.

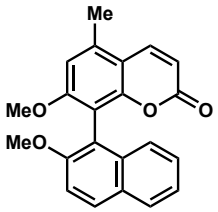

7-methoxy-8-(2-methoxynaphthalen-1-yl)-5-methyl-2*H*-chromen-2-one (48). Coumarin (**46**, 50.0 mg, 0.166 mmol, 1.00 equiv), commercial 2-methoxy-naphthalene-1-boronic acid (**47**; 66.9 mg, 0.331 mmol, 2.00 equiv), K_3PO_4 (105.4 mg, 0.497 mmol, 3.00 equiv), and approximately 5 mg activated 4.1 Å mol sieves were added to a dry round bottom flask. A stock solution of $Pd(OAc)_2$ (1.9 mg, 8.3 µmol, 5 mol %), and *S*-Phos (6.8 mg, 17 mmol, 10 mol %) in dry toluene (2 mL, 0.083 M) was prepared and stirred for 20 min at rt before transferring to the reaction vessel and heating to 110 °C. The reaction was monitored by TLC over 72 h. The reaction was cooled to rt, and passed through a silica plug with 1:1 ethyl acetate: hexanes as eluent, then concentrated to afford a golden solid. The crude material was purified by column chromatography using 0 to 30% ethyl acetate in hexanes. The desired product was recovered as 17 mg of a white glassy solid in a 30% yield. **^{1}H NMR** (800 MHz, acetone-*d*$_6$) δ 8.15 (d, *J* = 9.7 Hz, 1H), 8.00 (d, *J* = 9.0 Hz, 1H), 7.88 (d, *J* = 8.6 Hz, 0H), 7.53 (d, *J* = 9.0 Hz, 1H), 7.31 (qt, *J* = 6.6, 3.3 Hz, 2H), 7.23 (d, *J* = 8.3 Hz, 0H), 7.12 (s, 1H), 6.17 (d, *J* = 9.8 Hz, 1H), 3.83 (s, 3H), 3.75 (s, 3H), 2.68 (s, 3H); **^{13}C NMR** (200 MHz, acetone-*d*$_6$) δ 160.4, 160.0, 155.2, 153.9, 141.0, 137.6, 133.6, 129.7, 129.3, 128.0, 126.2, 124.5, 123.3, 115.5, 114.0, 112.0, 111.9, 110.8, 109.6,

56.0, 55.6, 18.0; **HRMS** (ESI) *m/z* calculated for $C_{22}H_{19}O_4^+$ [M+H]$^+$ 347.1278, found 347.1261.

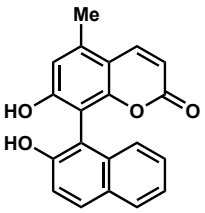

7-hydroxy-8-(2-hydroxynaphthalen-1-yl)-5-methyl-2*H*-chromen-2-one (42). Biaryl (**48**, 17 mg, 49 µmol, 1.0 equiv) was dissolved in dry CH_2Cl_2 (0.5 mL, 0.1 M) in a dry round bottom flask and cooled to –78 °C. A solution of 1 M BBr_3 in CH_2Cl_2 (200 µL, 200 µmol, 4.0 equiv) was added slowly, and the reaction was allowed to warm to room temperature and stir overnight. The reaction was quenched by the addition of water and pH adjusted to approximately 4.1 with aqueous saturated sodium bicarbonate, then extracted with ethyl acetate (10 mL x 3). The extracts were combined, washed with brine, dried over Na_2SO_4, and concentrated to an off-white solid as 15.3 mg of the target compound was isolated without further purification in a 98% yield. **^{1}H NMR** (600 MHz, CD_3OD) δ 8.17 (d, *J* = 9.6 Hz, 1H), 7.80 (t, *J* = 9.1 Hz, 2H), 7.26 (ddd, *J* = 6.9, 4.5, 1.8 Hz, 2H), 7.22 (d, *J* = 8.8 Hz, 1H), 7.21 – 7.16 (m, 1H), 6.88 (s, 1H), 6.18 (d, *J* = 9.6 Hz, 1H), 2.59 (s, 3H); **^{13}C NMR** (150 MHz, CD_3OD) δ 162.9, 159.4, 154.6, 152.8, 142.2, 13735, 134.0, 129.3, 128.8, 127.6, 125.8, 123.7, 122.3, 117.7, 114.2, 111.3, 111.2, 109.9, 108.9, 17.1; **HRMS** (ESI) *m/z* calculated for $C_{20}H_{15}O_4^+$ [M+H]$^+$ 319.0965, found 319.0970.

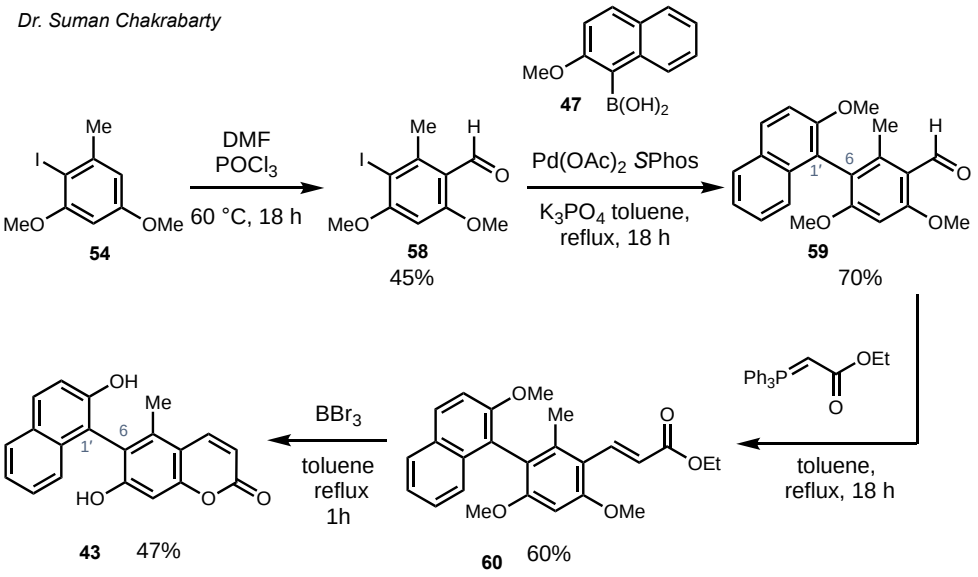

Supplemental Scheme S3.5. Synthesis of 6,1'-cross-coupled product **43**.

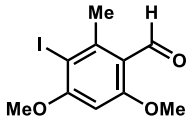

3-iodo-4,6-dimethoxy-2-methylbenzaldehyde (58). To an oven-dried 50 mL round-bottomed flask charged with a stir bar was added dry dimethylformamide (5 mL) under dry nitrogen atmosphere. The reaction mixture was cooled to 0 °C using an ice bath and $POCl_3$ (0.94 mL, 10.1 mmol, 2.00 equiv) was added dropwise. The ice bath was removed, and the resultant mixture was stirred at room temperature for 1 h. Subsequently, a solution of 1,3-dimethoxy-5-methylbenzene (**54**, synthesized via iodination of 3,5-dimethoxytoluene using N-iodosuccinimide; 1.40 g, 5.03 mmol, 1.00 equiv) in dry dimethylformamide (5 mL) was added to the reaction flask and the resultant mixture was stirred at 60 °C for 18 h. Afterwards, the reaction mixture was quenched with the addition of ice, basified to pH 13 using 10 M KOH and stirred at room temperature for 30 min. The reaction mixture was subsequently acidified to pH 2 using 5 M HCl and extracted with ethyl acetate (2 x 20 mL). The combined organic fractions were washed with water (20 mL), brine (20 mL), dried over anhydrous Na_2SO_4 and concentrated in vacuum. Flash chromatography over silica gel (gradient of 5-60% ethyl acetate in hexanes) to afford the desired product **58** (692 mg, 45% yield) as a yellow solid. TLC analysis (30% ethyl acetate in Hexanes) $\mathbf{R_f}$ = 0.5; **^{1}H NMR** (600 MHz, $CDCl_3$) δ 10.34 (1H, s), 6.32 (1H, s), 3.95 (3H,

s), 3.92 (3H, s), 2.78 (3H, s) ppm; **^{13}C NMR** (150 MHz, $CDCl_3$) δ 190.2, 165.3, 162.4, 146.3, 118.4, 92.6, 87.5, 56.6, 55.9, 26.2 ppm; **HRMS (ESI)** $(M+H)^+$ calculated for $C_9H_{12}IO_2^+$ = 306.9826, found = 306.9795 *m/z*.

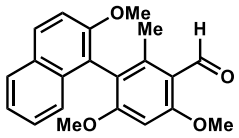

4,6-dimethoxy-3-(2-methoxynaphthalen-1-yl)-2-methylbenzaldehyde (59). To an oven-dried 50 mL round bottomed charged with a stir bar was added aryl iodide **58** (200 mg, 0.65 mmol, 1.0 equiv), 2-methoxy-naphthalene-1-boronic acid (**47**; 198 mg, 0.980 mmol, 1.50 equiv), K_3PO_4 (827 mg, 3.90 mmol, 6.00 equiv), $Pd(OAc)_2$ (29 mg, 0.13 mmol, 0.20 equiv) and *S*-Phos (107 mg, 0.260 mmol, 0.400 equiv). A reflux condenser and a Teflon septa were added and the resultant mixture was subjected to vacuum and then refilled with nitrogen. The degas cycle was carried out for a total of 5 times, following which dry toluene (13 mL) was added and the resultant mixture was stirred at room temperature for 30 min. The mixture was subsequently heated to reflux and was allowed to stir at 110 ˚C for a total of 18 h. Afterwards, the reaction mixture was cooled to room temperature and was quenched by the addition of saturated aqueous NH_4Cl (13 mL) and was extracted with ethyl acetate (2 x 20 mL). The combined organic layers were washed with brine (10 mL) and were concentrated under vacuum. Flash chromatography over silica gel (gradient of 5-70% ethyl acetate in hexanes) afforded the desired product **59** (152 mg, 70% yield) as a waxy solid. TLC (35% ethyl acetate in hexanes) $\mathbf{R_f}$ = 0.5; **^{1}H NMR** (600 MHz, $CDCl_3$) δ 10.66 (s, 1H), 7.90 (d, *J* = 9.0 Hz, 1H), 7.86 – 7.81 (m, 1H), 7.38 (d, *J* = 9.1 Hz, 1H), 7.32 (ddt, *J* = 9.7, 6.7, 3.3 Hz, 2H), 7.25 – 7.19 (m, 1H), 6.51 (s, 1H), 4.00 (s, 3H), 3.83 (s, 3H), 3.69 (s, 3H), 2.20 (s, 3H) ppm; **^{13}C NMR** (150 MHz, $CDCl_3$) δ 191.1, 165.1, 162.9, 154.5, 143.4, 133.6, 129.3, 129.1, 128.1, 126.4, 124.5, 123.5, 119.5, 118.8, 117.3, 113.7, 92.5, 56.7, 55.8, 55.8, 17.7 ppm; **HRMS (ESI)** $(M+H)^+$ calculated for $C_{21}H_{21}O_4^+$ = 337.1434, found = 337.1436 m/z.

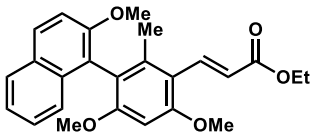

Ethyl (*E*)-3-(4,6-dimethoxy-3-(2-methoxynaphthalen-1-yl)-2-methylphenyl)acrylate (60). A mixture of aldehyde intermediate **59** (152 mg, 0.450 mmol) and Wittig reagent ethyl (triphenylphosphoranylidene)acetate (199 mg, 0.57 mmol, 1.20 equiv) were dissolved in toluene (4.5 mL) and the resultant mixture was refluxed under nitrogen for 18 h. Afterwards, the reaction mixture was concentrated under reduced pressure. Flash chromatography over silica gel (gradient of 5-50% ethyl acetate in hexanes) afforded the desired product **60** (110 mg, 47% yield) as a white solid. TLC (25% ethyl acetate in hexanes) $\mathbf{R_f}$ = 0.5; **^{1}H NMR** (600 MHz, $CDCl_3$) δ 8.00 (d, *J* = 16.1 Hz, 1H), 7.89 (d, *J* = 9.0 Hz, 1H), 7.85 – 7.80 (m, 1H), 7.38 (d, *J* = 8.9 Hz, 1H), 7.31 (m, 3H), 7.22 (dd, *J* = 7.8, 1.8 Hz, 1H), 6.67 (d, *J* = 16.1 Hz, 1H), 6.53 (s, 1H), 4.26 (q, J = 7.1 Hz, 2H), 3.99 (s, 3H), 3.84 (s, 3H), 3.66 (s, 3H), 2.00 (s, 3H), 1.33 (t, *J* = 7.1 Hz, 3H) ppm; **^{13}C NMR** (150 MHz, $CDCl_3$) δ 168.6, 160.4, 159.5, 154.4, 140.8, 139.3, 133.7, 129.1, 127.9, 126.3, 124.7, 123.4, 120.5, 119.7, 117.9, 115.4, 113.8, 93.1, 60.1, 56.7, 55.8, 55.4, 17.6, 14.4 ppm; **HRMS (ESI)** $(M+H)^+$ calculated for $C_{25}H_{27}O_5^+$ = 407.1853, found = 407.1853 m/z.

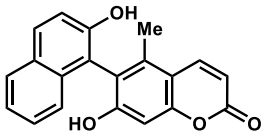

7-hydroxy-6-(2-hydroxynaphthalen-1-yl)-5-methyl-2H-chromen-2-one (43). This transformation was carried out with slight modifications of the original procedure[88] reported by Lavielle and coworkers as follows. To a solution of the intermediate **60** (110 mg, 0.270 mmol, 1.00 equiv) in dry toluene (2.7 mL) under an inert nitrogen atmosphere was added BBr_3 (0.20 mL, 2.2 mmol, 8.0 equiv) dropwise, and the resultant mixture was heated to reflux at 110 °C for 1 h. Afterwards, the reaction mixture was cooled to room temperature and subsequently to 0 °C using an ice bath and was quenched with the slow addition of water (5 mL; caution: significant exotherm noted). The quenched reaction mixture was stirred at room temperature for 30 min and was extracted with ethyl acetate (2 x 20 mL). The combined organic layers were washed with brine, dried over anhydrous

Na_2SO_4 and concentrated under vacuum. Flash chromatography on silica gel (gradient of 5-80% ethyl acetate in hexanes) affords the desired product **43** (40 mg, 47%) as a crystalline white solid: TLC (60% ethyl acetate in hexanes) $\mathbf{R_f}$ = 0.5; **^{1}H NMR** (600 MHz, $CDCl_3$) δ 7.93 (m, 2H), 7.90–7.85 (m, 1H), 7.40 (m, 2H), 7.34 (d, *J* = 8.9 Hz, 1H), 7.19 – 7.13 (m, 1H), 6.95 (s, 1H), 6.28 (d, *J* = 9.7 Hz, 1H), 5.53 (s, 1H), 5.32 (s, 1H), 2.15 (s, 3H) ppm; **^{13}C NMR** (150 MHz, $CDCl_3$) δ 161.2, 157.8, 156.6, 152.6, 140.9, 138.6, 132.85, 131.8, 129.4, 128.6, 127.9, 124.3, 123.3, 118.0, 117.1, 112.8, 112.5, 110.7, 101.9, 15.8 ppm; **HRMS (ESI)** $(M+H)^+$ calculated for $C_{20}H_{15}O_4^+$ = 319.0965, found = 319.0969 *m/z*.

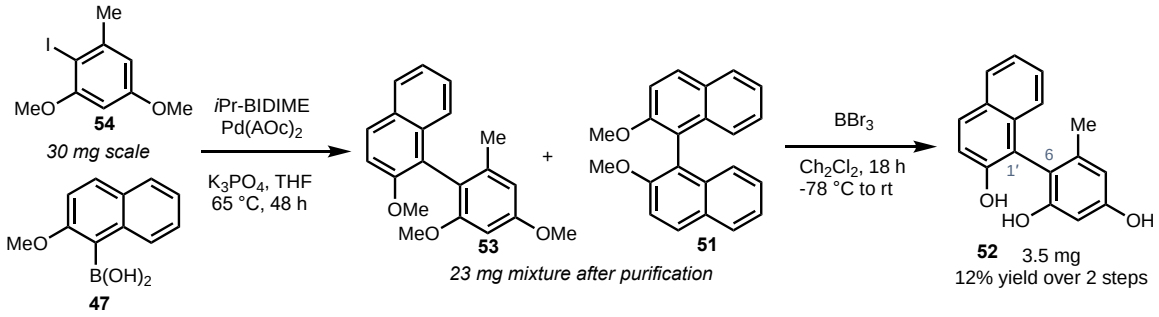

Supplemental Figure S3.3.6. Synthesis of 3,1'-cross-coupled product **52**.

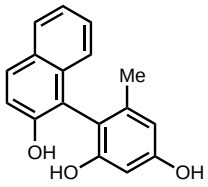

4-(2-hydroxynaphthalen-1-yl)-5-methylbenzene-1,3-diol (**52**): To a solution **54** (30.0 mg, 108 µmol, 1.0 equiv), boronic acid (**47**; 65.0 mg, 0.324 mmol, 3.0 equiv), K_3PO_4 (68.6 mg, 0.324, 3.0 equiv), $Pd(OAc)_2$ (5.0 mg, 22 µmol, 0.2 equiv), and iPr-BIDIME ((2R,3R)-3-(tert-butyl)-4-(2,6-dimethoxyphenyl)-2-isopropyl-2,3-dihydrobenzo[d][1,3]oxaphosphole, CAS#1477517-19-3, Strem Chemicals, 16.3 mg, 44 µmol, 0.40 equiv) were added to a dry round bottom flask. Dry THF (4.30 mL, 0.025 M) was added, and the reaction was heated to 65 °C for 48 h. The reaction was cooled, quenched with 1 M NaOH, and extracted with CH_2Cl_2 (10 mL x 3). The combined extracts were washed with brine, dried over Na_2SO_4, and concentrated to afford a brown solid. The crude material was purified by flash chromatography over silica gel with a gradient of 5 to 30% ethyl

acetate in hexanes, resulting in isolation of 23.1 mg of a mixture of **53** and **51**. The mixture was subjected to BBr_3 deprotection by dissolving in CH_2Cl_2, cooling to -78 °C, then BBr_3 (75.0 µL, 0.299 mmol, approximately 4.0 equiv) was added dropwise, and the reaction mixture was allowed to warm to rt and stirred for 18 h. The reaction was quenched by cooling to 0 °C, then adding water and stirring for 10 minutes. The pH was adjusted to approximately 4.0 by addition of aqueous saturated sodium bicarbonate, and extracted with ethyl acetate (10 mL x 3). The extracts were combined, washed with brine, dried over Na_2SO_4, and concentrated to a dark brown solid. The crude material was purified flash chromatography over silica gel 0 to 40% ethyl acetate in hexanes to recover 3.5 mg biaryl **52** as an off-white solid in a 12% yield over two steps.**^{1}H NMR** (400 MHz, Chloroform-*d*) δ 7.89 (d, *J* = 8.9 Hz, 1H), 7.87–7.82 (m, 1H), 7.43–7.34 (m, 2H), 7.31 (d, *J* = 9.0 Hz, 1H), 7.28 (s, 1H), 6.56–6.45 (m, 2H), 5.17 (s, 1H), 4.95 (s, 1H), 4.69 (s, 1H), 1.91 (s, 3H).

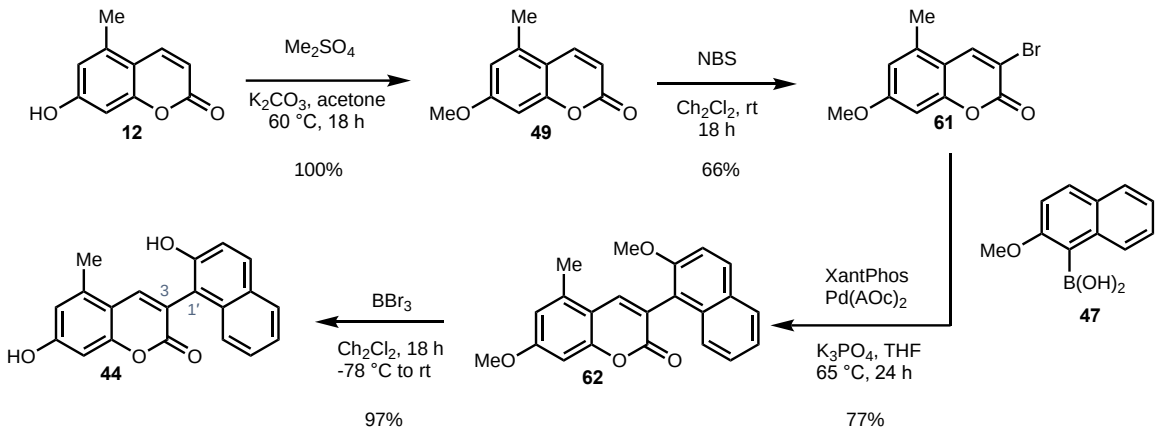

Supplemental Figure S3.7. Synthesis of 3,1'-cross-coupled product **44**.

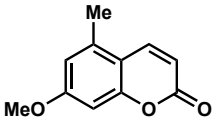

7-methoxy-5-methyl-2*H*-chromen-2-one (49):

Coumarin (**12**, 100 mg, 0.5676 mmol, 1.0 equiv) and K_2CO_3 (314 mg, 2.2705 mmol, 4.0 equiv) were added to a round bottom flask. Dry acetone (2 mL, 0.5M) was added at rt followed by Me_2SO_4 (135 µL, 1.4191 mmol, 2.5 equiv). The reaction was heated to 50 °C and allowed to stir overnight 16 h. The reaction was cooled to rt and quenched by stirring with 1 mL 1.0M NaOH for 10 minutes at rt. The reaction was then extracted with EtOAc

(10 mL x 3), extracts combined, washed with brine, dried over Na_2SO_4, and concentrated to a white solid, (110 mg, quantitative yield). Carried forward without further purification. **^{1}H NMR** (600 MHz, Chloroform-*d*) δ 7.82 (d, J = 9.7 Hz, 1H), 6.70 – 6.61 (m, 2H), 6.24 (d, J = 9.7 Hz, 1H), 3.84 (s, 3H), 2.47 (s, 3H).**^{13}C NMR** (151 MHz, Chloroform-*d*) δ 162.50, 161.47, 156.66, 140.61, 137.40, 114.08, 112.43, 111.71, 98.77, 55.76, 18.62., **HRMS** (ESI) *m/z* calculated for $C_{11}H_{11}O_3^+$ $[M+H]^+$ 191.0703, found 191.0705.

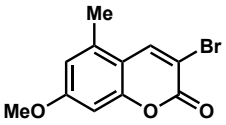

3-bromo-7-methoxy-5-methyl-2*H*-chromen-2-one (61). Coumarin (**49**, 92 mg, 0.48 mmol, 1.0 equiv; see page S10 for synthesis) was added to a round bottom flask and dissolved in dry CH_2Cl_2 (1.4 mL, 0.35 M). NBS (130 mg, 0.73 mmol, 1.5 equiv) added at room temperature under a stream of nitrogen and allowed to stir at room temperature overnight. The reaction was quenched with water and extracted with ethyl acetate (10 mL x 3). The extracts were combined, washed with brine, dried over Na_2SO_4, and concentrated to provide an off-white solid. The crude material was purified by flash chromatography over silica gel with a gradient of 0 to 40% ethyl acetate in hexanes. 86 mg of the desired compound was recovered as white solid in a 66% yield. **^{1}H NMR** (600 MHz, $CDCl_3$) δ 8.18 (s, 1H), 6.71 (s, 1H), 6.67 (s, 1H), 3.85 (s, 3H), 2.47 (s, 3H); **^{13}C NMR** (151 MHz, $CDCl_3$) δ 162.8, 157.7, 155.9, 142.0, 136.9, 114.7, 110.2, 107.3, 98.7, 55.9, 18.7; **HRMS** (ESI) *m/z* calculated for $C_{11}H_{10}BrO_3^+$ $[M+H]^+$ 268.9808, found 268.9811.

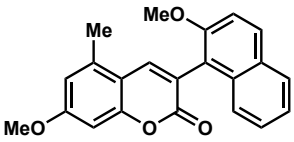

7-methoxy-3-(2-methoxynaphthalen-1-yl)-5-methyl-2*H*-chromen-2-one (62). Coumarin **61** (15 mg, 56 µmol, 1.0 equiv), boronic acid (**47**; 17 mg, 0.84 mmol, 1.5 equiv), K_3PO_4 (36 mg, 0.17, 3.0 equiv), $Pd(OAc)_2$ (2.5 mg, 11 µmol, 0.2 equiv), and XantPhos (4,5-Bis(diphenylphosphino)-9,9-dimethylxanthene, CAS# 161265-03-8, 13 mg, 22 µmol, 0.40 equiv) were added to a dry round bottom flask. Dry THF (2.2 mL, 0.025 M) was added, and the reaction was heated to 65 °C for 18 h. The reaction was cooled, quenched

with 1 M NaOH, and extracted with CH_2Cl_2 (10 mL x 3). The combined extracts were washed with brine, dried over Na_2SO_4, and concentrated to afford a reddish-brown solid. The crude material was purified by flash chromatography over silica gel with a gradient of 5 to 30% ethyl acetate in hexanes, resulting in isolation of 14.8 mg of the target compound as a white solid in a 77% yield. **^{1}H NMR** (600 MHz, $CDCl_3$) δ 7.93 (d, J = 9.0 Hz, 1H), 7.84 (d, J = 7.5 Hz, 2H), 7.67 (d, J = 8.5 Hz, 1H), 7.42 (ddd, J = 8.4, 6.7, 1.4 Hz, 1H), 7.39 – 7.34 (m, 2H), 6.79 (d, J = 2.4 Hz, 1H), 6.73 (d, J = 2.6 Hz, 1H), 3.93 (s, 3H), 3.89 (s, 3H), 2.45 (s, 3H); **^{13}C NMR** (151 MHz, $CDCl_3$) δ 162.3, 160.9, 156.5, 155.1, 141.3, 137.3, 133.4, 130.6, 129.3, 128.4, 127.1, 124.1, 123.8, 120.35, 118.4, 114.0, 113.6, 112.4, 98.6, 56.9, 55.8, 18.8; **HRMS** (ESI) *m/z* calculated for $C_{22}H_{19}O_4^+$ $[M+H]^+$ 347.1278, found 347.1284.

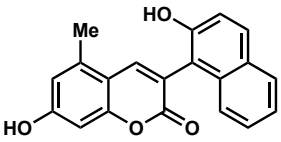

7-hydroxy-3-(2-hydroxynaphthalen-1-yl)-5-methyl-2*H*-chromen-2-one (44). Biaryl (**62**; 28 mg, 81 µmol, 1.0 equiv) was dissolved in dry CH_2Cl_2 (1.6 mL, 0.05 M) in a dry round bottom flask and cooled to –78 °C. BBr_3 (31 µL, 0.32 mmol, 4.0 equiv) was added dropwise, and the reaction mixture was allowed to warm to rt and stirred for 18 h. The reaction was quenched by cooling to 0 °C, then adding water and stirring for 10 minutes. The pH was adjusted to approximately 4.1 by addition of aqueous saturated sodium bicarbonate, and extracted with ethyl acetate (10 mL x 3). The extracts were combined, washed with brine, dried over Na_2SO_4, and concentrated to a brown solid. The crude material was purified flash chromatography over silica gel 7 to 60% ethyl acetate in hexanes to recover 25 mg biaryl **36** as a white solid in a 97% yield. **^{1}H NMR** (600 MHz, acetone-d_6) δ 8.91 (s, 2H), 8.00 (s, 1H), 7.87–7.82 (m, 2H), 7.60 (dd, J = 8.5, 1.1 Hz, 1H), 7.38 (ddd, J = 8.3, 6.7, 1.3 Hz, 1H), 7.31 (ddd, J = 8.0, 6.7, 1.2 Hz, 1H), 7.27 (d, J = 8.9 Hz, 1H), 6.77 (dd, J = 2.3, 1.0 Hz, 1H), 6.70 (d, J = 2.3 Hz, 1H), 2.50 (s, 3H). **^{13}C NMR** (150 MHz, acetone-d_6) δ 161.5, 160.8, 157.6, 153.8, 143.0, 139.2, 134.9, 130.7, 129.6, 128.9, 127.3, 125.0, 123.8, 120.0, 119.3, 116.7, 115.1, 112.5, 101.2, 18.6; **HRMS** (ESI) *m/z* calculated for $C_{20}H_{13}O_4^-$ $[M-H]^-$ 317.0819, found 317.0824.

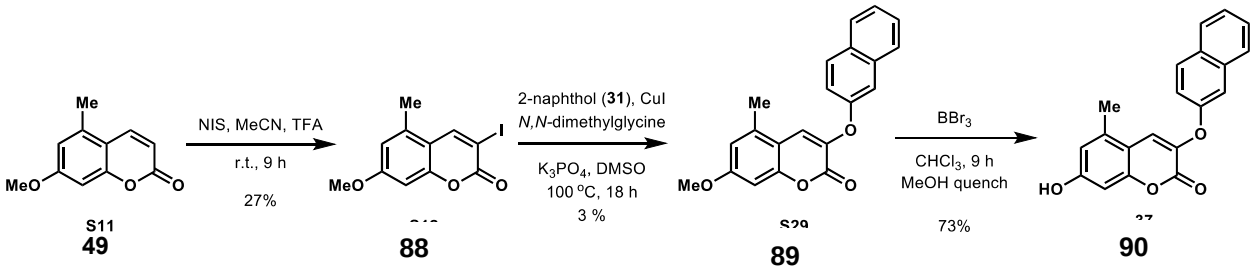

Supplemental Scheme S3.8. Synthesis of C–O cross-coupling product **37**.

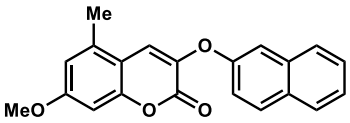

7-methoxy-5-methyl-3-(naphthalen-2-yloxy)-2H-chromen-2-one (89). The aryl iodide phenol coupling was carried out according to conditions previously reported by Maiti and Buchwald[89] as follows. To an oven-dried round bottomed flask charged with a stir bar was added iodide **88** (86 mg, 0.27 mmol, 1.00 equiv), 2-naphthol (**31**, 47 mg, 0.32 mmol, 1.2 equiv), copper iodide (10 mg, 20 mol %), *N,N*-dimethylglycine (11 mg, 40 mol %), dry K_3PO_4 (172 mg, 0.810 mmol, 3.00 equiv) and dry DMSO (1 mL). The resultant mixture was subjected to vacuum and back filled with nitrogen for a total of 3 times. The reaction mixture was heated to 100 ˚C for 18 h. Afterwards, the reaction mixture was cooled to room temperature, a saturated solution of NH_4Cl (20 mL) was added to the reaction mixture, and the resultant mixture was extracted with ethyl acetate (20 mL x 3). The combined organic extracts were washed with brine (20 mL), dried over Na_2SO_4 and concentrated in vacuum. Flash chromatography over silica gel (gradient of 5-40% ethyl acetate in hexanes) afforded the C–O cross-coupling product **89** (3.0 mg, 3.3% yield) as a white solid: TLC (20% ethyl acetate in hexanes) $\mathbf{R_f}$ = 0.5; **^{1}H NMR** (600 MHz, $CDCl_3$) δ 7.89 (d, J = 8.9 Hz, 1H), 7.86 (dd, J = 8.3, 1.3 Hz, 1H), 7.77 – 7.74 (m, 1H), 7.50 (ddd, J = 8.2, 6.8, 1.4 Hz, 1H), 7.45 (ddd, J = 8.1, 6.8, 1.3 Hz, 1H), 7.43 (s, 1H), 7.40 (d, J = 2.5 Hz, 1H), 7.35 (dd, J = 8.9, 2.5 Hz, 1H), 6.79 – 6.73 (m, 2H), 3.88 (s, 3H), 2.38 (s, 3H); **^{13}C NMR** (150 MHz, $CDCl_3$) δ 161.2, 157.8, 153.9, 153.5, 138.9, 136.6, 134.2, 130.6, 130.3, 127.8, 127.3, 126.8, 125.1, 123.2, 118.9, 114.4, 113.3, 111.3, 98.6, 55.7, 18.7; **HRMS (ESI)** $(M+H)^+$ calculated for $C_{21}H_{17}O_4^+$ = 333.1121, found = 333.1122 *m/z*.

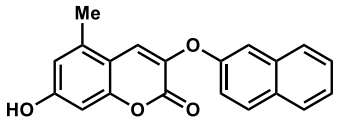

7-hydroxy-5-methyl-3-(naphthalen-2-yloxy)-2H-chromen-2-one (90). To a solution of intermediate **89** (3 mg, 9 µmol, 1 equiv) in dry CH_2Cl_2 (1 mL) at -78 ˚C was added BBr_3 (1 M solution in CH_2Cl_2; 0.45 mL, 50.0 equiv). The resultant mixture was stirred at room temperature overnight. Afterwards, the reaction mixture was carefully quenched with dry methanol, and the resultant mixture was concentrated under vacuum. The crude mixture was dissolved in dry methanol (1 mL) and the mixture was concentrated to dryness under vacuum. This process was repeated a total of 5 times to azeotropically remove $B(OMe)_3$. Afterwards, the crude mixture was dried overnight under vacuum to afford the deprotected C–O cross-coupling product **90** (2.1 mg, 73% yield) as a white solid: TLC (30% ethyl acetate in hexanes) $\mathbf{R_f}$ = 0.5; **^{1}H NMR** (800 MHz, DMSO-*d_6*) δ 10.45 (s, 1H), 8.19 (d, J = 8.5 Hz, 1H), 8.00 (d, J = 7.9 Hz, 1H), 7.96 (d, J = 9.0 Hz, 1H), 7.92 (s, 1H), 7.72 (ddd, J = 8.3, 6.8, 1.3 Hz, 1H), 7.56 (ddd, J = 8.0, 6.7, 1.1 Hz, 1H), 7.42 (d, J = 9.0 Hz, 1H), 6.71 (d, J = 2.3 Hz, 1H), 6.66 (d, J = 2.4 Hz, 1H), 2.39 (s, 3H); **^{13}C NMR** (200 MHz, DMSO-*d_6*) δ 160.4, 157.3, 154.2, 151.8, 138.3, 136.1, 132.7, 131.1, 129.86, 129.0, 128.9, 127.6, 126.1, 126.0, 117.6, 115.2, 110.3, 109.0, 100.6, 18.7; **HRMS (ESI)** calculated for $C_{20}H_{13}O_4^-$ = 713.0819, found = 317.0822 *m/z*.

<u>Analytical-scale generation of cross-coupled product standards by transesterification</u>

To determine the site-selectivity of selected KtnC-catalyzed cross-coupling reactions, standards were prepared by transesterification of dimers with known connectivity. Subjecting dimers containing a labile vinylogous methyl ester to a given alcohol in the presence of acid and heat created a statistical mixture of compounds that could be used on analytical scale with analysis by LC-MS without the need for isolation of individual species. This strategy allowed rapid access to standards with known connectivity for comparison to KtnC cross-coupled reactions, which is particularly attractive for generation of 6,6'-cross-coupled coumarin scaffolds which were synthetically intractable.

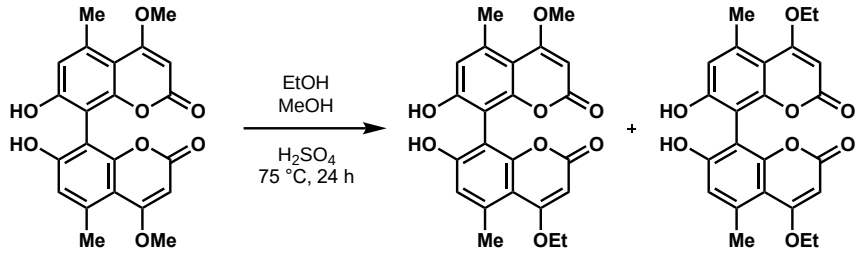

9, AA **32, AB** **68, BB**

Supplemental Scheme S3.9. 4,4-ethoxy-7,7'-dihydroxy-4'methoxy-5,5'-dimethyl-*2H,2H*'-[8,8'-bichromene]2,2'-dione (32). To an authentic standard of 7,7'-dihydroxy-4,4'-dimethoxy-5,5'-dimethyl-2*H*,2'*H*-[8,8'-bichromene]-2,2'-dione **9** (2.5 mg, 5.9 µmol, 1.0 equiv) was added methanol (200 µL, 29.4 µM), ethanol (200 µL, 29.4 µM), and concentrated H_2SO_4 (11 µL, 0.54 mM) in a 1-dram vial with stir bar. The vial was sealed and heated to 75 °C and monitored by LC-MS over 24 h. The crude mixture was used as an analytical standard. **HRMS** (ESI) calculated for $C_{23}H_{21}O_8^+$ $[M+H]^+$ = 425.1231, found = 425.1251 *m/z*.

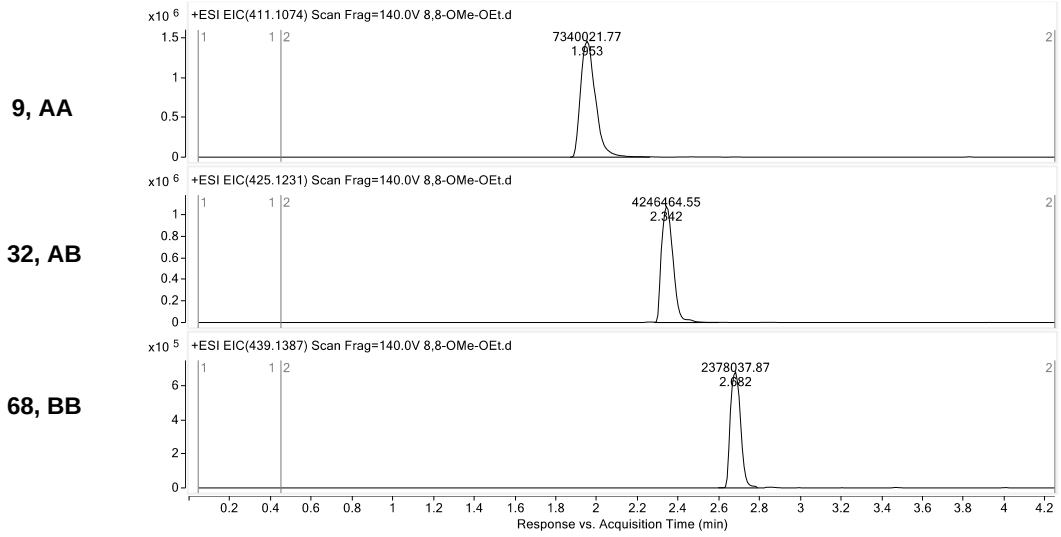

Supplemental Figure S3.10. Extracted ion chromatograms (EICs) of products with 8,8'-connectivity.

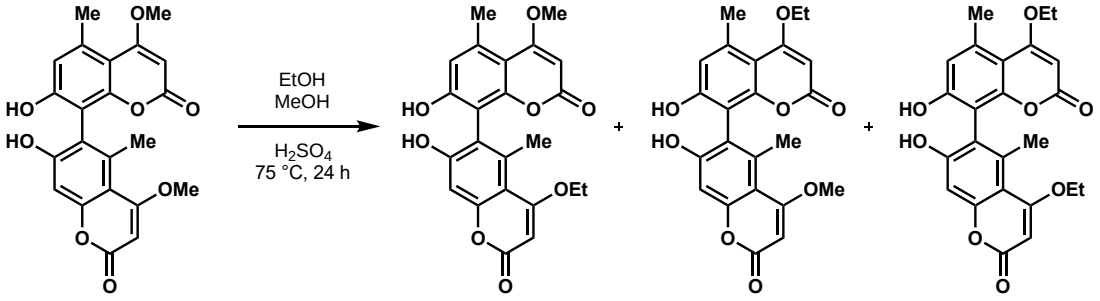

AA (**63**) AB (**91**) AB' (**92**) BB (**93**)

Supplemental Scheme S3.11. 4-ethoxy-7,7'-dihydroxy-4'-methoxy-5,5'-dimethyl-*2H,2H*'-[6,8'-bichromene]-2,2'-dione (91). To an authentic standard of 7,7'-dihydroxy-4,4'-dimethoxy-5,5'-dimethyl-2*H*,2'*H*-[6,8'-bichromene]-2,2'-dione **63** (0.95 mg, 0.22 µmol, 1.00 equiv) was added methanol (100 µL, 2.20 µM), ethanol (100 µL, 2.20 µM), and concentrated H_2SO_4 (6.0 µL, 0.037 mM) in a 1-dram vial with stir bar. The vial was sealed and heated to 75 °C and monitored by LC-MS over 24 h. The crude mixture was used as an analytical standard. **HRMS** (ESI) calculated for $C_{23}H_{21}O_8^+$ $[M+H]^+$ = 425.1231, found = 425.1227 *m/z*.

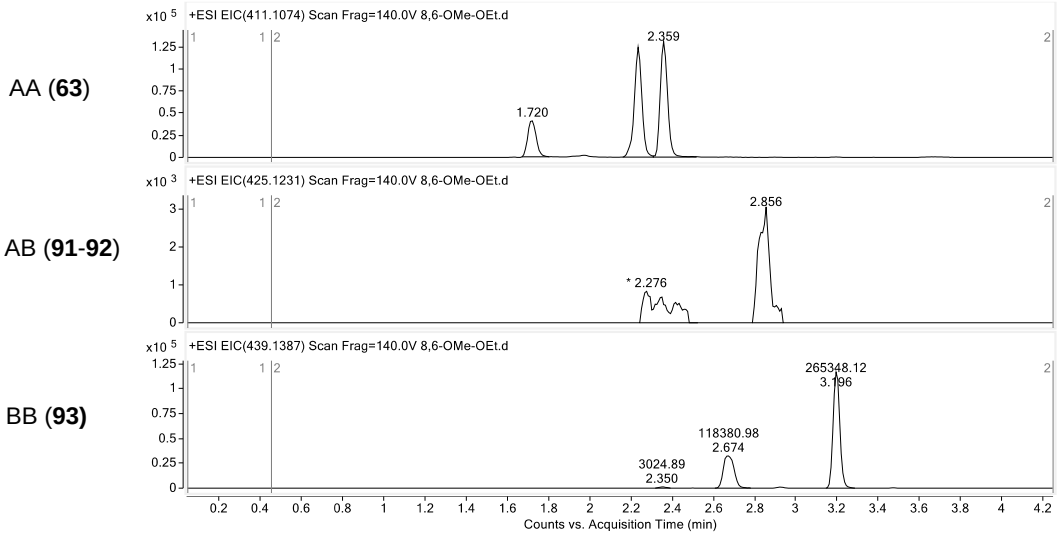

Supplemental Figure S3.12 Extracted ion chromatograms (EICs) of products with 8,6'- and 6,8'-connectivity.

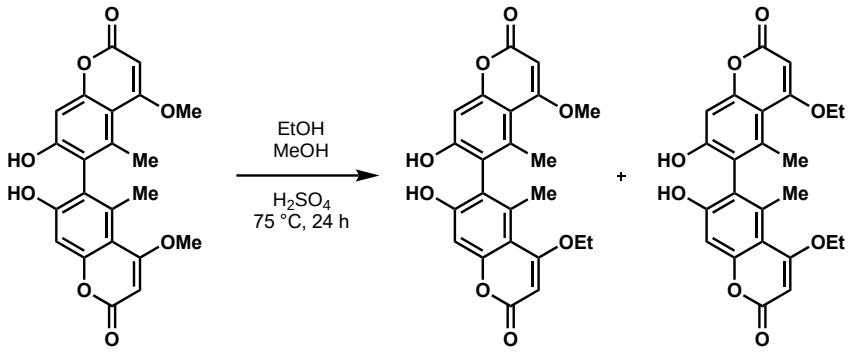

Supplemental Figure S3.13. 4-ethoxy-7,7'-dihydroxy-4'methoxy-5,5'-dimethyl-*2H,2H*'-[6,6'-bichromene]2,2'-dione (33). To an authentic standard of 7,7'-dihydroxy-4,4'-dimethoxy-5,5'-dimethyl-2*H*,2'*H*-[6,6'-bichromene]-2,2'-dione **64** (0.95 mg, 0.22 µmol, 1.0 equiv) was added methanol (100 µL, 2.2 µM), ethanol (100 µL, 2.2 µM), and concentrated H_2SO_4 (6.0 µL, 37 µM) in a 1 dram vial with stir bar. The vial was sealed and heated to 75 °C and monitored by LC-MS over 24 h. The crude mixture was used as an analytical standard. **HRMS** (ESI) calculated for $C_{23}H_{21}O_8^+$ $[M+H]^+$ = 425.1231, found = 425.1251 *m/z*.

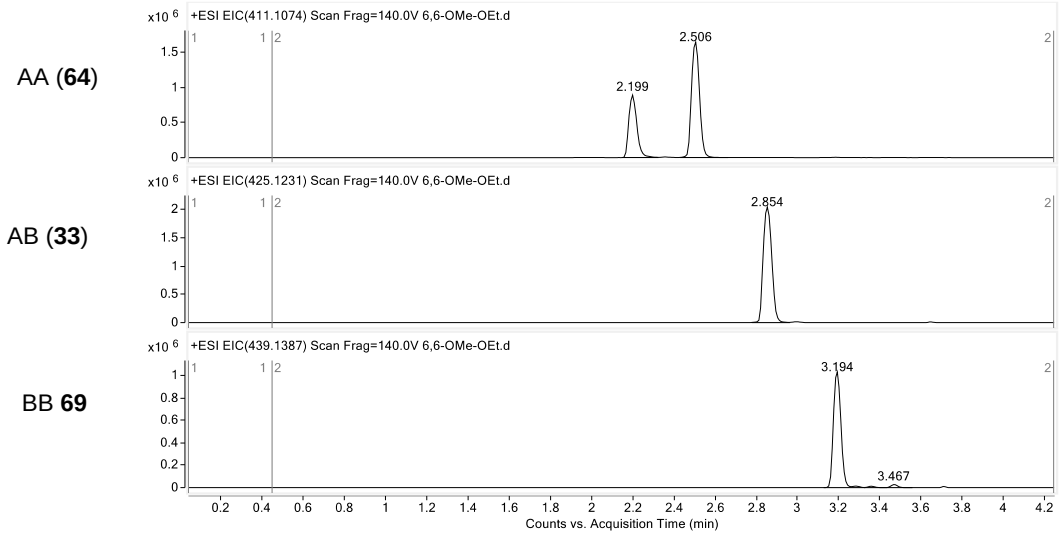

Supplemental Figure S3.14. Extracted ion chromatograms (EICs) of cross-coupled products with 6,6'-connectivity.

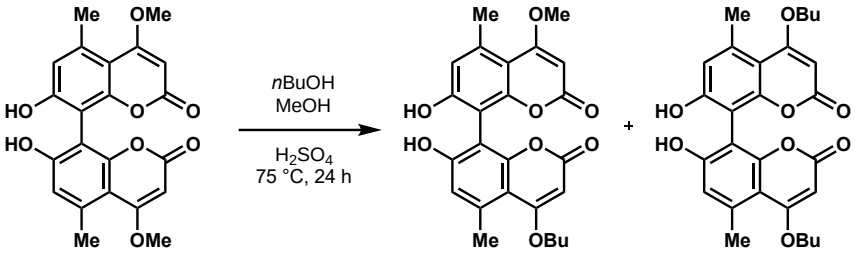

AA (**9**) AB (**34**) BB (**94**)

Supplemental Figure S3.15. 4-butoxy-7,7'-dihydroxy-4'methoxy-5,5'-dimethyl-*2H,2H*'-[8,8'-bichromene]2,2'-dione (34). To an authentic standard of 7,7'-dihydroxy-4,4'-dimethoxy-5,5'-dimethyl-2*H*,2'*H*-[8,8'-bichromene]-2,2'-dione **9** (2.5 mg, 5.5 µmol, 1.0 equiv) was added n-butanol (200 µL, 28.0 µM), *n*-butanol (200 µL, 28.0 µM), and concentrated H_2SO_4 (11 µL, 0.5 mM) in a 1 dram vial with stir bar. The vial was sealed and heated to 75 °C and monitored by LC-MS over 24 h. The crude mixture was used as an analytical standard. **HRMS** (ESI) calculated for $C_{25}H_{25}O_8^+$ $[M+H]^+$ = 453.1544, found = 453.1570 *m/z.*

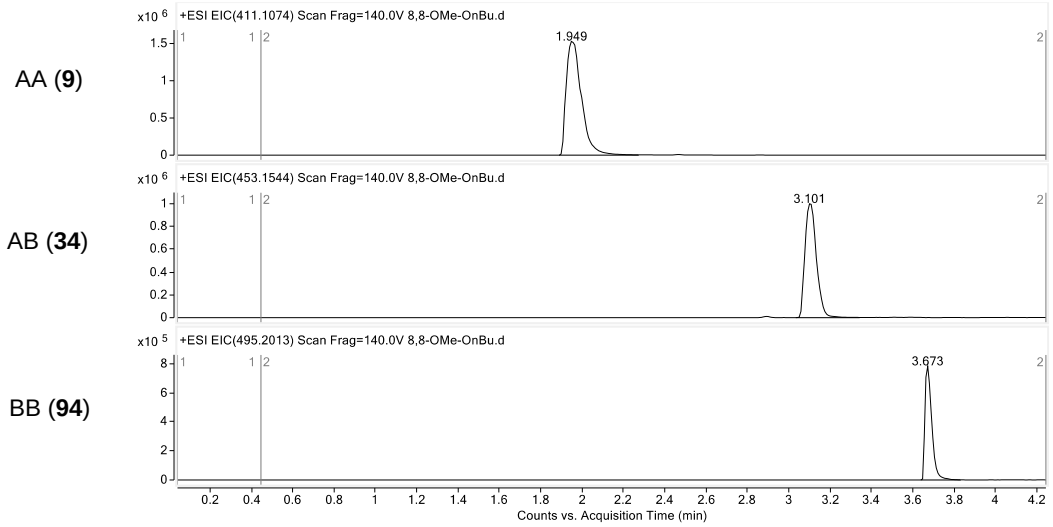

Supplemental Figure S3.16. Extracted ion chromatograms (EICs) of cross-coupled products with 8,8'-connectivity.

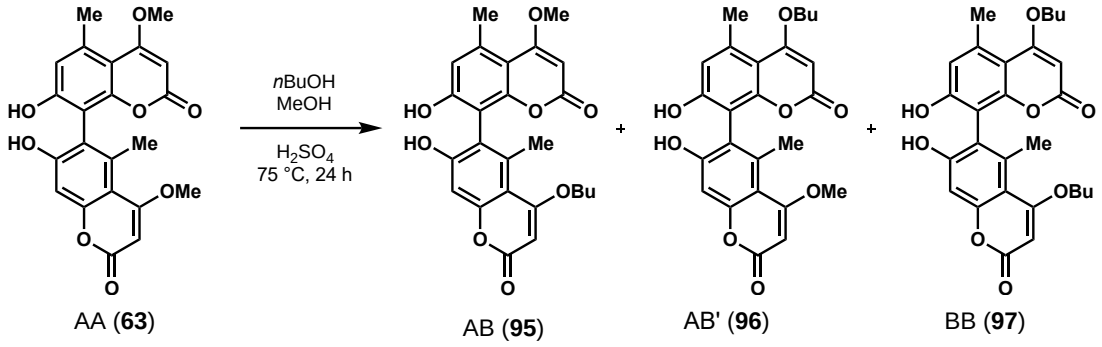

Supplemental Figure S3.17. 4-butoxy-7,7'-dihydroxy-4'-methoxy-5,5'-dimethyl-*2H,2H*'-[6,8'-bichromene]2,2'-dione (95). To an authentic standard of 7,7'-dihydroxy-4,4'-dimethoxy-5,5'-dimethyl-2*H*,2'*H*-[6,8'-bichromene]-2,2'-dione **63** (0.95 mg, 2.1 µmol, 1.0 equiv) was added methanol (100 µL, 21.0 µM), *n*-butanol (100 µL, 21.0 µM), and concentrated H_2SO_4 (6.0 µL, 0.35 mM) in a 1 dram vial with a stir bar. The vial was sealed and heated to 75 °C and monitored by LC-MS over 24 h. The crude mixture was used as an analytical standard. **HRMS** (ESI) calculated for $C_{25}H_{25}O_8^+$ $[M+H]^+$ = 453.1544, found = 453.3457 *m/z.*

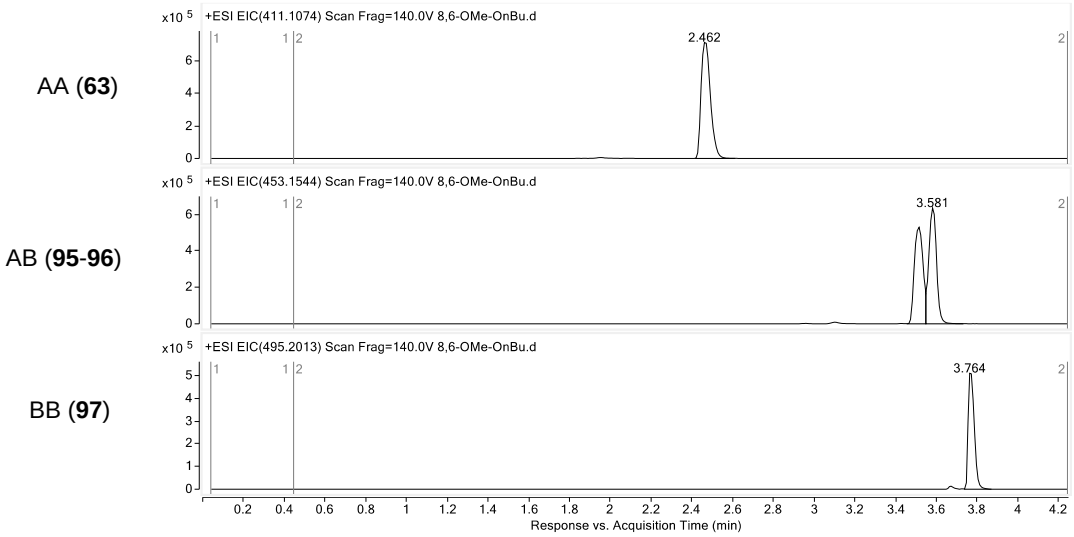

Supplemental Figure S3.18. Extracted ion chromatograms (EICs) of products with 8,6'- and 6,8'-connectivity.

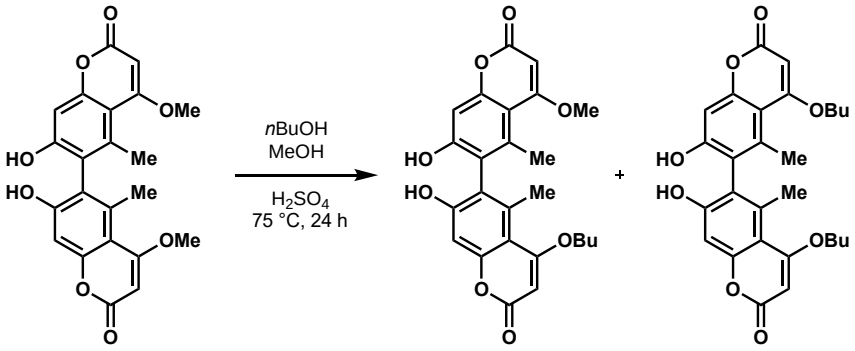

Supplemental Figure S3.19. 4-butoxy-7,7'-dihydroxy-4'methoxy-5,5'-dimethyl-*2H,2H*'-[6,6'-bichromene]-2,2'-dione (35). To an authentic standard of 7,7'-dihydroxy-4,4'-dimethoxy-5,5'-dimethyl-2*H*,2'*H*-[6,6'-bichromene]-2,2'-dione (**64**; 0.95 mg, 2.1 µmol, 1.0 equiv) was added methanol (100 µL, 21 µM), *n*-butanol (100 µL, 21.0 µM), and concentrated H_2SO_4 (6.0 µL, 0.35 mM) in a 1 dram vial with stir bar. The vial was sealed and heated to 75 °C and monitored by LC-MS over 24 h. The crude mixture was used as an analytical standard. **HRMS** (ESI) calculated for $C_{25}H_{25}O_8^+$ $[M+H]^+$ = 453.1544, found = 453.1567 *m/z.*

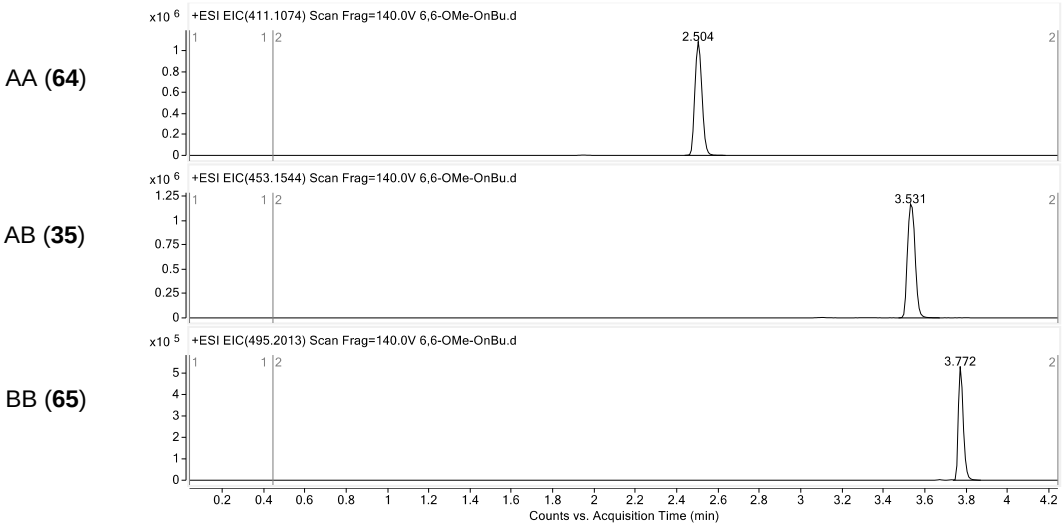

Supplemental Figure S3.20. Extracted ion chromatograms (EICs) of cross-coupled products with 6,6'-connectivity.

Chemical methods for oxidative cross-coupling

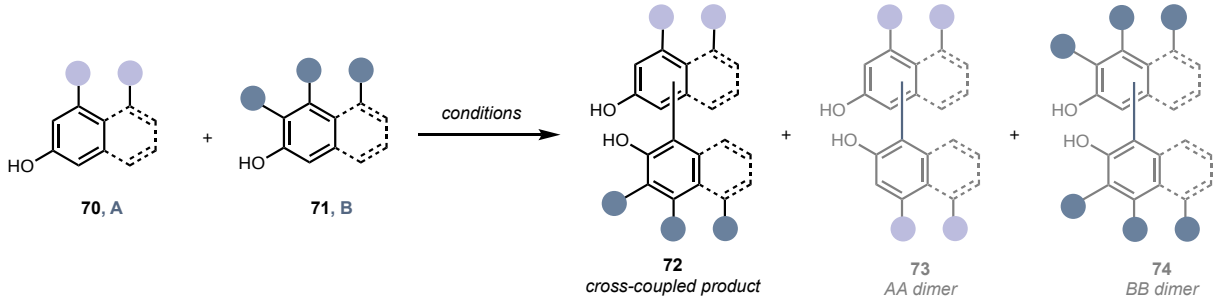

Entry	Phenols	(A) Cu(OH)Cl•TMEDA	(B) VOF_3	(C) $FeCl_3$	(D) Fe(TPP)Cl	(E) Cr-Salen-Cy
1	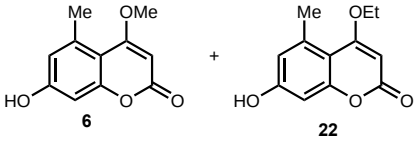	5% [a]	23% [a]	trace	trace	0%
2	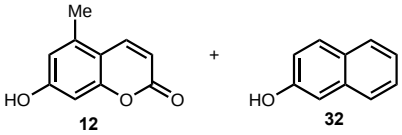	19% [b]	trace	0%	decomposition	trace
3	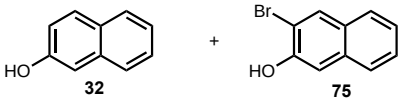	23%	5% [b]	6% [b]	decomposition	5%

Supplemental Figure S3.21. Experimental data for Figure 3.19. Oxidative cross-coupling reactions of different classes of phenols were benchmarked with transition metal catalysts.[90-97] Representative examples of coumarin–coumarin, coumarin–naphthol, and naphthol–naphthol cross-coupling reactions are included. Percent yields for isolated cross-coupled products are reported. [a]Relative percent conversion calculated by LC-MS. [b]Percent yield calculated by NMR. All reactions were screened on analytical scale and monitored by LC-MS to optimize conditions and determine general reactivity. LC-MS traces (Supplemental Figures S3.15-S3.29) detail the extracted ion chromatograms of the remaining starting materials, dimerized, and cross-coupled products formed in the reaction. Reactions that showed relative conversions of >5% to cross-coupled products were selected for further investigation.

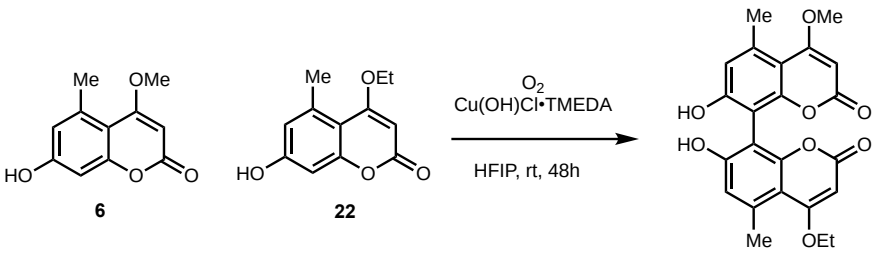

Entry 1a. To a solution of 7-hydroxy-4-methoxy-5-methyl-*2H*-chromen-2-one (**6**; 100 mg, 0.481 mmol, 1.00 equiv) and 4-ethoxy-7-hydroxy-5-methyl-2*H*-chromen-2-one (**22**; 107 mg, 0.481 mmol, 1.00 equiv) in hexafluoro-2-propanol (4.81 mL, 0.1 M) was added Di-μ-hydroxo-bis[(*N,N,N′,N′*-tetramethylethylenediamine)copper(II)] chloride, CAS# 30698-64-7, (Cu(OH)Cl•TMEDA, 113 mg, 0.481 mmol, 1.00 equiv) at room temperature and stirred for 48 h.[98] Upon addition of copper complex, reaction mixture turned a deep navy blue. The reaction was quenched with 2 mL 0.1 M HCl, which induced a color change from navy to green to light yellow. The reaction was diluted with deionized H_2O (30 mL), extracted with ethyl acetate (25 mL x 3) and 70% isopropanol was added to aid in emulsion separation (2 mL x 2). The combined organic extracts were washed with brine, dried over Na_2SO_4, then concentrated to a pale-yellow solid, 139 mg of crude material recovered as a mixture of unreacted starting materials, dimers, and one cross-coupled product. The mixture was analyzed by LC-MS to determine the connectivity of the cross-coupled product **32** using authentic standards generated by transesterification. **HRMS** (ESI) calculated for $C_{23}H_{19}O_8^-$ $[M-H]^-$ = 423.1085, found 423.1082 *m/z*.

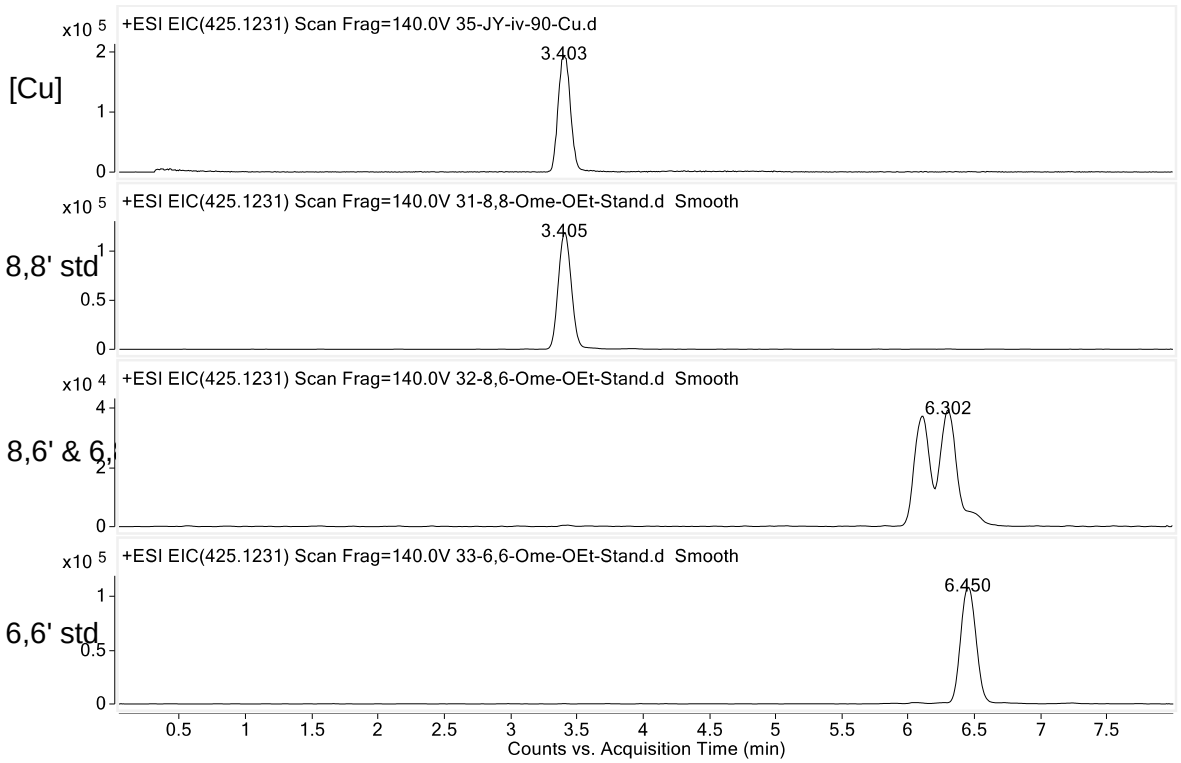

Supplemental Figure S3.22. Extracted ion chromatograms (EICs) of cross-coupled products (1A) compared to standards with 8,8'-, 8,6'- and 6,8'-, and 6,6'-isomers prepared by transesterification.

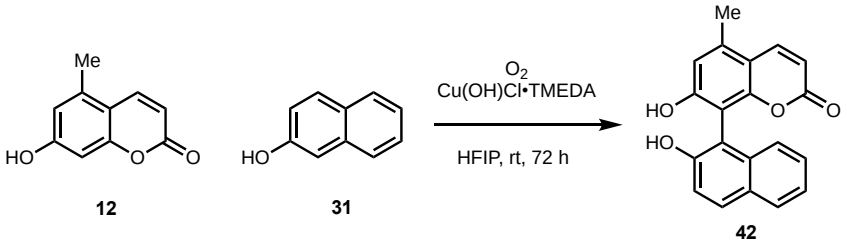

Entry 2a. To a solution of 7-hydroxy-5-methyl-2*H*-chromen-2-one (**12**, 50 mg, 0.28 mmol, 1.0 equiv) and 2-naphthol (**31**, 4.0 mg, 0.28 mmol, 1.0 equiv) in HFIP (2.8 mL, 0.10 M) was added Cu(OH)Cl•TMEDA (33 mg, 0.28 mmol, 1.0 equiv) at room temperature and stirred for 48 h.[98] Upon addition of copper complex, reaction mixture turned dark navy blue. The reaction mixture was quenched with 1 mL 0.1 M HCl, inducing a color change from navy to brownish yellow. The reaction was diluted with deionized H_2O (10 mL), extracted with ethyl acetate (15 mL x 3). The combined organic extracts were washed with brine, dried over Na_2SO_4, then concentrated under reduced pressure to afford 111 mg of a brown solid. To confirm the connectivity of the major cross-coupled species (**42**),

the crude reaction mixture was compared to authentic standards (see Supplemental Schemes S3-6) by LC-MS. The major product was determined to harbor the 8,1'-connectivity, with an unidentified isomeric minor product that did not match the retention times of available standards. The yield of the 8,1'-product was determined by ^{1}H NMR as 19% and was calculated by analysis of 20.5 mg of the crude reaction mixture in 1.0 mL of D_6-Acetone with 5.0 mg (0.0297 mmol) 1,3,5-trimethoxybenzene as an internal standard (Supplemental Figure S86). **HRMS** (ESI) calculated for $C_{20}H_{13}O_4^-$ [M-H]$^-$ = 317.0819, found = 317.0820 *m/z*.

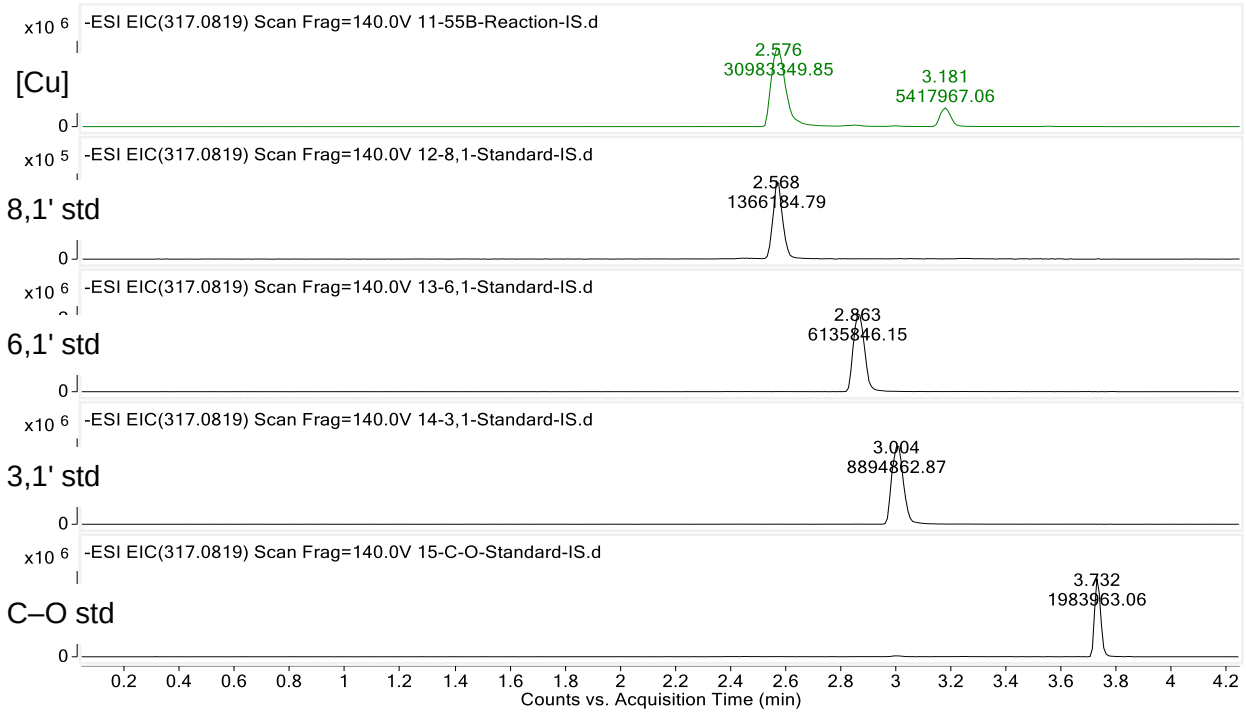

Supplemental Figure S3.23. Extracted ion chromatograms comparing 2A to product standards. The match in retention times confirms the 8,1'-connectivity as the major cross-coupled product.

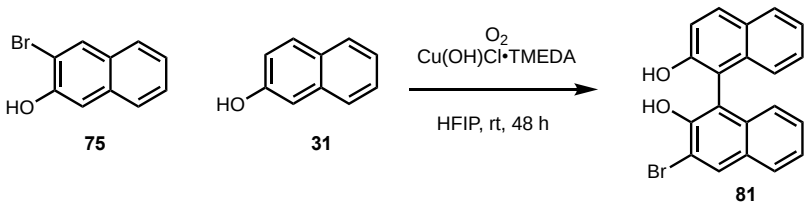

Entry 3a. To a solution of 3-bromo-2-naphthol (**75**, 116 mg, 0.520 mmol, 1.00 equiv) and 2-naphthol (**31**, 75 mg, 0.52 mmol, 1.0 equiv) in HFIP (5.2 mL, 0.10 M) was added Cu(OH)Cl•TMEDA (121 mg, 0.520 mmol, 1.00 equiv) at room temperature and stirred for 48 h. The reaction was quenched with 1 mL 0.1 M HCl and diluted with deionized H_2O (10 mL), extracted with ethyl acetate (25 mL x 3). The combined organic extracts were washed with brine, dried over Na_2SO_4, then concentrated under reduced pressure to afford 236 mg of a brown solid. The crude mixture was purified by flash chromatography over silica gel with a gradient of 5% to 30% ethyl acetate in hexanes, recovering 44 mg of cross-coupled product **81** as an off-white solid in a 23% yield with minor impurities. ^{1}H NMR (400 MHz, CDCl3) δ 8.28 (s, 1H), 7.97 (d, *J* = 8.9 Hz, 1H), 7.89 (d, *J* = 8.1 Hz, 1H), 7.82 (d, *J* = 8.2 Hz, 1H), 7.43–7.34 (m, 3H), 7.34–7.28 (m, 2H), 7.14 (d, *J* = 8.4 Hz, 1H), 7.10 (d, *J* = 8.3 Hz, 1H), 5.61 (s, 1H), 5.02 (s, 1H). All spectra obtained were consistent with literature values.[98-99] **HRMS** (ESI) calculated for $C_{20}H_{12}BrO_2^-$ [M-H]$^-$ = 363.0026, found 365.0007 *m/z.*

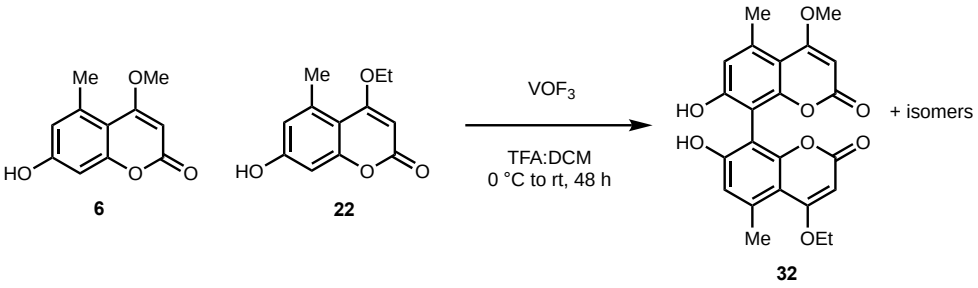

Entry 1b. To a solution of 7-hydroxy-4-methoxy-5-methyl-*2H*-chromen-2-one (**4**; 100 mg, 0.48 mmol, 1.0 equiv) and 4-ethoxy-7-hydroxy-5-methyl-2*H*-chromen-2-one (**18**; 107 mg, 0.480 mmol, 1.00 equiv) in dry CH_2Cl_2 (4.0 mL, 0.125 M) and trifluoroacetic acid (1 mL, 0.5 M) was added VOF_3 (120 mg, 0.97 mmol, 2.00 equiv) at 0 °C, then warmed to room temperature and stirred for 48 h.[93-96] Upon addition of the vanadium complex, the reaction mixture turned a deep navy blue. The reaction was quenched by addition of H_2O and extracted with ethyl acetate (15 mL x 3). The combined extracts were washed with brine, dried over Na_2SO_4, and concentrated under reduced pressure to afford a pale-yellow solid (112 mg). The reaction resulted in a complex, inseparable mixture of multiple dimers and cross-coupled products combined with remaining coumarin starting materials. The crude mixture was analyzed by LC-MS and percent conversions were calculated. The

connectivity of the major cross-coupled isomer (**32**) was determined by comparison of standards with known connectivity on analytical scale. **HRMS** (ESI) calculated for $C_{23}H_{19}O_8^-$ $[M-H]^-$ = 423.1085, found = 423.1085 *m/z.*

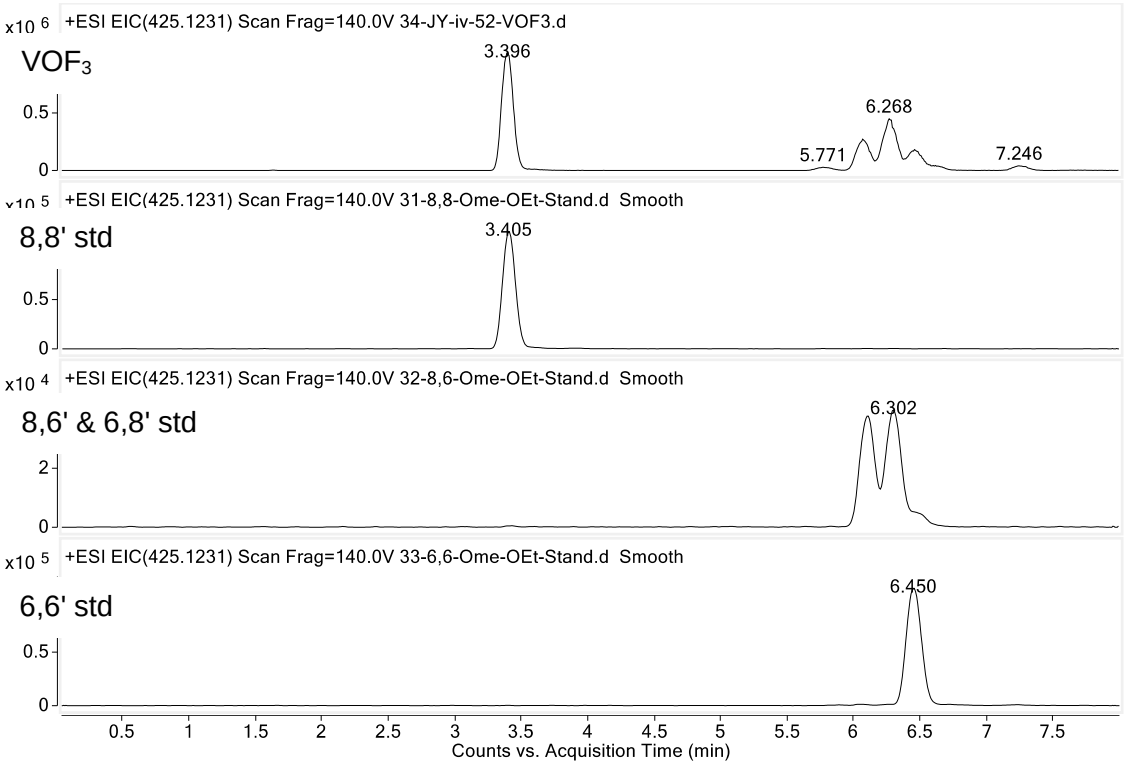

Supplemental Figure S3.24. Extracted ion chromatograms (EICs) of cross-coupled products (1B) compared to standards with 8,8'-, 8,6'- and 6,8'-, and 6,6'-isomers prepared by transesterification.

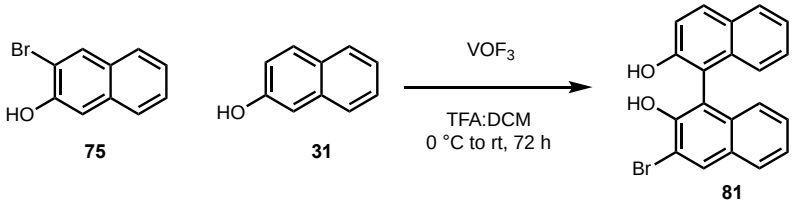

Entry 3b. To a solution of 3-bromo-2-naphthol (**75**, 77 mg, 0.35 mmol, 1.0 equiv) and 2-naphthol (**31**, 50.0 mg, 0.350 mmol, 1.00 equiv) in dry CH_2Cl_2 (2.80 mL, 0.125 M) and trifluoroacetic acid (0.7 mL, 0.5 M) was added VOF_3 (85 mg, 0.69 mmol, 2.0 equiv) at 0 °C, then warmed to room temperature and stirred for 48 h.[93-96] Upon addition of the vanadium complex, the reaction mixture gradually turned orange then green over 72 h. The reaction was quenched by addition of H_2O and extracted with ethyl acetate (25 mL x 3). The combined extracts were washed with brine, dried over Na_2SO_4, and concentrated

under vacuum to give a black solid (124 mg). The crude mixture was purified by flash chromatography over silica gel with a gradient of 0 to 25 % ethyl acetate in hexanes. The fractions contained a total of 5.8 mg of **81** in a 5% yield, calculated by comparison to an internal standard by ^{1}H NMR in $CDCl_3$. Fraction 2 (29 mg) contained 5.6 mg (33 µmol) of 1,3,5-trimethoxybenzene as an internal standard and 4.7 mg of **81**; combined fractions 3-5 (33 mg) contained 7.5 mg (45 µmol) of 1,3,5-trimethoxybenzene and 1.1 mg of **81**. **HRMS** (ESI) calculated for $C_{20}H_{12}BrO_2^-$ [M-H]$^-$ 363.0026, found = 317.0809 *m/z*.

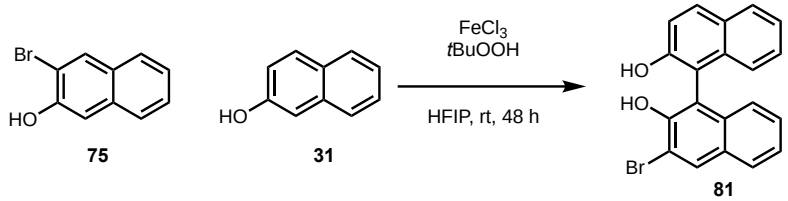

Entry 3c. To a solution of 3-bromo-2-naphthol (**75**, 116 mg, 0.520 mmol, 1.00 equiv) and 2-naphthol (**31**, 75.0 mg, 0.520 mmol, 1.00 equiv) in HFIP (5.2 mL, 0.10 M) was added anhydrous $FeCl_3$ (17 mg, 0.10 mmol, 0.20 equiv) and 75 µL *t*-BuOOH (70% solution, 0.57 mmol, 1.1 equiv) at room temperature and stirred for 48 h.[97] The reaction was quenched by the addition of water and the aqueous phase was extracted with ethyl acetate (25 mL x 3). The organic layers were combined, washed with brine, dried over Na_2SO_4, filtered, and evaporated under reduced pressure to afford 229 mg of a dark brown solid. The reaction resulted in a mixture of dimers and one major cross-coupled product. The crude mixture was purified by flash chromatography over silica gel with a gradient of 0 to 20% ethyl acetate in hexanes, resulting in mixed fractions. The fractions containing the cross-coupled product **81** were combined and concentrated under reduced pressure to afford 36.2 mg of a yellow solid. The yield was calculated as 6.4% using the entire 36.2 mg mixture in 1 mL $CDCl_3$ and 5 mg mesitylene (97% purity, 0.0404 mmol) as the internal standard (Supplemental Figure S88). **HRMS** (ESI) *m/z* calculated for $C_{20}H_{12}BrO_2^-$ [M-H]$^-$ 363.0026, found 363.0022 *m/z*.

General procedure for Fe(TPP)Cl mediated coupling (column D). Carried out on analytical scale only due to low or no formation of cross-coupled product. Each phenolic substrate was used in a 1:1 ratio (1 equiv each, 5 mg scale) and were dissolved in a solution of Fe(III)meso-tetraphenylporphine chloride, CAS# 16456-81-8 (Fe(TPP)Cl, 0.2

equiv) in HFIP (0.08 M), followed by addition of *t*-BuOOH (70%, 1.1 equiv) at room temperature.[100] Each reaction was stirred at room temperature and monitored by LC-MS over 48 h. Trace amounts (<2% conversion) of cross-coupled product or decomposition of starting materials was observed in each case, with detailed LC-MS traces shown in Supplemental Figures S3.24-S3.25.

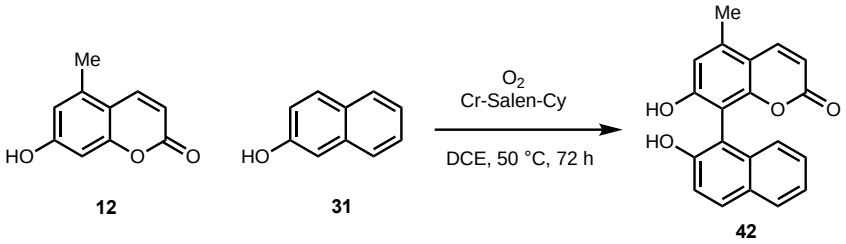

Entry 2e. To a solution of 7-hydroxy-5-methyl-2*H*-chromen-2-one (**12**; 50 mg, 0.28 mmol, 1.0 equiv) and 2-naphthol (**31**; 41 mg, 0.28 mmol, 1.0 equiv) in 1,2-dichloroethane (2.8 mL, 0.10 M) was added 18 mg (1R,2R)-(-)-[1,2-Cyclohexanediamino-*N,N'*-bis(3,5-di-t-butylsalicylidene)]chromium(III) chloride, CAS# 164931-83-3 (Cr-Salen-Cy, 28 µmol, 0.10 equiv) and heated to 50 °C for 72 h.[101] The reaction mixture was diluted with ethyl acetate, filtered through silica gel, and evaporated under reduced pressure to afford 97 mg of a dark brown solid. LC-MS analysis revealed that the reaction resulted in a mixture of dimers and multiple cross-coupled products. Analysis by ^{1}H NMR did not reveal significant formation of cross-coupled product, with only trace amounts of cross-coupled products observed by LC-MS.

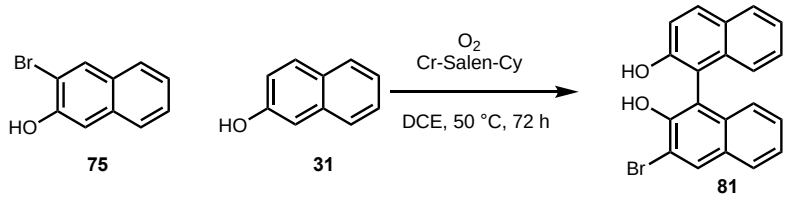

Entry 3e. To a solution of 3-bromo-2-naphthol (**75**; 116 mg, 0.520 mmol, 1.00 equiv) and 2-naphthol (**31**; 75.0 mg, 0.520 mmol, 1.00 equiv) in 1,2-dichloroethane (5.2 mL, 0.10 M) was added 33 mg Cr-Salen-Cy catalyst (52 µmol, 0.10 equiv) and heated to 50 °C for 72 h.[101] The reaction mixture was diluted with ethyl acetate, filtered through silica gel, and evaporated under reduced pressure to afford 223 mg of a dark brown solid. The reaction resulted in a mixture of dimers and one major cross-coupled product. The reaction was purified by flash chromatography over silica gel with a gradient of 0 to 20% ethyl acetate in hexanes, to provide 10.1 mg of **81** (5% yield) as a yellow solid with impurities. ^{1}H NMR

(600 MHz, CDCl3) δ 8.28 (s, 1H), 7.89 (d, *J* = 9.4 Hz, 1H), 7.83 (d, *J* = 8.2 Hz, 1H), 7.39 (dddd, *J* = 16.3, 8.1, 6.7, 1.1 Hz, 3H), 7.33 – 7.28 (m, 2H), 7.15 (d, *J* = 8.4 Hz, 1H), 7.10 (d, *J* = 8.4 Hz, 1H), 5.57 (s, 1H), 4.97 (s, 1H). All spectra obtained were consistent with literature values.[98-99] **HRMS** (ESI) calculated for $C_{20}H_{12}BrO_2^-$ $[M-H]^-$ = 363.0026, found = 363.0025 *m/z*.

LC-MS traces for chemical oxidative coupling reactions

Reactions were carried out on analytical scale and analyzed by LC-MS. For each reaction, extracted ion chromatograms (EICs) of the starting materials, A and B, cross-coupled products (AB), and dimers (AA and BB) are provided. The number of peaks for each product mass is used to assess the number of products formed in each reaction as separation of constitutional isomers is assumed.

Supplemental Figure S3.25. Oxidative cross-coupling of **6** and **22** by Cu(OH)Cl•TMEDA (**Supplemental Figure S3.21, Entry 1a**).

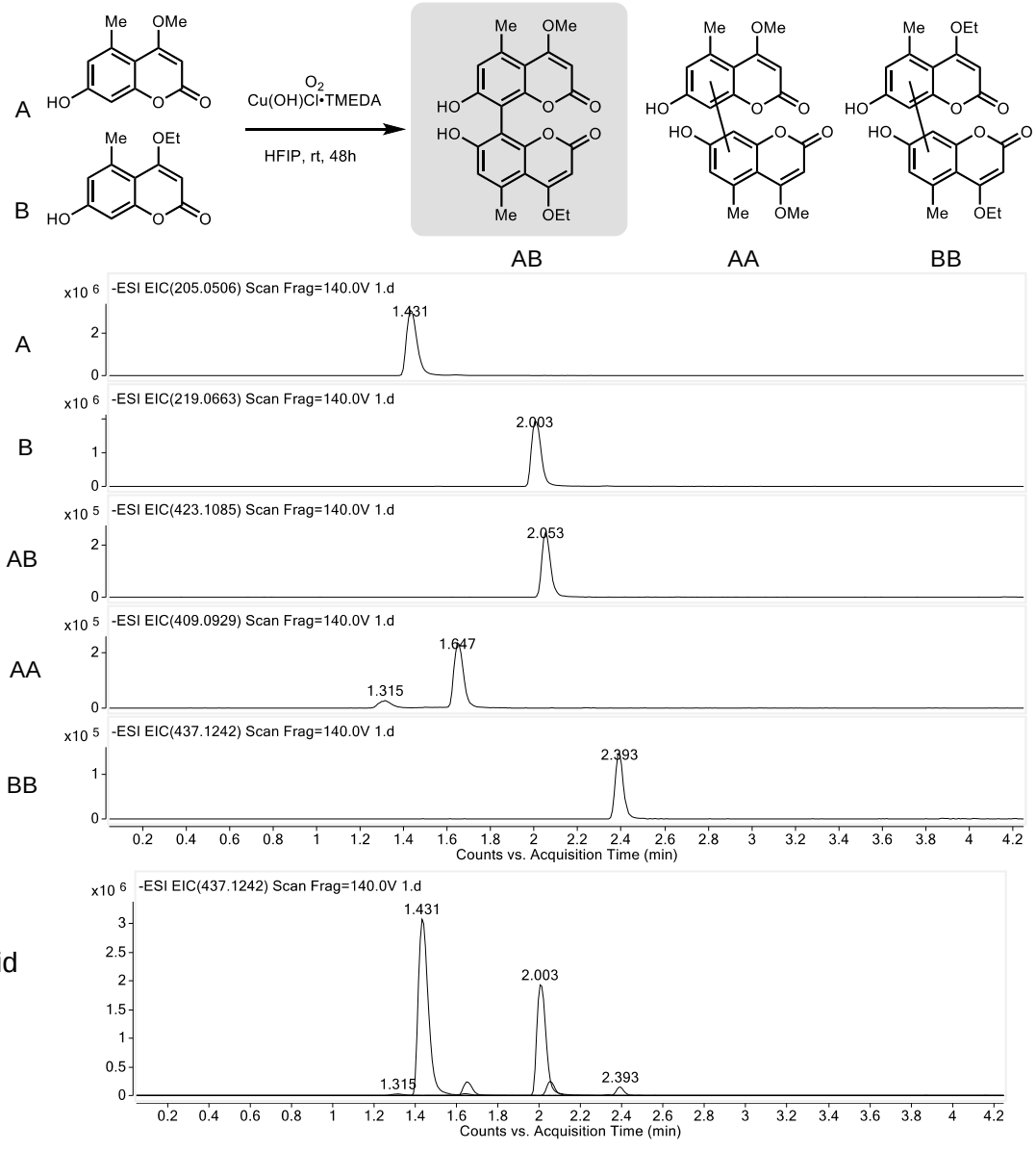

Supplemental Figure S3.26. Oxidative cross-coupling of **12** and **31** by Cu(OH)Cl•TMEDA (**Supplemental Figure S3.21, Entry 2a**).

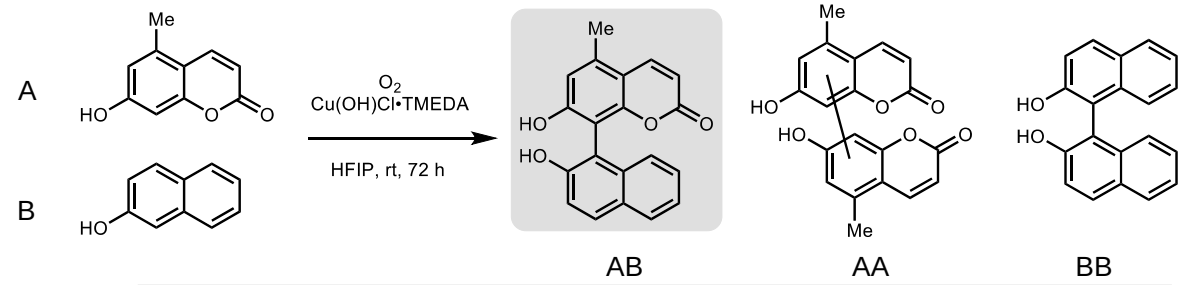

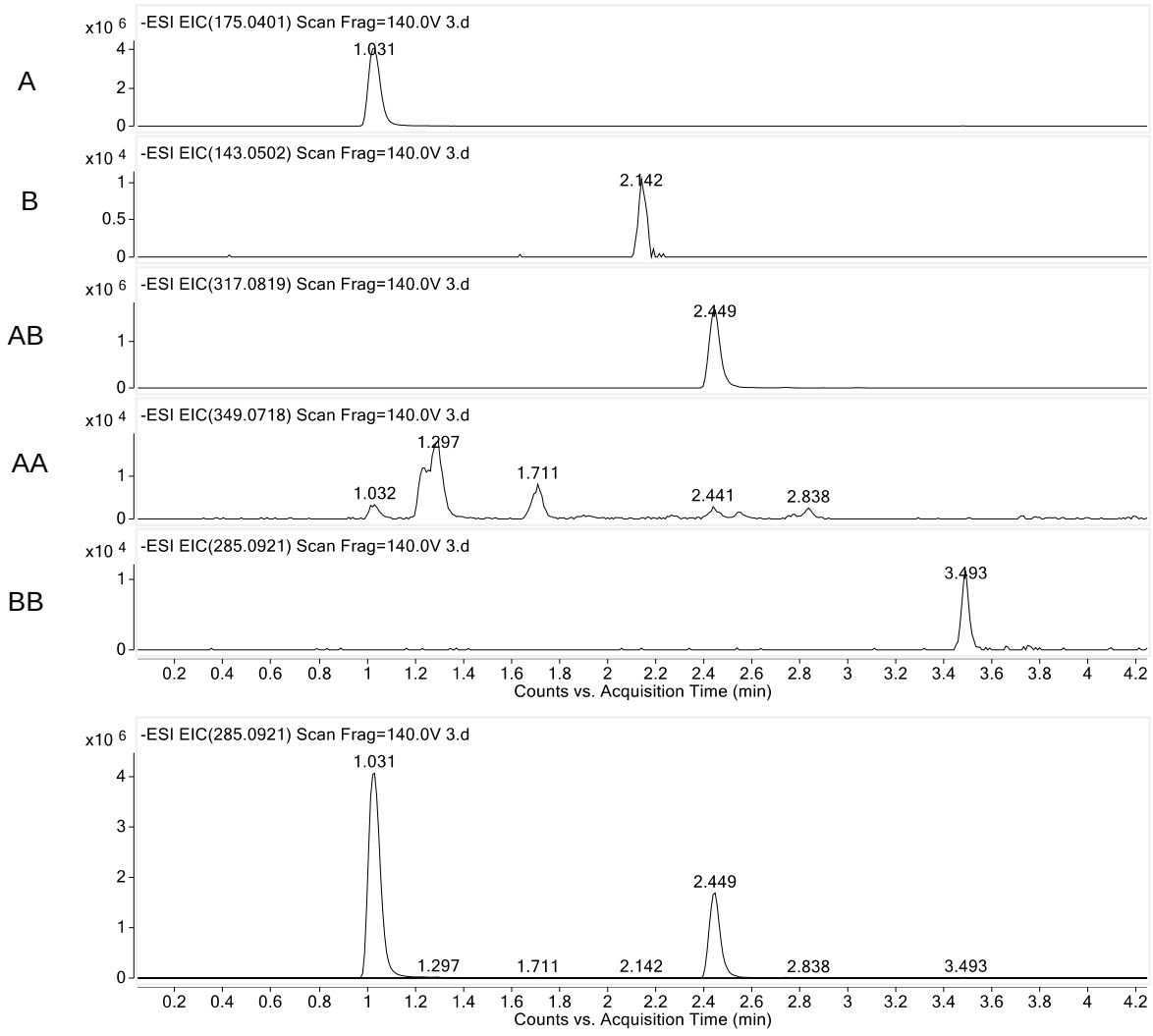

Supplemental Figure S3.27. Oxidative cross-coupling of **31** and **75** by Cu(OH)Cl•TMEDA (**Supplemental Figure S3.21, Entry 3a**).

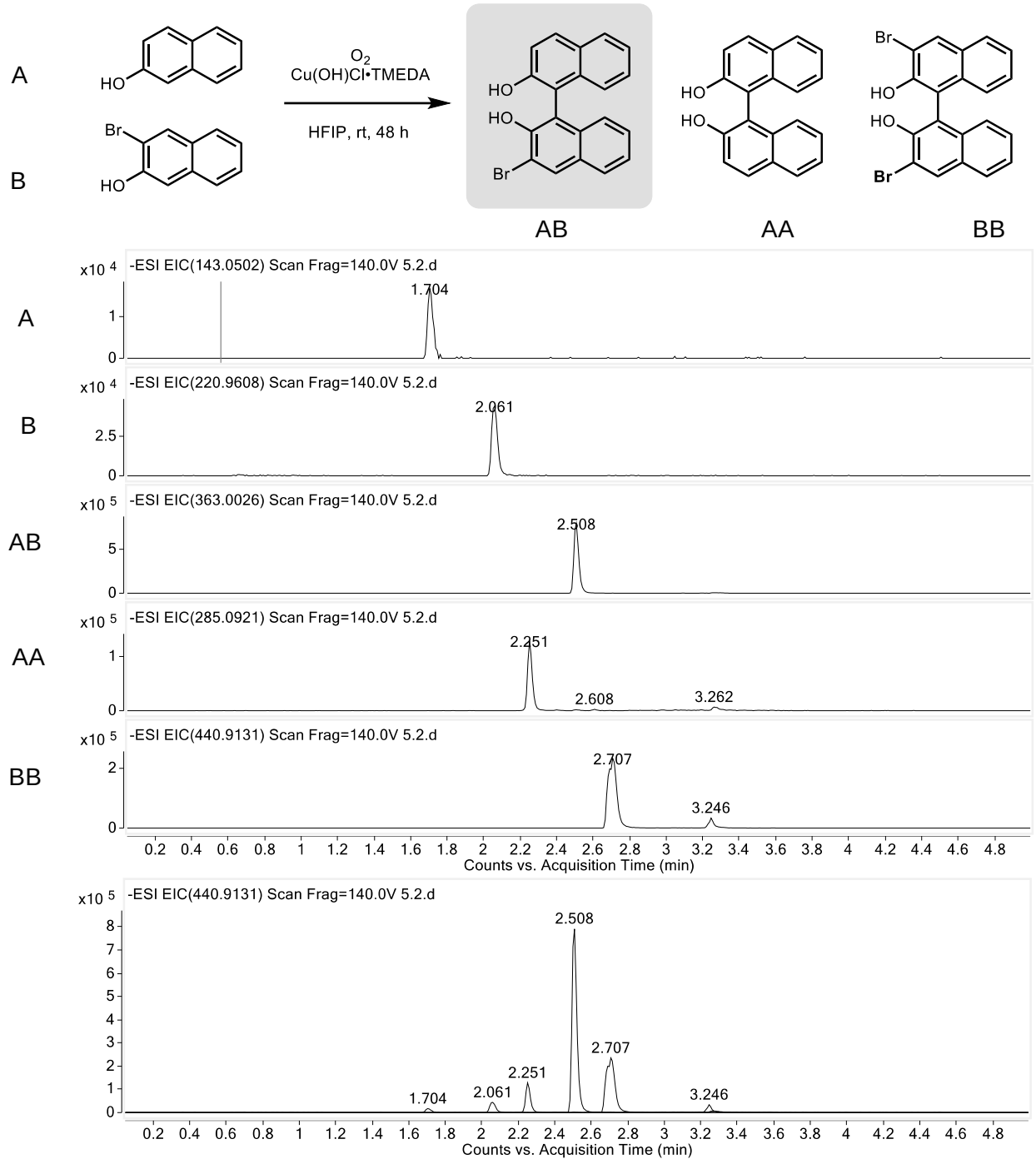

Supplemental Figure S3.28. Oxidative cross-coupling of **6** and **22** by VOF_3 (**Supplemental Figure S3.21, Entry 1b**).

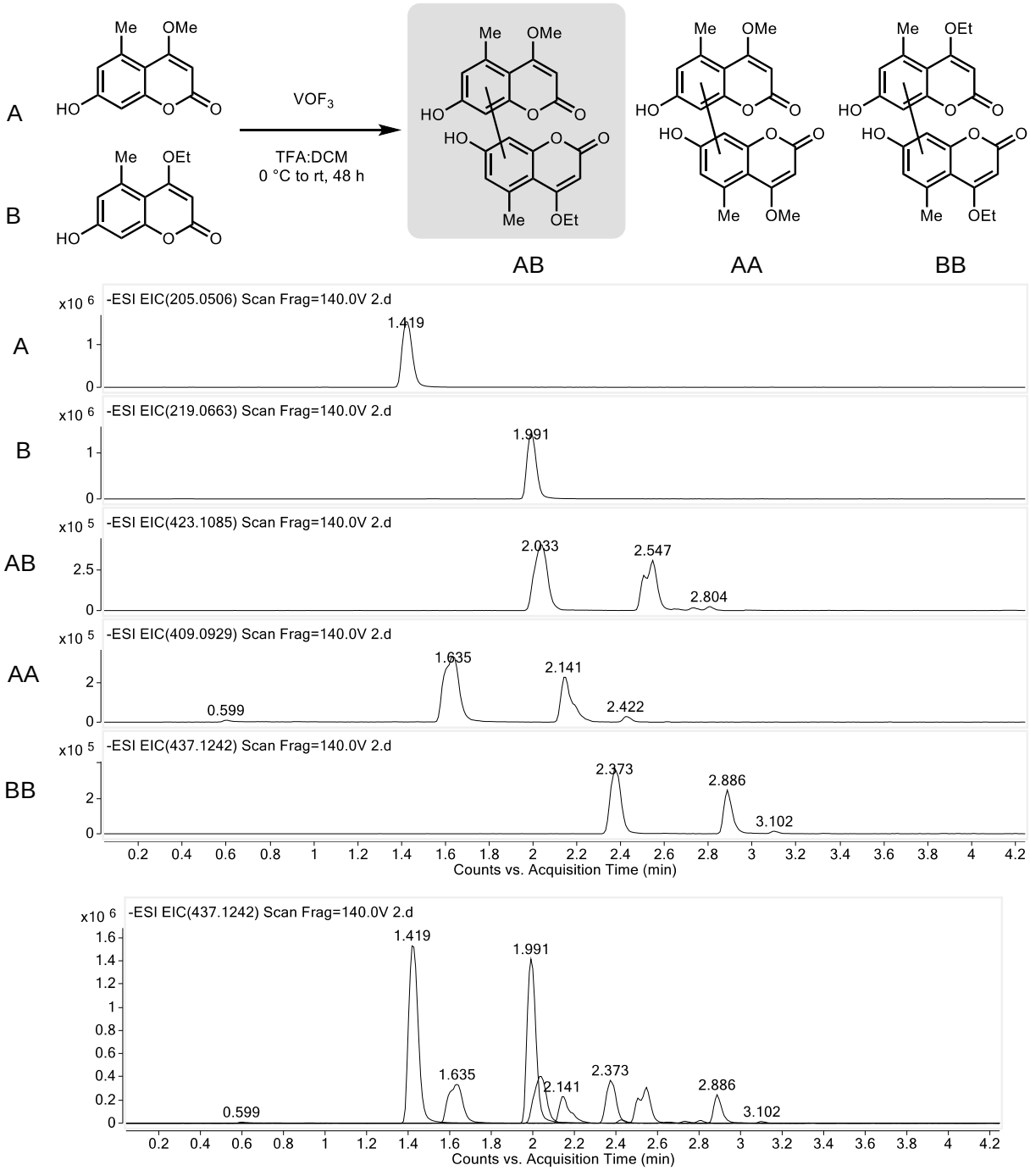

Supplemental Figure S3.29. Oxidative cross-coupling of **12** and **31** by VOF_3 (**Supplemental Figure S3.21, Entry 2b**).

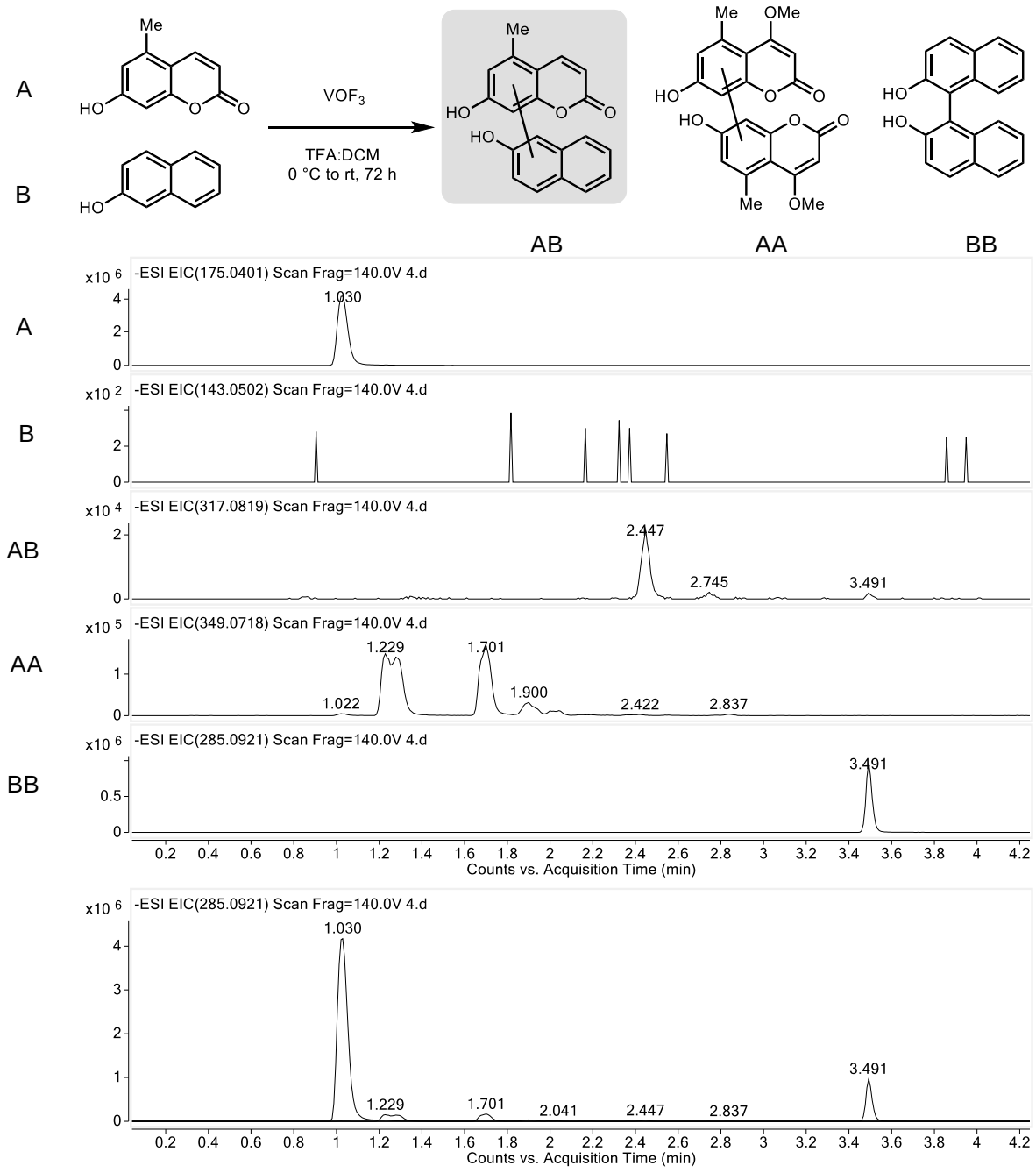

Supplemental Figure S3.30. Oxidative cross-coupling of **31** and **75** by VOF_3 (**Supplemental Figure S3.21, Entry 3b**).

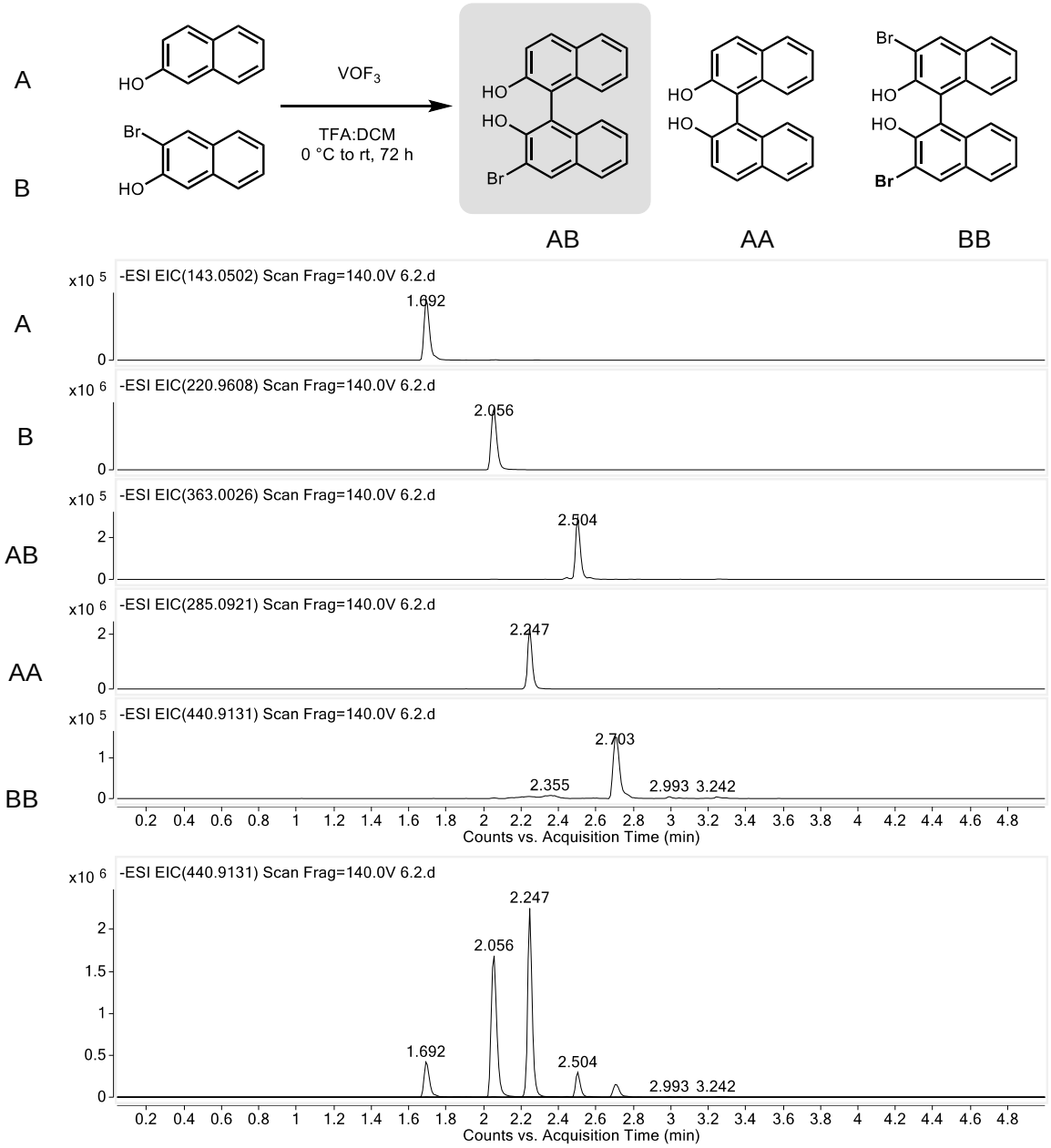

Supplemental Figure S3.31. Oxidative cross-coupling of **6** and **22** by $FeCl_3$ (**Supplemental Figure S3.21, Entry 1c**).

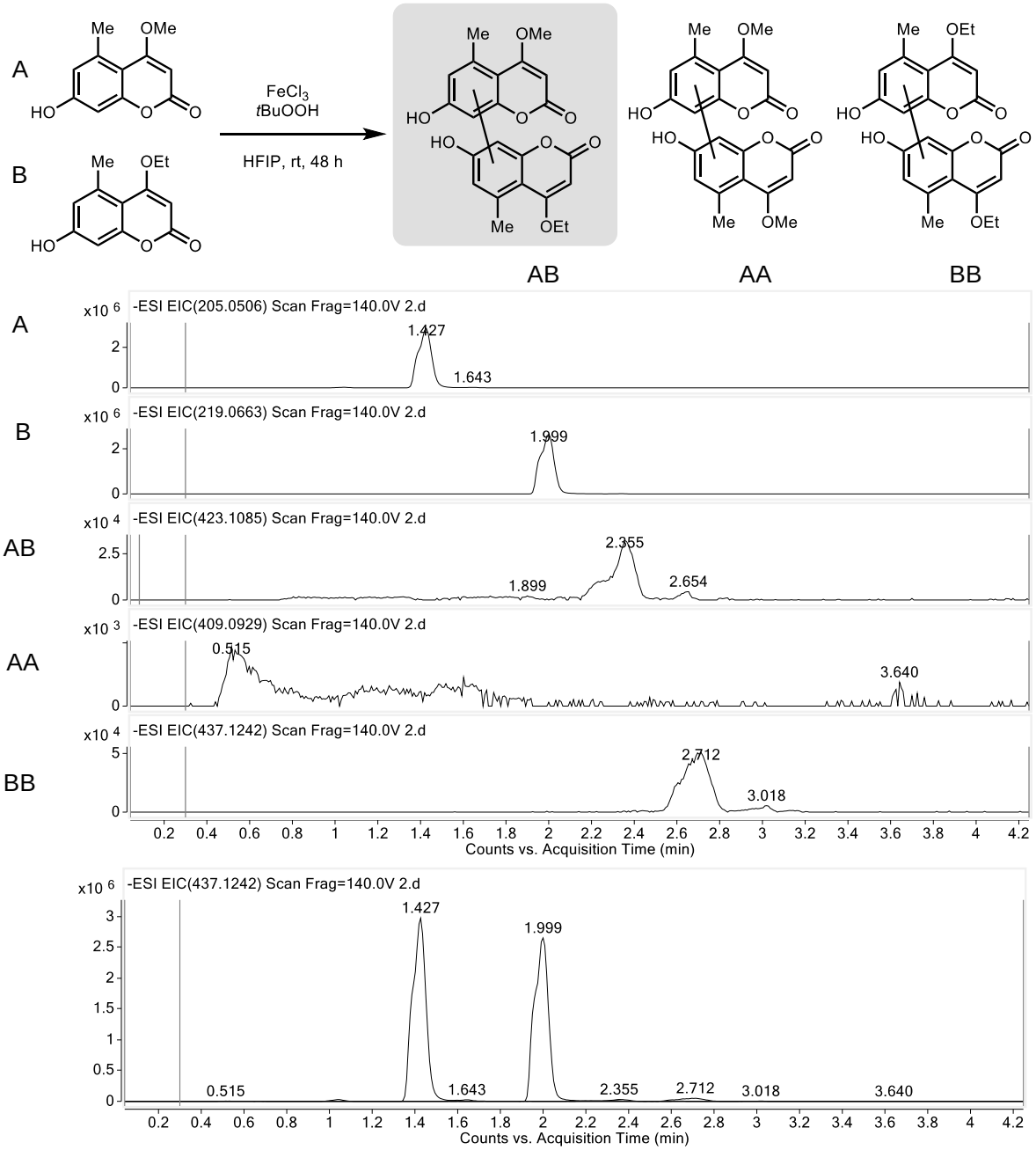

Supplemental Figure S3.32. Oxidative cross-coupling of **12** and **31** by $FeCl_3$ (**Supplemental Figure S3.21, Entry 2c**).

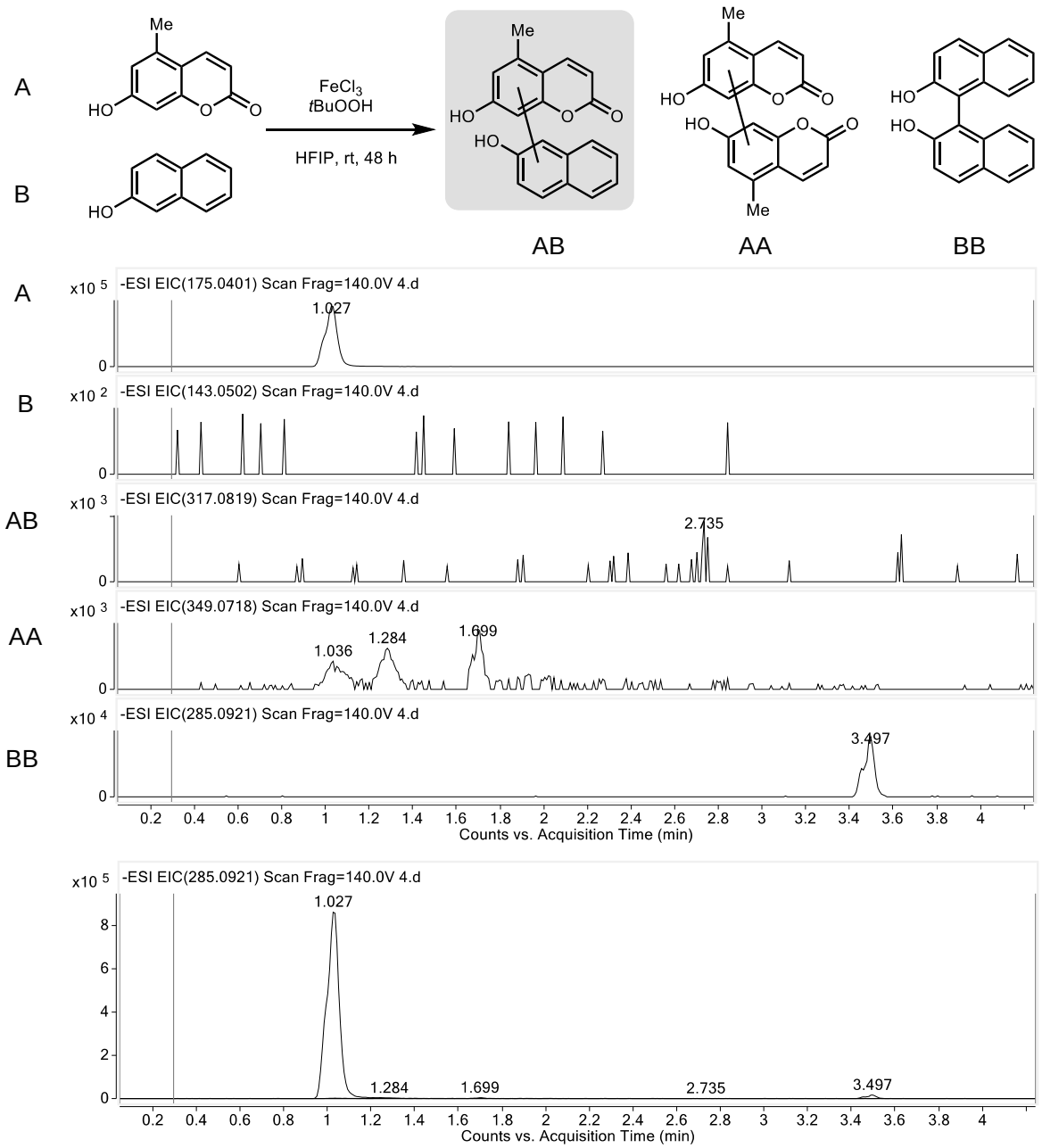

Supplemental Figure S3.33. Oxidative cross-coupling of **31** and **75** by $FeCl_3$ (**Supplemental Figure S3.21, Entry 3c**).

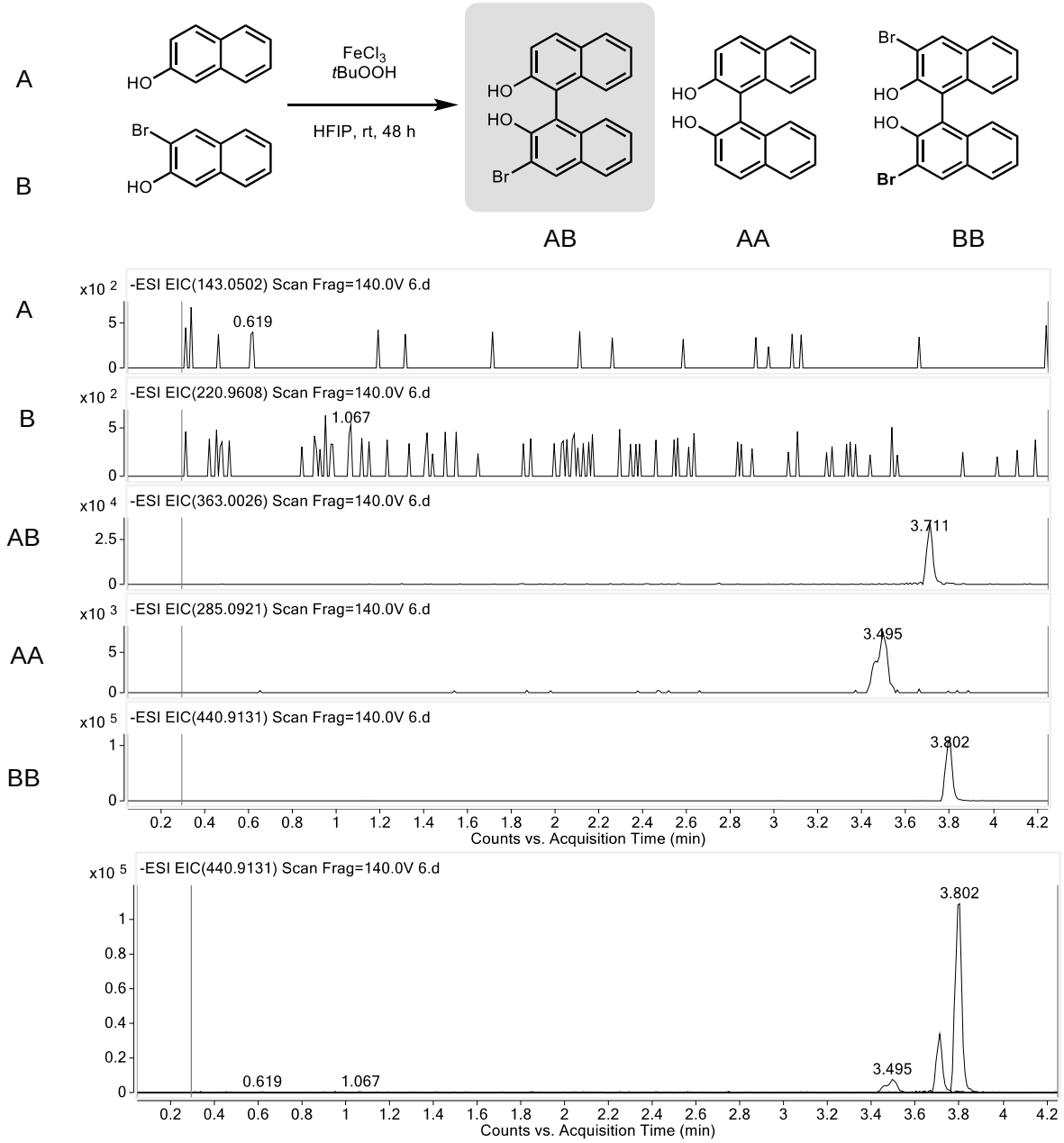

Supplemental Figure S3.34. Oxidative cross-coupling of **6** and **22** by Fe(TPP)Cl (**Supplemental Figure S3.21, Entry 1d**).

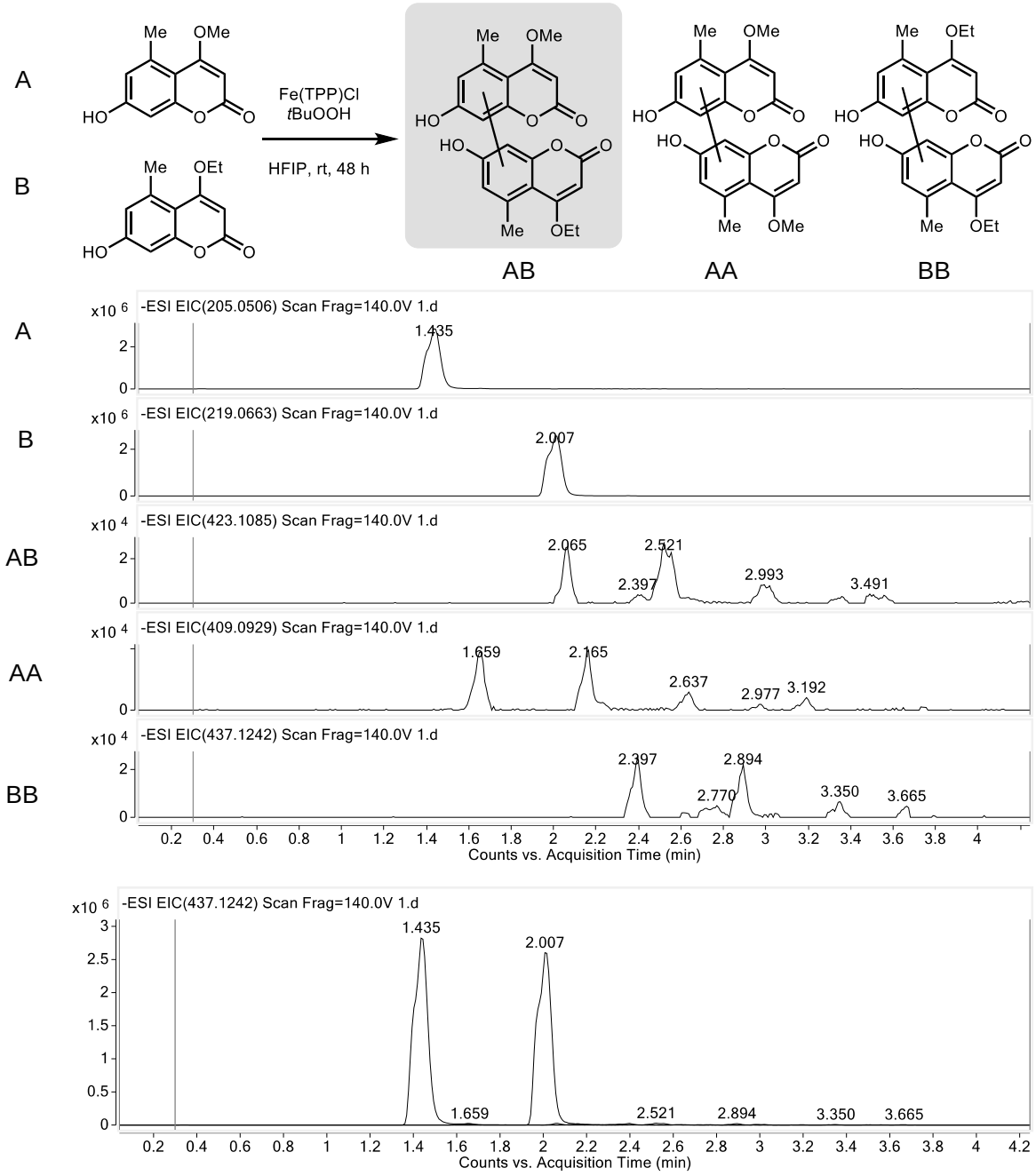

Supplemental Figure S3.35. Oxidative cross-coupling of **12** and **31** by Fe(TPP)Cl (**Supplemental Figure S3.21, Entry 2d**).

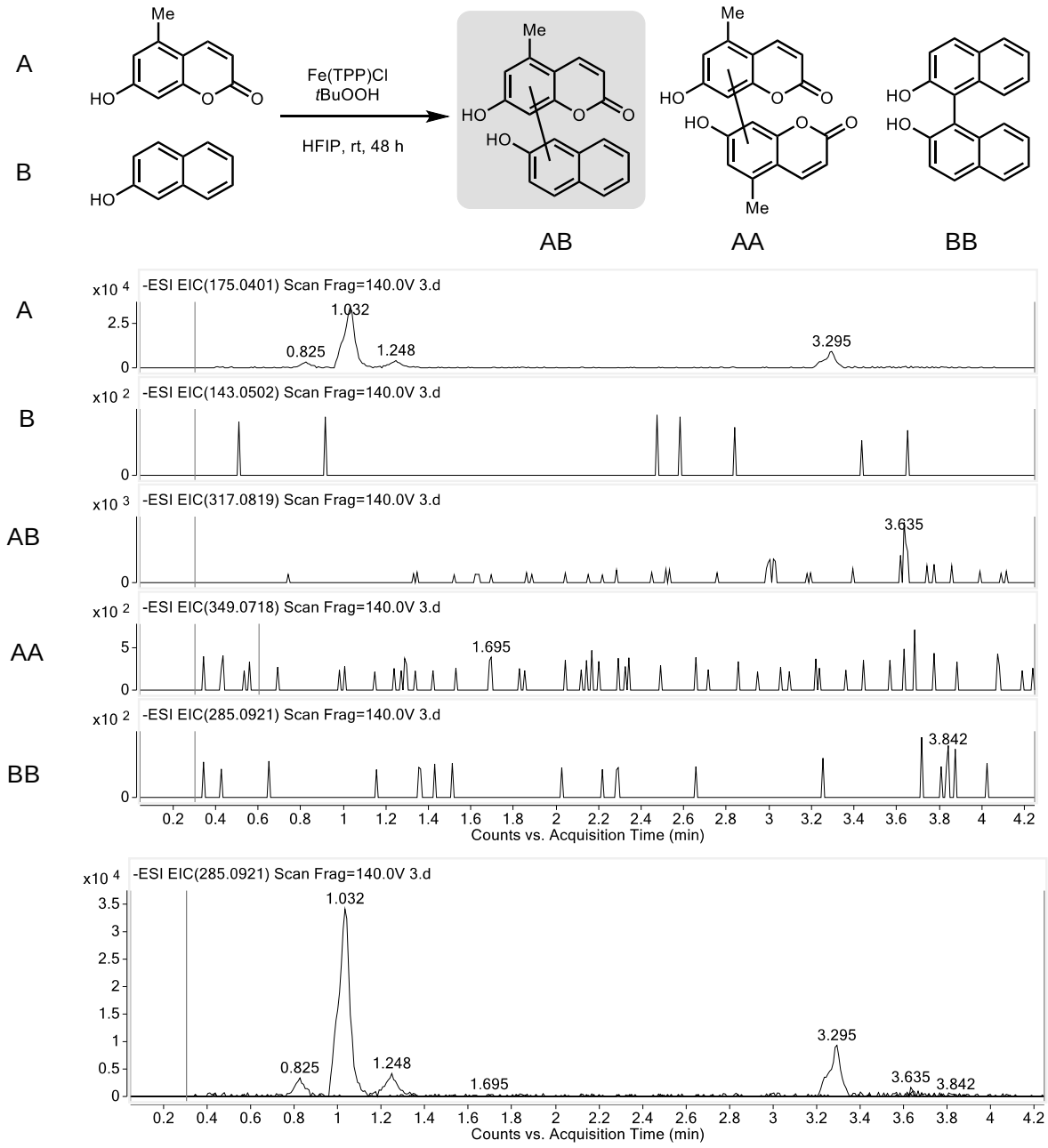

Supplemental Figure S3.36. Oxidative cross-coupling of **31** and **75** by Fe(TPP)Cl (**Supplemental Figure S3.21, Entry 3d**).

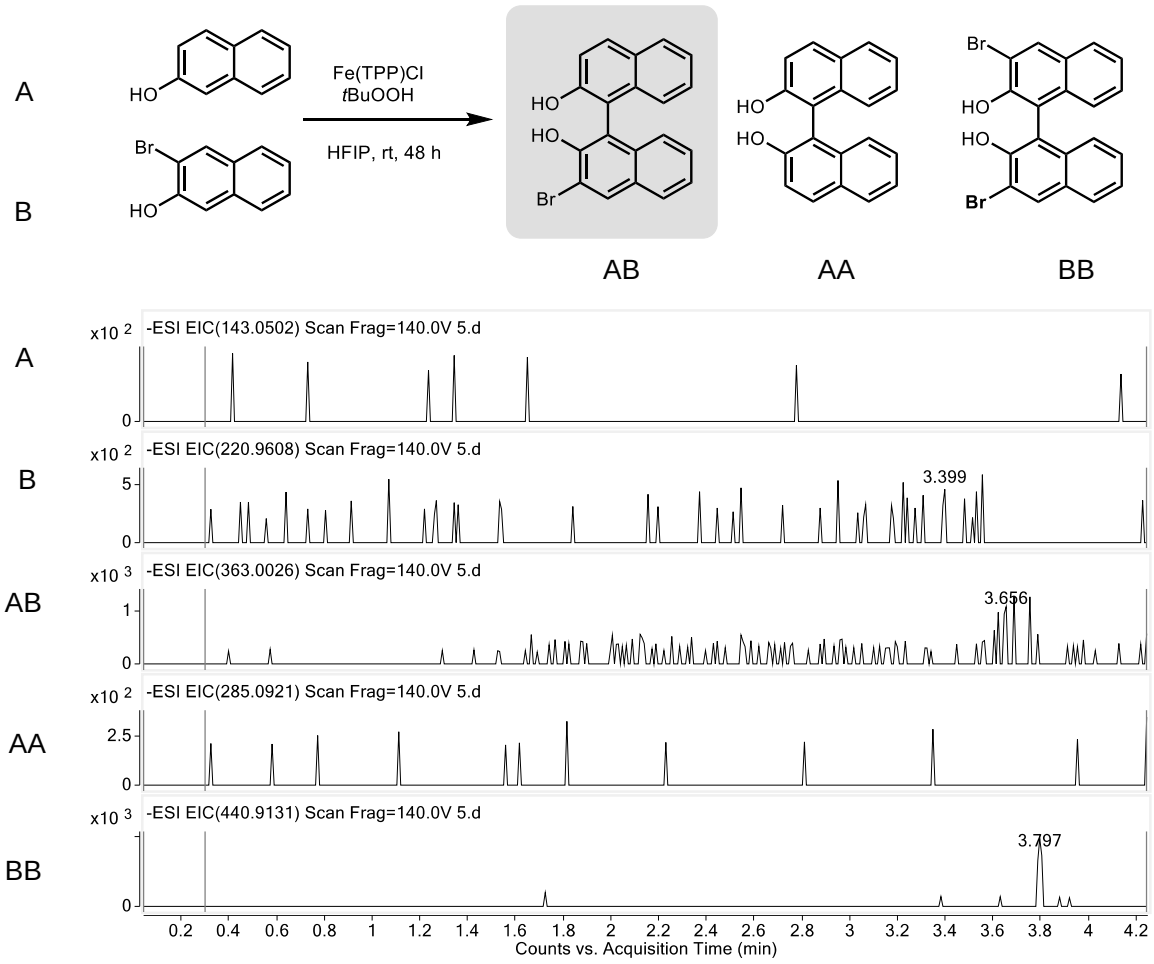

Supplemental Figure S3.37. Oxidative cross-coupling of **6** and **22** by Cr-Salen-Cy (**Supplemental Figure S3.21, Entry 1e**).

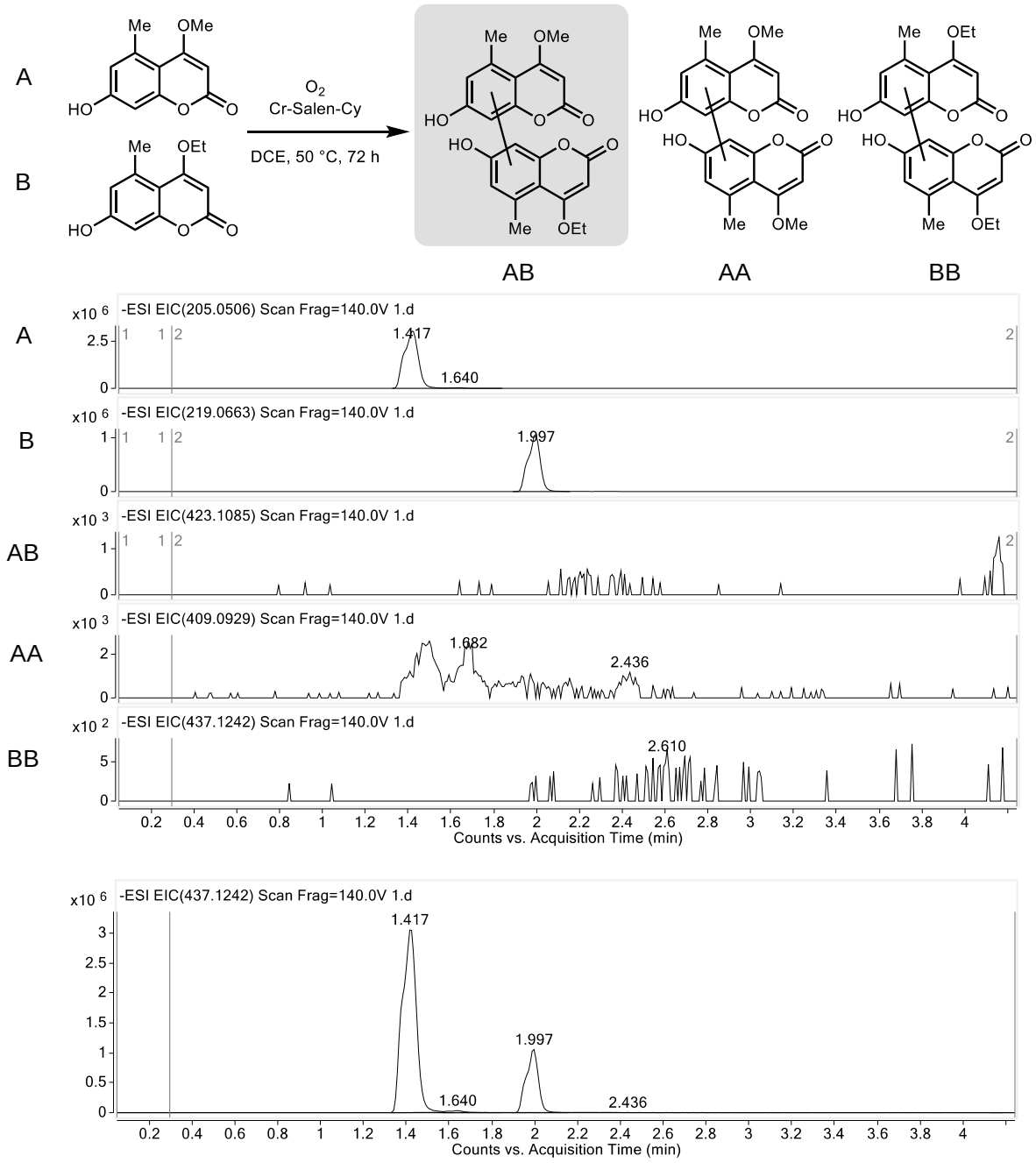

Supplemental Figure S3.38. Oxidative cross-coupling of **12** and **31** by Cr-Salen-Cy (**Supplemental Figure S3.21, Entry 2e**).

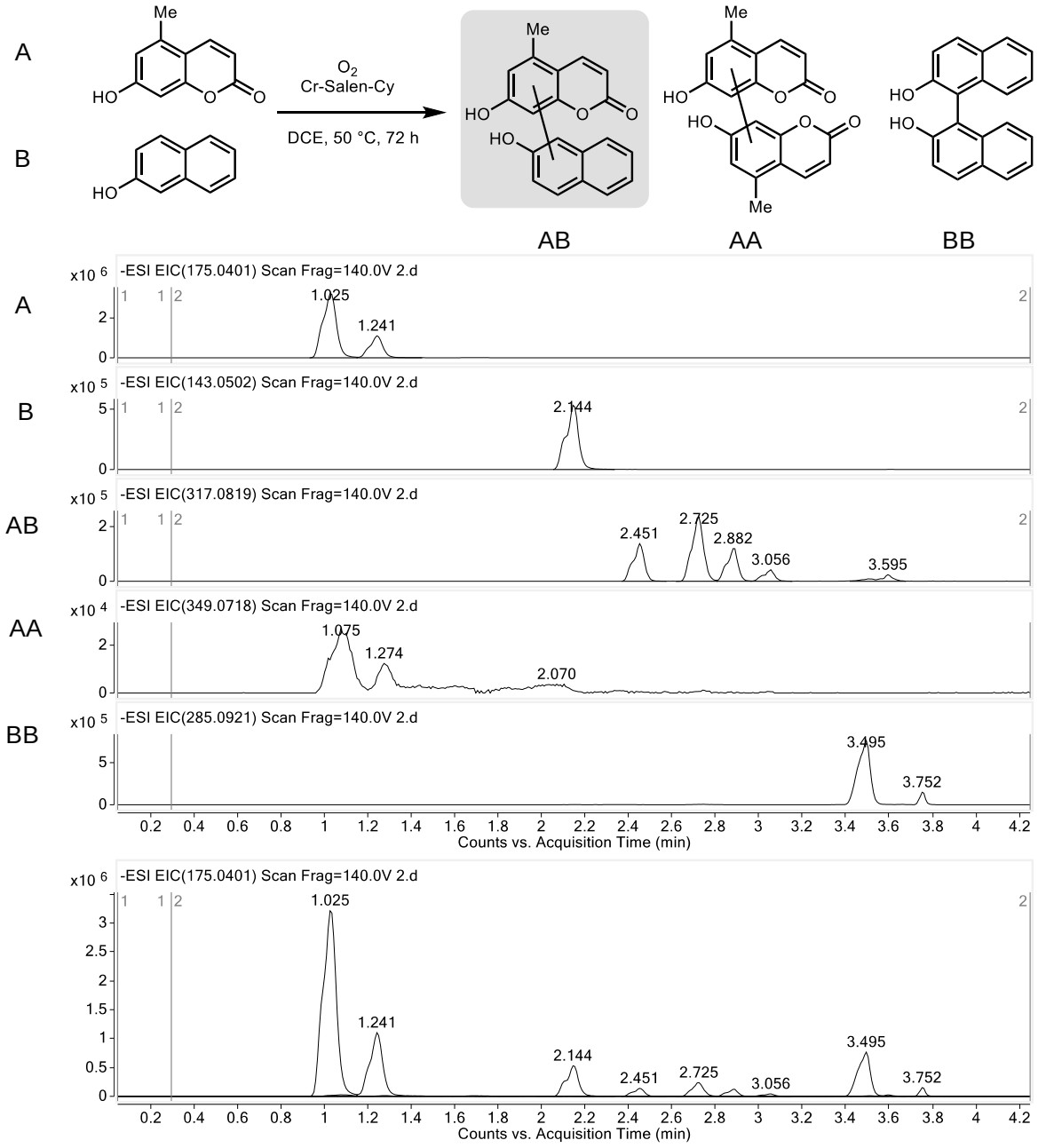

Supplemental Figure S3.39. Oxidative cross-coupling of **31** and **75** by Cr-Salen-Cy (**Supplemental Figure S3.21, Entry 3e**).

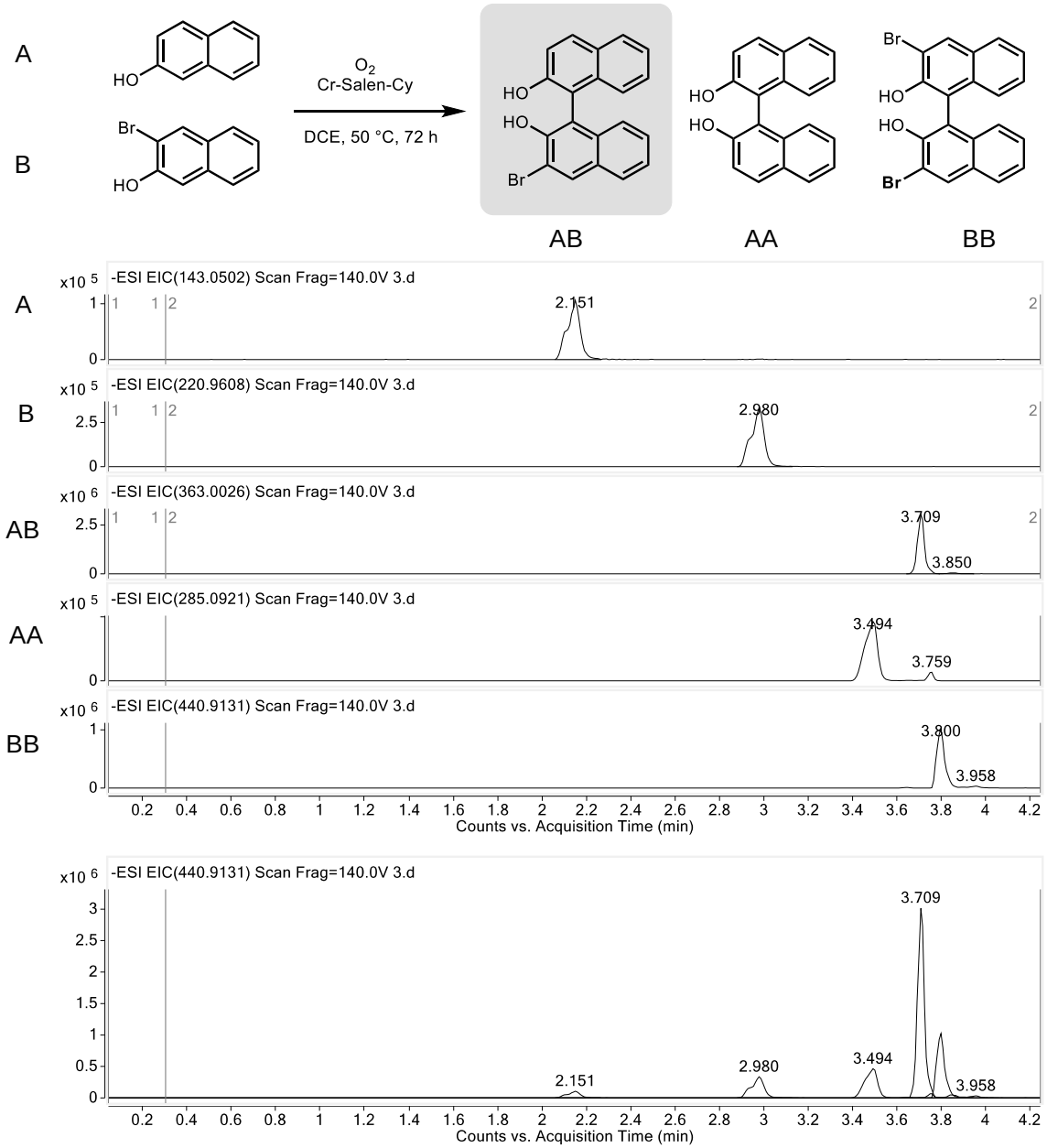

Biocatalytic reactions with fungal P450 KtnC

Methods for biocatalytic cross-couplings

General protocol. A colony of *P. pastoris* KM71 containing KtnC was inoculated in 6 mL BMG medium and grown overnight at 30 °C with shaking at 235 rpm. The culture was added to BMG medium (125 mL) and grown at 30 °C with shaking at 235 rpm until the optical density at 600 nm was in the range of 10-16. Cultures were induced for expression by resuspension in BMM medium to a final optical density of 30. Substrates were added to 24-well plates from a 25 or 50 mM stock in DMSO, followed by 1 mL aliquots of expression cultures. The 24 well plates were sealed with an adhesive cover and grown at 30 °C with shaking at 235 rpm for 48h and supplemented with 100 µL of 10X methanol (5% MeOH, 95% water) after 24 h. Reactions were carried out with final substrate concentrations in a 1:10 molar ratio (25 µM of **6** and 250 µM of coupling partner or 100 µM of **6** and 1000 µM coupling partner).

Supplemental Figure S3.40. Optimization of analytical-scale whole-cell biotransformations for oxidative cross-coupling. The effect of increasing concentration of coupling partner B on percent conversion to cross-coupled product (AB) was monitored by LC-MS and relative percent conversions were calculated (see below for analysis methods).

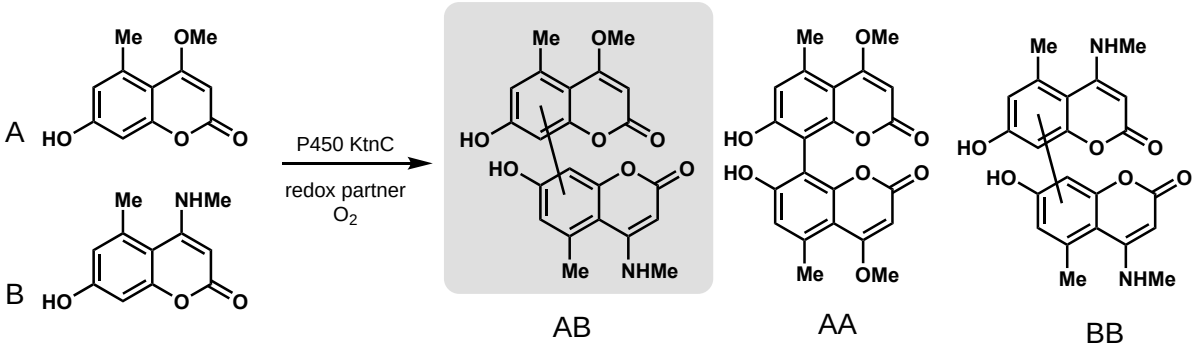

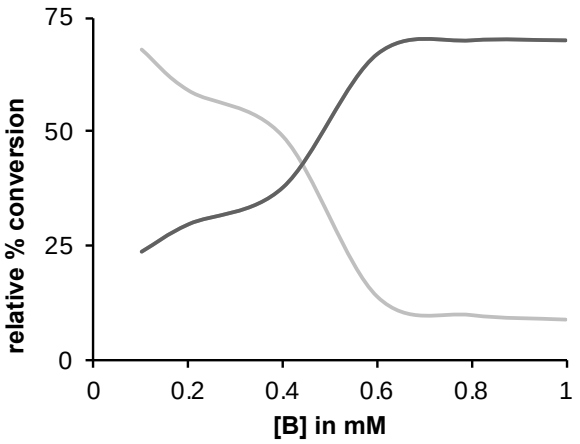

entry	[A]	[B]	% AA	% AB	AA:AB
1	0.1	0.1	68	24	3:1
2	0.1	0.2	59	30	2:1
3	0.1	0.4	49	38	1:1
4	0.1	0.6	14	67	1:5
5	0.1	0.8	10	70	1:7
6	0.1	1.0	9	70	1:7

[A] & [B] in mM, P. pastoris, 30 °C, 235 RPM, 2 d

Quantification of reaction conversion. Percent conversion was calculated based on consumption of coumarin starting material **6** and formation of coumarin dimer **9** compared to a standard curve with an internal standard. To generate the standard curves, a colony of *P. pastoris* KM71 was inoculated in 6 mL BMG medium and grown overnight at 30 °C with shaking at 235 rpm. The culture was added to BMG medium (125 to 200 mL) and grown at 30 °C with shaking at 235 rpm until the optical density at 600 nm was in the range of 9-14. Cultures were induced for expression by resuspension in BMM medium to a final optical density of 30. Solutions of starting material coumarin **6** and dimer product **9** were prepared in triplicate by serial dilution with DMSO. The stock solutions of standards were added to 24-well plates, followed by 1 mL aliquots of expression cultures with final concentrations from 0 up to 100 or 150 μM coumarin **6** and 0 to 50 or 75 μM dimer **9**. The 24-well plates were sealed with an adhesive cover and grown at 30 °C with shaking at 235 rpm for 48 h and supplemented with 100 μL of 10X methanol (5% MeOH, 95% water) after 24 h. The cultures were subjected to chemical lysis by the addition of 200 μL CelLytic Y Cell Lysis Reagent (Sigma) then incubated at 30 °C with shaking at 235 rpm for 30 min. An aliquot (50 μL) of the samples were removed and diluted with 150 μL methanol containing an internal standard, either 1,3,5-trimethoxybenzene with a final concentration of 300 μM or 4,4'-dihydroxybenzophenone for a final concentration of 40 μM. Precipitated yeast cells were pelleted by centrifugation (17,000 x *g* for 10 min), or filtered through Pall AcroPrep Advance 350 μL 0.2 um GHP Short Tip Natural PP 96-well filter plates by centrifugation (2000 rpm for 3 min). The samples were subjected to liquid

chromatography PDA spectrometry (UPLC) analysis performed on an Agilent 6230 time of flight mass spectrometer with a Dual AJS ESI source and an Agilent 1290 Infinity Series II diode array detector, autosampler, and binary pump, using one of the following conditions:

Method A. Waters Acquity UPLC HSS T3 1.8 µm C18, 2.1x50 mm column; positive mode; phase A = deionized water with 2 mM ammonium formate, pH = 3.5 and phase B = 95:5 acetonitrile: deionized water, v/v with 2 mM ammonium formate, pH = 3.5; method = 80% A held for 0.5min, to 45% A over 2.75 min, 10% A 100% A for 1.0 min, 254, 275, and 308 nm UV detection and 0.7 mL/min flow rate. Each injection was followed by equilibration at 80% A for 1 min.

Method B. Waters Acquity UPLC HSS T3 1.8 µm C18, 2.1x50 mm column; negative mode; phase A = 95:5 deionized water:acetonitrile B = 95:5 acetonitrile:deionized water; method = 80% A held for 0.5min, to 45% A over 2.75 min, 10% A 100% A for 1.0 min, 254, 275, and 308 nm UV detection and 0.7 mL/min flow rate. Each injection was followed by equilibration at 80% A for 1 min.

Method C. Waters Acquity UPLC HSS T3 1.8 µm C18, 2.1x50 mm column; negative mode; phase A = 100% deionized water with 0.1% formic acid: B = 95:5 acetonitrile:deionized water with 0.1% formic acid; method = 80% A held for 0.5min, to 45% A over 2.75 min, 10% A 100% A for 1.0 min, 254, 275, and 308 nm UV detection and 0.7 mL/min flow rate. Each injection was followed by equilibration at 80% A for 1 min.

Method D. Waters XBridge 3.5 µm C18, 2.1x150 mm column; positive mode; phase A = deionized water with 0.1% formic acid and phase B = 95:5 acetonitrile:deionized water with 0.1% formic acid; method = 85% A held for 1 min, 85% A to 20% A over 7 min, 20% A held for 1.5 min, and 0.4 mL/min flow rate, with either no UV detection or 254, 275, and 308 nm UV detection.

The percent conversion of the cross-coupled AB products was calculated with respect to the native coumarin **6** coupling partner by quantifying the concentration of remaining starting material A (native coumarin **6**) by standard curve, and the amount of coumarin dimer AA (dimer **9**) formed by standard curve. The concentration of the desired cross-coupled AB products was assumed to be comprised of the remaining. A species according to the formula:

1. $[A]_{start} = [A]_{remaining} + 2 \times [AA]_{formed} + [AB]_{formed}$

2. where $[AB]_{formed} = [A]_{start} - [A]_{remaining} - 2 \times [AA]_{formed}$

3. $\%\ AB = [AB]_{formed} / [A]_{start} * 100\%$

4. $\%\ AA = [AA]_{formed} / [AA]_{max} * 100\%$ where $[AA]_{max}$ is the theoretical maximum concentration possible

Standard curves for $[A]_{remaining}$ and $[AA]_{formed}$ were generated by using MassHunter software to process the raw data files. Extracted Ion Chromatograms to find peak integration of each species A, AA, and the internal standard (IS) with the peak integrations normalized by the internal standard (A/IS and AA/IS).

Standard curves and quantification of biocatalytic reactions

Supplemental Figure S3.41. Oxidative cross-coupling of **6** (A) with non-native partner (B) catalyzed by KtnC (**Figure 3.2**).

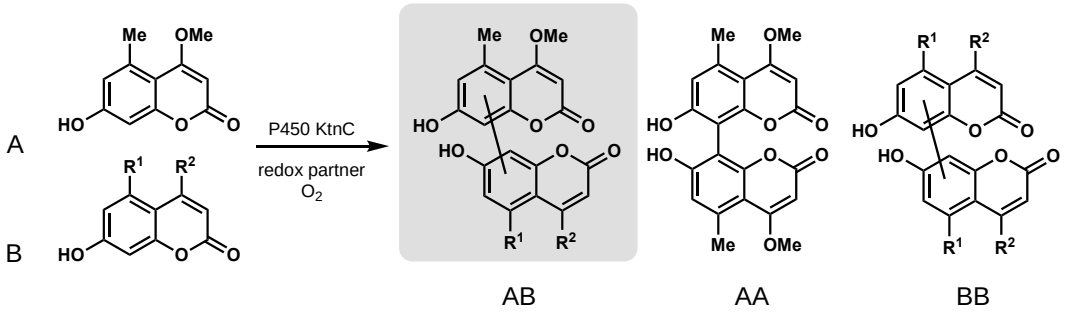

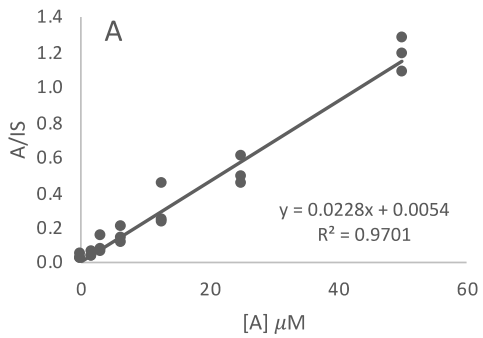

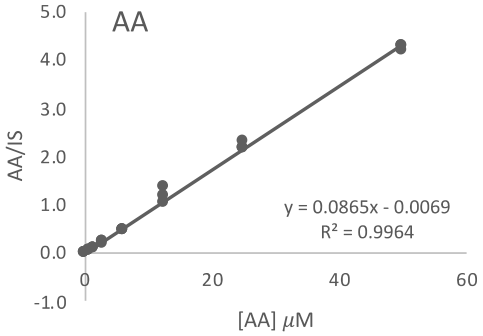

R1	R2	entry #	A/IS	AA/IS	$[A]_{remaining}$	$[AA]_{present}$	AB	% conv AB	average	% conv AA	average
Me	OEt	A1	0.01	0.05	1.67	0.64	22.05	88.19	87.3	5.12	4.7
		A2	0.03	0.04	2.32	0.53	21.62	86.49		4.24	
Me	OPr	A3	0.24	0.21	11.00	2.47	9.06	36.22	37.7	19.79	17.9
		A4	0.24	0.17	11.17	2.01	9.80	39.22		16.10	
Me	OiPr	A5	0.11	0.26	5.74	3.05	13.15	52.60	54.0	24.42	26.2
		A6	0.07	0.29	4.17	3.48	13.86	55.44		27.88	
Me	OBu	B1	0.07	0.34	3.94	3.96	13.14	52.56	49.7	31.70	34.5
		B2	0.07	0.40	3.97	4.66	11.70	46.80		37.30	

Supplemental Figure S3.42. Oxidative cross-coupling of **6** (A) with non-native partner (B) catalyzed by KtnC (**Figure 3.2**).

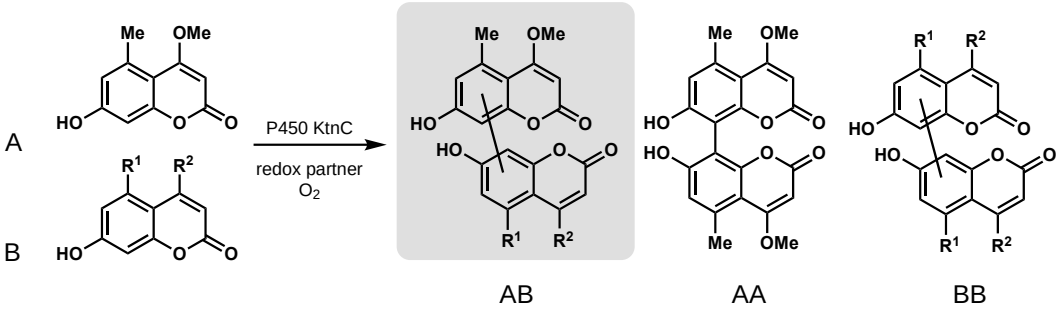

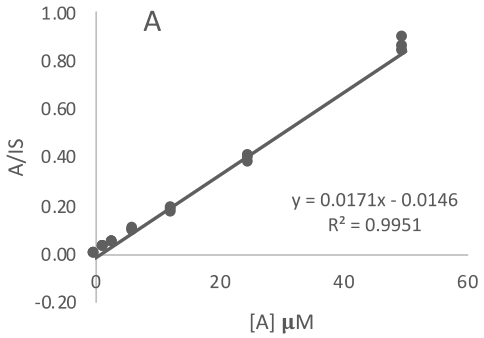

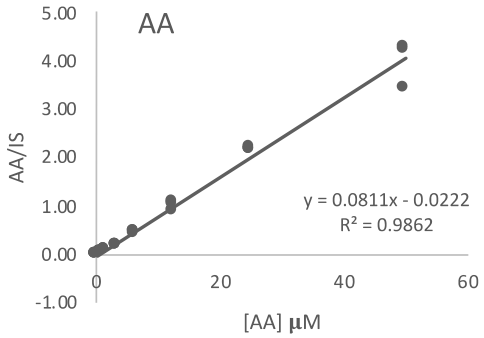

R1	R2	entry #	A/IS	AA/IS	$A_{remaining}$	$AA_{present}$	AB	% conv AB	average	% AA	average
Me	OtBu	B3	0.000	0.568	0.85302	7.27818	9.591	38.4	34.9	58.2	61.7
		B4	0.000	0.639	0.85302	8.15289	7.841	31.4		65.2	

Supplemental Figure S3.43. Oxidative cross-coupling of **6** (A) with non-native partner (B) catalyzed by KtnC (**Figure 3.2**).

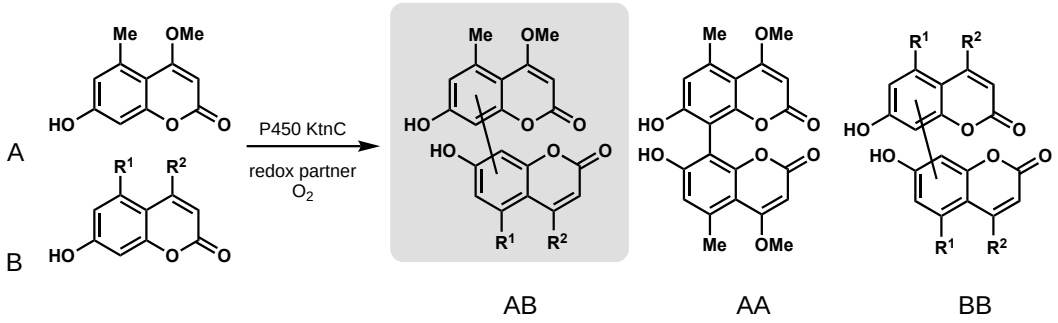

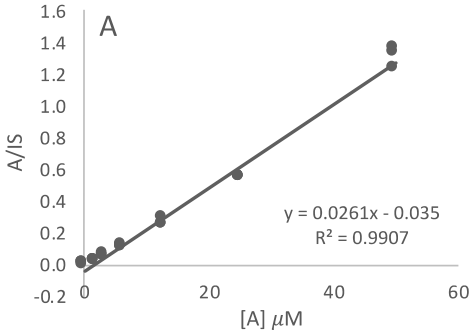

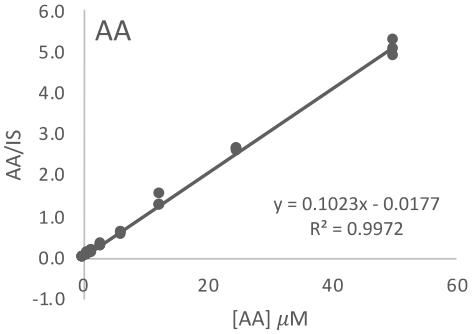

R1	R2	entry #	A/IS	AA/IS	$[A]_{remaining}$	$[AA]_{present}$	AB	% conv AB	average	% conv AA	average
H	OMe	A5	0.156	0.141	7.31570	1.54898	14.586	58.3	67.3	12.4	14.1
		A6	0.016	0.185	1.97117	1.98662	19.056	76.2		15.9	
Et	OMe	A1	0.371	0.009	15.55702	0.25933	8.924	35.7	31.0	2.1	2.2
		A2	0.431	0.013	17.84073	0.29776	6.564	26.3		2.4	
OH	OMe	C1	0.00	0.542	1.33926	5.46788	12.725	50.9	50.2	43.7	44.5
		C2	0.00	0.560	1.33926	5.64550	12.370	49.5		45.2	
Me	NHMe	A3	0.000	0.247	1.33926	2.58407	18.493	74.0	74.0	20.7	20.7
		A4	0.000	0.246	1.33926	2.57929	18.502	74.0		20.6	
Cl	OMe	C5	0.515	0.027	21.08830	0.43675	3.038	12.2	21.2	3.5	4.0
		C6	0.391	0.041	16.31739	0.57053	7.542	30.2		4.6	
Br	OMe	C3	0.396	0.016	16.50020	0.32768	7.844	31.4	29.9	2.6	2.7
		C4	0.414	0.017	17.21717	0.34356	7.096	28.4		2.7	
Me	H	B1	0.000	0.265	1.33926	2.76393	18.133	72.5	73.4	22.1	21.2
		B2	0.000	0.243	1.33926	2.54569	18.569	74.3		20.4	
H	Me	B3	0.000	0.494	1.33926	5.00279	13.655	54.6	54.0	40.0	40.6
		B4	0.000	0.510	1.33926	5.15688	13.347	53.4		41.3	
H	H	C1	0.000	0.706	1.33926	7.07236	9.516	38.1	39.0	56.6	55.7
		C2	0.000	0.683	1.33926	6.85020	9.960	39.8		54.8	

Supplemental Figure S3.44. Oxidative cross-coupling of **6** (A) with non-native **28** (B) catalyzed by KtnC (**Figure 3.2**).

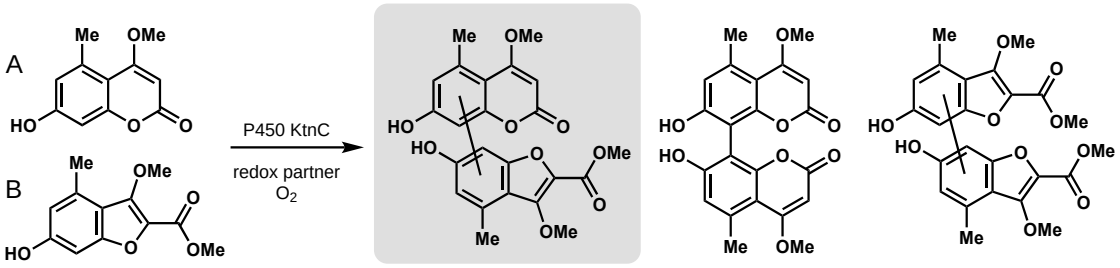

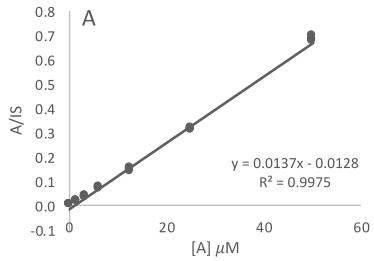

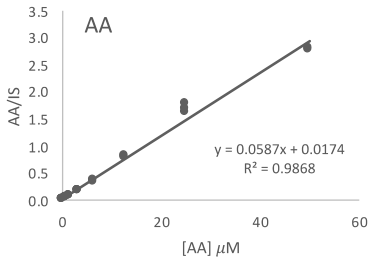

B partner	entry #	A/IS	AA/IS	$[A]_{remaining}$	$[AA]_{present}$	AB	% conv AB	average	% conv AA	average
benzofuran	B3	0.000	0.333	0.93431	5.38362	13.298	53.2	51.9	43.1	44.4
	B4	0.000	0.353	0.93431	5.70944	12.647	50.6		45.7	

Supplemental Figure S3.45. Oxidative cross-coupling of **6** (A) with non-native partner (B) catalyzed by KtnC (**Figure 3.2**).

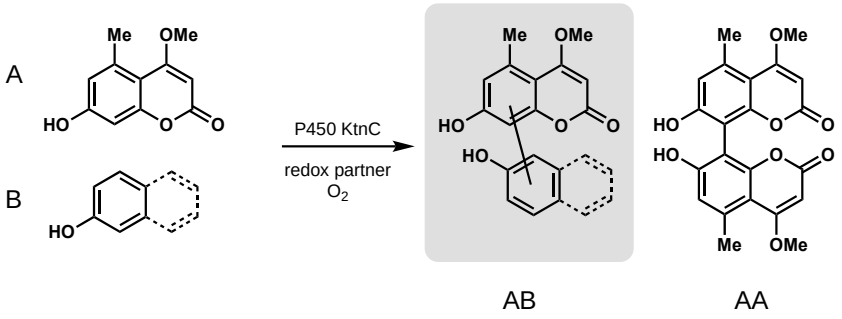

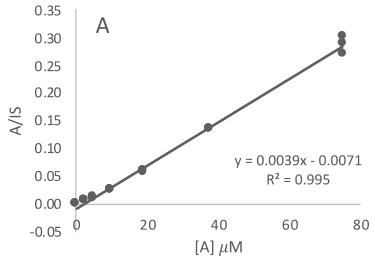

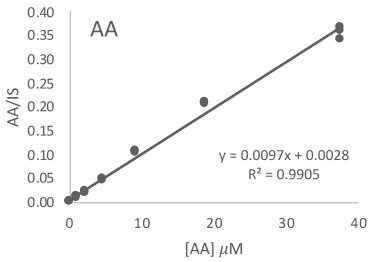

Phenol	entry #	A/IS	AA/IS	$[A]_{remaining}$	$[AA]_{present}$	AB	% conv AB	average	% conv AA	average
quinoline	C3	0.051	0.340	15.02189	34.84561	15.287	15.3	14.2	69.7	72.1
	C4	0.041	0.363	12.31828	37.27717	13.127	13.1		74.6	
2-naphthol	D1	0.121	0.322	33.02458	33.02720	0.921	0.9	2.0	66.1	65.1
	D2	0.119	0.314	32.72324	32.12063	3.035	3.0		64.2	
7-methoxy-2-naphthol	D3	0.250	0.051	66.52782	4.93853	23.595	23.6	20.3	9.9	10.5
	D4	0.272	0.056	72.05196	5.51253	16.923	16.9		11.0	
carbazole	D5	0.001	0.388	2.15328	39.77408	18.299	18.3	15.4	79.5	82.0
	D6	0.005	0.412	3.05648	42.24427	12.455	12.5		84.5	

Relative % yield calculations for Figures 3.3-3.6

Supplemental Figure S3.46. Oxidative cross-coupling of **22** (A) with non-native partner (B) catalyzed by KtnC (**Figure 3.3**).

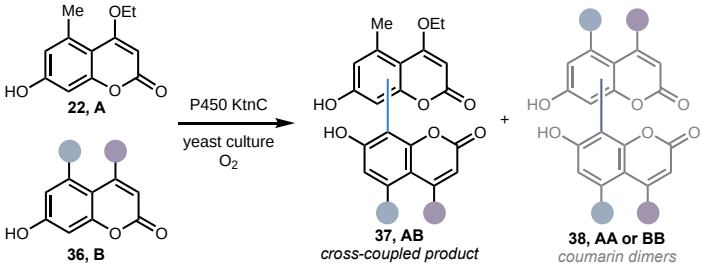

Peak areas:

R1	R2	A	AA	AB1	AB2	AB3	AB4
Me	OPr	721658	273609	31266	144577	26356	4040
		657074	206695	32628	145079	13525	
Me	OiPr	2165229	353294	373205	48616	14431	
		1869504	315643	344147			
Me	OBu	543337	246392	682922			
		579937	254793	695291			
Me	Me	523737	808202	69205	86007		
		715974	1022738	63014	51912	83207	
OH	OMe	963644	217958	1607003			
		1570325	420891	1626282			
Br	OMe	0	0				
		369104	23081	19697	57899		
Me	H	520821	531252	170472	26249	162253	12970
		517504	43971	151521	21900	141592	13414
H	OMe	724750	1004	17196	60862		
		690760	240	22324	22031		
Cl	OMe	309591	75526	8023	80661		
		368177	78751	8921	79025		
Me	NHMe	42493	11683	135281	56575	227557	
		72191	10098	124280	45087	218041	
H	H	523929	136650	261091	102338	8425	
		503291	29873	287562	95321	6031	

Calculations:

R1	R2	% total conversion	avg	% AA	avg	% AB1	avg	% AB2	avg	% AB3	avg	% AB4	avg	total % AB	avg
Me	OPr	51.1	49.5	37.1	34.9	2.1	2.4	9.8	10.6	1.8	1.4	0.3	0.1	14.0	14.6
		47.9		32.8		2.6		11.5		1.1		0.0		15.2	
Me	OiPr	34.5	34.4	21.4	21.8	11.3	11.7	1.5	0.7	0.4	0.2	0.0	0.0	13.2	12.6
		34.3		22.2		12.1		0.0		0.0		0.0		12.1	
Me	OBu	68.4	68.0	28.7	28.6	39.7	39.3	0.0	0.0	0.0	0.0	0.0	0.0	39.7	39.3
		67.5		28.6		39.0		0.0		0.0		0.0		39.0	
Me	Me	77.2	76.5	70.4	69.8	3.0	2.6	3.7	2.8	0.0	1.4	0.0	0.0	6.8	6.7
		75.8		69.1		2.1		1.8		2.8		0.0		6.7	
OH	OMe	67.9	64.5	14.5	17.7	53.4	46.9	0.0	0.0	0.0	0.0	0.0	0.0	53.4	46.9
		61.1		20.8		40.3		0.0		0.0		0.0		40.3	
Br	OMe	0.0	25.1	0.0	9.4	0.0	4.0	0.0	11.7	0.0	0.0	0.0	15.7	0.0	15.7
		25.1		9.4		4.0		11.7		0.0		15.7			
Me	H	73.4	59.0	54.3	31.9	8.7	12.5	1.3	1.8	8.3	11.7	0.7	1.0	19.0	27.1
		44.6		9.4		16.2		2.3		15.2		1.4		35.2	
H	OMe	9.9	8.0	0.2	0.2	2.1	2.6	7.6	5.3	0.0	0.0	0.0	0.0	9.7	7.9
		6.1		0.1		3.0		3.0		0.0		0.0		6.0	
Cl	OMe	43.6	41.8	27.5	26.6	1.5	1.5	14.7	13.8	0.0	0.0	0.0	0.0	16.1	15.2
		40.0		25.7		1.5		12.9		0.0		0.0		14.3	
Me	NHMe	91.2	88.1	4.8	4.5	27.9	26.9	11.7	10.5	46.9	46.2	0.0	0.0	86.4	83.6
		85.0		4.2		25.9		9.4		45.4		0.0		80.7	
H	H	55.2	51.2	23.4	14.8	22.3	26.3	8.8	9.4	0.7	0.7	0.0	0.0	31.8	36.3
		47.1		6.3		30.2		10.0		0.6		0.0		40.9	

Supplemental Figure S3.47. Oxidative cross-coupling of **14** (A) with non-native partner (B) catalyzed by KtnC (**Figure 3.4**).

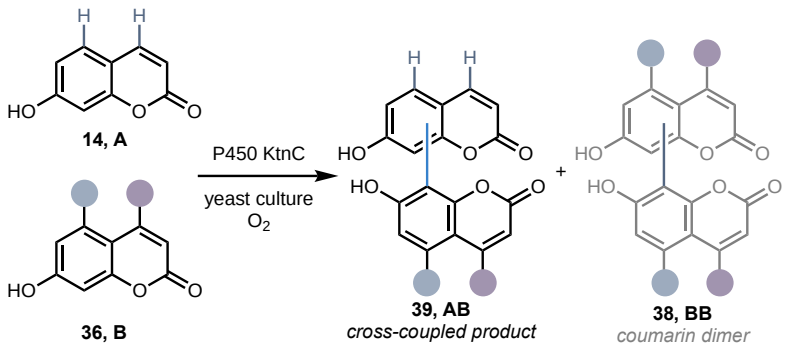

Peak areas:

R1	R2	A	AA	AB1	AB2	AB3	AB4
Me	NHMe	181355	185440	25285	3682	5945	14320
		171770	225851	19907	3683	4511	11304
Me	OEt	1669640	233965	88973	45515	4382	
		1608001	306353	95174	42087	3835	
Me	H	398203	8525	5380	1680		
		437297	12434	6441	1939		
Me	OBu	2132774	0	21543	13250	2643	
		2901616	0	10932	6595	1295	
Cl	OMe	697760	10291	2365	2956	1277	
		469623	11782	1852	1893	1076	

Calculations:

R1	R2	% total conversion	avg	% AA	avg	% AB1	avg	% AB2	avg	% AB3	avg	% AB4	avg	total % AB	avg
Me	NHMe	69.8	72.0	61.7	64.9	4.2	3.6	0.6	0.6	1.0	0.8	2.4	2.0	8.2	7.1
		74.1		68.1		3.0		0.6		0.7		1.7		5.9	
Me	OEt	26.7	29.3	20.6	23.2	3.9	4.0	2.0	1.9	0.2	0.2	0.0	0.0	6.1	6.0
		31.9		25.9		4.0		1.8		0.2		0.0		6.0	
Me	H	5.7	6.4	4.0	4.7	1.3	1.3	0.4	0.4	0.0	0.0	0.0	0.0	1.7	1.7
		7.1		5.3		1.4		0.4		0.0		0.0		1.8	
Me	OBu	1.7	1.2	0.0	0.0	1.0	0.7	0.6	0.4	0.1	0.1	0.0	0.0	1.7	1.2
		0.6		0.0		0.4		0.2		0.0		0.0		0.6	
Cl	OMe	3.7	4.7	2.8	3.8	0.3	0.3	0.4	0.4	0.2	0.2	0.0	0.0	0.9	0.9
		5.7		4.7		0.4		0.4		0.2		0.0		1.0	

Supplemental Figure S3.48. Oxidative cross-coupling of **A** with 7-hydroxyquinoline partner **29** (B) catalyzed by KtnC (**Figure 3.5**).

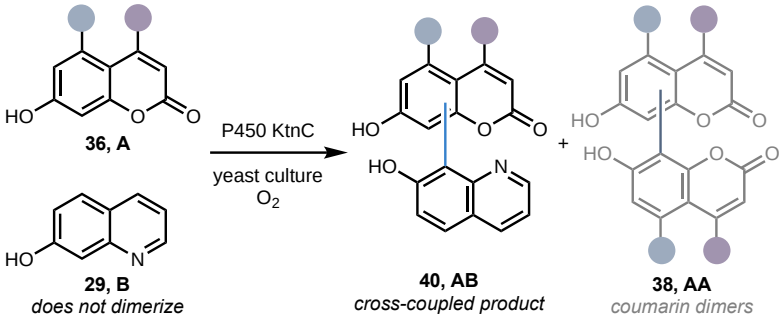

Peak areas:

R1	R2	A	AA	AB1	AB2	AB3	AB4
Me	Me	4233154	13506	696634	43495		
		4331161	9173	428519	26862		
H	H	525985	0	16300	6354	21214	5753
		576858	0	27133	11051	34828	9322
H	Me	1633797	2482	47393	30517	6879	
		1588117	2129	44016	30061	6494	
Me	NHMe	208884	267958	61669	27761	47578	190191
		248231	308789	41488	19028	33024	135922
Me	H	577313	36647	958481	50360	260049	168164
		589510	29599	891638	48779	244744	155231
Me	OEt	3039154	360694	197337	18865	35111	24726
		2755312	177028	212714	23885	22281	14131
Cl	OMe	544833	11840	13274	4173	4587	
		533117	10916	14306	4246	3730	
H	OMe	2066420	6798	55154	63263	17595	15668
		1985756	11751	122605	128357	33367	27682
Br	OMe	460500	7858	5608	1532	2294	3410
		310008	5442	8786	1711	2273	1983

Calculations:

R1	R2	% total conversion	avg	% AA	avg	AB1	AB2	AB3	AB4	total % AB	avg
Me	Me	15.3	12.6	0.5	0.5	13.9	0.9	0.0	0.0	14.8	12.1
		9.9		0.4		8.9	0.6	0.0	0.0	9.5	
H	H	8.6	10.6	0.0	0.0	2.8	1.1	3.7	1.0	8.6	10.6
		12.5		0.0		4.1	1.7	5.3	1.4	12.5	
H	Me	5.2	5.1	0.3	0.3	2.7	1.8	0.4	0.0	4.9	4.9
		5.1		0.3		2.6	1.8	0.4	0.0	4.8	
Me	NHMe	80.5	78.9	50.0	53.2	5.8	2.6	4.4	17.7	30.5	25.7
		77.3		56.4		3.8	1.7	3.0	12.4	21.0	
Me	H	72.3	71.4	3.5	3.2	45.9	2.4	12.5	8.1	68.8	68.1
		70.4		3.0		44.8	2.5	12.3	7.8	67.4	
Me	OEt	24.7	21.6	17.9	14.2	4.9	0.5	0.9	0.6	6.8	7.5
		18.5		10.5		6.3	0.7	0.7	0.4	8.1	
Cl	OMe	7.7	7.7	4.0	3.9	2.2	0.7	0.8	0.0	3.7	3.8
		7.6		3.8		2.5	0.7	0.6	0.0	3.9	
H	OMe	7.4	10.9	0.6	0.8	2.5	2.8	0.8	0.7	6.8	10.1
		14.5		1.0		5.3	5.5	1.4	1.2	13.4	
Br	OMe	5.8	6.7	3.2	3.2	1.1	0.3	0.5	0.7	2.6	3.5
		7.6		3.2		2.6	0.5	0.7	0.6	4.4	

Supplemental Figure S3.49. Oxidative cross-coupling of **A** with 2-naphthol partner **31** (B) catalyzed by KtnC (**Figure 3.6**).

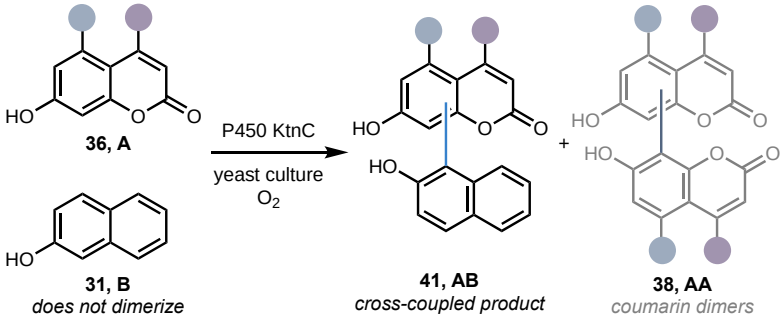

R1	R2	A	AA	AB1	AB2	% total conversion	avg	% AA	avg	% AB1	% AB2	total % AB	avg
Me	NHMe	47239	13469	3847		39.5	42.7	34.5	37.9	4.9	0.0	4.9	4.7
		219170	83813	10106	8290	45.9		41.4		2.5	2.0	4.5	
H	OMe	1160944	4396	5277		1.2	0.8	0.7	0.5	0.4	0.0	0.4	0.3
		1222816	1714	2360		0.5		0.3		0.2	0.0	0.2	
Me	H	411865	2099	7658	3600	3.6	3.2	1.0	0.8	1.8	0.8	2.6	2.4
		324324	1013	4305	2617	2.7		0.6		1.3	0.8	2.1	

Supplemental Figure S3.50. Oxidative cross-coupling of **9** with coupling partner **B** catalyzed by KtnC, DesC, or [Cu] (**Figure 3.20**).

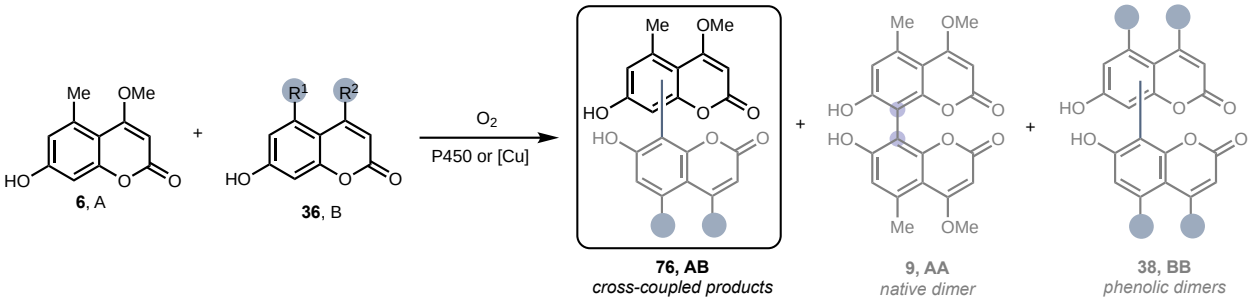

Substrate B	catalyst	A	AA	AB1	AB2	AB3	AB4	% total conversion	avg	% AA	avg	% AB1	% AB2	% AB3	% AB4	total % AB	avg
Me, OEt	KtnC	432151	4849702	2336988	1520700			96.9	96.2	69.3	68.1	16.7	10.9	0.0	0.0	27.6	28.0
	KtnC	660858	4844583	2459407	1668343			95.4		66.9		17.0	11.5	0.0	0.0	28.5	
	DesC	3384253	399939	391707	1257196	249348		44.4	46.8	13.2	15.1	6.4	20.7	4.1	0.0	31.2	31.7
	DesC	3110214	518950	462006	1251346	257400		49.2		17.0		7.6	20.5	4.2	0.0	32.2	
	[Cu] 1	2642215	42665	107683				6.8	6.8	3.0	3.0	3.8	0.0	0.0	0.0	3.8	3.8
Me, OPr	KtnC	226479	7461989	153807	131319	16627	18868	98.5	98.0	96.5	95.9	1.0	0.8	0.1	0.1	2.1	2.1
	KtnC	385795	7253549	153390	132602	14629	17062	97.5		95.4		1.0	0.9	0.1	0.1	2.1	
	DesC	1946538	2078100	11048	857186	391581	205464	74.3	79.0	54.9	58.7	0.1	11.3	5.2	2.7	19.4	20.3
	DesC	1176332	2263915	10860	896360	426634	197965	83.7		62.6		0.2	12.4	5.9	2.7	21.2	
	[Cu] 2	2386237	189046	641897				29.9	29.9	11.1	11.1	18.8	0.0	0.0	0.0	18.8	18.8
Me, OBu	KtnC	22829	7630183	77179	205742	16399		99.9	99.8	97.9	98.0	0.5	1.3	0.1	0.0	1.9	1.8
	KtnC	35861	7468569	69436	182120			99.8		98.1		0.5	1.2	0.0	0.0	1.7	
	DesC	1520718	2579451	38023	64251	19675		77.6	75.3	75.8	73.7	0.6	0.9	0.3	0.0	1.8	1.6
	DesC	1904893	2523122	29456	48887	21216		73.0		71.6		0.4	0.7	0.3	0.0	1.4	
	[Cu] 3	1949740	136105	7793	499597	62956		30.2		9.7		0.3	17.9	2.3	0.0	20.4	20.4
Me, NHMe	KtnC	536787	5731091	1257762	39462	90537	1991	96.0	94.0	85.6	83.3	9.4	0.3	0.7	0.0	10.4	10.7
	KtnC	1024854	5232015	1279078	27303	95488	18403	92.1		81.1		9.9	0.2	0.7	0.1	11.0	
	DesC	2229301	1804244	146144	29664	2263		62.9	64.1	60.0	61.2	2.4	0.5	0.0	0.0	3.0	2.9
	DesC	2318117	2075887	120913	54658	9743	5313	65.2		62.3		1.8	0.8	0.1	0.1	2.9	
	[Cu] 4	1980570	88612	104458	7295			12.7		7.8		4.6	0.3	0.0	0.0	4.9	4.9
OH, OMe	KtnC	2412460	6789122	820751				85.6	87.8	80.8	82.7	4.9	0.0	0.0	0.0	4.9	5.1
	KtnC	1399856	5836766	734563				89.9		84.5		5.3	0.0	0.0	0.0	5.3	
	DesC	2011506	2239077	535431	80213			71.7	71.9	63.0	62.9	7.5	1.1	0.0	0.0	8.7	8.9
	DesC	1768660	1989318	507423	75511			72.1		62.9		8.0	1.2	0.0	0.0	9.2	
	[Cu] 5	18963975	17657	104324	51398			1.0		0.2		0.5	0.3	0.0	0.0	0.8	0.8
H, OMe	KtnC	2550485	4804762	881331	558002			81.2	89.7	70.7	70.6	6.5	4.1	0.0	0.0	10.6	19.2
lots of BB	KtnC	308897	6229676	2926974	1978451			98.3		70.5		16.6	11.2	0.0	0.0	27.8	
	DesC	2834147	1473972	1274238	374972	471213	82227	64.5	64.9	36.9	36.7	16.0	4.7	5.9	1.0	27.6	28.2
	DesC	2943889	1547087	1381430	414896	539986	97226	65.2		36.5		16.3	4.9	6.4	1.1	28.7	
	[Cu] 6	8212383	1533750	14754	627806			31.1		25.7		0.1	5.3	0.0	0.0	5.4	5.4
Et, OMe	KtnC	876569	5731985	719835	442226	23186	32263	93.5	90.9	84.6	82.3	5.3	3.3	0.2	0.2	9.0	8.5
	KtnC	1606603	5472096	698064	381854	24785		88.2		80.1		5.1	2.8	0.2	0.0	8.1	
	DesC	2306336	1573398	184191	710706	329990	93995	65.9	62.5	46.5	43.9	2.7	10.5	4.9	1.4	19.5	18.6
	DesC	2701227	1367282	168800	623400	301120	84384	59.2		41.3		2.6	9.4	4.6	1.3	17.8	
	[Cu] 7	2299599	173175	422864				25.1		11.3		13.8	0.0	0.0	0.0	13.8	13.8
Cl, OMe	KtnC	3322935	3108651	404275	53052			66.8	78.3	62.2	76.0	4.0	0.5	0.0	0.0	4.6	2.3
no BB	KtnC	1242438	5462595					89.8		89.8		0.0	0.0	0.0	0.0	0.0	
	DesC	3658407	1112086	215862	301202	63743	4730	43.4	49.9	34.4	29.7	3.3	4.7	1.0	0.1	9.1	20.2
	DesC	3497835	1001791	2123270	323429	68291	4841	56.4		25.0		26.5	4.0	0.9	0.1	31.4	
	[Cu] 8	1553536	346376	2632	4155	10259		31.4		30.6		0.1	0.2	0.5	0.0	0.8	0.8
Br, OMe	KtnC	3503076	2877673	82837	12954	234588		63.5	65.3	60.0	61.6	0.9	0.1	2.4	0.0	3.4	3.7
	KtnC	3199160	3066853	138036	19410	217171		67.0		63.2		1.4	0.2	2.2	0.0	3.9	
	DesC	3481409	336993	26946	127094	18323	185400	22.9	27.2	14.9	19.4	0.6	2.8	0.4	4.1	7.9	7.8
	DesC	3726452	648565	37931	169672	26150	178970	31.5		23.9		0.7	3.1	0.5	3.3	7.6	
	[Cu] 9	1864628	454931	33045				33.6		32.4		1.2	0.0	0.0	0.0	1.2	1.2
Me, H	KtnC	2079971	5566401	919289	119029	152951	391003	85.9	86.4	75.2	75.6	6.2	0.8	1.0	2.6	10.7	10.7
	KtnC	1990483	5719947	946929	128548	153502	382728	86.8		76.1		6.3	0.9	1.0	2.5	10.7	
	DesC	2475655	2028364	854615	695605	67103	27566	69.7	71.0	49.6	50.2	10.5	8.5	0.8	0.3	20.1	20.8
	DesC	2343338	2144859	926963	769723	78055	31336	72.2		50.8		11.0	9.1	0.9	0.4	21.4	
	[Cu] 10	2318659	109215	100108	26074			12.9		8.2		3.8	1.0	0.0	0.0	4.7	4.7
H, Me	KtnC	189025	7055922	570715	285563	152998		98.8	99.3	92.2	91.8	3.7	1.9	1.0	0.0	6.6	7.5
	KtnC	40703	7111722	755161	362914	189927		99.7		91.3		4.8	2.3	1.2	0.0	8.4	
	DesC	2235714	2332726	388197	562265	150391	262196	72.9	72.4	56.5	56.1	4.7	6.8	1.8	3.2	16.5	16.4
	DesC	2185126	2168276	370589	524981	139749	228897	71.9		55.7		4.8	6.7	1.8	2.9	16.2	
	[Cu] 11	1737377	309256	90014	4620			29.1		25.2		3.7	0.2	0.0	0.0	3.9	3.9
H, H	KtnC	42380	7009911	111931	43090	10693	6647	99.7	99.8	98.5	98.5	0.8	0.3	0.1	0.0	1.2	1.3
	KtnC	23663	7030808	132827	51618	1788	9770	99.8		98.5		0.9	0.4	0.0	0.1	1.4	
	DesC	1878455	2720993	47592	67663	57247	23221	75.0	76.1	72.4	73.8	0.6	0.9	0.8	0.3	2.6	2.2
	DesC	1784552	2929900	36915	54603	43521	12600	77.1		75.2		0.5	0.7	0.6	0.2	1.9	
	[Cu] 12	1596838	259397	90765				27.6		23.5		4.1	0.0	0.0	0.0	4.1	4.1

Calculations for BB

Substrate B	catalyst	B	BB1	BB2	BB3	BB4	% total conversion	% BB1	% BB2	% BB3	% BB4	avg total BB
Me, OEt	KtnC	1234777	576617	698666			67.4	30.5	36.9			62.9
	KtnC	1776677	587921	663336			58.5	27.5	31.0			
	DesC	2536491	386257	63088	27082		27.3	22.1	3.6	1.6		27.9
	DesC	2249781	375251	48809	23563		28.5	23.9	3.1	1.5		
	[Cu] 1	3278200	66251				3.9	3.9				3.9
Me, OPr	KtnC	4618124	17429	25683	10247		2.3	0.7	1.1	0.4		2.3
	KtnC	4620553	16804	24814	11411		2.2	0.7	1.0	0.5		
	DesC	3935964	18718	8189			1.3	0.9	0.4	0.0		1.3
	DesC											
	[Cu] 2	3955085	480717				19.6	19.6				19.6
Me, NHMe	KtnC	85601	33142	4512	4400		49.6	39.1	5.3	5.2		50.4
	KtnC	105771	38192	6634	10788		51.3	35.2	6.1	9.9		
	DesC	no BB										5.7
	DesC	1868377	23509	6968	20588	5561	5.7	2.4	0.7	2.1	0.6	
	[Cu] 4	582470	20941	14500	116344		34.3	4.7	3.3	26.3		34.3
H, OMe	KtnC	3573082	427547				19.3	19.3				21.6
	KtnC	3283205	515078				23.9	23.9				
	DesC	2832608	316376	347035	106749		35.2	14.5	15.9	4.9		36.3
	DesC	3031824	343494	422717	139469		37.4	14.2	17.5	5.8		
	[Cu] 6	7832391	176569				4.3	4.3				4.3
Et, OMe	KtnC	3343719	1460485	88526	15235		48.3	45.1	2.7	0.5	0.0	46.1
	KtnC	3707615	1206243	199410	26600	12698	43.8	36.6	6.0	0.8	0.4	
	DesC	2978704	672288	37594	122171		35.8	29.0	1.6	5.3	0.0	37.2
	DesC	3208466	771729	64571	141828	27358	38.5	29.6	2.5	5.4	1.0	
	[Cu] 7	3972468	264943				11.8	11.8				11.8
Me, H	KtnC	5430689	246028	9349	76529	373374	20.6	7.2	0.3	2.2	10.9	19.6
	KtnC	5658117	213802	10265	67589	355195	18.6	6.2	0.3	1.9	10.2	
	DesC	4453076	190688	199698			14.9	7.3	7.6			14.4
	DesC	4511478	173677	189904			13.9	6.6	7.3			
	[Cu] 10	256181	17090	7226			16.0	11.2	4.7			16.0
H, Me	KtnC	5200373	8701	23613	8376		1.5	0.3	0.9	0.3		1.6
	KtnC	4881980	5315	31628	6309		1.7	0.2	1.3	0.3		
	DesC	4497081	69056	11694	6266	6753	4.0	2.9	0.5	0.3	0.3	4.0
	DesC	4349140	67460	13331	5132	5050	4.0	3.0	0.6	0.2	0.2	
	[Cu] 11	1111935	5811				1.0	1.0				1.0
H, H	KtnC	5599849	18455	393615			0.7	0.7				0.9
	KtnC	5580365	12723	73843	18903		1.1	0.5		0.7		
	DesC	8156453	8096	44971	11161		0.5	0.2		0.3		0.6
	DesC	5884395	7785	87246	16813		0.8	0.3		0.6		
	[Cu] 12	614424	8507	3813			3.9	2.7	1.2			3.9

Supplemental Figure S3.51. Oxidative cross-coupling of **9** with coupling partner **B** catalyzed by KtnC, DesC, or [Cu] (**Figure 3.22**).

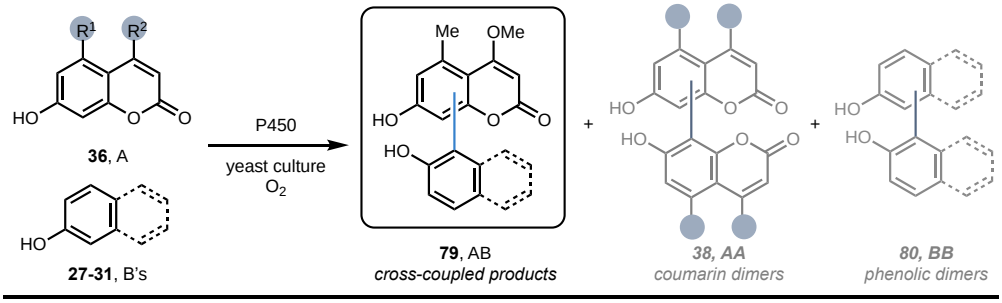

A	B	catalyst	A	AA	AB1	AB2	AB3	AB4	% total conversion	avg	% AA	avg	% AB1	% AB2	% AB3	% AB4	total % AB	avg
Native	2-naphthol	KtnC	17017	3775725	5115	4624			99.8	99.8	99.6	99.7	0.1	0.1	0.0	0.0	0.1	0.1
		KtnC	18512	4069879		5547			99.8		99.7		0.0	0.1	0.0	0.0	0.1	
		DesC	2273433	3943123			3786		77.6	78.1	77.6	78.1	0.0	0.0	0.0	0.0	0.0	0.0
		DesC	2229670	4104296			3752		78.6		78.6		0.0	0.0	0.0	0.0	0.0	
		[Cu] 1	8798387	71799	1226687				13.5		1.4		12.1	0.0	0.0	0.0	12.1	12.1
Native	7-Meo-2-naphthol	KtnC	27670	3687490					99.6	99.6	99.6	99.6	0.0	0.0	0.0	0.0	0.0	0.0
		KtnC	27260	3930452					99.7		99.7		0.0	0.0	0.0	0.0	0.0	
		DesC	2132030	4253947					80.0	76.6	80.0	76.6	0.0	0.0	0.0	0.0	0.0	0.0
		DesC	3102749	4236706					73.2		73.2		0.0	0.0	0.0	0.0	0.0	
		[Cu] 2	6348675	363263	1433114				25.4		8.5		16.8	0.0	0.0	0.0	16.8	16.8
Native	quinoline	KtnC	16397	3801012	33661	14604	9739	53204	99.8	99.8	98.3	98.4	0.4	0.2	0.1	0.7	1.4	1.4
		KtnC	23891	4183586	32757	17275	11494	54797	99.7		98.4		0.4	0.2	0.1	0.6	1.4	
		DesC	2389118	3938352				74710	76.9	77.8	76.2	77.1	0.0	0.0	0.0	0.7	0.7	0.7
		DesC	2177163	4001560				78285	78.8		78.0		0.0	0.0	0.0	0.8	0.8	
		[Cu] 3	7248147	2025296	6201119	558134			59.9		22.4		34.3	3.1	0.0	0.0	37.4	37.4
Native	carbazole	KtnC	19573	3986622	23409				99.8	99.7	99.5	99.5	0.3	0.0	0.0	0.0	0.3	0.2
		KtnC	27685	4173784	15519				99.7		99.5		0.2	0.0	0.0	0.0	0.2	
		DesC	2312866	4482182	21135	5317			79.5	79.4	79.3	79.1	0.2	0.0	0.0	0.0	0.2	0.3
		DesC	2398264	4571515	32947	7051			79.3		78.9		0.3	0.1	0.0	0.0	0.3	
		[Cu] 4	8514700	904766	5172				17.6		17.5		0.1	0.0	0.0	0.0	0.1	0.1
Native	benzofuran	KtnC	23158	4178785	13228	399898	85732	15851	99.7	91.7	94.0	86.3	0.1	4.5	1.0	0.2	5.8	5.4
		KtnC	1678402	4014740	12179	388345	91879	15300	83.6		78.6		0.1	3.8	0.9	0.1	5.0	
		DesC	3900380	3438476		938007	180407	85660	67.4	65.4	57.4	55.8	0.0	7.8	1.5	0.7	10.0	9.6
		DesC	4478309	3312226		859869	168887	80259	63.3		54.2		0.0	7.0	1.4	0.7	9.1	
		[Cu] 5	7271737	2622432		972039			46.1		38.9		0.0	7.2	0.0	0.0	7.2	7.2
OH, OMe	benzofuran	KtnC	3823129	798329	10212				29.6	31.7	29.4	31.5	0.2	0.0	0.0	0.0	0.2	0.2
		KtnC	3842467	974914	12872				33.8		33.6		0.2	0.0	0.0	0.0	0.2	
		DesC	3660201	888378	2014				32.7	33.8	32.7	33.7	0.0	0.0	0.0	0.0	0.0	0.0
		DesC	3572214	951673	2952				34.8		34.7		0.1	0.0	0.0	0.0	0.1	
		[Cu] 6	5758998	829225	9562				22.5	22.5	22.3	22.3	0.1	0.0	0.0	0.0	0.1	0.1
Me, H	7-Meo-2-naphthol	KtnC	9167357	2781285	128526	37727	140701	12889	39.1	38.6	37.0	36.4	0.9	0.3	0.9	0.1	2.1	2.2
		KtnC	9504081	2753398	142311	42964	156307	12563	38.1		35.8		0.9	0.3	1.0	0.1	2.3	
		DesC	8983022	2134561	14459	9435	27820		32.5	32.7	32.1	32.3	0.1	0.1	0.2	0.0	0.4	0.4
		DesC	9183349	2221665	15380	9036	30031		32.9		32.5		0.1	0.1	0.2	0.0	0.4	
		[Cu] 8	2141834	43166	316303	4689	29945		17.0	17.0	3.3	3.3	12.3	0.2	1.2	0.0	13.6	13.6
Me, H	quinoline	KtnC	8643138	4088564	197858	49371	55723	194360	50.1	51.2	47.2	48.2	1.1	0.3	0.3	1.1	2.9	3.0
		KtnC	8773086	4528354	246374	57674	63668	218099	52.4		49.2		1.3	0.3	0.3	1.2	3.2	
		DesC	8480063	2751914					39.4	40.3	39.4	40.3	0.0	0.0	0.0	0.0	0.0	0.0
		DesC	8317038	2924477					41.3		41.3		0.0	0.0	0.0	0.0	0.0	
		[Cu] 9	2594194	273862	7995781	2187641			80.5	80.5	4.1	4.1	60.0	16.4	0.0	0.0	76.4	76.4
H, OMe	quinoline	KtnC	5413462	957635	26718	48543	60881	45084	27.9	27.7	25.5	25.1	0.4	0.6	0.8	0.6	2.4	2.6
		KtnC	5419392	922670	31373	64955	72260	41778	27.5		24.7		0.4	0.9	1.0	0.6	2.8	
		DesC	4915760	4631350	9919			40914	65.5	64.2	65.1	63.8	0.1	0.0	0.0	0.3	0.4	0.4
		DesC	5739926	4834755	7433			53251	62.9		62.5		0.0	0.0	0.0	0.3	0.4	
		[Cu] 10	11649479	39365	4868013	448639			31.7		0.5		28.6	2.6	0.0	0.0	31.2	31.2
Me, NHMe	quinoline	KtnC	237080	202740	24775	45883			66.8	65.3	56.9	57.0	3.5	6.4	0.0	0.0	9.9	8.3
		KtnC	259111	203955	17251	30703			63.8		57.1		2.4	4.3	0.0	0.0	6.7	
		DesC	273850	416625		1620			75.3	75.7	75.2	75.6	0.0	0.1	0.0	0.0	0.1	0.2
		DesC	267652	425740		1944			76.1		76.0		0.0	0.2	0.0	0.0	0.2	
		[Cu] 11	2713068	33574	893810				26.2	26.2	1.8	1.8	24.3	0.0	0.0	0.0	24.3	24.3
H, H	quinoline	KtnC	11682201	12114	5703	5887	7449		0.4	0.4	0.2	0.2	0.0	0.1	0.1	0.0	0.2	0.2
		KtnC	11696334	16868	7497	6123	8735		0.5		0.3		0.1	0.1	0.1	0.0	0.2	
		DesC	11689482	4668			452		0.1	0.1	0.1	0.1	0.0	0.0	0.0	0.0	0.0	0.0
		DesC	11851876	6143	473				0.1		0.1		0.0	0.0	0.0	0.0	0.0	
		[Cu] 12	16902447	467024	8265598	1234431			38.2		3.4		30.2	4.5	0.0	0.0	34.8	34.8

LC-MS traces for biocatalytic reactions

Supplemental Figure S3.52. Oxidative cross-coupling of **6** and **11** by KtnC (**Figure 3.2**).

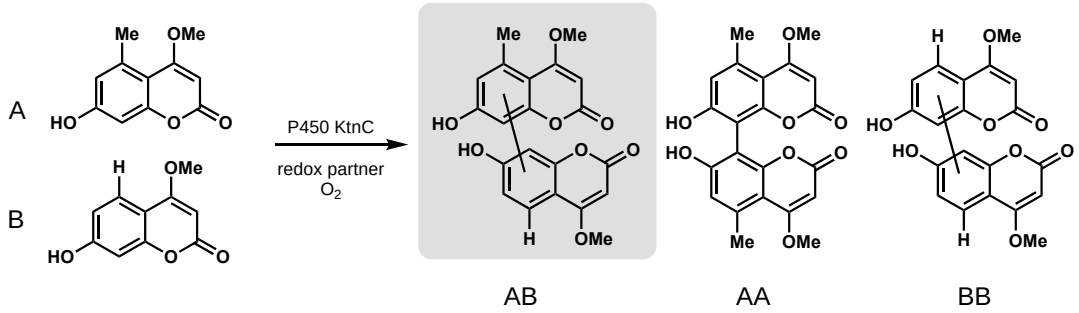

KtnC

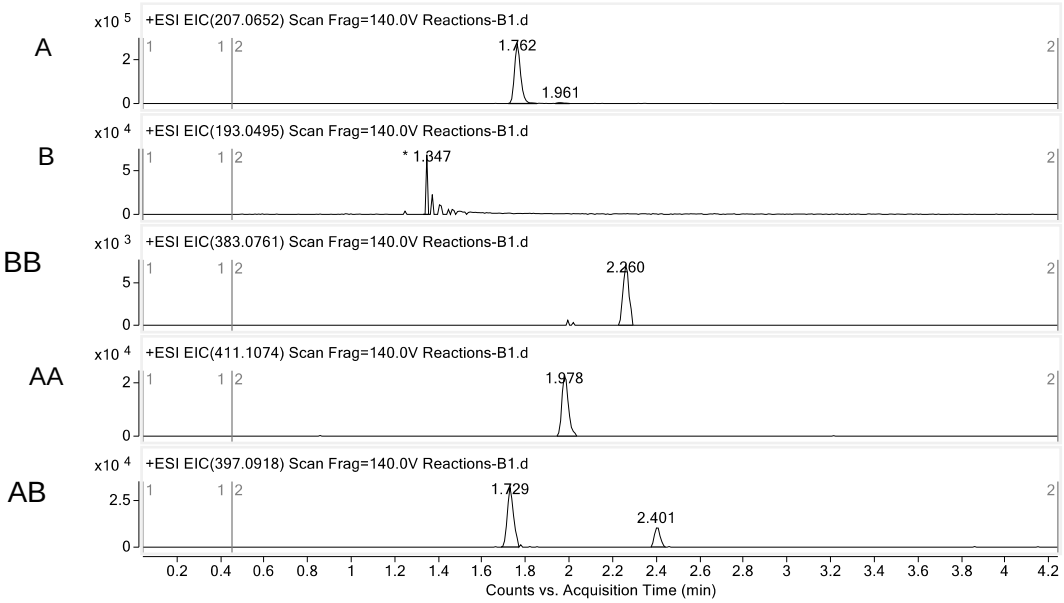

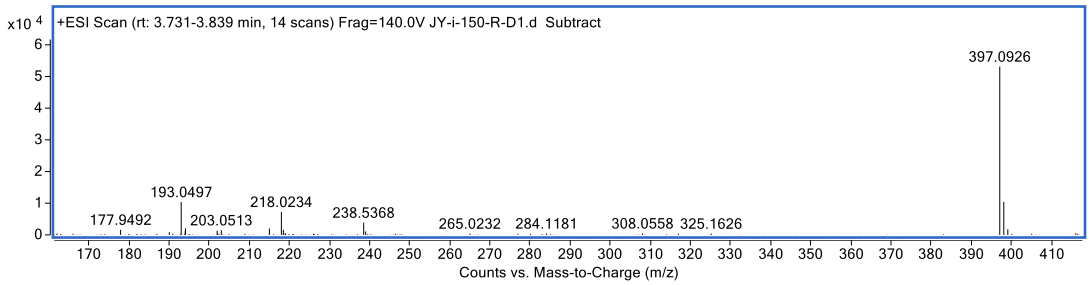

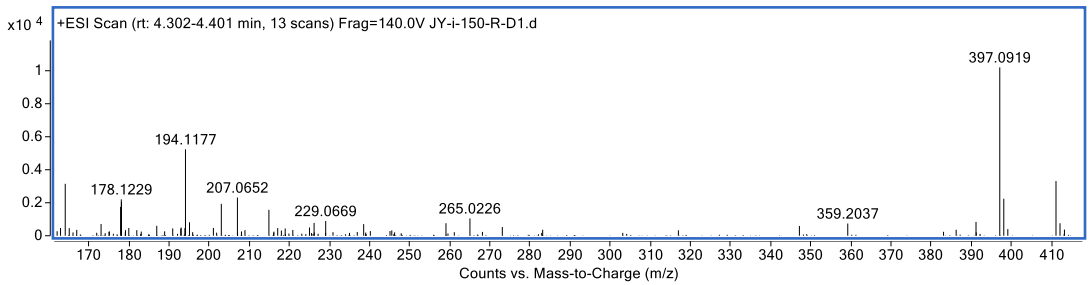

No Enzyme control

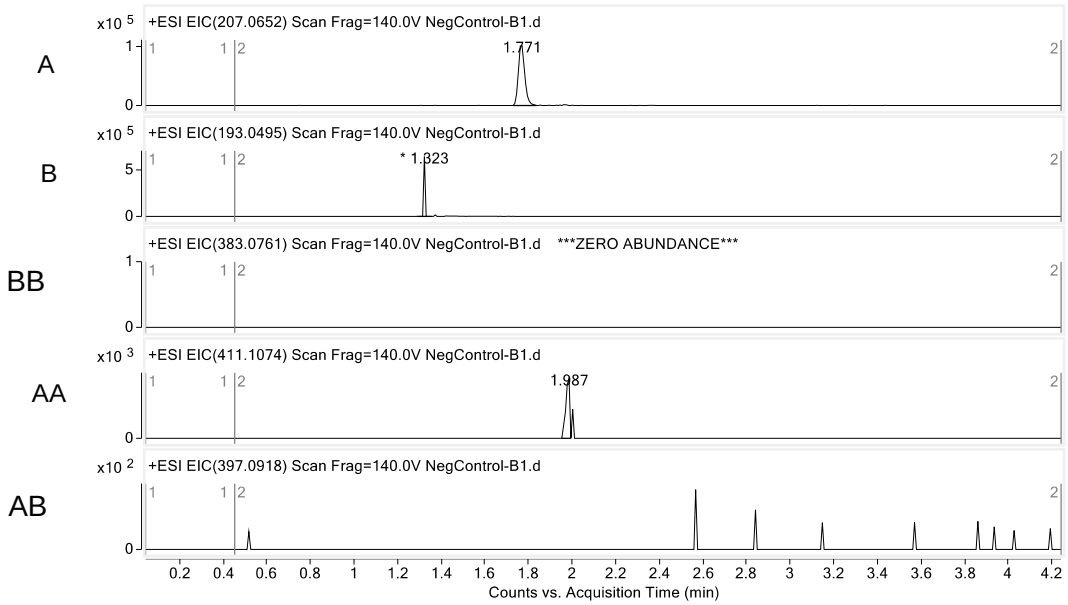

Supplemental Figure S3.53. Oxidative cross-coupling of **6** and **12** by KtnC (**Figure 3.2**).

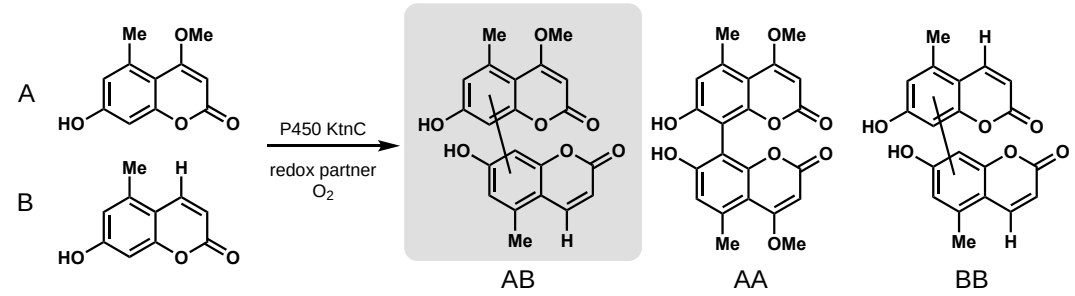

KtnC

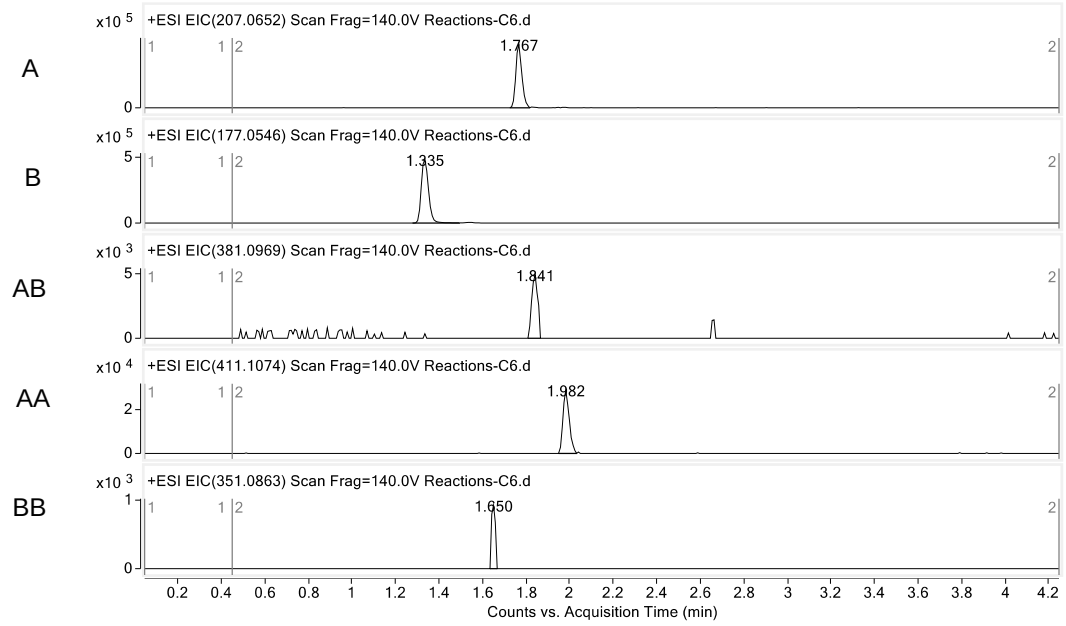

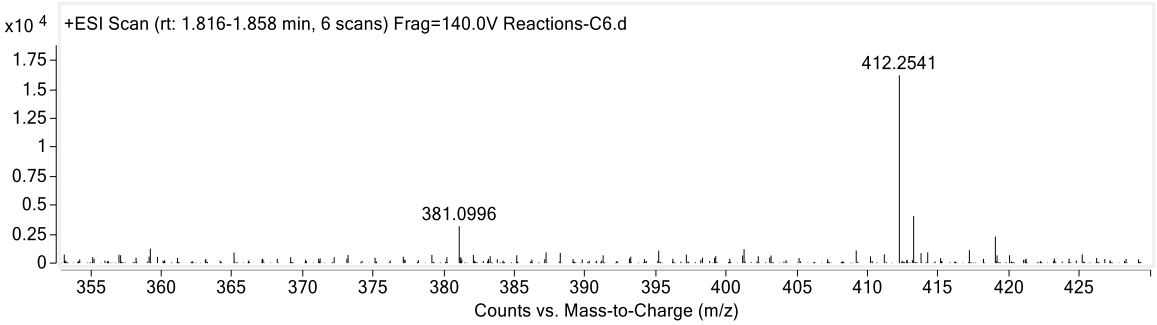

No Enzyme control

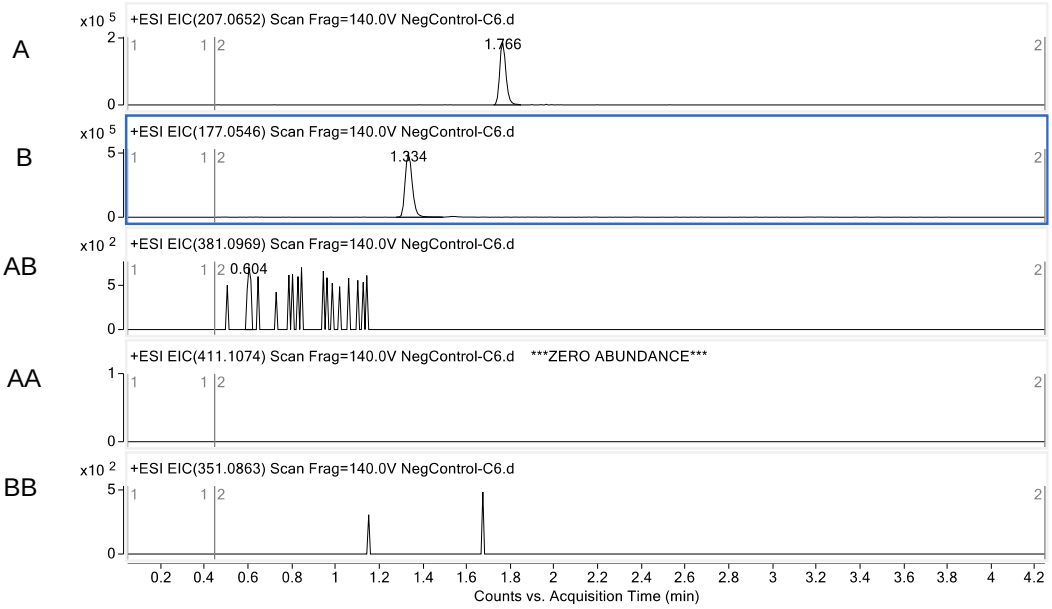

Supplemental Figure S3.54. Oxidative cross-coupling of **6** and **13** by KtnC (**Figure 3.2**).

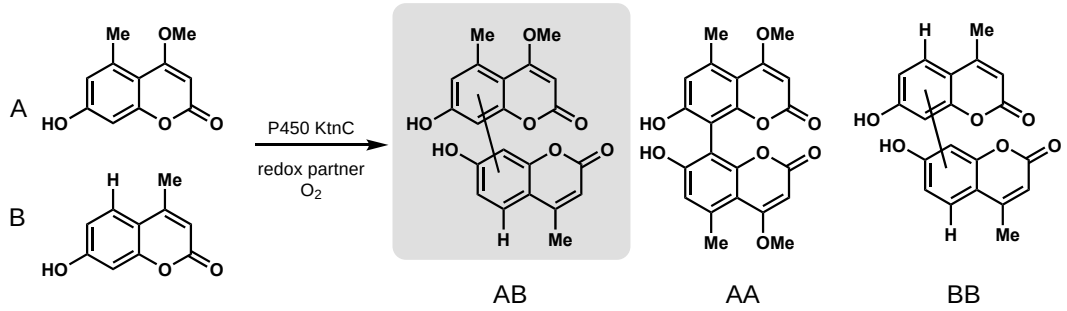

KtnC

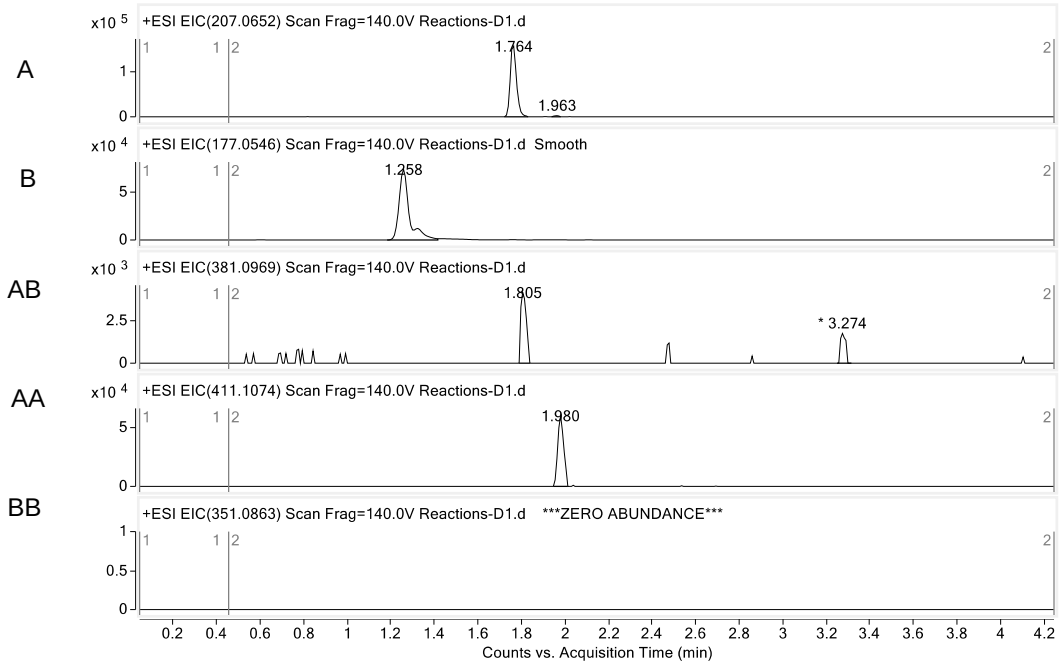

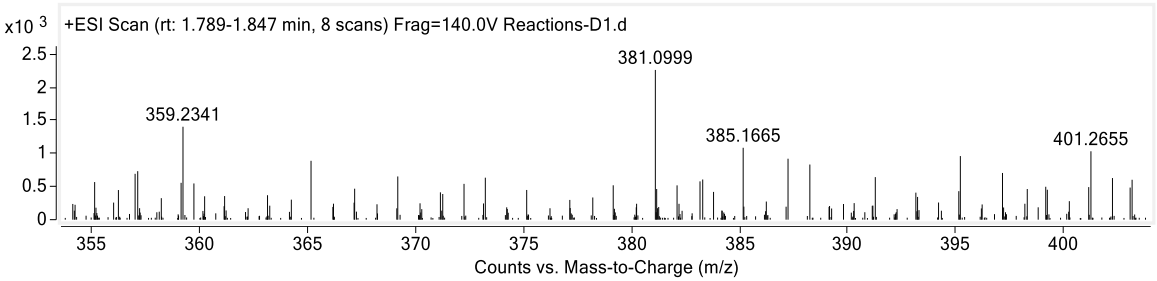

No Enzyme control

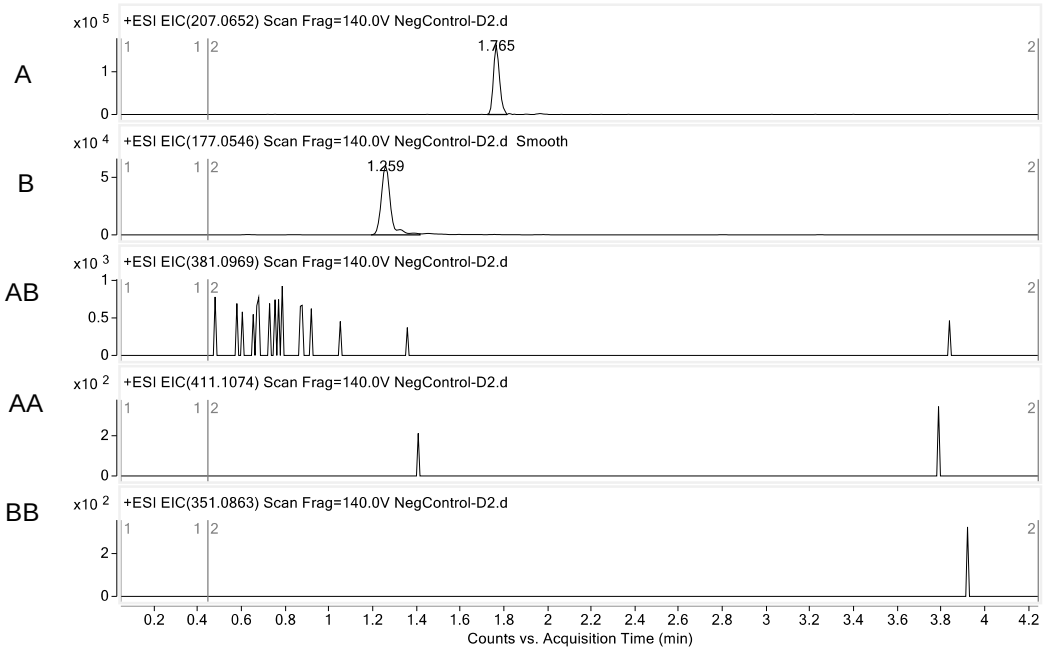

Supplemental Figure S3.55. Oxidative cross-coupling of **6** and **14** by KtnC (**Figure 3.2**).

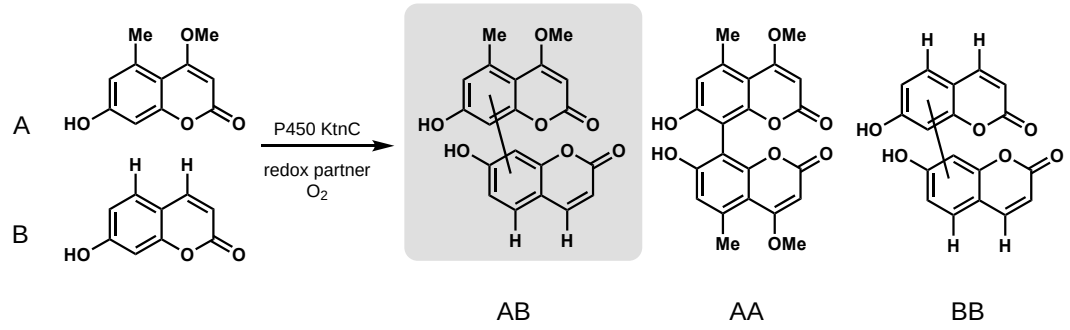

KtnC

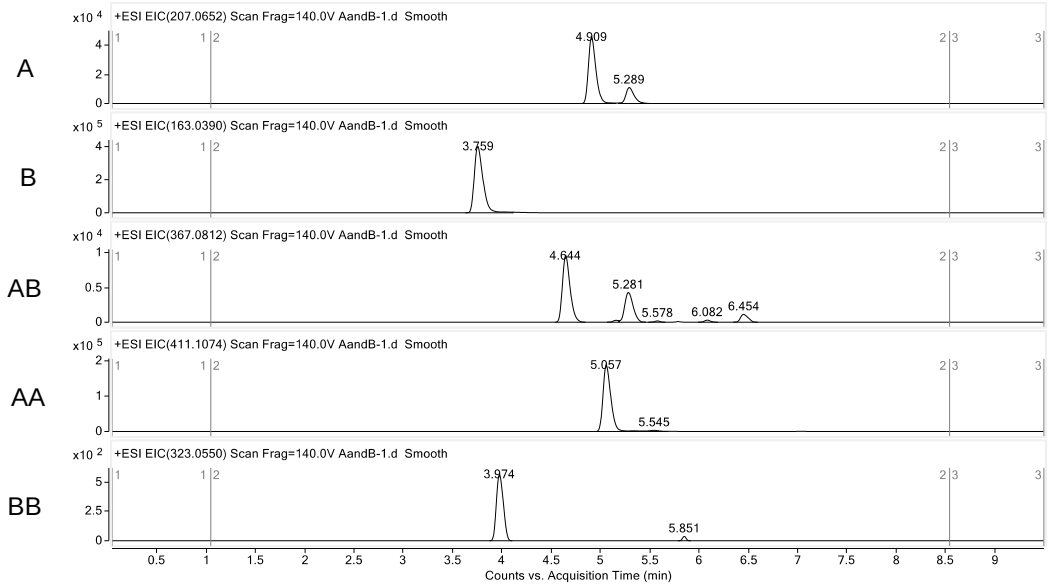

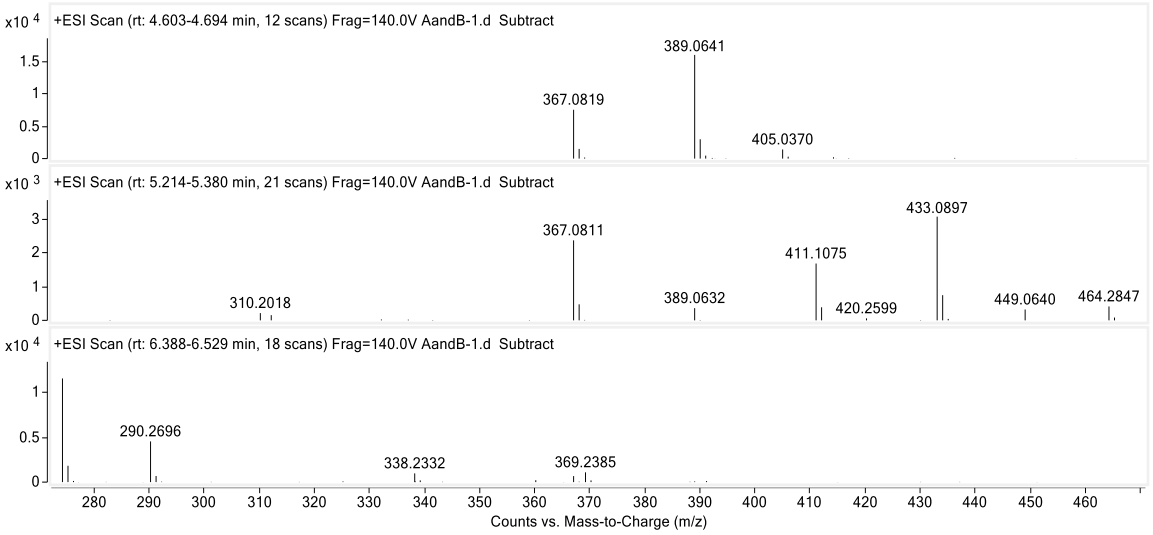

No Enzyme control

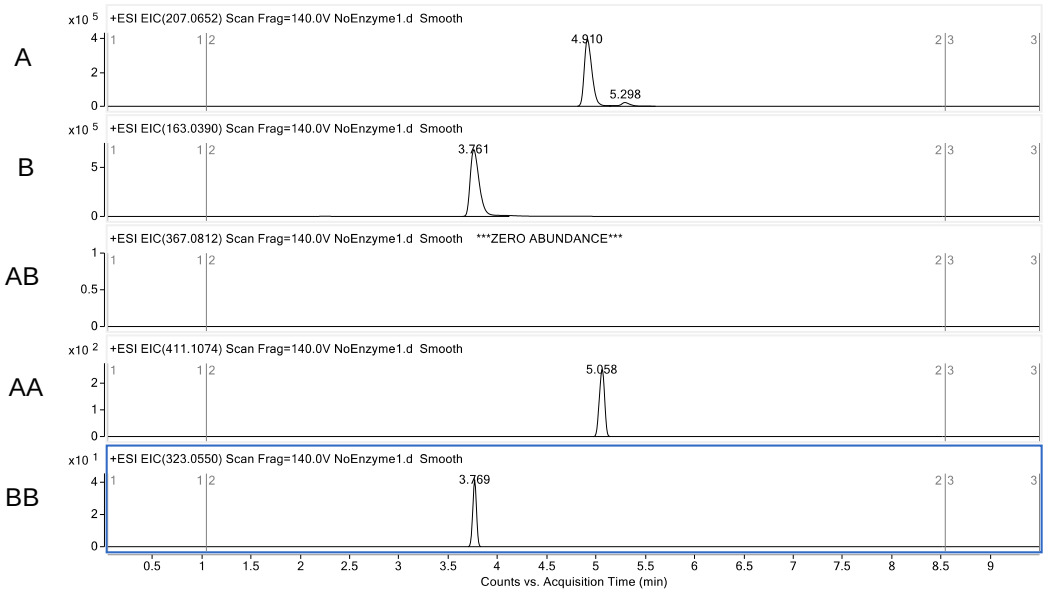

Supplemental Figure S3.56. Oxidative cross-coupling of **6** and **15** by KtnC (**Figure 3.2**).

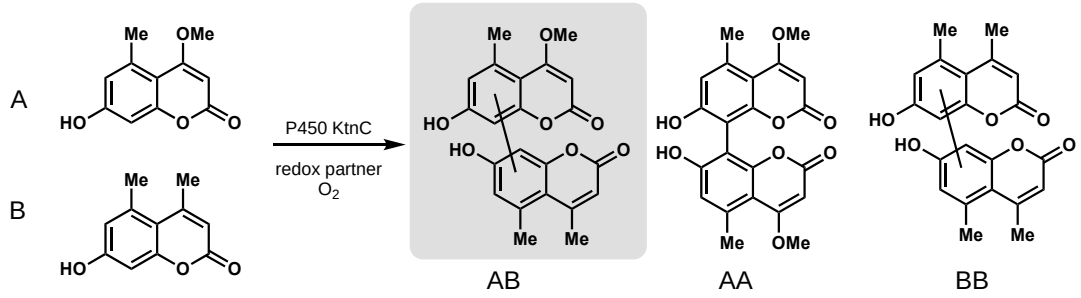

KtnC

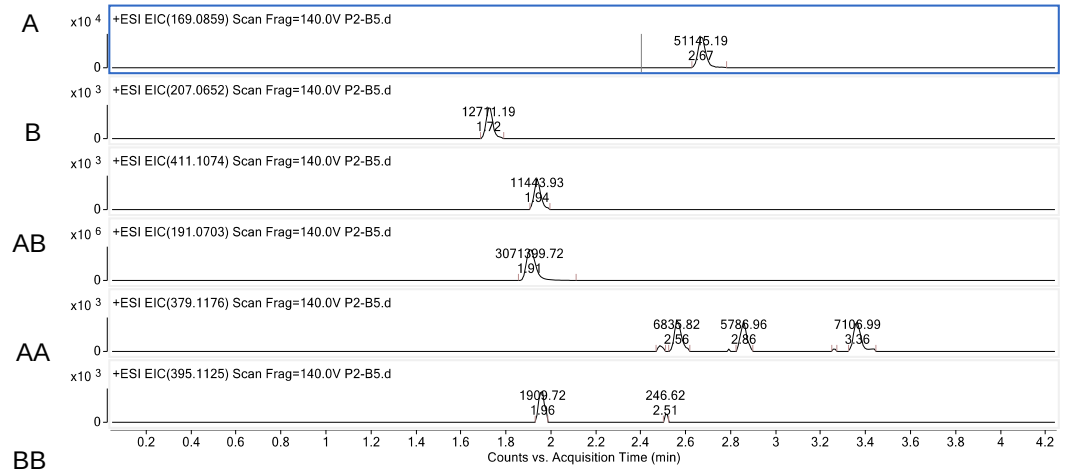

No Enzyme control

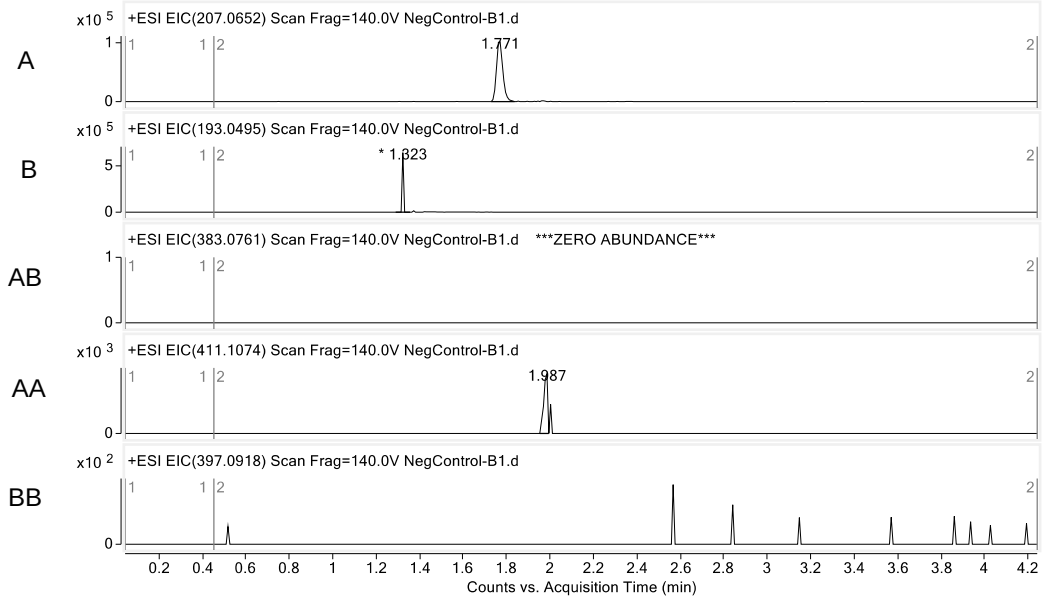

Supplemental Figure S3.57. Oxidative cross-coupling of **6** and **16** by KtnC (**Figure 3.2**).

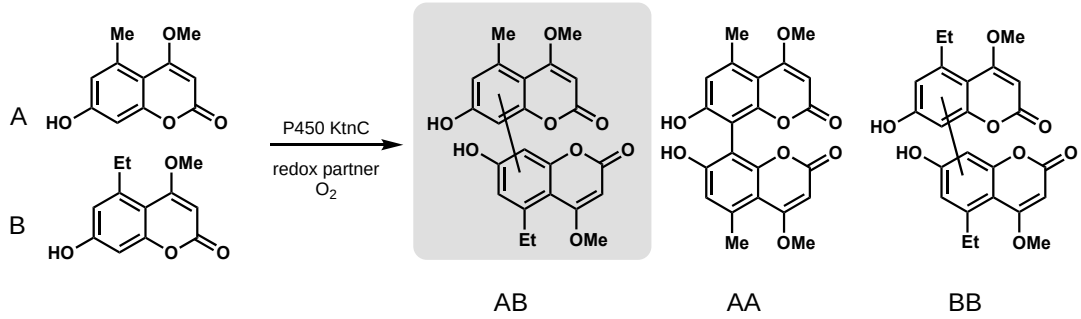

KtnC

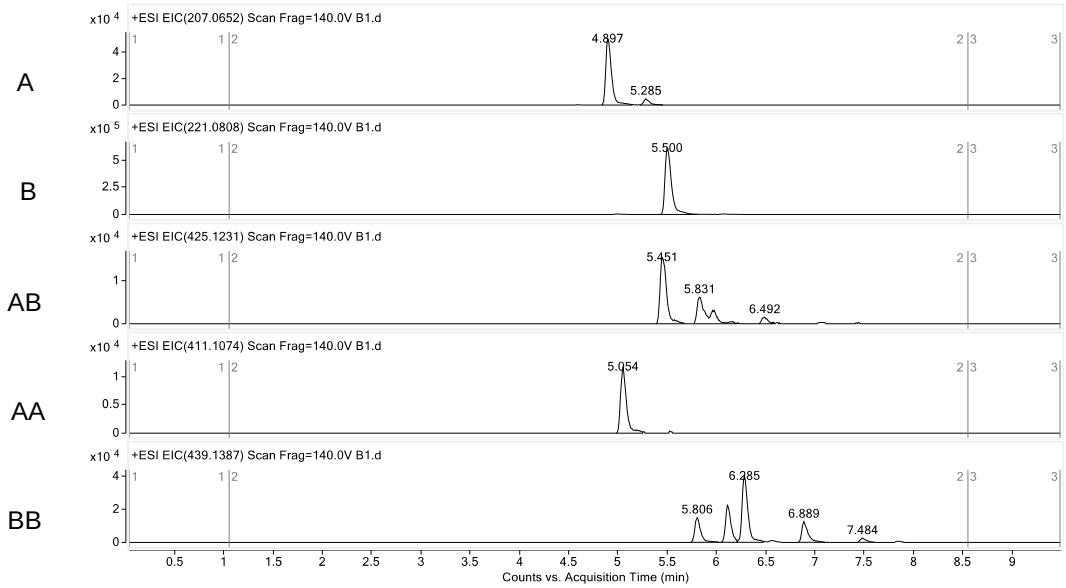

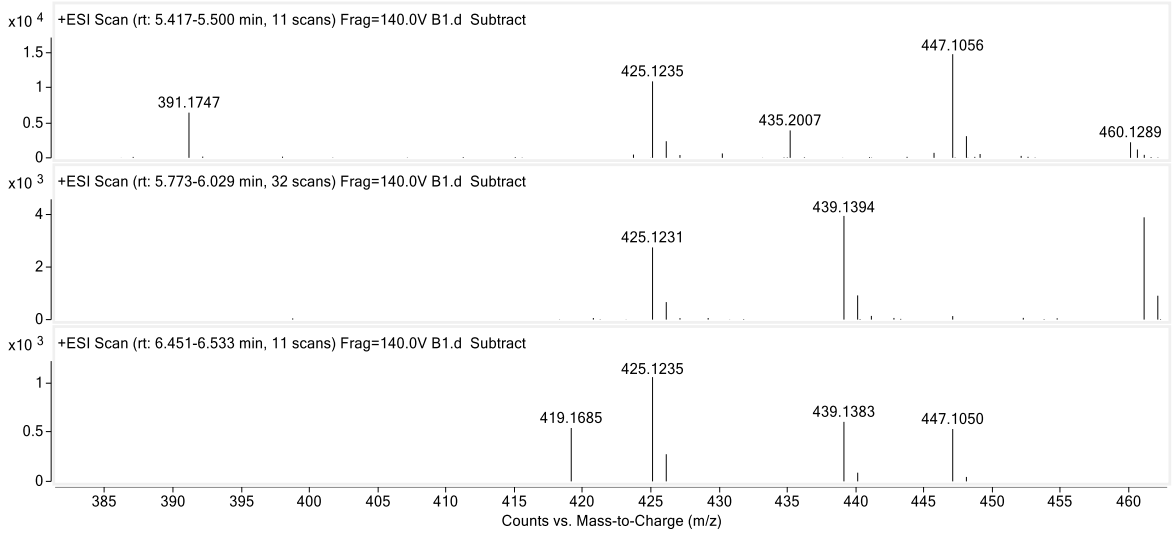

No Enzyme control

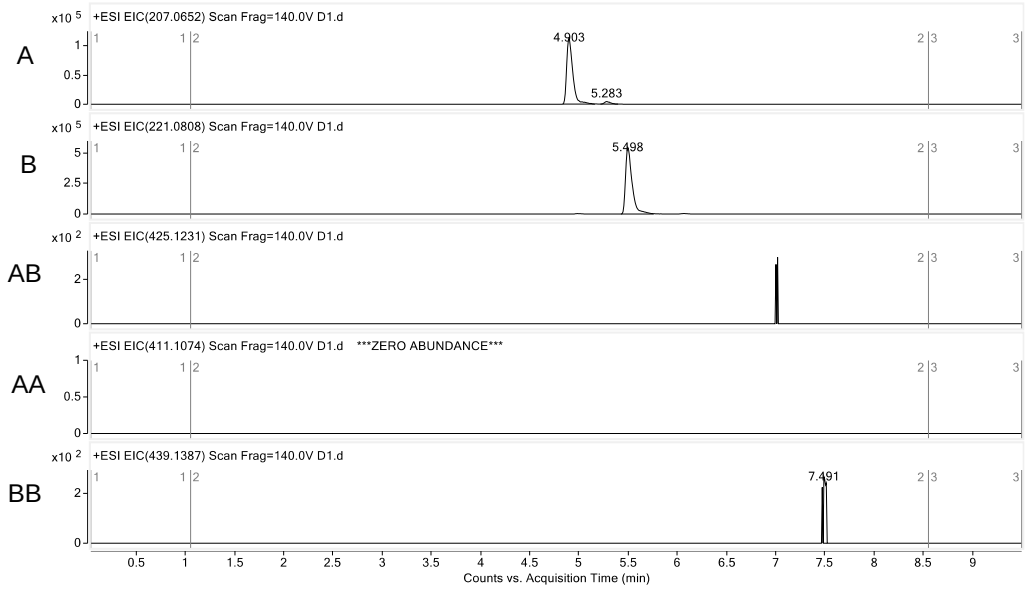

Supplemental Figure S3.58. Site-selectivity of oxidative cross-coupling of **6** and **17** by KtnC (**Figure 3.2**).

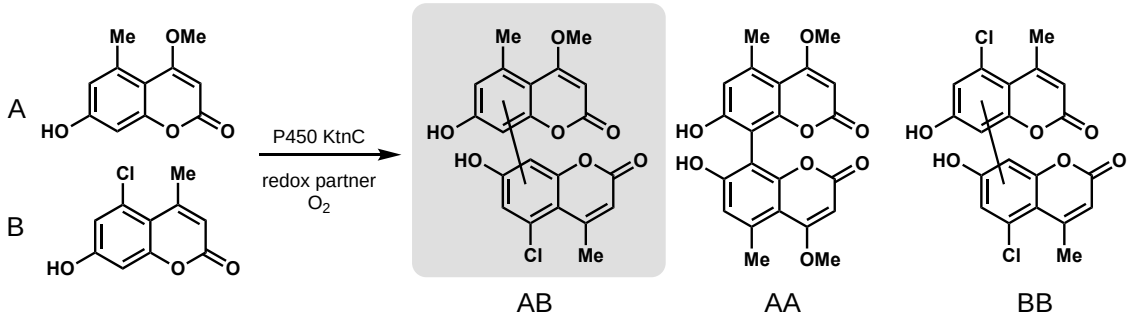

KtnC

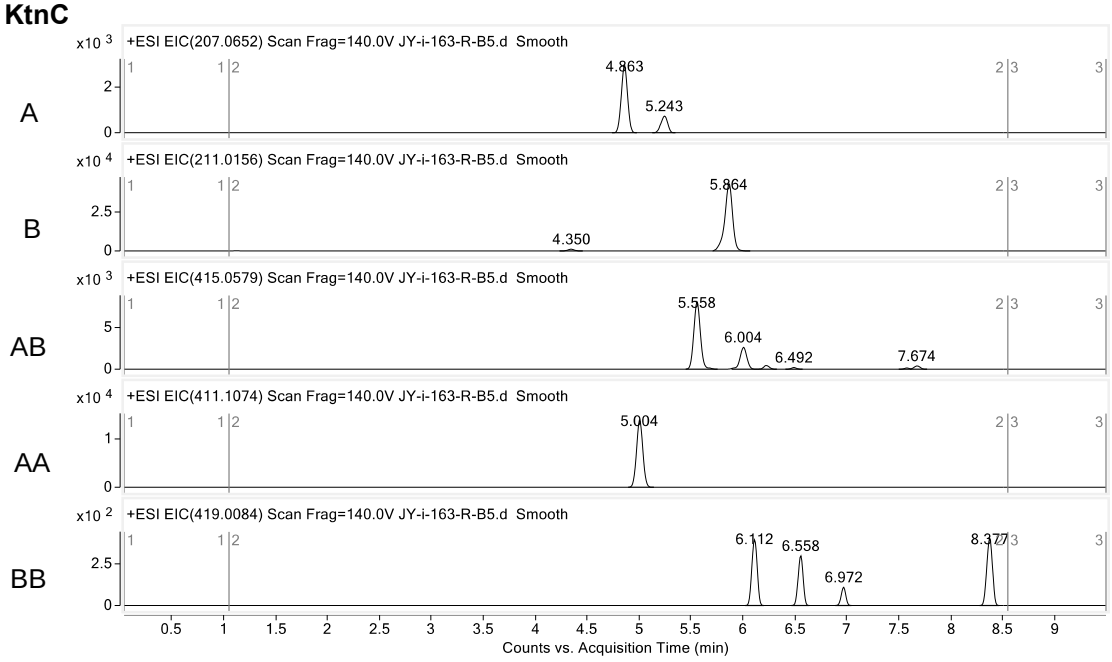

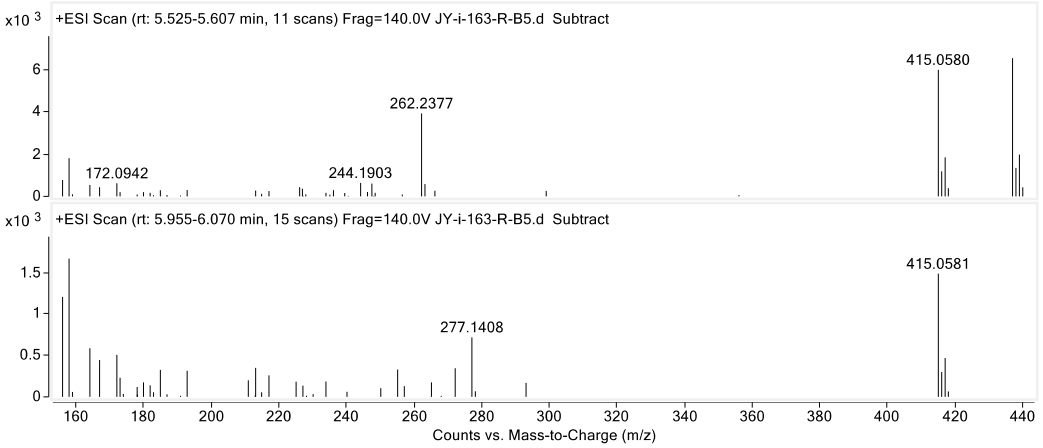

No Enzyme control

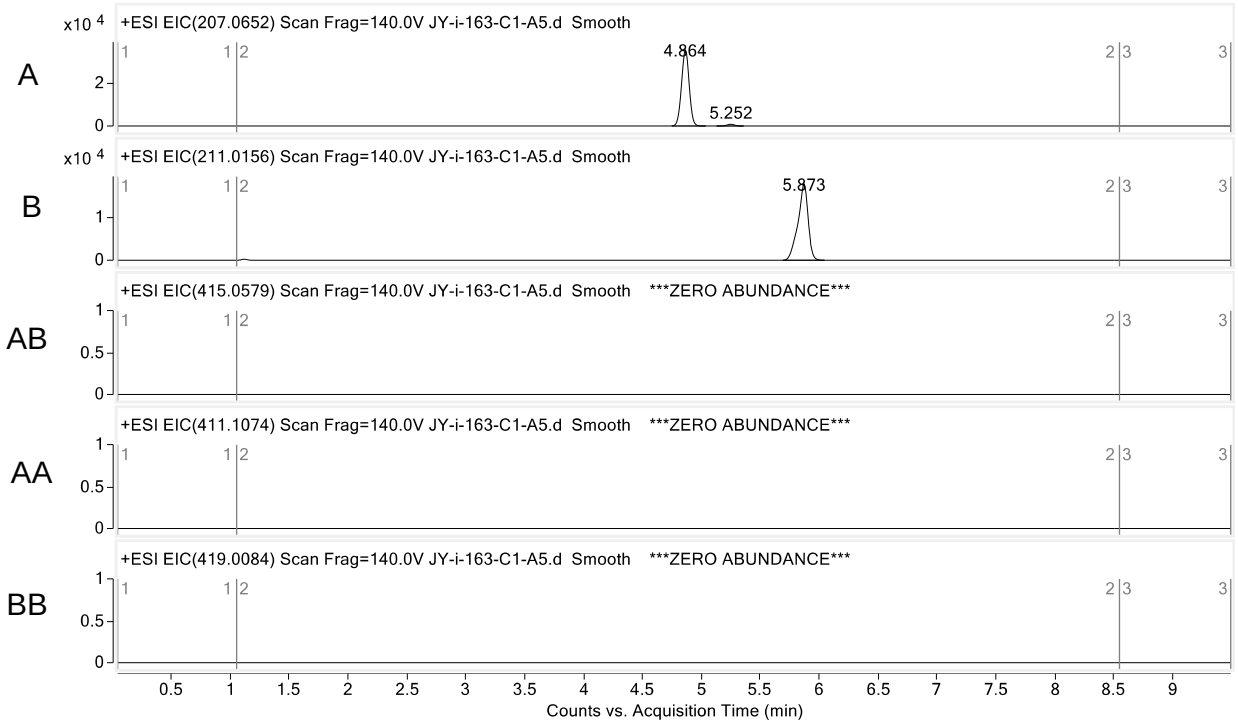

Supplemental Figure S3.59. Oxidative cross-coupling of **6** and **18** by KtnC (**Figure 3.2**).

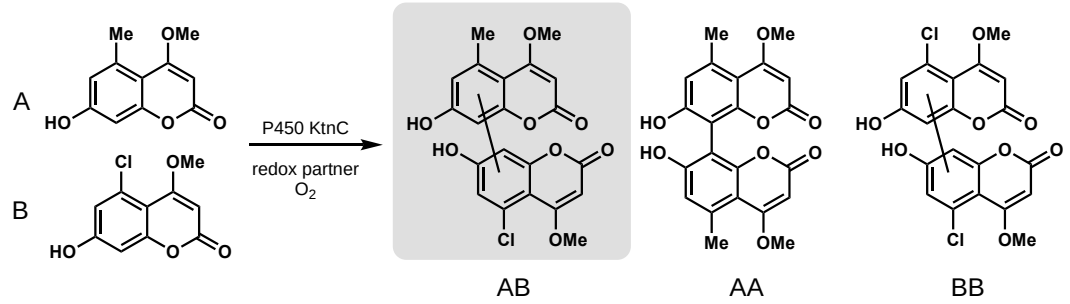

KtnC

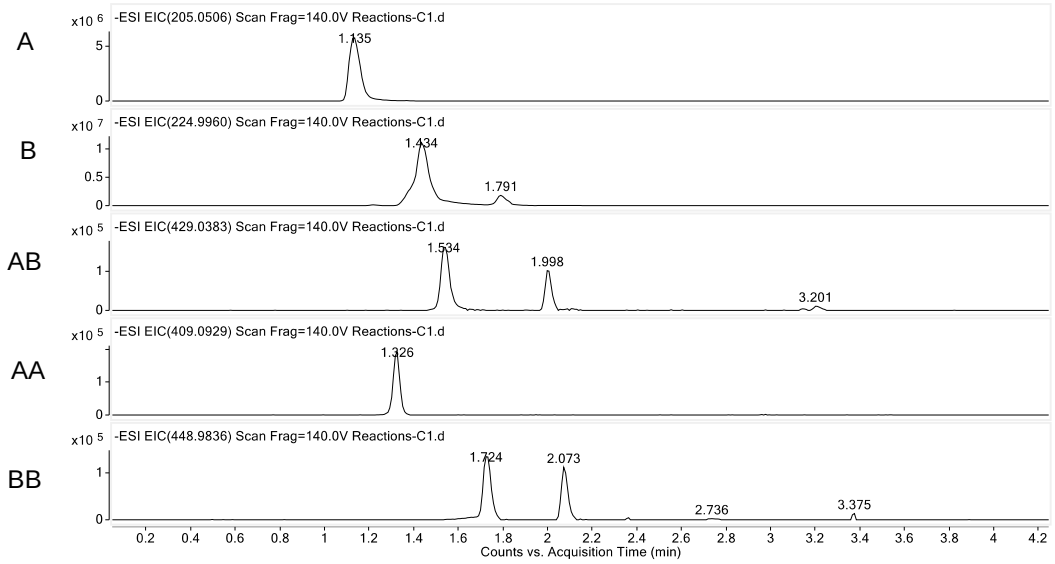

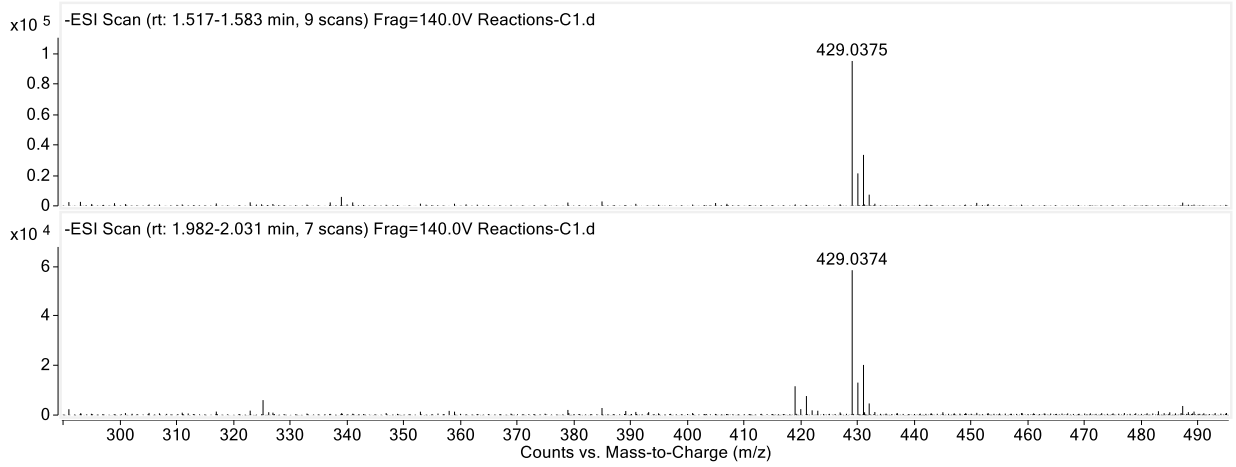

No Enzyme control

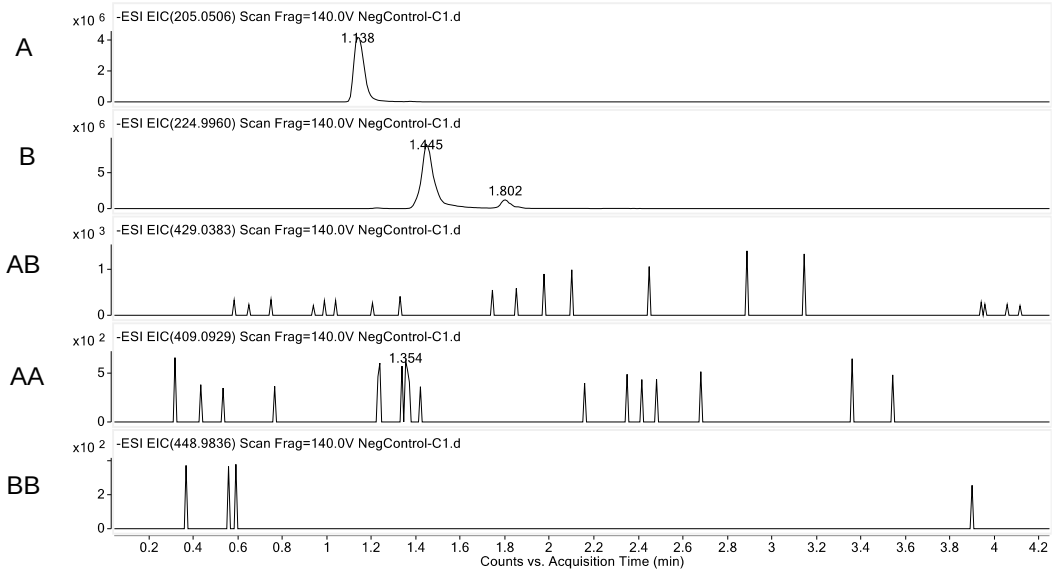

Supplemental Figure S3.60. Oxidative cross-coupling of **6** and **19** by KtnC (**Figure 3.2**).

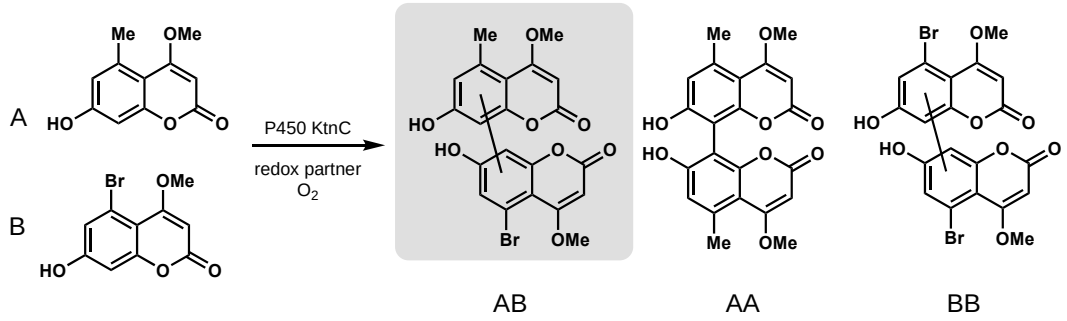

KtnC

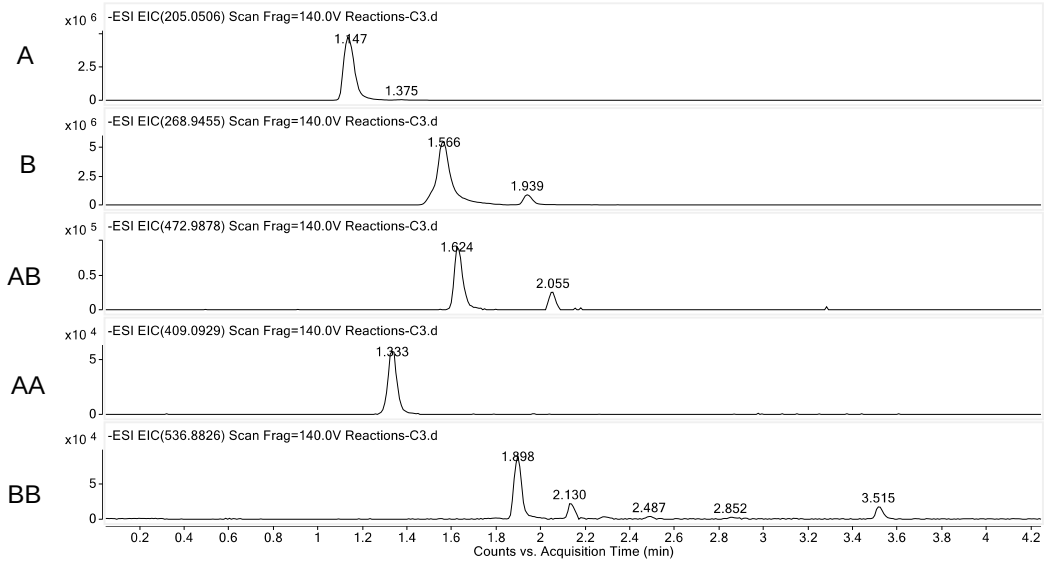

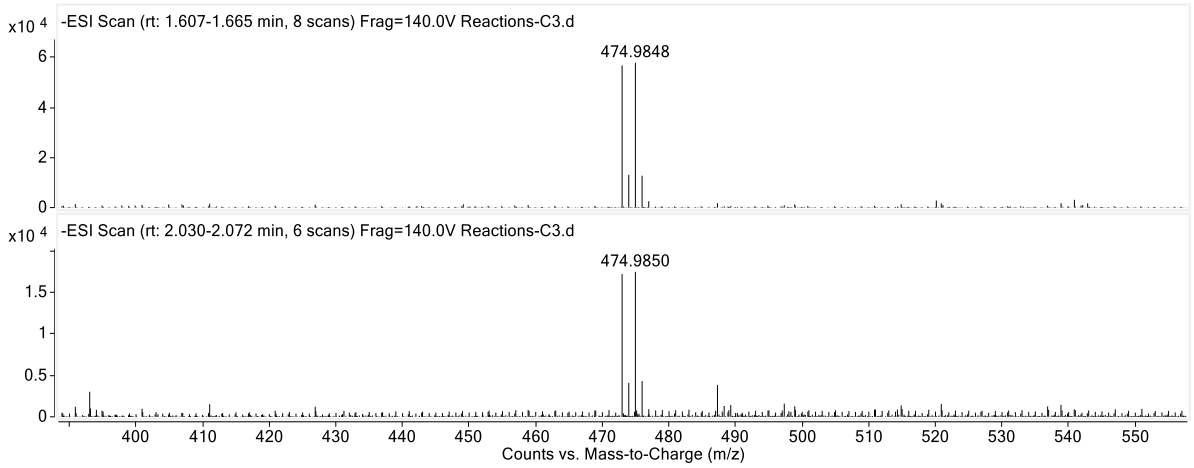

No Enzyme control

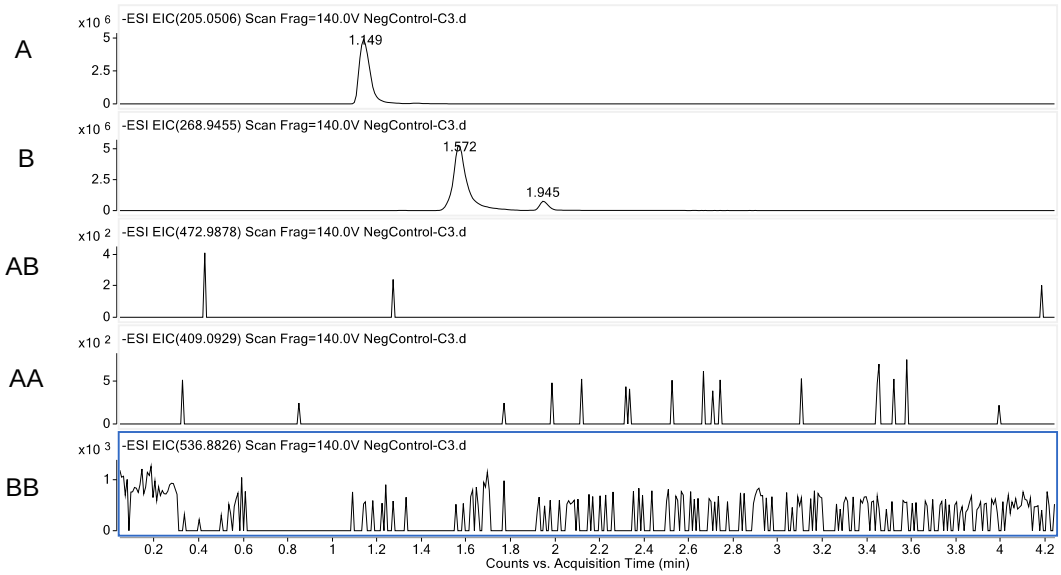

Supplemental Figure S3.61. Oxidative cross-coupling of **6** and **20** by KtnC (**Figure 3.2**).

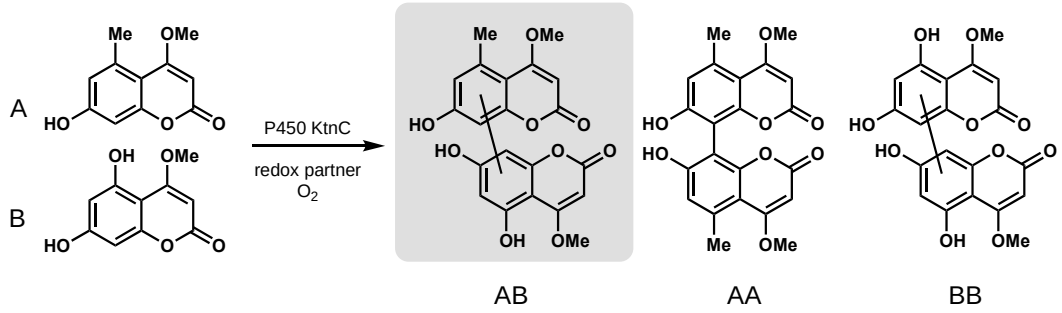

KtnC

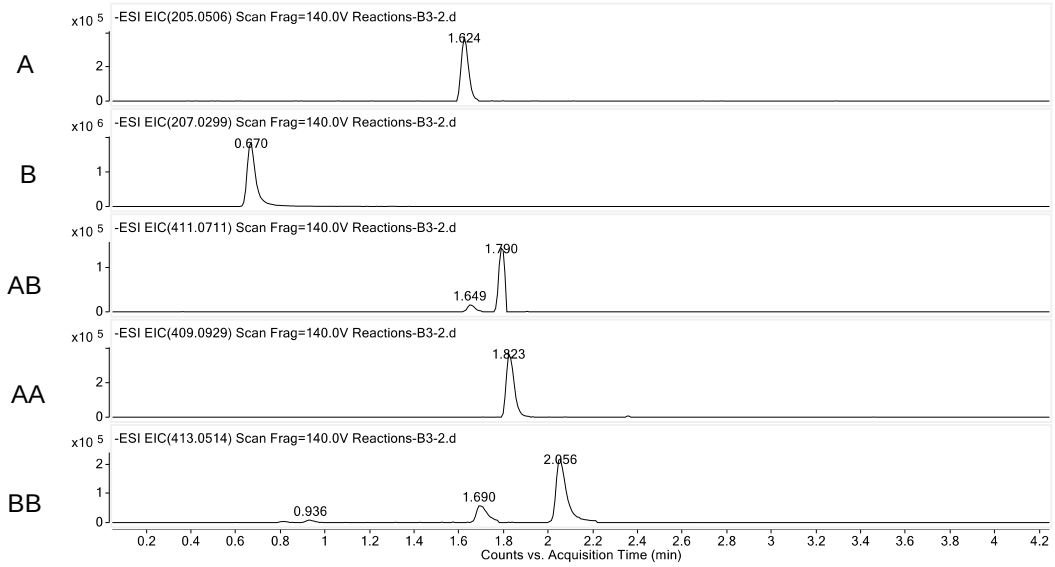

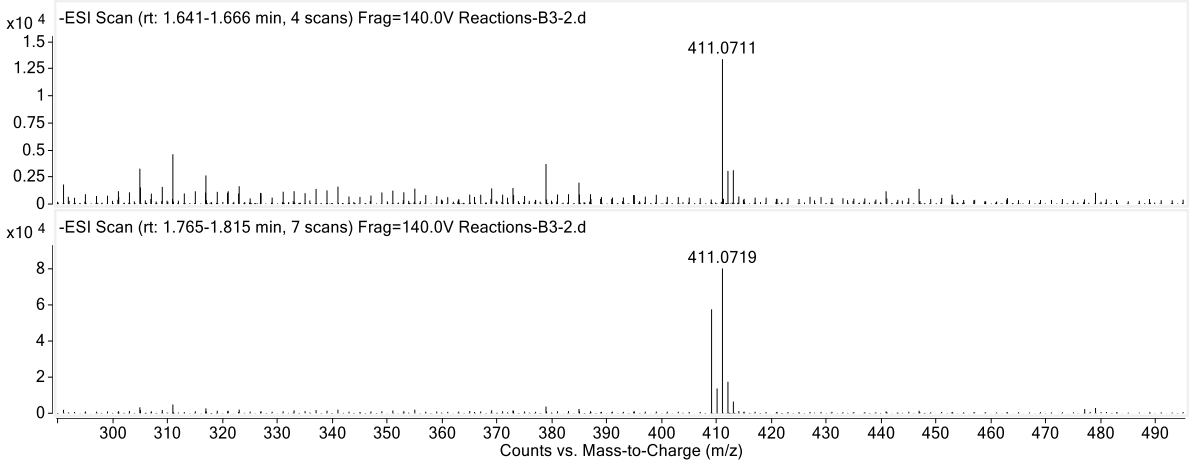

No Enzyme control

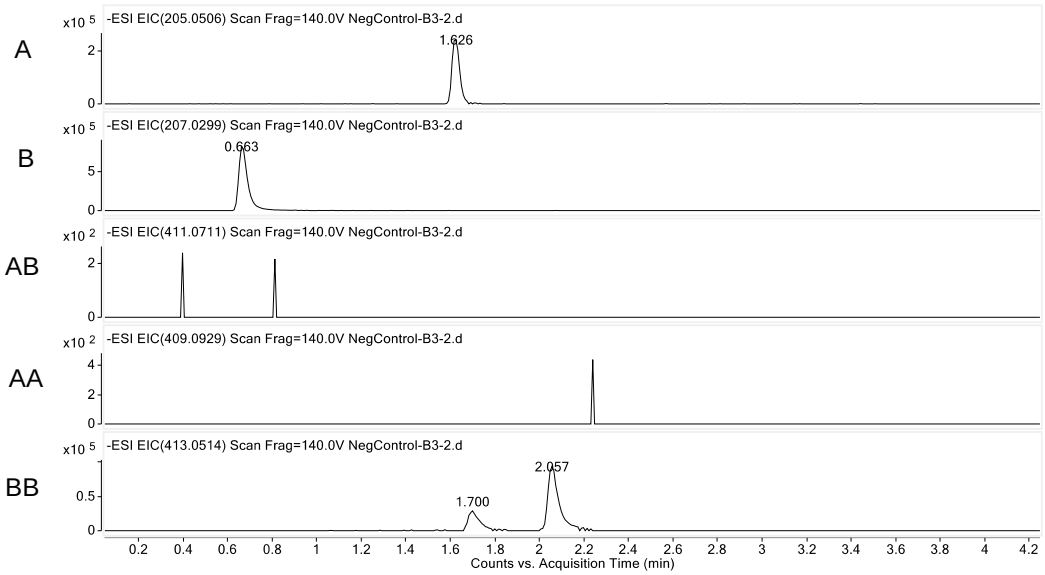

Supplemental Figure S3.62. Oxidative cross-coupling of **6** and **21** by KtnC (**Figure 3.2**).

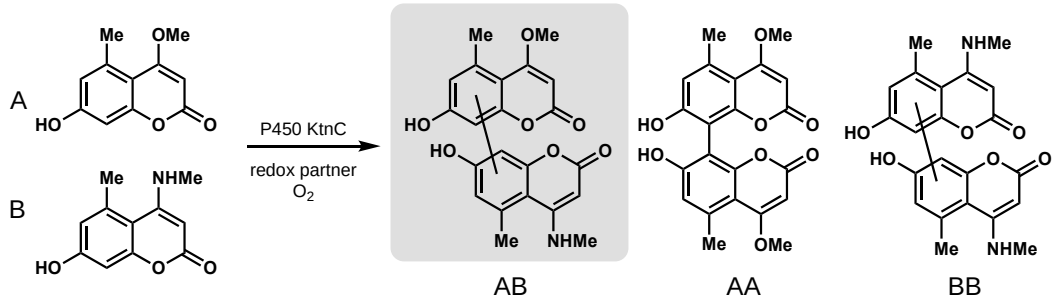

KtnC

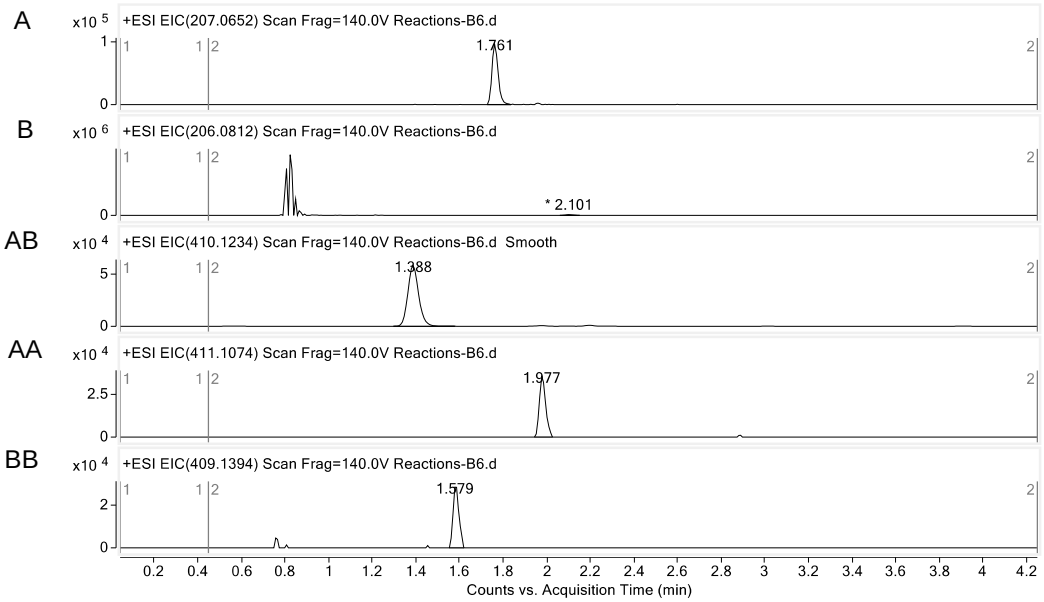

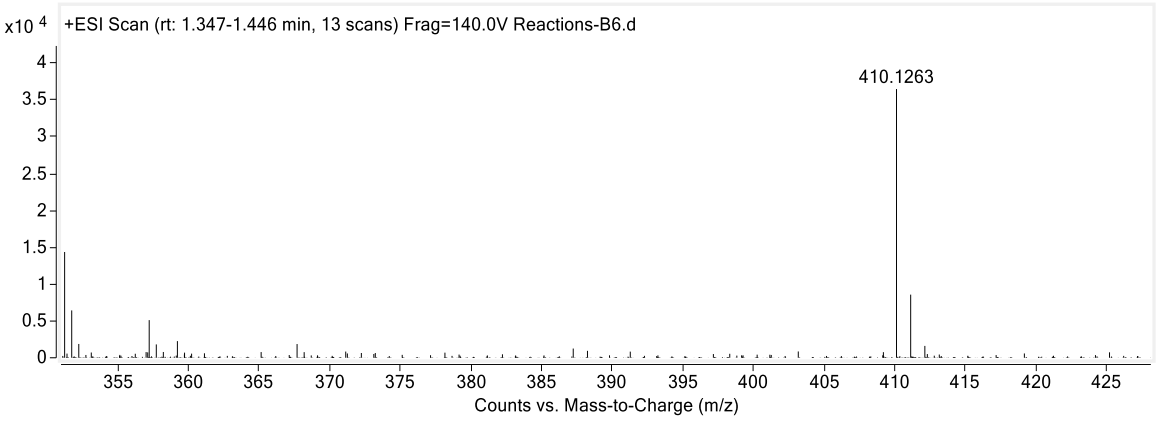

No Enzyme control

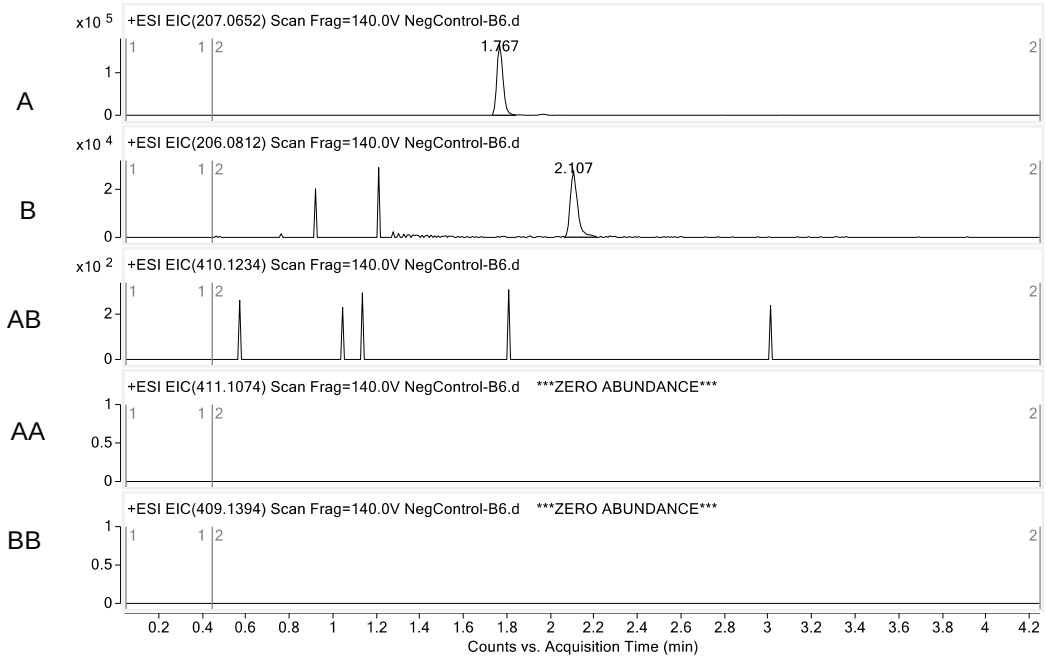

Supplemental Figure S3.63. Oxidative cross-coupling of **6** and **22** by KtnC (**Figure 3.2**).

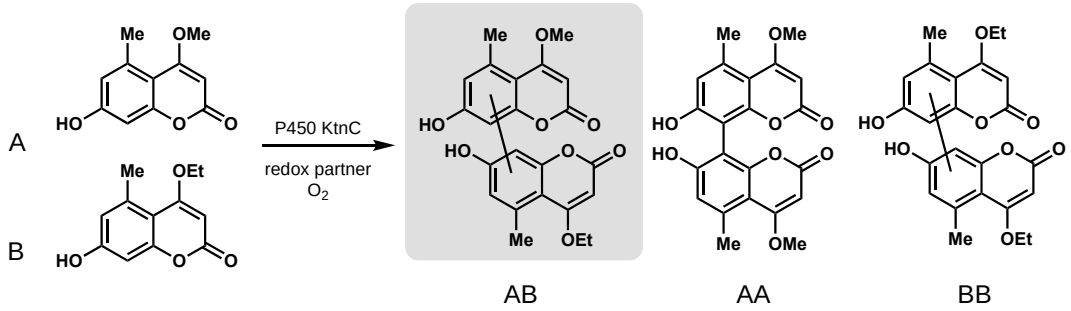

KtnC

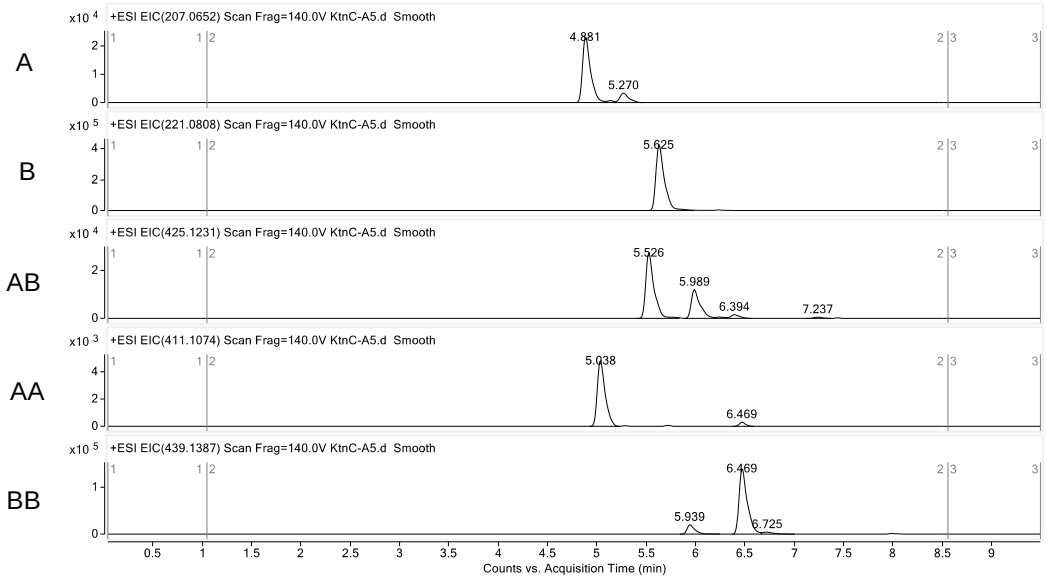

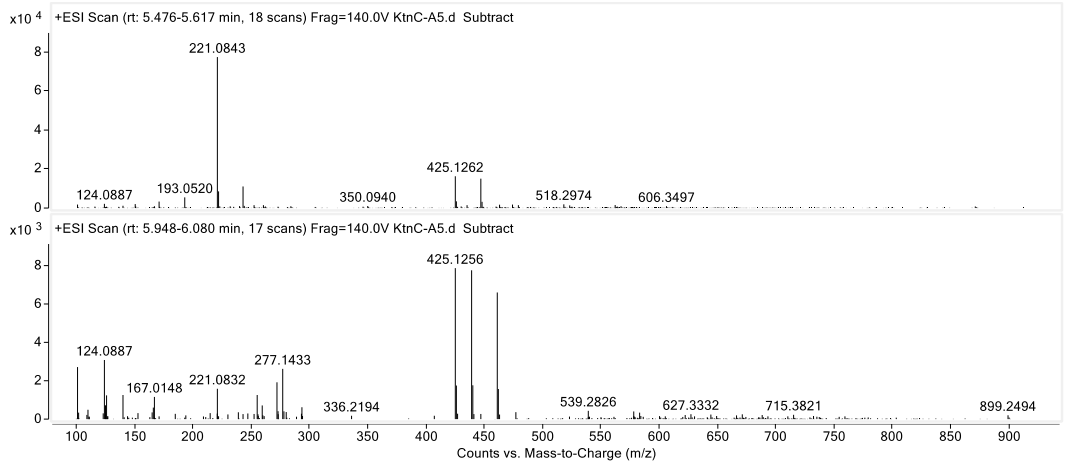

No Enzyme control

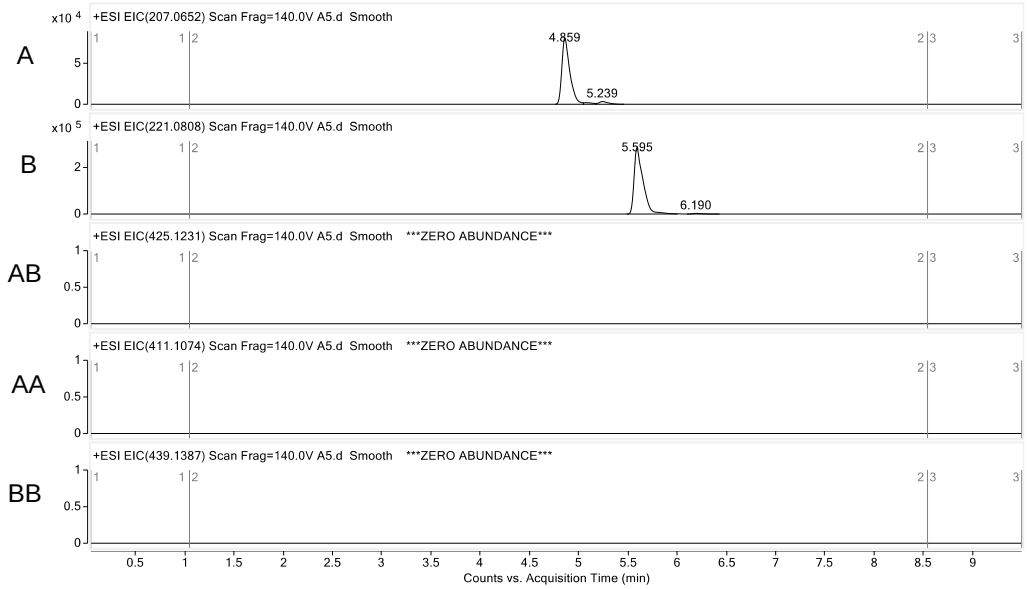

Supplemental Figure S3.64. Oxidative cross-coupling of **6** and **23** by KtnC (**Figure 3.2**).

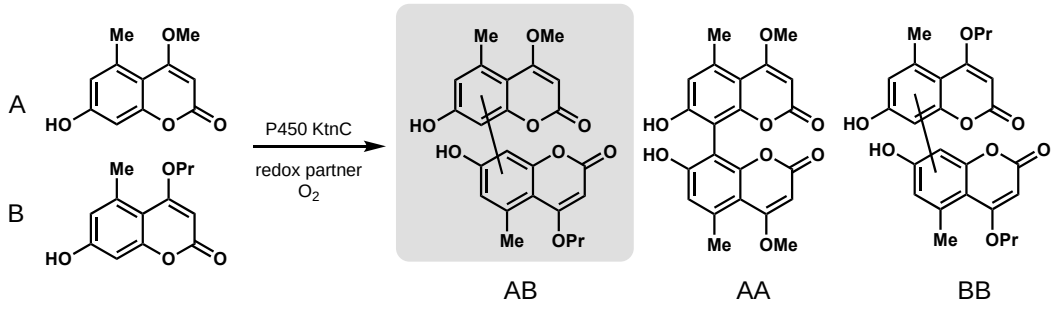

KtnC

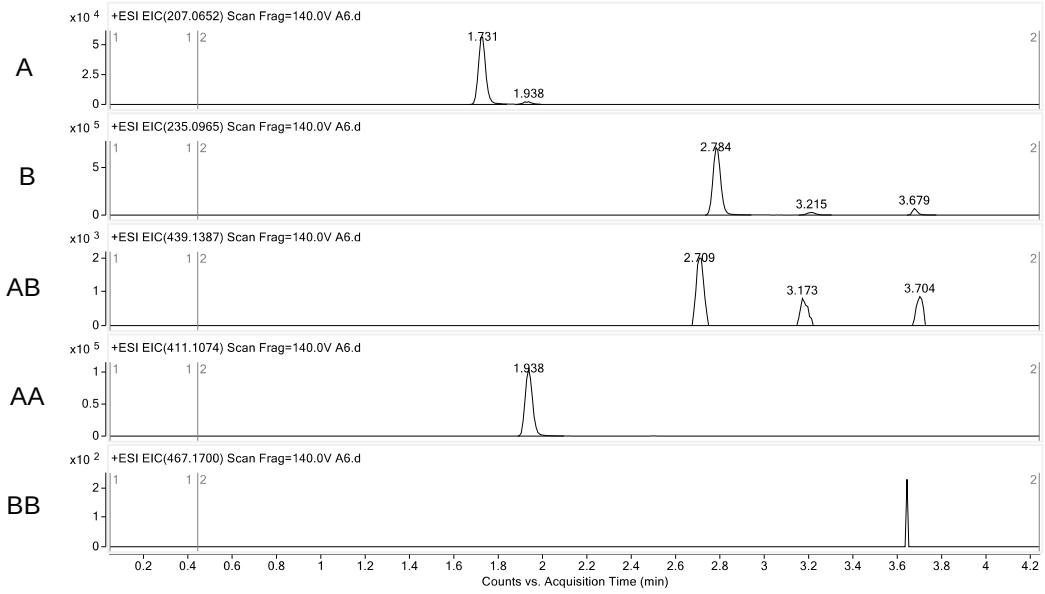

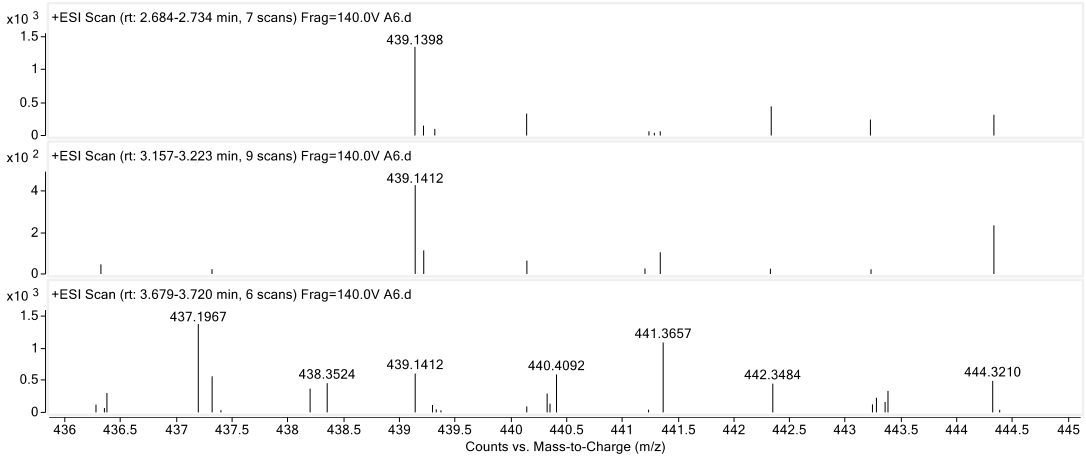

No Enzyme control

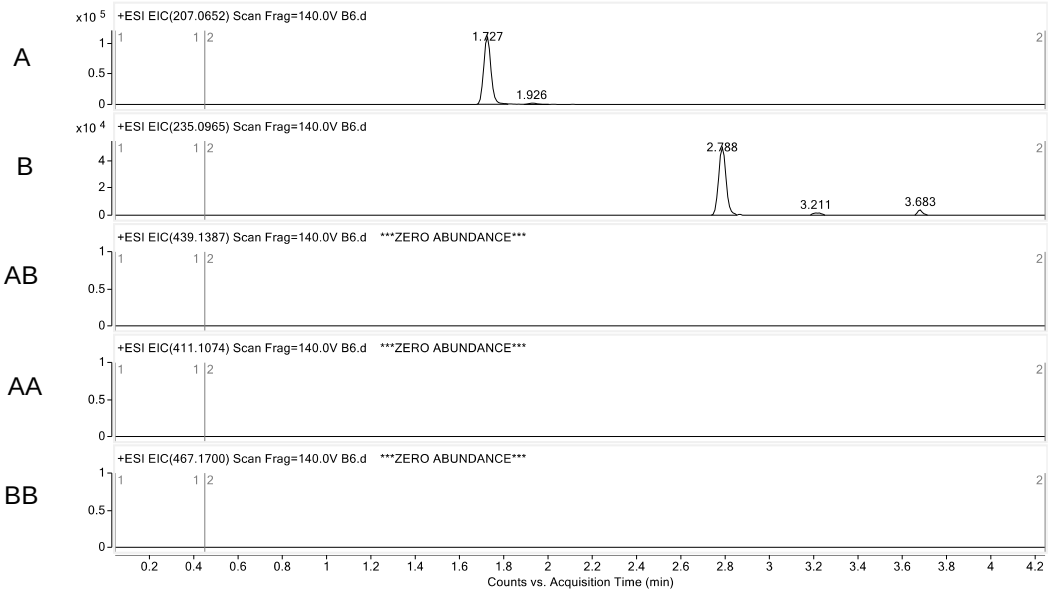

Supplemental Figure S3.65. Oxidative cross-coupling of **6** and **24** by KtnC (**Figure 3.2**).

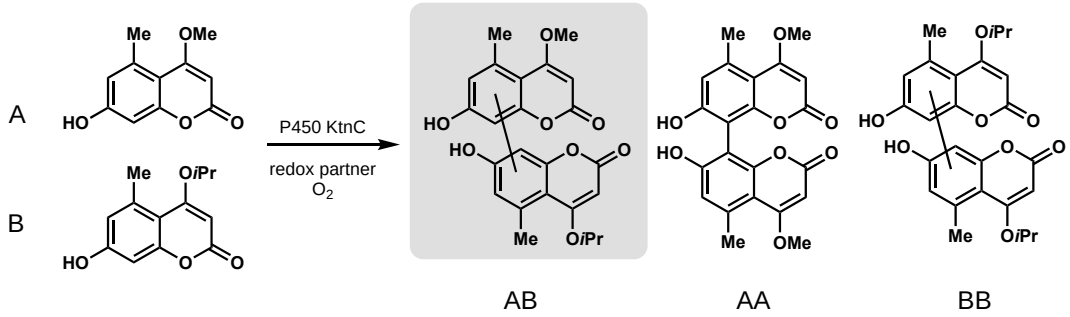

KtnC

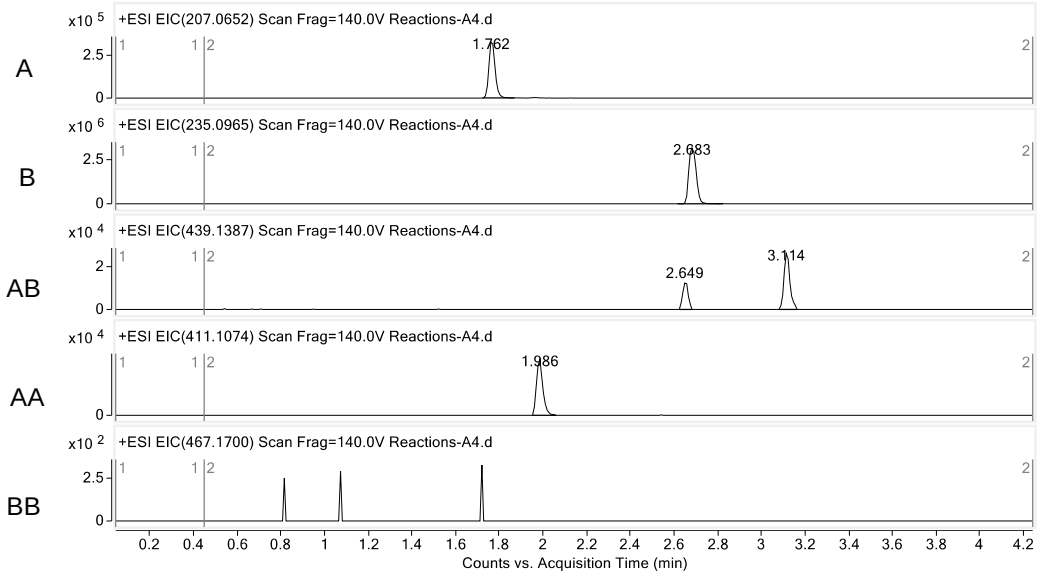

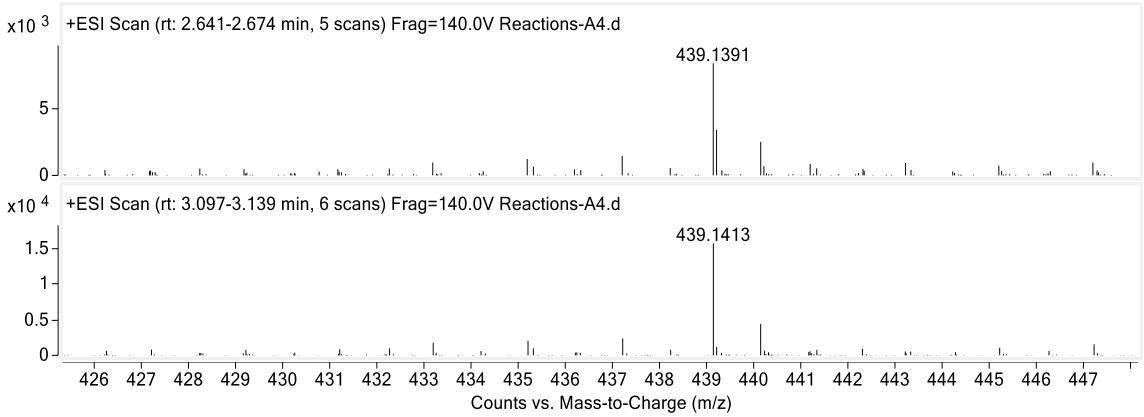

No Enzyme control

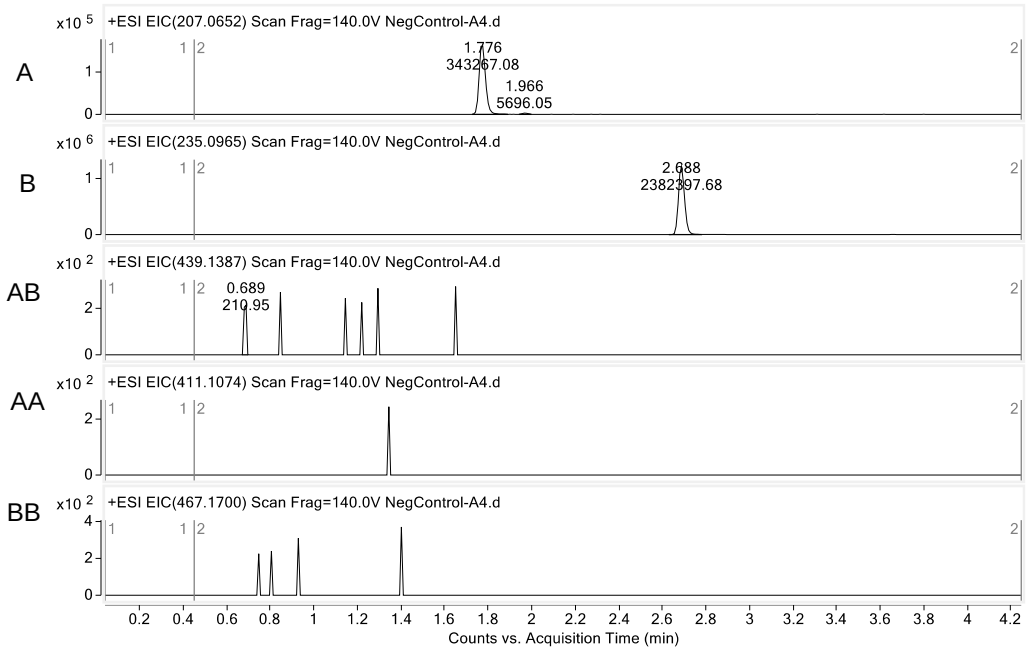

Supplemental Figure S3.66. Oxidative cross-coupling of **6** and **25** by KtnC (**Figure 3.2**).

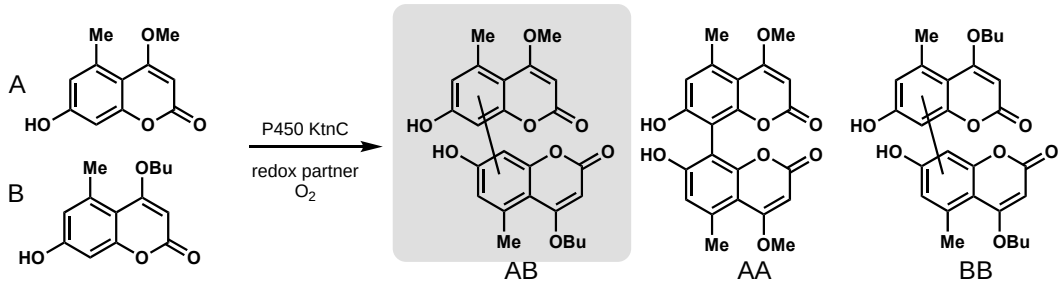

KtnC

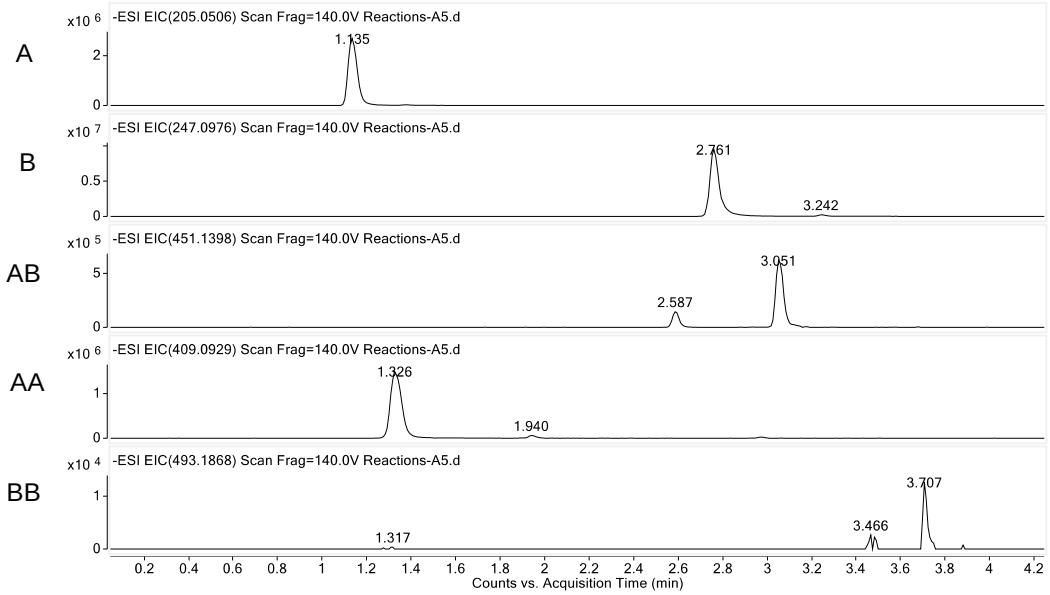

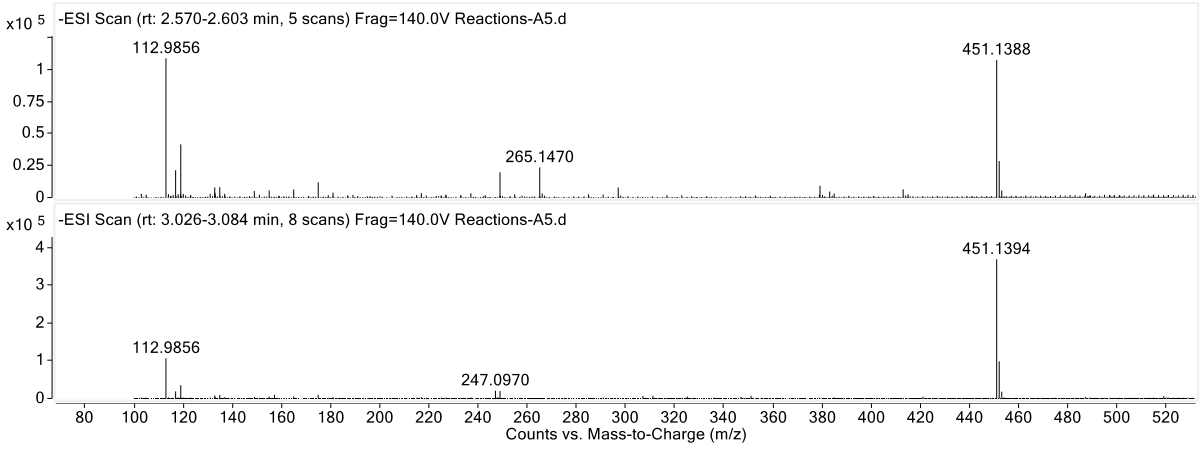

No Enzyme control

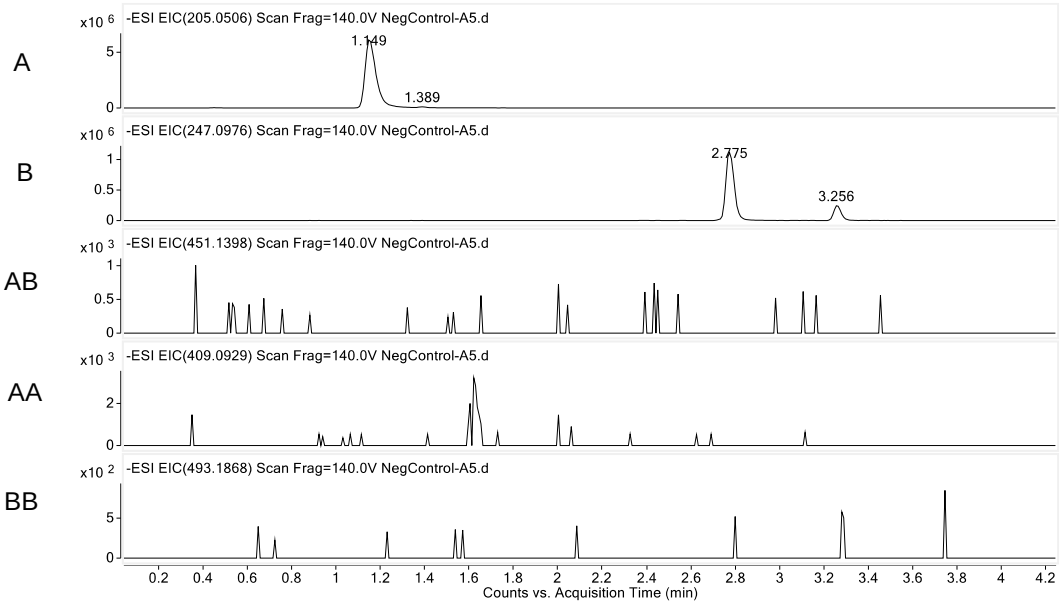

Supplemental Figure S3.67. Oxidative cross-coupling of **6** and **26** by KtnC (**Figure 3.2**).

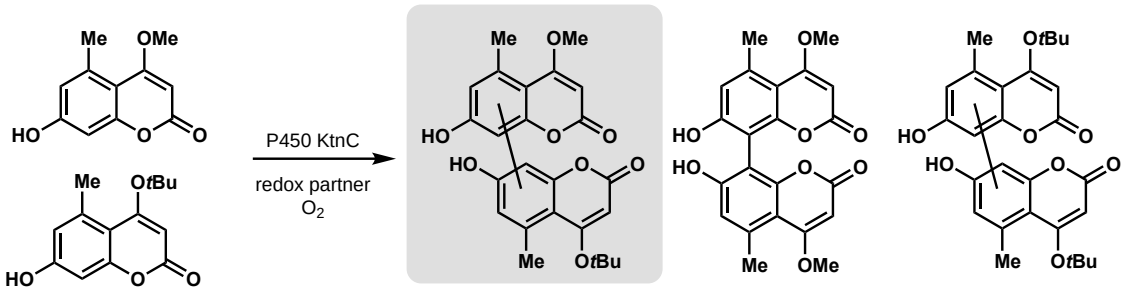

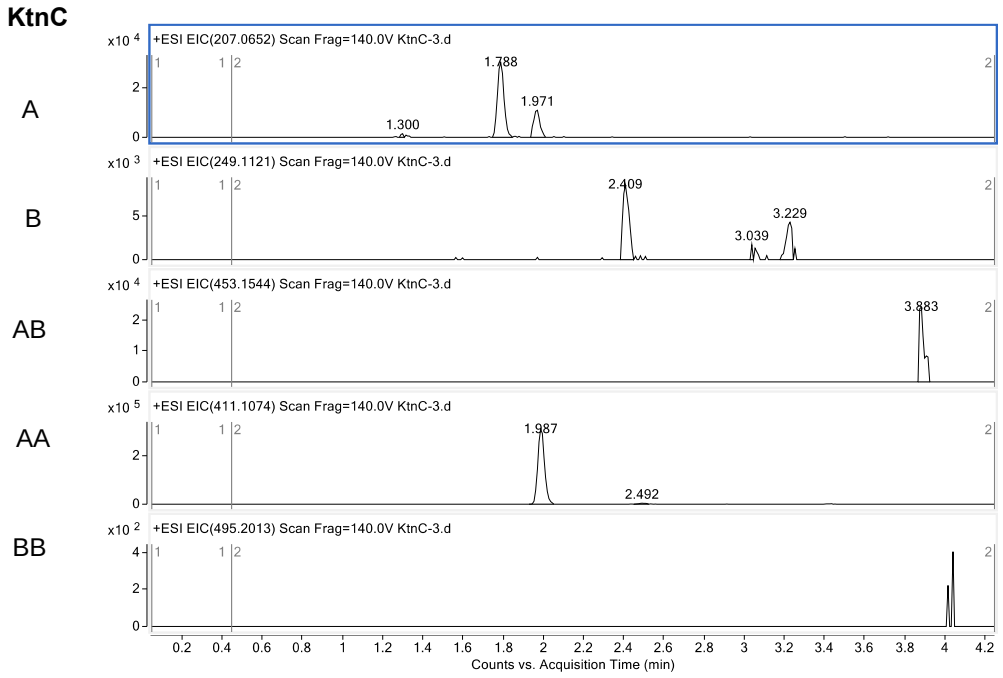

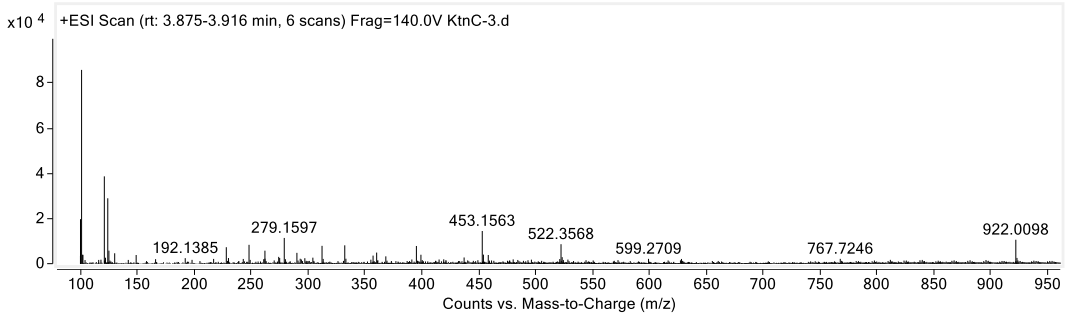

No Enzyme control

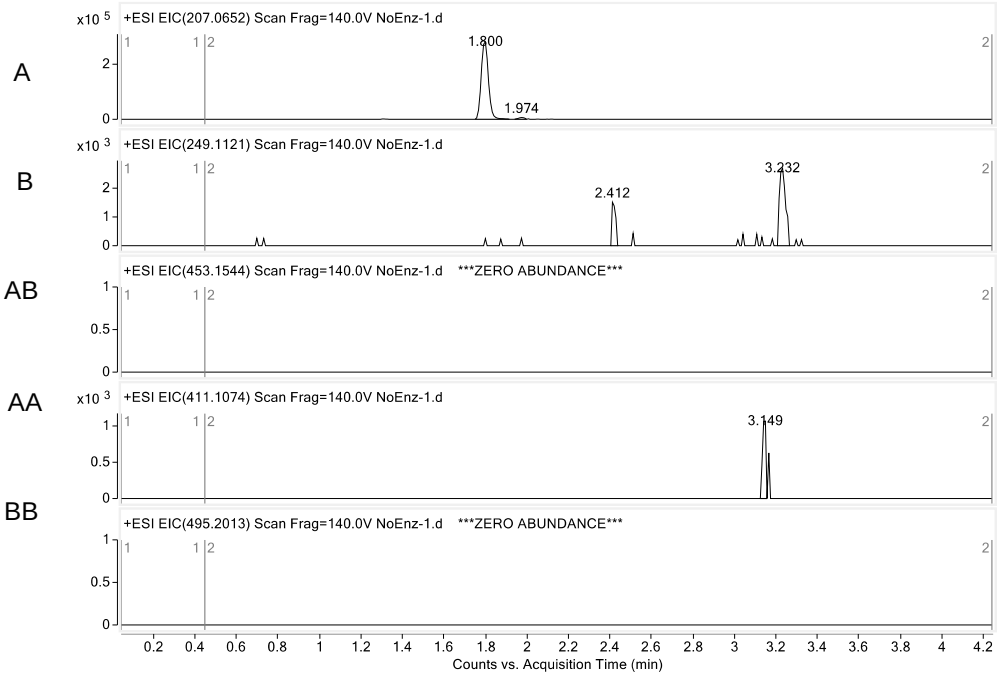

Supplemental Figure S3.68. Oxidative cross-coupling of **6** and **27** by KtnC (**Figure 3.2**).

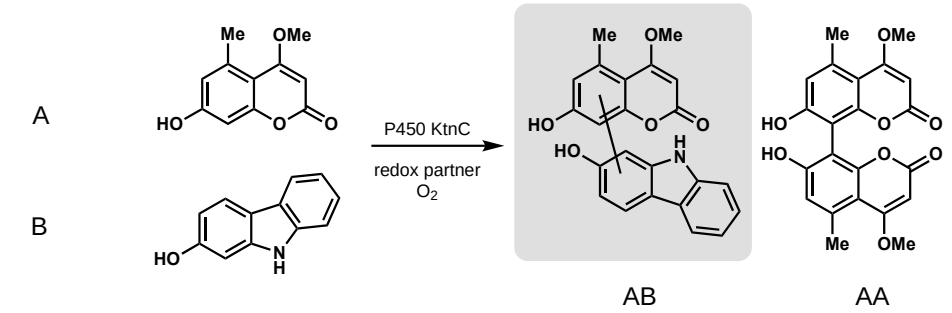

KtnC

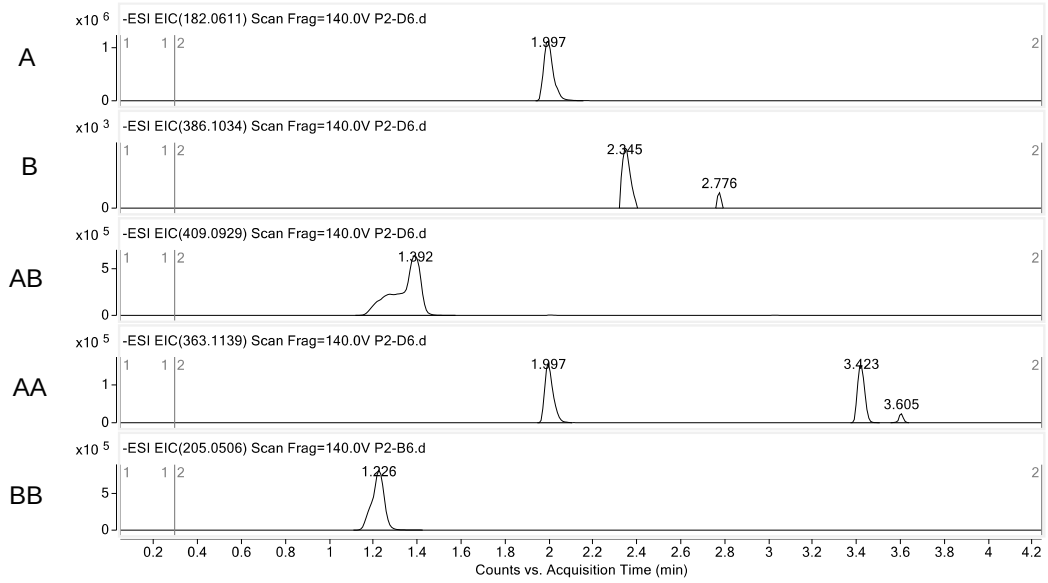

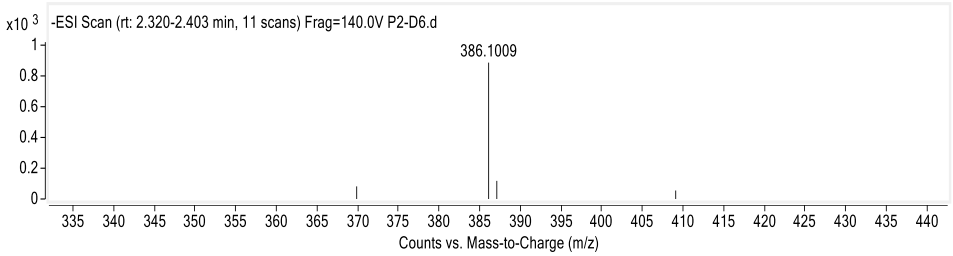

No Enzyme control

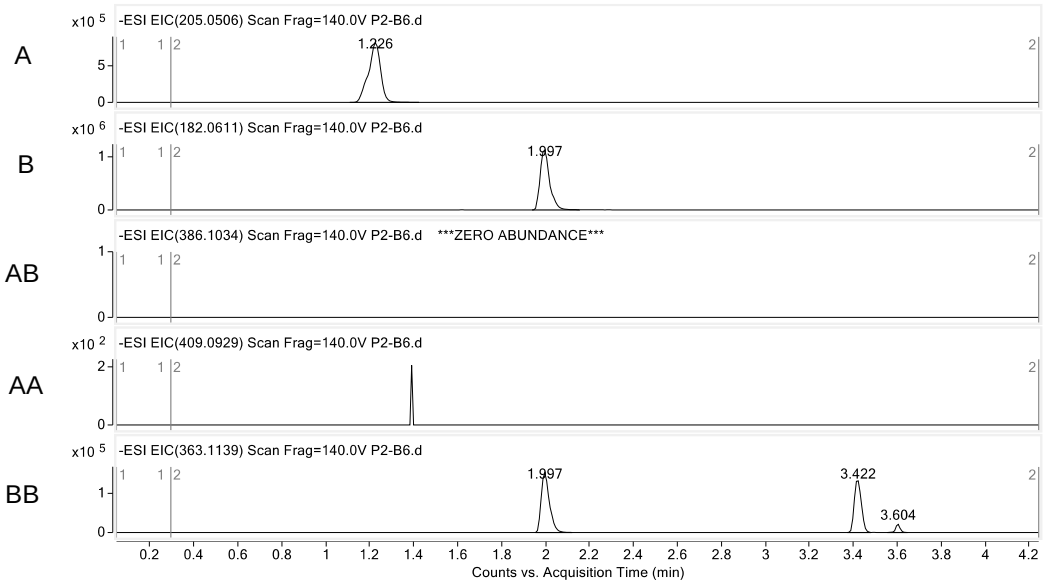

Supplemental Figure S3.69. Oxidative cross-coupling of **6** and **28** by KtnC (**Figure 3.2**).

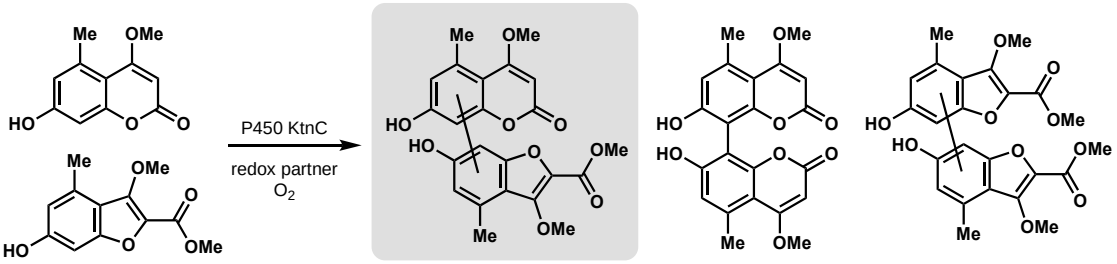

KtnC

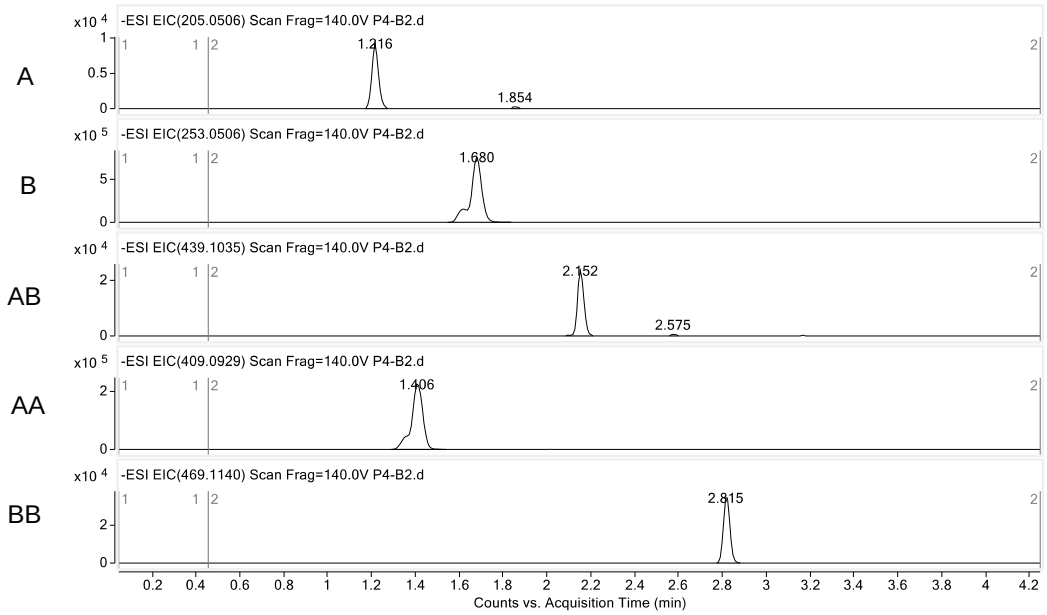

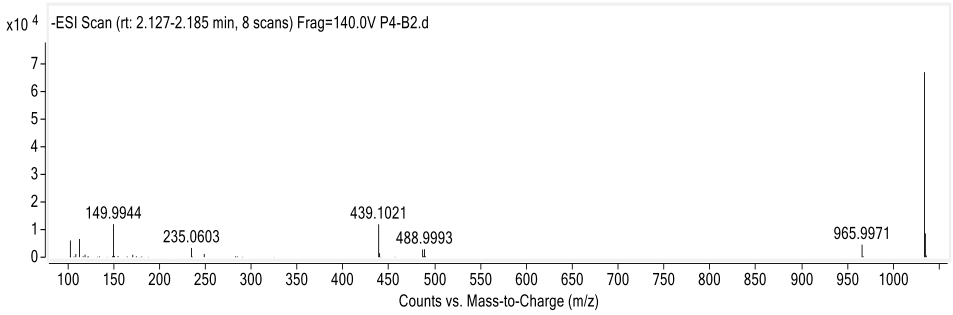

No Enzyme control

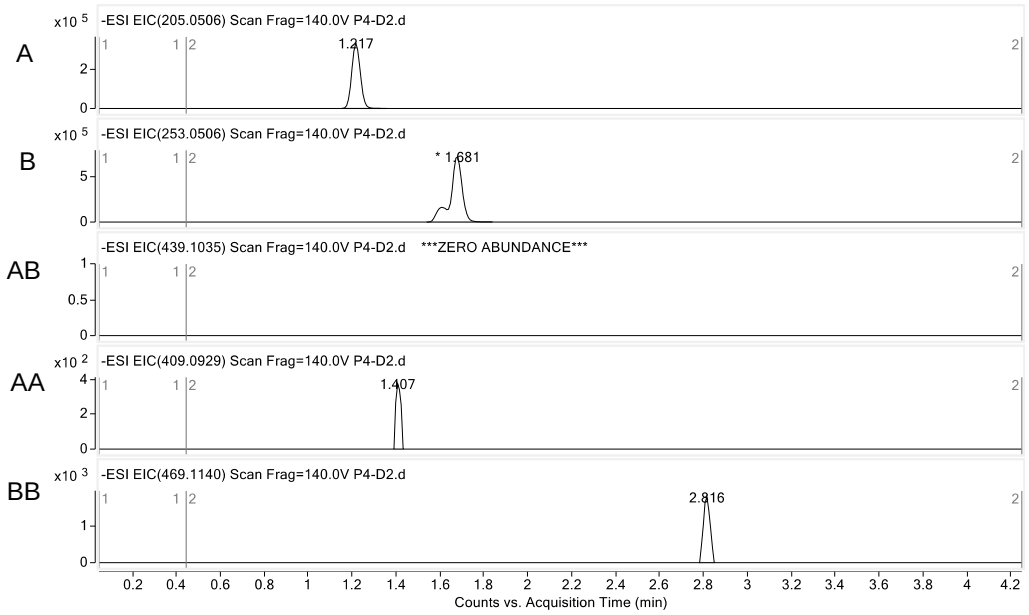

Supplemental Figure S3.70. Oxidative cross-coupling of **6** and **29** by KtnC (**Figure 3.2**).

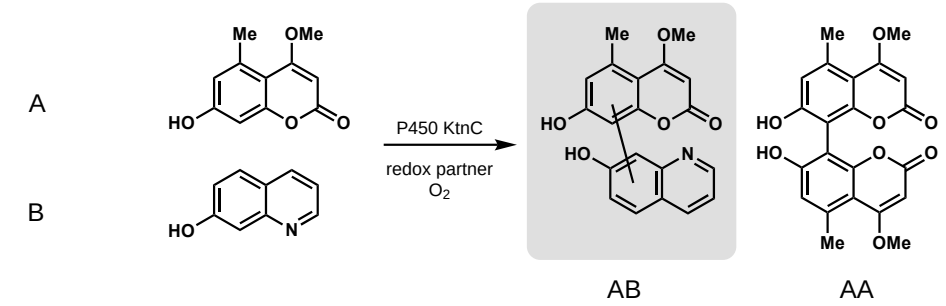

KtnC

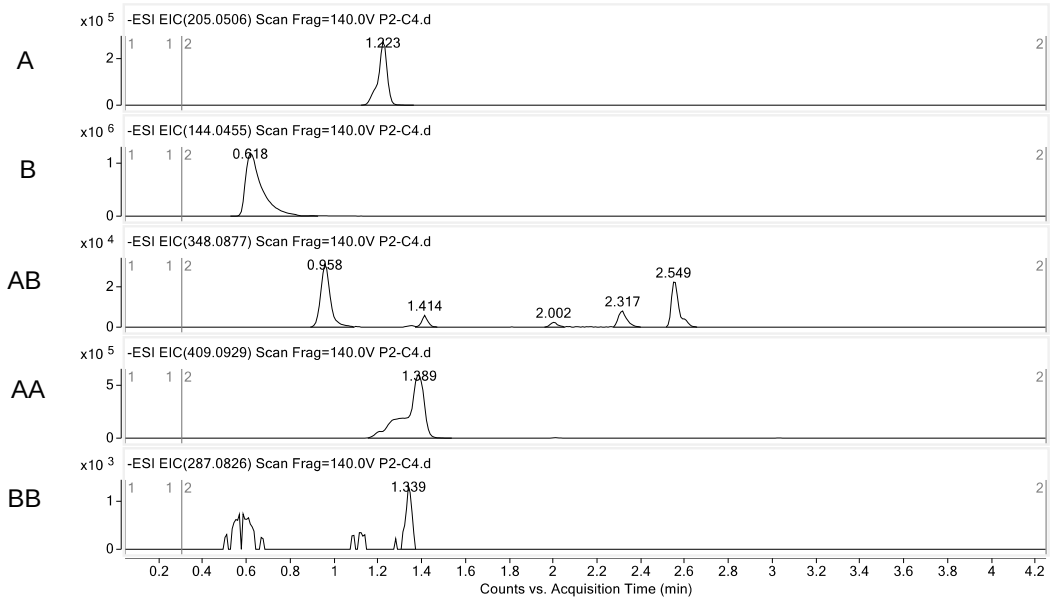

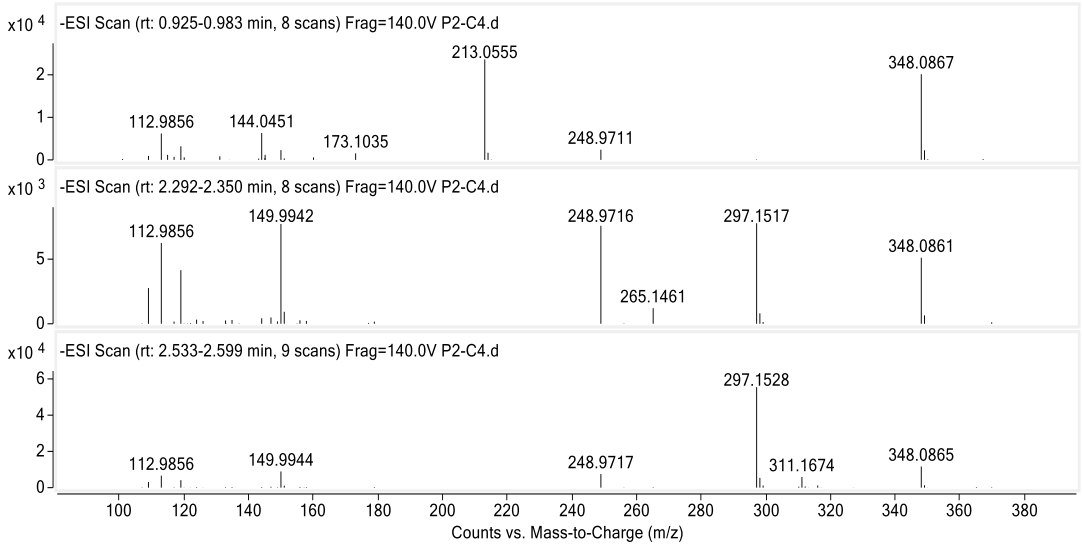

No Enzyme control

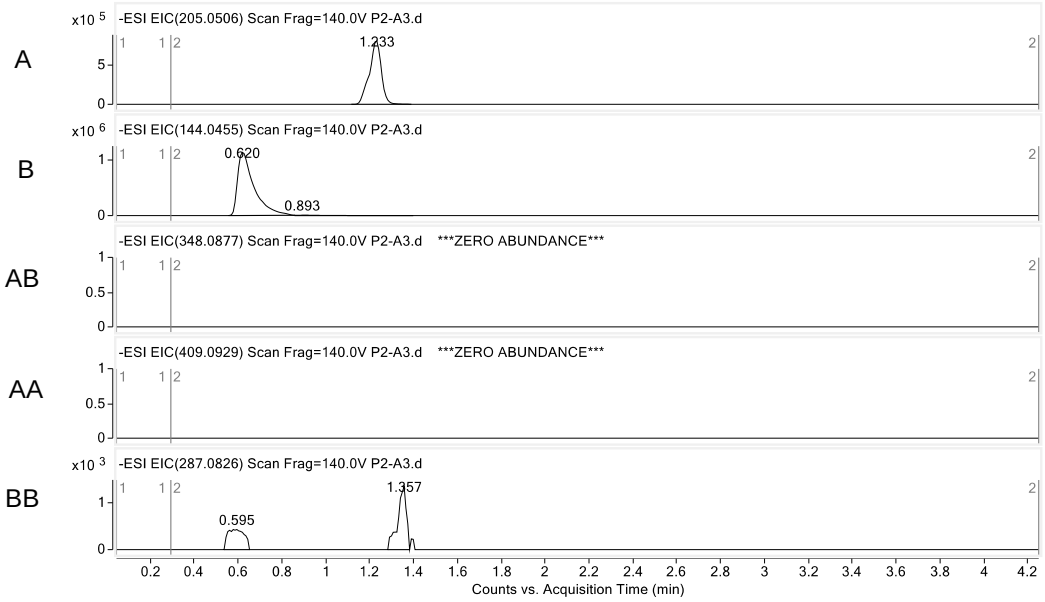

Supplemental Figure S3.71. Oxidative cross-coupling of **6** and **30** by KtnC (**Figure 3.2**).

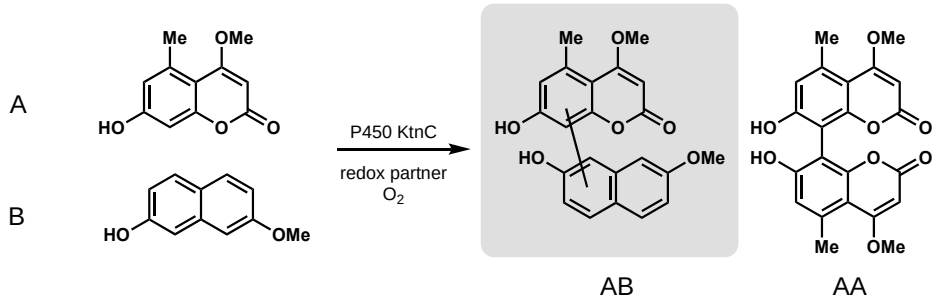

KtnC

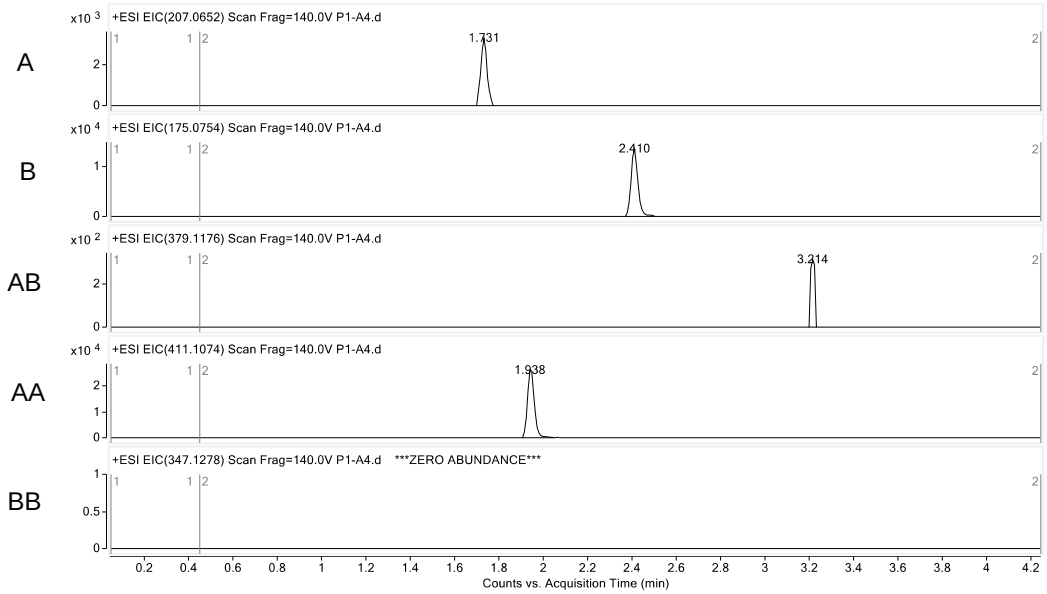

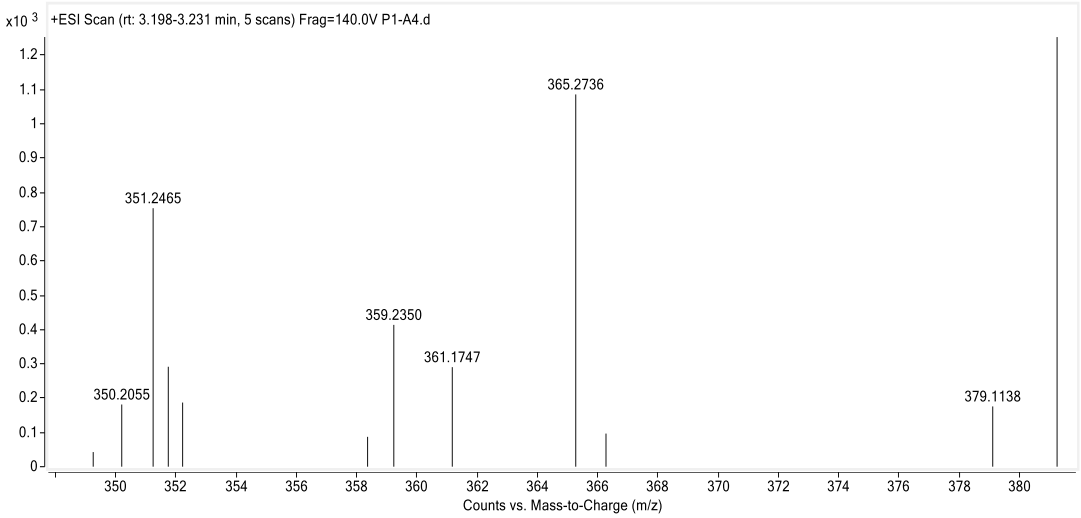

No Enzyme control

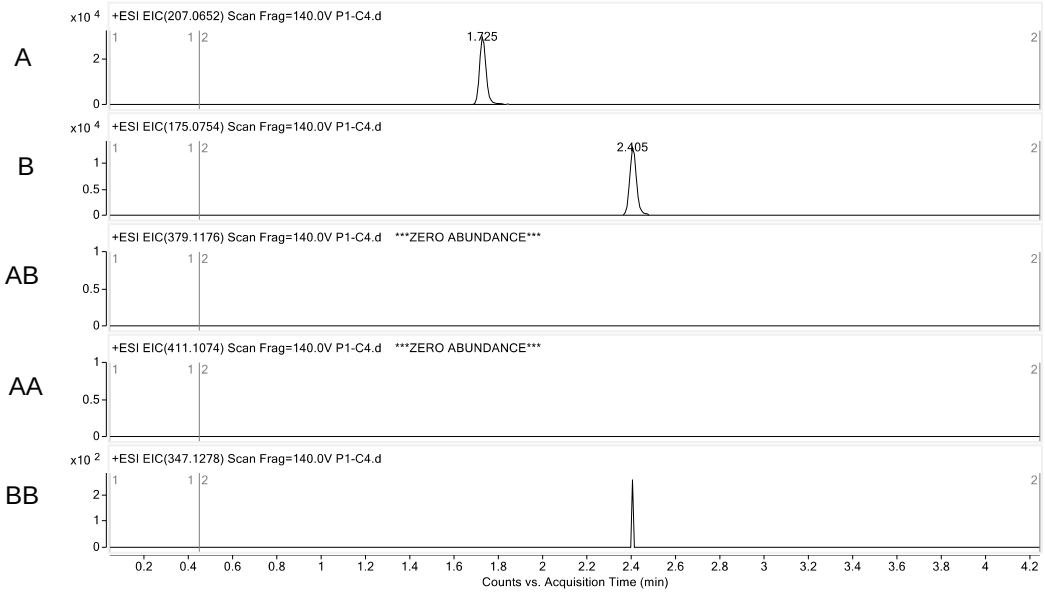

Supplemental Figure S3.72. Oxidative cross-coupling of **6** and **31** by KtnC (**Figure 3.2**).

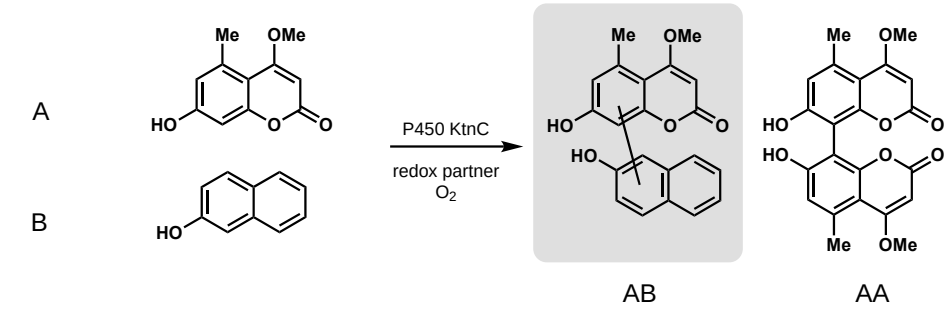

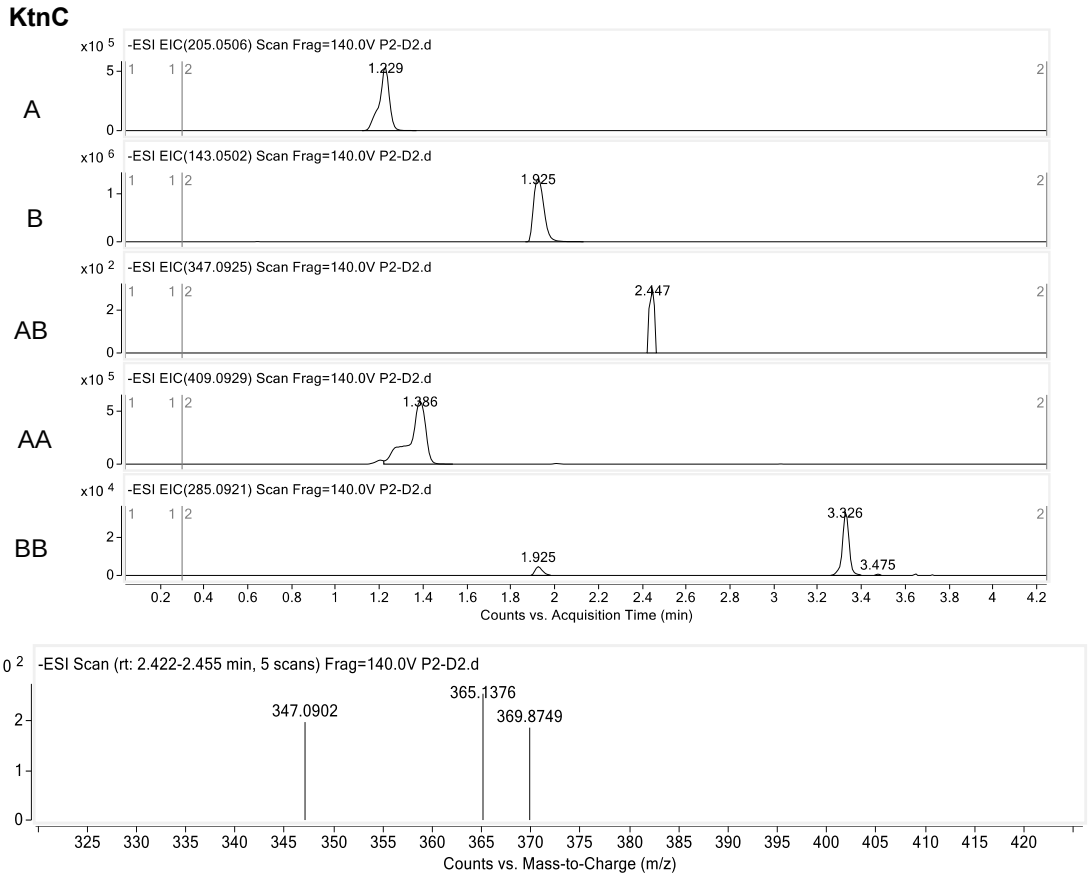

No Enzyme control

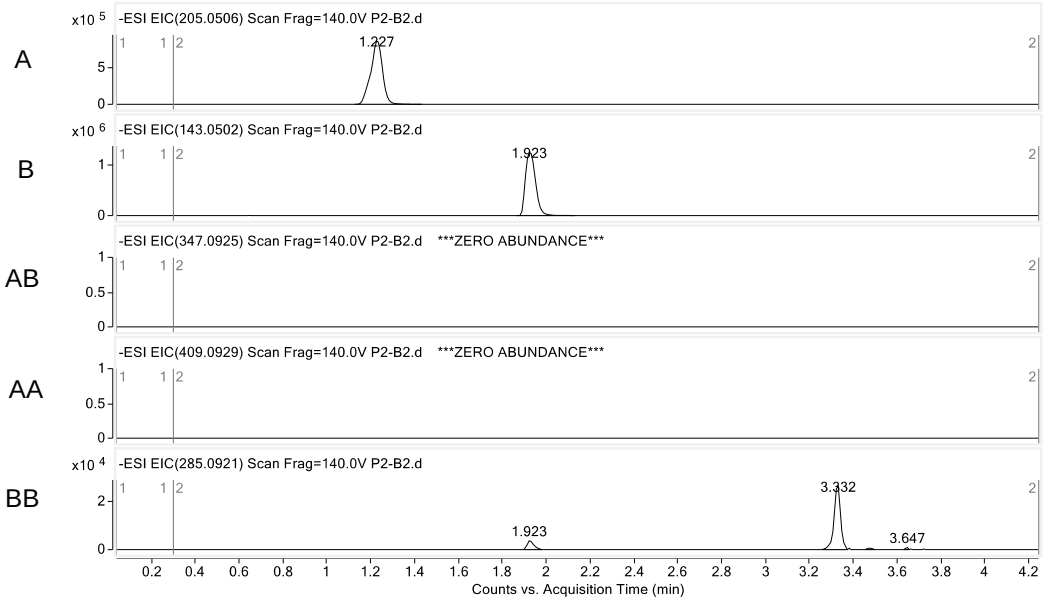

Supplemental Figure S3.73. Oxidative cross-coupling of **22** and **21** by KtnC (**Figure 3.3**).

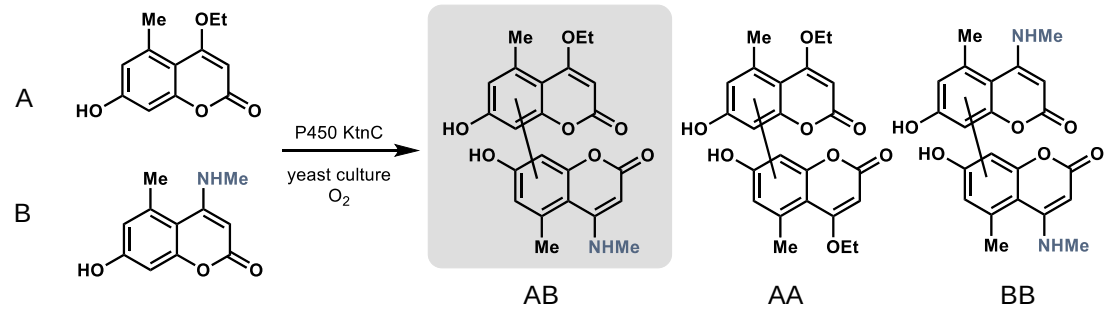

KtnC

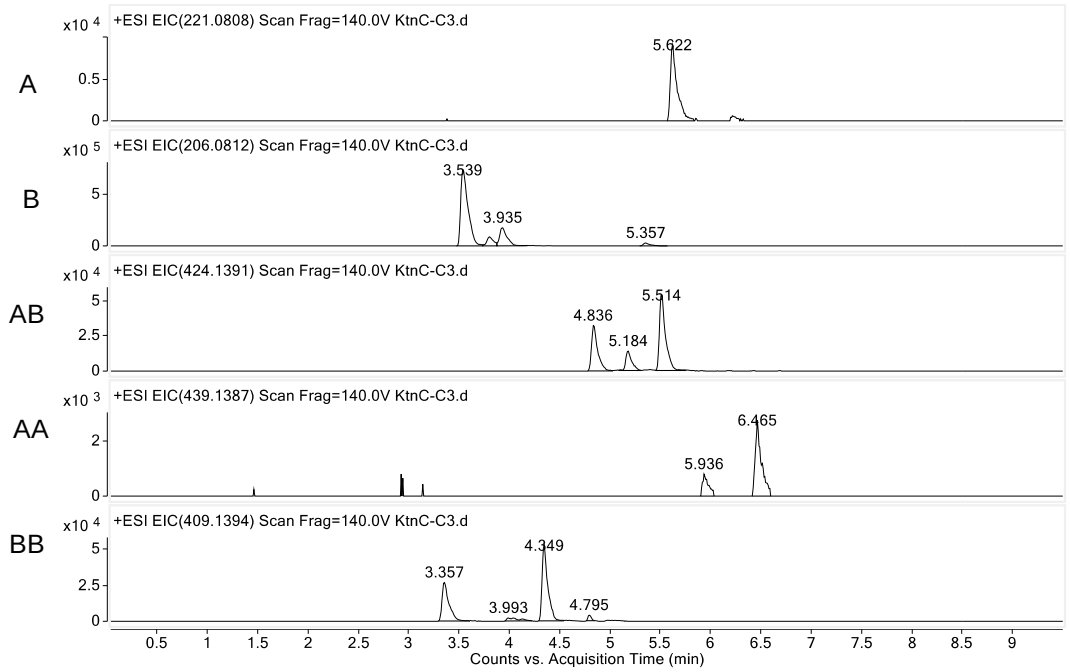

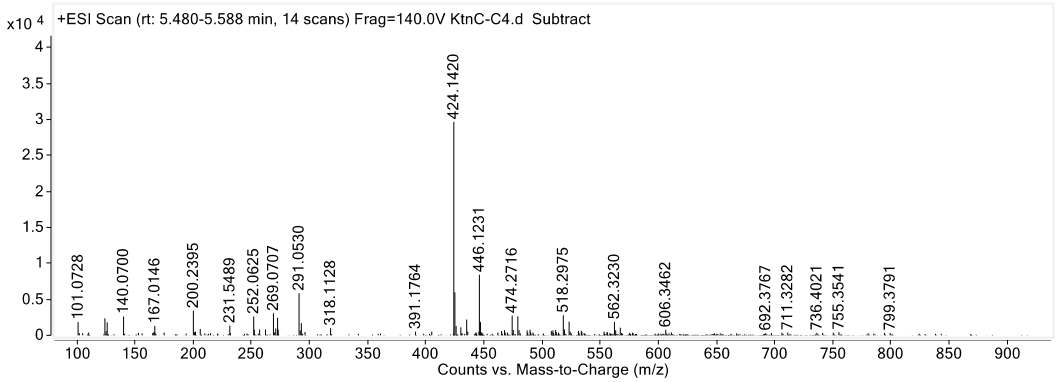

No Enzyme

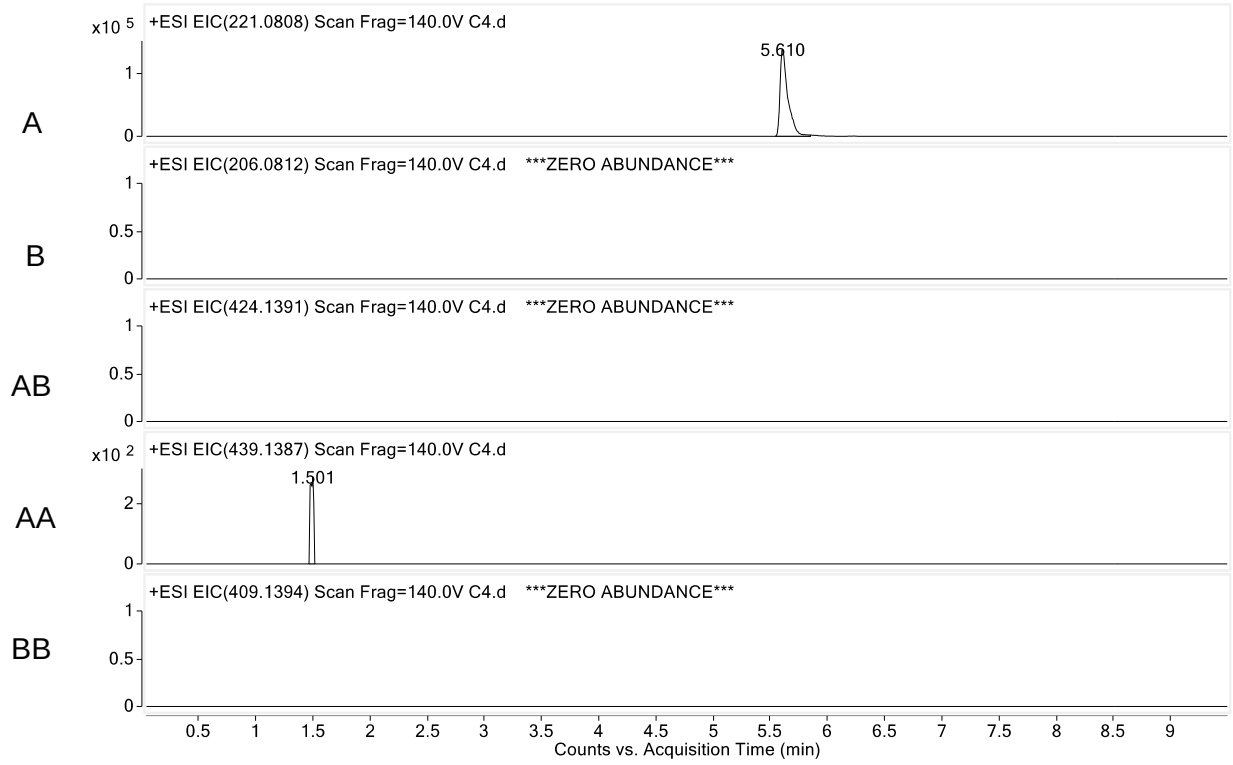
A
+ESI EIC(221.0808) Scan Frag=140.0V C4.d
x10 5
5.610
B
+ESI EIC(206.0812) Scan Frag=140.0V C4.d ***ZERO ABUNDANCE***
AB
+ESI EIC(424.1391) Scan Frag=140.0V C4.d ***ZERO ABUNDANCE***
AA
+ESI EIC(439.1387) Scan Frag=140.0V C4.d
x10 2
1.501
BB
+ESI EIC(409.1394) Scan Frag=140.0V C4.d ***ZERO ABUNDANCE***
0.5 1 1.5 2 2.5 3 3.5 4 4.5 5 5.5 6 6.5 7 7.5 8 8.5 9
Counts vs. Acquisition Time (min)

Supplemental Figure S3.74. Oxidative cross-coupling of **22** and **20** by KtnC (**Figure 3.3**).

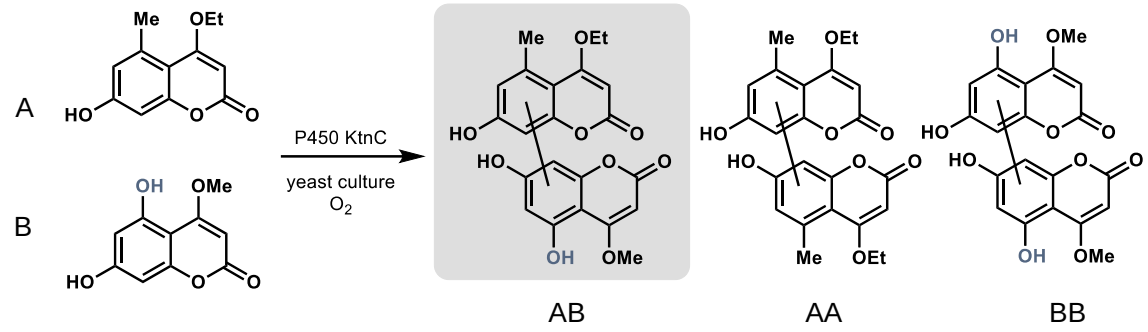

KtnC

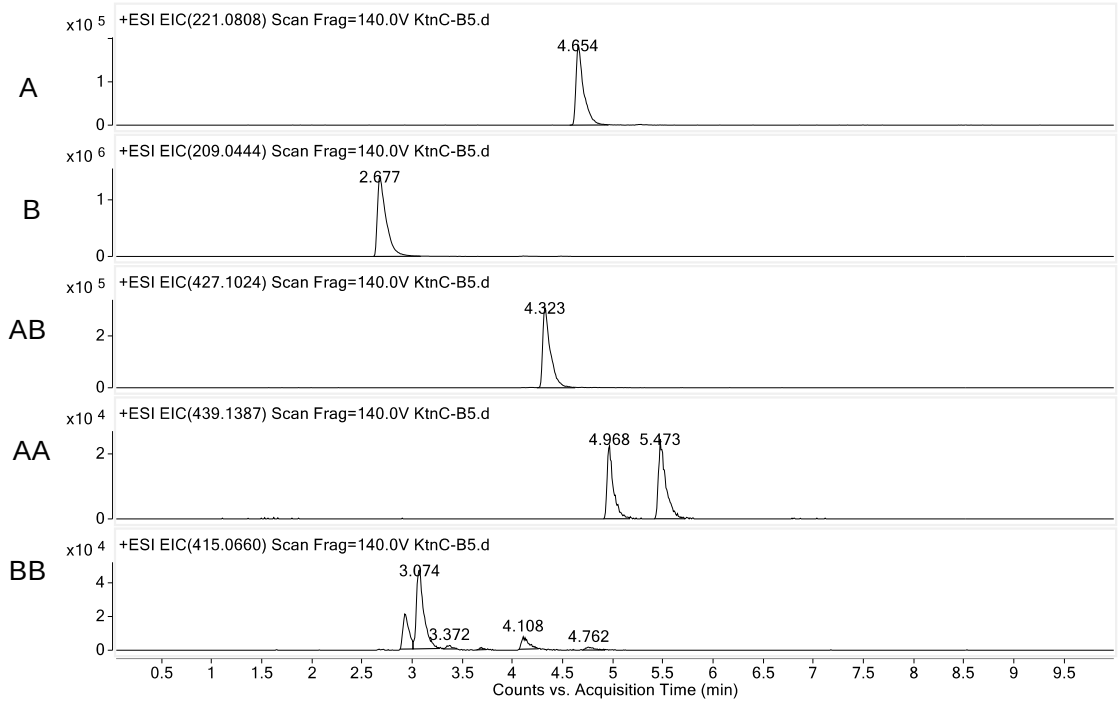

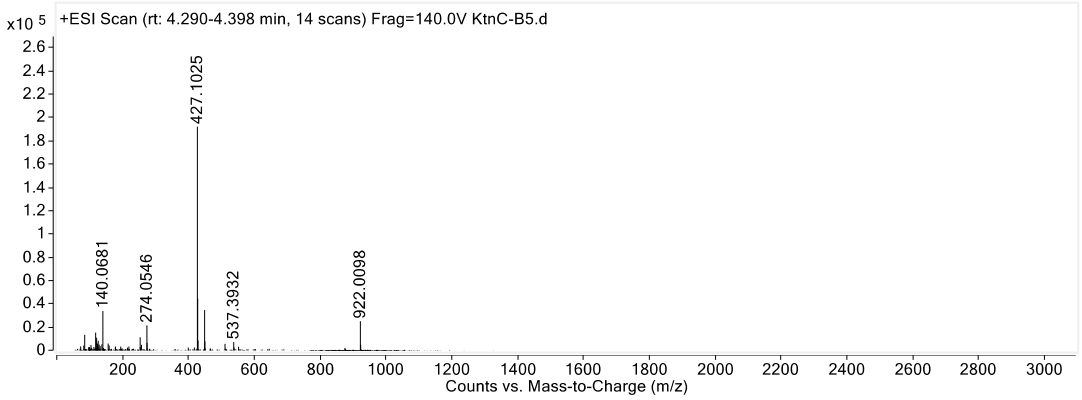

No enzyme

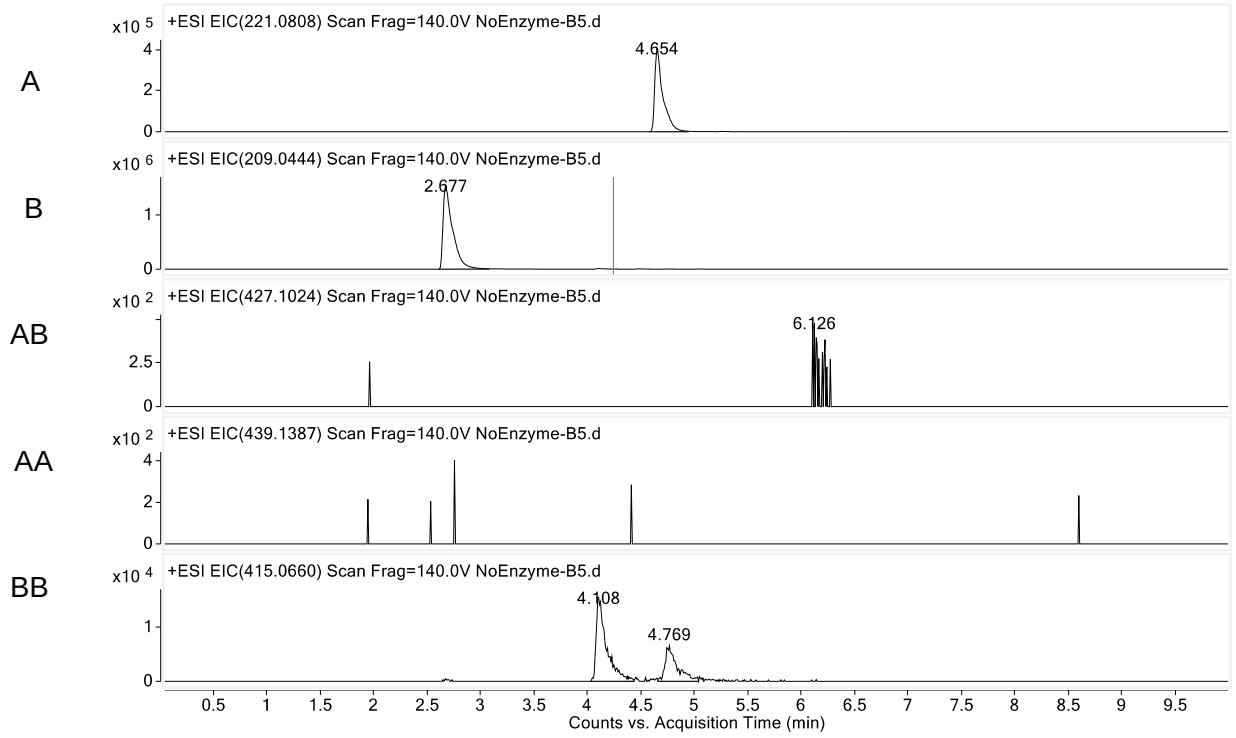
A
B
AB
AA
BB
+ESI EIC(221.0808) Scan Frag=140.0V NoEnzyme-B5.d
+ESI EIC(209.0444) Scan Frag=140.0V NoEnzyme-B5.d
+ESI EIC(427.1024) Scan Frag=140.0V NoEnzyme-B5.d
+ESI EIC(439.1387) Scan Frag=140.0V NoEnzyme-B5.d
+ESI EIC(415.0660) Scan Frag=140.0V NoEnzyme-B5.d
4.654
2.677
6.126
4.108
4.769
Counts vs. Acquisition Time (min)

Supplemental Figure S3.75. Oxidative cross-coupling of **22** and **14** by KtnC (**Figure 3.3**).

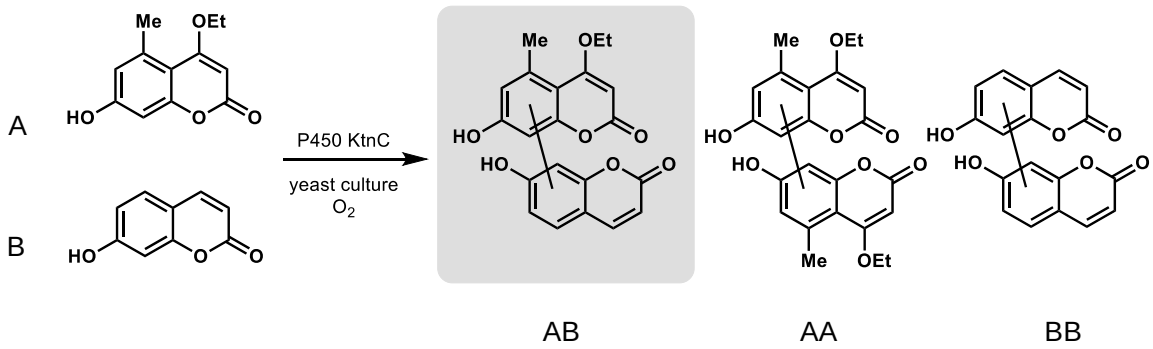

KtnC

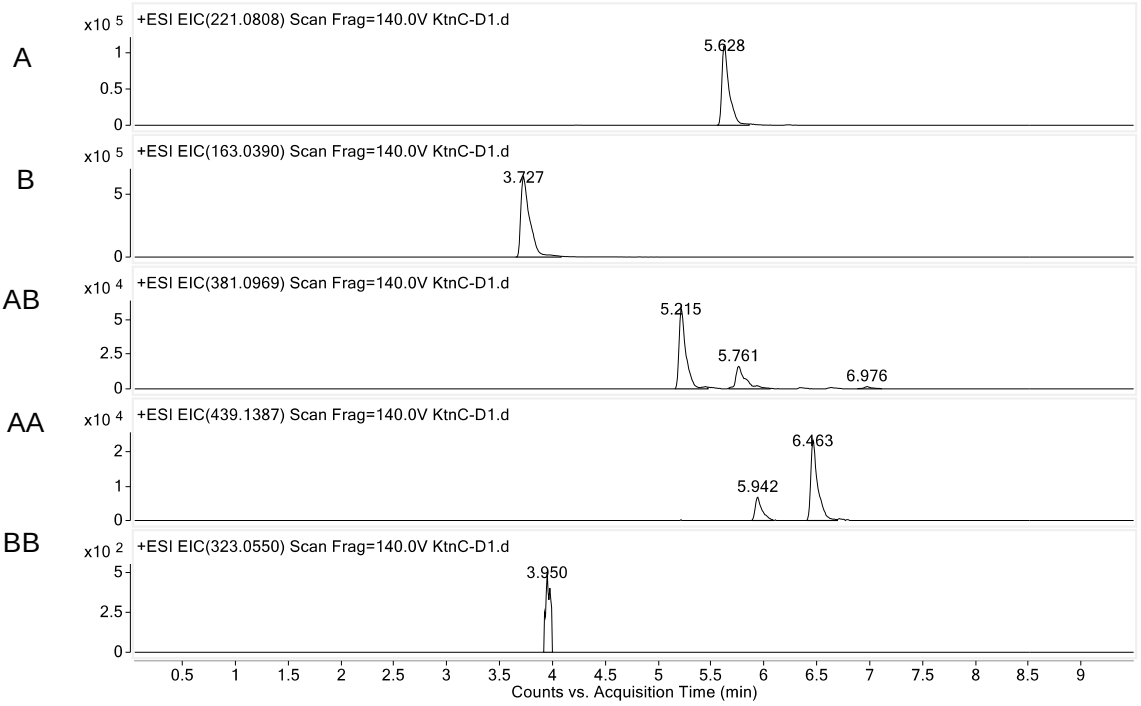

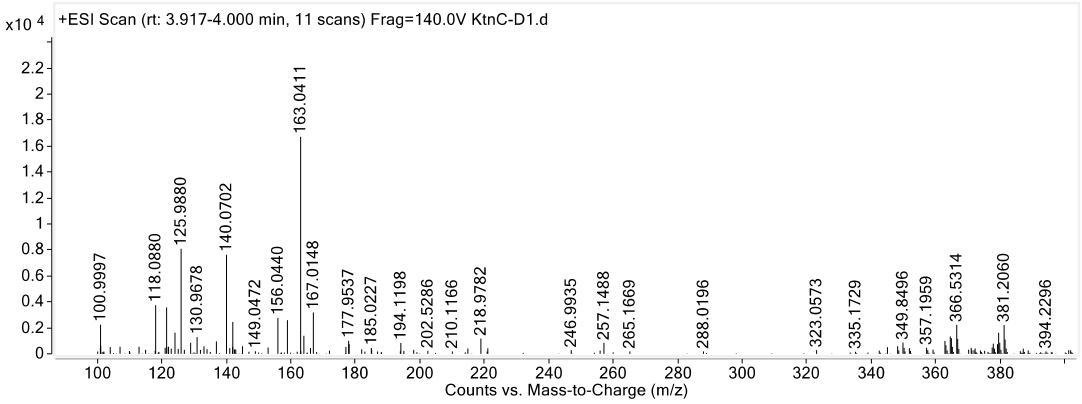

No enzyme

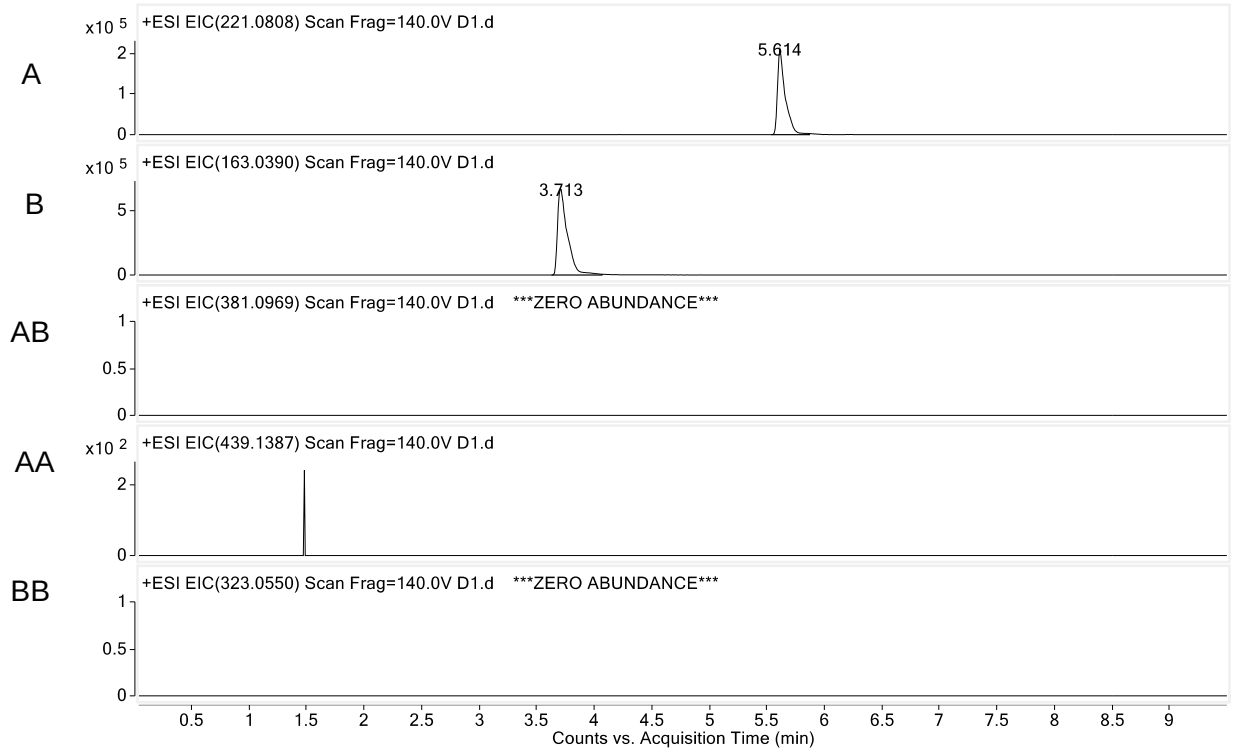
A
+ESI EIC(221.0808) Scan Frag=140.0V D1.d
x10 5
5.614
B
+ESI EIC(163.0390) Scan Frag=140.0V D1.d
x10 5
3.713
AB
+ESI EIC(381.0969) Scan Frag=140.0V D1.d ***ZERO ABUNDANCE***
AA
+ESI EIC(439.1387) Scan Frag=140.0V D1.d
x10 2
BB
+ESI EIC(323.0550) Scan Frag=140.0V D1.d ***ZERO ABUNDANCE***
Counts vs. Acquisition Time (min)

Supplemental Figure S3.76. Oxidative cross-coupling of **22** and **11** by KtnC (**Figure 3.3**).

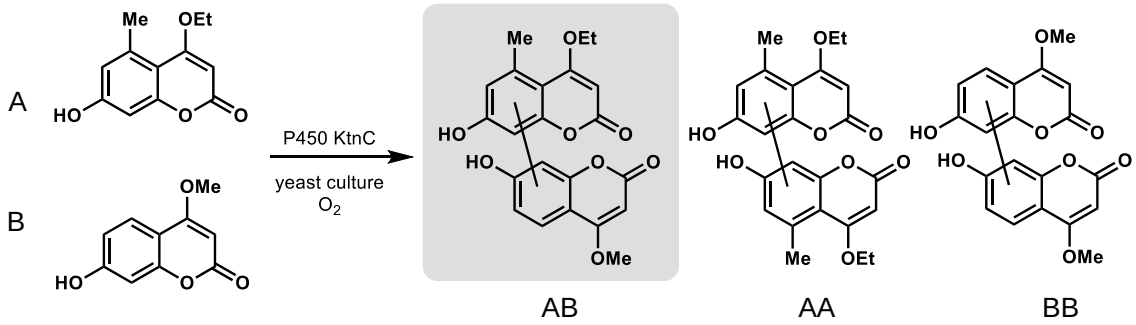

KtnC

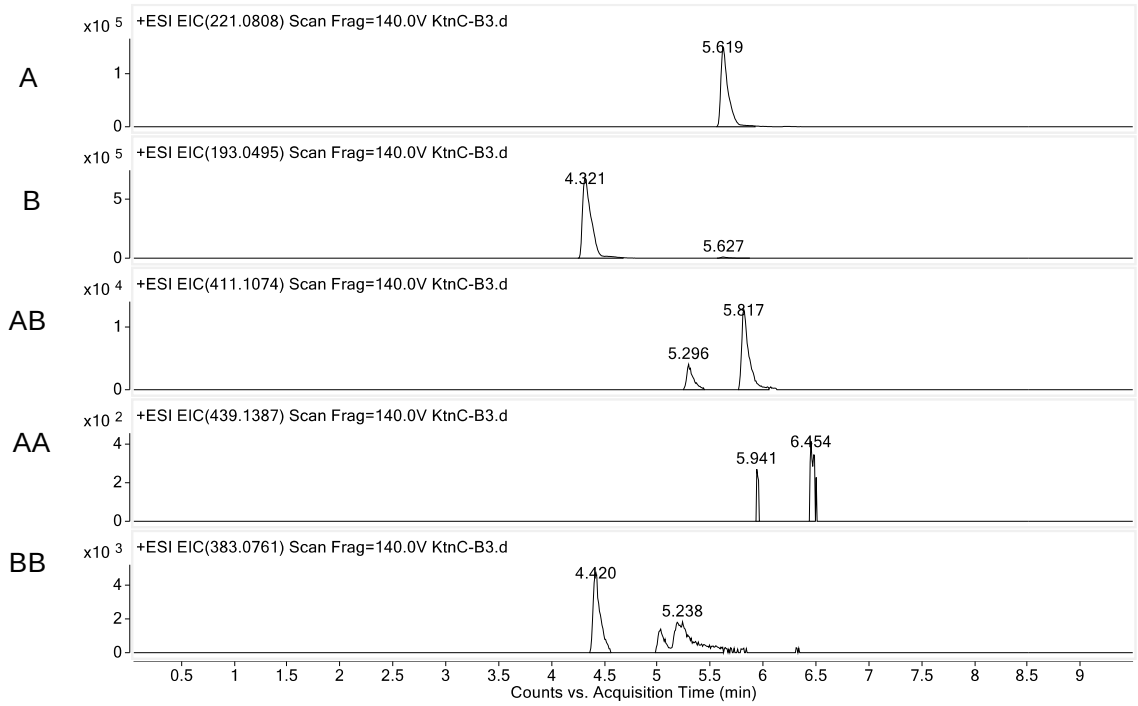

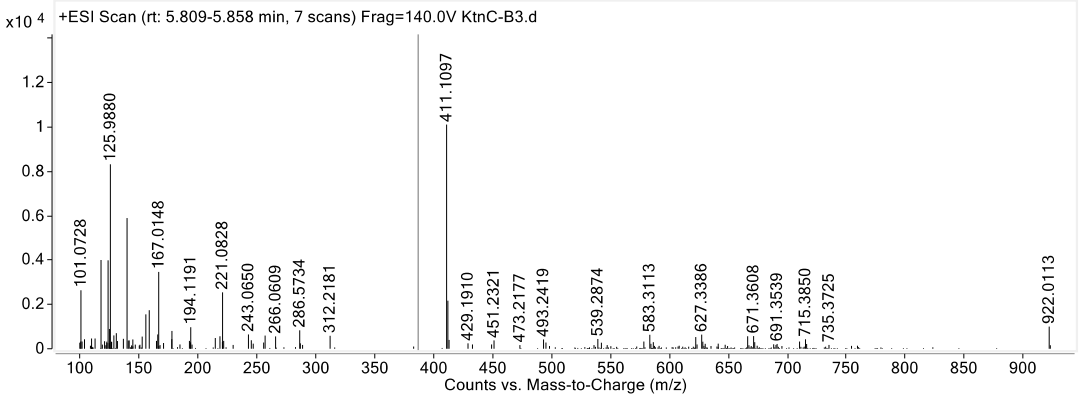

No enzyme

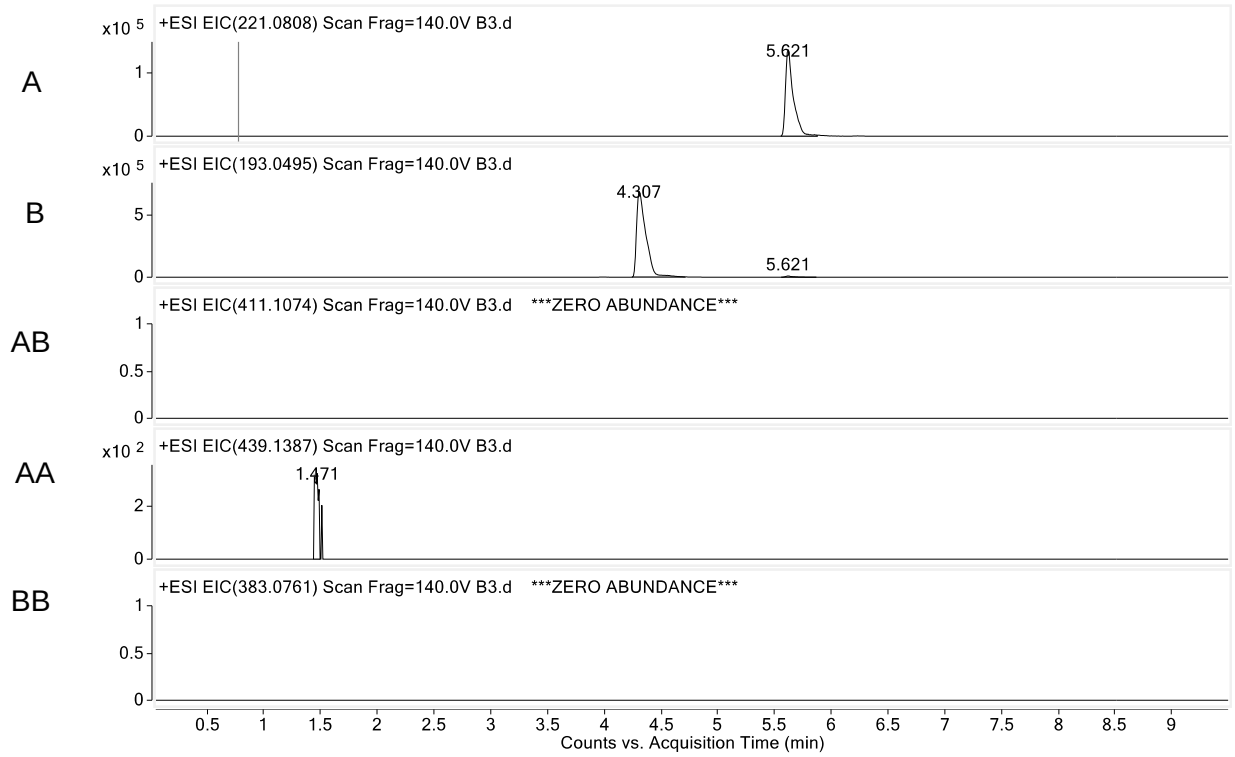
A
+ESI EIC(221.0808) Scan Frag=140.0V B3.d
x10 5
5.621
B
+ESI EIC(193.0495) Scan Frag=140.0V B3.d
x10 5
4.307
5.621
AB
+ESI EIC(411.1074) Scan Frag=140.0V B3.d ***ZERO ABUNDANCE***
AA
+ESI EIC(439.1387) Scan Frag=140.0V B3.d
x10 2
1.471
BB
+ESI EIC(383.0761) Scan Frag=140.0V B3.d ***ZERO ABUNDANCE***
Counts vs. Acquisition Time (min)

Supplemental Figure S3.77. Oxidative cross-coupling of **22** and **23** by KtnC (**Figure 3.3**).

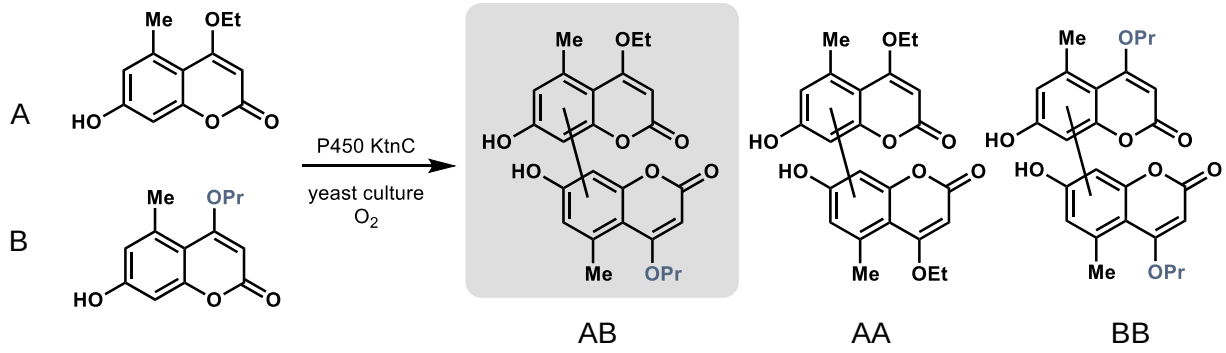

KtnC

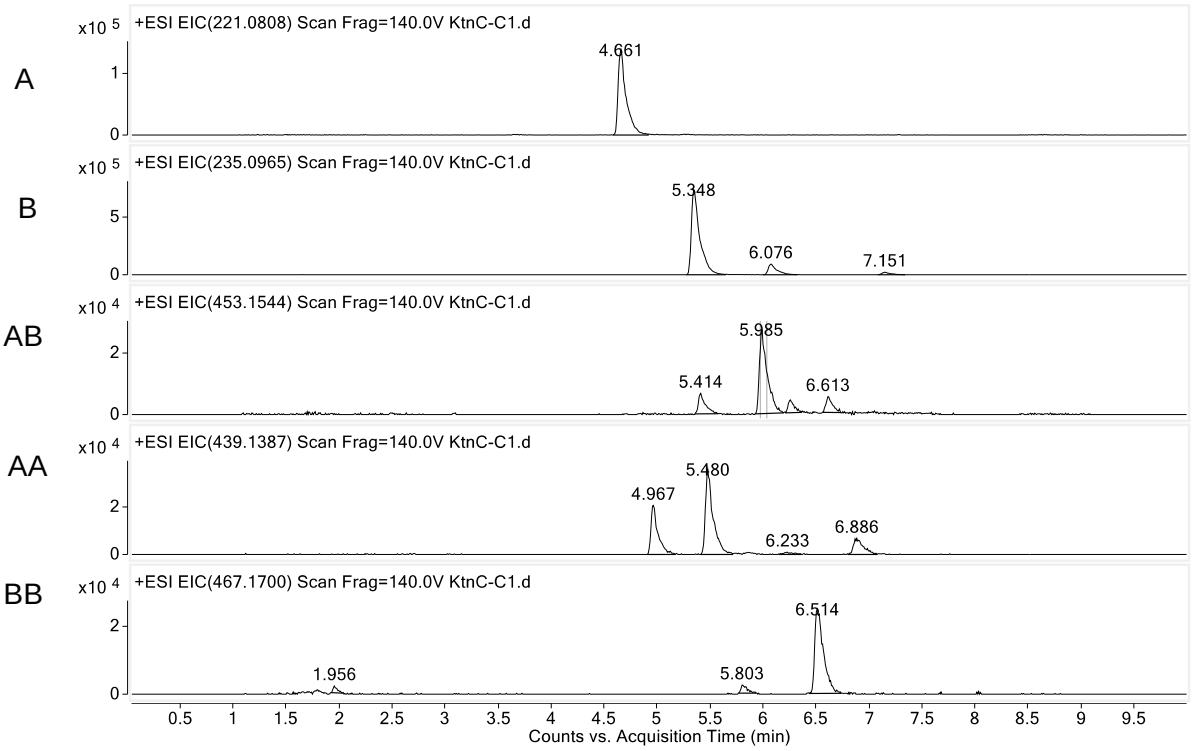

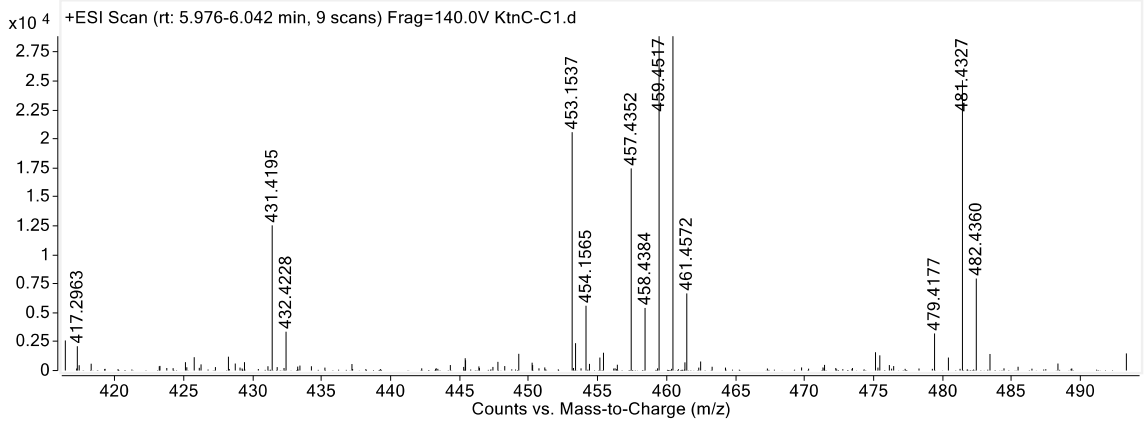

No enzyme

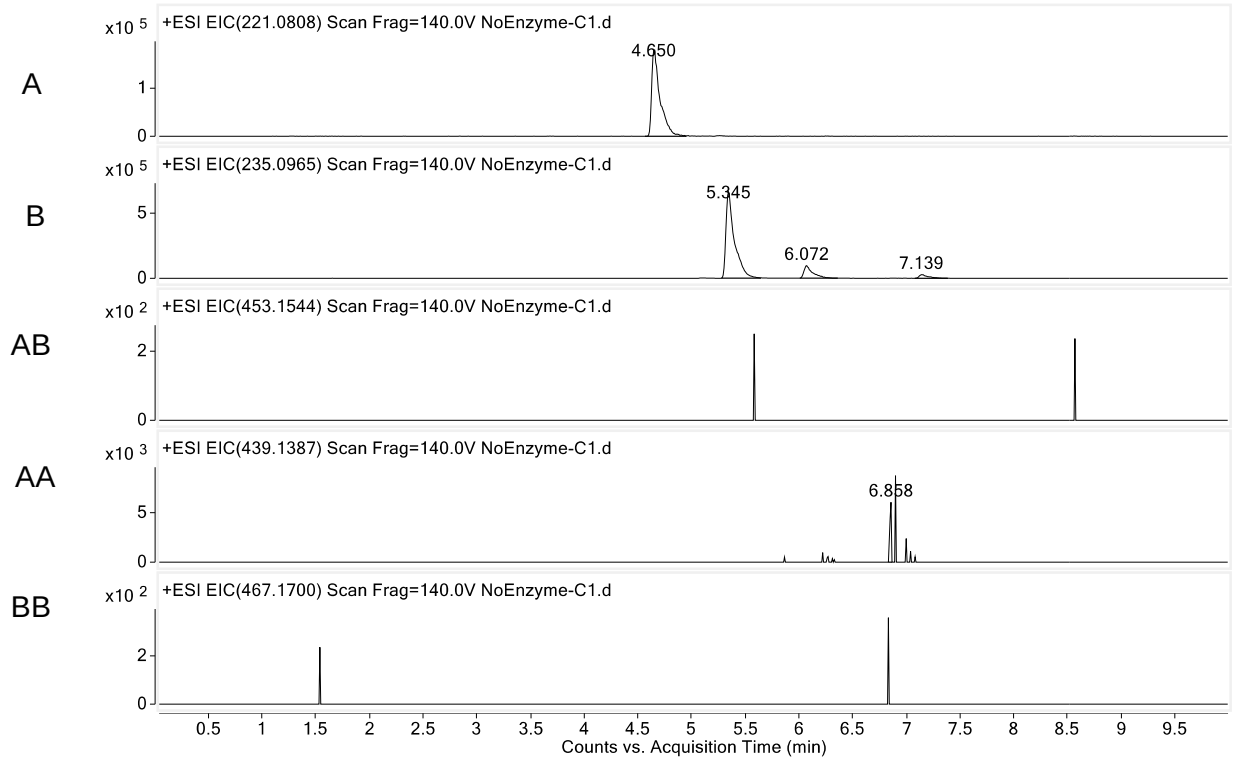
A
+ESI EIC(221.0808) Scan Frag=140.0V NoEnzyme-C1.d
x10 5
4.650
B
+ESI EIC(235.0965) Scan Frag=140.0V NoEnzyme-C1.d
x10 5
5.345
6.072
7.139
AB
+ESI EIC(453.1544) Scan Frag=140.0V NoEnzyme-C1.d
x10 2
AA
+ESI EIC(439.1387) Scan Frag=140.0V NoEnzyme-C1.d
x10 3
6.858
BB
+ESI EIC(467.1700) Scan Frag=140.0V NoEnzyme-C1.d
x10 2
0.5 1 1.5 2 2.5 3 3.5 4 4.5 5 5.5 6 6.5 7 7.5 8 8.5 9 9.5
Counts vs. Acquisition Time (min)

Supplemental Figure S3.78. Oxidative cross-coupling of **22** and **24** by KtnC (**Figure 3.3**).

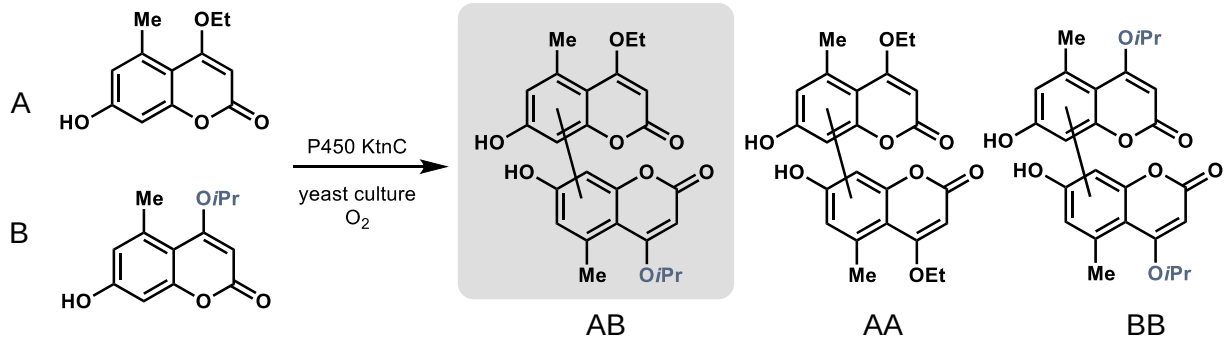

KtnC

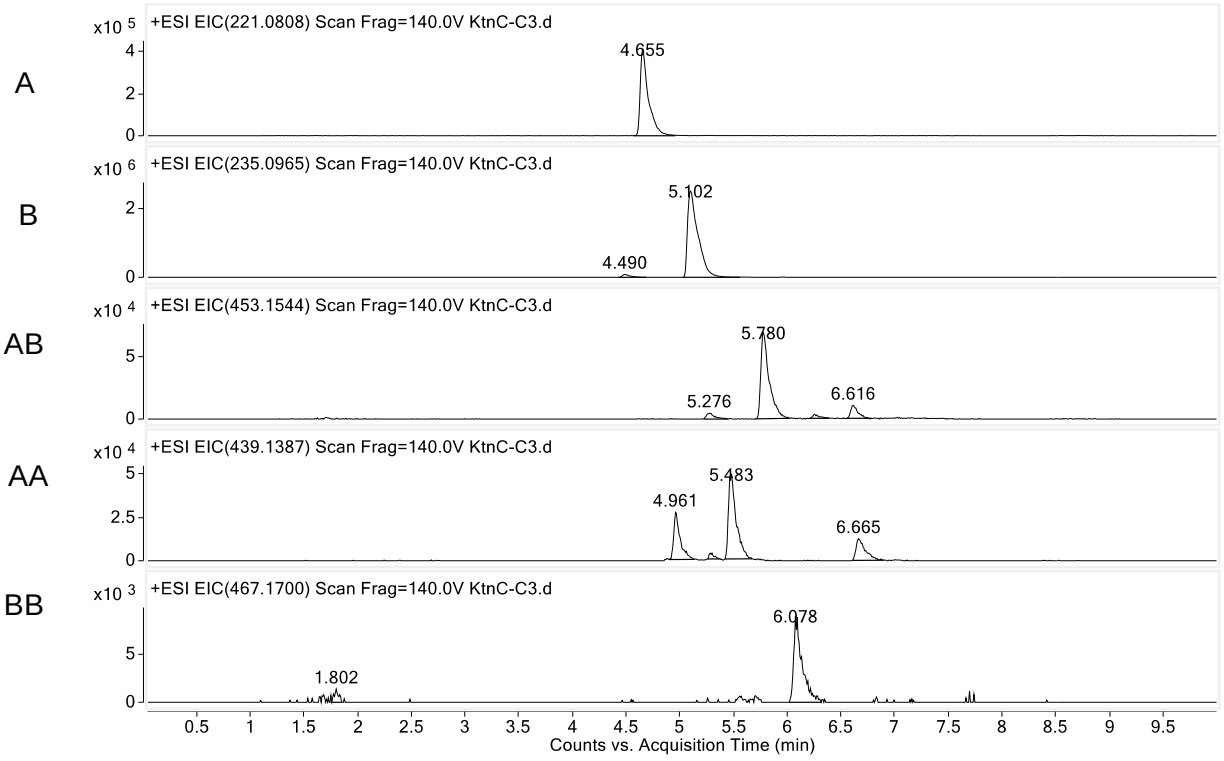

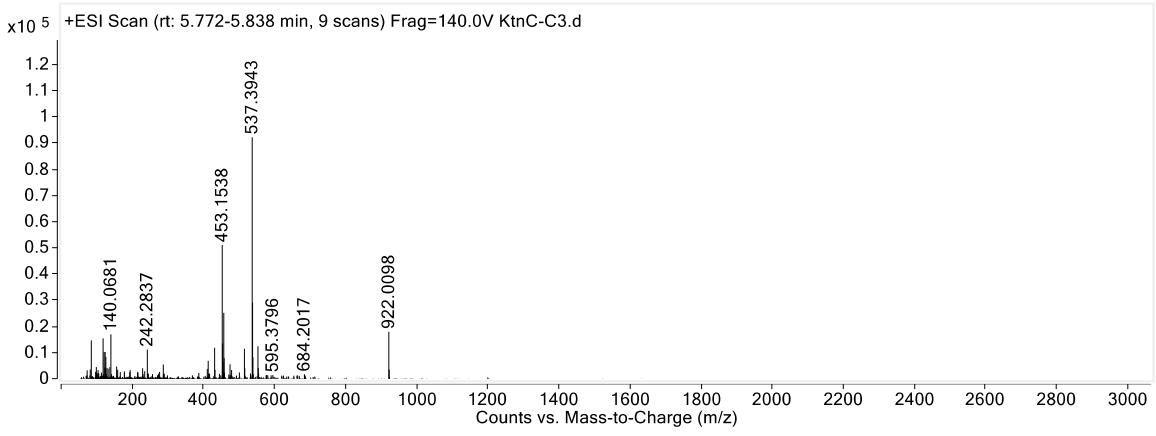

No enzyme

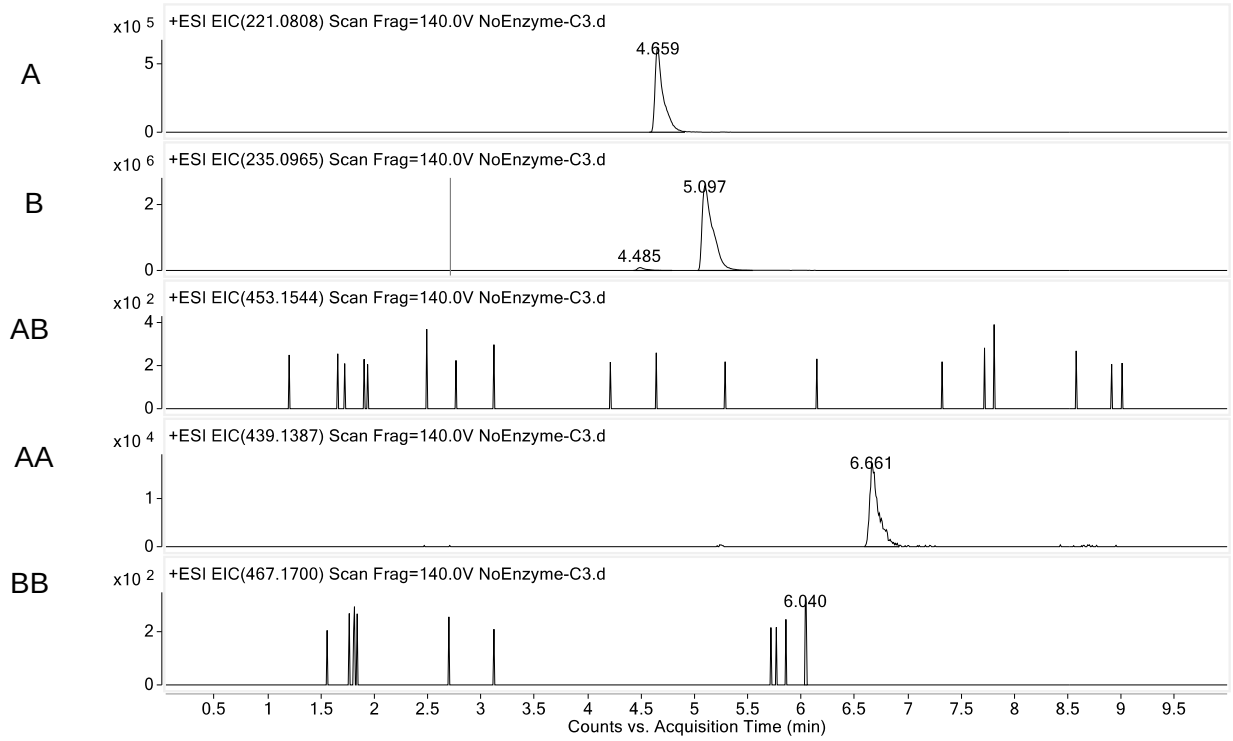
A
B
AB
AA
BB
+ESI EIC(221.0808) Scan Frag=140.0V NoEnzyme-C3.d
+ESI EIC(235.0965) Scan Frag=140.0V NoEnzyme-C3.d
+ESI EIC(453.1544) Scan Frag=140.0V NoEnzyme-C3.d
+ESI EIC(439.1387) Scan Frag=140.0V NoEnzyme-C3.d
+ESI EIC(467.1700) Scan Frag=140.0V NoEnzyme-C3.d
4.659
5.097
4.485
6.661
6.040
Counts vs. Acquisition Time (min)

Supplemental Figure S3.79. Oxidative cross-coupling of **22** and **25** by KtnC (**Figure 3.3**).

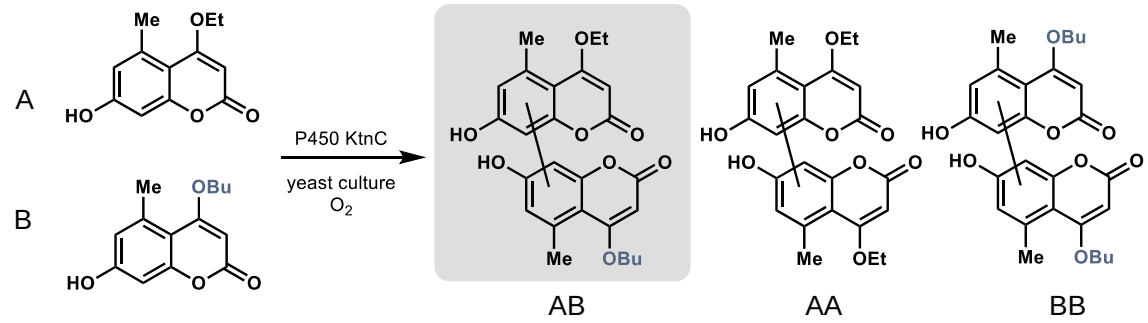

KtnC

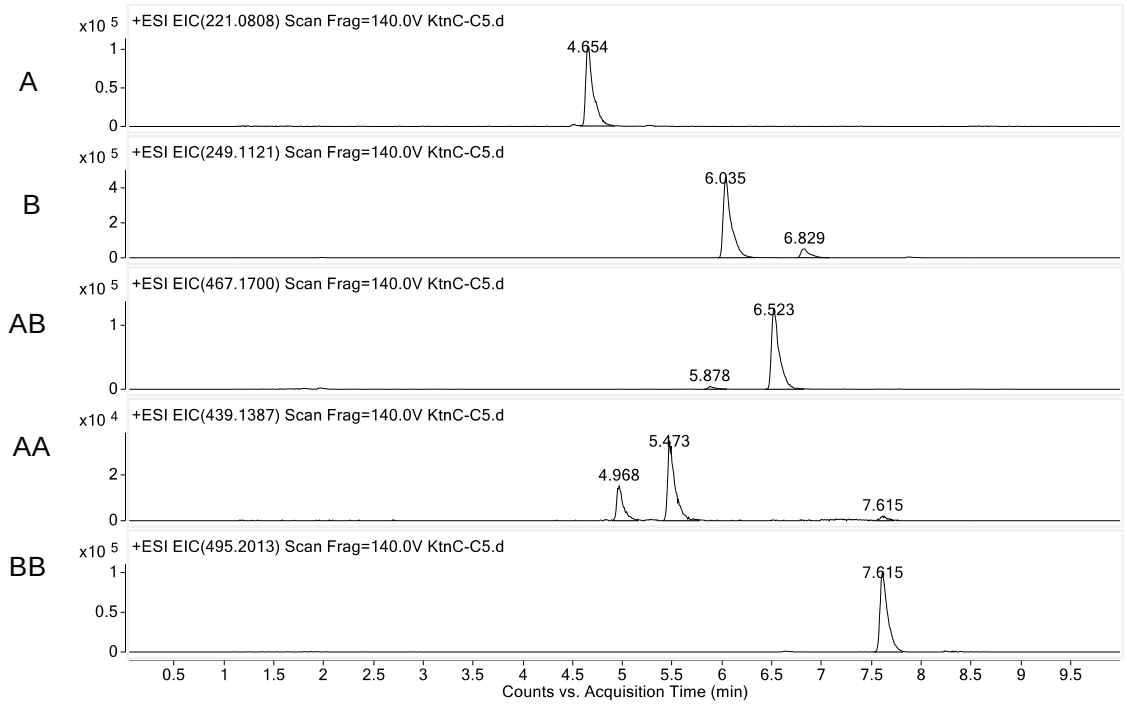

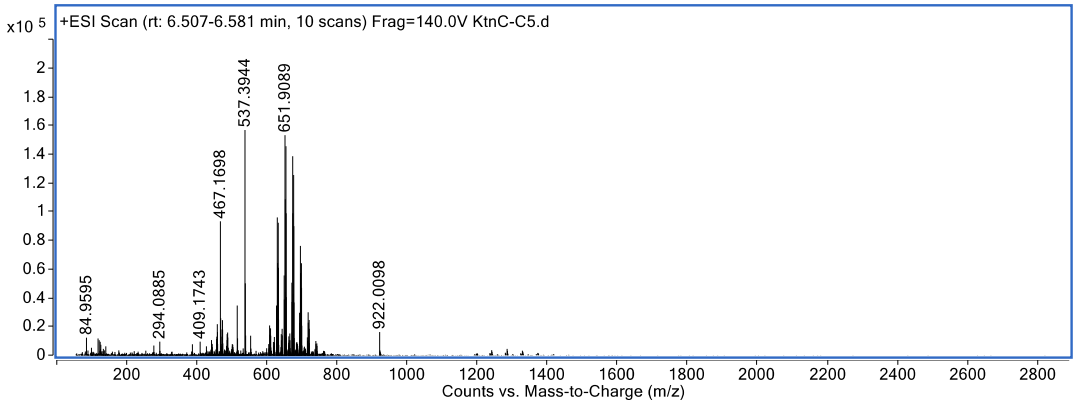

No enzyme

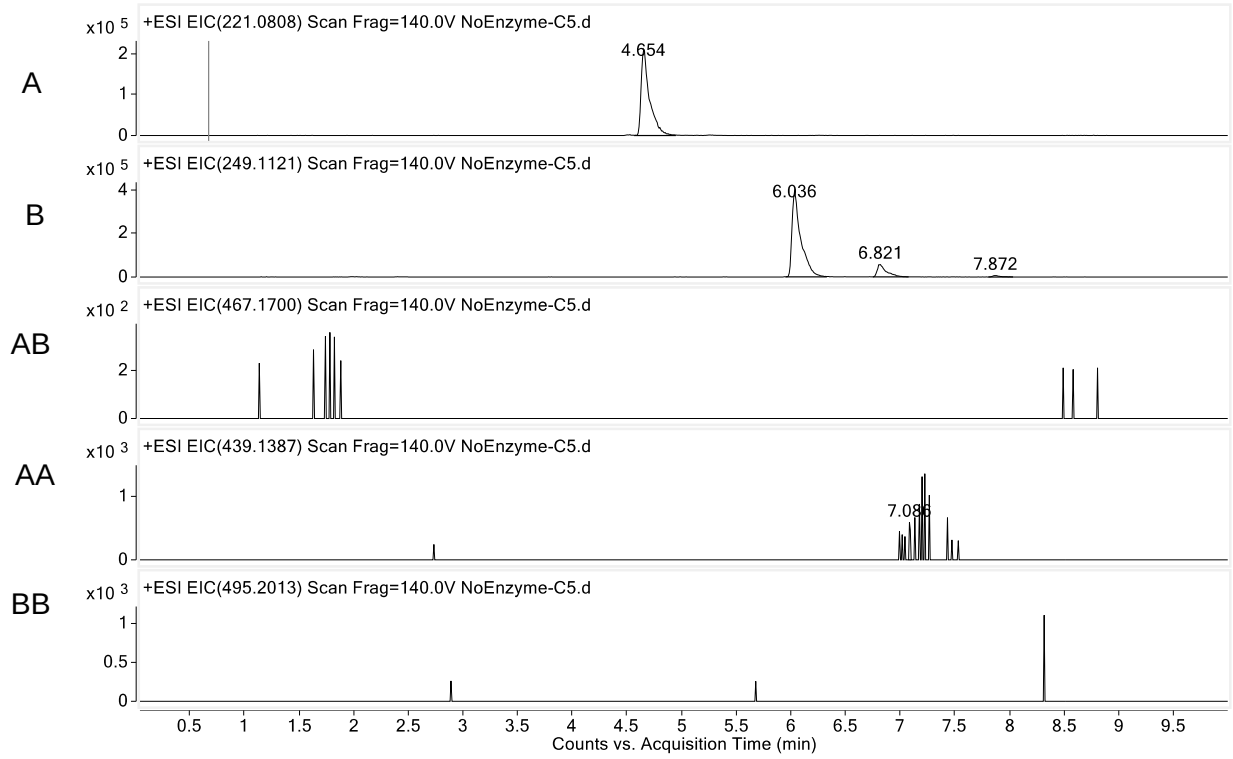
A
+ESI EIC(221.0808) Scan Frag=140.0V NoEnzyme-C5.d
x10 5
4.654
B
+ESI EIC(249.1121) Scan Frag=140.0V NoEnzyme-C5.d
x10 5
6.036
6.821
7.872
AB
+ESI EIC(467.1700) Scan Frag=140.0V NoEnzyme-C5.d
x10 2
AA
+ESI EIC(439.1387) Scan Frag=140.0V NoEnzyme-C5.d
x10 3
7.086
BB
+ESI EIC(495.2013) Scan Frag=140.0V NoEnzyme-C5.d
x10 3
Counts vs. Acquisition Time (min)

Supplemental Figure S3.80. Oxidative cross-coupling of **22** and **12** by KtnC (**Figure 3.3**).

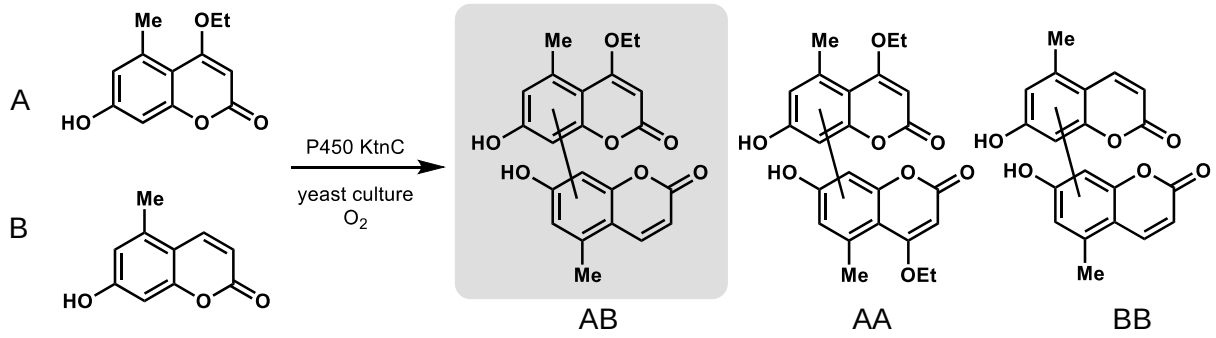

KtnC

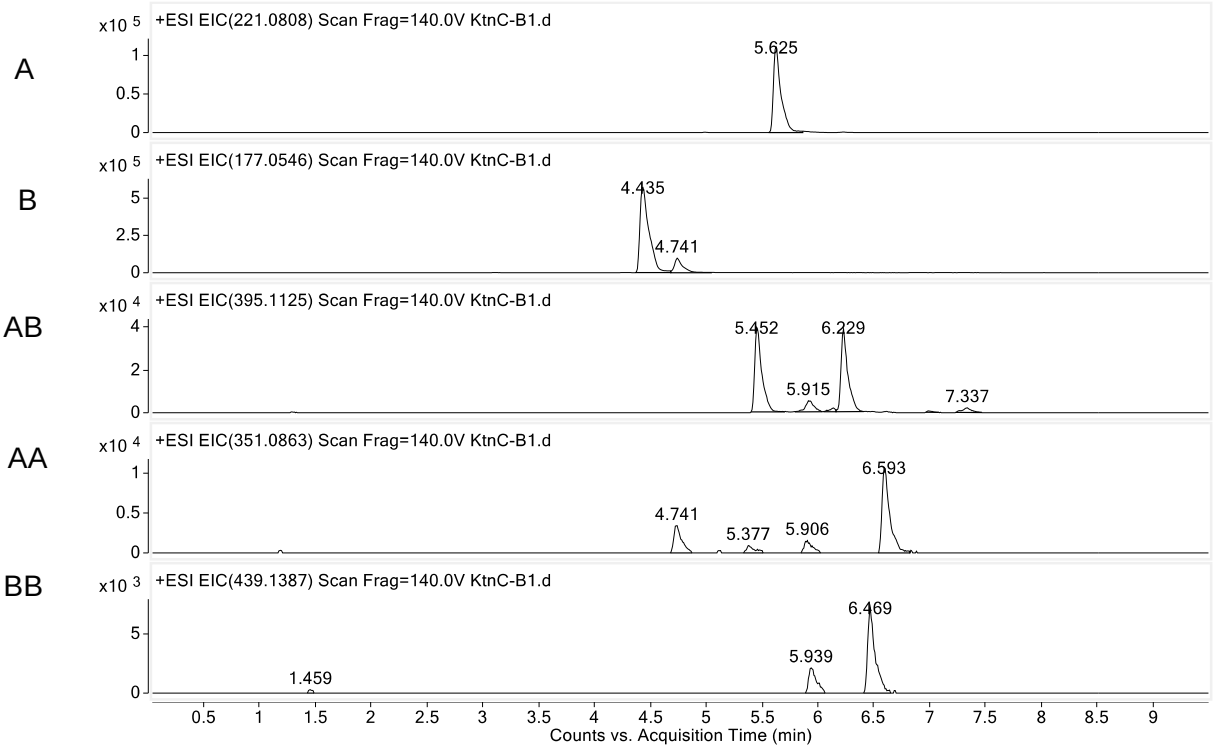

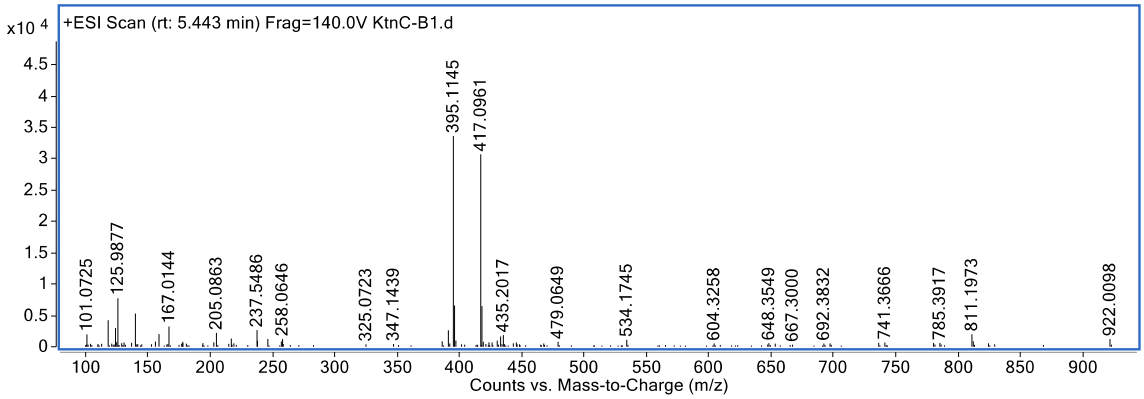

No enzyme

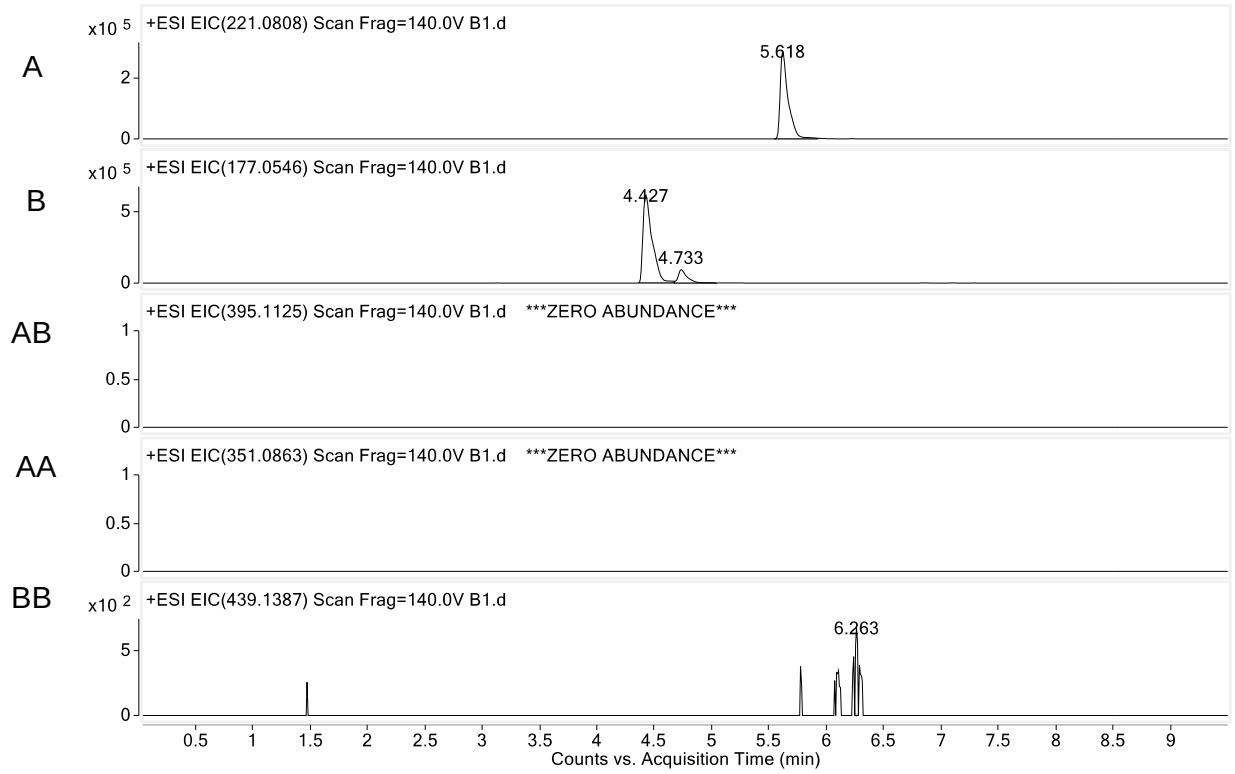
A
x10 5
+ESI EIC(221.0808) Scan Frag=140.0V B1.d
5.618
B
x10 5
+ESI EIC(177.0546) Scan Frag=140.0V B1.d
4.427
4.733
AB
+ESI EIC(395.1125) Scan Frag=140.0V B1.d ***ZERO ABUNDANCE***
AA
+ESI EIC(351.0863) Scan Frag=140.0V B1.d ***ZERO ABUNDANCE***
BB
x10 2
+ESI EIC(439.1387) Scan Frag=140.0V B1.d
6.263
Counts vs. Acquisition Time (min)

Supplemental Figure S3.81. Oxidative cross-coupling of **22** and **15** by KtnC (**Figure 3.3**).

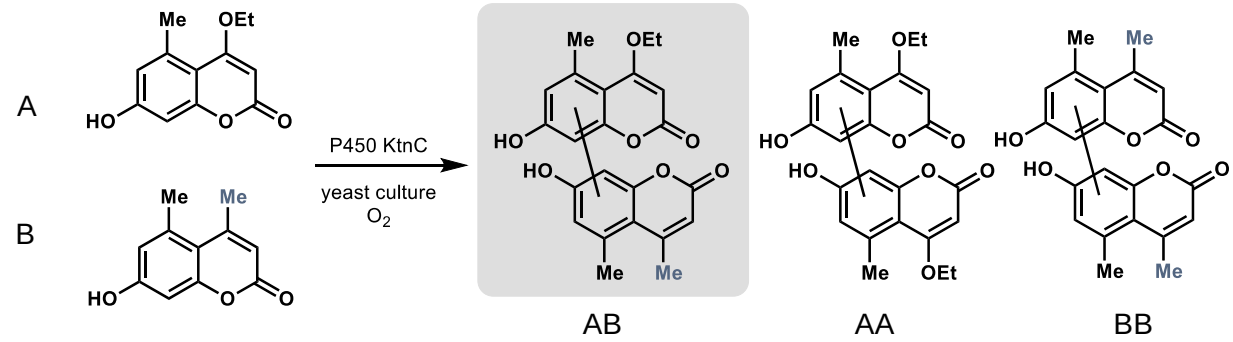

KtnC

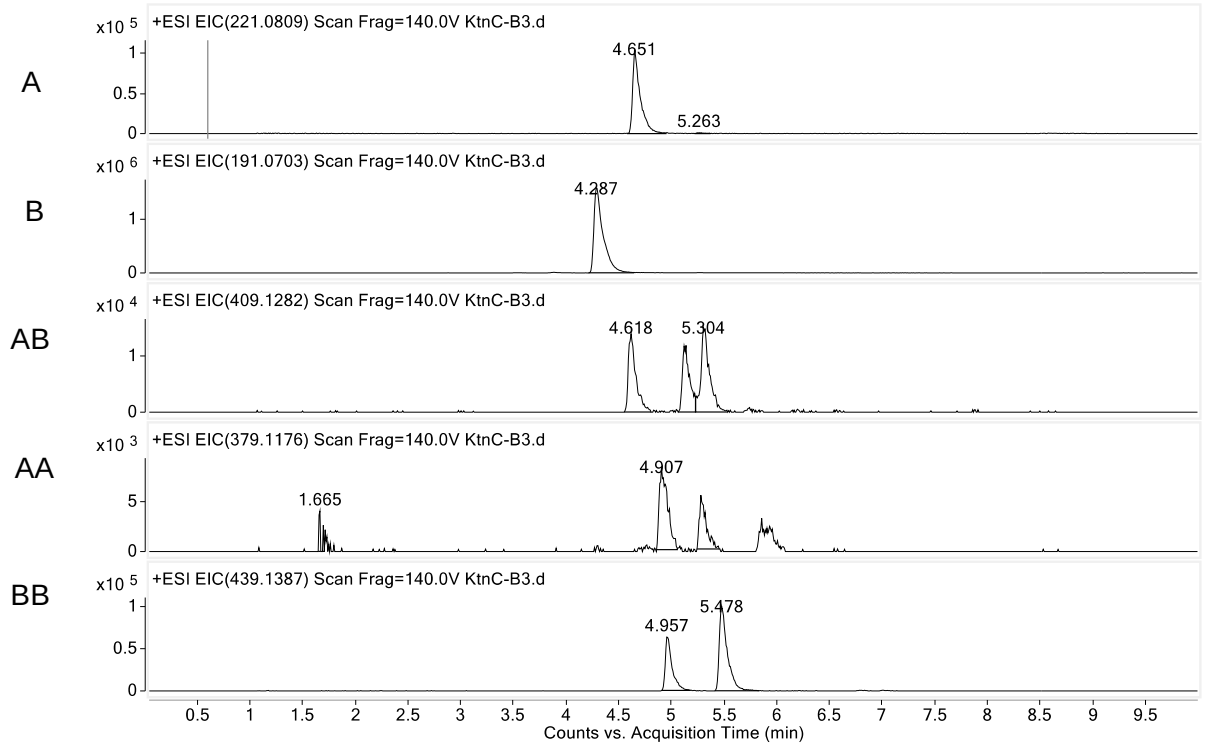

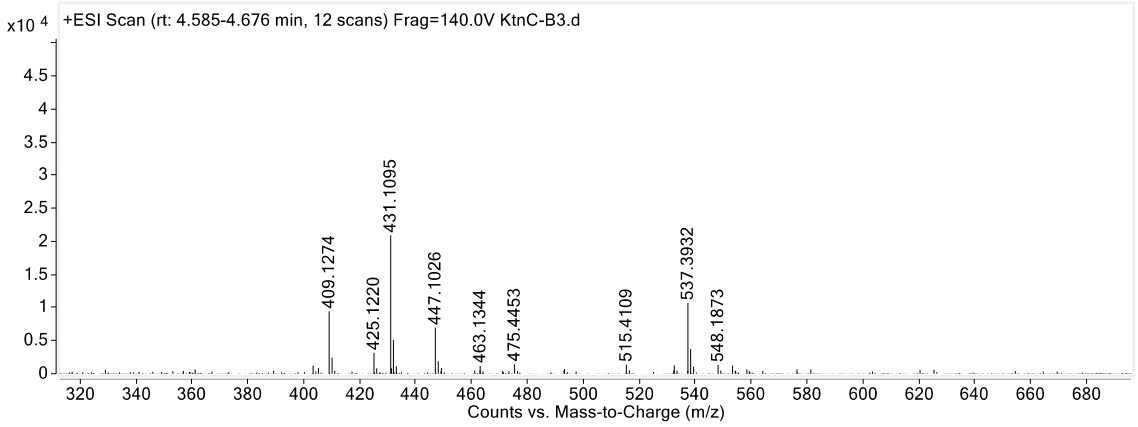

No enzyme

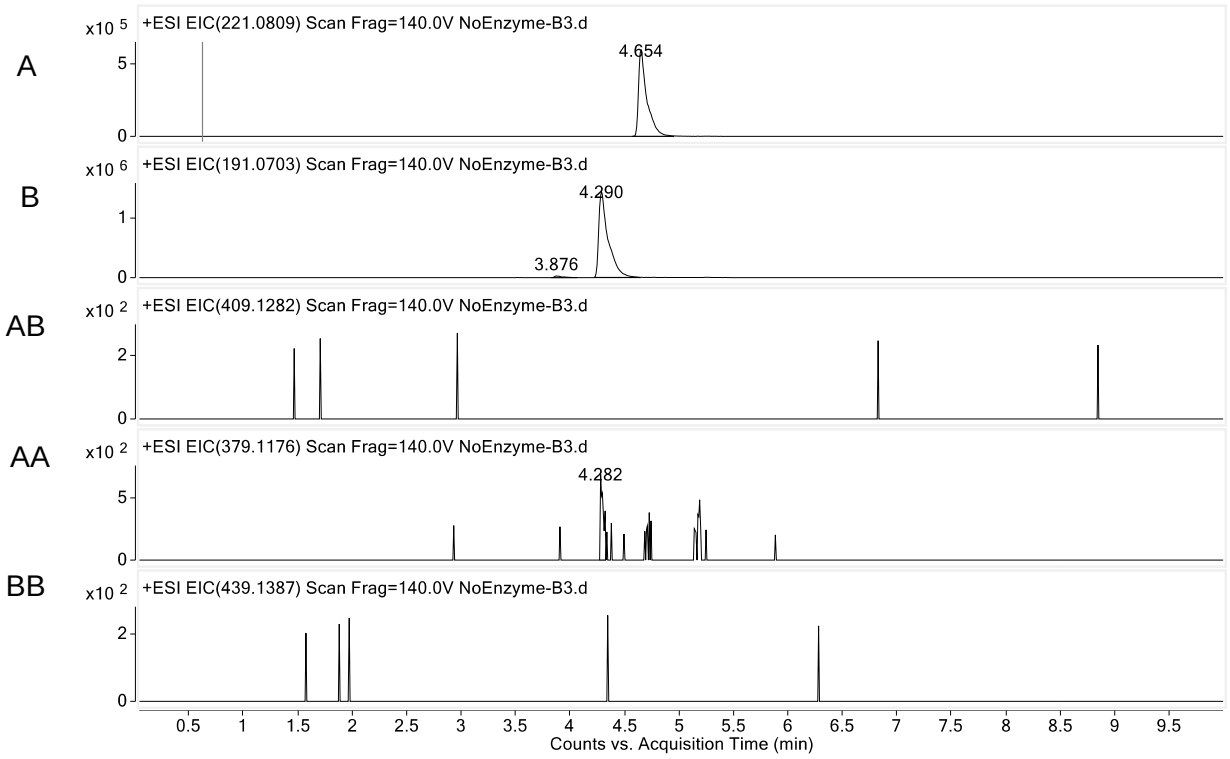
A
+ESI EIC(221.0809) Scan Frag=140.0V NoEnzyme-B3.d
x10 5
4.654
B
+ESI EIC(191.0703) Scan Frag=140.0V NoEnzyme-B3.d
x10 6
4.290
3.876
AB
+ESI EIC(409.1282) Scan Frag=140.0V NoEnzyme-B3.d
x10 2
AA
+ESI EIC(379.1176) Scan Frag=140.0V NoEnzyme-B3.d
x10 2
4.282
BB
+ESI EIC(439.1387) Scan Frag=140.0V NoEnzyme-B3.d
x10 2
0.5 1 1.5 2 2.5 3 3.5 4 4.5 5 5.5 6 6.5 7 7.5 8 8.5 9 9.5
Counts vs. Acquisition Time (min)

Supplemental Figure S3.82. Oxidative cross-coupling of **22** and **18** by KtnC (**Figure 3.3**).

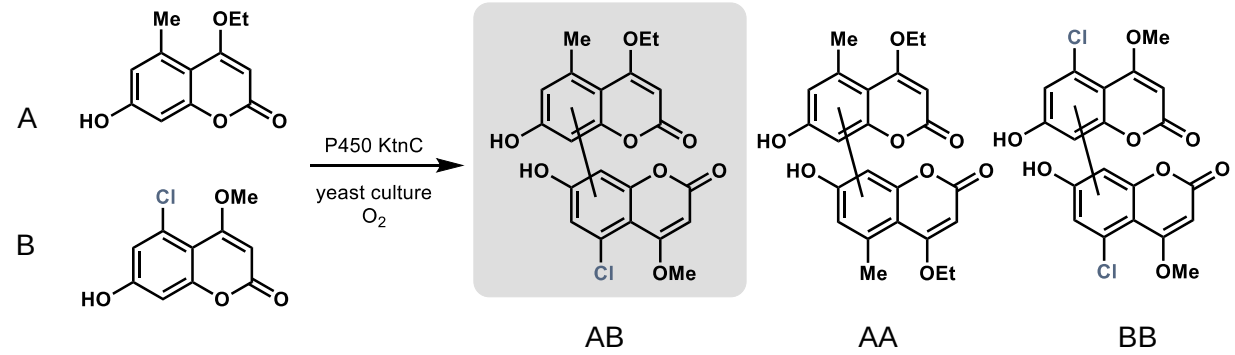

KtnC

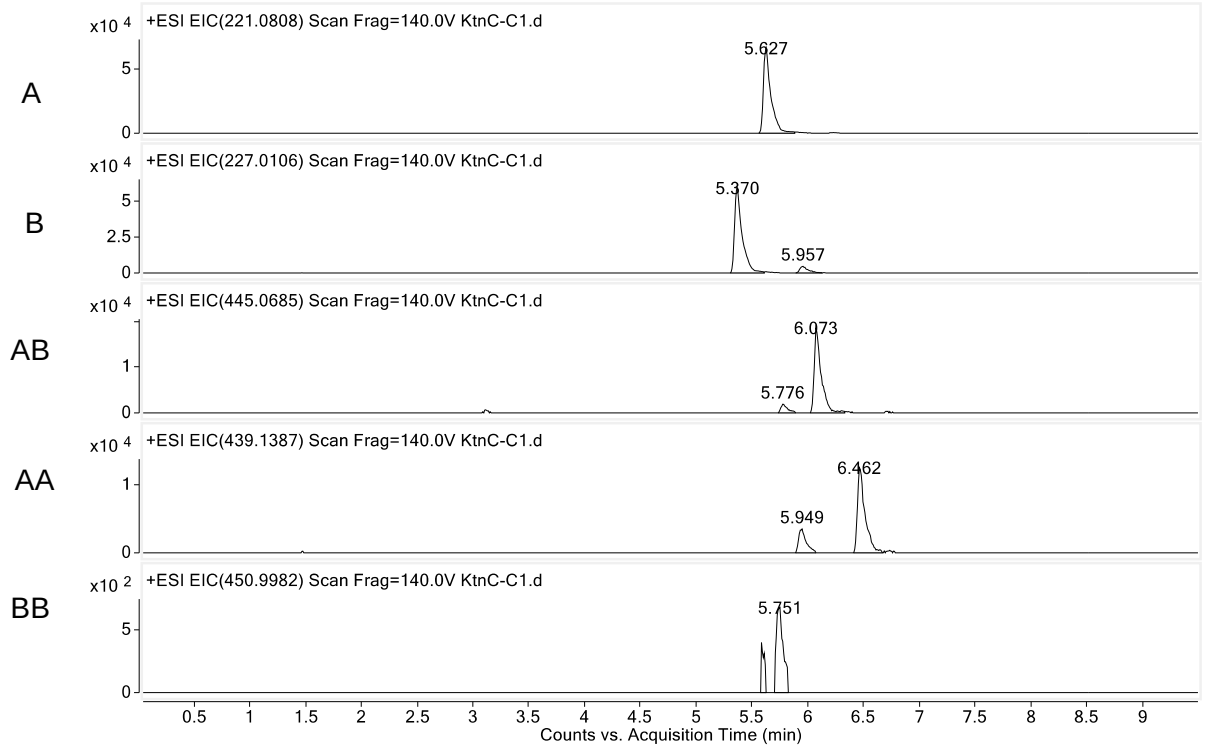

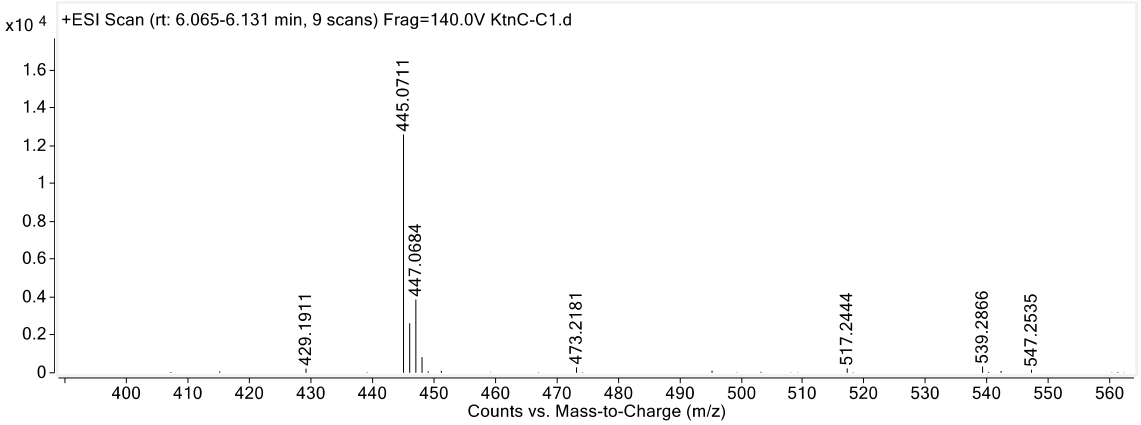

No enzyme

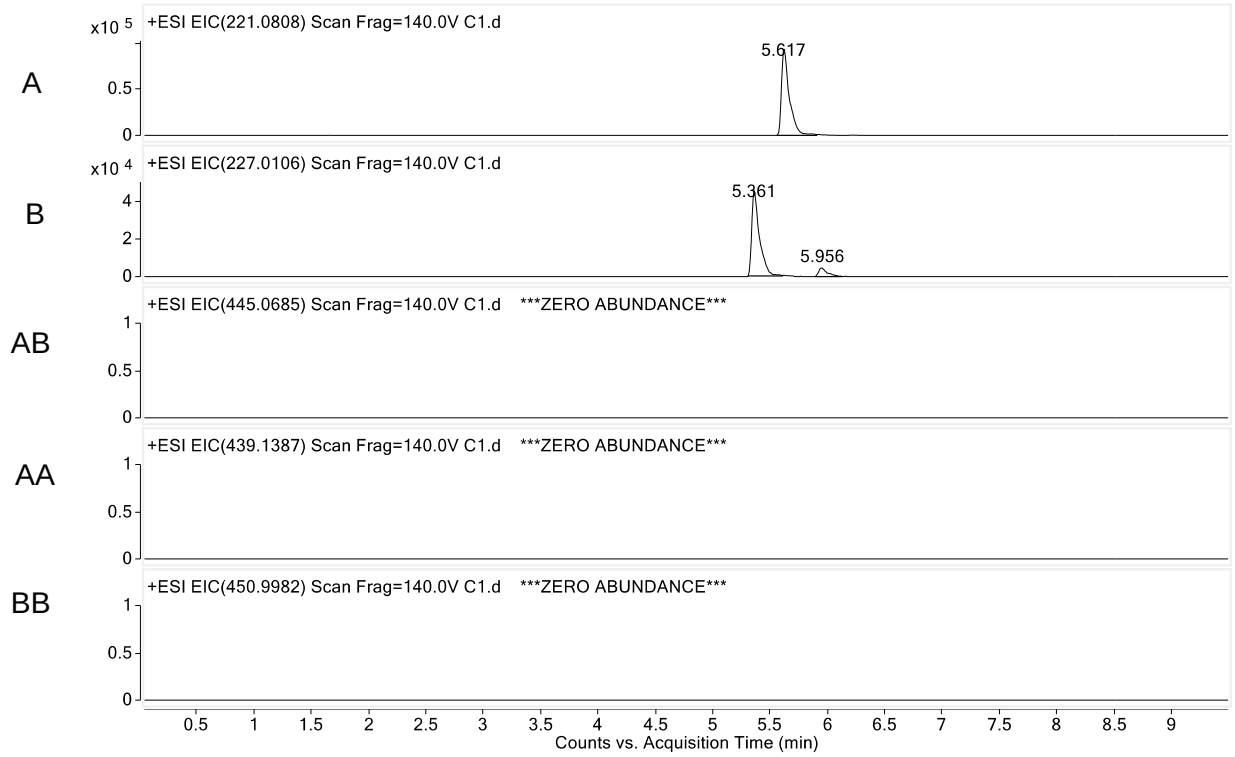
A
+ESI EIC(221.0808) Scan Frag=140.0V C1.d
x10 5
5.617
B
+ESI EIC(227.0106) Scan Frag=140.0V C1.d
x10 4
5.361
5.956
AB
+ESI EIC(445.0685) Scan Frag=140.0V C1.d ***ZERO ABUNDANCE***
AA
+ESI EIC(439.1387) Scan Frag=140.0V C1.d ***ZERO ABUNDANCE***
BB
+ESI EIC(450.9982) Scan Frag=140.0V C1.d ***ZERO ABUNDANCE***
Counts vs. Acquisition Time (min)

Supplemental Figure S3.83. Oxidative cross-coupling of **22** and **19** by KtnC (**Figure 3.3**).

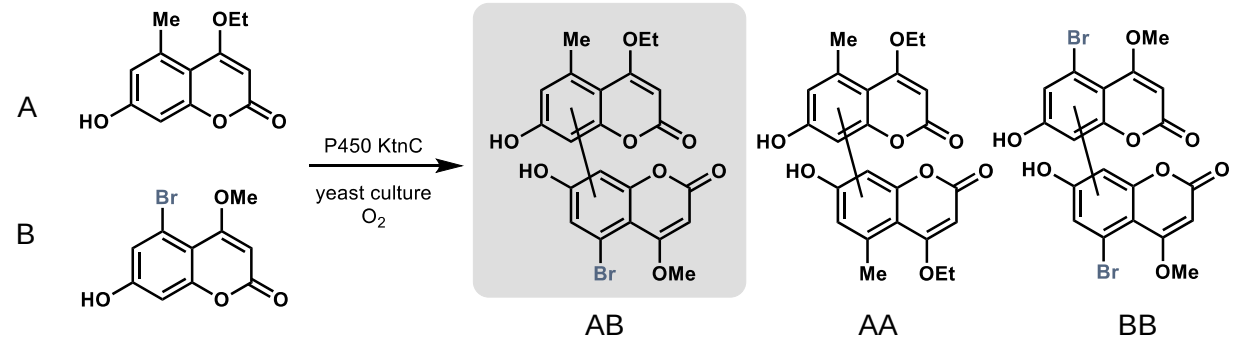

KtnC

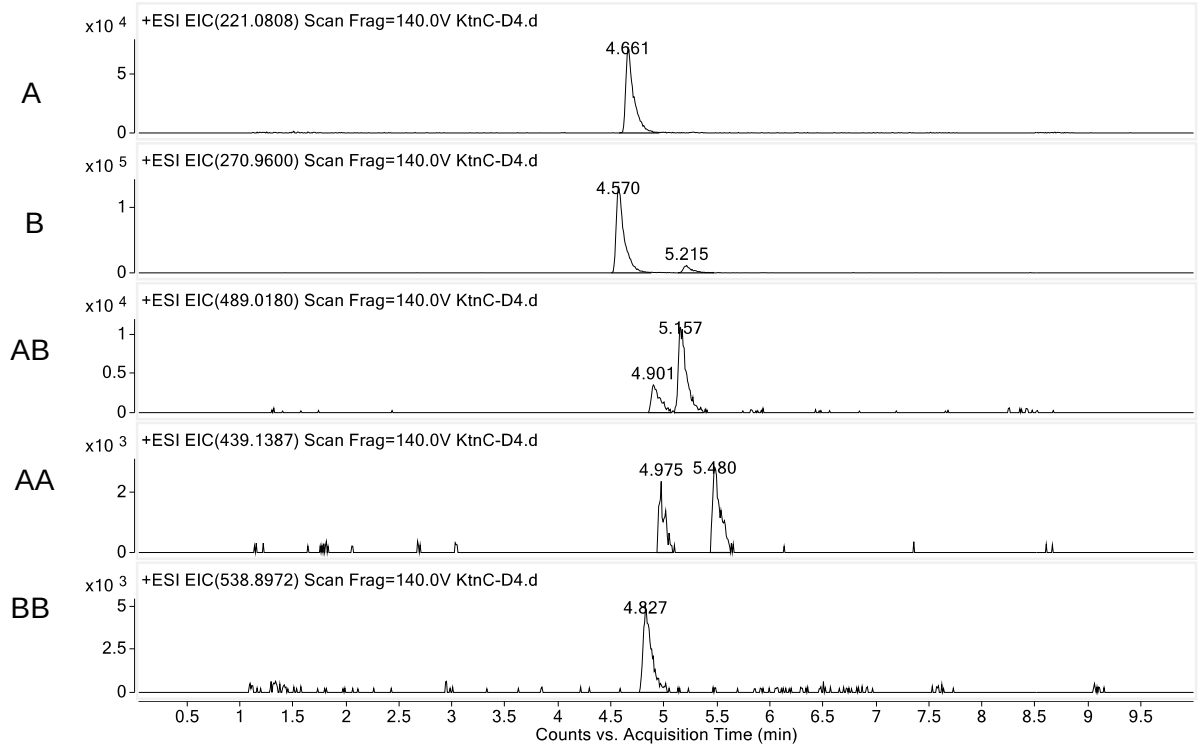

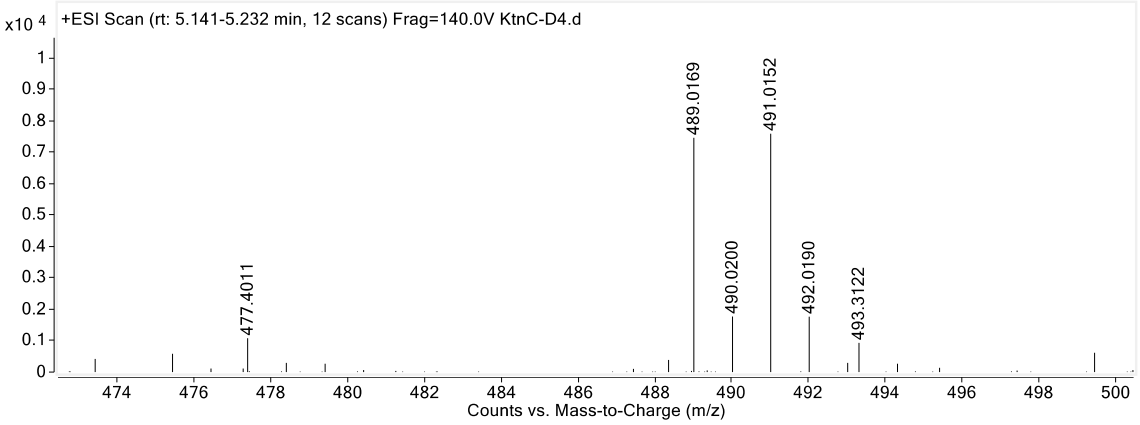

No enzyme

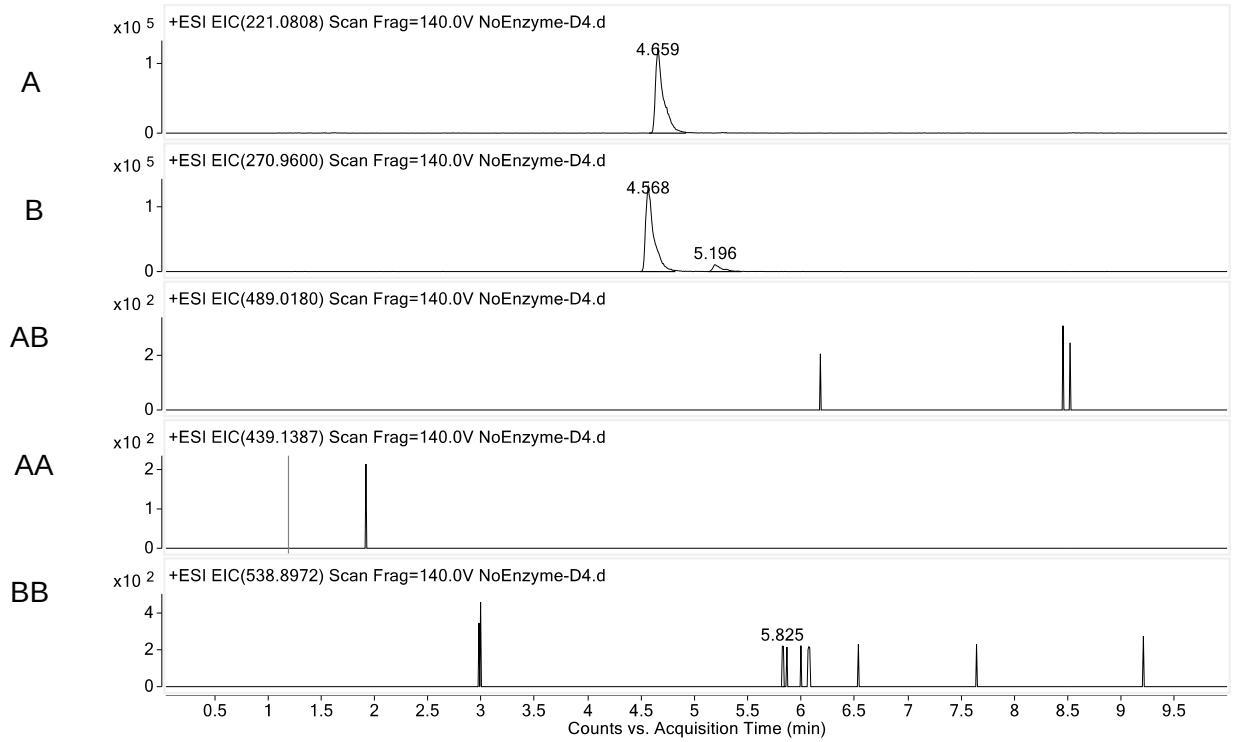
A
+ESI EIC(221.0808) Scan Frag=140.0V NoEnzyme-D4.d
x10 5
4.659
B
+ESI EIC(270.9600) Scan Frag=140.0V NoEnzyme-D4.d
x10 5
4.568
5.196
AB
+ESI EIC(489.0180) Scan Frag=140.0V NoEnzyme-D4.d
x10 2
AA
+ESI EIC(439.1387) Scan Frag=140.0V NoEnzyme-D4.d
x10 2
BB
+ESI EIC(538.8972) Scan Frag=140.0V NoEnzyme-D4.d
x10 2
5.825
0.5 1 1.5 2 2.5 3 3.5 4 4.5 5 5.5 6 6.5 7 7.5 8 8.5 9 9.5
Counts vs. Acquisition Time (min)

Supplemental Figure S3.84. Oxidative cross-coupling of **14** and **21** by KtnC (**Figure 3.4**).

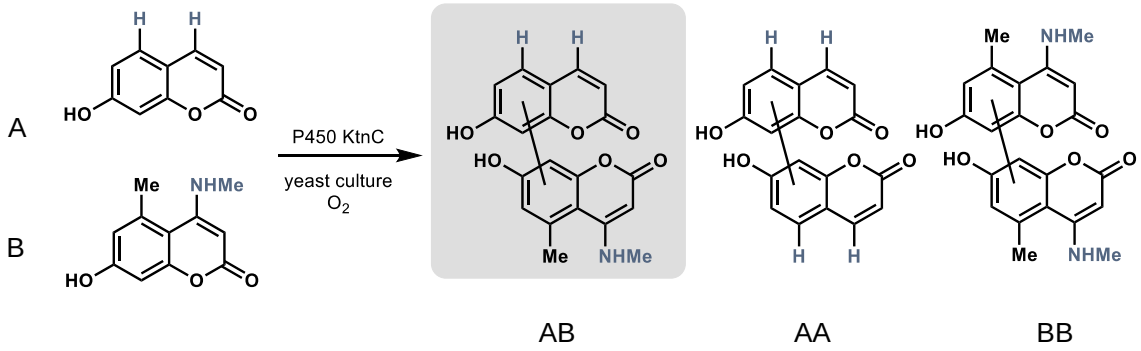

KtnC

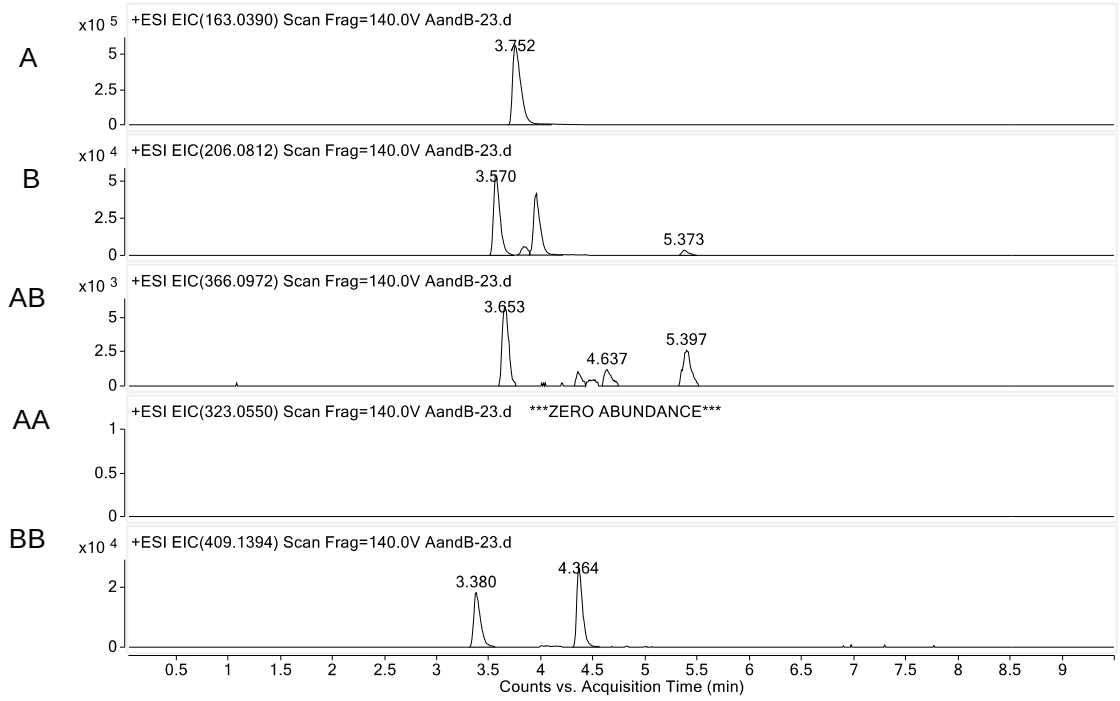

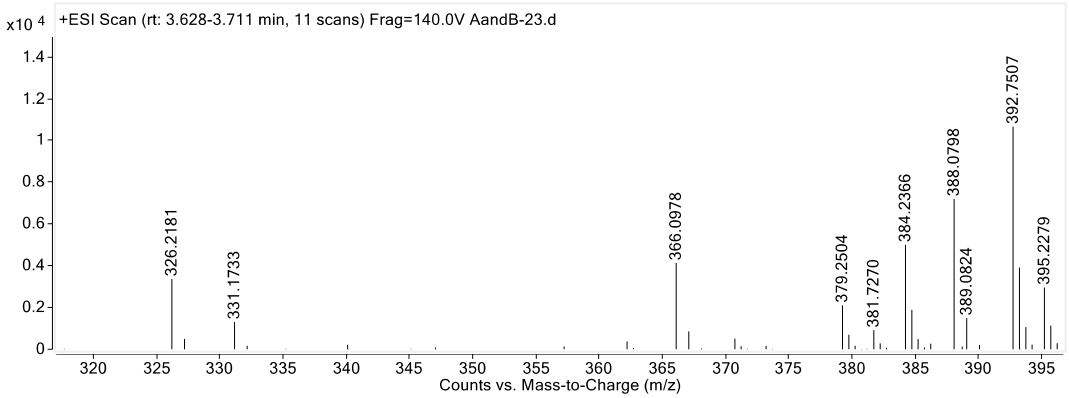

No enzyme

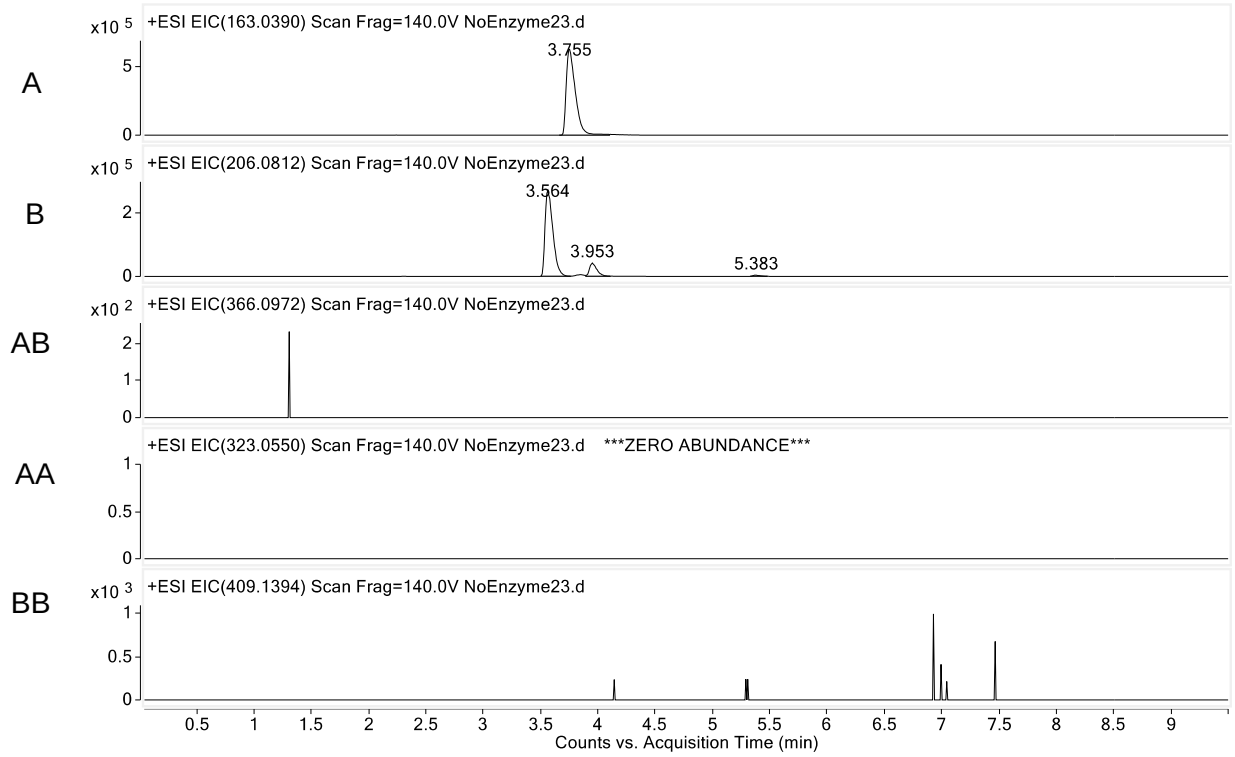
A
+ESI EIC(163.0390) Scan Frag=140.0V NoEnzyme23.d
x10 5
3.755
B
+ESI EIC(206.0812) Scan Frag=140.0V NoEnzyme23.d
x10 5
3.564
3.953
5.383
AB
+ESI EIC(366.0972) Scan Frag=140.0V NoEnzyme23.d
x10 2
AA
+ESI EIC(323.0550) Scan Frag=140.0V NoEnzyme23.d ***ZERO ABUNDANCE***
BB
+ESI EIC(409.1394) Scan Frag=140.0V NoEnzyme23.d
x10 3
Counts vs. Acquisition Time (min)

Supplemental Figure S3.85. Oxidative cross-coupling of **14** and **22** by KtnC (**Figure 3.4**).

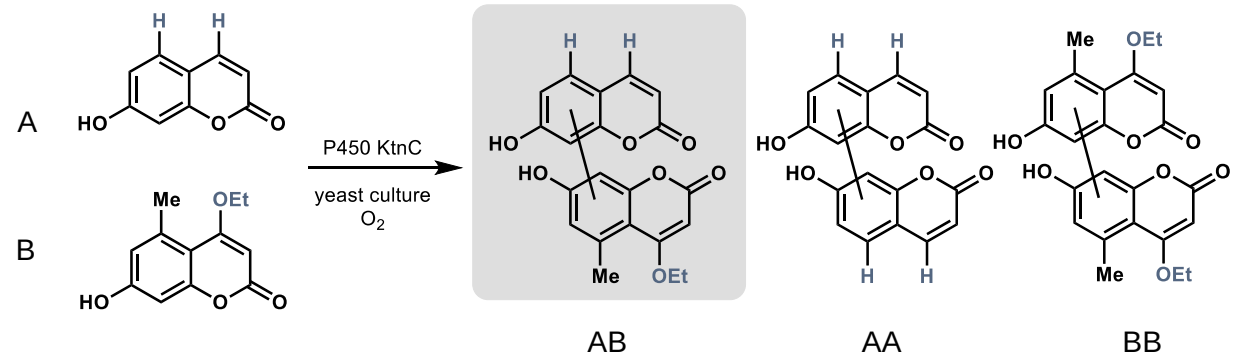

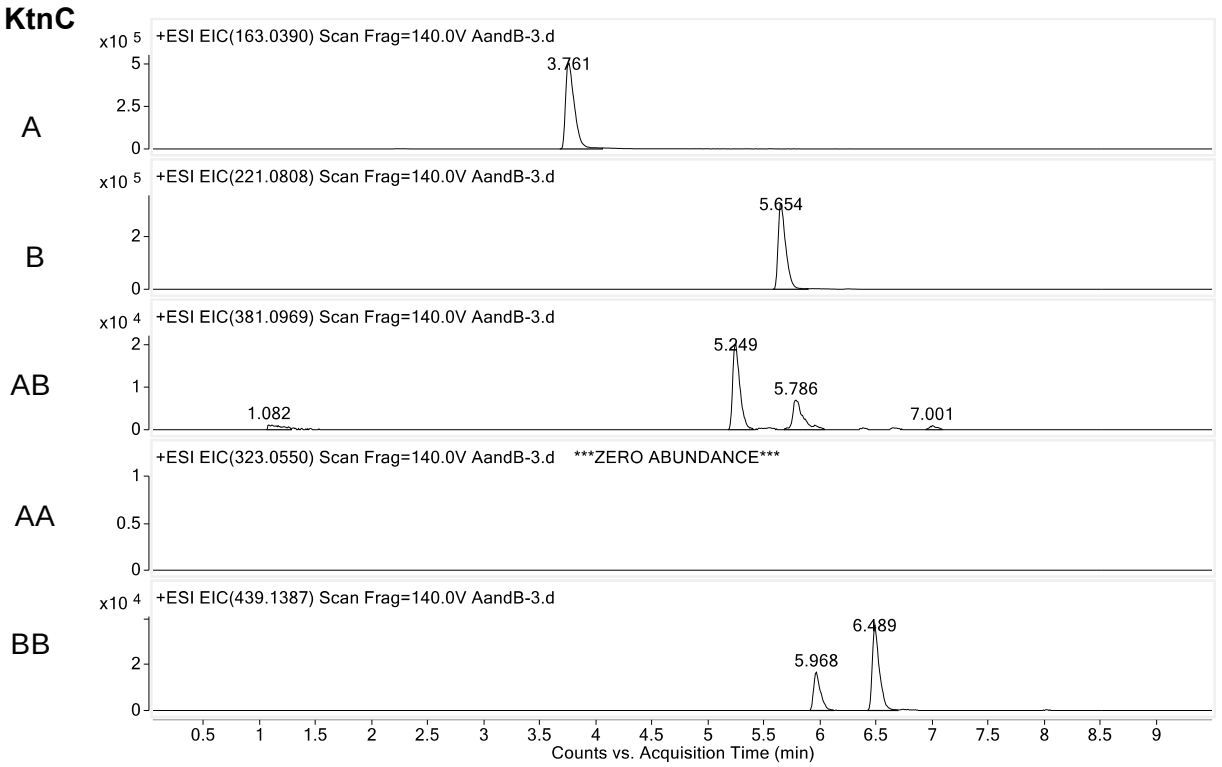

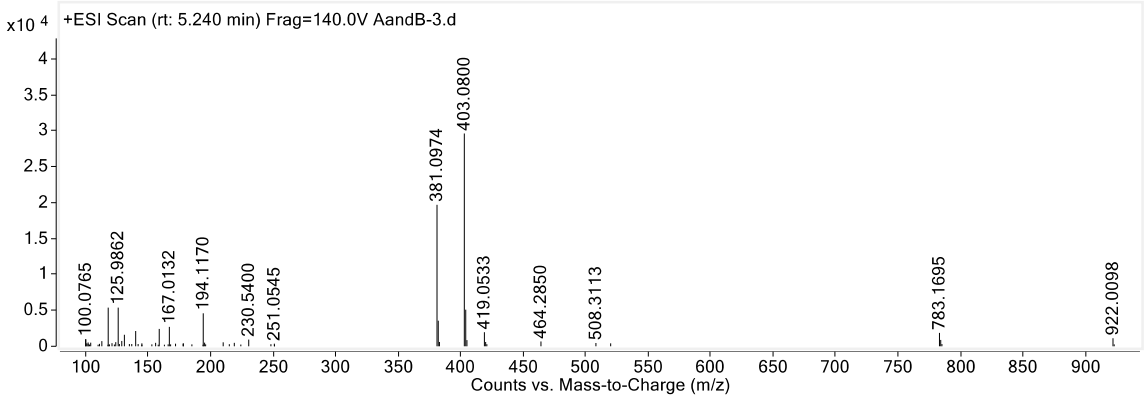

No enzyme

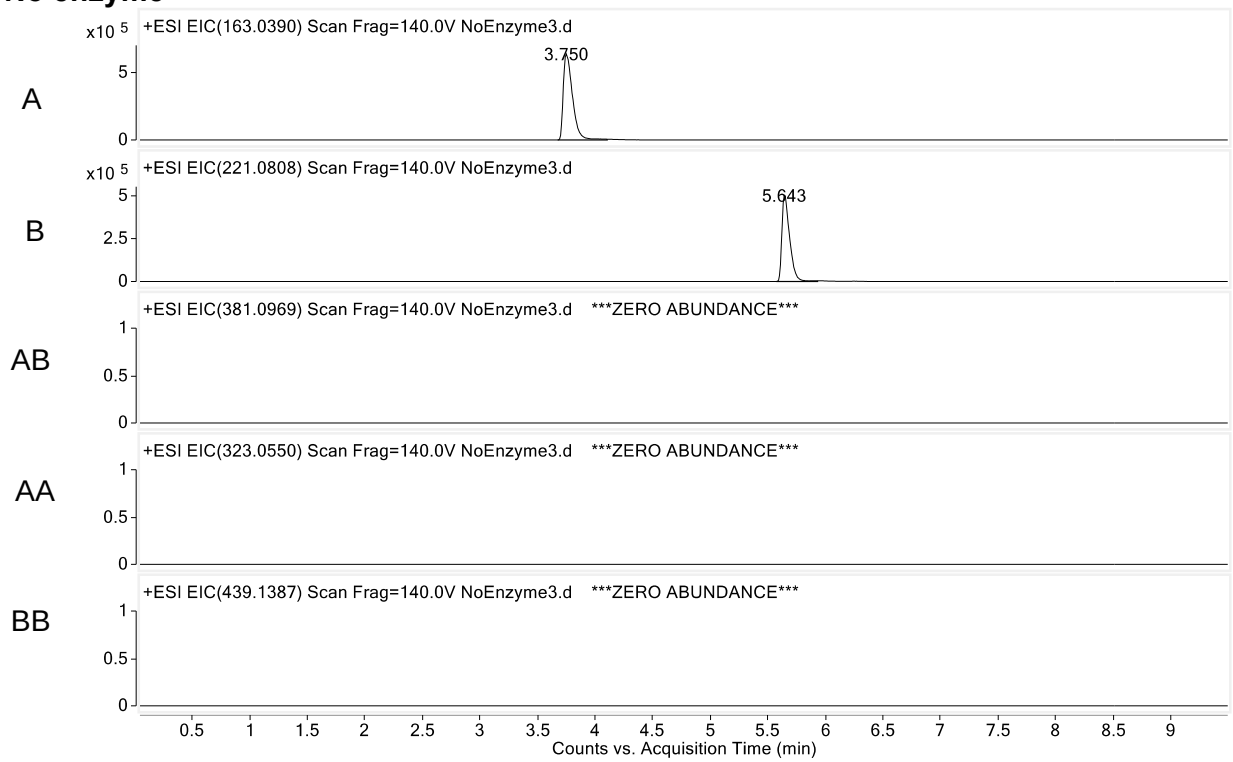
A
+ESI EIC(163.0390) Scan Frag=140.0V NoEnzyme3.d
x10 5
3.750
B
+ESI EIC(221.0808) Scan Frag=140.0V NoEnzyme3.d
x10 5
5.643
AB
+ESI EIC(381.0969) Scan Frag=140.0V NoEnzyme3.d ***ZERO ABUNDANCE***
AA
+ESI EIC(323.0550) Scan Frag=140.0V NoEnzyme3.d ***ZERO ABUNDANCE***
BB
+ESI EIC(439.1387) Scan Frag=140.0V NoEnzyme3.d ***ZERO ABUNDANCE***
Counts vs. Acquisition Time (min)

Supplemental Figure S3.86. Oxidative cross-coupling of **14** and **12** by KtnC (**Figure 3.4**).

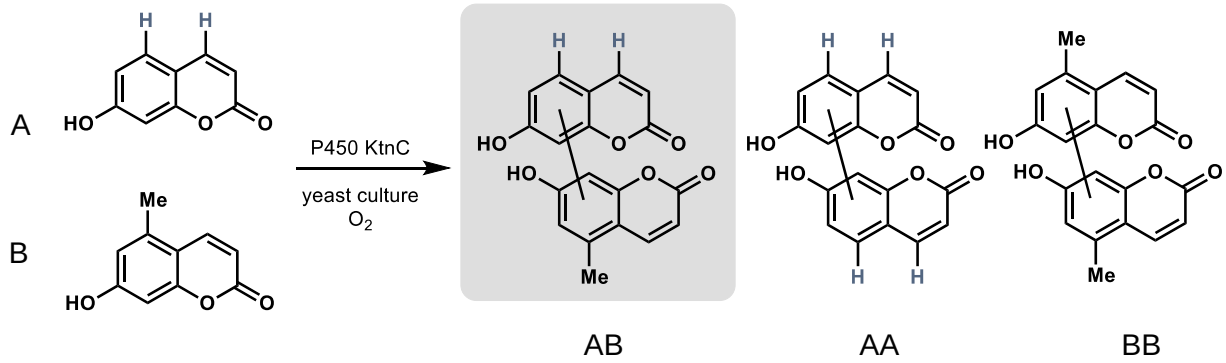

KtnC

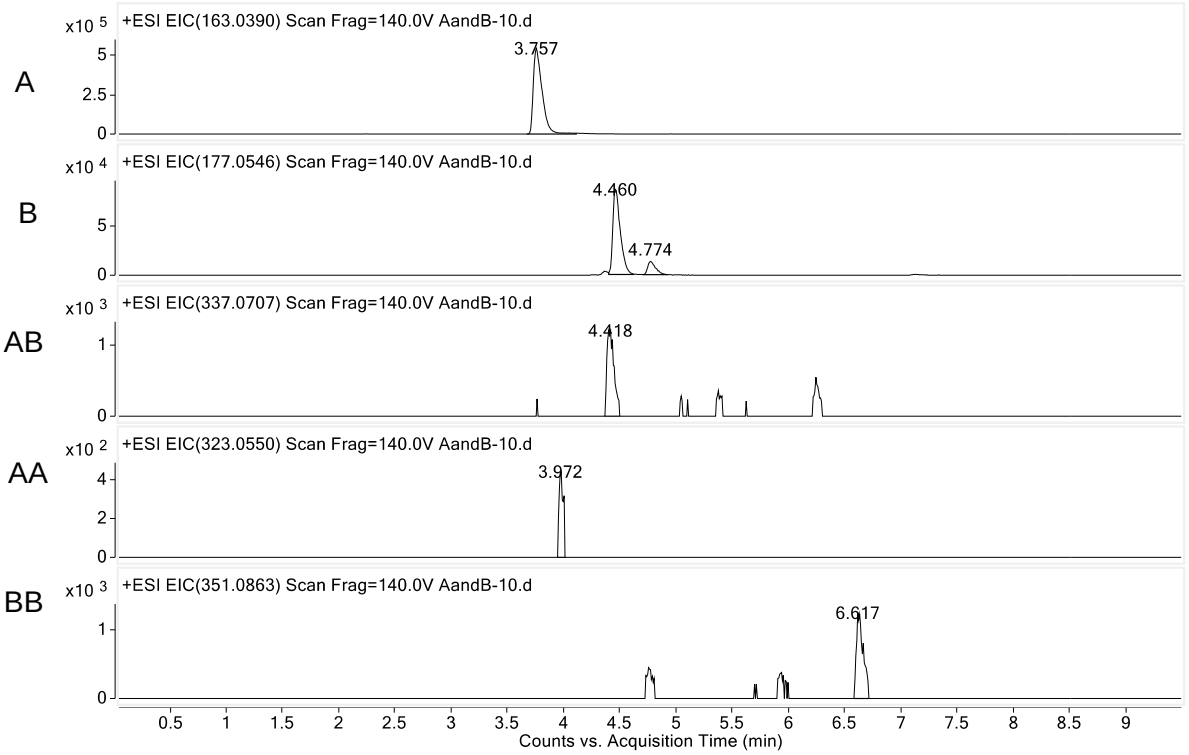

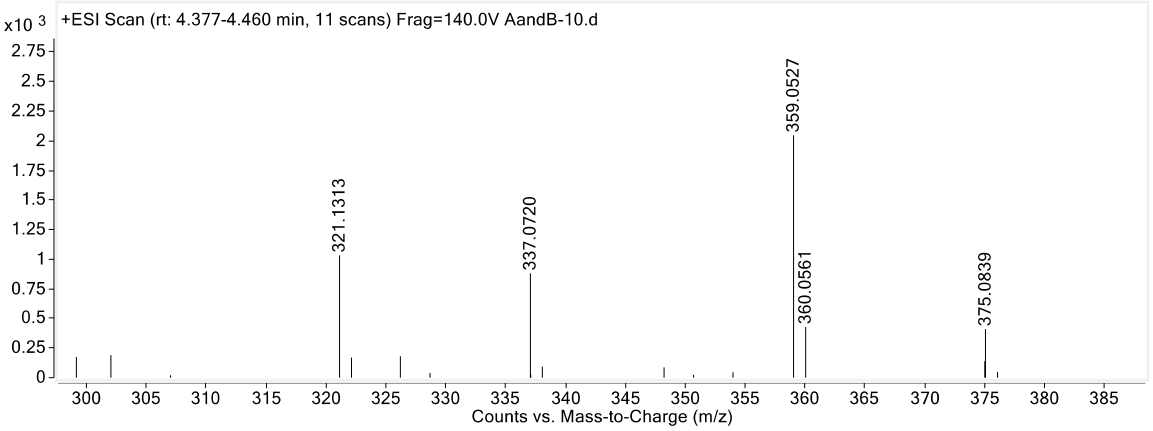

No enzyme

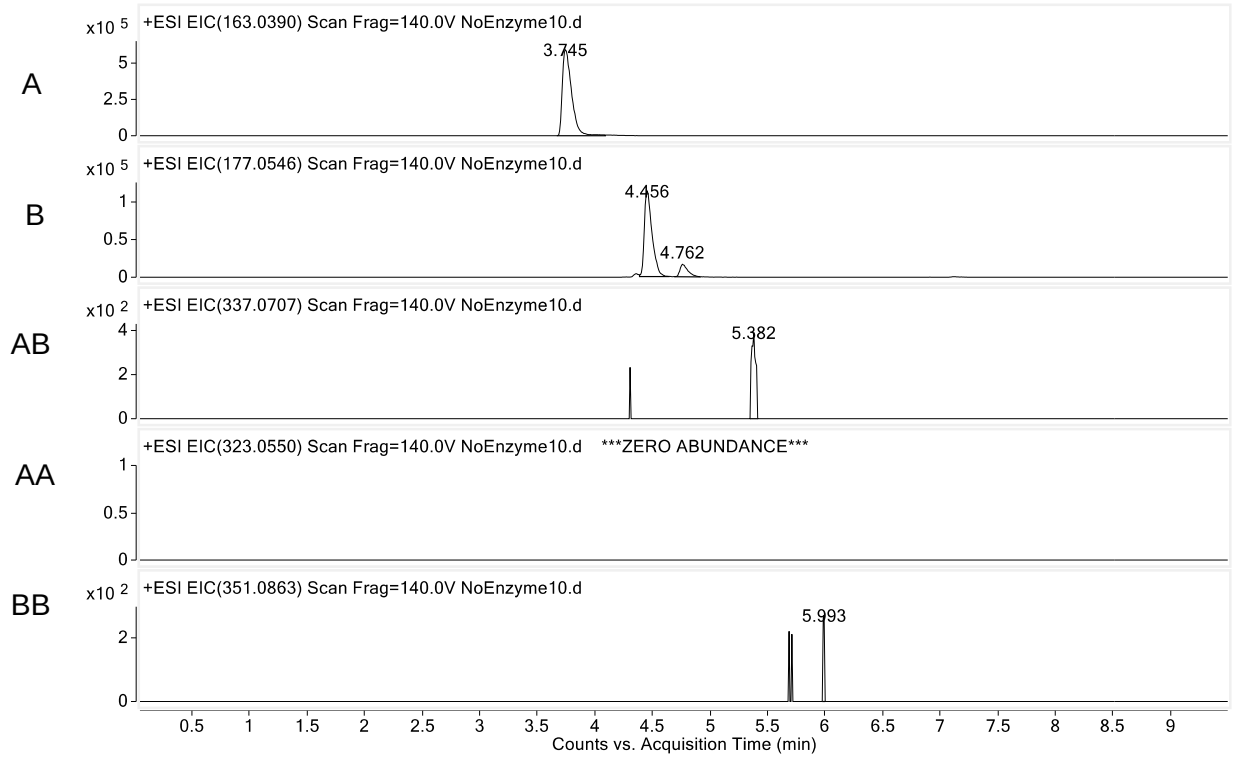
A
+ESI EIC(163.0390) Scan Frag=140.0V NoEnzyme10.d
x10 5
3.745
B
+ESI EIC(177.0546) Scan Frag=140.0V NoEnzyme10.d
x10 5
4.456
4.762
AB
+ESI EIC(337.0707) Scan Frag=140.0V NoEnzyme10.d
x10 2
5.382
AA
+ESI EIC(323.0550) Scan Frag=140.0V NoEnzyme10.d ***ZERO ABUNDANCE***
BB
+ESI EIC(351.0863) Scan Frag=140.0V NoEnzyme10.d
x10 2
5.993
Counts vs. Acquisition Time (min)

Supplemental Figure S3.87. Oxidative cross-coupling of **14** and **25** by KtnC (**Figure 3.4**).

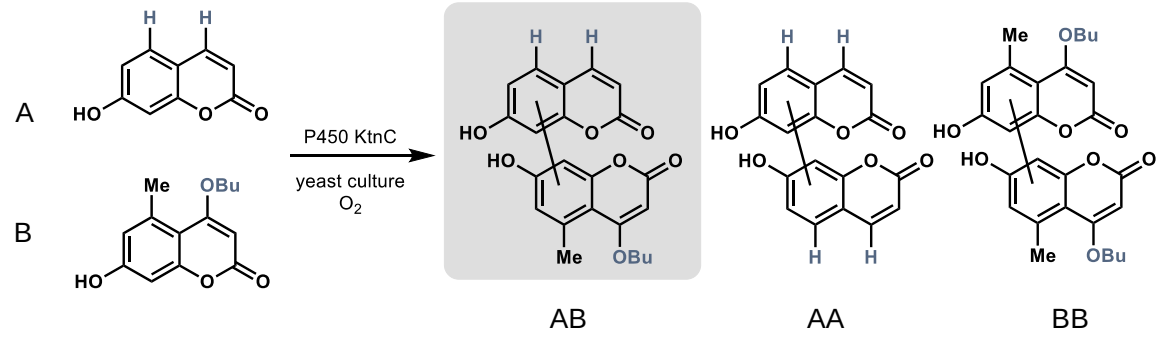

KtnC

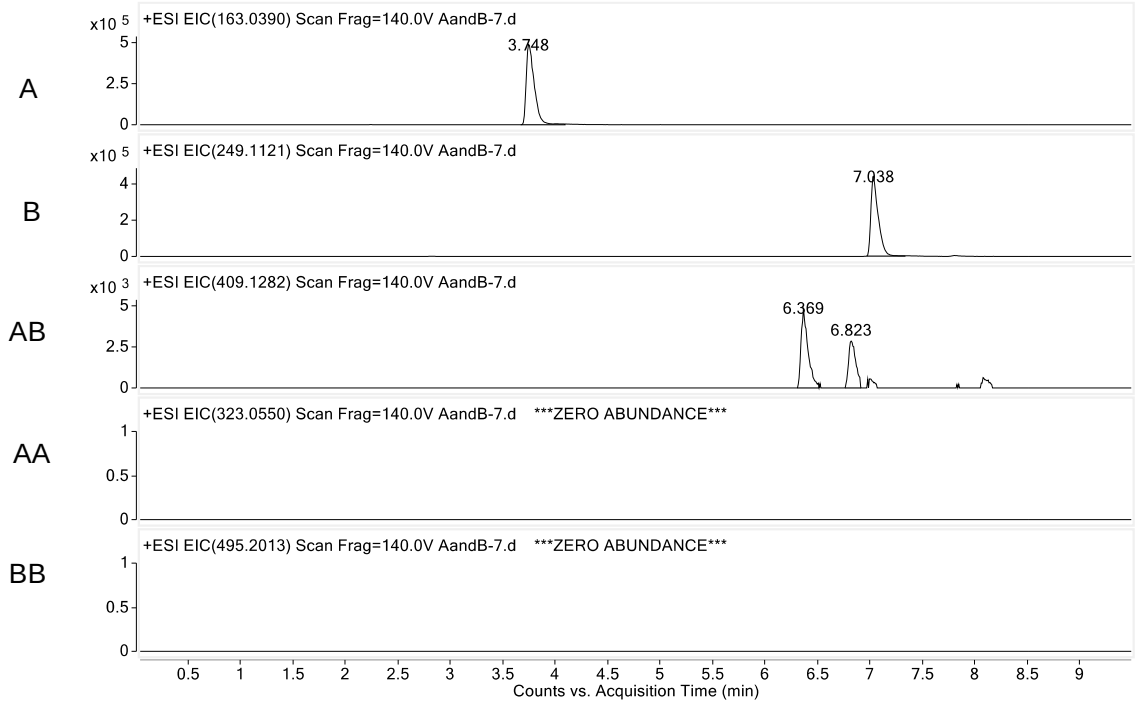

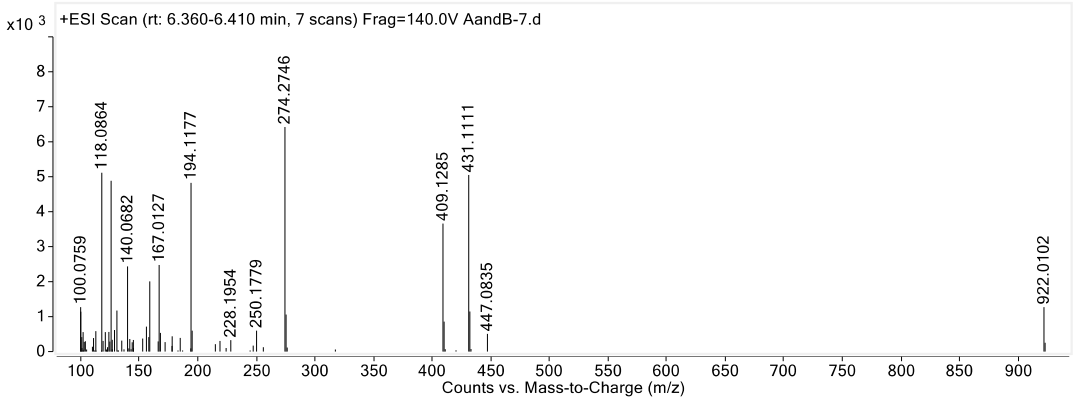

No enzyme

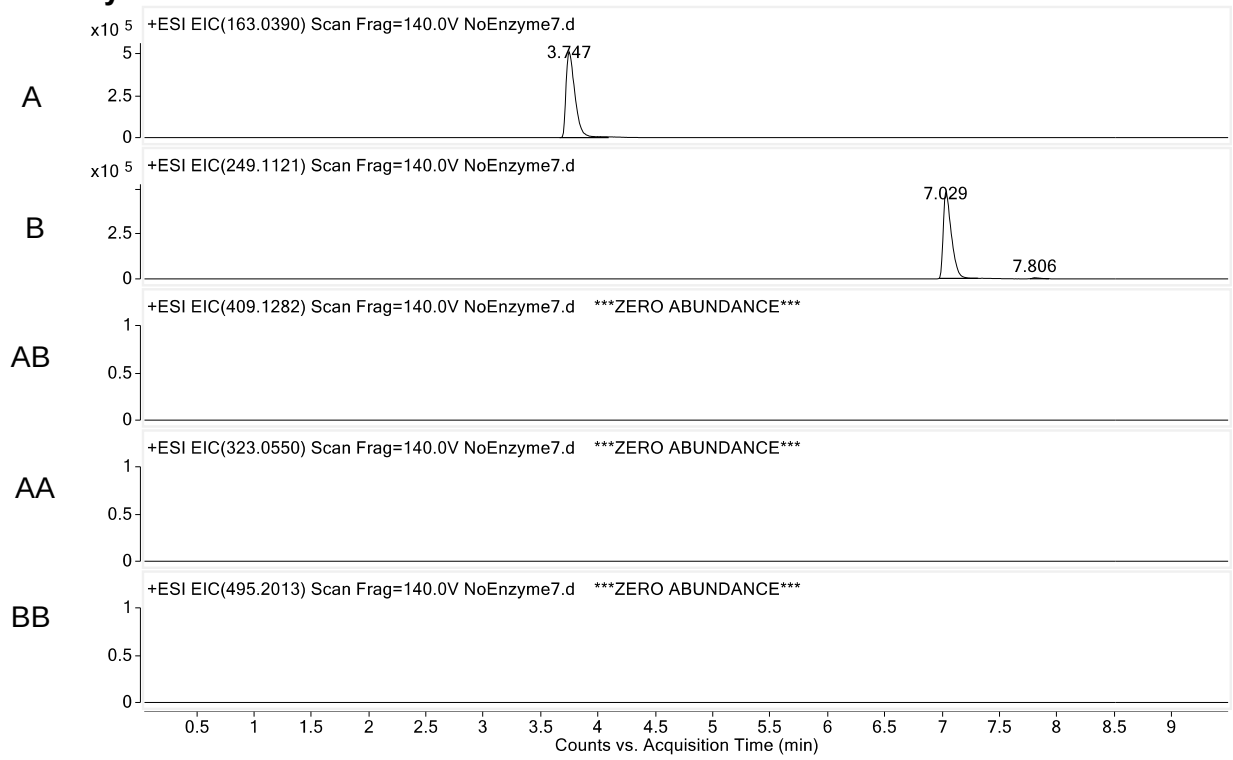
A
+ESI EIC(163.0390) Scan Frag=140.0V NoEnzyme7.d
x10 5
3.747
B
+ESI EIC(249.1121) Scan Frag=140.0V NoEnzyme7.d
7.029
7.806
AB
+ESI EIC(409.1282) Scan Frag=140.0V NoEnzyme7.d ***ZERO ABUNDANCE***
AA
+ESI EIC(323.0550) Scan Frag=140.0V NoEnzyme7.d ***ZERO ABUNDANCE***
BB
+ESI EIC(495.2013) Scan Frag=140.0V NoEnzyme7.d ***ZERO ABUNDANCE***
Counts vs. Acquisition Time (min)

Supplemental Figure S3.88. Oxidative cross-coupling of **14** and **18** by KtnC (**Figure 3.4**).

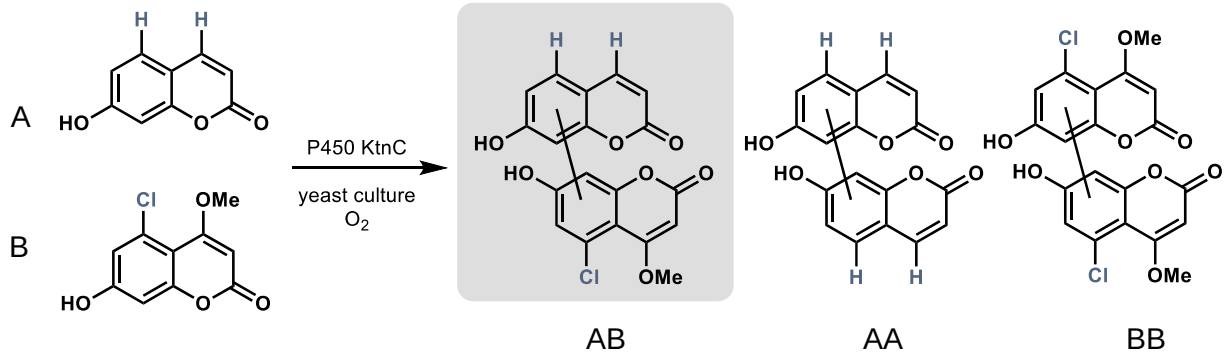

KtnC

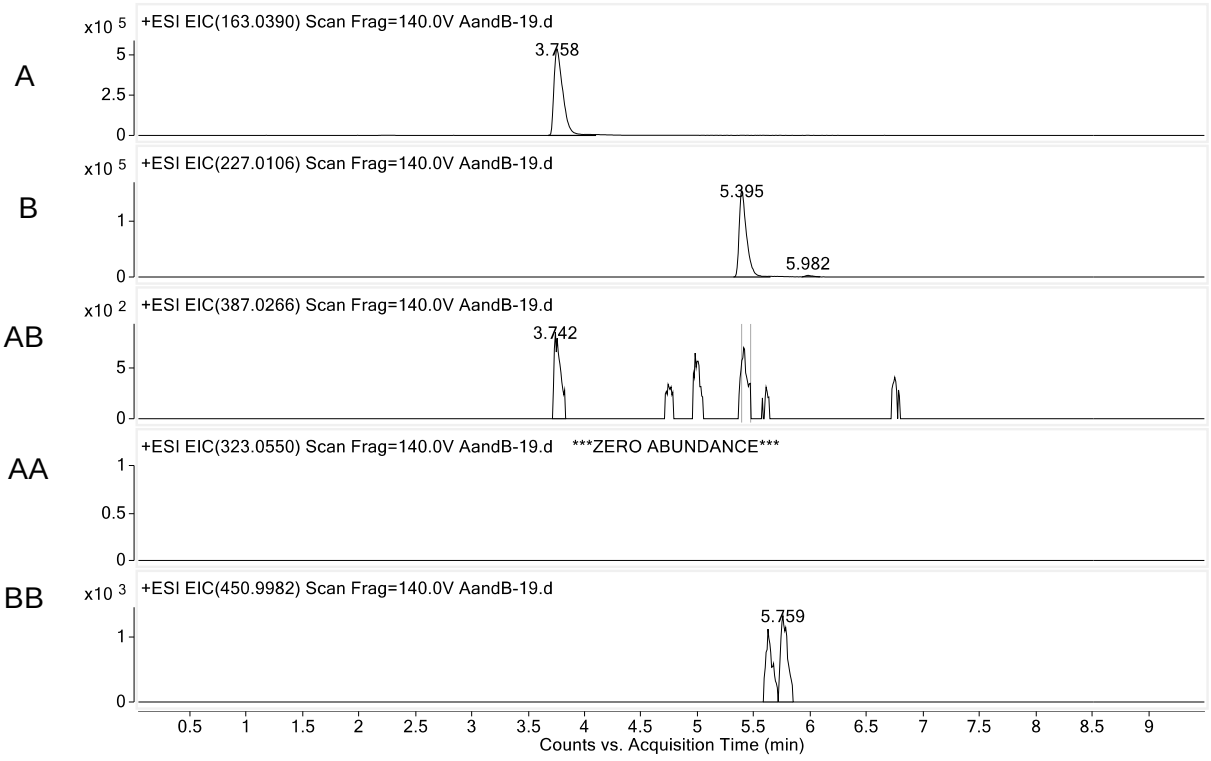

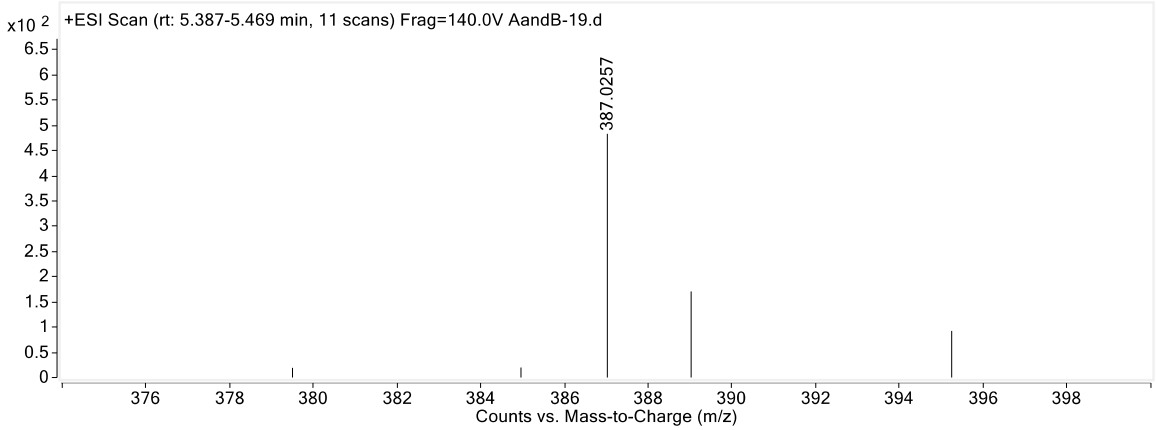

No enzyme

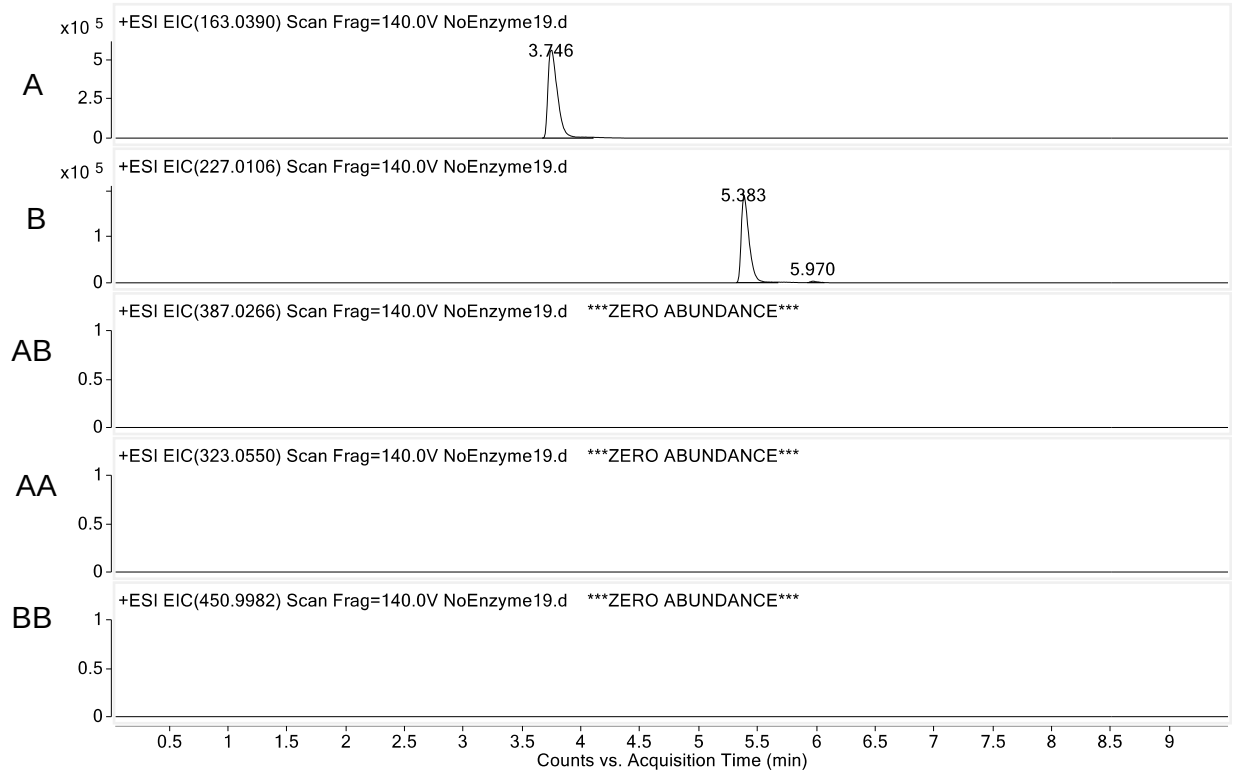
A
+ESI EIC(163.0390) Scan Frag=140.0V NoEnzyme19.d
x10 5
3.746
B
+ESI EIC(227.0106) Scan Frag=140.0V NoEnzyme19.d
x10 5
5.383
5.970
AB
+ESI EIC(387.0266) Scan Frag=140.0V NoEnzyme19.d ***ZERO ABUNDANCE***
AA
+ESI EIC(323.0550) Scan Frag=140.0V NoEnzyme19.d ***ZERO ABUNDANCE***
BB
+ESI EIC(450.9982) Scan Frag=140.0V NoEnzyme19.d ***ZERO ABUNDANCE***
Counts vs. Acquisition Time (min)

Supplemental Figure S3.89. Oxidative cross-coupling of **15** and **29** by KtnC (**Figure 3.5**).

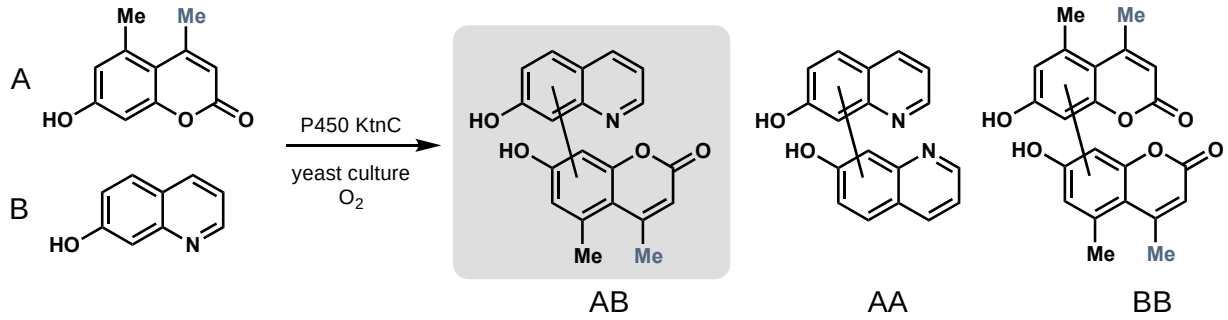

KtnC

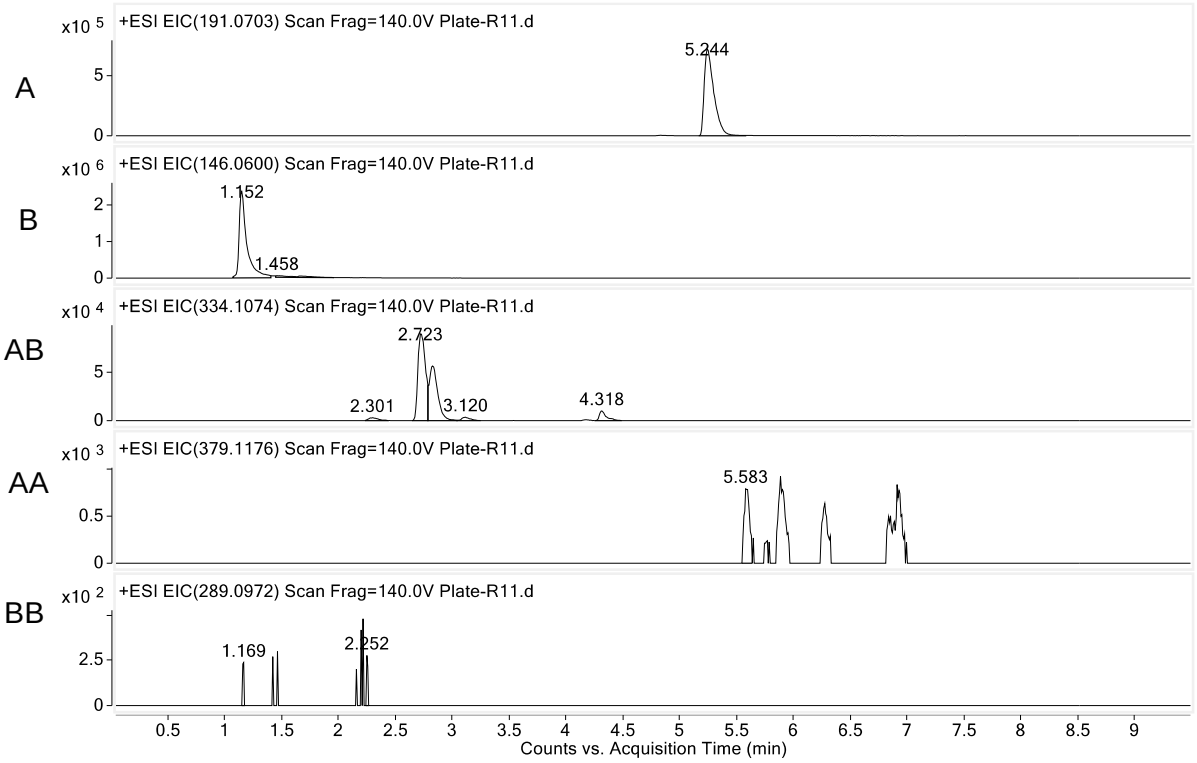

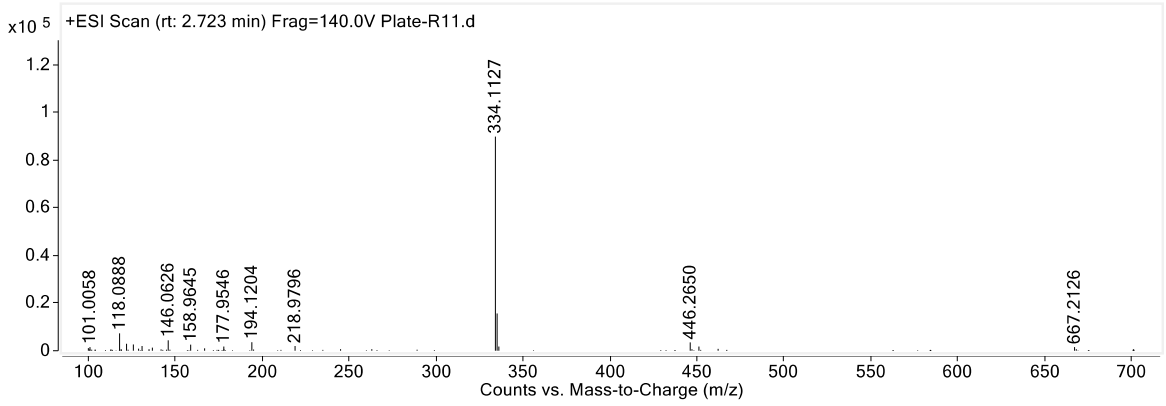

No enzyme

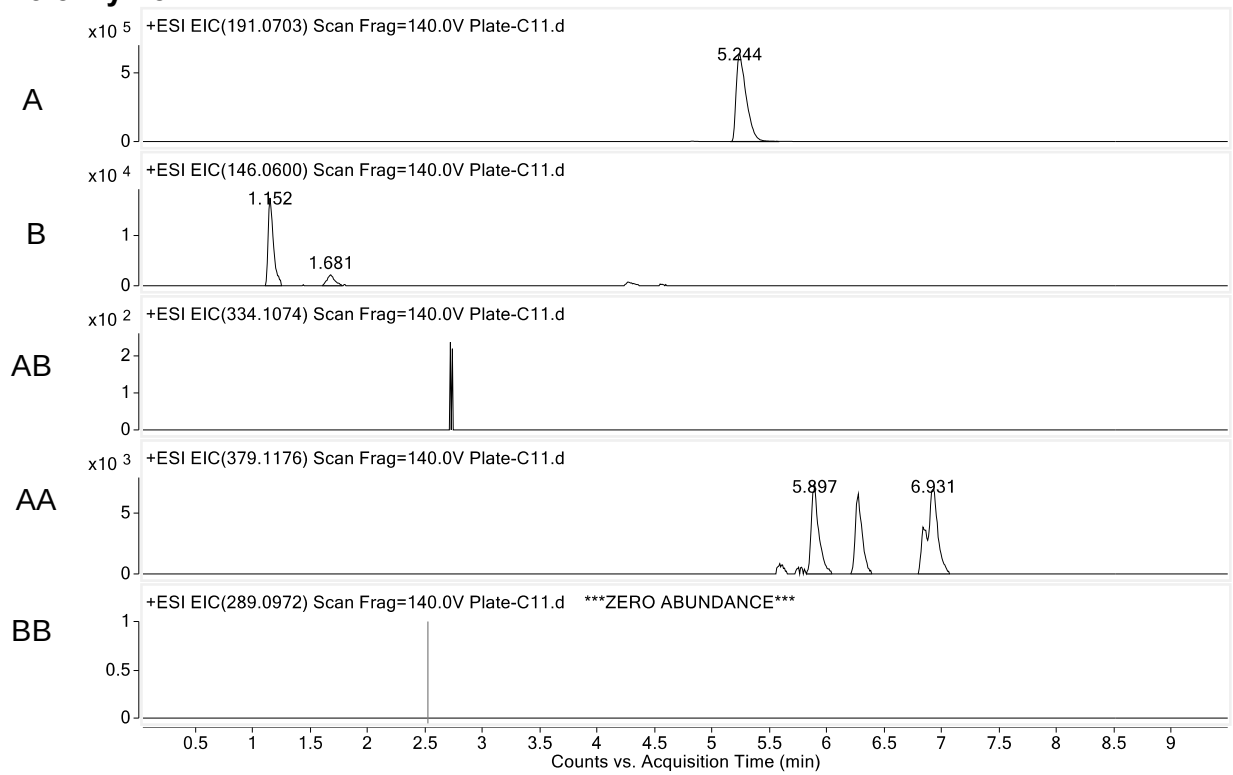
A
x10 5
+ESI EIC(191.0703) Scan Frag=140.0V Plate-C11.d
5.244
B
x10 4
+ESI EIC(146.0600) Scan Frag=140.0V Plate-C11.d
1.152
1.681
AB
x10 2
+ESI EIC(334.1074) Scan Frag=140.0V Plate-C11.d
AA
x10 3
+ESI EIC(379.1176) Scan Frag=140.0V Plate-C11.d
5.897
6.931
BB
+ESI EIC(289.0972) Scan Frag=140.0V Plate-C11.d ***ZERO ABUNDANCE***
0.5 1 1.5 2 2.5 3 3.5 4 4.5 5 5.5 6 6.5 7 7.5 8 8.5 9
Counts vs. Acquisition Time (min)

Supplemental Figure S3.90. Oxidative cross-coupling of **14** and **29** by KtnC (**Figure 3.5**).

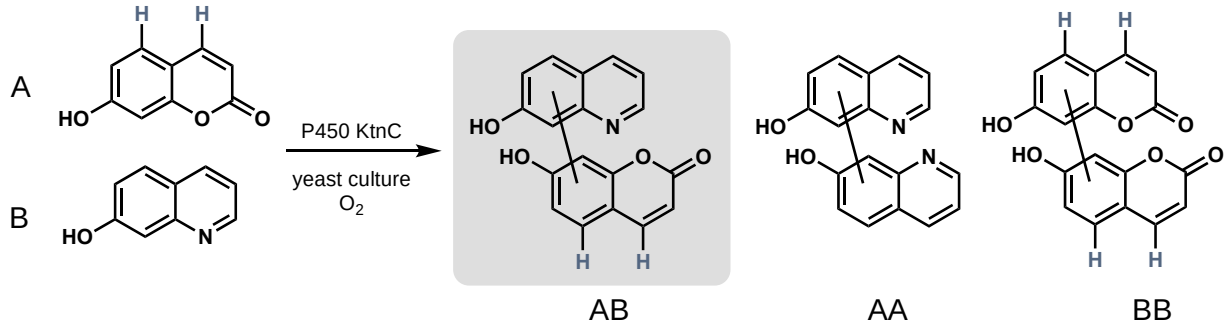

KtnC

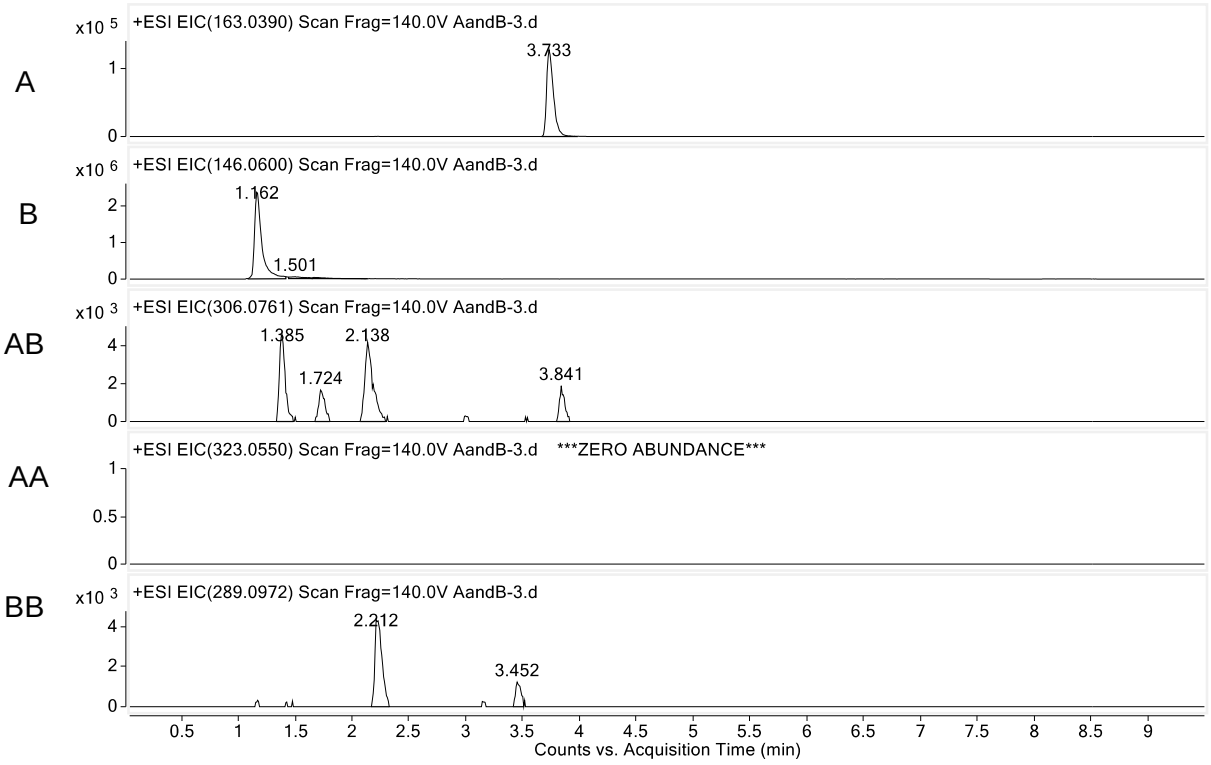

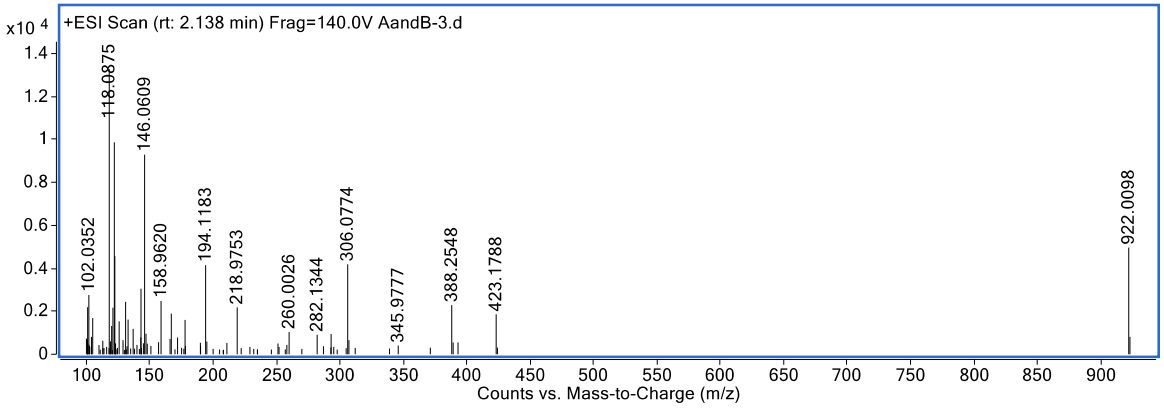

No enzyme

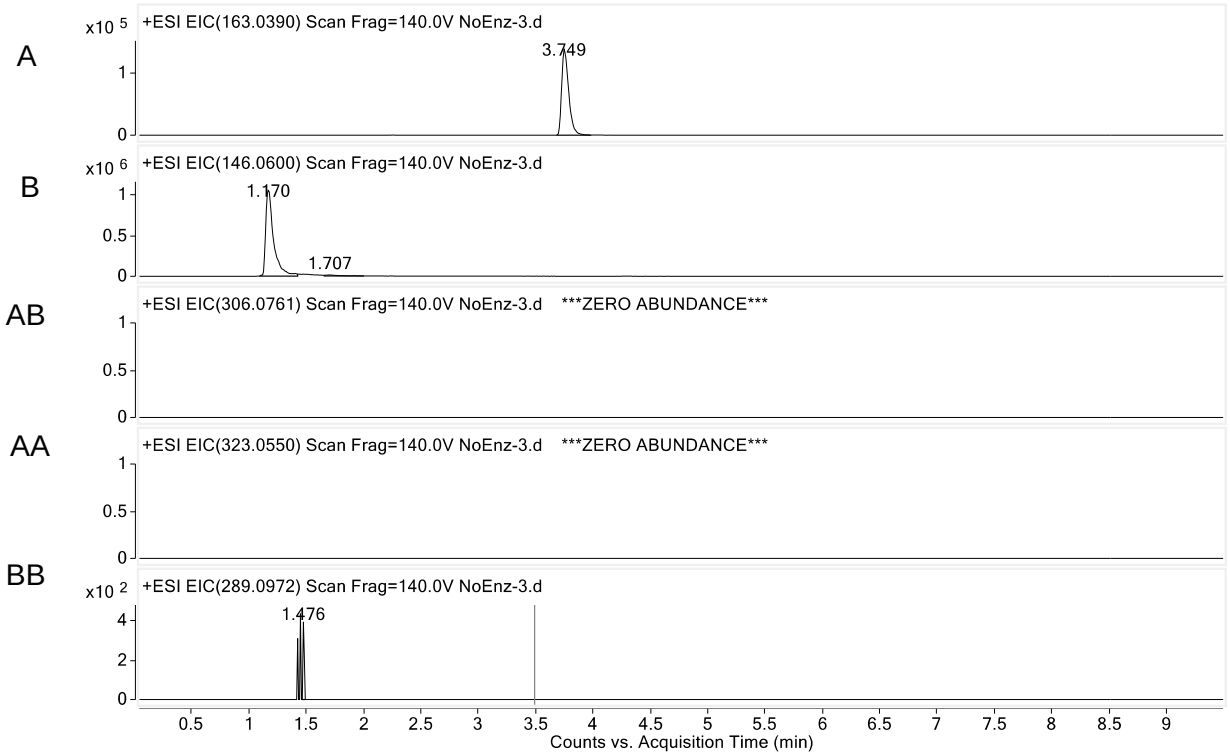
A
x10 5
+ESI EIC(163.0390) Scan Frag=140.0V NoEnz-3.d
3.749
B
x10 6
+ESI EIC(146.0600) Scan Frag=140.0V NoEnz-3.d
1.170
1.707
AB
+ESI EIC(306.0761) Scan Frag=140.0V NoEnz-3.d ***ZERO ABUNDANCE***
AA
+ESI EIC(323.0550) Scan Frag=140.0V NoEnz-3.d ***ZERO ABUNDANCE***
BB
x10 2
+ESI EIC(289.0972) Scan Frag=140.0V NoEnz-3.d
1.476
Counts vs. Acquisition Time (min)

Supplemental Figure S3.91. Oxidative cross-coupling of **13** and **29** by KtnC (**Figure 3.5**).

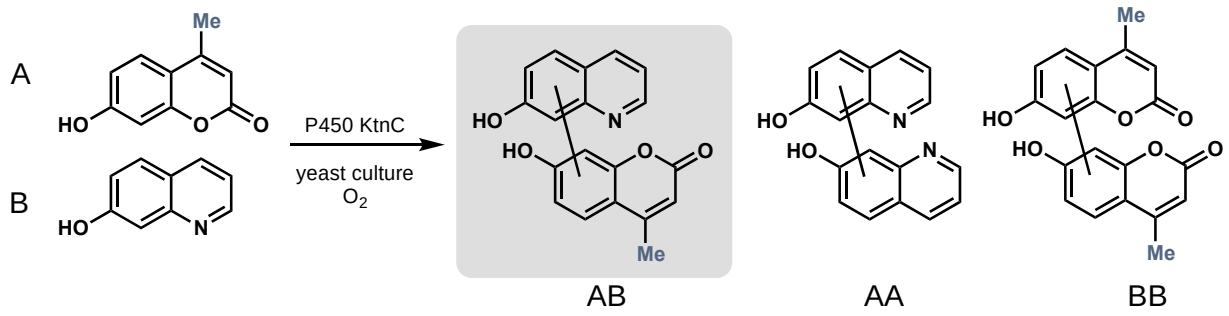

KtnC

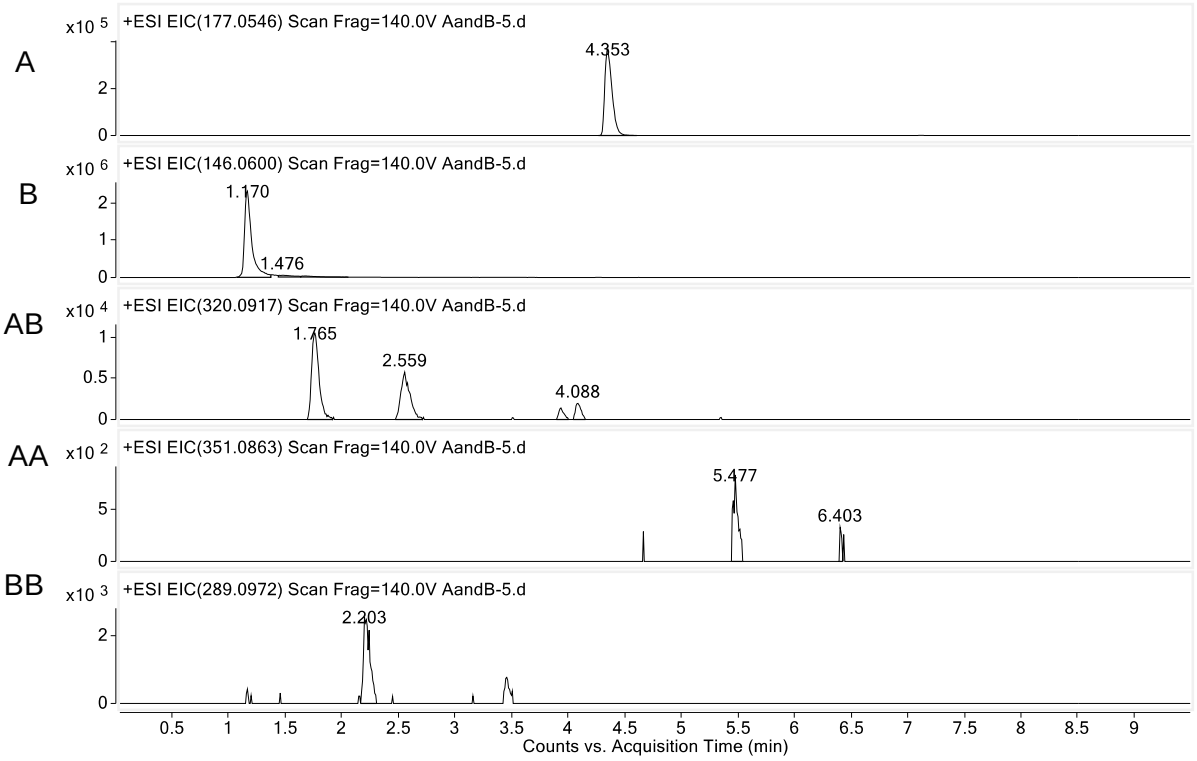

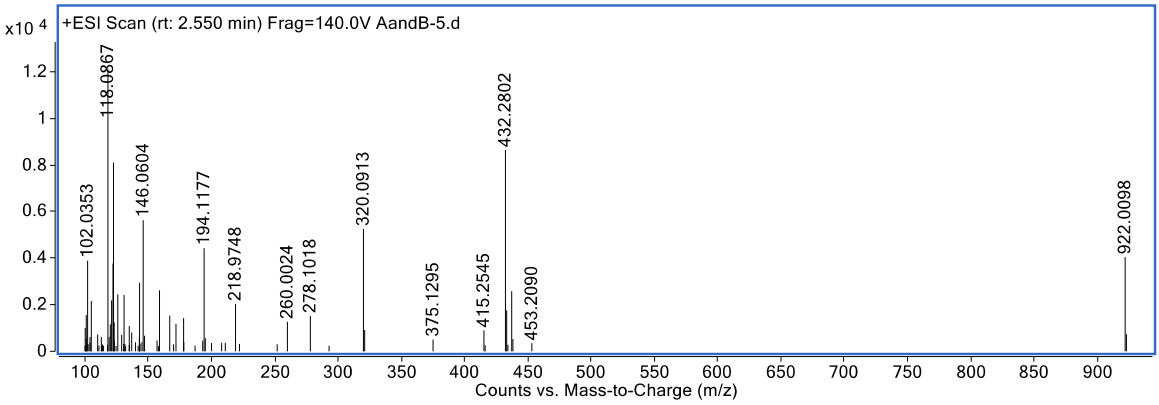

No enzyme

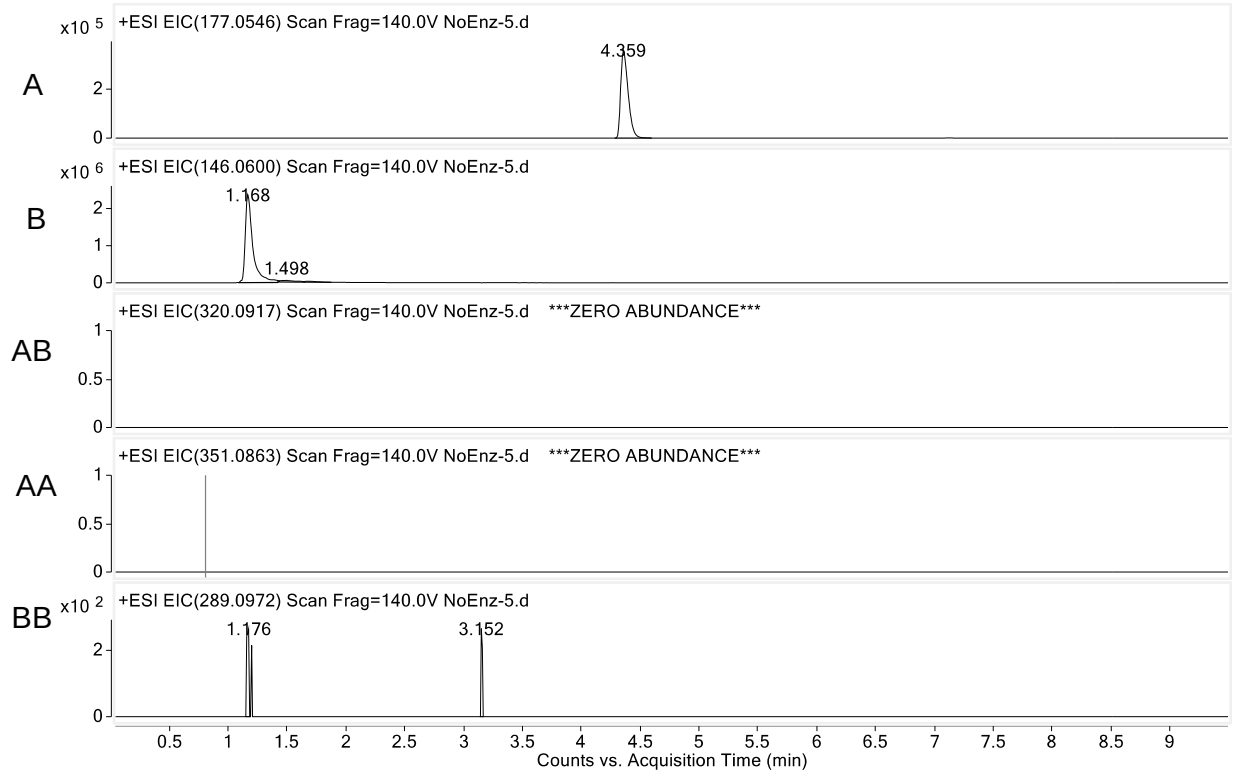
A
+ESI EIC(177.0546) Scan Frag=140.0V NoEnz-5.d
x10 5
4.359
B
+ESI EIC(146.0600) Scan Frag=140.0V NoEnz-5.d
x10 6
1.168
1.498
AB
+ESI EIC(320.0917) Scan Frag=140.0V NoEnz-5.d ***ZERO ABUNDANCE***
AA
+ESI EIC(351.0863) Scan Frag=140.0V NoEnz-5.d ***ZERO ABUNDANCE***
BB
+ESI EIC(289.0972) Scan Frag=140.0V NoEnz-5.d
x10 2
1.176
3.152
0.5 1 1.5 2 2.5 3 3.5 4 4.5 5 5.5 6 6.5 7 7.5 8 8.5 9
Counts vs. Acquisition Time (min)

Supplemental Figure S3.92. Oxidative cross-coupling of **21** and **29** by KtnC (**Figure 3.5**).

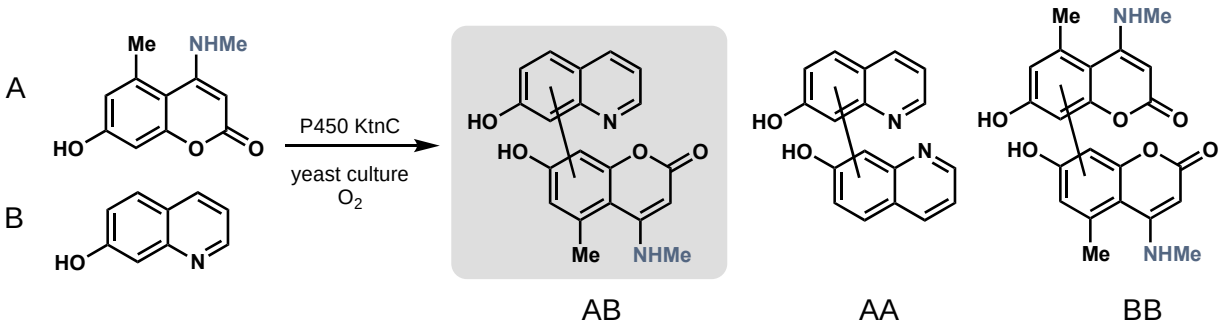

KtnC

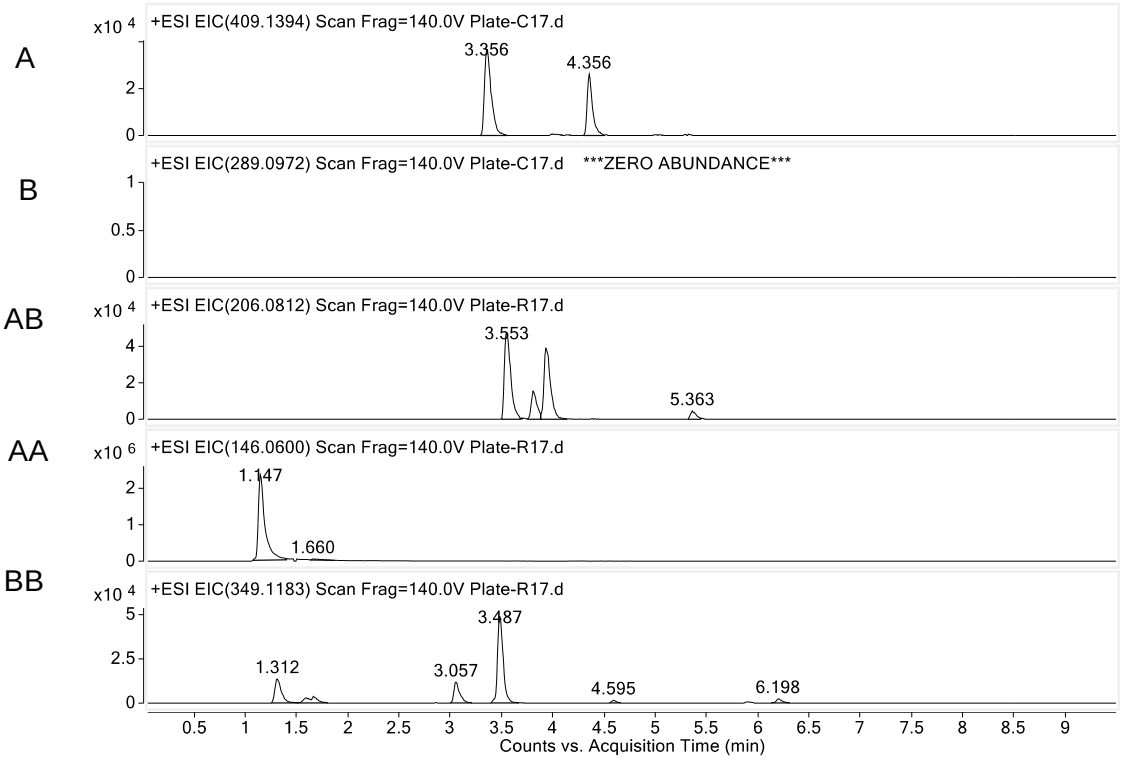

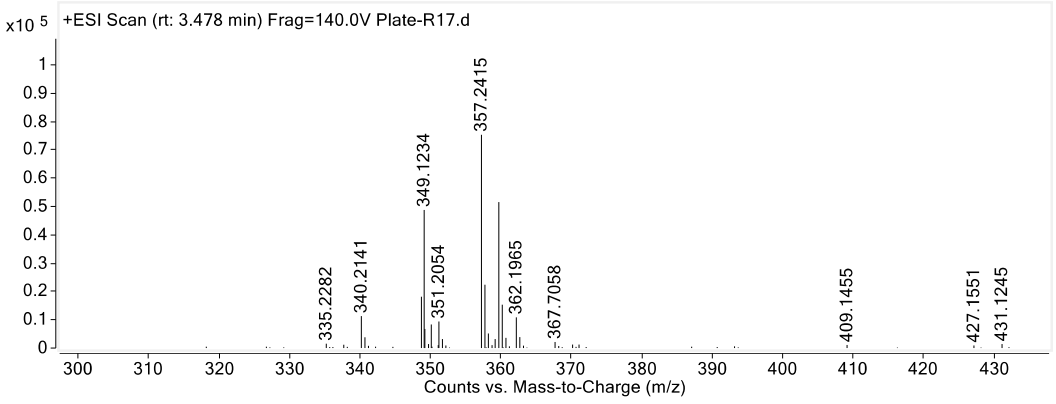

No enzyme

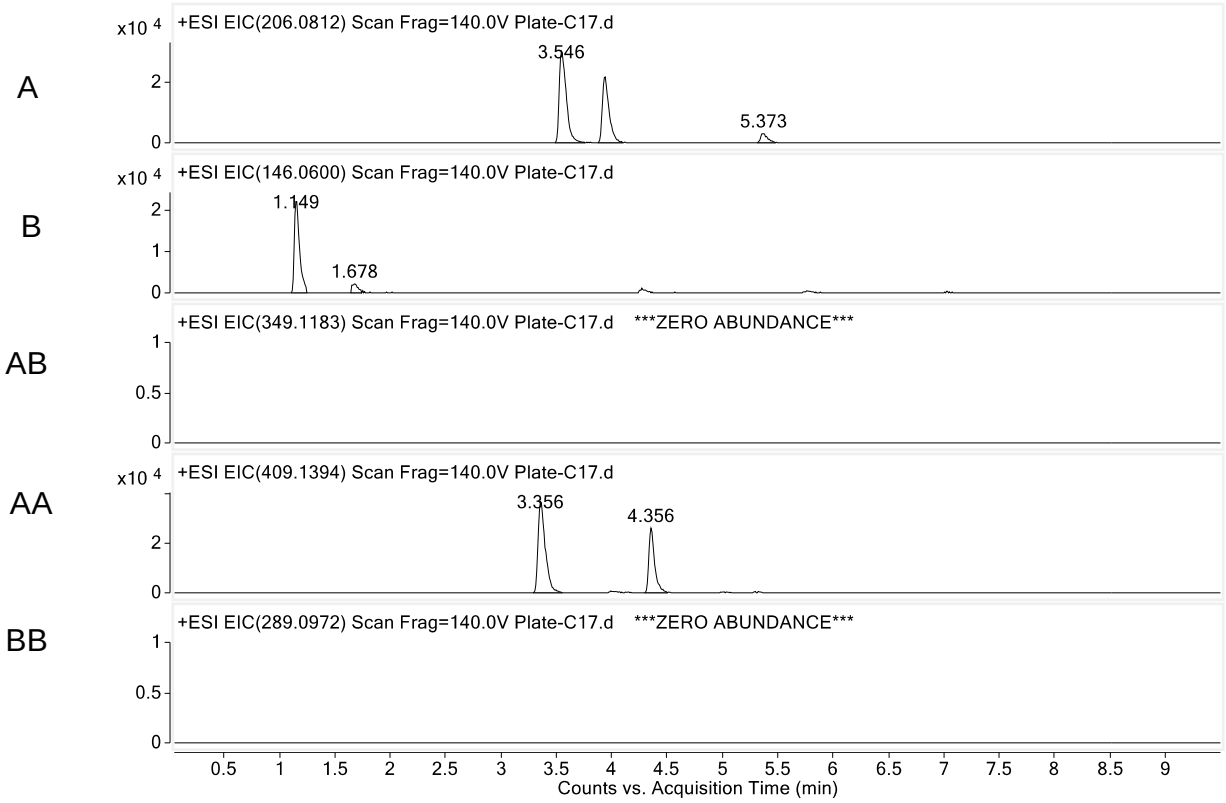
A
+ESI EIC(206.0812) Scan Frag=140.0V Plate-C17.d
x10 4
3.546
5.373
B
+ESI EIC(146.0600) Scan Frag=140.0V Plate-C17.d
x10 4
1.149
1.678
AB
+ESI EIC(349.1183) Scan Frag=140.0V Plate-C17.d ***ZERO ABUNDANCE***
AA
+ESI EIC(409.1394) Scan Frag=140.0V Plate-C17.d
x10 4
3.356
4.356
BB
+ESI EIC(289.0972) Scan Frag=140.0V Plate-C17.d ***ZERO ABUNDANCE***
Counts vs. Acquisition Time (min)

Supplemental Figure S3.93. Oxidative cross-coupling of **12** and **29** by KtnC (**Figure 3.5**).

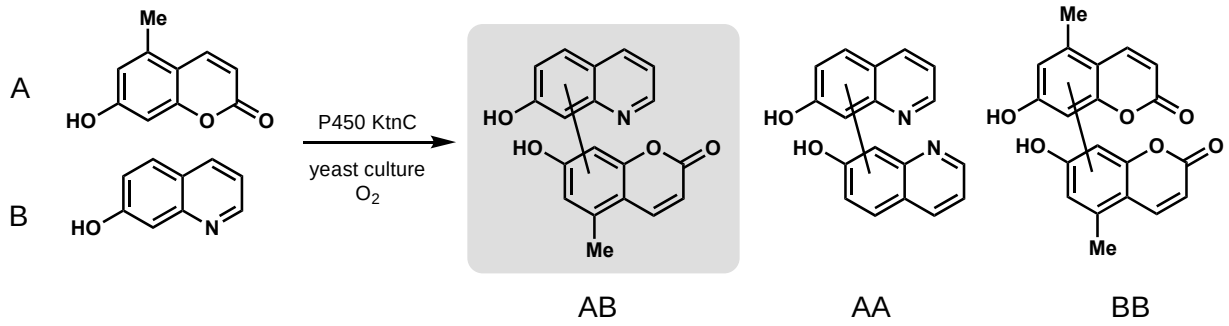

KtnC

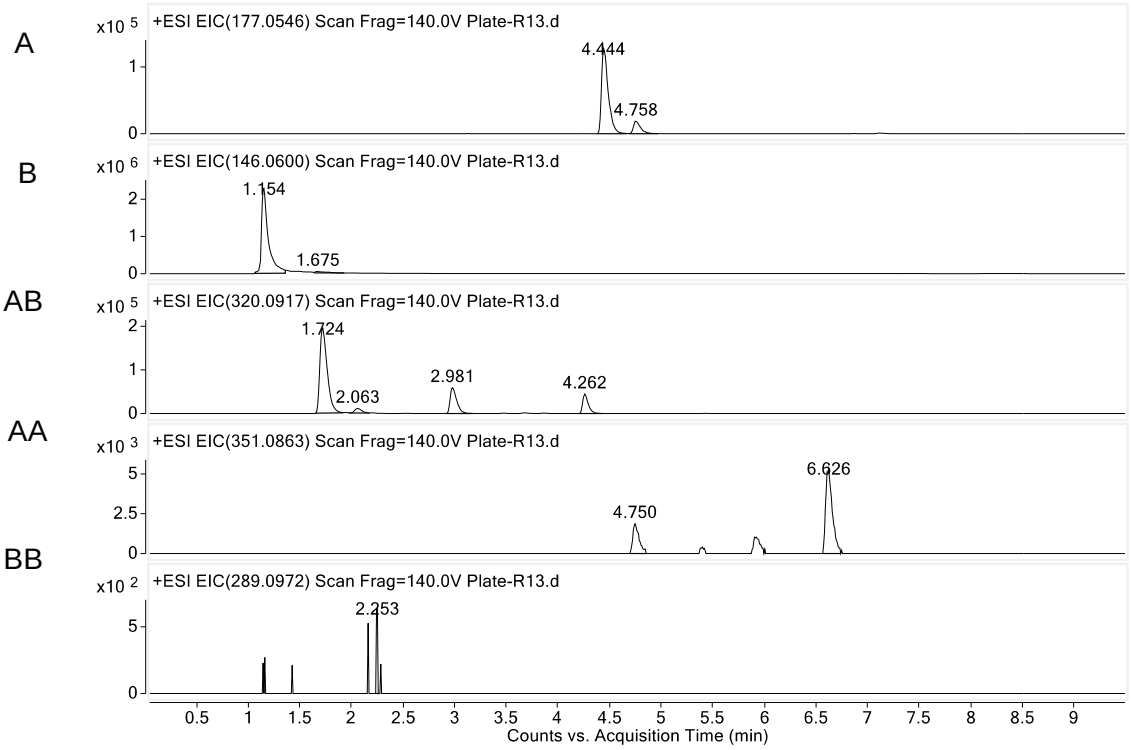

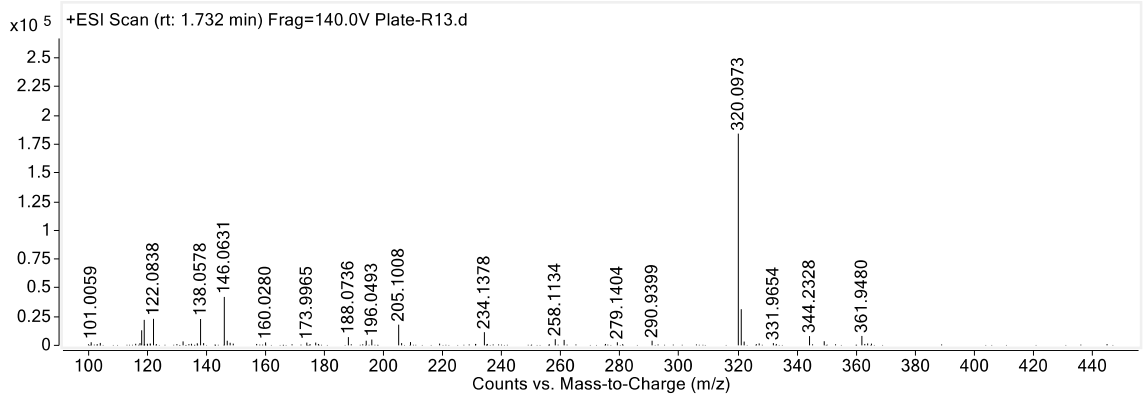

No enzyme

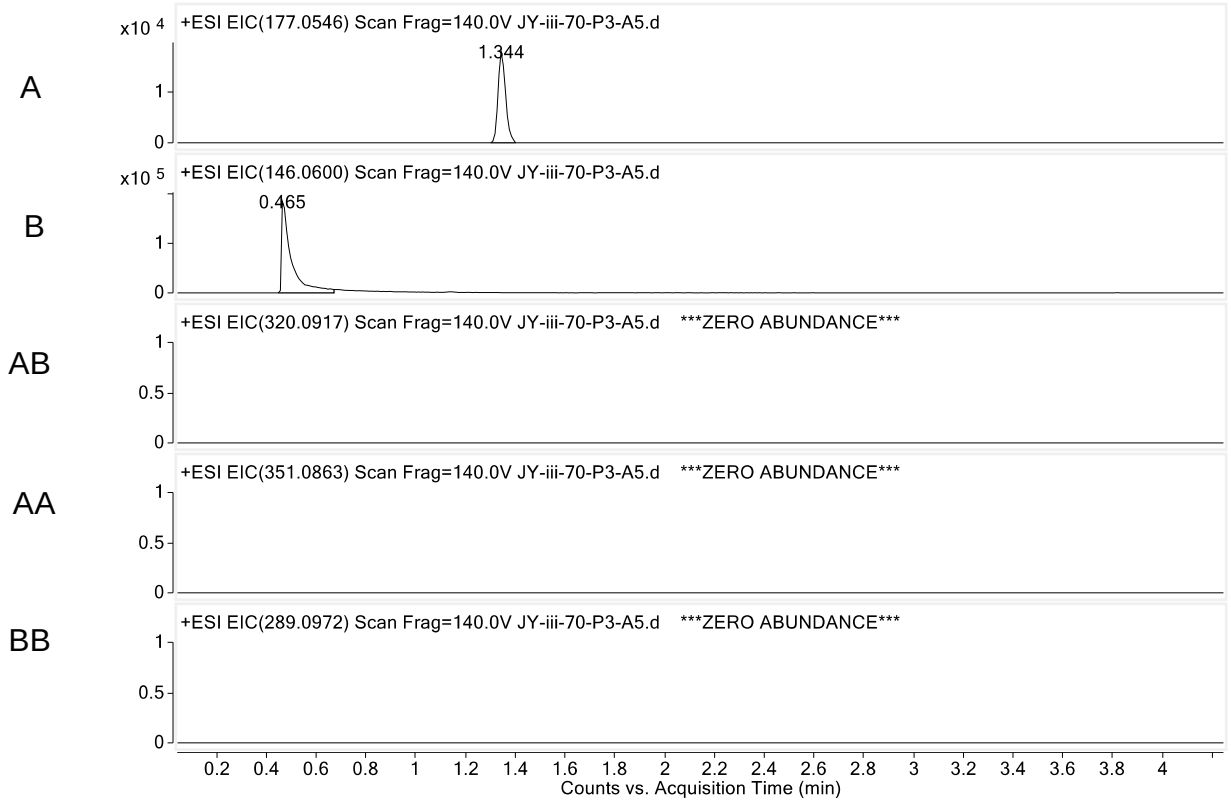
A
B
AB
AA
BB
x10 4
+ESI EIC(177.0546) Scan Frag=140.0V JY-iii-70-P3-A5.d
1.344
x10 5
+ESI EIC(146.0600) Scan Frag=140.0V JY-iii-70-P3-A5.d
0.465
+ESI EIC(320.0917) Scan Frag=140.0V JY-iii-70-P3-A5.d ***ZERO ABUNDANCE***
+ESI EIC(351.0863) Scan Frag=140.0V JY-iii-70-P3-A5.d ***ZERO ABUNDANCE***
+ESI EIC(289.0972) Scan Frag=140.0V JY-iii-70-P3-A5.d ***ZERO ABUNDANCE***
0.2 0.4 0.6 0.8 1 1.2 1.4 1.6 1.8 2 2.2 2.4 2.6 2.8 3 3.2 3.4 3.6 3.8 4
Counts vs. Acquisition Time (min)

Supplemental Figure S3.94. Oxidative cross-coupling of **22** and **29** by KtnC (**Figure 3.5**).

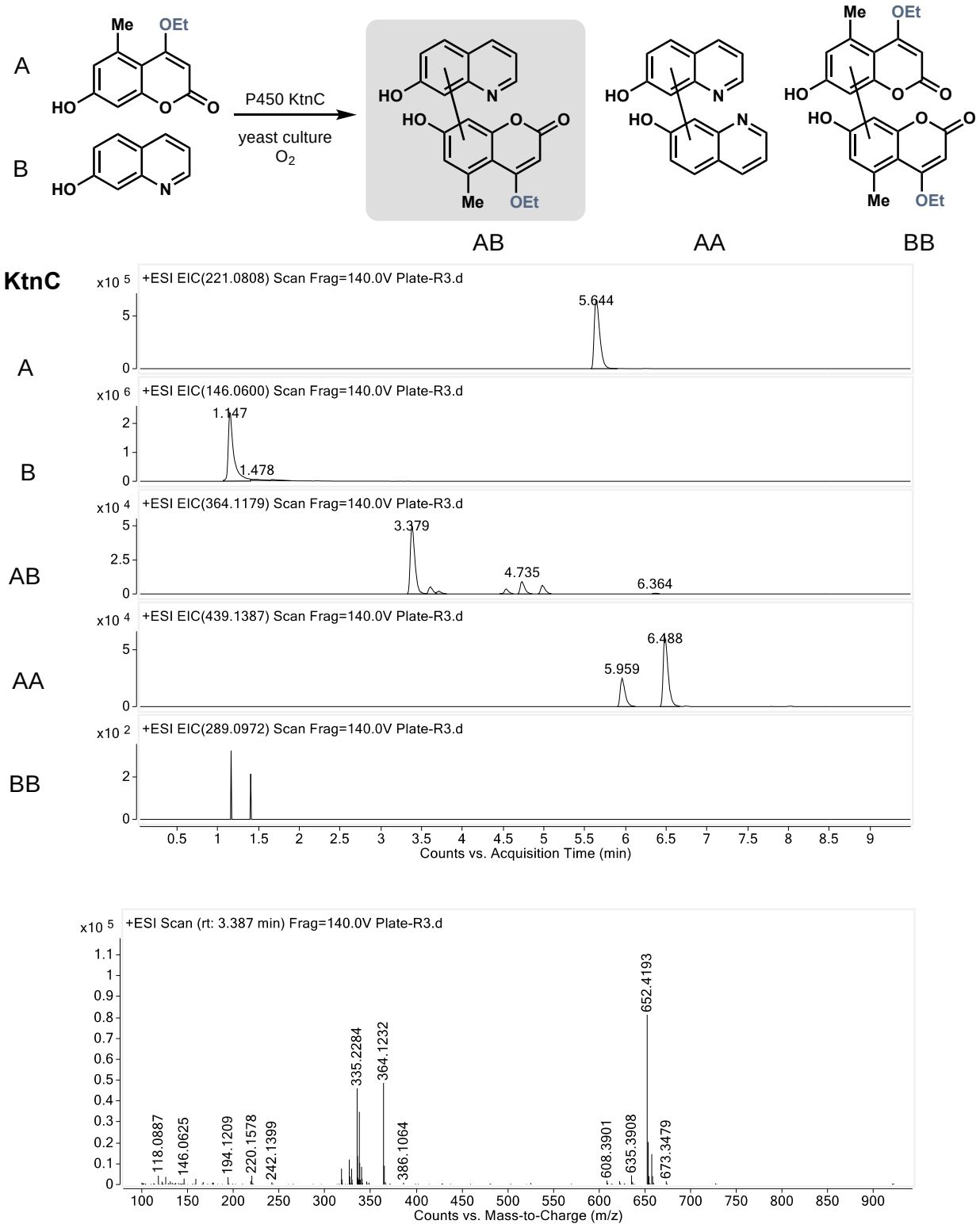

No enzyme

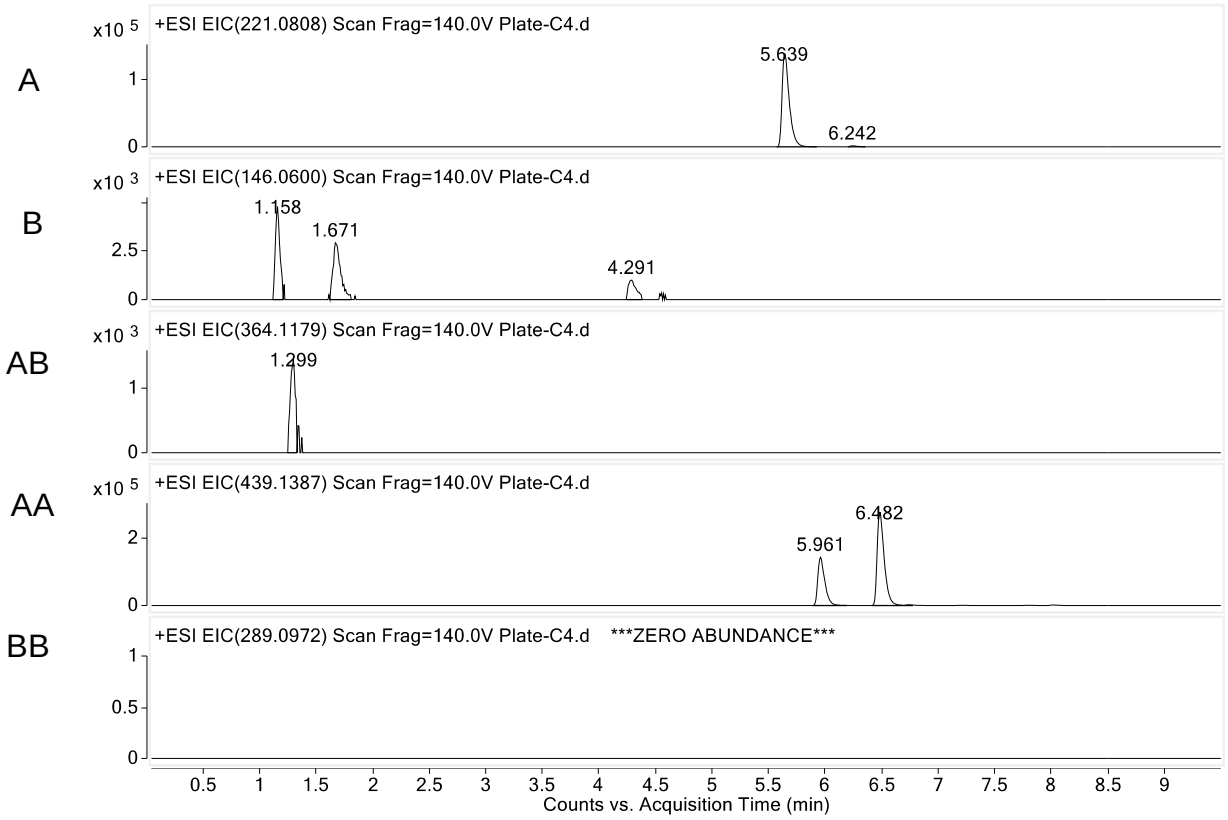
A
x10 5
+ESI EIC(221.0808) Scan Frag=140.0V Plate-C4.d
5.639
6.242
B
x10 3
+ESI EIC(146.0600) Scan Frag=140.0V Plate-C4.d
1.158
1.671
4.291
AB
x10 3
+ESI EIC(364.1179) Scan Frag=140.0V Plate-C4.d
1.299
AA
x10 5
+ESI EIC(439.1387) Scan Frag=140.0V Plate-C4.d
6.482
5.961
BB
+ESI EIC(289.0972) Scan Frag=140.0V Plate-C4.d ***ZERO ABUNDANCE***
Counts vs. Acquisition Time (min)

Supplemental Figure S3.95. Oxidative cross-coupling of **18** and **29** by KtnC (**Figure 3.5**).

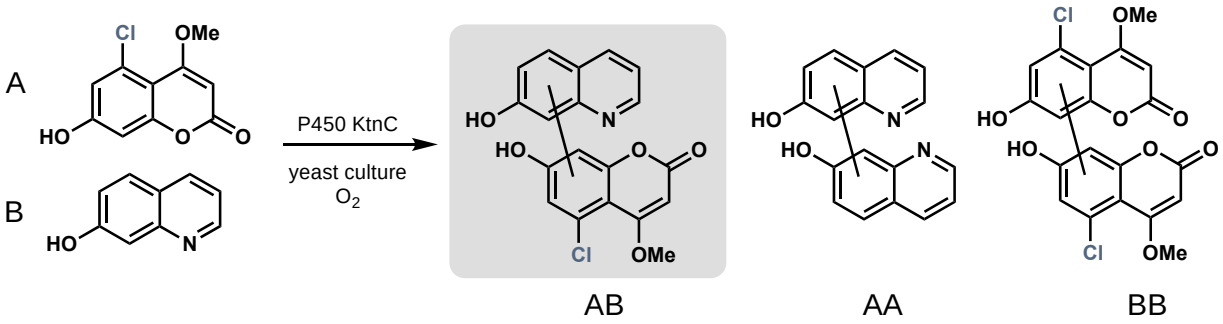

KtnC

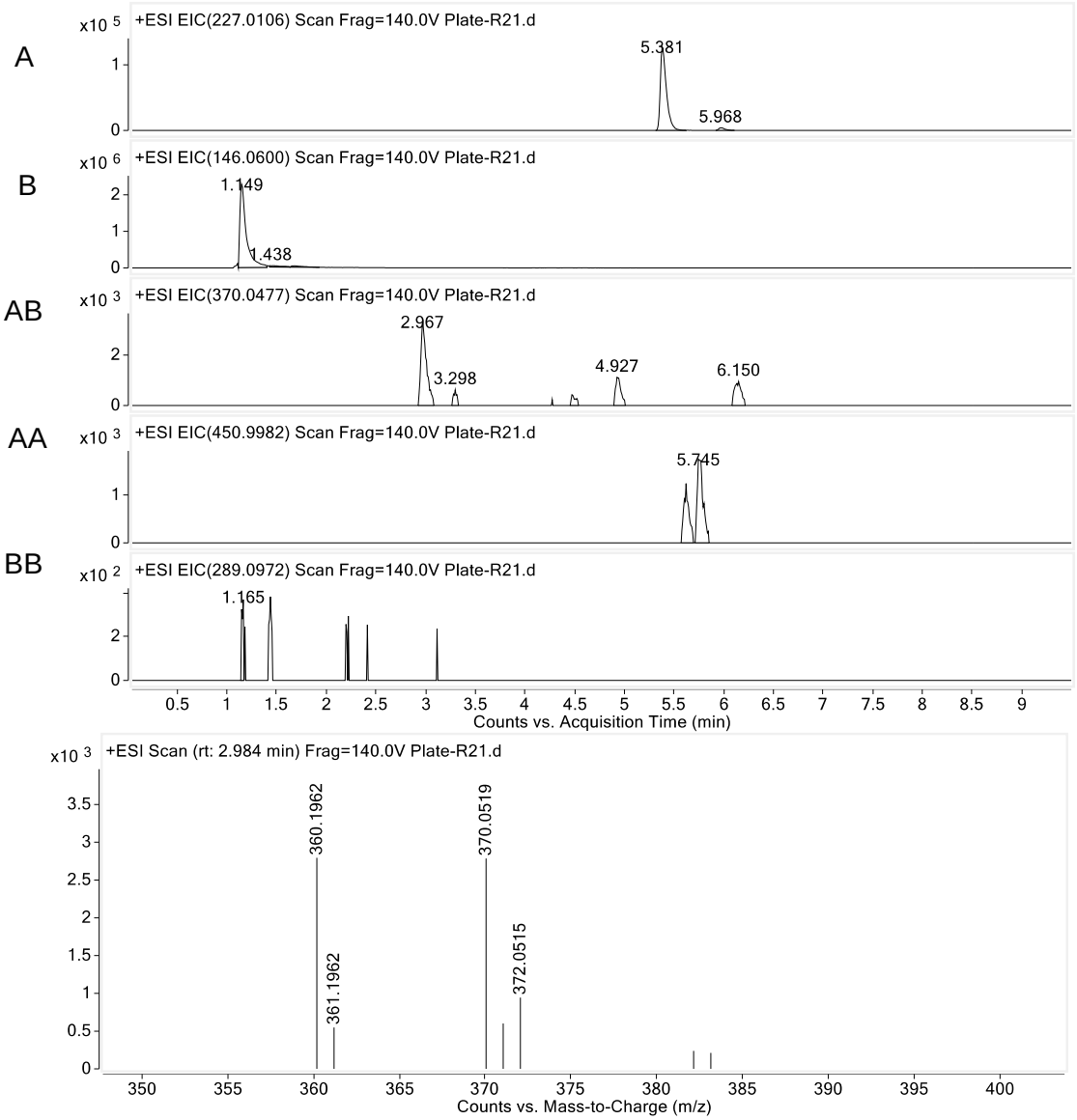

No enzyme

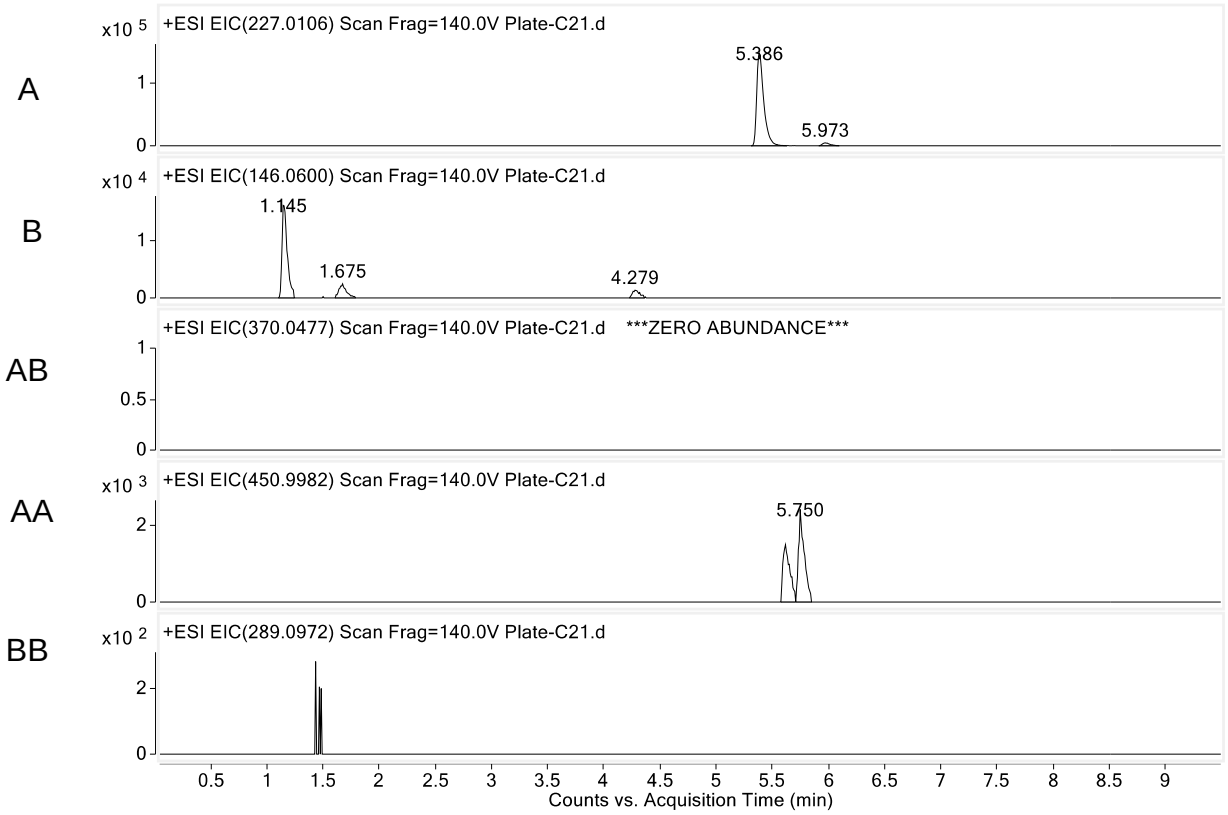
A
x10 5
+ESI EIC(227.0106) Scan Frag=140.0V Plate-C21.d
5.386
5.973
B
x10 4
+ESI EIC(146.0600) Scan Frag=140.0V Plate-C21.d
1.145
1.675
4.279
AB
+ESI EIC(370.0477) Scan Frag=140.0V Plate-C21.d ***ZERO ABUNDANCE***
AA
x10 3
+ESI EIC(450.9982) Scan Frag=140.0V Plate-C21.d
5.750
BB
x10 2
+ESI EIC(289.0972) Scan Frag=140.0V Plate-C21.d
0.5 1 1.5 2 2.5 3 3.5 4 4.5 5 5.5 6 6.5 7 7.5 8 8.5 9
Counts vs. Acquisition Time (min)

Supplemental Figure S3.96. Oxidative cross-coupling of **11** and **29** by KtnC (**Figure 3.5**).

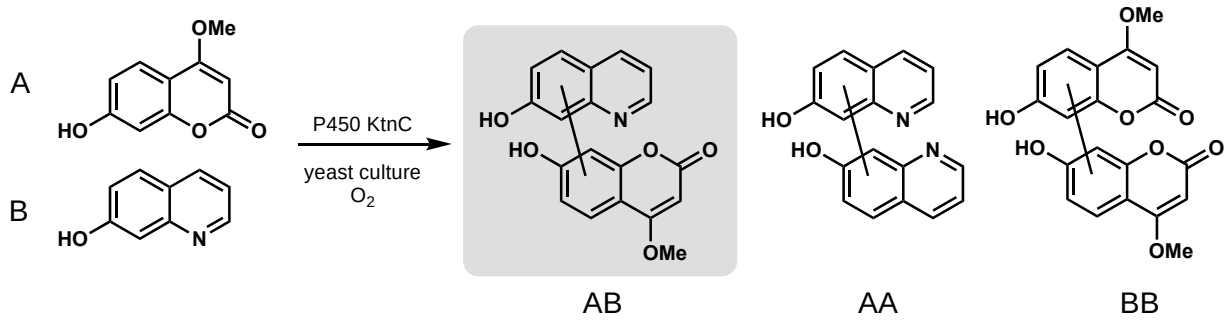

KtnC

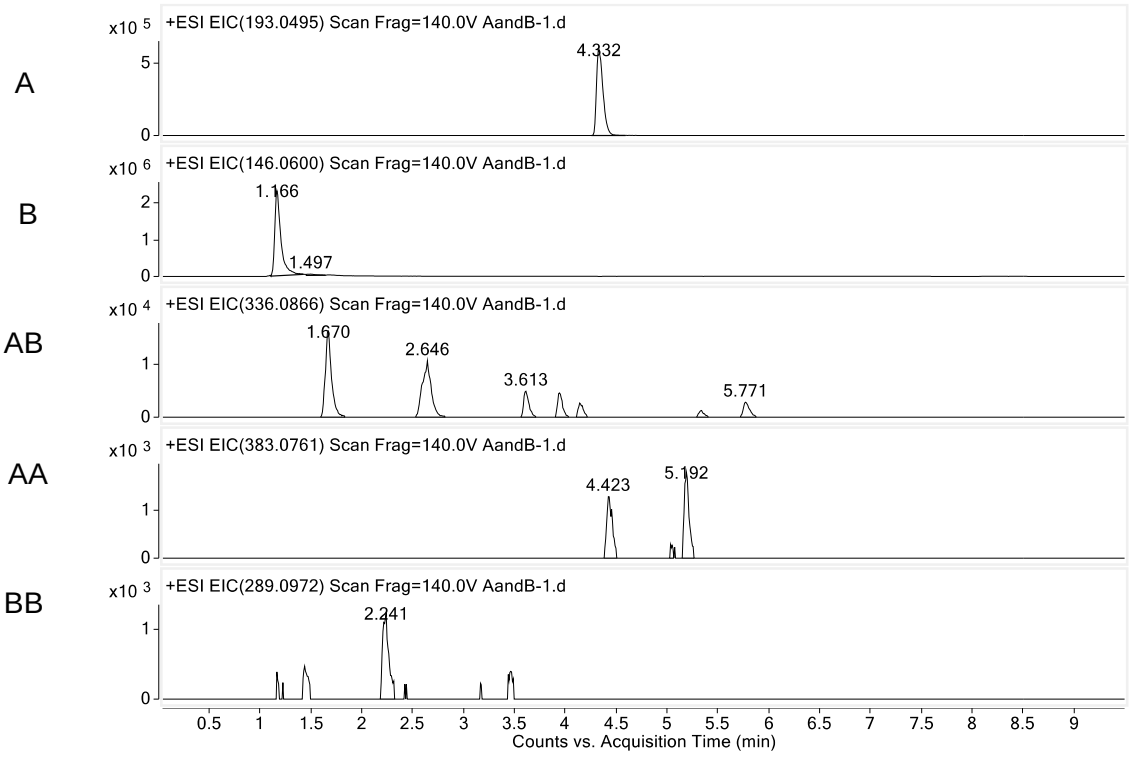

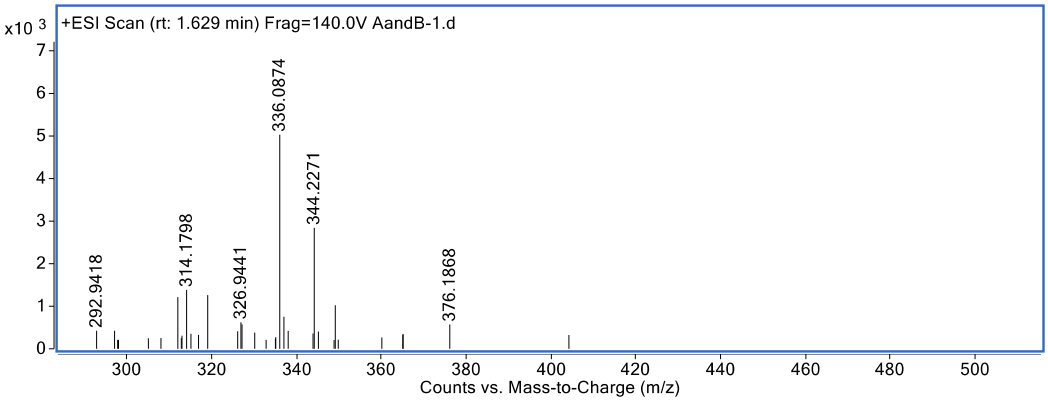

No enzyme

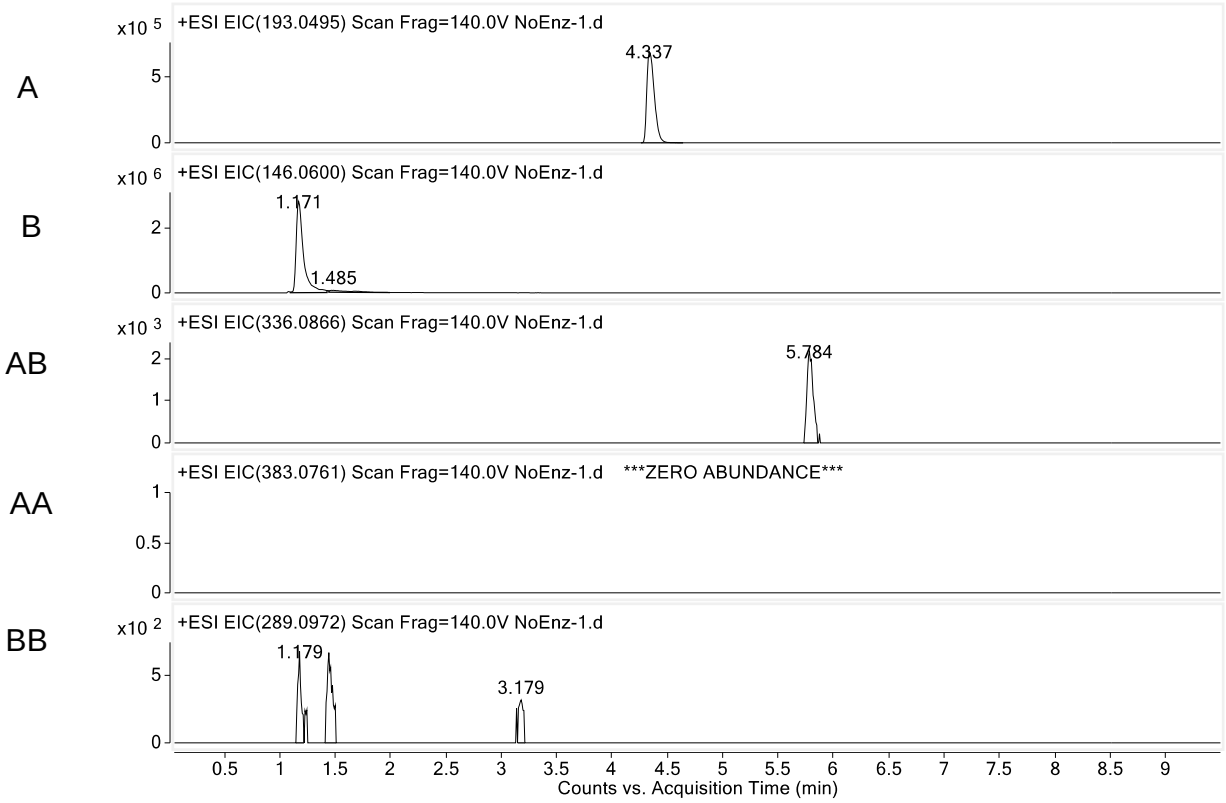
A
+ESI EIC(193.0495) Scan Frag=140.0V NoEnz-1.d
x10 5
4.337
B
+ESI EIC(146.0600) Scan Frag=140.0V NoEnz-1.d
x10 6
1.171
1.485
AB
+ESI EIC(336.0866) Scan Frag=140.0V NoEnz-1.d
x10 3
5.784
AA
+ESI EIC(383.0761) Scan Frag=140.0V NoEnz-1.d ***ZERO ABUNDANCE***
BB
+ESI EIC(289.0972) Scan Frag=140.0V NoEnz-1.d
x10 2
1.179
3.179
0.5 1 1.5 2 2.5 3 3.5 4 4.5 5 5.5 6 6.5 7 7.5 8 8.5 9
Counts vs. Acquisition Time (min)

Supplemental Figure S3.97. Oxidative cross-coupling of **19** and **29** by KtnC (**Figure 3.5**).

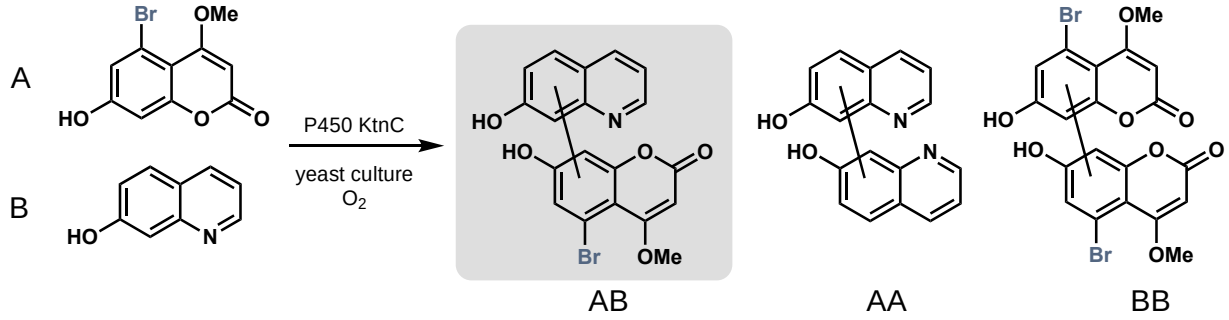

KtnC

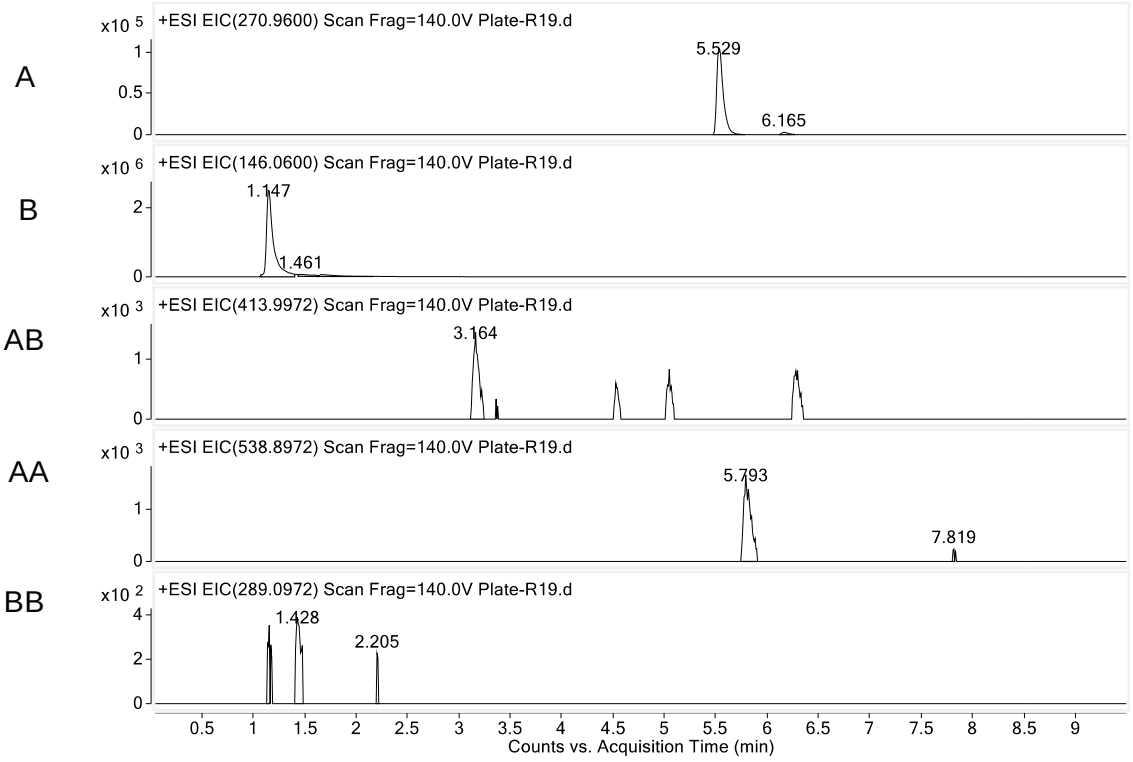

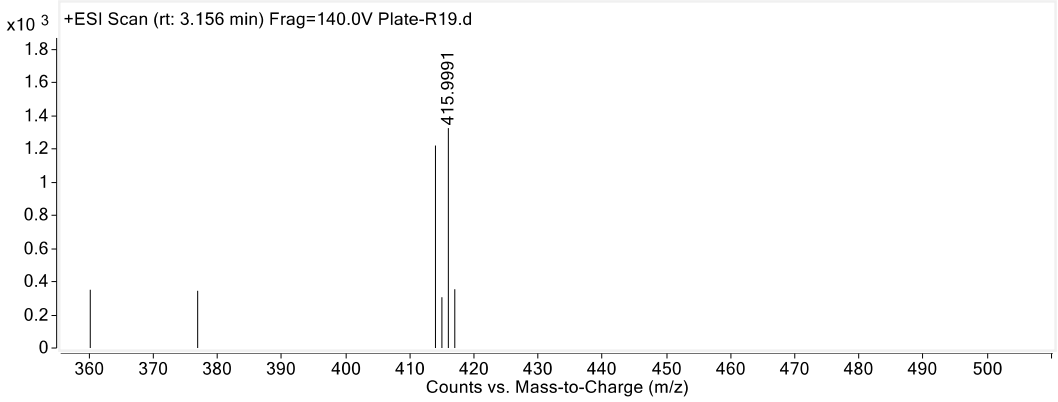

No enzyme

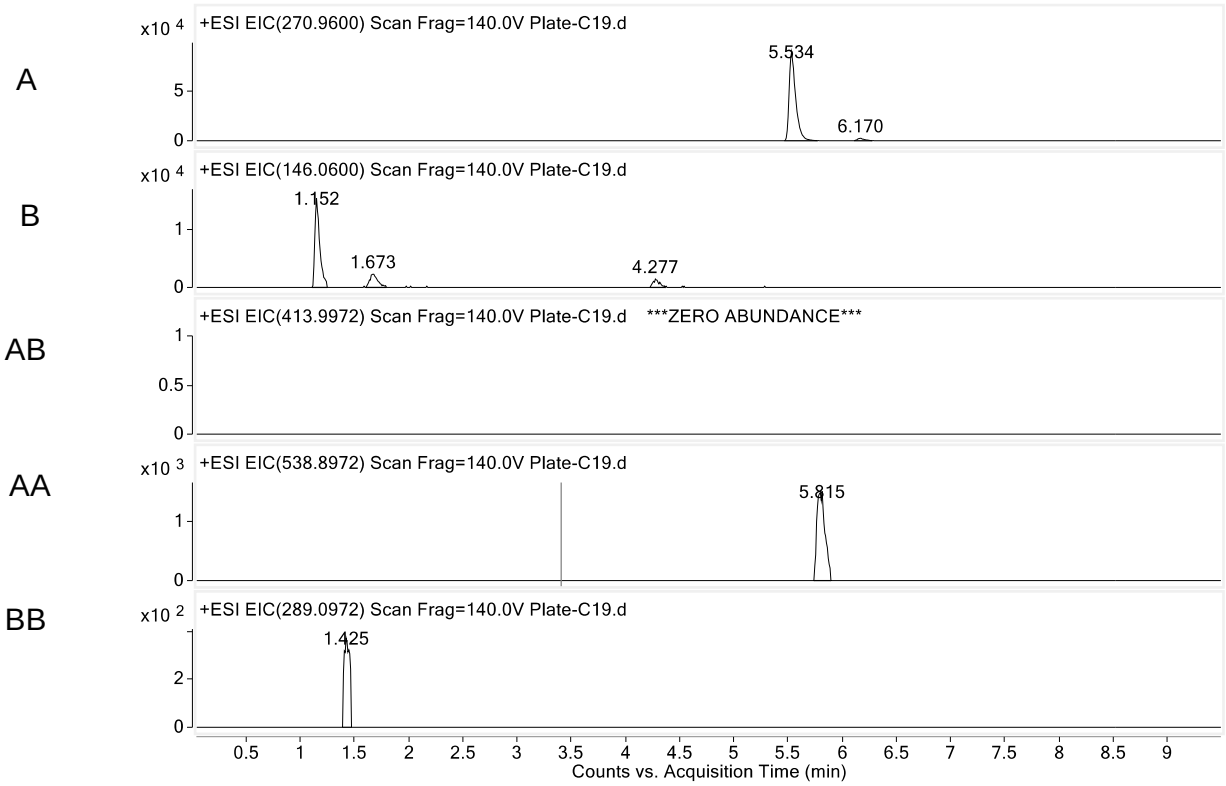
A
+ESI EIC(270.9600) Scan Frag=140.0V Plate-C19.d
x10 4
5.534
6.170
B
+ESI EIC(146.0600) Scan Frag=140.0V Plate-C19.d
x10 4
1.152
1.673
4.277
AB
+ESI EIC(413.9972) Scan Frag=140.0V Plate-C19.d ***ZERO ABUNDANCE***
AA
+ESI EIC(538.8972) Scan Frag=140.0V Plate-C19.d
x10 3
5.815
BB
+ESI EIC(289.0972) Scan Frag=140.0V Plate-C19.d
x10 2
1.425
0.5 1 1.5 2 2.5 3 3.5 4 4.5 5 5.5 6 6.5 7 7.5 8 8.5 9
Counts vs. Acquisition Time (min)

Supplemental Figure S3.98. Oxidative cross-coupling of **18** and **31** by KtnC (**Figure 3.6**).

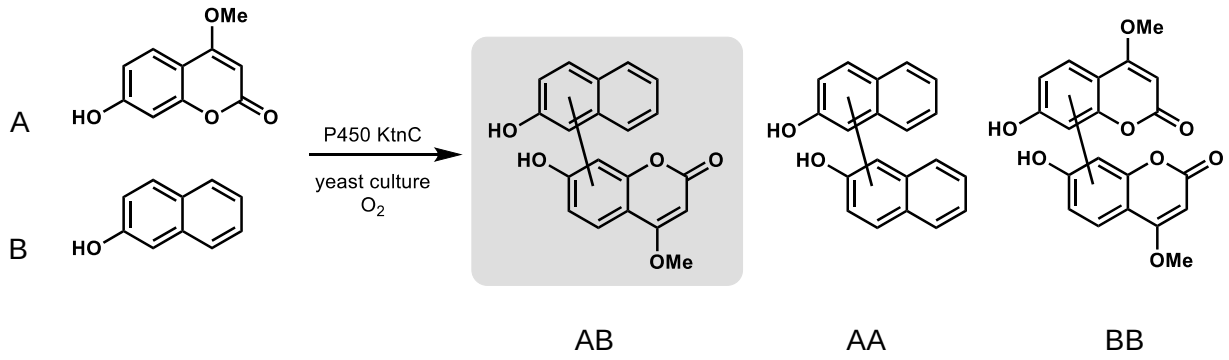

KtnC

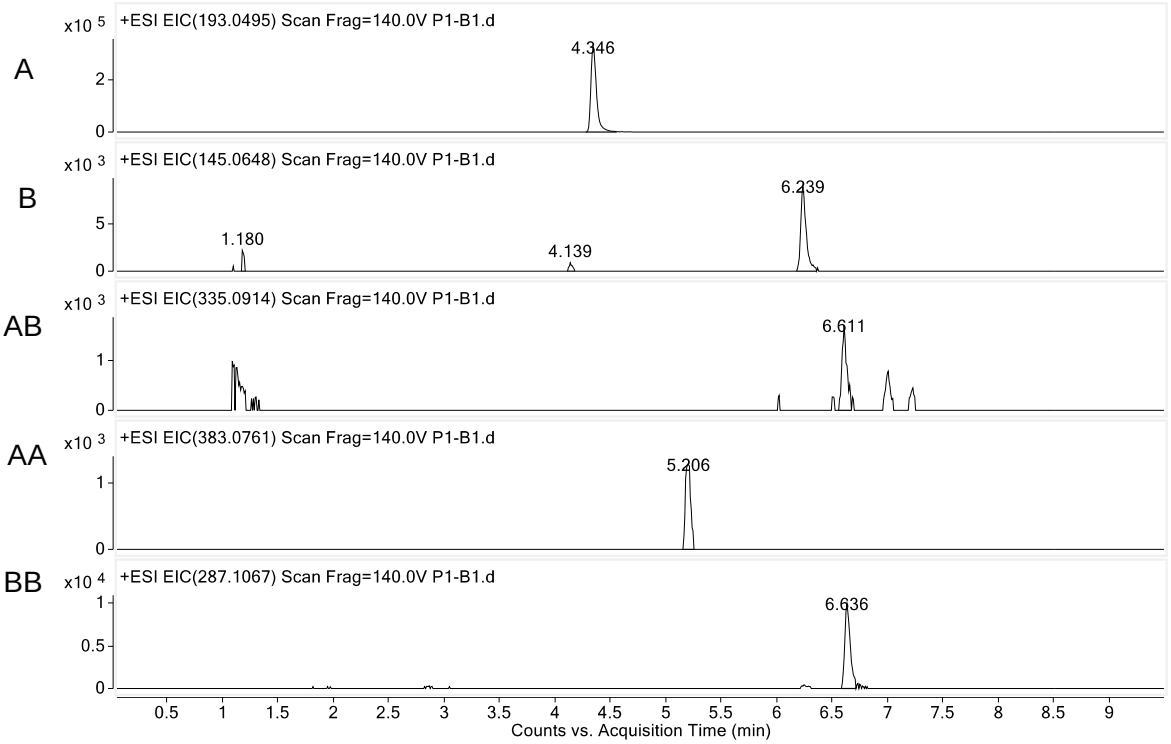

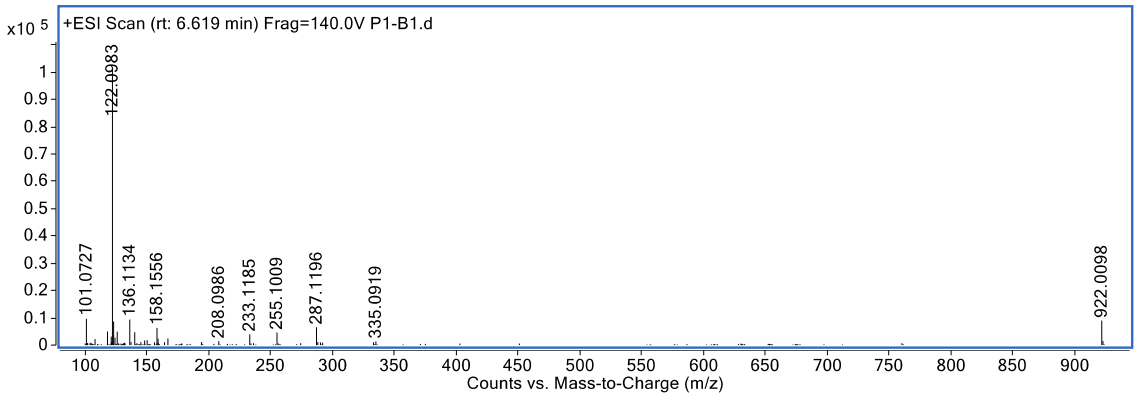

No enzyme

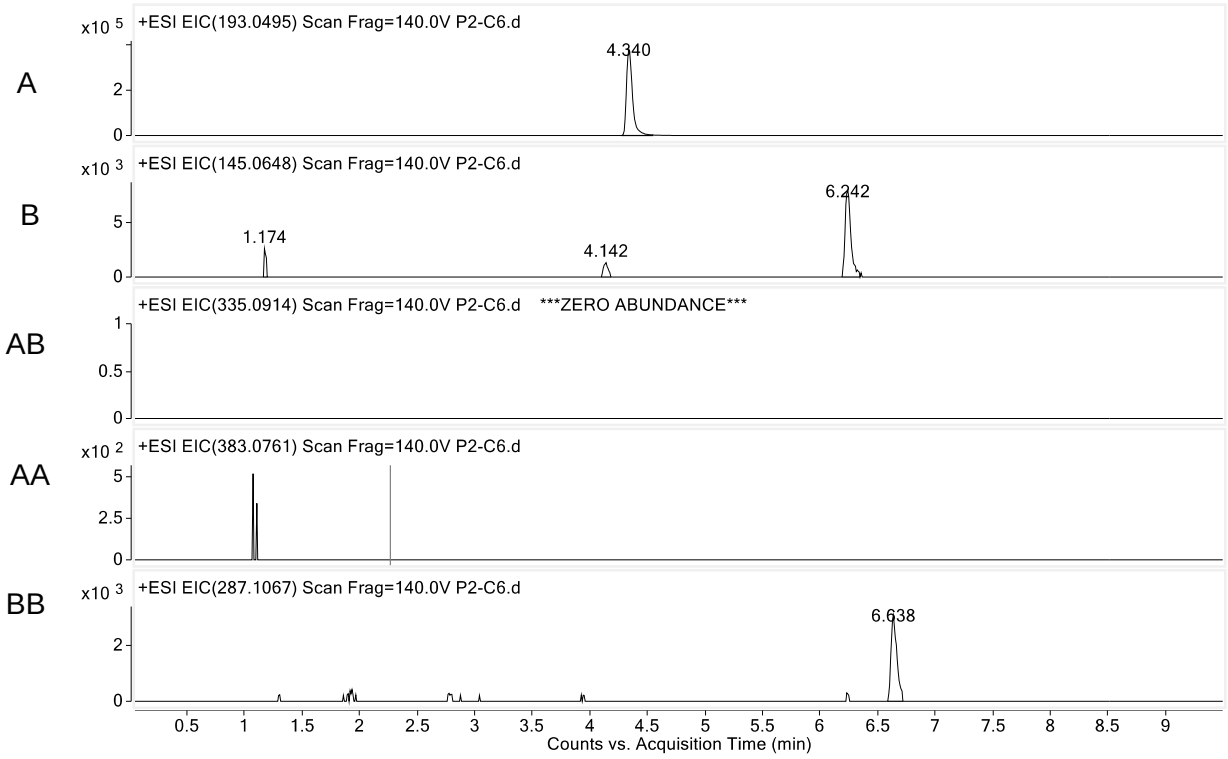
A
x10 5
+ESI EIC(193.0495) Scan Frag=140.0V P2-C6.d
4.340
B
x10 3
+ESI EIC(145.0648) Scan Frag=140.0V P2-C6.d
6.242
1.174
4.142
AB
+ESI EIC(335.0914) Scan Frag=140.0V P2-C6.d ***ZERO ABUNDANCE***
AA
x10 2
+ESI EIC(383.0761) Scan Frag=140.0V P2-C6.d
BB
x10 3
+ESI EIC(287.1067) Scan Frag=140.0V P2-C6.d
6.638
Counts vs. Acquisition Time (min)

Supplemental Figure S3.99. Oxidative cross-coupling of **12** and **31** by KtnC (**Figure 3.6**).

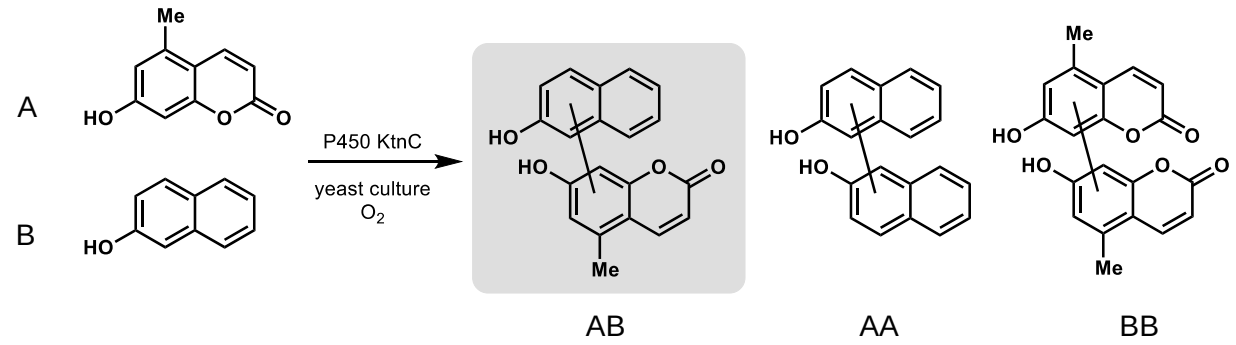

KtnC

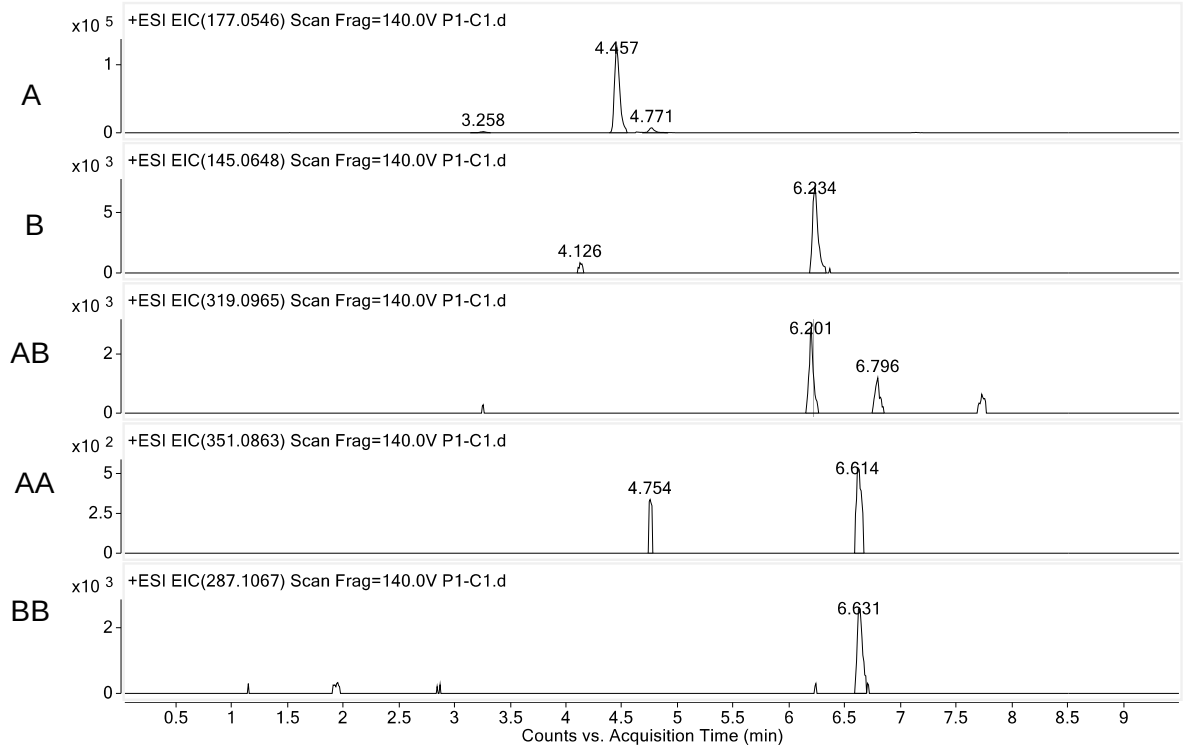

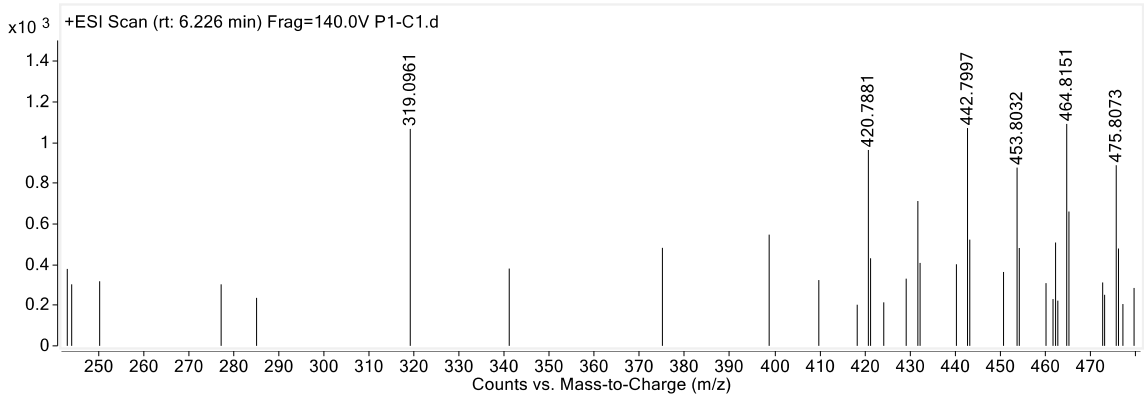

No enzyme

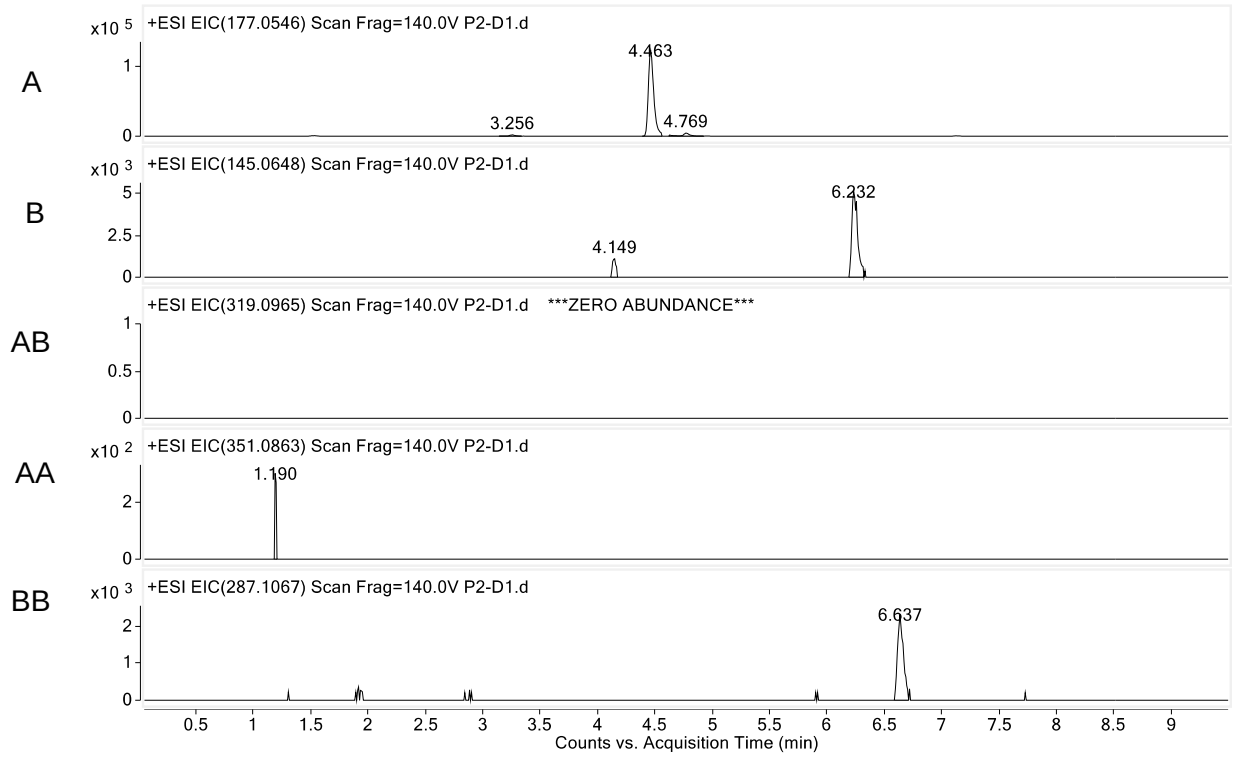
A
+ESI EIC(177.0546) Scan Frag=140.0V P2-D1.d
x10 5
4.463
3.256
4.769
B
+ESI EIC(145.0648) Scan Frag=140.0V P2-D1.d
x10 3
6.232
4.149
AB
+ESI EIC(319.0965) Scan Frag=140.0V P2-D1.d ***ZERO ABUNDANCE***
AA
+ESI EIC(351.0863) Scan Frag=140.0V P2-D1.d
x10 2
1.190
BB
+ESI EIC(287.1067) Scan Frag=140.0V P2-D1.d
x10 3
6.637
Counts vs. Acquisition Time (min)

Supplemental Figure S3.100. Oxidative cross-coupling of **21** and **31** by KtnC (**Figure 3.6**).

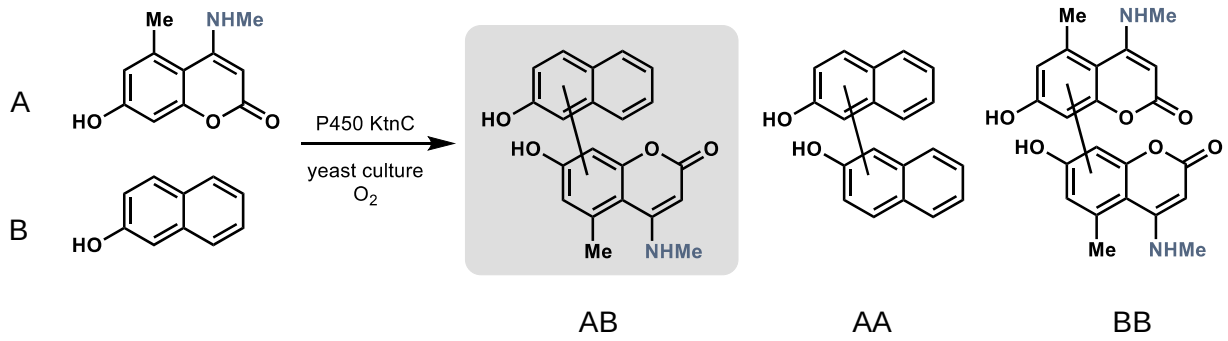

KtnC

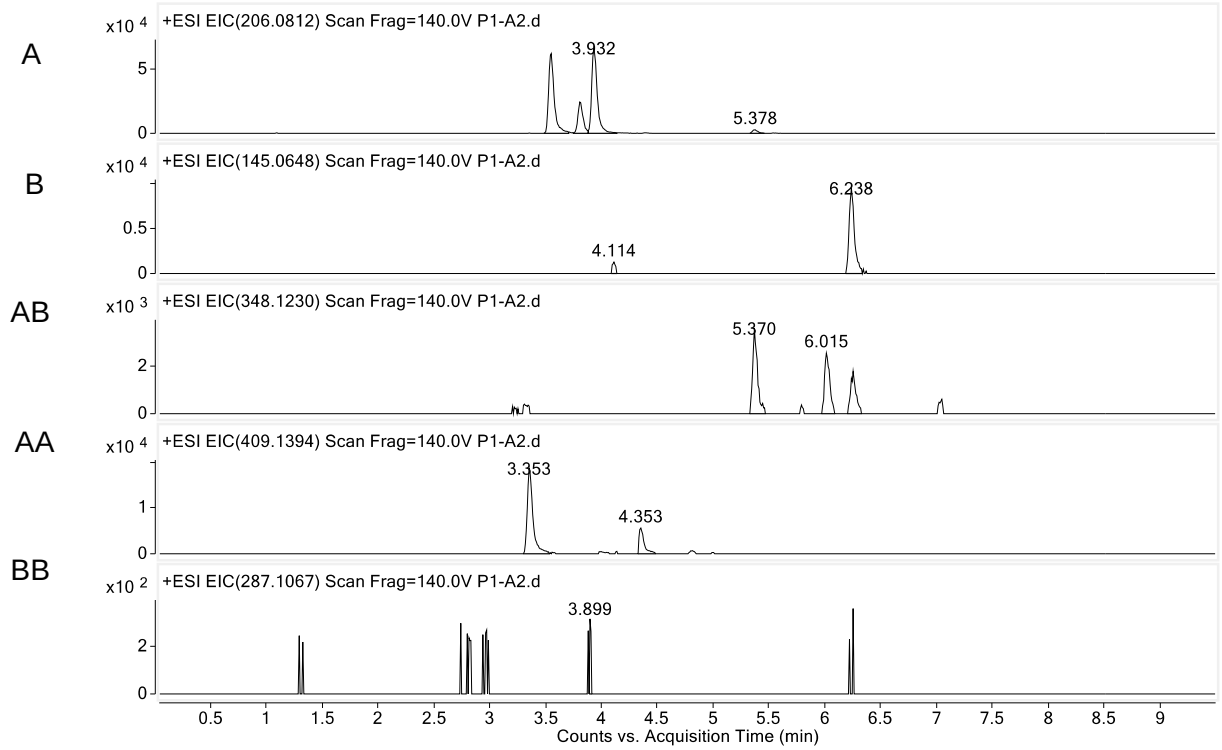

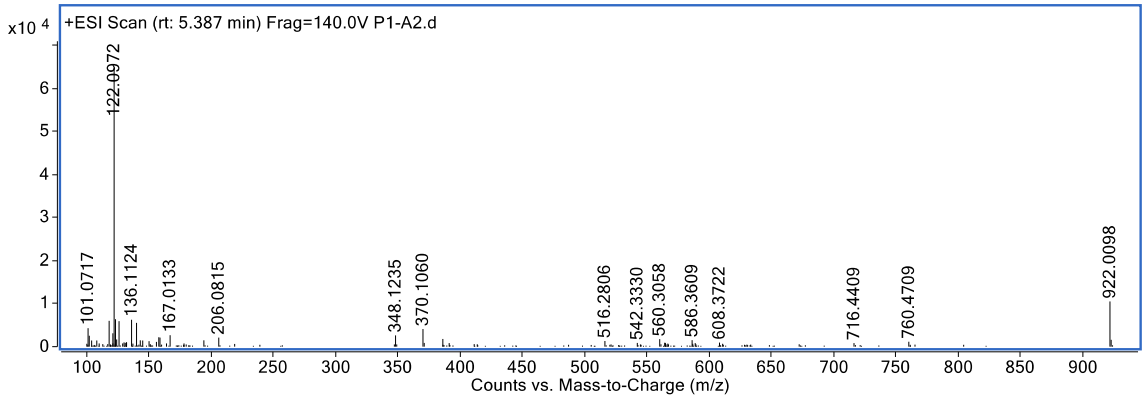

No enzyme

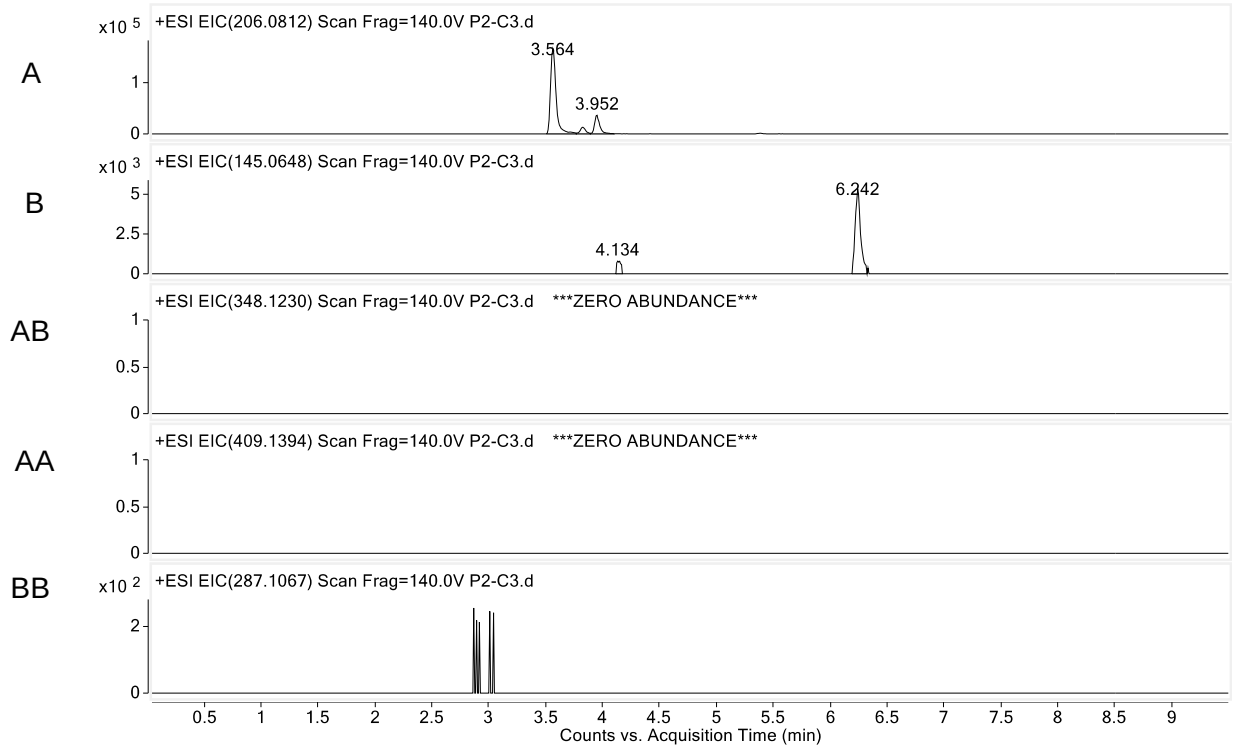
A
+ESI EIC(206.0812) Scan Frag=140.0V P2-C3.d
x10 5
3.564
3.952
B
+ESI EIC(145.0648) Scan Frag=140.0V P2-C3.d
x10 3
6.242
4.134
AB
+ESI EIC(348.1230) Scan Frag=140.0V P2-C3.d ***ZERO ABUNDANCE***
AA
+ESI EIC(409.1394) Scan Frag=140.0V P2-C3.d ***ZERO ABUNDANCE***
BB
+ESI EIC(287.1067) Scan Frag=140.0V P2-C3.d
x10 2
Counts vs. Acquisition Time (min)

Site- and atroposelectivity of biocatalytic reactions

Supplemental Figure S3.101. Site-selectivity of oxidative cross-coupling of **6** and **22** by KtnC (**Figure 3.2**).

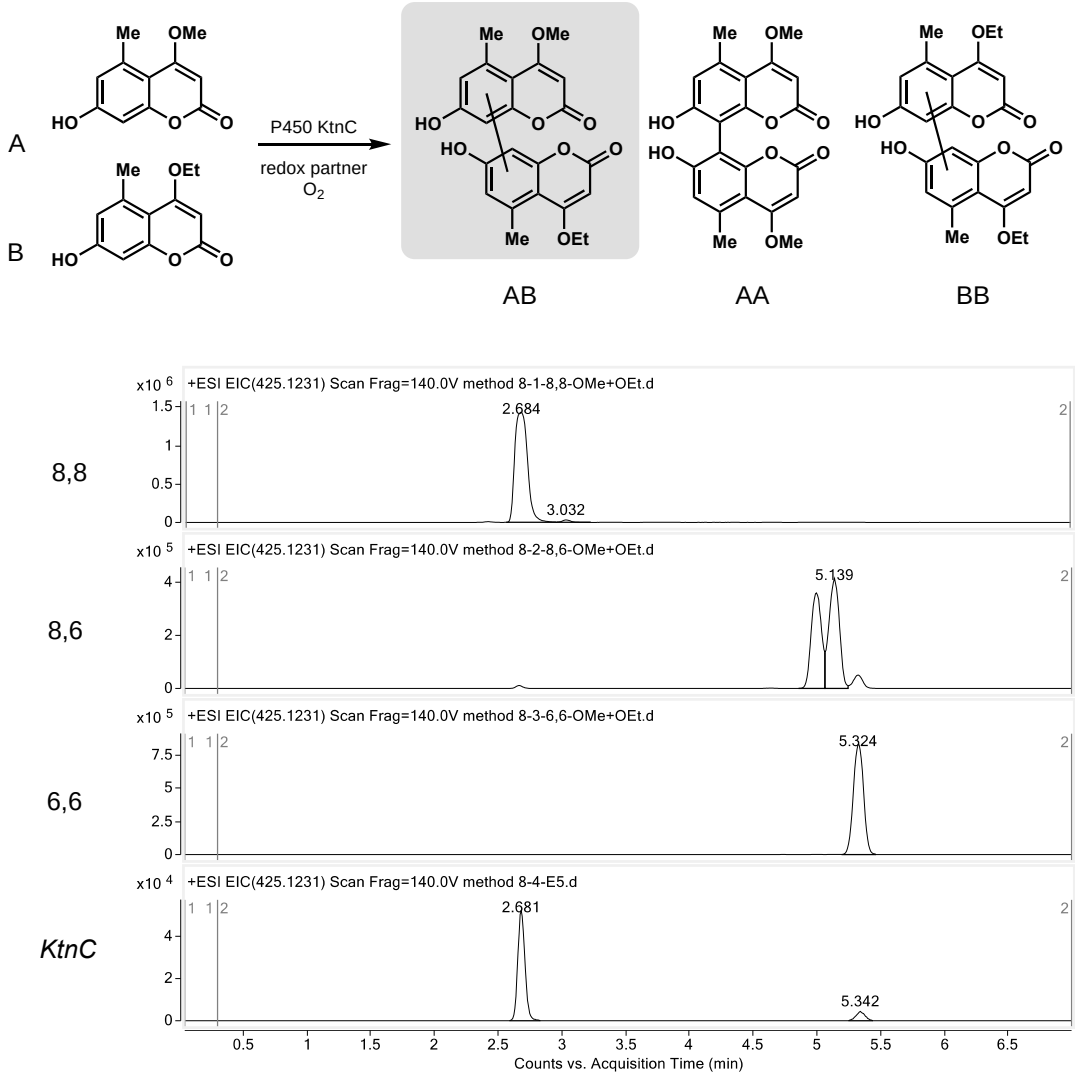

Supplemental Figure S3.102. Site-selectivity of oxidative cross-coupling of **6** and **25** by KtnC (**Figure 3.2**).

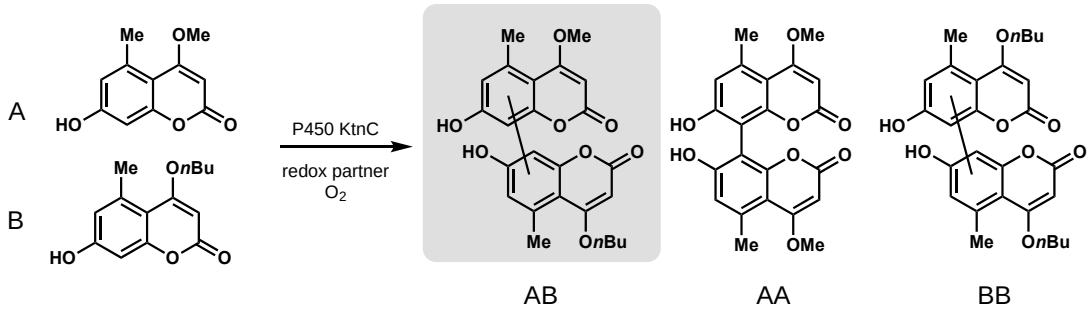

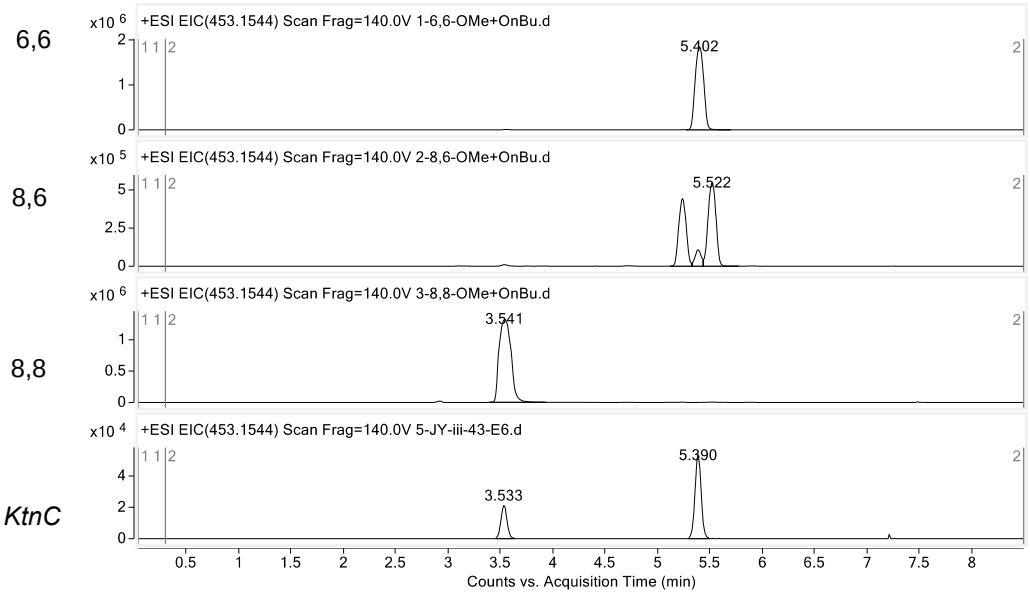

Supplemental Figure S3.103. Site-selectivity of oxidative cross-coupling of **12** and **31** by KtnC (**Figure 3.13**).

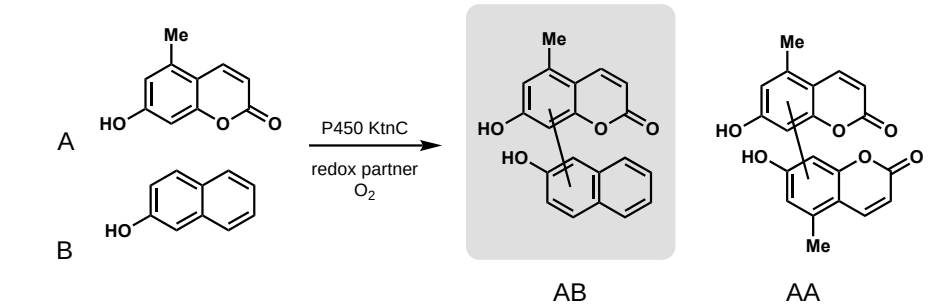

KtnC

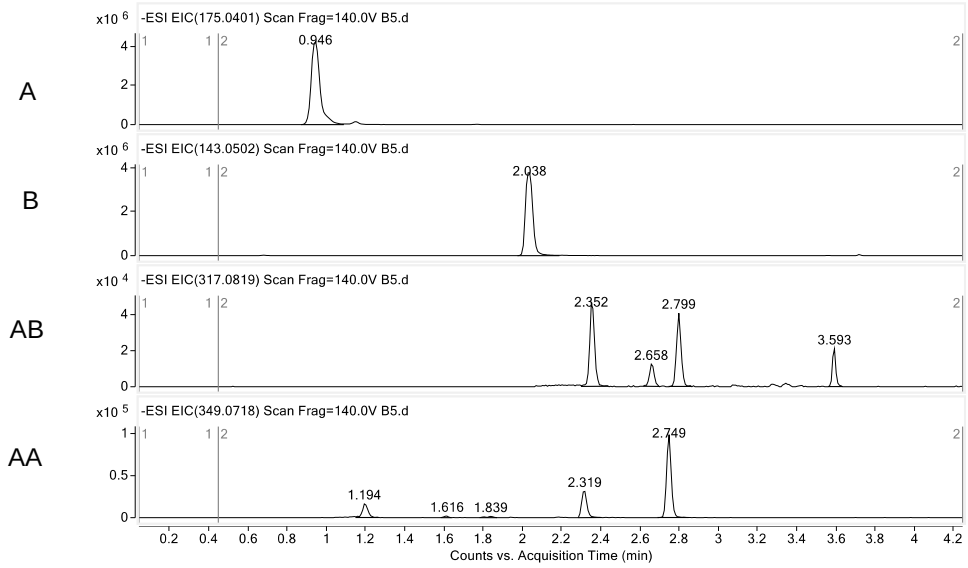

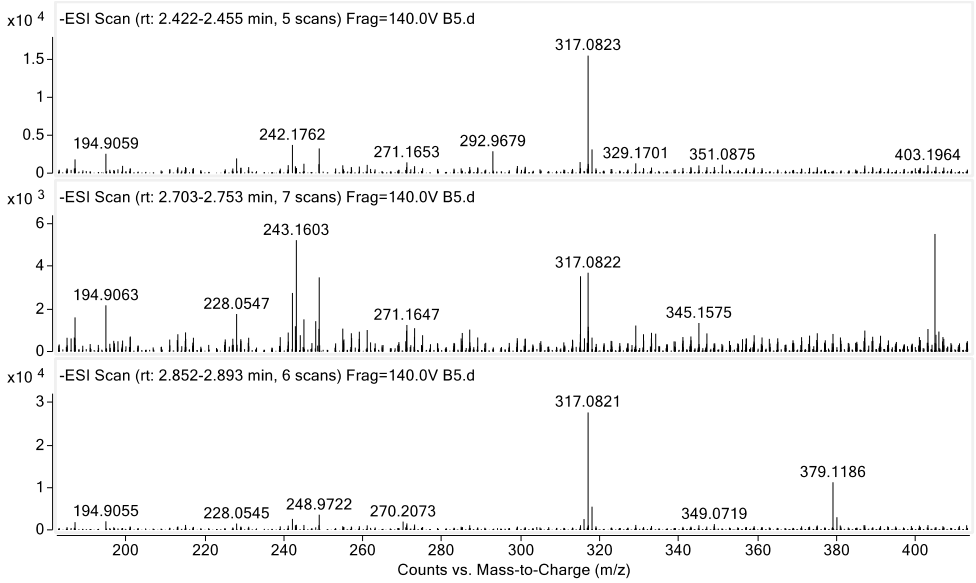

No enzyme control

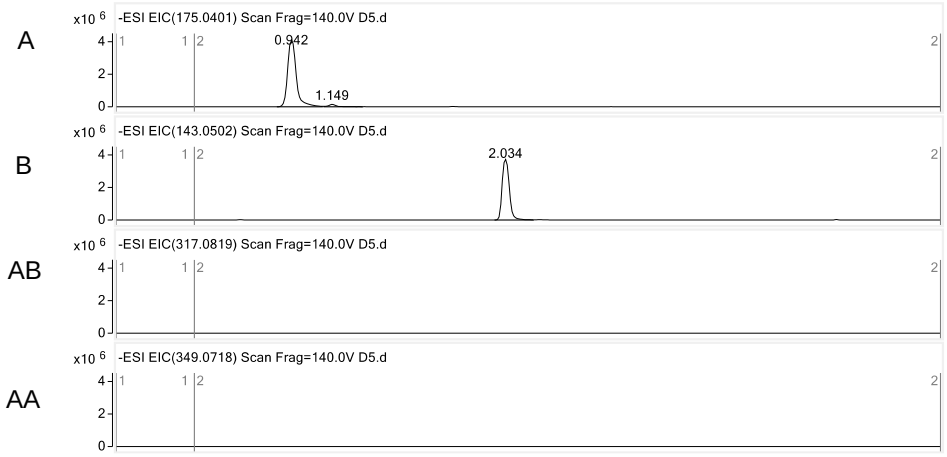

Supplemental Figure S3.104. Spiking of authentic standards into oxidative cross-coupling of **12** and **31** by KtnC to determine site-selectivity of biotransformation products (**Figure 3.13**).

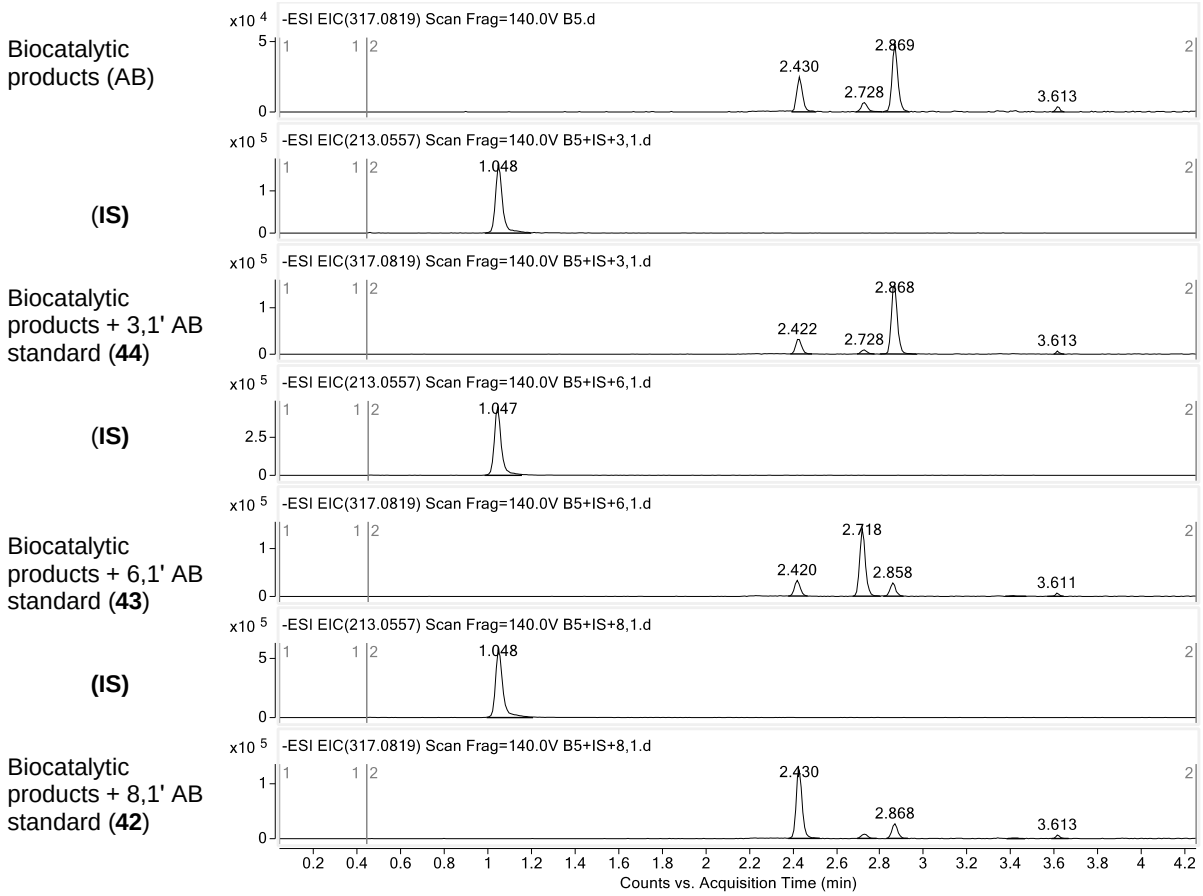

Supplemental Figure S3.105 Chiral resolution of **9** obtained from VOF_3 oxidative dimerization (top) and KtnC-catalyzed oxidative dimerization (bottom). Atropisomers were resolved using supercritical fluid chromatography with a CHIRALPAK OJ-H column (20% MeOH, CO_2, 3.5 mL/min).

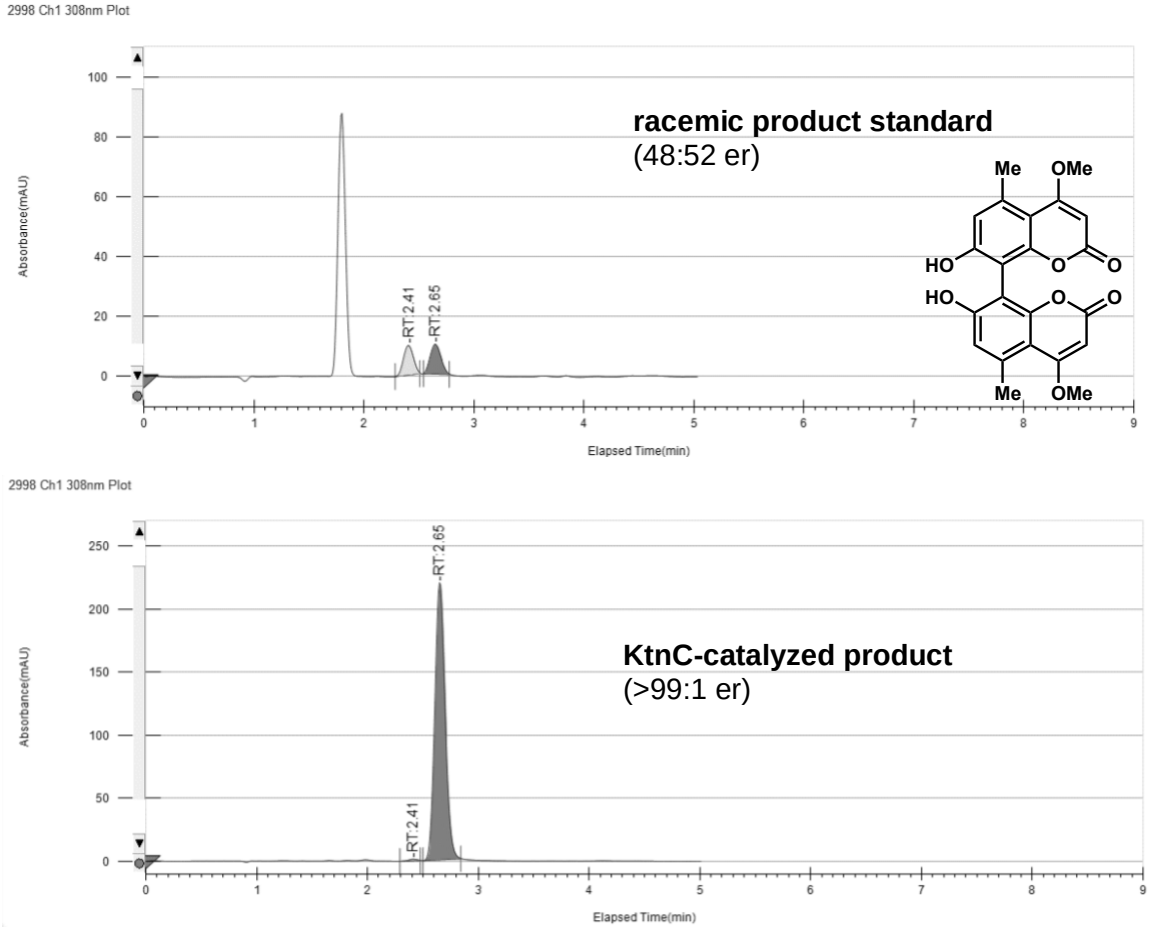

Supplemental Figure S3.106. Chiral resolution of **32** obtained from transesterification (top) and KtnC-catalyzed oxidative dimerization (bottom). Atropisomers were resolved using supercritical fluid chromatography with a CHIRALPAK OJ-H column (25% MeOH, CO_2, 3.5 mL/min).

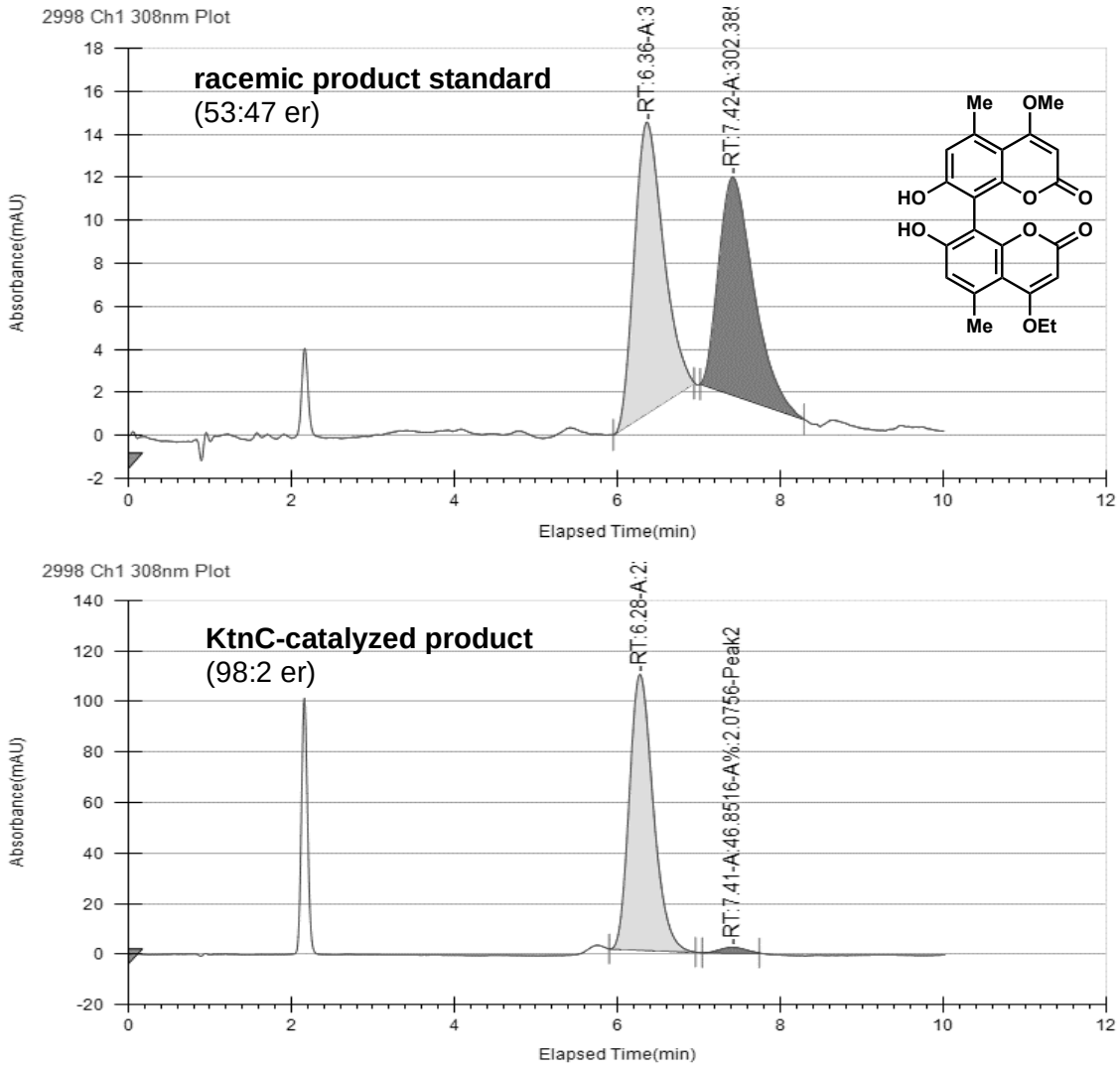

Supplemental Figure S3.107. Chiral resolution of **33** obtained from transesterification (top) and KtnC-catalyzed oxidative dimerization (bottom). Atropisomers were resolved using supercritical fluid chromatography with a CHIRALPAK OJ-H column (25% MeOH, CO_2, 3.5 mL/min).

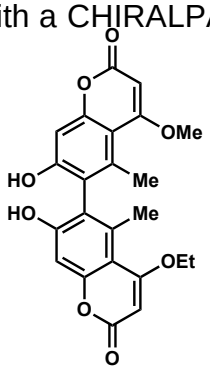

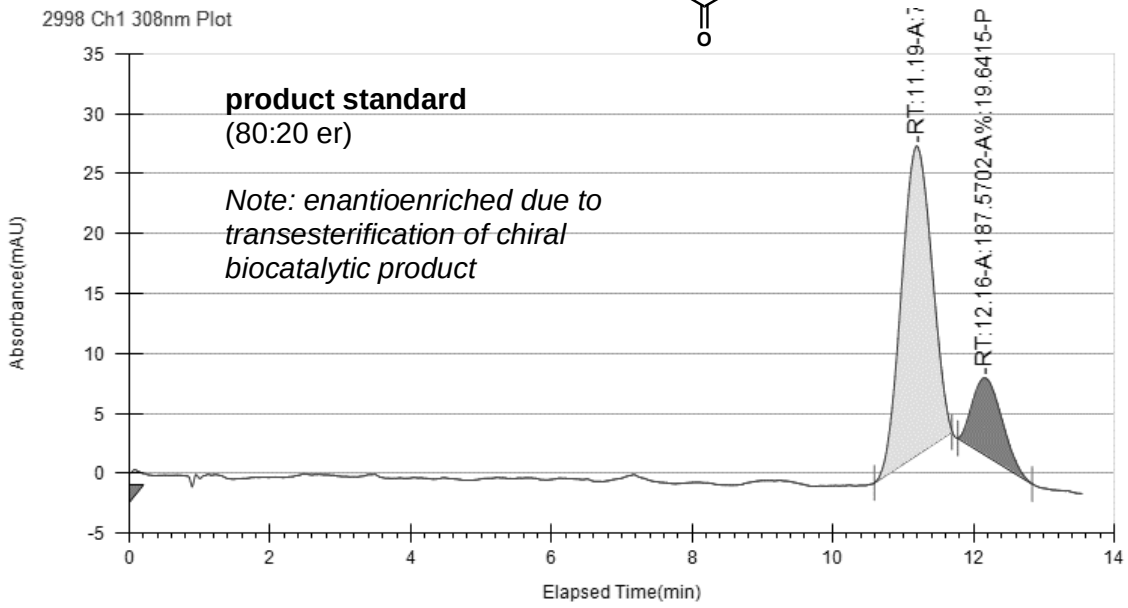

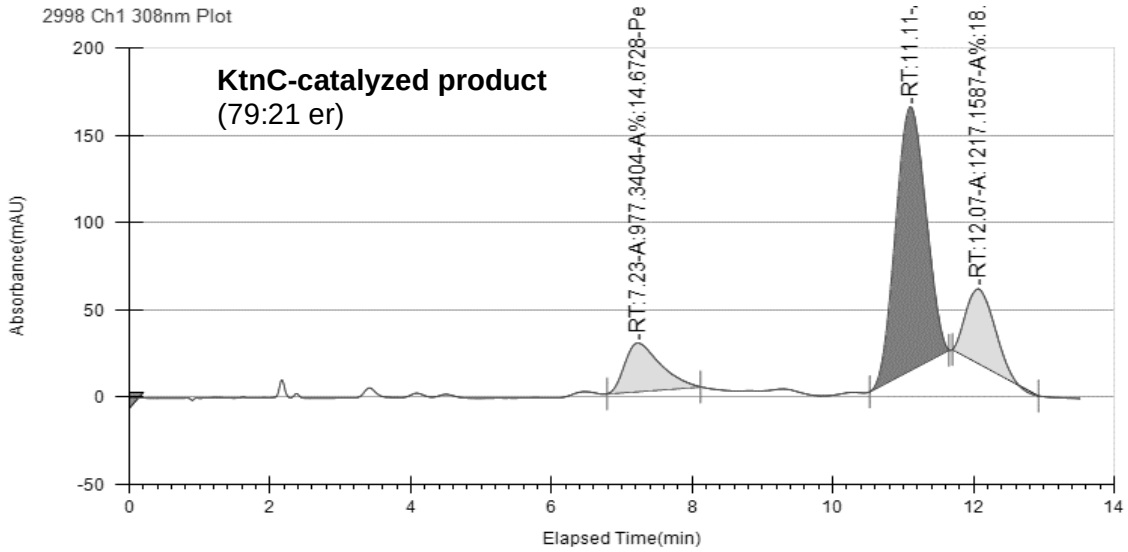

Supplemental Figure S3.108. Chiral resolution of **34** obtained from KtnC-catalyzed oxidative cross-coupling (top) and transesterification (bottom). Atropisomers were resolved by liquid chromatography PDA spectrometry (UPLC) analysis performed on an Agilent 6230 time of flight mass spectrometer with a Dual AJS ESI source and an Agilent 1290 Infinity Series II diode array detector, autosampler, and binary pump, using a Daicel Chiralpak IC-3, 4.6 x 150 mm, 3 µm column under the following conditions: negative mode, phase A = 95:5 deionized water:acetonitrile, B = 95:5 acetonitrile:deionized water; method = 80% A to 0% A over 12.0 min, held at 0% A for 3.0 min, to 80% A over 2.0 minutes. Total of 17.0 minutes with a 1.5 mL/min flow rate, and heating to 30 °C.

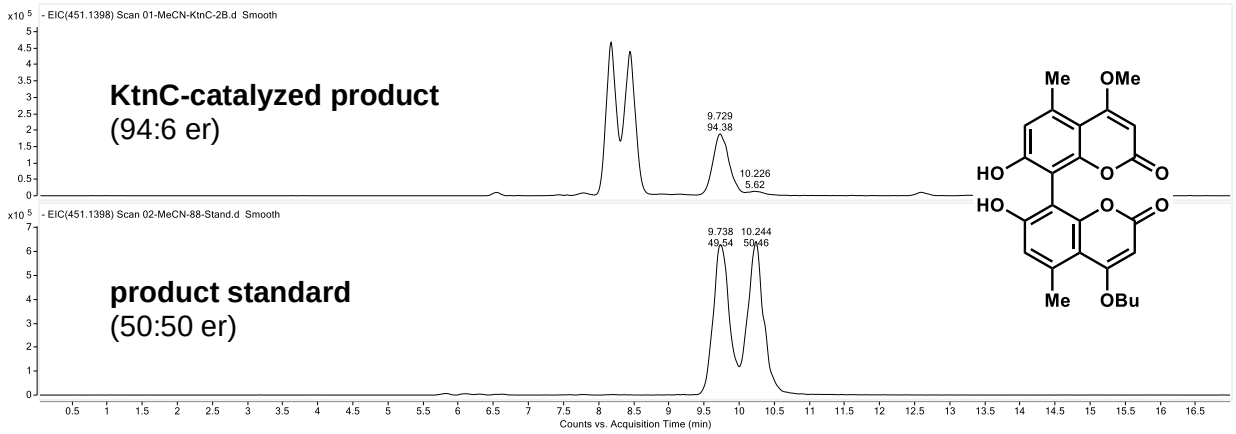

Supplemental Figure S3.109. Chiral resolution of **35** obtained from KtnC-catalyzed oxidative cross-coupling (top) and transesterification (bottom). Atropisomers were resolved by liquid chromatography PDA spectrometry (UPLC) analysis performed on an Agilent 6230 time of flight mass spectrometer with a Dual AJS ESI source and an Agilent 1290 Infinity Series II diode array detector, autosampler, and binary pump, using a Daicel Chiralpak IC-3, 4.6 x 150 mm, 3 µm column under the following conditions: negative mode, phase A = 95:5 deionized water:acetonitrile, B = 95:5 acetonitrile:deionized water; method = 80% A to 0% A over 85.0 min, held at 0% A for 3.0 min, to 80% A over 1.0 minutes, held at 80% A for 1.0 minutes. Total of 90.0 minutes with a 1.5 mL/min flow rate, and heating to 30 °C.

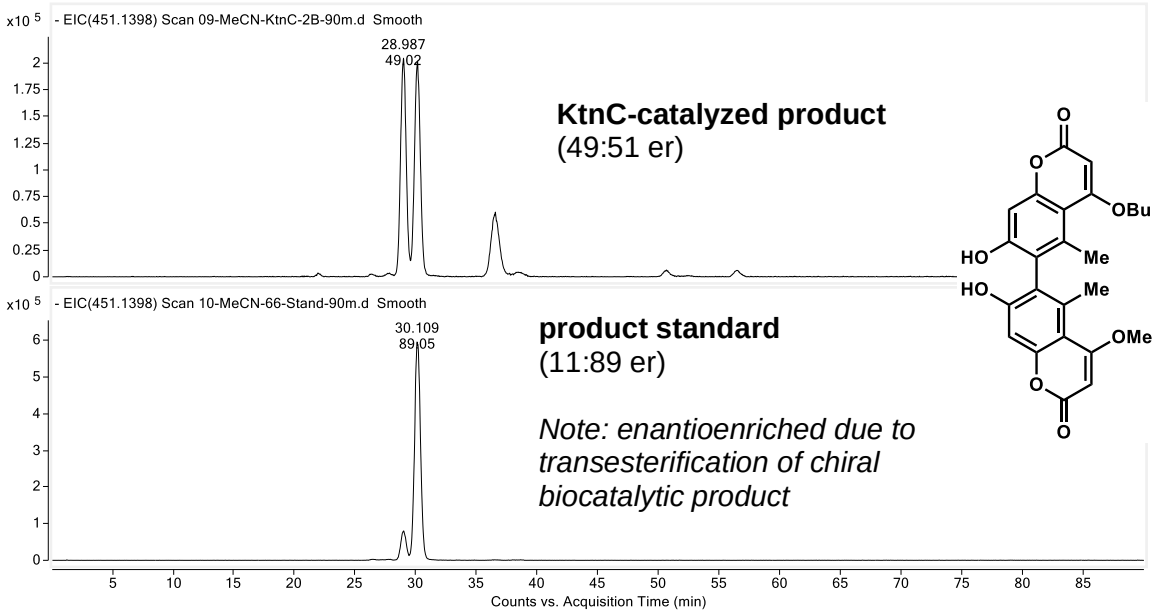

The absolute configurations of compounds **32**-**35** were reported previously.[102]

Preparative scale biocatalytic reactions

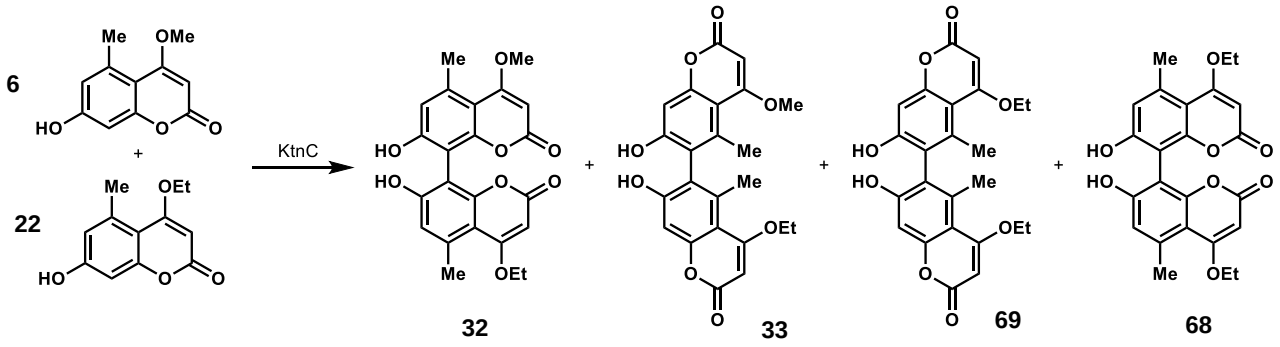

Supplemental Figure S3.110. KtnC-catalyzed cross-coupling of 7-hydroxy-4-methoxy-5-methyl-*2H*-chromen-2-one (6) and 4-ethoxy-7-hydroxy-5-methyl-*2H*-chromen-2-one (22). Cultures containing KtnC were grown to an optical density at 600 nm of 13.2. The biotransformation was performed according to the general procedure in *P. pastoris*, in 2 x 500 mL BMM media at 0.2 mmol **6** (41.2 mg) and 1.0 mmol **22** (220.2 mg) was halted after 96 h (88% conversion). The cell pellet was separated from the supernatant and frozen with liquid nitrogen. The aqueous supernatant was acidified with 1 M HCl (10 mL) and extracted with IPA and ethyl acetate (3x). The organic layers were combined, washed with brine, dried over Na_2SO_4, filtered, and evaporated under reduced pressure. The pellet was ground with a cold mortar and pestle (chilled at –78 °C), acidified with 1 M HCl (5 mL), and extracted with IPA and ethyl acetate by stirring for 2 h. The organic layer was decanted, and the aqueous layer was extracted with IPA and ethyl acetate (2x). The combined organic layers were washed with brine, dried over Na_2SO_4, filtered, and evaporated under reduced pressure. The crude solids were purified by flash column chromatography (8:3:1 toluene/ethyl acetate/formic acid v/v) then reversed-phase (Phenomenex Kinetex 5 µm C18, 150 x 21.2 mm column) under the following conditions: mobile phase A = deionized water + 0.1% formic acid and B = acetonitrile + 0.1% formic acid; method = 70% A for 5 min, 70% A to 65% A over 2.0 min, 65% A for 5.0 min, 65% A to 60% A over 2.0 min, 60% A for 5.0 min, 60% A to 40% A over 5.0 min, 40% A for 2.0 min, 40% A to 10% A over 4.0 min, 10% A for 1.0 min, 254 and 308 nm UV detection and 12 mL/min flow rate. The 8,8'-cross-coupled product **23** and substrate co-eluted as a 3:1 mixture from 11.6-15.0 min to provide 6.8 mg (6.8% yield, cross-coupled product). The 6,6'-cross-coupled product **33** and 8,8'-product **68** co-eluted as a 1:1 mixture from

16.6-19.6 min to provide 5.8 mg (2.8 mg, 3.3% isolated yield **33** and 3.0 mg, 1.4% isolated yield **68**, respectively). The 6,6'-product **69** eluted from 21.6-25.3 min to provide 9.4 mg (4.3% isolated yield).

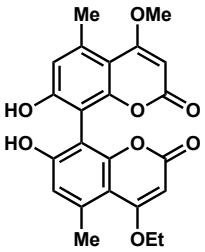

4-ethoxy-7,7'-dihydroxy-4'-methoxy-5,5'-dimethyl-*2H,2'H*-[8,8'-bichromene'-2,2'-dione (32). **^{1}H NMR** (400 MHz, $(CD_3)_2O$) δ6.76 (s, 2H), 5.50 (s, 1H), 5.45 (s, 1H), 4.25 (q, *J* = 7.0, 2H), 4.02 (s, 3H), 2.67 (s, 3H), 2.64 (s, 3H), 1.54 (t, *J* = 7.0, 3H); **^{1}H NMR** (600 MHz, $(CD_3)SO$) δ 10.32 (s, 2H), 6.71 (s, 2H), 5.57 (s, 1H), 5.53 (s, 1H), 4.18 (q, *J* = 7.1, 2H), 3.94 (s, 3H), 2.62 (s, 3H), 2.59 (s, 3H), 1.44 (t, *J* = 6.9, 3H); **^{13}C NMR** (150 MHz, $(CD_3)SO$) δ169.7, 168.7, 161.8, 161.7, 158.7, 158.7, 154.0, 154.0, 137.1, 137.0, 115.7, 115.7, 106.0, 106.0, 105.8, 105.8, 86.6, 86.4, 65.3, 56.5, 23.4, 23.2, 14.0; **98:2 er** (see Supplemental Figure S61); **HRMS** (ESI) calculated for $C_{23}H_{21}O_8^+$ $[M+H]^+$ = 425.1231, found 425.1236 *m/z*.

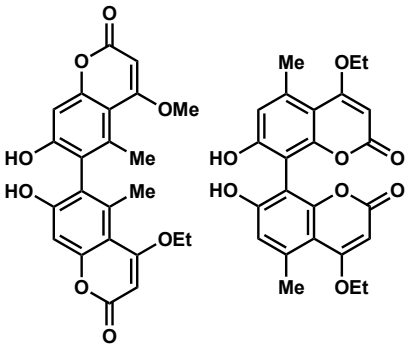

4-ethoxy-7,7'-dihydroxy-4'methoxy-5,5'-dimethyl-*2H,2H*'-[6,6'-bichromene]-2,2'-dione (33) and 4,4'-ethoxy-7,7'-dihydroxy-5,5'-dimethyl-*2H,2H*'-[8,8'-bichromene]-2,2'-dione (68), 1:1 ratio: **^{1}H NMR** (600 MHz, CD_3OD) δ 6.72 (s, 2H), 5.63 (s, 2H), 4.19 (t, *J* = 6.3, 4H), 2.33 (s, 6H), 1.87 (q, *J* = 7.0, 6.5, 4H, 1.54 (q, *J* =7.7, 4H), 1.00 (t, *J* = 7.4, 6H); cross-coupled-product **24**, 79:21 er; **HRMS** (ESI) calculated for $C_{23}H_{21}O_8^+$ $[M+H]^+$ =

425.1231, found = 425.1239 *m/z*, and for $C_{24}H_{23}O_8^+$ $[M+H]^+$ = 439.1387, found = 439.1395 *m/z*.

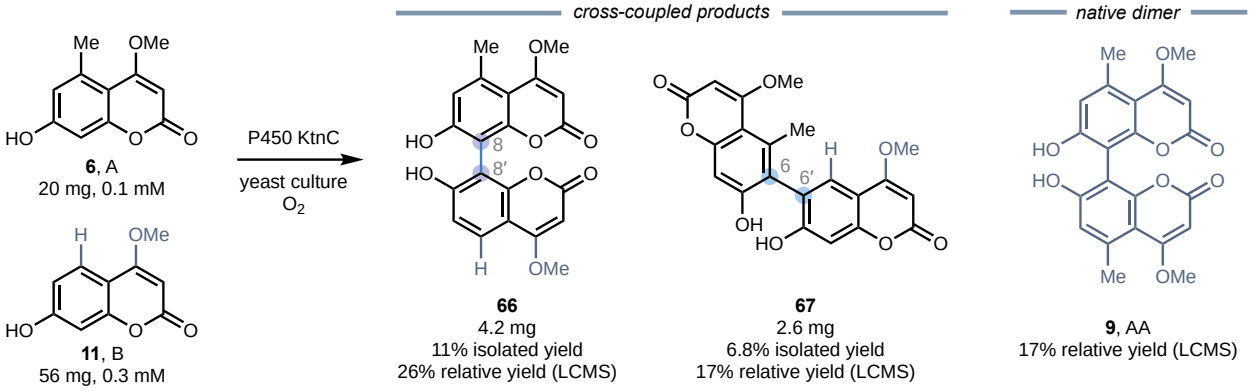

Supplemental Figure S3.111. KtnC-catalyzed cross-coupling of 7-hydroxy-4-methoxy-5-methyl-*2H*-chromen-2-one (6) and 7-hydroxy-4-methoxy-2*H*-chromen-2-one (11). Cultures containing KtnC were grown to an optical density at 600 nm of 13.2. The biotransformation was performed according to the general procedure in *S. cerevisiae*, in 2 x 500 mL H- minimal media at 0.1 mmol **6** (20.0 mg) and 0.3 mmol **11** (56.1 mg) was halted after 96 h (43% conversion). The supernatant and pellet were extracted with ethyl acetate (3x). The organic layers were combined, washed with brine, dried over Na_2SO_4, filtered, and evaporated under reduced pressure. The crude solids were purified by flash column chromatography (8:3:1 toluene/ethyl acetate/formic acid v/v) then reversed-phase (Phenomenex Kinetex 5 µm C18, 150 x 21.2 mm column) under the following conditions: mobile phase A = deionized water + 0.1% formic acid and B = acetonitrile + 0.1% formic acid; method = 70% A for 5 min, 70% A to 65% A over 2.0 min, 65% A for 5.0 min, 65% A to 60% A over 2.0 min, 60% A for 5.0 min, 60% A to 40% A over 5.0 min, 40% A for 2.0 min, 40% A to 10% A over 4.0 min, 10% A for 1.0 min, 254 and 308 nm UV detection and 12 mL/min flow rate. The 8,8'-cross-coupled product **66** was recovered as an off-white solid (4.2 mg) for a yield of 11% yield. The 6,6'-cross-coupled product **67** was recovered as an yellowish-brown solid (2.6 mg) for a yield of 6.8% yield.

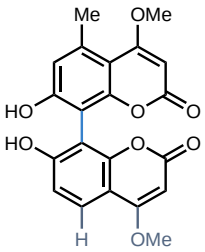

7,7'-dihydroxy-4,4'-dimethoxy-5-methyl-2*H*,2'*H*-[8,8'-bichromene]-2,2'-dione (66): **^{1}H NMR** (600 MHz, Methanol-d_4) δ 7.78 (d, J = 8.8 Hz, 1H), 6.94 (d, J = 8.8 Hz, 1H), 6.75 (s, 1H), 5.63 (s, 1H), 5.59 (s, 1H), 4.04 (s, 3H), 4.01 (s, 3H), 2.68 (s, 3H). **HRMS** (ESI) calculated for $C_{21}H_{17}O_8^+$ $[M+H]^+$ = 397.0918, found = 397.0926 *m/z*.

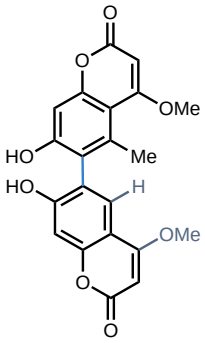

7,7'-dihydroxy-4,4'-dimethoxy-5-methyl-2*H*,2'*H*-[6,6'-bichromene]-2,2'-dione (67): **^{1}H NMR** (600 MHz, Methanol-d_4) δ 8.54 (s, 1H), 7.48 (s, 1H), 6.83 (s, 1H), 6.71 (s, 1H), 5.67 (s, 1H), 5.65 (s, 1H), 4.01 (s, 3H), 3.99 (s, 3H), 2.37 (s, 3H). **HRMS** (ESI) calculated for $C_{21}H_{17}O_8^+$ $[M+H]^+$ = 397.0918, found = 397.0919 *m/z*.

^{1}H NMR and ^{13}C NMR spectra of compounds

S3.112. 82: ^{1}H NMR (400 MHz, DMSO-d_6)

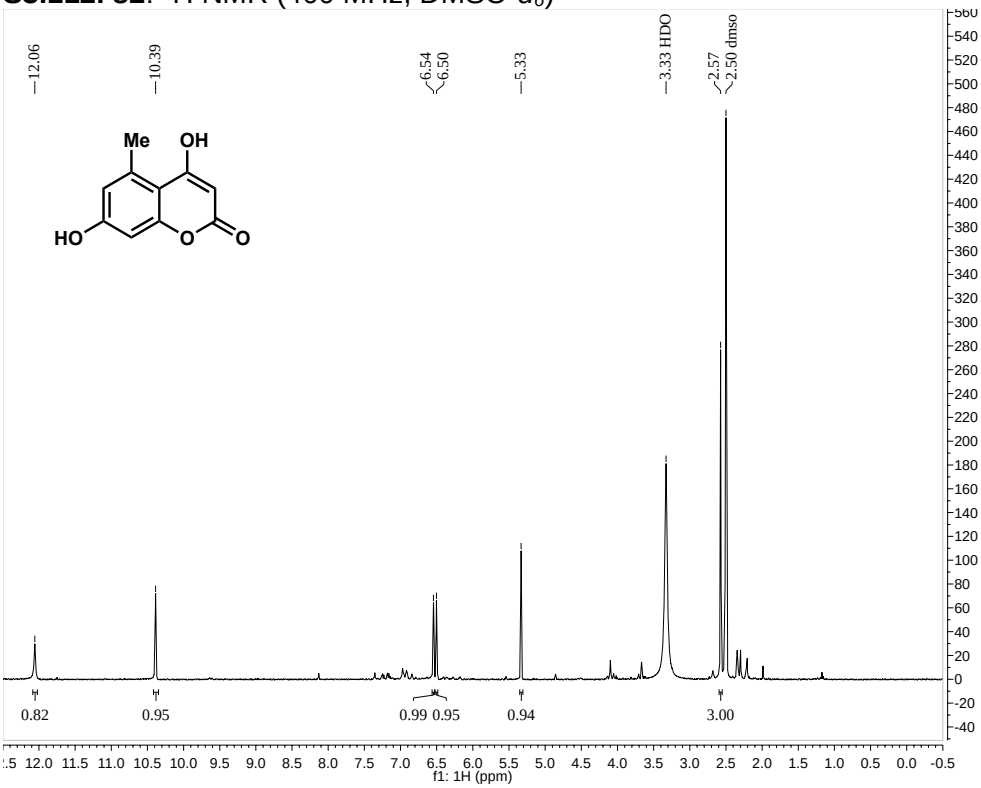

82: ^{13}C NMR (150 MHz, DMSO-d_6)

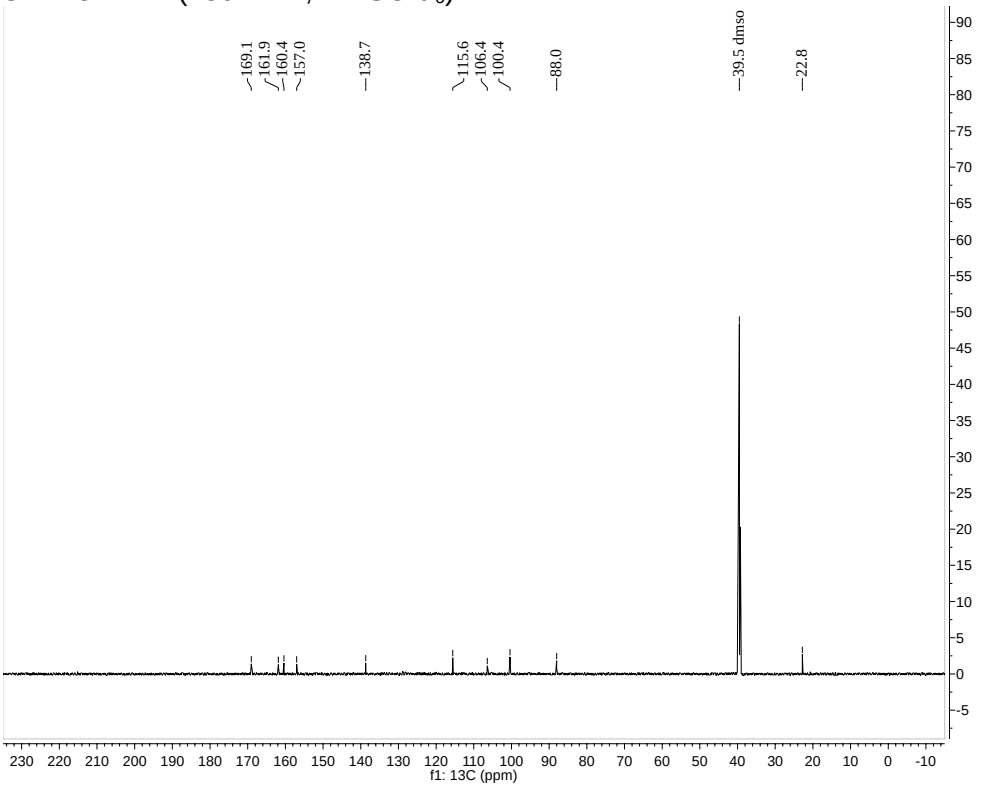

S3.113. 11: ^{1}H NMR (600 MHz, DMSO-d_6)

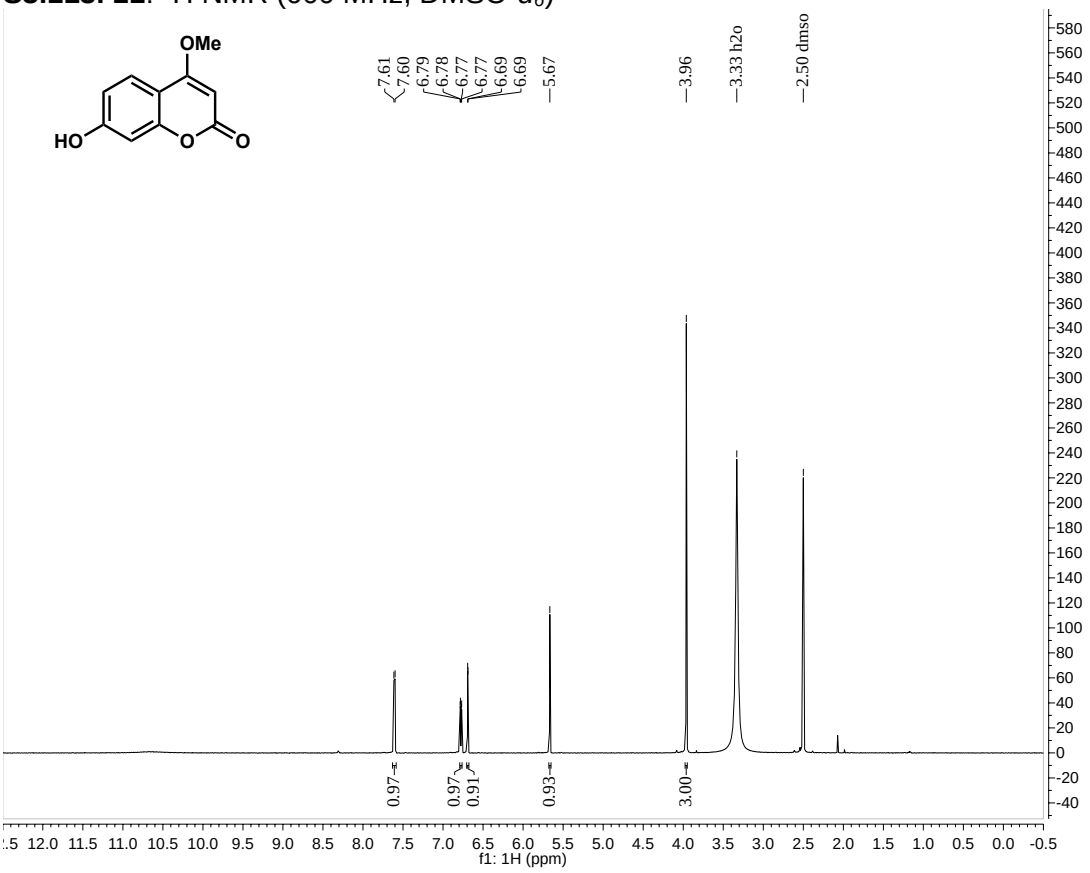

S3.114. 12: ^{1}H NMR (400 MHz, DMSO-d_6)

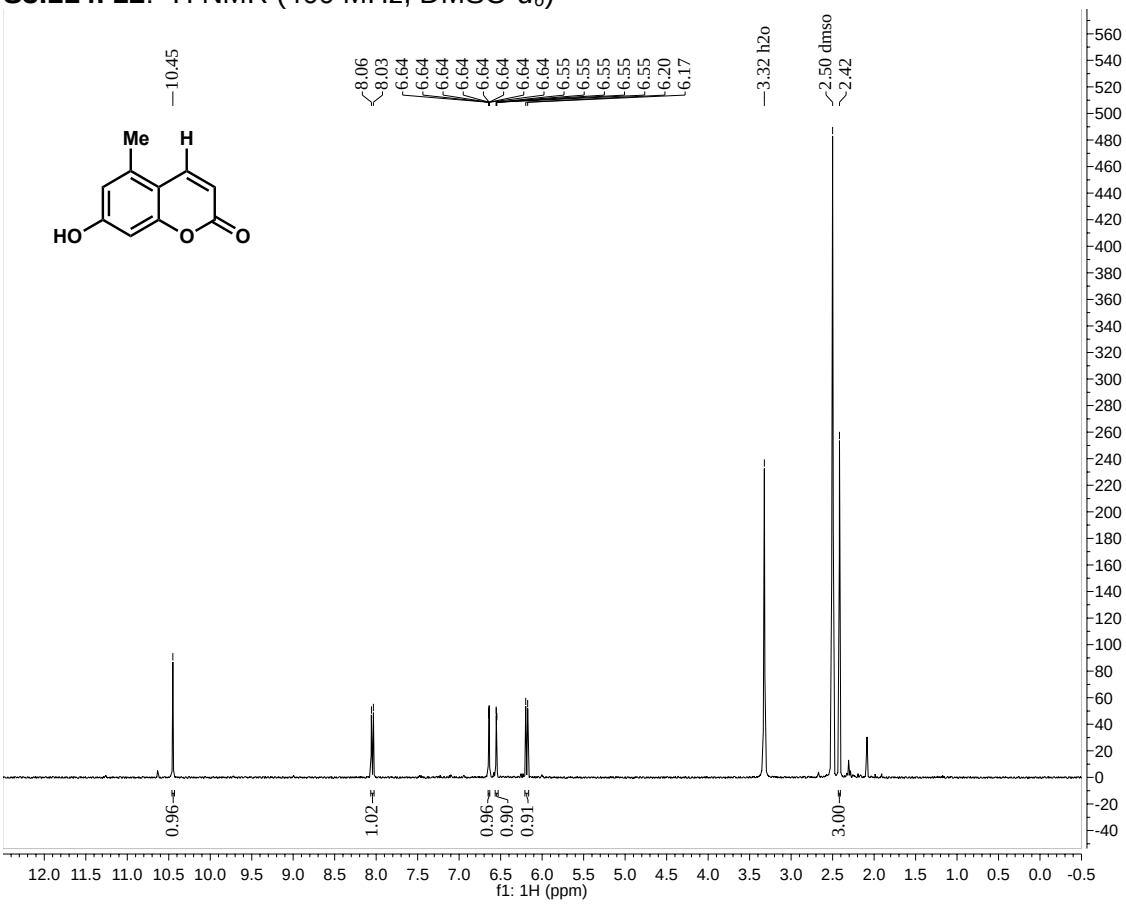

S3.115. 83: ^{1}H NMR (400 MHz, acetone-d_6)

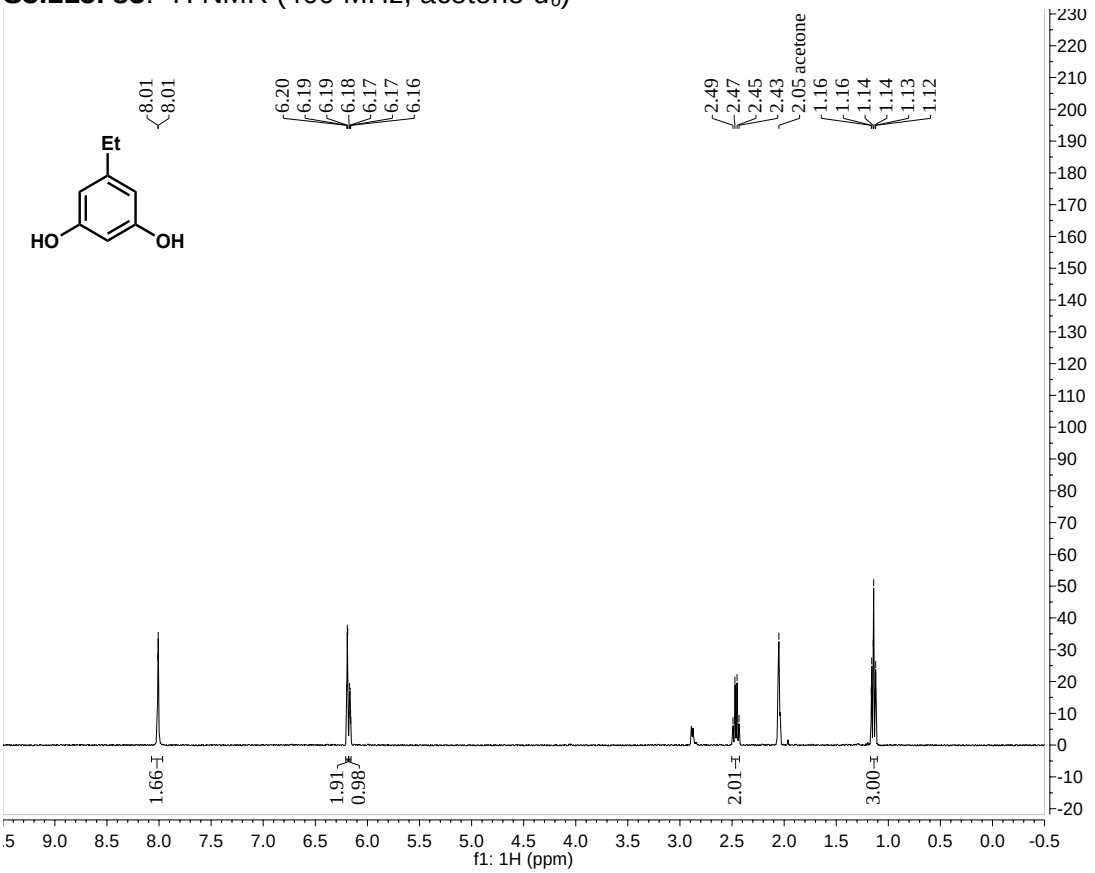

S3.116. 84: ^{1}H NMR (600 MHz, DMSO-d_6)

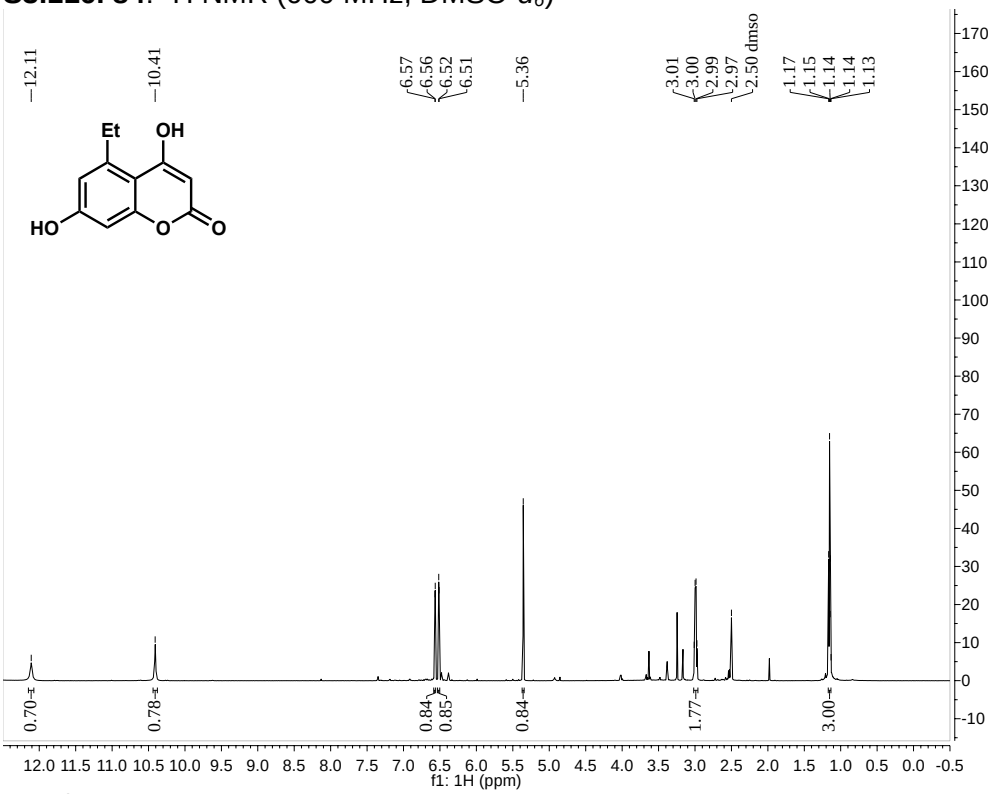

84: ^{13}C NMR (150 MHz, DMSO-d_6)

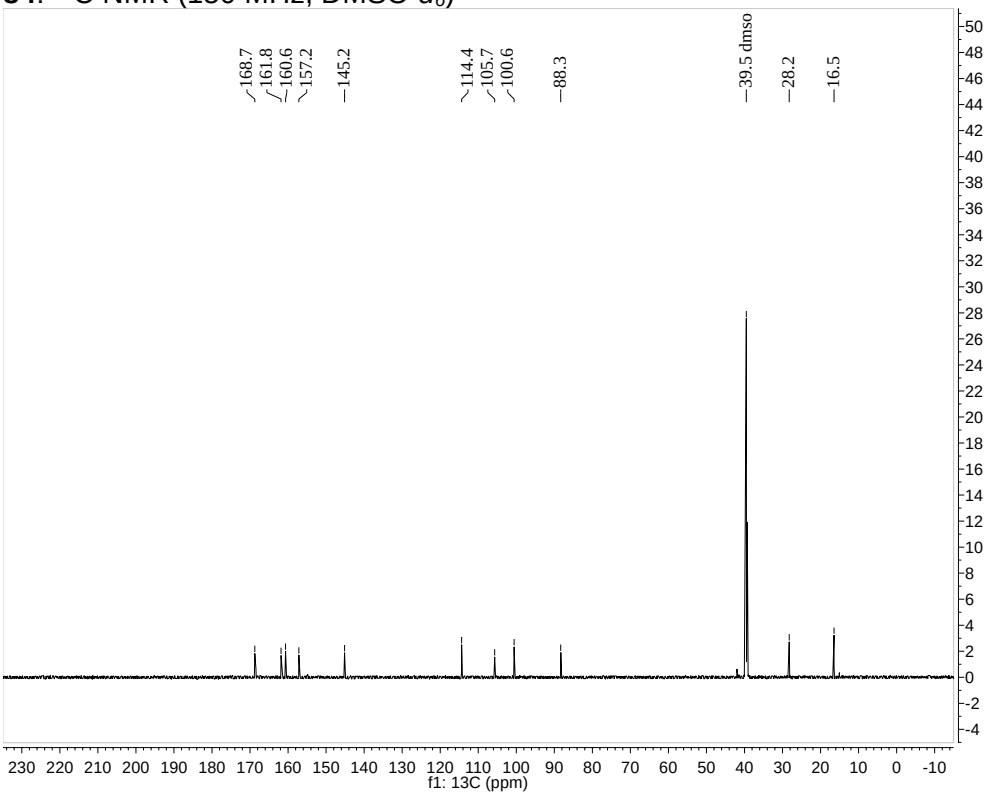

S3.117. 16: ^{1}H NMR (600 MHz, DMSO-d_6)

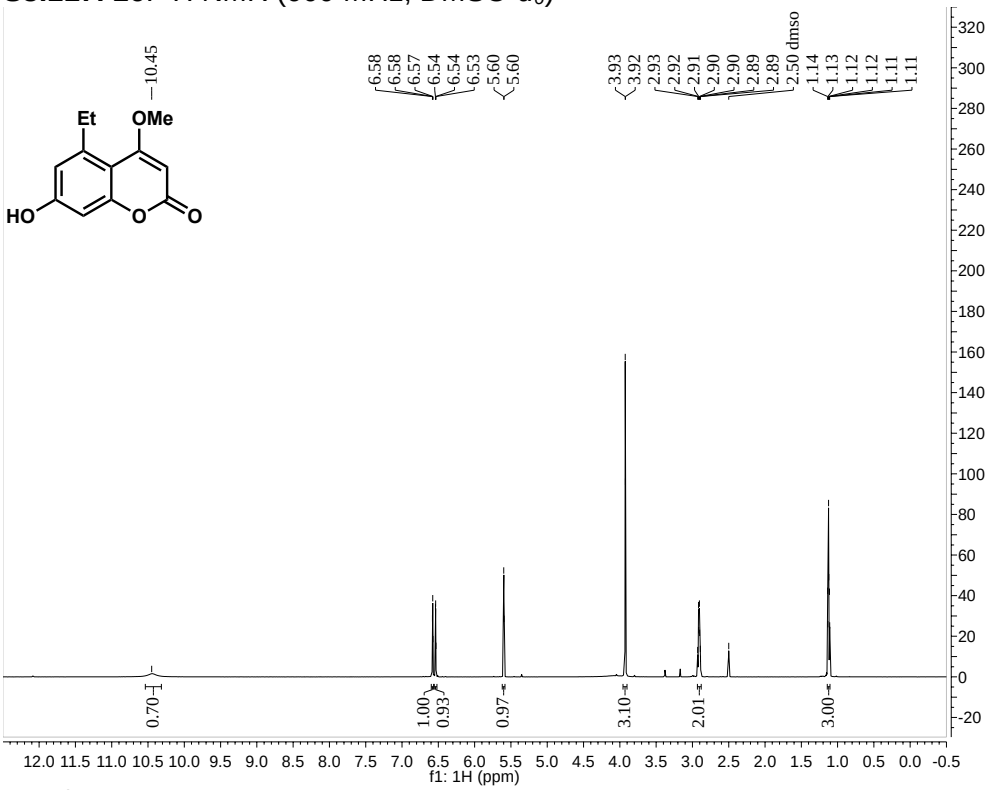

16: ^{13}C NMR (150 MHz, DMSO-d_6)

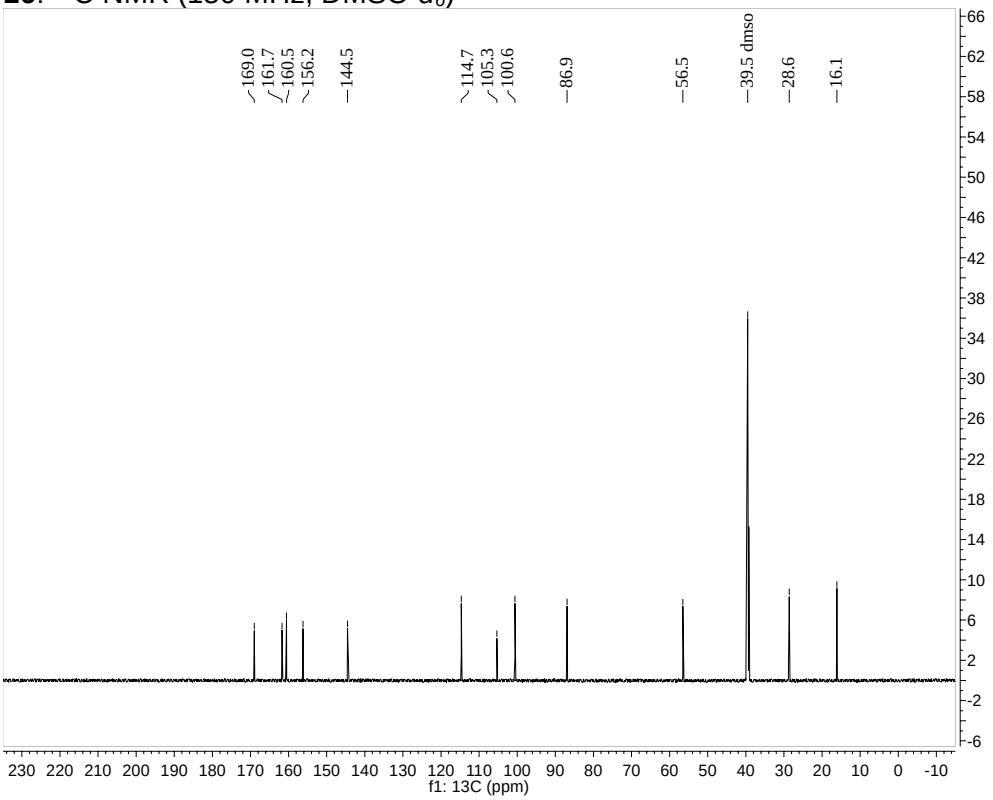

S3.118. 85: ^{1}H NMR (400 MHz, CD_3OD)

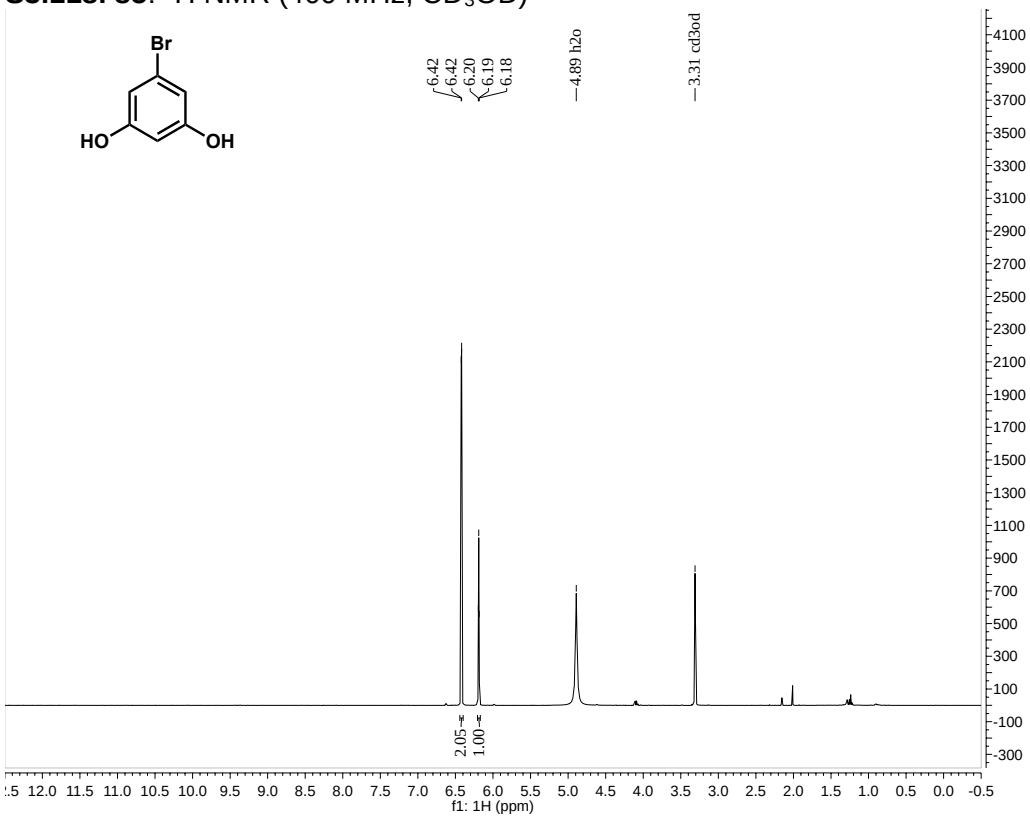

S3.119. 19: ^{1}H NMR (600 MHz, DMSO-d_6)

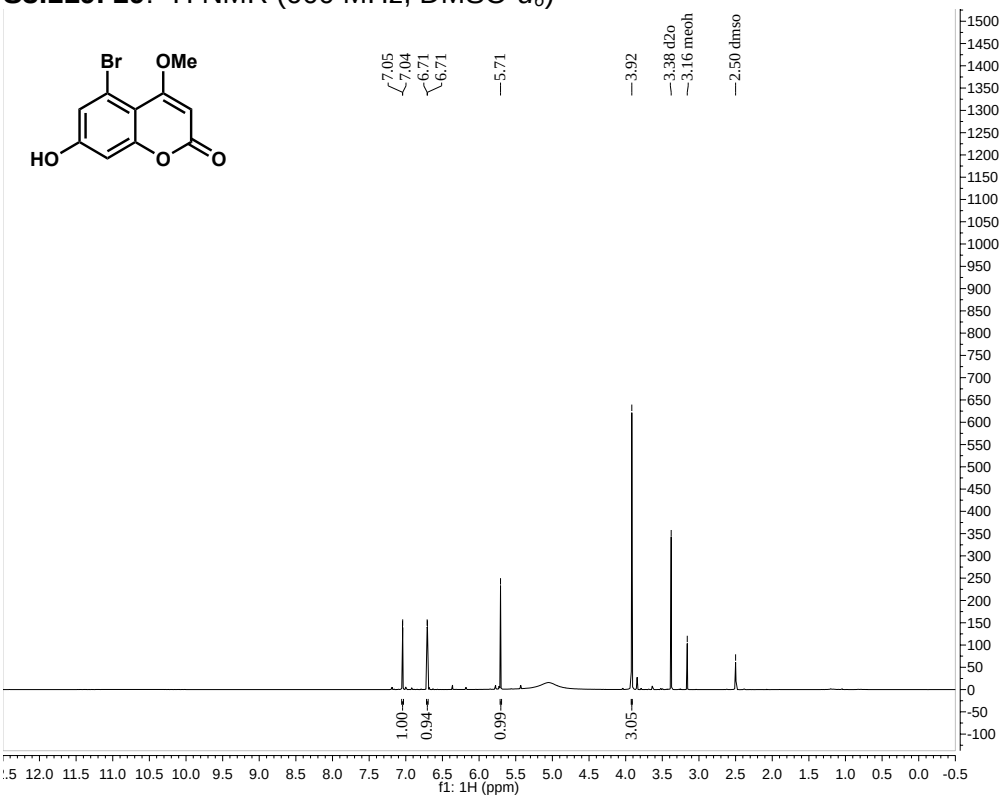

19: ^{13}C NMR (150 MHz, DMSO-d_6)

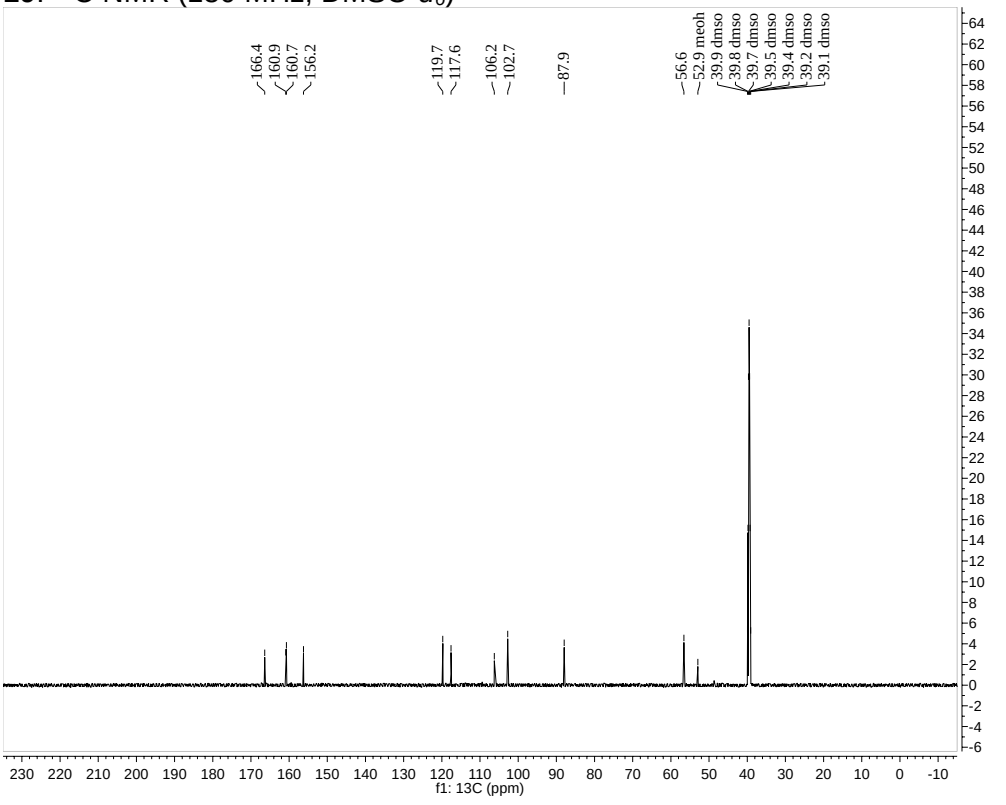

S3.120. 86: ^{1}H NMR (600 MHz, DMSO-d_6)

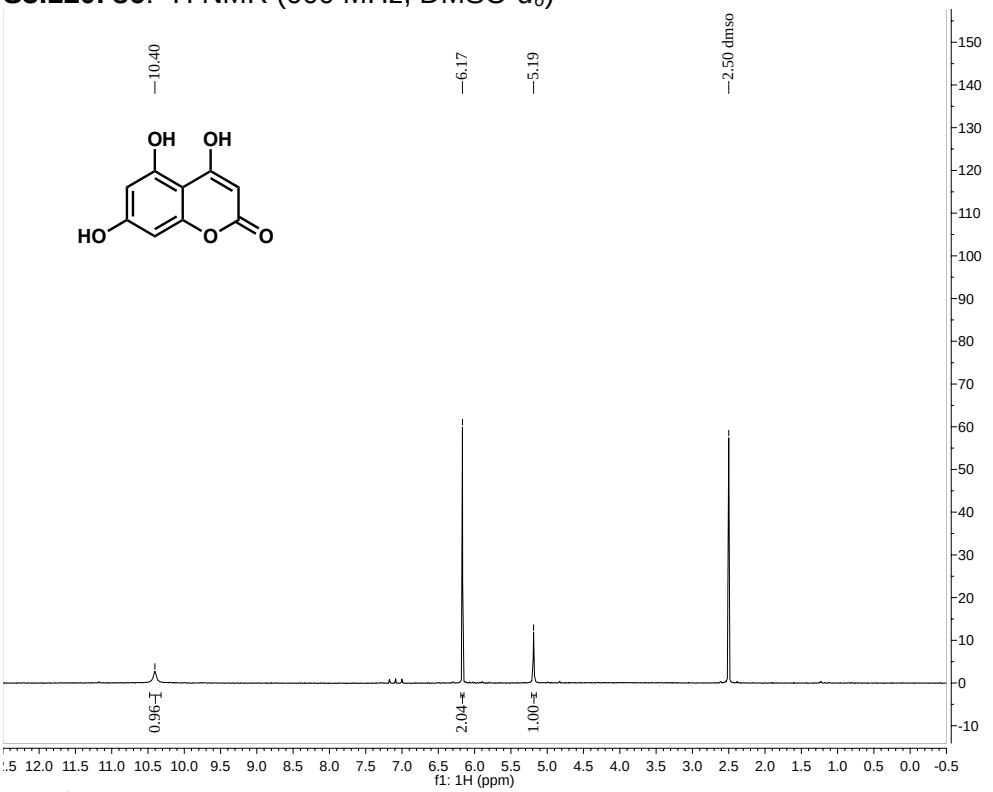

86: ^{13}C NMR (150 MHz, DMSO-d_6)

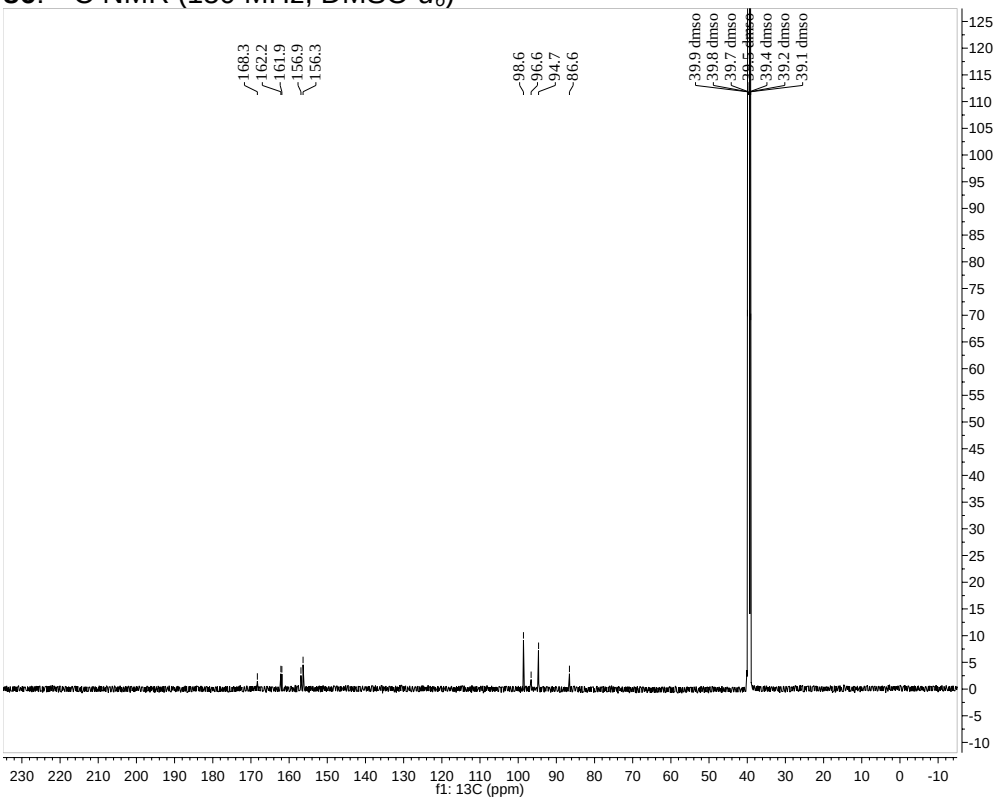

S3.121. 20: ^{1}H NMR (600 MHz, DMSO-d_6)

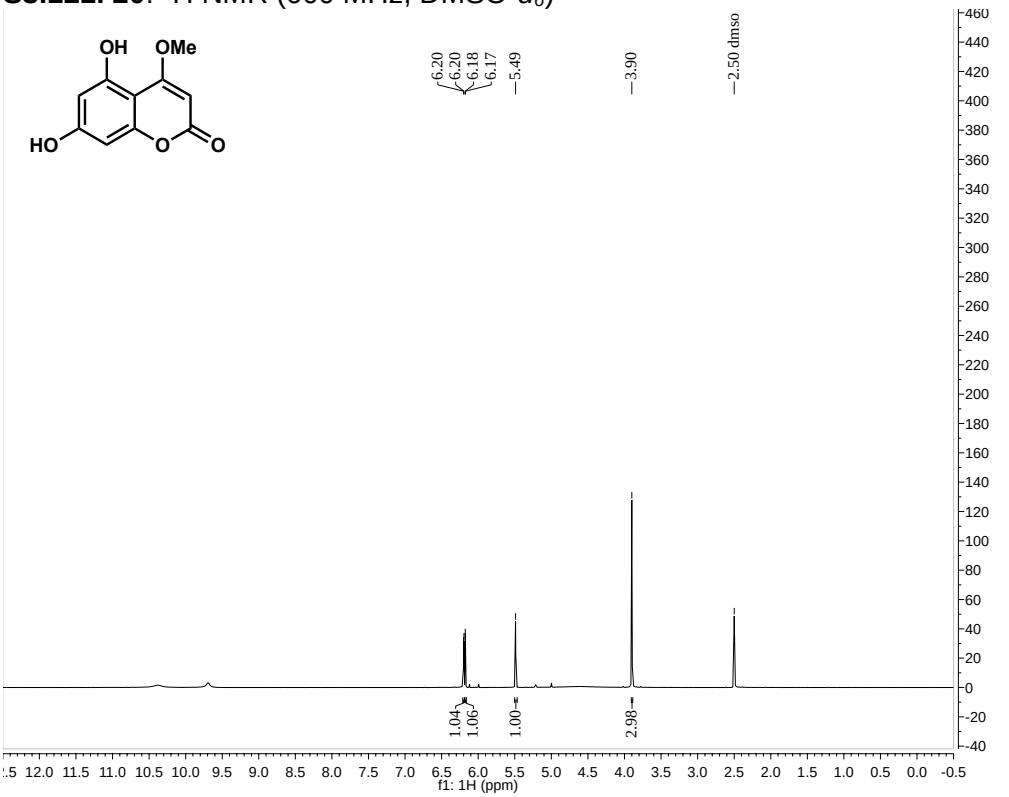

20: ^{13}C NMR (150 MHz, DMSO-d_6)

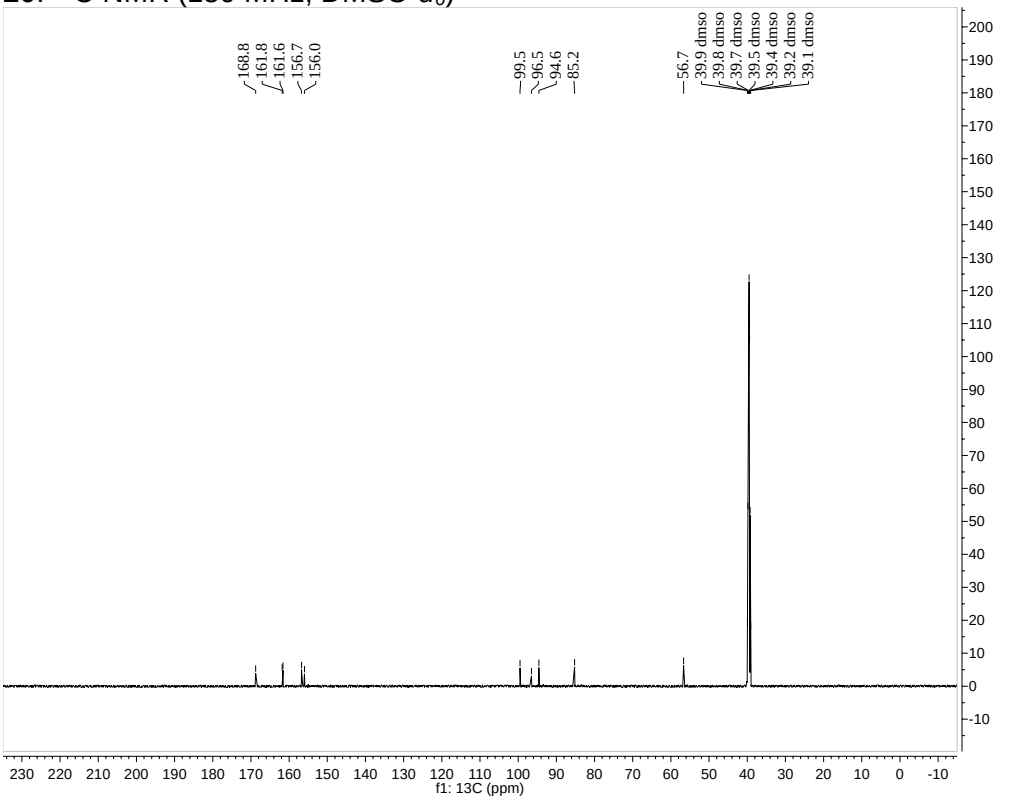

S3.122. 24: ^{1}H NMR (600 MHz, acetone-d_6)

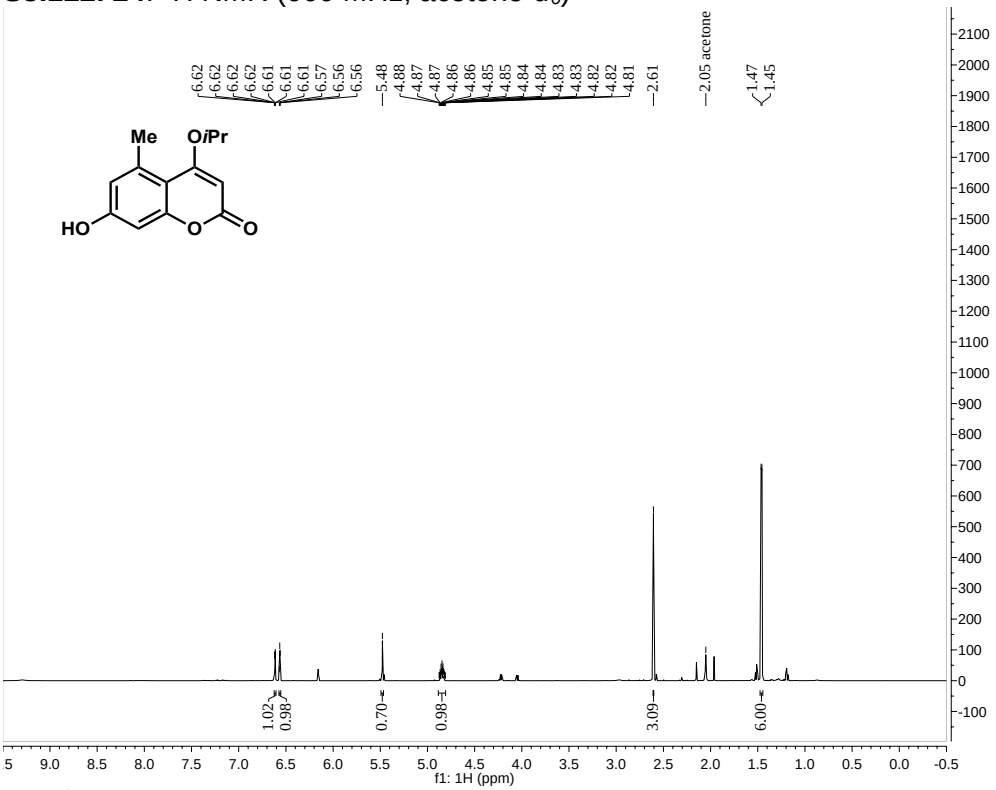

24: ^{13}C NMR (150 MHz, acetone-d_6)

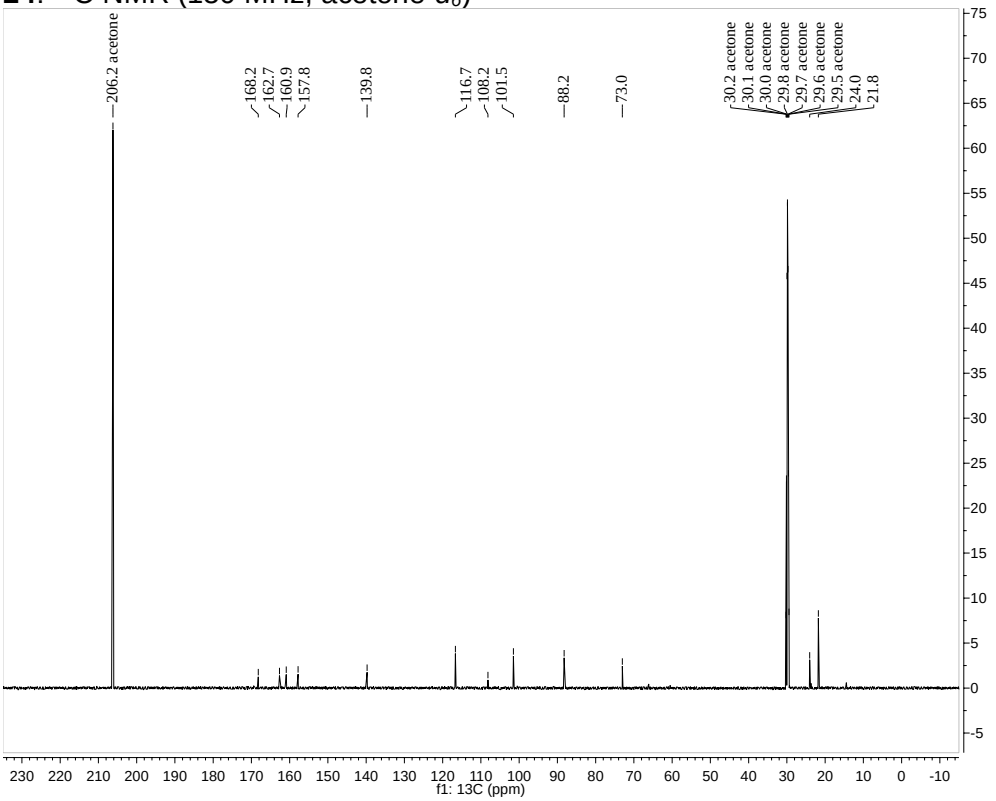

S3.123. 26: ^{1}H NMR (600 MHz, Acetone-d_6)

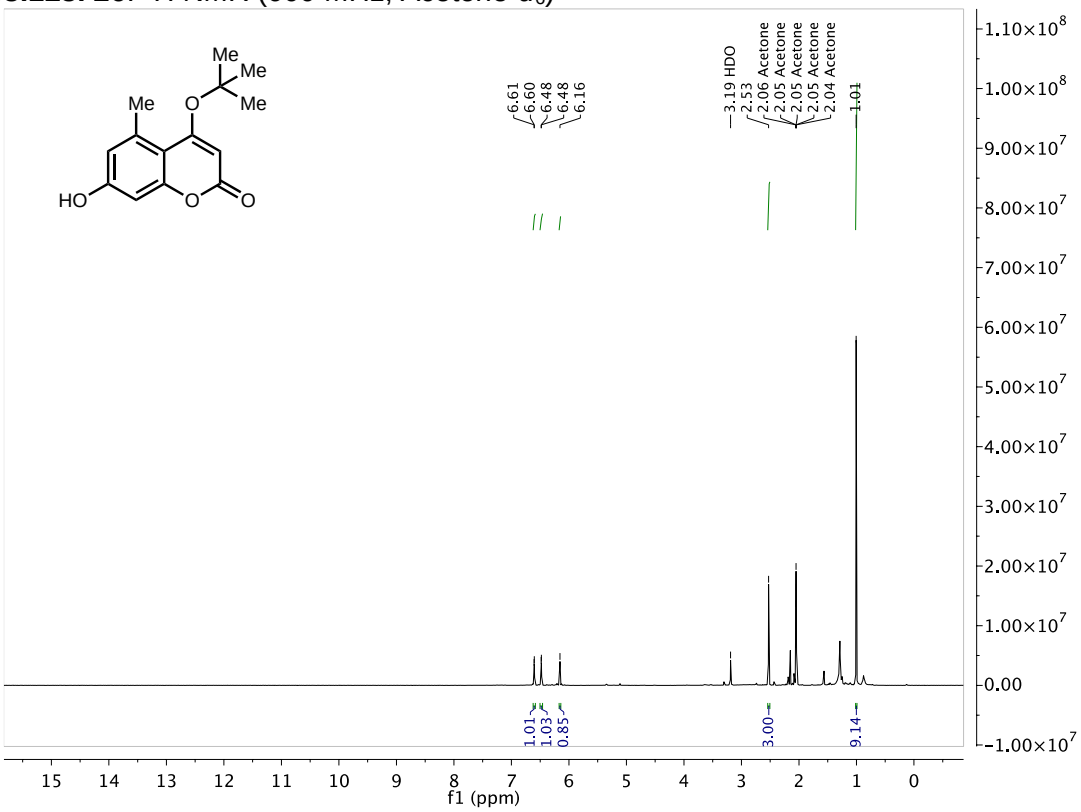

26: ^{13}C NMR (150 MHz, Acetone-d_6)

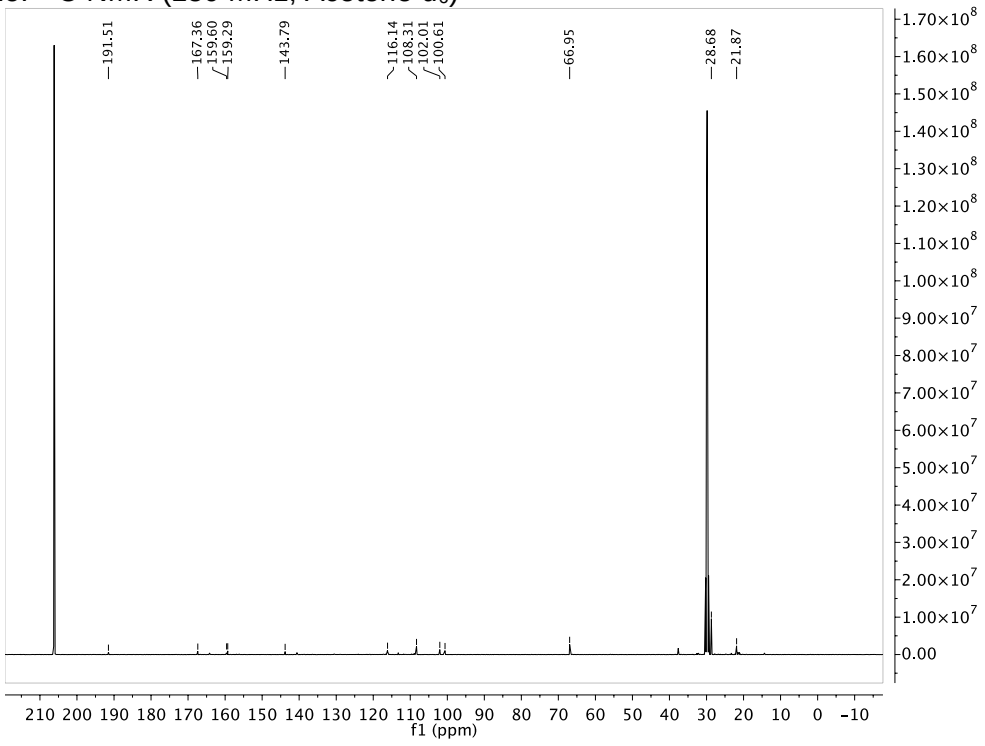

Supplemental Figure S3.124. Crude ^{1}H NMR (600 MHz, acetone-d_6) from oxidative cross-coupling of **12** and **31** (**Figure 3.19, Entry 2a**).

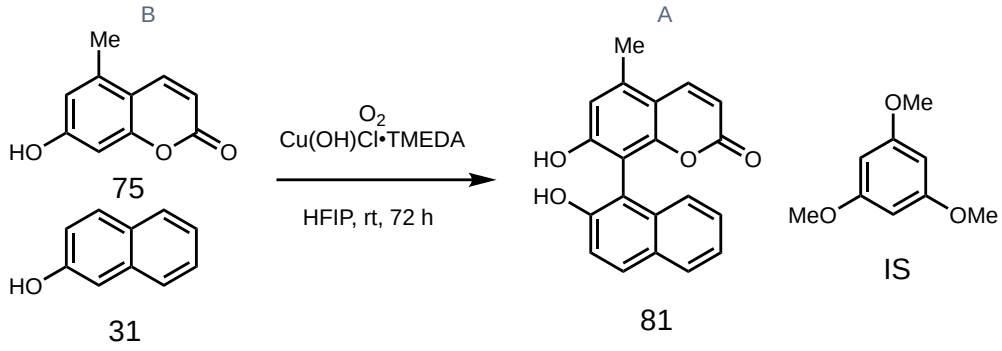

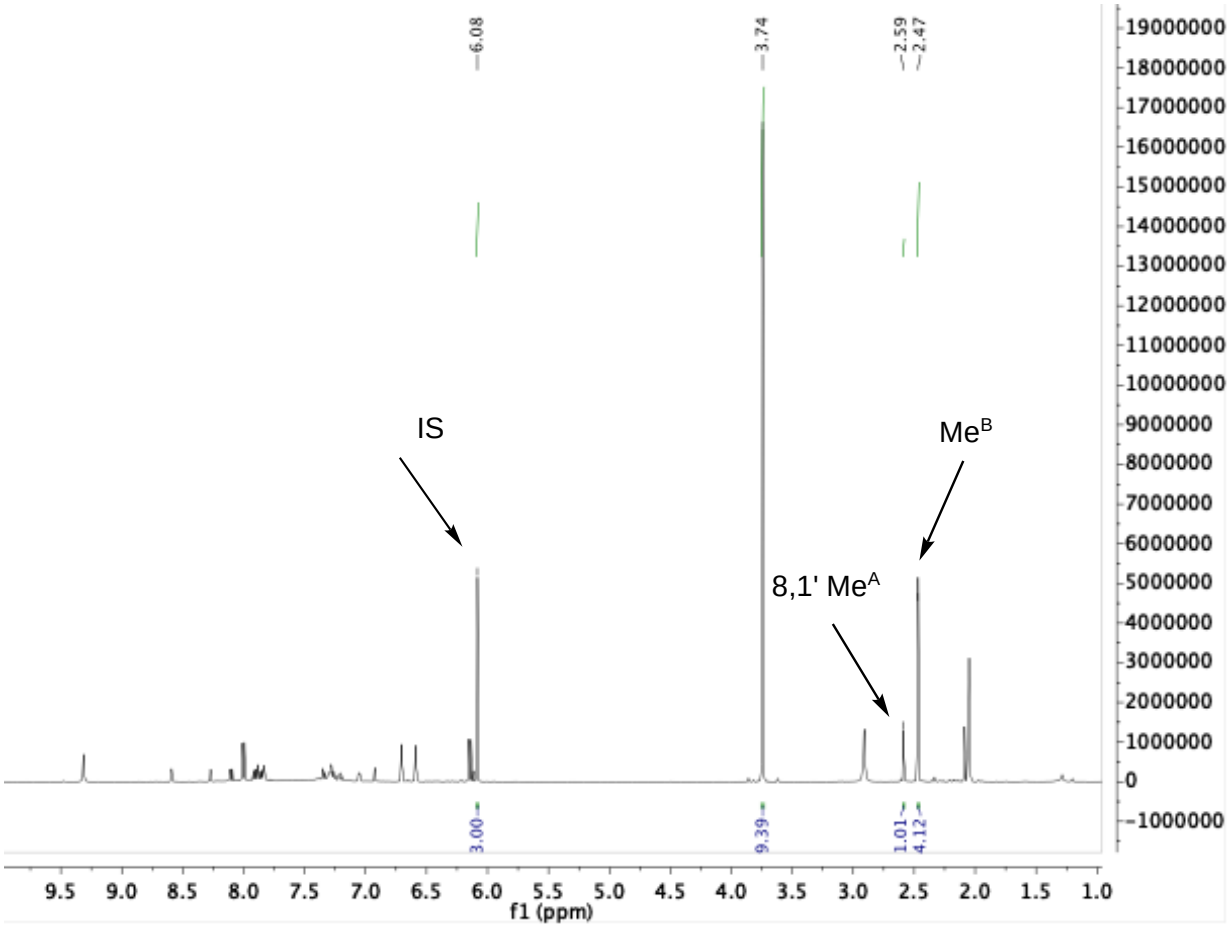

mg crude	mg sample	mg IS	mmol IS	Molar ratio	mg 8,1' sample	mg 8,1' reaction
111	20.5	5.0	0.029	0.336	3.2	17.3

Supplemental Figure S3.125. Crude ^{1}H NMR (600 MHz, $CDCl_3$) from oxidative cross-coupling of **75** and **31** (**Figure 3.19, Entry 3b**).

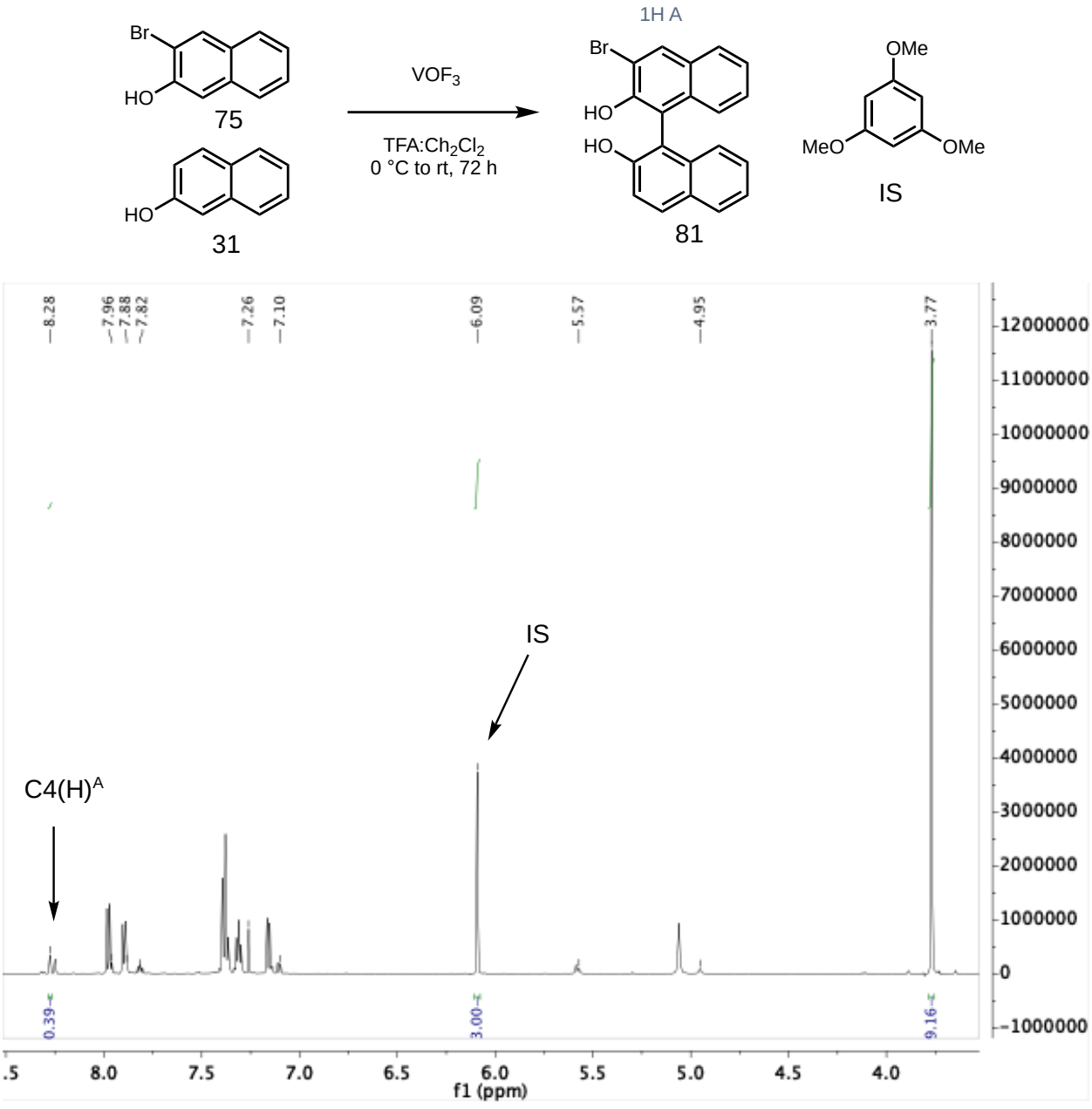

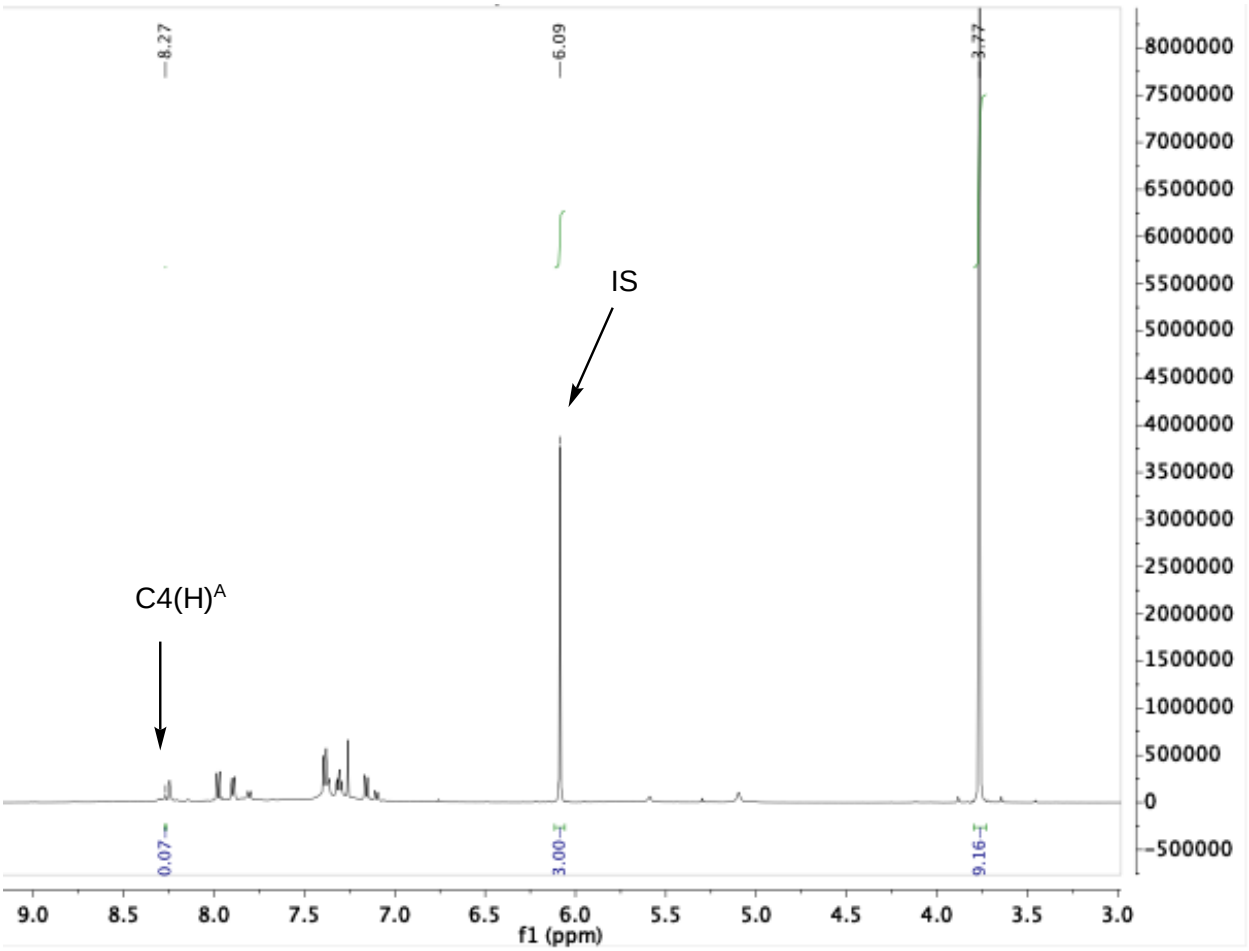

Fraction	mg fraction	mg IS	mmol IS	Molar ratio	mmol 8,1'	mg 8,1'
2	28.6	5.60	0.033	0.39	0.013	4.7
3-5	33.4	7.50	0.045	0.07	0.003	1.1

Supplemental Figure S3.126. Crude ^{1}H NMR (600 MHz, $CDCl_3$) from oxidative cross-coupling of **75** and **31** (**Figure 3.19, Entry 3c**).

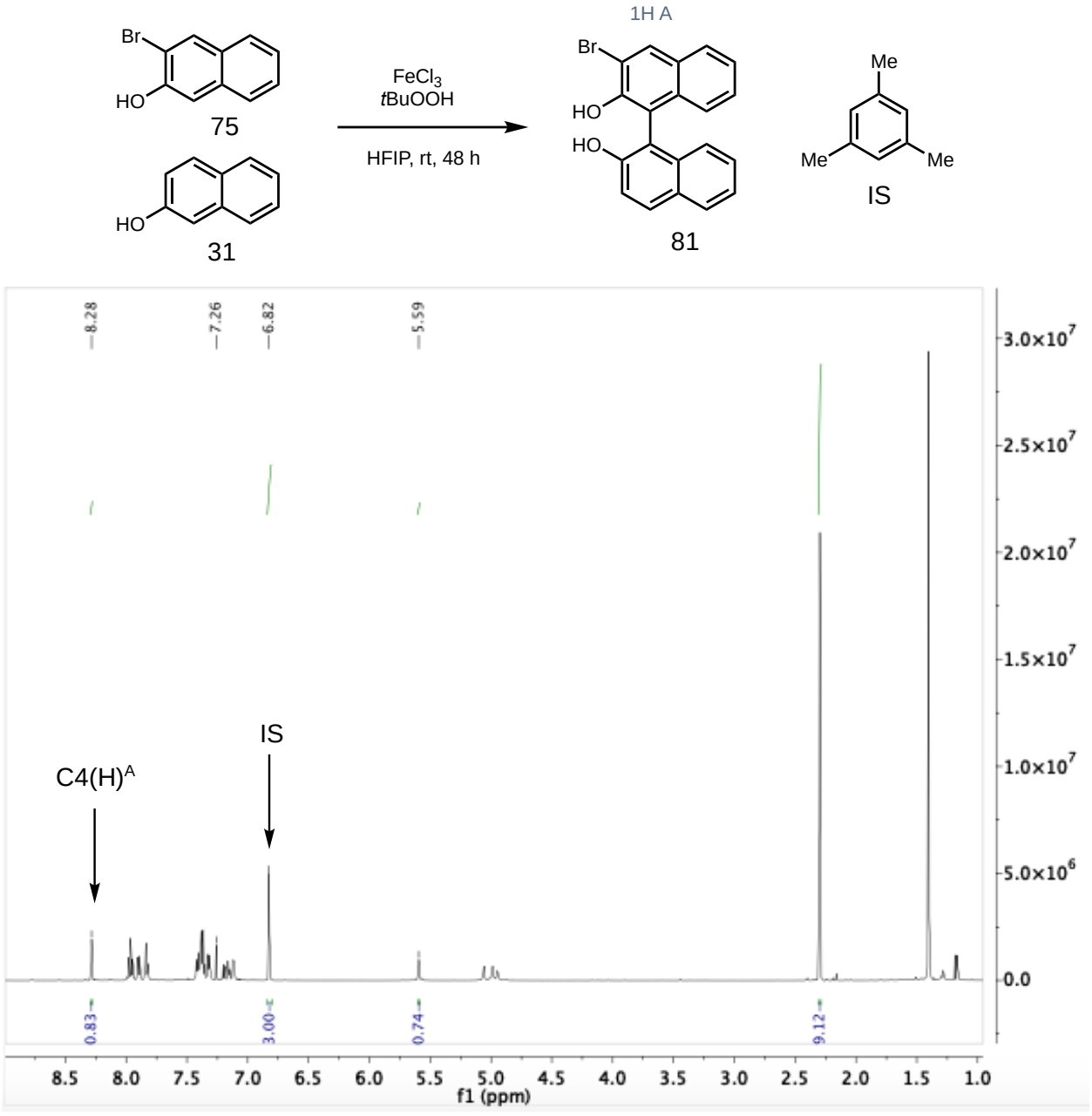

fractions	mg sample	mg IS (97% purity)	mmol IS	Molar ratio	mmol 8,1'	mg 8,1'
4 & 5	36.2	5.0	0.0404	0.83	0.0335	17.3

S3.127. **9**: ^{1}H NMR (400 MHz, DMSO-d_6)

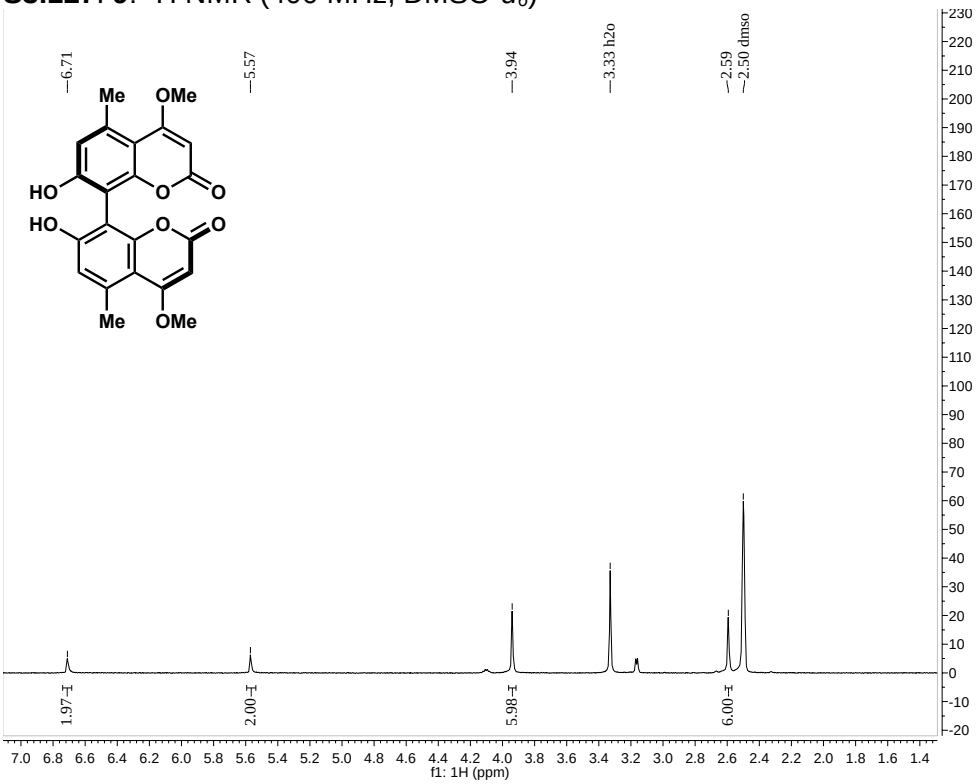

^{1}H NMR (400 MHz, CD_3OD)

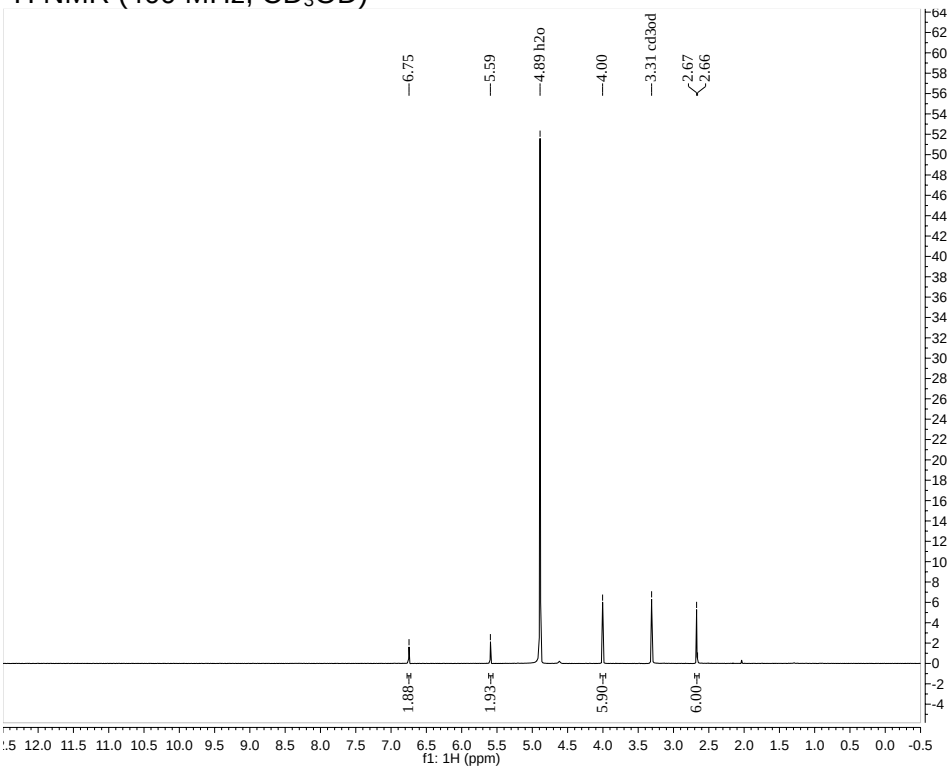

S3.128. **63**: ^{1}H NMR (400 MHz, DMSO-d_6)

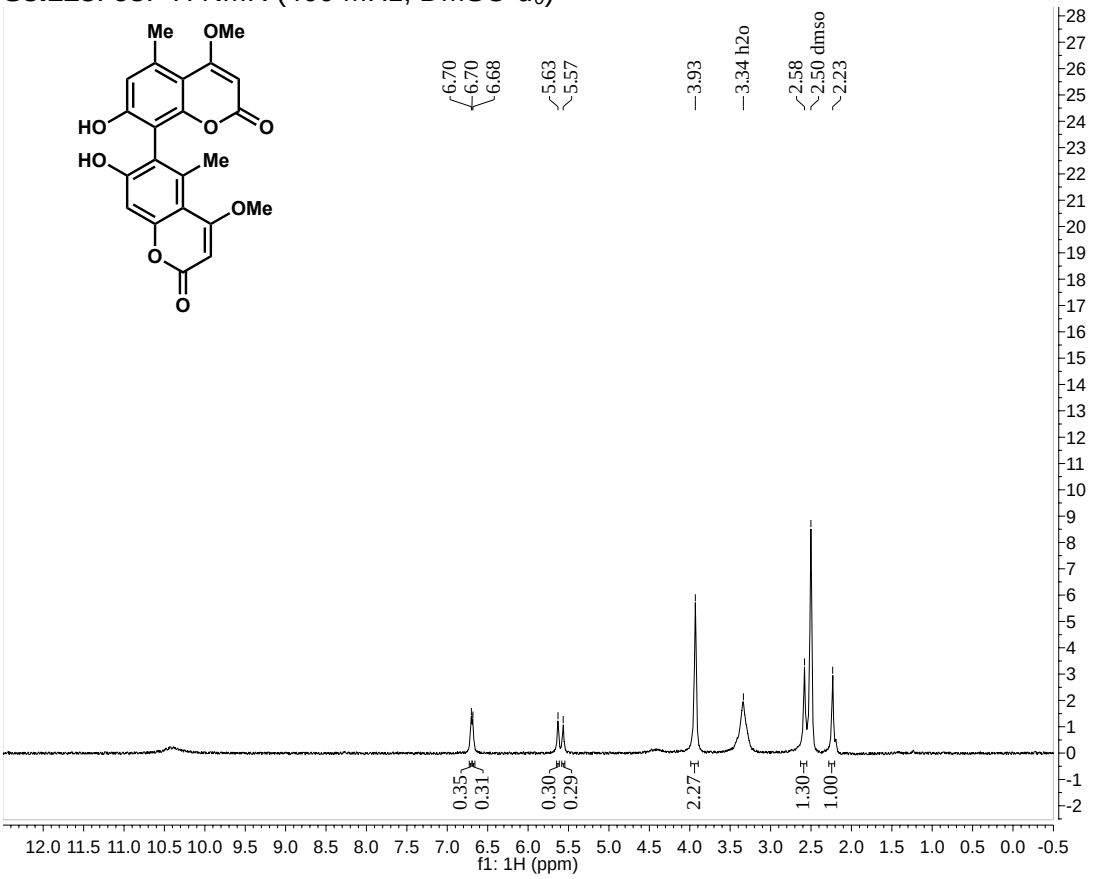

S3.129. **32**: ^{1}H NMR (400 MHz, CD_3OD)

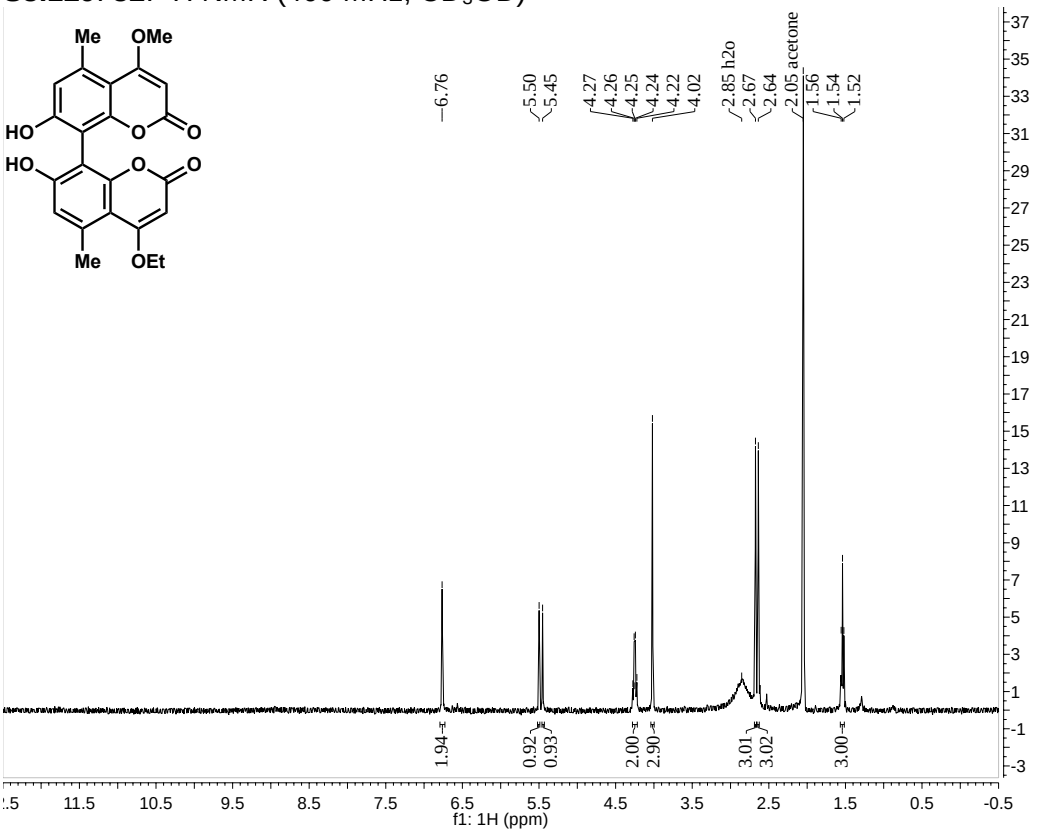

32: ^{1}H NMR (600 MHz, DMSO-d_6)

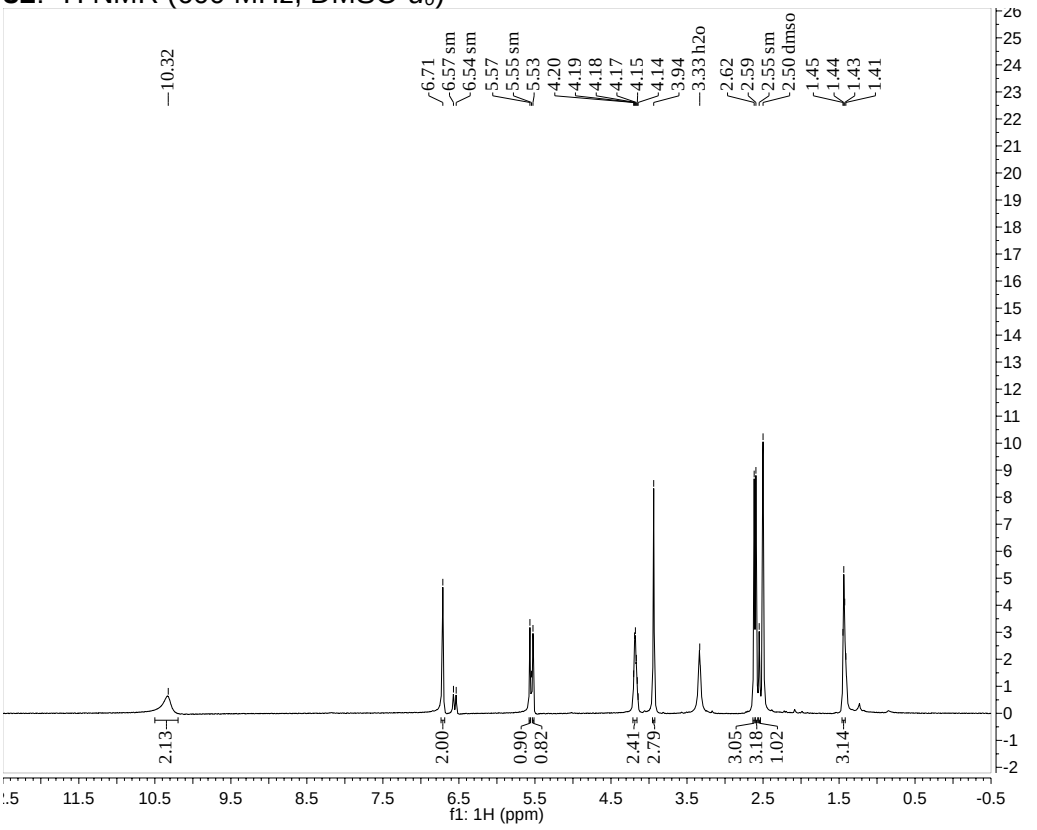

32: ^{13}C NMR (150 MHz, DMSO-d_6)

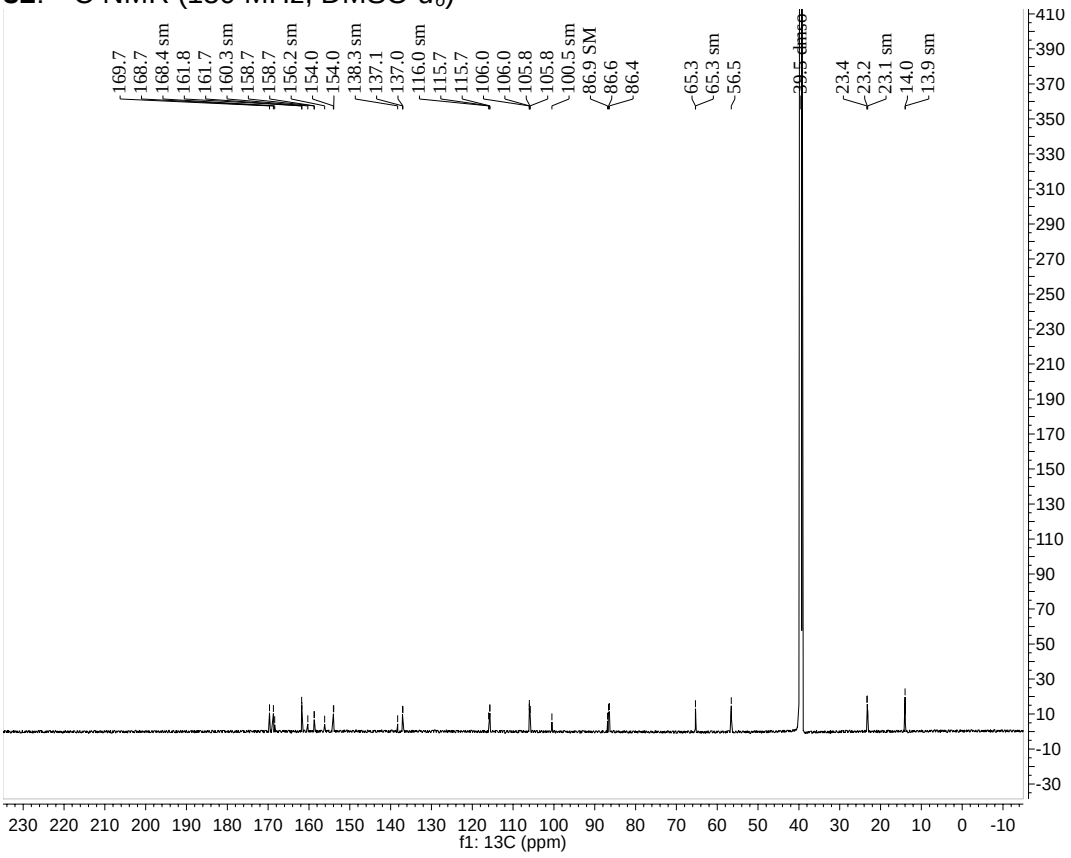

S3.130. **69**: ^{1}H NMR (600 MHz, CD_3OD)

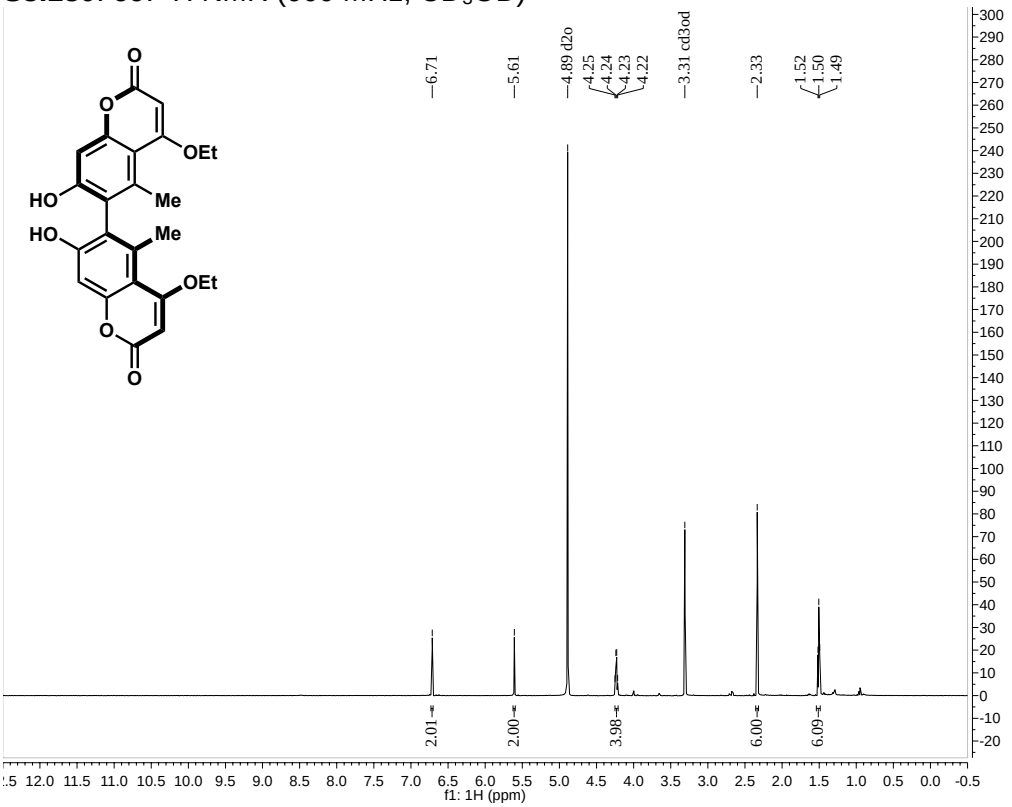

69: ^{13}C NMR (150 MHz, CD_3OD)

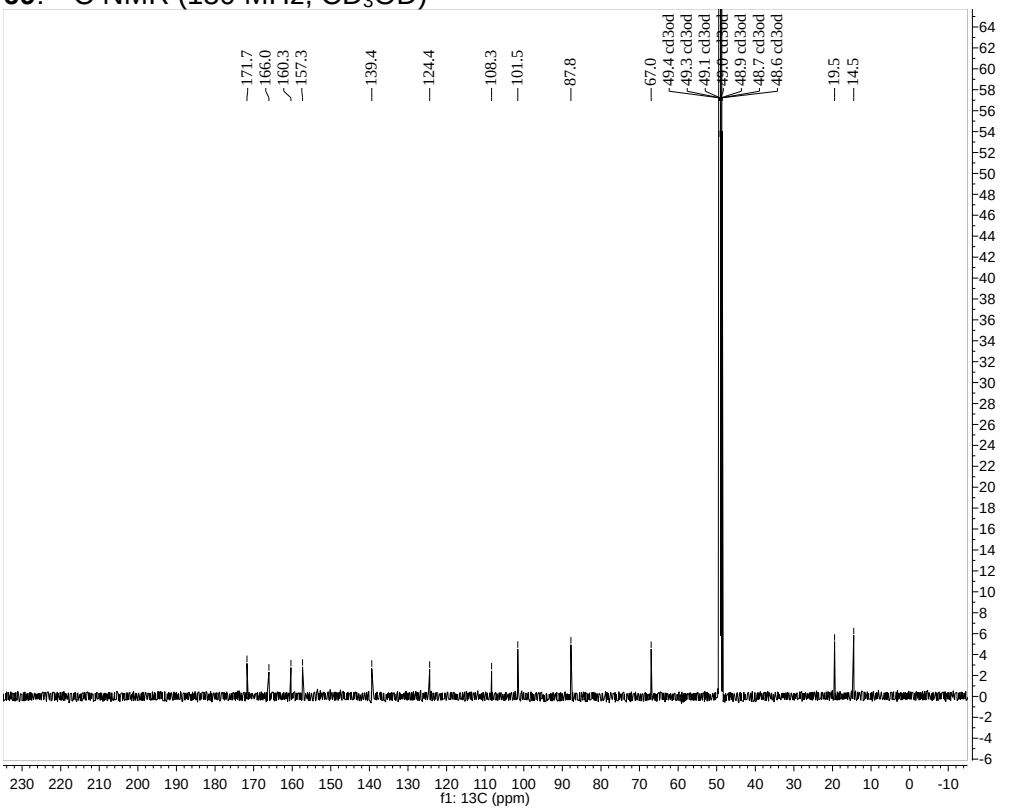

S.3.131. **64**. ^{1}H NMR (400 MHz, CD_3OD)

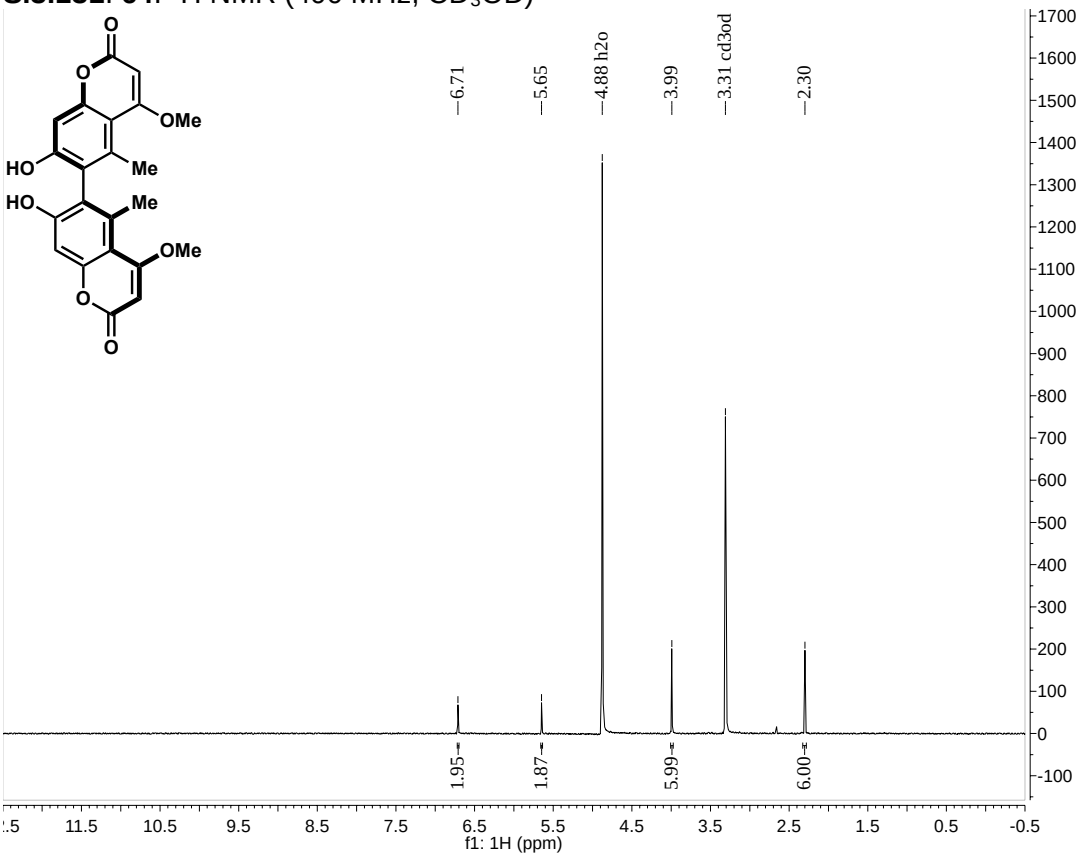

S3.132. **33**: ^{1}H NMR (400 MHz, CD_3OD)

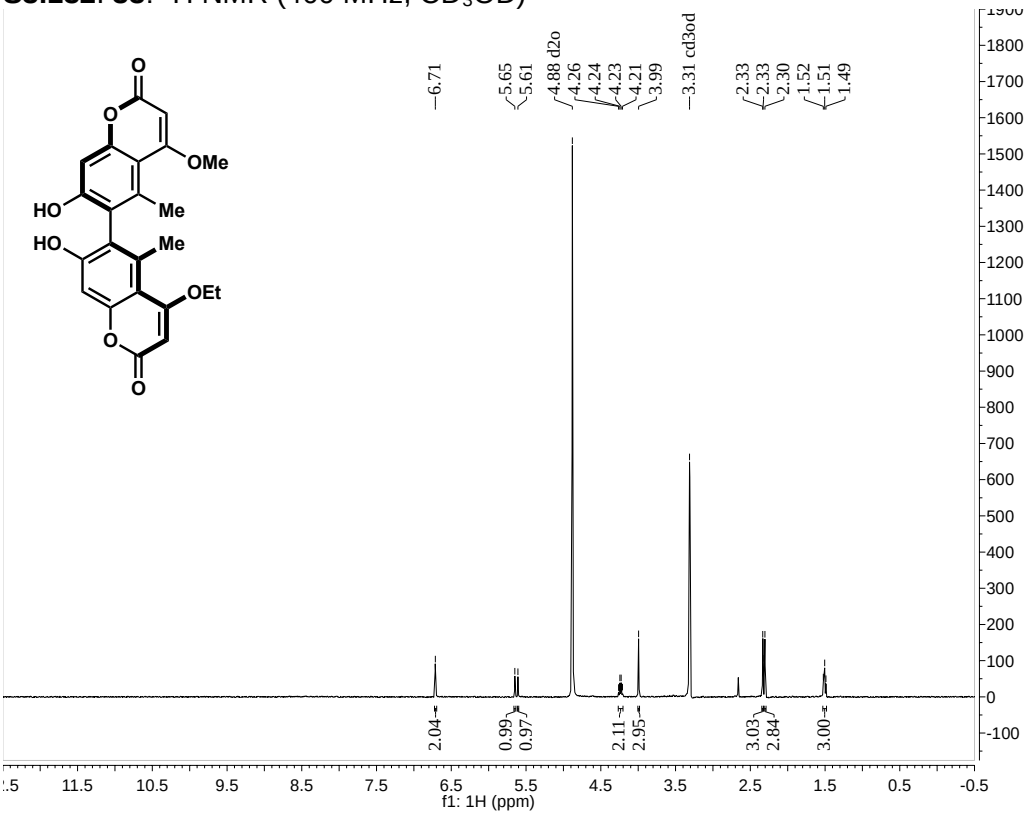

33: ^{13}C NMR (150 MHz, CD_3OD)

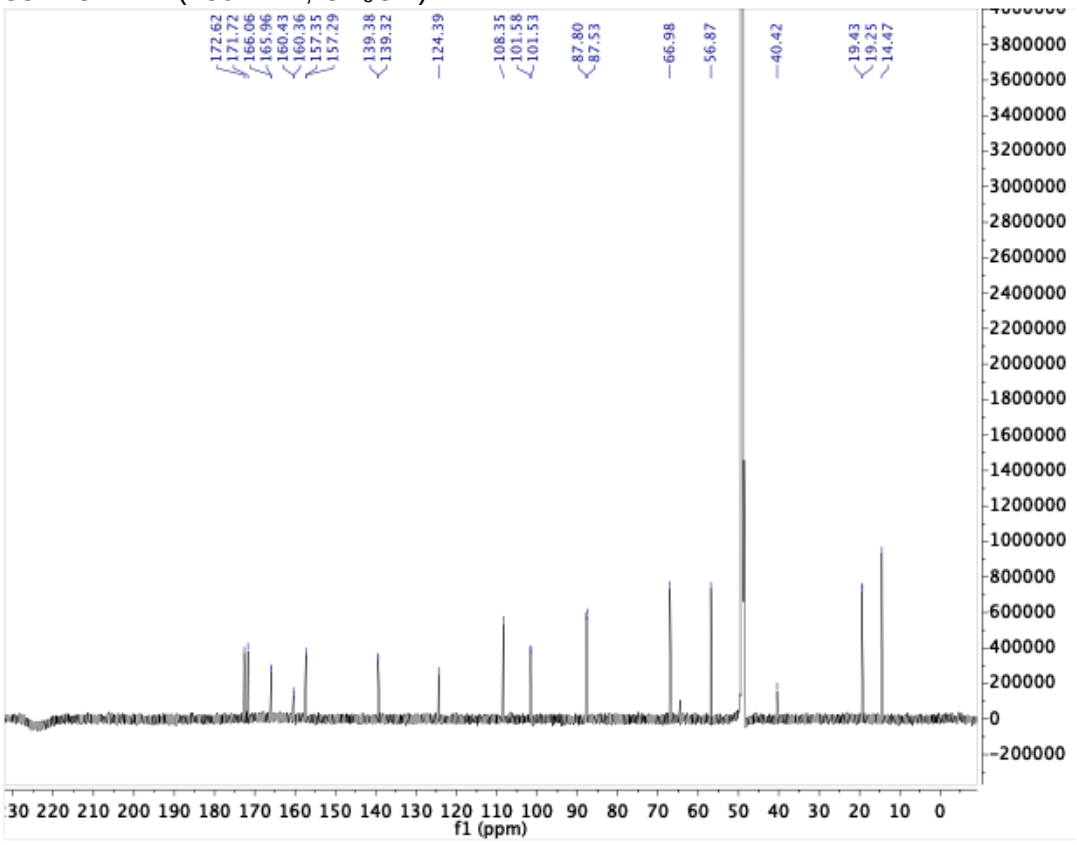

S3.133. **87**: ^{1}H NMR (400 MHz, Methanol-d_4)

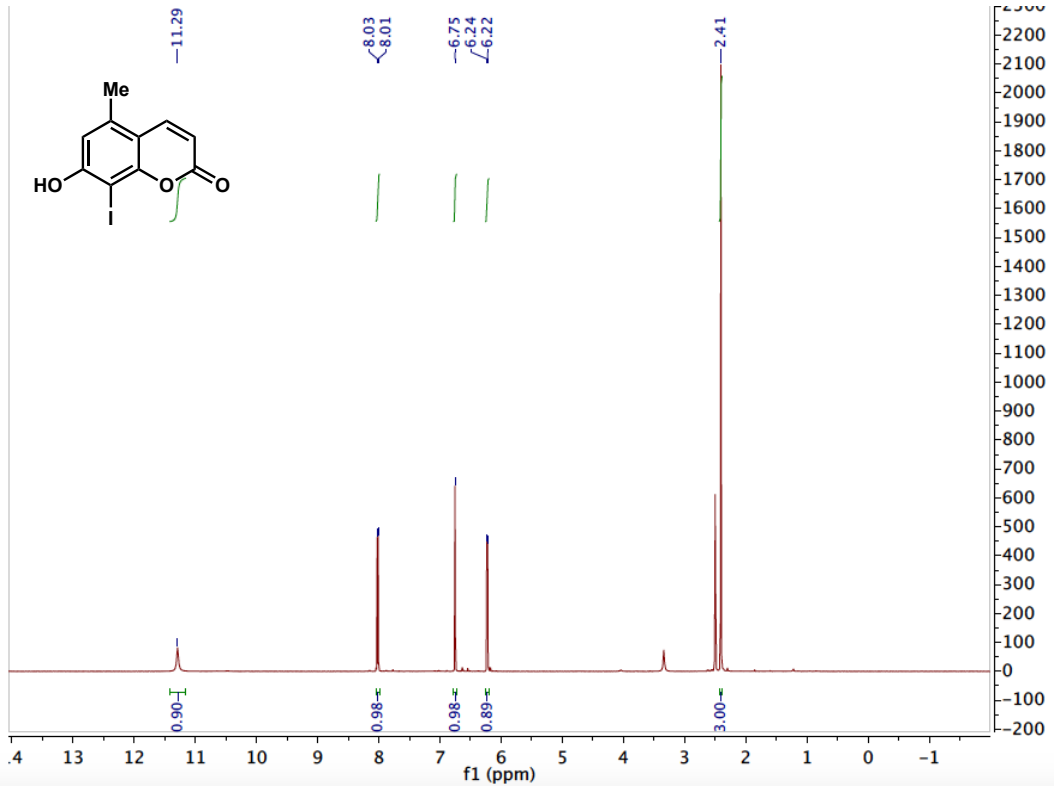

87: ^{13}C NMR (150 MHz, DMSO-d_6)

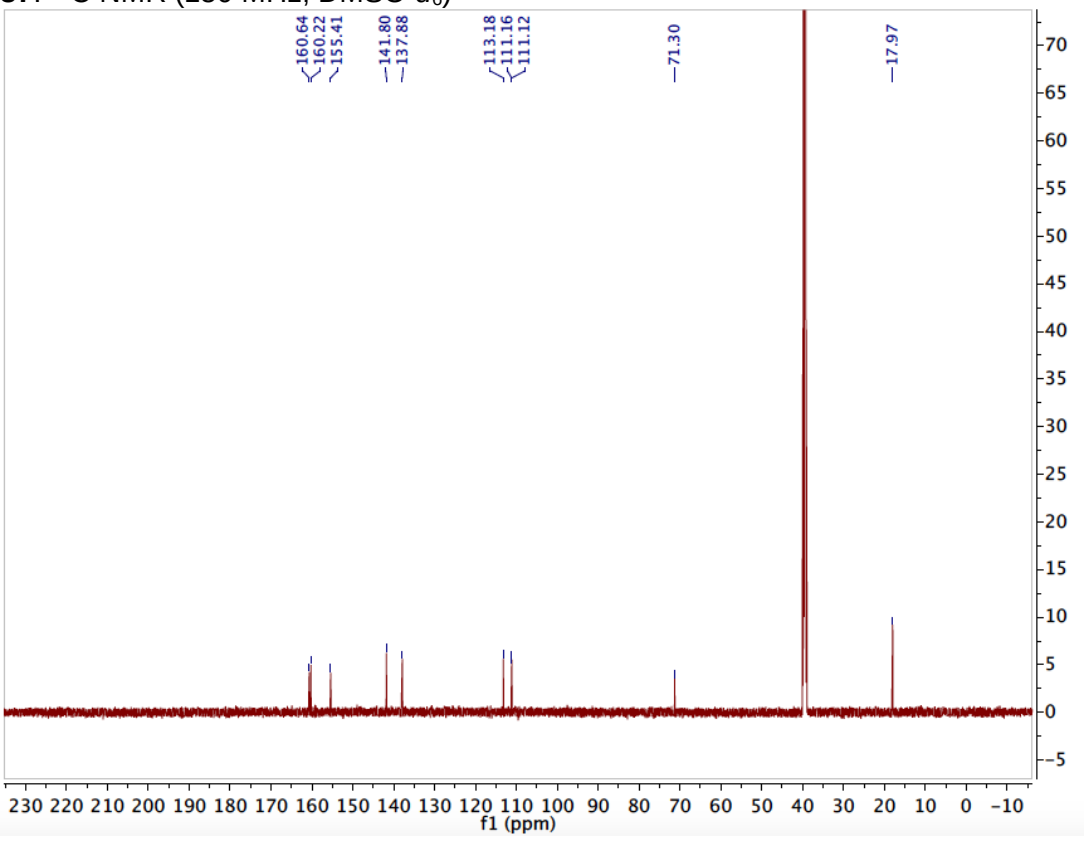

S3.134. **46**. ^{1}H NMR (600 MHz, CDCl3)

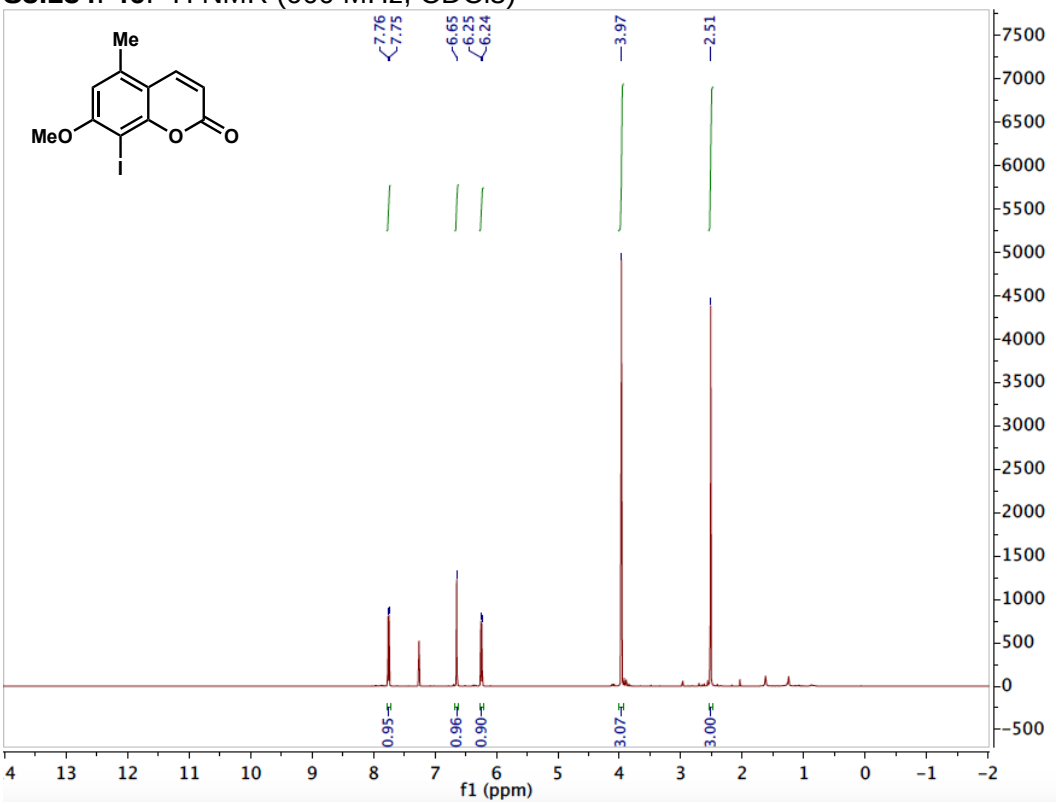

46: ^{13}C NMR (150 MHz, CDCl3)

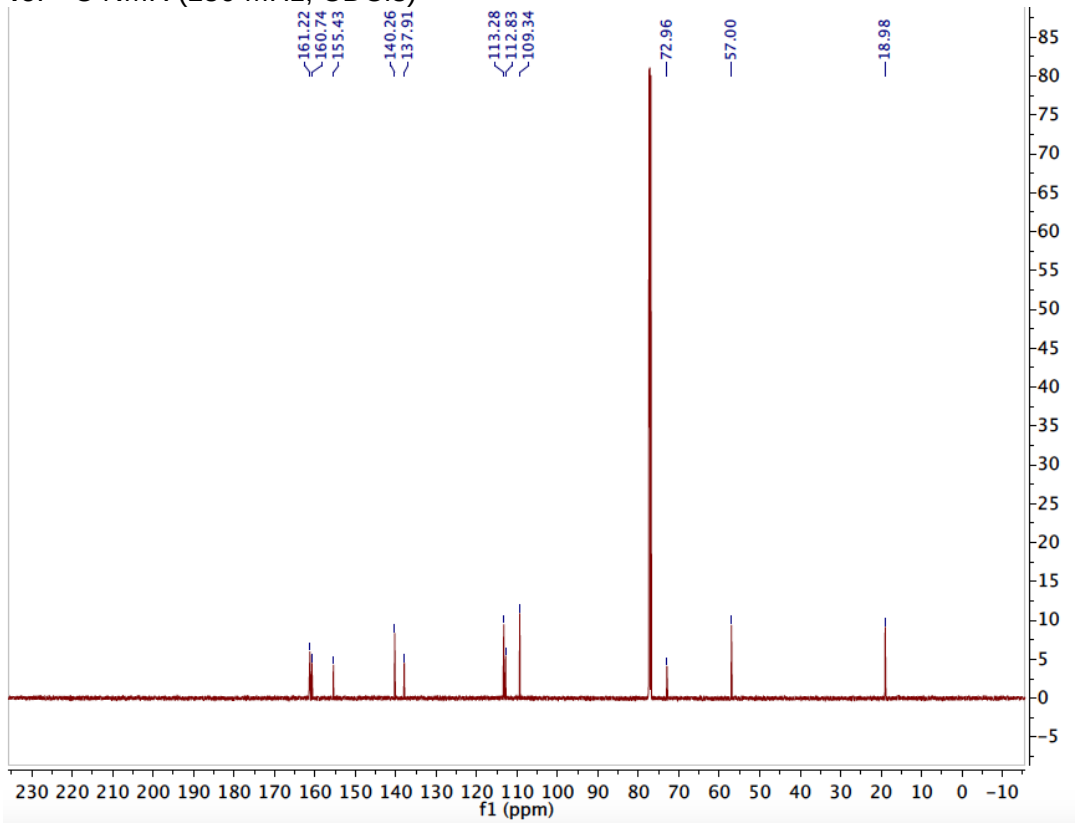

S3.135. **48**: ^{1}H NMR (800 MHz, acetone-d_6)

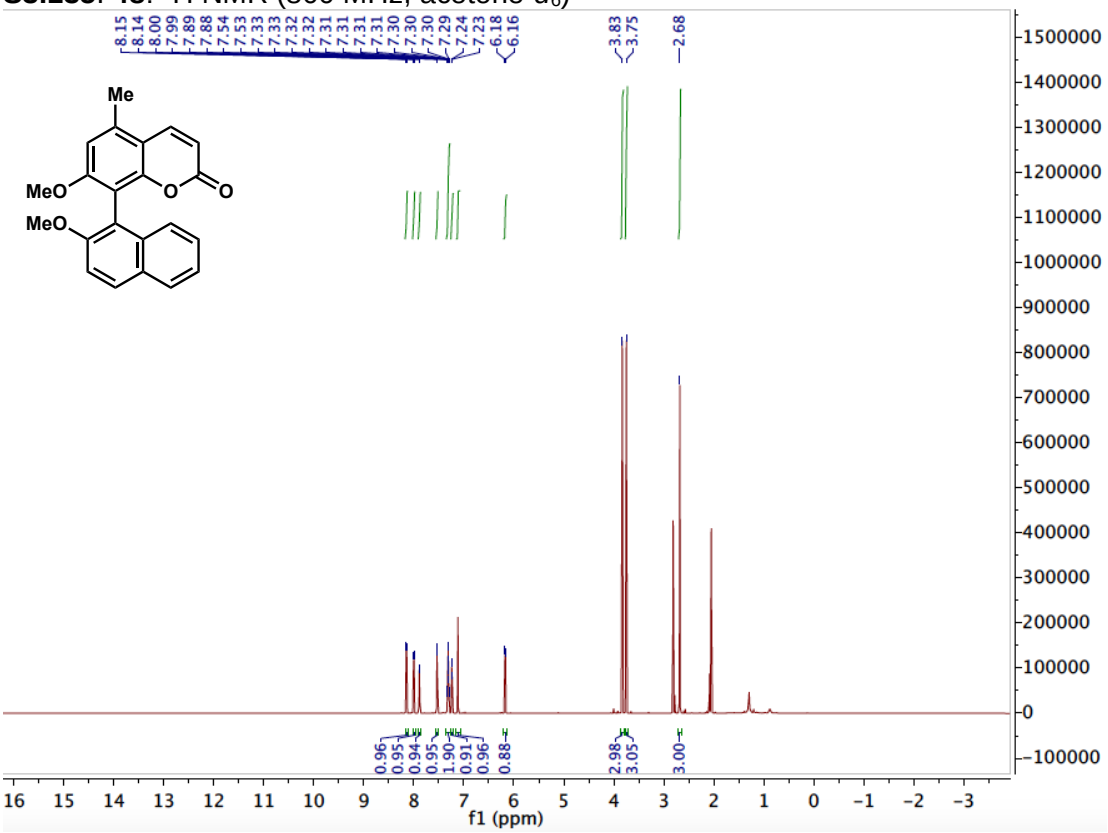

48: ^{13}C NMR (200 MHz, acetone-d_6)

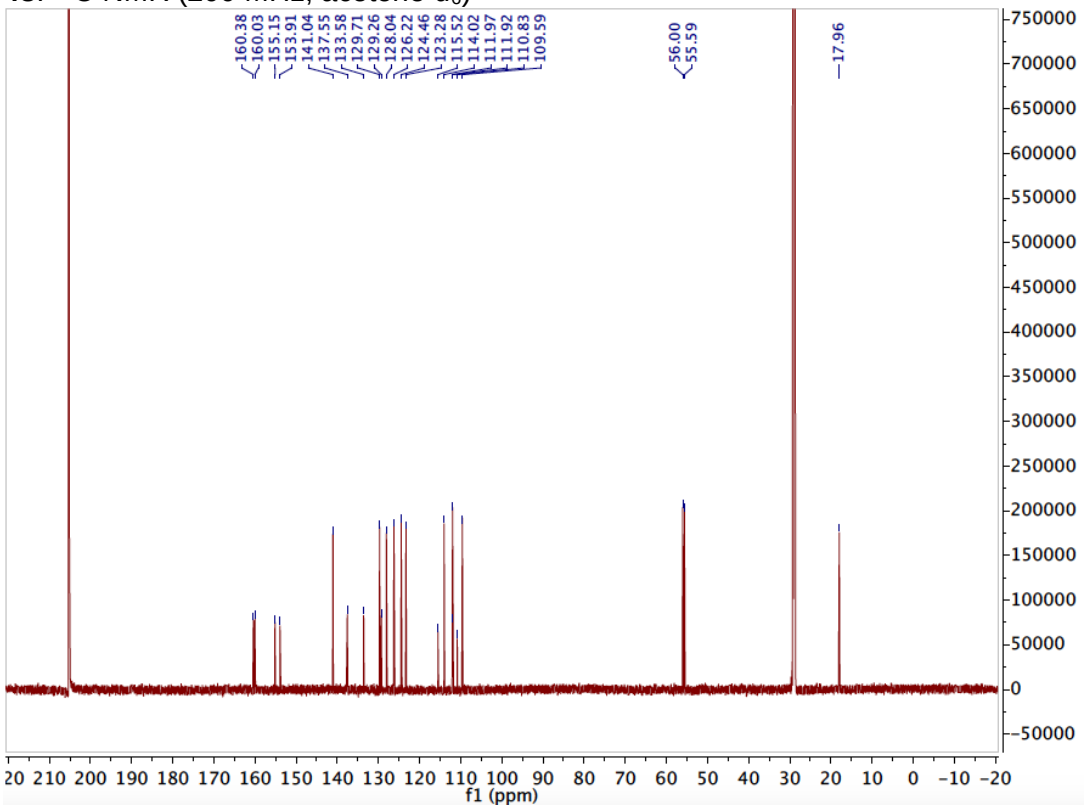

S3.136. **42**: ^{1}H NMR (600 MHz, Methanol-d_4)

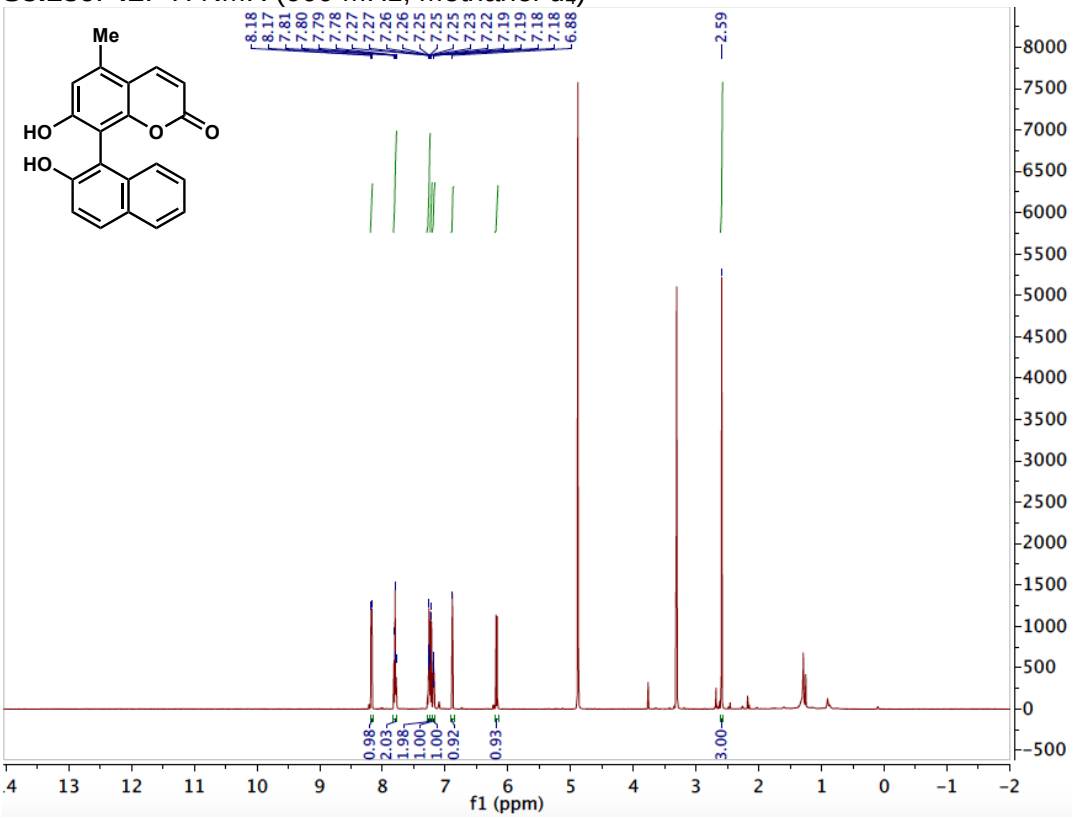

42: ^{13}C NMR (150 MHz, Methanol-d_4)

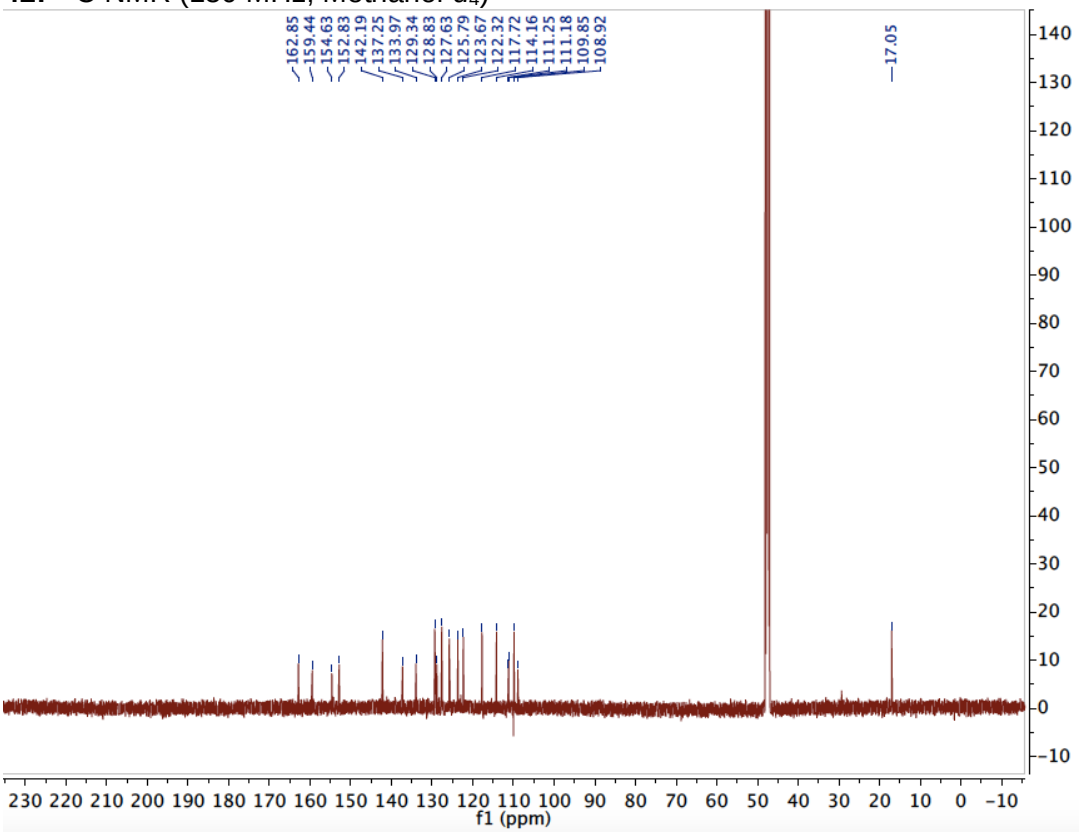

S3.137. **58**: ^{1}H NMR (600 MHz, ($CDCl_3$)

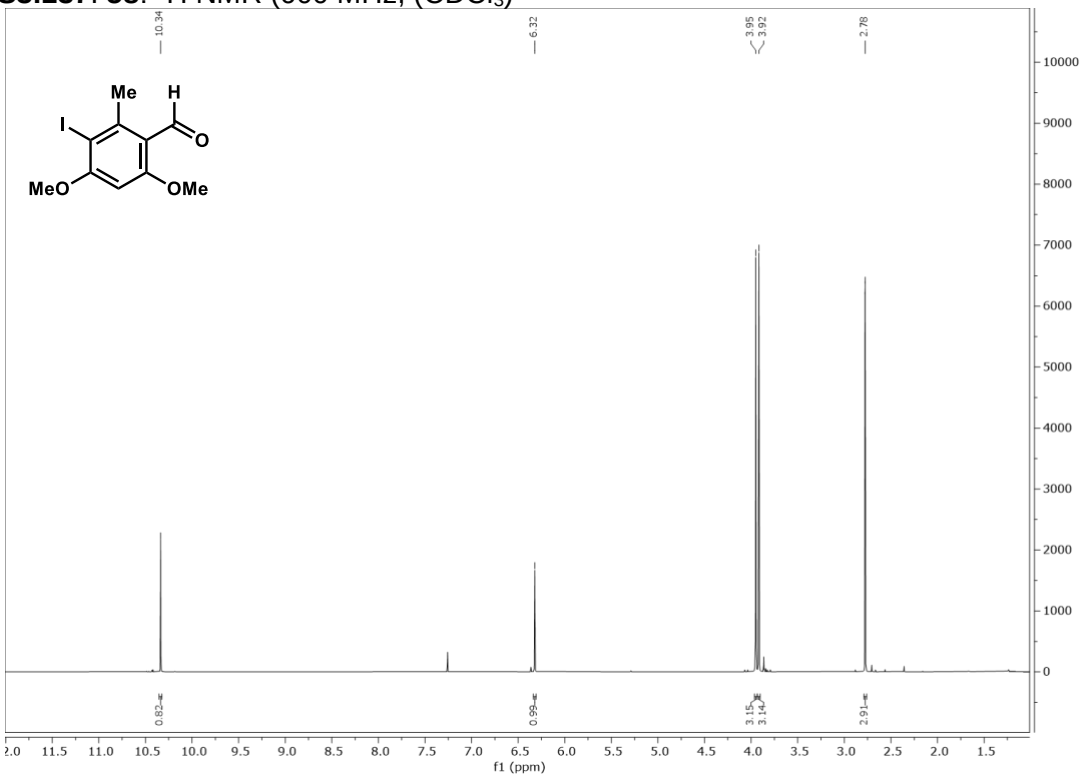

58: ^{13}C NMR (150 MHz, ($CDCl_3$)

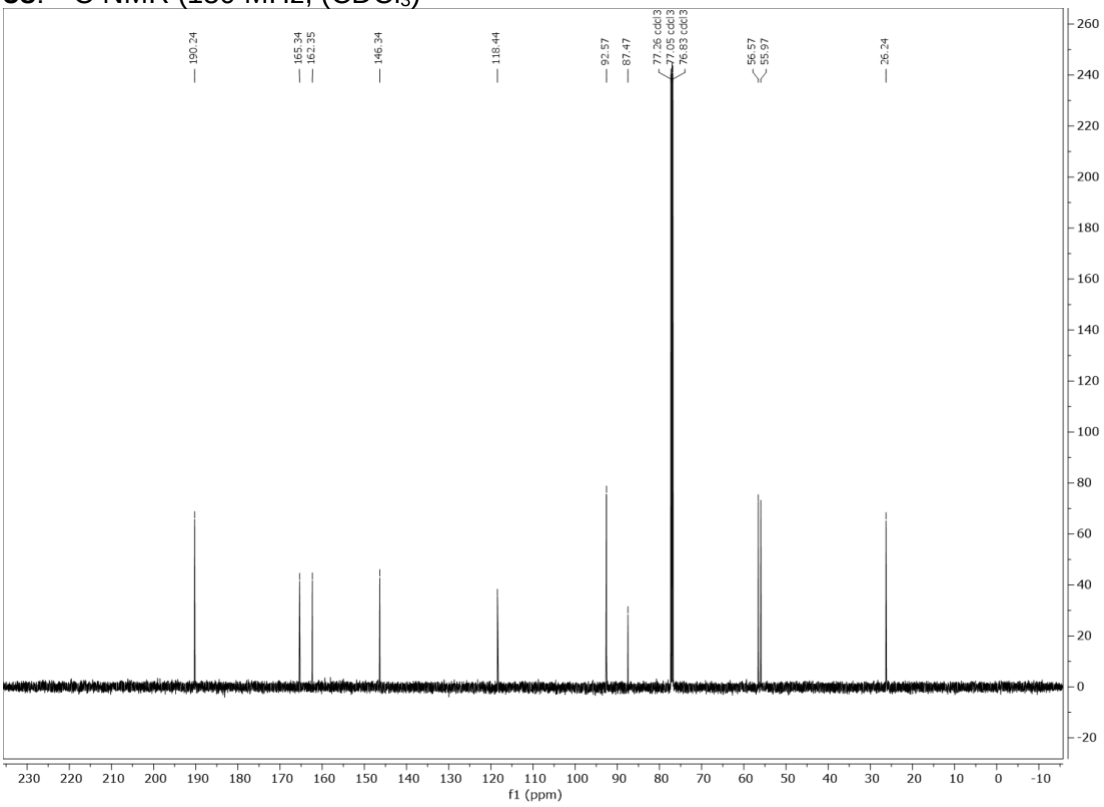

S3.138. **59**: ^{1}H NMR (600 MHz, ($CDCl_3$)

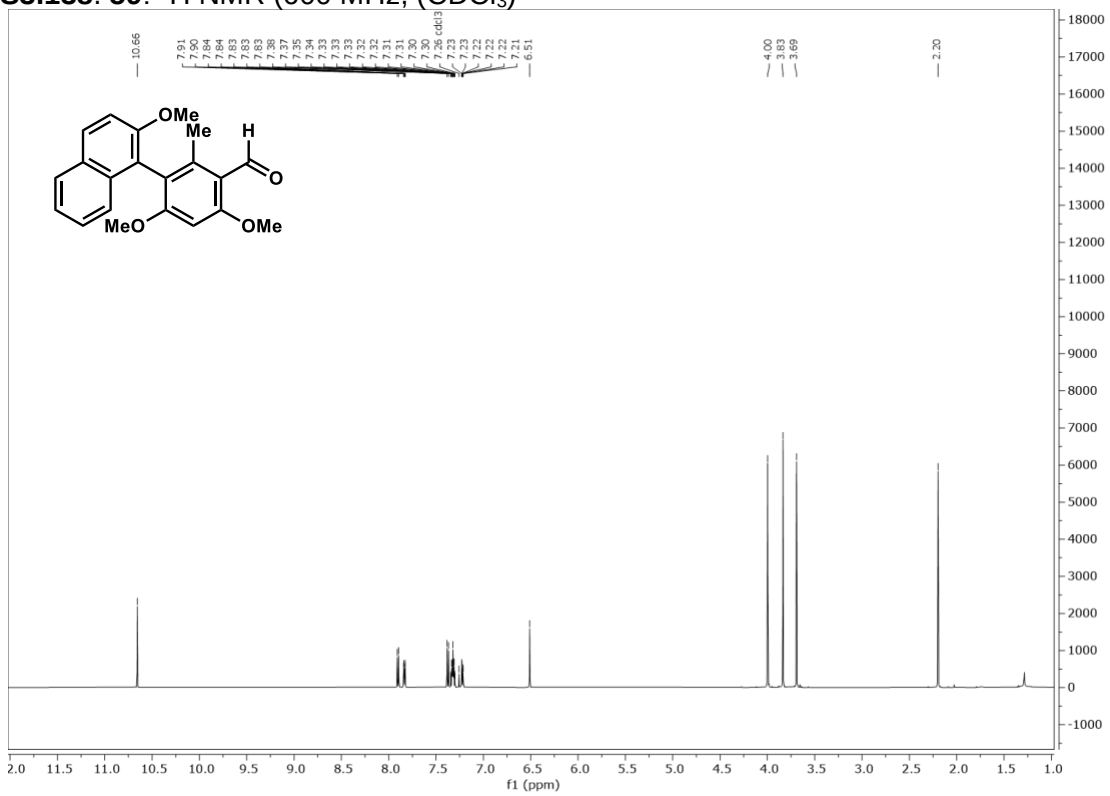

59: ^{13}C NMR (150 MHz, ($CDCl_3$)

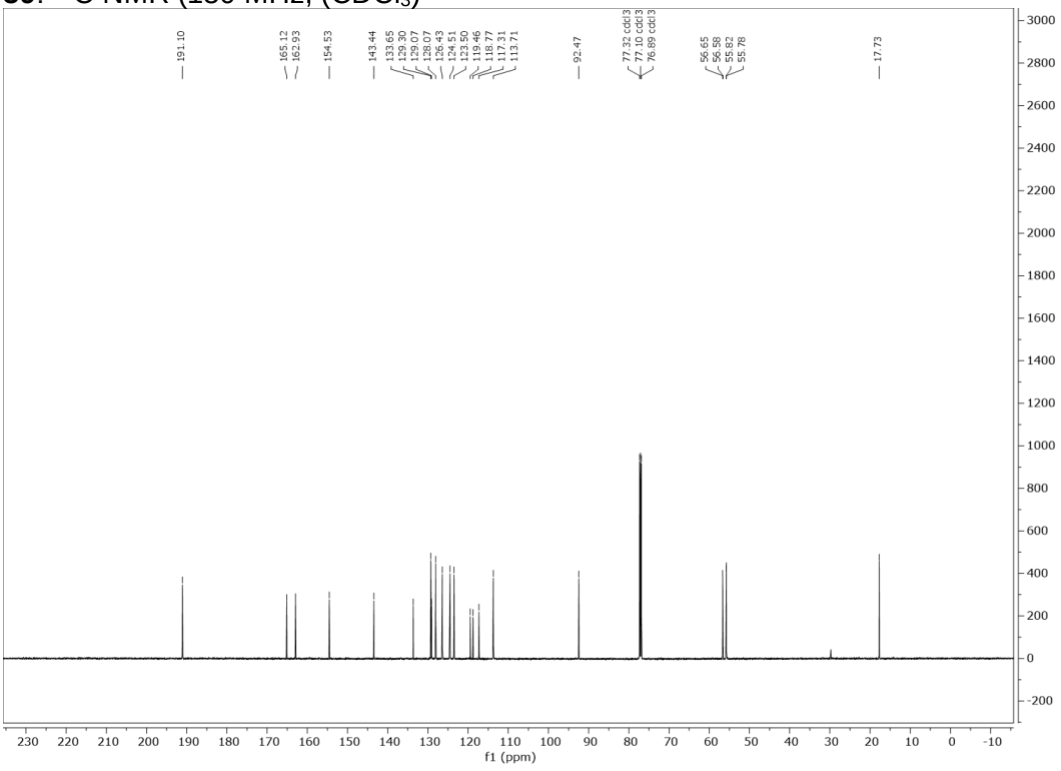

S3.139. **60**: ^{1}H NMR (600 MHz, $CDCl_3$)

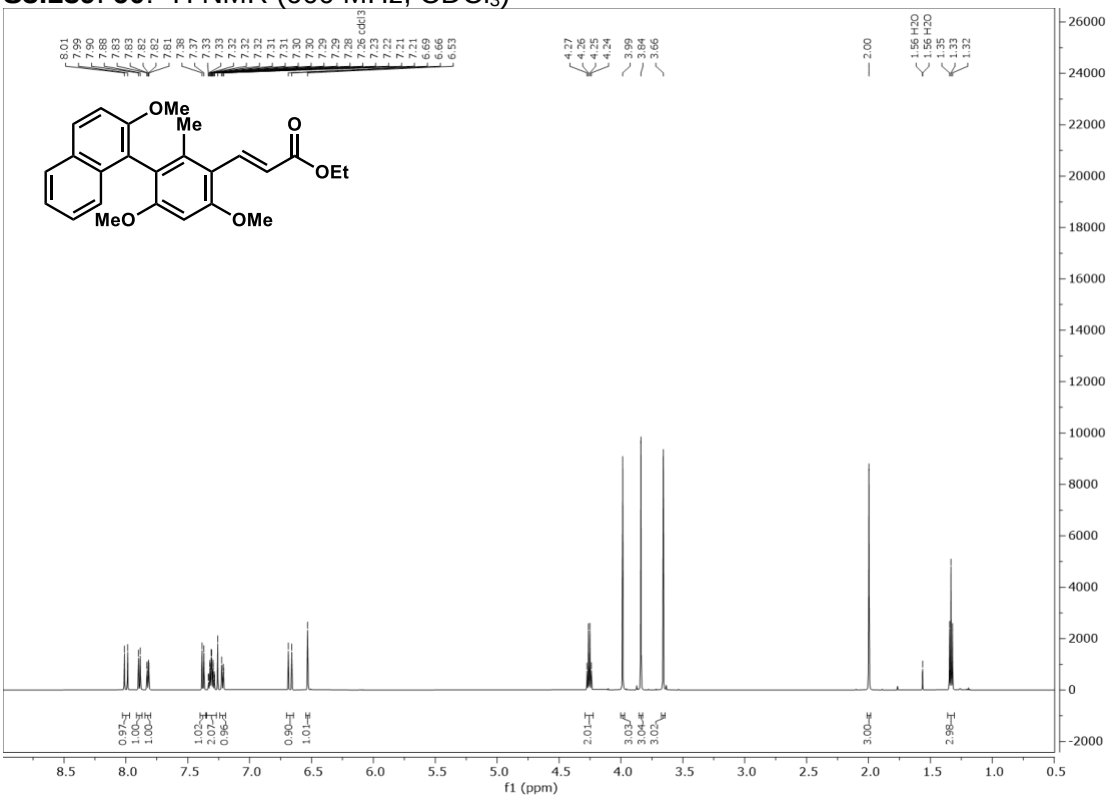

60: ^{13}C NMR (600 MHz, $CDCl_3$)

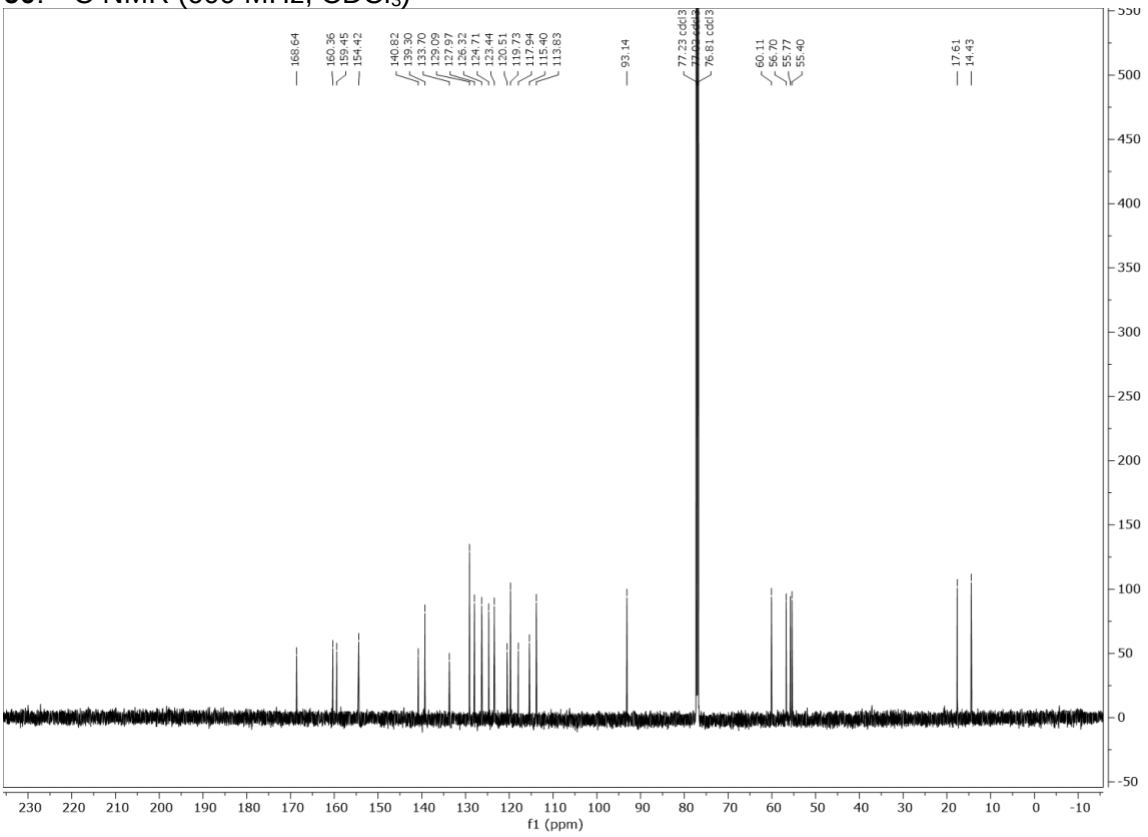

S3.140. **43**: ^{1}H NMR (600 MHz, ($CDCl_3$)

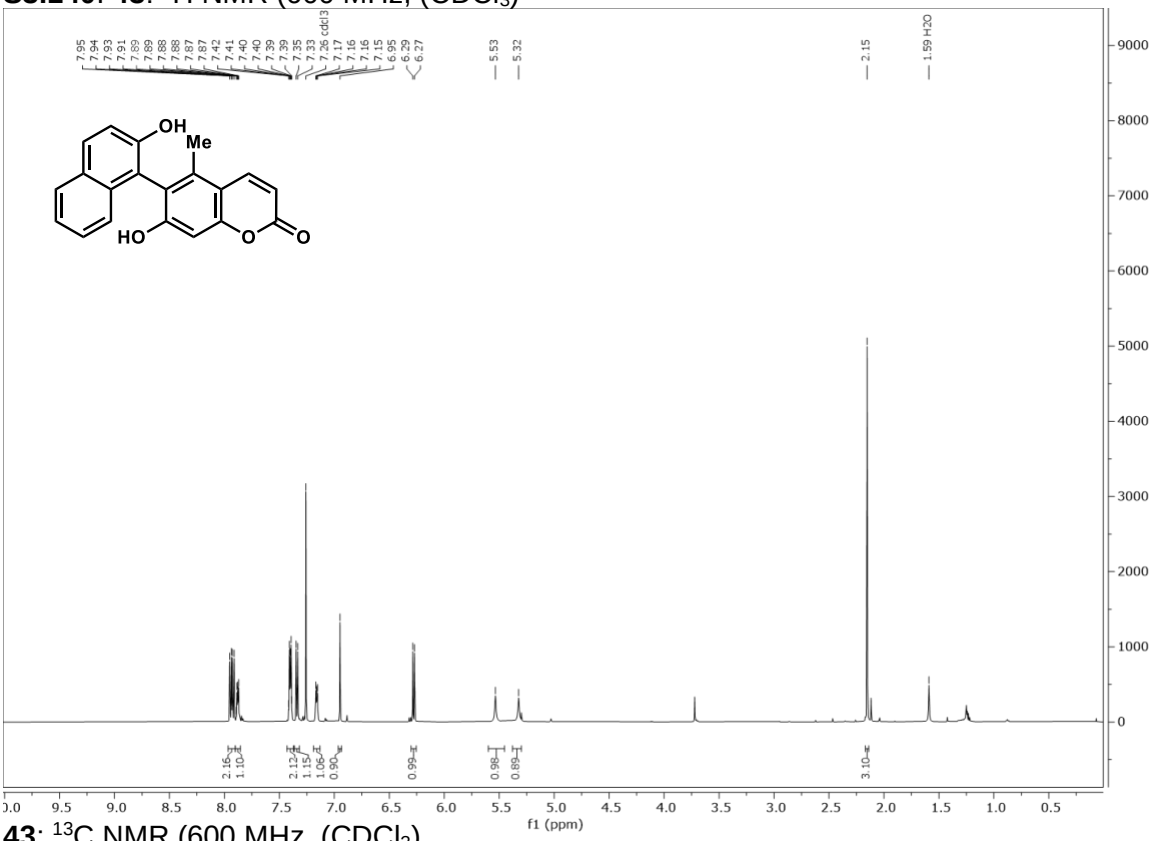

43: ^{13}C NMR (600 MHz, ($CDCl_3$)

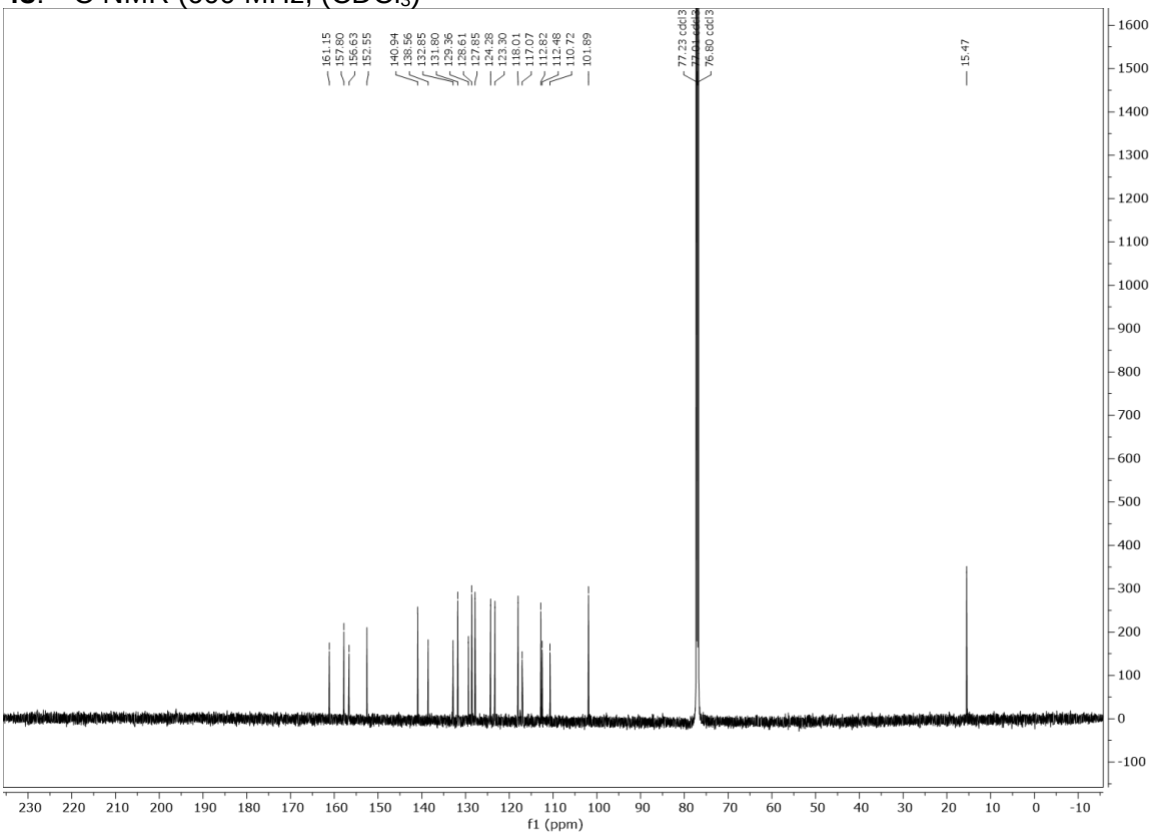

S3.141. **52**: ^{1}H NMR (400 MHz, Chloroform-*d*)

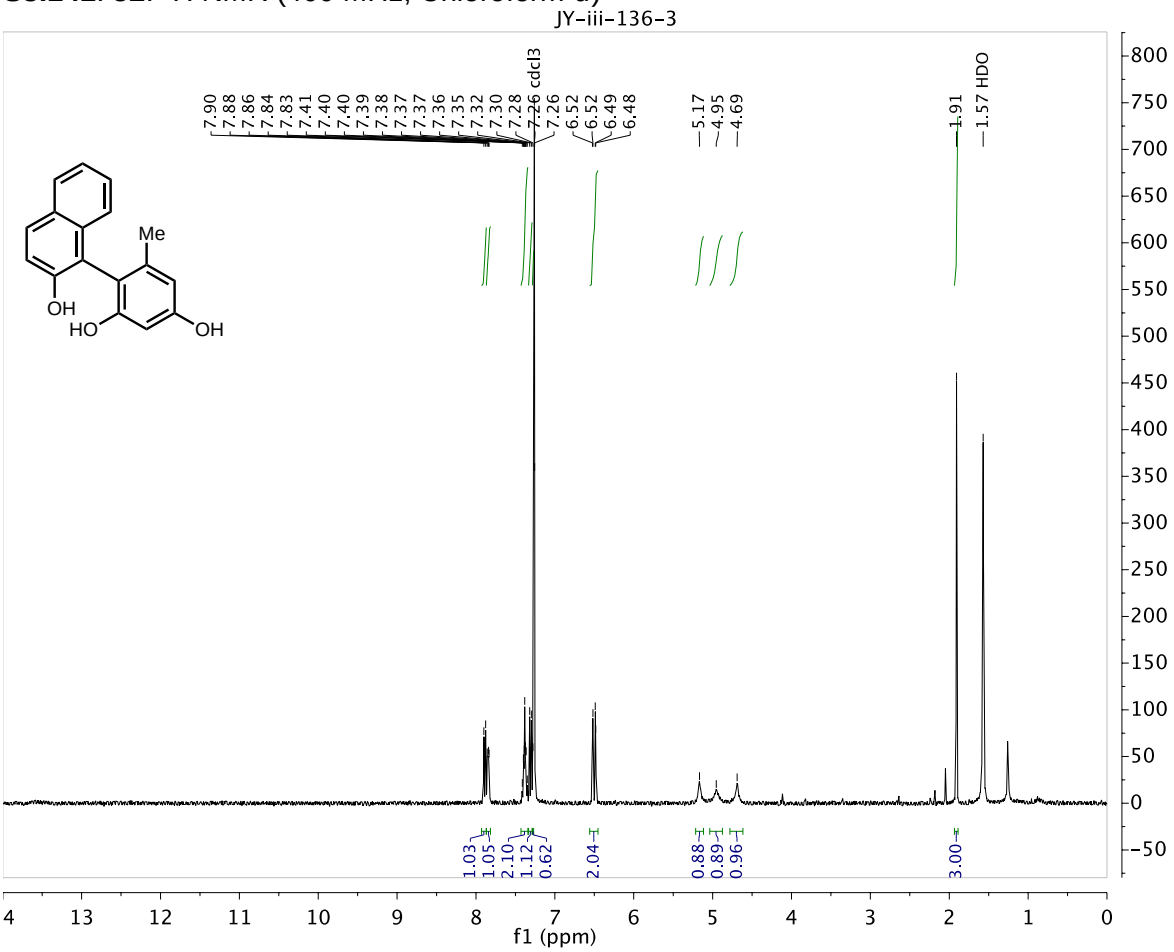

S3.142. **61**: ^{1}H NMR (600 MHz, CDCl3)

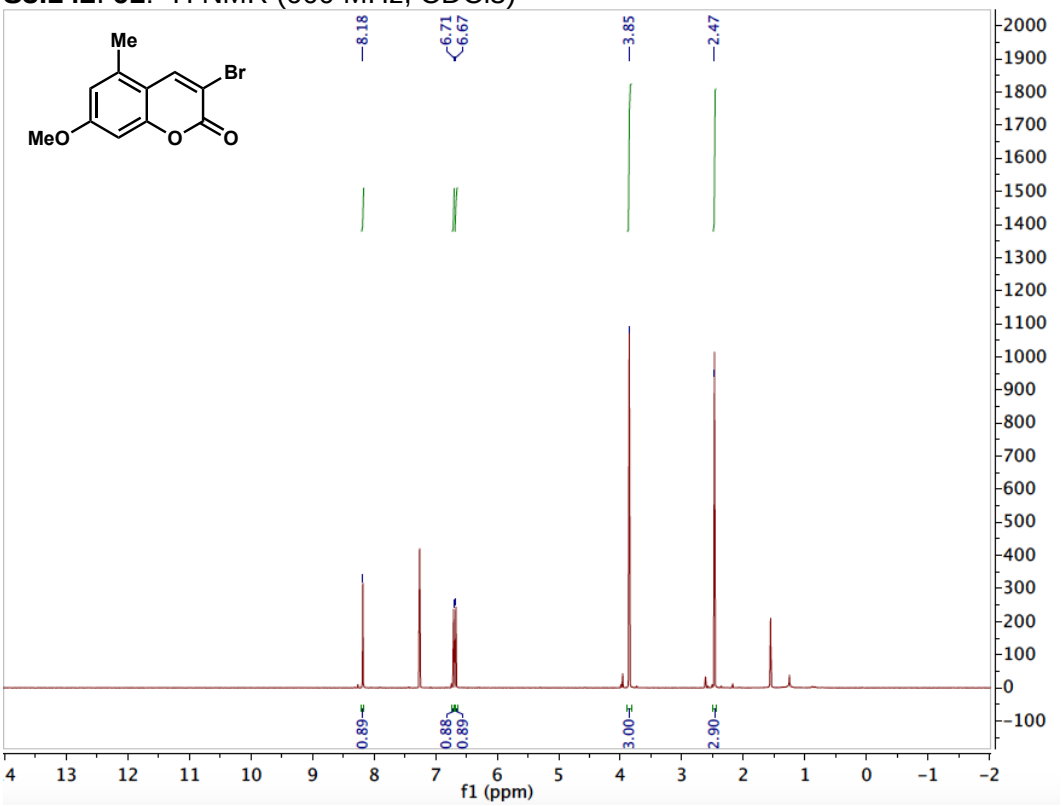

61: ^{13}C NMR (150 MHz, CDCl3)

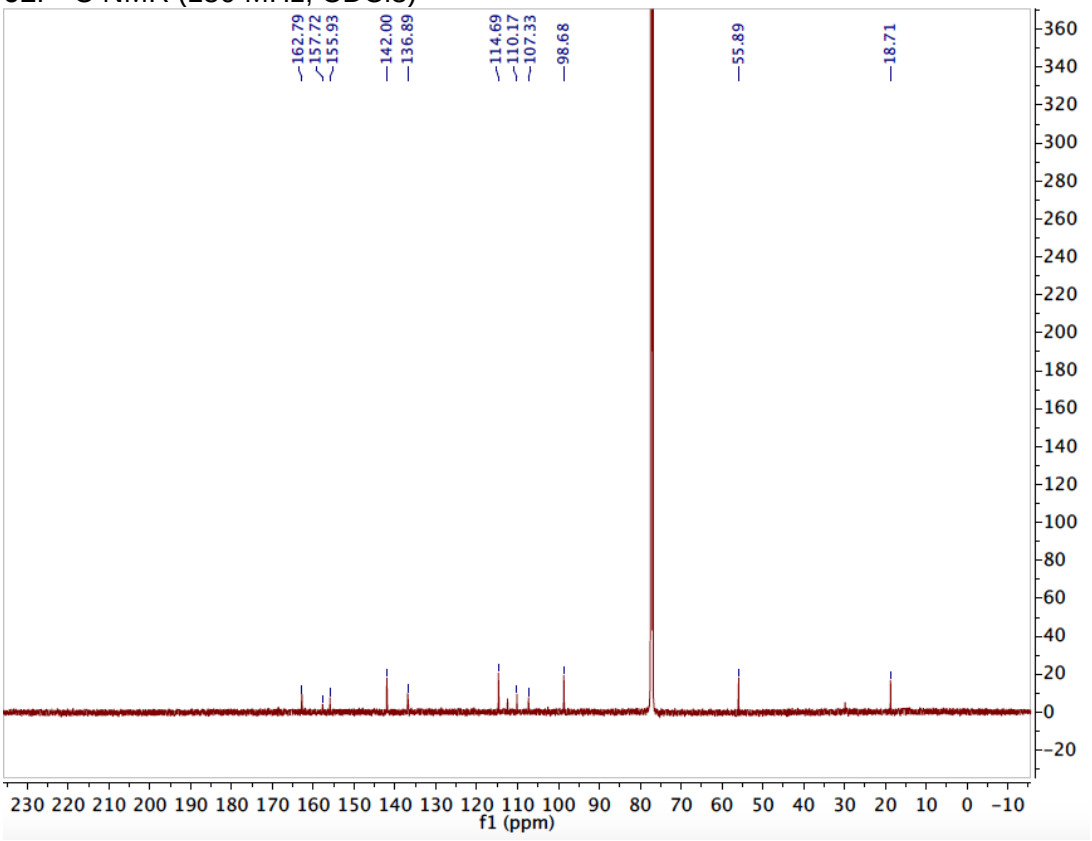

S3.143. **62**: ^{1}H NMR (600 MHz, CDCl3)

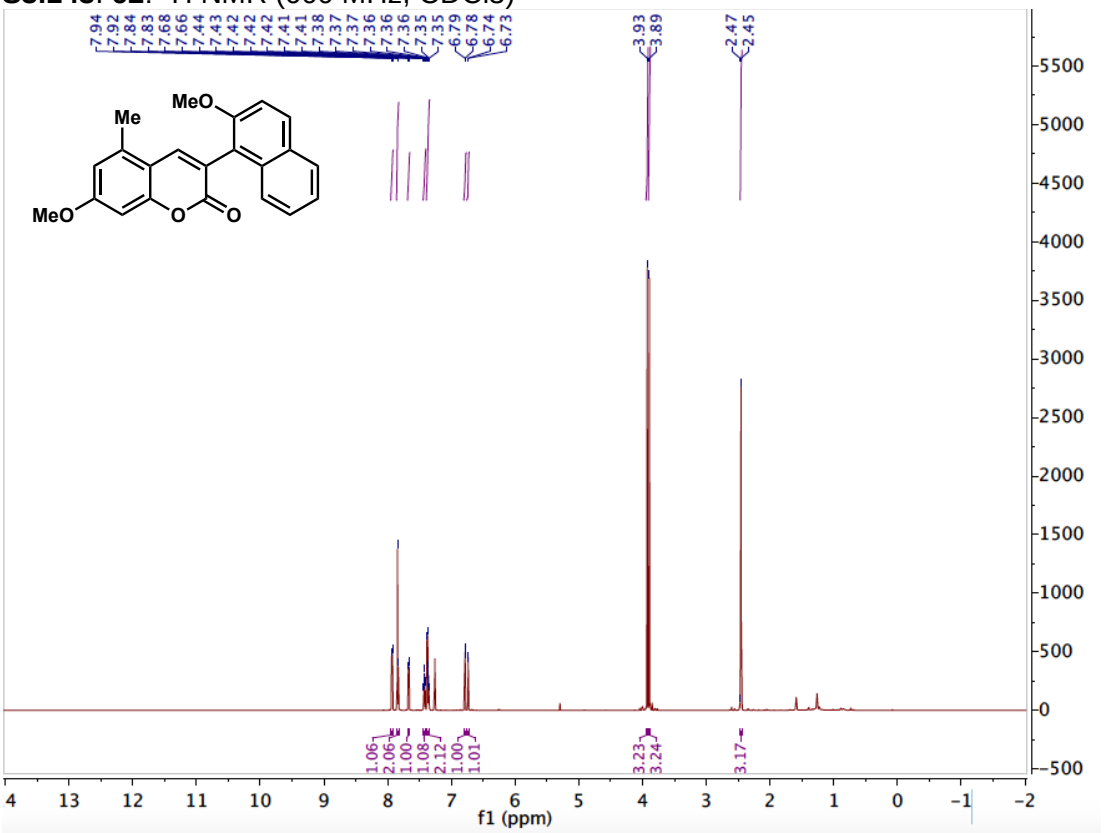

62: ^{13}C NMR (150 MHz, CDCl3)

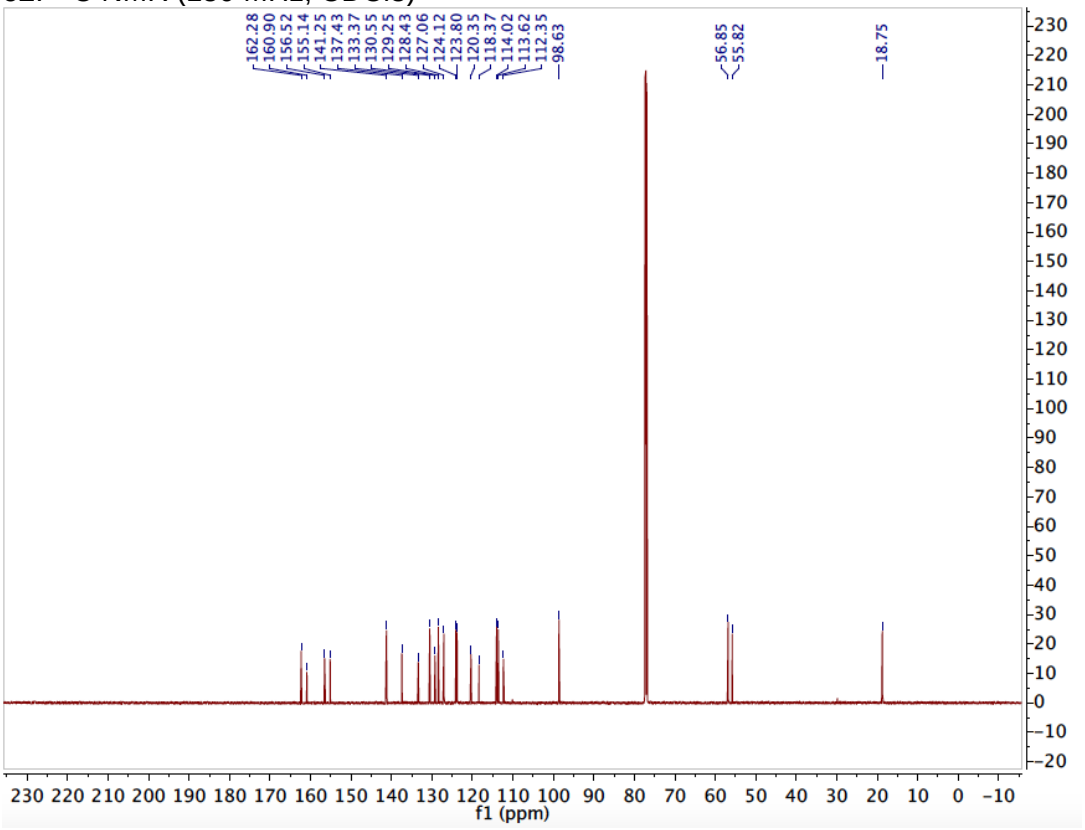

S3.144. **44**: ^{1}H NMR (600 MHz, acetone-d_6)

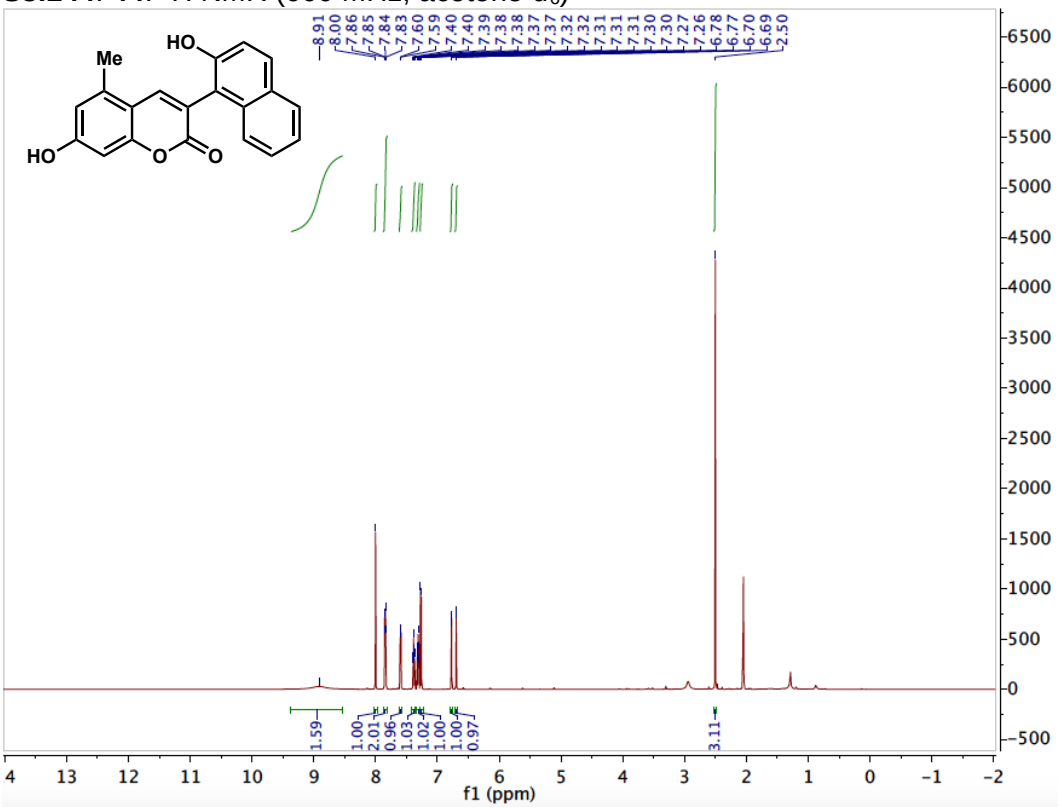

44: ^{13}C NMR (150 MHz, acetone-d_6)

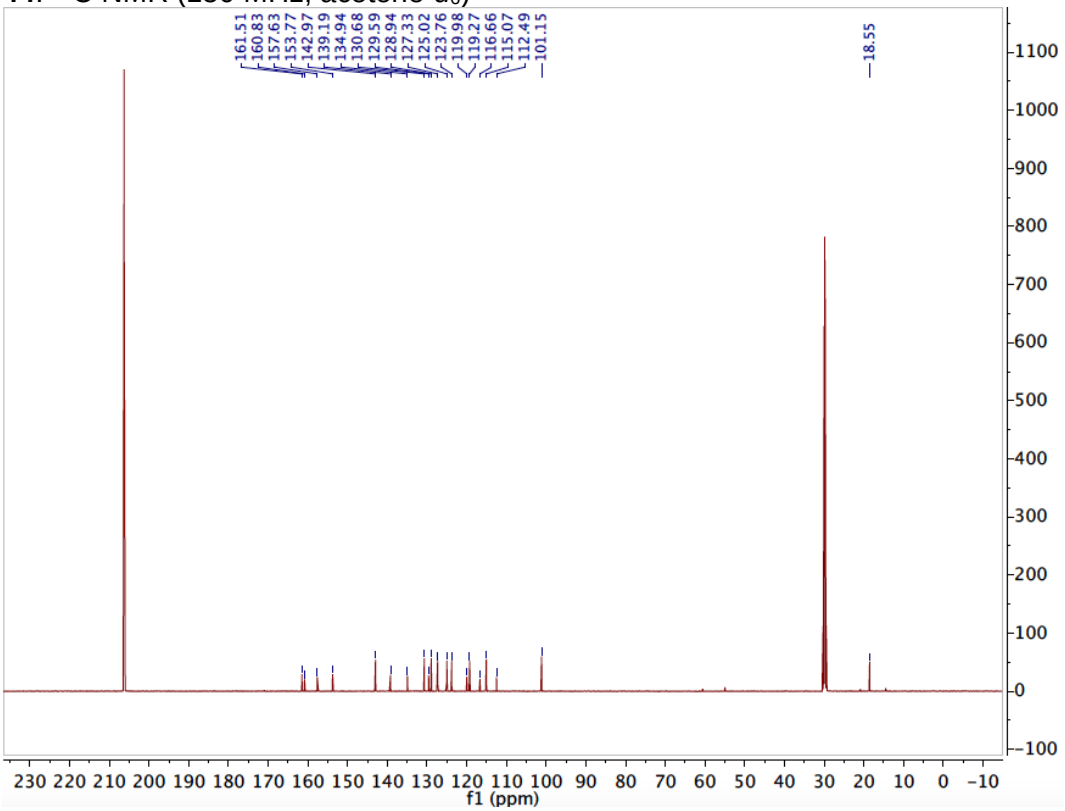

S3.145. **89**: ^{1}H NMR (600 MHz, $CDCl_3$)

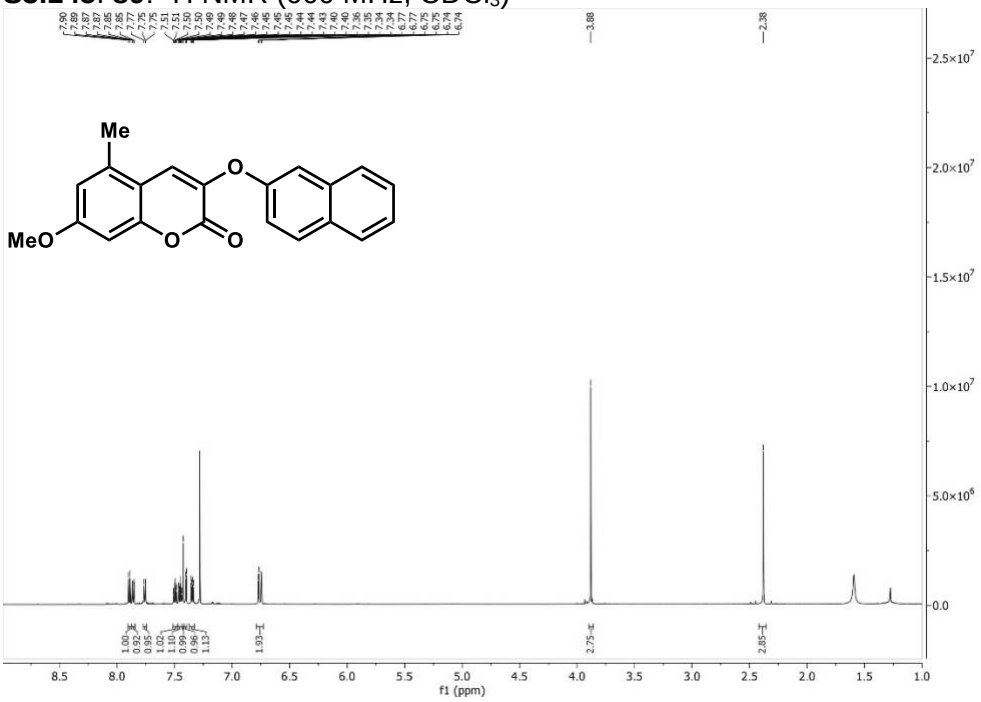

89: ^{13}C NMR (150 MHz, $CDCl_3$)

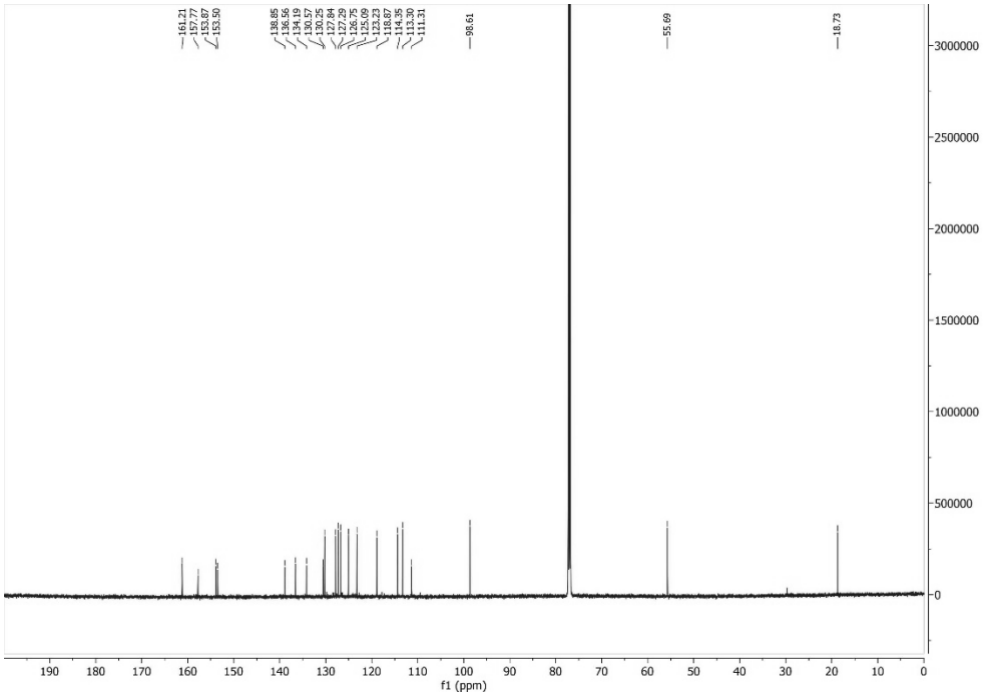

S3.146. **90**: ^{1}H NMR (800 MHz, DMSO-d_6)

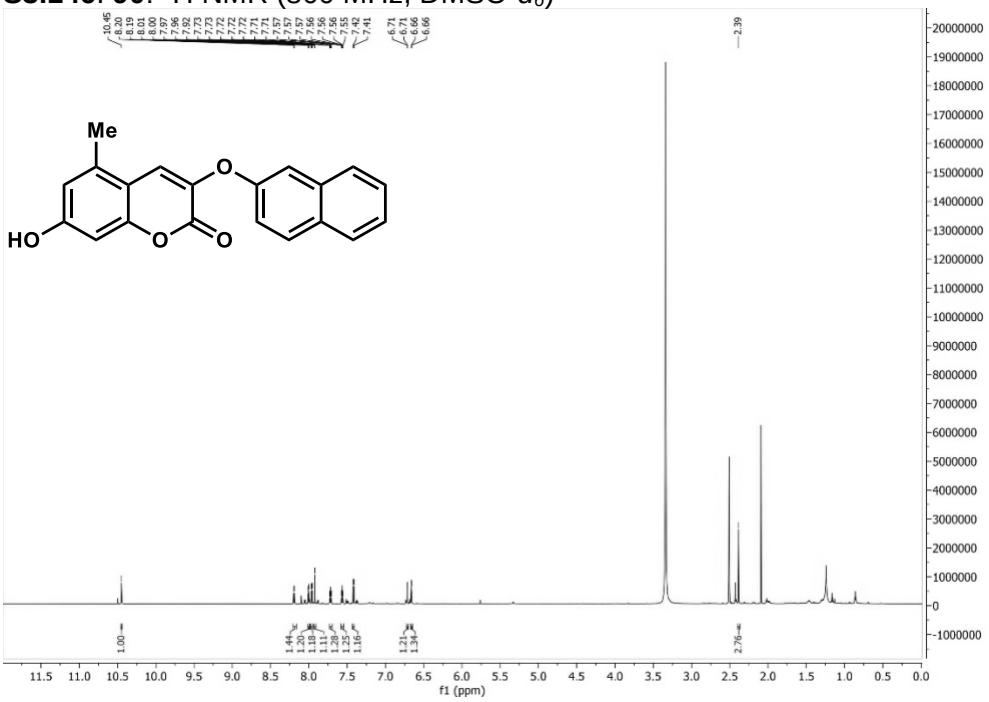

90: ^{13}C NMR (200 MHz, DMSO-d_6)

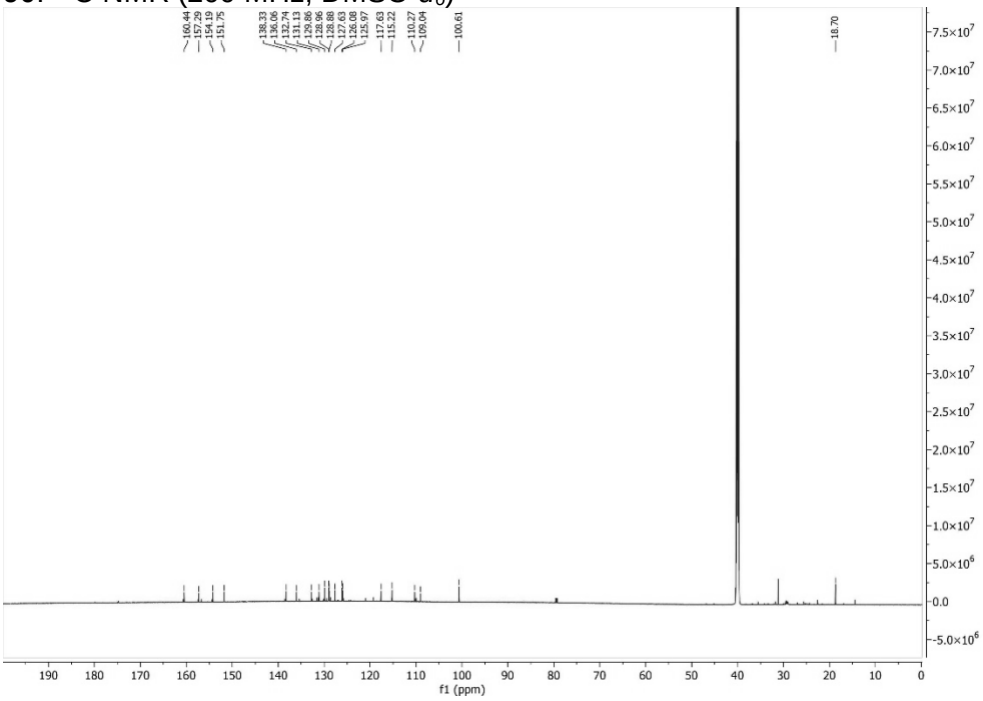

S3.147. **68**: ^{1}H NMR (600 MHz, CD_3OD)

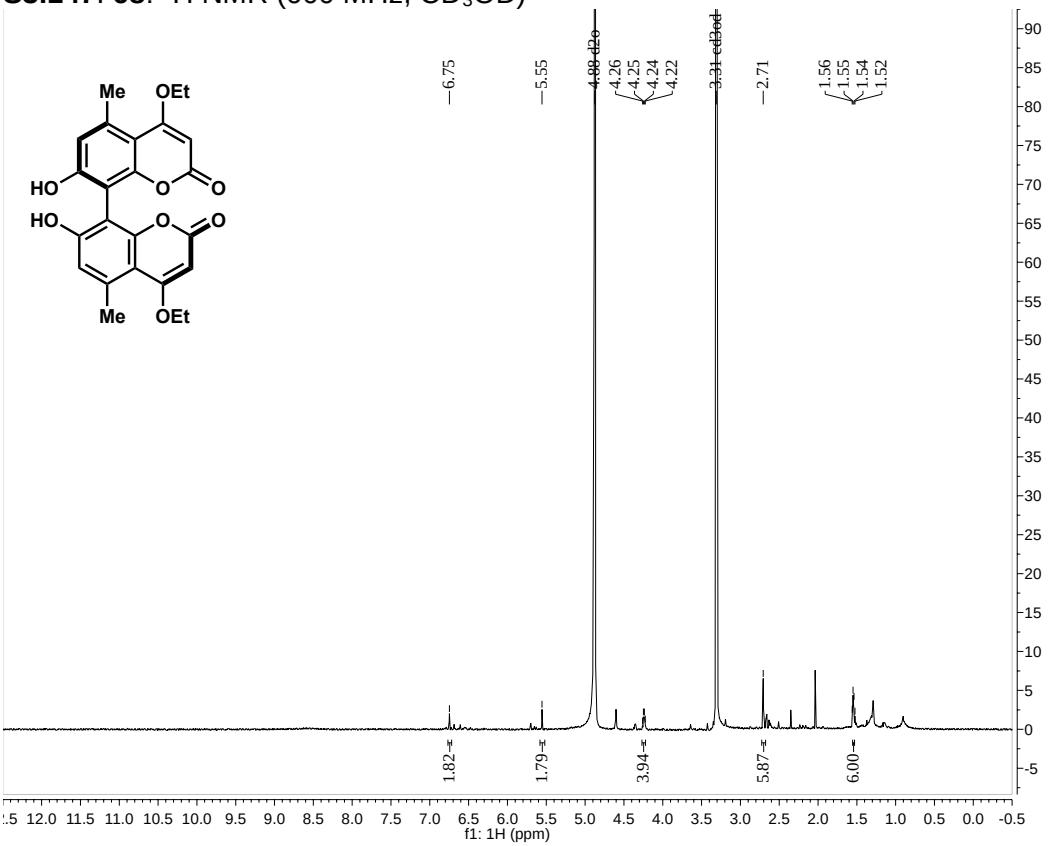

68: ^{1}H NMR (600 MHz, acetone-d_6)

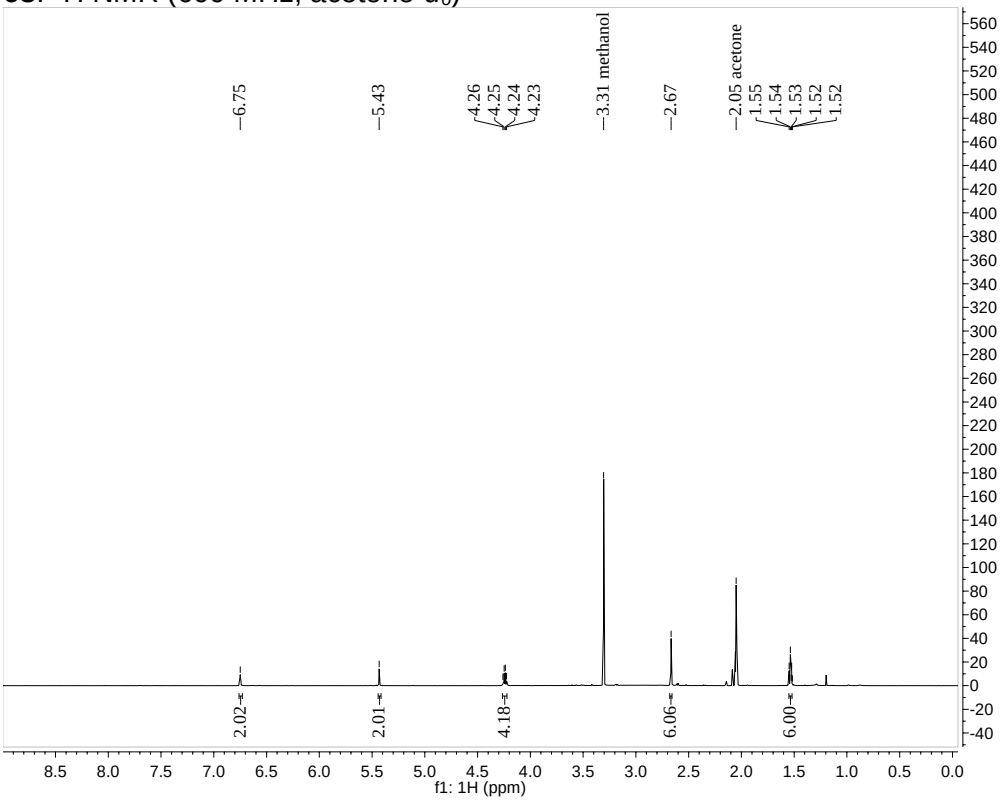

68: ^{13}C NMR (150 MHz, acetone-d_6)

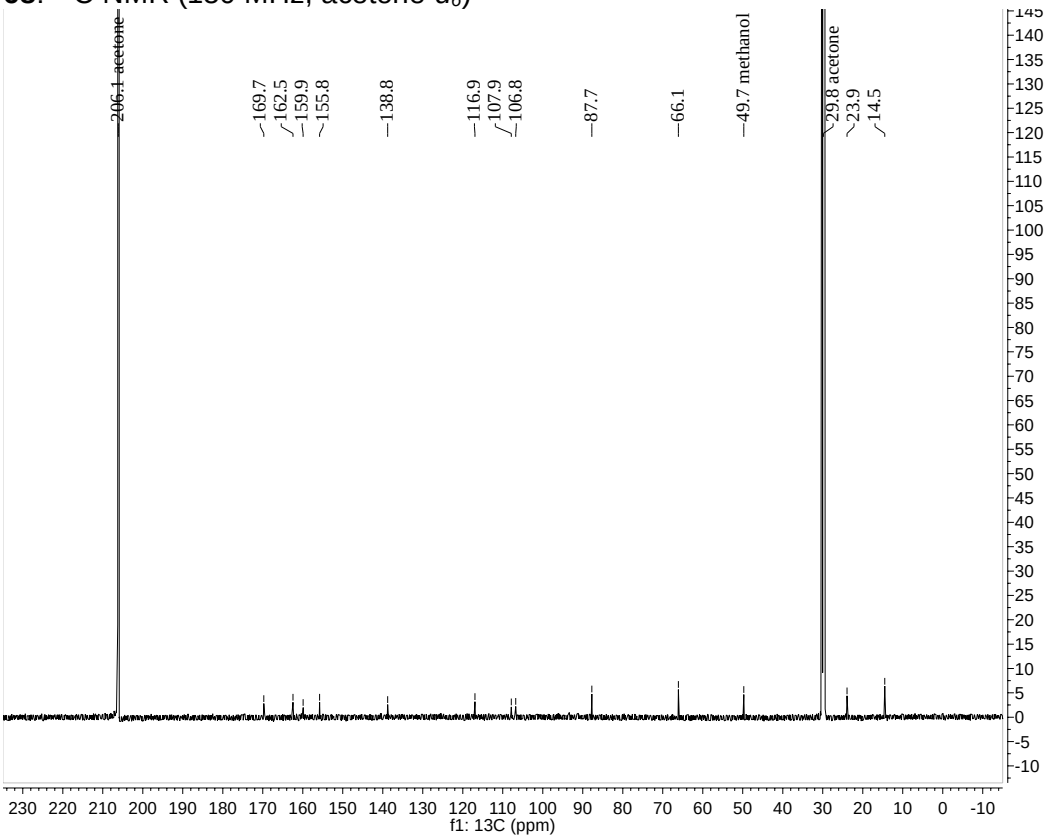

S3.148. 66: ^{1}H NMR (600 MHz, CD_3OD)

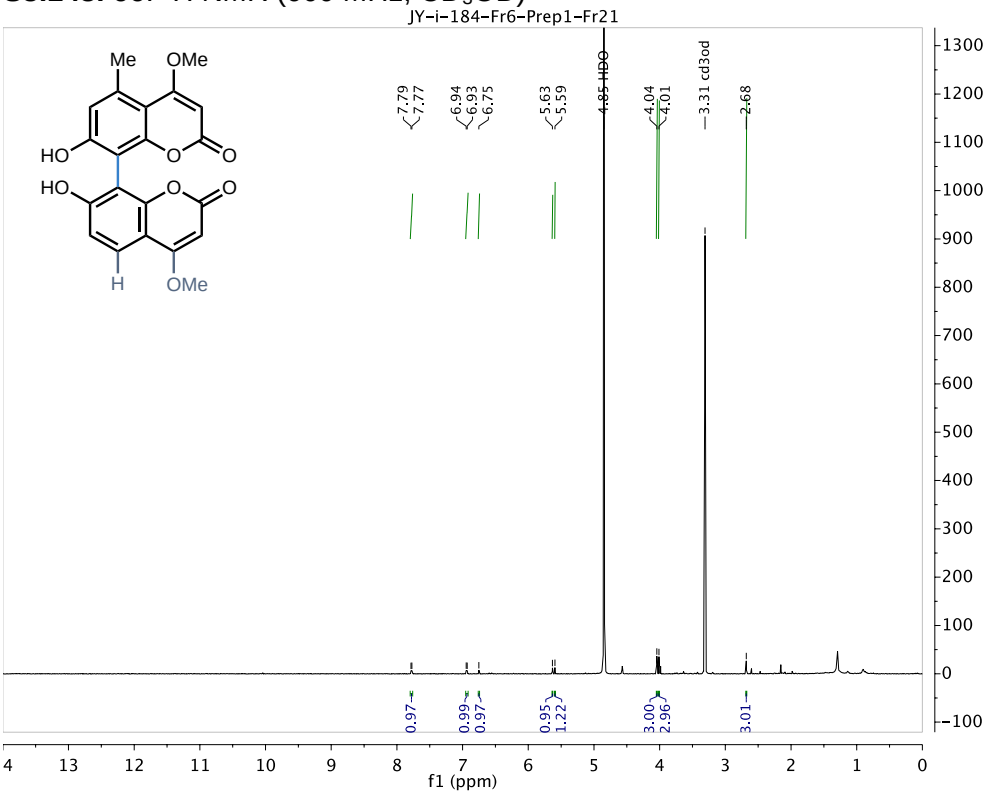

S3.149. 67: ^{1}H NMR (600 MHz, CD_3OD)

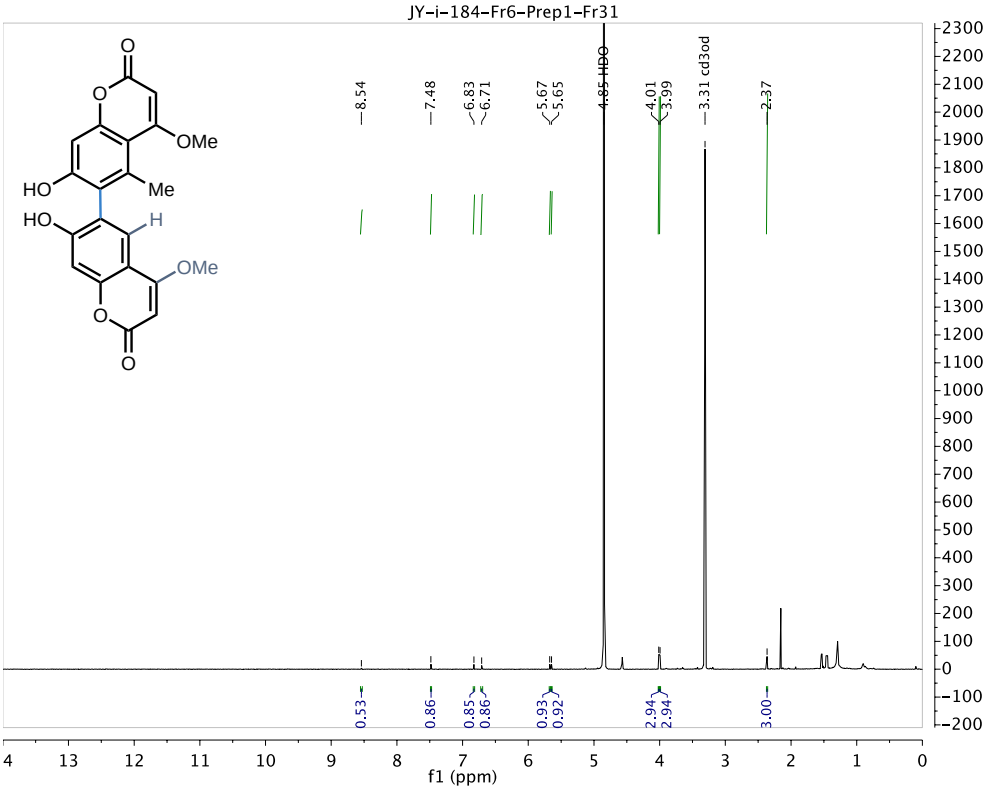

3.12 References

1. Yet, L., *Privileged Structures in Drug Discovery: Medicinal Chemistry and Synthesis*. First ed.; John Wiley & Sons, Inc.: Hoboken, NJ, 2018.

2. Yoon, T. P.; Jacobsen, E. N., Privileged chiral catalysts. *Science* **2003,** *299* (5613), 1691-1693.

3. Ashenhurst, J. A., Intermolecular oxidative cross-coupling of arenes. *Chem. Soc. Rev.* **2010,** *39* (2), 540-548.

4. Kozlowski, M. C., Oxidative coupling in complexity building transforms. *Acc. Chem. Res.* **2017,** *50* (3), 638-643.

5. Yang, Y.; Lan, J.; You, J., Oxidative C–H/C–H coupling reactions between two (hetero)arenes. *Chem. Rev.* **2017,** *117* (13), 8787-8863.

6. Wu, S. K.; Snajdrova, R.; Moore, J. C.; Baldenius, K.; Bornscheuer, U. T., Biocatalysis: Enzymatic Synthesis for Industrial Applications. *Angew. Chem.-Int. Edit.* **2021,** *60* (1), 88-119.

7. Woodley, J. M., New frontiers in biocatalysis for sustainable synthesis. *Curr Opin Green Sust* **2020,** *21*, 22-26.

8. Liu, J.; Liu, A.; Hu, Y., Enzymatic dimerization in the biosynthetic pathway of microbial natural products. *Nat. Prod. Rep.* **2021,** *38* (8), 1469-1505.

9. Yin; Liebscher, J., Carbon−carbon coupling reactions catalyzed by heterogeneous palladium catalysts. *Chem. Rev.* **2007,** *107* (1), 133-173.

10. Boström, J.; Brown, D. G.; Young, R. J.; Keserü, G. M., Expanding the medicinal chemistry synthetic toolbox. *Nat. Rev. Drug Discov.* **2018,** *17* (10), 709-727.

11. Yin, J.; Rainka, M. P.; Zhang, X.-X.; Buchwald, S. L., A highly active Suzuki catalyst for the synthesis of sterically hindered biaryls: novel ligand coordination. *J. Am. Chem. Soc.* **2002,** *124* (7), 1162-1163.

12. Cammidge, A. N.; Crépy, K. V. L., Synthesis of chiral binaphthalenes using the asymmetric Suzuki reaction. *Tetrahedron* **2004,** *60* (20), 4377-4386.

13. Buchwald Martin, R., S. L., Palladium-catalyzed Suzuki−Miyaura cross-coupling reactions employing dialkylbiaryl phosphine ligands. *Acc. Chem. Res.* **2008,** *41* (11), 1461-1473.

14. Valente, C.; Çalimsiz, S.; Hoi, K. H.; Mallik, D.; Sayah, M.; Organ, M. G., The development of bulky palladium NHC complexes for the most-challenging cross-coupling reactions. *Angew. Chem. Int. Ed.* **2012,** *51* (14), 3314-3332.

15. Patel, N. D.; Sieber, J. D.; Tcyrulnikov, S.; Simmons, B. J.; Rivalti, D.; Duvvuri, K.; Zhang, Y.; Gao, D. A.; Fandrick, K. R.; Haddad, N.; Lao, K. S.; Mangunuru, H. P. R.; Biswas, S.; Qu, B.; Grinberg, N.; Pennino, S.; Lee, H.; Song, J. J.; Gupton, B. F.; Garg, N. K.; Kozlowski, M. C.; Senanayake, C. H., Computationally assisted mechanistic investigation and development of Pd-catalyzed asymmetric Suzuki–Miyaura and Negishi cross-coupling reactions for tetra-*ortho*-substituted biaryl synthesis. *ACS Catal.* **2018,** *8* (11), 10190-10209.

16. Ackermann, L.; Potukuchi, H. K.; Althammer, A.; Born, R.; Mayer, P., Tetra-*ortho*-substituted biaryls through palladium-catalyzed Suzuki−Miyaura couplings with a diaminochlorophosphine ligand. *Org. Lett.* **2010,** *12* (5), 1004-1007.

17. Brown, D. G.; Boström, J., Analysis of past and present synthetic methodologies on medicinal chemistry: where have all the new reactions gone? *J. Med. Chem.* **2016,** *59* (10), 4443-4458.

18. Lee, Y. E.; Cao, T.; Torruellas, C.; Kozlowski, M. C., Selective oxidative homo- and cross-coupling of phenols with aerobic catalysts. *J. AM. Chem. Soc.* **2014,** *136* (19), 6782-6785.

19. Nieves-Quinones, Y.; Paniak, T. J.; Lee, Y. E.; Kim, S. M.; Tcyrulnikov, S.; Kozlowski, M. C., Chromium-salen catalyzed cross-coupling of phenols: mechanism and origin of the selectivity. *J. Am. Chem. Soc.* **2019,** *141* (25), 10016-10032.

20. Shalit, H.; Dyadyuk, A.; Pappo, D., Selective oxidative phenol coupling by iron catalysis. *J. Org. Chem.* **2019,** *84* (4), 1677-1686.

21. Reiss, H.; Shalit, H.; Vershinin, V.; More, N. Y.; Forckosh, H.; Pappo, D., Cobalt(II)[salen]-catalyzed selective aerobic oxidative cross-coupling between electron-rich phenols and 2-naphthols. *J. Org. Chem.* **2019,** *84* (12), 7950-7960.

22. Röckl, J. L.; Schollmeyer, D.; Franke, R.; Waldvogel, S. R., Dehydrogenative anodic C−C coupling of phenols bearing electron-withdrawing groups. *Angew. Chem. Int. Ed.* **2020,** *59* (1), 315-319.

23. Kang, H.; Herling, M. R.; Niederer, K. A.; Lee, Y. E.; Vasu Govardhana Reddy, P.; Dey, S.; Allen, S. E.; Sung, P.; Hewitt, K.; Torruellas, C.; Kim, G. J.; Kozlowski, M. C., Enantioselective vanadium-catalyzed oxidative coupling: development and mechanistic insights. *J. Org. Chem.* **2018,** *83* (23), 14362-14384.

24. Libman, A.; Shalit, H.; Vainer, Y.; Narute, S.; Kozuch, S.; Pappo, D., Synthetic and predictive approach to unsymmetrical biphenols by iron-catalyzed chelated radical–anion oxidative coupling. *J. Am. Chem. Soc.* **2015,** *137* (35), 11453-11460.

25. Morimoto, K.; Sakamoto, K.; Ohshika, T.; Dohi, T.; Kita, Y., Organo-iodine(III)-catalyzed oxidative phenol-arene and phenol-phenol cross-coupling reaction. *Angew. Chem. Int. Ed.* **2016,** *55* (11), 3652-3656.

26. More, N. Y.; Jeganmohan, M., Oxidative cross-coupling of two different phenols: an efficient route to unsymmetrical biphenols. *Org. Lett.* **2015,** *17* (12), 3042-3045.

27. Egami, H.; Katsuki, T., Iron-catalyzed asymmetric aerobic oxidation: oxidative coupling of 2-naphthols. *J. Am. Chem. Soc.* **2009,** *131* (17), 6082-6083.

28. Hovorka, M.; Günterova, J.; Zavada, J., Highly selective oxidative cross-coupling of substituted 2-naphthols: a convenient approach to unsymmetrical 1, 1′-binaphthalene-2, 2′-diols. *Tet. Lett.* **1990,** *31* (3), 413-416.

29. Li, X.; Hewgley, J. B.; Mulrooney, C. A.; Yang, J.; Kozlowski, M. C., Enantioselective oxidative biaryl coupling reactions catalyzed by 1, 5-diazadecalin metal complexes: efficient formation of chiral functionalized BINOL derivatives. *J. Org. Chem.* **2003,** *68* (14), 5500-5511.

30. Tian, J.-M.; Wang, A.-F.; Yang, J.-S.; Zhao, X.-J.; Tu, Y.-Q.; Zhang, S.-Y.; Chen, Z.-M., Copper-complex-catalyzed asymmetric aerobic oxidative cross-coupling of 2-naphthols:

enantioselective synthesis of 3,3′-substituted C1-symmetric BINOLs. *Angew. Chem. Int. Ed.* **2019,** *58* (32), 11023-11027.

31. Bringmann, G.; Price Mortimer, A. J.; Keller, P. A.; Gresser, M. J.; Garner, J.; Breuning, M., Atroposelective synthesis of axially chiral biaryl compounds. *Angew. Chem. Int. Ed.* **2005,** *44* (34), 5384-5427.

32. Kočovský, P.; Vyskočil, Š.; Smrčina, M., Non-symmetrically substituted 1,1‘-binaphthyls in enantioselective catalysis. *Chem. Rev.* **2003,** *103* (8), 3213-3246.

33. Kozlowski, M. C.; Morgan, B. J.; Linton, E. C., Total synthesis of chiral biaryl natural products by asymmetric biaryl coupling. *Chem. Soc. Rev.* **2009,** *38* (11), 3193-3207.

34. Bringmann, G.; Gulder, T.; Gulder, T. A. M.; Breuning, M., Atroposelective total synthesis of axially chiral biaryl natural products. *Chem. Rev.* **2011,** *111* (2), 563-639.

35. Aldemir, H.; Richarz, R.; Gulder, T. A., The biocatalytic repertoire of natural biaryl formation. *Angew. Chem. Int. Ed.* **2014,** *53* (32), 8286-8293.

36. Mate, D. M.; Alcalde, M., Laccase: a multi-purpose biocatalyst at the forefront of biotechnology. *Microb. Biotechnol.* **2017,** *10* (6), 1457-1467.

37. Sagui, F.; Chirivì, C.; Fontana, G.; Nicotra, S.; Passarella, D.; Riva, S.; Danieli, B., Laccase-catalyzed coupling of catharanthine and vindoline: an efficient approach to the bisindole alkaloid anhydrovinblastine. *Tetrahedron* **2009,** *65* (1), 312-317.

38. Obermaier, S.; Thiele, W.; Fürtges, L.; Müller, M., Enantioselective phenol coupling by laccases in the biosynthesis of fungal dimeric naphthopyrones. *Angew. Chem. Int. Ed.* **2019,** *58* (27), 9125-9128.

39. Fasan, R., Tuning P450 enzymes as oxidation catalysts. *ACS Catal.* **2012,** *2* (4), 647-666.

40. Noji, M.; Nakajima, M.; Koga, K., A new catalytic system for aerobic oxidative coupling of 2-naphthol derivatives by the use of CuCl-amine complex: a practical synthesis of binaphthol derivatives. *Tet. Lett.* **1994,** *35* (43), 7983-7984.

41. Nakajima, M., Synthesis and application of novel biaryl compounds with axial chirality as catalysts in enantioselective reactions. *Yakugaku Zasshi* **2000,** *120* (1), 68-75.

42. Wu, X.; Iwata, T.; Scharf, A.; Qin, T.; Reichl, K. D.; Porco, J. A., Asymmetric synthesis of gonytolide A: strategic use of an aryl halide blocking group for oxidative coupling. *J. Am. Chem. Soc.* **2018,** *140* (18), 5969-5975.

43. Feldman, K. S.; Ensel, S. M., Ellagitannin chemistry. Preparative and mechanistic studies of the biomimetic oxidative coupling of galloyl esters. *J. Am. Chem. Soc.* **1994,** *116* (8), 3357-3366.

44. Langeslay, R. R.; Kaphan, D. M.; Marshall, C. L.; Stair, P. C.; Sattelberger, A. P.; Delferro, M., Catalytic applications of vanadium: a mechanistic perspective. *Chem. Rev.* **2018,** *119* (4), 2128-2191.

45. Hirao, T., Vanadium in modern organic synthesis. *Chem. Rev.* **1997,** *97* (8), 2707-2724.

46. Kupchan, S. M.; Dhingra, O. P.; Kim, C.-K., Efficient intramolecular monophenol oxidative coupling. *J. Org. Chem.* **1978,** *43* (21), 4076-4081.

47. Buchwald M. R.; S. L., Palladium-catalyzed Suzuki-Miyaura cross-coupling reactions employing dialkylbiaryl phosphine ligands. *Acc Chem Res* **2008,** *41* (11), 1461-73.

48. Patel, N. D.; Sieber, J. D.; Tcyrulnikov, S.; Simmons, B. J.; Rivalti, D.; Duvvuri, K.; Zhang, Y.; Gao, D. A.; Fandrick, K. R.; Haddad, N.; Lao, K. S.; Mangunuru, H. P. R.; Biswas, S.; Qu, B.; Grinberg, N.; Pennino, S.; Lee, H.; Song, J. J.; Gupton, B. F.; Garg, N. K.; Kozlowski, M. C.; Senanayake, C. H., Computationally Assisted Mechanistic Investigation and Development of Pd-Catalyzed Asymmetric Suzuki-Miyaura and Negishi Cross-Coupling Reactions for Tetra-ortho-Substituted Biaryl Synthesis. *ACS Catal* **2018,** *8* (11), 10190-10209.

49. Barder, T. E.; Biscoe, M. R.; Buchwald, S. L., Structural Insights into Active Catalyst Structures and Oxidative Addition to (Biaryl)phosphine−Palladium Complexes via Density Functional Theory and Experimental Studies. *Organometallics* **2007,** *26* (9), 2183-2192.

50. Barder, T. E.; Walker, S. D.; Martinelli, J. R.; Buchwald, S. L., Catalysts for Suzuki−Miyaura Coupling Processes: Scope and Studies of the Effect of Ligand Structure. *J. Am. Chem. Soc.* **2005,** *127* (13), 4685-4696.

51. Yin, J.; Rainka, M. P.; Zhang, X. X.; Buchwald, S. L., A highly active Suzuki catalyst for the synthesis of sterically hindered biaryls: novel ligand coordination. *J Am Chem Soc* **2002,** *124* (7), 1162-3.

52. Castanet, A. S.; Colobert, F.; Broutin, P. E.; Obringer, M., Asymmetric Suzuki cross-coupling reaction: chirality reversal depending on the palladium-chiral phosphine ratio. *Tetrahedron-Asymmetry* **2002,** *13* (6), 659-665.

53. Cammidge, A. N.; Crépy, K. V. L., The first asymmetric Suzuki cross-coupling reaction. *Chemical Communications* **2000,** (18), 1723-1724.

54. Zhao, Q.; Li, C.; Senanayake, C. H.; Tang, W., An efficient method for sterically demanding Suzuki-Miyaura coupling reactions. *Chemistry* **2013,** *19* (7), 2261-5.

55. Tang, W. J.; Patel, N. D.; Xu, G. Q.; Xu, X. B.; Savoie, J.; Ma, S. L.; Hao, M. H.; Keshipeddy, S.; Capacci, A. G.; Wei, X. D.; Zhang, Y. D.; Gao, J. J.; Li, W. J.; Rodriguez, S.; Lu, B. Z.; Yee, N. K.; Senanayake, C. H., Efficient Chiral Monophosphorus Ligands for Asymmetric Suzuki-Miyaura Coupling Reactions. *Org. Lett.* **2012,** *14* (9), 2258-2261.

56. Yang, H.; Sun, J. W.; Gu, W.; Tang, W. J., Enantioselective Cross-Coupling for Axially Chiral Tetra-ortho-Substituted Biaryls and Asymmetric Synthesis of Gossypol. *J. Am. Chem. Soc.* **2020,** *142* (17), 8036-8043.

57. Wurtz, S.; Glorius, F., Surveying Sterically Demanding N-Heterocyclic Carbene Ligands with Restricted Flexibility for Palladium-catalyzed Cross-Coupling Reactions. *Accounts Chem. Res.* **2008,** *41* (11), 1523-1533.

58. Dufert, M. A.; Billingsley, K. L.; Buchwald, S. L., Suzuki-Miyaura Cross-Coupling of Unprotected, Nitrogen-Rich Heterocycles: Substrate Scope and Mechanistic Investigation. *J. Am. Chem. Soc.* **2013,** *135* (34), 12877-12885.

59. Cammidge, A. N.; Crepy, K. V., Application of the Suzuki reaction as the key step in the synthesis of a novel atropisomeric biphenyl derivative for use as a liquid crystal dopant. *J Org Chem* **2003,** *68* (17), 6832-5.

60. Altenhoff, G.; Goddard, R.; Lehmann, C. W.; Glorius, F., Sterically demanding, bioxazoline-derived N-heterocyclic carbene ligands with restricted flexibility for catalysis. *J Am Chem Soc* **2004,** *126* (46), 15195-201.

61. Lundgren, R. J.; Stradiotto, M., Addressing Challenges in Palladium-Catalyzed Cross-Coupling Reactions Through Ligand Design. *Chem-Eur J* **2012,** *18* (32), 9758-9769.

62. Huttel, W.; Nieger, M.; Muller, M., A short and efficient total synthesis of the naturally occurring coumarins siderin, kotanin, isokotanin A and desertorin C. *Synthesis-Stuttgart* **2003,** (12), 1803-1808.

63. Heravi, M. M.; Khaghaninejad, S.; Mostofi, M., Pechmann Reaction in the Synthesis of Coumarin Derivatives. *Adv Heterocycl Chem* **2014,** *112*, 1-50.

64. Xu, G. Q.; Fu, W. Z.; Liu, G. D.; Senanayake, C. H.; Tang, W. J., Efficient Syntheses of Korupensamines A, B and Michellamine B by Asymmetric Suzuki-Miyaura Coupling Reactions. *J. Am. Chem. Soc.* **2014,** *136* (2), 570-573.

65. Zhao, H. P.; Yan, B.; Peterson, L. B.; Blagg, B. S. J., 3-Arylcoumarin Derivatives Manifest Anti-proliferative Activity through Hsp90 Inhibition. *Acs Med Chem Lett* **2012,** *3* (4), 327-331.

66. Sethna, S. M.; Shah, N. M., The Chemistry of Coumarins. *Chem. Rev.* **1945,** *36* (1), 1-62.

67. Mazzaferro, L. S.; Huttel, W.; Fries, A.; Muller, M., Cytochrome P450-Catalyzed Regio- and Stereoselective Phenol Coupling of Fungal Natural Products. *J. Am. Chem. Soc.* **2015,** *137* (38), 12289-12295.

68. Li, Y.; Li, Q., Photochemically reversible and thermally stable axially chiral diarylethene switches. *Org Lett* **2012,** *14* (17), 4362-5.

69. Qu, S.; Greenhalgh, M. D.; Smith, A. D., Isothiourea-Catalysed Regioselective Acylative Kinetic Resolution of Axially Chiral Biaryl Diols. *Chem-Eur J* **2019,** *25* (11), 2816-2823.

70. Noji, M.; Nakajima, M.; Koga, K., A New Catalytic-System for Aerobic Oxidative Coupling of 2-Naphthol Derivatives by the Use of Cucl-Amine Complex - a Practical Synthesis of Binaphthol Derivatives. *Tetrahedron Letters* **1994,** *35* (43), 7983-7984.

71. Shalit, H.; Dyadyuk, A.; Pappo, D., Selective Oxidative Phenol Coupling by Iron Catalysis. *J Org Chem* **2019,** *84* (4), 1677-1686.

72. Shalit, H.; Libman, A.; Pappo, D., meso-Tetraphenylporphyrin Iron Chloride Catalyzed Selective Oxidative Cross-Coupling of Phenols. *J. Am. Chem. Soc.* **2017,** *139* (38), 13404-13413.

73. Narute, S.; Parnes, R.; Toste, F. D.; Pappo, D., Enantioselective Oxidative Homocoupling and Cross-Coupling of 2-Naphthols Catalyzed by Chiral Iron Phosphate Complexes. *J Am Chem Soc* **2016,** *138* (50), 16553-16560.

74. Egami, H.; Matsumoto, K.; Oguma, T.; Kunisu, T.; Katsuki, T., Enantioenriched Synthesis of C-1-Symmetric BINOLs: Iron-Catalyzed Cross-Coupling of 2-Naphthols and Some Mechanistic Insight. *J. Am. Chem. Soc.* **2010,** *132* (39), 13633-13635.

75. Egami, H.; Katsuki, T., Iron-Catalyzed Asymmetric Aerobic Oxidation: Oxidative Coupling of 2-Naphthols. *J. Am. Chem. Soc.* **2009,** *131* (17), 6082-+.

76. Nieves-Quinones, Y.; Paniak, T. J.; Lee, Y. E.; Kim, S. M.; Tcyrulnikov, S.; Kozlowski, M. C., Chromium-Salen Catalyzed Cross-Coupling of Phenols: Mechanism and Origin of the Selectivity. *J Am Chem Soc* **2019,** *141* (25), 10016-10032.

77. Lee, Y. E.; Cao, T.; Torruellas, C.; Kozlowski, M. C., Selective Oxidative Homo- and Cross-Coupling of Phenols with Aerobic Catalysts. *J. Am. Chem. Soc.* **2014,** *136* (19), 6782-6785.

78. Hubbard, J. S.; Harris, T. M., Condensations at the 6 position of the methyl ester and the dimethylamide of 3, 5-dioxohexanoic acid via 2, 4, 6-trianions. *J. Org. Chem.* **1981,** *46* (12), 2566-2570.

79. Xie, S.-S.; Wang, X.; Jiang, N.; Yu, W.; Wang, K. D.; Lan, J.-S.; Li, Z.-R.; Kong, L.-Y., Multi-target tacrine-coumarin hybrids: cholinesterase and monoamine oxidase B inhibition properties against Alzheimer's disease. *Eur. J. Med. Chem.* **2015,** *95*, 153-165.

80. Cao, J.-L.; Shen, S.-L.; Yang, P.; Qu, J., A catalyst-free one-pot construction of skeletons of 5-methoxyseselin and alloxanthoxyletin in water. *Org. Lett.* **2013,** *15* (15), 3856-3859.

81. Linusson, A.; Gottfries, J.; Olsson, T.; Örnskov, E.; Folestad, S.; Nordén, B.; Wold, S., Statistical molecular design, parallel synthesis, and biological evaluation of a library of thrombin inhibitors. *J. Med. Chem.* **2001,** *44* (21), 3424-3439.

82. Chaudhuri, D.; Sigmund, E.; Meyer, A.; Röck, L.; Klemm, P.; Lautenschlager, S.; Schmid, A.; Yost, S. R.; Van Voorhis, T.; Bange, S., Metal-free OLED triplet emitters by side-stepping Kasha's rule. *Angew. Chem. Int. Ed.* **2013,** *52* (50), 13449-13452.

83. Pandey, G.; Muralikrishna, C.; Bhalerao, U., Mushroom tyrosinase catalysed synthesis of coumestans, bebzofuranderivatives and related heterocyclic compounds. *Tetrahedron* **1989,** *45* (21), 6867-6874.

84. Cutler, H. G.; Crumley, F. G.; Cox, R. H.; Hernandez, O.; Cole, R. J.; Dorner, J. W., Orlandin: a nontoxic fungal metabolite with plant growth inhibiting properties. *J. Agric. Food Chem.* **1979,** *27* (3), 592-595.

85. Nozawa, K.; Seyea, H.; Nakajima, S.; Udagawa, S.-i.; Kawai, K.-i., Studies on fungal products. Part 10. Isolation and structures of novel bicoumarins, desertorins A, B, and C, from *Emericella desertorum*. *J. Chem. Soc.* **1987**, 1735-1738.

86. Laakso, J. A.; Narske, E. D.; Gloer, J. B.; Wicklow, D. T.; Dowd, P. F., Isokotanins AC: new bicoumarins from the sclerotia of *Aspergillus alliceus*. *J. Nat. Prod.* **1994,** *57* (1), 128-133.

87. Devji, T.; Reddy, C.; Woo, C.; Awale, S.; Kadota, S.; Carrico-Moniz, D., Pancreatic anticancer activity of a novel geranylgeranylated coumarin derivative. *Bioorg. Med. Chem. Lett.* **2011,** *21* (19), 5770-5773.

88. Dubuffet, T.; Loutz, A.; Lavielle, G., An efficient large scale synthesis of coumarins by a dealkylative boron-mediated ring closure of 3-(ortho-methoxyaryl) propenoic esters. *Syn. Comm.* **1999,** *29* (6), 929-936.

89. Maiti, D.; Buchwald, S. L., Cu-catalyzed arylation of phenols: synthesis of sterically hindered and heteroaryl diaryl ethers. *J. Org. Chem.* **2010,** *75* (5), 1791-1794.

90. Yang, Y.; Lan, J.; You, J., Oxidative C–H/C–H coupling reactions between two (hetero)arenes. *Chem. Rev.* **2017,** *117* (13), 8787-8863.

91. Noji, M.; Nakajima, M.; Koga, K., A new catalytic system for aerobic oxidative coupling of 2-naphthol derivatives by the use of CuCl-amine complex: a practical synthesis of binaphthol derivatives. *Tet. Lett.* **1994,** *35* (43), 7983-7984.

92. Nakajima, M., Synthesis and application of novel biaryl compounds with axial chirality as catalysts in enantioselective reactions. *Yakugaku Zasshi* **2000,** *120* (1), 68-75.

93. Wu, X.; Iwata, T.; Scharf, A.; Qin, T.; Reichl, K. D.; Porco, J. A., Asymmetric synthesis of gonytolide A: strategic use of an aryl halide blocking group for oxidative coupling. *J. Am. Chem. Soc.* **2018,** *140* (18), 5969-5975.

94. Feldman, K. S.; Ensel, S. M., Ellagitannin chemistry. Preparative and mechanistic studies of the biomimetic oxidative coupling of galloyl esters. *J. Am. Chem. Soc.* **1994,** *116* (8), 3357-3366.

95. Langeslay, R. R.; Kaphan, D. M.; Marshall, C. L.; Stair, P. C.; Sattelberger, A. P.; Delferro, M., Catalytic applications of vanadium: a mechanistic perspective. *Chem. Rev.* **2018,** *119* (4), 2128-2191.

96. Hirao, T., Vanadium in modern organic synthesis. *Chem. Rev.* **1997,** *97* (8), 2707-2724.

97. Libman, A.; Shalit, H.; Vainer, Y.; Narute, S.; Kozuch, S.; Pappo, D., Synthetic and predictive approach to unsymmetrical biphenols by iron-catalyzed chelated radical–anion oxidative coupling. *J. Am. Chem. Soc.* **2015,** *137* (35), 11453-11460.

98. Qu, S.; Greenhalgh, M. D.; Smith, A. D., Isothiourea-catalysed regioselective acylative kinetic resolution of axially chiral biaryl diols. *Chem. Eur. J.* **2019**.

99. Li, Y.; Li, Q., Photochemically reversible and thermally stable axially chiral diarylethene switches. *Org. Lett.* **2012,** *14* (17), 4362-4365.

100. Shalit, H.; Libman, A.; Pappo, D., *meso*-Tetraphenylporphyrin iron chloride catalyzed selective oxidative cross-coupling of phenols. *J. Am. Chem. Soc.* **2017,** *139* (38), 13404-13413.

101. Lee, Y. E.; Cao, T.; Torruellas, C.; Kozlowski, M. C., Selective oxidative homo-and cross-coupling of phenols with aerobic catalysts. *J. Am. Chem. Soc.* **2014,** *136* (19), 6782-6785.

102. Zetzsche, L.; Yazarians, J.; Chakrabarty, S.; Hinze, M.; Lukowski, A.; Joyce, L.; Narayan, A.; Murray, L., Biocatalytic oxidative cross-coupling reactions for biaryl bond formation. **2021**. 10.33774/chemrxiv-2021-v0bv6-v2.

Chapter 4: KtnC Protein Engineering for Enhanced Site-selectivity

4.1 Summary

To overcome the challenges accessing the 6,6'-cross-coupled coumarin product bearing the same connectivity as the natural product isokotanin C[1-2] (**5**), a high throughput directed evolution strategy was developed to engineer P450 variants with improved activity and selectivity. Enzyme libraries were generated through semi-rational mutagenesis,[3] wherein beneficial mutations were identified through site-scanning saturation mutagenesis of active site residues.[4] The reactions were analyzed in a tier-one screen by UPLC-DAD or by high throughput RapidFire-mass spectrometry, followed by a tier-two screen employing LC-MS. Over two rounds of evolution, the chemoselectivity and site-selectivity of the P450-mediated reaction were enhanced in comparison to wild type KtnC. A variant possessing two substitutions, P333G and L422V, provided a 3-fold increase in the percent yield of the desired 6,6'-cross-coupled coumarin product. The first substitution, P333G, improved site-selectivity at the expense of percent yield, whereas the L422V substitution increased percent yield but produced some erosion in site-selectivity.

4.2 Introduction

Multiple species of fungi have been implicated in the oxidative dimerization of coumarin **1** in the atroposelective biosynthesis of sterically hindered biaryl natural products.[5-7] Select enzymes responsible for this biosynthetic step have been characterized and reported as cytochrome P450s KtnC and DesC,[6] whereas others are proposed as putative P450 enzymes[2, 7] that provide complementary site-selectivity (Fig 4.1). With three potential sites of bond formation on coumarin **1** at the three, six and eight

positions, six dimeric isomers are possible. The P450s KtnC and DesC were determined to be the oxidative coupling enzymes responsible for the dimerization of coumarin **1** to the natural products (*P*)-orlandin (**2**) and (*M*)-desertorin A (**3**), bearing the 8,8' and 8,6'-connectivities, respectively. Putative P450 enzymes AfvE[8] and BicC[6, 9] were identified in the gene clusters of two different bicoumarin producing *Aspergillus* fungi and were hypothesized to be responsible for producing the 8,3' and 6,6'-isomers (Fig 4.1, **4** and **5**), respectively, however, their functions have not been characterized experimentally as the P450s KtnC and DesC.

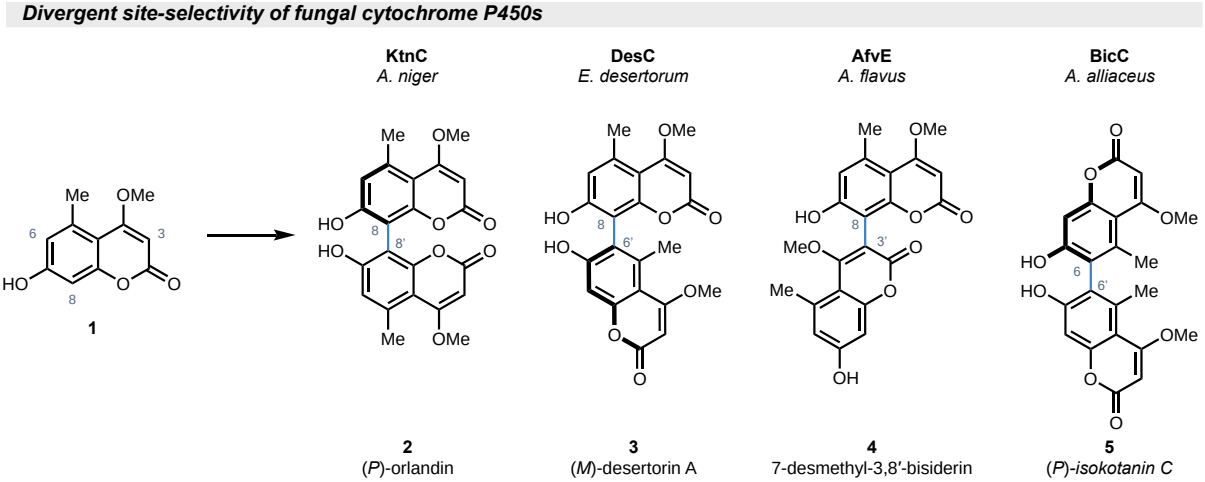

Figure 4.1: Catalyst controlled site- and atroposelectivity in Nature.
Fungal cytochrome P450s catalyze the oxidative dimerization of coumarins selectively. The enzymes responsible for the 3,8' and 6,6' isomers have been proposed in biosynthetic gene clusters of the producing organisms.

The isolation, characterization, and synthesis of symmetrical bicoumarin dimers have been extensively reported, with numerous methods to access natural products the with 8,8', 8,6', and 6,6'-isomers.[1-2, 6, 10-15] In the synthesis of fungal secondary metabolites isokotanins with the 6,6'-configuration (Fig 4.1, **5**), commonly employed strategies rely on building the sterically hindered biaryl bond between two functionalized phenols, then constructing the coumarin ring in subsequent steps.[10-12] However, the synthesis of cross-coupled products in this class of compounds poses an outstanding challenge. In our hands, strategies to synthesize cross-coupled coumarin atropisomers by direct oxidative coupling were explored but were not successful for the synthesis of 6,6' cross-coupled coumarins (Fig 4.2A). Coumarins with similar stereoelectronic properties, **1** and **6**, were combined with different small molecule oxidants commonly used for this chemistry.[16-23] In all reactions, the desired cross-coupled products were not isolable due to low yields and

the formation of multiple dimeric products. A copper catalyst[23] provided 5% relative yield of the 8,8'-cross-coupled isomer, with dimeric products AA and BB as the major products. This catalyst was site-selective with only one 8,8'-isomer formed of each species. Overall, the reaction lacked chemoselectivity and suffered from low yields. Vanadium(III)trifluoride,[24] which excels in the dimerization of coumarins, was not chemo- or site-selective, and although trace amounts of the desired 6,6'-isomer (**8**) were formed, the major products were the 8,8' (**7**) and 8,6'-isomers (not shown), including dimeric and cross-coupled products, resulting in a complex, inseparable mixture. With both copper and vanadium catalysts, the reactivity was governed by inherent electronic properties of the coumarins, and due to the lack of a substantial difference electronically between **1** and **6**, the reactions were not chemoselective, with mixtures of cross-coupled and dimeric

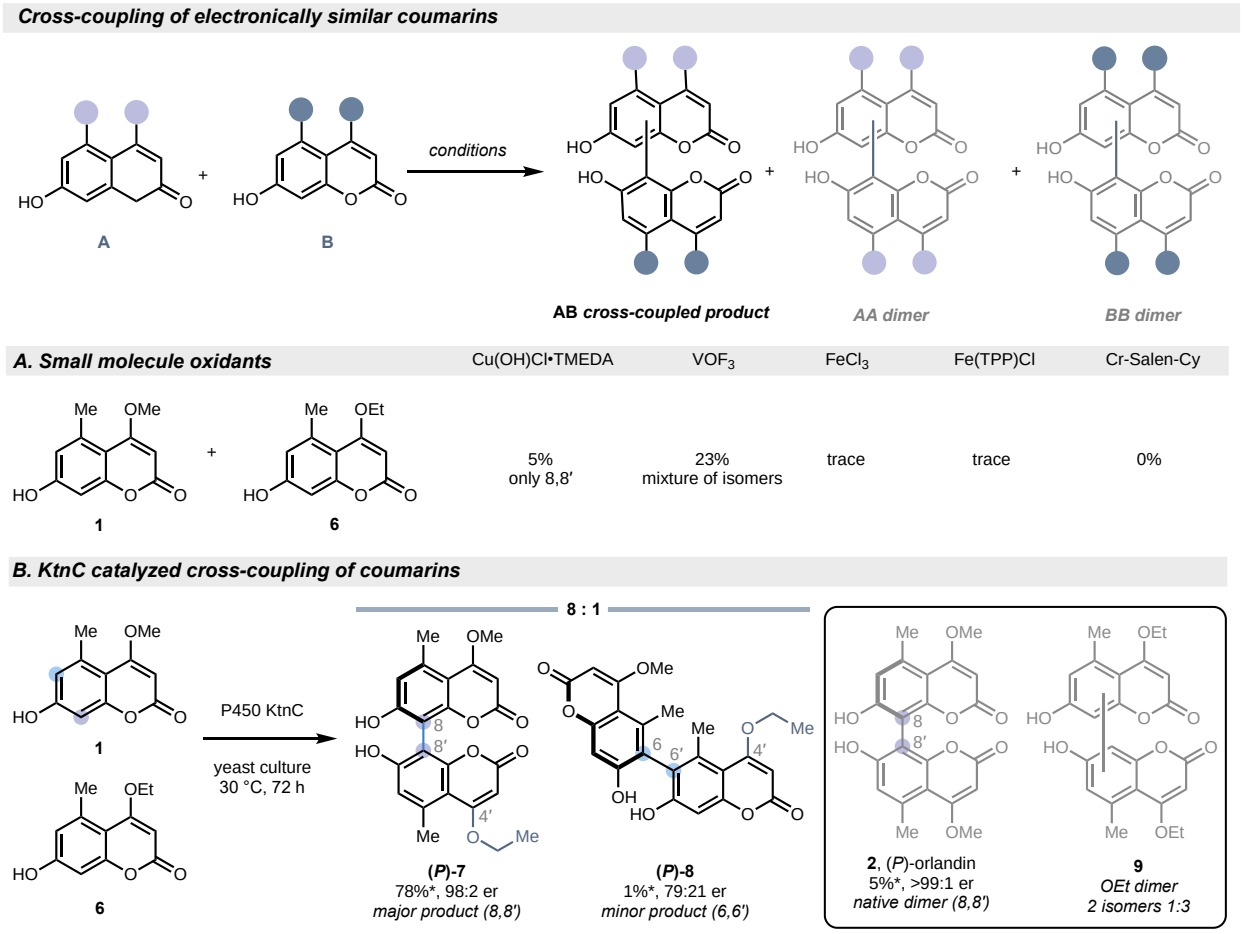

Figure 4.2: Cross-coupling of structurally and electronically similar coumarins.
A. Small molecule catalysts used in cross-coupling of coumarins **1** and **6** resulted in inseparable mixtures. Percent relative yields calculated by LC-MS. B. KtnC catalyzed cross-coupling: *P. pastoris* cells expressing KtnC in the presence of **1** and **6** combined in a 1:10 molar ratio, 100 µM **1** at 30°C with shaking at 235 rpm for 72 h, reported as percent conversions.

products occurring in both reactions. Trace amounts of cross-coupled products are formed with iron catalysts,[19-20] and no reactivity was observed with the chromium catalyst.[17, 25]

The challenge of overriding innate reactivity and selectivity in direct oxidative coupling reactions has limited the reliable use of this method for convergent synthetic approaches. Previously, we demonstrated that a biocatalytic solution could overcome the hurdles in reactivity of an oxidative cross-coupling reaction by surpassing electronic limitations to achieve catalyst-controlled selectivity in biaryl coupling reactions.[26] In contrast to small molecule mediated oxidative coupling reactions, we developed a biocatalytic method that was selective for cross-coupling of coumarins **1** and **6** atroposelectively (Fig 4.2B). Small amounts of the native dimer (**2**) were observed, and dimerization of the coupling partner (**6**) added in excess was also present (**9**), however, the cross-coupled product was formed preferentially under the reaction conditions. Although the major product of the cross-coupling reaction was the 8,8'-isomer (*P*)-**7**, a minor product with the 6,6'-connectivity, (*P*)-**8**, was also observed.

The engineering of P450 KtnC to a variant, LcX5, was recently disclosed.[26] The new variant enhanced the site-selectivity and percent yield of biocatalytic cross-coupling reaction with coumarin **10** and 2-naphthol (**11**, Fig 4.3). The variant produced a 92-fold improvement in the yield of product **12** compared to wild type KtnC, and further engineering produced an atroposelective variant, LcX7.[26] This engineering campaign resulted in a biocatalyst (top left) that outperformed the methods employed by traditional synthesis with transition metal catalysts and Suzuki cross-coupling (combining **13** and **14**), demonstrating the tunability of P450s for

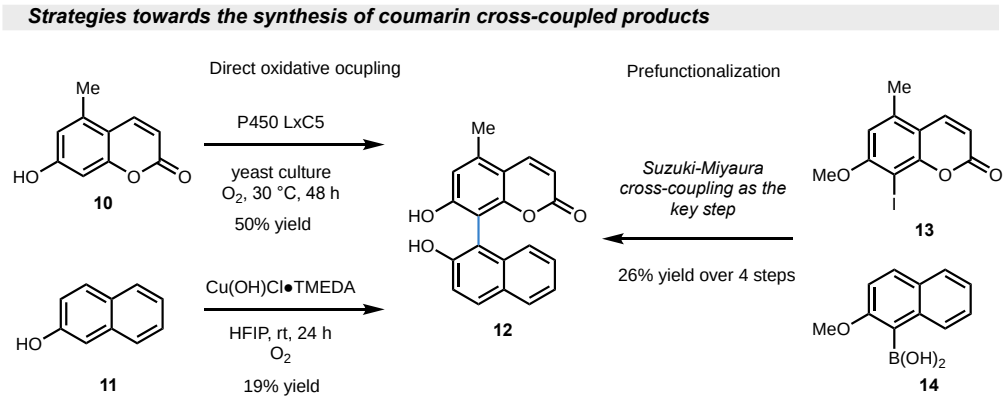

Figure 4.3: Synthesis of cross-coupled coumarin products.
The biocatalytic method using KtnC variant LxC5 was superior to direct oxidative coupling with a small molecule oxidant and by a prefunctionalization strategy utilizing a Suzuki-Miyaura cross-coupling reaction as the key step.

oxidative cross-coupling reactions. With the synthetic challenge of synthesizing cross-coupled coumarin products with the 6,6'-connectivity, we hypothesized that KtnC could be engineered for this desired selectivity. The ability to directly cross-couple two phenolic substrates with similar structural and electronic features is challenging using traditional synthetic methods. For cases in which there is a large difference in the oxidation potential of two phenolic substrates, cross-coupling is predictable and can proceed favorably. However, mixtures of products results when little or no difference in the substrates' oxidation potential exists,[21, 27] posing a challenge in chemoselectivity (dimerization versus cross-coupling) as well. By engineering a biocatalyst, we hypothesized that these limitations in chemo- and site-selectivity could be removed.

4.3 Directed evolution of KtnC

To overcome these challenges in the cross-coupling reaction of coumarins, we developed a high throughput directed evolution strategy to identify P450 variants with both improved activity and selectivity for the target reaction. Enzyme libraries were generated through semi-rational mutagenesis, wherein beneficial mutations were identified through site-scanning saturation mutagenesis of active site residues and then folded together in combinatorial libraries made by combinatorial site-directed mutagenesis.[4] This engineering strategy generated thousands of variants in each round of evolution, with each variant harboring one or several mutations within 12 Å of the predicted substrate-binding region in the active site. Reactions with these engineered protein libraries were performed as yeast biotransformations in 96-well plates and analyzed by UPLC-DAD or by high throughput RapidFire-mass spectrometry for total cross-coupled product formation. Reaction mixtures containing higher levels of cross-coupled product formation were then analyzed for site-selectivity in a second-tier screen using standard LC-MS. Ultimately, this two-tier mass spectrometry-based screen enabled rapid identification of variants with improved activity and selectivity for the target cross-coupling reaction.

Biotransformations were initially optimized for cross-coupled product formation by adding the non-native coupling partner **6** in excess (Fig 4.2B) to cultures of *Pichia pastoris*

expressing KtnC to achieve high percent conversion. This strategy is often employed to favor cross-coupling in small molecule mediated oxidative cross-coupling reactions but not atom economical and ultimately undesirable. Adding the non-native coumarin coupling partner in a 1:10 molar ratio was not practical on preparative scale, and to improve the synthetic utility and scalability of the reaction, a 1:1 molar ratio of the substrates was desired. The reaction was optimized in *Saccharomyces cerevisiae* to benchmark this ratio of substrates **1** and **6** (Fig 4.4). As anticipated, the major product of the reaction was the native dimer (**2**), formed in a 32% yield, and the yield of cross-coupled products were reduced significantly. The 8,8'-isomer (**7**) was formed as the major cross-coupled product in 21% yield. The desired, minor 6,6'-isomer (**8**) was formed in 13% yield. Dimerization of coumarin **6** was also observed producing a 15% yield of **9**, with two isomeric products formed in a 1:3 ratio.

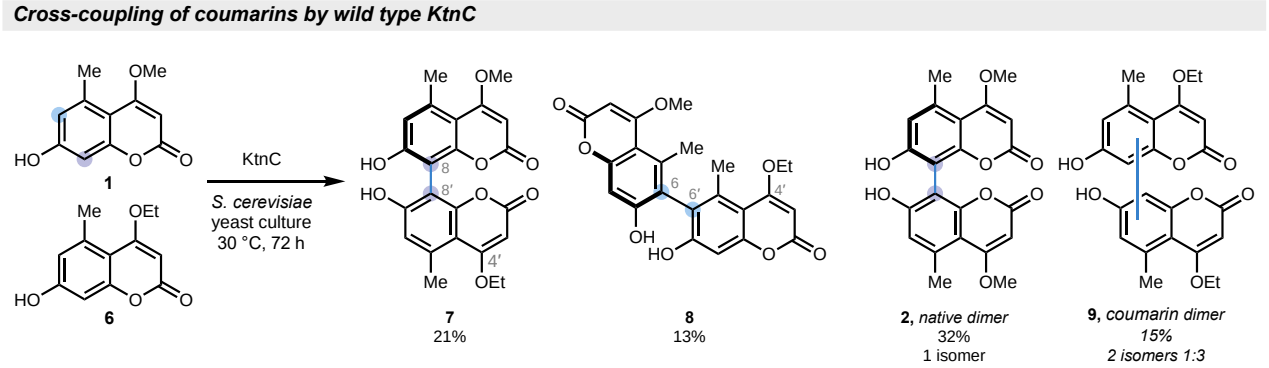

Figure 4.4: KtnC catalyzed cross coupling in *S. cerevisiae*.
KtnC catalyzed cross-coupling: *S. cerevisiae* cells expressing KtnC in the presence of **1** and **6** combined in a 1:1 molar ratio, 100 µM each at 30 °C with shaking at 235 rpm for 72 h, reported as relative percent yields.

Two analytical methods for a tier-one screen were developed. The first utilized UPLC separation coupled with a DAD detector, and the second was developed for high throughput reaction screening by RapidFire-mass spectrometry. Both methods were sufficient for identifying variant hits and required a tier-two screen to validate hits by LC-ToF MS, however the key benefit in RapidFire screening was speed. For comparison, screening one 96-well plate by RapidFire-MS required roughly 40 minutes, in comparison to the UPLC-DAD method requiring 11 hours, with a typical library comprised of 20 x 96-well plates. However, library screening could still be achieved by UPLC-DAD without access to the RapidFire-MS instrument (see Supplementalsection S4.3).

In the first round of evolution, biotransformations were screened to identify new variants of the gene encoding KtnC that provided improved site-selectivity for the 6,6'-isomer. The data from tier-one and tier-two screens were arranged in a waterfall plot to compare the fold-improvement scores and to identify the variant with desired reactivity (Fig 4.5). In the tier-one screen (red), the peak of product **8** was normalized with an internal standard (IS, 3-bromo-2-naphthol) and compared to the positive control to calculate the fold-improvement scores. The fold-improvement scores were plotted, and the top 96 variants were chosen to move to the tier-two screen for analysis by LC-ToF MS. In the tier-two screen, the relative percent yields of products, both dimers and all cross-coupled products, were calculated and plotted as fold-improvement compared to the template wild-type KtnC. Two options to categorize hits were compared (right, purple and chartreuse). The fold-improvement scores of the ratio of the desired 6,6'-isomer and the 8,8'-isomer were plotted (purple) as a measure of the site-selectivity of the reaction. Alternatively, the fold-improvement score of the relative percent yield to the desired product was also calculated and plotted (chartreuse) as a measure of

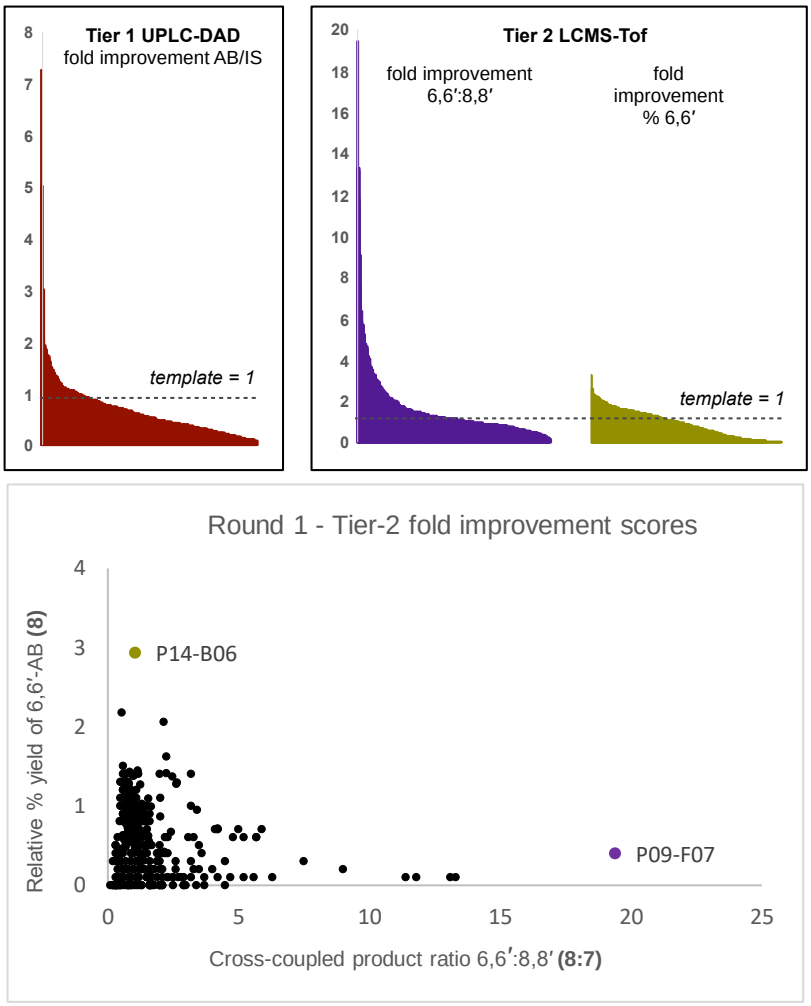

Figure 4.5: Screening results of round one engineering.
Results from tier-one and tier-two screens, with fold-improvement (FI) scores calculated relative to wild-type KtnC. Conditions: *S. cerevisiae* cells in 96-well plates expressing KtnC variants in the presence of **1** and **6** combined in a 1:1 molar ratio, 300 μM each at 30 °C with shaking at 235 rpm for 72 h. Top fold-improvement scores in tier-two screen: ratio of 66:88 AB products: 19 FI, relative percent yield to 6,6' product **8**: 1.5 FI.

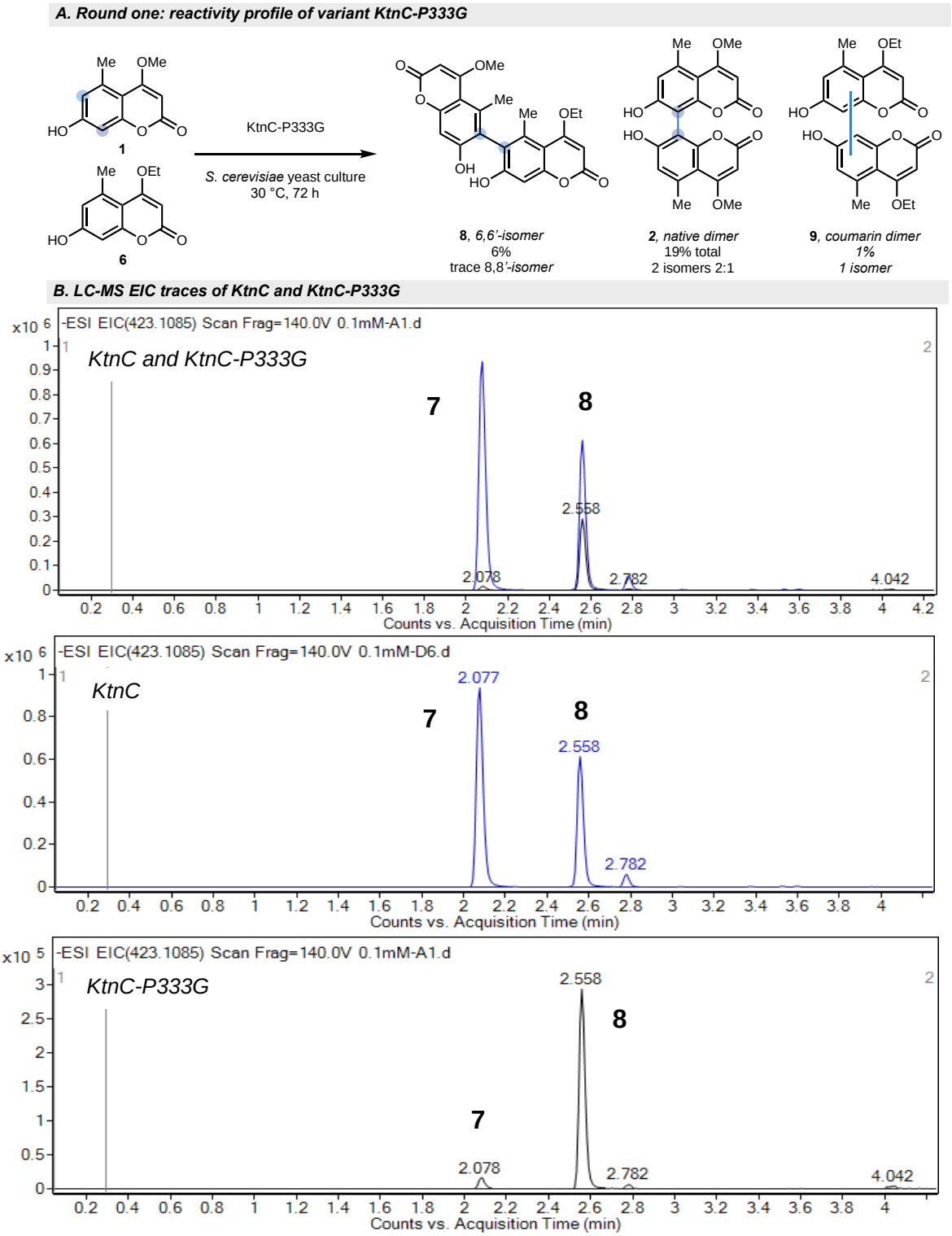

Figure 4.6: KtnC-P333G variant cross-coupling in *S. cerevisiae*.
A. KtnC-P333G catalyzed cross-coupling: *S. cerevisiae* cells expressing KtnC in the presence of **1** and **6** combined in a 1:1 molar ratio, 100 µM each at 30°C with shaking at 235 rpm for 72 h, reported as relative percent yields. B. Extracted ion chromatograms of the cross-coupled product mass. Top trace overlaid KtnC (blue trace) and KtnC-P333G (black trace), with peaks for cross-coupled 8,8'-product **7** and 6,6'-product **8** highlighted.

the activity of the enzyme for the desired product. Comparing the two plots, we found that there was modest improvement in activity (1.5 fold-improvement relative percent yield), but substantial improvement in the selectivity (19 fold-improvement).

After validating the results from the tier-one and tier-two screens, a variant, P333G, was identified with improved chemoselectivity and site-selectivity for the desired product isomer, at the expense of lower total activity (Fig 4.6A). The selective variant displayed a reduction in the formation of the native dimer (**2**) and non-native dimer, with only trace amounts of the 8,8'-cross-coupled product (**7**) normally formed as the major product with wild type KtnC biotransformations (Fig 4.6B). However, the relative percent yield to the desired product was reduced to 6% from 13% yield with wild-type KtnC. This trade-off was judged acceptable due to the enhanced site-selectivity, and the reduction of dimerization of both substrates, but was not ideal. A new coumarin dimer was also observed, and while the total conversion to coumarin dimers was reduced, the new dimer of coumarin **1** was formed as a minor product in a 2:1 ratio (12% **2** and 7% of the new isomer).

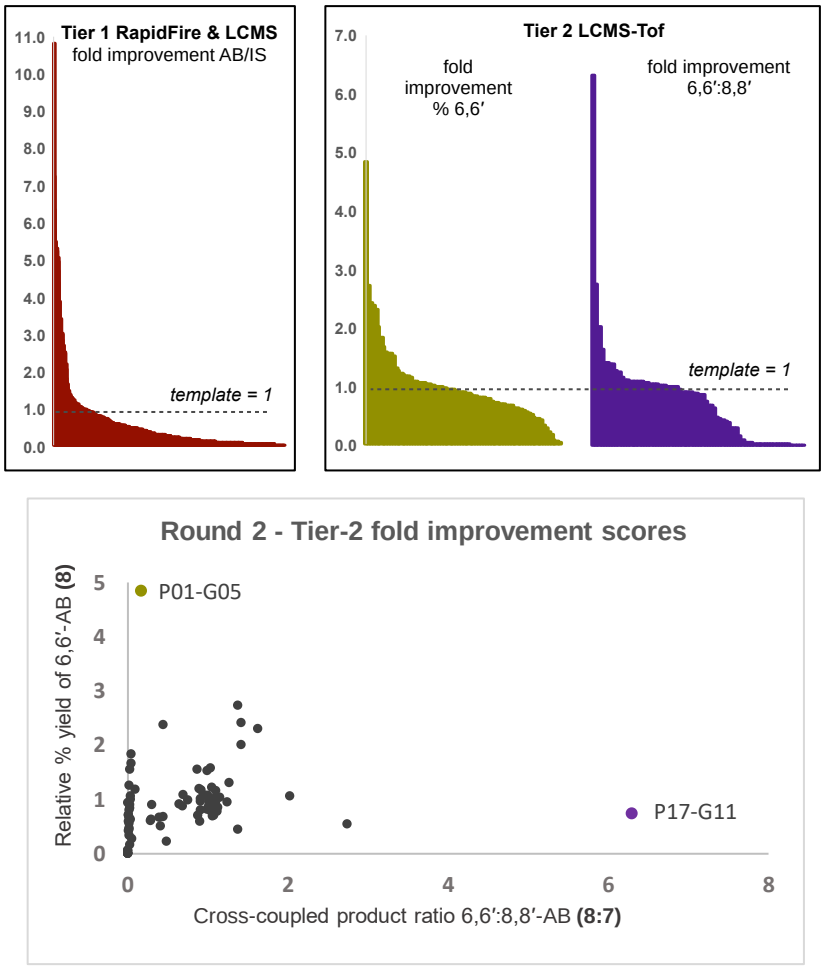

Figure 4.7: Screening results of round two engineering.
Results from tier-one and tier-two screens, with fold-improvement (FI) scores calculated relative to KtnC-P333G. Conditions: *S. cerevisiae* cells in 96-well plates expressing KtnC in the presence of **1** and **6** combined in a 1:1 molar ratio, 100 µM each at 30 °C with shaking at 235 rpm for 72 h. Top FI scores in tier-two screen: relative percent yield to 6,6'-product **8**: 4.8 FI.

In round two, a tier-one screen utilizing RapidFire-MS was utilized, which allowed the screening of 20 reaction plates (96-well) in less than 10 hours. The peak areas

corresponding to the cross-coupled product mass (AB) for each plate were normalized with an internal standard (IS, 4,4'-dihydroxybenzophenone) and organized into a waterfall plot (Fig 4.7, red). The top 96 hits from the tier-one screen were selected for analysis by Tof-LC MS in a tier-two screen, and the fold-improvement scores for both relative percent yield to the desired product (purple, % 6,6'-AB) and selectivity (chartreuse, 6,6'/8,8'-AB) were calculated and plotted. We observed variants with improved relative percent yield, reaching nearly 5-fold improvement over the template, P333G, and selective variants approaching 7-fold improvement in the ratio of cross-coupled products. However, as observed in round one, the most selective variants were not the most active. Increased activity was selected moving forward, and the tier-two hits were selected for validation and sequencing.

A variant was identified that was substantially more active than wild type KtnC, and the activity lost in round one was recovered. The variant KtnC-P333G-L422V showed an increase in the relative percent yield of the 6,6'-isomer (**8**), while mostly maintaining the selectivity profile established in round one. The new variant KtnC-P333G-L422V was less selective, with 9% conversion to the 8,8'-isomer (**7**), compared to only trace amounts of this product in round one with variant KtnC-P333G. No change in the total amount of the dimers of coumarin **1** was noted (19% in round one with KtnC-P333G and 17% total in round two with KtnC-P333G-L422V), with the minor dimeric product observed in a 3:1 ratio with the expected 8,8'-dimer (**2**). The erosion of selectivity in the dimerization reactions was initially attributed to the first mutation, P333G, and all the new variants from

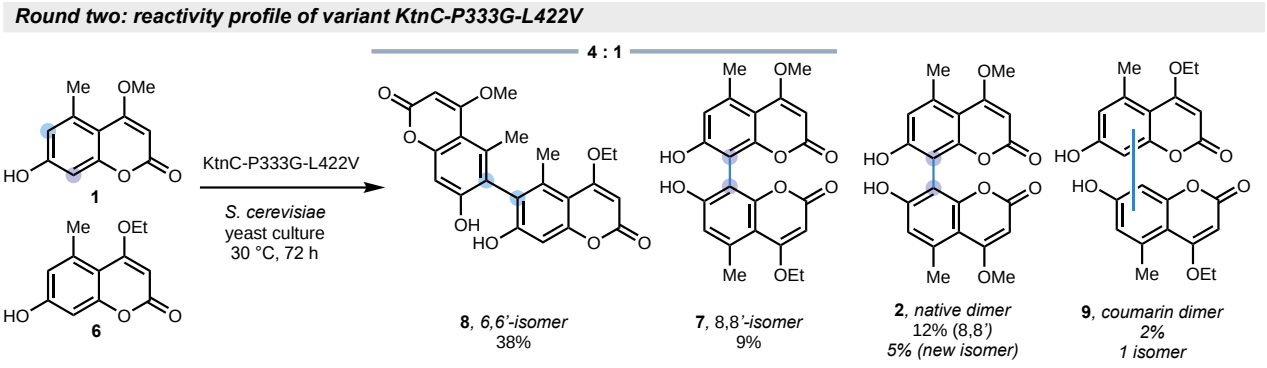

Figure 4.8: KtnC-P333G-L422V variant cross-coupling in *S. cerevisiae*.
A. KtnC-P333G-L422V catalyzed cross-coupling: *S. cerevisiae* cells expressing KtnC in the presence of **1** and **6** combined in a 1:1 molar ratio, 100 µM each at 30°C with shaking at 235 rpm for 72 h, reported as relative percent yields.

round two profiled in the validation stage formed two product dimers (Fig 4.9, AA1 and

AA2). However, this trend was also present in variant KtnC-G333P-F328L which underwent a reversion to lose the first mutation incorporated in round one. All of the round two hits validated were more active for the desired cross-coupling product, but not as selective (Fig 4.9, fold-improvement scores).

Two rounds of engineering were performed. In the initial round a KtnC variant was identified that was more selective (KtnC-P333G), producing the desired 6,6'-cross-coupled product exclusively in a 6% relative yield and a reduction in competing dimerization, albeit at the expense of percent yield (KtnC 13% down to 6%). The second round of engineering sought to increase the percent yield of the reaction while maintaining selectivity, and a second substitution (L422V) was identified that increased the amount of the desired product 7-fold to 38%. The second round of evolution provided a more active biocatalyst, JYxC2, but a regression in the site-selectivity was observed, with the 8,1'-product (**7**) formed in a 9% relative yield.

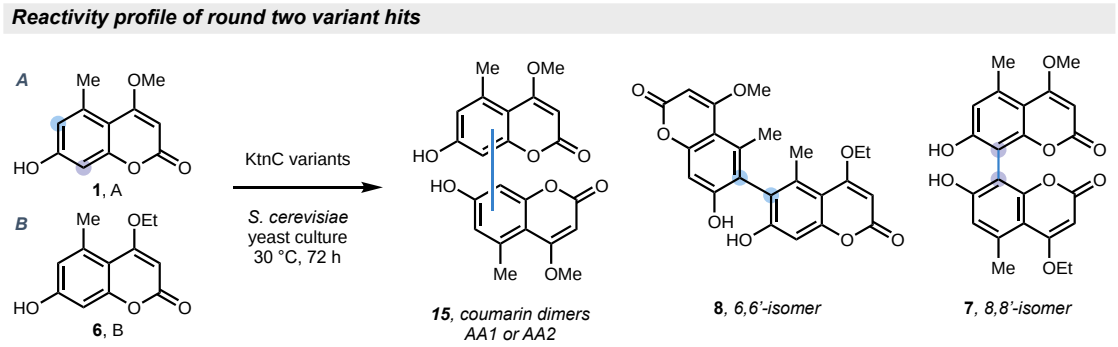

New dimer products observed

96 RXN Well	%AA1	%AA2	total %AA	%AB1 - 88	%AB2 - 66	fold impr %66	total %AB	*Mutation*
P01-A07	24	12	35.9	0.9	12.2	2.3	13	N132K
P01-D04	23	10	32.7	0.8	12.1	2.2	13	L323V
P01-G05	**12**	**5**	**16.8**	**9.0**	**37.9**	**7.0**	**47**	**L422V**
P15-C05	17	18	35.6	0.6	16.1	3.0	17	F328L, G333P
P20-B08	22	16	38.3	0.8	12.1	2.2	13	S120T

Figure 4.9: KtnC variant reactivity in round two.
New dimeric products observed with round two variants, AA1 and AA2. Relative percent yields, coumarin dimers (AA's), and cross-coupled products (AB's). Fold-improvement scores for relative percent yield calculated for cross-coupled product **8**.

4.4 Combinatorial library

A combinatorial library was engineered from template KtnC-P333G to combine the hits from library round one to fold in the mutations that were identified as beneficial in initial screening. In round one, nine unique mutations were identified as hits, comprised of mutations that provided better selectivity (entry 1, 29 fold-improvement) or higher percent yield (entries 2 and 4, 3 fold-improvement) of the desired 6,6'-isomer (Fig 4.10).

Primers were designed to incorporate these mutations (see Supplementaltable S4.2-S4.3) and the mutations were successfully incorporated into the DNA library. Five 96-well plates were screened with RapidFire-MS as the tier-one screen, and Tof-LC-MS as the tier-two screen (Fig 4.11). Fold-improvement scores were low in comparison to round one evolution at less than 2 fold-improvement over KtnC-P333G (red).

Looking at the tier-two fold-improvement scores of both the percent yield of the desired product (chartreuse) and the ratio of 6,6':8,8'-cross-coupled products (purple), there was little improvement over the variant KtnC-P333G in both metrics. Less general

A. Round one reactivity of validated hits and sequencing

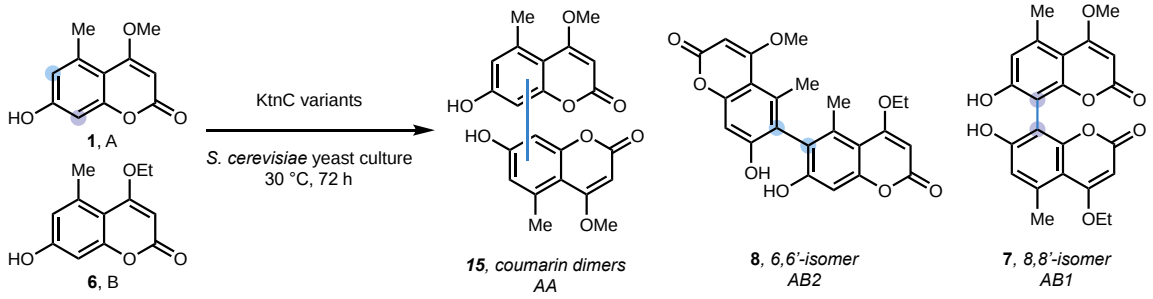

B. Calculated relative percent yields and sequencing data

entry	96 well plate	total %AA	%AB1 - 88	%AB2 - 66	fold improvement	%AB3	total %AB	ratio AB 66:88	fold improvement	Mutation
1	**P9-F7**	**19.1**	**0.3**	**6.0**	**0.5**	**0.1**	**6.4**	**17.3**	**28.8**	**P333G**
2	P12-C9	27.9	13.7	10.2	3.1	2.5	26.4	0.7	0.3	Y99K
3	P4-B2	8.2	2.8	6.9	0.5	0.5	10.2	2.5	4.2	L253G
4	P13-D2	26.8	8.3	10.7	3.2	1.5	20.6	1.3	0.6	S513G
5	P9-A8	6.3	0.4	1.5	0.1	0.0	1.8	4.2	6.9	P515R
6	P10-D7	12.4	0.8	3.2	0.3	0.1	4.0	4.2	6.9	P515G
7	P4-C1	8.1	2.7	6.3	0.5	0.5	9.5	2.3	3.8	P515L
8	P7-F2	13.3	1.3	2.6	0.2	0.0	3.9	2.0	3.3	P515W
9	P7-G8	19.5	1.1	3.9	0.3	0.1	5.2	3.4	5.7	Y517E

Figure 4.10: Sequencing results of round one hits.
Nine mutations were identified in round one engineering that were potential hits. Fold improvement scores calculated compared to wild type KtnC positive controls.

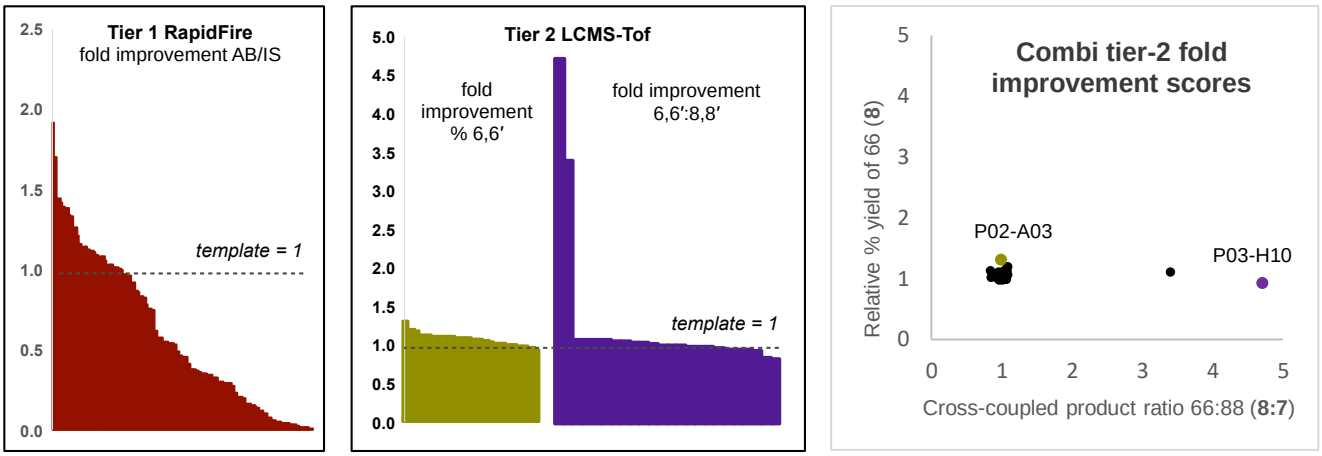

Figure 4.11: Screening results of round one combinatorial library engineering.
Results from tier-one and tier-two screens, with fold-improvement (FI) scores calculated relative to KtnC-P333G. Conditions: *S. cerevisiae* cells in 96-well plates expressing KtnC in the presence of **1** and **6** combined in a 1:1 molar ratio, 100 µM each at 30 °C with shaking at 235 rpm for 72 h.

activity was observed in the tier-one screen, with most variants resulting in no activity (see Supplementaltraces S4.18-S4.22). The top hits were validated and sequenced (Fig 4.12), and were found to be template KtnC-P333G, apart from one variant that incorporated an additional mutation, P515L, however this variant was not more active than the template controls. We hypothesized that the combination of mutations may be deleterious to enzyme activity, however, more evidence is needed to support this claim.

Combinatorial library sequencing data						
entry	***RF fold improv***	**%AA**	**%AB1 8,8′**	**%AB2 6,6′**	**fold impr % 6,6′**	***Mutation***
P02_C08	1.1	15	0.4	6.6	1.4	template
P02_G05	1.4	15	0.4	6.7	1.4	template
P03_H10	1.3	12	0.1	5.3	1.1	P515L
P04_B06	1.1	12	0.1	5.4	1.1	template

Table 4.1: Screening results of the combinatorial library.
Results from validation of the combinatorial library, with fold-improvement (FI) scores calculated relative to KtnC-P333G. Conditions: *S. cerevisiae* cells in 96-well plates expressing KtnC in the presence of **1** and **6** combined in a 1:1 molar ratio, 100 µM each at 30°C with shaking at 235 rpm for 72 h.

4.5 Discussion and conclusions

Two mutations were identified that improved both the site-selectivity and percent yield of the desired 6,6'-product. However, as observed in previous engineering

campaigns, optimization of the different types of selectivity simultaneously can be challenging.[26] In the initial rounds of engineering of LxC5-7 variants, an increase in the total amount of cross-coupled product was selected for improvement in the first rounds of evolution. Although there was increased cross-coupled product, the site-selectivity suffered, and an undesired C–O isomer was formed as one of the major products along with the desired 8,1'-isomer. Additional rounds of evolution were required to regain site-selectivity. In this campaign, site-selectivity was chosen as the initial selectivity feature to enhance with engineering, and a similar inverse relationship was observed – with increased selectivity, a reduction in reactivity was noted. When enhanced reactivity (percent yield of the 6,6'-cross-coupled product) was selected in round two, a variant was identified with higher percent yield, but at the expense of site selectivity, although the major product remained the desired 6,6'-isomer (see Fig 4.12).

In the cross-coupling of two electronically and structurally similar coumarins, the multiple types of selectivity must be controlled, including the chemoselectivity (dimerization over cross-coupling), site-selectivity (the formation of one desired isomer), atroposelectivity in tetra-*ortho*-substituted biaryls, and the general reactivity (percent yield). The P450 enzyme KtnC showed some activity towards the formation of an isokotanin type connectivity, forming a cross-coupled product with the 6,6'-connectivity as a minor product (Fig 4.13A). Over two rounds of evolution, improvement in the site-selectivity and percent yield of **8** was achieved, from an initial relative percent conversion of 13% to 38% (Fig 4.14B-C). Whereas KtnC variant JYxC2 achieved both an increase in the percent yield and the site-selectivity compared to wild-type KtnC, switching the major product from the 8,8' to the 6,6'-isomer and suppressing dimerization, additional rounds of evolution are required to further enhance the biocatalysts selectivity and yield. A careful analysis of the different features of selectivity should be considered during an evolution campaign, and the complexity of achieving all types of selectivity can be challenging to balance. More data on the substitutions associated with enhancement of each type of selectivity would be helpful to identify trends and potentially guide future engineering campaigns. The atroposelectivity of the reaction was not considered, due to limitations in the chiral separation of the two isomeric products, however, as the atroposelectivity was observed to decrease over rounds of evolution towards LxC5,[26] thus, it is important to

develop analytical methods to measure the enantioselectivity across each round of evolution for this reaction.

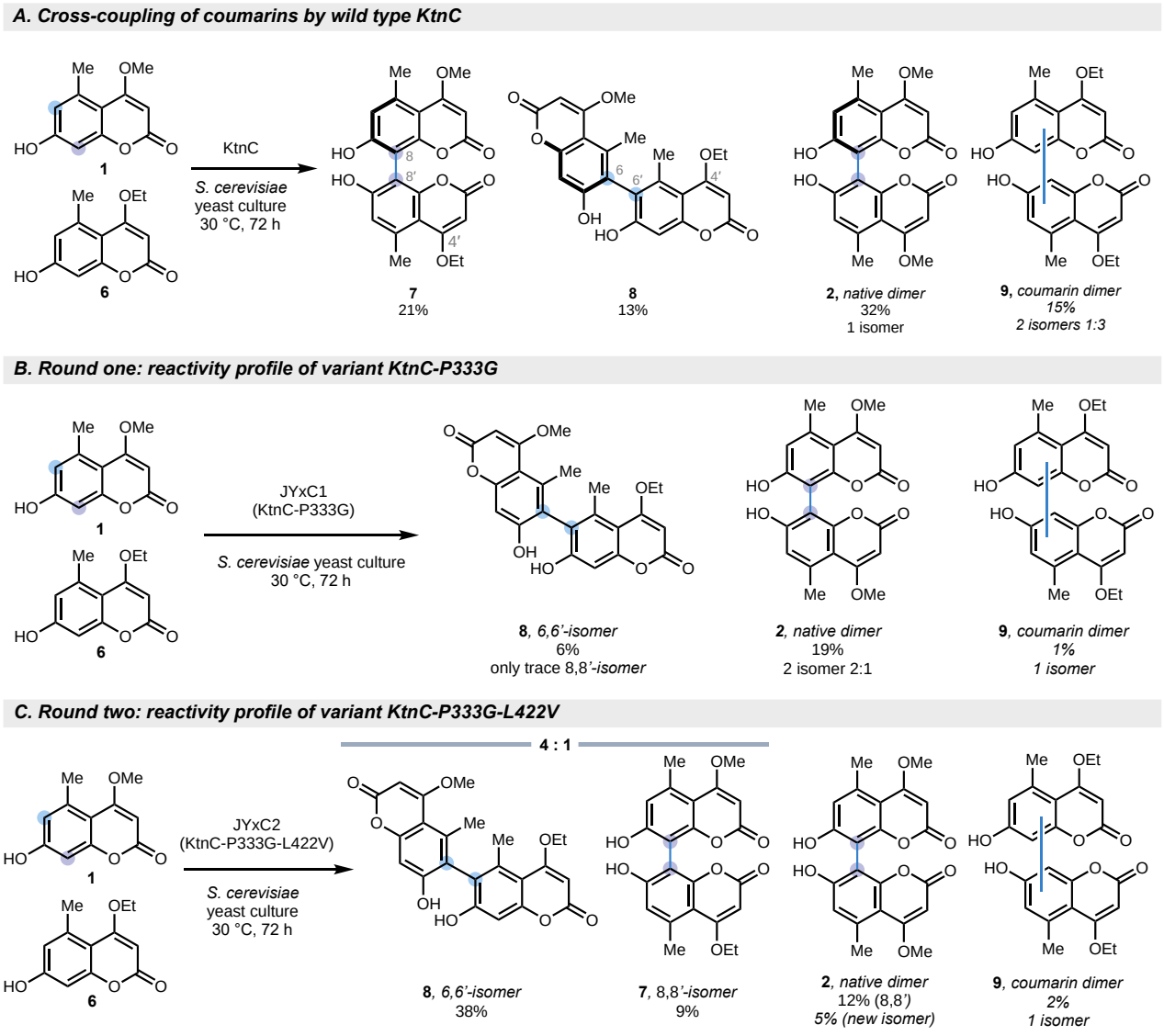

Figure 4.12: KtnC evolution over two rounds of engineering.
Starting point (A) through two rounds of engineering (B and C), values expressed as percent relative yields. A. Wild-type KtnC catalyzed the cross-coupling of coumarin **1** and **6** to form **8** in a 13% yield as a complex mixture of competing cross-coupled (**7** and **8**) and dimer byproducts (**2** and **9**). B. Round one variant KtnC-P333G selected for the enhanced selectivity for the desired 6,6'-product **8**. C. Round two variant KtnC-P333G-L422V provided a nearly 3-fold increase over wild type KtnC for the desired 6,6'-product **8.**

4.6 Experimental

Directed evolution of fungal P450 KtnC

Generation of KtnC variant libraries *Protocol developed by Lara Zetzsche*

Selection of active site residues to target. A homology model for KtnC was generated using Phyre2 (Supplemental Figure S4.1a). All residues within ~12 Å of predicted substrate binding region in the KtnC homology model active site were selected in PyMOL (command: “select bca. KtnC within 12 of substrate”). Any residues with >95% conservation based on a MAFFT alignment with up to 5,000 other sequences were removed from the pool of selected residues. The radius of the active site sphere was reduced incrementally until a total of 96 residues with ≤95% conservation were selected within an 11.25 Å radius (Supplemental Figure S4.1b).

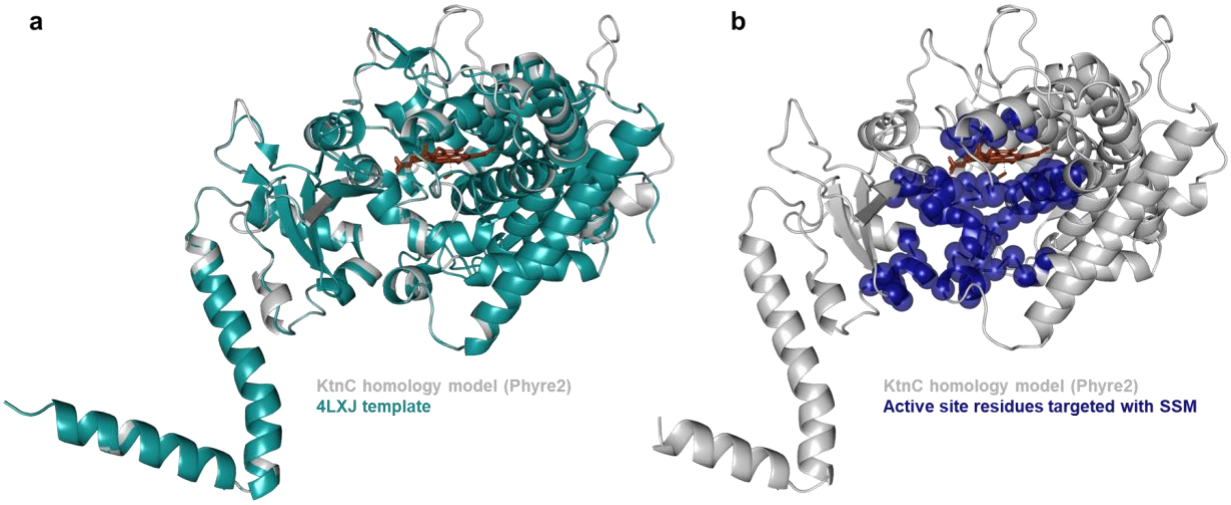

Supplemental Figure S4.1 Homology models. (a) Homology model of KtnC (gray) and based on 23% identity with lanosterol 14-alpha demethylase from *S. cerevisiae* (PDB 4LXJ; teal). (b) Residues selected for SSM within active site sphere.

Library generation workflow

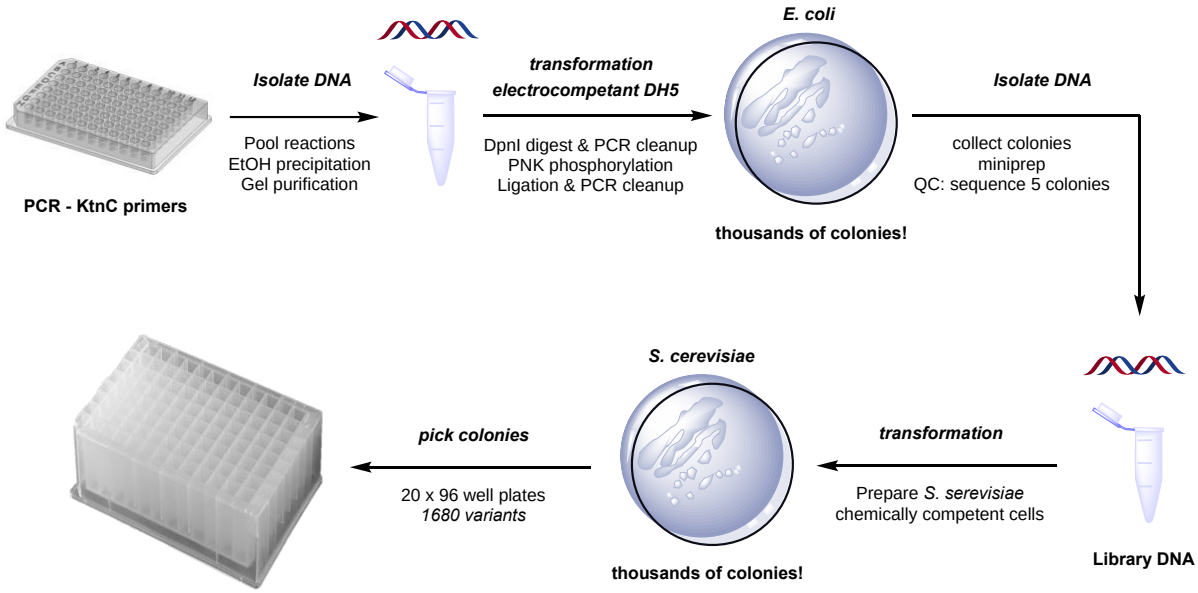

Supplemental Figure S4.2 Library generation workflow with individual steps outlined.

Site-saturation mutagenesis. Degenerate forward and reverse primers were designed for each of the 96 active site residues being targeted and purchased from IDT (Supplemental Table S4.1). Blunt-end whole-plasmid PCRs were set up in a 96-well PCR plate, with each 25-uL reaction containing 1X HF Phusion buffer, 4% DMSO, 400 µM dNTPs, 0.1 ng/µL template plasmid, 0.4 units Phusion DNA polymerase, 3 µM degenerate forward primer, and 3 µM reverse primer. The reaction conditions were programmed as follows: 98 °C denaturation for 2 min; 25 cycles of 98 °C for 20 s, 56 °C for 20 sec, 72 °C for 4.5 min; and a final 72 °C extension for 10 min. After amplification, 10 µL of each PCR product was pooled in a single tube. The crude PCR product mixture was concentrated using standard ethanol-based DNA precipitation procedures and purified by gel extraction from a 0.8% agarose gel using Qiagen spin columns. Any residual template DNA was digested in 1X Cutsmart buffer with 2 µL DpnI (NEB) overnight at 37 °C and removed with a PCR clean-up using Qiagen spin columns. The linear DNA fragments were phosphorylated in 1X T4 DNA ligase (NEB) buffer with 2 µL PNK enzyme (NEB) at 37 °C for 30 min. T4 ligase enzyme (1 µL, NEB) was added directly to the phosphorylation reaction and incubated at room temperature for 2 h. Salts were removed

from the ligation reaction with a PCR clean-up using Qiagen spin columns. High efficiency electrocompetent 5-alpha *E. coli* cells (NEB) were transformed with 2 µL of the clean DNA using standard electroporation protocols. Resulting colonies were grown up and miniprepped to give a plasmid DNA library. *S. cerevisiae* strain BY4742 cells were prepared for transformation with the plasmid DNA library through a standard protocol for lithium acetate transformations. Transformed cells were plated on histidine dropout plates containing 2% glucose and incubated at 25 °C for 3 d. Resulting colonies were used directly in library screening.

Multiple site-directed mutagenesis. Forward primers were designed to flank desired mutation with >15 complementary nucleotides on either side of mutation and purchased from IDT (Supplemental Table S4.3). Equimolar amounts of each of the forward primers were combined and diluted down to 5 µM. PCRs were performed with the QuikChange Lightning Multi Site-Directed Mutagenesis Kit (Agilent) according to their recommended protocols. After amplification, 1 µL of the supplied DpnI was added and the digestion reaction was incubated at 37 °C for 1 h. High efficiency electrocompetent 5-alpha *E. coli* cells (NEB) were transformed with 2 µL of the digested reaction using standard electroporation protocols. Resulting colonies were grown up and miniprepped to give a plasmid DNA library. *S. cerevisiae* strain BY4742 cells were prepared for transformation with the plasmid DNA library through a standard protocol for lithium acetate transformations. Transformed cells were plated on histidine dropout plates containing 2% glucose and incubated at 25 °C for 3 d. Resulting colonies were used directly in library screening.

Supplemental Table S4.1 Primers used for site-saturation mutagenesis of KtnC active site residues. Primers from round 1 (Rd1) were reused in subsequent rounds unless the sequence lost complementarity to the template DNA due to new mutations being carried forward. Codons that were edited to accommodate mutations added to the template DNA are highlighted in blue.

Mutation		*forward primer (5' to 3')*		*reverse primer (5' to 3')*
R62X	Rd1	NNKCCAAAGCTACGATGGAAGCG	Rd1	CATGTAGCTACCCTCGTCTACAATC
K64X	Rd1	NNKCTACGATGGAAGCGCTTCG	Rd1	TGGCCGCATGTAGCTACCC
L65X	Rd1	NNKCGATGGAAGCGCTTCGA	Rd1	CTTTGGCCGCATGTAGCTAC
R66X	Rd1	NNKTGGAAGCGCTTCGATGC	Rd1	TAGCTTTGGCCGCATGTAGC
W67X	Rd1	NNKAAGCGCTTCGATGCGG	Rd1	TCGTAGCTTTGGCCGCA
K68X	Rd1	NNKCGCTTCGATGCGGAGAA	Rd1	CCATCGTAGCTTTGGCCG
R69X	Rd1	NNKTTCGATGCGGAGAAAGAGTATG	Rd1	CTTCCATCGTAGCTTTGGCC
F70X	Rd1	NNKGATGCGGAGAAAGAGTATGCG	Rd1	GCGCTTCCATCGTAGCTTTG
D71X	Rd1	NNKGCGGAGAAAGAGTATGCGAGA	Rd1	GAAGCGCTTCCATCGTAGC
A72X	Rd1	NNKGAGAAAGAGTATGCGAGAGCATATC	Rd1	ATCGAAGCGCTTCCATCG
E73X	Rd1	NNKAAAGAGTATGCGAGAGCATATCAGC	Rd1	CGCATCGAAGCGCTTCC
Y76X	Rd1	NNKGCGAGAGCATATCAGCAGTACA	Rd1	CTCTTTCTCCGCATCGAAGC
R93X	Rd1	NNKATGCAGAATGATAATTATGGCATTG	Rd1	GATCGCATAAGGTTTCCCTGC
M94X	Rd1	NNKCAGAATGATAATTATGGCATTGTGC	Rd1	CCGGATCGCATAAGGTTTCC
Q95X	Rd1	NNKAATGATAATTATGGCATTGTGCTTC	Rd1	CATCCGGATCGCATAAGGTT
D97X	Rd1	NNKAATTATGGCATTGTGCTTCCC	Rd1	ATTCTGCATCCGGATCGC
Y99X	Rd1	NNKGGCATTGTGCTTCCCTTAAAC	Rd1	ATTATCATTCTGCATCCGGATCG
I101X	Rd1	NNKGTGCTTCCCTTAAACTCAGCAA	Rd1	GCCATAATTATCATTCTGCATCCG
W111X	Rd1	NNKAGGTCTCTACCACACGACCAGC	Rd1	TTCCTTTGCTGAGTTTAAGGGA
R112X	Rd1	NNKTCTCTACCACACGACCAGCTG	Rd1	CCATTCCTTTGCTGAGTTTAAGG
S120X	Rd1	NNKTTTCTTCAAGCCTTGGCAGA	Rd1	CAGCTGGTCGTGTGGTAGAGA
F121X	Rd1	NNKCTTCAAGCCTTGGCAGAGTTT	Rd1	GCTCAGCTGGTCGTGTGGT
L122X	Rd1	NNKCAAGCCTTGGCAGAGTTTGC	Rd1	AAAGCTCAGCTGGTCGTGTG
Q123X	Rd1	NNKGCCTTGGCAGAGTTTGCG	Rd1	AAGAAAGCTCAGCTGGTCGTG
A124X	Rd1	NNKTTGGCAGAGTTTGCGGATAT	Rd1	TTGAAGAAAGCTCAGCTGGTCG
L125X	Rd1	NNKGCAGAGTTTGCGGATATGAACA	Rd1	GGCTTGAAGAAAGCTCAGCTG
A126X	Rd1	NNKGAGTTTGCGGATATGAACATGTAC	Rd1	CAAGGCTTGAAGAAAGCTCAGC
E127X	Rd1	NNKTTTGCGGATATGAACATGTACTGC	Rd1	TGCCAAGGCTTGAAGAAAGC
F128X	Rd1	NNKGCGGATATGAACATGTACTGCG	Rd1	CTCTGCCAAGGCTTGAAGAAA
A129X	Rd1	NNKGATATGAACATGTACTGCGACGTC	Rd1	AAACTCTGCCAAGGCTTGAAG
D130X	Rd1	NNKATGAACATGTACTGCGACGTCA	Rd1	CGCAAACTCTGCCAAGGC
M131X	Rd1	NNKAACATGTACTGCGACGTCACG	Rd1	ATCCGCAAACTCTGCCAAG
N132X	Rd1	NNKATGTACTGCGACGTCACGGA	Rd1	CATATCCGCAAACTCTGCCA
M133X	Rd1	NNKTACTGCGACGTCACGGACA	Rd1	GTTCATATCCGCAAACTCTGCC
Y134X	Rd1	NNKTGCGACGTCACGGACAGG	Rd1	CATGTTCATATCCGCAAACTCTG
D139X	Rd1	NNKAGGACACCCATTGAAGCTGTT	Rd1	CGTGACGTCGCAGTACATGTT
P142X	Rd1	NNKATTGAAGCTGTTCATAGTTGCAACA	Rd1	TGTCCTGTCCGTGACGTCG
I143X	Rd1	NNKGAAGCTGTTCATAGTTGCAACAAC	Rd1	GGGTGTCCTGTCCGTGACG
V146X	Rd1	NNKCATAGTTGCAACAACGCTGAATC	Rd1	AGCTTCAATGGGTGTCCTGTC
L203X	Rd1	NNKCTCGGACCAGATACAGCCCC	Rd1	CAAGGCCATAGTAACCGTTGAG
R232X	Rd1	NNKACGGGATATCCGCGCA	Rd1	TCGATAACAACTGCTCATAATTGC
G234X	Rd1	NNKTATCCGCGCATCCTGCG	Rd1	CGTTCGTCGATAACAACTGCTC
Y235X	Rd1	NNKCCGCGCATCCTGCG	Rd1	TCCCGTTCGTCGATAACAAC
P236X	Rd1	NNKCGCATCCTGCGGCCA	Rd1	ATATCCCGTTCGTCGATAACAA
R237X	Rd1	NNKATCCTGCGGCCATTCGT	Rd1	CGGATATCCCGTTCGTCG
I238X	Rd1	NNKCTGCGGCCATTCGTGTG	Rd1	GCGCGGATATCCCGTTC

L239X	Rd1	NNKCGGCCATTCGTGTGGC	Rd1	GATGCGCGGATATCCCG
R240X	Rd1	NNKCCATTCGTGTGGCGCTT	Rd1	CAGGATGCGCGGATATCC
P241X	Rd1	NNKTTCGTGTGGCGCTTTTCG	Rd1	CCGCAGGATGCGCGG
F242X	Rd1	NNKGTGTGGCGCTTTTCGTCC	Rd1	TGGCCGCAGGATGCG
L253X	Rd1	NNKAGGAAACACTTATCTCTCGTGAGAGA	Rd1	ATTTCGGCATTCGGACGA
D321X	Rd1	NNKGATCTCATTTTCTACCATTTCGAAC	Rd1	TGCCAGCAACTGTACCTGTGC
D322X	Rd1	NNKCTCATTTTCTACCATTTCGAACTCTG	Rd1	ATCTGCCAGCAACTGTACCTGT
L323X	Rd1	NNKATTTTCTACCATTTCGAACTCTGTAAA	Rd1	ATCATCTGCCAGCAACTGTACC
I324X	Rd1	NNKTTCTACCATTTCGAACTCTGTAAA**CC**	Rd1	GAGATCATCTGCCAGCAACTGT
	Rd2	NNKTTCTACCATTTCGAACTCTGTAAA**GG**		
F325X	Rd1	NNKTACCATTTCGAACTCTGTAAA**CCG**	Rd1	AATGAGATCATCTGCCAGCAAC
	Rd2	NNKTACCATTTCGAACTCTGTAAA**GGG**	Rd1	
Y326X	Rd1	NNKCATTTCGAACTCTGTAAA**CCG**AC	Rd1	GAAAATGAGATCATCTGCCAGC
	Rd2	NNKCATTTCGAACTCTGTAAA**GGG**AC		
H327X	Rd1	NNKTTCGAACTCTGTAAA**CCG**ACCG	Rd1	GTAGAAAATGAGATCATCTGCCAGC
	Rd2	NNKTTCGAACTCTGTAAA**GGG**ACCG		
F328X	Rd1	NNKGAACTCTGTAAA**CCG**ACCGCA	Rd1	ATGGTAGAAAATGAGATCATCTGCC
	Rd2	NNKGAACTCTGTAAA**GGG**ACCGCA		
E329X	Rd1	NNKCTCTGTAAA**CCG**ACCGCATTC	Rd1	GAAATGGTAGAAAATGAGATCATCTG
	Rd2	NNKCTCTGTAAA**GGG**ACCGCATTC		
L330X	Rd1	NNKTGTAAA**CCG**ACCGCATTCAA	Rd1	TTCGAAATGGTAGAAAATGAGATCA
	Rd2	NNKTGTAAA**GGG**ACCGCATTCAA		
C331X	Rd1	NNKAAA**CCG**ACCGCATTCAACA	Rd1	GAGTTCGAAATGGTAGAAAATGAGA
	Rd2	NNKAAA**GGG**ACCGCATTCAACA		
K332X	Rd1	NNK**CCG**ACCGCATTCAACATCA	Rd1	ACAGAGTTCGAAATGGTAGAAAATG
	Rd2	NNK**GGG**ACCGCATTCAACATCA		
P333X	Rd1	NNKACCGCATTCAACATCATCTTCC	Rd1	TTTACAGAGTTCGAAATGGTAGAAAA
T334X	Rd1	NNKGCATTCAACATCATCTTCCAGC	Rd1	**CGG**TTTACAGAGTTCGAAATGG
			Rd2	**CCC**TTTACAGAGTTCGAAATGG
F336X	Rd1	NNKAACATCATCTTCCAGCTGTATGC	Rd1	TGCGGT**CGG**TTTACAGAGTTC
			Rd2	TGCGGT**CCC**TTTACAGAGTTC
D393X	Rd1	NNKATCTCCGGTTTTGTCAGCTTTC	Rd1	GTACAGTCGAAAGGTCTCCTTTGT
I394X	Rd1	NNKTCCGGTTTTGTCAGCTTTCG	Rd1	ATCGTACAGTCGAAAGGTCTCCT
S395X	Rd1	NNKGGTTTTGTCAGCTTTCGCCG	Rd1	GATATCGTACAGTCGAAAGGTCTCC
G396X	Rd1	NNKTTTGTCAGCTTTCGCCGTG	Rd1	GGAGATATCGTACAGTCGAAAGGT
F397X	Rd1	NNKGTCAGCTTTCGCCGTGTCA	Rd1	ACCGGAGATATCGTACAGTCGA
V398X	Rd1	NNKAGCTTTCGCCGTGTCATGA	Rd1	AAAACCGGAGATATCGTACAGTCG
S399X	Rd1	NNKTTTCGCCGTGTCATGAAACC	Rd1	GACAAAACCGGAGATATCGTACA
F400X	Rd1	NNKCGCCGTGTCATGAAACCTC	Rd1	GCTGACAAAACCGGAGATATCG
R401X	Rd1	NNKCGTGTCATGAAACCTCTTACTCTAAA	Rd1	AAAGCTGACAAAACCGGAGATA
I421X	Rd1	NNKTTATTGTCTCCATGTCGGAATGT	Rd1	TGTACCGGGACGAAGAGACA
L422X	Rd1	NNKTTGTCTCCATGTCGGAATGTCC	Rd1	GATTGTACCGGGACGAAGAGA
L423X	Rd1	NNKTCTCCATGTCGGAATGTCCA	Rd1	TAAGATTGTACCGGGACGAAGA
S424X	Rd1	NNKCCATGTCGGAATGTCCATTTG	Rd1	CAATAAGATTGTACCGGGACGA
P425X	Rd1	NNKTGTCGGAATGTCCATTTGGA	Rd1	AGACAATAAGATTGTACCGGGACG
C426X	Rd1	NNKCGGAATGTCCATTTGGATCC	Rd1	TGGAGACAATAAGATTGTACCGG
T468X	Rd1	NNKTTTTCTCATGGAGCGGGC	Rd1	CAAGAACGTGAGCGAGGTGG
F469X	Rd1	NNKTCTCATGGAGCGGGCAG	Rd1	TGTCAAGAACGTGAGCGAGG
S470X	Rd1	NNKCATGGAGCGGGCAGCT	Rd1	AAATGTCAAGAACGTGAGCGA

A473X	Rd1	NNKGGCAGCTGTCCCGCG	Rd1	TCCATGAGAAAATGTCAAGAACG
G474X	Rd1	NNKAGCTGTCCCGCGCGG	Rd1	CGCTCCATGAGAAAATGTCAA
S475X	Rd1	NNKTGTCCCGCGCGGG	Rd1	GCCCGCTCCATGAGAAAA
P477X	Rd1	NNKGCGCGGGTTCTCGCT	Rd1	ACAGCTGCCCGCTCCA
F511X	Rd1	NNKACCAGTGGTCCGGTCTATATGC	Rd1	TCCATAGGGTAGTATCTCCTTCTGC
T512X	Rd1	NNKAGTGGTCCGGTCTATATGCCTAA	Rd1	GAATCCATAGGGTAGTATCTCCTTCTG
S513X	Rd1	NNKGGTCCGGTCTATATGCCTAATCC	Rd1	GGTGAATCCATAGGGTAGTATCTCC
G514X	Rd1	NNKCCGGTCTATATGCCTAATCCATC	Rd1	ACTGGTGAATCCATAGGGTAGTATCT
P515X	Rd1	NNKGTCTATATGCCTAATCCATCAGTGATG	Rd1	ACCACTGGTGAATCCATAGGG
V516X	Rd1	NNKTATATGCCTAATCCATCAGTGATGA	Rd1	CGGACCACTGGTGAATCCA
Y517X	Rd1	NNKATGCCTAATCCATCAGTGATGATG	Rd1	GACCGGACCACTGGTGAATC
M518X	Rd1	NNKCCTAATCCATCAGTGATGATGAGA	Rd1	ATAGACCGGACCACTGGTGAA

Combinatorial library

KtnC_P333G sequence

Mutations incorporated in bold, template mutation (P333G) highlighted in blue

ATGGCAGTTCATGTACCATTCAGCATCCACCACGTCGTGGATATCGGCATTTCCACCGGCCCGG
TAGTCATTGTCCTCGTTCTCCTATTCGGGTTGGCTGTCGTGGGATCCGACAGCCTTGATGGATG
GTGGCAGAAAAGAGCCTTGAGAGGCATTCCGATTGTAGACGAGGGTAGCTACATGCGGCCAAAG
CTACGATGGAAGCGCTTCGATGCGGAGAAAGAGTATGCGAGAGCATATCAGCAGTACACAAAAG
CAGGGAAACCTTATGCGATCCGGATGCAGAATGATAAT**TAT**GGCATTGTGCTTCCCTTAAACTC
AGCAAAGGAATGGAGGTCTCTACCACACGACCAGCTGAGCTTTCTTCAAGCCTTGGCAGAGTTT
GCGGATATGAACATGTACTGCGACGTCACGGACAGGACACCCATTGAAGCTGTTCATAGTTGCA
ACAACGCTGAATCATTAAACATCCTCAATAAGCTTCTCGCCCGGGAAACCGATACAGCCTTATC
TCAGATTTTCGAGCAGCCTACAGGAAAAGACTGGAAGGAATTGAACACACTGCAGACAATCCTC
TCCTTATGCTCAACGGTTACTATGGCCTTGCTCCTCGGACCAGATACAGCCCCTGACCCGGTGC
TCCACCACCATTCGACGTCTTTTGGCGAAGCAATTATGAGCAGTTGTTATCGACGAACGGGATA
TCCGCGCATCCTGCGGCCATTCGTGTGGCGCTTTTCGTCCGAATGCCGAAAT**CTG**AGGAAACAC
TTATCTCTCGTGAGAGAGAGACTTGTTCCTGAGGTTGCGCGCCGTGTCGCAGCTGCACGAGCGG
CGGATAAAACCAAGGACGTACGCCCATCTTCATTGTTGGACGCACTGATCGCGGCGGCCTTCGA
CAACGGCAGCTTAAGCCCAGATGACCAAGGCAGAAATGATGCAGCACAGGTACAGTTGCTGGCA
GATGATCTCATTTTCTACCATTTCGAACTCTGTAAA**GGG**ACCGCATTCAACATCATCTTCCAGC
TGTATGCCATCATGGACCACCCAGAGTACAAGGCTCCTCTCCGAGAGGAGGCACTCCAAGCCTT
GAAGCTCACCAATGGTGACTGGACCGTTGAAACTCTGAAGCACGCTCCCAAGTTAGAAAGCTTT
ACAAAGGAGACCTTTCGACTGTACGATATCTCC**GGT**TTTGTCAGCTTTCGCCGTGTCATGAAAC
CTCTTACTCTAAACTCCATCGGCCTGTCTCTTCGTCCCGGTACAATCTTATTGTCTCCATGTCG
GAATGTCCATTTGGATCCCGAGATCTATGAAGACCCGACAACTTTCAATGGCTACCGCTTCTAC
GACTCCAGCCGCGAGGTCTGCTCTCCACGCGTGGCAACCACCTCGCTCACGTTCTTGACATTTT
CTCATGGAGCGGGCAGCTGTCCCGCGCGGGTTCTCGCTACTCAAATTTGTCGGACGATCTTCAT
CAAGTTCCTGTTGCAGTACGACGTAGAACCTGTGCAGAAGGAGATACTACCCTATGGATTCACC
AGTGGT**CCG**GTC**TAT**ATGCCTAATCCATCAGTGATGATGAGAATCCGGCCAAGAAGTGACGGGA
AG

Supplemental Table S4.2 and S4.3 Primers for multiple site-directed mutagenesis combinatorial libraries. Mutated codons highlighted in blue.

S4.2

entry	*Mutation*	*codon*	*KtnC (wt)*	*KtnC-combi*
1	Y99K	295	tat	AAG
2	L253G	757	ctg	GGG
3	G396R	1186	ggt	AGG
4	S513G	1537	agt	GGG
5	P515R	1543	ccg	AGG
6	P515G	1543	ccg	GGG
7	P515L	1543	ccg	TTG
8	P515W	1543	ccg	TGG
9	Y517E	1549	tat	GAG

S4.3

Mutation(s)	*primer (5' to 3')*
Y99K	CCGGATGCAGAATGATAATAAGGGCATTGTGCTTCCCTTAAACTC
L253G	TCCGAATGCCGAAATGGGAGGAAACACTTATCTCTCGTG
G396R	CTGTACGATATCTCCAGGTTTGTCAGCTTTCGCCGTGTC
S513G	CCCTATGGATTCACCGGGGGTCCGGTCTATATG
S513G, S515X	CCCTATGGATTCACCGGGGGTNNGGTCTATATGCCTAATCCATCAG
S513G, S515X, P515G	CTACCCTATGGATTCACCGGGGGTNNGGTCGAGATGCCTAATCCATCAGTG
P515X	CTATGGATTCACCAGTGGTNNGGTCTATATGCCTAATCCATC
Y517E	GATTCACCAGTGGTCCGGTCGAGATGCCTAATCCATC
P515X, Y517E	CTACCCTATGGATTCACCAGTGGTNNGGTCGAGATGCCTAATCCATC

***E. coli* colony sequencing**	
1	S513G, P515K
2	L253G
3	Y517E
4	S513G, P515W, Y99K
5	S513G, P515V
6	G396R
7	Y99k, G396R
8	template

***S. cerevisiae* sequencing**	
1	P515Q
2	S513G, P515R, Y517E
3	G396R, S513G, P515A, Y517E
4	Y99k, G396R
5	G396R, P515G
6	L253G
7	L253G, G396R
8	G396R, P515E

Supplemental Table S4.4 Combinatorial library sequencing validation. Quality control sequencing of combi library colonies after both transformation steps in the library

generation workflow. Eight colonies were selected after each transformation to validate the incorporation of the expected mutations.

Screening KtnC variant libraries

High throughput biotransformations. Histidine dropout minimal media containing 4% glucose was added to each well of up to 20 sterile 96-well culture plates (VWR) to a volume of 500 µL. *S. cerevisiae* library colonies were inoculated into each well of the plate except for row E, which was reserved for *S. cerevisiae* KtnC template positive control colonies (rows E1-E10) and negative control wells (E11 and E12). Cultures were grown overnight at 30 °C with shaking at 350 rpm, 3mm radius, and 85% humidity. Culture plates were centrifuged at 2,000 x *g* for 15 min to pellet cells and the growth media was removed. Cells were resuspended with 250 µL of histidine dropout minimal media containing 6% galactose and 100 µM each substrate. Biotransformations were incubated at 30 °C with shaking at 350 rpm for 2-3 days. Reactions were quenched with the addition of 2-3 equivalents of methanol and centrifugation at 2,000 x *g* for 20 min. The resulting supernatant was used for mass spectrometry analysis.

Tier-one screening methods

UPLC-DAD screen for activity. Library reactions were analyzed for total cross-coupling activity in a high-throughput tier 1 screening using an Agilent 6230 spectrometer with an Agilent G7117A Infinity Series II diode array detector, autosampler, and binary pump. Library samples were prepared by diluting the library samples 3:1 in methanol containing 150 µM 3-bromo-2-naphthol (internal standard) in shallow 96-well plates (Waters). The reaction products were separated and analyzed under the following conditions:

Waters Acquity Premier HSS T3 1.8 µm C18, 2.1 x 50 mm column. Phase A = 95:5 water:acetonitrile; phase B = 95:5 acetonitrile: water. The pump was programmed as follows: 25% B to 35% B over 2.5 min, hold at 35% B for 1.5 min, to 100% B over 1.0 min, to 25% B over 0.5 min. The flow rate was set to 0.6 mL/min flow rate, the column was heated to 50 °C.

The peak areas at 322 nm for internal standard and 6,6'-cross-coupled product were collected for each sample using the MassHunter Qualitative Analysis 10.0 software. The product peak areas were normalized with the internal standard (calculated as product/internal standard) and the average resulting from the template reactions (wells E1-E10) for each plate (n=10) was set to 1.0. The calculations for the variant reactions were normalized to the template reactions, giving fold improvement scores for each variant.

Method development and optimization. Screening by UPLC-DAD required higher substrate concentrations for detection, and conditions for biotransformations were optimized to balance conversion to products and the lower limit of detection for the analytes after reaction workup.

Wild Type KtnC reactivity screen. 96 well plate biotransformations in *S. cerevisiae* Optimization of substrate concentration for analysis by UPLC tier one screen.

Supplemental table S4.5 Wild-type reactions 96-well plate screen. Relative percent yield calculated as averages of 12 replicates for each condition.

96 well plate reaction layout														relative % yield by LC-MS		
	1	2	3	4	5	6	7	8	9	10	11	12	volume	AA dimer	8,8' AB	6,6' AB
A	negative control NO ENZYME 100 µM												250 µL	0.0	-	-
B	positive control KtnC 100 µM Native												250 µL	27.3	-	-
C	KtnC 50 µM Native A + 50 µM Me, OEt B												250 µL	10.8	1.9	0.7
D	KtnC 100 µM Native A + 100 µM Me, OEt B												250 µL	13.1	3.0	0.9
E	KtnC 150 µM Native A + 150 µM Me, OEt B												250 µL	8.5	2.1	0.7
F	KtnC 200 µM Native A + 200 µM Me, OEt B												250 µL	3.9	1.8	0.7
G	KtnC 300 µM Native A + 300 µM Me, OEt B												250 µL	13.8	4.4	1.1
H	KtnC 500 µM Native A + 500 µM Me, OEt B												250 µL	4.5	1.2	0.5

Initial attempts were carried out to optimize the reaction in a 96 well plate format with A and B in a 1:1 ratio at different concentrations. The reaction was low yielding, and the desired 6,6'-isomer (**8**, AB) was at best 1% relative yield. The samples were then screened by UPLC, but after quenching and dilution, no product was detectable. The

reactions were repeated (Supplemental Table S4.6), with the concentration of **1** (A) and **6** (B) increased. Reaction conditions were chosen based on 6,6'-AB/IS and the number of equivalents of methanol for quenching/dilution was also tested.

Supplemental Table S4.6 Optimization of substrate concentrations for UPLC screening analysis.

96 well plate reaction layout													UPLC peak area		
	1	2	3	4	5	6	7	8	9	10	11	12	volume	Area 66	Area IS	AA/IS
A	negative control NO ENZYME 100 µM												250 µL	NA		
B	Positive control KtnC 100 µM Native												250 µL	NA		
C	KtnC 250 µM Native + 250 µM Me, OEt												250 µL	31.735	83.604	0.380
D	KtnC 300 µM Native + 300 µM Me, OEt												250 µL	34.365	87.486	0.393
E	KtnC 400 µM Native + 400 µM Me, OEt												250 µL	22.891	49.752	0.460
F	KtnC 500 µM Native + 500 µM Me, OEt												250 µL	46.200	60.325	0.766
G	KtnC 750 µM Native + 750 µM Me, OEt												250 µL	38.164	63.792	0.598
H	KtnC 250 µM Native + 750 µM Me, OEt												250 µL	42.680	80.648	0.529
control - culture tube, 0.1 mM A & B													1 mL	29.88	77.261	0.387

At higher concentrations the desired 6,6'-peak (**8**, AB) was detectable by UPLC. An internal standard, 3-bromo-2-naphthol (IS), was chosen for its late retention time without overlap with other species.

Row E and F were both detectable by UPLC (S4.6), but row F had the highest AB/IS and was chosen as the reaction substrate concentration conditions moving forward.

Tier-1 UPLC screening method development

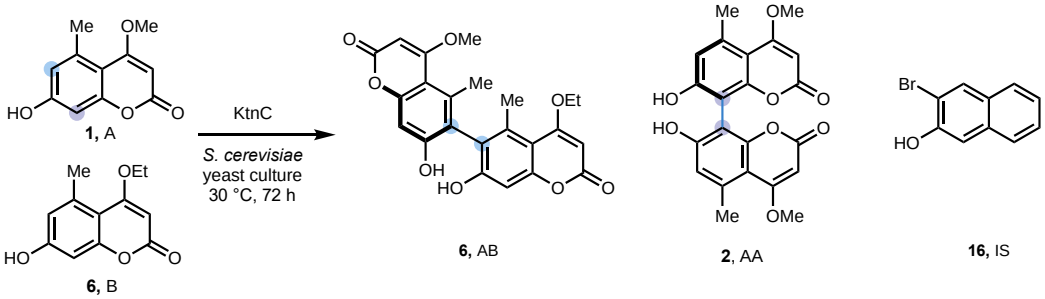

Supplemental Figure S4.3 Reaction scheme for UPLC method development. UPLC methods were developed to separate the desired AB product **6** from the substrates **1** (A) and **6** (B), and dimeric product **2** (AA), and internal standard **16** (IS).

Supplemental Figure S4.4 Negative control, no enzyme.

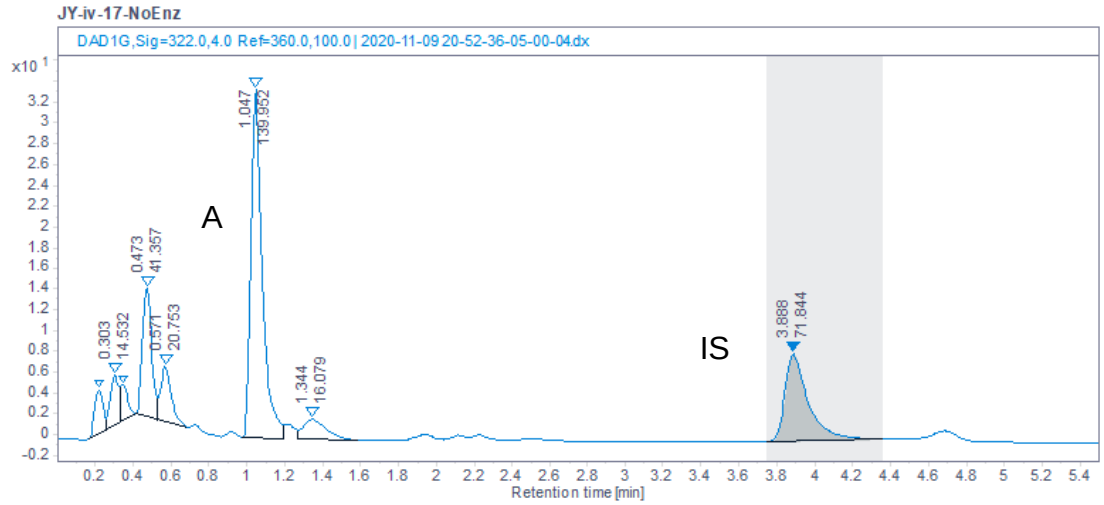

Supplemental Figure S4.5 Positive: KtnC with native substrate only.

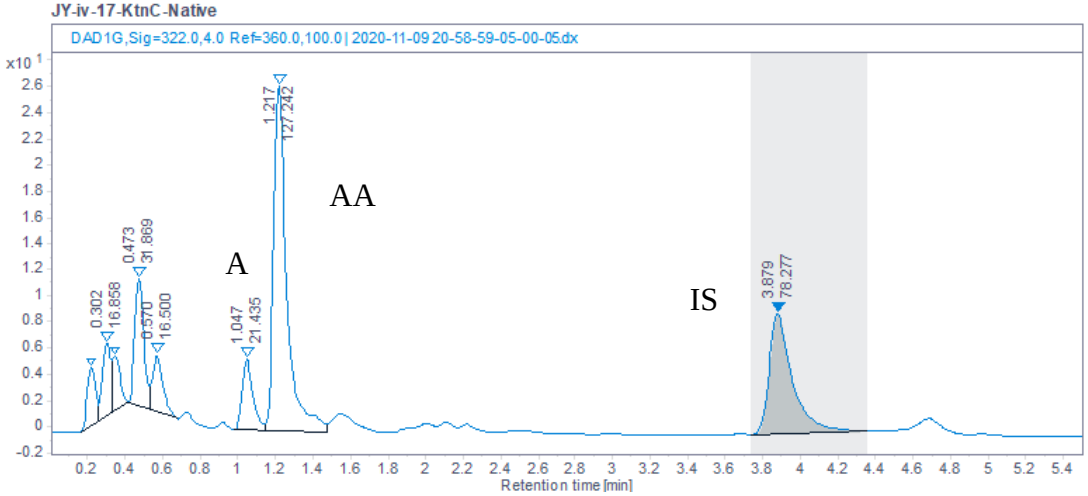

Supplemental Figure S4.6 Positive control 2 - KtnC with A and B in culture tubes.

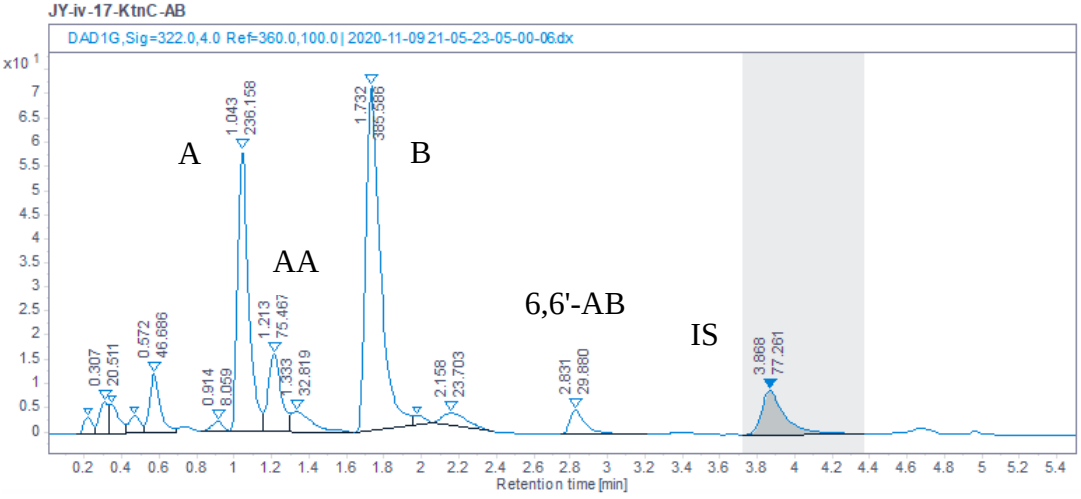

Supplemental Figure S4.7 6,6'-AB (**8**) authentic standard (300 µM).

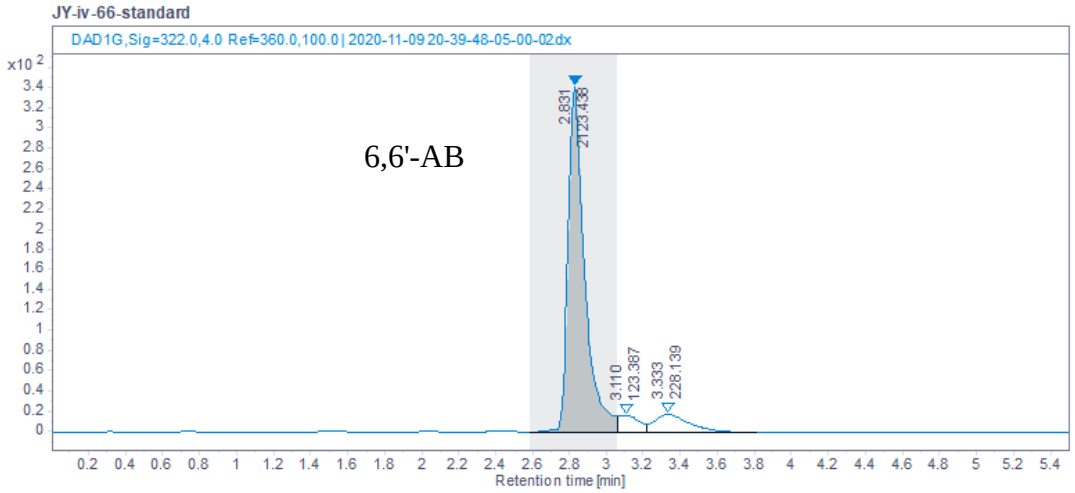

Supplemental Figure S4.8 3-bromo-2-naphthol internal standard (300 µM).

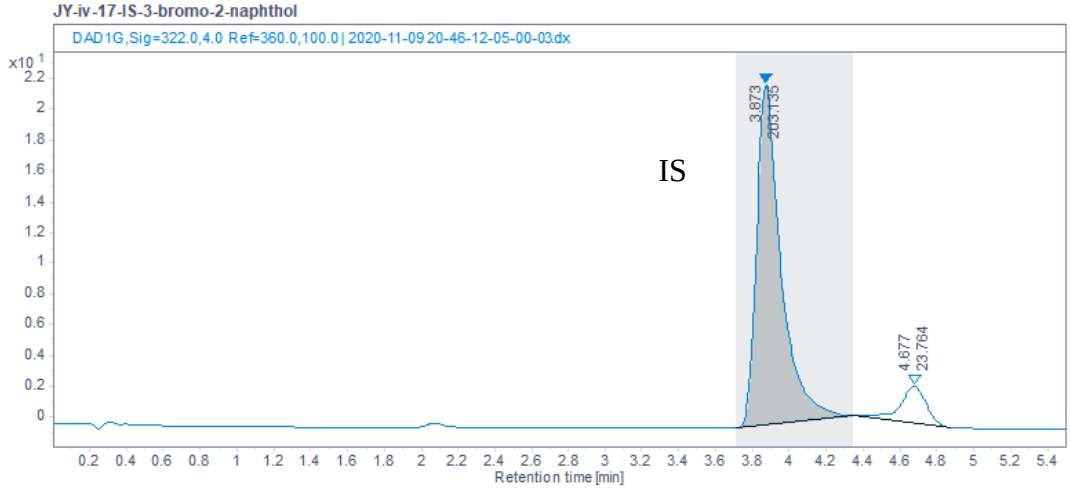

Reaction workup optimization. Dilution factors of 1 to 3 equivalents (equiv) methanol were added to the biotransformations to quench the reactions and prepare samples for UPLC analysis.

Supplemental Figure S4.9 1 equiv MeOH.

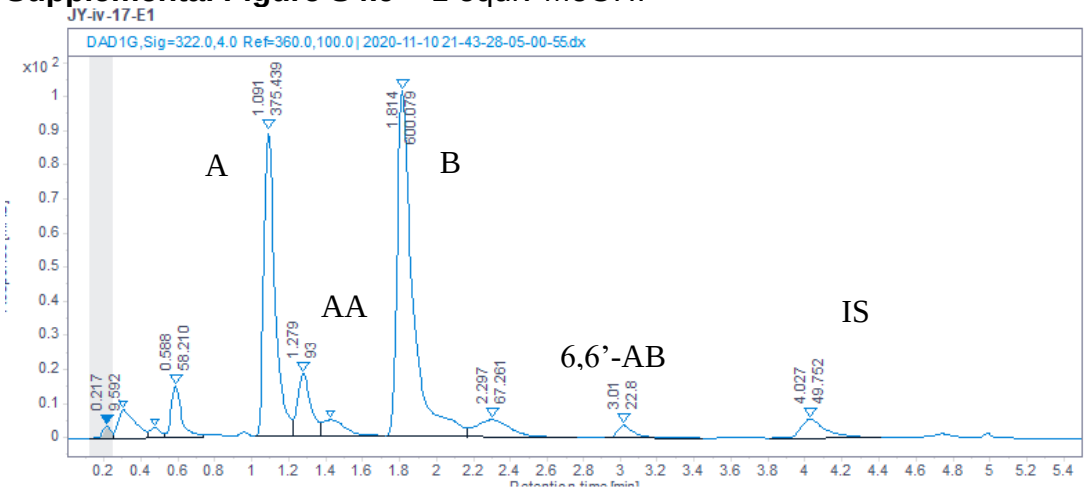

Supplemental Figure S4.10 2 equiv MeOH

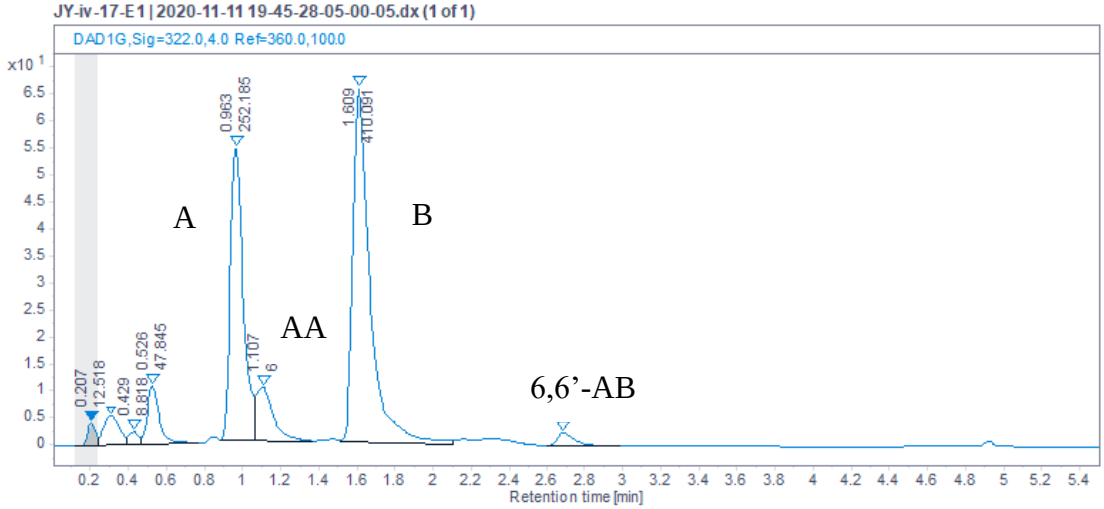

Supplemental Figure S4.11 3 equiv MeOH

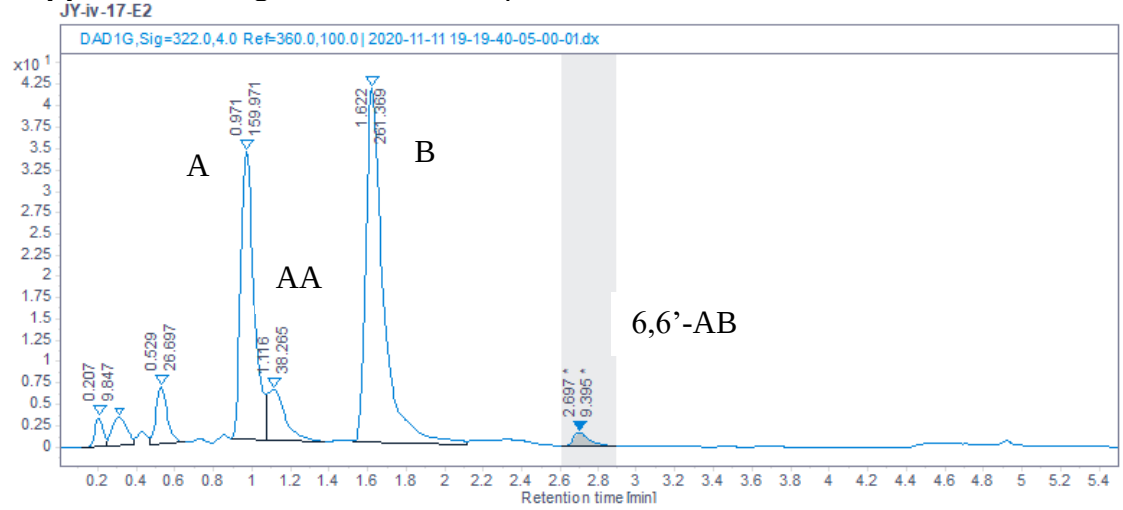

At 3 equiv of methanol, the desired product peak was still detectable, and this was the dilution factor that was used going forward. Reactions were quenched with 3 equiv methanol with a final concentration of 200-300 µM internal standard in the screening of reactions plates.

High throughput LC-MS screen for activity. Reactions were subjected to liquid chromatography PDA spectrometry (UPLC) analysis performed on an Agilent 6230 time of flight mass spectrometer with a Dual AJS ESI source and an Agilent 1290 Infinity Series II diode array detector, autosampler, and binary pump. The reaction products were analyzed under the following conditions:

To determine the site-selectivity of the biotransformations, samples were analyzed by negative mode on a Waters Acquity Premier HSS T3 1.8 µm C18, 2.1 x 50 mm column. Phase A = 95:5 water:acetonitrile; phase B = 95:5 acetonitrile: water. The pump was programmed as follows: 40% B to 50% B over 1.0 min, to 100% B over 0.01 min, held at 100% B for 0.24 min. The flow rate was set to 0.7 mL/min flow rate, the column was heated to 50 °C, and each injection was followed by equilibration at 40% B for 0.25 min.

The MassHunter software was used to extract ion chromatograms of the substrates and product masses to characterize the relative percent yield and site-selectivity of the reactions. Variants that gave the desired site-selectivity were carried forward to the hit validation and sequencing step.

High throughput RapidFire-MS screen for activity. Library reactions were analyzed for total cross-coupling activity in a high-throughput tier-one screen utilizing an Agilent RapidFire 365 High throughput Mass Spectrometry System linked to an Agilent 6545 Q-TOF. Library samples were prepared by diluting the library samples 2:1 in water containing 600 nM 4,4**'**-dihydroxybenzophenone (internal standard) in shallow 96-well plates (Axygen) and heat-sealed with pierceable aluminum covers (Agilent). Each RapidFire injection was programmed as follows: 0.6 s to aspirate the sample, 3 s to load the sample onto the C4 cartridge with water (0.5 mL/min), 8 s to elute the sample from the cartridge using 90% acetonitrile buffered with 10 mM ammonium formate pH 8 (0.8 mL/min), and 0.5 s to re-equilibrate.

The peak areas for the extracted ion chromatograms for the internal standard and the cross-coupled product were collected for each sample using the MassHunter Qualitative Analysis 10.0 software. The cross-coupled product peak areas were normalized with the internal standard, and the average resulting from the template reactions (wells E1-E10) for each plate (n=10) was set to 1.0. The product peaks for the variant reactions were normalized to the template reactions, giving fold improvement scores for each variant.

Tier-two LC-Tof MS screen for selectivity. Reactions identified as hits (set by the fold improvement score) were subjected to liquid chromatography PDA spectrometry (UPLC) analysis performed on an Agilent 6230 time of flight mass spectrometer with a Dual AJS ESI source and an Agilent 1290 Infinity Series II diode array detector, autosampler, and binary pump. The reaction products were separated and analyzed under the following conditions:

To determine site-selectivity of reaction, samples were analyzed by negative mode on a Waters Acquity Premier HSS T3 1.8 µm C18, 2.1 x 50 mm column. Phase A = 95:5 water:acetonitrile; phase B = 95:5 acetonitrile: water. The pump was programmed as follows: 25% B to 35% B over 6.0 min, to 25% B for 1.5 min, then held at 35% B for 0.5 min. The flow rate was set to 0.7 mL/min flow rate, the column was heated to 50 °C.

MassHunter software was used to extract ion chromatograms of the substrate and product masses to characterize the relative percent yield and site-selectivity of the reactions. Variants that gave the desired activity and site-selectivity were carried forward to the hit validation and sequencing step.

Hit validation and sequencing. Hit variants that were selected in a tier-one screen were validated by growing cultures from glycerol stocks of the respective cells harboring the variants, repeating biotransformations (n=3), and analyzing reactions by TOF-LC-MS using previously described procedures. Variants that showed improvement over the template after validation were sequenced to identify the active site mutations. Plasmid DNA was isolated from *S. cerevisiae* using the Zymoprep Yeast Plasmid Miniprep II kit.

The resulting plasmid DNA was used to transform DH5α *E. coli* cells. Clean plasmid DNA was isolated from DH5α cells using QIAGEN miniprep kit and sent to GENEWIZ for Sanger sequencing. The sequence for the top hit from each round was used as the template for the following round.

Mutated variant sequences

Round 1 variant: KtnC-P333G

ATGGCAGTTCATGTACCATTCAGCATCCACCACGTCGTGGATATCGGCATTTCCACCGGCCCGG
TAGTCATTGTCCTCGTTCTCCTATTCGGGTTGGCTGTCGTGGGATCCGACAGCCTTGATGGATG
GTGGCAGAAAAGAGCCTTGAGAGGCATTCCGATTGTAGACGAGGGTAGCTACATGCGGCCAAAG
CTACGATGGAAGCGCTTCGATGCGGAGAAAGAGTATGCGAGAGCATATCAGCAGTACACAAAAG
CAGGGAAACCTTATGCGATCCGGATGCAGAATGATAATTATGGCATTGTGCTTCCCTTAAACTC
AGCAAAGGAATGGAGGTCTCTACCACACGACCAGCTGAGCTTTCTTCAAGCCTTGGCAGAGTTT
GCGGATATGAACATGTACTGCGACGTCACGGACAGGACACCCATTGAAGCTGTTCATAGTTGCA
ACAACGCTGAATCATTAAACATCCTCAATAAGCTTCTCGCCCGGGAAACCGATACAGCCTTATC
TCAGATTTTCGAGCAGCCTACAGGAAAAGACTGGAAGGAATTGAACACACTGCAGACAATCCTC
TCCTTATGCTCAACGGTTACTATGGCCTTGCTCCTCGGACCAGATACAGCCCCTGACCCGGTGC
TCCACCACCATTCGACGTCTTTTGGCGAAGCAATTATGAGCAGTTGTTATCGACGAACGGGATA
TCCGCGCATCCTGCGGCCATTCGTGTGGCGCTTTTCGTCCGAATGCCGAAATCTGAGGAAACAC
TTATCTCTCGTGAGAGAGAGACTTGTTCCTGAGGTTGCGCGCCGTGTCGCAGCTGCACGAGCGG
CGGATAAAACCAAGGACGTACGCCCATCTTCATTGTTGGACGCACTGATCGCGGCGGCCTTCGA
CAACGGCAGCTTAAGCCCAGATGACCAAGGCAGAAATGATGCAGCACAGGTACAGTTGCTGGCA
GATGATCTCATTTTCTACCATTTCGAACTCTGTAAA**GGG**ACCGCATTCAACATCATCTTCCAGC
TGTATGCCATCATGGACCACCCAGAGTACAAGGCTCCTCTCCGAGAGGAGGCACTCCAAGCCTT
GAAGCTCACCAATGGTGACTGGACCGTTGAAACTCTGAAGCACGCTCCCAAGTTAGAAAGCTTT
ACAAAGGAGACCTTTCGACTGTACGATATCTCCGGTTTTGTCAGCTTTCGCCGTGTCATGAAAC
CTCTTACTCTAAACTCCATCGGCCTGTCTCTTCGTCCCGGTACAATCTTATTGTCTCCATGTCG
GAATGTCCATTTGGATCCCGAGATCTATGAAGACCCGACAACTTTCAATGGCTACCGCTTCTAC
GACTCCAGCCGCGAGGTCTGCTCTCCACGCGTGGCAACCACCTCGCTCACGTTCTTGACATTTT
CTCATGGAGCGGGCAGCTGTCCCGCGCGGGTTCTCGCTACTCAAATTTGTCGGACGATCTTCAT
CAAGTTCCTGTTGCAGTACGACGTAGAACCTGTGCAGAAGGAGATACTACCCTATGGATTCACC
AGTGGTCCGGTCTATATGCCTAATCCATCAGTGATGATGAGAATCCGGCCAAGAAGTGACGGGA
AG

MAVHVPFSIHHVVDIGISTGPVVIVLVLLFGLAVVGSDSLDGWWQKRALRGIPIVDEGSYMRPK
LRWKRFDAEKEYARAYQQYTKAGKPYAIRMQNDNYGIVLPLNSAKEWRSLPHDQLSFLQALAEF
ADMNMYCDVTDRTPIEAVHSCNNAESLNILNKLLARETDTALSQIFEQPTGKDWKELNTLQTIL
SLCSTVTMALLLGPDTAPDPVLHHHSTSFGEAIMSSCYRRTGYPRILRPFVWRFSSECRNLRKH
LSLVRERLVPEVARRVAAARAADKTKDVRPSSLLDALIAAAFDNGSLSPDDQGRNDAAQVQLLA
DDLIFYHFELCK**G**TAFNIIFQLYAIMDHPEYKAPLREEALQALKLTNGDWTVETLKHAPKLESF
TKETFRLYDISGFVSFRRVMKPLTLNSIGLSLRPGTILLSPCRNVHLDPEIYEDPTTFNGYRFY

DSSREVCSPRVATTSLTFLTFSHGAGSCPARVLATQICRTIFIKFLLQYDVEPVQKEILPYGFT
SGPVYMPNPSVMMRIRPRSDGK

Round 2 variant: KtnC-P333G-L422V

ATGGCAGTTCATGTACCATTCAGCATCCACCACGTCGTGGATATCGGCATTTCCACCGGCCCGG
TAGTCATTGTCCTCGTTCTCCTATTCGGGTTGGCTGTCGTGGGATCCGACAGCCTTGATGGATG
GTGGCAGAAAAGAGCCTTGAGAGGCATTCCGATTGTAGACGAGGGTAGCTACATGCGGCCAAAG
CTACGATGGAAGCGCTTCGATGCGGAGAAAGAGTATGCGAGAGCATATCAGCAGTACACAAAAG
CAGGGAAACCTTATGCGATCCGGATGCAGAATGATAATTATGGCATTGTGCTTCCCTTAAACTC
AGCAAAGGAATGGAGGTCTCTACCACACGACCAGCTGAGCTTTCTTCAAGCCTTGGCAGAGTTT
GCGGATATGAACATGTACTGCGACGTCACGGACAGGACACCCATTGAAGCTGTTCATAGTTGCA
ACAACGCTGAATCATTAAACATCCTCAATAAGCTTCTCGCCCGGGAAACCGATACAGCCTTATC
TCAGATTTTCGAGCAGCCTACAGGAAAAGACTGGAAGGAATTGAACACACTGCAGACAATCCTC
TCCTTATGCTCAACGGTTACTATGGCCTTGCTCCTCGGACCAGATACAGCCCCTGACCCGGTGC
TCCACCACCATTCGACGTCTTTTGGCGAAGCAATTATGAGCAGTTGTTATCGACGAACGGGATA
TCCGCGCATCCTGCGGCCATTCGTGTGGCGCTTTTCGTCCGAATGCCGAAATCTGAGGAAACAC
TTATCTCTCGTGAGAGAGAGACTTGTTCCTGAGGTTGCGCGCCGTGTCGCAGCTGCACGAGCGG
CGGATAAAACCAAGGACGTACGCCCATCTTCATTGTTGGACGCACTGATCGCGGCGGCCTTCGA
CAACGGCAGCTTAAGCCCAGATGACCAAGGCAGAAATGATGCAGCACAGGTACAGTTGCTGGCA
GATGATCTCATTTTCTACCATTTCGAACTCTGTAAA**GGG**ACCGCATTCAACATCATCTTCCAGC
TGTATGCCATCATGGACCACCCAGAGTACAAGGCTCCTCTCCGAGAGGAGGCACTCCAAGCCTT
GAAGCTCACCAATGGTGACTGGACCGTTGAAACTCTGAAGCACGCTCCCAAGTTAGAAAGCTTT
ACAAAGGAGACCTTTCGACTGTACGATATCTCCGGTTTTGTCAGCTTTCGCCGTGTCATGAAAC
CTCTTACTCTAAACTCCATCGGCCTGTCTCTTCGTCCCGGTACAATC**GTG**TTGTCTCCATGTCG
GAATGTCCATTTGGATCCCGAGATCTATGAAGACCCGACAACTTTCAATGGCTACCGCTTCTAC
GACTCCAGCCGCGAGGTCTGCTCTCCACGCGTGGCAACCACCTCGCTCACGTTCTTGACATTTT
CTCATGGAGCGGGCAGCTGTCCCGCGCGGGTTCTCGCTACTCAAATTTGTCGGACGATCTTCAT
CAAGTTCCTGTTGCAGTACGACGTAGAACCTGTGCAGAAGGAGATACTACCCTATGGATTCACC
AGTGGTCCGGTCTATATGCCTAATCCATCAGTGATGATGAGAATCCGGCCAAGAAGTGACGGGA
AG

MAVHVPFSIHHVVDIGISTGPVVIVLVLLFGLAVVGSDSLDGWWQKRALRGIPIVDEGSYMRPK
LRWKRFDAEKEYARAYQQYTKAGKPYAIRMQNDNYGIVLPLNSAKEWRSLPHDQLSFLQALAEF
ADMNMYCDVTDRTPIEAVHSCNNAESLNILNKLLARETDTALSQIFEQPTGKDWKELNTLQTIL
SLCSTVTMALLLGPDTAPDPVLHHHSTSFGEAIMSSCYRRTGYPRILRPFVWRFSSECRNLRKH
LSLVRERLVPEVARRVAAARAADKTKDVRPSSLLDALIAAAFDNGSLSPDDQGRNDAAQVQLLA
DDLIFYHFELCK**G**TAFNIIFQLYAIMDHPEYKAPLREEALQALKLTNGDWTVETLKHAPKLESF
TKETFRLYDISGFVSFRRVMKPLTLNSIGLSLRPGTI**V**LSPCRNVHLDPEIYEDPTTFNGYRFY
DSSREVCSPRVATTSLTFLTFSHGAGSCPARVLATQICRTIFIKFLLQYDVEPVQKEILPYGFT
SGPVYMPNPSVMMRIRPRSDGK

Supplemental data for the combinatorial library

Supplemental Figures S4.11-S4.16. The tier-one RapidFire-MS traces showed little activity. EIC traces of the cross-coupled product masses shown for plates P01-P05.

Supplemental Figure S4.12 P01

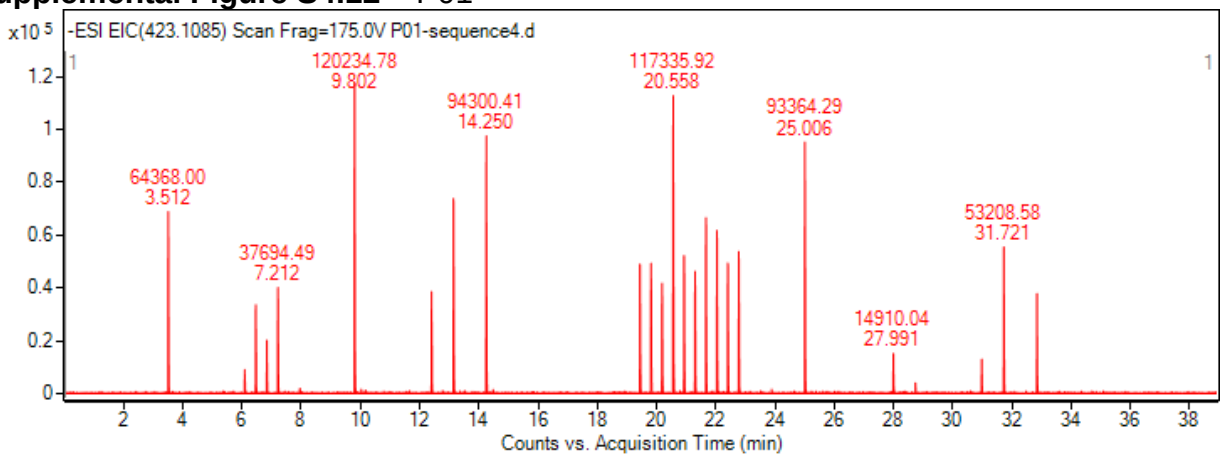

Supplemental Figure S4.13 P02

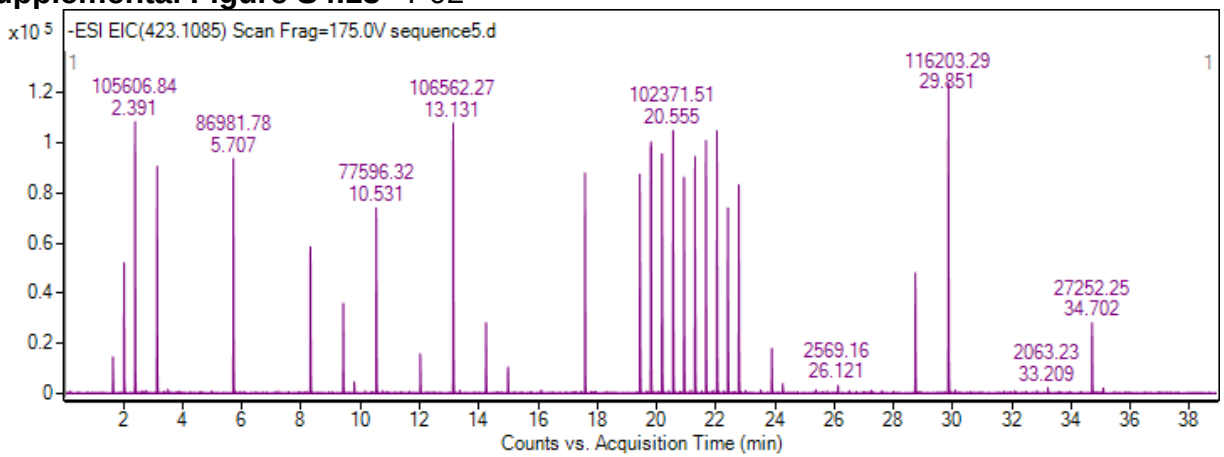

Supplemental Figure S4.14 P03

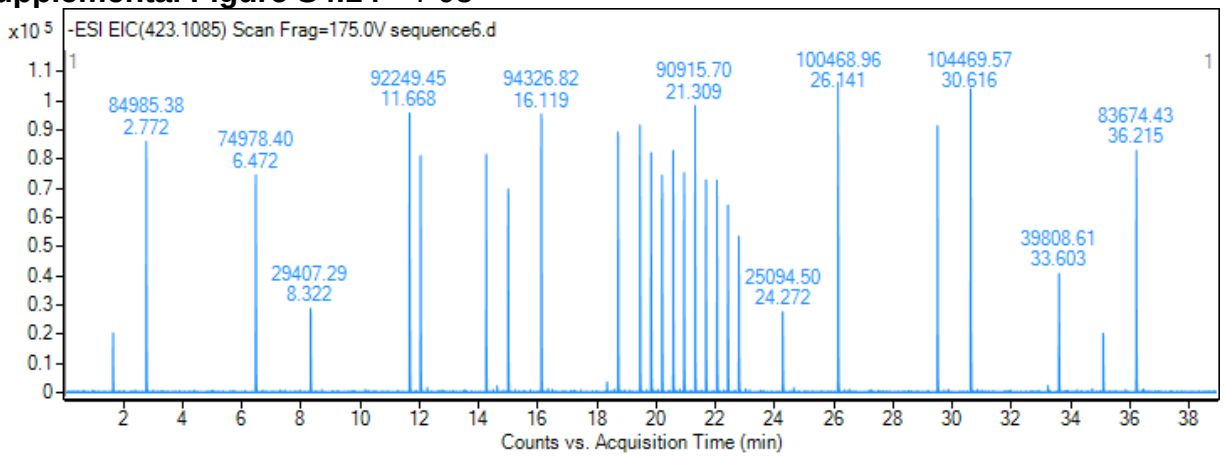

Supplemental Figure S4.15 P04

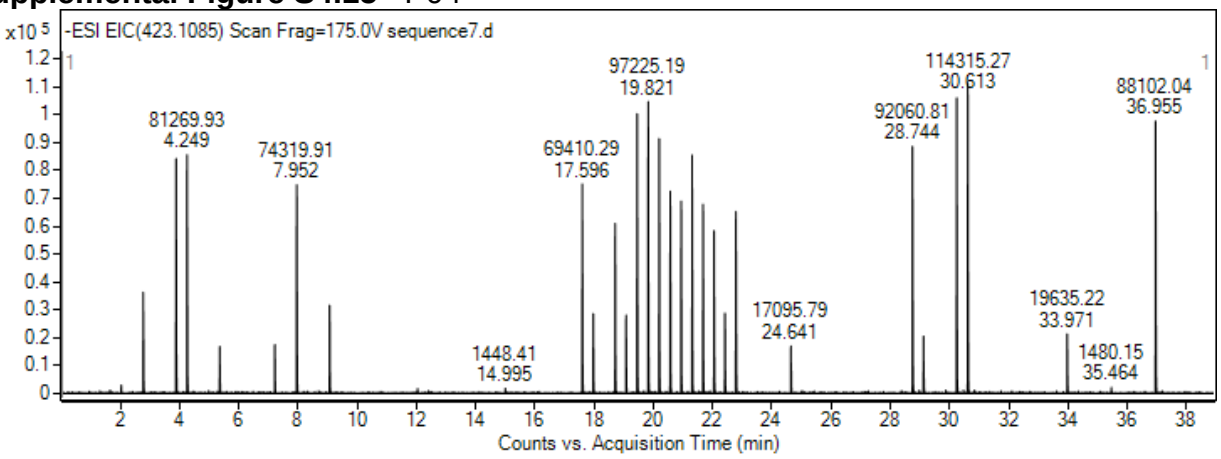

Supplemental Figure S4.16 P05

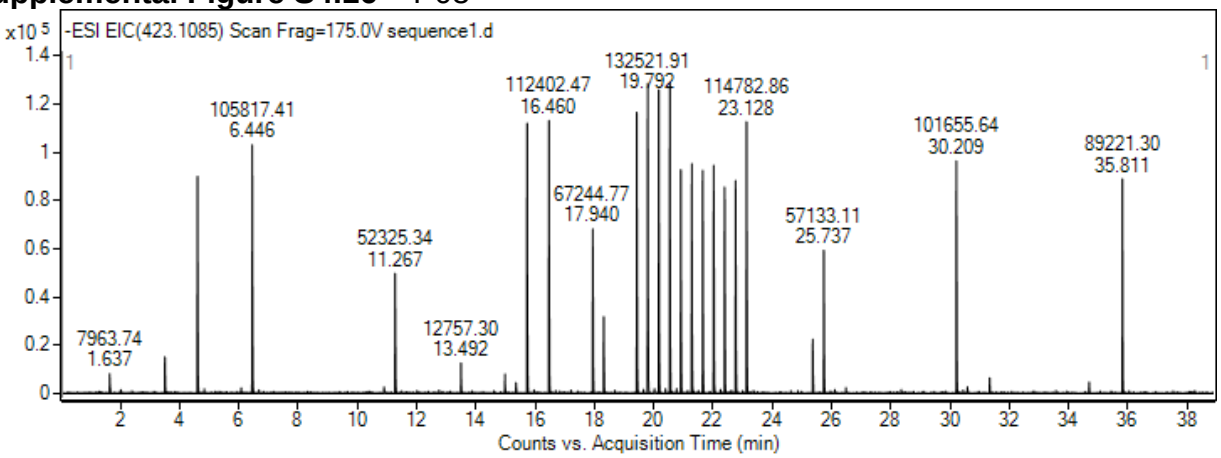

4.7 References

1. Laakso, J. A.; Narske, E. D.; Gloer, J. B.; Wicklow, D. T.; Dowd, P. F., Isokotanins New Bicoumarins from *Aspergillus-Alliaceus*. *J. Nat. Prod.* **1994,** *57* (1), 128-133.

2. Girol, C. G.; Fisch, K. M.; Heinekamp, T.; Gunther, S.; Huttel, W.; Piel, J.; Brakhage, A. A.; Muller, M., Regio- and Stereoselective Oxidative Phenol Coupling in *Aspergillus niger*. *Angewandte Chemie Int. Edition* **2012,** *51* (39), 9788-9791.

3. Lutz, S., Beyond directed evolution-semi-rational protein engineering and design. *Curr Opin Biotech* **2010,** *21* (6), 734-743.

4. Chen, M. M. Y.; Snow, C. D.; Vizcarra, C. L.; Mayo, S. L.; Arnold, F. H., Comparison of random mutagenesis and semi-rational designed libraries for improved cytochrome P450 BM3-catalyzed hydroxylation of small alkanes. *Protein Eng. Des. Sel.* **2012,** *25* (4), 171-178.

5. Huttel, W.; Muller, M., Regio- and stereoselective intermolecular phenol coupling enzymes in secondary metabolite biosynthesis. *Natural Product Reports* **2021,** *38* (5), 1011-1043.

6. Mazzaferro, L. S.; Huttel, W.; Fries, A.; Muller, M., Cytochrome P450-Catalyzed Regio- and Stereoselective Phenol Coupling of Fungal Natural Products. *J. Am. Chem. Soc.* **2015,** *137* (38), 12289-12295.

7. Huttel, W.; Muller, M., Regio- and stereoselective intermolecular oxidative phenol coupling in kotanin biosynthesis by Aspergillus niger. *ChemBioChem* **2007,** *8* (5), 521-9.

8. Cary, J. W.; Han, Z.; Yin, Y.; Lohmar, J. M.; Shantappa, S.; Harris-Coward, P. Y.; Mack, B.; Ehrlich, K. C.; Wei, Q.; Arroyo-Manzanares, N.; Uka, V.; Vanhaecke, L.; Bhatnagar, D.; Yu, J.; Nierman, W. C.; Johns, M. A.; Sorensen, D.; Shen, H.; De Saeger, S.; Di Mavungu, J. D.; Calvo, A. M., Transcriptome Analysis of Aspergillus flavus Reveals veA-Dependent Regulation of Secondary Metabolite Gene Clusters, Including the Novel Aflavarin Cluster. *Eukaryot. Cell* **2015,** *14* (10), 983-997.

9. Kjaerbolling, I.; Vesth, T.; Frisvad, J. C.; Nybo, J. L.; Theobald, S.; Kildgaard, S.; Petersen, T. I.; Kuo, A.; Sato, A.; Lyhne, E. K.; Kogle, M. E.; Wiebenga, A.; Kun, R. S.; Lubbers, R. J. M.; Makela, M. R.; Barry, K.; Chovatia, M.; Clum, A.; Daum, C.; Haridas, S.; He, G. F.; LaButti, K.; Lipzen, A.; Mondo, S.; Pangilinan, J.; Riley, R.; Salamov, A.; Simmons, B. A.; Magnuson, J. K.; Henrissat, B.; Mortensen, U. H.; Larsen, T. O.; de Vries, R. P.; Grigoriev, I. V.; Machida, M.; Baker, S. E.; Andersen, M. R., A comparative genomics study of 23 Aspergillus species from section Flavi. *Nature Communications* **2020,** *11* (1).

10. Buchi, G.; Klaubert, D. H.; Shank, R. C.; Weinreb, S. M.; Wogan, G. N., Structure and Synthesis of Kotanin and Desmethylkotanin, Metabolites of Aspergillus-Glaucus. *J. Org. Chem.* **1971,** *36* (8), 1143-&.

11. Huttel, W.; Nieger, M.; Muller, M., A short and efficient total synthesis of the naturally occurring coumarins siderin, kotanin, isokotanin A and desertorin C. *Synthesis-Stuttgart* **2003,** (12), 1803-1808.

12. Bringmann, G.; Hinrichs, J.; Henschel, P.; Kraus, J.; Peters, K.; Peters, E. M., Atropo-enantioselective synthesis of the natural bicoumarin (+)-isokotanin A via a configurationally stable biaryl lactone. *European Journal of Organic Chemistry* **2002,** *2002* (6), 1096-1106.

13. Graff, J.; Debande, T.; Praz, J.; Guenee, L.; Alexakis, A., Asymmetric bromine-lithium exchange: application toward the synthesis of natural product. *Org. Lett.* **2013,** *15* (16), 4270-3.

14. Nozawa, K.; Nakajima, S.; Kawai, K.; Udagawa, S.; Miyaji, M., Bicoumarins from Ascostromata of *Petromyces Alliaceus*. *Phytochemistry* **1994,** *35* (4), 1049-1051.

15. Cutler, H. G.; Crumley, F. G.; Cox, R. H.; Hernandez, O.; Cole, R. J.; Dorner, J. W., Orlandin - Nontoxic Fungal Metabolite with Plant-Growth Inhibiting Properties. *J. Agr. Food Chem.* **1979,** *27* (3), 592-595.

16. Tian, J. M.; Wang, A. F.; Yang, J. S.; Zhao, X. J.; Tu, Y. Q.; Zhang, S. Y.; Chen, Z. M., Copper-Complex-Catalyzed Asymmetric Aerobic Oxidative Cross-Coupling of 2-Naphthols: Enantioselective Synthesis of 3,3'-Substituted C1-Symmetric BINOLs. *Angew Chem Int Ed Engl* **2019,** *58* (32), 11023-11027.

17. Lee, Y. E.; Cao, T.; Torruellas, C.; Kozlowski, M. C., Selective Oxidative Homo- and Cross-Coupling of Phenols with Aerobic Catalysts. *J. Am. Chem. Soc.* **2014,** *136* (19), 6782-6785.

18. Reiss, H.; Shalit, H.; Vershinin, V.; More, N. Y.; Forckosh, H.; Pappo, D., Cobalt(II)[salen]-Catalyzed Selective Aerobic Oxidative Cross-Coupling between Electron-Rich Phenols and 2-Naphthols. *J Org Chem* **2019,** *84* (12), 7950-7960.

19. Shalit, H.; Dyadyuk, A.; Pappo, D., Selective Oxidative Phenol Coupling by Iron Catalysis. *J. Org. Chem.* **2019,** *84* (4), 1677-1686.

20. Shalit, H.; Libman, A.; Pappo, D., meso-Tetraphenylporphyrin Iron Chloride Catalyzed Selective Oxidative Cross-Coupling of Phenols. *J. Am. Chem. Soc.* **2017,** *139* (38), 13404-13413.

21. Libman, A.; Shalit, H.; Vainer, Y.; Narute, S.; Kozuch, S.; Pappo, D., Synthetic and Predictive Approach to Unsymmetrical Biphenols by Iron-Catalyzed Chelated Radical-Anion Oxidative Coupling. *J. Am. Chem. Soc.* **2015,** *137* (35), 11453-11460.

22. Wu, X.; Iwata, T.; Scharf, A.; Qin, T.; Reichl, K. D.; Porco, J. A., Asymmetric synthesis of gonytolide A: strategic use of an aryl halide blocking group for oxidative coupling. *J. Am. Chem. Soc.* **2018,** *140* (18), 5969-5975.

23. Noji, M.; Nakajima, M.; Koga, K., A New Catalytic-System for Aerobic Oxidative Coupling of 2-Naphthol Derivatives by the Use of CuCl-Amine Complex. *Tetrahedron Letters* **1994,** *35* (43), 7983-7984.

24. Hirao, T., Vanadium in modern organic synthesis. *Chem. Rev.* **1997,** *97* (8), 2707-2724.

25. Nieves-Quinones, Y.; Paniak, T. J.; Lee, Y. E.; Kim, S. M.; Tcyrulnikov, S.; Kozlowski, M. C., Chromium-Salen Catalyzed Cross-Coupling of Phenols: Mechanism and Origin of the Selectivity. *J Am Chem Soc* **2019,** *141* (25), 10016-10032.

26. Zetzsche, L.; Yazarians, J.; Chakrabarty, S.; Hinze, M.; Lukowski, A.; Joyce, L.; Narayan, A.; Murray, L., Biocatalytic oxidative cross-coupling reactions for biaryl bond formation. **2021.** DOI:10.33774/chemrxiv-2021-v0bv6-v2.

27. Kocovsky, P.; Vyskocil, S.; Smrcina, M., Non-symmetrically substituted 1,1'-binaphthyls in enantioselective catalysis. *Chem. Rev.* **2003,** *103* (8), 3213-46.

Chapter 5: Summary and Outlook

5.1 Summary

Biaryl bonds with hindered rotation are abundant in natural products, drugs, materials, and ligands. Their three-dimensional structure impacts the function of this diverse group of stereoisomers (Figure 5.1A).[1-3] Atroposelective biaryl bond formation remains a challenging transformation in modern chemistry.[4] Although numerous methods have been developed, each has limitations that impede their reliable incorporation into synthetic routes and into target compounds. The most widely utilized routes, transition metal catalyzes cross-coupling reactions, excel in building biaryl C–C bonds that are less sterically demanding, with methods for cross-coupling arenes with mono, di, and tri-*ortho*-substituents disclosed.[5-6] Tetra-*ortho*-substitution patterns are considerably more challenging and are typically not general (Figure 5.1B, left).[7-8]

In contrast, direct oxidative coupling of phenols provides a more direct route to the formation of sterically hindered biaryl bonds but is overrepresented with examples of dimerizations while cross-coupling reactions remain more challenging (Figure 5.1B, right).[9] Direct oxidative coupling can be achieved with a wide range of transition metal catalyst and metal free oxidants and offers an attractive alternative without the need for additional synthetic steps to install functional handles at the site of bond formation or protecting group manipulations, but the method is impeded by the need to control multiple layers of selectivity. To be effective, control over the chemoselectivity (homocoupling *vs.* cross-coupling, and C–C *vs.* C–O or C–N coupling), site-selectivity (in the formation of one desired product isomer), and atroposelectivity of the reactions must be achieved for formation of the desired biaryl bond on demand. This requirement for different forms of selectivity, which is dictated by innate steric and electronic properties of the starting materials in small molecule catalyzed cross-coupling reactions, has limited the use of direct oxidative coupling in the formation of sterically hindered and electronically

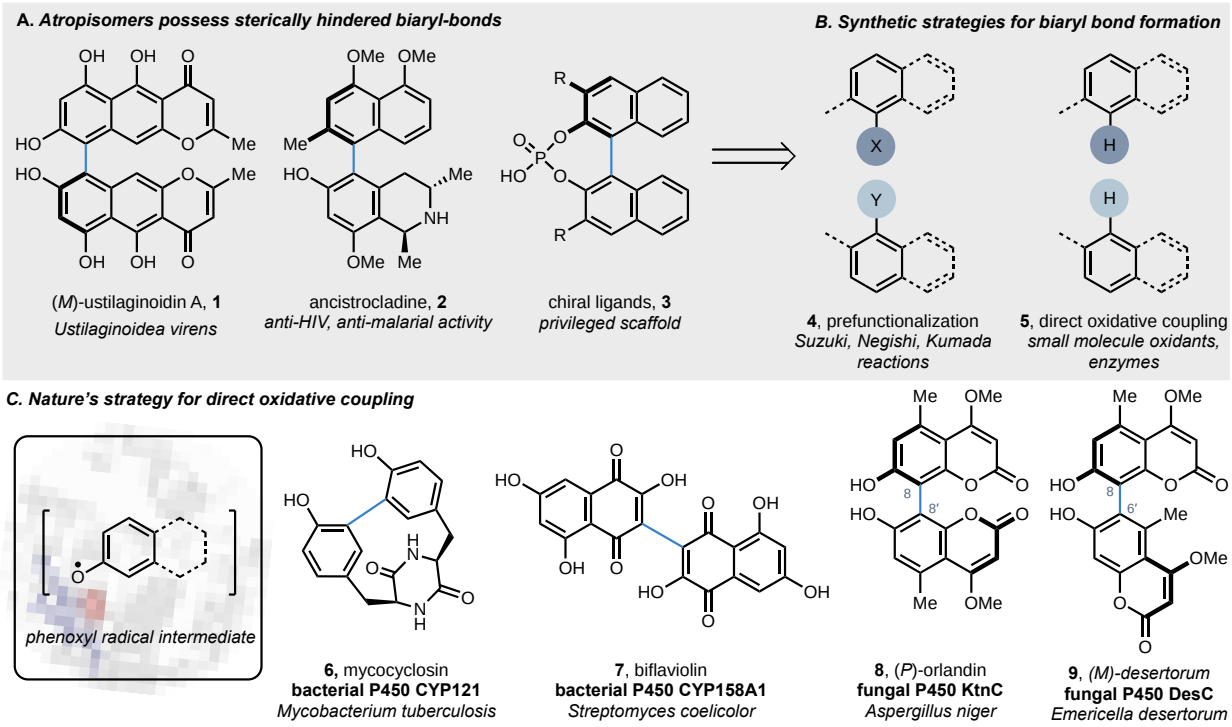

Figure 5.1: Strategies for the synthesis of atropisomers
A. Sterically hindered biaryl bonds in natural products and privileged ligand scaffolds. B. Traditional synthetic methods employed for the formation of biaryl bonds. C. Nature's enzymatic tools in the biosynthesis of natural product atropisomers through direct oxidative dimerization of phenols.

unfavorable combinations.[10-12] However, Nature has developed numerous enzymes, such as cytochromes P450 (P450s), capable of selective direct oxidative coupling reactions, controlling the chemo, site- and atroposelectivity through binding of the substrates within an enzyme active site (Figure 5.1C).[13] Although examples of oxidative coupling enzymes have been identified and biochemically characterized, these enzymes are rarely investigated beyond their native reactivity for synthesis of compounds outside the biosynthetic pathway of the host organism. The investigation and development of oxidative coupling biocatalysts for non-native dimerization reactions and cross-coupling of phenols remains an underexplored and underutilized tool in synthesis.[13] Thus, we sought to develop a biocatalytic method for oxidative dimerization and cross-coupling of coumarins and phenols leveraging the exquisite site- and atroposelectivity of the fungal P450 enzymes KtnC and DesC, taking inspiration from the divergent selectivity displayed in the biosynthesis of **8** and **9**.

The heterologous expression of the genes encoding fungal P450 enzymes KtnC and DesC in both *S. cerevisiae* and *P. pastoris* were performed in the development of a

new platform for biocatalytic oxidative dimerization and cross-coupling reactions. Extensive optimization studies for the biocatalytic reaction were implemented in the method development phase to enhance the percent yields of the reactions on both analytical and preparative scale, including testing growth, induction, and expression conditions in yeast, and exploring the effect of substrate concentration and ratios on reactivity (Figure 5.2A). To enable the exploration of the substrate scope and selectivity of the fungal P450 enzymes KtnC and DesC, analytical methods were developed that were critical in quantifying the relative percent yields, percent conversions, and percent yields of the biocatalytic reactions. LC-MS was employed as the primary tool for reaction discovery and in the structural assignment of products that were synthetically intractable or not isolable from preparative scale reactions for direct characterization of the products. The analytical methods developed allowed for the rapid screening of conditions and substrates in high throughput (96 well plates) or semi-high throughput (24 well plates) formats (Figure 5.2B). Refinement of three analysis methods for analytical scale reactions

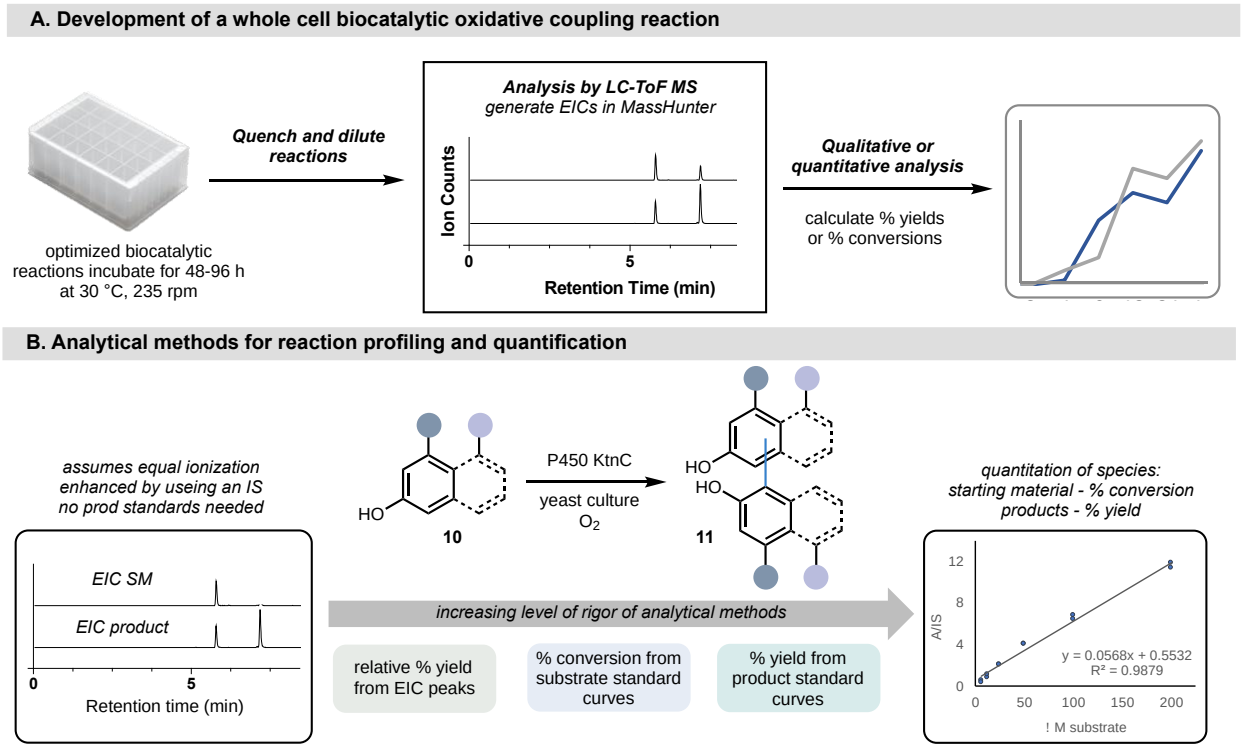

Figure 5.2: Development of a biocatalytic platform for oxidative coupling reactions in yeast and analytical methods for reaction analysis.
A. Optimization of the heterologous host yeast strain, growth, and induction of protein expression were conducted. B. Analytical methods for substrate scope exploration in the dimerization and cross-coupling reactions were developed and implemented in reaction profiling and quantitation.

provided tools to quantify and compare product formation in dimerization and cross-coupling reactions.

Initial exploration of the substrate scopes of KtnC and DesC revealed the enzymes were promiscuous and could be employed for oxidative dimerizations of coumarins, in some cases with good site- and enantioselectivity (Figure 5.3A-C, also see Chapter 2, Figure 2.9 for experimental details). Site-selectivity trends were observed in the dimerization of coumarins with increasing steric bulk of vinylogous ester functional

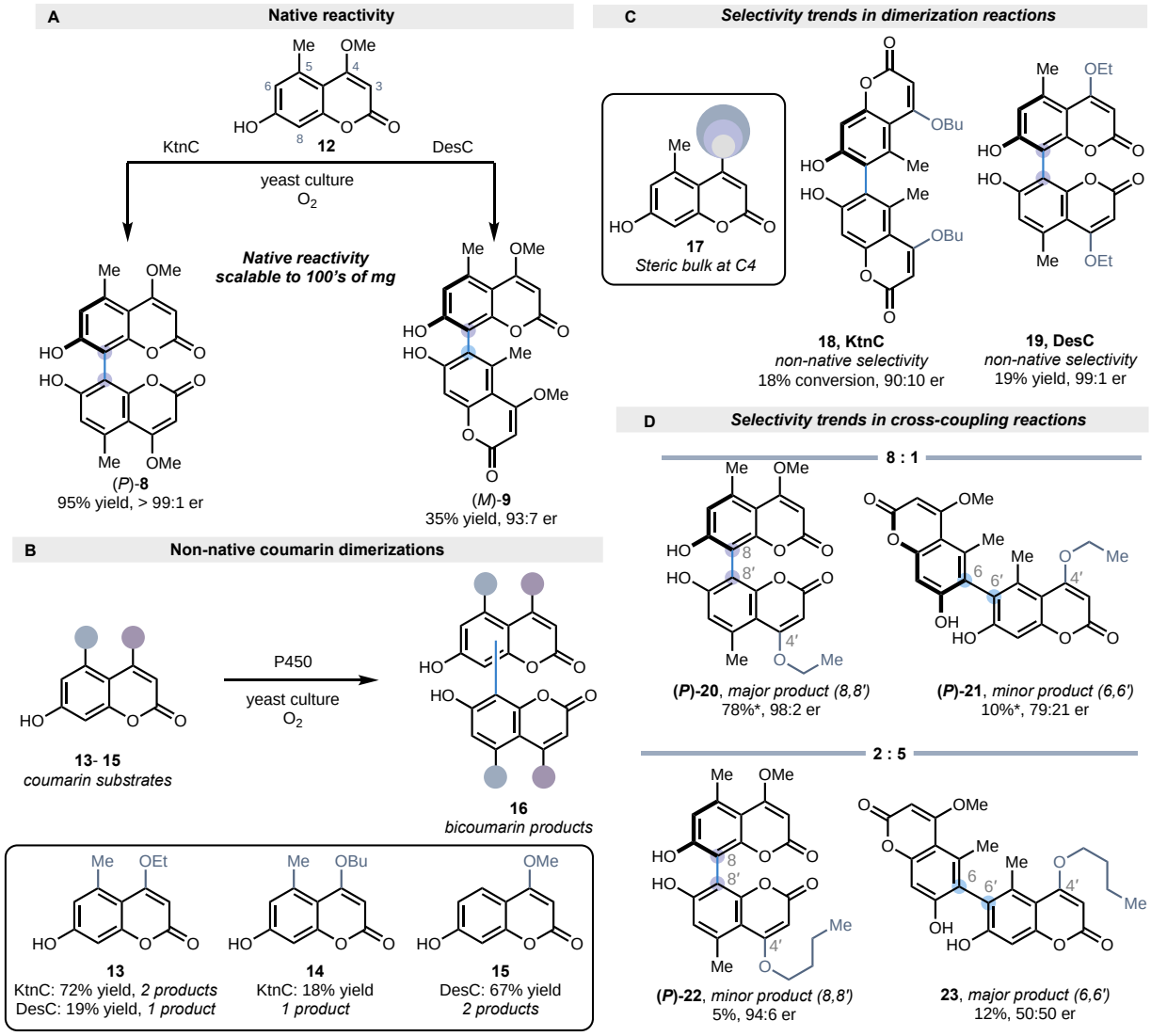

Figure 5.3: P450 catalyzed oxidative dimerization and cross-coupling reactions
A. Initial efforts to enhance the expression of P450s in Pichia pastoris allowed for the preparative scale dimerization reactions of the native substrate **12** with KtnC and DesC. B. The dimerization reaction with non-native coumarins. C. Site-selectivity of bulky coumarins switched from 8,8' to the desirable 6,6'-connectivity with KtnC, and from 8,6' to 8,8'-connectivity with DesC. D. A similar trend was observed in cross-coupling reactions of bulky coumarins with KtnC, with the major product switching from 8,8' to the 6,6'-connectivity.

groups, leading to the discovery of novel selectivity in wild-type KtnC in the formation of 6,6'-isomers in non-natural substrates bearing large groups at the C4 position (Figure 5.3C). New reactivity was discovered in wild-type KtnC for the oxidative cross-coupling of coumarins, a promising proof-of-concept outside the native functionality of the enzymes. Similar trends in site-selectivity were observed in the KtnC cross-coupling reactions of coumarins with greater steric bulk at the C4 position (Figure 5.3D, see also Chapter 3, Figure 3.2 for experimental details). Tuning the vinylogous ester group allowed for the

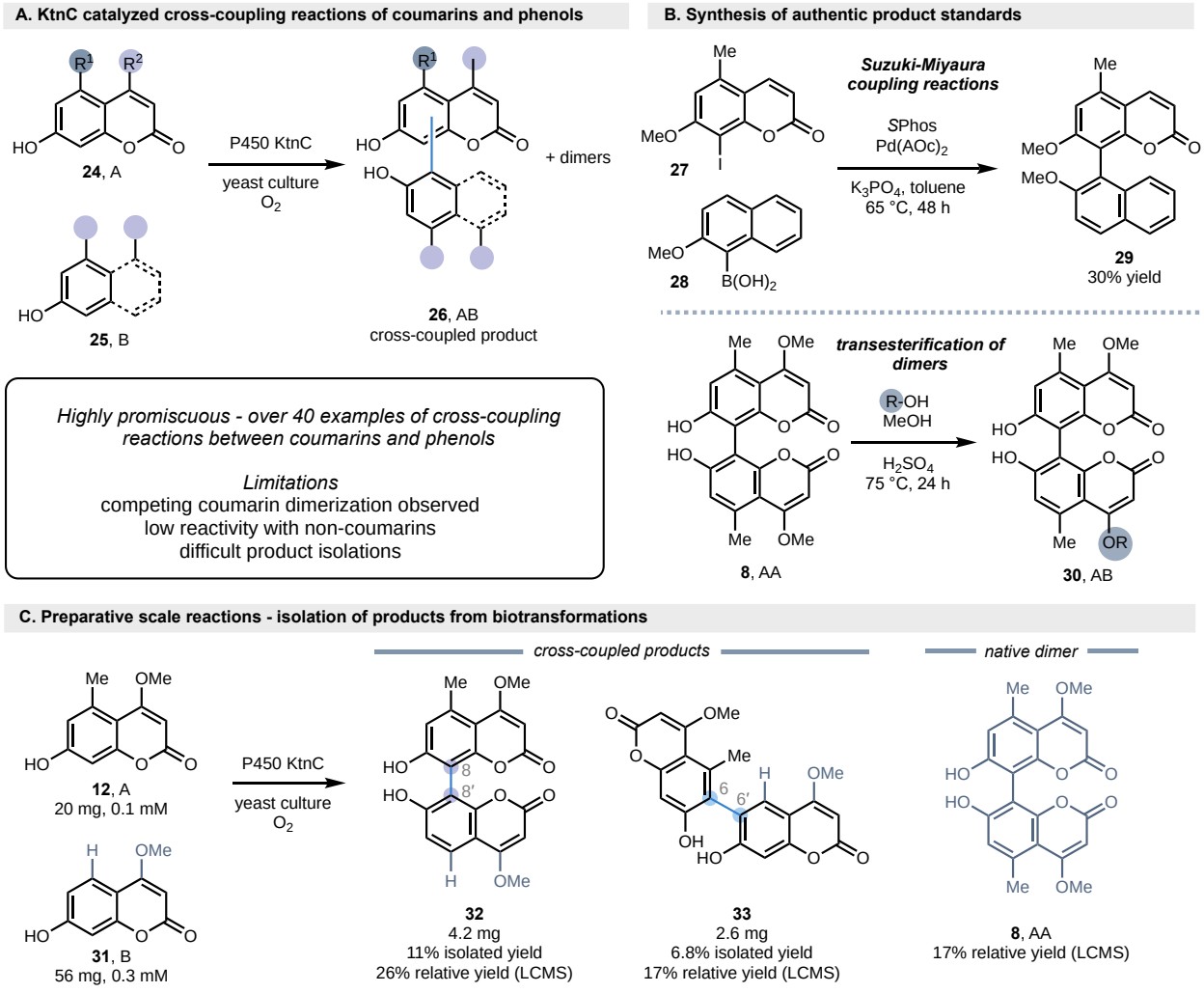

Figure 5.4: P450 catalyzed oxidative dimerization and cross-coupling reactions
A. Initial efforts to optimize the expression of P450s in *Pichia pastoris* allowed for the preparative scale dimerization reactions of the native substrate **12** with KtnC and DesC. B. The dimerization reaction with non-native coumarins. C. Site-selectivity of bulky coumarins switched from 8,8' (**8**) to the desirable 6,6'-connectivity (**18**) with KtnC, and from 8,6' (**9**) to 8,8'-connectivity (**19**) with DesC. D. A similar trend was observed in cross-coupling reactions of bulky coumarins with KtnC, with the major product switching from 8,8 to the 6,6'-connectivity (**23**).

synthesis of bicoumarins with 6,6'-connectivity (**18**, **21**, and **23**), compounds which were otherwise difficult to synthesize through traditional chemical methods.

The cross-coupling reaction was further developed and examples of over 40 unique substrate combinations were demonstrated, including coupling between non-native coumarins and phenols (5.4A) from excellent (up to 78%) to low percent (1%) yields and conversions. To identify the products in enzymatic reactions that could not be scaled up and isolated, two main strategies were employed for the synthesis of product standards for comparison by LC-MS (Figure 5.4B). Conditions for Suzuki-Miyaura cross-coupling reactions were screened and identified for the synthesis of the tetra-*ortho*-substituted biaryl **29** in a 30% yield, with the ligand *S*Phos proving the most general and highly active in the sterically hindered cross-coupling of coumarins and naphthol fragments. Coumarin-coumarin cross-coupled products were not accessible through Suzuki-Miyaura coupling, and direct oxidative coupling provided only some of the potential product isomers. Transesterification of coumarin dimers of known connectivity was employed, creating analytical standards that were used to identify the connectivity of analytical scale enzymatic cross-coupling reactions by LC-MS. In cross-coupling reactions with relative percent yields above 30%, preparative scale reactions were attempted with limited success (Figure 5.4C, also see Chapter 3, Figures 3.16–3.18 for experimental details). In the KtnC catalyzed cross-coupling reaction of **12** and **31**, two products were isolated in low yields, 11% **32** and 7% **33**, after two rounds of purification. The disparity between calculated relative percent yields and isolated yields highlighted some of the challenges of preparative scale biotransformations in this platform, namely, the loss of products to incomplete extractions from whole-cell biotransformation culture, and the need for iterative purification steps due to the formation of multiple products. Although some limitations were encountered, the range of reactivity of wild-type KtnC across numerous substrate combinations, and the potential for access to 6,6'-isomeric products was advantageous, providing an excellent starting point for further development of the platform with protein engineering.

The ability to improve the reactivity of the cross-coupling reaction to build rare 6,6'-isomers between two structurally and electronically similar coumarin substrates **12** and **13** was desired. The wild-type KtnC catalyzed biotransformation was an unselective

reaction producing up to five products, two cross-coupled isomers (**20** and **21**, 34% combined yield) and three dimeric products (**8** and **34**), with dimeric products making up the majority of the products (47% combined yield, Figure 5.5A). Additionally, the major cross-coupled product **20** possessed the 8,8'-connectivity, formed in a roughly 2:1 ratio with the more desirable 6,6'-isomer **21**. I sought to test the hypothesis that KtnC variants could provide enhanced selectivity by directed evolution of wild-type KtnC and

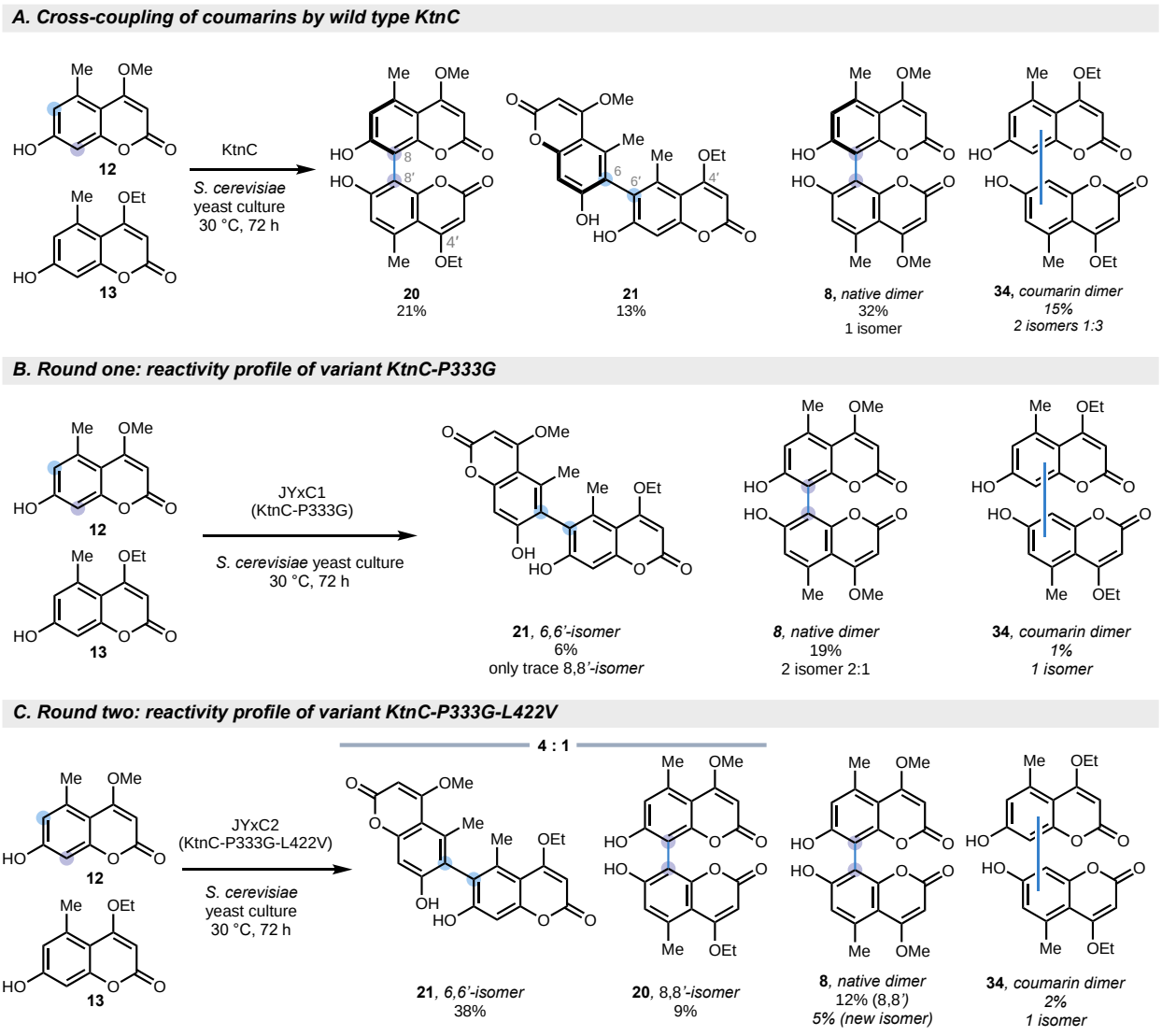

Figure 5.5: Protein engineering to improve the selectivity of P450 catalyzed cross-coupling reaction
A. Wild-type KtnC formed product **21** as the minor cross-coupled product, with dimers **8** and **34** as the major product in the reaction carried out with substrates in a 1:1 ratio. B. Round 1 of evolution identified a substitution, P333G, that enhanced the site-selectivity and chemoselectivity of the reaction. The desired product **21** was the sole cross-coupled product, with a substantial reduction in dimerization. C. Round 2 recovered the reactivity of the biotransformation, increasing from 6% to 38%, **21** however at the expense of the chemoselectivity and site-selectivity.

demonstrating the tunability of the selectivity of the reaction over two rounds of protein engineering.

Two enzyme libraries were generated through semi-rational mutagenesis,[14] wherein beneficial mutations were identified through site-scanning saturation mutagenesis of active site residues.[15] The reactions were analyzed in a tier-one screen by UPLC-DAD or by high throughput RapidFire-mass spectrometry, followed by a tier-two screen employing LC-MS. Over two rounds of evolution, the chemoselectivity and site-selectivity of the P450-mediated reaction were enhanced in comparison to wild type KtnC (Figure 5.5B-C). A variant possessing two substitutions, P333G and L422V, provided a 3-fold increase from 13% relative percent yield to 38% of the desired 6,6'-cross-coupled coumarin product **21**. Notably, the chemo- and site-selectivity of the biocatalyst was also improved (Figure 5.5C), with less than half of the dimerization products observed (14% in round 2 compared to 47% with wild-type KtnC). The atroposelectivity of the reaction was not considered, due to limitations in the chiral separation of the two isomeric products, however, as the atroposelectivity was observed to decrease over rounds of evolution towards LxC5,[16] thus, it is important to develop analytical methods to measure the enantioselectivity across each round of evolution for this reaction. These examples highlight the tunability of the biocatalytic platform, offering an advantage over small molecule synthesis through the potential catalyst control over reactivity, chemo- and site-selectivity.

5.2 Future directions

Although a vast amount of information on the reactivity of fungal P450 enzyme KtnC has been uncovered, several limitations in the biocatalytic platform are apparent. The first is in reactivity, for example, KtnC accepts a wide range of coumarins in dimerization and cross-coupling reactions, however, this activity rapidly declines with other phenolic substrates (see Figure 3.2B in Chapter 3). Second, we observed some instances of chemoselectivity in select reactions, however, many cross-coupling reactions still dimerize one or both coumarin coupling partners, a similar problem encountered in small molecule catalyzed direct oxidative coupling reactions of phenols.

This competing dimerization and lack of chemoselectivity on the surface presents little advantage over commonly employed chemical oxidants, however, looking at details of the product distributions that are formed in the biocatalytic reaction suggests catalyst control, a feature uncommon in most small molecule methods. Lastly, the limitations in whole-cell preparative scale reactions hinder the platform's general scalability, as we encountered considerable hurdles in the product isolation steps. This becomes a non-issue when conversion is high and the reaction is selective, for example, in biocatalytic reactions with variant LxC5 which achieves 50% yield of a single cross-coupled product without dimerized products, however, the challenges in scalability with KtnC and DesC remain a hurdle to their synthetic utility.[16]

Despite these limitations, the biocatalytic platform for oxidative phenolic cross-coupling reactions has demonstrated potential with wild-type enzymes, and the ability to be engineered for improvements in reactivity. With a vast number of P450 enzymes sequences encoding enzymes that potentially catalyze this desirable reaction, there is room for further exploration and growing possibility that our original goals in developing this reaction will be realized. In particular, two avenues present that path forward: (1) the tunable nature of the biocatalysts that has been demonstrated in this work, and (2) the growing number of sequences available for applying the same principles demonstrated with the KtnC biocatalytic reaction to new enzymes. Thus, the ability to engineer the biocatalysts for the desired reactivity profile presents a powerful advantage over small molecule methods. Bioinformatic tools for uncovering new and related enzymes with sequence similarity networks, using genome mining to identify new enzymes in biosynthetic pathways, and advances in computational biology, such as protein structure predictions, machine learning, and computational modeling, all present an opportunity to further expand the chemical versatility and synthetic utility of P450 oxidative phenolic coupling reactions.[17-19]

Future directions for this project, and for biocatalytic oxidative phenolic coupling in general, should focus on improving the scalability and selectivity of the reactions to make this transformation useful as a reliable tool in modern synthesis. To achieve that goal, expanding the substrate scopes of known oxidative coupling enzymes would be helpful in identifying new reactivity outside the native biotransformations the enzymes evolved

for. This could be accomplished by screening numerous enzymes for new chemistry with panels of phenolic substrates. Screening enzymes and numerous substrates and substrate combinations creates a large dataset, which would be valuable for data mining to uncover reactivity trends and serve as a record for new reactions that could be developed into key steps in synthetic routes to classes of natural products or drugs. Next, after identifying new reactions of interest, applying protein engineering would enhance the desired selectivity. Lastly, exploring new heterologous hosts, engineering proteins that are readily expressed and purified to allow *in vitro* reactions, and exploring P450s from bacterial organisms could all contribute to developing an alternative to whole-cell biotransformations in yeast to enhance reaction scalability.

Beyond increasing percent yield and controlling selectivity, this platform enables the fragment coupling of two phenols, but has presently not been extended to simple phenols that possess a single aromatic ring. Further expanding the substrate scope beyond coumarins is a critical step in the development of the platform and could be achieved by screening new enzymes or protein engineering. Given the ubiquity of C_1 and C_2 symmetric BINOL type ligands[20-23] in asymmetric catalysis, one future goal could focus on developing new biocatalysts for cross-coupling unsymmetric naphthol-type phenols, which currently present a synthetic challenge. Beyond targeting reactions that are difficult to achieve, potential uses for this chemistry in the key site- and stereo-determining step in biaryl coupling could be applied in complex molecule synthesis, specifically where asymmetric cross-coupling or arenes provides a desirable synthetic strategy.

Lastly, deeper mechanistic questions underlying the C–C coupling in the enzyme active sight are ripe for exploration. As discussed in Chapters 1 and 2, several plausible mechanistic hypotheses, such as the diradical coupling, radical-addition, and PCET, and cationic mechanisms are proposed.[13, 24-28] Due to the difficulty in obtaining crystal structures of membrane bound P450 enzymes of interest, detailed mechanistic studies have not been possible for the majority of the enzymes known to carry out this transformation. However, with the advances in computational tools for structure prediction including AlphaFold, the ability to model enzymes, substrates, and reactions is possible and could provide additional mechanistic insight. Answering these fundamental questions could aid in developing this biocatalytic platform further.

5.3 References

1. Bringmann, G.; Mortimer, A. J. P.; Keller, P. A.; Gresser, M. J.; Garner, J.; Breuning, M., Atroposelective synthesis of axially chiral biaryl compounds. *Angew. Chem. Int. Edit.* **2005,** *44* (34), 5384-5427.

2. LaPlante, S. R.; Edwards, P. J.; Fader, L. D.; Jakalian, A.; Hucke, O., Revealing Atropisomer Axial Chirality in Drug Discovery. *ChemMedchem* **2011,** *6* (3), 505-513.

3. Clayden, J.; Moran, W. J.; Edwards, P. J.; LaPlante, S. R., The Challenge of Atropisomerism in Drug Discovery. *Angew. Chem. Int. Edit.* **2009,** *48* (35), 6398-6401.

4. Bringmann, G.; Gulder, T.; Gulder, T. A. M.; Breuning, M., Atroposelective total synthesis of axially chiral biaryl natural products. *Chem. Rev.* **2011,** *111* (2), 563-639.

5. Buchwald, M. R.; S. L., Palladium-catalyzed Suzuki-Miyaura cross-coupling reactions employing dialkylbiaryl phosphine ligands. *Acc. Chem. Res.* **2008,** *41* (11), 1461-73.

6. Barder, T. E.; Biscoe, M. R.; Buchwald, S. L., Structural Insights into Active Catalyst Structures and Oxidative Addition to (Biaryl)phosphine−Palladium Complexes via Density Functional Theory and Experimental Studies. *Organometallics* **2007,** *26* (9), 2183-2192.

7. Wurtz, S.; Glorius, F., Surveying Sterically Demanding N-Heterocyclic Carbene Ligands with Restricted Flexibility for Palladium-catalyzed Cross-Coupling Reactions. *Acc. Chem. Res.* **2008,** *41* (11), 1523-1533.

8. Patel, N. D.; Sieber, J. D.; Tcyrulnikov, S.; Simmons, B. J.; Rivalti, D.; Duvvuri, K.; Zhang, Y.; Gao, D. A.; Fandrick, K. R.; Haddad, N.; Lao, K. S.; Mangunuru, H. P. R.; Biswas, S.; Qu, B.; Grinberg, N.; Pennino, S.; Lee, H.; Song, J. J.; Gupton, B. F.; Garg, N. K.; Kozlowski, M. C.; Senanayake, C. H., Computationally Assisted Mechanistic Investigation and Development of Pd-Catalyzed Asymmetric Suzuki-Miyaura and Negishi Cross-Coupling Reactions for Tetra-ortho-Substituted Biaryl Synthesis. *ACS Catal* **2018,** *8* (11), 10190-10209.

9. Kozlowski, M. C., Oxidative Coupling in Complexity Building Transforms. *Accounts Chem. Res.* **2017,** *50* (3), 638-643.

10. Kocovsky, P.; Vyskocil, S.; Smrcina, M., Non-symmetrically substituted 1,1'-binaphthyls in enantioselective catalysis. *Chem Rev* **2003,** *103* (8), 3213-46.

11. Shalit, H.; Dyadyuk, A.; Pappo, D., Selective Oxidative Phenol Coupling by Iron Catalysis. *J Org Chem* **2019,** *84* (4), 1677-1686.

12. Libman, A.; Shalit, H.; Vainer, Y.; Narute, S.; Kozuch, S.; Pappo, D., Synthetic and predictive approach to unsymmetrical biphenols by iron-catalyzed chelated radical–anion oxidative coupling. *J. Am. Chem. Soc.* **2015,** *137* (35), 11453-11460.

13. Huttel, W.; Muller, M., Regio- and stereoselective intermolecular phenol coupling enzymes in secondary metabolite biosynthesis (vol 38, pg 1011, 2021). *Natural Product Reports* **2021,** *38* (7), 1408-1408.

14. Lutz, S., Beyond directed evolution-semi-rational protein engineering and design. *Curr Opin Biotech* **2010,** *21* (6), 734-743.

15. Chen, M. M. Y.; Snow, C. D.; Vizcarra, C. L.; Mayo, S. L.; Arnold, F. H., Comparison of random mutagenesis and semi-rational designed libraries for improved cytochrome P450 BM3-catalyzed hydroxylation of small alkanes. *Protein Eng. Des. Sel.* **2012,** *25* (4), 171-178.

16. Zetzsche, L.; Yazarians, J.; Chakrabarty, S.; Hinze, M.; Lukowski, A.; Joyce, L.; Narayan, A.; Murray, L., Biocatalytic oxidative cross-coupling reactions for biaryl bond formation. **2021**. DOI: 10.33774/chemrxiv-2021-v0bv6-v2.

17. Chavali, A. K.; Rhee, S. Y., Bioinformatics tools for the identification of gene clusters that biosynthesize specialized metabolites. *Briefings in Bioinformatics* **2018,** *19* (5), 1022-1034.

18. Keilwagen, J.; Hartung, F.; Paulini, M.; Twardziok, S. O.; Grau, J., Combining RNA-seq data and homology-based gene prediction for plants, animals and fungi. *Bmc Bioinformatics* **2018,** *19*.

19. Roumpeka, D. D.; Wallace, R. J.; Escalettes, F.; Fotheringham, I.; Watson, M., A Review of Bioinformatics Tools for Bio-Prospecting from Metagenomic Sequence Data. *Frontiers in Genetics* **2017,** *8*.

20. Wencel-Delord, J.; Panossian, A.; Leroux, F. R.; Colobert, F., Recent advances and new concepts for the synthesis of axially stereoenriched biaryls. *Chem. Soc. Rev.* **2015,** *44* (11), 3418-3430.

21. Egami, H.; Matsumoto, K.; Oguma, T.; Kunisu, T.; Katsuki, T., Enantioenriched Synthesis of C-1-Symmetric BINOLs: Iron-Catalyzed Cross-Coupling of 2-Naphthols and Some Mechanistic Insight. *J. Am. Chem. Soc.* **2010,** *132* (39), 13633-13635.

22. Brunel, J. M., BINOL: A versatile chiral reagent. *Chem. Rev.* **2005,** *105* (3), 857-897.

23. Chen, Y.; Yekta, S.; Yudin, A. K., Modified BINOL ligands in asymmetric catalysis. *Chem. Rev.* **2003,** *103* (8), 3155-3211.

24. Dumas, V. G.; Defelipe, L. A.; Petruk, A. A.; Turjanski, A. G.; Marti, M. A., QM/MM study of the C-C coupling reaction mechanism of CYP121, an essential Cytochrome p450 of *Mycobacterium tuberculosis*. *Proteins* **2014,** *82* (6), 1004-1021.

25. Zhao, B.; Guengerich, F. P.; Bellamine, A.; Lamb, D. C.; Izumikawa, M.; Lei, L.; Podust, L. M.; Sundaramoorthy, M.; Kalaitzis, J. A.; Reddy, L. M.; Kelly, S. L.; Moore, B. S.; Stec, D.; Voehler, M.; Falck, J. R.; Shimada, T.; Waterman, M. R., Binding of two flaviolin substrate molecules, oxidative coupling, and crystal structure of Streptomyces coelicolor A3(2) cytochrome P450 158A2. *Journal of Biological Chemistry* **2005,** *280* (12), 11599-11607.

26. Yu, X.; Liu, F.; Zou, Y.; Tang, M. C.; Hang, L.; Houk, K. N.; Tang, Y., Biosynthesis of Strained Piperazine Alkaloids: Uncovering the Concise Pathway of Herquline A. *J. Am. Chem. Soc.* **2016,** *138* (41), 13529-13532.

27. Grandner, J. M.; Cacho, R. A.; Tang, Y.; Houk, K. N., Mechanism of the P450-Catalyzed Oxidative Cyclization in the Biosynthesis of Griseofulvin. *ACS Catal.* **2016,** *6* (7), 4506-4511.

28. Lin, H. C.; McMahon, T. C.; Patel, A.; Corsello, M.; Simon, A.; Xu, W.; Zhao, M. X.; Houk, K. N.; Garg, N. K.; Tang, Y., P450-Mediated Coupling of Indole Fragments To Forge Communesin and Unnatural Isomers. *J. Am. Chem. Soc.* **2016,** *138* (12), 4002-4005.